catalysts

Immobilized Biocatalysts

Edited by
Peter Grunwald

Printed Edition of the Special Issue Published in *Catalysts*

www.mdpi.com/journal/catalysts

MDPI

Immobilized Biocatalysts

Immobilized Biocatalysts

Special Issue Editor

Peter Grunwald

MDPI • Basel • Beijing • Wuhan • Barcelona • Belgrade

Special Issue Editor
Peter Grunwald
University of Hamburg
Germany

Editorial Office
MDPI
St. Alban-Anlage 66
Basel, Switzerland

This is a reprint of articles from the Special Issue published online in the open access journal *Catalysts* (ISSN 2073-4344) from 2017 to 2018 (available at: https://www.mdpi.com/journal/catalysts/special_issues/Immobilized_Biocatalysts)

For citation purposes, cite each article independently as indicated on the article page online and as indicated below:

LastName, A.A.; LastName, B.B.; LastName, C.C. Article Title. *Journal Name* **Year**, *Article Number*, Page Range.

ISBN 978-3-03897-318-8 (Pbk)
ISBN 978-3-03897-319-5 (PDF)

Articles in this volume are Open Access and distributed under the Creative Commons Attribution (CC BY) license, which allows users to download, copy and build upon published articles even for commercial purposes, as long as the author and publisher are properly credited, which ensures maximum dissemination and a wider impact of our publications. The book taken as a whole is © 2018 MDPI, Basel, Switzerland, distributed under the terms and conditions of the Creative Commons license CC BY-NC-ND (http://creativecommons.org/licenses/by-nc-nd/4.0/).

Contents

About the Special Issue Editor

Peter Grunwald studied chemistry at the University of Saarbrücken and the University of Hamburg, Germany, where he graduated in the field of high-frequency spectroscopy, and then became a staff member of the Institute of Physical Chemistry. After receiving his PhD in physical chemistry from the Department of Chemistry at the University of Hamburg, he founded a biotechnology research group. He was appointed professor in 2001. His research interests focus on the preparation and properties of immobilized enzymes, the kinetics of enzymes in organic solvents, and interactions between biocatalysts and heavy metal ions. Prof. Grunwald is also interested in chemical education, including curriculum development. He is the editor of a biocatalysis series and the author of a biocatalysis textbook.

Preface to "Immobilized Biocatalysts"

This book provides an updated overview of immobilized biocatalysts (enzymes and whole cells) presenting modern techniques for their fabrication together with a variety of interesting actual applications.

The enzymes, the immobilization of which is described in the different articles, belong to the enzyme classes EC 1 (glucose oxidase, cyclohexanone monooxygenase, horseradish peroxidase, ketoreductase, glucose dehydrogenase, and laccase), EC 2 (hypoxanthine–guanine–xanthine phosphoribosyltransferase, aminotransferase, cellulose synthase), EC 3 (cellulase, β-amylase, various lipases, an esterase, invertase, endo-β-N-acetylglucosaminidase, β-fructofuranosidase, and the protease ficin), and to EC 4 (hydroxynitril lyase). Immobilized whole cells include those of Escherichia coli, Gram-positive Planococcus sp. S5, Rhodotorula mucilaginosa, Gram-negative Enterobacter aerogenes, Komagataeibacter xylinum B-12429 cells, and baker's yeast lysates.

The book starts with a variety of review articles. The first one is an overview of the industrial application of (immobilized) biocatalysts in areas such as the pharmaceutical, food and beverage industries, as well as the energy sector (biofuel production and natural gas conversion). The authors discuss how the next generation of immobilized biocatalysts will be coined by the overlap of technical expertise in enzyme immobilization, protein, and process engineering to improve industrial processes with respect to product yield, market profitability, and environmental-friendliness. A review, written with the aim of providing an orientation for selecting appropriate support materials with tailored properties for the preparation of highly effective biocatalytic systems and their application in different processes deals with the pros and cons of a large variety of inorganic and organic as well as hybrid and composite materials including nano-supports. To the rather new hybrid materials belong metal–organic frameworks (MOFs) characterized by a vast structural and functional tunability. They are reviewed here with respect to their usability as platforms for enzyme immobilization, and the different applications of these enzyme@MOF hybrid materials. This is followed by a research paper where the authors demonstrate the in situ self-assembly of Zn/adenine hybrid nano-coordination polymers as a simple one-step immobilization method, resulting in highly active catalysts with excellent reusability.

In connection with the application of immobilized redox enzymes for sensing applications, as well as for energy conversion, direct electron transfer by tunneling between enzymes and conductive surfaces is of high importance. This requires controlling enzyme orientation at planar electrodes. The factors influencing the proper orientation together with various analytical methods for the characterization and quantification of the desired orientation is the topic of a further review. Related to this, a paper about the construction of an amperometric biosensor for the co-detection of dopamine and glucose may be of interest. As a novel matrix for enzyme immobilization, polyelectrolyte complex beads prepared from a two-step reaction of oppositely-charged polymers turned out to be well-suited for entrapping recombinant E. coli cells overexpressing cyclohexanone monooxygenase. A two-enzyme system consisting of a ketoreductase and glucose dehydrogenase immobilized inside polyvinyl alcohol (PVA) gel particles served to catalyze the asymmetric reduction of keto esters to optically active hydroxy esters. Rhodotorula mucilaginosa is a very active and selective whole-cell biocatalyst for the asymmetric reduction of various aromatic ketones to the desired chiral alcohols; for cell immobilization, agar, calcium alginate, PVA-alginate, and chitosan were employed. Enterobacter aerogenes expressing the ataA gene encoding the adhesive protein of Acinetobacter sp. Tol 5 simplified and accelerated the immobilization of the whole-cell catalysts on polyurethane foam and was shown to be well-suited for biological hydrogen production.

Other articles describe the application of immobilized biocatalysts for the degradation of pollutants, e.g., the nonsteroidal anti-inflammatory drug naproxen by means of the Gram-positive bacterium Planococcus sp. S5 immobilized onto a loofah sponge. A lipase from Thermomyces lanuginosus was used to degrade the micro-pollutant bisphenol A in contaminated water; a commercial macroporous melamine formaldehyde foam served as the immobilization support. Highly stable and reusable cross-linked enzyme aggregates (CLEAs) of the thermostable esterase estUT1 of the bacterium Ureibacillus thermosphaericus, co-expressed with an E. coli chaperone team, were prepared for the removal of organophosphate insecticides such as malathion from municipal wastewater. In another article, the application of the CLEA-technique for maltose production with starch from cassava bagasse with crosslinked -amylase is reported, and in a review article, techniques for the preparation of CLEAs, including the co-immobilization of different enzymes together with a variety of biotechnological application examples demonstrating their economic and environmental benefits are discussed.

Lipases have attracted high scientific attention because they not only hydrolyze carboxylic ester bonds, but also cause esterification, interesterification, and transesterification reactions in nonaqueous media. An example is a low-temperature ethyl hexanoate synthesis by means of an acyl transfer reaction with an antarctic Pseudomonas AMS8 lipase in toluene. A new immobilization method making use of SiO2 xerogel and nanocarbon-in-silica composites was successfully tested with lipases catalyzing the esterification of fatty acids with aliphatic alcohols. A one-step encapsulation method for synthesizing X-shaped zeolitic imidazolate frameworks (ZIF-8) and immobilizing Rhizomucor miehei lipase for the biocatalytic production of biodiesel showed a 26-fold increase in activity with soybean oil as the substrate compared to the free enzyme, a conversion yield of 95.6% under optimum conditions; 84.7% of the initial activity was preserved after 10 cycles. The isolation and purification of two Fusarium verticillioides lipases through adsorption using octadecyl Sepabeads and octyl Sepharose resins resulted in a three-fold increase in activity, with potential for industrial application. A new strategy to mitigate the often unfavorable interaction of enzymes with the solid support is the genetic fusion of T4-lysozyme to the N-terminus of enzymes to be immobilized; the T4-lysozyme acts as an inert shield in covalent immobilization and leads to retention or even significant improvement in the rescued activity.

Further application examples discussed in this book are the immobilization of the hydroxynitrile lyase from Prunus amygdalus on Celite R-633, which very successfully catalyzes the conversion of benzaldehyde to R-mandelonitrile, or that of endo-β-N-acetylglucosaminidase from the commensal Bifidobacterium infantis for the release of bioactive N-glycans, which might be of use as prebiotics or anti-pathogenic factors. A recombinant β-fructofuranosidase from the yeast Xanthophyllomyces dendrorhous that was expressed in Pichia pastoris and immobilized within PVA lenticular particles turned out to be well-suited to the synthesis of various neo-fructooligosaccharides. Hypoxanthine–guanine–xanthine phosphoribosyltransferase from Thermus thermophilus HB8 was immobilized onto glutaraldehyde-activated MagReSyn®Amine magnetic iron oxide porous microparticles by different strategies for the one-pot, one-step production of dietary nucleotides. Graphene oxide grafted with the hydrophobic spacer p-β-sulfuric acid ester ethyl sulfone aniline for the covalent immobilization of cellulase led to a significant increase in the enzyme's half-life; the whole immobilization procedure was finished after 10 min with an immobilization yield and efficiency of above 90%. Komagataeibacter xylinum B-12429 cells immobilized in PVA cryogel turned out to be well-suited to the production of bacterial crystalline cellulose from various renewable biomass sources. An inorganic/organic hybrid support, TiO2–lignin, was employed for the immobilization of a cellulase from Aspergillus niger. The hybrid support contributed to a significant improvement of the enzyme's thermal and chemical stability. Finally, the contribution of different yeast-surface-display techniques for the creation of engineered strains for application in consolidated bioprocessing (CBP) is reviewed elaborately. CBP combines

cellulase production, enzymatic hydrolysis, and microbial fermentation into a single operation to convert lignocellulosic biomass to platform chemicals such as ethanol.

In conclusion, this book should be of great interest to all those involved in the various aspects of this topic, which are discussed in the research and review articles written by renowned researchers. They introduce new immobilization procedures, novel support materials and application areas, thereby meeting the state of the art of both scientific and technical standards.

Peter Grunwald

Special Issue Editor

catalysts

MDPI

Editorial

Immobilized Biocatalysts

Peter Grunwald

Department of Physical Chemistry, University of Hamburg, Grindelallee 117, D-20146 Hamburg, Germany; grunwald@chemie.uni-hamburg.de

Received: 28 August 2018; Accepted: 4 September 2018; Published: 9 September 2018

1. Definitions, Historical Aspects, and Perspectives

An application-related definition for immobilized enzymes was given by Chibata in 1978 [1]: they are "enzymes physically confined or localized in a certain defined region of space with retention of their catalytic activities which can be used repeatedly and continuously"; this also holds in essence for immobilized cells.

The immobilization of biocatalysts or other bioactive components often means their transformation from a soluble to an insoluble state by attaching them to an insoluble carrier material or by encapsulating the catalysts within a polymer matrix of synthetic or natural origin. This may result in a significant change of the native catalyst's properties. For an explanation of the observed modified reaction behavior, the laws of heterogeneous kinetics have to be applied [2,3].

Examples of immobilized biocatalysts (enzymes and whole cells) were known since about 100 years. One of the first papers in this field was a report by Nelson and Griffin [4] on the adsorption of yeast invertase onto charcoal; the catalyst remained active in this state and catalyzed the hydrolysis of sucrose. However, the great practical importance of these findings was not recognized until several decades later; pioneering research began with the work of Grubhofer and Schleith [5], Bernfeld and Wan [6], or Katchalski-Katzir et al. [7], to name but a few. Since then, the number of publications increased significantly and research in this area of enzyme technology has not lost any of its topicality until to date. Application fields are numerous and steadily increasing. Immobilization of biocatalysts is not only important for an economical application of biocatalysts in (organic) synthesis, but also for the construction of biosensors or use of immobilized biocatalysts in wastewater treatment [8–10]. Furthermore, site-selective immobilization is a key step for on-chip enzyme assays, a topic excellently reviewed by Wong et al. [11]. A combination of biocatalysis with nanotechnology led, for example, in the recent past, to the development of nanocarriers for therapeutic proteins; these nanoconjugates are able to cross the blood–brain barrier and enable the treatment of diseases of the central nervous system (CNS), such as lysosomal storage diseases associated with cognitive impairment or CNS tumors [12–14].

An application of biocatalysts in immobilized form has several advantages: they may be reused several times, reducing the costs for a biocatalyst, and thus, of the entire process. The procedure often results in enhanced (thermal) stability, and spoiling of the obtained products is avoided. Regardless, up to now, large-scale applications of immobilized biocatalysts are still rather rare, and an immobilization procedure characterized by a general applicability does not seem to exist; the opinion that each biocatalyst needs a tailor-made immobilization procedure is widespread. Nonetheless, there are some outstanding examples of industrial application. The first one was the immobilization of aminoacylase by use of diethylaminoethyl (DEAE)–Sephadex as a solid support for the stereoselective hydrolysis of *N*-acyl-D,L-amino acids, developed in 1969 by Chibata et al., Tanabe Seiyaku Co., Japan [15], and the same group succeeded in establishing a large-scale industrial process for the amino acid L-aspartate production from ammonium fumarate by entrapment of L-asparate ammonialyase-containing *Escherichia coli* cells [16,17]. Actual examples of industrial processes performed in presence of robust immobilized enzymes were discussed by Thum et al. [18].

For further recently published reviews, see, e.g., Homaei et al. [19], Liese and Hilterhaus [20], Sheldon and van Pelt [21], Zucca and Sunjust [22], Mohamad et al. [23], and Kim et al. [24], as well as Rehm et al. [25] and Bernal et al. [26], with the latter two dealing with new strategies to integrate enzyme immobilization and protein engineering.

2. This Special Issue

When I was asked to overtake the role of a Guest Editor for this Special Issue, although feeling honored, I first declined against the background of other obligations. Now looking back on these months of acquiring possible authors for this project, I do not regret the invested time. This is particular due to the wonderful and uncomplicated cooperation with the Assistant Editor Adela Liao and her competent team. Moreover, I owe particular thanks to all the authors who contributed their excellent papers to this Special Issue that is comprised of twenty-nine articles, among them six reviews, covering many important aspects of this topic together with a variety of new approaches.

The enzymes, the immobilization of which is described in the different articles, belong to the enzyme classes EC 1 (glucose oxidase, cyclohexanone monooxygenase, horseradish peroxidase, ketoreductase, glucose dehydrogenase, and laccase), EC 2 (hypoxanthine–guanine–xanthine phosphoribosyltransferase and aminotransferase), EC 3 (cellulase, β-amylase, various lipases, invertase, endo-β-*N*-acetylglucosaminidase, β-fructofuranosidase, and the protease ficin), and to EC 4 (hydroxynitril lyase). Immobilized whole cells include those of *Escherichia coli*, Gram-positive *Planococcus* sp. S5, *Rhodotorula mucilaginosa*, Gram-negative *Enterobacter aerogenes*, *Komagataeibacter xylinum* B-12429 cells, and baker's yeast lysates.

In more detail, Bracco et al. [27] immobilized the hydroxynitrile lyase from *Prunus amygdalus* on Celite R-633 for catalyzing very successfully the conversions of benzaldehyde to *R*-mandelonitrile; the immobilized enzyme was recycled up to ten times. A paper supporting glycoproteomic investigations was presented by Cohen et al. [28]. These researchers immobilized endo-β-*N*-acetylglucosaminidase from the commensal *Bifidobacterium infantis* for the release of bioactive *N*-glycans which might be of use as prebiotics or anti-pathogenic factors. The immobilized enzyme also catalyzed the cleavage of neutral glycans from whey proteins. Musa et al. [29] reported a low-temperature ethyl hexanoate synthesis by means of an acyl transfer reaction with an antarctic *Pseudomonas* AMS8 Lipase as catalyst in toluene that worked optimally at 20 °C. The product is employed as a synthetic flavor ester in the food, beverage, and cosmetic and pharmaceutical industries. According to Míguez et al. [30], a recombinant β-fructofuranosidase from the yeast *Xanthophyllomyces dendrorhous* that was expressed in *Pichia pastoris* turned out to be well suited for the synthesis of various neo-fructooligosaccharides such as neokestose, 1-kestose, neonystose, and blastose in a batch reactor at 30 °C. The β-fructofuranosidase was immobilized in polyvinyl alcohol lenticular particles, and could be reused for at least seven cycles without loss of activity. The tetrameric hypoxanthine–guanine–xanthine phosphoribosyltransferase from *Thermus thermophilus* HB8 was immobilized by del Arco et al. [31] onto glutaraldehyde-activated MagReSyn®Amine magnetic iron-oxide porous microparticles (M*Tt*HGXPRT) by different strategies for the one-pot, one-step production of dietary nucleotides. The best variant showed negligible loss of activity at 60 °C during 24 h, and a reusability of up to seven cycles. Graphene oxide was grafted by Gao and coworkers [32] with the hydrophobic spacer *p*-β-sulfuric acid ester, ethyl sulfone aniline, for the covalent immobilization of cellulase. After optimizing the reaction conditions, the whole procedure was finished already after 10 min with an immobilization yield and efficiency of above 90%. At 50 °C, the half-life of the cellulase immobilized by this new approach was six-fold higher than that of the free cellulase. The potential this method may have for the immobilization of other enzymes needs to be clarified. Another new immobilization method described by Kovalenko et al. [33] makes use of SiO_2 xerogel and nanocarbons-in-silica composites for an entrapment of baker's yeast lysates. The authors tested theses carriers with invertase and lipase activity of the enzymatically active components. The invertase activity increased by a factor of about six in the presence of multi-walled carbon nanotubes (CNTs) inside the xerogel, whereas the lipase activity tested via esterification of

fatty acids with aliphatic alcohols increased by a factor of nearly two. The lipase-active composite CNTs-in-silica biocatalysts operated without loss of activity for more than one thousand hours.

With the aim of degrading the nonsteroidal anti-inflammatory drug naproxen, Dzionek et al. [8] immobilized the Gram-positive bacterium *Planococcus* sp. S5 onto a loofah sponge. This conjugate degraded naproxen efficiently for 55 days without significant damage and disintegration of the carrier, and in higher concentrations than free cells did. Barley β-amylase is, among others, important for maltose production. Araujo-Silva et al. [34] prepared immobilized β-amylase in the form of cross-linked enzyme aggregates using bovine serum albumin or soy protein isolate as feeder proteins to reduce diffusion problems and to successfully obtain maltose from converting the residual starch contained in cassava bagasse. A two-enzyme system developed by Petrovičová and colleagues [35], consisting of ketoreductase and glucose dehydrogenase immobilized inside of polyvinyl alcohol (PVA) gel particles, served to catalyze the asymmetric reduction of keto esters to optically active hydroxy esters. The catalyst could be used 18 times with minimal loss of activity and complete conversion of a model substrate. The described storage conditions enabled the retention of 80% activity after about 10 months. High-throughput screening performed by Liu et al. [36] revealed *Rhodotorula mucilaginosa* as a very active and selective whole-cell biocatalyst for the asymmetric reduction of various aromatic ketones to the desired chiral alcohols. For cell immobilization, agar, calcium alginate, PVA-alginate, and chitosan were employed as support matrices; pH tolerance and thermal stability were improved. Cells immobilized on agar retained 90% activity after 60 days of storage at 4 °C and could be reused six times without loss of activity. Biological hydrogen production by microbial cells is an actual research area. Nakatani and coworkers [37], for this purpose, immobilized *Enterobacter aerogenes* expressing the *ataA* gene encoding the adhesive protein of *Acinetobacter* sp. Tol 5 on polyurethane foam, thereby simplifying and accelerating the immobilization of whole-cell catalysts. The total H_2 production was 0.6 mol/mol glucose at a production rate in the flow reactor of 42 $mL \cdot h^{-1} \cdot L^{-1}$.

An application example of biocatalyst immobilization for wastewater treatment was provided by Samoylova et al. [9]. They prepared stable cross-linked enzyme aggregates (CLEAs) of the thermostable esterase, estUT1, of the bacterium *Ureibacillus thermosphaericus*, and used these CLEAs for removal of the organophosphate insecticide, malathion. High operational stability and activity of the esterase was achieved by its coexpression with an *E. coli* chaperone team. Siar et al. [38] investigated experimental parameters influencing activity and stability of a ficin extract immobilized onto glutaraldehyde-activated agarose beads. An optimal immobilization yield with 80% was achieved at pH 9 and maximum enzyme loading was about 70 mg/g. Using casein as a substrate, the activity of the biocatalyst was 30%. The obtained results suggested a complex inactivation mechanism of the immobilized enzyme as a function of reaction conditions. An actual topic is the biocatalytic production of biodiesel. An attractive procedure reported by Adnan and coworkers [39] relies on a one-step encapsulation method for synthesizing X-shaped zeolitic imidazolate frameworks (ZIF-8) and immobilizing *Rhizomucor miehei* lipase. The conjugate showed a 26-fold increase in activity with soybean oil as a substrate compared to the free enzyme, and a conversion yield of 95.6% under optimal conditions; 84.7% of the initial activity was preserved after 10 cycles. Dell Antonio Facchini et al. [40] isolated and purified two *Fusarium verticillioides* lipases through adsorption using octadecyl Sepabeads and octyl Sepharose resins which resulted in a three-fold increase in activity. The catalysts were investigated with respect to their ability to release *S*-enantiomers from substrates, and their transesterification capacity. The obtained results indicate industrial applicability of the immobilized lipases. A new strategy to mitigate the often unfavorable interaction of enzymes with the solid support is the genetic fusion of T4-lysozyme to the *N*-terminus of enzymes to be immobilized. Planchestainer and coworkers [41] demonstrated with different enzyme-fusion conjugates that the T4-lysozyme acts as an inert shield in covalent immobilization and leads to the retention of or even significant improvement in the rescued activity.

Bergman and colleagues [42] provided a method for temporally resolving the transients of vesicular neurotransmitter release and fluctuations of metabolites such as glucose, thereby improving

understanding of the regulation of neuronal activity. For this purpose, they developed an amperometric biosensor for co-detection of dopamine and glucose. The device enabled visualization of fluctuations in glucose and dopamine concentrations at a millisecond time scale. *Komagataeibacter xylinum* B-12429 cells immobilized in polyvinyl-alcohol cryogel turned out to be well suited for the production of bacterial crystalline cellulose from various renewable biomass sources as reported by Stepanov and Efremenko [43]. The cellulose passed through the pores of the cryogel matrix into the medium resulting in a continuous production. The immobilized cells retained 100% metabolic activity for at least 10 working cycles. An inorganic/organic hybrid support TiO_2–lignin was employed by Zdarta et al. [44] for the immobilization of a cellulase from *Aspergillus niger*. As is to be seen from the fact that the half-life of the immobilized cellulase was five times that of the free enzyme and over 90% of its initial catalytic was retained after ten repeated cycles, the hybrid support contributed to a significant improvement of the enzyme's thermal and chemical stability. Allertz et al. [10] presented the first application of commercial macroporous melamine formaldehyde foam Basotect® for covalent and adsorptive enzyme immobilization after pretreatment of the carrier surface. The immobilization conditions for laccase from *Trametes versicolor* and the lipase from *Thermomyces lanuginosus* were optimized, and the immobilized laccase was shown to be able to degrade 80% of the micro-pollutant bisphenol A in contaminated water. A novel matrix for enzyme immobilization, polyelectrolyte complex beads prepared from a two-step reaction of oppositely charged polymers, was developed by Krajčovič et al. [45] for entrapping recombinant *E. coli* cells overexpressing cyclohexanone monooxygenase. The immobilizate exhibited high operational stability and reusability, e.g., in connection with the oxidation of *rac*-bicyclo[3.2.0]hept-2-en-6-one to the respective lactones. Liang et al. [46] demonstrated with glucose oxidase (GOx) and horseradish peroxidase as examples that in situ self-assembly of Zn/adenine hybrid nano coordination polymers provides a simple one-step immobilization method, resulting in highly active catalysts with excellent reusability. The immobilized GOx could also be used in connection with a glucose biosensor, detecting the substrate selectively down to 1.84 μM.

This Special Issue also contains six review articles. Chapman et al. [47] provided an overview of the industrial application of (immobilized) biocatalysts in areas such as pharmaceutical, food, and beverage industries, as well as the energy sector (biofuel production and natural gas conversion). The authors discuss how the next generation of immobilized biocatalysts will be coined by the overlap of technical expertise in enzyme immobilization, protein, and process engineering to improve industrial processes with respect to product yield, market profitability, and environmental friendliness. Immobilized redox enzymes are employed for sensing applications, as well as for energy conversion. In this connection, direct electron transfer by tunneling between enzymes and conductive surfaces is of high importance. This requires controlling enzyme orientation at planar electrodes. Hitaishi et al. [48] review all the factors influencing a proper orientation together with various analytical methods for characterization and quantification of the desired orientation. The review contributed by Yamaguchi and colleagues [49] deals with techniques for the preparation of cross-linked enzyme aggregates (CLEAs), including co-immobilization of different enzymes. CLEAs often combine the advantages of immobilized enzymes such as high catalytic activities, good storage, and operational stabilities, as well as good reusability. A variety of biotechnological application examples are given demonstrating their economic and environmental benefits. Metal–organic frameworks (MOFs) are porous hybrid materials consisting of metal ions or clusters and organic ligands, and are characterized by a vast structural and functional tunability. Wang et al. [50] review these MOFs as platforms for enzyme immobilization, and the different applications of these enzyme–MOF hybrid materials. The improvement of catalytic activity and robustness of MOF-encapsulated enzymes compared to their free counterparts is discussed in detail. Consolidated bioprocessing (CBP) combines cellulases production, enzymatic hydrolysis, and microbial fermentation into a single operation to convert lignocellulosic biomass to platform chemicals such as ethanol. Tabañag and colleagues [51] reviewed the contribution of different yeast-surface-display techniques for the creation of correspondingly engineered strains. Finally,

Zdarta et al. [52] discuss the pros and cons of a large variety of inorganic and organic, as well as hybrid and composite, materials including nano supports, used for the immobilization of biocatalysts. The review was written with the aim of providing an orientation for selecting appropriate support materials with tailored properties for the preparation of highly effective biocatalytic systems and their application in different processes.

In conclusion, the Special Issue "Immobilized Biocatalysts" should be of great interest for all those involved in the various aspects of this topic, which are discussed in the contributions and review articles. They introduce new immobilization procedures, as well as novel support materials and applications, thereby meeting the state of the art of both scientific and technical standards.

Conflicts of Interest: The author declare no conflict of interest.

References

1. Chibata, I. (Ed.) *Immobilized Enzymes, Research and Development*; Kodansha: Tokyo, Japan, 1978.
2. Buchholz, K.; Kasche, V.; Bornscheuer, U.T. *Biocatalysts and Enzyme Technology*; WILEY-VCH Verlag GmbH & Co., KGaA: Weinheim, Germany, 2005.
3. Grunwald, P. *Biocatalysis: Biochemical Fundamentals and Applications*; World Scientific Publishing Pte. Ltd.: Singapore, 2017.
4. Nelson, J.M.; Griffin, E.G. Adsorption of invertase. *J. Am. Chem. Soc.* **1916**, *38*, 1109–1115. [CrossRef]
5. Grubhofer, N.; Schleith, L. Modified ion exchangers as specific adsorbents. *Naturwissenschaften* **1953**, *40*, 508–512. [CrossRef]
6. Bernfeld, P.; Wan, J. Antigens and enzymes made insoluble by entrapping them into lattices of synthetic polymers. *Science* **1963**, *142*, 678–679. [CrossRef] [PubMed]
7. Katchalski-Katzir, E.; Silman, E.H.; Goldman, R. Effect of the microenvironment on the mode of action of immobilized enzymes. *Adv. Enzymol.* **1971**, *34*, 445–536.
8. Dzionek, A.; Wojcieszyńska, D.; Hupert-Kocurek, K.; Adamczyk-Habrajska, M.; Guzik, U. Immobilization of *Planococcus* sp. S5 strain on the loofah sponge and Its application in naproxen removal. *Catalysts* **2018**, *8*, 176. [CrossRef]
9. Samoylova, Y.V.; Sorokina, K.N.; Piligaev, A.V.; Parmon, V.N. Preparation of stable cross-linked enzyme aggregates (CLEAs) of a *Ureibacillus thermosphaericus* esterase for application in malathion removal from wastewater. *Catalysts* **2018**, *8*, 154. [CrossRef]
10. Allertz, P.J.; Berger, S.; Sellenk, G.; Dittmer, C.; Dietze, M.; Stahmann, K.-P.; Salchert, K. Approaching immobilization of enzymes onto open Porous Basotect®. *Catalysts* **2017**, *7*, 359. [CrossRef]
11. Wong, L.S.; Khan, F.; Micklefield, J. Selective covalent protein immobilization: Strategies and applications. *Chem. Rev.* **2009**, *109*, 4025–4053. [CrossRef] [PubMed]
12. Peluffo, H.; Unzueta, U.; Negro-Demontel, M.L.; Xu, Z.; Váquez, E.; Ferrer-Miralles, N.; Villaverde, A. BBB-targeting, protein-based nanomedicines for drug and nucleic acid delivery to the CNS. *Biotechnol. Adv.* **2015**, *33*, 277–287. [CrossRef] [PubMed]
13. Reynolds, J.L.; Mahato, R.I. Nanomedicines for the treatment of CNS diseases. *J. Neuroimmune Pharmacol.* **2017**, *12*, 1–5. [CrossRef] [PubMed]
14. DeMarino, C.; Schwab, A.; Pleet, M.; Mathiesen, A.; Friedman, J.; El-Hage, N.; Kashanchi, F. Biodegradable Nanoparticles for Delivery of therapeutics in CNS Infection. *J. Neuroimmune Pharmacol.* **2017**, *12*, 31–50. [CrossRef] [PubMed]
15. Chibata, I.; Tosa, T.; Sato, T.; Mori, T. Production of L-amino acids by aminoacylase adsorbed on DEAE-Sephadex. *Methods Enzymol.* **1976**, *44*, 746–759. [PubMed]
16. Chibata, I.; Tosa, T.; Sato, T. Immobilized aspartase-containing microbial cells: Preparation and enzymatic properties. *Appl. Microbiol.* **1974**, *27*, 878–885. [PubMed]
17. Tosa, T.; Sato, T.; Mori, T.; Chibata, I. Basic Studies for Continuous Production of L-Aspartic Acid by Immobilized Escherichia coli Cells. *Appl. Microbiol.* **1974**, *27*, 886–889. [PubMed]
18. Thum, O.; Hellmers, F.; Ansorge-Schumacher, M. Industrial Applications of Robust Enzyme Preparations. In *Industrial Biocatalysis*; Grunwald, P., Ed.; Pan Stanford Series on Biocatalysis; Pan Stanford Publishing Pte. Ltd.: Singapore, 2014; Volume 1.

19. Homaei, A.A.; Sariri, R.; Vianello, F.; Stevanato, R. Enzyme immobilization: An update. *J. Chem. Biol.* **2013**, *6*, 185–205. [CrossRef] [PubMed]
20. Liese, A.; Hilterhaus, L. Evaluation of immobilized enzymes for industrial applications. *Chem. Soc. Rev.* **2013**, *42*, 6236–6249. [CrossRef] [PubMed]
21. Sheldon, R.A.; van Pelt, S. Enzyme immobilization in biocatalysis: Why, what and how. *Chem. Soc. Rev.* **2013**, *42*, 6223–6235. [CrossRef] [PubMed]
22. Zucca, P.; Sanjust, E. Inorganic Materials as Supports for Covalent Enzyme Immobilization: Methods and Mechanisms. *Molecules* **2014**, *19*, 14139–14194. [CrossRef] [PubMed]
23. Mohamad, N.R.; Marzuki, N.H.C.; Buang, N.A.; Huyop, F.; Wahab, R.A. An overview of technologies for immobilization of enzymes and surface analysis techniques for immobilized enzymes. *Biotechnol. Biotechnol. Equip.* **2015**, *29*, 205–220. [CrossRef] [PubMed]
24. Kim, K.H.; Lee, O.K.; Lee, E.Y. Nano-immobilized biocatalysts for biodiesel production from renewable and sustainable resources. *Catalysts* **2018**, *8*, 68.
25. Bernal, C.; Rondriguez, K.; Martínez, R. Integrating enzyme immobilization and protein engineering: An alternative path for the development of novel and improved industrial biocatalysts. *Biotechnol. Adv.* **2018**, *36*, 1470–1480. [CrossRef] [PubMed]
26. Rehm, F.B.H.; Chen, S.; Rehm, B.H.A. Bioengineering toward direct production of immobilized enzymes: A paradigm shift in biocatalyst design. *Bioengineered* **2018**, *9*, 6–11. [CrossRef] [PubMed]
27. Bracco, P.; Torrelo, G.; Noordam, S.; de Jong, G.; Hanefeld, U. Immobilization of *Prunus amygdalus* Hydroxynitrile Lyase on Celite. *Catalysts* **2018**, *8*, 287. [CrossRef]
28. Cohen, J.L.; Karav, S.; Barile, D.; de Moura Bell, J.M.L.N. Immobilization of an endo-β-*N*-acetylglucosaminidase for the release of bioactive *N*-glycans. *Catalysts* **2018**, *8*, 278. [CrossRef]
29. Musa, N.; Latip, W.; Abd Rahman, R.N.Z.; Salleh, A.B.; Mohamad Ali, M.S. Immobilization of an Antarctic Pseudomonas AMS8 Lipase for Low Temperature Ethyl Hexanoate Synthesis. *Catalysts* **2018**, *8*, 234. [CrossRef]
30. Míguez, N.; Gimeno-Pérez, M.; Fernández-Polo, D.; Cervantes, F.V.; Ballesteros, A.O.; Fernández-Lobato, M.; Ribeiro, M.H.; Plou, F.J. Immobilization of the β-fructofuranosidase from *Xanthophyllomyces dendrorhous* by nntrapment in polyvinyl alcohol and its application to neo-fructooligosaccharides production. *Catalysts* **2018**, *8*, 201. [CrossRef]
31. Del Arco, J.; Martínez-Pascual, S.; Clemente-Suárez, V.J.; Corral, O.J.; Jordaan, J.; Hormigo, D.; Perona, A.; Fernández-Lucas, J. One-Pot, One-Step Production of Dietary Nucleotides by Magnetic Biocatalysts. *Catalysts* **2018**, *8*, 184. [CrossRef]
32. Gao, J.; Lu, C.-L.; Wang, Y.; Wang, S.-S.; Shen, J.-J.; Zhang, J.-X.; Zhang, Y.-W. Rapid immobilization of cellulase onto graphene oxide with a hydrophobic spacer. *Catalysts* **2018**, *8*, 180. [CrossRef]
33. Kovalenko, G.A.; Perminova, L.V.; Beklemishev, A.B.; Parmon, V.N. Heterogeneous biocatalysts prepared by immuring enzymatic active components inside silica xerogel and nanocarbons-in-silica composites. *Catalysts* **2018**, *8*, 177. [CrossRef]
34. Araujo-Silva, R.; Mafra, A.C.O.; Rojas, M.J.; Kopp, W.; de Campos Giordano, R.; Fernandez-Lafuente, R.; Tardioli, P.W. Maltose production using starch from cassava bagasse catalyzed by cross-linked β-amylase aggregates. *Catalysts* **2018**, *8*, 170. [CrossRef]
35. Petrovičová, T.; Markošová, K.; Hegyi, Z.; Smonou, I.; Rosenberg, M.; Rebroš, M. Co-Immobilization of Ketoreductase and Glucose Dehydrogenase. *Catalysts* **2018**, *8*, 168. [CrossRef]
36. Liu, H.; Duan, W.-D.; de Souza, F.Z.R.; Liu, L.; Chen, B.-S. Asymmetric ketone reduction by immobilized *Rhodotorula mucilaginosa*. *Catalysts* **2018**, *8*, 165. [CrossRef]
37. Nakatani, H.; Ding, N.; Ohara, Y.; Hori, K. Immobilization of *Enterobacter aerogenes* by a trimeric autotransporter adhesin, AtaA, and Its application to biohydrogen production. *Catalysts* **2018**, *8*, 159. [CrossRef]
38. Siar, E.-H.; Arana-Peña, S.; Barbosa, O.; Zidoune, M.N.; Fernandez-Lafuente, R. Immobilization/stabilization of ficin extract on glutaraldehyde-activated agarose beads. Variables that control the final stability and activity in protein hydrolyses. *Catalysts* **2018**, *8*, 149. [CrossRef]
39. Adnan, M.; Li, K.; Xu, L.; Yan, Y. X-shaped ZIF-8 for immobilization *Rhizomucor miehei* lipase via encapsulation and its application toward biodiesel production. *Catalysts* **2018**, *8*, 96. [CrossRef]

40. Facchini, F.D.A.; Pereira, M.G.; Vici, A.C.; Filice, M.; Pessela, B.C.; Guisan, J.M.; Fernandez-Lorente, G.; Polizeli, M.L.T.M. Immobilization effects on the catalytic properties of two *Fusarium verticillioides* lipases: Stability, hydrolysis, transesterification and enantioselectivity improvement. *Catalysts* **2018**, *8*, 84. [CrossRef]
41. Planchestainer, M.; Padrosa, D.R.; Contente, M.L.; Paradisi, F. Genetically fused T4L acts as a shield in covalent enzyme immobilisation enhancing the rescued activity. *Catalysts* **2018**, *8*, 40. [CrossRef]
42. Bergman, J.; Mellander, L.; Wang, Y.; Cans, A.-S. Co-detection of dopamine and glucose with high temporal resolution. *Catalysts* **2018**, *8*, 34. [CrossRef]
43. Stepanov, N.; Efremenko, E. "Deceived" concentrated immobilized cells as biocatalyst for intensive bacterial cellulose production from various sources. *Catalysts* **2018**, *8*, 33. [CrossRef]
44. Zdarta, J.; Jędrzak, A.; Klapiszewski, L.; Jesionowski, T. Immobilization of cellulase on a functional inorganic–organic hybrid support: Stability and kinetic study. *Catalysts* **2017**, *7*, 374. [CrossRef]
45. Krajčovič, T.; Bučko, M.; Vikartovská, A.; Lacík, I.; Uhelská, L.; Chorvát, D.; Neděla, V.; Tihlaříková, E.; Gericke, M.; Heinze, T.; et al. Polyelectrolyte complex beads by novel two-step process for improved performance of viable whole-cell Baeyer-Villiger monoxygenase by immobilization. *Catalysts* **2017**, *7*, 353. [CrossRef]
46. Liang, H.; Sun, S.; Zhou, Y.; Liu, Y. In-situ self-assembly of zinc/adenine hybrid nanomaterials for enzyme immobilization. *Catalysts* **2017**, *7*, 327. [CrossRef]
47. Chapman, J.; Ismail, A.E.; Dinu, C.Z. Industrial applications of enzymes: Recent advances, techniques, and outlooks. *Catalysts* **2018**, *8*, 238. [CrossRef]
48. Hitaishi, V.P.; Clement, R.; Bourassin, N.; Baaden, M.; de Poulpiquet, A.; Sacquin-Mora, S.; Ciaccafava, A.; Lojou, E. Controlling redox enzyme orientation at planar electrodes. *Catalysts* **2018**, *8*, 192. [CrossRef]
49. Yamaguchi, H.; Kiyota, Y.; Miyazaki, M. Techniques for preparation of cross-linked enzyme aggregates and their applications in bioconversions. *Catalysts* **2018**, *8*, 174. [CrossRef]
50. Wang, Q.; Lian, X.; Fang, Y.; Zhou, H.-C. Applications of immobilized bio-catalyst in metal-organic frameworks. *Catalysts* **2018**, *8*, 166. [CrossRef]
51. Tabañag, I.D.F.; Chu, I.-M.; Wei, Y.-H.; Tsai, S.L. The role of yeast-surface-display techniques in creating biocatalysts for consolidated bioprocessing. *Catalysts* **2018**, *8*, 94. [CrossRef]
52. Zdarta, J.; Meyer, A.S.; Jesionowski, T.; Pinelo, M. A general overview of support materials for enzyme immobilization: Characteristics, properties, practical utility. *Catalysts* **2018**, *8*, 92. [CrossRef]

© 2018 by the author. Licensee MDPI, Basel, Switzerland. This article is an open access article distributed under the terms and conditions of the Creative Commons Attribution (CC BY) license (http://creativecommons.org/licenses/by/4.0/).

catalysts

MDPI

Review

Industrial Applications of Enzymes: Recent Advances, Techniques, and Outlooks

Jordan Chapman, Ahmed E. Ismail * and Cerasela Zoica Dinu *

Department of Chemical and Biomedical Engineering, Benjamin M. Statler College of Engineering and Mineral Resources, West Virginia University, P.O. Box 6102, Morgantown, WV 26506, USA; jschapman@mix.wvu.edu

* Correspondence: ahmed.ismail@mail.wvu.edu (A.E.I.); cerasela-zoica.dinu@mail.wvu.edu (C.Z.D); Tel.: +1-304-293-9338 (C.Z.D); Fax: +1-304-293-4139(C.Z.D)

Received: 5 May 2018; Accepted: 30 May 2018; Published: 5 June 2018

Abstract: Enzymes as industrial biocatalysts offer numerous advantages over traditional chemical processes with respect to sustainability and process efficiency. Enzyme catalysis has been scaled up for commercial processes in the pharmaceutical, food and beverage industries, although further enhancements in stability and biocatalyst functionality are required for optimal biocatalytic processes in the energy sector for biofuel production and in natural gas conversion. The technical barriers associated with the implementation of immobilized enzymes suggest that a multidisciplinary approach is necessary for the development of immobilized biocatalysts applicable in such industrial-scale processes. Specifically, the overlap of technical expertise in enzyme immobilization, protein and process engineering will define the next generation of immobilized biocatalysts and the successful scale-up of their induced processes. This review discusses how biocatalysis has been successfully deployed, how enzyme immobilization can improve industrial processes, as well as focuses on the analysis tools critical for the multi-scale implementation of enzyme immobilization for increased product yield at maximum market profitability and minimum logistical burden on the environment and user.

Keywords: enzyme; immobilization; industrial applications; scale-up; techno-economic analysis; life cycle

1. Introduction

Enzymes are highly efficient biocatalysts researched for industrial-scale catalysis because of their several distinct advantages that range from their operation in milder reaction conditions, to their exceptional product selectivity, and to their lower environmental and physiological toxicity [1–4]. The above listed advantages were shown to translate into reduced operating costs when they were effectively employed as biocatalysts in chemical processes. As such, their lower energy requirements, mitigation of waste generation, and simplified production routes [1,3,5] have been partially realized in the pharmaceutical, food, and beverage industries [6–12]. Further work remains however to demonstrate that biocatalysis is economically competitive in other industries, such as natural gas conversion and biofuel production [13–19]. Moreover, across the various industries where biocatalysis can be used, a recurring barrier persists, i.e., the application of enzyme catalysis in chemical processes is limited by the lack of enzyme stability at high temperatures or in turbulent flow regimes, as well as in potentially toxic solvents [20–27]. Thus, concentrated approaches spanning over various disciplines are focusing on the identification and production of robust, stable biocatalysts suitable for application in a broader range of industrial settings [1,3,20–29].

This review focuses on how enzyme catalysis has been advantageously used in chemical processes and which industries can further exploit enzyme catalysis for improved outcomes. Further, this review contains an in-depth discussion of the latest enzyme immobilization techniques,

how enzyme immobilization can aid in the realization of fully optimized biocatalysts, and the combination of technical expertise that will drive the scale-up of these economically competitive immobilized-biocatalytic processes for industrial applications.

2. Enzyme Implementation: A Societal Need

The pharmaceutical, food and beverage, detergent, and biofuel industries have reaped the advantages of enzyme catalysis in commercial-scale applications, while other industries, such as natural gas conversion and fine chemical production, are only recently considering their use [1–4]. In industrial-scale chemical production, the benefits of biocatalysis are often multifaceted, and as such, enzymes are attractive catalysts owing to mild reaction conditions, high product selectivity, and low environmental impact, and thus have been employed for both simplified chemical synthesis routes and improved chemical process economics [1,3,5]; Table 1 illustrates the broad applications of enzyme catalysis throughout various industries.

Table 1. Industrial applications of enzyme catalysis.

Sector	Enzymes	Applications	References
Pharmaceuticals	Nitrile hydratase, transaminase, monoamine oxidase, lipase, penicillin acylase	Synthesis of intermediates for production of active pharmaceutical ingredients	[2,4,30–38]
Food Processing	Trypsin, amylase, glucose isomerase, papain, pectinase	Conversion of starch to glucose, production of high fructose corn syrup, production of prebiotics, debittering of fruit juice	[2,5,9–12,39–43]
Detergent	Protease, lipase, amylase, cellulase	Stain removal, removal of fats and oils, color retention,	[44–48]
Biofuels	Lipase, cellulase, xylanase	Production of fatty acid methyl esters, decomposition of lignocellulotic material for bioethanol production	[18,19,44,49–57]
Paper and Pulp	Lipase, cellulase, xylanase	Removal of lignin for improved bleaching, improvement in fiber properties	[2,4,44,58–61]

Though the advantages of biocatalysis are numerous, commercial enzyme catalysis is used only if it affords a process improved economics of operation [5]. According to Business Communication Company (BCC) Research, the global enzyme market is projected to grow from $5.01 billion in 2016 to $6.32 billion in 2021 (Figure 1), with market trends predicting a shift toward increased technical enzyme production including those used in textile, paper, leather, and biodiesel industries where excess waste generation incurs fines from environmental agencies [44]. Such market projections were shown to be largely driven by process development in enzymatic biofuel production, which present good opportunities for the scale-up of immobilized biocatalysts [44,49].

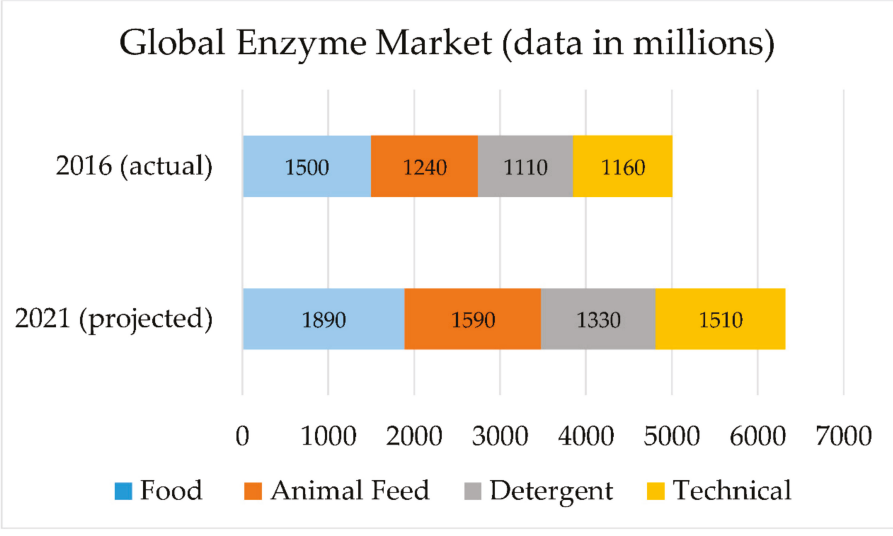

Figure 1. Global enzyme market in 2016 (top) and projected global enzyme market in 2021 (bottom). Figure adapted from data included in Ref. [44].

3. Enzyme Immobilization for Expanded Scope of Implementation

Studies in enzyme immobilization, i.e., the attachment of the biocatalyst to a material with desired physical, chemical, electrical, or mechanical properties, have shown that immobilizing biocatalysts can improve their activity and stability across a broader range of operating conditions, with the additional functionality being imparted depending upon both the method of immobilization as well as the inherent properties of the materials used in such immobilization [49,62–66]. It was further demonstrated that the immobilized biocatalysts are novel in that their application simultaneously also allows for a reduced number of processing steps due to the facile separation of the biocatalyst itself from its reaction mixture, their retention of catalytic activity, and the resulting appreciable degree of reusability [5,20–27]. Table 2 lists both the common advantages and disadvantages associated with the use of an immobilized biocatalyst, as highlighted in previous research.

Table 2. Advantages and disadvantages of enzyme immobilization.

Advantages	Disadvantages
Functionality for use in continuous processes	Loss of enzyme activity
Improved stability in broader range of operating conditions (e.g., pH, temperature etc.)	Immobilization of enzyme in undesired conformation and subsequent loss of activity
Facile separation of enzyme from product	Cost of carrier and additional preparation materials and methods, as well as laborious training strategies
Reusability of enzyme	Mass transfer limitations
Immobilization in preferred conformation and at preferred location	Laborious and time-consuming immobilization processes

Determining the appropriateness of implementing immobilized biocatalysis on an industrial scale requires a critical evaluation of both technical and economic factors as well as of the process in consideration. Often, the benefits of immobilization must be multiple-fold to see an improvement over the economics of free enzyme-catalyzed processes [5]. As such, efficient enzyme immobilization depends critically on

techniques that afford high degrees of stability and reusability, as well as additional functionality without significant hindrances to enzyme activity and product selectivity [49,62–66].

Three main immobilization techniques (Figure 2) have been largely reported in the literature, namely carrier-bound attachment, encapsulation or entrapment, and the formation of crosslinked enzyme aggregates [20–27]. Two kinetic parameters are often calculated for an immobilized enzyme to assess the effects of immobilization on the enzyme's catalytic efficiency when compared to the non-immobilized enzyme counterpart, i.e., the Michaelis constant K_m and maximal reaction velocity V_{max}. K_m compares the rates of substrate-enzyme binding and dissociation with smaller values of K_m suggesting that binding dominates and indicating higher enzyme-substrate affinity [1]. V_{max} measures the rate at which an enzyme converts the substrate to product, and when controlled for catalytic mass, the value of V_{max} is an appropriate measure of catalytic activity [1].

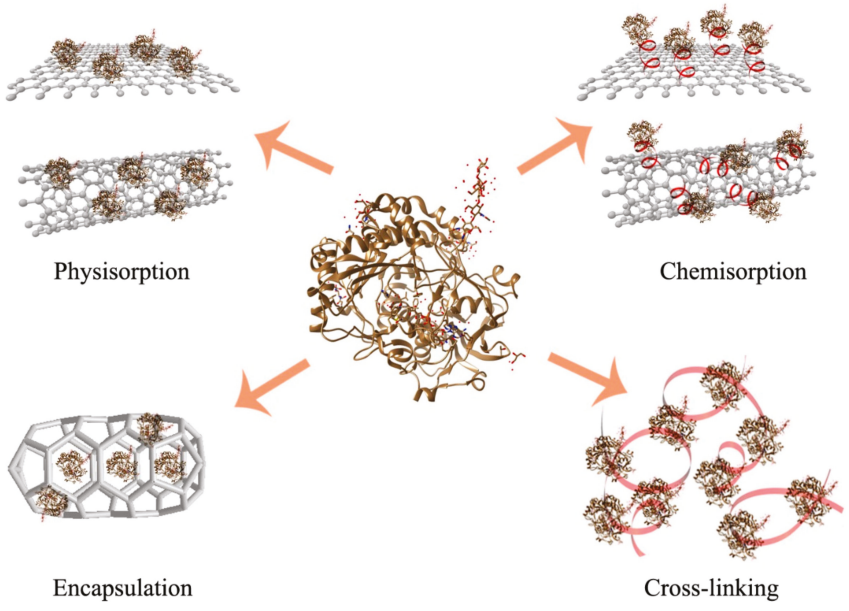

Figure 2. Schematic of different enzyme immobilization techniques. The crystal structure of Glucose Oxidase (GOx) isolated from Aspergillus Niger was used as a model enzyme (PDB ID: 3QVP) [67]. Physical and covalent immobilization techniques are discussed relative to flat nanosupport graphene and curved nanosupport, carbon nanotube respectively. Encapsulation is discussed relative to a pore geometry higher than the diameter of the enzyme, while cross-linking is illustrated relative to the distance between two individual GOx.

3.1. Carrier-Bound Enzyme Immobilization through Both Physical and Chemical Binding

Carrier-bound enzyme immobilization is characterized by the attachment of the biocatalyst onto a prefabricated solid material with the appropriate immobilization methods being selected to allow for optimization of the catalytic performance [5,68]. The two common methods of carrier-bound enzyme immobilization are physisorption and chemisorption, with physical adsorption offering the benefit of a generally universal, facile immobilization method, since the binding mechanism is not dependent on a site-specific chemical reaction between the enzyme and the support [49], while the covalent bonding requires site-specific chemical interactions between the enzyme and the support or the use of a cross-linking reagent [17].

Even though a wide range of both organic and inorganic supports, including ceramics and metal oxides [69,70], nanomaterials [68,71–75], and polymers [76–84] have been investigated as supports for enzyme immobilization [24], the application of such physically adsorbed enzyme-support conjugates is limited by enzyme leaching as well as a decrease in the enzyme's catalytic efficiency [24]. Falus et al., for instance, reported the immobilization of subtilisin A onto various silica gels for the continuous production of racemic N-Boc-phenylalanine ethyl thioester, an important pharmaceutical intermediate [83]. Subtilisin A was physisorbed to surface-grafted silica gel and used as packing in three reactors in series for the dynamic kinetic resolution of racemic N-Boc-phenylalanine ethyl thioester. At optimal conditions, the continuous flow process yielded a 97% conversion of the substrate at an enantiomeric excess of 99.5%, with the immobilized subtilisin A retaining catalytic activity after 120 h in continuous flow operation. The improved activity retention and shelf life was reported to be up to 1 year and was attributed to the increased thermostability of the enzyme upon physisorption [83].

Burkholderia sp. lipase, an enzyme widely studied for the production of biodiesel, was immobilized onto magnetic nanoparticles and evaluated for its catalytic activity. Tran et al. found that methyl-grafted Fe_3O_4-SiO_2 nanocomposites had a high affinity for lipase (29.5 mg lipase g^{-1} nanocomposite being adsorbed) most likely due to the porous structure of the silica coating. A higher K_m value and lower V_{max} value were however reported for the immobilized enzyme, thus indicating that the immobilization process decreased both the catalytic activity and its efficiency, likely due to the non-specific attachment and deformation of the enzyme active site and its increased mass transfer resistance. The immobilization also allowed for the improved reusability and separation of lipase in the transesterification of olive oil with methanol to produce fatty acid methyl esters (FAMEs). Physisorption of lipase onto magnetic methyl-grafted Fe_3O_4-SiO_2 nanoparticles was shown to retain significant activity for up to 10 reaction cycles owing to its increased stability from multi-point hydrophobic interactions with grafted methyl groups [70].

Zhang et al. reported on the immobilization of catalase onto carbon nanotubes for application in nanoelectronics, biosensing, and high-resolution imaging. Carbon nanotubes have been extensively studied as supports for enzymes due to their high surface area-to-volume ratio and biocompatibility [72]. An optimal enzyme loading (1.88 mg m^{-2}) was found for the physisorption of catalase onto oxidized single wall nanotubes (O-SWNT). A K_m value for O-SWNT-catalase conjugates, relative to that of the free enzyme, was reported to be 27.0%, indicating that the adsorptive interactions induced conformational changes in the secondary structure of the enzyme, as confirmed by Fourier transformation infrared spectroscopy and circular dichroism (CD) analyses. V_{max} for O-SWNT-catalase conjugates was reported to be 6.3 times lower than that of free enzyme. An analysis of CD spectra for immobilized catalase suggested that hydrogen bonding between enzyme and O-SWNT caused increased enzyme rigidity and therefore increased activity retention [72]. Lastly, Nidetzky's group has shown that chimeras of target enzymes can be combined with silica binding modules (SBM) through noncovalent interaction and become very tightly attached to such underivatized glass, even at physiological pH conditions. Moreover, the research has shown that the immobilized enzymes displayed full biological activity, suggesting that their binding to such a glass surface could be controlled through their specific orientation at the SBM interface [85,86].

Immobilization via covalent attachment was shown to offer strong chemical bonding that prevents significant enzyme leaching and further mitigates the loss of enzyme active sites [1]. Covalent binding methods are however more intensive and chemically harsher than physical adsorption, often requiring activation steps capable of inducing enzyme denaturation [87]. Further, the selection of an enzyme to be covalently immobilized must be carefully evaluated to ensure optimal catalytic efficiency, and as such, the enzyme-support covalent bond, for instance, should not affect the amino acids associated with the enzyme active site, or the immobilization method may cause loss of catalytic activity [87].

Zhu and Sun successfully immobilized lipase from *Candida rugosa* onto poly(vinyl alcohol-co-ethylene) (PVA-co-PE) nanofibrous membranes via glutaraldehyde activation for hydrolysis of p-nitrophenyl palmitate [75]. It was determined that covalent bonding caused an increase in K_m and

a decrease in V_{max} due to slower substrate diffusion and decreased enzyme mobility at the interface. Immobilized lipase was also found to retain nearly 90% of its activity after incubation in a phosphate buffer system at 55 °C for 75 min, while free enzymes were found to retain only approximately 20% of their initial activity. Significantly more activity than free lipase was also retained after 30 days of storage at 4 °C most likely due to a decrease in denaturation [75].

Kuo et al. reported on the immobilization of the same enzyme for the synthesis of 2-phenylethyl acetate, the major aromatic ester of rose fragrance. In this study, lipase was covalently bonded to polyvinylidene fluoride (PVDF) membrane, activated via 1,4-diaminobutane and glutaraldehyde, resulting in an enzyme loading of 1.71 mg enzyme g^{-1} PVDF. The immobilization technique also led to improved catalytic activity with only slightly hindered catalytic efficiency in n-hexane, likely due to the preservation of the tertiary structure in the organic medium resulting from covalent immobilization [77]. Complementarily, a study by Mendes et al. demonstrated that the optimal immobilization protocol among carrier-binding methods for lipase from *Penicillium camembertii* is covalent attachment to an epoxy-silica-polyvinyl alcohol composite. The covalently bound lipase was found to have a lower, less variable enzyme loading capacity than the physically adsorbed lipase. Moreover, the optimal case for covalently bound lipase yielded a hydrolytic activity nearly double that of physical adsorption as well as a greater activity retention. Covalent attachment of lipase to epoxy-silica-polyvinyl alcohol also resulted in improved thermostability compared to that of free lipase [88].

Epoxide hydrolase (EH) has also been studied for its potential application in the synthesis of high-value, enantiomerically pure pharmaceutical intermediates and other bioactive molecules. Petri et al., for instance, proposed the covalent attachment of EH from *Aspergillus niger* to epoxide-activated silica gel for the enantioselective hydrolysis of p-nitrostyrene oxide. Immobilization onto the silica gel resulted in a relatively high immobilization yield of nearly 70%, and the immobilized EH was found to retain about 90% of its activity relative to free EH, as well as good storage stability over the span of few months. The covalent immobilization of EH caused no decrease in the enantiomeric selectivity of p-nitrostyrene oxide hydrolysis and markedly improved the stability of EH in organic solvent of 20% DMSO [89].

Nanomaterials have been studied as supports for biocatalysts due to minimal mass transport limitations and high specific surface area for volume-efficient catalysis [22,68]. Li et al., for instance, used an electrospun polyacrylonitrile-glycopolymer nanofibrous membrane as a support for covalent binding of catalase from bovine liver. Immobilized catalase activity was about 50% of that of the free catalase, but was found to be stable across broader ranges of temperatures and pHs. It was also found that covalently immobilized catalase retained approximately 80% relative activity after storage at 4 °C for 30 days, whereas free catalase retained no relative activity when in the same conditions [68]. Alptekin et al. optimized a protocol of the chemical attachment of catalase onto Eupergit C, a macroporous derivative of methacrylamide reported to be chemically and mechanically stable as a catalyst for operation in batch and plug flow reactors. The ratio of K_{cat} to K_m was calculated to assess the catalytic efficiency of free and immobilized catalase and was found to be nearly 2 orders of magnitude, thus suggesting that the immobilized enzyme was less efficient in converting the substrate to product. However, immobilization was shown to improve enzyme shelf life and operational stability as a biocatalyst in batch and plug flow reactors. Studies showed that immobilized catalase retained nearly 78% of initial activity when measured 28 days after immobilization, whereas free catalase was inactive after only 11 days of storage. Furthermore, immobilized catalase retained 50% activity at 82 min in a plug flow reactor [90].

3.2. Enzyme Entrapment

Enzyme entrapment is the immobilization of a biocatalyst into carriers of varying degrees of porosity and permeability [27]. Enzymes immobilized via entrapment exhibit improved stability due to intensified control of their microenvironment and were also shown to be more catalytically active at higher temperatures in organic solvents, as well as easily separated from substrate-product reaction mixture [87].

Immobilization via entrapment in a variety of carriers, e.g., sol gels, hydrogels, polymers, nanomaterials, has been researched for the employment of biocatalysts in the synthesis of organic compounds and for novel biosensing systems [64,66]. Complementarily, the immobilization of lipase has been proposed for application in the production of flavor and fragrance chemicals, as well. Ferraz et al., for instance, investigated the viability of geranyl propionate synthesis using lipase from *Penicillium crustosum* as biocatalyst. Lipase was entrapped in beads nearly 0.5 cm in diameter via a crosslinking reaction between calcium chloride and sodium alginate. Calcium-alginate beads containing lipase were optimized further for geraniol and propionate conversion, as well as tested for reusability. Results show that the activity retention of immobilized lipase decreased linearly with respect to the number of cycles of use, suggesting that activity loss was due to enzyme leaching during each cycle [91]. Risso et al. studied the same entrapment method for the immobilization of inulinase from *Kluyveromyces marxianus*, an important biocatalyst in the production of high fructose syrups. Inulinase, entrapped in calcium-alginate beads, was characterized by the determination of its kinetic parameters, as well as its thermostability and pH stability in varying degrees of organic solvents. The K_m value of immobilized inulinase was found to be significantly less than that of free inulinase at optimal mass fractions of organic solvent, while the $V_{\max}$ value of immobilized inulinase was comparable to that of free inulinase in the same conditions. However, mass transfer resistances, which would likely be the rate-limiting process, were not considered in the kinetic analysis of the immobilized biocatalyst [92].

Arica et al. proposed the entrapment of catalase from bovine liver in thermally reversible cylinders of poly(isopropylacrylamide-co-hydroxyethylmethacrylate) for reactor system applications. Immobilized catalase exhibited a decrease in catalytic activity and enzyme-substrate affinity, and retained less activity at higher temperatures than free catalase. It was also found that an increase in temperature caused for a decrease in hydrogel swelling and higher mass transfer resistance. The apparent kinetic parameters of the immobilized catalase were largely attributed to the temperature-dependent behavior of the hydrogel carrier itself. The entrapment technique allowed for enzyme reusability and increased storage stability. Immobilized catalase also showed 78% activity retention after storage at 4 °C for 20 days, while free catalase retained none of its activity in the same storage conditions. Furthermore, hydrogel-entrapped catalase was found to retain approximately 95% activity for 6 cycles in the batch reactor system [93].

Singh et al. studied the apparent kinetic and stabilizing effects of the encapsulation of bovine liver catalase in hollow silica nanoparticles (HSNPs). No absorption peaks were observed for catalase or hydrogen peroxide in the supernatant liquid isolated from the immobilization procedure, thus indicating an immobilization yield of nearly 100%. It was further determined that the encapsulation technique decreased both enzyme's activity and enzyme-substrate affinity. However, immobilized catalase showed significantly improved stability throughout a broad range of pHs and temperature conditions. Free catalase was completely denatured when tested for activity at 70 °C, while encapsulated catalase was found to have optimal catalytic activity at 80 °C. The encapsulation of catalase within HSNPs—rather than the physical adsorption of catalase onto HSNPs—was demonstrated by the thermostability results for immobilized enzyme. It is expected that physically adsorbed enzyme would show a loss of catalytic activity near the denaturation temperature of free enzyme [94].

Yan et al. reported the successful nanogel encapsulation of bovine carbonic anhydrase (BCA), a metalloenzyme that is studied for applications in carbon capture and biocatalytic enrichment of natural gas where industrial application is limited by the almost total loss of enzyme catalytic activity at 63 °C due to the irreversible aggregation of BCA. Acryloylation and subsequent in-situ polymerization of BCA to form single BCA nanogels were performed, thus imparting molecular structural stability to the enzyme while mitigating mass transfer limitations. BCA nanogels exhibited similar catalytic activity as free BCA and showed significant retention of activity at temperatures greater than 63 °C. It was also determined that nanogel encapsulation preserved the secondary structure of BCA, therefore inhibiting irreversible aggregation and allowing for catalytic activity even at 81 °C [95].

Enzyme entrapment in biocompatible nanoparticles and solid supports has also been reported as a novel approach for the improvement of enzyme activity as a result of biocatalyst-carrier interactions. Studies of enzyme entrapment in solid carriers have shown that for optimal immobilization conditions it is possible to "lock" immobilized enzymes into more catalytically active conformations [96]. Prakasham et al., for instance, investigated the kinetic parameters and stability of amylase entrapped in matrices comprised of nickel-impregnated silica paramagnetic particles. It was observed that the entrapped amylase had more rapid starch hydrolysis than the free amylase, for all the tested pHs and temperature conditions. A lower K_m value was however recorded for the immobilized amylase, most probably indicating that the entrapment technique yielded a more efficient, robust biocatalyst [96].

Wu et al. reported on the facile co-immobilization of enzymes glucose oxidase (GOx) and horseradish peroxidase (HRP) into a metal-organic framework. The entrapment was performed by mixing solutions of zinc nitrate, GOx, and HRP, and 2-methylimidazole at ambient conditions for 0.5 h resulted in the enzyme-embedded zeolitic imidazolate framework (GOx&HRP/ZIF-8). The catalytic activity of such conjugate was compared to that of a mixture of GOx/ZIF-8 and HRP/ZIF-8 to determine any changes in efficiency as resulted from the co-immobilization technique. Analysis showed that GOx&HRP/ZIF-8 exhibited a 2 times higher activity than the mixture of single-immobilized conjugates due to a significant decrease in mass transfer resistance. Furthermore, GOx&HRP/ZIF-8 were found to retain significantly more activity than free enzyme in organic solvent and when stored at room temperature [97]. Currently however, the successful scale-up of entrapped enzymes for biocatalysis is prevented by mass transfer limitations of substrate through carrier material, enzyme leaching, and low total catalytic mass of enzyme-carrier conjugate [24]. Lastly, Lin et al. reported on the entrapment of HRP in inorganic interfaces made with cooper phosphate supports and in aqueous solution. Results showed that the hierarchical flower-like spherical structures considerably enhanced enzyme's activity relative to that of the free enzyme in solution. In addition, the hybrid interfaces also exhibited excellent reusability and reproducibility even when several cycles for evaluating the active hydrogen peroxide (H_2O_2) release were performed [98].

3.3. Cross-Linked Enzyme Aggregates

Enzyme immobilization via the formation of cross-linked enzyme aggregates (CLEAs), one of the newest class of immobilization techniques, has also been researched considerably since its development [99] for application in industrial biotransformations of fine chemicals and pharmaceuticals [24]. The general preparation of CLEAs is carried out via the aggregation of given soluble enzymes when using a precipitating reagent, such as ammonium sulfate [100–102], acetone [103], ethanol [102], or tert-butanol [100], followed by the subsequent copolymerization of enzyme aggregates with a cross-linking agent, most frequently glutaraldehyde [62,99–109]. However, analysis showed that aggregate cross-linking is not a universal immobilization method and should thus be optimized for each target biocatalyst, with the precipitating and cross-linking agents having to be selected carefully to ensure that immobilization does not adversely affect enzyme activity [62,100–103,105].

CLEAs were shown to offer the benefits of enhanced shelf life and operational stability, reusability, and exceptional resistance to the leaching of immobilized biocatalyst in aqueous media, while not suffering from substrate diffusion limitations that could potentially reduce catalytic activity [100]. In certain instances, CLEAs were shown to possess higher catalytic activities than the corresponding free enzymes, and this phenomenon, known as hyperactivation, was attributed to the aggregation of enzyme in a pre-organized tertiary structure that rendered it permanently insoluble upon cross-linking [24]. Thus, CLEAs showed a large potential for application in industrial-scale processes owing to high catalytic productivity and inexpensive immobilization methods [24]. However, the successful scale-up of applications were dependent on improving CLEA's mechanical properties while better defining separation criteria for continuous processes [24].

Specifically, Lai et al. reported the direct formation (from fermentation broth) and stability analysis of CLEAs with lipase from *Penicillium expansum* (PEL) in various solvents, for the production of biodiesel from corn and microalgal oil, respectively. In this study, PEL-CLEAs were found to be less catalytically active than free PEL, likely due to mass transfer limitations of the large substrate molecules. PEL-CLEAs also showed an improved stability over free PEL at increased temperatures and in various conditions of pH. The clumping of PEL-CLEAs and loss of enzyme active sites was however determined to cause a decrease in the yield of biodiesel. PEL-CLEAs also exhibited substantial activity retention in nonaqueous solutions, suggesting that the immobilization method can be geared toward industrial production of biodiesel [106].

Nguyen and Yang produced combined cross-linked enzyme aggregates (combi-CLEAs) of GOx and HRP for the catalysis of a cascade chemical reaction applicable to glucose detection biosystems [105] and pharmaceutical wastewater treatment [109]. The combi-CLEAs were optimized for the cross-linking density and mass ratio of GOx to HRP for ensuring maximal catalytic activity and enzyme stability. Upon optimization, combi-CLEAs showed similar catalytic activity relative to free enzymes, but lower values of K_m were most likely a result of two factors: the distance of mass transfer for hydrogen peroxide intermediate, which was substantially reduced by the co-immobilization technique; and the cross-linking of GOx, resulting in decreased inhibition in the presence of H_2O_2 [105].

Vafiadi et al. reported similarly promising results for the use of combi-CLEAs on three commercial enzyme mixtures exhibiting feruloyl esterase activity. The authors reported on the immobilization via aggregate cross-linking and assessed its kinetic activity relative to free enzyme in ternary mixtures of n-hexane, 1-butanol, and water. Combi-CLEAs were designed to retain maximal catalytic activity by the evaluation of 10 aggregating agents, while the efficiency was optimized by varying the concentration of the cross-linking agent. A product yield of 97% was reported upon the enzyme's precipitation via ammonium sulfate and cross-linking at a glutaraldehyde concentration of 100 mM. The use of ammonium sulfate with this precipitating agent was found to be advantageous because its solvation is an endothermic reaction. Notably, the activity of enzyme aggregates prior to cross-linking were found to be higher than that of the free enzyme, supporting evidence that suggests suitable immobilization techniques can lock enzymes in highly active conformations. Furthermore, combi-CLEAs were easily separated from the reaction mixture containing unreacted methyl ferulic esters, synthesized 1-butyl ferulate by centrifugation and later reused for furuloyl esterase activity, though the immobilized enzymes showed poor activity retention and stability [102].

Martins et al. formed magnetic cross-linked enzyme aggregates (mCLEAs) from rhamnopyranosidase (Rhmnase), a hydrolytic enzyme applicable in the production of valuable pharmaceutical compounds such as lipoprotein associated phospholipase A2 inhibitors, which are administered in the treatment of atherosclerosis [110]. Such magnetic aggregates were evaluated for their catalytic activity with different cross-linking and precipitating agents and subsequently compared to CLEAs@Rhmnase for reusability in a batch reactor system. CLEAs@Rhmnase were found to retain nearly 100% activity after 5 reutilization cycles of 24 h each, however, the CLEAs@Rhmnase showed a significant loss in activity after 7 reutilization cycles. Conversely, mCLEAs@Rhmnase showed an initial loss in activity of approximately 40% after one reutilization cycle and near constant activity thereafter, likely due to the higher physical stability of the magnetic aggregates. Additionally, mCLEAs@Rhmnase were shown to be more catalytically active and efficient than CLEAs@Rhmnase, suggesting that the selection of immobilization materials should be critically assessed for ensuring high biocatalytic turnover. It was determined that magnetic enzyme aggregates are more suitable biocatalysts for a scaled up process owing to improved reusability and stability [104].

Zhao et al. reported the use of CLEAs of *Pseudomonas* sp. lipase (CLEA-PSL) as a biocatalyst for the enantioselective resolution of (*S*)-*N*-(2-ethyl-6-methylphenyl) alanine, a chemical precursor in the production of widely used herbicides [111]. Precipitation and cross-linking conditions were optimized for the formation of CLEA-PSL, and kinetic parameters were determined for free and immobilized lipase, respectively. CLEA-PSL were found to be more active than the free lipase, and it was also

noted that 48 h were required for free lipase to reach a substrate conversion of 50%, while only 12 h were needed for the immobilized lipase to achieve the same conversion and enantiomeric excess. The time difference was presumably due to an induced change to a more catalytically active enzyme conformation upon immobilization. The evaluation of kinetic parameters determined that CLEA-PSL also showed an improved affinity for substrate, most likely due to the changes in the enzyme's secondary structure caused by immobilization. Lastly, the immobilized lipase was found to be more thermostable than the free lipase and retained nearly 80% of its initial activity after ten reutilization cycles in a batch reactor and with no reported loss of enantioselectivity [103].

Enzyme aggregate cross-linking has also been proposed as a method to improve biocatalysts that are currently employed on an industrial scale. Illanes et al., for instance, implemented CLEAs from recombinant penicillin acylase for the production of cephalexin with increased enzyme stability and global productivity (g cephalexin g^{-1} biocatalyst). Free penicillin acylase was found to require a lesser reaction time, but CLEAs were advantageous for preservation of enzyme activity. Free enzyme retained 50% residual activity after 30 h, while CLEAs retained an equal amount of activity after 78 h. Furthermore, CLEAs were found to have an increased total specific productivity (135.5 g cephalexin g^{-1} biocatalyst) than that of free penicillin amylase (of only 40.1 g cephalexin g^{-1} biocatalyst) with such an increase in the reusability, justifying a slight loss of catalytic activity due to an overall increase in the production potential of cephalexin [101].

Lastly, the intramolecular cross-linking of non-aggregated enzymes has been investigated as a method of inducing increased rigidity to and preventing non-specific protein-protein associations of multimeric enzymes, thus preserving catalytic activity when coupled with another immobilization method [112–114]. Dinu et al. demonstrated that cross-linking of perhydrolase S54V (AcT), i.e., an enzyme that catalyzes the perhydrolysis of propylene glycol diacetate to decontaminant agent peracetic acid, allowed for the novel integration of nanobiocatalytic conjugates with latex-based paint that led to the formation of a bioactive decontaminating composite. The study also found that AcT, cross-linked with polyfunctional aldehyde dextran, retained a greater degree of catalytic activity when covalently bound to single walled carbon nanotubes (SWNTs) as compared to covalent bonding of AcT to SWNTs. The superior activity retention of AcT was attributed to cross-linking with aldehyde dextran that conferred increased rigidity to the enzyme and led to the preservation of its secondary structure upon covalent immobilization onto SWNTs [112].

4. Intensified Approach for Designing Improved Biocatalysts

The combination of different technical expertizes has allowed for the improved design of immobilized biocatalytic processes, but profitability seems to remain the determining factor for further enzyme-induced process development and implementation [5,115,116]. For instance, significant progress was made in protein design via directed evolutionary approaches, with such progress allowing for improved activity, stability, and substrate affinity, as well as reduced costs to isolate enzymes [1,3,23,28,29]. Directed evolution requires the administration of random mutations to the amino acids constituting an enzyme, which could be employed through chemical mutagenesis or DNA shuffling, followed by screening for the desired phenotype and the isolation of genes coding for any identified improved genetic variant [3]. As a result of such an advance, research teams have been successful not only in developing biocatalysts that may be deployed at high temperatures and extreme pH conditions, but also biocatalysts that have catalytic activities of several orders of magnitudes greater than those of naturally occurring ones [1,3,29]. For instance, researchers at Codexis and Merck successfully used such multiple iterations to increase enzyme-substrate affinity and to design an economically competitive enzyme-catalyzed process for subtilisin, a pharmaceutical used for diabetes treatment [2]. However, while progress in protein engineering has helped drive increased applications in industrial enzyme catalysis, it has not addressed all limitations, like the poor mechanical stability and limited reusability of the biocatalysts, the costs associated with their in vitro production, or further adoption in commercial-scale processes [5,20–27].

Molecular dynamics simulations (MDS) provide atomic level understanding of phenomena that determine the physical and catalytic characteristics of an immobilized biocatalyst [117–121]. Studies of molecular dynamics simulations, which carry out numerical integration of Newton's laws of motion at an atomistic scale, have been used to predict the structures and catalytic properties of enzymes at the molecular level, which have been extended to research in enzyme immobilization where accurate characterization of enzyme-carrier interactions provides insight into binding mechanisms [117–120]. An understanding of atomistic-level interactions has led to the development of efficient and optimized biodevices. For instance, Franca et al. were able to determine through MDS that the active site of acetyl co-enzyme A carboxylase (ACC) had a positive surface potential. This insight into ACC was used to devise an optimal electrostatic adsorption of ACC onto an AFM tip for improved biodevice functionality [119].

Basso et al. performed molecular simulations on endo- and exoinulinase to explain differences in regioselectivity between the two structures. Analyses of the three-dimensional structures were subsequently used to formulate an optimal immobilized biocatalyst that showed hyperactivity when compared to its native structure [118]. Qu et al. employed molecular simulations of a hydrolase MfphA adsorbed onto single walled carbon nanotubes (SWNTs) for verification of and insight into analytical results. Molecular modeling results illustrated preferred binding of two particular amino acids Trp201 and Met81 to carbon nanotubes, thus resulting in a loss of hydrolase activity due to blocking of the active site [117]. Studies using molecular simulations have illustrated the utility of computational modeling in optimization of immobilization techniques to reduce lab material costs and create insight into molecular phenomena for the development of optimal immobilized biocatalysts [117–120].

These analyses show that the adoption of critical evaluation criteria for immobilized enzyme processes on multiple scales—including molecular-level modeling and analysis, life cycle assessments, and techno-economic analyses—is paramount for economical scale-up [5,44,50–52,117–120]. Ultimately, the appropriateness of immobilized biocatalyst for industrial processes boils down to the fruition of additional profitability with the immobilized form of an enzyme often having to hold multiple benefits over free enzyme for process economics that could overcome the additional costs and constraints associated with the immobilization to a reduced loss of catalytic activity, while balancing the cost used for covering the possible materials to be used as supports [5,116].

Glucose Isomerase: A Model for Enzyme Immobilization

The immobilization of glucose isomerase (GI) is considered an excellent model for commercial application of an immobilized enzyme where GI efficiently catalyzes the conversion of d-glucose to d-fructose in the production of high-fructose syrup (HFCS) [122]. The enzymatic production of HFCS was previously determined to be more economically competitive than conventional chemical methods requiring alkaline catalysis due to improved product quality, simplified production route, and reduction of undesired byproducts such as mannose and psicose [122].

Much research has been done on immobilization of GI since its development and first industrial use in 1967. A broad range of immobilized GI products have been sold by producers like Genencor, DuPont, Novozymes SA, and Solvay, and continued progress in GI immobilization has yielded iterative improvements in the production of HFCS using immobilized GI as biocatalyst [5]. In most contemporary processes, HFCS is produced in continuous fixed bed reactors containing immobilized GI as catalytic packing, which results in a mixture of nearly 42% d-fructose, 50% d-glucose, and small amounts of other sugars, and a 55% mixture of d-fructose—required for commercial application as sweetener—is attained via chromatographic enrichment [5]. The success of immobilized GI is rooted in the biochemical properties of the enzyme as well as the technological developments that allowed for the commercialization of the immobilized enzyme-catalyzed process. Currently, the production of HFCS is the largest industrial process employing an immobilized biocatalyst, with a nearly 10 million tons produced per year [5]. Studies showed that the temperature-dependent position of isomerization equilibrium, along with the relatively high K_m value of GI, were two of the biochemical factors that drove the development of an immobilized enzyme process to improve upon a free enzyme process.

At higher temperatures the equilibrium of the isomerization is shifted to favor higher yields of fructose, so the use of thermostable immobilized enzyme allowed for improved yields of HFCS. Immobilized GI allowed for implementation in continuous processes, which proved to be advantageous, as the high-concentration throughput of substrate helped to overcome the low efficiency of enzyme-substrate binding indicated by the low K_m of GI. Furthermore, the production cost of GI was significant at the time of development, as the immobilization of GI decreased the total amount required for HFCS production by allowing for enzyme reuse [5]. The GI-catalyzed process is being further researched for the employment of thermostable enzyme with good activity retention at 90 °C, at which point the equilibrium conditions shift such that a 55% mixture of fructose can be obtained, obviating the need for chromatographic enrichment in the process [5].

5. Environmental Impact Assessment and Economic Approaches for Enzyme Implementation in Industrial Catalysis

While the development of highly efficient immobilized biocatalyst is the short-term goal of lab-scale research, critical economic and environmental evaluations of immobilized enzyme-catalyzed processes are required to determine the suitability of an immobilized enzyme for scale-up [50–52]. In such a context, life-cycle assessments (LCAs) and techno-economic analyses (TEAs) are increasingly important tools as a growing number of immobilized enzymes are assessed for commercial-scale biocatalytic processes [5].

LCAs are used to identify process energy and material requirements, as well as waste and emissions, which are subsequently used to analyze the sustainability and environmental impact of a process. The use of enzymes in industrial processes is often associated with reduced consumption of energy, chemical inputs, and waste streams. For example, using phospholipase to degum vegetable oil led to a decrease of 44 tons of equivalent CO_2 generation per 1000 tons of oil produced, due to improvement in oil yield and a subsequent decrease in feedstock requirements [5]. In another study, the enzymatic production of biodiesel reduced the amount of steam needed to preheat feedstock due to milder reaction conditions, and also improved each measure of environmental impact, including human toxicity, ozone depletion, and global warming potential [50]. Immobilized enzyme-catalyzed processes have been found to further reduce the environmental burden of free enzyme-catalyzed processes [51]. Raman et al. performed LCA on production of biofuel from alkali catalyst, free lipase, and immobilized lipase to determine an optimally sustainable process. Both free lipase and immobilized lipase reduced process energy consumption when scaled to 1000 kg per year production due to milder reaction conditions. Furthermore, the immobilized lipase was reported to improve the free-enzyme catalyzed process because its reuse reduced consumption of carbohydrates and the minerals required for its free form production [51]. The general decrease in material and energy consumption exhibited by enzymatic processes, as a result of reduction of energy consumption, indicates that biocatalytic processes are potentially both more environmentally benign and economically lucrative. However, LCA does not account for productivity or process economics, and thus is insufficient as a standalone metric for process implementation.

TEAs study the economic viability of a process based on technology readiness and process economics such as utilities, feedstocks, labor, and capital investments [52]. Olafsson et al. reported a TEA for a comparison of integrated and off-site cellulase catalysis in fermentation of lignocellulosic material for ethanol production. The authors found that off-site production of ethanol using similar technologies was a more economically competitive option due to the production of more marketable byproducts [52]. Analysis showed that while profitability remains the critical driving force of process development, TEAs and LCAs in combination are invaluable tools for the full diagnosis of both benefits and drawbacks associated with scale-up of biocatalytic processes.

6. Pertinent Examples of Enzymes Application in Industrial Catalysis

6.1. Pharmaceuticals Industry

Enzyme catalysis has been successfully used for the production of pharmaceutically active chemicals at the industrial scale. The most significant advantages enzyme catalysis holds over conventional catalysis are the high regio-, chemo-, and stereoselectivities at which enzymes convert substrate to product [2,123]. A high degree of product specificity is largely desirable in such pharmaceutical processes due to the streamlining of product synthesis routes and subsequent improvement in process economics [8,30]. For example, the production of many pharmaceuticals requires the introduction and subsequent removal of protecting groups from pharmaceutically active ingredient intermediates to ensure adequate product selectivity. The use of appropriate enzymes not only obviates such steps, but has also been shown to yield higher enantiomeric excesses of desired stereoisomers [8]. Furthermore, enzyme-catalyzed synthesis routes often reduced or eliminated the need for chemically harsh substances or high-temperature conditions that can otherwise require intense process safety considerations [2].

The interdisciplinary approach that allowed for the economically advantageous implementation of biocatalysis on the industrial scale is highlighted by the development of the enzyme-catalyzed synthesis of sitagliptin, a drug marketed by Merck for type II diabetes treatment [31]. Sitagliptin is a dipeptidyl peptidase-4 inhibitor that prevents an increase in the blood-retinal barrier and inhibits diabetes-induced tight junction disassembly [32]. Conventional synthesis of sitagliptin requires a high-pressure hydrogenation of enamine via a rhodium-based catalyst and subsequent carbon treatment to remove trace amounts of rhodium, yielding sitagliptin in 97% enantiomeric excess (e.e.) [100]. Research teams at Codexis and Merck conducted extensive protein engineering to produce an R-selective transaminase (R-ATA) from *Arthrobacter* sp. capable of converting 200 g L^{-1} of prositagliptin ketone to sitagliptin in dimethyl sulfoxide (DMSO) in greater than 99.95% e.e. [33]. In addition to a yield of higher enantiomeric purity, the enzyme-catalyzed route had 10% increased yield and a 53% increase in productivity (kg sitagliptin L^{-1} day^{-1}), and also eliminated the need for a rare heavy metal-based catalyst that necessitated purification and special equipment necessary for high-pressure operation [31].

Codexis and Merck have also invested heavily in research for scale-up of a monoamine oxidase (MAO)-catalyzed process for enantiomerically pure desymmetrization of a bicyclic proline intermediate, an important precursor in the synthesis of boceprevir, a NS3 protease inhibitor used for treatment of chronic hepatitis C infections [2,34]. Conventional synthesis of bicyclic proline is an intensive process requiring an excess of metal-based oxidant and reductant through 8 reaction steps; the enantioselective, MAO-catalyzed synthesis of the intermediate is an attractive alternative with the potential to greatly reduce operation time and waste generation [30]. Although significant improvements in MAO activity, solubility, and thermostability were achieved through protein engineering via 4 rounds of evolution involving the introduction of random mutations and subsequent screening for desired phenotypes, the addition of bisulfate to the MAO-catalyzed process for the capture of imine compounds was necessary to mitigate its irreversible inhibition [30].

The combination of biocatalysts genetically, engineered for robust catalytic capabilities and topological process optimizations, illustrates the overlap of technical expertise needed for successful scale-up of enzyme catalysis [2,5]. As such, the enzyme-catalyzed process showed several marked improvements over the conventional synthesis of the intermediate when compared at the same scale, namely decreases of 59.8% in raw materials, 32.8% in water, and 63.1% in process waste per unit of product synthesized [30]. Though further work is needed for economically feasible industrial-scale implementation, the comparison between the conventional synthesis and the MAO-catalyzed synthesis route suggests that enzyme catalysis could greatly improve over current industry standards and outcomes.

In a study by Hayes et al., authors reported an improved commercial-scale synthesis route for (*S*,*S*)-reboxetine succinate, a noradrenergic anti-depressant for the treatment of fibromyalgia in the latter stages of development at Pfizer [35,36]. The production of reboxetine requires an acetylation of diol intermediate. However, conventional synthesis routes rely on classical chemical acetylation that suffers from di-acetylation and poor enantioselectivity, therefore generating considerable amounts of unwanted byproducts [2]. The proposed generation synthesis route successfully employed *Candida antartica* lipase B, an active, commercially available enzyme, for the highly enantioselective acetylation of diol intermediate [36]. The lipase-catalyzed process resulted in the selective mono-acetylation of diol intermediate with 98% regioselectivity and greater than 99% yield. Furthermore, it was possible for the enzyme to be removed from the reaction mixture via simple filtration, and it thus maintained high regioselectivity at the lab scale upon reuse, all at low costs [36]. As such, the new generation synthesis route resulted in a 58% improvement in the commercial product yield of (*S*,*S*)-reboxetine succinate and a nearly 1300 MT year^{-1} reduction in process waste at peak process throughput [36].

Because lipases can hydrolyze a broad spectrum of substrates, they have been researched as biocatalysts for many other pharmaceutical syntheses [7,36,37]. Martinez et al., for instance, proposed a new-generation synthesis route for the industrial-scale production of pregabalin, a neuroactive drug exhibiting anticonvulsant, pain killing, and anti-anxiety activity used for the treatment of epilepsy, anxiety, and social phobia [37,38]. The proposed route utilized lipolase, a commercially available lipase, for the selective hydrolysis and subsequent separation of the *S*-enantiomer intermediate from the *R*-enantiomer for conversion to pregabalin via decarboxylation [37]. While screening for industrial enzyme increased selectivity and reduced waste generation, several process optimizations allowed for the improved process economics of such a new-generation route. The addition of Ca^{2+} and Zn^{2+} mitigated lipolase inactivation by forming complexes with chemical species that acted as enzyme inhibitors. In addition, the rapid phase splitting of *S*-enantiomer from R-enantiomer enabled racemization and thus efficient reuse of starting material [37]. The new-generation synthesis route resulted in a 40–45% increase in yield of pregabalin at 99.5% purity and 99.75% e.e. Furthermore, the amount of waste generated per kilogram of product yielded was calculated to be just 20% that of the classical route [37].

6.2. The Food-Water-Fuel Nexus

The large-scale production of biofuels, i.e., fuels derived from biomass, animal fats, waste oils, and other renewable resources that encompass chemical products such as bioalcohols, biodiesel, biosynthetic oils, and biogas, has been recognized for its potential to supplement or replace fossil fuels, particularly as oil reserves are depleted to meet global energy demands [18,49]. The benefits of economically feasible biofuel production are two-fold: biofuel offers improved sustainability over traditional fuel sources as well as significantly reduces the environmental impact owing to its lower emission of carbon monoxide, nitrogen oxides, sulfur oxides, and particulate matter [18]. According to British Petroleum (BP), global production of biofuels rose by an average of 14.1% from 2006 to 2016, illustrating the growing impact that biofuels have on the world energy landscape [124]. While government incentives have helped to drive industry-scale biofuel production, the economic viability of biofuel production will be determined by the development of processes that efficiently use waste from agriculture and industry as feedstock, thus side-stepping the ethical dilemma of using fresh water and land resources for fuel production [125]. Numerous technologies exist for the conversion of raw biological materials to usable, high-energy bioproducts with most production routes requiring either the transesterification of oils or the esterification of fatty acids [5,18]. The traditional chemical process uses sodium methoxide for conversion of plant oil triglycerides to fatty acid methyl esters (FAMEs), which subsequently results in a product contaminated with high alkali salt content requiring costly purification [5].

The use of lipase as a biocatalyst for esterification was researched for its efficiency at mild reaction conditions and high-purity product yields and was proposed to eliminate the need for purification. However, for biofuel production, economical implementation of such an enzymatic process requires efficient recovery and reuse of lipase due to the required scale of production, therefore necessitating an immobilized enzyme [5,49].

A prominent trend in the production of biofuels is the design of processes based on inexpensive, largely abundant starting materials because cheap feedstock is one of the biggest driving forces in the profitability of biofuels processes [19]. The biggest such feedstock is lignocellulosic biomass—made up of lignin, cellulose, and hemicellulose—due to its massive abundance and wide range of sources including crop residues, softwood and hardwood, herbaceous biomass, and municipal solid waste [19]. The most difficult technical barrier required to unlock lignocellulosic biomass is however the extensive mechanical or chemical pretreatment required to further enable the processing of cellulose in lignocellulosic biomass via hydrolysis to glucose and subsequent conversion to bioethanol via whole-cell fermentation [126–128]. Current research suggests that ionic liquids, i.e., salts that exist in molten states at temperatures below 100 °C with strong chemical and thermal stabilities and extremely low vapor pressures, will play a key role in the development of processes that viably release cellulose from lignocellulosic material [126–128].

Chemical conversion of cellulose to glucose requires the use of diluted acids and high temperatures, which implies high energy inputs to result in the generation of a significant amount of unwanted byproducts [19]. A more ideal approach is the use of cellulase, i.e., a mixture of hydrolytic enzymes that act synergistically in the conversion of cellulosic material, for the selective enzymatic hydrolysis of cellulose to glucose, which requires longer reaction time but leads to improved yield from the subsequent fermentation due to a low generation of unwanted byproduct [19,53–55]. The economically viable scale-up of cellulase-catalyzed cellulose conversion to glucose for bioethanol production is limited by poor biocatalyst recovery, slow enzyme-catalyzed reaction rates, and low biocatalyst stability under industrial operation conditions [54,55]. Therefore, immobilized cellulase is a requirement for industrial catalysis, particularly considering the acid pretreatment required for cellulose [55].

Reported lab-scale work on the immobilization of cellulase illustrates the potential for the employment of cellulase for biodiesel production. Khorshidi et al., for instance, showed that immobilized cellulase was significantly more active than free cellulase at lower pH conditions and at higher temperatures, showing that the immobilization technique can functionalize biocatalyst at industrial conditions [54]. Lima et al. found that immobilized cellulase had increased thermostability when compared to free cellulase and retained nearly 70% of its initial activity after eight cycles of converting cellulosic biomass to glucose. The significant activity retention of immobilized cellulose suggests that immobilization techniques can improve process economics by allowing for efficient reuse of biocatalyst [56].

In 2006, Hainabaichuan Co. Ltd. (Guangzhou, China) began processing waste palm oils and waste edible oils for lipase-catalyzed production of 20,000 tons of biodiesel per year and subsequent scale-up to 40,000 tons per year in 2008 [49]. Lvming Environmental Technology Co. Ltd.(Shanghai, China) implemented a commercially available immobilized lipase as a catalyst in a FAME production line with an annual capacity of 10,000 tons in 2007 [57]. The enzymatic reaction, designed for a feedstock of high acid value (AVN160 mg KOH g^{-1}) waste cooking oil, was carried out in a stirred tank reactor at an enzyme loading of 0.4% relative to charged substrate, which led to a FAME yield of 90% at optimal conditions [57]. Piedmont Biofuels announced in 2012 the successful scale-up of a continuous enzymatic transesterification of free fatty acids (FFAs) via immobilized *Candida antarctica* lipase B for biodiesel production; the enzymatic reaction eliminated the need for caustic stripping of the chemical intermediate due to its high product selectivity [5].

6.3. Natural Gas Conversion

Recent advances in the extraction and recovery of natural gas resources have made accessible vast reserves of natural gas in North America [129]. A review of world energy production and energy

markets by BP reported a proven reserve of nearly 8.7 trillion m^3 of natural gas in the US alone [124]. Additionally, production of natural gas in the US comprises over 20% of global natural gas production at 750 billion m^3 in 2016 [124].

The composition of natural gas is 80–95% methane with varying degrees of heavier hydrocarbons, but methane has a relatively low market value due to difficulties in storage and transportation as well as limited use as fuel [129,130]. The low market value and high greenhouse gas potential of methane have initiated a surge in research and development of technologies that can be employed to convert methane to high-quality, value-added chemicals.

Much current research on the economically viable use of methane as feedstock is focused on conversion to methanol, which can be more readily converted to olefins and other valuable hydrocarbons [130,131]. Current processes for a traditional chemical conversion of methane to methanol, such as steam reformation and the Fischer-Tropsch process, are limited by several significant drawbacks. The chemical conversion route requires the use of high-temperature, high-pressure unit operations as well as noble metal catalysts, resulting in a poor selectivity of methanol [130]. The low yield of methanol necessitates a large process throughput in order to overcome large capital cost investments, thus the process is only profitable at a massive scale, thus placing further constrictions on process employment due to the difficulty of transporting methane from an extraction site to a production plant [129,130].

The use of the biocatalyst methane monooxygenase (MMO), for the conversion of methane to methanol, has recently gained interest in the wave of expanding natural gas extraction. MMO has been shown to convert methane to methanol at ambient conditions with selectivity approaching 100% and thus has been researched for the scale-up of methane conversion, considering its multiple advantages over the chemical conversion route [14,129–131]. The high selectivity of MMO-catalyzed methanol production eases the intensity of product separation and could significantly reduce the number of steps required in the conversion process. Furthermore, the enzymatic reaction occurs at mild reaction conditions, and could thus cut back on costs associated with heating, pressurization, and other feedstock conditioning steps [129,130].

Much lab-scale research remains to assess the MMO-catalyzed conversion of methane for industrial applications because isolation of MMO is an intensive process, suggesting it may be beneficial to immobilize the enzyme for reuse. Blanchette et al. reported the use of a 3D printed microbioreactor with immobilized MMO as packing for continuous methane conversion to methanol. Although immobilized MMO retained good activity through 20 consecutive reuses, the overall product yield was significantly less than the biocatalytic mass required for methane conversion [129]. Ultimately, enzymatic conversion of methane to methanol is a developing technology with several major hurdles to overcome before successful economic scale-up. Due to the inexpensive costs of methane and methanol, enzyme-catalyzed process must be efficient to ensure economic viability. Currently, low catalytic activity of MMO is a significant limiting factor [14,15,129–131]. Furthermore, a more intensive examination of process configurations is required to mitigate the mass transfer limitations that arise from the low solubility of oxygen and methane in aqueous media [130].

6.4. Food and Beverage Industry

In many instances, traditional chemical synthesis routes are not viable for food products due to reagent toxicity and complex reaction chemistries that result in unfavorable process economics [11]. Biocatalysts, on the other hand, present an opportunity for simplified, efficient production routes that mitigate the need for harsh substances, and thus are more economically competitive [9–11,132]. As such, the use of biocatalysts in food and beverage processes dates back thousands of years to the advents of culinary practices like wine and cheese making [10]. In modern times, the widespread use of enzymes in food and beverage industries for food quality preservation or modification is one of the earliest successful industrial applications of biocatalysis, observed in beer fermentation, juice debittering, and bread baking [133]. The replacement of conventional chemical treatment with enzyme-catalyzed pathways for conversion of starch to glucose and fructose first took place several decades ago [12,122].

The conventional production route requires temperatures up to 175 °C and considerable pressurization, whereas biocatalytic processes can be carried out at temperatures near 100 °C and at ambient pressure via sequential α-amylase-catalyzed reactions encompassing both liquefaction and saccharification steps [122]. In addition to milder reaction conditions, the multi-enzymatic process resulted in higher product selectivity and therefore allowed for better defined production routes for varying sugar products like maltose, fructose syrup, and crystalline sugar, as dictated by biocatalyst selection [122].

An emerging trend is the use of enzyme catalysis for commercial-scale production of probiotics, artificial sweeteners, and rare sugars [2]. Probiotics, such as oligosaccharides, lactulose, lactilol hydrolysates, and inulin, are non-digestible food additives that stimulate growth of gut bacteria and can reportedly improve human health [2,9,133]. Dietary supplement producers have become particularly interested in simple, efficient enzyme-catalyzed synthesis routes of probiotics due to above-average projected market growth and accompanying increase in demand [2,9]. Yakult Honsha Co. Ltd. of Japan and Friesland Food Domo of The Netherlands, among others, have carried out commercial-scale, enzyme-catalyzed production of galacto-oligosaccharides (GOS), a lucrative probiotic with digestive health benefits and use as low-calorie sweeteners [9]. GOS are produced by transgalactosylation simultaneous to hydrolysis of lactose via β-galactosidase; lab-scale results have shown GOS yields near 40% for free enzyme, while immobilized enzymes show the potential for larger yields of up to 50% through implementation in a continuous system resulting in decreased product inhibition [9].

The enzymatic production of protein hydrosylates for use as nutritional supplements and flavor enhancers has been developed due to milder reaction conditions and increased control over product formation relative to traditional chemical routes [133]. When hydrolyzed, a parent protein forms biofunctional peptides exhibiting antioxidant, antimicrobial, and antihypertensive properties, among other therapeutic effects [132,133]. The production of fish protein hydrolysates from seafood processing waste via papain, a proteolytic enzyme derived from papaya that has found widespread industrial application, has garnered attention recently because the process is a potential solution for minimizing pollution from fishing industries [39]. Additionally, papain has been researched as a biocatalyst for production of protein hydrosylates from Chinese walnuts; lab-scale work on papain catalysis has shown moderate yields and purities of hydrosylates, and peptides obtained from produced hydrosylates showed good antioxidant properties [40].

6.5. Flavors and Aromas Industry

Biocatalytic processes economically and environmentally advantageous to conventional chemical processes are in development for commercial-scale production of fragrance compounds, flavor compounds, and aromatics. The chemical structures of such substances are often characterized by regio-, chemo-, or stereoselective positioning of functional groups like alcohols, aldehydes, ketones, and esters; thus, scale-up of efficient enzyme-catalyzed processes for production of aromatic compounds is a potentially lucrative endeavor, particularly in light of promising global market projections for flavors and fragrances [42].

Lipase enzymes play an integral role in the development of biocatalytic fragrance and flavor production due to its capability to transfer acyl groups from esters to other nucleophiles [42]. Though most progress has been in bench-scale synthesis of aroma esters, the results suggest that a combination of protein engineering and process engineering can facilitate scale-up to profitable industrial processes. For instance, Vosmann et al. achieved a 94% conversion of oleic acid selectively to benzyl oleate with benzyl alcohol as an acyl acceptor in 1 h using a commercially available lipase, which illustrates strong product specificity that could make enzymatic conversion advantageous [41]. Badgujar et al. reached 99% conversion of vinyl propionate to p-cresyl propionate in 1.5 h via immobilized lipase in heptane, highlighting that certain immobilization techniques could functionalize lipase for implementation in industrial environments [43]. However, further work to achieve more efficient, robust biocatalytic reactions is required before enzymatic production of aromatic esters can be scaled to larger process throughputs [41–43].

6.6. Detergents Industry

Successful employment of biocatalysts is cited as the driving force of production of cost effective, environmentally benign detergents [44]. In the instance of the detergents industry it should be noted that enzymes are a product rather than a chemical process-specific catalyst. Nonetheless, favorable market trends in the detergents' industry reinforce the underlying view that biocatalytic products are inherently safer and more sustainable than traditional chemical products that pose health and safety risks [44–46]. Alkaline proteases—which are effective in the removal of protein stains and the cleaving of damaged cotton fibers—isolated from microbial sources comprise significant portions of multiple detergents produced and sold at commercial scale by manufacturers like Novozymes SA, Kao Corporation, and Genecor International [45]. The high reaction specificity of enzymatic reactions further mitigates damage to fabrics and surfaces that is characteristic of chemically harsh detergent agents [47]. Furthermore, the ratio of catalytically active enzymes in detergent mixtures are optimized for specific detergent applications; for instance, dishwashing detergents often contain varying degrees of amylase and lipase intended for the removal of starch food deposits and fats and oils, respectively [47,48].

7. Projections of Economic Growth and Implementation Potential

The market for industrially relevant enzymes—including those applied in food, animal feed, detergent, and technical industries—is expected to grow globally through 2021 at an annual growth rate of 4.7%. Development of novel enzyme technologies, increased demand for naturally made food products, and policy requiring larger shares of renewable energy sources like biofuels [44] are not only becoming an alternative but an implementation reality. Of these categories, enzymes used in technical industries such as papers, textiles, leathers, and biofuels comprise the greatest potential for use of immobilized biocatalysts owing to process-oriented application [44]. Thus, market projections for technical enzymes are a reasonable indicator of process development for biocatalytic processes designed for commercial-scale production lines.

The most significant driving force in projected market growth for technical enzymes is renewed interest in enzyme-catalyzed biofuel production using lignocellulosic materials, which is a direct result of stricter environmental regulations [44]. In this regard, enzymes used in biofuels processes represent the largest portion of the technical enzyme market, which is dominated by two major players, Novozymes and Danisco/DuPont [44]. In 2015, DuPont and Quad County Corn Processors signed a multiyear contract for the production of bioethanol from cellulosic material in corn kernel fiber; the same year, DuPont acquired enzyme production technology assets from Dyadic, which is expected to further drive process development in the technical enzyme sector [44]. The same technologies are being investigated for further integration into paper and pulp industries, where xylanase, catalase, and lipase are frequently used for biomechanical pulping, de-inking of recycled fibers, and modification of fiber properties [58–61].

The bulk of the global technical enzyme market is reported for markets in Europe, the Middle East, and Africa (EMEA) at nearly 35% of the global share in 2016 [44]. However, strong market growth is projected for North America and Asia-Pacific, with annual growth rates of 6.8% for North America and 7.9% for the Asia-Pacific region through 2021 (Figure 3) [44]. Furthermore, the technical enzyme market is expected to overtake the EMEA market as the largest global segment of the market by 2021, suggesting progress in process development will largely take place in the Asia-Pacific region and in North America through 2021 [44].

If further progress is to be achieved, optimizing the structure-function relationships of enzyme-based conjugates while minimizing the production costs of the individual components (i.e., support and biocatalysts), as well as the implementation costs of the biocatalytic process is imperious (Figure 4). The modification of conventional schemes for enzyme immobilization and integration will not only need to facilitate product yield but, furthermore, optimize the process' metrics to thus limit logistical burden to both the environment and the individual [134–136]. Coupling or transient enzyme-driven reactions will also aim to reduce any public pressure associated with implementation of fossil fuels and thus lead a safer and eco-friendly solution for industrial revolution.

The challenges and opportunities associated with enzyme catalysis implementation will not only have to consider profit and marketability, but it will further have to consider integration of biomimetic approaches or "one pot" processes that could allow for efficiency, profitability, reusability and stability, all under the complexity of multi-chain driven specific reactions.

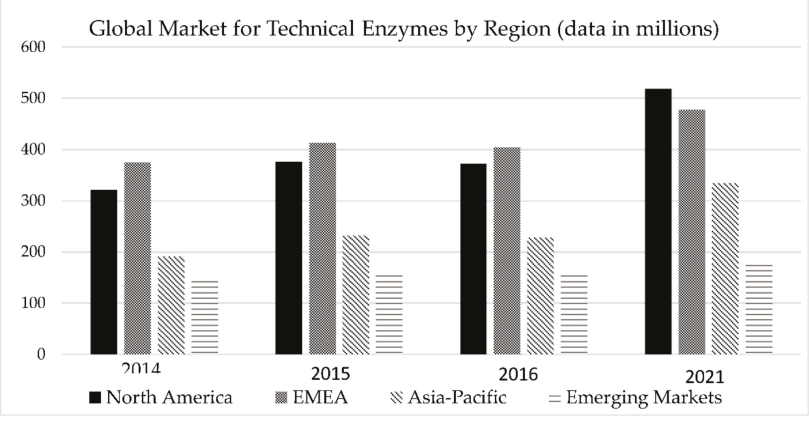

Figure 3. Global market growth projections for technical enzymes by geographical regions.

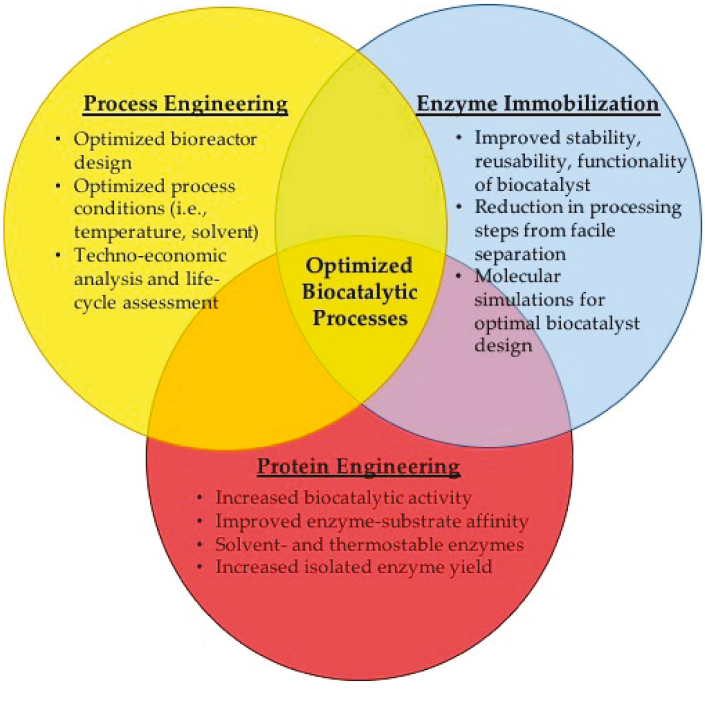

Figure 4. Schematic representation of a multidisciplinary approach aimed to define optimal biocatalytic processes. Implementation of biocatalysts in industrial technologies will have to not only consider optimization of the enzyme functionality but further, lead to increase in enzyme operational stability at the interface with supports used for immobilization.

8. Conclusions

Commercial-scale enzyme catalysis has been implemented in several industries such as pharmaceutical and foods with recent trends for biofuel production and natural gas conversion. Product yield in such industries was shown to be governed by enzymatic catalysis being implemented in milder process conditions and under less energy consumption, with reduced waste generation, exceptional high product selectivity to result in improvements in process economics and environmental sustainability.

The scale-up of enzymatic processes is however largely hampered by limitations in biocatalyst stability. To that end, enzyme immobilization was proposed and researched as an attractive approach for expanding the scope of enzyme catalysis and improved process efficiency. Critical examination of strategies for immobilization are still need to facilitate the development of optimal enzymes while holistic knowledge of economic driving forces to surround process development are still required for appropriateness of enzyme catalysis implementation in commercial-scale processes. The successful industrial application of new generation immobilized biocatalysts ultimately will be defined by critical analysis of immobilized enzyme processes, where overlap of expertise in protein engineering, enzyme immobilization, process engineering and life cycle analysis is paramount. Future implementation prospects will need to account for the structure-function relationship both at the level of the enzyme and the platform used in the immobilization as well as the optimized product yield at low implementation costs and with conjunction of experimental and computational approaches for an integrated combinatorial strategy.

Author Contributions: Proposed conceptualization of the paper: J.C; Feedback on the conceptualization: C.Z.D. and A.E.I; Writing of the paper draft: J.C.; J.C., C.Z.D. and A.E.I revised the manuscript; All authors have approved the final manuscript.

Funding: This work was funded by the National Science Foundation (NSF) grant 1454230.

Acknowledgments: The authors acknowledge the work of Xiao Hu for Figure 2. Molecular graphics were performed with the UCSF Chimera package. Chimera is developed by the Resource for Biocomputing, Visualization, and Informatics at the University of California, San Francisco (supported by NIGMS P41-GM103311).

Conflicts of Interest: The authors declare no conflict of interest.

References

1. Bommarius, A.S.; Paye, M.F. Stabilizing biocatalysts. *Chem. Soc. Rev.* **2013**, *42*, 6534–6565. [CrossRef] [PubMed]
2. Choi, J.-M.; Han, S.-S.; Kim, H.-S. Industrial applications of enzyme biocatalysis: Current status and future aspects. *Biotechnol. Adv.* **2015**, *33*, 1443–1454. [CrossRef] [PubMed]
3. Madhavan, A.; Sindhu, R.; Binod, P.; Sukumaran, R.K.; Pandey, A. Strategies for design of improved biocatalysts for industrial applications. *Bioresour. Technol.* **2017**, *245*, 1304–1313. [CrossRef] [PubMed]
4. Roy, I.; Prasad, S. Converting Enzymes into Tools of Industrial Importance. *Recent Pat. Biotechnol.* **2017**, *12*, 33–56.
5. DiCosimo, R.; McAuliffe, J.; Poulose, A.J.; Bohlmann, G. Industrial use of immobilized enzymes. *Chem. Soc. Rev.* **2013**, *42*, 6437–6474. [CrossRef] [PubMed]
6. Sun, H.; Zhang, H.; Ang, E.L.; Zhao, H. Biocatalysis for the synthesis of pharmaceuticals and pharmaceutical intermediates. *Bioorgan. Med. Chem.* **2017**, *26*, 1275–1284. [CrossRef] [PubMed]
7. Patel, R.N. Biocatalysis for synthesis of pharmaceuticals. *Bioorganic Med. Chem.* **2017**, *26*, 1252–1274. [CrossRef] [PubMed]
8. Huisman, G.W.; Collier, S.J. On the development of new biocatalytic processes for practical pharmaceutical synthesis. *Curr. Opin. Chem. Biol.* **2013**, *17*, 284–292. [CrossRef] [PubMed]
9. Panesar, P.S.; Kumari, S.; Panesar, R. Biotechnological approaches for the production of prebiotics and their potential applications. *Crit. Rev. Biotechnol.* **2013**, *33*, 345–364. [CrossRef] [PubMed]
10. Fernandes, P. Enzymes in Food Processing: A Condensed Overview on Strategies for Better Biocatalysts. *Enzyme Res.* **2010**. [CrossRef] [PubMed]

11. Akoh, C.C.; Chang, S.-W.; Lee, G.-C.; Shaw, J.-F. Biocatalysis for the Production of Industrial Products and Functional Foods from Rice and Other Agricultural Produce. *J. Agric. Food Chem.* **2008**, *56*, 10445–10451. [CrossRef] [PubMed]
12. Kapoor, S.; Rafiq, A.; Sharma, S. Protein engineering and its applications in food industry. *Crit. Rev. Food Sci. Nutr.* **2017**, *57*, 2321–2329. [CrossRef] [PubMed]
13. Pellis, A.; Cantone, S.; Ebert, C.; Gardossi, L. Evolving biocatalysis to meet bioeconomy challenges and opportunities. *New Biotechnol.* **2018**, *40*, 154–169. [CrossRef] [PubMed]
14. Strong, P.J.; Kalyuzhnaya, M.; Silverman, J.; Clarke, W.P. A methanotroph-based biorefinery: Potential scenarios for generating multiple products from a single fermentation. *Bioresour. Technol.* **2016**, *215*, 314–323. [CrossRef] [PubMed]
15. Fei, Q.; Guarnieri, M.T.; Tao, L.; Laurens, L.M.L.; Dowe, N.; Pienkos, P.T. Bioconversion of natural gas to liquid fuel: Opportunities and challenges. *Biotechnol. Adv.* **2014**, *32*, 596–614. [CrossRef] [PubMed]
16. Noraini, M.Y.; Ong, H.C.; Badrul, M.J.; Chong, W.T. A review on potential enzymatic reation for biodiesel production from algae. *Renew. Sustain. Energy Rev.* **2014**, *39*, 24–34. [CrossRef]
17. Asgher, M.; Shahid, M.; Kamal, S.; Iqbal, H.M.N. Recent trends and valorization of immobilization strategies and ligninolytic enzymes by industrial biotechnology. *J. Mol. Catal. B Enzym.* **2014**, *101*, 56–66. [CrossRef]
18. Liew, W.H.; Hassim, M.H.; Ng, D.K.S. Review of evolution, technology and sustainability assessments of biofuel production. *J. Clean. Prod.* **2014**, *71*, 11–29. [CrossRef]
19. Cardona, C.A.; Quintero, J.A.; Paz, I.C. Production of bioethanol from sugarcane bagasse: Status and perspectives. *Bioresour. Technol.* **2010**, *101*, 4745–4766. [CrossRef] [PubMed]
20. Grigoras, A.G. Catalase immobilization—A review. *Biochem. Eng. J.* **2017**, *117*, 1–20. [CrossRef]
21. Cao, S.; Xu, P.; Ma, Y.; Yao, X.; Yao, Y.; Zong, M.; Li, X.; Lou, W. Recent advances in immobilized enzymes on nanocarriers. *Chin. J. Catal.* **2016**, *37*, 1814–1823. [CrossRef]
22. Ansari, S.A.; Husain, Q. Potential applications of enzymes immobilized on/in nano materials: A review. *Biotechnol. Adv.* **2012**, *30*, 512–523. [CrossRef] [PubMed]
23. Misson, M.; Zhang, H.; Jin, B. Nanobiocatalyst advancements and bioprocessing applications. *Interface* **2015**, *12*, 20140891. [CrossRef] [PubMed]
24. Sheldon, R.A. Enzyme Immobilization: The Quest for Optimum Performance. *Adv. Synth. Catal.* **2007**, *349*, 1289–1307. [CrossRef]
25. Mehta, J.; Bhardwaj, N.; Bhardwaj, S.K.; Kim, K.-H.; Deep, A. Recent advances in enzyme immobilization techniques: Metal-organic frameworks as novel substrates. *Coord. Chem. Rev.* **2016**, *322*, 30–40. [CrossRef]
26. Cipolatti, E.P.; Valerio, A.; Henriques, R.O.; Moritz, D.E.; Ninow, J.L.; Freire, D.M.G.; Manoel, E.A.; Fernandez-Lafuente, R.; Oliveira, D.D. Nanomaterials for biocatalyst immobilization—State of the art and future trends. *RSC Adv.* **2016**, *6*, 104675–104692. [CrossRef]
27. Bezerra, C.S.; Lemos, C.M.G.D.F.; Sousa, M.D.; Goncalves, L.R.B. Enzyme immobilization onto renewable polymeric matrixes: Past, present and future trends. *J. Appl. Polym. Sci.* **2015**, *132*. [CrossRef]
28. Tracewell, C.A.; Arnold, F.H. Directed enzyme evolution: Climbing fitness peaks on amino acid at a time. *Curr. Opin. Chem. Biol.* **2009**, *13*, 3–9. [CrossRef] [PubMed]
29. Chao, F.-A.; Morelli, A.J.C.H., III; Churchfield, L.; Hagmann, L.N.; Shi, L.; Masterson, L.R.; Sarangi, R.; Veglia, G.; Seelig, B. Structure and dynamics of a primordial catalytic fold generated by in vitro evolution. *Nat. Chem. Biol.* **2013**, *9*, 81–83. [CrossRef] [PubMed]
30. Li, T.; Liang, J.; Ambrogelly, A.; Brennan, T.; Gloor, G.; Huisman, G.; Lalonde, J.; Lekhal, A.; Mijts, B.; Muley, S.; et al. Efficient, chemoenzymatic process for manufacture of the boceprevir bicyclic [3.1.0]proline intermediate based on amine oxidase-catalyzed desymmetrization. *J. Am. Chem. Soc.* **2012**, *134*, 6467–6472. [CrossRef] [PubMed]
31. Desai, A.A. Sitagliptin manufacture: A compelling tale of green chemistry, process intensification, and industrial asymmetric catalysis. *Angew. Chem. Int. Ed.* **2011**, *50*, 1974–1976. [CrossRef] [PubMed]
32. Goncalves, A.; Almeida, L.; Silva, A.P.; Fontes-Ribeiro, C.; Ambrosio, A.F.; Cristovao, A.; Fernandes, R. The dipeptidyl peptidase-4 (dpp-4) inhibitor sitagliptin ameliorates retinal endothelial cell dysfunction triggered by inflammation. *Biomed. Pharmacother.* **2018**, *102*, 833–838. [CrossRef] [PubMed]
33. Savile, C.K. Biocatalytic asymmetric synthesis of chiral amines from ketones applied to sitagliptin manufacture. *Science* **2010**, *329*, 305–309. [CrossRef] [PubMed]

34. Kjellin, M.; Wesslen, T.; Lofblad, E.; Lennerstrand, J.; Lannergard, A. The effect of the first-generation hcv-protease inhibitors boceprevir and telaprevir and the relation to baseline ns3 resistance mutations in genotype 1: Experience from a small swedish cohort. *Upsala J. Med. Sci.* **2018**, *123*, 50–56. [CrossRef] [PubMed]
35. Krell, H.V.; Leuchter, A.F.; Cook, I.A.; Abrams, M. Evaluation of reboxetine, a noradrenergic antidepressant, for the treatment of fibromyalgia and chronic low back pain. *Psychosomatics* **2005**, *46*, 379–384. [CrossRef] [PubMed]
36. Hayes, S.T.; Assaf, G.; Checksfield, G.; Cheung, C.; Critcher, D.; Harris, L.; Howard, R.; Mathew, S.; Regius, C.; Scotney, G.; et al. Commercial synthesis of (s,s0-reboxetine succinate: A journey to find the cheapest commercial chemistry for manufacture. *Org. Process Res. Dev.* **2011**, *15*, 1305–1314. [CrossRef]
37. Martinez, C.A.; Hu, S.; Dumond, Y.; Tao, J.; Kelleher, P.; Tully, L. Development of a Chemoenzymatic Manufacturing Process for Pregabalin. *Org. Process Res. Dev.* **2008**, *12*, 392–398. [CrossRef]
38. Marouf, H.M. Effect of Pregabalin Premedication on Emergence Agitation in Children after Sevoflurane Anesthesia: A Randomized Controlled Study. *Anesth. Essays Res.* **2018**, *12*, 31–35. [CrossRef] [PubMed]
39. Elavarasan, K.; Shamasundar, B.A. Effect of oven drying and freeze drying on the antioxidant and functional properties of protein hydrosylates derived from freshwater fish (Cirrhinus mrigala) using papain enzyme. *J. Food Sci. Technol.* **2016**, *53*, 1303–1311. [CrossRef] [PubMed]
40. Liu, M.-C.; Yang, S.-J.; Hong, D.; Yang, J.-P.; Liu, M.; Lin, Y.; Huang, C.-H.; Wang, C.-J. A simple and convenient method for the preparation of antioxidant peptides from walnut (Juglans regia L.) protein hydrosylates. *Chem. Cent. J.* **2016**, *10*, 39. [CrossRef] [PubMed]
41. Vosmann, K.; Wiege, B.; Weitkamp, P.; Weber, N. Preparation of lipophilic alkyl (hydroxy)benzoates by solvent-free lipase-catalyzed esterification and transesterification. *Appl. Microbiol. Biotechnol.* **2008**, *80*, 29–36. [CrossRef] [PubMed]
42. SA, A.G.A.; Meneses, A.C.D.; Araujo, P.H.H.D.; Oliveira, D.D. A review on enzymatic synthesis of aromatic esters used as flavor ingredients for food, cosmetics an pharmaceutical industries. *Trends Food Sci. Technol.* **2017**, *69*, 95–105. [CrossRef]
43. Badgujar, K.C.; Pai, P.A.; Bhanage, B.M. Enhanced biocatalytic activity of immobilized Pseudomonas cepacia lipase under sonicated condition. *Bioprocess Biosyst. Eng.* **2016**, *39*, 211–221. [CrossRef] [PubMed]
44. Dewan, S.S. *Global Markets for Enzymes in Industrial Applications*; BCC Research: Wellesly, MA, USA, 2017.
45. Kumar, D.; Savitri; Thakur, N.; Verma, R.; Bhalla, T.C. Microbial Proteases and Application as Laundry Detergent Additive. *Res. J. Microbiol.* **2008**, *3*, 661–672. [CrossRef]
46. Alfa, M.J.; Jackson, M. A new hydrogen peroxide-based medical-device detergent with germicidal properties: Comparison with enzymatic cleaners. *AJIC* **2001**, *29*, 168–177. [CrossRef] [PubMed]
47. Singh, R.; Kumar, M.; Mittal, A.; Mehta, P.K. Microbial enzymes: Industrial progress in 21st century. *3 Biotech* **2016**, *6*, 174. [CrossRef] [PubMed]
48. Li, S.; Yang, X.; Yang, S.; Zhu, M.; Wang, X. Technology Prospecting on Enzymes: Application, Marketing and Engineering. *Comput. Struct. Biotechnol. J.* **2012**, *2*, e201209017. [CrossRef] [PubMed]
49. Zhang, B.; Weng, Y.; Xu, H.; Mao, Z. Enzyme immobilization for biodiesel production. *Appl. Microbial. Biotechnol.* **2012**, *93*, 61–67. [CrossRef] [PubMed]
50. Harding, K.G.; Dennis, J.S.; Blottnitz, H.V.; Harrison, S.T.L. A life-cycle comparison between inorganic and biological catalysis for the production of biodiesel. *J. Clean. Prod.* **2007**, *16*, 1368–1378. [CrossRef]
51. Raman, J.K.; Ting, V.F.W.; Pogaku, R. Life cycle assessment of biodiesel production using alkali, soluble and immobilized enzyme catalyst processes. *Biomass Bioenergy* **2011**, *35*, 4221–4229. [CrossRef]
52. Olofsson, J.; Barta, Z.; Borjesson, P.; Wallberg, O. Integrating enzyme fermentation in lignocellulosic ethanol production: Life-cycle assessment and techno-economic analysis. *Biotechnol. Biofuels* **2017**, *10*, 51. [CrossRef] [PubMed]
53. Yue, F.; Jian-xin, J.; Li-wei, Z. Recent developments in activities, utilization and sources of cellulase. *For. Stud. China* **2009**, *11*, 202–207.
54. Khorshidi, K.J.; Lenjannezhadian, H.; Jamalan, M.; Zeinali, M. Preparation and characterization of nanomagnetic cross-linked cellulase aggregates for cellulose bioconversion. *J. Chem. Technol. Biotechnol.* **2016**, *91*, 539–546. [CrossRef]
55. Taherzadeh, M.J.; Karimi, K. Enzyme-based hydrolysis processes for ethanol from lignocellulosic materials: A review. *BioResources* **2007**, *2*, 707–738.

56. Lima, J.S.; Araujo, P.H.H.; Sayer, C.; Souza, A.A.U.; Viegas, A.C.; Oliveira, D.D. Cellulase immobilization on magnetic nanoparticles encapsulated in polymer nanospheres. *Bioprocess Biosyst. Eng.* **2017**, *40*, 511–518. [CrossRef] [PubMed]
57. Tan, T.; Lu, J.; Nie, K.; Deng, L.; Wang, F. Biodiesel production with immobilized lipase: A review. *Biotechnol. Adv.* **2010**, *28*, 628–634. [CrossRef] [PubMed]
58. Bhat, M.K. Cellulases and related enzymes in biotechnology. *Biotechnol. Adv.* **2000**, *18*, 355–383. [CrossRef]
59. Kuhad, R.C.; Gupta, R.; Singh, A. Microbial Cellulases and Their Industrial Applications. *Enzyme Res.* **2011**, *2011*. [CrossRef] [PubMed]
60. Hasan, F.; Shah, A.A.; Hameed, A. Industrial applications of microbial lipases. *Enzyme Microb. Technol.* **2006**, *39*, 235–251. [CrossRef]
61. Bajpai, P. Application of Enzymes in the Pulp and Paper Industry. *Biotechnol. Prog.* **1999**, *15*, 147–157. [CrossRef] [PubMed]
62. Sheldon, R.A. Characteristic features and biotechnological applications of cross-linked enzyme aggregates (cleas). *Appl. Microbial. Biotechnol.* **2011**, *92*, 467–477. [CrossRef] [PubMed]
63. Jesionowski, T.; Zdarta, J.; Krajewska, B. Enzyme immobilization by adsorption: A review. *Adsorption* **2014**, *20*, 801–821. [CrossRef]
64. Betancor, L.; Luckarift, H.R. Bioinspired enzyme encapsulation for biocatalysis. *Trends Biotechnol.* **2008**, *26*, 566–572. [CrossRef] [PubMed]
65. Feng, W.; Ji, P. Enzymes immobilized on carbon nanotubes. *Biotechnol. Adv.* **2011**, *29*, 889–895. [CrossRef] [PubMed]
66. Chauhan, G.S. Evaluation of nanogels as supports for enzyme immobilization. *Polym. Int.* **2014**, *63*, 1889–1894. [CrossRef]
67. Kommoju, P.R.; Chen, Z.W.; Bruckner, R.C.; Mathews, F.S.; Jorns, M.S. Probing oxygen activation sites in two flavoprotein oxidases using chloride as an oxygen surrogate. *Biochemistry* **2011**, *50*, 5521–5534. [CrossRef] [PubMed]
68. Li, Y.; Quan, J.; Branford-White, C.; Williams, G.R.; Wu, J.-X.; Zhu, L.-M. Electrospun polyacrylonitrile-glycopolymer nanofibrous membranes for enzyme immobilization. *J. Mol. Catal. B Enzym.* **2012**, *76*, 15–22. [CrossRef]
69. Kumar, D.; Nagar, S.; Bhushan, I.; Kumar, L.; Parshad, R. Covalent immobilization of organic solvent tolerant lipase on aluminum oxide pellets and its potential application in esterification reaction. *J. Mol. Catal. B Enzym.* **2013**, *87*, 51–61. [CrossRef]
70. Tran, D.-T.; Chen, C.-L.; Chang, J.-S. Immobilization of Burkholderia sp. lipase on ferric silica nanocomposite for biodiesel production. *J. Biotechnol.* **2012**, *158*, 112–119. [CrossRef] [PubMed]
71. Premaratne, G.; Nerimetla, R.; Matlock, R.; Sunday, L.; Koralege, R.S.H.; Ramsey, J.D.; Krishnan, S. Stability, scalability, and reusability of a volume efficient biocatalytic system constructed on magnetic nanoparticles. *Catal. Sci. Technol.* **2016**, *6*, 2361–2369. [CrossRef] [PubMed]
72. Zhang, C.; Luo, S.; Chen, W. Activity of catalase adsorbed to carbon nanotubes: Effects of carbon nanotube surface properties. *Talanta* **2013**, *113*, 142–147. [CrossRef] [PubMed]
73. Edwards, J.V.; Prevost, N.T.; Condon, B.; French, A.; Wu, Q. Immobilization of lysozyme-cellulose amide-linked conjugates on cellulose I and II cotton nanocrystalline preparations. *Cellulose* **2012**, *19*, 495–506. [CrossRef]
74. Hong, J.; Xu, D.; Gong, P.; Yu, J.; Ma, H.; Yao, S. Covalent-bonded immobilization of enzyme on hydrophilic polymer covering magnetic nanogels. *Microporous Mesoporous Mater.* **2008**, *109*, 470–477. [CrossRef]
75. Zhu, J.; Sun, G. Lipase immobilization on glutaraldehyde-activated nanofibrous membranes for improved enzyme stabilities and activities. *React. Funct. Polym.* **2012**, *72*, 839–845. [CrossRef]
76. Ottone, C.; Bernal, C.; Serna, N.; Illanes, A.; Wilson, L. Enhanced long-chain fatty alcohol oxidation by immobilization of alcohol dehydrogenase from *S. cerevisiae*. *Appl. Microbiol. Biotechnol.* **2017**, *102*, 237–247. [CrossRef] [PubMed]
77. Kuo, C.-H.; Chen, G.-J.; Chen, C.-I.; Liu, Y.-C.; Shieh, C.-J. Kinetics and optimization of lipase-catalyzed synthesis of rose fragrance 2-phenylethyl acetate through transesterification. *Process Biochem.* **2014**, *49*, 437–444. [CrossRef]

78. Tomke, P.D.; Rathod, V.K. Ultrasound assisted lipase catalyzed synthesis of cinnamyl acetate via transesterification reaction in a solvent free medium. *Ultrason. Sonochemistry* **2015**, *27*, 241–246. [CrossRef] [PubMed]
79. Eberhardt, A.M.; Pedroni, V.; Volpe, M.; Ferreira, M.L. Immobilization of catalase from Aspergillus niger on inorganic and biopolymeric supports for H_2O_2 decomposition. *Appl. Catal. B Environ.* **2004**, *47*, 153–163. [CrossRef]
80. Homaei, A.A.; Sajedi, R.H.; Sariri, R.; Seyfzadeh, S.; Stevanato, R. Cysteine enhances activity and stability of immobilized papain. *Amino Acids* **2010**, *38*, 937–942. [CrossRef] [PubMed]
81. Dincer, A.; Telefoncu, A. Improving the stability of cellulase by immobilization on modified polyvinyl alcohol coated chitosan beads. *J. Mol. Catal. B Enzym.* **2007**, *45*, 10–14. [CrossRef]
82. Lopez-Gallego, F.; Betancor, L.; Hidalgo, A.; Dellamora-Ortiz, G.; Mateo, C.; Fernandez-Lafuente, R.; Guisan, J.M. Stabilization of different alcohol oxidases via immobilization and post immobilization techniques. *Enzyme Microb. Technol.* **2007**, *40*, 278–284. [CrossRef]
83. Falus, P.; Cerioli, L.; Bajnoczi, G.; Boros, Z.; Weiser, D.; Nagy, J.; Tessaro, D.; Servi, S.; Poppe, L. A Continuous-Flow Cascade Reactor System for Subtilisin A-Catalyzed Dynamic Kinetic Resolution of N-tert-butyloxy-carbonylphenylalanine Ethyl Thioester with Benzylamine. *Adv. Synth. Catal.* **2016**, *358*, 1608–1617. [CrossRef]
84. Knezevic, Z.; Milosavic, N.; Bezbradica, D.; Jakovljevic, Z.; Prodanovic, R. Immobilization of lipase from Candida rugosa on Eupergit C supports by covalent attachment. *Biochem. Eng. J.* **2006**, *30*, 269–278. [CrossRef]
85. Bolivar, J.M.; Nidetzky, B. Positively Charged Mini-Protein Z_{basic2} as a Highly Efficient Silica Binding Module: Opportunities for Enzyme Immobilization on Unmodified Silica Supports. *Langmuir* **2012**, *28*, 10040–10049. [CrossRef] [PubMed]
86. Bolivar, J.M.; Nidetzky, B. Smart enzyme immobilization in microstructured reactors. *Microreactors* **2013**, *31*, 50–54.
87. Zhao, X.; Qi, F.; Yuan, C.; Du, W.; Liu, D. Lipase-catalyzed process for biodiesel production: Enzyme immobilization, process simulation and optimization. *Renew. Sustain. Energy Rev.* **2015**, *44*, 182–197. [CrossRef]
88. Mendes, A.A.; Freitas, L.; Carvalho, A.K.F.D.; Oliveira, P.C.D.; Castro, H.F.D. Immobilization of a Commercial Lipase from Penicillium camembertii (Lipase G) by Different Strategies. *Enzyme Res.* **2011**. [CrossRef] [PubMed]
89. Petri, A.; Marconcini, P.; Salvadori, P. Efficient immobilization of epoxide hydrolase onto silica gel and use in the enantioselective hydrolysis of racemic para-nitrostyrene oxide. *J. Mol. Catal. B Enzym.* **2005**, *32*, 219–224. [CrossRef]
90. Alptekin, O.; Tukel, S.S.; Yildirim, D.; Alagoz, D. Immobilization of catalase onto Eupergit C and its characterization. *J. Mol. Catal. B Enzym.* **2010**, *64*, 177–183. [CrossRef]
91. Ferraz, L.I.R.; Possebom, G.; Alvez, E.V.; Cansian, R.L.; Paroul, N.; Oliveira, D.D.; Treichel, H. Application of home-made lipase in the production of geranyl propionate by esterification of geraniol and propionic acid in solvent-free system. *Biocatal. Agric. Biotechnol.* **2015**, *4*, 44–48. [CrossRef]
92. Risso, F.V.A.; Mazutti, M.A.; Treichel, H.; Costa, F.; Maugeri, F.; Rodrigues, M.I. Effect of Organic Solvent on the Characteristics of Free and Immobilized Inulinase from Kluyveromyces marxianus ATCC 16045. *Food Technol. Biotechnol.* **2010**, *48*, 143–150.
93. Arica, M.Y.; Oktem, H.A.; Oktem, Z.; Tuncel, S.A. Immobilization of catalase in poly(isopropylacrylamide-co-hydroxythylmethacrylate) thermally reversible hydrogels. *Polym. Int.* **1999**, *48*, 879–884. [CrossRef]
94. Singh, H.P.; Gupta, N.; Sharma, R.K. Hollow Silica Nanoparticles as Support for Catalase Enzyme Immobilization. *Catal. Lett.* **2013**, *143*, 1304–1311. [CrossRef]
95. Yan, M.; Liu, Z.; Lu, D.; Liu, Z. Fabrication of Single Carbonic Anhydrase Nanogel against Denaturation and Aggregation at High Temperature. *Biomacromolecules* **2007**, *8*, 560–565. [CrossRef] [PubMed]
96. Prakasham, R.S.; Devi, G.S.; Rao, C.S.; Sivakumar, V.S.S.; Sathish, T.; Sarma, P.N. Nickel-Impregnated Silica Nanoparticle Synthesis and Their Evaluation for Biocatalyst Immobilization. *Appl. Biochem. Biotechnol.* **2010**, *160*, 1888–1895. [CrossRef] [PubMed]

97. Wu, X.; Ge, J.; Yang, C.; Hou, M.; Liu, Z. Facile synthesis of multiple enzyme-containing metal-organic frameworks in a biomolecule friendly environment. *Chem. Commun.* **2015**, *51*, 13408–13411. [CrossRef] [PubMed]
98. Lin, Z.; Xiao, Y.; Wang, L.; Yin, Y.; Zheng, J.; Yang, H.; Chen, G. Facile synthesis of enzyme-inorganic hybrid nanoflowers and their application as an immobilized trypsin reactor for highly efficient protein digestion. *RSC Adv.* **2014**, *4*, 13888–13891. [CrossRef]
99. Cao, L.; Rantwijk, F.V.; Sheldon, R.A. Cross-Linked Enzyme Aggregates: A Simple and Effective Method for the Immobilization of Penicillin Acylase. *Org. Lett.* **2000**, *2*, 1361–1364. [CrossRef] [PubMed]
100. Sheldon, R.A. Cross-Linked Enzyme Aggregates as Industrial Biocatalysts. *Org. Process Res. Dev.* **2011**, *15*, 213–223. [CrossRef]
101. Illanes, A.; Wilson, L.; Altamirano, C.; Cabrera, Z.; Alvarez, L.; Aguirre, C. Production of cephalexin in organic medium at high substrate concentrations with CLEA of penicillin acylase and PGA-450. *Enzyme Microb. Technol.* **2007**, *40*, 195–203. [CrossRef]
102. Vafiadi, C.; Topakas, E.; Christakopoulos, P. Preparation of multipurpose cross-linked enzyme aggregates and their application to production of alkyl ferulates. *J. Mol. Catal. B Enzym.* **2008**, *54*, 35–41. [CrossRef]
103. Zhao, L.; Zheng, L.; Gao, G.; Jia, F.; Cao, S. Resolution of N-(2-ethyl-6-methyl-phenyl) alanine via cross-linked aggregates of Pseudomonas sp. Lipase. *J. Mol. Catal. B Enzym.* **2008**, *54*, 7–12. [CrossRef]
104. Martins, S.L.; Albuquerque, B.F.; Nunes, M.A.P.; Ribeiro, M.H.L. Exploring magnetic and imprinted cross-linked enzyme aggregates of rhamnopyranosidase in microbioreactors. *Bioresour. Technol.* **2018**, *249*, 704–712. [CrossRef] [PubMed]
105. Nguyen, L.T.; Yang, K.-L. Combined cross-linked enzyme aggregates of horseradish peroxidase and glucose oxidase for catalyzing cascade chemical reactions. *Enzyme Microb. Technol.* **2017**, *100*, 52–59. [CrossRef] [PubMed]
106. Lai, J.-Q.; Hu, Z.-L.; Sheldon, R.A.; Yang, Z. Catalytic performance of cross-linked enzyme aggregates of Penicillium expansum lipase and their use as a catalyst for biodiesel production. *Process Biochem.* **2012**, *47*, 2058–2063. [CrossRef]
107. Nuijens, T.; Cusan, C.; Schepers, A.C.H.M.; Kruijtzer, J.A.W.; Rijkers, D.T.S.; Liskamp, R.M.J.; Quaedflieg, P.J.L.M. Enzymatic synthesis of activated esters and their subsequent use in enzyme-based peptide synthesis. *J. Mol. Catal. B Enzym.* **2011**, *71*, 79–84. [CrossRef]
108. Cui, J.-D.; Zhang, S.; Sun, L.-M. Cross-Linked Enzyme Aggregates of Phenylalanine Ammonia Lyase: Novel Biocatalysts for Synthesis of L-Phenylalanine. *Appl. Biochem. Biotechnol.* **2012**, *167*, 835–844. [CrossRef] [PubMed]
109. Taboada-Puig, R.; Junghanns, C.; Demarche, P.; Moreira, M.T.; Feijoo, G.; Lema, J.M.; Agathos, S.N. Combined cross-linked enzyme aggregates from versatile peroxidase and glucose oxidase: Production, partial characterization and application for the elimination of endocrine disruptors. *Bioresour. Technol.* **2011**, *102*, 6593–6599. [CrossRef] [PubMed]
110. Thirkettle, J. SB-253514 and Analogues; Novel Inhibitors of Lipoprotein Associated Phospholipase A_2 Produced by Pseudomonas fluorescens DSM 11579. *J. Antibiot.* **2000**, *53*, 733–735. [CrossRef] [PubMed]
111. O'Connell, P.J.; Harms, C.T.; Allen, J.R.F. Metolachlor, S-metolachlor and their role within sustainable weed management. *Crop Prot.* **1998**, *17*, 207–212. [CrossRef]
112. Dinu, C.Z.; Borkar, I.V.; Bale, S.S.; Campbell, A.S.; Kane, R.S.; Dordick, J.S. Perhydrolase-nanotube-paint sporicidal composites stabilized by intramolecular crosslinking. *J. Mol. Catal. B Enzym.* **2012**, *75*, 20–26. [CrossRef]
113. Ren, T.; Mao, Z.; Moya, S.E.; Gao, C. Immobilization of Enzymes on 2-Hydroxyethylm Methacrylate and Glycidyl Methacrylate Copolymer Brushes. *Chem. Asian. J.* **2014**, *9*, 2132–2139. [CrossRef] [PubMed]
114. Fuentes, M.; Segura, R.L.; Abian, O.; Betancor, L.; Hidalgo, A.; Mateo, C.; Fernandez-Lafuente, R.; Guisan, J.M. Determination of protein-protein interactions through aldehyde-dextran intermolecular cross-linking. *Proteomics* **2004**, *4*, 2602–2607. [CrossRef] [PubMed]
115. Liese, A.; Hilterhaus, L. Evaluation of immobilized enzymes for industrial applications. *Chem. Soc. Rev.* **2013**, *42*, 6236–6249. [CrossRef] [PubMed]
116. Dach, R.; Song, J.J.; Roschangar, F.; Samstag, W.; Senanayake, C.H. The Eight Criteria Defining a Good Chemical Manufacturing Process. *Org. Process Res. Dev.* **2012**, *16*, 1697–1706. [CrossRef]

117. Zhou, H.; Qu, Y.; Chunlei; Kong; Li, D.; Shen, E.; Ma, Q.; Zhang, X.; Wang, J.; Zhou, J. Catalytic performance and molecular dynamic simulation of immobilized C-C bond hydrolase based on carbon nanotube matrix. *Colloids Surfaces B Biointerfaces* **2014**, *116*, 365–371. [CrossRef] [PubMed]
118. Basso, A.; Spizzo, P.; Ferrario, V.; Knapic, L.; Savko, N.; Braiuca, P.; Ebert, C.; Ricca, E.; Calabro, V.; Gardossi, L. Endo- and Exo-Inulinases: Enzyme-Substrate Interaction and Rational Immobilization. *Biotechnol. Prog.* **2010**, *26*, 397–405. [CrossRef] [PubMed]
119. Franca, E.F.; Leite, F.L.; Cunha, R.A.; Oliveira, O.N., Jr.; Freitas, L.C.G. Designing and enzyme-based nanobiosensor using molecular modeling techniques. *Phys. Chem. Chem. Phys.* **2011**, *13*, 8894–8899. [CrossRef] [PubMed]
120. Mathpati, A.C.; Vyas, V.K.; Bhanage, B.M. Kinetic resolution of 1,2-diols using immobilized Burkholderia cepacia lipase: A combined experimental and molecular dynamics investigation. *J. Biotechnol.* **2017**, *262*, 1–10. [CrossRef] [PubMed]
121. Allen, M.P.; Teldesley, D.J. *Computer Simulations of Liquids*; Oxford University Press: New York, NY, USA, 1987.
122. Maarel, M.J.E.C.V.D.; Veen, B.V.D.; Uitdehaag, J.C.M.; Leemhuis, H.; Dijkhuizen, L. Properties and applications of starch-converting enzymes of the alpha-amylase family. *J. Biotechnol.* **2002**, *94*, 137–155. [CrossRef]
123. Rasor, J.P.; Voss, E. Enzyme-catalyzed processes in pharmaceutical industry. *Appl. Catal. A Gen.* **2001**, *221*, 145–158. [CrossRef]
124. Petroleum, British. *BP Statistical Review of World Energy*; Petroleum, British: London, UK, 2017.
125. Qiu, C.; Colson, G.; Escalante, C.; Wetzstein, M. Considering macroeconomic indicators in the food before fuel nexus. *Energy Econ.* **2012**, *34*, 2021–2028. [CrossRef]
126. Rabideau, B.D.; Ismail, A.E. Mechanisms of hydrogen bond formation between ionic liquids and cellulose and the influence of water content. *Phys. Chem. Chem. Phys.* **2015**, *17*, 5767–5775. [CrossRef] [PubMed]
127. Viell, J.; Inouye, H.; Szekely, N.K.; Frielinghaus, H.; Marks, C.; Wang, Y.; Anders, N.; Spiess, A.C.; Makowski, L. Multi-scale processes of beech wood disintegration and pretreatment with 1-ethyl-3-methylimidazolium acetate/water mixtures. *Biotechnol. Biofuels* **2016**, *9*, 7. [CrossRef] [PubMed]
128. Pinkert, A.; Marsh, K.N.; Pang, S.; Staiger, M.P. Ionic Liquids and Their Interaction with Cellulose. *Chem. Rev.* **2009**, *109*, 6712–6728. [CrossRef] [PubMed]
129. Blanchette, C.D.; Knipe, J.M.; Stolaroff, J.K.; DeOtte, J.R.; Oakdale, J.S.; Maiti, A.; Lenhardt, J.; Sirajuddin, S.; Rosenzweig, A.C.; Baker, S.E. Printable enzyme-embedded materials for methane to methanol conversion. *Nat. Commun.* **2016**, *7*, 11900. [CrossRef] [PubMed]
130. Stone, K.A.; Hilliard, M.V.; He, Q.P.; Wang, J. A mini review on bioreactor configurations and gas transfer enhancements for biochemical methane conversion. *Biochem. Eng. J.* **2017**, *128*, 83–92. [CrossRef]
131. Strong, P.J.; Xie, S.; Clarke, W.P. Methane as a Resource: Can the Methanotrophs Add Value? *Environ. Sci. Technol.* **2015**, *49*, 4001–4018. [CrossRef] [PubMed]
132. Agyei, D.; Danquah, M.K. Industrial-scale manufacturing of pharmaceutical-grade bioactive peptides. *Biotechnol. Adv.* **2011**, *2011*, 272–277. [CrossRef] [PubMed]
133. Fernandez-Lucas, J.; Castaneda, D.; Hormigo, D. New trends for a classical enzyme: Papain, a biotechnological success story in the food industry. *Trends Food Sci. Technol.* **2017**, *68*, 91–101. [CrossRef]
134. Lima-Ramos, J.; Tufvesson, P.; Woodley, J.M. Application of environmental and economic metrics to guide the development of biocatalytic processes. *Green Process. Synth.* **2014**, *3*, 195–213. [CrossRef]
135. Tufvesson, P.; Lima-Ramos, J.; Haque, N.A.; Gernaey, K.V.; Woodly, J.M. Advances in the Process Development of Biocatalytic Processes. *Org. Process Res. Dev.* **2013**, *17*, 1233–1238. [CrossRef]
136. Sheldon, R.A.; Woodley, J.M. Role of Biocatalysis in Sustainable Chemistry. *Chem. Rev.* **2018**, *118*, 801–838. [CrossRef] [PubMed]

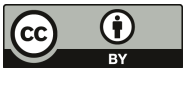

© 2018 by the authors. Licensee MDPI, Basel, Switzerland. This article is an open access article distributed under the terms and conditions of the Creative Commons Attribution (CC BY) license (http://creativecommons.org/licenses/by/4.0/).

catalysts

MDPI

Review

A General Overview of Support Materials for Enzyme Immobilization: Characteristics, Properties, Practical Utility

Jakub Zdarta [1,2,*], Anne S. Meyer [2], Teofil Jesionowski [1] and Manuel Pinelo [2]

[1] Institute of Chemical Technology and Engineering, Faculty of Chemical Technology, Poznan University of Technology, Berdychowo 4, PL-60965 Poznan, Poland; teofil.jesionowski@put.poznan.pl

[2] Center for BioProcess Engineering, Department of Chemical and Biochemical Engineering, Technical University of Denmark, Søltofts Plads 229, DK-2800 Kgs. Lyngby, Denmark; am@kt.dtu.dk (A.S.M.); mp@kt.dtu.dk (M.P.)

* Correspondence: jakub.zdarta@put.poznan.pl; Tel.: +48-616-653-747

Received: 19 January 2018; Accepted: 21 February 2018; Published: 24 February 2018

Abstract: In recent years, enzyme immobilization has been presented as a powerful tool for the improvement of enzyme properties such as stability and reusability. However, the type of support material used plays a crucial role in the immobilization process due to the strong effect of these materials on the properties of the produced catalytic system. A large variety of inorganic and organic as well as hybrid and composite materials may be used as stable and efficient supports for biocatalysts. This review provides a general overview of the characteristics and properties of the materials applied for enzyme immobilization. For the purposes of this literature study, support materials are divided into two main groups, called *Classic* and *New materials*. The review will be useful in selection of appropriate support materials with tailored properties for the production of highly effective biocatalytic systems for use in various processes.

Keywords: enzymes; enzyme immobilization; inorganic and organic supports; hybrid materials; biocatalysts and bioprocesses

1. Introduction

Enzymes are well-known as highly effective and efficient catalysts of a wide variety of processes characterized by high selectivity and activity. Additionally, enzymes may reduce the number of reaction steps and quantities of hazardous solvents needed and thus make a process more inexpensive and environmentally friendly [1]. For these reasons enzymes have become extremely important catalysts which exhibit great potential in many practical applications in industries ranging from food to pharmaceuticals [2]. The use of enzymes in multiple catalytic processes has resulted in studies leading to significant improvement of the enzyme properties. One of the most important and widely used techniques is enzyme immobilization in which catalysts are attached to a solid support that is insoluble in the reaction mixture [3]. The greatest advantage of immobilization is that it significantly improves the stability of the biomolecules under various reaction conditions and enhances the reusability of biomolecules over successive catalytic cycles [4]. Moreover, after binding the enzyme molecules, the catalysts change from a homogeneous to a heterogeneous form, which facilitates simple separation of the biocatalytic system from the reaction mixture and results in products of higher purity [5,6]. Various immobilization techniques have been developed, including adsorption, covalent binding, entrapment, encapsulation and cross-linking [7]. These differ in the type and character of the interactions formed and in the form and type of the support materials used. Selection of the most appropriate immobilization method and support material depends strongly on the type and conditions

of the catalytic process as well as the type of the enzyme [8]. However, it should be emphasized that the selection of the support materials is the most crucial challenge due to the major impact the support material may have on the properties of the biocatalytic system.

A very broad variety of materials of various origins can be used as supports for enzyme immobilization. These materials may, in general, be divided into organic, inorganic and hybrid or composite. The support should protect the enzyme structure against harsh reaction conditions and thus help the immobilized enzyme to retain high catalytic activity [9]. Moreover, use of a suitable material, for example hydrophobic carriers in lipase immobilization, may additionally increase the activity of the biocatalyst [10,11]. However, there are some limitations in this area, because the matrix must not have a negative effect on the structure of the enzyme and should not disturb the enzyme more than is required to create stable enzyme–matrix interactions. Additionally, there should be affinity between the functional groups of the two materials to allow the formation of these enzyme–matrix interactions and effective binding of the enzyme to the support. This is particularly important in the case of covalent immobilization [12]. The carrier should expose the active sites of the catalyst for easy attachment of substrate molecules and to reduce diffusional limitations of the substrates and products [13]. The main required features of support materials for effective enzyme immobilization are summarized in Figure 1.

Figure 1. Main features of support materials used for enzyme immobilization.

Nevertheless, it should be remembered that the appropriate selection of a matrix is directly related to the type of enzyme and to the process in which the biocatalytic system will be used. For the purposes of this literature review, the materials used as supports for enzyme immobilization have been classified as *Classic materials* (Section 2), which are the most commonly used and *New materials*, which offer especially desirable properties (Section 3). The latter type is also currently used

in immobilization and not only allow effective enzyme binding but also increase the applicability of the resulting biocatalytic systems.

2. *Classic Support Materials* for Enzyme Immobilization

Since the beginning of the work to develop the immobilization techniques, there has been a need to define a group of materials to which enzymes may be attached. In general, materials have been sought which offer high stability, availability, relatively low price and high affinity to the bound enzymes. A wide variety of materials of both inorganic and organic origin have been evaluated as effective supports for biocatalysts and are classified for the purposes of this review as *Classic materials* (Figure 2). Although *Classic materials* have been less frequently applied in recent years, they remain an important group of materials used for the immobilization of enzymes.

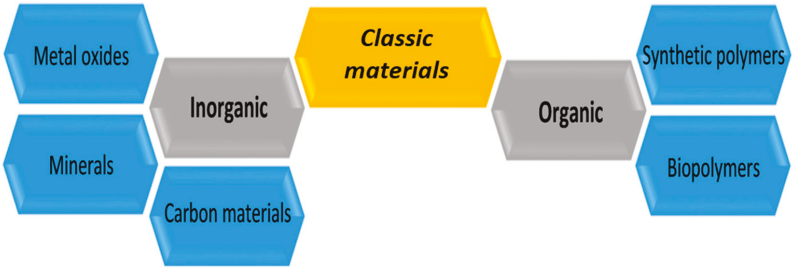

Figure 2. Selected examples of *Classic materials* of inorganic and organic origin used for enzyme immobilization.

2.1. Inorganic Materials

2.1.1. Silica and Inorganic Oxides

Silica is one of the most frequently used inorganic support materials for enzyme immobilization. Its high thermal and chemical resistance and good mechanical properties make it a suitable material for many practical applications. Silica offers good sorption properties due to its high surface area and porous structure. These properties allow effective enzyme attachment and reduce diffusional limitations [14,15]. Moreover, the presence of many hydroxyl groups on the surface of silica facilitates enzyme attachment and favours its functionalization with surface modifying agents such as glutaraldehyde or 3-aminopropyltriethoxysilane (APTES) [16]. Another advantage of this material is that it can be used in many different forms. Enzymes belonging to many catalytic classes, for example oxidoreductases, transferases, hydrolases and isomerases, have been immobilized with the use of sol-gel silica, fumed silica, colloidal silica nanoparticles and silica gel as supports [17–21]. The biocatalytic systems obtained demonstrate high catalytic activity retention and good thermal and pH resistance. For example, lipases immobilized on a silica gel matrix and on mesoporous silica retained respectively 91% and 96% of the activity of the free enzyme [22,23].

In previous studies, among other inorganic oxides, titanium, aluminium and zirconium oxides have also been used for the immobilization of many enzymes, for example lipase, cysteine, urease and α-amylase [24–27]. These supports are known for their high stability, mechanical resistance and good sorption capacity. Moreover, these materials are inert under various reaction conditions, which facilitates their application as supports for various classes of enzymes. Due to the presence of many hydroxyl groups on their surface, these materials are highly hydrophilic; this enhances enzyme immobilization and surface modification modified that favours the formation of relatively stable enzyme–matrix interactions.

2.1.2. Mineral Materials

Minerals are also used as support materials to produce recoverable biocatalytic systems with enhanced enzyme stability under reaction conditions. They are abundant in nature, are easily available, offer high biocompatibility and can be used as obtained without further advanced treatment and purification, which makes them relatively cheap [28]. Moreover, the presence of many functional groups (such as –OH, COOH, C=O, –SH, $–NH_2$) on the surface of the minerals allows the formation even of covalent bonds between the enzyme and the support and facilitates modification of the minerals. When additional functional groups are introduced, the adhesion area and hydrophobicity of the support increases while steric hindrances may be reduced [29]. The minerals used as supports for enzyme immobilization are mainly clay materials such as bentonite, halloysite, kaolinite, montmorillonite and sepiolite [30–32] though the group also includes the mineral hydroxyapatite known as calcium apatite [33,34]. In theory, enzymes belonging to many catalytic classes can be attached without limitation to the surface of mineral materials but in practice the most often immobilized are lipases, α-amylases, tyrosinases and glucose oxidases. Enzymes immobilized on minerals are used mainly in environmental engineering for waste and wastewater treatment as well as in biosensors to improve linear range and detection limit [35]. For example, according to Chrisnasari et al., glucose oxidase immobilized on bentonite modified by tetramethylammonium hydroxide retains over 50% of its initial activity after five repeated catalytic cycles [36].

2.1.3. Carbon-Based Materials

Carbon-based materials such as activated carbons and unmodified and modified charcoals have been used as effective and valuable support materials in enzyme immobilization, especially during the last two decades. The well-developed porous structure of these materials, with pores of various sizes and volumes and the high surface area (up to 1000 m^2/g) mean that these materials contain numerous contact sites on their surface for enzyme immobilization [37]. High adsorption capacity, the abundance of many functional groups and minimal release of fine particulate matter make carbon-based materials suitable carriers for the adsorption immobilization of various enzymes [38]. For example, unmodified charcoal support was used for the immobilization of amyloglucosidase. The immobilized enzyme when used for starch hydrolysis without any additional treatment retained over 90% of the free enzyme catalytic activity [39]. According to Silva et al. use of activated carbon for adsorption attachment of pancreatin allows a total immobilization yield that results in the creation of biocatalytic systems with good catalytic properties [40].

2.2. Organic Materials

It is well known that there is no universal support material suitable for all enzymes for all of their applications. Inorganic carriers have certain limitations, such as limited biocompatibility, lower affinity to biomolecules and reduced possibilities to create various geometrical shapes. Moreover, a cross-linking agent such as glutaraldehyde is usually required to create covalent bond between the enzyme and an inorganic support. Due to these reasons, some materials of organic origin are also used for the immobilization of various enzymes under different immobilization protocols. In general, organic support materials can be divided into two groups: (i) synthetic materials (mainly polymers) and (ii) renewable materials obtained from natural sources (biopolymers). Both groups have been widely used since the beginning of enzyme immobilization for the attachment of different types of biocatalysts.

2.2.1. Synthetic Polymers

The greatest advantage of synthetic polymers as support materials is that the monomers that build the polymeric chain can be selected according to the requirements of the enzyme and process in which the product of immobilization will be used [41,42]. The type and quantity of the monomers

determine the chemical structure and properties of the polymer. The composition of the monomers strongly affects the solubility, porosity, stability and mechanical properties of the polymer. A chemical feature that is directly related to the monomer structure is the presence of reactive chemical moieties in the polymeric chain. A very wide range of verified chemical functional groups may be observed in the structure of polymers. They include, for example, carbonyl, carboxyl, hydroxyl, epoxy, amine and diol groups, as well as strongly hydrophobic alkyl groups and trialkyl ammine moieties [43,44]. These groups facilitate effective enzyme binding and also functionalization of the polymer surface. The type of functional groups determines whether the enzyme is anchored to the matrix via for example adsorption or by the formation of covalent bonds, since it is mainly these two types of immobilization that take place when synthetic polymeric supports are used. Additionally, the type and quantity of functional groups determine the hydrophobic/hydrophilic character of the matrix and therefore its ability to form polar or hydrophobic interactions with the enzyme [45]. Moreover, by using polymeric supports, control of the length of the matrix–enzyme spacers has been achieved. Longer spacers allow the enzyme to retain higher conformational flexibility, while shorter spacers can protect the biomolecules against thermal inactivation and reduce leaching of the enzyme [46].

Various polymer materials can be used as effective supports and improve properties of the immobilized enzyme such as thermal stability and reusability. The polymer layers play a very important role in protecting the active sites of the enzyme from negative effects of the ingredients of the reaction mixture and the process conditions. However, it should be noted that synthesis of a polymer with the desired properties and functional groups is usually a time-consuming and costly process. Different polymers containing various functional groups have been used for enzyme immobilization. For example, α-amylase was covalently immobilized on polyaniline via –NH groups, while tyrosinase was immobilized via –NH and C=O groups on polyamide 66 (Nylon 66) without any linkers [47,48]. In another study, commercial lipase was immobilized by covalent binding on strongly hydrophobic polystyrene microspheres activated by epoxy groups [49]. In a hydrophobic environment, lipase exhibits extremely high catalytic properties which are related to the phenomenon called interfacial activation. Furthermore, polyurethane foam has been used for covalent immobilization of inulinase [50]. Bai et al. used polyvinyl alcohol modified by glutaraldehyde as a support for the immobilization of laccase via –OH groups. After immobilization, as a result of the strong interactions, the product was characterized by good storage stability and reusability which make it suitable for use in biosensors to detect bisphenol A [51]. Glucose oxidase, an antimicrobial enzyme, was immobilized on amino- and carboxyl-plasma-activated polypropylene film. The introduction of these groups enhanced the affinity of the polymer to the enzyme [52]. Commercially available ion exchange resins—for example Amberlite and Sepabeads—have also been used, respectively, for the immobilization of enzymes such as α-amylase and alcohol dehydrogenase [53,54].

2.2.2. Biopolymers

An alternative to the use of synthetic polymers as matrices for enzymes is the use of biopolymers—polymers of natural origin. Biopolymers include carbohydrates but also proteins such as albumin and gelatin [55]. Materials such as collagen, cellulose, keratins and carrageenan as well as chitin, chitosan and alginate are examples of biopolymers used for immobilization [56–59]. Biopolymers possess a unique set of properties, from biodegradability to harmless products, biocompatibility and non-toxicity, to an outstanding affinity to proteins, which make them suitable supports for enzymes [60]. Their natural origin and biocompatibility minimizes their negative impact on the structure and properties of enzymes and thus the immobilized proteins retain high catalytic activities. Furthermore, the availability of reactive functional groups in their structure—mainly hydroxyl but also amine and carbonyl moieties—enables direct reaction between the enzyme and matrix and facilitates modification of their surface [61]. Above all, however, these materials are renewable and easy to obtain; in many cases they are by-products of various industries, which makes them inexpensive and reduces the costs associated with the immobilization process [62]. Biopolymers

are used for immobilization by adsorption and covalent binding; however, their ability to create various geometrical configurations and propensity for gel formation mean that they are also used for immobilization by encapsulation and entrapment.

Chitosan on the basis of a literature survey can be considered the most frequently used biopolymer for enzyme immobilization. Chitosan can be applied in various forms and shapes. For example, Shi et al. used chitosan microspheres cross-linked by glutaraldehyde for the immobilization of nuclease, which is an important enzyme in genetic engineering [63]. In another study, glucose isomerase was adsorbed in macroporous chitosan beads prepared by chelation with various metal ions [64]. As reported by Kim et al. cellulose nanocrystals obtained from cotton linter cellulose can be used for immobilization by non-specific adsorption interactions of *Candida rugosa* lipase with high loading efficiency [65], whilst lipase was immobilized by entrapment by Tumturk et al. using κ-carrageenan hydrogels [66]. Vegetable and marine sponges characterized by an open fibrous network that reduces diffusional limitations have also been used as matrices for the immobilization of lipases, mainly via hydrogen bonds [67,68]. It may be concluded that biopolymers can be used to immobilize enzymes belonging to various catalytic classes with the retention of good catalytic properties. Moreover, the produced biocatalytic systems offer improved thermal stability and in general are noted for their good reusability.

Special attention should also be paid to alginates. Their remarkable abilities for gelation, mainly using sodium or calcium ions and for the creation of capsules in which single or multiple enzymes can be immobilized, mean that these materials are used principally for encapsulation and entrapment [69]. However, due to the relatively low mechanical stability of alginate gels and diffusional limitations in the transport of the substrates and products, their utilization in immobilization is restricted to a few applications only [70]. For example, Betigeri and Neau immobilized lipase in calcium alginate beads by entrapment, while Kocaturk and Yagar encapsulated polyphenol oxidase in copper alginate beads and obtained high immobilization yields [71,72]. The products exhibited good catalytic activity retention but their reusability was poor due to leaching of the enzyme from the matrix.

Agarose is a popular choice among biopolymers for use in enzyme immobilization. This linear heteropolysaccharide biopolymer consists of β-D-galactose and 3,6-anhydro-α-L-galactose units, linked by β-1-4 glycosidic and α-1-3 glycosidic bonds [73]. Like alginates, agarose also exhibits great ability for gelation which can occur at temperatures of agarose solution below 35 °C, without addition of any ions and results in formation of highly ordered stable and rigid structures [74]. It is worth mentioning that the 3-D architecture of this hydrophilic material remains almost unaltered in the presence of various organic solvents and does not shrink or swell under such conditions [75]. The ability of agarose gel to form various forms, such as beads, capsules or fibres, has led to this organic support material being of the great interest for industrial applications. For example, Prakash and Jaiswal used agarose beads for simple physical entrapment of thermostable α-amylase. The practical application of the resulting biocatalytic system was tested for removal of starch stains from clothes and the reusability of agarose immobilized enzyme was found to be up to five cycles [76]. In another study, a cross-linked agarose bead support highly activated with aldehyde groups was applied for multipoint covalent attachment of the commercial enzyme Depol™ 333MDP (β-1,4-endoxylanase). A high immobilization efficiency of over 85% was observed and the immobilized enzyme showed significant improvement of thermal stability compared to free protein [77].

2.3. Summary of Classic Materials

Classic materials used for enzyme immobilization of both inorganic and organic origin have been described in the above sections. Inorganic support materials, such as inorganic oxides, minerals or carbon-based materials, are characterized mainly by good thermal and chemical stability as well as by excellent mechanical resistance. These materials are also known for their good sorption properties which are a result of their well-developed porous structure and usually high surface area that ensures numerous contact sites for effective enzyme immobilization. In contrast, synthetic polymers and

biopolymers, also grouped under *Classic materials*, offer numerous functional groups that facilitate even covalent binding of enzymes without cross-linking agents. Additionally, biopolymers are usually characterized by high protein affinity as well as biocompatibility that limits negative effects of the support on the structure of enzymes. Moreover, irrespective of their origin, *Classic materials* for enzymes immobilization are usually abundant in nature (mineral, biopolymers) or are easy to synthesize (inorganic oxides, synthetic polymers) which makes them relatively cheap. These facts have meant that these support materials still play an important role as carriers for use for immobilization of enzymes.

The *Classic materials* and types of enzymes that may be immobilized using of these supports are summarized in Table 1 together with information about immobilization type, cross-linking agents and binding group.

Table 1. Summary and selected examples of *Classic materials* of both inorganic and organic origin applied for enzymes immobilization.

Support Material	Binding Groups	Cross-Linking Agent	Immobilization Type	Immobilized Enzyme	Reference
Inorganic Materials					
Sol-gel silica	–OH	–	adsorption	lipase from *Aspergillus niger*	[20]
Silica gel	–OH, C=O	glutaraldehyde	covalent binding	commercial lipase	[22]
γAl_2O_3	–OH	–	adsorption	cysteine proteinases from *Solanum granuloso-leprosum*	[25]
ZrO_2	–OH	–	adsorption	α-amylase from *Bacillus subtilis*	[26]
Montmorillonite	–OH	3-aminopropyl-triethoxysilane	covalent binding	glucoamylase from *Aspergillus niger*	[31]
Hydroxyapatite	–OH	–	adsorption	glucose oxidase from *Aspergillus niger*	[34]
Bentonite	–OH, $–NH_2$	tetramethyl ammonium hydroxide	covalent binding	glucose oxidase from *Aspergillus niger*	[36]
Commercial activated carbon	–OH, C=O	–	adsorption	cellulose from *Aspergillus niger*	[37]
Activated charcoal	–OH, C=O, COOH	–	adsorption	papain	[38]
Activated charcoal	–OH, C=O, COOH	–	adsorption	amyloglucosidase	[39]
Organic materials					
polyaniline	–N–H, C=O	glutaraldehyde	covalent binding	α-amylase	[47]
polystyrene	C=O, epoxy groups	poly(glycidyl methacrylate)	covalent binding	lipase	[49]
poly(vinyl alcohol)	–OH, C=O	glutaraldehyde	covalent binding	laccase from *Trametes versicolor*	[51]
polypropylene	–OH	plasma activated	covalent binding	Glucose oxidase	[52]
Cellulose nanocrystals	–OH	–	adsorption	lipase from *Candida rugosa*	[65]
Luffa cylindrica sponges	–OH, C=O, COOH	–	adsorption	lipase from *Aspergillus niger*	[67]
chitosan	–OH, $–NH_2$	–	entrapment	lipase from *Candida rugosa*	[71]
agarose	–OH	–	entrapment	α-amylase	[76]

3. *New Support Materials* for Enzyme Immobilization

Possibilities for practical applications of immobilized enzymes are continuing to grow. For this reason, discovery and use of *New materials* with desired properties, tailored to particular enzymes, has recently become extremely important. These materials, of both organic and inorganic origin, are characterized by exceptional thermal and chemical stability and very good mechanical properties. Moreover, these support materials are produced in various morphological shapes with controllable particle sizes, usually at nanoscale, which make them suitable for use with enzymes. Furthermore, these materials possess remarkable quantities of various functional groups, corresponding to the chemical groups of the proteins, which enhance enzyme binding and surface modification [78]. However, particularly during the last decade, scientific attention has been directed towards hybrid and composite materials, which combine properties of both composite precursor types and thus maximize their advantages [79]. Hence, with the use of *New materials* (see Figure 3) as enzyme supports, control of the technological process is improved, the immobilized enzymes exhibit enhanced catalytic efficiency

and the purity and quality of the reaction products increase compared to the processes catalysed by enzymes immobilized using the *Classic materials*.

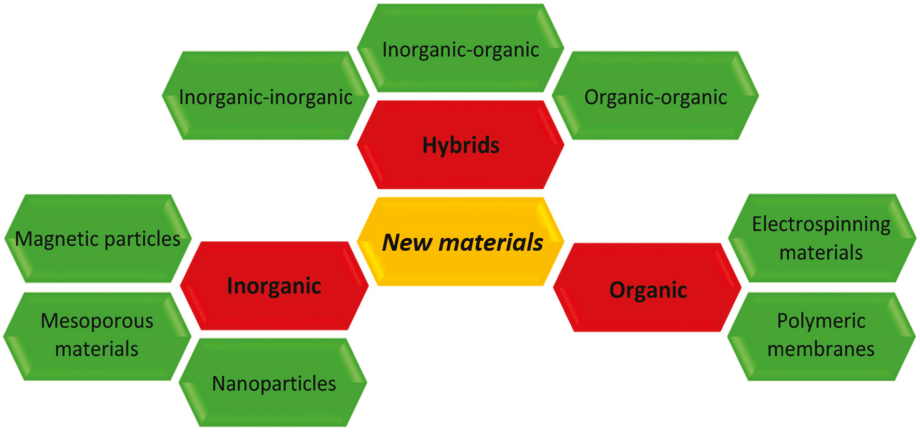

Figure 3. Selected examples of *New materials* of inorganic, organic and hybrid origin, applied for enzyme immobilization.

3.1. Inorganic Materials

3.1.1. Magnetic Particles

The separation of biocatalysts from the reaction mixture after the catalytic process is one of the crucial problems that must be solved when immobilized enzymes are used. One possible solution is attachment of the enzyme molecules to magnetic iron oxide nanoparticles (MNPs) and simple separation of the biocatalytic system with the use of an external magnetic field [80]. MNPs are also known for their large surface area and the abundance of hydroxyl groups on their surface which enables their easy modification and strong (covalent) binding of the enzyme. These are very important features. High mechanical stability and low porosity, however, which minimize steric hindrances, are also relevant for the creation of a stable enzyme–matrix biocatalytic system [81]. According to Netto et al. many enzymes grouped within the oxidoreductases, hydrolases or transferases can be immobilized on the surface of magnetic nanoparticles to create generally stable systems offering high reusability and easy separation from the reaction mixture [82]. There are several examples that demonstrate these advantages. Mehrasbi et al. immobilized lipase on magnetic nanoparticles functionalized with 3-glycidoxypropyltrimethoxysilane. The immobilized enzyme when used to catalyse the production of biodiesel from waste cooking oil, maintained 100% of its initial activity even after six reaction cycles [83]. In another study, Aber et al. immobilized glucose oxidase by adsorption on unmodified MNPs and used the resulting system for decolourization of Acid Yellow 12. After 15 catalytic cycles the immobilized glucose oxidase retained more than 90% of its initial properties [84]. Atacan et al. used magnetic nanoparticles, pre-treated with gallic acid, for the covalent immobilization of trypsin. Their results showed that the MNPs-trypsin biocatalyst can degrade bovine serum albumin with high efficiency [85].

3.1.2. Mesoporous Materials

A feature that distinguishes mesoporous supports from other materials used for enzyme immobilization is the possibility of tailoring the properties of the support to the biomolecules by adjusting the synthesis conditions and obtaining matrices with a desired pore structure [86,87].

These kinds of carriers contain mesopores with diameters of usually 2 to 50 nm, with a narrow and regular pore arrangement, surface areas as high as 1500 m^2/g and pore volumes of around 1.5 cm^3/g, which make them suitable supports for various biomolecules [88]. Enzymes can be immobilized on mesoporous materials by covalent binding or by encapsulation. In both techniques of immobilization, however, the enzyme is placed in the pores of the support, which means that the structure of the protein is protected and good catalytic properties are generally retained. When the enzyme is located in the pores of the carrier, diffusional limitations must also be taken into account because the transport of substrates and products is restricted [89]. Nevertheless, in view of their water insolubility, thermal and chemical stability, hydrophilicity and the presence of sufficient chemical groups for the binding of catalysts, mesoporous materials fulfil most of the requirements for effective enzyme matrices [90].

Materials such as zeolites, carbons and sol-gel matrices, as well as precipitated and ordered mesoporous oxides are included in the mesoporous group [91–93]. For example, various mesoporous silica materials are frequently used. Lipases from *Candida antarctica* and from *Candida rugosa* have been immobilized via non-specific interactions without any intermediate agents on SBA 15 and MCM 41 mesoporous silica, respectively and used as catalysts in organic synthesis [94,95]. The reusability of the immobilized enzymes was found to be significantly improved, because they could be reused for at least five reaction cycles without significant loss of their activity. SBA 15 and MCM 41 silicas were also used for adsorption immobilization of alkaline protease [96]. The immobilized enzyme attained its maximum loading (589.43 mg/g) when SBA 15 silica was used. The products of immobilization also had good pH and temperature stability. In another study, Mangrulkar et al. immobilized tyrosinase on the mesoporous silica MCM-41 and used the resulting biocatalytic system for the detection of phenol. The lowest concentration of phenol detectable by the immobilized tyrosinase was found to be 1 mg/L [97]. As mentioned above, mesoporous materials can also be used for enzyme encapsulation. Wang and Caruso used mesoporous silica spheres for the immobilization of catalase, protease and peroxidase and showed that after immobilization the lifetime of all tested enzymes was improved compared to their free forms [98].

3.1.3. Nanoparticles

Nanoparticles of both inorganic and organic origin with diameters of up to 30 nm have been extensively studied in recent years as potential supports for enzyme immobilization. However, for the purpose of this review, attention is focused on nanoparticles of inorganic origin as these materials are attracting growing interest due to the fact that they generally significantly improve the immobilization yield and the efficiency of the biocatalytic system obtained [99,100]. Nanoparticles provide a large surface area for enzyme binding that leads to higher loading of the enzyme on the matrix surface and increased immobilization yield. The greatest advantage, however, of nanoparticles over other inorganic materials is their ability to minimize diffusional limitations. Enzyme molecules are attached to the surface of the nonporous particles and their active sites are exposed for wide contact with substrates [101,102]. This means that biocatalytic systems based on nanoparticles usually provide high catalytic activity retention [103].

Various inorganic nanomaterials such as nanogold [104] and graphene [105] can be used as matrices for enzyme immobilization. Most frequently, however, inorganic oxide nanoparticles are used. For example, Hou et al. used titania nanoparticles for the immobilization of carbonic anhydrase by glutaraldehyde and immobilized over 160 mg of the enzyme per gram of the matrix. The product was used for biomimetic conversion of CO_2 [106]. In another study, lipase from *Rhizomucor miehei* was covalently immobilized on silica nanoparticles modified by octyltriethoxysilane and glycidoxypropyltrimethoxysilane. The immobilized lipase proved to be a very thermostable biocatalyst [107]. Notably, both biocatalytic systems achieved over 90% catalytic activity retention.

3.1.4. Ceramic Materials

Ceramic materials are known for their extremely high resistance to temperature, pressure and chemicals (organic solvents, bases, acids). These features make them very promising materials for use as supports for industrial applications of immobilized enzymes [108]. Ceramic supports also offer good mechanical stability. Hence, when the enzymes become catalytically inactive, they can be relatively easily regenerated and used for the immobilization of a new biocatalyst [109]. Hydroxyl groups are mainly present on the surface of these materials. This favours mainly adsorption immobilization of enzymes, based on non-specific interactions. For covalent attachment of biomolecules, additional surface modification is necessary. Ceramic materials such as alumina, zirconia, titania, silica, iron oxide and calcium phosphate have been used as biomolecule carriers. It should be added that these materials can also be used in the form of ceramic foam or composite (TiO_2/Al_2O_3) ceramic membranes [110,111].

Ebrahimi et al. physically immobilized β-galactosidase using a ceramic material in the form of a membrane as a support. The system was used to catalyse a transgalactosylation reaction of lactose to produce galactosyl-oligosaccharides. The immobilized enzyme was used for continuous production of oligosaccharides and its efficiency reached 40% under optimal process parameters [112]. Wang et al. immobilized horseradish peroxidase on a ceramic material (cordierite) which had been modified by *N*-β-amino-ethyl-γ-aminopropyl-trimethoxysilane for covalent attachment of the enzyme. The biocatalytic system was used to remove oil from wastewater. The highest recorded removal efficiency was close to 92% and the system exhibited good reusability [113].

3.1.5. Carbon Nanotubes

Carbon nanotubes are a new type of support material that has been more and more widely used in recent years. Both single-walled and multi-walled carbon nanotubes are characterized by an ordered, nonporous structure, large surface area and biocompatibility. Moreover, they exhibit outstanding thermal, chemical and mechanical resistance [114,115]. Carbon nanotubes are also relatively amenable to functionalization to further increase their affinity to enzymes and favour the formation of strong enzyme–matrix interactions [116]. Unlike other materials, carbon nanotubes enhance the transfer of electrons between the substrate and the immobilized enzyme. They are thus most frequently used for the immobilization of oxidoreductases and are applied in biosensors for the detection of various compounds such as phenol and its mono- and multi-substituent derivatives, bisphenols or pharmaceuticals, i.e., diclofenac or tetracycline. However, other groups of enzymes (transferases and hydrolases) have also been immobilized with the use of carbon nanotubes [117,118].

In one reported study, glucose oxidase was immobilized on carbon nanotubes and further cross-linked with chitosan. The results confirmed that the transfer rate of electrons was strongly enhanced [119]. In another study α-glucosidase was covalently immobilized on multi-walled carbon nanotubes functionalized by amine groups. The system so obtained was used in a biosensor for measuring the antidiabetic potential of medicinal plants [120]. The immobilized enzymes used in both biosensors exhibited greatly improved sensitivity and time of response and thus better detecting properties. The biosensors also offered relatively good storage stability as indicated by their activity which remained almost unaltered over 30 days.

3.1.6. Graphene and Graphene Oxide

Graphene and graphene oxide (GO) among carbon-based materials have also attracted great attention as support materials for enzymes. This interest reflects their unique features such as biodegradability, two-dimensional structure, high surface area and pore volume as well as good thermal and chemical stability [121]. Additionally, the presence of many various functional groups, such as carboxylic (COOH), hydroxyl (–OH) or epoxide groups, facilitates creation of strong enzyme-matrix interactions without linking agents or modification of the graphene surface [122]. Due to these features, enzymes like lipases [123] or peroxidases [124] can be immobilized on GO

surfaces mainly by adsorption, covalent binding or entrapment [125]. It is also worth mentioning that graphene-based materials may even enhance enzyme biocatalytic activity. Moreover, graphene-based supports are characterized by antioxidant properties and may enhance removal of free radicals (i.e., hydroxyl or dithiocyanate) from reaction mixtures [126]. This results in improved protection of enzyme molecules from inactivation.

For example, horseradish peroxidase (HRP) was covalently immobilized on reduced graphene oxide nanoparticles functionalized with glutaraldehyde. Kinetic parameters (turnover number (k_{cat}) and catalytic efficiency (k_{cat}/K_M)) of the immobilized enzyme increased after its attachment, thus demonstrating enhancement of the catalytic properties of the HRP. Moreover, reusability was also significantly improved, as indicated by immobilized enzyme which maintained over 70% of its initial activity after 10 catalytic cycles [127]. In another study, D-psicose 3-epimerase (DPEase) was immobilized on non-modified graphene oxide and applied for production of the rare sugar D-psicose, an epimer of D-fructose. After immobilization, the efficiency of biocatalytic conversion of D-fructose to D-psicose was improved. Thermal stability of immobilized DPEase was also significantly enhanced, as the graphene-bounded enzyme exhibiting a half-life of 720 min that was 180 times higher than the half-life of free D-psicose 3-epimerase (4 min) [128].

3.2. Organic Materials

As already mentioned, the properties of the immobilized enzyme are strongly dependent on the structure and characteristics of the matrix. In general, the organic materials classified here as *New materials* are mainly the same materials and containing very similar chemical groups as those described in Section 2.2. However, here these organic materials appear in completely different forms and as a result have very different properties. These materials may for example be used in the form of single particles, fibres of nanometre size, or membranes. These supports increase the performance, efficiency and stability of the immobilized biomolecules and render the latter more reusable. Moreover, control of the process is improved and processes can be carried out in a continuous manner, which makes them cost-effective [129]. Hence, biocatalytic systems based on these materials can become attractive for applications in industrial-scale processes. Selected cases of the use of *New materials* of organic origin for enzyme immobilization are discussed below.

3.2.1. Electrospun Materials

The great potential of electrospun materials as supports for enzyme immobilization results from their many functional and structural advantages. These materials are known for their length (electrospun nanofibers), uniformity of diameter and diversity of composition. They also have high porosity and surface areas, which lead to high enzyme loading [130]. The nanometre sizes of these materials provide additional benefits mainly related to low hindrance of mass transfer and reduced diffusional limitations. As a result, the efficiency of the immobilized enzyme can be increased. Electrospun support materials are also known for other useful properties, for example their biocompatibility, nontoxicity, biodegradability, high mechanical strength and hydrophilicity, which make them suitable matrices for various types of biocatalysts [131,132]. It should also be noted that due to the presence of various functional moieties on their surface, electrospun nanomaterials can be easily modified to favour enzyme attachment and increase the activity of the enzyme [133]. A very wide range of synthetic polymers such as poly(vinyl alcohol), polystyrene, polyacrylamide and polyurethane, as well as biopolymers such as chitin, chitosan, alginate and cellulose, may be used to produce electrospun carriers [134–136]. Their great advantage over other matrices is the fact that because of the variety of materials used to produce electrospun supports, they can be obtained with properties tailored to the enzyme and the process. Enzymes can be immobilized on these materials by adsorption and covalent binding (surface attachment) as well as by encapsulation carried out at the same time as the support is formed, which additionally reduces the costs of the process [137].

For example, Canbolat et al. used poly(ε-caprolactone) to immobilize catalase by encapsulation using layering methods. Moreover, to enhance the catalytic activity of the enzyme, its molecules were combined with cyclodextrin before immobilization. The results indicated that the addition of cyclic oligosaccharides had a positive effect on the catalytic properties of the biocatalyst. It should also be noted that immobilization by encapsulation results in higher stability of the catalase because the enzyme is protected from negative effects of the reaction conditions [138]. Weiser et al. used polyvinyl alcohol nanofibers for the immobilization by entrapment of five different types of lipase for the kinetic resolution of racemic secondary alcohols by acylation in inorganic media. The study proved that the activity of all tested lipases was enhanced by stabilization of the active conformation of the enzyme. Furthermore, after immobilization of the biomolecules, the turnover frequency of the reaction increased due to a reduction in mass transfer limitations, which was directly related to the structural properties of the polymeric nanofibers [139]. In another study, poly(vinyl alcohol) or polylactic acid nanofibers in the form of a membrane were used for adsorption immobilization of *Candida antarctica* lipase B. The biocatalytic system was used for the kinetic resolution of 1-phenylethanol and 1-phenyl acetate. Polyvinyl alcohol membrane with immobilized lipase may be used in both organic and water media; however, the lipase immobilized on polylactic acid fibres preserved higher activity and exhibited higher enantiomer selectivity. Nevertheless, due to the protection afforded by the nanofibers, both immobilized systems demonstrated excellent stability even over 10 reaction cycles [140].

3.2.2. Polymeric Membranes

As has been described above, polymeric materials can be used in enzyme immobilization in the form of beads, powders, fibres or foams. However, in recent years there has been growing interest in the use of commercially available polymeric membranes. This is mainly because they have easily tuneable properties which make them suitable for many groups of enzymes [141,142]. These membranes have a large surface area that allows efficient enzyme attachment. The membranes also offer good porosity as well as well-defined pore sizes and structure, which facilitate the immobilization of biomolecules not only on the surface of the support but also in its pores [143]. The reaction mixture passing through the membrane therefore has relatively easy access to the active sites of the enzyme, which reduces diffusional limitations. Moreover, membranes with tailored properties can easily be prepared in different shapes and various geometrical configurations [144]. The membranes are also generally insoluble and are known for their mechanical stability, hence they fulfil the requirements for performing as suitable carriers for enzyme immobilization.

Many types of synthetic polymers can be used for the preparation of membranes, for example poly(vinyl alcohol), polyurethane and poly(vinylidene fluoride) [145,146]. However, membranes made from biopolymers, for example from chitosan or cellulose, can also be used as enzyme support materials [147]. Depending on the type of material used, various functional groups are present in the membrane that not only favour effective enzyme immobilization but also enable modification of the membrane for covalent binding of biomolecules. It should also be noted that in addition to membranes obtained on a laboratory scale, commercially available ultra- and nanofiltration membranes can also be used for enzyme immobilization and examples such as GR51PP, NF270 and NTR7450 may be mentioned [148–150]. However, the greatest advantage of polymeric membranes as biomolecule support matrices, in comparison with other materials, is the fact that no additional separation and purification of the reaction mixture is required; the catalytic process can take place and products can be isolated from the reaction mixture in the same step [151]. It is also worth noting that polymeric membranes, as supports for enzymes, play a crucial role particularly in the case of enzymatic membrane reactors (EMR).

3.3. Hybrid and Composite Materials

In the light of the above-mentioned unique features and properties of inorganic and organic matrices, many studies have been carried out with the aim of combining them to maximize their

benefits. The possibility of selecting and combining precursors to meet the requirements of a given enzyme and the process in which it is to be used facilitates more precise control of the enzyme immobilization process. Additionally, the biocatalytic systems thus produced can be used in a wider range of practical applications [152]. Combined and reinforced materials usually exhibit properties not observed for their individual components. Hybrids and composites usually make it possible to stabilize the interactions between an enzyme and a support and make biocatalysts more mechanically resistant and stable under reaction conditions. It should be added that hybrid supports in general provide a suitable environment for biomolecules that favours the retention of high catalytic properties by the immobilized enzyme, makes the biocatalytic system reusable and protects it against conformational changes during storage [153]. An additional benefit of the use of composite supports is the fact that these materials are suitable for enzymes belonging to all catalytic classes. Hence, in the quest for support materials for enzyme immobilization, particular attention should be paid to hybrid or composite materials obtained by the conjugation of: (i) organic-organic; (ii) inorganic-inorganic, or (iii) organic-inorganic precursors.

3.3.1. Organic-Organic Hybrids

As described above, many types of polymers of synthetic and natural origin can be used as supports for enzymes. However, to increase their usability, they can be combined to obtain products with enhanced properties which are better suited to the enzyme and the technological process. Organic-organic hybrids may be synthesized by connecting together the following: (i) two synthetic materials, for example polyaniline and polyacrylonitrile, polyethyleneimine, with epoxy-activated acrylate copolymer or poly(acrylic acid) and polyvinyl alcohol [154–156]; (ii) a synthetic polymer with a biopolymer, such as poly(acrylic acid) and cellulose, polyvinyl alcohol and chitosan, or polyaniline and chitosan [157–159]; (iii) two biopolymers, such as chitosan and alginate, chitin and lignin or cellulose and dextran [160–162]. For instance, combining a synthetic polymer having good pH and thermal resistance and mechanical stability with a biopolymer known for its biocompatibility and high affinity to biocatalysts and using the resulting hybrid as an enzyme support, could result in a stable, reusable biocatalytic system with the retention of good catalytic properties [163]. Additionally, through appropriate selection of precursors, the hydrophobic/hydrophilic character of the matrix can be controlled to increase the strength of the interactions formed between the enzyme and support and to enhance the catalytic activity of the biomolecule [164]. The greatest advantage of these materials is the possibility of forming them into various shapes and sizes. The materials can be used as enzyme supports in the form of particles, fibres, tubes, beads, membranes or sheets [165–167]. The wide variety of available organic-organic hybrids makes these materials suited for immobilization of enzymes belonging to all catalytic classes by adsorption, covalent binding and also by entrapment or encapsulation [168,169]. For example, two monomers, polylactic acid and polyethylene glycol, were used to produce micro- or nanofibers by an electrospinning technique. The material thus produced had high porosity, a large surface area, the ability to incorporate functional additives, which are all excellent properties as a matrix for enzyme attachment. In the study, alkaline phosphatase was immobilized via biotin-streptavidin interactions on surface of the matrix. The bound enzyme exhibited good stability and reusability over a long storage time so this system may be a promising platform for the development of biosensors [170]. Polyvinyl alcohol–hypromellose is an example of an organic hybrid produced by merging a synthetic polymer with a semisynthetic biopolymer which is an inert derivative of methylcellulose. This material was used for the immobilization of lipase from *Burkholderia cepacia* without any cross-linkers. The resulting biocatalytic system was used for the synthesis of phenethyl butyrate in nonpolar medium and proved to be a successful catalyst, achieving 99% conversion of the phenethyl alcohol and vinyl butyrate used as substrates. The protective effect of the polymeric hybrid support resulted in the retention of high catalytic activity by the immobilized lipase and the activation energy of the reaction was found to be lower when the immobilized enzyme was used [171]. Matto and Husain employed a calcium alginate–starch hybrid gel as a carrier for

adsorption immobilization and entrapment of peroxidase. The presence of many hydroxyl groups in the starch structure enhanced the surface attachment of the enzyme, while the capacity of alginate for gelation favoured the entrapment of peroxidase. The entrapped enzyme was found to be significantly more stable against pH, temperature, solvents and inhibitors like urea or heavy metals, compared to the surface-immobilized enzyme. Moreover, this form of immobilized peroxidase retained over 70% of its original activity even after seven repeated reaction cycles [172]. In a study by Abdulla and Ravindra, equal proportions of alginate and κ-carrageenan were used to produce a novel biopolymeric hybrid for lipase immobilization by entrapment. The resulting biocatalyst was employed in biodiesel production from *Jatropha* oil and ethanol. Under optimal process conditions, total transesterification of triglycerides to fatty acid ethyl esters was achieved. This biocatalytic system also demonstrated good reusability as indicated by retention of over 75% of its initial activity after six cycles. The results suggest that lipase immobilized on an alginate–κ-carrageenan hybrid could be an efficient and environmentally friendly biocatalyst for biodiesel production [173]. Another application of a composite built from two biopolymers was reported by Nupur et al. who combined chitosan and calcium alginate and used the resulting hybrid in the form of beads for entrapment immobilization of penicillin G amidase (PGA). The immobilized PGA demonstrated high thermal and storage stability and good reusability. The enzyme entrapped in alginate–chitosan hybrid beads was found to have several advantages and could be used in the organic synthesis of 6-aminopenicillanic acid with high efficiency [174].

3.3.2. Organic-Inorganic Hybrids

A very wide range of materials of both organic and inorganic origin can be combined to create hybrid or composite supports for the immobilization of enzymes. The most frequently used inorganic precursors include silica, inorganic oxides such as zinc and titanium oxides, as well as minerals, carbon materials and magnetic nanoparticles [175–178]. They can be combined with polymers of synthetic origin, for example polyacrylonitrile, polyethyleneimine and polyvinyl alcohol [179,180], as well as with biopolymers such as chitosan, lignin and alginate [181,182]. These materials are mainly used for the adsorption or covalent immobilization of hydrolases, oxidoreductases and transferases but the encapsulation of these enzymes in carriers of this type has also been reported [183]. Organic-inorganic hybrids display great potential as support materials for enzymes; such hybrids provide good stability and mechanical resistance and very high affinity to biological molecules. The high stability and often also chemical inertness are related to features of the inorganic precursor. The good ability to bind enzymes is due to the organic components since synthetic polymers and biopolymers have many functional moieties in their structures that are able to interact with the chemical groups of biocatalysts [184]. As a result of their stability and functionality, hybrids in this group can be used for many practical applications, which is their greatest advantage. Many different combinations of organic and inorganic substances have been used to produce functional organic-inorganic composites and hybrids for enzyme immobilization. For example, Zhao et al. combined the stability and mechanical resistance of silica with the biocompatibility and gelation properties of chitosan and achieved immobilization of glucose isomerase on silica–chitosan hybrid microspheres via simple in situ encapsulation. The immobilized enzyme was further used as a catalyst for the conversion of glucose to fructose. The relative activity of the enzyme was found to be above 90% over a wide pH range of 6–8, a temperature range of 40–80 °C, a storage time of 3 months and after 15 repeated catalytic cycles [185]. In another study, a silica–dialdehyde starch (SiO_2-DAS) mixed hybrid, offering high enzyme binding capacity due to the presence of polysaccharide in the structure, was used for the immobilization of cellulose. The product maintained higher activity over broader pH and temperature ranges than the free enzyme. Moreover, the immobilized cellulase exhibited higher affinity to the substrates as well as better reusability and storage stability. This product might therefore be used as an effective biocatalyst for cellulose bioconversion [186]. Miranda et al. reported the synthesis of an eco-friendly poly-L-leucine-rehydrated hydrotalcite nanohybrid material and its effective use for tyrosinase immobilization without bifunctional linkers. They used the resulting biocatalytic system in

the asymmetric epoxidation reaction of chalcone. The nanohybrid-based biocatalyst exhibited excellent activity and enantioselectivity. The product also demonstrated good reusability, with unaltered activity after five consecutive runs. Thus, this biocatalytic system could find potential applications in protein engineering, biomedicine and catalysis [187]. Chang et al. combined natural clay composed of montmorillonite and layer silicates with chitosan, which exhibits good gelation abilities. The inorganic-organic hybrid was further cross-linked with glutaraldehyde and finally applied in the form of wet and dry beads for the immobilization of *β*-glucosidase. The covalently bound enzyme exhibited high stability over wide pH and temperature ranges. Additionally, the properties of wet and dry beads were compared and it was found that use of the dried materials led to higher catalytic efficiency [188]. In another study, the conductive properties of carbon nanospheres were combined with the gelation ability of sodium alginate for entrapment immobilization of glucose oxidase and its use for biosensing of glucose. Under optimal measurement conditions, the biosensor achieved very good performance for glucose over a wide linear concentration range, with a detection limit of 0.5 μM. The biosensor also exhibited satisfactory reproducibility and good long-term stability [189].

3.3.3. Inorganic-Inorganic Hybrids

Besides the types discussed above, inorganic-inorganic hybrid and composite materials also possess many features which make them interesting potential supports for enzyme immobilization. In general, inorganic hybrids exhibit good pH and thermal stability, mechanical resistance and chemical inertness. Moreover, their precursors are easily available and in many cases their synthesis is simple and hence relatively cheap [190]. A variety of functional groups such as carbonyl (C=O), carboxyl (COOH), amine ($–NH_2$) and epoxy are present on the surface of inorganic-inorganic materials, although the most frequently observed are hydroxyl (–OH) groups. These groups determine the hydrophilic character of inorganic composite supports and increase their affinity to biomolecules [191]. Additionally, the presence of many functional groups enhances immobilization efficiency and allows easy functionalization of the surface [192]. Besides simple modification, the presence of various chemical moieties allows the production of combined materials with desired technological features and high affinity for enzymes, which makes these materials promising for practical applications. For example, sol-gel derived silica was combined with multi-walled carbon nanotubes (MWCNTs) and used for the non-specific immobilization of lipase from *Candida rugosa*. The biocatalytic system thus obtained was applied in esterification reactions in organic media, with high efficiencies. The immobilized lipase also exhibited good reusability as indicated by almost unaltered initial activity after five catalytic cycles due to the protective effect of the MWCNTs [193]. In another study, Zhu et al. used carboxyl-functionalized silica-coated magnetic nanoparticles (SCMNPs) as a carrier for covalent immobilization of porcine pancreatic lipase. The addition of the magnetic nanoparticles to the composite enabled easy separation of the biocatalytic system from the reaction mixture using a magnetic field. The immobilized lipase exhibited enhanced activity compared to the free enzyme and good thermal resistance, with high catalytic efficiency at 70 °C [194].

The presence of many functional moieties enables the attachment of enzymes belonging to many catalytic classes, including hydrolases and oxidoreductases [195,196] and the potential use of all known immobilization techniques. For example, glucose oxidase was entrapped in nanozeolites combined with magnetic nanoparticles and multi-walled carbon nanotubes [197]. In another case, *β*-glucosidase, *α*-chymotrypsin and lipase B from *Candida antarctica* were successfully covalently immobilized on the surface of magnetic nanoparticles activated by *N*,*N*-disuccinimidyl carbonate [198]. In general, silica is one of the most commonly used precursors for inorganic hybrids. However, other inorganic components such as inorganic oxides, minerals, clays, noble metal nanoparticles and carbon-based materials may also act as precursors for inorganic-inorganic enzyme supports [199–202]. An interesting example of an inorganic-inorganic composite used for enzyme immobilization is a combination of calcium carbonate and gold nanoparticles ($CaCO_3$-AuNPs). This support was used by Li et al. for adsorption immobilization of horseradish peroxidase and further to produce a mediator-free hydrogen

peroxide biosensor. Due to the good electrical conductivity of the $CaCO_3$-AuNPs inorganic hybrid, as well as the favourable orientation of the enzyme molecules on the surface of the matrix, the biosensor exhibited strong activity toward H_2O_2 reduction and achieved a good linear response over a wide range of hydrogen peroxide concentrations and a relatively low limit of detection (1.0×10^{-7} M) [203]. In another study, the ability of carbon nanotubes to direct electron transfer and the high surface area of titanium dioxide were exploited to create TiO_2–carbon nanotube microparticles for adsorption immobilization of glucose oxidase by non-specific interactions. The immobilized enzyme was further used to build a biosensor for glucose detection. Electrochemical analysis showed the biosensor to have high efficiency, sensitivity and reproducibility and the capacity to detect glucose up to concentrations of 3 mM [204]. In another such system, multi-walled carbon nanotubes provided a highly porous conductive network that enhanced electrochemical transduction, while $CaCO_3$ acted as a host carrier for immobilization of tyrosinase by entrapment. This inorganic hybrid with immobilized enzyme was used as a highly effective and sensitive dopamine or catechol biosensor. The biocatalytic system was shown to be resistant to the effects of inhibitors and interferents and its parameters remained unaltered in the presence of uric and ascorbic acid [205].

3.4. Summary of New Materials

Table 2 summarizes the most important types of *New materials* and enzymes that may be immobilized by using these carriers. Moreover, information about binding groups, immobilization type or cross-linking agents are also presented.

Table 2. Summary and selected examples of *New materials* of inorganic, organic and hybrid origin applied for enzymes immobilization.

Support Material	Binding Groups	Cross-Linking Agent	Immobilization Type	Immobilized Enzyme	Reference
Inorganic Materials					
magnetic nanoparticles	epoxy groups	3-glycidoxypropyl-trimethoxylsilane	covalent binding	lipase from *Candida antarctica*	[83]
	–OH	–	adsorption	glucose oxidase from *Aspergillus niger*	[84]
silica SBA-15	–OH	–	adsorption	alkaline protease	[96]
mesoporous silica	–OH	–	encapsulation	catalase	[98]
silica mesoporous nanoparticles	epoxy groups	3-glycidoxypropyl-trimethoxylsilane	covalent binding	lipase from *Rhizomucor miehei*	[107]
TiO_2 nanoparticles	–OH	–	adsorption	carbonic anhydrase	[106]
cordierite	$–NH_2$	*N*-*β*-aminoethyl-*γ*-aminopropyl-trimethoxysilane	covalent binding	horseradish peroxidase	[113]
multi-walled carbon nanotubes	$–NH_2$	3-aminopropyl-triethoxysilane	covalent binding	α-glucosidase	[120]
reduced graphene oxide	C=O	glutaraldehyde	covalent binding	horseradish peroxidase	[127]
Organic materials					
electrospinning fibres of polycaprolactone	C=O	-	adsorption	catalase	[138]
electrospinning nanofibers of polyvinyl alcohol	–OH	-	encapsulation	lipase from *Burkholderia cepacia*	[140]
polyethersulphone membrane	-	-	adsorption	Phosphotriesterase lactonase from *Sulfolobus solfataricus*	[145]
NTR7450 membrane	-	-	adsorption	casein glycomacropeptide	[150]
Hybrid/composite materials					
polyaniline-polyacrylonitrile composite	–N–H	-	encapsulation	glucose oxidase	[154]
cellulose-poly(acrylic acid) fibres	–OH, COOH	-	covalent binding	horseradish peroxidase	[157]
chitosan-alginate beads	$–NH_2$, –OH	-	entrapment	amyloglucosidase	[160]
graphene oxide-Fe_3O_4	–OH, C=O	cyanuric chloride	covalent binding	glucoamylase	[177]
silica-lignin	–OH, C=O	-	adsorption	glucose oxidase form *Aspergillus niger*	[178]
polyacrylonitrile-multi-walled carbon nanotubes	–N–H, C=O, –OH	*N*-Hydroxy-succinimide	covalent binding	catalase	[179]
silica-graphene oxide particles	–OH, C=O	*N*-Hydroxy-succinimide	covalent binding	cholesterol oxidase	[199]
ZnO-SiO_2 nanowires	–OH	–	cross-linking	horseradish peroxidase	[202]
$CaCO_3$-gold nanoparticles	–OH, C=O	–	adsorption	horseradish peroxidase	[203]

New materials with tailored properties are increasingly frequently used as supports for enzymes both due to limitations in application of *Classic materials* and also to improve the properties of the immobilized enzymes. Materials belonging to the *New materials* group can facilitate easy separation of biocatalytic systems from reaction mixtures (magnetic nanoparticles) or enable avoidance of enzyme particles overloading on the surface of the carrier (nanoparticles and mesoporous materials). Moreover, materials such as graphene or graphene oxide enhance transfer of electrons between immobilized enzyme and substrate and result in increased catalytic activity of the biomolecules. The greatest advantage of the materials of organic origin classified as *New materials* is that they can be formed in various geometrical shapes such as fibres or membranes and reduce diffusional limitations and improve the efficiency of the biocatalytic processes. Within *New materials*, there is continuing and growing interest in hybrid materials. Hybrid supports may be synthesized through the combination of precursors of different origin and their properties can be tailored to the requirements of the biocatalysts as well as to the technological process in which the product will be used after immobilization. Hybrid supports are characterized by good thermal and chemical stability and mechanical resistance and usually ensure stable, covalent binding of the enzyme.

4. Summary

Inorganic materials such as inorganic oxides, minerals and carbon-based materials and materials of organic origin, including synthetic and natural polymers, may be classified as *Classic support materials* used for the immobilization of enzymes. These carriers are characterized by good stability under harsh reaction conditions, high availability or relatively simple synthesis and consequently low price. In general, these groups of support materials can be used for the immobilization of all classes of enzymes through the use of all immobilization techniques although adsorption immobilization is the most common. In view of the properties of these materials, the formation of highly specific interactions between the enzyme and the support is usually limited. Therefore, immobilization is based on non-specific hydrogen interactions. In some cases, however, where for example there is a high affinity of functional groups, the formation of covalent bonds cannot be excluded. The wide use of *Classic materials* as supports for enzymes is also linked to the more cost-effective immobilization process since these carriers do not require complicated preparation procedures and immobilization is usually fast and simple. *Classic materials* will continue to play a significant role as supports for the immobilization of enzymes from many catalytic classes for many practical applications ranging from the synthesis of highly pure chemical compounds to food processes and wastewater treatment.

The wide group of support materials which for the purposes of this review are called *New materials* for enzyme immobilization can offer properties designed for particular enzymes or for the requirements of a given technological process. These materials have come into use due to certain defects of the *Classic materials* and to the relatively low efficiencies of catalytic conversions carried out with biocatalysts bound to *Classic materials*. Inorganic materials in the *New materials* group include magnetic nanoparticles, which enhance fast and simple separation of the immobilized enzyme from the reaction mixture by means of an external magnetic field and mesoporous materials with a hierarchic pore structure, which ensures the uniform distribution of biomolecules in the matrix pores and thus reduces overloading of the enzymes and maintains catalytic activity at a high level. There are also materials of organic origin, such as electrospun membranes; depending on the material used for their production, these materials can significantly increase the transfer of electrons, which is a key step in many biocatalytic transformations. However, special interest particularly in recent years has been paid to applications of hybrid and composite *New materials* for enzyme immobilization. As has been described, these materials are synthesized from combinations of precursors of inorganic, organic and mixed inorganic and organic origin. They are designed to offer high stability, good affinity for enzymes and the presence of many chemical functional groups compatible with the chemical moieties present in the protein structure. Because of these features, biomolecules are attached mainly via covalent bonds and this ensures the good reusability and operational stability of the resulting biocatalytic

systems. *New materials* will be employed more and more extensively in the future for immobilization of enzymes. Their applications will not be limited to the creation of biocatalytic systems for use in synthesis; hybrids and composite materials will also be used to production of biocatalytic cells and biosensors for the detection of various compounds in medicine and in environmental monitoring, as well as for remediation of hazardous compounds.

It should be emphasized that in presented literature review the materials have been considered regardless of the type/mode of enzyme immobilization methodology employed, thus the treatise is universal with respect to this regard. However, for creation of stable and efficient biocatalytic systems, the attachment technique must be optimized individually for the specific enzyme, the specific material and the biocatalytic process to be employed.

Acknowledgments: This work was supported by research grant funds from the National Science Center, Poland, in accordance with decision no. DEC-2015/19/N/ST8/02220.

Author Contributions: Jakub Zdarta researched the literature and wrote the manuscript; Anne S. Meyer, Teofil Jesionowski and Manuel Pinelo discussed ideas and edited the manuscript.

Conflicts of Interest: The authors declare no conflict of interest. The funding sponsors had no role in the design of the study; in the collection, analysis, or interpretation of data; in the writing of the manuscript; or in the decision to publish the results.

References

1. Cowan, D.A.; Fernandez-Lafuente, R. Enhancing the functional properties of thermophilic enzymes by chemical modification and immobilization. *Enzyme Microb. Technol.* **2011**, *49*, 326–346. [CrossRef] [PubMed]
2. Wohlgemuth, R. Biocatalysis—Key to sustainable industrial chemistry. *Curr. Opin. Biotechnol.* **2010**, *21*, 713–724. [CrossRef] [PubMed]
3. Jesionowski, T.; Zdarta, J.; Krajewska, B. Enzymes immobilization by adsorption: A review. *Adsorption* **2014**, *20*, 801–821. [CrossRef]
4. Zhang, Y.; Ge, J.; Liu, Z. Enhanced activity of immobilized or chemically modified enzymes. *ACS Catal.* **2015**, *5*, 4503–4513. [CrossRef]
5. Marzadori, C.; Miletti, S.; Gessa, C.; Ciurli, S. Immobilization of jack bean urease on hydroxyapatite: Urease immobilization on alkaline soils. *Soil Biol. Biochem.* **1998**, *30*, 1485–1490. [CrossRef]
6. Mateo, C.; Palomo, J.M.; Fernandez-Lafuente, G.; Guisan, J.M.; Fernandez-Lafuente, R. Improvement of enzyme activity, stability and selectivity via immobilization techniques. *Enzyme Microb. Technol.* **2007**, *40*, 1451–1463. [CrossRef]
7. Sheldon, R.A. Enzyme immobilization: The quest for optimum performance. *Adv. Synth. Catal.* **2007**, *49*, 1289–1307. [CrossRef]
8. Guzik, U.; Hupert-Kocurek, K.; Wojcieszynska, D. Immobilization as a strategy for improving enzyme properties—Application to oxidoreductases. *Molecules* **2014**, *19*, 8995–9018. [CrossRef] [PubMed]
9. Sheldon, R.A.; van Pelt, S. Enzyme immobilisation in biocatalysis: Why, what and how? *Chem. Soc. Rev.* **2013**, *42*, 6223–6235. [CrossRef] [PubMed]
10. Rodrigues, R.C.; Berenguer-Murcia, A.; Fernandez-Lafuente, R. Coupling chemical modification and immobilization to improve the catalytic performance of enzymes. *Adv. Synth. Catal.* **2011**, *353*, 2216–2238. [CrossRef]
11. Cao, L. *Carrier-Bound Immobilized Enzymes*; Wiley-VCH: Weinheim, Germany, 2005.
12. Fernandez-Lafuente, R. Stabilization of multimeric enzymes: Strategies to prevent subunit dissociation. *Enzyme Microb. Technol.* **2009**, *45*, 405–418. [CrossRef]
13. Wong, L.S.; Khan, F.; Micklefield, J. Selective covalent protein immobilization: Strategies and applications. *Chem. Rev.* **2009**, *109*, 4025–4053. [CrossRef] [PubMed]
14. Jesionowski, T. Preparation of colloidal silica from sodium metasilicate solution and sulphuric acid in emulsion medium. *Colloids Surf. A* **2001**, *190*, 153–165. [CrossRef]
15. Jesionowski, T.; Krysztafkiewicz, A. Preparation of the hydrophilic/hydrophobic silica particles. *Colloids Surf. A* **2002**, *207*, 49–58. [CrossRef]

16. Zucca, P.; Sanjust, E. Inorganic materials as supports for covalent enzyme immobilization: Methods and mechanisms. *Molecules* **2014**, *19*, 14139–14194. [CrossRef] [PubMed]
17. Kramer, M.; Cruz, J.C.; Pfromm, P.H.; Rezac, E.; Czermak, P. Enantioselective transestrification by *Candida antarctica* lipase B immobilized on fumed silica. *J. Biotechnol.* **2010**, *150*, 80–86. [CrossRef] [PubMed]
18. Falahati, M.; Mamani, L.; Sabuory, A.A.; Shafiee, A.; Foroumadi, A.; Badiei, A.R. Aminopropyl functionalized cubic Ia3d mesoporous silica nanoparticle as an efficient support for immobilization of superoxide dismutase. *Biochim. Biophys. Acta* **2011**, *1814*, 1195–1202. [CrossRef] [PubMed]
19. Godjevargova, T.; Nenkova, R.; Konsulov, V. Immobilization of glucose oxidase by acronitrile copolymer coated silica supports. *J. Mol. Catal. B* **2006**, *38*, 59–64. [CrossRef]
20. Zdarta, J.; Sałek, K.; Kołodziejczak-Radzimska, A.; Siwińska-Stefańska, K.; Szwarc-Rzepka, K.; Norman, M.; Klapiszewski, Ł.; Bartczak, P.; Kaczorek, E.; Jesionowski, T. Immobilization of *Amano Lipase A* onto Stöber silica surface: Process characterization and kinetic studies. *Open Chem.* **2015**, *13*, 138–148. [CrossRef]
21. Kołodziejczak-Radzimska, A.; Zdarta, J.; Jesionowski, T. Physicochemical and catalytic properties of acylase I from *Aspergillus melleus* immobilized on amino- and carbonyl-grafted Stöber silica. *Biotechnol. Prog.* **2018**. [CrossRef] [PubMed]
22. Narwal, S.K.; Saun, N.K.; Gupta, R. Characterization and catalytic properties of free and silica-bound lipase: A comparative study. *J. Oleo Sci.* **2014**, *63*, 599–603. [CrossRef] [PubMed]
23. Zou, B.; Hua, Y.; Cui, F.; Jiang, L.; Yu, D.; Huang, H. Effect of surface modification of low cost mesoporous SiO_2 carriers on the properties of immobilized lipase. *J. Colloids Interface Sci.* **2014**, *417*, 210–216. [CrossRef] [PubMed]
24. Foresti, M.L.; Valle, G.; Bonetto, R.; Ferreira, M.L.; Briand, L.E. FTIR, SEM and fractal dimension characterization of lipase B from *Candida antarctica* immobilized onto titania at selected conditions. *Appl. Surf. Sci.* **2010**, *256*, 1624–1635. [CrossRef]
25. Vallés, D.; Furtado, S.; Villadóniga, C.; Cantera, A.M.B. Adsorption onto alumina and stabilization of cysteine proteinases from crude extract of solanum granuloso-leprosum fruits. *Process Biochem.* **2011**, *46*, 592–598. [CrossRef]
26. Reshmi, R.; Sanjay, G.; Sugunan, S. Immobilization of α-amylase on zirconia: A heterogeneous biocatalyst for starch hydrolysis. *Catal. Commun.* **2007**, *8*, 393–399. [CrossRef]
27. Yang, Z.; Si, S.; Zhang, C. Study on the activity and stability of urease immobilized ontonanoporous alumina membranes. *Microporous Mesoporous Mater.* **2008**, *111*, 359–366. [CrossRef]
28. Ghiaci, M.; Aghaei, H.; Soleimanian, S.; Sedaghat, M.E. Enzyme immobilization Part 1. Modified bentonite as a new and efficient support for immobilization of *Candida rugose* lipase. *Appl. Clay Sci.* **2009**, *43*, 289–295. [CrossRef]
29. Mbouguen, J.K.; Ngameni, E.; Walcarius, A. Organoclay-enzyme film electrodes. *Anal. Chim. Acta* **2006**, *578*, 145–155. [CrossRef] [PubMed]
30. An, N.; Zhou, C.H.; Zhuang, X.Y.; Tong, D.S.; Yu, W.H. Immobilization of enzymes on clay minerals for biocatalysts and biosensors. *Appl. Clay Sci.* **2015**, *114*, 283–296. [CrossRef]
31. Sanjay, G.; Sugunan, S. Acid activated montmorillonite: An efficient immobilization support for improving reusability, storage stability and operational stability of enzymes. *J. Porous Mater.* **2008**, *15*, 359–367. [CrossRef]
32. Sedaghat, M.E.; Ghiaci, M.; Aghaei, H.; Soleimanian-Zad, S. Enzyme immobilization. Part 4. Immobilization of alkaline phosphatase on Na-sepiolite and modified sepiolite. *Appl. Clay Sci.* **2009**, *46*, 131–135. [CrossRef]
33. Zdarta, J.; Budzińska, K.; Kołodziejczak-Radzimska, A.; Klapiszewski, Ł.; Siwińska-Stefańska, K.; Bartczak, P.; Piasecki, A.; Maciejewski, H.; Jesionowski, T. Hydroxyapatite as a support in protease immobilization process. *Physicochem. Probl. Miner. Process.* **2015**, *51*, 633–646.
34. Salman, S.; Soundararajan, S.; Safina, G.; Satoh, I.; Danielsson, B. Hydroxyapatite as a novel reversible in situ adsorption matrix for enzyme thermistor-based FIA. *Talanta* **2008**, *77*, 490–493. [CrossRef]
35. Zhou, C.H.; Keeling, J. Fundamental and applied research on clay minerals: From climate and environment to nanotechnology. *Appl. Clay Sci.* **2013**, *74*, 3–9. [CrossRef]
36. Chrisnasari, R.; Wuisan, Z.G.; Budhyantoro, A.; Widi, R.K. Glucose oxidase immobilization on TMAH-modified bentonite. *Indones. J. Chem.* **2015**, *15*, 22–28. [CrossRef]
37. Daoud, F.B.O.; Kaddour, S.; Sadoun, T. Adsorption of cellulose *Aspergillus niger* on a commercial activated carbon: Kinetics and equilibrium studies. *Colloids Surf. B Biointerface* **2010**, *75*, 93–99. [CrossRef] [PubMed]

38. Dutta, S.; Bhattacharyya, A.; De, P.; Ray, P.; Basu, S. Removal of mercury from its aqueous solution using charcoal-immobilized papain (CIP). *J. Hazard. Mater.* **2009**, *172*, 888–896. [CrossRef] [PubMed]
39. Rani, A.S.; Das, M.L.M.; Satyanarayana, S. Preparation and characterization of amyloglucosidase adsorbed on activated charcoal. *J. Mol. Catal. B Enzym.* **2000**, *10*, 471–476. [CrossRef]
40. Silva, V.D.M.; De Marco, L.M.; Delvivo, F.M.; Coelho, J.V.; Silvestre, M.P.C. Immobilization of pancreatin in activated carbon and in alumina for preparing whey hydrolysates. *Acta Sci. Health Sci.* **2005**, *27*, 163–169.
41. Hanefeld, U.; Gardossi, L.; Magner, E. Understanding Enzyme Immobilisation. *Chem. Soc. Rev.* **2009**, *38*, 453–468. [CrossRef] [PubMed]
42. Maksym, P.; Tarnacka, M.; Dzienia, A.; Matuszek, K.; Chrobok, A.; Kaminski, K.; Paluch, M. Enhanced polymerization rate and conductivity of ionic liquid-based epoxy resin. *Macromolecules* **2017**, *50*, 3262–3272. [CrossRef]
43. Kirk, O.; Christensen, M.W. Lipases from *Candida antarctica*: Unique biocatalysts from a unique origin. *Org. Process Res. Dev.* **2002**, *6*, 446–451. [CrossRef]
44. Ferrario, V.; Ebert, C.; Knapic, L.; Fattor, D.; Basso, A.; Spizzo, P.; Gardossi, L. Conformational changes of lipases in aqueous media: A comparative computational study and experimental implications. *Adv. Synth. Catal.* **2011**, *353*, 2466–2480. [CrossRef]
45. Basso, A.; Braiuca, P.; Cantone, S.; Ebert, C.; Linda, P.; Spizzo, P.; Caimi, P.; Hanefeld, U.; Degrassi, G.; Gardossi, L. In silico analysis of enzyme surface and glycosylation effect as a tool for efficient covalent immobilisation of CalB and PGA on Sepabeads. *Adv. Synth. Catal.* **2007**, *349*, 877–886. [CrossRef]
46. Cantone, S.; Ferrario, V.; Corici, L.; Ebert, C.; Fattor, D.; Spizzo, P.; Gardossi, L. Efficient immobilisation of industrial biocatalysts: Criteria and constraints for the selection of organic polymeric carriers and immobilisation methods. *Chem. Soc. Rev.* **2013**, *42*, 6262–6276. [CrossRef] [PubMed]
47. Ashly, P.C.; Joseph, M.J.; Mohanan, P.V. Activity of diastase α-amylase immobilized on polyanilines (PANIs). *Food Chem.* **2011**, *127*, 1808–1813. [CrossRef]
48. Jimenez Hamann, M.C.; Saville, B.A. Enhancement of tyrosinase stability by immobilization on Nylon 66. *Food Bioprod. Process Trans. Inst. Chem. Eng. C* **1996**, *74*, 47–52.
49. Wang, W.; Zhou, W.; Li, J.; Hao, D.; Su, Z.; Ma, G. Comparison of covalent and physical immobilization of lipase in gigaporous polymeric microspheres. *Bioprocess Biosys. Eng.* **2015**, *38*, 2107–2115. [CrossRef] [PubMed]
50. Silva, M.F.; Rigo, D.; Mossi, V.; Dallago, R.M.; Henrick, P.; Kuhn, G.D.O.; Rosa, C.D.; Oliveira, D.; Oliveira, J.V.; Treichel, H. Evaluation of enzymatic activity of commercial inulinase from *Aspergillus niger* immobilized in polyurethane foam. *Food Bioprod. Process.* **2013**, *91*, 54–59. [CrossRef]
51. Bai, X.; Gu, H.; Chen, W.; Shi, H.; Yang, B.; Huang, X.; Zhang, Q. Immobilized laccase on activated poly(vinyl alcohol) microspheres for enzyme thermistor application. *Appl. Biochem. Biotechnol.* **2014**, *173*, 1097–1107. [CrossRef] [PubMed]
52. Vartiainen, J.; Rättö, M.; Paulussen, S. Antimicrobial activity of glucose oxidase-immobilized plasma-activated polypropylene films. *Packag. Technol. Sci.* **2005**, *18*, 243–251. [CrossRef]
53. Kumari, A.; Kayastha, A.M. Immobilization of soybean (*Glycine max*) α-amylase onto chitosan and amberlite MB-150 beads: Optimization and characterization. *J. Mol. Catal. B Enzym.* **2011**, *69*, 8–14. [CrossRef]
54. Alsafadi, D.; Paradisi, F. Covalent immobilization of alcohol dehydrogenase (ADH2) from *Haloferaxvol canii*: How to maximize activity and optimize performance of halophilic enzymes. *Mol. Biotechnol.* **2014**, *56*, 240–247. [CrossRef] [PubMed]
55. Elnashar, M.M.M. *Biotechnology of Biopolymers*; InTech: London, UK, 2011.
56. Horchani, H.; Aissa, I.; Ouertani, S.; Zarai, Z.; Gargouri, Y.; Sayari, A. Staphylococcal lipases: Biotechnological applications. *J. Mol. Catal. B Enzyme* **2012**, *76*, 125–132. [CrossRef]
57. Vijayaraghavan, K.; Yamini, D.; Ambika, V.; Sravya Sowdamini, N. Trends in inulinase production—A review. *Crit. Rev. Biotechnol.* **2009**, *29*, 67–77. [CrossRef] [PubMed]
58. Homaei, A.A.; Sariri, R.; Vianello, F.; Stevanato, R. Enzyme immobilization: An update. *J. Chem. Biol.* **2013**, *6*, 185–205. [CrossRef] [PubMed]
59. Tischer, W.; Wedekind, F. Immobilized enzymes: Methods and applications. *Top. Curr. Chem.* **1999**, *200*, 95–126.
60. Krajewska, B. Application of chitin- and chitosan-based materials for enzyme immobilizations: A review. *Enzyme Microb. Technol.* **2004**, *35*, 126–139. [CrossRef]

61. Kurita, K. Controlled functionalization of the polysaccharide chitin. *Prog. Polym. Sci.* **2001**, *26*, 1921–1971. [CrossRef]
62. Peter, M. Applications and environmental aspects of chitin and chitosan. *J. Macromol. Sci.* **1995**, *32*, 629–640. [CrossRef]
63. Shi, L.E.; Tang, Z.X.; Yi, Y.; Chen, J.S.; Xiong, W.Y.; Ying, G.Q. Immobilization of nuclease p1 on chitosan micro-spheres. *Chem. Biochem. Eng. Q.* **2011**, *25*, 83–88.
64. Cahyaningrum, S.E.; Herdyastusi, N.; Maharani, D.K. Immobilization of glucose isomerase in surface-modified chitosan gel beads. *Res. J. Pharm. Biol. Chem. Sci.* **2014**, *5*, 104–111.
65. Kim, H.J.; Park, S.; Kim, S.H.; Kim, J.H.; Yu, H.; Kim, H.J.; Yang, Y.H.; Kan, E.; Kim, Y.H.; Lee, S.H. Biocompatible cellulose nanocrystals as supports to immobilize. *J. Mol. Catal. B Enzym.* **2015**, *12*, 170–178. [CrossRef]
66. Tumturk, H.; Karaca, N.; Demirel, G.; Sahin, F. Preparation and application of poly(*N*,*N*-dimethylacrylamide-co-acrylamide) and poly(*N*-isopropylacrylamide-co-acrylamide)/κ-Carrageenan hydrogels for immobilization of lipase. *Int. J. Biol. Macromol.* **2007**, *40*, 281–285. [CrossRef] [PubMed]
67. Zdarta, J.; Jesionowski, T. *Luffa cylindrica* sponges as a thermally and chemically stable support for *Aspergillus niger* lipase. *Biotechnol. Prog.* **2016**, *32*, 657–665. [CrossRef] [PubMed]
68. Zdarta, J.; Norman, M.; Smułek, W.; Moszyński, D.; Kaczorek, E.; Stelling, A.L.; Ehrlich, H.; Jesionowski, T. Spongin-based scaffolds from *Hippospongia communis* demosponge as an effective support for lipase immobilization. *Catalysts* **2017**, *7*, 147. [CrossRef]
69. Hwang, E.T.; Gu, M.B. Enzyme stabilization by nano/microsized hybrid materials. *Eng. Life Sci.* **2013**, *13*, 49–61. [CrossRef]
70. Coradin, T.; Nassif, N.; Livage, J. Silica-alginate composites for microencapsulation. *Appl. Microbiol. Biotechnol.* **2003**, *61*, 429–434. [CrossRef] [PubMed]
71. Betigeri, S.S.; Neau, S.H. Immobilization of lipase using hydrophilic polymers in the form of hydrogel beads. *Biomaterials* **2002**, *51*, 3627–3636. [CrossRef]
72. Kocaturk, S.; Yagar, H. Optimization of polyphenol oxidase immobilization in copper alginate beads. *Artif. Cells Blood Substit. Biotechnol.* **2010**, *38*, 157–163. [CrossRef] [PubMed]
73. Sin Ball, S.G.; Morell, M.K. From bacterial glycogen to starch: Understanding the biogenesis of the plant starch granule. *Annu. Rev. Plant Biol.* **2003**, *54*, 207–233. [CrossRef] [PubMed]
74. Delattre, C.; Fenoradosoa, T.A.; Michaud, P. Galactans: An overview of their most important sourcing and applications as natural polysaccharides. *Braz. Arch. Biol. Technol.* **2011**, *54*, 1075–1092. [CrossRef]
75. Porath, J.; Axén, R. Immobilization of enzymes to agar, agarose, and sephadex support. *Methods Enzymol.* **1976**, *44*, 19–45. [PubMed]
76. Prakash, O.; Jaiswal, N. Immobilization of a thermostable α-amylase on agarose and agar matrices and its application in starch stain removal. *World Appl. Sci. J.* **2011**, *13*, 572–577.
77. De Oliveira, S.M.; Moreno-Perez, S.; Romero-Fernandez, M.; Fernandez-Lorente, G.; Rocha-Martin, J.; Guisan, J.M. Immobilization and stabilization of commercial β-1,4-endoxylanase Depol™ 333MDP by multipoint covalent attachment for xylan hydrolysis: Production of prebiotics (xylo-oligosaccharides). *Biocatal. Biotransform.* **2018**, *36*, 141–150. [CrossRef]
78. Singh, V.; Srivastava, P.; Singh, A.; Singh, D.; Malviya, T. Polysaccharide-silica hybrids: Design and applications. *Polym. Rev.* **2016**, *56*, 113–136. [CrossRef]
79. Grigoras, A.G. Catalase immobilization—A review. *Biochem. Eng. J.* **2017**, *117*, 1–20. [CrossRef]
80. Cao, M.; Li, Z.; Wang, J.; Ge, W.; Yue, T.; Li, R.; Colvin, V.L.; Yu, W.W. Food related applications of magnetic iron oxide nanoparticles: Enzyme immobilization, protein purification, and food analysis. *Trends Food Sci. Technol.* **2012**, *27*, 47–56. [CrossRef]
81. Li, X.S.; Zhu, G.T.; Luo, Y.B.; Yuan, B.F.; Feng, Y.Q. Synthesis and applications of functionalized magnetic materials in sample preparation. *TrAC Trends Anal. Chem.* **2013**, *45*, 233–247. [CrossRef]
82. Netto, C.G.C.M.; Toma, H.E.; Andrade, L.H. Superparamagnetic nanoparticles as versatile carriers and supporting materials for enzymes. *J. Mol. Catal. B Enzym.* **2013**, *85–86*, 71–92. [CrossRef]
83. Mehrasbi, M.R.; Mohammadi, J.; Peyda, M.; Mohammadi, M. Covalent immobilization of *Candida antarctica* lipase on core-shell magnetic nanoparticles for production of biodiesel from waste cooking oil. *Renew. Energy* **2017**, *101*, 593–602. [CrossRef]

84. Aber, S.; Mahmoudikia, E.; Karimi, A.; Mahdizadeh, F. Immobilization of glucose oxidase on Fe_3O_4 magnetic nanoparticles and its application in the removal of Acid Yellow 12. *Water Air Soil Pollut.* **2016**, *227*, 93–104. [CrossRef]
85. Atacan, K.; Cakiroglu, B.; Ozacar, M. Improvement of the stability and activity of immobilized trypsin on modified Fe_3O_4 magnetic nanoparticles for hydrolysis of bovine serum albumin and its application in the bovine milk. *Food Chem.* **2016**, *212*, 460–468. [CrossRef] [PubMed]
86. Schuth, F. Endo- and exotemplating to create high-surface-area inorganic materials. *Angew. Chem. Int. Ed.* **2003**, *42*, 3604–3622. [CrossRef] [PubMed]
87. Matuszek, K.; Chrobok, A.; Latos, P.; Markiton, M.; Szymańska, K.; Jarzębski, A.; Swadźba-Kwaśny, M. Silica-supported chlorometallate(III) ionic liquids as recyclable catalysts for Diels-Alder reaction under solventless conditions. *Catal. Sci. Technol.* **2016**, *6*, 8129–8137. [CrossRef]
88. Hartmann, M. Ordered mesoporous materials for bioadsorption and biocatalysis. *Chem. Mater.* **2005**, *17*, 4577–4593. [CrossRef]
89. Fan, J.; Lei, J.; Wang, L.; Yu, C.; Tu, B.; Zhao, D. Rapid and high-capacity immobilization of enzymes based on mesoporous silicas with controlled morphologies. *Chem. Commun.* **2003**, *17*, 2140–2141. [CrossRef]
90. Yiu, H.H.P.; Wright, P.A.; Botting, N.P. Enzyme immobilisation using siliceous mesoporous molecular sieves. *Microporous Mesoporous Mater.* **2001**, *44–45*, 763–765. [CrossRef]
91. Schuth, F. Non-siliceous mesostructured and mesoporous materials. *Chem. Mater.* **2001**, *13*, 3184–3195. [CrossRef]
92. Moritz, M.; Geszke-Moritz, M. Mesoporous materials as multifunctional tools in biosciences: Principles and applications. *Mater. Sci. Eng. C* **2015**, *49*, 114–151. [CrossRef] [PubMed]
93. Catalano, P.N.; Wolosiuk, A.; Soler-Illia, G.J.A.A.; Bellino, M.G. Wired enzymes in mesoporous materials: A benchmark for fabricating biofuel cells. *Bioelectrochemistry* **2015**, *106*, 14–21. [CrossRef] [PubMed]
94. Cai, C.; Gao, Y.; Liu, Y.; Zhong, N.; Liu, N. Immobilization of *Candida antarctica* lipase B onto SBA-15 and their application in glycerolysis for diacylglycerols synthesis. *Food Chem.* **2012**, *212*, 205–212. [CrossRef] [PubMed]
95. Chen, Y.; Xu, Y.; Wu, X.M. Efficient improving the activity and enantioselectivity of *Candida rugosa* lipase for the resolution of naproxen by enzyme immobilization on MCM-41 mesoporous molecular sieve. *Int. J. Bioautom.* **2015**, *19*, 325–334.
96. Zhuang, H.; Dong, S.; Zhang, T.; Tang, N.; Xu, N.; Sun, B.; Liu, J.; Zhang, M.; Yuan, Y. Study on alkaline protease immobilized on mesoporous materials. *Asian J. Chem.* **2014**, *26*, 1139–1144.
97. Mangrulkar, P.A.; Yadav, R.; Meshram, J.S.; Labhsetwar, N.K.; Rayalu, S.S. Tyrosinase-immobilized MCM-41 for the detection of phenol. *Water Air Soil Pollut.* **2012**, *223*, 819–825. [CrossRef]
98. Wang, Y.; Caruso, F. Mesoporous silica spheres as supports for enzyme immobilization and encapsulation. *Chem. Mater.* **2005**, *17*, 953–961. [CrossRef]
99. Jia, H.; Zhu, G.; Wang, P. Catalytic behaviors of enzymes attached to nanoparticles: The effect of particle mobility. *Biotechnol. Bioeng.* **2003**, *84*, 406–414. [CrossRef] [PubMed]
100. Kim, J.; Grate, J.W.; Wang, P. Nanostructures for enzyme stabilization. *Chem. Eng. Sci.* **2006**, *61*, 1017–1026. [CrossRef]
101. Cipolatti, E.P.; Valerio, A.; Henriques, R.A.; Moritz, D.E.; Ninow, J.L.; Freire, D.M.G.; Manoel, E.A.; Fernandez-Lafuente, R.; de Oliveira, D. Nanomaterials for biocatalyst immobilization—State of the art and future trends. *RSC Adv.* **2016**, *6*, 104675–104692. [CrossRef]
102. Hu, C.; Wang, N.; Zhang, W.; Zhang, S.; Meng, Y.; Yu, X. Immobilization of *Aspergillus terreus* lipase in self-assembled hollow nanospheres for enantioselective hydrolysis of ketoprofen vinyl ester. *J. Biotechnol.* **2015**, *194*, 12–18. [CrossRef] [PubMed]
103. Wang, X.; Shi, J.; Li, Z.; Zhang, S.; Wu, H.; Jiang, Z.; Yang, C.; Tian, C. Facile one-pot preparation of chitosan/calcium pyrophosphate hybrid microflowers. *ACS Appl. Mater. Interface* **2014**, *6*, 14522–14532. [CrossRef] [PubMed]
104. Kotal, M.; Srivastava, S.K.; Matiti, T.K. Fabrication of gold nanoparticle assembled polyurethane microsphere template in trypsin immobilization. *J. Nanosci. Nanotechnol.* **2011**, *11*, 10149–10157. [CrossRef] [PubMed]
105. Bolibok, P.; Wiśniewski, M.; Roszek, K.; Terzyk, A.P. Controlling enzymatic activity by immobilization on graphene oxide. *Sci. Nat.* **2017**, *104*, 36. [CrossRef] [PubMed]

106. Hou, J.; Dong, G.; Xiao, B.; Malassigne, C.; Chen, V. Preparation of titania based biocatalytic nanoparticles and membranes for CO_2 conversion. *J. Mater. Chem. A* **2015**, *3*, 3332–3342. [CrossRef]
107. Garmroodi, M.; Mohammadi, M.; Ramazani, A.; Ashjari, M.; Mohammadi, J.; Sabour, B.; Yousefi, M. Covalent binding of hyper-activated *Rhizomucor miehei* lipase (RML) on hetero-functionalized siliceous supports. *Int. J. Biol. Macromol.* **2016**, *86*, 208–215. [CrossRef] [PubMed]
108. Ota, S.; Miyazaki, S.; Matsuoka, H.; Morisato, K.; Shintani, Y.; Nakanishi, K. High-throughput protein digestion by trypsin-immobilized monolithic silica with pipette-tip formula. *J. Biochem. Biophys. Meth.* **2007**, *70*, 57–62. [CrossRef] [PubMed]
109. de Cazes, M.; Belleville, P.; Mougel, M.; Kellner, H.; Sanchez-Marcano, J. Characterization of laccase-grafted ceramic membranes for pharmaceuticals degradation. *J. Membr. Sci.* **2015**, *476*, 384–393. [CrossRef]
110. Caldas, E.M.; Novatzky, D.; Deon, M.; de Menezes, E.W.; Hertz, P.F.; Costa, T.M.H.; Arenas, L.T.; Benvenutt, E.V. Pore size effect in the amount of immobilized enzyme for manufacturing carbon ceramic biosensor. *Microporous Mesoporous Mater.* **2017**, *247*, 95–102. [CrossRef]
111. Pazouki, M.; Zamani, F.; Khalili, M. Development of clay foam ceramic as a support for fungi immobilization for biodiesel production. *Int. J. Eng. Trans. B Appl.* **2014**, *27*, 1691–1696.
112. Ebrahimi, M.; Placido, L.; Engel, L.; Shams Ashaghi, K.; Czermak, P. A novel ceramic membrane reactor system for the continuous enzymatic synthesis of oligosaccharides. *Desalination* **2010**, *250*, 1105–1108. [CrossRef]
113. Wang, W.; Li, Z.; Li, W.; Wu, J. Horseradish peroxidase immobilized on the silane-modified ceramics for the catalytic oxidation of simulated oily water. *Sep. Purif. Technol.* **2012**, *89*, 206–211. [CrossRef]
114. Titirici, M.M.; White, R.J.; Brun, N.; Budarin, V.L.; Su, D.S.; Del Monte, F.; Clark, J.H.; MacLachlan, M.J. Sustainable carbon materials. *Chem. Soc. Rev.* **2015**, *44*, 250–290. [CrossRef] [PubMed]
115. Hong, G.; Diao, S.; Antaris, A.L.; Dai, H. Carbon nanomaterials for biological imaging and nanomedicinal therapy. *Chem. Rev.* **2015**, *115*, 10816–10906. [CrossRef] [PubMed]
116. Pedrosa, V.A.; Paliwal, S.; Balasubramanian, S.; Nepal, D.; Davis, V.; Wild, J.; Ramanculov, E.; Simonian, A. Enhanced stability of enzyme organophosphate hydrolase interfaced on the carbon nanotubes. *Colloids Surf. B Biointerface* **2010**, *77*, 69–74. [CrossRef] [PubMed]
117. Wan, X.; Zhang, C.; Yu, D.; Huang, H.; Hu, Y. Enzyme immobilized on carbon nanotubes. *Prog. Chem.* **2015**, *27*, 1251–1259.
118. Markiton, M.; Boncel, S.; Janas, D.; Chrobok, A. Highly active nanobiocatalyst from lipase noncovalently immobilized on multiwalled carbon nanotubes for Baeyer-Villiger synthesis of lactones. *ACS Sustain. Chem. Eng.* **2017**, *8*, 1685–1691. [CrossRef]
119. Liu, Y.; Wang, M.; Zhao, F.; Xu, Z.; Dong, S. The direct electron transfer of glucose oxidase and glucose biosensor based on carbon nanotubes/chitosan matrix. *Biosens. Bioelectron.* **2005**, *21*, 984–988. [CrossRef] [PubMed]
120. Mohiuddin, M.; Arbain, D.; Islam, A.K.M.S.; Ahmad, M.S.; Ahmad, M.N. Alpha-glucosidase enzyme biosensor for the electrochemical measurement of antidiabetic potential of medicinal plants. *Nanoscale Res. Lett.* **2016**, *95*, 1–12. [CrossRef] [PubMed]
121. Zhang, Y.; Wu, C.; Guo, S.; Zhang, J. Interactions of graphene and graphene oxide with proteins and peptides. *Nanotechnol. Rev.* **2013**, *2*, 27–45. [CrossRef]
122. Zhang, C.; Chen, S.; Alvarez, P.J.J.; Chen, W. Reduced graphene oxide enhances horseradish peroxidase stability by serving as radical scavenger and redox mediator. *Carbon* **2018**, *94*, 531–538. [CrossRef]
123. Pavlidis, I.V.; Vorhaben, T.; Tsoufis, T.; Rudolf, P.; Bornscheuer, U.T.; Gournis, D.; Stamatis, H. Development of effective nanobiocatalytic systems through the im mobilization of hydrolases on functionalized carbon-based nanomaterials. *Bioresour. Technol.* **2012**, *115*, 164–171. [CrossRef] [PubMed]
124. Zhang, J.; Zhang, J.; Zhang, F.; Yang, H.; Huang, X.; Liu, H.; Guo, S. Graphene oxide as a matrix for enzyme immobilization. *Langmuir* **2010**, *26*, 6083–6085. [CrossRef] [PubMed]
125. Tseng, C.; Liao, C.; Sun, Y.; Peng, C.; Tzen, J.T.C.; Guo, R.; Liu, J. Immobilization of *Clostridium cellulolyticum*. *J. Agric. Food Chem.* **2014**, *62*, 6771–6776. [CrossRef] [PubMed]
126. Lee, K.H.; Lee, B.; Hwang, S.J.; Lee, J.U.; Cheong, H.; Shin, K.; Hur, N.H. Large scale production of highly conductive reduced graphene oxide sheets by a solvent-free low temperature reduction. *Carbon* **2014**, *69*, 327–335. [CrossRef]

127. Vineh, M.B.; Saboury, A.A.; Poostchi, A.A.; Rashidi, A.M.; Parivar, K. Stability and activity improvement of horseradish peroxidase by covalent immobilization on functionalized reduced graphene oxide and biodegradation of high phenol concentration. *Int. J. Biol. Macromol.* **2018**, *106*, 1314–1322. [CrossRef] [PubMed]
128. Dedania, S.R.; Patel, M.J.; Patel, D.M.; Akhani, R.C. Immobilization on graphene oxide improves the thermal stability and bioconversion efficiency of D-psicose 3-epimerase for rare sugar production. *Enzyme Microb. Technol.* **2017**, *107*, 49–56. [CrossRef] [PubMed]
129. Bhushani, J.A.; Anandharamakrishnan, V. Electrospinning and electrospraying techniques: Potential food based applications. *Trends Food Sci. Technol.* **2014**, *38*, 21–33. [CrossRef]
130. Wang, Z.G.; Wan, L.S.; Liu, Z.M.; Huang, X.J.; Xu, Z.K. Enzyme immobilization on electrospun polymer nanofibers: An overview. *J. Mol. Catal. B Enzym.* **2009**, *56*, 189–195. [CrossRef]
131. Dai, Y.; Yao, J.; Song, Y.; Liu, X.; Wang, S.; Yuan, Y. Enhanced performance of immobilized laccase in electrospun fibrous membranes by carbon nanotubes modification and its application for bisphenol A removal from water. *J. Hazard. Mater.* **2016**, *317*, 485–493. [CrossRef] [PubMed]
132. Liang, D.; Hsiao, B.S.; Chu, B. Functional electrospun nanofibrous scaffolds for biomedical applications. *Adv. Drug Deliv. Rev.* **2007**, *59*, 1392–1412. [CrossRef] [PubMed]
133. Bhardwaj, N.; Kundu, S.C. Electrospinning: A fascinating fiber fabrication technique. *Biotechnol. Adv.* **2010**, *28*, 325–347. [CrossRef] [PubMed]
134. Wong, D.E.; Dai, M.; Talbert, J.N.; Nugen, S.R.; Goddard, J.M. Biocatalytic polymer nanofibers for stabilization and delivery of enzymes. *J. Mol. Catal. B Enzym.* **2014**, *110*, 16–22. [CrossRef]
135. Lee, K.Y.; Jeong, L.; Kang, Y.O.; Lee, S.J.; Park, W.H. Electrospinning of polysaccharides for regenerative medicine. *Adv. Drug Deliv. Rev.* **2009**, *61*, 1020–1032. [CrossRef] [PubMed]
136. Yoo, H.S.; Kim, J.; Park, T.G. Surface-functionalized electrospun nanofibers for tissue engineering and drug delivery. *Adv. Drug Deliv. Rev.* **2009**, *61*, 1033–1042. [CrossRef] [PubMed]
137. Kim, J.; Grate, J.W.; Wang, P. Nanobiocatalysis and its potential applications. *Trends Biotechnol.* **2008**, *26*, 639–646. [CrossRef] [PubMed]
138. Canbolat, M.F.; Savas, H.B.; Gultekin, F. Improved catalytic activity by catalase immobilization using γ-cyclodextrin and electrospun PCL nanofibers. *J. Appl. Sci.* **2017**, *134*, 318–326. [CrossRef]
139. Weiser, D.; Soti, P.L.; Banoczi, G.; Bodai, V.; Kiss, B.; Gellert, A.; Nagy, Z.K.; Koczka, B.; Szilagyi, A.; Marosi, G.; et al. Bioimprinted lipases in PVA nanofibers as efficient immobilized biocatalysts. *Tetrahedron* **2016**, *72*, 7335–7342. [CrossRef]
140. Soti, P.L.; Weiser, D.; Vigh, T.; Nagy, Z.K.; Poppe, L.; Maros, G. Electrospun polylactic acid and polyvinyl alcohol fibers as efficient and stable nanomaterials for immobilization of lipases. *Bioprocess. Biosyst. Eng.* **2016**, *39*, 449–459. [CrossRef] [PubMed]
141. Handayani, N.; Loos, K.; Wahyuningrum, D.; Buchari, M.; Zulfikar, M.A. Immobilization of *Mucor miehei* lipase onto macroporous aminated polyethersulfone membrane for enzymatic reactions. *Membranes* **2012**, *2*, 198–213. [CrossRef] [PubMed]
142. Orregoa, C.E.; Salgadoa, N.; Valenciab, J.S.; Giraldoc, G.I.; Giraldod, O.H.; Cardonae, C.A. Novel chitosan membranes as support for lipases immobilization: Characterization aspects. *Carbohydr. Polym.* **2010**, *79*, 9–16. [CrossRef]
143. Kuo, C.H.; Chen, G.J.; Kuo, T.Y.; Liu, Y.C.; Shieh, C.J. Optimum lipase immobilized on diamine-grafted PVDF membrane and its characterization. *Ind. Eng. Chem. Res.* **2012**, *51*, 5141–5147. [CrossRef]
144. Gupta, S.; Bhattacharya, A.; Murthy, C.N. Tune to immobilize lipases on polymer membranes: Techniques, factors and prospects. *Biocatal. Agricultur. Biotechnol.* **2013**, *2*, 171–190. [CrossRef]
145. Vitola, G.; Mazzei, R.; Fontananova, E.; Porzio, E.; Manco, G.; Gaeta, S.N.; Giorno, L. Polymeric biocatalytic membranes with immobilized thermostable phosphotriesterase. *J. Membr. Sci.* **2016**, *516*, 144–151. [CrossRef]
146. Donato, L.; Algieri, C.; Rizzi, A.; Giorno, L. Kinetic study of tyrosinase immobilized on polymeric membrane. *J. Membr. Sci.* **2014**, *454*, 346–350. [CrossRef]
147. Konovalova, V.; Guzikevich, K.; Burban, A.; Kujawski, W.; Jarzynka, K.; Kujawa, J. Enhanced starch hydrolysis using α-amylase immobilized on cellulose ultrafiltration affinity membrane. *Carbohydr. Polym.* **2016**, *152*, 710–717. [CrossRef] [PubMed]
148. Luo, J.; Meyer, A.S.; Jonsson, G.; Pinelo, M. Fouling-induced enzyme immobilization for membrane reactors. *Bioresour. Technol.* **2013**, *147*, 260–268. [CrossRef] [PubMed]

149. Luo, J.; Marpani, F.; Brites, R.; Frederiksen, L.; Meyer, A.S.; Jonsson, G.; Pinelo, M. Directing filtration to optimize enzyme immobilization in reactive membranes. *J. Membr. Sci.* **2014**, *459*, 1–11. [CrossRef]
150. Luo, J.; Nordvang, R.T.; Morthensen, S.T.; Zeuner, B.; Meyer, A.S.; Mikkelsen, J.D.; Pinelo, M. An integrated membrane system for the biocatalytic production of 3′-sialyllactose from dairy by-products. *Bioresour. Technol.* **2014**, *166*, 9–16. [CrossRef] [PubMed]
151. Morthensen, S.T.; Luo, J.; Meyer, A.S.; Jørgensen, H.; Pinelo, M. High performance separation of xylose and glucose by enzyme assisted nanofiltration. *J. Membr. Sci.* **2015**, *492*, 107–115. [CrossRef]
152. Liu, W.F.; Wei, L.N. Research progress on carbonic anhydrase immobilization. *J. Mol. Catal.* **2016**, *30*, 182–197.
153. Yang, X.-Y.; Tian, G.; Jiang, N.; Su, B.L. Immobilization technology: A sustainable solution for biofuel cell design. *Energy Environ. Sci.* **2012**, *5*, 5540–5563. [CrossRef]
154. Xue, H.; Shen, Z.; Li, C. Improved selectivity and stability of glucose biosensor based on in situ electropolymerized polyaniline–polyacrylonitrile composite film. *Biosens. Bioelectron.* **2005**, *20*, 2330–2334. [CrossRef] [PubMed]
155. Rajdeo, K.; Harini, T.; Lavanya, K.; Fadnavis, N.W. Immobilization of pectinase on reusable polymer support for clarification of apple juice. *Food Bioprod. Process.* **2016**, *99*, 12–19. [CrossRef]
156. Sui, C.-H.; Wang, Z.-Y.; Wei, Y.-Q.; Wang, C. Immobilization of glucoamylase onto electrospun PAA/PVA microfibrous membrane by active ester method. *Chin. J. Process Eng.* **2016**, *16*, 494–499.
157. Riccardi, C.M.; Kasi, R.M.; Kumar, C.V. Nanoarmoring of enzymes by interlocking in cellulose fibers with poly(acrylic acid). *Method. Enzymol.* **2017**, *590*, 475–500.
158. Badgujar, K.C.; Bhanage, B.M. Investigation of deactivation thermodynamics of lipase immobilized on polymeric carrier. *Bioprocess Biosyst. Eng.* **2017**, *40*, 717–757. [CrossRef] [PubMed]
159. Yavuz, A.G.; Uygun, A.; Bhethanabotla, V.R. Preparation of substituted polyaniline/chitosan composites by in situ electropolymerization and their application to glucose sensing. *Carbohydr. Polym.* **2010**, *81*, 712–719. [CrossRef]
160. Pervez, S.; Aman, A.; Qader, S.A. Role of two polysaccharide matrices on activity, stability and recycling efficiency of immobilized fungal amyloglucosidase of GH15 family. *Int. J. Biol. Macromol.* **2017**, *96*, 70–77. [CrossRef] [PubMed]
161. Zdarta, J.; Klapiszewski, Ł.; Wysokowski, M.; Norman, M.; Kołodziejczak-Radzimska, A.; Moszyński, D.; Ehrlich, H.; Maciejewski, H.; Stelling, A.L.; Jesionowski, T. Chitin-lignin material as a novel matrix for enzyme immobilization. *Mar. Drugs* **2015**, *13*, 2424–2446. [CrossRef] [PubMed]
162. De Paula, R.C.M.; Feitosa, J.P.A.; Paula, H.C.B. Polysaccharide based copolymers as supramolecular systems in biomedical applications. *Curr. Drug. Targets* **2015**, *16*, 1591–1605. [CrossRef]
163. Kara, F.; Aksoy, E.A.; Calamak, S.; Hasirci, N.; Aksoy, S. Immobilization of heparin on chitosan-grafted polyurethane films to enhance anti-adhesive and antibacterial properties. *J. Bioact. Compat. Polym.* **2016**, *31*, 72–90. [CrossRef]
164. Shen, L.; Cheng, K.C.K.; Schroeder, M.; Yang, P.; Marsh, E.N.G.; Lahann, J.; Chen, Z. Immobilization of enzyme on a polymer surface. *Surf. Sci.* **2016**, *648*, 53–59. [CrossRef]
165. Zucca, P.; Fernandez-Lafuente, R.; Sanjust, E. Agarose and its derivatives as supports for enzyme immobilization. *Molecules* **2016**, *21*, 1577. [CrossRef] [PubMed]
166. Schulze, A.; Breite, D.; Kim, Y.; Schmidt, M.; Thomas, I.; Went, M.; Fischer, K.; Prager, A. Bio-Inspired polymer membrane surface cleaning. *Polymers* **2017**, *9*, 97. [CrossRef]
167. Huang, J.; Kaner, R.B. A general chemical route to polyaniline nanofibers. *J. Am. Chem. Soc.* **2004**, *126*, 851–855. [CrossRef] [PubMed]
168. Lai, J.; Yi, Y.; Zhua, P.; Shen, J.; Wu, K.; Zhang, L.; Liu, J. Polyaniline-based glucose biosensor: A review. *J. Electroanal. Chem.* **2016**, *782*, 138–153. [CrossRef]
169. Fang, L.; Liang, B.; Yang, G.; Hu, Y.; Zhu, Q.; Ye, X. Study of glucose biosensor lifetime improvement in 37 °C serum based on PANI enzyme immobilization and PLGA biodegradable membrane. *Biosens. Bioelectron.* **2014**, *56*, 91–96. [CrossRef] [PubMed]
170. Kumar, M.; Rahikainen, R.; Unruh, D.; Hytönen, V.P.; Delbruck, C.; Sindelar, R.; Renz, F. Mixture of PLA–PEG and biotinylated albumin enables immobilization of avidins on electrospun fibers. *J. Biomed. Mater. Res. A* **2017**, *105*, 356–362. [CrossRef] [PubMed]

171. Badgujar, K.C.; Bhanage, B.M. Solvent stability study with thermodynamic analysis and superior biocatalytic activity of *Burkholderia cepacia* lipase immobilized on biocompatible hybrid matrix of poly(vinyl alcohol) and hypromellose. *J. Phys. Chem. B* **2014**, *118*, 14808–14819. [CrossRef] [PubMed]
172. Matto, M.; Husain, Q. Calcium alginate-starch hybrid support for both surface immobilization and entrapment of bitter gourd (*Momordicacharantia*) peroxidase. *J. Mol. Catal. B Enzym.* **2009**, *57*, 164–170. [CrossRef]
173. Abdulla, R.; Ravindra, P. Immobilized *Burkholderia cepacia* lipase for biodiesel production from crude *Jatropha curcas* L. oil. *Biomass Bioenergy* **2013**, *56*, 8–13. [CrossRef]
174. Nupur, N.; Ashish, M.; Mira Das, D. Preparation and biochemical property of penicillin G amidase-loaded alginate and alginate/chitosan hydrogel beads. *Recent Pat. Biotechnol.* **2016**, *10*, 121–132. [CrossRef] [PubMed]
175. Li, J.; Wu, H.; Liang, Y.; Jiang, Z.; Jiang, Y.; Zhang, L. Facile fabrication of organic-inorganic hybrid beads by aminated alginate enabled gelation and biomimetic mineralization. *J. Biomater. Sci-Polym. E* **2013**, *24*, 119–134. [CrossRef] [PubMed]
176. Li, L.; Ma, L.; Li, H. Characteristics of magnetic microspheres and its application in enzyme immobilization. *J. Clin. Reh. Tissue Eng. Res.* **2008**, *12*, 8198–8200.
177. Amirbandeh, M.; Taheri-Kafrani, A. Immobilization of glucoamylase on triazine-functionalized Fe_3O_4/graphene oxide nanocomposite: Improved stability and reusability. *Int. J. Biol. Macromol.* **2016**, *93*, 1183–1191. [CrossRef] [PubMed]
178. Jędrzak, A.; Rębiś, T.; Klapiszewski, Ł.; Zdarta, J.; Milczarek, G.; Jesionowski, T. Carbon paste electrode based on functional GO_x/silica-lignin systemto prepare an amperometric glucose biosensor. *Sens. Actuators B* **2018**, *256*, 176–185. [CrossRef]
179. Wan, L.S.; Ke, B.B.; Xu, Z.K. Electrospun nanofibrous membranes filled with carbon nanotubes for redox enzyme immobilization. *Enzyme Microb. Technol.* **2008**, *42*, 332–339. [CrossRef]
180. Barros, A.E.L.; Almeida, A.M.P.; Carvalho, L.B., Jr.; Azevedo, W.M. Polysiloxane/PVA-glutaraldehyde hybrid composite as solid phase or immunodetections by ELISA. *Braz. J. Med. Biol. Res.* **2002**, *35*, 459–463. [CrossRef]
181. Shah, N.; Ul-Islam, M.; Khattak, W.A.; Park, J.K. Overview of bacterial cellulose composites: A multipurpose advanced material. *Carbohyd. Polym.* **2013**, *98*, 1585–1598. [CrossRef] [PubMed]
182. Zdarta, J.; Klapiszewski, Ł.; Jędrzak, A.; Nowicki, M.; Moszyński, D.; Jesionowski, T. Lipase B from *Candida antarctica* immobilized on a silica-lignin matrix as a stable and reusable biocatalytic system. *Catalysts* **2017**, *7*, 14. [CrossRef]
183. Vatsyayan, P.; Bordoloi, S.; Goswami, P. Large catalase based bioelectrode for biosensor application. *Biophys. Chem.* **2010**, *153*, 36–42. [CrossRef] [PubMed]
184. Zhang, S.; Jiang, Z.; Zhang, W.; Wang, X.; Shi, J. Polymer-inorganic microcapsules fabricated by combining biomimetic adhesion and bioinspired mineralization and their use for catalase immobilization. *Biochem. Eng. J.* **2015**, *93*, 281–288. [CrossRef]
185. Zhao, H.; Cui, Q.; Shah, V.; Xu, J.; Wang, T. Enhancement of glucose isomerase activity by immobilizing on silica/chitosan hybrid microspheres. *J. Mol. Catal. B Enzym.* **2016**, *126*, 18–23. [CrossRef]
186. Guo, M.; Yao, S.S.; Gao, X.Y.; Fu, X.P. Preparation and enzymological properties of SiO_2-DAS immobilized cellulose. *J. Chem. Eng. Chin.* **2015**, *29*, 1407–1414.
187. Miranda, R.A.; Llorca, J.; Medina, F.; Sueiras, J.E.; Segarra, A.M. Asymmetric epoxidation of chalcone catalyzed by reusable poly-L-leucine immobilized on hydrotalcite. *J. Catal.* **2011**, *282*, 65–73. [CrossRef]
188. Chang, M.Y.; Kao, H.C.; Juang, R.S. Thermal inactivation and reactivity of β-glucosidase immobilized on chitosan–clay composite. *Int. J. Biol. Macromol.* **2008**, *43*, 48–53. [CrossRef] [PubMed]
189. Han, E.; Li, X.; Cai, J.R.; Cui, H.Y.; Zhang, X.A. Development of highly sensitive amperometric biosensor for glucose using carbon nanosphere/sodium alginate composite matrix for enzyme immobilization. *Anal. Sci.* **2014**, *30*, 897–902. [CrossRef] [PubMed]
190. Ambrogio, M.W.; Thomas, C.R.; Zhao, Y.-L.; Zink, J.I.; Stoddart, J.F. Mechanized silica nanoparticles: A new frontier in theranostic nanomedicine. *Acc. Chem. Res.* **2011**, *44*, 903–913. [CrossRef] [PubMed]
191. Yuce-Dursun, B.; Cigil, A.B.; Dongez, D.; Kahraman, M.V.; Ogan, A.; Demir, S. Preparation and characterization of sol-gel hybrid coating films for covalent immobilization of lipase enzyme. *J. Mol. Catal. B Enzym.* **2016**, *127*, 18–25. [CrossRef]

192. Zniszczoł, A.; Herman, A.P.; Szymańska, K.; Mrowiec-Białoń, J.; Walczak, K.Z.; Jarzębski, A.; Boncel, S. Covalently immobilized lipase on aminoalkyl-, carboxy- and hydroxy-multi-wall carbon nanotubes in the enantioselective synthesis of Solketal esters. *Enzyme Microb. Technol.* **2016**, *87*, 61–69. [CrossRef] [PubMed]
193. Lee, S.H.; Doan, T.T.N.; Won, K.; Ha, S.H.; Koo, Y.M. Immobilization of lipase within carbon nanotube–silica composites for non-aqueous reaction systems. *J. Mol. Catal. B Enzym.* **2010**, *62*, 169–172. [CrossRef]
194. Zhu, Y.T.; Ren, X.Y.; Liu, Y.M.; Wei, Y.; Qing, L.S.; Liao, X. Covalent immobilization of porcine pancreatic lipase on carboxyl-activated magnetic nanoparticles: Characterization and application for enzymatic inhibition assays. *Mater. Sci. Eng. C* **2014**, *38*, 278–285. [CrossRef] [PubMed]
195. Lei, Z.; Liu, X.; Ma, L.; Liu, D.; Zhang, H.; Wang, Z. Spheres-on-sphere silica microspheres as matrix for horseradish peroxidase immobilization and detection of hydrogen peroxide. *RSC Adv.* **2015**, *5*, 38665–38672. [CrossRef]
196. Bian, S.; Wu, H.; Jiang, X.; Long, Y.; Chen, Y. Syntheses and applications of hybrid mesoporous silica membranes. *Prog. Chem.* **2014**, *26*, 1352–1360.
197. Nenkova, R.; Wu, J.; Zhang, Y.; Godjevargova, T. Evaluation of immobilization techniques for the fabrication of nanomaterial-based amperometric glucose biosensors. *Anal. Lett.* **2015**, *48*, 1297–1310. [CrossRef]
198. Zlateski, V.; Fuhrer, R.; Koehle, F.M.; Wharry, S.; Zeltner, M.; Stark, W.J.; Moody, T.S.; Grass, R.N. Efficient magnetic recycling of covalently attached enzymes on carbon-coated metallic nanomagnets. *Bioconj. Chem.* **2014**, *25*, 677–684. [CrossRef] [PubMed]
199. Abraham, S.; Srivastava, S.; Kumar, V.; Pandey, S.; Rastogi, P.K.; Nirala, N.R.; Kashyap, S.; Srivastava, S.K.; Singh, V.N.; Ganesan, V.; et al. Enhanced electrochemical biosensing efficiency of silica particles supported on partially reduced graphene oxide for sensitive detection of cholesterol. *J. Electroanal. Chem.* **2015**, *757*, 65–72. [CrossRef]
200. Shoja, Y.; Rafati, A.A.; Ghodsi, J. Enzymatic biosensor based on entrapment of D-amino acid oxidase on gold nanofilm/MWCNTs nanocomposite modified glassy carbon electrode by sol-gel network: Analytical applications for D-alanine in human serum. *Enzyme Microb. Technol.* **2017**, *100*, 20–27. [CrossRef] [PubMed]
201. Fidal, V.T.K.P.; Inguva, S.; Krishnamurthy, S.; Marsili, E.; Mosnier, J.P.; Chandra, T.S. Mediator-free interaction of glucose oxidase, as model enzyme for immobilization, with Al-doped and undoped ZnO thin films laser-deposited on polycarbonate supports. *Enzyme Microb. Technol.* **2017**, *96*, 67–74.
202. Sun, H.; Jin, X.; Long, N.; Zhang, R. Improved biodegradation of synthetic azo dye by horseradish peroxidase cross-linked on nano-composite support. *Int. J. Biol. Macromol.* **2017**, *95*, 1049–1055. [CrossRef] [PubMed]
203. Li, F.; Feng, Y.; Wang, Z.; Yang, L.; Zhuo, L.; Tang, B. Direct electrochemistry of horseradish peroxidase immobilized on the layered calcium carbonate-gold nanoparticles inorganic hybrid composite. *Biosens. Bioelectron.* **2010**, *25*, 2244–2248. [CrossRef] [PubMed]
204. Lopes, J.H.; Colson, F.X.; Barralet, J.E.; Merle, G. Electrically wired enzyme/TiO_2 composite for glucose detection. *Mater. Sci. Eng. C* **2017**, *76*, 991–996. [CrossRef] [PubMed]
205. Bujduveanu, M.R.; Yao, W.; LeGoff, A.; Gorgy, K.; Shan, D.; Diao, G.W.; Ungureanu, E.M.; Cosnier, S. Multiwalled carbon nanotube-$CaCO_3$ nanoparticle composites for the construction of a tyrosinase-based amperometric dopamine biosensor. *Electroanalysis* **2013**, *25*, 613–619. [CrossRef]

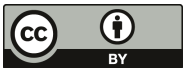

© 2018 by the authors. Licensee MDPI, Basel, Switzerland. This article is an open access article distributed under the terms and conditions of the Creative Commons Attribution (CC BY) license (http://creativecommons.org/licenses/by/4.0/).

catalysts

MDPI

Review

Applications of Immobilized Bio-Catalyst in Metal-Organic Frameworks

Qi Wang, Xizhen Lian, Yu Fang and Hong-Cai Zhou *

Department of Chemistry, Texas A&M University, P.O. Box 30012, College Station, TX 77842-3012, USA; qi.wang@chem.tamu.edu (Q.W.); xizhen.lian@chem.tamu.edu (X.L.); yu.fang@chem.tamu.edu (Y.F.)
* Correspondence: zhou@chem.tamu.edu; Tel.: +1-979-845-4034

Received: 9 April 2018; Accepted: 18 April 2018; Published: 20 April 2018

Abstract: Immobilization of bio-catalysts in solid porous materials has attracted much attention in the last few decades due to its vast application potential in ex vivo catalysis. Despite the high efficiency and selectivity of enzymatic catalytic processes, enzymes may suffer from denaturation under industrial production conditions, which, in turn, diminish their catalytic performances and long-term recyclability. Metal-organic frameworks (MOFs), as a growing type of hybrid materials, have been identified as promising platforms for enzyme immobilization owing to their enormous structural and functional tunability, and extraordinary porosity. This review mainly focuses on the applications of enzyme@MOFs hybrid materials in catalysis, sensing, and detection. The improvements of catalytic activity and robustness of encapsulated enzymes over the free counterpart are discussed in detail.

Keywords: metal-organic frameworks (MOFs); enzyme immobilization; bio-catalyst; conversion; sensing

1. Introduction

The history of utilizing bio-catalysts in production dates back to thousands of years ago when human learned to make alcohol from sugar via fermentation with the addition of yeast or other microorganisms. With the fusion of ideas from modern protein chemistry and molecular biology, enzymes, as nature's catalysts, have been extensively applied in industrial production, such as drug and food production [1–3]. However, these applications are limited by the relatively low stability of enzymes, for example, weak thermal stability and high sensitivity to pH changes, which results in the lack of long-term recyclability and difficulty of separating enzymes from products [4,5]. A possible strategy to overcome these issues is heterogeneously immobilizing enzymes on solid supports, which keeps enzymes in the confined microenvironment and prevents enzymes from denaturing [6–8].

Metal-organic frameworks (MOFs) are an emerging porous materials assembled by the coordination of metal ions or clusters with organic linkers [9–11]. MOFs are highly tunable platforms in terms of structure and functionality [12,13]. Thus, MOFs have shown promising potentials in gas adsorption and separation, catalysis, photosynthesis, biomedicine, and so on [14–25]. The high surface area, large pore volume, and high stability of MOFs indicate that they are ideal for enzyme immobilization [26–30]. This review mainly focuses on the applications of immobilized enzyme@MOFs materials in biomimetic catalysis and conversion, sensing, and detection. The performance of immobilized enzymes will be compared with the free counterparts and the merits imparted from immobilization will be discussed.

2. Applications of Enzyme@MOFs Materials in Catalysis, Sensing, and Detection

Due to the high selectivity nature of enzymes, the applications of immobilized enzyme@MOFs materials are mainly for catalysis, sensing, and detection. Immobilized enzymes are separated by

the pores of MOFs, which avoids their aggregation and facilitates high conversion rate. In addition, the physical confinement of the immobilized enzymes by the cavity wall of MOFs prevents the occurrence of protein denaturation.

The synthetic approaches of enzyme@MOF materials also play a key role in their practical performances, especially in the aspect of promoting substrate diffusion and prohibiting enzyme leaching. Typically, the synthetic approaches can be classified into two major categories: one-pot synthesis and post-synthetic immobilization. One-pot synthesis, also known as biomineralization or co-precipitation, encapsulates the enzymes in the material through the formation of coordination porous shell structures. The core-shell structure creates diffusion pathways for substrates contacting the encapsulated enzymes. Post-synthetic immobilizations, including the formation of covalent and non-covalent bonds between MOF and enzymes, also provides strong host-guest interactions and accessible enzyme active sites.

2.1. Biomimetic Catalysis and Conversion

2.1.1. Chemical Conversion

Park et al. reported the covalent attachment of enhanced green fluorescent protein (EGFP) and *Candida-antarctica*-lipase-B (CAL-B) in 1D ($[(Et_2NH_2)(In(pda)_2)]$, pda = 1,4-phenylenediacetate), 2D ($[Zn(bpydc)(H_2O)(H_2O)]_n$, bpydc = 2,2′-bipyridine 5,5′-dicarboxylate), and 3D (IRMOF-3) MOFs [31] The carboxylate groups on the MOF surface were first activated and then reacted with the amino groups on the enzymes (Figure 1). The catalytic activity of the immobilized CAL-B was verified through transesterification of (±)-1-phenylethanol. CAL-B immobilized on IRMOF-3 showed 10^3-fold higher activity than that of free CAL-B, while maintaining the same enantioselectivity. The authors proposed that the confined spaces in MOFs allow substrates to access enzymes more efficiently. Moreover, after three catalytic cycles, no significant decrease of enzymatic activity was observed.

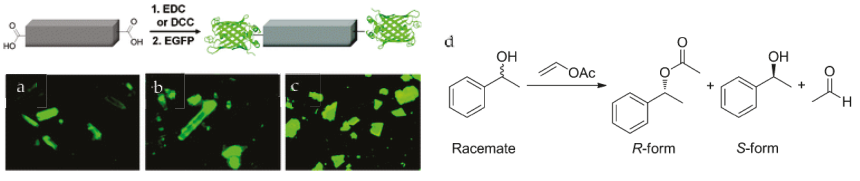

Figure 1. Schematic representation of the bioconjugation of the 1D-polymer, $[(Et_2NH_2)(In(pda)_2)]_n$, with EGFP. Fluorescence microscopic images of EGFP coatedMOFs. (**a**) 1D + EGFP; (**b**) 2D + EGFP; (**c**) 3D + EGFP. An Olympus WIB filter set (λ_{em} = 460–490 nm; λ_{em} > 515 nm) was used for recording the fluorescence [31]; and (**d**) the catalytic reaction of racemate and the product enantiomers. Reproduced from [31] with permission from the Royal Society of Chemistry, copyright 2011.

Ma group first reported the immobilization of MP-11 into a mesoporous MOF, Tb-mesoMOF $[Tb_{16}(tatb)_{16}$, tatb = triazine-1,3,5-tribenzoate], consisting of cages with diameters of 0.9, 3.0, and 4.1 nm (Figure 2) [32]. After the loading of MP-11, the 3.0 and 4.1 nm cavities disappeared, while the 0.9 nm pore still existed, indicating the occupation of the enzyme in large pores and the accessible small pores for substrate diffusion. The BET surface area of Tb-mesoMOF drops from 1935 m^2/g to 400 m^2/g after MP-11 loading of 19.1 μmol/g. MCM-41, a mesoporous silica material with a lower surface area at ~1000 m^2/g and a lower loading of 3.4 μmol/g [33], was also applied for MP-11 encapsulation. The MP-11@Tb-mesoMOF catalyzed the oxidation of 3,5-di-tert-butyl-catechol in the presence of H_2O_2. In comparison to free MP-11 and MP-11@MCM-41, MP-11@Tb-mesoMOF showed a much higher conversion percentage, reaction rate, and better recyclability after seven cycles. Proved by the bathochromic shift of the immobilized MP-11 in Tb-mesoMOF compared to free MP-11,

the hydrophobic interactions between the hydrophobic nanocage of Tb-mesoMOF and MP-11 were attributed to the better performance of MP-11@Tb-mesoMOF over free MP-11.

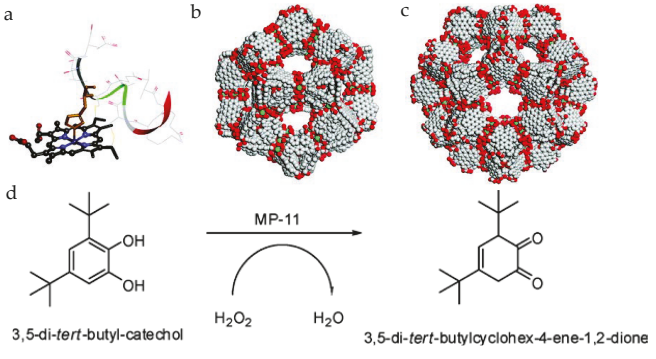

Figure 2. (**a**) Molecular structure of MP-11 (obtained from the solution structure of PDB 1OCD); (**b**) the 3.9 nm-diameter cage; (**c**) the 4.7 nm-diameter cage in Tb-mesoMOF; and (**d**) the reaction scheme for oxidation of 3,5-di-t-butylcatechol to *o*-quinone [32]. Reproduced from [32] with permission from American Chemical Society, copyright 2011.

Zhou and co-workers reported two mesoporous MOFs, PCN-332 and -333, composed of M_3O clusters and tritopic linkers (Figure 3) [34]. PCN-333(Al) showed good stability in a pH range of 3–9 and exhibited hierarchical cavities with sizes of 1.1 nm, 4.2 nm, and 5.5 nm. The mesoporous cages functioned as single-molecule traps (SMTs) to encapsulate HRP and Cyt-c, whereas MP-11 as a smaller enzyme was immobilized by multiple-enzyme encapsulation (MEE). PCN-333(Al) demonstrated record-high enzyme loading capacity and much better recyclability than porous silicate materials, for example, SBA-15. In particular, PCN-333(Al) immobilized HRP and Cyt-c exhibited stronger substrate affinity and improved catalytic performance over free enzymes owing to the separation of enzymes in the cages, which prevents the undesirable self-aggregation during the reaction.

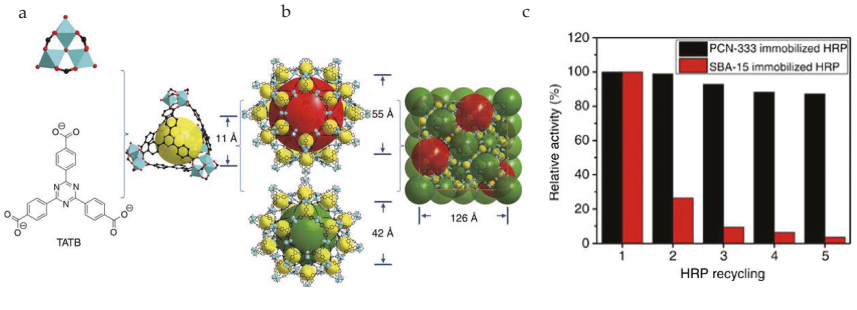

Figure 3. (**a**) Ligand and cluster used in PCN-333; (**b**) Three different cages in PCN-333; (**c**) Catalytic activity of immobilized enzymes in each recycle test [34]. Reproduced from [34] with permission from Springer Nature, copyright 2015.

Falcaro et al. provided a biomineralization approach to encapsulate biomacromolecules in ZIF-8 [35]. The ZIF-8/proteins were simply prepared by soaking the protein in 2-methylimidazole aqueous solution and mixed with zinc acetate aqueous solution. The activity of ZIF-8/HRP was examined by monitoring the rate of H_2O_2 decomposition with pyrogallol as the hydrogen donor, which can be converted to a yellowish product, purpurogallin. Owing to the excellent stability of ZIF-8, the coated DNA, proteins, and enzymes exhibited much-improved chemical and thermal stability.

For example, the immobilized HRP maintained its catalytic activity in boiling water (100 °C) or in boiling DMF (153 °C).

2.1.2. Protein Digestion and Chemical Degradation

Trypsin is a commonly-used protease that catalyzes protein digestion and transformation into peptides for proteomics analysis and industrial production. The practical application of trypsin often suffers from the long running time (18–24 h) and self-digestion in the reaction media [36] Immobilization on MOFs is capable of preventing the self-digestion and improve their recyclability. Unlike most of the catalytic reactions for chemical conversions, the substrates of trypsin are proteins, which are typically larger than the pore size of MOFs. Thus, trypsin is normally attached to the surface of MOFs instead of encapsulated inside of the pores to allow better substrate accessibility. Bovine serum albumin (BSA) digestion is usually used as the model reaction.

Lin and Huang et al. reported a novel trypsin-FITC@MOF bioreactor that showed high protein digestion efficiency [37]. Trypsin was first modified with fluorescein isothiocyanate dye (FITC) by bioconjugation via microwave. Then, FITC was trapped in the cavity of CYCU-4 ([Al(OH)(SDC)], SDC = 4,4′-stilbenedicarboxylic acid) through strong π-π interaction and hydrogen bonding between FITC and MOF linker. In the BSA digestion test, FITC@CYCU-4 obtained 47 matched peptides and 72% sequence coverage confirmed by nanoLC-MS^2 followed with Mascot database searching. These results were comparable to free trypsin-FITC. The same group also reported a similar dye-assisted enzyme immobilization method utilizing a small molecular dye, 4-chloro-7-nitrobenzofurazan (NBD) [38]. The dye-modified trypsin exhibited the best activities when immobilized on CYCU-4 and UiO-66, which demonstrated 69–71% conversion percentage even after five consecutive catalytic cycles. On the contrary, NBD-FITC@MIL-100 or MIL-101 only demonstrated moderate activities. This can be ascribed to the size mismatch between NBD and the cavities of MOFs (MIL-100 or MIL-101).

The same group synthesized covalent linkage trypsin-MOF composite (Figure 4) [39]. MIL-101(Cr), MIL-88B(Cr), and MIL-88B-NH_2(Cr) were firstly activated by *N*,*N*′-dicyclohexylcarbodiimide (DCC) and then conjugated with trypsin through the formation of peptide bonds. The digestion of BSA was performed with the assistance of ultrasonication for 2 min. Trypsin-MIL-88B-NH_2(Cr) showed much higher amino acid sequence coverage percentage and more matched peptides than the other two composites. This can be ascribed to the higher substrate affinity of MIL-88B-NH_2 through the hydrogen bond between the surface amino groups on MOF and the protein. The BSA digestion result of trypsin-MIL-88B-NH_2 was similar to that of free trypsin, indicating that the immobilization did not compromise enzyme activity or substrate accessibility.

Hupp and Farha et al. reported the encapsulation of organophosphorus acid anhydrolase (OPAA), a nerve agent detoxifying enzyme, by using PCN-128y ($[Zr_6O_4(OH)_8(ettc)_2]$, ettc = (4′,4″,4‴,4⁗-(ethene-1,1,2,2-tetrayl)tetrakis-([1,1′-biphenyl]-4-carboxylate)) (Figure 5) [40]. PCN-128y is a water-stable MOF that possesses 4.4 nm mesoporous 1-D channels. Diisopropyl fluorophosphate (DFP), a less toxic nerve agent simulant, and Soman, an extremely toxic nerve agent, were detoxified by OPAA@PCN-128y. PCN-128y achieved 12 wt % loading of OPAA. Both free OPAA and immobilized OPAA reached the conversion percentage of 80–90% for DFP. The immobilized OPAA demonstrated a considerably better conversion percentage than free OPAA at elevated temperature and after three days. The hierarchical structure of PCN-128y allows it to host OPAA in the large channels and has an efficient mass transfer of reactant and product in the smaller channels.

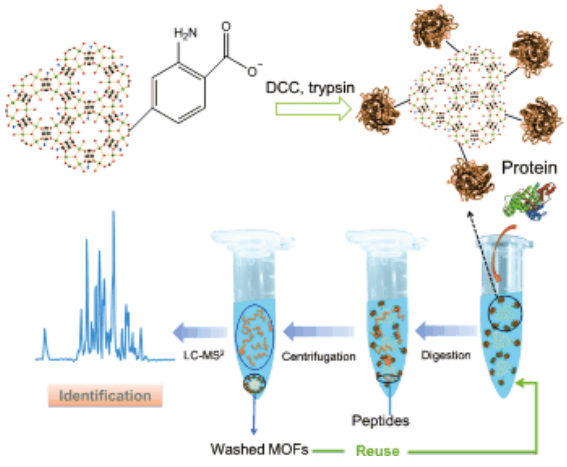

Figure 4. Schematic of trypsin immobilization on MIL-88B-NH_2(Cr), protein digestion through trypsin-MOF, and identification by LC-MS^2. Reproduced from [39] with permission from John Wiley and Sons, copyright 2012.

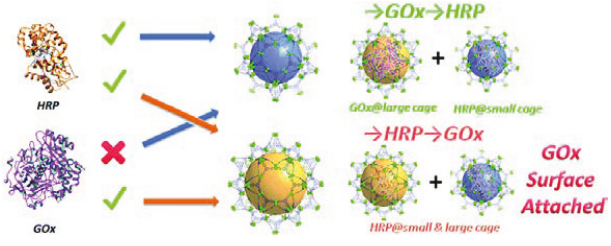

Figure 5. Schematic of the results of the stepwise encapsulation of GOx and HRP with different loading orders in PCN-888. Reproduced from [41] with permission from Royal Society of Chemistry, copyright 2016.

2.1.3. Tandem Reaction with Multiple Enzymes

Tandem reaction is a chemical process that comprises at least two consecutive reactions [42]. The products of the previous step become the substrates in the next step of the reaction under the same condition without the necessity of isolating the intermediates. Thus, compared with single enzyme immobilization, more delicate designs are needed to immobilize multiple enzymes in the same system to catalyze tandem reactions.

Inspired by the hierarchical structure and ligand extension strategy, PCN-888 was rationally designed as a tandem nanoreactor that possessed even larger cavities for the co-encapsulation of HRP and GOx (Figure 5) [41]. The loading order of the two enzymes (GOx first, HRP second) was essential for the preparation of the bi-enzyme nanoreactor. The reversed order would end up loading HRP in both large and intermediate pores and attaching GOx only on the MOF surface. In the bi-enzyme system, GOx catalyzed the oxidation of glucose by oxygen, yielding gluconolactone and hydrogen peroxide. The latter was the substrate in the conversion of ABTS to $ABTS^+$ catalyzed by HRP. The generation of $ABTS^+$, as monitored by UV–VIS spectroscopy at 403 nm, was utilized to trace the reaction. The leaching of enzymes from PCN-888 was negligible, which could be due to the presence of the π-π interaction between the enzyme and the conjugated heptazine core and terminal benzene rings on the ligands.

A recent work by Zhou et al. reported the encapsulation of two antioxidative enzymes, SOD and CAT, in fluorescent nanoscale PCN-333 (FNPCN-333) for the removal of toxic reactive oxygen species from human cells [43]. SOD catalyzes the disproportionation of superoxide and generates hydrogen peroxide and oxygen. Hydrogen peroxide is further decomposed into water and oxygen catalyzed by CAT. The loading of SOD and CAT was conducted in a similar stepwise manner. The as-synthesized "nanofactory" was tested to be stable in the acidic environment and was enzymatically functional in endocytic organelles. Compared with free enzymes, the enzyme@MOF nanofactory demonstrated intracellular enzymatic activity for up to a week, thanks to the MOF protection against the proteolytic digestion and acidic organelle environment.

2.2. Applications in Sensing and Detection

Bio-catalyst immobilized sensing and detection devices, in other words, biosensors, are of great interest in the field of glucose monitoring, food analysis, cancer diagnosis, etc. Especially, glucose biosensors account for approximately 85% of the entire biosensor market owing to the great need of millions of daily diabetics test to monitor blood glucose levels [44]. GOx, GDH, and hexokinase are three of commonly-used enzymes for glucose measurements [45]. The general aim of the design of a biosensor is to allow quick and convenient testing at the point of concern or care where the sample is procured. This requires the enzymes of the biosensors to be stable and functional in an unnatural environment. Thus, MOFs are considered as promising immobilization matrices to effectively protect the enzymes against perturbations.

Mao and Yang et al. utilized a series of zeolitic imidazolate frameworks (ZIFs), including ZIF-7, -8, -67, -68, and -70, as the matrices to immobilize methylene green (MG) and GDH as biosensors (Figure 6) [46]. To prepare the biosensor, a MG/ZIF composite was drop-coated on a glassy carbon electrode and then GDH was coated. Among the five ZIFs, MG/ZIF-70 composite biosensor showed the best performance with a glucose sensitivity linear range of 0.1–2 mM and a sensitivity of 54 mA M^{-1} cm^{-2}. In addition, this ZIF-based biosensor demonstrated a quick response and high selectivity for in vivo monitoring of glucose in the cerebral system.

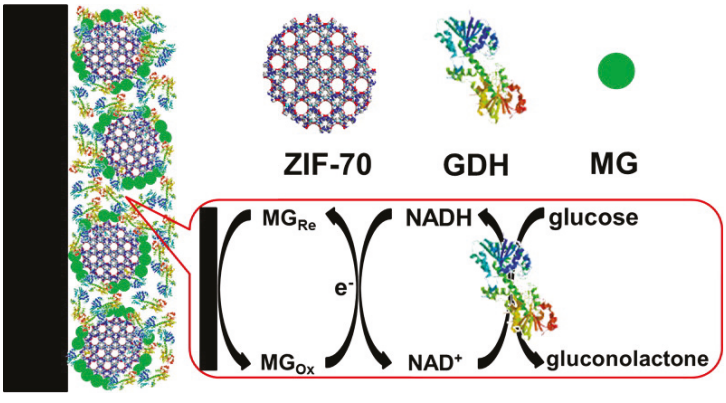

Figure 6. Schematic of the design of ZIF-70-based electrochemical biosensor. Reproduced from [46] with permission from American Chemical Society, copyright 2013.

Mass transfer and electron transfer are two fundamental factors for an effective biosensor. Legrand and Steunou et al. incorporated Pt nanoparticles (PtNP) together with GOx in the MIL-100(M) (M = Fe, Cr, Al) and MIL-127(Fe) in order to improve the conductivity [47]. The sensor was assembled by successive deposition of MOFs and GOx on the surface of PtNP-CIE (CIE = carbon ink electrode). Among all the MOFs applied, MIL-100(Fe) based biosensor exhibited the best performance, which was

likely owing to a synergism of the structural properties of MIL-100(Fe) and the catalytic properties of Fe^{3+}. The glucose sensitivity was determined to be 71 mA M^{-1} cm^{-2} and the response time was under 5 s. The sensors based on other MOFs presented non-linear relationships in the range of low glucose concentration and much longer response times.

Liu et al. reported a composite that was prepared using amino-containing MOF (MIL-101(Al)-NH_2) as the host support to anchor Hemin as an enzyme mimic in order to simulate the peptidic microenvironment in the native peroxidase [48]. The oxidation of 3,3,5,5-tetramethylbenzidine (TMB) by H_2O_2 and the oxidation of glucose catalyzed by GOx were used to evaluate its performance. TMB oxidation demonstrated a linear range with the concentration of H_2O_2 from 5.0 μM to 200 μM (R^2 = 0.994). For the glucose detection, it was observed to have a linear range from 10 μM to 300 μM (R^2 = 0.993).

3. Conclusions

In summary, we reviewed a variety of applications of MOF-based immobilized bio-catalysts in chemical conversion, protein digestion, tandem reaction, sensing, and detection. MOFs, as the porous solid supports, normally provide the separation of enzymes (in other words, avoiding aggregation), shielding for enzymes against perturbation conditions, cavity micro-environment that may benefit MOF-enzyme interaction and substrate diffusion, and potential catalytic sites from metal clusters or organic linkers. These benefiting factors, in turn, offer better reusability and better catalytic activity compared to free enzymes. However, it is worth noting that even though this area has been studied for almost a decade, there is still a large gap between benchtop results and practical applications. Many of the catalytic reactions and protein digestion cases are proof-of-concept models at ex vivo conditions. The specific interaction sites between the framework of MOFs and biocatalysts are largely unknown. The same statement can be made for the exact effect of the confined environment in MOF cavities on the diffusion of the substrate and product. The size matching between MOFs' pores and enzymes plays a key role in the encapsulation approach as shown in some examples mentioned. The large enzyme may not be able to enter small MOF pores via post-synthetic method, whereas small enzymes may suffer from leaching problems in large pores. The rational design of MOFs that matches the size of enzymes well and provides excellent substrates/products would be of great interest for future study. In addition, few reported examples have shown the capability to immobilize multiple enzymes in one MOF system for tandem reactions. The development of the multi-enzyme systems would have the potential to gain more commercial popularity owing to their multifunctionalities.

Acknowledgments: This work was supported by the Robert A. Welch foundation through the Welch Endowed Chair to HJZ (A-0030) and the Strategic Transformative Research Program, College of Science, Texas A&M University.

Author Contributions: This is a review paper. Q.W. and X.L. discussed the scope and the content of the review. Q.W. wrote the manuscript. X.L. and Y.F. edited the manuscript.

Conflicts of Interest: The authors declare no conflict of interest.

Abbreviations

ABTS	2,2′-Azino-bis(3-ethylbenzothiazoline-6-sulphonic acid)
BPYDC	2,2′-bipyridine 5,5′-dicarboxylate
BSA	Bovine serum albumin
CAL-B	Candida-antarctica-lipase-B
CAT	Catalase
CIE	Carbon ink electrode
CYCU	Chung Yuan Christian University
Cyt c	Cytochrome c

DMF	*N*,*N*′-Dimethylformimade
EDC	1-Ethyl-3-(3-dimethylaminopropyl)carbodiimide
EGFP	Enhanced green fluorescent protein
ETTC	4′,4″,4‴,4⁗-(ethene-1,1,2,2-tetrayl)tetrakis-([1,1′-biphenyl]-4-carboxylate)
FITC	Fluorescein isothiocyanate
GDH	Glucose dehydrogenase
GOx	Glucose oxidase
HRP	Horseradish peroxidase
MCM	Mobil Composition of Matter
MEE	Multi-enzyme encapsulation
MG	Methylene green
MOF	Metal organic framework
MP-11	Microperoxidase-11
NBD	4-Chloro-7-nitrobenzofurazan
NP	Nanoparticle
OPAA	Organophosphorus acid anhydrolase
PCN	Porous coordination network
PDA	1,4-phenylenediacetic acid
SDC	4,4′-stilbenedicarboxylic acid
SEE	Single-enzyme encapsulation
SOD	Superoxide dismutase
TATB	Triazine-1,3,5-tribenzoate
TMB	Tetramethylbenzidine
ZIF	Zeolitic imidazolate frameworks

References

1. Bornscheuer, U.T.; Huisman, G.W.; Kazlauskas, R.J.; Lutz, S.; Moore, J.C.; Robins, K. Engineering the third wave of biocatalysis. *Nature* **2012**, *485*, 185–194. [CrossRef] [PubMed]
2. Cooper, G.M.; Hausman, R.E. *The Cell: A Molecular Approach*, 3rd ed.; ASM Press: Washington, DC, USA; Sinauer Associates: Sunderland, MA, USA, 2004.
3. Schmid, A.; Dordick, J.S.; Hauer, B.; Kiener, A.; Wubbolts, M.; Witholt, B. Industrial biocatalysis today and tomorrow. *Nature* **2001**, *409*, 258–268. [CrossRef] [PubMed]
4. Majewski, M.B.; Howarth, A.J.; Li, P.; Wasielewski, M.R.; Hupp, J.T.; Farha, O.K. Enzyme encapsulation in metal-organic frameworks for applications in catalysis. *CrystEngComm* **2017**, *19*, 4082–4091. [CrossRef]
5. Lian, X.; Fang, Y.; Joseph, E.; Wang, Q.; Li, J.; Banerjee, S.; Lollar, C.; Wang, X.; Zhou, H.C. Enzyme-MOF (metal-organic framework) composites. *Chem. Soc. Rev.* **2017**, *46*, 3386–3401. [CrossRef] [PubMed]
6. Zhou, Z.; Hartmann, M. Recent progress in biocatalysis with enzymes immobilized on mesoporous hosts. *Top. Catal.* **2012**, *55*, 1081–1100. [CrossRef]
7. Zhou, Z.; Hartmann, M. Progress in enzyme immobilization in ordered mesoporous materials and related applications. *Chem. Soc. Rev.* **2013**, *42*, 3894–3912. [CrossRef] [PubMed]
8. Xu, C.-P.; Yun, J.W. Influence of aeration on the production and the quality of the exopolysaccharides from *Paecilomyces tenuipes* C240 in a stirred-tank fermenter. *Enzym. Microb. Technol.* **2004**, *35*, 33–39. [CrossRef]
9. Zhou, H.C.; Long, J.R.; Yaghi, O.M. Introduction to metal-organic frameworks. *Chem. Rev.* **2012**, *112*, 673–674. [CrossRef] [PubMed]
10. Zhou, H.C.; Kitagawa, S. Metal-organic frameworks (MOFs). *Chem. Soc. Rev.* **2014**, *43*, 5415–5418. [CrossRef] [PubMed]
11. Qin, J.S.; Yuan, S.; Wang, Q.; Alsalme, A.; Zhou, H.C. Mixed-linker strategy for the construction of multifunctional metal-organic frameworks. *J. Mater. Chem. A* **2017**, *5*, 4280–4291. [CrossRef]
12. Perry Iv, J.J.; Perman, J.A.; Zaworotko, M.J. Design and synthesis of metal-organic frameworks using metal-organic polyhedra as supermolecular building blocks. *Chem. Soc. Rev.* **2009**, *38*, 1400–1417. [CrossRef] [PubMed]

13. Tranchemontagne, D.J.; Mendoza-Cortes, J.L.; O'Keeffe, M.; Yaghi, O.M. Secondary building units, nets and bonding in the chemistry of metal-organic frameworks. *Chem. Soc. Rev.* **2009**, *38*, 1257–1283. [CrossRef] [PubMed]
14. Lee, J.Y.; Farha, O.K.; Roberts, J.; Scheidt, K.A.; Nguyen, S.T.; Hupp, J.T. Metal–organic framework materials as catalysts. *Chem. Soc. Rev.* **2009**, *38*, 1450–1459. [CrossRef] [PubMed]
15. Long, J.R.; Yaghi, O.M. The pervasive chemistry of metal-organic frameworks. *Chem. Soc. Rev.* **2009**, *38*, 1213–1214. [CrossRef] [PubMed]
16. Cozzolino, A.F.; Brozek, C.K.; Palmer, R.D.; Yano, J.; Li, M.; Dincă, M. Ligand redox non-innocence in the stoichiometric oxidation of Mn_2(2,5-dioxidoterephthalate) (Mn-MOF-74). *J. Am. Chem. Soc.* **2014**, *136*, 3334–3337. [CrossRef] [PubMed]
17. Hirai, K.; Reboul, J.; Morone, N.; Heuser, J.E.; Furukawa, S.; Kitagawa, S. Diffusion-coupled molecular assembly: Structuring of coordination polymers across multiple length scales. *J. Am. Chem. Soc.* **2014**, *136*, 14966–14973. [CrossRef] [PubMed]
18. Sumida, K.; Rogow, D.L.; Mason, J.A.; McDonald, T.M.; Bloch, E.D.; Herm, Z.R.; Bae, T.-H.; Long, J.R. Carbon dioxide capture in metal–organic frameworks. *Chem. Rev.* **2012**, *112*, 724–781. [CrossRef] [PubMed]
19. Murray, L.J.; Dinca, M.; Long, J.R. Hydrogen storage in metal-organic frameworks. *Chem. Soc. Rev.* **2009**, *38*, 1294–1314. [CrossRef] [PubMed]
20. Yanai, N.; Kitayama, K.; Hijikata, Y.; Sato, H.; Matsuda, R.; Kubota, Y.; Takata, M.; Mizuno, M.; Uemura, T.; Kitagawa, S. Gas detection by structural variations of fluorescent guest molecules in a flexible porous coordination polymer. *Nat. Mater.* **2011**, *10*, 787–793. [CrossRef] [PubMed]
21. Rosi, N.L.; Eckert, J.; Eddaoudi, M.; Vodak, D.T.; Kim, J.; O'Keeffe, M.; Yaghi, O.M. Hydrogen storage in microporous metal-organic frameworks. *Science* **2003**, *300*, 1127–1129. [CrossRef] [PubMed]
22. Zhao, X.; Xiao, B.; Fletcher, A.J.; Thomas, K.M.; Bradshaw, D.; Rosseinsky, M.J. Hysteretic adsorption and desorption of hydrogen by nanoporous metal-organic frameworks. *Science* **2004**, *306*, 1012–1015. [CrossRef] [PubMed]
23. Horcajada, P.; Gref, R.; Baati, T.; Allan, P.K.; Maurin, G.; Couvreur, P.; Férey, G.; Morris, R.E.; Serre, C. Metal–organic frameworks in biomedicine. *Chem. Rev.* **2012**, *112*, 1232–1268. [CrossRef] [PubMed]
24. Zhang, T.; Lin, W. Metal-organic frameworks for artificial photosynthesis and photocatalysis. *Chem. Soc. Rev.* **2014**, *43*, 5982–5993. [CrossRef] [PubMed]
25. Bosch, M.; Sun, X.; Yuan, S.; Chen, Y.P.; Wang, Q.; Wang, X.; Zhou, H.C. Modulated synthesis of metal-organic frameworks through tuning of the initial oxidation state of the metal. *Eur. J. Inorg. Chem.* **2016**, *2016*, 4368–4372. [CrossRef]
26. Wang, X.; Makal, T.A.; Zhou, H.-C. Protein immobilization in metal–organic frameworks by covalent binding. *Aust. J. Chem.* **2014**, *67*, 1629–1631. [CrossRef]
27. Raja, D.S.; Liu, W.-L.; Huang, H.-Y.; Lin, C.-H. Immobilization of protein on nanoporous metal-organic framework materials. *Comments Inorg. Chem.* **2015**, *35*, 331–349. [CrossRef]
28. Mehta, J.; Bhardwaj, N.; Bhardwaj, S.K.; Kim, K.-H.; Deep, A. Recent advances in enzyme immobilization techniques: Metal-organic frameworks as novel substrates. *Coord. Chem. Rev.* **2016**, *322*, 30–40. [CrossRef]
29. Chen, Y.; Ma, S. Biomimetic catalysis of metal-organic frameworks. *Dalton Trans.* **2016**, *45*, 9744–9753. [CrossRef] [PubMed]
30. Gkaniatsou, E.; Sicard, C.; Ricoux, R.; Mahy, J.-P.; Steunou, N.; Serre, C. Metal-organic frameworks: A novel host platform for enzymatic catalysis and detection. *Mater. Horiz.* **2017**, *4*, 55–63. [CrossRef]
31. Jung, S.; Kim, Y.; Kim, S.J.; Kwon, T.H.; Huh, S.; Park, S. Bio-functionalization of metal-organic frameworks by covalent protein conjugation. *Chem. Commun.* **2011**, *47*, 2904–2906. [CrossRef] [PubMed]
32. Lykourinou, V.; Chen, Y.; Wang, X.-S.; Meng, L.; Hoang, T.; Ming, L.-J.; Musselman, R.L.; Ma, S. Immobilization of mp-11 into a mesoporous metal–organic framework, mp-11@mesomof: A new platform for enzymatic catalysis. *J. Am. Chem. Soc.* **2011**, *133*, 10382–10385. [CrossRef] [PubMed]
33. Hartmann, M. Ordered mesoporous materials for bioadsorption and biocatalysis. *Chem. Mater.* **2005**, *17*, 4577. [CrossRef]
34. Feng, D.; Liu, T.-F.; Su, J.; Bosch, M.; Wei, Z.; Wan, W.; Yuan, D.; Chen, Y.-P.; Wang, X.; Wang, K.; et al. Stable metal-organic frameworks containing single-molecule traps for enzyme encapsulation. *Nat. Commun.* **2015**, *6*, 5979. [CrossRef] [PubMed]

35. Liang, K.; Ricco, R.; Doherty, C.M.; Styles, M.J.; Bell, S.; Kirby, N.; Mudie, S.; Haylock, D.; Hill, A.J.; Doonan, C.J.; et al. Biomimetic mineralization of metal-organic frameworks as protective coatings for biomacromolecules. *Nat. Commun.* **2015**, *6*, 7240. [CrossRef] [PubMed]
36. Casadonte, F.; Pasqua, L.; Savino, R.; Terracciano, R. Smart trypsin adsorption into *N*-(2-aminoethyl)-3-aminopropyl-modified Mesoporous Silica for Ultra Fast protein digestion. *Chem. Eur. J.* **2010**, *16*, 8998–9001. [CrossRef] [PubMed]
37. Liu, W.-L.; Lo, S.-H.; Singco, B.; Yang, C.-C.; Huang, H.-Y.; Lin, C.-H. Novel trypsin-FITC@MOF bioreactor efficiently catalyzes protein digestion. *J. Mater. Chem. B* **2013**, *1*, 928–932. [CrossRef]
38. Liu, W.-L.; Wu, C.-Y.; Chen, C.-Y.; Singco, B.; Lin, C.-H.; Huang, H.-Y. Fast multipoint immobilized MOF bioreactor. *Chem. Eur. J.* **2014**, *20*, 8923–8928. [CrossRef] [PubMed]
39. Shih, Y.-H.; Lo, S.-H.; Yang, N.-S.; Singco, B.; Cheng, Y.-J.; Wu, C.-Y.; Chang, I.H.; Huang, H.-Y.; Lin, C.-H. Trypsin-immobilized metal–organic framework as a biocatalyst in proteomics analysis. *ChemPlusChem* **2012**, *77*, 982–986. [CrossRef]
40. Li, P.; Moon, S.-Y.; Guelta, M.A.; Harvey, S.P.; Hupp, J.T.; Farha, O.K. Encapsulation of a nerve agent detoxifying enzyme by a mesoporous zirconium metal–organic framework engenders thermal and long-term stability. *J. Am. Chem. Soc.* **2016**, *138*, 8052–8055. [CrossRef] [PubMed]
41. Lian, X.; Chen, Y.-P.; Liu, T.-F.; Zhou, H.-C. Coupling two enzymes into a tandem nanoreactor utilizing a hierarchically structured MOF. *Chem. Sci.* **2016**, *7*, 6969–6973. [CrossRef] [PubMed]
42. Tietze, L.F.; Beifuss, U. Sequential transformations in organic chemistry: A synthetic strategy with a future. *Angew. Chem. Int. Ed. Engl.* **1993**, *32*, 131–163. [CrossRef]
43. Lian, X.; Erazo-Oliveras, A.; Pellois, J.-P.; Zhou, H.-C. High efficiency and long-term intracellular activity of an enzymatic nanofactory based on metal-organic frameworks. *Nat. Commun.* **2017**, *8*, 2075. [CrossRef] [PubMed]
44. Wang, J. Electrochemical glucose biosensors. *Chem. Rev.* **2008**, *108*, 814–825. [CrossRef] [PubMed]
45. Yoo, E.-H.; Lee, S.-Y. Glucose biosensors: An overview of use in clinical practice. *Sensors (Basel)* **2010**, *10*, 4558. [CrossRef] [PubMed]
46. Ma, W.; Jiang, Q.; Yu, P.; Yang, L.; Mao, L. Zeolitic imidazolate framework-based electrochemical biosensor for in vivo electrochemical measurements. *Anal. Chem.* **2013**, *85*, 7550–7557. [CrossRef] [PubMed]
47. Patra, S.; Hidalgo Crespo, T.; Permyakova, A.; Sicard, C.; Serre, C.; Chausse, A.; Steunou, N.; Legrand, L. Design of metal organic framework-enzyme based bioelectrodes as a novel and highly sensitive biosensing platform. *J. Mater. Chem. B* **2015**, *3*, 8983–8992. [CrossRef]
48. Qin, F.-X.; Jia, S.-Y.; Wang, F.-F.; Wu, S.-H.; Song, J.; Liu, Y. Hemin@metal-organic framework with peroxidase-like activity and its application to glucose detection. *Catal. Sci. Technol.* **2013**, *3*, 2761–2768. [CrossRef]

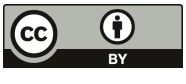

© 2018 by the authors. Licensee MDPI, Basel, Switzerland. This article is an open access article distributed under the terms and conditions of the Creative Commons Attribution (CC BY) license (http://creativecommons.org/licenses/by/4.0/).

catalysts

MDPI

Communication

In-Situ Self-Assembly of Zinc/Adenine Hybrid Nanomaterials for Enzyme Immobilization

Hao Liang †, Shanshan Sun †, Yan Zhou and Yanhui Liu *

State Key laboratory of Chemical Resource Engineering, Beijing University of Chemical Technology, 15 Beisanhuan East Road, Chaoyang District, Beijing 100029, China; starslh@163.com (H.L.); shanshansun3785@163.com (S.S.); zhouyan@mail.buct.edu.cn (Y.Z.)

* Correspondence: liuyh@mail.buct.edu.cn; Tel.: +86-10-6442-1335

† These two authors contributed equally to this work.

Received: 16 October 2017; Accepted: 27 October 2017; Published: 3 November 2017

Abstract: In this study, a one-step and facile immobilization of enzymes by self-assembly of zinc ions and adenine in aqueous solution with mild conditions was reported. Enzymes, such as glucose oxidase (GOx) and horseradish peroxidase (HRP), could be efficiently encapsulated in Zn/adenine coordination polymers (CPs) with high loading capacity over 90%. When the enzyme was immobilized by CPs, it displayed high catalytic efficiency, high selectivity and enhanced stability due to the protecting effect of the rigid framework. As a result, the relative activity of Zn/adenine nano-CP-immobilized GOx increased by 1.5-fold at pH 3 and 4-fold at 70 to 90 °C, compared to free GOx. The immobilized GOx had excellent reusability (more than 90% relative activity after being reused eight times). Furthermore, the use of this system as a glucose biosensor was also demonstrated by co-immobilization of two enzymes, detecting glucose down to 1.84 μM with excellent selectivity. The above work indicated that in-situ self-assembly of Zn/adenine CPs could be a simple and efficient method for biocatalyst immobilization.

Keywords: adenine; enzyme; self-assembly; coordination polymers; immobilization

1. Introduction

Enzymes are a typical class of biocatalysts, having been used in a variety of scientific and technical areas. For instance, they have wide applications in the fields of fine and bulk chemicals, foods, pharmaceutical science, cosmetics, textiles and paper industries, due to their high catalytic activity, high selectivity, low toxicity and water solubility [1–6]. However, the disadvantages of free enzymes, including high cost, poor operational stability and challenges in recovery and reuse, have limited industrial applications of enzymes [7]. To solve these issues, immobilization techniques are considered, because binding of free enzymes to supports limits their mobility [8]. What is more, some immobilized enzymes could show more robust activity than free enzymes [9–12].

Conventional immobilization methods are generally divided into four main categories; adsorption, covalent binding, entrapment and cross-linking [13–22]. However, there are several disadvantages in the conventional immobilization methods, such as the lack of effective reusability, difficulties in immobilization, a severe loss of enzymatic activity due to the blocking of the active site of the enzyme, restricted flexibility and mass-transfer limitations between the enzyme and substrate [13]. Therefore, some new methods and materials to immobilize enzymes have been developed.

Coordination polymers (CPs), formed by metal ions and bridging organic ligands, have recently received considerable attention and are considered as new functional composite materials [23–27]. Because of their mild polymerization conditions, porosity and high guest-entrapment efficiency [11], CPs could play important roles in many fields, including catalysis [12], biological detection [28], imaging [29,30], gas storage [31] and drug delivery [32].

In nature, biomolecules normally have excellent metal-coordination properties [33]. Up to now, various types of biomolecules, such as nucleotides [34], proteins [35], peptides [36], amino acids [37] and nucleobases [38] have been used as the ligands to construct CPs. It also has been demonstrated that some CPs are capable of adsorbing and entrapping a broad range of molecules, due to their good biocompatibility and porosity [34,39]. Adenine, as an important naturally occurring nitrogen heterocycle present in nucleic acids [40], has multiple possible metal-binding modes [41–43]. It has been reported that adenine could coordinate with Zn [44], Au [45], Ag [46], Co [47] or Cu [48] to form CPs with diversified morphology and structure. However, most of the researchers just studied the structure of these materials, and very few have studied the encapsulating adaptability of CPs and the activity of guests after they were entrapped. What is more, those CPs that have been reported were formed by harsh reaction conditions, complicated syntheses and with high cost [44–48].

In this work, we reported a convenient, efficient and high-capacity immobilization method for enzymes by the entrapment of glucose oxidase (GOx) and horseradish peroxidase (HRP) within Zn/adenine CPs. We used adenine and zinc in aqueous solution without adding other linkers to form CPs by in-situ self-assembly. Fourier transform infrared spectroscopy (FTIR), X-ray diffraction (XRD), scanning electron microscopy (SEM) and transmission electron microscopy (TEM) were performed to characterize the CPs. After the CPs was confirmed with promising encapsulating capacity, we use them to immobilize enzymes. The enzyme activity, pH and thermostability of immobilized enzymes were also investigated. The results revealed that the immobilized enzymes showed high catalytic efficiency, enhanced stability and recyclable usability. Besides, a highly sensitive and selective biosensor for glucose was prepared using the CPs to co-immobilize glucose oxidase and horseradish peroxidase for an enzyme cascade system. The Zn/adenine CPs were promising for enzyme immobilization.

2. Results and Discussion

2.1. Preparation and Characterization of Zn/Adenine Complexes

We first tested the in-situ self-assembly of zinc ions and adenine. The synthesis of the Zn/adenine composite was performed by mixing zinc chloride solution, adenine and 4-(2-hydroxyethyl)-1-piperazineethanesulfonic acid (HEPES) buffer at room temperature. Then, a white solid precipitate quickly appeared. To understand the formation of the coordination complexes, the coordination of Zn^{2+} and adenine was studied in different concentrations of HEPES (Figure S1a). The amounts of Zn/adenine composite increased with increasing HEPES concentration (Figure S1b). High HEPES concentration was beneficial to the formation of complexes. The coordination of Zn^{2+} and adenine was also studied in different pH and ionic strength. As shown in Figure S1c, the yield of Zn/adenine composites reached the maximum at pH 7.8. Low pH leads to the protonation of adenine [40], which would inhibit the coordination of Zn^{2+} ions. Then, the self-assembly reaction was performed at different ionic strengths. It could be found that the amounts of Zn/adenine composite increased with increasing NaCl concentration (Figure S1d). The solubility of adenine in aqueous solution was weakened in high ionic-strength solutions, and it would intensify the reaction of Zn^{2+} ions and adenine [34].

To gain a further understanding of the Zn/adenine composite, we characterized CPs by FTIR, XRD, SEM and TEM. As shown in Figure 1a, the shift of the IR band may suggest coordination interactions between Zn^{2+} and N_9 (from 1418.4 cm^{-1} in adenine to 1401.2 cm^{-1} in the coordination polymer) [45]. The 1671.8 cm^{-1} band of adenine was considered to arise from the NH_2 scissoring vibrational mode [45]. The corresponding NH_2 IR band of the coordination polymer was observed at 1643.0 cm^{-1}. The shift of the NH_2 IR band could be attributed to the C_6–NH_2 coordination with Zn^{2+}. The assignments of FTIR spectra of adenine and Zn/adenine complexes were listed (Table S1). According to the results of XRD (Figure 1b), no sharp diffraction peaks were observed in Zn/adenine complexes, indicating the amorphous nature of Zn/adenine complexes. This may be caused by the asymmetric chemical structure of nucleobases and high coordination flexibility of zinc ions [40].

The SEM photo (Figure 1c) and TEM photo (Figure 1d) revealed that the microstructure of CPs resembles a stack of nanoparticles. From the images, we also can re-confirm the amorphous nature of the nano CPs. Zn^{2+} ions and adenine may firstly form nanoparticles, and then these nanoparticles assemble together (Figure S2). Finally, the stoichiometry of Zn/adenine CPs determined by the titration experiment was adenine:Zn^{2+} = 1:2 (Figure S3). We considered that adenine bridges four Zn^{2+} ions through the N_3, N_7, N_9 and NH_2 sites, forming a framework structure (Figure 2). This coordination mode is very similar to the one observed by Hui Wei et al. [45].

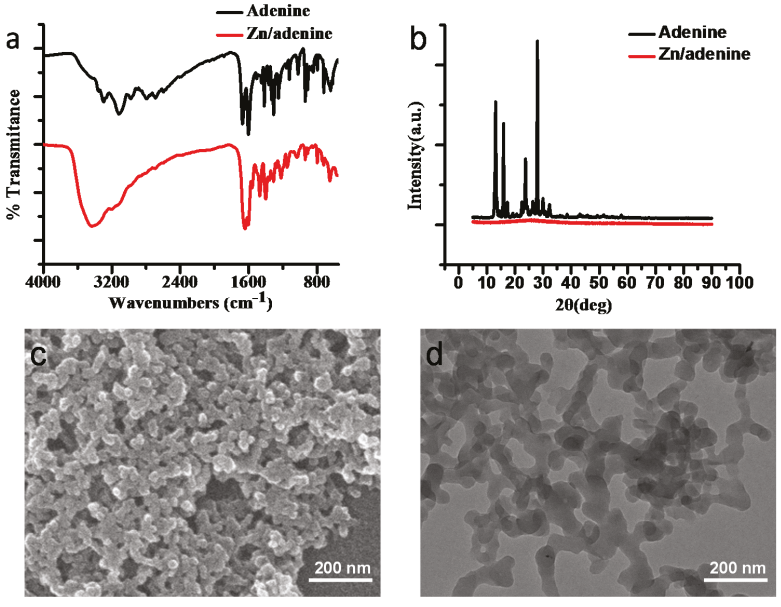

Figure 1. (**a**) The fourier transform infrared spectroscopy (FTIR) spectra of adenine and Zn/adenine complexes; (**b**) X-ray diffraction (XRD) patterns of powdery adenine and Zn/adenine complexes; (**c**) Scanning electron microscopy (SEM) image of Zn/adenine complexes (magnification = 30,000); (**d**) Transmission electron microscopy (TEM) image of Zn/adenine complexes.

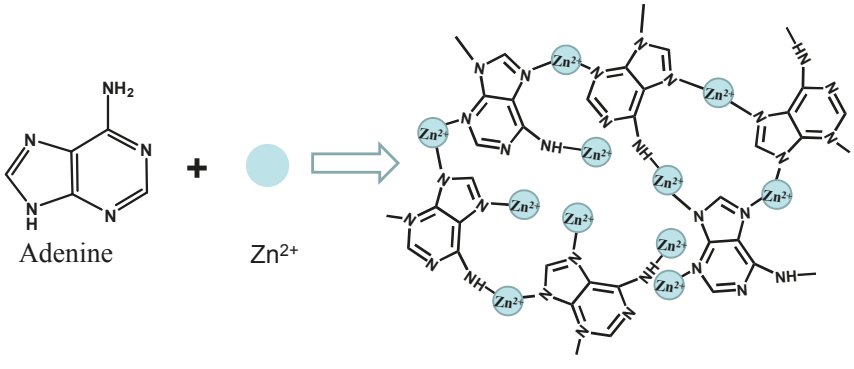

Figure 2. A scheme of Zn^{2+} reacting with adenine, forming CPs.

2.2. Encapsulation Property of Zn/Adenine Complexes

After confirming the self-assembled properties of Zn^{2+} ions and adenine, we next tested the in-situ entrapping ability of the composites using three kinds of guests (water-soluble small dyes, proteins and nanoparticles). The encapsulation ratios of guests in nano CPs were calculated by measuring the absorption intensity in the supernatant. All of the guests were encapsulated at a high efficiency (Figure 3a). For water-soluble small dyes, both of the Orange G and Amido black 10B could be encapsulated by the CPs, but the degree was different (Figure 3a). In Amido black 10B, the absorption peak almost completely disappeared in the supernatant, while in Orange G the absorption peak was left at ~30% in the supernatant (Figure S4). To study the binding capacity of Zn^{2+}/adenine to proteins, fluorescein-labeled bovine serum albumin (BSA, pI = 4.7) was next used. As shown in Figure 3a, more than 79% of BSA was efficiently entrapped. After encapsulating, the fluorescence was almost fully attenuated due to the nano-CP entrapping (Figure S4). This suggested that Zn/adenine complexes could be able to efficiently encapsulate protein molecules.

The above successes in trapping water-soluble small dyes and proteins prompted us to further investigate nanoparticles as guests. Citrate-capped 13 nm Au nanoparticles (NPs) were mixed with adenine and $ZnCl_2$. After adding adenine, bluish–violet precipitation formed. The encapsulation ratio of Au NPs in CPs was calculated by measuring the absorption intensity in the supernatant (Figure S4). There was almost no absorption in the supernatant of Au–Zn/adenine complexes, suggesting successful encapsulation. As shown in Figure 3b, the entrapped Au NPs could also be observed by transmission electron microscopy (TEM). The round and dark nanoparticles were the Au NPs, which were entrapped by the Zn/adenine complexes. According to the above results, a diverse range of guest molecules including water-soluble small dyes, proteins and gold NPs could be encapsulated in Zn/adenine nano CPs with high loading capacity.

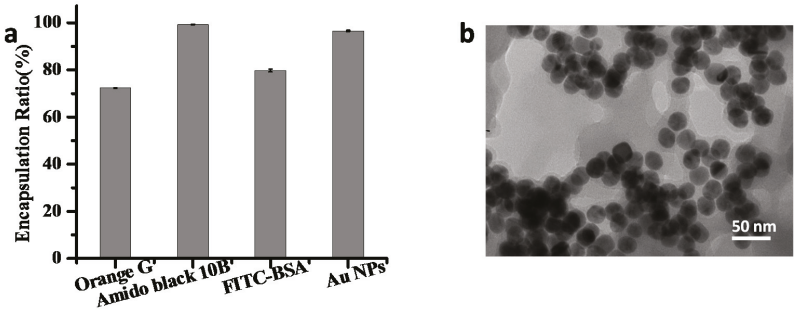

Figure 3. (**a**) The encapsulation ratios of different guests in the nano CPs; (**b**) the TEM image of the Au nanoparticles entrapped by Zn/adenine complexes.

2.3. Immobilization of Single Enzyme

Next, we employed glucose oxidase (GOx) and horseradish peroxidase (HRP) as guest molecules to test the enzyme immobilization property of the Zn/adenine complexes. The loading efficiency of GOx and HRP was 93% and 92%, respectively (Figure 4a). In our system, the immobilized enzymes showed about 20% increase in catalytic activity compared to free enzymes in solution (Figure 4a). High enzyme stability is important in applications [49–51]. High temperature and extreme pH are the major reasons for enzyme deactivation. The stability of the GOx–Zn/adenine complexes was examined at different pH values (from 3 to 10, Figure 4b) and temperatures (from 30 to 90 °C, Figure 4c) and compared with that of the free GOx in solution. The activity of the GOx–Zn/adenine complexes was more stable compared to that of the free enzymes with respect to pH. Especially at pH 3, the immobilized GOx showed a 1.5-fold increase in relative activity compared to free GOx. When the

temperature was higher, the immobilized enzyme exhibited higher activity compared with the free enzyme. As a result, the relative activity of Zn/adenine nano CP-immobilized GOx increased by 4-fold at 70 to 90 °C, compared to free GOx. The confinement of the proteins within the rigid structure of the CPs prevented protein denaturation caused by thermal fluctuations of proteins in solution [52]. Thus, the Zn/adenine complexes could protect enzymes from deactivation under heat and acid conditions. We considered that the rigid structure of the nano CPs would increase the structural stability of the embedded enzymes, thus improving the enzymes' stabilities. We also tested the recycling of the GOx–Zn/adenine complexes. The immobilized enzyme can be easily collected by centrifugation after the reaction, and can be redispersed well by vortex mixing. Results indicated that the GOx–Zn/adenine complexes could reach a relative activity of more than 90% after being reused eight times (Figure 4d).

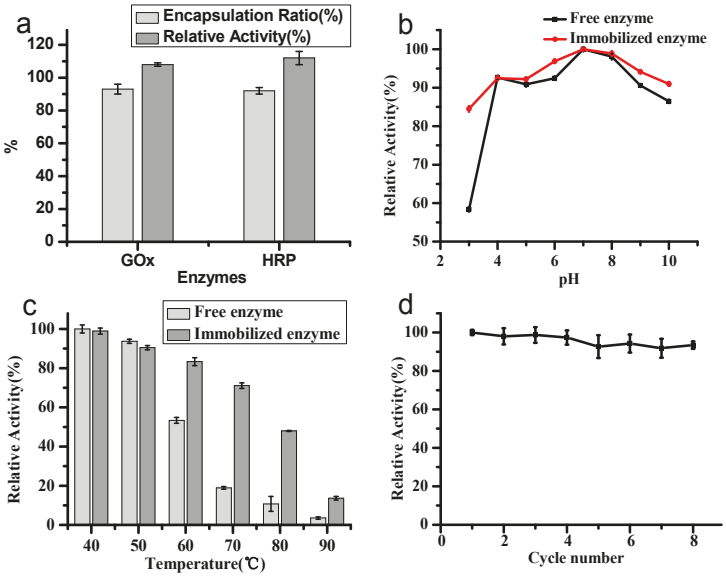

Figure 4. (**a**) Ratio of encapsulated glucose oxidase (GOx) and horseradish peroxidase (HRP) by the Zn/adenine complexes, and the relative activity of the two immobilized enzymes compared to the free enzymes; stability of the GOx–Zn/adenine complexes compared with the equivalent free enzymes (**b**) at different pH values at 25 °C; (**c**) at different temperatures; (**d**) relative activity of GOx–Zn/adenine complexes after reusing for 8 cycles.

2.4. Co-Immobilization of GOx and HRP

After establishing the feasibility of using the Zn/adenine complexes for single-enzyme immobilization, co-immobilization of multiple enzymes was further performed. Co-immobilization of multiple enzymes could enhance the overall reaction efficiency and specificity, and omit the isolation of reaction intermediates [10]. GOx specifically converts glucose to gluconic acid and produces H_2O_2 as a byproduct, which is a co-substrate for HRP to oxidize 2,2′-azinobis(3-ethylbenzothiazoline-6-sulfonic acid) diammonium salt (ABTS) [52]. Therefore, based on the above studies, GOx and HRP were chosen for a cascade reaction. The total immobilization ratio was over 90%, measured by the Bradford assay. The catalytic activities of the co-localized GOx and HRP in the Zn/adenine complexes were evaluated by reacting with glucose using ABTS as a chromogenic substrate, and they were compared with the same concentration of free GOx and HRP. However, the relative activity of single enzymes on their own was just half of the activity of the co-immobilized enzymes. The selectivity for glucose was confirmed by monitoring the absorbance at 414 nm in the presence of various competing compounds (Figure 5a).

Different concentrations of glucose were used to measure the sensitivity of the sensor. Figure 5b illustrates a good linearity between the absorbance and the concentration of glucose in the range of 0–100 μM (R^2 = 0.995). The concentration of limit of detection C_{LOD} can be expressed as a function of S (slope of the curve) and S_B (a standard deviation): $C_{LOD} = 3S_B/S$ [35]. In the experiment, S_B was determined to be calculated by three sets of blank signals, and S was 0.0049. Calculated according to the formula, the limit of detection (LOD) was determined to be 1.84 μM, which is lower than some of the previously reported colorimetric glucose sensors [35,53].

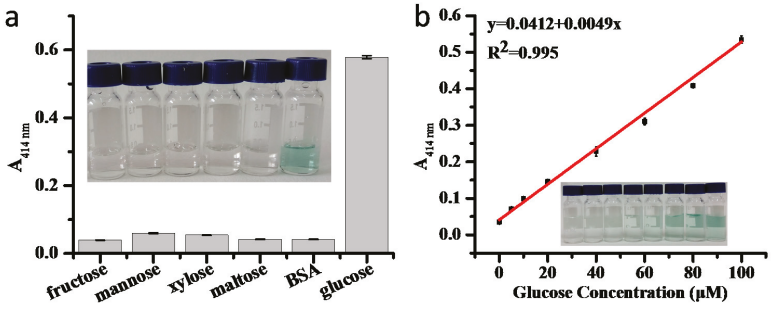

Figure 5. (**a**) The selectivity of the GOx–HRP–Zn/adenine complexes for 100 μM glucose in comparison to 100 μM fructose, mannose, xylose, maltose and 1 mg/mL bovine serum albumin (BSA) (inset: photographs of the samples.); (**b**) detection of glucose in solutions with glucose concentrations of 0–100 μM (absorbance at 414 nm was measured after incubation in solution for 10 min at room temperature) (inset: photographs of the samples).

3. Materials and Methods

3.1. Materials

Adenine, zinc chloride, sodium chloride, 2,2′-azinobis(3-ethylbenzothiazoline-6-sulfonic acid) diammonium salt (ABTS), Fe_3O_4 NPs, 4-(2-hydroxyethyl)-1-piperazineethanesulfonic acid (HEPES), Orange G, Amido black 10B, fluorescein isothiocyanate (FITC), horseradish peroxidase (HRP) and bovine serum albumin (BSA) were purchased from Aladdin Industrial Corporation. $HAuCl_4 \cdot 4H_2O$ was supplied by Sinopharm Chemical Reagent Co., Ltd. (Shanghai, China). Glucose, fructose, mannose, xylose, sucrose, sodium hydroxide, hydrochloric acid and hydrogen peroxide were purchased from Beijing Chemical Works. Glucose oxidase (GOx) was purchased from Amresco (Scottsdale, AZ, USA). Milli-Q water was used to prepare all the buffers and solutions.

3.2. Preparation of Zn and Adenine Coordinated Complexes

In a typical experiment, the Zn/adenine complexes were prepared by mixing 100 μL $ZnCl_2$ (45 mM), 100 μL adenine (15 mM) and 500 μL HEPES buffer (100 mM, pH 7.4). The volume of the system was 1 mL, and water was added to make up. After 2 h at room temperature, the samples were centrifuged at 10,000 rpm for 5 min and washed with Milli-Q water to remove remaining chemicals.

3.3. Study of the Zn/Adenine Complexes at Different Concentrations and pH of Buffer, as Well as Different Ionic Strengths

Different concentrations of HEPES buffer (pH 7.4, 0.1 M) and different pH of HEPES buffer were prepared. The Zn/adenine complexes were prepared by 500 μL buffer mixed with 100 μL adenine solution (15 mM) and 100 μL $ZnCl_2$ (45 mM). To quantify the weight of precipitations, all the samples were centrifuged, dried under 60 °C and weighed. The content of adenine remained in the supernatant was measured using UV-vis spectroscopy at 260 nm by the standard curve (Figure S5). The influence of

ionic strength was also studied. Appropriate NaCl solution (2 mM) was added into the reaction system to enhance ionic strength. The weight of precipitation and residue ratio of adenine were measured by the aforementioned method. In the experiments, the concentration of HEPES was 10, 20, 30, 40 or 50 mM. The different pH values were 6.8, 7.2, 7.4, 7.8 or 8.2. The concentration of NaCl was 100, 200, 300, 400 or 500 mM.

3.4. Stoichiometry and Structural Characterization of Zn/Adenine Complexes

The reaction ratio of adenine obtained by mixing aqueous $ZnCl_2$ (5 mL in water) and aqueous adenine (5 mL in 0.1 M HEPES buffer at pH 7.4) was plotted as a function of mixed ratio. Conditions (in reaction mixtures): [adenine] = 1.5 mM, [$ZnCl_2$] = 0, 0.75, 1.5, 2.25, 3.0, 4.5, 6.0, 7.5 and 9.0 mM. It was mixed for about two hours, and centrifuged to separate the supernatant and precipitate. The amount of adenine remained in the supernatant was measured using UV-vis spectroscopy at 260 nm.

Fourier transform infrared spectroscopy (FTIR) spectra of adenine and Zn/adenine complexes were obtained on a FTIR spectrometer (8700/Continuum XL Imaging Microscope, Nicolet, Waltham, MA, USA) with measuring wavelength ranging from 4000 to 550 cm^{-1}.

Powder X-ray diffraction (XRD) patterns of adenine and Zn/adenine complexes were determined by powder X-ray diffraction (D8 Advance X-ray diffractometer, Bruker, Karlsruhe, Germany) with a Cu Kα anode (λ = 0.15406 nm) at 40 kV and 40 mA.

Scanning electron microscopy (SEM) images of samples were taken on a S-4700 scanning electron microscope (Hitachi, Tokyo, Japan) at an accelerating voltage of 10.0 kV. Samples for SEM measurements were prepared by pipetting a drop of the solution of the coordination complexes onto a cover glass and drying on a filter paper.

Transmission electron microscopy (TEM) was performed on a Hitachi H-800 transmission electron microscope (Hitachi, Tokyo, Japan). The sample was prepared by pipetting a drop of the solution of the Zn/adenine complexes onto a 230 mesh carbon copper grid and drying on a filter paper. The Au–Zn/adenine complexes were prepared by the same method.

3.5. Encapsulation Experiment

Adenine (15 mM, 100 μL) and dye (5 mM, 10 μL), or fluorescein-labeled bovine serum albumin (FITC–BSA) (5 mg/mL, 10 μL), or Au NPs (13 nm, 10 nM, 100 μL), or Fe_3O_4 NPs (5 mg/mL, 100 μL) were mixed with HEPES buffer (0.1 M, pH 7.4, 500 μL). Then, 100 μL $ZnCl_2$ (45 mM) was added. The products were collected by centrifugation at 10,000 rpm/min for 5 min. The dyes and Au NPs in the supernatant were quantified using UV-vis spectrometry (UV-2450, Shimadzu). The FITC–BSA in the supernatant was measured by the fluorescence intensity (485/535 nm) by a microplate reader (Infinite F200 Pro, TECAN, Männedorf, Switzerland).

3.6. Immobilization of Single Enzymes

The aqueous solution of GOx (1 mg/mL) and the aqueous solution of HRP (1 mg/mL) was prepared and stored at 4 °C. Immobilization of the enzymes within the Zn/adenine complexes was performed by firstly mixing 100 μL of 15 mM adenine aqueous solution, 500 μL of HEPES buffer (0.1 M, pH 7.4), and 100 μL of enzymes. Then, 100 μL of $ZnCl_2$ (45 mM) in water was quickly added and mixed. After 2 h, the immobilized enzymes were collected by centrifugation at 10,000 rpm for 5 min. The amounts of protein incorporated into the Zn/adenine complexes were measured by the Coomassie brilliant blue method.

For the GOx activity assay, 200 μL of glucose (20 mM) solution and 200 μL of ABTS (0.5 mM) were mixed with 20 μL of free GOx (100 μg/mL) or 22 μL of the suspension of the immobilized GOx (containing the same amount of protein compared with free GOx). Then, 40 μL of HRP (100 μg/mL) were added. The mixed samples were incubated at room temperature for 5 min. The reaction was monitored with a UV/vis spectrometer at 414 nm. For the HRP activity assay, 200 μL ABTS (0.5 mM)

and 200 μL H_2O_2 (0.9 mM) were added into 0.5 μg free enzyme and equivalent immobilized enzyme, respectively. The mixed samples were incubated at room temperature for 5 min. The absorbance was recorded at 414 nm.

3.7. Enzyme Stability Test

For stability test at different pH values, the free GOx and the suspension of GOx–Zn/adenine complexes were added into 1 mL of various pH solutions for 4 h. Then, the enzymatic activity was measured by recording the absorbance at 414 nm. To test stability at different temperatures, free and immobilized enzymes were incubated at 30–90 °C for 30 min. To test the recycling of the GOx–Zn/adenine complexes, the reaction was performed for 5 min, and the immobilized enzyme was separated by centrifugation. The supernatant was measured by recording the absorbance at 414 nm. Then, new substrate and other solution were added to start the new cycle of the reaction for 5 min. The above steps were repeated several times to observe the change of the activity. In all the experiments, the error bars were calculated based on the standard deviation from three independent measurements.

3.8. Co-Immobilization of GOx and HRP

Co-immobilization of enzymes within the Zn/adenine complexes was performed by mixing 100 μL 15 mM adenine aqueous solution with 500 μL HEPES (100 mM, pH 7.4). Then, 50 μL GOx and HRP (1 mg/mL each) were added by vortex mixing. Finally, 100 μL $ZnCl_2$ (45 mM) was quickly added and mixed. After 2 h, the immobilized enzymes were collected by centrifugation at 10,000 rpm for 5 min. In co-immobilization, the total immobilized protein ratio (i.e., percentage of immobilized protein) was measured by the Coomassie brilliant blue method.

3.9. Glucose Detection with GOx–HRP–Zn/Adenine Complexes

Different concentrations of glucose (750 μL) and 1 mM ABTS (750 μL) were added into 500 μL of the suspension of GOx–HRP–Zn/adenine complexes. The samples were then incubated at room temperature for 10 min. The reaction solution was centrifuged at 10,000 rpm for 3 min, and the absorbance of the supernatants at 414 nm was measured by using a UV-1100 spectrophotometer. The selectivity was determined by the absorbance of the supernatants using 100 μM glucose as the substrate, compared with 100 μM xylose, fructose, mannose, or galactose, or 1 mg/mL BSA.

4. Conclusions

In summary, we presented a one-step, facile and general method for immobilization of enzymes by a typical metal–organic nano coordination polymer. The zinc/adenine hybrid nanomaterials were formed by self-assembly of zinc ions and adenine in aqueous solution with mild conditions. The Zn/adenine CPs showed a good adaptive encapsulating ability. A diverse range of guests, including water-soluble small dyes, proteins and nanoparticles, could be encapsulated in the nano CPs. All these guests were loaded at a high capacity. Indeed, the loading efficiency of enzymes was over 90%. The GOx–Zn/adenine complexes displayed high catalytic efficiency, high selectivity and enhanced stability due to the protecting effect of the rigid framework. As a result, the relative activity of Zn/adenine nano-CP-immobilized GOx increased by 1.5-fold at pH 3 and 4-fold at 70 to 90 °C, compared to free GOx. Moreover, the immobilized GOx could reach a relative activity of more than 90% after being reused eight times. The use of this system as a glucose biosensor was also demonstrated by co-immobilization of two enzymes, detecting glucose down to 1.84 μM with excellent selectivity. The high sensitivity, stability and recyclable usability of the immobilized enzymes against free enzymes make this method promising for biocatalyst immobilization.

Supplementary Materials: The following are available online at www.mdpi.com/2073-4344/7/11/327/s1, Figure S1: (a) a photograph of Zn^{2+} reacting with adenine in different concentrations of pH 7.4 HEPES buffer. The CP precipitant weight and the adenine percentage remained in the supernatant after Zn^{2+} reacted with adenine

and centrifugation of the samples in different concentrations of pH 7.4 HEPES buffer (b), in different HEPES pH (c) and in different ionic strengths (d); Figure S2: (a) SEM image of Zn/adenine complexes (magnification = 12,000), (b) TEM image of Zn/adenine complexes; Figure S3: The obtained titration curve of the stoichiometry of experiment. Conditions (in reaction mixtures): [adenine] = 1.5 mM, [$ZnCl_2$] = 0, 0.75, 1.5, 2.25, 3.0, 4.5, 6.0, 7.5, and 9.0 mM; Figure S4: UV-vis spectra of Amido black 10B (a) and Orange G (b), and the supernatant after Zn/adenine-complex encapsulation; (c) Photographs of the samples of fluorescein-labeled bovine serum albumin (FITC–BSA) encapsulated in Zn/adenine complexes and the control; (d) UV-vis spectra of the supernatant of Au NPs in HEPES buffer, Au NPs with Zn, with adenine and after Zn/adenine complexes encapsulated (inset: photographs of the samples); Figure S5: The standard curve of adenine with good linearity; Table S1: Assignments of FTIR spectra of adenine and Zn/adenine complexes.

Acknowledgments: This work was supported by the Beijing Natural Science Foundation (2162030), the Beijing Natural Science Foundation-Beijing Municipal Education Commission Joint Funding project (KZ201710020014), the fund of the Beijing Laboratory for Food Quality and Safety (Beijing Technology and Business University), the National Natural Science Foundation of China (21606014), the Double First-rate Program (ylkxj03) and the 111 Project (B13005).

Author Contributions: Hao Liang, Shanshan Sun, Yan Zhou and Yanhui Liu conceived and designed experiments, analyzed the data, and wrote the manuscript.

Conflicts of Interest: The authors declare no conflict of interest. The founding sponsors had no role in the design of the study; in the collection, analyses, or interpretation of data; in the writing of the manuscript, or in the decision to publish the results.

References

1. Bornscheuer, U.T.; Huisman, G.W.; Kazlauskas, R.J.; Lutz, S.; Moore, J.C.; Robins, K. Engineering the third wave of biocatalysis. *Nature* **2012**, *485*, 185–194. [CrossRef] [PubMed]
2. Choi, J.M.; Han, S.S.; Kim, H.S. Industrial applications of enzyme biocatalysis: Current status and future aspects. *Biotechnol. Adv.* **2015**, *33*, 1443–1454. [CrossRef] [PubMed]
3. Kirk, O.; Borchert, T.V.; Fuglsang, C.C. Industrial enzyme applications [review]. *Curr. Opin. Biotechnol.* **2002**, *13*, 345–351. [CrossRef]
4. Mateo, C.; Palomo, J.M.; Fernandez-Lorente, G.; Guisan, J.M.; Fernandez-Lafuente, R. Improvement of enzyme activity, stability and selectivity via immobilization techniques. *Enzyme Microb. Technol.* **2007**, *40*, 1451–1463. [CrossRef]
5. Tran, D.N.; Balkus, K.J.B., Jr. Perspective of recent progress in immobilization of enzymes. *ACS Catal.* **2011**, *1*, 956–968. [CrossRef]
6. Wu, X.; Hou, M.; Ge, J. Metal-organic frameworks and inorganic nanoflowers: A type of emerging inorganic crystal nanocarrier for enzyme immobilization. *Catal. Sci. Technol.* **2015**, *5*, 5077–5085. [CrossRef]
7. Cao, S.; Xu, P.; Ma, Y.; Yao, X.; Yao, Y.; Zong, M.; Li, X.; Lou, W. Recent advances in immobilized enzymes on nanocarriers. *Chin. J. Catal.* **2016**, *37*, 1814–1823. [CrossRef]
8. Altinkaynak, C.; Tavlasoglu, S.; Ÿzdemir, N.; Ocsoy, I. A new generation approach in enzyme immobilization: Organic-inorganic hybrid nanoflowers with enhanced catalytic activity and stability. *Enzyme Microb. Technol.* **2016**, *93–94*, 105–112. [CrossRef] [PubMed]
9. Li, C.; Jiang, S.; Zhao, X.; Liang, H. Co-immobilization of enzymes and magnetic nanoparticles by metal-nucleotide hydrogelnanofibers for improving stability and recycling. *Molecules* **2017**, *22*, 179. [CrossRef] [PubMed]
10. Liang, H.; Jiang, S.; Yuan, Q.; Li, G.; Wang, F.; Zhang, Z.; Liu, J. Co-immobilization of multiple enzymes by metal coordinated nucleotide hydrogel nanofibers: Improved stability and an enzyme cascade for glucose detection. *Nanoscale* **2016**, *8*, 6071–6078. [CrossRef] [PubMed]
11. Liang, H.; Liu, B.; Yuan, Q.; Liu, J. Magnetic iron oxide nanoparticle seeded growth of nucleotide coordinated polymers. *ACS Appl. Mater. Interfaces* **2016**, *8*, 15615–15622. [CrossRef] [PubMed]
12. Lyu, F.; Zhang, Y.; Zare, R.N.; Ge, J.; Liu, Z. One-pot synthesis of protein-embedded metal-organic frameworks with enhanced biological activities. *Nano Lett.* **2014**, *14*, 5761–5765. [CrossRef] [PubMed]
13. Brady, D.; Jordaan, J. Advances in enzyme immobilisation. *Biotechnol. Lett.* **2009**, *31*, 1639. [CrossRef] [PubMed]
14. Govardhan, C.P. Crosslinking of enzymes for improved stability and performance. *Curr. Opin. Biotechnol.* **1999**, *10*, 331–335. [CrossRef]

15. Kim, J.; Grate, J.W.; Wang, P. Nanostructures for enzyme stabilization. *Chem. Eng. Sci.* **2006**, *61*, 1017–1026. [CrossRef]
16. Lei, C.; Shin, Y.; Magnuson, J.K.; Fryxell, G.; Lasure, L.L.; Elliott, D.C.; Liu, J.; Ackerman, E.J. Characterization of functionalized nanoporous supports for protein confinement. *Nanotechnology* **2006**, *17*, 5531–5538. [CrossRef] [PubMed]
17. Nadar, S.S.; Rathod, V.K. Magnetic macromolecular cross linked enzyme aggregates (cleas) of glucoamylase. *Enzyme Microb. Technol.* **2016**, *83*, 78–87. [CrossRef] [PubMed]
18. Schoevaart, R.; Wolbers, M.W.; Golubovic, M.; Ottens, M.; Kieboom, A.P.; Van, R.F.; La, V.D.W.; Sheldon, R.A. Preparation, optimization, and structures of cross-linked enzyme aggregates (cleas). *Biotechnol. Bioeng.* **2004**, *87*, 754–762. [CrossRef] [PubMed]
19. Shah, S.; Sharma, A.; Gupta, M.N. Preparation of cross-linked enzyme aggregates by using bovine serum albumin as a proteic feeder. *Anal. Biochem.* **2006**, *351*, 207–213. [CrossRef] [PubMed]
20. Sheldon, R.A. Cross-linked enzyme aggregates (cleas): Stable and recyclable biocatalysts. *Biochem. Soc. Trans.* **2007**, *35*, 1583–1587. [CrossRef] [PubMed]
21. Sheldon, R.A.; Van, P.S. Enzyme immobilisation in biocatalysis: Why, what and how. *Chem. Soc. Rev.* **2013**, *42*, 6223–6235. [CrossRef] [PubMed]
22. Wang, M.; Bao, W.J.; Wang, J.; Wang, K.; Xu, J.J.; Chen, H.Y.; Xia, X.H. A green approach to the synthesis of novel "desert rose stone"-like nanobiocatalytic system with excellent enzyme activity and stability. *Sci. Rep.* **2014**, *4*, 6606. [CrossRef] [PubMed]
23. Cook, T.R.; Zheng, Y.R.; Stang, P.J. Metal-organic frameworks and self-assembled supramolecular coordination complexes: Comparing and contrasting the design, synthesis and functionality of metal-organic materials. *Chem. Rev.* **2013**, *113*, 734–777. [CrossRef] [PubMed]
24. Wang, J.; Cohen Stuart, M.A.; Marcelis, A.T.M.; Colomb-Delsuc, M.; Otto, S.; van der Gucht, J. Stable polymer micelles formed by metal coordination. *Macromolecules* **2012**, *45*, 7179–7185. [CrossRef]
25. Wang, X.; McHale, R. Metal-containing polymers: Building blocks for functional (nano)materials. *Macromol. Rapid Commun.* **2010**, *31*, 331–350. [CrossRef] [PubMed]
26. Whittell, G.R.; Hager, M.D.; Schubert, U.S.; Manners, I. Functional soft materials from metallopolymers and metallosupramolecular polymers. *Nat. Mater.* **2011**, *10*, 176–188. [CrossRef] [PubMed]
27. Zhang, W.-X.; Liao, P.-Q.; Lin, R.-B.; Wei, Y.-S.; Zeng, M.-H.; Chen, X.-M. Metal cluster-based functional porous coordination polymers. *Coord. Chem. Rev.* **2015**, *293–294*, 263–278. [CrossRef]
28. Tan, H.; Zhang, L.; Ma, C.; Song, Y.; Xu, F.; Chen, S.; Wang, L. Terbium-based coordination polymer nanoparticles for detection of ciprofloxacin in tablets and biological fluids. *ACS Appl. Mater. Interfaces* **2013**, *5*, 11791–11796. [CrossRef] [PubMed]
29. Taylor, K.M.; Jin, A.; Lin, W. Surfactant-assisted synthesis of nanoscale gadolinium metal–organic frameworks for potential multimodal imaging. *Angew. Chem. Int. Ed.* **2008**, *47*, 7722–7725. [CrossRef] [PubMed]
30. Liu, D.; Huxford, R.C.; Lin, W. Phosphorescent nanoscale coordination polymers as contrast agents for optical imaging. *Angew. Chem. Int. Ed.* **2011**, *50*, 3696–3700. [CrossRef] [PubMed]
31. Tran, L.D.; Feldblyum, J.I.; Wong-Foy, A.G.; Matzger, A.J. Filling pore space in a microporous coordination polymer to improve methane storage performance. *Langmuir* **2015**, *31*, 2211–2217. [CrossRef] [PubMed]
32. Gao, P.F.; Zheng, L.L.; Liang, L.J.; Yang, X.X.; Li, Y.F.; Huang, C.Z. A new type of ph-responsive coordination polymer sphere as a vehicle for targeted anticancer drug delivery and sustained release. *J. Mater. Chem. B* **2013**, *1*, 3202–3208. [CrossRef]
33. Liu, Y.; Tang, Z. Nanoscale biocoordination polymers: Novel materials from an old topic. *Chemistry* **2012**, *18*, 1030–1037. [CrossRef] [PubMed]
34. Liang, H.; Zhang, Z.; Yuan, Q.; Liu, J. Self-healing metal-coordinated hydrogels using nucleotide ligands. *Chem. Commun.* **2015**, *51*, 15196–15199. [CrossRef] [PubMed]
35. Sun, J.; Ge, J.; Liu, W.; Lan, M.; Zhang, H.; Wang, P.; Wang, Y.; Niu, Z. Multi-enzyme co-embedded organic-inorganic hybrid nanoflowers: Synthesis and application as a colorimetric sensor. *Nanoscale* **2014**, *6*, 255–262. [CrossRef] [PubMed]
36. Mantion, A.; Massüger, L.; Rabu, P.; Palivan, C.; McCusker, L.B.; Taubert, A. Metal-peptide frameworks (mpfs): "Bioinspired" metal organic frameworks. *J. Am. Chem. Soc.* **2008**, *130*, 2517–2526. [CrossRef] [PubMed]

37. Imaz, I.; Rubio-Martínez, M.; Saletra, W.J.; Amabilino, D.B.; Maspoch, D. Amino acid based metal-organic nanofibers. *J. Am. Chem. Soc.* **2009**, *131*, 18222–18223. [CrossRef] [PubMed]
38. Moussatova, A.; Vázquez, M.-V.; Martínez, A.; Dolgounitcheva, O.; Zakrzewski, V.G.; Ortiz, J.V.; Pedersen, D.B.; Simard, B. Theoretical study of the structure and bonding of a metal—DNA Base complex: Al-guanine. *J. Phys. Chem. A* **2003**, *107*, 9415–9421. [CrossRef]
39. Wang, F.; Liu, B.; Huang, P.-J.J.; Liu, J. Rationally designed nucleobase and nucleotide coordinated nanoparticles for selective DNA adsorption and detection. *Anal. Chem.* **2013**, *85*, 12144–12151. [CrossRef] [PubMed]
40. Verma, S.; Mishra, A.K.; Kumar, J. The many facets of adenine: Coordination, crystal patterns, and catalysis. *Acc. Chem. Res.* **2010**, *43*, 79–91. [CrossRef] [PubMed]
41. Bakkali, H.E.; Castiñeiras, A.; Garcíasantos, I.; Gonzálezpérez, J.M.; Niclósgutiérrez, J. Metallo-supramolecular structures by self-assembly through weak interactions in mixed ligand metal complexes of adenine and malonate. *Cryst. Growth Des.* **2015**, *14*, 249–260. [CrossRef]
42. Navarro, J.A.R.; Lippert, B. Molecular architecture with metal ions, nucleobases and other heterocycles. *Coord. Chem. Rev.* **1999**, *185*, 653–667. [CrossRef]
43. Singh, P. The family of n 9 -adenine: New entry for adenine-benzamide conjugates linked via versatile spacers. *J. Chem. Sci.* **2014**, *126*, 159–167. [CrossRef]
44. An, J.; Geib, S.J.; Rosi, N.L. Cation-triggered drug release from a porous zinc-adeninate metal-organic framework. *J. Am. Chem. Soc.* **2009**, *131*, 8376–8377. [CrossRef] [PubMed]
45. Wei, H.; Li, B.; Du, Y.; Shaojun Dong, A.; Wang, E. Nucleobase-metal hybrid materials: Preparation of submicrometer-scale, spherical colloidal particles of adenine-gold(iii) via a supramolecular hierarchical self-assembly approach. *Chem. Mater.* **2007**, *21*, 2987–2993. [CrossRef]
46. And, C.S.P.; Verma, S. A luminescent silver-adenine metallamacrocyclic quartet. *J. Am. Chem. Soc.* **2006**, *128*, 400–401.
47. Burneo, I.; Stylianou, K.C.; Rodríguez-Hermida, S.; Juanhuix, J.; Fontrodona, X.; Imaz, I.; Maspoch, D. Two new adenine-based co(II) coordination polymers: Synthesis, crystal structure, coordination modes, and reversible hydrochromic behavior. *Cryst. Growth Des.* **2015**, *15*, 3182–3189. [CrossRef]
48. Garcíaterán, J.P.; Castillo, O.; Luque, A.; Garcíacouceiro, U.; Pascual Román, A.; Lezama, L. An unusual 3d coordination polymer based on bridging interactions of the nucleobase adenine. *Inorg. Chem.* **2004**, *43*, 4549–4551. [CrossRef] [PubMed]
49. Ge, J. Protein-inorganic hybrid nanoflowers. *Nat. Nanotechnol.* **2012**, *7*, 428–432. [CrossRef] [PubMed]
50. Ge, J.; Lu, D.; Liu, Z.; Liu, Z. Recent advances in nanostructured biocatalysts. *Biochem. Eng. J.* **2009**, *44*, 53–59. [CrossRef]
51. Kim, J.; Grate, J.W.; Wang, P. Nanobiocatalysis and its potential applications. *Top. Catal.* **2012**, *108*, 639–646. [CrossRef]
52. Wu, X.; Ge, J.; Yang, C.; Hou, M.; Liu, Z. Facile synthesis of multiple enzyme-containing metal-organic frameworks in a biomolecule-friendly environment. *Chem. Commun.* **2015**, *51*, 13408–13411. [CrossRef] [PubMed]
53. Mu, J.; Wang, Y.; Zhao, M.; Zhang, L. Intrinsic peroxidase-like activity and catalase-like activity of Co_3O_4 nanoparticles. *Chem. Commun.* **2012**, *48*, 2540–2542. [CrossRef] [PubMed]

© 2017 by the authors. Licensee MDPI, Basel, Switzerland. This article is an open access article distributed under the terms and conditions of the Creative Commons Attribution (CC BY) license (http://creativecommons.org/licenses/by/4.0/).

catalysts

MDPI

Review

Controlling Redox Enzyme Orientation at Planar Electrodes

Vivek Pratap Hitaishi [1], Romain Clement [1], Nicolas Bourassin [2], Marc Baaden [2], Anne de Poulpiquet [1], Sophie Sacquin-Mora [2], Alexandre Ciaccafava [3] and Elisabeth Lojou [1,*]

[1] National Center for Scientific Research (CNRS), Aix Marseille University, BIP, UMR 7281, 31 Chemin Aiguier, 13009 Marseille, France; vhitaishi@imm.cnrs.fr (V.P.H.); rclement@imm.cnrs.fr (R.C.); adepoulpiquet@imm.cnrs.fr (A.d.P.)

[2] Laboratoire de Biochimie Théorique, National Center for Scientific Research (CNRS), UPR9080, Université Paris Diderot, Sorbonne Paris Cité, PSL Research University, 13 rue Pierre et Marie Curie, 75005 Paris, France; bourassin@ibpc.fr (N.B.); baaden@ibpc.fr (M.B.); Sophie.Sacquin-Mora@ibpc.fr (S.S.-M.)

[3] Chemistry and Biology of Membranes and Nanoobjects, UMR 5248 CNRS, University of Bordeaux, Bat. B14 allée Geoffroy St. Hilaire, 33600 Pessac, France; a.ciaccafava@cbmn.u-bordeaux.fr

* Correspondence: lojou@imm.cnrs.fr; Tel.: +33-4-91-16-41-44

Received: 13 April 2018; Accepted: 28 April 2018; Published: 4 May 2018

Abstract: Redox enzymes, which catalyze reactions involving electron transfers in living organisms, are very promising components of biotechnological devices, and can be envisioned for sensing applications as well as for energy conversion. In this context, one of the most significant challenges is to achieve efficient direct electron transfer by tunneling between enzymes and conductive surfaces. Based on various examples of bioelectrochemical studies described in the recent literature, this review discusses the issue of enzyme immobilization at planar electrode interfaces. The fundamental importance of controlling enzyme orientation, how to obtain such orientation, and how it can be verified experimentally or by modeling are the three main directions explored. Since redox enzymes are sizable proteins with anisotropic properties, achieving their functional immobilization requires a specific and controlled orientation on the electrode surface. All the factors influenced by this orientation are described, ranging from electronic conductivity to efficiency of substrate supply. The specificities of the enzymatic molecule, surface properties, and dipole moment, which in turn influence the orientation, are introduced. Various ways of ensuring functional immobilization through tuning of both the enzyme and the electrode surface are then described. Finally, the review deals with analytical techniques that have enabled characterization and quantification of successful achievement of the desired orientation. The rich contributions of electrochemistry, spectroscopy (especially infrared spectroscopy), modeling, and microscopy are featured, along with their limitations.

Keywords: metalloenzymes; enzyme immobilization; enzyme orientation; electrodes; bioelectrocatalysis

1. Introduction: Interest in and Limitation of Bioelectrocatalysis Based on Immobilized Redox Enzymes

1.1. Fundamental Issue: Understanding Energy Chains, and the Mechanism of Biocatalysis Involving Redox Enzymes

Electron Transfer (ET) is an essential process allowing a variety of microorganisms to find energy for growth. Depending on its environment, and especially on the available substrates, a given microorganism may find its energy through a combination of different metabolic pathways. A variety of redox proteins and enzymes are involved in those energy chains, displaying a variety of structural motifs, cofactors, and metal content. Many of these individual proteins and enzymes can be identified, and fully characterized in vitro. The way they interact in vivo to fulfill the ET chain, however,

often remains obscure. Furthermore, for a given metabolic pathway, some redox chains are favored for a given organism, and some proteins or enzymes may be over- or under-expressed. Depending on the environment or on the type of microorganism, one protein can replace another one as electron donor or acceptor for a specific process. Photosynthesis is one relevant example for which the involvement of one protein over another varies depending on the considered species (such as algae, cyanobacteria, or plants) [1]. Heme- (cytochrome c_6) or copper-containing proteins (plastocyanin), on the one hand, and FeS cluster- or flavin mononucleotide-containing proteins (flavodoxin), on the other hand, act as electron transfer shuttles allowing the coupling of water oxidation to $NADP^+$ reduction by photosystem I/photosystem II systems. Respiration of some exotic microorganisms known as extremophiles is also pertinent in this respect (Figure 1A). Although the latter are very interesting because they are sources of enzymes exhibiting outstanding properties, such as resistance to high temperatures, low pH, and high salinity, their electron pathways are far from being understood. In the respiratory chain of the acidophilic bacterium *Acidithiobacillus ferrooxidans*, two similar cupredoxins with close redox potentials are found, one soluble in the periplasm and the other anchored to the membrane. The reason for such redundancy in the electron pathway from ferrous oxidation to O_2 reduction is still unclear, despite many years of research on the organism [2]. Another relevant organism is *Aquifex aeolicus*, a hyperthermophilic ancestral bacterium which can sustain energy for growth from H_2 or H_2S oxidation coupled to either O_2 or sulfur reduction [3]. This feature leads to an intricate energy chain involving many enzymes interacting to sequentially transfer electrons within short timescales. Last, but not least, intramolecular ET also occurs inside an enzyme to transfer the electrons from the active site, where transformation of the substrate occurs, to the surface of the enzyme. In many cases, for huge enzymes in particular, the distance the electron must be transferred across is optimized by the maturation and incorporation of cofactors.

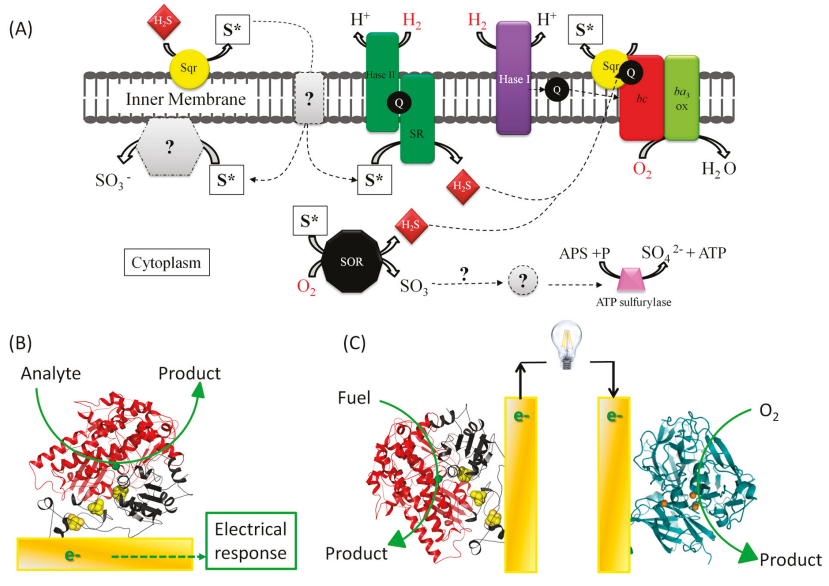

Figure 1. Electron transfer (ET) involving immobilized enzymes on interfaces: from metabolic ET chains (**A**) to biosensors (**B**) and enzymatic fuel cells (**C**). (**A**) is a schematic view of *A. aeolicus* metabolisms adapted from [3].

These few examples illustrate how the complexity of electron transfer pathways requires specific approaches to acquire some knowledge regarding the productive interaction between the involved

enzymes and proteins. Common methods to analyze these fast ET processes include stop flow or chemical quench flow methods, as well as pulse radiolysis. Electrochemistry is another method of choice to quantify the rate of electron transfer processes. Not only can intramolecular ET within one protein be determined, but also the intermolecular ET between two interacting proteins can be characterized. The electron flow is then recorded as a current, which is related to the efficiency of the catalysis when an enzyme is involved. Furthermore, studying the ET between one protein and a conductive surface can mimic in vivo ET, because many of these processes occur at the surfaces of the interacting partners, or at the interface with the substrate. Interestingly, chemical functionalization of electrochemical interfaces has been a very active research field during the last years, since it provides a broad range of functionalities that will help to tune the interaction with a specific protein. Use of electrochemistry, however, requires as a first step the immobilization of the proteins or enzymes on conductive solid surfaces which act as electrodes, with the ultimate goal of keeping the protein structure as functional as possible.

1.2. The Applicative Issue: Use of Redox Enzymes Immobilized on Solid Conductive Supports for Biosensors, Bioreactors, and Biofuel Cells

Beyond fundamental knowledge of microorganism energy chains, the control and the functional immobilization of redox enzymes on conductive solid supports have found great interest in many environmentally friendly "green" biotechnological devices.

For these applications, the enzymes must be immobilized on the solid electrode surface in order to avoid diffusion into the biodevices, thereby losing the desired electrons, and compromising their effectiveness [4]. Among the currently developed biodevices, electrochemical biosensors have been the subject of extensive research for many years (Figure 1B). They have been preferred to other sensors such as those based on optical transduction because of the low cost and fast response of the electrochemical transduction. Large improvements in the detection limit down to fM concentrations, sensitivity, specificity, and stability of the biosensors have been achieved (see review [5] and references therein). This accomplishment is due to the identification and purification of new redox enzymes that are able to act as a recognition element, combined with the development of new conductive matrices for their efficient immobilization, essentially on the basis of large-surface-area nanomaterials. Electrochemical biosensors are used in many different domains, among which medical applications [5], food safety, and environmental monitoring [6] are those undergoing the largest developments. The earliest electrochemical biosensor for biomedical applications dates back to 1962, and uses the redox enzyme glucose oxidase to measure sugar in blood [7]. The increasing knowledge of the parameters that control enzymatic activity on electrodes has enabled the design of the current commercially available «finger-pricking» approach, and has opened the way to implantable glucose biosensors. Advanced technology allows us to now envision the integration of the glucose bioelectrochemical sensor in a smartphone platform, simplifying the lives of diabetic patients [8]. Furthermore, it is possible to measure glucose in other fluids than blood, i.e., interstitial liquid, urine, saliva, sweat, or ocular fluid [9]. These last developments have led to the design of new robust enzyme-decorated bioelectrodes, such as flexible electrodes [10]. Many other targets are detectable by electrochemical enzyme-based biosensors, such as nitric oxide [11], cholesterol [12], urea [13], or influenza virus [14]. In the domain of the environment, bioremediation is a process that involves redox enzymes for cleanup [15]. Oxygenases and multicopper oxidases (MCOs) are, for example, very efficient in the degradation of chlorinated and phenolic compounds. In this case, it should be productive to immobilize the enzyme on a conductive support to promote bioremediation by use of electrochemical methods.

More recent applications in the domain of bioreactors for fine chemistry have found great interest in the original use of redox enzymes immobilized on conductive supports. The two following examples illustrate this increasing research field nicely. A mandatory step for wide use of enzymes in biocatalysis is the regeneration of nicotinamide adenine dinucleotide phosphate, known under its redox couple $NADP^+$/NADPH. Actually, this cofactor is required for the function of a large number of identified

enzymes that are efficient in industrial processes such as the production of alcohols, hydroxylation of aromatic compounds, hydrolysis of triglycerides, or Baeyer–Villiger reactions [16]. Economic considerations impose the regeneration of NADPH, as it is costly to synthesize it. Among the methods explored for that purpose, electrochemical ones would be of great interest thanks to their low cost and simplicity. In this case, the activity of enzymes immobilized on various electrodes would be one attractive way to regenerate the cofactor. The second example is the electrochemical reduction of CO_2 into fuel products, with the additional advantage of providing a method for CO_2 sequestration. Biology offers natural biocatalysts able to achieve CO_2 reduction with high efficacy. Although the current research mostly focuses on whole microorganisms colonizing electrodes [17], encouraging results have been reported on the activity of specific enzymes [18]. Here, the mandatory step would again be the functional immobilization of the enzyme on the electrode surface.

Finally, one emerging domain where the immobilization of redox enzymes is mandatory is the sustainable production of electricity. Fuel cells can be considered as green devices for electricity generation, since they produce no greenhouse gases. However, the transformation of H_2 and O_2 at the anode and cathode of the fuel cell requires catalysts based on expensive noble metals such as platinum. Some redox enzymes are known to catalyze fuel oxidation and oxidant reduction with high efficiency and specificity. This possibility opens the route for the development of the so-called enzymatic fuel cells, where the catalysts are the redox enzymes (Figure 1C). Two main categories of biofuel cells exist, mainly depending on the intended application and on the fuel used, with the oxidant being, in most cases, oxygen. The proof of concept of the first biofuel cell category appeared more than 40 years ago. It is based on the oxidation of glucose by flavin-based glucose oxidase or cellulose dehydrogenase. Many applications are targeted. As an illustration, one can cite biobatteries, small enough to be implanted in blood for feeding medical devices, such as a glucose biosensor or an insulin delivering pump, biobatteries implanted on ocular lenses to monitor ocular pressure, or biobatteries stuck on the skin to monitor lactate in sweat. Recent reviews report the major current developments in that type of biofuel cells [19]. A more recent concept uses the same fuel as in platinum-based fuel cells, with the aim of enhanced power output compared with sugar/O_2 enzymatic fuel cells. Here, hydrogen oxidation is carried out by the highly efficient hydrogenases, whose active site is composed of nickel and iron atoms. Coupled to MCOs for oxygen reduction, H_2/O_2 biofuel cells display an open circuit voltage of around 1.1 V, depending on the origin of the enzymes, which is the highest ever reported for biofuel cells [20]. Late development of this new biofuel cell generation relies on the hydrogenases themselves, which—intrinsically—are very sensitive to oxygen. This sensitivity was observed for most of the enzymes known before the identification of some extremophilic hydrogenases from microorganisms able to sustain energy from a hydrogen–oxygen metabolism. These latter hydrogenases were demonstrated to be oxygen-tolerant and, moreover, resistant to carbon monoxide, opening the way to their use as biocatalysts in fuel cells. This second category of biofuel cells could be employed to power environmental sensors, with an additional advantage over platinum-based fuel cells. Indeed, thanks to the specificity and properties of some hydrogenases, it becomes possible to use nonpure H_2, as hydrogen produced from biomass or waste. Recent research shows that high current densities in the order of 10 mA/cm^2, and all the most high currents reported (up to 1 A per mg of enzyme) can be reached, which is very promising [21].

1.3. Limitations of Bioelectrocatalysis: Stability, Wiring, and Interrelationships

For both fundamental research and applied perspectives described earlier, the main first step is the productive immobilization of redox enzymes on electrochemical interfaces. The aim is to optimize the ET rates both for intermolecular and interfacial ET, in order to ultimately optimize bioelectrocatalysis efficiency. Concomitantly, stabilization of the enzymes once immobilized would be desired. Many recent reviews analyze the issues relative to protein behavior once immobilized on solid supports [22]. Although no general rules can be formulated, it is plausible to expect that the interaction between the solid support and the enzyme may cause an alteration in protein structure and/or

flexibility, hence modifying its properties. Depending on the enzyme and on the support, enhanced stability and activity, or, on the contrary, destabilization may be observed. Immobilization may prevent enzyme aggregation, thus enhancing catalysis when compared with free enzymes in solution. Proper immobilization on a solid support mimicking the enzyme native environment may improve enzyme activity. Here, we particularly want to highlight the specific aspects of trying to perform conductive electron transfer processes by using a conductive surface for enzyme immobilization. With this goal in mind, additional principles have to be taken into account, and some of the general rules admitted for an efficient and stable immobilization process no longer hold. As an example, it is expected that in order to achieve high catalysis efficiency, nonredox enzymes must be oriented with the active site turning to the opposite side of the solid surface to facilitate substrate access. In the case of ET however, the situation is the opposite, since the ET rate strongly depends on the distance between the electrode and the active site. Hence, an orientation of the enzyme with the active site as close as possible to the solid surface will be targeted. This situation will be discussed further in the following. Along the same lines, it is also admitted that deleterious interactions between an enzyme and a surface should be avoided by introducing a linker on the enzyme. In the case of ET, however, this linker introduces an additional distance that can be prejudicial to the ET efficiency. Furthermore, the enzymes on conductive supports will be subjected to electric fields, as soon as the bioelectrode is polarized at the required operational potential. This operational condition implies that redox enzymes on solid electrodes must not only resist various nonphysiological environments (salt concentration, nonbuffered solution, etc.) but also resist high current flow, or a wide range of redox potentials.

These general considerations clearly illustrate that redox enzyme immobilization on solid electrochemical interfaces raises issues that are different from the general issues of enzyme immobilization on solid supports. The goal of the present review is to describe these specific aspects, and it will focus on the main parameters that govern the functional immobilization of redox enzymes on electrodes, as well as the current tools available to rationalize and control these parameters. We will limit our discussion to planar electrodes, for which fundamental studies of immobilized redox enzymes are more relevant, as discussed hereafter.

2. Interfacial Electron Transfer: Why Is Orientation a Key Issue?

The maturation of the idea to use redox enzymes in biodevices was driven in parallel by the increasing understanding of the ET mechanism in the context of biological processes [23]. According to Marcus theory, the ET rate k_{ET} between an electron acceptor and an electron donor is a function of the potential difference between the electron acceptor and donor, given as the Gibbs free energy of activation (ΔG), and of the reorganization energy [24]. k_{ET} can be expressed as $k_{ET} = \alpha(r)v\, e^{-\Delta G/RT}$, where αv depends on the electronic coupling between the reactants, with the transmission coefficient α exponentially varying with the distance r separating the donor and the acceptor. Based on this theory, the maximum distance of electron tunneling between donor and acceptor was estimated to be 20 Å [23,25]. Actually, this is the distance which is reached through complex formation between the active sites of two interacting proteins. The upper distance limit of 20 Å is also observed in many enzymes for the separation of active sites and electronic relays, although electrons can travel longer distances through conserved aromatic residues of the protein moiety [26]. As a consequence, the intramolecular ET does not limit the catalysis since k_{ET} is much higher than catalytic constants [27]. Considering now the electrode as the donor or the acceptor, the rule can be extended to define the limiting distance separating it from the enzyme for ET. As enzyme diameters are on the order of a few nm, active sites are often more distant from the surface than the predicted maximal distance for fast ET within the electrode. The consequence is that for interfacial ET to proceed, it is mandatory to place the active site at a distance compatible with ET, using controlled tethering to the surface. Because the active site is often protected from the external environment by deep embedding inside the protein moiety, one has to play with the electronic relays inside the enzyme which allow fast intramolecular ET. The electron entry or exit point will be the particular electronic relay on the surface of the enzyme that

must be located at a close distance from the electrode (Figure 2). The molecular-level features favoring a specific orientation can be determined based on the examination of the crystallographic structure of the enzyme, possibly in combination with molecular modeling approaches [28]. Nevertheless, it is experimentally very difficult to succeed in a single-point attachment of an enzyme on an electrode surface. The immobilization of the protein will often lead to a distribution of enzyme orientations. Even in the case of enzyme immobilization through specific anchors grafted on the enzymes (this will be discussed below), one cannot exclude ET through a variety of pathways because of enzyme flexibility on the surface. As the interfacial electron transfer constant k_0 between the enzyme and the electrode surface depends on the distance of the electron tunneling, the distribution in the enzyme orientations creates a dispersion of this constant that may lie in the range between k_{min} and $k_{max} = k_0$. In the case of ahomogeneous distribution of enzyme orientations we have $k_{min} = k_0 \exp(-\beta d_0)$, where βd_0 is a parameter that represents the dispersion of possible orientations the enzyme molecules may adopt while maintaining electron exchange with the electrode. The βd_0 parameter governs the shape of the electrochemical signals as modeled by Armstrong's group [29], and reported in recent papers for the analysis of the ET of immobilized enzymes [30].

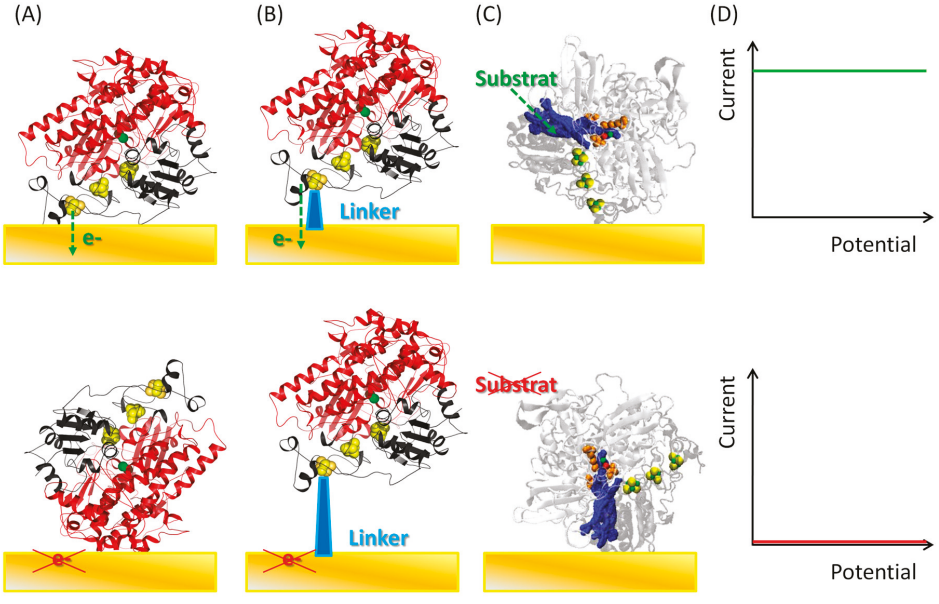

Figure 2. Schemes of enzyme immobilization conditions (**A**–**C**) allowing or precluding a direct electrical connection (DET) (**D**) at an electrochemical interface. (**A**) Illustrates how the distance between the active site, or a surface electronic relay, of an adsorbed enzyme and the electrode influences DET; (**B**) Illustrates the effect of the length of a linker used for enzyme immobilization on DET; (**C**) Illustrates the effect of the substrate channel access upon enzyme immobilization on DET.

Note that the enzyme orientation on the electrode is not only a key issue for interfacial electron transfer, but is also essential to facilitate the diffusion of substrates and products within the enzyme internal cavity network toward the catalytic site. Molecular Dynamics simulations on [NiFe] hydrogenases from *A. aeolicus* and *Desulfovibrio fructosovorans* have shown how these two homologous enzymes display their own specific internal tunnel network [31]. In the case of the membrane-bound *A. aeolicus* hydrogenase, all the substrate entry points are located on the same side of the enzyme's surface. As a consequence, the enzyme's adsorption on an electrode with the wrong

orientation might result in the shielding of some parts of its surface, such that a small substrate could no longer use it as an entry point to reach the active site.

3. The Key Components

3.1. Properties of Redox Proteins

Enzymes are large biomolecules that are abundantly found in living organisms with great variety and very specific functions. As biocatalysts, enzymes accelerate reactions by decreasing their activation energy. They are composed of one or more long chains of amino acid residues displaying a vast array of functions within organisms, including catalyzing metabolic reactions, DNA replication, and responding to stimuli. The structure of such proteins stands out as complex but with a high degree of organization compared to small molecules, as required to fulfill high selectivity. This structure/function relationship will have strong impact on further functional enzyme immobilization. Tertiary structures form by folding of the α-helix and pleating of the ß-sheet in such a way as to achieve maximum stability or the lowest energy state. The final shape of the protein is stabilized by various interactions, including hydrogen bonding, disulfide bonds, ionic bonds, Van der Waals, and hydrophobic interactions. Coarse-grain modeling approaches can provide useful insight on the thermal unfolding of surface-immobilized enzymes [32]. More generally, how the immobilization will alter this structure is, of course, of great importance.

Among enzymes, redox enzymes are those proteins whose established role is to convert a substrate along an energy chain through electron exchange. They consist of a redox center, required for their bioactivity, with the ability to either accept or donate electrons. Different types of redox centers can be found in redox enzymes, ranging from metal-based ones (Ni, Fe, Mo, Cu, etc. . . .) to inorganic ones such as flavin adenine dinucleotide (FAD), acting as a cofactor. In metalloenzymes, the metal ion is usually held by coordinate-covalent bonds on the amino acid side chains or inorganic ligands, or is bound to a prosthetic group (e.g., heme). The redox active center is very often embedded in the polypeptide structure, which protects it against hostile environments but, from a conductive point of view, insulates it. Different strategies have been used during maturation to succeed in a fast intramolecular ET, which is not limiting compared with the catalytic efficiency; this is illustrated hereafter by some relevant examples, widely studied in the literature (Figure 3).

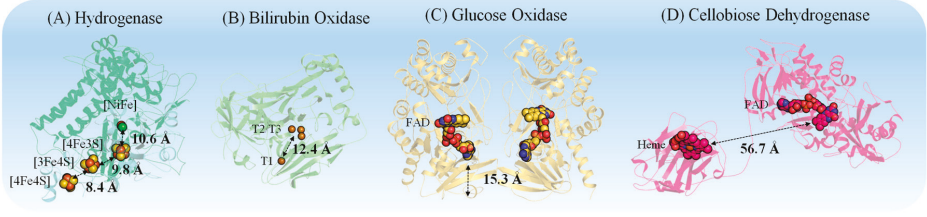

Figure 3. Representation of relevant distances for intramolecular and interfacial ET in several redox enzymes: metal center to metal center, metal center to cofactor, or cofactor to protein surface. (**A**) *A. aeolicus* hydrogenase model [31]; (**B**) Bilirubin oxidase (pdb ID: 2XLL); (**C**) Glucose oxidase (pdb ID: 1CF3); (**D**) Cellobiose dehydrogenase (pdb ID: 4QI7).

MCOs [33] such as laccases (LAC), bilirubin oxidases (BOD), or cuprous oxidase (CueO) are copper-containing enzymes that efficiently catalyze oxygen (O_2) reduction directly to water [34]. BODs and LACs are found in fungi, plants, and bacteria, where they catalyze the oxidation of bilirubin to biliverdin and the oxidation of polyphenol compounds, respectively. O_2 reduction requires four copper sites which differ by their ligand coordination and geometry: one T1 Cu, and a trinuclear cluster composed of one T2 Cu center coupled to a binuclear T3 Cu center [34]. Physiologically, electrons

are received from the substrate to the T1 Cu, and are transferred through a histidine–cysteine bridge to the trinuclear cluster 12–14 Å away, where O_2 reduction takes place [35]. In a mimicking way, one can imagine how an electrode can provide the electrons instead of the physiological substrate, which means that the electrode has to be wired to the copper T1.

Hydrogenases (Hases) are the enzymes that catalyze the reversible oxidation of molecular hydrogen (H_2) and reduction of protons. They are found in the periplasm or cytoplasm of various microorganisms, in many different environments, where their main role is to provide energy for the organisms by oxidation of molecular hydrogen. Hases are subclassified into three different types based on the active site metal content: iron–iron Hases, nickel–iron Hases, and iron Hases [36]. The [FeFe]-Hases are more specifically involved in H_2 production from proton reduction, whereas [NiFe]-Hases are more efficient in H_2 oxidation [37]. In the latter case, the [NiFe] active site, where the hydrogen binds, is buried deep inside the large subunit. To transfer the electrons from/to the active site, 3 FeS clusters less than 13 Å distant from each other constitute a conductive line in the small subunit towards/from the surface of the enzyme. Hydrogen reaches the active site through well-defined hydrophobic channels, [38] whereas avenues for proton evacuation are not yet so clearly identified. If one wants to immobilize such an enzyme, two conditions need to be met: (i) wire the enzyme to the electrode via the FeS cluster located closest to the surface of the protein; and (ii) make sure the channels for the substrate access and products removal are accessible.

Glucose oxidase (Gox) is the most studied redox enzyme so far, and catalyzes the oxidation of β-D-glucose to D-glucono-1,5-lactone and hydrogen peroxide using molecular oxygen. It is a large dimeric protein with a molecular weight of 160 kDa and an average diameter of 8 nm, containing one tightly bound FAD per monomer as a cofactor [39]. The FAD cofactor is deeply embedded inside the protein matrix. In addition, it was experimentally shown that the FAD molecule is located in a cavity deeper than 8 Å [40]. Various attempts have been made to establish the wiring between the active center of GOx and various electrodes [41]. However, many discrepancies in the results are reported, and uncertainty remains regarding the retention of the conformation of the enzymes.

Cellobiose dehydrogenases catalyze the oxidation of various saccharides into lactones. Their strategy to transfer electrons is different from Gox as each monomer consists in two domains, one with a FAD cofactor and the other with a heme. ET proceeds physiologically from the substrate to the FAD cofactor and finally to the heme. The latter is accessible to the solvent, and is connected to the FAD domain through a flexible linker [42], which can be a great advantage if using this type of enzyme on an electrode surface.

These few examples clearly indicate that the strategy required to succeed in the ET from/to the enzyme to/from the electrochemical interface will largely depend on the structure and specific features of the enzyme. Apart from fast intramolecular ET achieved thanks to electronics relays within the enzyme, ET between physiological partners in a given chain, or between the substrate and the enzyme, is facilitated by specific recognition surfaces involving both hydrophobic and hydrophilic moieties [43]. As illustrations, the third, surface-exposed FeS cluster in the [NiFe]-Hases from *Desulfovibrio* is surrounded by an acidic patch composed of glutamic amino acid residues, which recognize a lysine-rich environment of the interacting heme of the physiological partner, a cytochrome c_3 [31,44]. This electrostatic interaction allows both partners to come to a close distance which then induces fast intermolecular ET. Various other striking examples of electrostatic-driven protein–protein interactions for efficient ET are documented in the literature: interaction between cytochrome *c* oxidase and cytochrome *c* [45], sulfite reductase and ferredoxin [46], cytochrome P450 and putidaredoxin [47], and NADH-cytochrome b_5 reductase and Fe(III)-cytochrome b_5 [48]. Also, the Cu T1 in LACs is inserted in a hydrophobic pocket which allows favorable interaction with its natural organic substrates [49]. The knowledge of such recognition interfaces will become a key issue once a rational approach to immobilize enzymes on electrodes is envisioned.

Furthermore, from the 3D structure of given redox enzymes, it is possible to calculate the surface electrostatic potential distribution which indicates the existence of dipole moments [50]. A dipole

moment, in the simplest case, is a vector quantity representing the separation of two opposite electrical charges. The magnitude of this quantity is equal to the distance between the charges multiplied by the charge. The direction of the vector is from negative to positive charge. In the general case, the dipole moment can be computed by the formula $\vec{\mu} = \sum_i q_i \times \vec{r_i}$, with $\vec{\mu}$ as the overall dipole moment generated by i charges, q_i as the magnitude of each partial charge i, and r_i as the position vector of charge i. Such calculations provide an initial understanding for preferential orientations of immobilized enzymes on electrodes, a feature that may be exploited to favor high ET rates. Another key aspect of enzymes is their internal cavity network that enables the diffusion of substrates/reaction products between the solvent and the enzyme's catalytic site, and which can also be investigated via modeling and free energy calculation [51]. From a theoretical perspective, the ET itself can be simulated using a wealth of different techniques involving mixed Quantum–Classical molecular dynamics (MD) simulations, Quantum Mechanics/Molecular Mechanics (QM/MM) approaches, or numerous Density Functional Theory (DFT) variants [52].

3.2. Conductive Electrode Surfaces

A large variety of electrodes are available, displaying high electric conductivity and mechanical and thermal stability. During the last years, a great deal of research has focused on the immobilization of redox enzymes in and on 3D conductive materials. The idea underlying the use of high surface area/volume materials is to enhance the loading of redox enzymes and, hence, the current for biocatalysis. Carbon-based materials such as carbon nanotubes, carbon nanofibers, carbon felt, or metal nanoparticles have been demonstrated to act as a very efficient host matrix [53]. It is also expected that tuning the size of the pores of the matrix may help in the stabilization of the enzyme by multipoint anchoring [54]. The control of enzyme loading and specific activity in such large-area materials is, however, in most cases hampered by the lack of methods able to monitor one individual enzyme in the matrix. In addition, homogeneous distribution and orientation of enzymes in the 3D network is rarely achieved. Nonetheless, it is worth mentioning the original work of Vincent's group, who set up a Protein Film Infrared Electrochemistry (PFIRE) method for the monitoring of the enzyme conformation entrapped in carbon black particles [55]. Mazurenko et al. also reported the resolution of enzyme partitions in carbon felts [21]. Nevertheless, it appears more relevant to study the immobilization of redox enzymes on more planar electrodes, to achieve easier control of the enzyme conformation, and to overcome mass transport and substrate partition issues arising from the surface meso- or nanoporosity which induces local variation of substrates and products (such as local acidification, for example) and complexifies the whole process. The notion of planarity itself must be discussed here. Given an average size of enzymes in few nanometer ranges, all materials that present macroporosity should be considered as planar from the enzyme immobilization point of view. However, macroporosity is most often accompanied by mesoporosity, in which the enzyme is connected through many points. Any porous materials should thus be considered as nonplanar.

Smooth metal surfaces like Au, Ag, and Pt, or more complex surfaces such as indium–tin–oxide (ITO), or flat carbon-based surfaces such as glassy carbon can be used for the immobilization of redox enzymes, as well. However, even these surfaces considered as planar present a roughness factor that may influence enzyme immobilization. Few studies report the effect of roughness on bioelectrocatalysis. It is worth noting the work from Thorum et al. in which roughness was induced on a gold electrode to force protruding of functionalities required to get access to the enzyme active site [56]. Gold supports/electrodes of different geometries are commercially available and are the model supports for analytic and surface-addressing techniques like Surface Plasmon Resonance (SPR), Quartz Crystal Microbalance (QCM), Polarization Modulation Infrared Reflectance Absorption Spectroscopy (PMIRRAS), Surface-Enhanced Infrared Absorption (SEIRA), and ellipsometry. As the chip used in these methods can also serve as the electrode for electrochemical sensing, the gold surface appears all the more relevant when dealing with redox enzyme immobilization. In principle, single-crystal/monocrystalline gold surfaces should be used in all these techniques because they

provide a controlled gold surface at the atomic level. However, the reusability of the surface is critical, whereas improved understanding of surface pretreatment for polycrystalline gold allows preparing reproducible surfaces [57]. Hence, polycrystalline gold surfaces, where the distribution of metal atoms is nonuniform throughout the electrode surface, are very handy. Surface treatment provides surface control and promotes their wide use for protein electrochemistry [58]. Electrochemical cleaning by cycling in H_2SO_4 solution between −0.35 V and +1.5 V vs. Ag/AgCl allows calculating of the real electroactive surface area by integrating the gold oxide reduction peak at +0.9 V, taking into account a charge of 390 $\mu C \cdot cm^{-2}$ for the reduction of a gold oxide monolayer [59]. The roughness factor can thus be calculated ($R_f = A_{electroactive}/A_{geometric}$), which represents the difference between the projected geometric surface area and the electro-accessible surface area. R_f takes values around 2 to 5 depending on the kind of surface considered and the cleaning procedure [60].

Several spectroscopic methods have been coupled to electrochemistry taking advantage of conductive biocompatible materials. Surface-enhanced vibrational spectroscopies benefit from nanostructuration of the metal (Au or Ag) to increase their sensitivity (enhancement factor in absorption: 10^2–10^6) [61]. Because of the nanostructuration surface, here also a roughness factor can be calculated ($R_f = A_{real}/A_{geometric}$); the geometric area ($A_{geometric}$) represents a flat surface while the real area (A_{real}) is experimentally accessible, for example, via electrochemistry or AFM [60,62,63]. On the other hand, infrared spectroscopy based on reflection absorption techniques requires flat reflective surfaces [64]. While monocrystalline gold remains the most commonly used support, it was recently shown that despite lower-intensity infrared signals, glassy carbon is a promising alternative for broadening the applications related to electrochemistry [65].

A molecular-level picture of these surfaces can be obtained through modeling approaches such as MD simulations. Interestingly, the last decade has seen the development of numerous force fields (FF), specifically parameterized to model a large variety of solid surfaces [28]. Amongst the material models that are now accessible to computational chemists, one can mention metallic surfaces (Ag, Al, Au, Cu, Ni, Pb, Pd, Pt), for which Lennard-Jones potentials for nonbonded interactions have been developed [66]. Gold in particular can be modeled in common simulation codes such as GROMACS and NAMD using either the GolP atomistic force field [67] or the METAL/INTERFACE force field [68]. Additional materials of interest for bioelectrochemistry can be modeled such as silica [69], but also graphite [70] or carbon nanotubes [71]. These latter materials cannot be considered as planar surfaces, however. An important issue when studying the adsorption of biomolecules with considerable dipole moments, such as redox enzymes, is the surface polarization, which can contribute to up to 20% of the total binding energy between the protein and the surface [72]. This aspect is taken into account in the GolP-CHARMM FF for gold surfaces [73]. Another FF that incorporates polarization is the AMOEBA FF [74], which was already extended to model peptides on a graphene surface [75]. Still, development efforts in that field are mostly directed towards solvated biomolecules, and a lot remains to be done for the simulation of interfaces.

3.3. Interaction between Enzyme and Conductive Surface: How Can It Be Modulated?

Enzymes can be immobilized on the electrode surfaces following different processes including simple adsorption, entrapment in a complex matrix such as redox polymers, and covalent binding [76,77]. Among the challenges of immobilizing enzymes onto electrodes, preserving the native conformation and catalytic properties, and providing good electrical connection and relative stability are of outmost importance. In this respect, one philosophy of immobilizing enzymes is based on considering the electrode as a surrogate to the known physiological partner of the enzyme: a substrate, a cofactor, heme- or [Fe-S]-based protein shuttles, etc. To get a proper enzyme immobilization for the optimum ET, mimicking physiological interactions between partners, it is thus of great importance to gain the possibility to tune the interactions between enzymes and the electrode surface. Two main options exist when trying to tune the interactions between a redox enzyme and an electrode: (i) chemical functionalization of the electrode surface; and (ii) engineering the enzyme.

3.3.1. Electrode Functionalization

Several methods have been developed to add surface chemical functions to planar electrodes [78] (Figure 4). Concerning gold surfaces, the most widely used functionalization is achieved through self-assembled monolayers (SAMs). SAMs are usually formed by spontaneous adsorption of sulfur. Alkanethiols, or dialkyl disulfides or sulfides possess high affinity for the surface of gold (but also for platinum or silver), with a bond energy of RS-Au of ~40 kcal·mol^{-1} [79]. This adsorption results in well-defined organic surfaces with desirable and alterable chemical functionalities, controlled simply by changing the terminal group of the thiol chain. The modification of a gold electrode with SAMs provides a choice of positive/negative/hydrophobic terminal functional groups such as –COOH, –NH_2, –SO_3H, –CH_3, and –OH. In addition, the knowledge of the pKa of the terminal moieties allows chemical control on the electrode surface. As examples, pKa values of 6.0 [80] and 6.9 [81] for SAMs of 11-mercaptoundecanoic acid (MUA) and 4-aminothiophenol (4ATP) groups on gold were determined, respectively. Dependence of the pKa of –NH_2-based SAMs on thiol chain length was also reported [82].

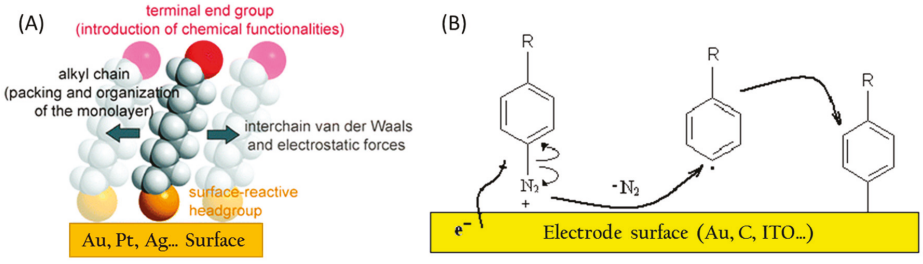

Figure 4. Representation of (**A**) self-assembled monolayer [83] and (**B**) scheme for electrografting of diazonium salts on electrode surfaces (Au, C or Indium Tin Oxide (ITO)) with alterable terminal chemical functionality.

Their ease of preparation from millimolar thiol solutions makes SAMs attractive candidates for surface tailoring. A surface coverage of the order of pmol·cm^{-2} is generally achieved and adsorption stops at the level of monolayer coverage [84]. This surface coverage, as well as compactness and organization of the layer, shows, however, dependence on the type of thiol molecules, nature of the metal surface, immobilization time, and thiol concentration [85]. Longer adsorption time and longer thiol chains are expected to provide a more organized SAM layer by decreasing pinhole defects or conformational defects in the alkane chains [86,87]. Long-chain thiols are expected to form well-organized assemblies due to stabilizing van der Waals interaction along the adsorbed chain. On the contrary, presence of long chains may screen their mobility in the solution and, hence, their accessibility to the metal surface. It was recently proposed that fast and repeated changes on applied potential pulses relative to potential of zero charge cause an ion stirring effect [88] which has an influence on the SAM formation kinetics. Immobilization of biomolecules on SAMs has been critically reviewed [89]. The possibility to prepare mixed SAMs is an added advantage, where homogeneous or separated phases of different thiols may allow the site-specific binding of enzyme to the surface [90].

Besides this, silane-based SAMs on ITO electrodes have been used owing to their simple preparation, good reproducibility, and high stability [91]. ITO, being low cost, highly stable, and transparent, is a very useful material as an electrode due to its electrical and optical properties [92] and plays an important role especially for biosensor technology [93]. The silane-based chemicals act as cross-linkers because they contain Si–O bonds which react with the surface hydroxyl groups of ITO where the end groups of silane act as an immobilization matrix for biomolecules.

However, the use of SAMs for redox enzyme immobilization also raises critical issues. The first is linked to the ET process through the SAM itself, which can become a limiting step and control

the whole ET process. As developed above, the efficiency of ET, given by the ET rate constant k_{ET}, is found to be a function of the distance d between the electrode surface and the redox species. A study related to the kinetics of ET between a gold electrode and a SAM of thiol of variable length confirms the exponential dependence of the rate constant on the chain length [94], according to $k_{ET} = k^{\circ} \exp[-\beta d]$. In the case of SAMs, an additional parameter is the surface coverage, θ, after SAM formation. For a complete monolayer of SAM without any defects (θ = 1), the mechanism of ET is tunneling, as the monolayer shows blocking behavior. Therefore, the expression for the ET rate constant can be read as $k_{tunnel} = k^{\circ} \exp[-\beta d]$, where k° is the rate constant for a bare electrode, β is the constant of electron transfer through tunneling, and d the thickness of the SAM. This is the case for chemisorption of long-chain thiols on a gold surface, which usually results in well-organized monolayers with minor defects due to effective van der Waals interactions along the carbon chains [95]. Another mechanism is based on a membrane-like behavior of the SAM, so that redox species can permeate through the monolayer, and ET to/from the electrode takes place. This kinetic process is controlled by the partition coefficient, κ, between the solution and the membrane, the diffusion coefficient, D_f, in the membrane, and the kinetics of material transport at the film/solution interface with a rate constant, $k_{interface}$ [96]. In the presence of pinhole defects within the SAM, another ET pathway may be effective due to diffusion of the redox species through the defect sites to the electrode. This alternative transfer may operate in the case of short thiol chains which are expected to display less organized layers. All these ET phenomena may take place in parallel and an effective rate constant will reflect the relative contributions of the different pathways [97] (Figure 5). As an implication, for ET to proceed, a balance is needed between a sufficiently high ET rate and sufficient organization to be able to obtain a controlled SAM. This can be reasonably achieved by maintaining the length of thiols comprising around 6–8 carbons [98].

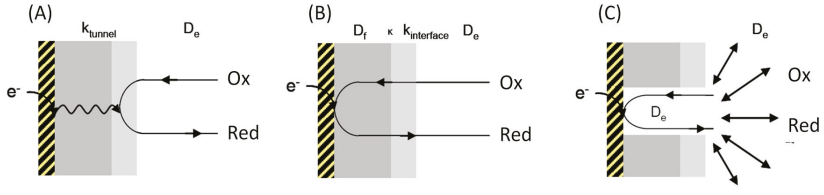

Figure 5. ET processes through a self-assembled monolayer (SAM) (in grey) formed on an electrode. (**A**) Tunneling ET process through a compact SAM; (**B**) ET through a SAM behaving as a membrane. ET will be controlled by a partition coefficient at the membrane/solution interface and by the diffusion coefficient inside the membrane; (**C**) ET proceeds through defects in the SAM. D_e and D_f are the diffusion coefficients in the electrolyte and in the SAM, respectively. Ox and Red designate a redox couple in solution. Adapted from [96].

The second critical issue is linked to the poor stability of the SAM, especially when the potential of the electrode is polarized to extreme values of potentials [99]. The Au–S bond is found to be stable only in a small potential window i.e., −0.6 to +0.6 V vs. Ag/AgCl [100]. Thiol-based SAMs are also sensitive to heating, and their thermal stability is limited to 400 K [101]. Above this temperature, thiol molecules start to desorb in the form of disulfides, suggesting that the Au–S bond is weaker than the S–C bond of thiols [102]. Some discrepancy, however, exists about the thermal stability of monolayers of thiol [103]. SAMs formed by long-chain thiols appear to be more thermally stable due to their well-organized nature on the surface [104].

As a consequence of the poor stability of the Au–S bond, a carbon–gold (Au–C) bond should be preferred [105]. Reduction of aryl-based diazonium salts is a widely used method to prepare functionalized surfaces, not only on carbon, but also on gold electrodes [106–108]. The interest in such modifications concerns the wide range of functional groups available that are associated

to high stability over a large potential window. Formation of mixed monolayers by successive electrochemical reductions from a mixture of diazonium salts presents an added advantage towards surface functionalization [109,110]. The disadvantage is the difficulty to stop the reaction at the monolayer formation. Electrografting of aryl compounds on electrode surfaces is based on the formation and attachment of highly reactive aryl radicals. However, polymerization between two aryl radicals, and their chemical reaction with already adsorbed aryl molecules may compromise the quality of the monolayer. Possible control of the monolayer can be achieved by utilizing a so-called "protecting–deprotecting" approach, where a bulky group protects the functional group, avoiding both the formation of disordered multilayers and possible reaction of functional end groups with aryl radicals. Organization of the monolayer is typically controlled by the size of the protecting group [111]. On the other hand, the chemical substituent groups attached to the benzene ring of diazonium salt can significantly affect the electrografting of these molecules on the electrode surface, first due to their size and second due to their nucleophilic/electrophilic nature. QCM measurement was used to probe the thickness of the electrodeposited aryl organic layer on an Au electrode, and suggested that the large size of the substituent and its steric hindrance typically led to the formation of thin layers [112]. A recent study related to the kinetics of electrografting on gold surfaces also suggested that the presence of an electron-attracting group increases the rate of reaction of the aryl radical on the gold surface [113], whereas the presence of an electron-donating group slows down the grafting process, thereby offering control over the possibility to form monolayers. It should be noted that a mixed layer of aromatic diazonium salt and thiol can be advantageously used, as demonstrated in the case of LAC on gold electrodes. A submonolayer of aryl groups was formed to minimize multilayer formation by aryl radical attack, while full electrode coverage was achieved by further thiol adsorption [114].

Other tools to functionalize planar electrodes are noteworthy. Among additional immobilization strategies, a variety of amines can be covalently attached to the electrode surface through their electrooxidation onto the electrode [115]. Immobilization via in vivo natural enzyme substrate can be used alternatively to significantly increase electrocatalytic activity relative to simple protein adsorption on the electrode. Bilirubin is the natural substrate for BODs, which is in vivo oxidized to biliverdin with the reduction of oxygen to water. BOD was immobilized on a pyrolytic graphite (PG) electrode prefunctionalized by bilirubin, and a twofold increase in electrocatalytic activity in terms of current was reported compared to a bare PG electrode [116].

Infrared spectroscopy is a perfect tool to monitor an electrode functionalization and to judge the quality of the immobilization procedure regarding its impact on the protein structure. IR spectroelectrochemistry allows simultaneous monitoring of electrochemical signals and infrared spectra reflecting the secondary structure of the enzyme (Amide I and Amide II bands centered at ~1650 cm^{-1} and ~1550 cm^{-1}, respectively). However, one important aspect when choosing an immobilization procedure is to avoid spectral interference between the immobilizing molecules and the enzymatic system to study. Since the electrode material used in spectroelectrochemical experiments is a metal (gold or silver), SAMs are the common platform used for enzyme immobilization. The spectral overlap between a SAM and a protein is usually negligible since the main signals arising from the alkyl chain are located in the high wavenumber region of the spectra (2800 cm^{-1}–3000 cm^{-1}). However, one has to pay attention to the chemical head group of the SAM, especially amine functions (N–H bending mode of primary amines from 1650–1580 cm^{-1}) and carboxylic functions (C=O stretching mode from 1760–1690 cm^{-1}). This issue is compounded when much more complex modifications of the electrode are required. This problem has been tackled in a very elegant manner for the immobilization of a membrane protein—the bacterial respiratory ubiquinol/cytochrome bo_3 (cyt bo_3) [117]. In this study, a tethered bilayer lipid membrane (tBLM) was used to immobilize cyt bo_3. The commonly used lipid tether cholesteryl (2-(2-(2- mercaptoethoxy)ethoxy)ethyl)carbamate (CPEO3), which serves as an anchor for the lipid bilayer, contains a carbamate function that strongly overlaps with the protein signals. In this respect, the authors have successfully synthesized a novel molecule WK3SH (dihydrocholesteryl (2-(2-(2-ethoxy)ethoxy)ethanethiol), an IR transparent variant of

CPEO3 lacking the carbamate function, thereby suppressing interferences with signals arising from the secondary structure of the enzyme. This effort allowed the challenging monitoring of a transmembrane proton gradient generated by cyt bo_3 catalytic activity.

3.3.2. Enzyme Engineering

Engineering on the enzymes can alternatively serve to tune the interaction between bare or functionalized electrodes. Although very elegant, this strategy has been less employed so far, mainly because it can affect both stability and activity of the protein before and after immobilization. However, unlike nonspecific adsorption where multipoint connections between enzymes and electrodes are possible, site-specific attachment can provide an orientational immobilization that will also dictate the distance between the enzyme active site and the electrode surface [118–120]. The approach can thus maximize the rate of direct ET, with low distribution of ET rates. The basic approach is to use genetic engineering to introduce linkers on the functional proteins, then immobilize these protein molecules on the electrode via the linkers. The electrodes have to be chemically modified accordingly to specifically react with the labeled enzyme.

A classical site-specific immobilization method relies on the introduction of affinity tags like polyhistidine tags (His-tag), which are widely used in biochemistry for protein purification. His-tags have six sequential histidine residues that can chelate metals like Cu, Ni, or Co [121], or can favor the electrostatic interactions towards hydrophilic surfaces [122]. The issue here is to evaluate the effect of such site-specific immobilization of genetically engineered protein molecules compared to random immobilization on the interfacial ET efficiency. With His-tags being quite long linkers, the increased distance may impede the ET, or on the contrary may induce required flexibility of the immobilized enzymes. Oriented immobilization could be obtained via the formation of ternary metal chelate complexes between metalated nitriloacetic acid (NTA), such as a Cu-NTA functionality on the electrode, and His-tagged recombinant proteins. Balland et al. designed a short-length NTA-terminated alkane thiol to immobilize His-tagged LAC on a gold electrode through copper ligandation [121]. Both N- and C-terminal His-tagged LACs were studied with the expectation of a more favorable orientation of LAC through the C-terminal labeling which is closer to the Cu T1. Although catalysis of O_2 reduction was reported in the presence of a redox mediator, no direct current could be obtained even in the most favorable C-terminal modification. This result strongly suggested that His-tag labeling at the C-terminal or N-terminal sequences in LAC does not allow Cu T1 to approach the electrode at a tunneling distance. In another study, deletion of a flexible 10-amino-acid sequence at the C-terminal end of a two-domain-type LAC was performed to expose the Cu T1. Labeling with a His-tag was additionally introduced in the mutated enzyme [122]. The catalytic activity of the wild-type LAC was compared to the mutated one, once immobilized on Au electrodes modified by SAM displaying various chemical functionalities [122]. Direct wiring of the enzymes was achieved and explained by the proximity of the C-terminal end to the Cu T1 in the LAC under study. Despite the fact that no significant difference in the surface concentration between adsorbed WT or mutants exists, direct electrochemical activity was reported to be much higher on mutated enzymes due to the oriented immobilization of genetically engineered enzymes. Li and collaborators introduced a cysteine-6-His-tag either at the C-terminal or N-terminal end of a LAC for an oriented immobilization on gold electrodes. The strategy was based on different distances to the Cu T1 or Cu T2/T3 between C-Ter and N-Ter. Based on the quantification of produced H_2O_2 during O_2 reduction, the authors proposed that a different orientation was obtained depending on the C-Ter or N-Ter grafting. It must be noticed, however, that no clear catalytic signals could be observed in both cases, underlining most probably a slow ET independently of the immobilization strategy [123]. These three related examples illustrate the difficulty to rationalize the efficient immobilization of engineered enzymes for electrocatalysis.

Other peptides have potential binding properties for different types of surfaces. These peptides are expected to bind to surfaces by noncovalent interaction, and can exhibit high affinity and selectivity [124]. They are mostly selected by the phage display peptide library [125]. Few binding

peptides display some affinity for material surfaces of interest for electrochemistry, such as for graphene [126], carbon nanostructures [127], and gold [128,129]. Some peptides are already used to anchor enzymes on different types of surfaces such as alkaline phosphatase on a gold surface [129]. Currently, these peptides are not used to immobilize and orient redox enzymes on electrode surfaces, but they could provide a robust method to bind the enzyme at a different part of the protein. However, this binding method could also suffer from inhibition of the ET because of the length of the linker.

The publications just described above engineered only the N-terminal or C-terminal end. It should be interesting to have possibilities of mutation at other targeted parts of the enzyme, eventually closer to the active site, or at any locations on the enzyme surface in order to relate the position at which the enzyme is immobilized to the ET rate. As a recent illustration, cellobiose dehydrogenase from *Myriococcum thermophilum* has been shown to be an ideal candidate for site-directed mutagenesis. Having no surface cysteine residues, this amino acid was introduced at specific surface locations in view of the oriented immobilization [130]. "Thiol-ene" click chemistry between the thiol group available on the cysteine moieties and vinyl groups grafted on the electrode was successfully exploited for site-specific covalent linkage. The cysteine moieties were introduced on the dehydrogenase domain in such a way that two different orientations of the active site (the heme group of the flexible cytochrome domain) were ensured upon immobilization. An increase in electrocatalytic activity in terms of current for site-directed covalent immobilization was reported compared to physical adsorption, in a ratio ~7, thus indicating favorable enzyme loading on the electrode. Interestingly, a significant difference in current output was also observed between the two different grafting localizations, suggesting a control of the orientation of the enzyme. In the same way, a fungal laccase presenting a unique surface lysine residue close to the T1 Cu site was immobilized on planar electrodes [131]. This strategy can be applied in all the cases where a unique surface residue can be genetically engineered. However, site-specific protein engineering is sometimes limited by the available sites on the protein surface and/or because such modifications might alter the function or structure of the protein. Homology modeling can also be used to design new mutants with enhanced catalytic activity and immobilization yield on a surface. This was the case in the work of Gao et al. who performed site-directed mutagenesis on formate dehydrogenase immobilized on nanoparticles [132].

An attractive new strategy is the use of noncanonical amino acids (ncAAs) like propargyl-L-lysine (PrK), which can be genetically introduced at desired locations on the enzyme [133] (Figure 6). Moreover, a unique alkyne chemical handle of ncAAs will ensure a covalent linkage of the mutated enzymes with the modified electrode via click chemistry [133]. By varying the length and position of the linker on the *E. coli* CueO, the distance of the enzyme's electroactive site relative to the glassy carbon electrode was controlled [134]. It was shown that (i) site-directed anchorage was more efficient for direct O_2 reduction than nonspecific immobilization; and (ii) labeling far from the active site was not favorable to high catalysis efficiency. However, it was also emphasized that the ET efficiency was not directly related to the distance between the active site and the electrode, suggesting that other pathways such as ET through the structure of the protein may be involved. In that particular study, one can wonder whether the flexibility of the linker could be a major factor governing the overall ET.

The effectiveness of oriented immobilization and electrochemical operational stability for these genetically modified enzymes on electrode surfaces certainly depends upon the immobilization strategy. In case of chelation between a histidine moiety on the modified protein and Cu–NTA ligands on the electrode, stability can be affected by dissociation of the Cu ion from the NTA-modified electrodes induced by competitive binding with the His-tag on the enzyme [135]. In comparison, the operational stability of bioelectrodes prepared by covalent conjunction using click chemistry between cysteine-modified protein and vinyl groups of the electrode lasts up to a few days [130].

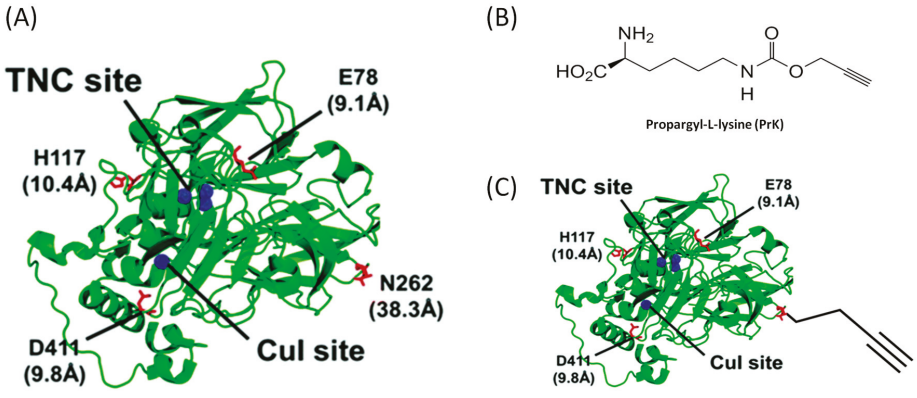

Figure 6. (**A**) 3D structure of cuprous oxidase (CueO) including the two redox centers (blue spheres). The four noncanonical amino acids (nCAAs) incorporation sites are labeled in red; (**B**) Chemical structure of Propargyl-L-lysine (PrK); (**C**) Genetically modified enzyme offering a unique alkyne moiety for site-specific attachment to electrodes via click chemistry [134].

4. How to Probe Enzyme Orientation on an Electrode

4.1. Electrochemistry

Electrochemical techniques are the ideal tools to study both intramolecular ET within an enzyme and interfacial ET between the enzymes and the electrodes. Theoretically, using cyclic voltammetry and chronoamperometry, kinetic parameters of the catalysis can be quantified. However, the type of kinetic data which can be obtained is linked to the type of interaction between the enzyme and the electrode, and especially to the enzyme's orientation [136]. Enzyme/electrode interaction is of utmost importance because the ET rate is exponentially dependent on the distance between the redox active center and the electrochemical interface, as predicted by the Marcus theory [24,137]. Fifteen years ago, most electrochemical studies involved the enzymes in combination with their physiological partners, or artificial redox partners, either diffusing or co-immobilized with the enzymes [138]. Unlike the observation of the redox signals for small proteins such as cytochrome *c* or ferredoxins [139], it was thought at that time that the size of the enzyme and the burying of the active site would preclude any direct electrical connection. Instead, the redox partners play the role of electron shuttles between the active site and the electrode, in a similar way as they are doing physiologically. Then, the so-called mediated catalytic current (MET) gave access to second-order rate constants between many different redox enzymes and their partners, and also allowed the demonstration of pseudo-specificity of the catalysis [140]. However, such a mediated electron transfer system has several disadvantages in terms of thermodynamic loss between the mediator and the enzyme, decreased efficiency due to potential mediator leaking, and difficulty to design a simplified system. The increasing knowledge of the arrangement of the active centers, of the cofactors, and of the distribution of surface charges and hydrophobic patches for an increasing number of redox enzymes has allowed the determination of the key parameters for their favorable orientation on functionalized electrodes. Hence, a direct electrical connection (DET) can be achieved, although many redox enzymes are still electrochemically silent. In some cases, the determination of the surface coverage of the enzymes participating in the catalysis, then the quantification of the catalytic constant k_{cat}, Michaelis constant (K_M), or inhibition constants was achieved [141]. This advanced analysis is mostly observed, however, on nanostructured electrodes, such as carbon nanotube- or gold nanoparticle-modified electrodes, that are able to enhance the loading of enzymes, thus increasing the detection signals. Interestingly, studying the MET/DET ratio appears to be relevant for the evaluation of the distribution of the orientation of the enzymes on

the electrode [136]. In addition, being a relative value, the MET/DET ratio is free from errors caused by the variation of adsorbed enzyme amount [30]. This strategy was applied to various enzymes immobilized on thiol-based SAMs and allowed to determine the surface chemistry on the electrode able to promote DET. One can cite relevant studies that analyzed the catalytic efficiency of *A. aeolicus* [NiFe]-Hase [142] on negative, positive, or hydrophobic SAMs on gold, of *D. gigas* Hase on positive SAM on gold [143], of *R. eutropha* [NiFe]-Hase on negative SAM on silver [61], of *Trametes hirsuta* LAC on neutral hydrophobic SAM on gold [144], of *Cerrena unicolor* C139 LAC positive SAM on gold [107], or of *Myrothecium verrucaria* BOD on positive or negative SAMs on gold [145] (Figure 7). In the latter paper, electrochemistry was coupled to SPR demonstrating that the switching between DET over MET when adsorption was performed either on negative or positive SAM was effectively linked to a different enzyme orientation and not to different enzyme loading. A similar study based on the coupling between electrochemistry and QCM to investigate O_2 reduction catalysis by *M. verrucaria* BOD further concluded with an optimum enzyme density on the SAM–Au electrode for direct catalysis [146].

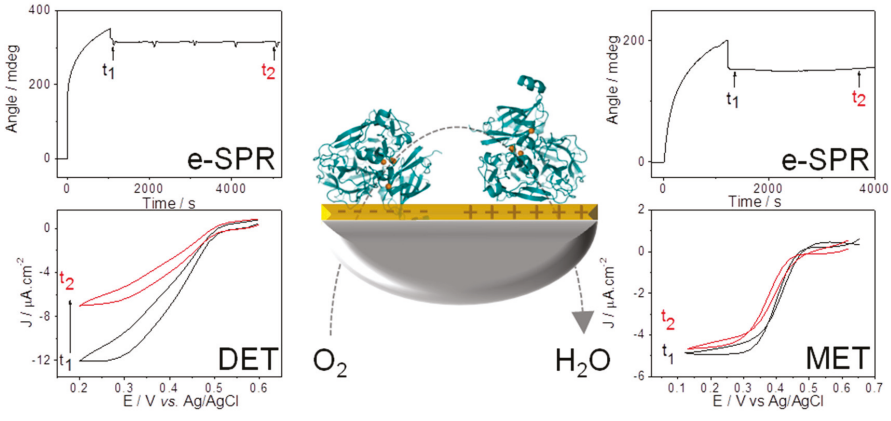

Figure 7. Coupling SPR with electrochemistry allowed the demonstration of a different orientation of the *M. verrucaria* bilirubin oxidase (BOD) according to the charge of the electrode controlling the type of ET process for enzymatic O_2 reduction. On either positive (**Right**) or negative (**Left**) SAM-modified gold electrodes, surface adsorption of the enzyme is successful. However, negatively charged SAM (**Left**) allows direct ET (DET), while positively charged SAM (**Right**) requires a redox mediator for catalysis (MET). Adapted from [145].

4.2. Spectroscopies

Thanks to specific surface selection rules [147], infrared techniques such as SEIRA and IRRAS spectroscopies have been successfully used in order to evaluate the orientation of redox enzymes immobilized onto electrodes. In those methods, the electromagnetic field propagates in a perpendicular direction to the metal surface. Therefore, the chemical groups with a dipole moment oriented perpendicular to the metal surface will exhibit the highest intensity of IR absorption, whereas the ones with a dipole moment parallel to the surface will show no absorption at all. For dipole moments lying in between, the intensity of the IR signal will depend on its angle with the surface normal. In proteins, the main secondary structure elements are α-helices and β-sheets, associated with specific amide I (C=O stretching mode, N–H bending) and amide II (combination of N–H bending and C–N stretching) spatial arrangements. Consequently, while the amide I dipole moment of an α-helix lies parallel to the α-helix itself, its amide II component is perpendicular. For β-sheets, the situation is reversed for the main amide I and amide II components. As a consequence of this surface selection rule, the intensity

ratio between Amide I and Amide II bands brings information regarding the orientation of the enzyme provided that a structure or a model of the enzyme is available [148] (Figure 8).

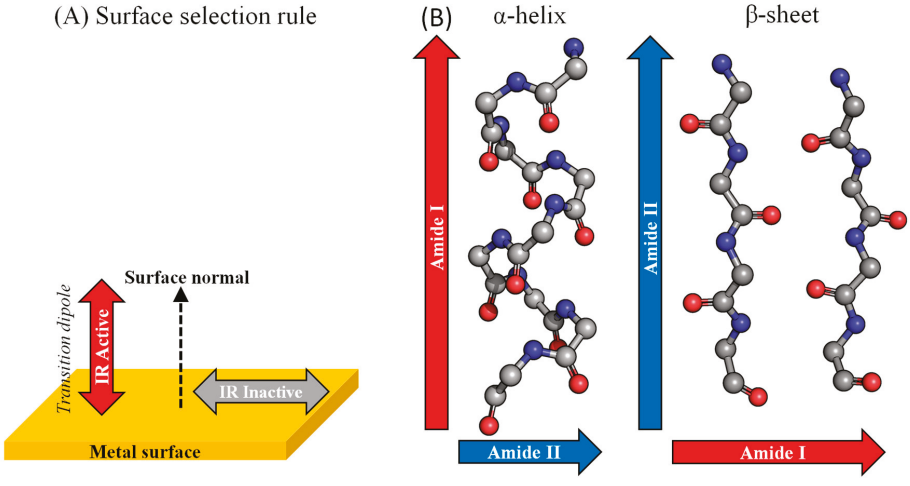

Figure 8. (**A**) Scheme representing the surface selection rule. Molecules with a transition dipole moment perpendicular to the metal surface exhibit the highest IR intensity while the parallel ones show no IR absorption; (**B**) Backbones of α-helix and β-sheet secondary structure elements with C=O and C–N highlighted in red and blue, respectively. Arrows show the direction of dipole moment depending on the type of chemical bond—amide I or amide II—relative to the secondary structure.

Surface-Enhanced Infrared Absorption (SEIRA) spectroscopy was used in combination with MD simulations to observe and rationalize the immobilization in a controlled orientation of membrane-bound [NiFe]-Hase from *Ralstonia eutropha* [149]. The membrane-bound Hase from *D. vulgaris* Hildenborough was reconstituted onto a SAM-modified gold electrode with a subsequent addition of a lipid membrane, either below or above the enzyme [150]. Immobilization on top of the membrane led to a great freedom of movement of the immobilized enzyme as indicated by the wide variation in the ratio of amide I to amide II between reproduced experiments. In the other configuration with the enzyme below the membrane, the direct interaction between the enzyme and the SAM-modified gold electrode led to a ratio of amide I to amide II close to 1, reproducible between experiments, indicating a more uniform immobilization procedure. Similarly, the different orientations adopted by a LAC depending on its covalent or noncovalent binding to the electrode [144] were monitored by SEIRA spectroscopy.

Polarization Modulated Infrared Reflection Absorption Spectroscopy (PM-IRRAS) allowed the observation of different orientations of the membrane-bound Hase of *A. aeolicus* [142]. Indeed, depending on the physico-chemical properties of the SAM-modified gold electrode (hydrophilic or hydrophobic), the intensity of the ratio of amide I to amide II varied, reflecting different orientations of the enzyme. Moreover, on the basis of simulations, those ratios could be correlated to the angle of the α-helices (main secondary structure element) present in the enzyme with respect to the normal of the electrode, giving an idea of the absolute orientation of the enzyme. Those results provided a structural interpretation of the electrochemical behavior of *A. aeolicus* Hase alternating between pure MET or a mixed DET + MET process depending on the physicochemical properties of the electrode. Similarly, PM-IRRAS was used to study the orientation of LAC onto SAM-modified gold electrodes depending on the charges of the SAM headgroup [107]. Different orientations correlated with electrochemical signals were observed with significantly higher catalytic signal for LAC immobilized on positively charged

surfaces. The same authors studied various immobilization procedures comprising hydrophilic SAM (mercapto ethanol), lipidic SAM (Dipalmitoylphosphatidylglycerol), and charged diazonium salts. They were able to conclude that orientations of LAC with β-sheets lying parallel to the electrode were associated with electrochemical response for O_2 reduction [151]. BOD from *M. verracuria* BOD was recently studied in a combined study including PM-IRRAS [145]. Despite drastically different electrochemical signals for O_2 reduction depending on the charges of SAM-modified electrodes, similar spectral features were observed for the amide region. This apparent discrepancy was rationalized on the basis of the particular topology consisting of a repeated β-barrel motif in the *M. verracuria* BOD.

4.3. Microscopy

Studying protein orientation with AFM [152] was proposed quite early, though in an indirect way. Using antibodies that bind to a specific region of the protein and measuring the volume of the protein/protein complex allows us to decipher if the antibody is present and, therefore, to deduce the orientation of the protein. Similarly, measuring by AFM the height profile of the protein-modified electrode after incubation in an antibody solution could also indicate the presence or absence of antibody, and therefore give clues about the protein orientation. However, if this technique has sometimes been used for simple redox proteins, to the best of our knowledge this has never been applied to enzymes. On the other hand, very few studies report the use of microscopy for direct evaluation of enzyme orientation. Actually, the direct measure of height profiles by AFM without antibody is a valuable method only if one dimension of the enzyme is characteristic. Hence, no information about the orientation can be obtained when globular enzymes are studied. LAC immobilization on mixed SAMs was, for example, studied using AFM, which gave information regarding enzyme distribution on the electrode surface. However, since these enzymes are recorded as quasi-spheres, the method would not be useful to determine their orientation [153]. In another example, *A. aeolicus* membrane-bound Hase immobilized on hydrophobic SAM was examined with AFM. Once again, approximately 3 nm high spherical features were observed, thus indicating the presence of a monolayer of enzyme but not which orientation was adopted [142]. A similar result was obtained with another globular enzyme—*R. eutropha* membrane-bound Hase—immobilized on a gold electrode [149].

However, an STM study, as well as three examples where AFM proved useful in determining enzyme orientation, are worth mentioning. The cytochrome *c* nitrite reductase from *E. coli*, a decaheme-containing homodimer with asymmetric dimensions, was adsorbed at an Au (111) electrode. STM was used to measure the lateral dimension of the immobilized enzymes and thus inform about their orientation [154]. This approach demonstrated that a distribution of orientations is adopted and that the enzymes possibly immobilize as monomers and dimers. A recombinant horseradish peroxidase bearing His- or Cys-tags at different positions with respect to the heme active site was attached to a gold electrode via the tag [155]. AFM measurements were performed in liquid (in 150 µL PBS), i.e., in an environment able to preserve the enzyme native structure (as far as it can be preserved on a solid surface). Various height profiles of the tagged proteins were measured on an Au (111) surface, indicating that different binding points lead to different orientations of the proteins. Furthermore, this observation was consistent with the different heterogeneous ET rates between enzyme and electrode recorded in electrochemical experiments.

The orientation of the [NiFeSe] membrane-bound Hase from *D. vulgaris* Hildenborough on a gold electrode modified with SAMs and a lipid bilayer was further studied by combining AFM and electrochemistry [156]. This Hase is characterized by the presence of a lipidic tail at the opposite of the distal 4Fe4S cluster—the exit point of electrons. The enzyme is elongated and the longest dimension corresponds to the axis 4Fe4S cluster-lipidic tail. When the electrode, first modified with SAMs and a lipid bilayer, was incubated in a Hase solution, AFM showed the apparition of globules whose height suggested that the Hase's longer dimension was vertically oriented. This orientation happened only when the lipidic tail was present, and not when the soluble form of the enzyme was studied instead.

Since only MET was possible in electrochemistry, this observation indicated that the lipidic tail was inserted in the lipid bilayer. On the contrary, when the electrode was co-incubated in a solution of Hase and phospholipids, AFM indicated a flat surface with deep holes. After dissolution of the lipid bilayer with surfactants, globular features corresponding to Hase molecules were recovered. Since in this second case DET was allowed, the 4Fe4S was supposed to be oriented towards the electrode, while the Hase lipidic tail was inserted in the lipid bilayer on top of it. The same enzyme was combined with *E. coli* F_1F_0 ATP-synthase inserted in the lipid bilayer overhanging it. This whole machinery allowed the use of H_2 as a fuel to produce the proton gradient necessary for ATP synthesis. The F_1F_0 ATP-synthase consists of a large soluble domain and a smaller membrane domain. The presence and the size of protrusions on top of the lipid bilayer recorded by AFM indicated a unique orientation of F_1F_0 ATP-synthase with its soluble domain directed towards the outer of the membrane [157].

Finally, the bacterial respiratory complex I from *Rhodothermus marinus* was reconstituted in a biomimetic membrane on a gold electrode. The complex is a single protein (NADH-menaquinone oxidoreductase) consisting of two L-shaped domains [158]. The complex in its native form was first inserted in liposomes before incubation of the SAM-modified gold electrode in the proteoliposome suspension. A lipid membrane with protrusions of 6–8 nm was evidenced by AFM. This distance is consistent with the hydrophilic part of the protein extending outside the lipid membrane, although the size is smaller than that evidenced by X-ray crystallography (13 nm), suggesting that the L structure is flexible (Figure 9).

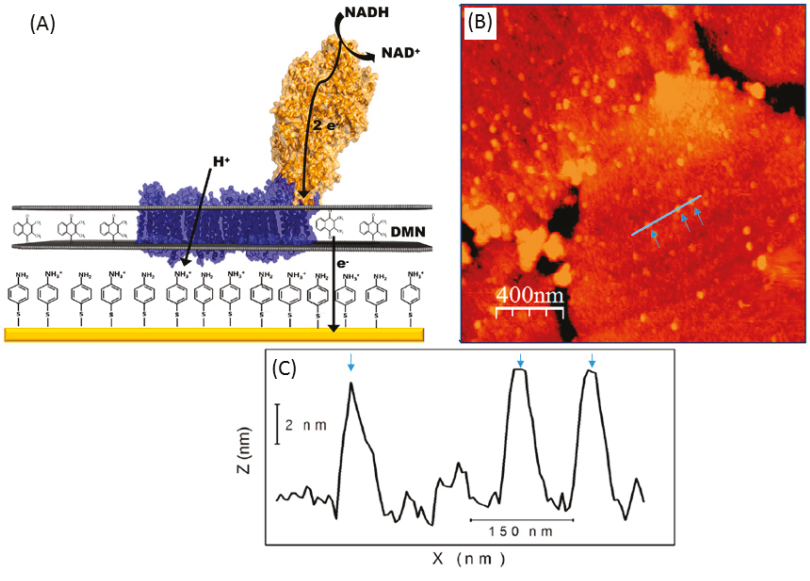

Figure 9. AFM study of the NADH-oxidizing respiratory complex I reconstituted in a phospholipid bilayer on a gold electrode. (**A**) Schematic representation of the reconstitution. The gold electrode is modified with 4-aminothiophenol and the phospholipid bilayer contains the redox mediator 2,3-dimethyl-1,4-naphtoquinone; (**B**) Tapping-mode AFM topography of a gold plate modified with 4-aminothiophenol to which complex I has been immobilized; (**C**) Z-axis profile across the line drawn in (**B**). The arrows indicate features whose height corresponds to the arm of complex I protruding outside the membrane (yellow structure in (**A**)). Adapted with permission from [158].

4.4. Modeling

To study functionalized electrode surfaces for enzyme immobilization, modeling approaches offer a window into the detailed surface interactions at the molecular level [28]. Several approaches can be used to predict the preferred orientation of enzymes on surfaces by modeling. SAM-functionalized gold surfaces have been modeled in numerous simulation works on enzyme–surface interactions, for example, to probe the enzyme binding orientation as a function of the surface charge [149]. Matanovic et al. used a combination of Density Functional Theory (DFT) and docking simulations to study the oriented interaction between bilirubin oxidase and a graphene electrode functionalized with bilirubin [159].

Sampling all relevant configurations sufficiently is one of the inherent challenges of such methods. ProtPOS (Prediction of Protein Preferred Orientation on a Surface) is software designed to predict the preferential orientations of a protein adsorbed on a surface. Its approach is to search for low-energy protein–surface conformations [160]. The use of a particle swarm optimization (PSO) algorithm allows fast computation of the energies of protein poses in every rotational and translational degree of freedom of the protein–surface complex [161]. The stochastic character of the PSO algorithm makes several runs necessary, with each run returning the lowest energy orientation of the protein on the surface that can be fed into MD simulations with a wide range of software—such as GROMACS [162] or AMBER [163,164].

More generally, the search for a global minimum in the enzyme–surface interaction energy landscape is a classic way to handle the question of protein orientation on a surface [165], and can be addressed via several modeling schemes such as parallel tempering Monte Carlo [166], docking via Brownian Dynamics Simulations [167], or MD simulations [168]. In their recent study on β-galactosidase grafted on a hydrophilic surface, Li et al. used coarse-grain MD simulations to probe the enzyme orientation and its catalytic activity as a function of the surface's hydrophilicity [169]. Such coarse-grain approaches have been developed for modeling protein–surface interactions because they allow an increase in the time and length scales that are accessible during simulations [28]. While coarse-grain representations can successfully address issues such as proteins binding on surfaces [161], or folding [32], they are, however, unable to deal with oxido-reduction processes and could not be used to describe ET between surfaces and enzymes until now.

When enzymes are immobilized on a surface via covalent bonds, for example, in the case of laccase bound on a SAM-functionalized gold surface, one can also determine the enzyme orientation by identifying the protein surface residue that will form the lowest energy bond with the SAM via calculations [169]. Bioinformatics tools represent another useful approach to determine a suitable orientation for enzymes immobilized on a surface in order to promote direct electron transfer, for example, by identifying hydrophobic patches on the protein surface [170].

5. Factors Driving the Oriented Immobilization at an Electrode

5.1. Importance of Electrostatic Interactions to Drive the Oriented Immobilization for Fast ET

As discussed in Section 3.1, electrostatic interactions are a major factor governing the stabilization of physiological protein–protein or protein–substrate interactions. In the context of intermolecular ET, it is therefore an essential parameter that needs to be evaluated and controlled in order to induce a proper orientation for an efficient electron transfer. Those interactions should inspire and guide the bioelectrochemist willing to achieve a physiological-like protein immobilization. Thus, when a molecular structure of the redox enzyme is available, calculations of the dipole moment of the enzyme might give hints for a rational approach to immobilize the targeted redox enzyme. In cases where the enzyme has a strong dipole moment, the preferential adsorption orientation can be predicted based on the surface chemistry of the electrode [171], while enzymes with less stable dipole moments can display several stable adsorption orientations [149]. Several computational studies on [NiFe]-Hases from various species have highlighted the importance of the enzyme dipole for

determining its orientation on a charged electrode [149]. In particular, the weak, fluctuating dipole moment in the membrane-bound [NiFe]-Hase from *A. aeolicus* enables the enzyme to adsorb efficiently on both negatively and positively charged surfaces [172]. BODs and LACs have been the subject of many studies highlighting the role of dipole moments in their oriented immobilization. For example, the orientation of laccase from *T. versicolor* adsorbed on charged SAMs was shown to be controlled by the enzyme's dipole moment and the distribution of charged patches all over the protein surface [173] (Figure 10).

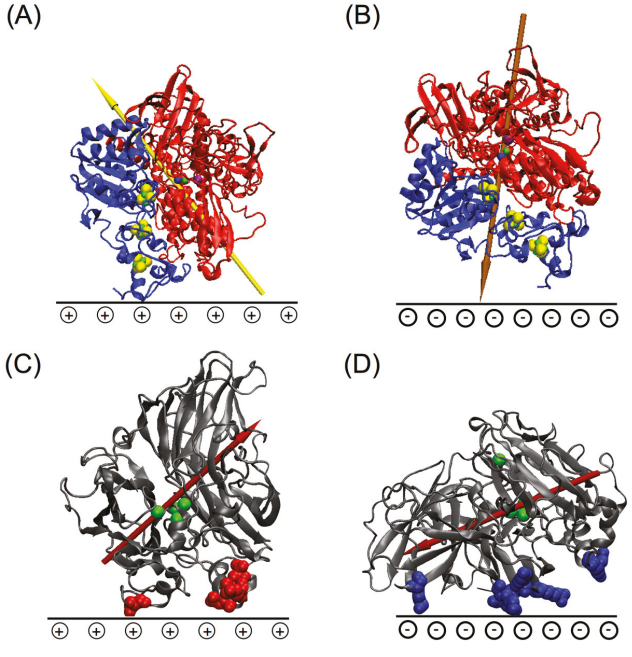

Figure 10. The fluctuating dipole moment of the [NiFe]-Hase from *A. aeolicus* enables it to adsorb efficiently on both positively and negatively charged surfaces (panels (**A**) and (**B**), respectively) [172]. On the other hand, the strong dipole moment in the LAC from *T. versicolor* leads to different enzyme orientations on positively and negatively charged surfaces (panels (**C**) and (**D**), respectively) [173]. Negatively charged residues interacting with the surface are shown as red van der Waals spheres in panel (**C**), while positively charged residues are shown in blue in panel (**D**).

The oriented immobilization on electrode surfaces presenting different charges of two different BODs, one from a fungus (*M. verrucaria*) and the other from a bacterium (*Bacillus pumilus*), was shown to be controlled by the variation of their dipole moments as a function of pH [30]. Hence, direct connection of *M. verrucaria* BOD was obtained upon adsorption at pH 6 on negatively charged surfaces, in relation with a dipole moment pointing towards the T1 Cu, while only mediated catalytic current was obtained on positively charged surfaces [145]. On the contrary, *B. pumilus* BOD, with a dipole moment directed toward the opposite side of the T1 Cu in all the pH range, was unable to achieve any direct connection on negatively charged surfaces. This last example clearly demonstrates that the dipole moment is the key property driving the orientation, much more than the global surface charge which is similar for the two BODs.

Electrostatic control of the orientation of enzymes was reported in other papers, although a direct link with dipole moments was not underlined. Modeling studies highlight the crucial role played

by the surface charge for effective reactions at the interface. For example, the hexameric tyrosine coordinated protein (HTHP) will adsorb in a nonproductive orientation for DET on positively charged SAMs [174]. In their work on sulfite oxidase adsorbing on SAMs, Utesch et al. showed how the solution ionic strength impacts the enzyme adsorption [175]. High ionic strengths tend to inhibit the interaction between the cyt b_5 domain and the SAMs both by competitive adsorption between ions and the cytochrome units, and by the shielding of the electrostatic attraction between the enzyme and the surface. The same group also investigated the effect of the protonation degree of the SAM surface on the immobilization of a [NiFe]-Hase [171]. They showed how the number of contacts between the SAM and negatively charged areas on the enzyme surface increase with the SAM ionization level. The strength of the enzyme/surface interaction is proportional to the SAM degree of protonation. However, MD simulations show that a high (50%) protonation degree of the SAM induces conformation changes in the enzyme that might be detrimental to its catalytic activity. However, one should note that, from a simulation perspective, the vast majority of modeling studies dealing with protein–solid surface systems concerns peptides grafted on surfaces, while the larger, more complex redox enzymes have, until now, attracted much less attention. Electrochemistry was thus the main method used throughout. Ulstrup et al. extensively studied the electrochemical behavior of four MCOs (three LACs, i.e., *Coprinus cinereus* (CcL), *Myceliophthora thermophila* (MtL), and *Streptomyces coelicolor* (ScL) as well as BOD from *M. verrucaria*) on different SAMs terminated by methyl, carboxylate, and amino groups [176]. A clear DET signal for catalytic reduction was reported for *M. verrucaria* BOD and CcL immobilized on negative carboxylate SAMs, and for ScL immobilized on positive or hydrophobic SAMs. No catalytic current could be obtained for MtL on any SAMs. Such observations demonstrate the clear sensitivity of a given enzyme to the local chemistry of the electrode surface more likely due to their electrostatic interactions. Enzymes having negative (ScL) or positive (*M. verrucaria* BOD, CcL) surface charge around the copper T1 active site are adsorbed on positive or negative SAMs, respectively, in a DET-type orientation derived by electrostatic interactions between opposite charges. Hydrophobic interactions have also featured for ScL immobilization on octanethiol SAMs, typically due to the hydrophobic environment around the active site along with negative surface charges. Although MtL is structurally similar to *M. verrucaria* BOD, no clear DET on any SAM surface indicates an entirely different environment around the Cu T1. Oriented immobilization of a [FeFe]-Hase from *Clostridium acetobutylicum* having large positive surface regions was achieved at negative SAMs on gold electrodes [177]. On the contrary, an oxygen-tolerant [NiFe]-Hase from *R. eutropha* adopted favorable orientation for DET-type electrocatalysis on 6-amino-1-hexanethiol coated gold electrodes [149]. This Hase being homologous to *A. aeolicus* Hase, one can suspect that the dipole moment of the enzyme may explain such a result.

5.2. Effect of Covalent Attachment

Covalent attachment is viewed as a general solution to avoid enzyme leaching from the electrochemical interface. The presence of amino, carboxylate, or hydroxyl groups within the amino acid moieties of an enzyme is exploited for covalent binding. SAMs on gold also offer a variety of terminal chemical functionalities that permit ease of covalent conjunction. For covalent attachment, carbodiimide chemistry is the most popular one, where water-soluble 1-(3-dimethylaminopropyl)-3-ethylcarbodiimide hydrochloride (EDC) and N-hydroxysuccinimide (NHS) reagents are commonly used [178,179]. The issue here is whether the covalent attachment will preclude any specific orientation of the enzyme, and hence decrease the ET efficiency. Actually, covalent attachment may result in multipoint attachment of the enzyme as more than one surface functional group may participate during bond formation. Consequently, the relative position achieved by immobilized enzymes is random and enzymes adopt nonuniform distribution orientations.

Infrared spectroscopy is a valuable tool to monitor the formation of a covalent bond between an immobilized enzyme and a linker. The EDC/NHS coupling reaction catalyzing the formation of amide bonds between the amino groups of a linker molecule on the surface of the Au electrode and

the carboxylic acid groups of a LAC was performed [144]. As a result of this covalent attachment, an absorption band appeared at 1737 cm^{-1}, typical of a carbonyl group, confirming the formation of covalent amide bonds between the amino-terminated linker of the gold electrode and the carboxylic functions of the LAC exposed to the solvent. Surface-Enhanced Raman Scattering (SERS) was used to monitor the covalent attachment of the azido-modified horseradish peroxidase onto gold electrodes modified with an alkynyl complex—1,4-dialkynylbenzene (DEB). The success of the click chemistry reaction was evidenced by the disappearance of the azide band of the enzyme involved in the covalent bond with the DEB monolayer [180]. Rudiger et al. reported higher operational stability compared to adsorbed enzymes when *D. gigas* [Ni-Fe]-Hase was covalently attached to gold electrodes modified with a SAM of 4-aminothiophenol. After 80 h of continuous operation, 25% of the initial current was maintained. A clear DET signal confirmed that the immobilization method favors an orientation where the active site of the enzyme faces the electrode surface [143]. Gutierrez-Sanchez et al. reported similar higher operational stability for covalent conjunction of *M. verucaria* BOD to gold electrodes modified by carboxylate-terminated SAM [145]. This result was obtained by coupling SPR to electrochemistry, and was unexpected since it was also demonstrated that before covalent attachment, the decrease in the catalytic signal was not related to any enzyme desorption from the gold surface. This observation clearly demonstrates that covalent binding induces some rigidification of the structure which is favorable to enzyme stability once immobilized. However, with the same *M. verucaria* BOD enzyme and on the same type of negative SAM on gold, Blanford et al. did not find any improvement of stability of the catalytic signal after covalent linking, and even showed a decrease in the magnitude of the current [181]. Actually, characteristics of the immobilized systems, including surface coverage, electrocatalytic activity, and stability of the proteins are considerably affected by the type of bond formed between electrode and protein, which is driven by the immobilization method. In the two cases just reported, the binding reaction was performed in two different ways. In the first case, the enzyme was first oriented according to electrostatic interaction on the SAM-modified gold electrode, and then the coupling reaction was performed. In the second case, the activated ester was first immobilized on the gold electrodes before enzyme coupling.

5.3. Effect of Enzyme Partition

In vivo, catalytic reactions mostly occur in an enzyme-crowded environment. It can thus be suspected that the density of enzymes on the electrode interface might impact the catalysis efficiency. The enzyme surface packing on the electrode could also influence its redox potential. For example, MD simulations and quantum calculations performed on cytochrome *c* covalently bound on a bare gold surface have shown that crowding of the proteins can raise their redox potential to around 100 mV [182]. This effect would be due to the change in the polarizability of the enzyme's environment, where much less polarizable proteins replace water. Concomitantly, enzyme surface density may alter enzyme orientation because of interactions between neighboring molecules. At the same time, such interactions may impede important functional movements. McArdle et al. used electrochemistry coupled to QCM with dissipation analysis to explore the effect of *M. verucaria* BOD molecular density on catalytic activity and layer rigidity. An optimum concentration of enzymes to be adsorbed was found as a balance between rates of adsorption, enzyme denaturation, and reorientation [146]. One way to vary the enzyme density at planar electrodes is to use mixed SAMs composed of different thiol derivatives. These SAMs are usually prepared by co-adsorption from a solution containing different thiol components onto an electrode surface. Mixed SAMs present stronger overall polarization than pure SAMs as a consequence of antiparallel orientation of dipoles within the SAM. In case of electrostatic binding of enzymes, this polarization induces an enhanced amount of enzyme loading [183]. Many studies dedicated to enzymatic electrocatalysis use mixed SAMs, although the partition of the thiols in such mixed layers is not straightforward, and a detailed relationship between the SAM mixed chemistry and the enzyme activity is rarely provided. Actually, dilution of two different thiols may result in homogeneous [184], or phase-separated monolayers [185]. It is

noteworthy that Traunsteiner et al. used electrochemistry to study the effect of the structure of a mixed SAM obtained by the dilution of short-chain thiols with a longer thiol chain, the linker, on the binding and catalytic efficiency of *T. versicolor* LAC (Figure 11). The linker was chosen to fit the Cu T1 pocket and to bind LAC in a favorable orientation for electrocatalysis. The arrangement of the linker was visualized by high-resolution STM, showing two configurations as a function of water content in the thiol solutions. In case of separated domains of the linker and the short thiol chain, very small catalytic current was observed, contrary to the high current obtained when LAC was immobilized on homogeneous mixed SAM. In the latter case, it was suggested that the isolation of the linker by short thiol molecules improved the binding of LAC [153].

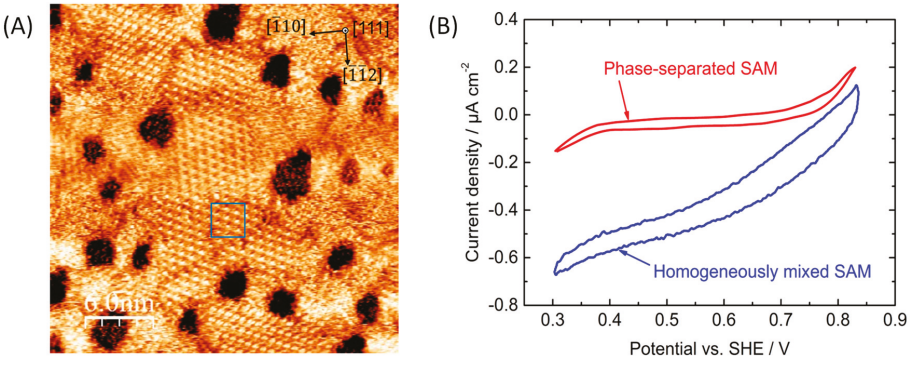

Figure 11. (**A**) EC-STM image showing homogeneous phase of a mixed SAM on Au(111) and (**B**) CVs of *T. versicolor* LAC immobilized on the homogeneously mixed SAM (blue) and the phase-separated SAM (red) on Au(111) in oxygen-saturated solution [153].

5.4. Effect of Potential, Electric Field

Electrical potential is a major parameter which controls redox enzyme activity, but also the formation of inactive states, or reactivation processes, by modulating the redox state of the active site. In addition to electrostatic interactions between charged species (either electrode or enzyme) induced by pH-dependent surface chemistry, electrical potential may also influence the enzyme conformation and orientation (and, hence, catalysis) in two different ways. First, performing the adsorption of the enzyme under an applied potential may have an impact on the orientation by creating an electric field around the enzyme. Second, imposing a potential once the enzyme is adsorbed on an electrode surface should affect its orientation and even its conformation by changing the charge in the environment of the enzyme. These two processes have been explored in only rare papers.

Proteins can be divided into hard and soft proteins depending on the conformational entropy of their structure. It was shown by ellipsometry and MD simulations that soft proteins, such as glucose oxidase, are less sensitive to changes in the conformation under applied potential once immobilized on a solid surface [186]. CueO [187] and fructose dehydrogenase (FDH) [188] adsorbed on a bare gold electrode at potentials around the potential of zero charge (E_{pzc}) showed the highest direct catalytic activity, suggesting a more favorable enzyme orientation. For both enzymes, DET activity decreased when enzymes were allowed to adsorb at electrode potentials far from the E_{pzc}. Different behavior as a function of the adsorbed potential was observed depending on the surface of the gold electrode, either bare, or modified by a hydrophobic thiol layer. The proposed model explains how the electrostatic interaction between the enzymes and the electrode in the electric double layer affects the orientation, but also the stability of the adsorbed enzymes. Lopez et al. immobilized *M. verrucaria* BOD on bare and nanocrystalline gold electrodes via potential pulse-assisted immobilization [189].

An increase in the direct catalytic current was observed compared to the electrode simply prepared by drop casting of enzyme, likely from a preferential orientation of *M. verrucaria* BOD.

The effect of electrode potential on protein immobilization after enzyme adsorption has also been investigated. Change in enzyme orientation upon application of a potential on the membrane-bound Hase from *R. eutropha* was monitored by spectroelectrochemistry [149]. Indeed, as discussed above, application of a negative potential below the E_{PZC} of the SAM-coated Au electrode confirms a reorientation of a fraction of the enzyme population in a more favorable configuration for DET, leading finally to an increase in catalytic current. On the other hand, possible deleterious side effects induced by the application of potential have been evidenced [190]. In the case of the anaerobic [NiFe]-Hase from *D. vulgaris* Miyazaki F, continuous potential application leads to a decrease in the intensity arising from the infrared markers of the active site (one C≡O and two C≡N ligands). Remarkably, the signal intensity arising from amide I and amide II bands reflecting the structural integrity of the enzyme remains constant, suggesting a targeted destruction of the active site. The authors suggest the in situ generation of ROS reacting with the active site and leading to its destruction. This experimental dataset argues against the widely used "film loss" explanation. Besides this, catalytic current dependence on the electrochemical methods used emphasized that cyclic voltammetry induced a faster decrease in the current for O_2 reduction by *M. verrucaria* BOD with time than did chronopotentiometry, suggesting a clear influence of the applied potential on the current stability [181]. The interfacial electric field has also been pointed out to affect the redox potential of enzymes. A SEIRA study of the type II NADH: Quinone Oxidoreductase from *E. coli* immobilized on SAM-modified gold electrodes outlined a substantial increase in the redox potential of the enzyme (~140 mV) [191]. The authors attributed this upshift in potential to an electric-field-driven stabilization of the flavin cofactor. This interpretation was supported by previous similar observations on tetraheme cytochromes c_3 [192].

6. Future Directions: Towards Rational Bioelectrode Design

We have reviewed how to control the orientation of redox enzymes on electrochemical interfaces. This step is mandatory to achieve a fast ET process and maximize the quantity of loaded enzymes on the surface. Success in such oriented immobilization is particularly important for practical applications as it will enable higher sensitivity for biosensors as well as higher current densities—and, hence, power densities—for biofuel cells. Fundamental understanding of the physiological processes in which redox enzymes are involved for ET is essential if one wants to provide the best tailored immobilization procedure. Protein–protein interactions can be investigated using numerous modeling tools, especially to identify potential interaction partners, and to determine the structure of protein assemblies on a surface [193] and the stability over time of these complexes. In particular, the modeling of protein complexes permits the identification of conformational changes induced by protein binding, which are likely to have a noticeable effect on the enzyme's biological function. Key parameters that may yield some degree of control over the orientation of enzymes may be deduced. The molecular bases for functional orientation of common and largely used enzymes are now available. This is the case for BOD and LAC, the enzymes widely used for O_2 reduction. This is also the case for Hases, which have been studied in depth on different types of planar electrodes. However, many enzymes, particularly less broadly used ones, remain silent in electrochemistry, which illustrates that the sole examination of the structure of an enzyme is not sufficient to describe the immobilization and ET phenomenon in its full complexity. The influence of tags used for purification, and surfactants in the case of membrane proteins, may play an essential role in enzyme orientation which is often underestimated.

One important issue that still needs to be further investigated is the effect of the orientation required for DET on the conformation and dynamics of the immobilized enzyme. Electrostatic interactions are most often required to guide a proper orientation of the enzyme yielding a high ET rate constant. Whether these interactions can affect the native conformation, or even denature the enzymes, is still an open question. From a theoretical perspective, molecular modeling approaches provide us

with a detailed picture on the molecular level of how the surface/protein interaction can control the enzymes' orientation, and eventually impact their conformation and internal dynamics. In addition, quantum calculation can help determine potential modifications of the enzymes' redox properties and catalytic activity when they are immobilized on the electrode surface. Some experimental works already clearly state change in the conformation of enzymes upon immobilization on an electrode. As a relevant illustration, the two highly homologous membrane-bound [NiFe]-Hases from *A. aeolicus* and *R. eutropha* display completely different behavior on highly negatively charged electrode surfaces [194]. Recovering of the catalytic signal for H_2 oxidation after surfactant addition in the *R. eutropha* Hase sample suggested that the absence of a surfactant compared to the *A. aeolicus* Hase sample induced structural changes of the enzyme because of the strong electrostatic interactions. LAC and BOD immobilized for DET on gold electrodes were shown to face potential-induced structural changes as revealed by SERRS and ellipsometry experiments [58,141]. QCM and dual-polarization interferometry studies of BOD immobilized on negative SAM-based gold electrodes highlighted that deformation required for DET should lead to a decrease in activity at high enzyme concentrations [146].

To improve the understanding and control of the molecular details involved in protein–electrode interaction, it is now mandatory to develop new methods that are able to relate in real time electrocatalytic activity to enzyme loading, enzyme partition, and enzyme conformation and dynamics. However, very few works nowadays report such coupled methods. One exception is SPR and QCM coupled to electrochemistry, the so-called e-SPR and e-QCM approaches that were already developed to correlate enzyme loading to activity [145,181]. Such coupled methods established for the first time the relation between the amount of deposited enzymes and the enzymatic activity. They also allowed a definite demonstration that a decrease in catalytic currents was not a result of enzyme leaking in most cases, but was due to other processes. Whether these other processes involved are reorientation, change in conformation, or denaturation must be now elucidated. Further developments in orientation-sensitive spectroelectrochemical methods such as PMIRRAS and Plasmon Waveguide Resonance [195], a much more sensitive variant of SPR able to measure affinity and kinetics of interaction, are currently running. They may allow us to relate the conformation of the enzyme or reorientation to its activity. To characterize the overall surface topology, fluorescence microscopy, or AFM approaches, should also be coupled to electrochemistry to constitute a map of enzyme localization on an electrode surface, and visualize the real effect of enzyme density. Such approaches require technological set ups that are currently under investigation for other redox systems than enzymes, but may be applied to redox enzymes in the near future [196]. Sampling issues remain a bottleneck in the simulation of enzyme–surface interactions, in particular, for investigating processes taking place on a large range of length and time scales. Therefore, the development of enhanced sampling methods and multiscale approaches represents a central challenge for studying such complex systems. Finally, sensitive electrochemical methods have to be developed to search for noncatalytic signals, allowing us to access the real amounts of enzymes effectively participating in the catalysis.

With that objective and to enhance the signal-to-noise ratio, electrochemical interfaces other than planar electrodes should be used. However, one should define for which conditions the key parameters for a specific enzyme orientation obtained on flat electrodes could be extended to more complex electrodes, and beyond to 3D nanostructures. A few recently reported examples demonstrated the ability to transfer the determined molecular basis for DET from a planar to a more complex-structured electrode. The physicochemical properties of the SAM-modified gold electrodes obtained in the case of *M. verrucaria* BOD were transposed to functionalized nanoporous gold [197], as well as to functionalized carbon nanotubes films [30]. The requirement of an aromatic linker to anchor LAC via the Cu T1 was confirmed on films made of gold nanoparticles [198]. Catalysis with *A. aeolicus* Hase immobilized on carbon nanotubes presenting different surface chemistry highlighted good correlation with catalytic currents observed on the corresponding SAM functionality on planar gold electrodes. Agreement between the magnitudes of the catalytic current as a function of the surface chemistry on the carbon nanotubes with theoretical modeling of the dipole moment of the enzyme was also

demonstrated [194]. Nevertheless, only a low percentage, around 10%, of the loaded enzymes were electrically connected in the 3D structure [21], which suggests that other parameters than a correct enzyme orientation for DET drive catalysis in 3D conductive structures. One should be aware of the heterogeneity of electrochemical interfaces such as those formed by carbon nanotubes or carbon particles. Indeed, on such surfaces the walls of the carbon nanotubes are hydrophobic. Chemical functions are created upon carbon nanotube oxidative treatment or after π-binding of aromatic derivatives, yielding surfaces presenting various functionalities. The multiporosity displayed by 3D conductive surface must also be taken into account. Such a property is expected to be suitable for electrocatalysis, with macroporosity (pore diameter more than 50 nm) allowing fast substrate transport and mesoporosity allowing stable enzyme encapsulation. In the case when the pore is of the same dimension as the enzyme, one can expect that electrical connection of the enzyme might be efficient independently of its orientation, with the functionalities on the material serving only for stable anchorage [199]. In this case, however, transport processes should play a key role, both to provide a sufficient level of substrate to the enzyme and to permit fast evacuation of the product to avoid enzyme inhibition. This means that efficient bioelectrocatalysis will be achieved through a balance between electrical connection of a high amount of redox enzymes, protection of the enzymes in a suitable conductive structure, and substrate availability.

Acknowledgments: This work was supported by ANR (ENZYMOR-ANR-16-CE05-0024) and by the "Initiative d'Excellence" program from the French State (Grant "DYNAMO", ANR-11-LABX-0011-01).

Conflicts of Interest: The authors declare no conflict of interest.

References

1. Mellor, S.B.; Vavitsas, K.; Nielsen, A.Z.; Jensen, P.E. Photosynthetic fuel for heterologous enzymes: The role of electron carrier proteins. *Photosynth. Res.* **2017**, *134*, 329–342. [CrossRef] [PubMed]
2. Ilbert, M.; Bonnefoy, V. Insight into the evolution of the iron oxidation pathways. *Biochim. Biophys. Acta Bioenerg.* **2013**, *1827*, 161–175. [CrossRef] [PubMed]
3. Guiral, M.; Aussignargues, C.; Prunetti, L.; Infossi, P.; Ilbert, M.; Giudici-Orticoni, M.T. The energy sulfur metabolism of the hyperthermophilic bacterium *Aquifex aeolicus*. *Biochim. Biophys. Acta Bioenerg.* **2012**, *1817*, S155. [CrossRef]
4. Moehlenbrock, M.J.; Minteer, S.D. Extended lifetime biofuel cells. *Chem. Soc. Rev.* **2008**, *37*, 1188–1196. [CrossRef] [PubMed]
5. Maduraiveeran, G.; Sasidharan, M.; Ganesan, V. Electrochemical sensor and biosensor platforms based on advanced nanomaterials for biological and biomedical applications. *Biosens. Bioelectron.* **2018**, *103*, 113–129. [CrossRef] [PubMed]
6. Justino, C.I.L.; Duarte, A.C.; Rocha-Santos, T.A.P. Recent Progress in Biosensors for Environmental Monitoring: A review. *Sensors* **2017**, *17*, 2918. [CrossRef] [PubMed]
7. Clark, L.C.; Lyons, C. Electrode systems for continuous monitoring in cardiovascular surgery. *Ann. N. Y. Acad. Sci.* **1962**, *102*, 29–45. [CrossRef] [PubMed]
8. Bandodkar, A.J.; Imani, S.; Nunez-Flores, R.; Kumar, R.; Wang, C.Y.; Mohan, A.M.V.; Wang, J.; Mercier, P.P. Re-usable electrochemical glucose sensors integrated into a smartphone platform. *Biosens. Bioelectron.* **2018**, *101*, 181–187. [CrossRef] [PubMed]
9. Bruen, D.; Delaney, C.; Florea, L.; Diamond, D. Glucose Sensing for Diabetes Monitoring: Recent Developments. *Sensors* **2017**, *17*, 1866. [CrossRef] [PubMed]
10. Bandodkar, A.J.; Wang, J. Non-invasive wearable electrochemical sensors: A review. *Trends Biotechnol.* **2014**, *32*, 363–371. [CrossRef] [PubMed]
11. Santharaman, P.; Venkatesh, K.A.; Vairamani, K.; Benjamin, A.R.; Sethy, N.K.; Bhargava, K.; Karunakaran, C. ARM-microcontroller based portable nitrite electrochemical analyzer using cytochrome *c* reductase biofunctionalized onto screen printed carbon electrode. *Biosens. Bioelectron.* **2017**, *90*, 410–417. [CrossRef] [PubMed]

12. Huang, Y.; Tan, J.; Cui, L.J.; Zhou, Z.D.; Zhou, S.F.; Zhang, Z.H.; Zheng, R.; Xue, Y.W.; Zhang, M.X.; Li, S.S.; et al. Graphene and Au NPs co-mediated enzymatic silver deposition for the ultrasensitive electrochemical detection of cholesterol. *Biosens. Bioelectron.* **2018**, *102*, 560–567. [CrossRef] [PubMed]
13. Jakhar, S.; Pundir, C.S. Preparation, characterization and application of urease nanoparticles for construction of an improved potentiometric urea biosensor. *Biosens. Bioelectron.* **2018**, *100*, 242–250. [CrossRef] [PubMed]
14. Anik, U.; Tepeli, Y.; Diouani, M.F. Fabrication of Electrochemical Model Influenza A Virus Biosensor Based on the Measurements of Neuroaminidase Enzyme Activity. *Anal. Chem.* **2016**, *88*, 6151–6153. [CrossRef] [PubMed]
15. Sharma, B.; Dangi, A.K.; Shukla, P. Contemporary enzyme based technologies for bioremediation: A review. *J. Environ. Manag.* **2018**, *210*, 10–22. [CrossRef] [PubMed]
16. Morrison, C.S.; Armiger, W.B.; Dodds, D.R.; Dordick, J.S.; Koffas, M.A.G. Improved strategies for electrochemical 1,4-NAD(P)H_2 regeneration: A new era of bioreactors for industrial biocatalysis. *Biotechnol. Adv.* **2018**, *36*, 120–131. [CrossRef] [PubMed]
17. Bajracharya, S.; Srikanth, S.; Mohanakrishna, G.; Zacharia, R.; Strik, D.; Pant, D. Biotransformation of carbon dioxide in bioelectrochemical systems: State of the art and future prospects. *J. Power Sources* **2017**, *356*, 256–273. [CrossRef]
18. Hadj-Said, J.; Pandelia, M.E.; Leger, C.; Fourmond, V.; Dementin, S. The Carbon Monoxide Dehydrogenase from Desulfovibrio vulgaris. *Biochim. Biophys. Acta Bioenerg.* **2015**, *1847*, 1574–1583. [CrossRef] [PubMed]
19. Gamella, M.; Koushanpour, A.; Katz, E. Biofuel cells—Activation of micro- and macro-electronic devices. *Bioelectrochemistry* **2018**, *119*, 33–42. [CrossRef] [PubMed]
20. Mazurenko, I.; Wang, X.; de Poulpiquet, A.; Lojou, E. H_2/O_2 enzymatic fuel cells: From proof-of-concept to powerful devices. *Sustain. Energy Fuels* **2017**, *1*, 1475–1501. [CrossRef]
21. Mazurenko, I.; Monsalve, K.; Infossi, P.; Giudici-Orticoni, M.T.; Topin, F.; Mano, N.; Lojou, E. Impact of substrate diffusion and enzyme distribution in 3D-porous electrodes: A combined electrochemical and modelling study of a thermostable H_2/O_2 enzymatic fuel cell. *Energy Environ. Sci.* **2017**, *10*, 1966–1982. [CrossRef]
22. Hoarau, M.; Badieyan, S.; Marsh, E.N.G. Immobilized enzymes: Understanding enzyme—Surface interactions at the molecular level. *Org. Biomol. Chem.* **2017**, *15*, 9539–9551. [CrossRef] [PubMed]
23. Winkler, J.R.; Gray, H.B. Electron flow through metalloproteins. *Chem. Rev.* **2013**, *114*, 3369–3380. [CrossRef] [PubMed]
24. Marcus, R.A.; Sutin, N. Electron transfers in chemistry and biology. *Biochim. Biophys. Acta* **1985**, *811*, 265–322. [CrossRef]
25. Moser, C.C.; Keske, J.M.; Warncke, K.; Farid, R.S.; Dutton, P.L. Nature of biological electron-transfer. *Nature* **1992**, *355*, 796–802. [CrossRef] [PubMed]
26. Bostick, C.D.; Mukhopadhyay, S.; Pecht, I.; Sheves, M.; Cahen, D.; Lederman, D. Protein bioelectronics: A review of what we do and do not know. *Rep. Prog. Phys.* **2018**, *81*, 026601. [CrossRef] [PubMed]
27. Page, C.C.; Moser, C.C.; Chen, X.X.; Dutton, P.L. Natural engineering principles of electron tunnelling in biological oxidation-reduction. *Nature* **1999**, *402*, 47–52. [CrossRef] [PubMed]
28. Ozboyaci, M.; Kokh, D.B.; Corni, S.; Wade, R.C. Modeling and simulation of protein-surface interactions: Achievements and challenges. *Q. Rev. Biophys.* **2016**, *49*, e4. [CrossRef] [PubMed]
29. Léger, C.; Bertrand, P. Direct electrochemistry of redox enzymes as a tool for mechanistic studies. *Chem. Rev.* **2008**, *108*, 2379–2438. [CrossRef] [PubMed]
30. Mazurenko, I.; Monsalve, K.; Rouhana, J.; Parent, P.; Laffon, C.; Goff, A.L.; Szunerits, S.; Boukherroub, R.; Giudici-Orticoni, M.-T.; Mano, N. How the intricate interactions between carbon nanotubes and two bilirubin oxidases control direct and mediated O_2 reduction. *ACS Appl. Mater. Interfaces* **2016**, *8*, 23074–23085. [CrossRef] [PubMed]
31. Oteri, F.; Baaden, M.; Lojou, E.; Sacquin-Mora, S. Multiscale simulations give insight into the hydrogen in and out pathways of [NiFe]-hydrogenases from *Aquifex aeolicus* and Desulfovibrio fructosovorans. *J. Phys. Chem. B* **2014**, *118*, 13800–13811. [CrossRef] [PubMed]
32. Ogorzalek, T.L.; Wei, S.; Liu, Y.; Wang, Q.; Brooks, C.L., III; Chen, Z.; Marsh, E.N.G. Molecular-level insights into orientation-dependent changes in the thermal stability of enzymes covalently immobilized on surfaces. *Langmuir* **2015**, *31*, 6145–6153. [CrossRef] [PubMed]

33. Mano, N.; de Poulpiquet, A. O_2 Reduction in Enzymatic Biofuel Cells. *Chem. Rev.* **2018**, *118*, 2392–2468. [CrossRef] [PubMed]
34. Sakurai, T.; Kataoka, K. Basic and applied features of multicopper oxidases, CueO, bilirubin oxidase, and laccase. *Chem. Rec.* **2007**, *7*, 220–229. [CrossRef] [PubMed]
35. Solomon, E.I.; Augustine, A.J.; Yoon, J. O_2 Reduction to H_2O by the multicopper oxidases. *Dalton Trans.* **2008**, *30*, 3921–3932. [CrossRef] [PubMed]
36. Lubitz, W.; Ogata, H.; Rüdiger, O.; Reijerse, E. Hydrogenases. *Chem. Rev.* **2014**, *114*, 4081–4148. [CrossRef] [PubMed]
37. Fontecilla-Camps, J.C.; Volbeda, A.; Cavazza, C.; Nicolet, Y. Structure/function relationships of [NiFe]-and [FeFe]-hydrogenases. *Chem. Rev.* **2007**, *107*, 4273–4303. [CrossRef] [PubMed]
38. Wang, P.-H.; Best, R.B.; Blumberger, J. Multiscale simulation reveals multiple pathways for H_2 and O_2 transport in a [NiFe]-hydrogenase. *J. Am. Chem. Soc.* **2011**, *133*, 3548–3556. [CrossRef] [PubMed]
39. Wilson, R.; Turner, A. Glucose oxidase: An ideal enzyme. *Biosens. Bioelectron.* **1992**, *7*, 165–185. [CrossRef]
40. Hecht, H.; Schomburg, D.; Kalisz, H.; Schmid, R. The 3D structure of glucose oxidase from Aspergillus niger. Implications for the use of GOD as a biosensor enzyme. *Biosens. Bioelectron.* **1993**, *8*, 197–203. [CrossRef]
41. Zebda, A.; Gondran, C.; Le Goff, A.; Holzinger, M.; Cinquin, P.; Cosnier, S. Mediatorless high-power glucose biofuel cells based on compressed carbon nanotube-enzyme electrodes. *Nat. Commun.* **2011**, *2*, 370. [CrossRef] [PubMed]
42. Ludwig, R.; Ortiz, R.; Schulz, C.; Harreither, W.; Sygmund, C.; Gorton, L. Cellobiose dehydrogenase modified electrodes: Advances by materials science and biochemical engineering. *Anal. Bioanal. Chem.* **2013**, *405*, 3637–3658. [CrossRef] [PubMed]
43. Secundo, F. Conformational changes of enzymes upon immobilisation. *Chem. Soc. Rev.* **2013**, *42*, 6250–6261. [CrossRef] [PubMed]
44. Sugimoto, Y.; Kitazumi, Y.; Shirai, O.; Nishikawa, K.; Higuchi, Y.; Yamamoto, M.; Kano, K. Electrostatic roles in electron transfer from NiFe hydrogenase to cytochrome c_3 from Desulfovibrio vulgaris Miyazaki F. *Biochim. Biophys. Acta Proteins Proteom.* **2017**, *1865*, 481–487. [CrossRef] [PubMed]
45. Shimada, S.; Shinzawa-Itoh, K.; Baba, J.; Aoe, S.; Shimada, A.; Yamashita, E.; Kang, J.Y.; Tateno, M.; Yoshikawa, S.; Tsukihara, T. Complex structure of cytochrome *c*-cytochrome *c* oxidase reveals a novel protein-protein interaction mode. *EMBO J.* **2017**, *36*, 291–300. [CrossRef] [PubMed]
46. Kim, J.Y.; Kinoshita, M.; Kume, S.; Gt, H.; Sugiki, T.; Ladbury, J.E.; Kojima, C.; Ikegami, T.; Kurisu, G.; Goto, Y.; et al. Non-covalent forces tune the electron transfer complex between ferredoxin and sulfite reductase to optimize enzymatic activity. *Biochem. J.* **2016**, *473*, 3837–3854. [CrossRef] [PubMed]
47. Andralojc, W.; Hiruma, Y.; Liu, W.M.; Ravera, E.; Nojiri, M.; Parigi, G.; Luchinat, C.; Ubbink, M. Identification of productive and futile encounters in an electron transfer protein complex. *Proc. Natl. Acad. Sci. USA* **2017**, *114*, E1840–E1847. [CrossRef] [PubMed]
48. Kollipara, S.; Tatireddy, S.; Pathirathne, T.; Rathnayake, L.K.; Northrup, S.H. Contribution of Electrostatics to the Kinetics of Electron Transfer from NADH-Cytochrome b_5 Reductase to Fe(III)-Cytochrome b_5. *J. Phys. Chem. B* **2016**, *120*, 8193–8207. [CrossRef] [PubMed]
49. Cracknell, J.A.; Vincent, K.A.; Armstrong, F.A. Enzymes as working or inspirational electrocatalysts for fuel cells and electrolysis. *Chem. Rev.* **2008**, *108*, 2439–2461. [CrossRef] [PubMed]
50. Felder, C.E.; Prilusky, J.; Silman, I.; Sussman, J.L. A server and database for dipole moments of proteins. *Nucleic Acids Res.* **2007**, *35*, W512–W521. [CrossRef] [PubMed]
51. Topin, J.; Rousset, M.; Antonczak, S.; Golebiowski, J. Kinetics and thermodynamics of gas diffusion in a NiFe hydrogenase. *Proteins Struct. Funct. Bioinform.* **2012**, *80*, 677–682. [CrossRef] [PubMed]
52. Narth, C.; Gillet, N.; Cailliez, F.; Lévy, B.; de la Lande, A.L. Electron transfer, decoherence, and protein dynamics: Insights from atomistic simulations. *Acc. Chem Res.* **2015**, *48*, 1090–1097. [CrossRef] [PubMed]
53. Mazurenko, I.; de Poulpiquet, A.; Lojou, E. Recent developments in high surface area bioelectrodes for enzymatic fuel cells. *Curr. Opin. Electrochem.* **2017**, *5*, 74–84. [CrossRef]
54. Mazurenko, I.; Clément, R.; Byrne-Kodjabachian, D.; de Poulpiquet, A.; Tsujimura, S.; Lojou, E. Pore size effect of MgO-templated carbon on enzymatic H_2 oxidation by the hyperthermophilic hydrogenase from *Aquifex aeolicus*. *J. Electroanal. Chem.* **2018**, *812*, 221–226. [CrossRef]

55. Ash, P.A.; Liu, J.; Coutard, N.; Heidary, N.; Horch, M.; Gudim, I.; Simler, T.; Zebger, I.; Lenz, O.; Vincent, K.A. Electrochemical and Infrared Spectroscopic Studies Provide Insight into Reactions of the NiFe Regulatory Hydrogenase from Ralstonia eutropha with O_2 and CO. *J. Phys. Chem. B* **2015**, *119*, 13807–13815. [CrossRef] [PubMed]
56. Thorum, M.S.; Anderson, C.A.; Hatch, J.J.; Campbell, A.S.; Marshall, N.M.; Zimmerman, S.C.; Lu, Y.; Gewirth, A.A. Direct, Electrocatalytic Oxygen Reduction by Laccase on Anthracene-2-methanethiol-Modified Gold. *J. Phys. Chem. Lett.* **2010**, *1*, 2251–2254. [CrossRef] [PubMed]
57. Feng, G.; Niu, T.; You, X.; Wan, Z.; Kong, Q.; Bi, S. Studies on the effect of electrode pretreatment on the coverage of self-assembled monolayers of dodecanethiol on gold by electrochemical reductive desorption determination. *Analyst* **2011**, *136*, 5058–5063. [CrossRef] [PubMed]
58. Pankratov, D.; Sotres, J.; Barrantes, A.; Arnebrant, T.; Shleev, S. Interfacial behavior and activity of laccase and bilirubin oxidase on bare gold surfaces. *Langmuir* **2014**, *30*, 2943–2951. [CrossRef] [PubMed]
59. Trasatti, S.; Petrii, O. Real surface area measurements in electrochemistry. *Pure Appl. Chem.* **1991**, *63*, 711–734. [CrossRef]
60. Monsalve, K.; Roger, M.; Gutierrez-Sanchez, C.; Ilbert, M.; Nitsche, S.; Byrne-Kodjabachian, D.; Marchi, V.; Lojou, E. Hydrogen bioelectrooxidation on gold nanoparticle-based electrodes modified by *Aquifex aeolicus* hydrogenase: Application to hydrogen/oxygen enzymatic biofuel cells. *Bioelectrochemistry* **2015**, *106*, 47–55. [CrossRef] [PubMed]
61. Sezer, M.; Millo, D.; Weidinger, I.M.; Zebger, I.; Hildebrandt, P. Analyzing the catalytic processes of immobilized redox enzymes by vibrational spectroscopies. *IUBMB Life* **2012**, *64*, 455–464. [CrossRef] [PubMed]
62. Buividas, R.; Fahim, N.; Juodkazytė, J.; Juodkazis, S. Novel method to determine the actual surface area of a laser-nanotextured sensor. *Appl. Phys. A* **2014**, *114*, 169–175. [CrossRef]
63. Fang, S.-U.; Hsu, C.-L.; Hsu, T.-C.; Juang, M.-Y.; Liu, Y.-C. Surface roughness-correlated SERS effect on Au island-deposited substrate. *J. Electroanal. Chem.* **2015**, *741*, 127–133. [CrossRef]
64. Mendelsohn, R.; Mao, G.; Flach, C.R. Infrared Reflection-Absorption Spectroscopy: Principles and Applications to Lipid-Protein Interaction in Langmuir Films. *Biochim. Biophys. Acta* **2010**, *1798*, 788–800. [CrossRef] [PubMed]
65. Dongmo, S.; Wittstock, G.; Christoffers, J.; Brand, I. In situ determination of potential-driven structural changes in a redox-active plumbagin polymer film on a glassy carbon electrode using PM IRRAS under electrochemical control. *Electrochim. Acta* **2017**, *255*, 298–308. [CrossRef]
66. Heinz, H.; Vaia, R.; Farmer, B.; Naik, R. Accurate simulation of surfaces and interfaces of face-centered cubic metals using 12−6 and 9−6 Lennard-Jones potentials. *J. Phys. Chem. C* **2008**, *112*, 17281–17290. [CrossRef]
67. Iori, F.; Di Felice, R.; Molinari, E.; Corni, S. GolP: An atomistic force-field to describe the interaction of proteins with Au (111) surfaces in water. *J. Comput. Chem.* **2009**, *30*, 1465–1476. [CrossRef] [PubMed]
68. Heinz, H.; Lin, T.-J.; Kishore Mishra, R.; Emami, F.S. Thermodynamically consistent force fields for the assembly of inorganic, organic, and biological nanostructures: The INTERFACE force field. *Langmuir* **2013**, *29*, 1754–1765. [CrossRef] [PubMed]
69. Kubiak-Ossowska, K.; Jachimska, B.; Mulheran, P.A. How Negatively Charged Proteins Adsorb to Negatively Charged Surfaces: A Molecular Dynamics Study of BSA Adsorption on Silica. *J. Phys. Chem. B* **2016**, *120*, 10463–10468. [CrossRef] [PubMed]
70. Mücksch, C.; Urbassek, H.M. Molecular dynamics simulation of free and forced BSA adsorption on a hydrophobic graphite surface. *Langmuir* **2011**, *27*, 12938–12943. [CrossRef] [PubMed]
71. Trohalaki, S.; Pachter, R.; Luckarift, H.; Johnson, G. Immobilization of the Laccases from *Trametes versicolor* and *Streptomyces coelicolor* on Single-wall Carbon Nanotube Electrodes: A Molecular Dynamics Study. *Fuel Cells* **2012**, *12*, 656–664. [CrossRef]
72. Heinz, H.; Jha, K.C.; Luettmer-Strathmann, J.; Farmer, B.L.; Naik, R.R. Polarization at metal–biomolecular interfaces in solution. *J. R. Soc. Interface* **2011**, *8*, 220–232. [CrossRef] [PubMed]
73. Wright, L.B.; Rodger, P.M.; Corni, S.; Walsh, T.R. GolP-CHARMM: First-principles based force fields for the interaction of proteins with Au (111) and Au (100). *J. Chem. Theory Comput.* **2013**, *9*, 1616–1630. [CrossRef] [PubMed]
74. Shi, Y.; Xia, Z.; Zhang, J.; Best, R.; Wu, C.; Ponder, J.W.; Ren, P. Polarizable atomic multipole-based AMOEBA force field for proteins. *J. Chem. Theory Comput.* **2013**, *9*, 4046–4063. [CrossRef] [PubMed]

75. Akdim, B.; Pachter, R.; Kim, S.S.; Naik, R.R.; Walsh, T.R.; Trohalaki, S.; Hong, G.; Kuang, Z.; Farmer, B.L. Electronic properties of a graphene device with peptide adsorption: Insight from simulation. *ACS Appl. Mater. Interfaces* **2013**, *5*, 7470–7477. [CrossRef] [PubMed]
76. Datta, S.; Christena, L.R.; Rajaram, Y.R.S. Enzyme immobilization: An overview on techniques and support materials. *3 Biotech* **2013**, *3*, 1–9. [CrossRef] [PubMed]
77. Mohamad, N.R.; Marzuki, N.H.C.; Buang, N.A.; Huyop, F.; Wahab, R.A. An overview of technologies for immobilization of enzymes and surface analysis techniques for immobilized enzymes. *Biotechnol. Biotechnol. Equip.* **2015**, *29*, 205–220. [CrossRef] [PubMed]
78. Arya, S.K.; Prusty, A.K.; Singh, S.; Solanki, P.R.; Pandey, M.K.; Datta, M.; Malhotra, B.D. Cholesterol biosensor based on *N*-(2-aminoethyl)-3-aminopropyl-trimethoxysilane self-assembled monolayer. *Anal. Biochem.* **2007**, *363*, 210–218. [CrossRef] [PubMed]
79. Ulman, A. Formation and structure of self-assembled monolayers. *Chem. Rev.* **1996**, *96*, 1533–1554. [CrossRef] [PubMed]
80. Jin, B.; Wang, G.-X.; Millo, D.; Hildebrandt, P.; Xia, X.-H. Electric-field control of the pH-dependent redox process of cytochrome *c* immobilized on a gold electrode. *J. Phys. Chem. C* **2012**, *116*, 13038–13044. [CrossRef]
81. Bryant, M.A.; Crooks, R.M. Determination of surface pKa values of surface-confined molecules derivatized with pH-sensitive pendant groups. *Langmuir* **1993**, *9*, 385–387. [CrossRef]
82. Marmisollé, W.A.; Capdevila, D.A.; de la Llave, E.; Williams, F.J.; Murgida, D.H. Self-Assembled Monolayers of NH_2-Terminated Thiolates: Order, pK_a, and Specific Adsorption. *Langmuir* **2013**, *29*, 5351–5359. [CrossRef] [PubMed]
83. Gooding, J.J.; Ciampi, S. The molecular level modification of surfaces: From self-assembled monolayers to complex molecular assemblies. *Chem. Soc. Rev.* **2011**, *40*, 2704–2718. [CrossRef] [PubMed]
84. Dubois, L.H.; Nuzzo, R.G. Synthesis, structure, and properties of model organic surfaces. *Ann. Rev. Phys. Chem.* **1992**, *43*, 437–463. [CrossRef]
85. Love, J.C.; Estroff, L.A.; Kriebel, J.K.; Nuzzo, R.G.; Whitesides, G.M. Self-assembled monolayers of thiolates on metals as a form of nanotechnology. *Chem. Rev.* **2005**, *105*, 1103–1170. [CrossRef] [PubMed]
86. Schwartz, D.K. Mechanisms and kinetics of self-assembled monolayer formation. *Ann. Rev. Phys. Chem.* **2001**, *52*, 107–137. [CrossRef] [PubMed]
87. Porter, M.D.; Bright, T.B.; Allara, D.L.; Chidsey, C.E. Spontaneously organized molecular assemblies. 4. Structural characterization of n-alkyl thiol monolayers on gold by optical ellipsometry, infrared spectroscopy, and electrochemistry. *J. Am. Chem. Soc.* **1987**, *109*, 3559–3568. [CrossRef]
88. Jambrec, D.; Conzuelo, F.; Estrada-Vargas, A.; Schuhmann, W. Potential-Pulse-Assisted Formation of Thiol Monolayers within Minutes for Fast and Controlled Electrode Surface Modification. *ChemElectroChem* **2016**, *3*, 1484–1489. [CrossRef]
89. Samanta, D.; Sarkar, A. Immobilization of bio-macromolecules on self-assembled monolayers: Methods and sensor applications. *Chem. Soc. Rev.* **2011**, *40*, 2567–2592. [CrossRef] [PubMed]
90. Mondal, P.C.; Fontanesi, C. Electrochemistry of Metalloproteins Attached through Functional Self-Assembled Monolayers on Gold and Ferromagnetic Electrodes. *ChemPhysChem* **2018**, *19*, 60–66. [CrossRef] [PubMed]
91. Aydın, E.B.; Sezgintürk, M.K. Indium Tin Oxide (ITO): A promising material in biosensing technology. *TrAC Trends Anal. Chem.* **2017**, *97*, 309–315. [CrossRef]
92. Vashist, S.K.; Lam, E.; Hrapovic, S.; Male, K.B.; Luong, J.H. Immobilization of antibodies and enzymes on 3-aminopropyltriethoxysilane-functionalized bioanalytical platforms for biosensors and diagnostics. *Chem. Rev.* **2014**, *114*, 11083–11130. [CrossRef] [PubMed]
93. Yoshioka, K.; Kato, D.; Kamata, T.; Niwa, O. Cytochrome P450 modified polycrystalline indium tin oxide film as a drug metabolizing electrochemical biosensor with a simple configuration. *Anal. Chem.* **2013**, *85*, 9996–9999. [CrossRef] [PubMed]
94. Smalley, J.F.; Feldberg, S.W.; Chidsey, C.E.; Linford, M.R.; Newton, M.D.; Liu, Y.-P. The kinetics of electron transfer through ferrocene-terminated alkanethiol monolayers on gold. *J. Phys. Chem.* **1995**, *99*, 13141–13149. [CrossRef]
95. Xu, J.; Li, H.; Zhang, Y. Relationship between electronic tunneling coefficient and electrode potential investigated by using self-assembled alkanethiol monolayers on gold electrodes. *J. Phys. Chem.* **1993**, *97*, 11497–11500. [CrossRef]

96. Mokrani, C.; Fatisson, J.; Guerente, L.; Labbe, P. Structural characterization of (3-mercaptopropyl)sulfonate monolayer on gold surfaces. *Langmuir* **2005**, *21*, 4400–4409. [CrossRef] [PubMed]
97. Liu, B.; Bard, A.J.; Mirkin, M.V.; Creager, S.E. Electron transfer at self-assembled monolayers measured by scanning electrochemical microscopy. *J. Am. Chem. Soc.* **2004**, *126*, 1485–1492. [CrossRef] [PubMed]
98. Chi, Q.J.; Zhang, J.D.; Andersen, J.E.T.; Ulstrup, J. Ordered assembly and controlled electron transfer of the blue copper protein azurin at gold (111) single-crystal substrates. *J. Phys. Chem. B* **2001**, *105*, 4669–4679. [CrossRef]
99. Beulen, M.W.; Kastenberg, M.I.; van Veggel, F.C.; Reinhoudt, D.N. Electrochemical stability of self-assembled monolayers on gold. *Langmuir* **1998**, *14*, 7463–7467. [CrossRef]
100. Ovchinnikova, S.; Medvedev, A.Z. Desorption of octanethiol from gold electrode surface during its electrochemical cleaning. *Russ. J. Electrochem.* **2015**, *51*, 287–293. [CrossRef]
101. Stettner, J.; Winkler, A. Characterization of alkanethiol self-assembled monolayers on gold by thermal desorption spectroscopy. *Langmuir* **2010**, *26*, 9659–9665. [CrossRef] [PubMed]
102. Rzeźnicka, I.I.; Lee, J.; Maksymovych, P.; Yates, J.T. Nondissociative chemisorption of short chain alkanethiols on Au (111). *J. Phys. Chem. B* **2005**, *109*, 15992–15996. [CrossRef] [PubMed]
103. Ossowski, J.; Nascimbeni, G.; Żaba, T.; Verwüster, E.; Rysz, J.; Terfort, A.; Zharnikov, M.; Zojer, E.; Cyganik, P. Relative Thermal Stability of Thiolate-and Selenolate-Bonded Aromatic Monolayers on the Au (111) Substrate. *J. Phys. Chem. C* **2017**, *121*, 28031–28042. [CrossRef]
104. Wang, Y.; Solano Canchaya, J.G.; Dong, W.; Alcami, M.; Busnengo, H.F.; Martin, F. Chain-Length and Temperature Dependence of Self-Assembled Monolayers of Alkylthiolates on Au (111) and Ag (111) Surfaces. *J. Phys. Chem. A* **2014**, *118*, 4138–4146. [CrossRef] [PubMed]
105. Guo, L.; Ma, L.; Zhang, Y.; Cheng, X.; Xu, Y.; Wang, J.; Wang, E.; Peng, Z. Spectroscopic Identification of the Au–C Bond Formation upon Electroreduction of an Aryl Diazonium Salt on Gold. *Langmuir* **2016**, *32*, 11514–11519. [CrossRef] [PubMed]
106. Vacca, A.; Mascia, M.; Rizzardini, S.; Palmas, S.; Mais, L. Coating of gold substrates with polyaniline through electrografting of aryl diazonium salts. *Electrochim. Acta* **2014**, *126*, 81–89. [CrossRef]
107. Olejnik, P.; Palys, B.; Kowalczyk, A.; Nowicka, A.M. Orientation of laccase on charged surfaces. Mediatorless oxygen reduction on amino-and carboxyl-ended ethylphenyl groups. *J. Phys. Chem. C* **2012**, *116*, 25911–25918. [CrossRef]
108. Hetemi, D.; Pinson, J. Surface functionalisation of polymers. *Chem. Soc. Rev.* **2017**, *46*, 5701–5713. [CrossRef] [PubMed]
109. Santos, L.; Ghilane, J.; Lacroix, J.C. Formation of mixed organic layers by stepwise electrochemical reduction of diazonium compounds. *J. Am. Chem. Soc.* **2012**, *134*, 5476–5479. [CrossRef] [PubMed]
110. Santos, L.; Mattiuzzi, A.; Jabin, I.; Vandencasteele, N.; Reniers, F.O.; Reinaud, O.; Hapiot, P.; Lhenry, S.B.; Leroux, Y.; Lagrost, C. One-Pot Electrografting of Mixed Monolayers with Controlled Composition. *J. Phys. Chem. C* **2014**, *118*, 15919–15928. [CrossRef]
111. Leroux, Y.R.; Hapiot, P. Nanostructured monolayers on carbon substrates prepared by electrografting of protected aryldiazonium salts. *Chem. Mater.* **2013**, *25*, 489–495. [CrossRef]
112. Zhang, X.; Rösicke, F.; Syritski, V.; Sun, G.; Reut, J.; Hinrichs, K.; Janietz, S.; Rappich, J. Influence of the para-substitutent of benzene diazonium salts and the solvent on the film growth during electrochemical reduction. *Z. Phys. Chem.* **2014**, *228*, 557–573. [CrossRef]
113. Bouden, S.; Pinson, J.; Vautrin-Ul, C. Electrografting of diazonium salts: A kinetics study. *Electrochem. Commun.* **2017**, *81*, 120–123. [CrossRef]
114. Pita, M.; Gutierrez-Sanchez, C.; Olea, D.; Velez, M.; Garcia-Diego, C.; Shleev, S.; Fernandez, V.M.; De Lacey, A.L. High Redox Potential Cathode Based on Laccase Covalently Attached to Gold Electrode. *J. Phys. Chem. C* **2011**, *115*, 13420–13428. [CrossRef]
115. Alam, M.T.; Gooding, J.J. Modification of carbon electrode surfaces. In *Electrochemistry of Carbon Electrodes*; Wiley: Hoboken, NJ, USA, 2016; Volume 16.
116. Cracknell, J.A.; McNamara, T.P.; Lowe, E.D.; Blanford, C.F. Bilirubin oxidase from Myrothecium verrucaria: X-ray determination of the complete crystal structure and a rational surface modification for enhanced electrocatalytic O_2 reduction. *Dalton Trans.* **2011**, *40*, 6668–6675. [CrossRef] [PubMed]

117. Wiebalck, S.; Kozuch, J.; Forbrig, E.; Tzschucke, C.C.; Jeuken, L.J.C.; Hildebrandt, P. Monitoring the Transmembrane Proton Gradient Generated by Cytochrome bo_3 in Tethered Bilayer Lipid Membranes Using SEIRA Spectroscopy. *J. Phys. Chem. B* **2016**, *120*, 2249–2256. [CrossRef] [PubMed]
118. Wu, J.C.Y.; Hutchings, C.H.; Lindsay, M.J.; Werner, C.J.; Bundy, B.C. Enhanced enzyme stability through site-directed covalent immobilization. *J. Biotechnol.* **2015**, *193*, 83–90. [CrossRef] [PubMed]
119. Rueda, N.; dos Santos, J.; Ortiz, C.; Torres, R.; Barbosa, O.; Rodrigues, R.C.; Berenguer-Murcia, Á.; Fernandez-Lafuente, R. Chemical modification in the design of immobilized enzyme biocatalysts: Drawbacks and opportunities. *Chem. Rec.* **2016**, *16*, 1436–1455. [CrossRef] [PubMed]
120. Hibino, Y.; Kawai, S.; Kitazumi, Y.; Shirai, O.; Kano, K. Mutation of heme *c* axial ligands in D-fructose dehydrogenase for investigation of electron transfer pathways and reduction of overpotential in direct electron transfer-type bioelectrocatalysis. *Electrochem. Commun.* **2016**, *67*, 43–46. [CrossRef]
121. Balland, V.; Hureau, C.; Cusano, A.M.; Liu, Y.; Tron, T.; Limoges, B. Oriented Immobilization of a Fully Active Monolayer of Histidine-Tagged Recombinant Laccase on Modified Gold Electrodes. *Chemistry* **2008**, *14*, 7186–7192. [CrossRef] [PubMed]
122. Tsujimura, S.; Asahi, M.; Goda-Tsutsumi, M.; Shirai, O.; Kano, K.; Miyazaki, K. Direct electron transfer to a metagenome-derived laccase fused to affinity tags near the electroactive copper site. *Phys. Chem. Chem. Phys.* **2013**, *15*, 20585–20589. [CrossRef] [PubMed]
123. Li, Y.; Zhang, J.; Huang, X.; Wang, T. Construction and direct electrochemistry of orientation controlled laccase electrode. *Biochem. Biophys. Res. Commun.* **2014**, *446*, 201–205. [CrossRef] [PubMed]
124. Care, A.; Bergquist, P.L.; Sunna, A. Solid-binding peptides: Smart tools for nanobiotechnology. *Trends Biotechnol.* **2015**, *33*, 259–268. [CrossRef] [PubMed]
125. Shiba, K. Natural and artificial peptide motifs: Their origins and the application of motif-programming. *Chem. Soc. Rev.* **2010**, *39*, 117–126. [CrossRef] [PubMed]
126. Cui, Y.; Kim, S.N.; Jones, S.E.; Wissler, L.L.; Naik, R.R.; McAlpine, M.C. Chemical Functionalization of Graphene Enabled by Phage Displayed Peptides. *Nano Lett.* **2010**, *10*, 4559–4565. [CrossRef] [PubMed]
127. Nguyen, P.Q.; Botyanszki, Z.; Tay, P.K.R.; Joshi, N.S. Programmable biofilm-based materials from engineered curli nanofibres. *Nat. Commun.* **2014**, *5*, 4945. [CrossRef] [PubMed]
128. Hnilova, M.; Oren, E.E.; Seker, U.O.S.; Wilson, B.R.; Collino, S.; Evans, J.S.; Tamerler, C.; Sarikaya, M. Effect of Molecular Conformations on the Adsorption Behavior of Gold-Binding Peptides. *Langmuir* **2008**, *24*, 12440–12445. [CrossRef] [PubMed]
129. Khatayevich, D.; Gungormus, M.; Yazici, H.; So, C.; Cetinel, S.; Ma, H.; Jen, A.; Tamerler, C.; Sarikaya, M. Biofunctionalization of materials for implants using engineered peptides. *Acta Biomater.* **2010**, *6*, 4634–4641. [CrossRef] [PubMed]
130. Al-Lolage, F.A.; Meneghello, M.; Ma, S.; Ludwig, R.; Bartlett, P.N. A flexible method for the stable, covalent immobilization of enzymes at electrode surfaces. *ChemElectroChem* **2017**, *4*, 1528–1534. [CrossRef]
131. Lalaoui, N.M.; Rousselot-Pailley, P.; Robert, V.; Mekmouche, Y.; Villalonga, R.; Holzinger, M.; Cosnier, S.; Tron, T.; Le Goff, A. Direct electron transfer between a site-specific pyrene-modified laccase and carbon nanotube/gold nanoparticle supramolecular assemblies for bioelectrocatalytic dioxygen reduction. *ACS Catal.* **2016**, *6*, 1894–1900. [CrossRef]
132. Gao, X.; Ni, K.; Zhao, C.; Ren, Y.; Wei, D. Enhancement of the activity of enzyme immobilized on polydopamine-coated iron oxide nanoparticles by rational orientation of formate dehydrogenase. *J. Biotechnol.* **2014**, *188*, 36–41. [CrossRef] [PubMed]
133. Guan, D.; Kurra, Y.; Liu, W.; Chen, Z. A click chemistry approach to site-specific immobilization of a small laccase enables efficient direct electron transfer in a biocathode. *Chem. Commun.* **2015**, *51*, 2522–2525. [CrossRef] [PubMed]
134. Schlesinger, O.; Pasi, M.; Dandela, R.; Meijler, M.M.; Alfonta, L. Electron transfer rate analysis of a site-specifically wired copper oxidase. *Phys. Chem. Chem. Phys.* **2018**, *20*, 6159–6166. [CrossRef] [PubMed]
135. Johnson, D.L.; Martin, L.L. Controlling protein orientation at interfaces using histidine tags: An alternative to Ni/NTA. *J. Am. Chem. Soc.* **2005**, *127*, 2018–2019. [CrossRef] [PubMed]
136. Milton, R.D.; Minteer, S.D. Direct enzymatic bioelectrocatalysis: Differentiating between myth and reality. *J. R. Soc. Interface* **2017**, *14*. [CrossRef] [PubMed]
137. Marcus, R.A. Electron transfer reactions in chemistry. Theory and experiment. *Rev. Mod. Phys.* **1993**, *65*, 599. [CrossRef]

138. Lojou, E.; Cutruzzola, F.; Tegoni, M.; Bianco, P. Electrochemical study of the intermolecular electron transfer to *Pseudomonas aeruginosa* cytochrome cd_1 nitrite reductase. *Electrochim. Acta* **2003**, *48*, 1055–1064. [CrossRef]
139. Dos Santos, M.M.C.; de Sousa, P.M.P.; Goncalves, M.L.S.; Krippahl, L.; Moura, J.J.G.; Lojou, E.; Bianco, P. Electrochemical studies on small electron transfer proteins using membrane electrodes. *J. Electroanal. Chem.* **2003**, *541*, 153–162. [CrossRef]
140. Pedroso, H.A.; Silveira, C.M.; Almeida, R.M.; Almeida, A.; Besson, S.; Moura, I.; Moura, J.J.G.; Almeida, M.G. Electron transfer and docking between cytochrome cd_1 nitrite reductase and different redox partners—A comparative study. *Biochim. Biophys. Acta Bioenerg.* **2016**, *1857*, 1412–1421. [CrossRef] [PubMed]
141. Dagys, M.; Laurynėnas, A.; Ratautas, D.; Kulys, J.; Vidžiūnaitė, R.; Talaikis, M.; Niaura, G.; Marcinkevičienė, L.; Meškys, R.; Shleev, S. Oxygen electroreduction catalysed by laccase wired to gold nanoparticles via the trinuclear copper cluster. *Energy Environ. Sci.* **2017**, *10*, 498–502. [CrossRef]
142. Ciaccafava, A.; Infossi, P.; Ilbert, M.; Guiral, M.; Lecomte, S.; Giudici-Orticoni, M.T.; Lojou, E. Electrochemistry, AFM, and PM-IRRA Spectroscopy of Immobilized Hydrogenase: Role of a Hydrophobic Helix in Enzyme Orientation for Efficient H_2 Oxidation. *Angew. Chem. Int. Ed.* **2012**, *51*, 953–956. [CrossRef] [PubMed]
143. Rudiger, O.; Gutierrez-Sanchez, C.; Olea, D.; Pereira, I.A.C.; Velez, M.; Fernandez, V.M.; De Lacey, A.L. Enzymatic Anodes for Hydrogen Fuel Cells based on Covalent Attachment of Ni-Fe Hydrogenases and Direct Electron Transfer to SAM-Modified Gold Electrodes. *Electroanalysis* **2010**, *22*, 776–783. [CrossRef]
144. Vaz-Dominguez, C.; Pita, M.; de Lacey, A.L.; Shleev, S.; Cuesta, A. Combined ATR-SEIRAS and EC-STM Study of the Immobilization of Laccase on Chemically Modified Au Electrodes. *J. Phys. Chem. C* **2012**, *116*, 16532–16540. [CrossRef]
145. Gutierrez-Sanchez, C.; Ciaccafava, A.; Blanchard, P.Y.; Monsalve, K.; Giudici-Orticoni, M.T.; Lecomte, S.; Lojou, E. Efficiency of Enzymatic O_2 Reduction by Myrothecium verrucaria Bilirubin Oxidase Probed by Surface Plasmon Resonance, PMIRRAS, and Electrochemistry. *ACS Catal.* **2016**, *6*, 5482–5492. [CrossRef]
146. McArdle, T.; McNamara, T.P.; Fei, F.; Singh, K.; Blanford, C.F. Optimizing the Mass-Specific Activity of Bilirubin Oxidase Adlayers through Combined Electrochemical Quartz Crystal Microbalance and Dual Polarization Interferometry Analyses. *ACS Appl. Mater. Interfaces* **2015**, *7*, 25270–25280. [CrossRef] [PubMed]
147. Osawa, M.; Ataka, K.-I.; Yoshii, K.; Nishikawa, Y. Surface-Enhanced Infrared Spectroscopy: The Origin of the Absorption Enhancement and Band Selection Rule in the Infrared Spectra of Molecules Adsorbed on Fine Metal Particles. *Appl. Spectrosc.* **1993**, *47*, 1497–1502. [CrossRef]
148. Jiang, X.; Zaitseva, E.; Schmidt, M.; Siebert, F.; Engelhard, M.; Schlesinger, R.; Ataka, K.; Vogel, R.; Heberle, J. Resolving voltage-dependent structural changes of a membrane photoreceptor by surface-enhanced IR difference spectroscopy. *Proc. Natl. Acad. Sci. USA* **2008**, *105*, 12113–12117. [CrossRef] [PubMed]
149. Heidary, N.; Utesch, T.; Zerball, M.; Horch, M.; Millo, D.; Fritsch, J.; Lenz, O.; von Klitzing, R.; Hildebrandt, P.; Fischer, A.; et al. Orientation-controlled electrocatalytic efficiency of an adsorbed oxygen-tolerant hydrogenase. *PLoS ONE* **2015**, *10*, e0143101. [CrossRef] [PubMed]
150. Gutiérrez-Sanz, O.; Marques, M.; Pereira, I.A.C.; De Lacey, A.L.; Lubitz, W.; Rüdiger, O. Orientation and Function of a Membrane-Bound Enzyme Monitored by Electrochemical Surface-Enhanced Infrared Absorption Spectroscopy. *J. Phys. Chem. Lett.* **2013**, *4*, 2794–2798. [CrossRef]
151. Olejnik, P.; Pawłowska, A.; Pałys, B. Application of Polarization Modulated Infrared Reflection Absorption Spectroscopy for electrocatalytic activity studies of laccase adsorbed on modified gold electrodes. *Electrochim. Acta* **2013**, *110*, 105–111. [CrossRef]
152. Bergkvist, M.; Carlsson, J.; Oscarsson, S. A method for studying protein orientation with atomic force microscopy using relative protein volumes. *J. Phys. Chem. B* **2001**, *105*, 2062–2069. [CrossRef]
153. Traunsteiner, C.; Sek, S.; Huber, V.; Valero-Vidal, C.; Kunze-Liebhaeuser, J. Laccase immobilized on a mixed thiol monolayer on Au (111)—Structure-dependent activity towards oxygen reduction. *Electrochim. Acta* **2016**, *213*, 761–770. [CrossRef]
154. Gwyer, J.D.; Zhang, J.; Butt, J.N.; Ulstrupy, J. Voltammetry and in situ scanning tunneling microscopy of cytochrome *c* nitrite reductase on Au (111) electrodes. *Biophys. J.* **2006**, *91*, 3897–3906. [CrossRef] [PubMed]
155. Kartashov, A.V.; Serafini, G.; Dong, M.; Shipovskov, S.; Gazaryan, I.; Besenbacher, F.; Ferapontova, E.E. Long-range electron transfer in recombinant peroxidases anisotropically orientated on gold electrodes. *Phys. Chem. Chem. Phys.* **2010**, *12*, 10098–10107. [CrossRef] [PubMed]

156. Gutierrez-Sanchez, C.; Olea, D.; Marques, M.; Fernandez, V.M.; Pereira, I.A.C.; Velez, M.; De Lacey, A.L. Oriented Immobilization of a Membrane-Bound Hydrogenase onto an Electrode for Direct Electron Transfer. *Langmuir* **2011**, *27*, 6449–6457. [CrossRef] [PubMed]
157. Gutierrez-Sanz, O.; Natale, P.; Marquez, I.; Marques, M.C.; Zacarias, S.; Pita, M.; Pereira, I.A.C.; Lopez-Montero, I.; De Lacey, A.L.; Velez, M. H-2-Fueled ATP Synthesis on an Electrode: Mimicking Cellular Respiration. *Angew. Chem. Int. Ed.* **2016**, *55*, 6216–6220. [CrossRef] [PubMed]
158. Gutierrez-Sanz, O.; Olea, D.; Pita, M.; Batista, A.P.; Alonso, A.; Pereira, M.M.; Velez, M.; De Lacey, A.L. Reconstitution of Respiratory Complex I on a Biomimetic Membrane Supported on Gold Electrodes. *Langmuir* **2014**, *30*, 9007–9015. [CrossRef] [PubMed]
159. Matanovic, I.; Babanova, S.; Chavez, M.S.; Atanassov, P. Protein–Support Interactions for Rationally Designed Bilirubin Oxidase Based Cathode: A Computational Study. *J. Phys. Chem. B* **2016**, *120*, 3634–3641. [CrossRef] [PubMed]
160. Ngai, J.C.; Mak, P.-I.; Siu, S.W. ProtPOS: A python package for the prediction of protein preferred orientation on a surface. *Bioinformatics* **2016**, *32*, 2537–2538. [CrossRef] [PubMed]
161. Liu, J.; Yu, G.; Zhou, J. Ribonuclease A adsorption onto charged self-assembled monolayers: A multiscale simulation study. *Chem. Eng. Sci.* **2015**, *121*, 331–339. [CrossRef]
162. Kutzner, C.; Pall, S.; Fechner, M.; Esztermann, A.; de Groot, B.L.; Grubmuller, H. Best bang for your buck: GPU nodes for GROMACS biomolecular simulations. *J. Comput. Chem.* **2015**, *36*, 1990–2008. [CrossRef] [PubMed]
163. Salomon-Ferrer, R.; Case, D.A.; Walker, R.C. An overview of the Amber biomolecular simulation package. *Wiley Interdiscip. Rev. Comput. Mol. Sci.* **2013**, *3*, 198–210. [CrossRef]
164. Ponder, J.W.; Case, D.A. Force fields for protein simulations. *Adv. Protein Chem.* **2003**, *66*, 27–85. [PubMed]
165. Makrodimitris, K.; Masica, D.L.; Kim, E.T.; Gray, J.J. Structure prediction of protein−solid surface interactions reveals a molecular recognition motif of statherin for hydroxyapatite. *J. Am. Chem. Soc.* **2007**, *129*, 13713–13722. [CrossRef] [PubMed]
166. Xie, Y.; Zhou, J.; Jiang, S. Parallel tempering Monte Carlo simulations of lysozyme orientation on charged surfaces. *J. Chem. Phys.* **2010**, *132*, 02B602. [CrossRef] [PubMed]
167. Brancolini, G.; Kokh, D.B.; Calzolai, L.; Wade, R.C.; Corni, S. Docking of ubiquitin to gold nanoparticles. *ACS Nano* **2012**, *6*, 9863–9878. [CrossRef] [PubMed]
168. Zheng, J.; Li, L.; Chen, S.; Jiang, S. Molecular simulation study of water interactions with oligo (ethylene glycol)-terminated alkanethiol self-assembled monolayers. *Langmuir* **2004**, *20*, 8931–8938. [CrossRef] [PubMed]
169. Li, Y.; Ogorzalek, T.L.; Wei, S.; Zhang, X.; Yang, P.; Jasensky, J.; Brooks, C.L.; Marsh, E.N.G.; Chen, Z. Effect of immobilization site on the orientation and activity of surface-tethered enzymes. *Phys. Chem. Chem. Phys.* **2018**, *20*, 1021–1029. [CrossRef] [PubMed]
170. Cazelles, R.; Lalaoui, N.; Hartmann, T.; Leimkühler, S.; Wollenberger, U.; Antonietti, M.; Cosnier, S. Ready to use bioinformatics analysis as a tool to predict immobilisation strategies for protein direct electron transfer (DET). *Biosens. Bioelectron.* **2016**, *85*, 90–95. [CrossRef] [PubMed]
171. Utesch, T.; Millo, D.; Castro, M.A.; Hildebrandt, P.; Zebger, I.; Mroginski, M.A. Effect of the protonation degree of a self-assembled monolayer on the immobilization dynamics of a [NiFe] hydrogenase. *Langmuir* **2013**, *29*, 673–682. [CrossRef] [PubMed]
172. Oteri, F.; Ciaccafava, A.; De Poulpiquet, A.; Baaden, M.; Lojou, E.; Sacquin-Mora, S. The weak, fluctuating, dipole moment of membrane-bound hydrogenase from *Aquifex aeolicus* accounts for its adaptability to charged electrodes. *Phys. Chem. Chem. Phys.* **2014**, *16*, 11318–11322. [CrossRef] [PubMed]
173. Liu, J.; Xie, Y.; Peng, C.; Yu, G.; Zhou, J. Molecular Understanding of Laccase Adsorption on Charged Self-Assembled Monolayers. *J. Phys. Chem. B* **2017**, *121*, 10610–10617. [CrossRef] [PubMed]
174. Peng, L.; Utesch, T.; Yarman, A.; Jeoung, J.H.; Steinborn, S.; Dobbek, H.; Mroginski, M.A.; Tanne, J.; Wollenberger, U.; Scheller, F.W. Surface-Tuned Electron Transfer and Electrocatalysis of Hexameric Tyrosine-Coordinated Heme Protein. *Chemistry* **2015**, *21*, 7596–7602. [CrossRef] [PubMed]
175. Utesch, T.; Sezer, M.; Weidinger, I.M.; Mroginski, M.A. Adsorption of sulfite oxidase on self-assembled monolayers from molecular dynamics simulations. *Langmuir* **2012**, *28*, 5761–5769. [CrossRef] [PubMed]

176. Climent, V.; Zhang, J.; Friis, E.P.; Østergaard, L.H.; Ulstrup, J. Voltammetry and single-molecule in situ scanning tunneling microscopy of laccases and bilirubin oxidase in electrocatalytic dioxygen reduction on Au (111) single-crystal electrodes. *J. Phys. Chem. C* **2011**, *116*, 1232–1243. [CrossRef]
177. Madden, C.; Vaughn, M.D.; Díez-Pérez, I.; Brown, K.A.; King, P.W.; Gust, D.; Moore, A.L.; Moore, T.A. Catalytic turnover of [FeFe]-hydrogenase based on single-molecule imaging. *J. Am. Chem. Soc.* **2011**, *134*, 1577–1582. [CrossRef] [PubMed]
178. Xia, N.; Xing, Y.; Wang, G.; Feng, Q.; Chen, Q.; Feng, H.; Sun, X.; Liu, L. Probing of EDC/NHSS-mediated covalent coupling reaction by the immobilization of electrochemically active biomolecules. *Int. J. Electrochem. Sci.* **2013**, *8*, 2459–2467.
179. Palazon, F.; Montenegro Benavides, C.; Léonard, D.; Souteyrand, E.l.; Chevolot, Y.; Cloarec, J.-P. Carbodiimide/NHS derivatization of COOH-terminated SAMs: Activation or byproduct formation? *Langmuir* **2014**, *30*, 4545–4550. [CrossRef] [PubMed]
180. Ran, Q.; Peng, R.; Liang, C.; Ye, S.; Xian, Y.; Zhang, W.; Jin, L. Covalent immobilization of horseradish peroxidase via click chemistry and its direct electrochemistry. *Talanta* **2011**, *83*, 1381–1385. [CrossRef] [PubMed]
181. Singh, K.; McArdle, T.; Sullivan, P.R.; Blanford, C.F. Sources of activity loss in the fuel cell enzyme bilirubin oxidase. *Energy Environ. Sci.* **2013**, *6*, 2460–2464. [CrossRef]
182. Zanetti-Polzi, L.; Daidone, I.; Bortolotti, C.A.; Corni, S. Surface packing determines the redox potential shift of cytochrome *c* adsorbed on gold. *J. Am. Chem. Soc.* **2014**, *136*, 12929–12937. [CrossRef] [PubMed]
183. Krzemiński, Ł.; Cronin, S.; Ndamba, L.; Canters, G.W.; Aartsma, T.J.; Evans, S.D.; Jeuken, L.J.C. Orientational Control over Nitrite Reductase on Modified Gold Electrode and Its Effects on the Interfacial Electron Transfer. *J. Phys. Chem. B* **2011**, *115*, 12607–12614. [CrossRef] [PubMed]
184. Kakiuchi, T.; Iida, M.; Gon, N.; Hobara, D.; Imabayashi, S.-I.; Niki, K. Miscibility of adsorbed 1-undecanethiol and 11-mercaptoundecanoic acid species in binary self-assembled monolayers on Au (111). *Langmuir* **2001**, *17*, 1599–1603. [CrossRef]
185. Smith, R.K.; Reed, S.M.; Lewis, P.A.; Monnell, J.D.; Clegg, R.S.; Kelly, K.F.; Bumm, L.A.; Hutchison, J.E.; Weiss, P.S. Phase separation within a binary self-assembled monolayer on Au {111} driven by an amide-containing alkanethiol. *J. Phys. Chem. B* **2001**, *105*, 1119–1122. [CrossRef]
186. Benavidez, T.E.; Torrente, D.; Marucho, M.; Garcia, C.D. Adsorption of Soft and Hard Proteins onto OTCEs under the Influence of an External Electric Field. *Langmuir* **2015**, *31*, 2455–2462. [CrossRef] [PubMed]
187. Sugimoto, Y.; Kitazumi, Y.; Tsujimura, S.; Shirai, O.; Yamamoto, M.; Kano, K. Electrostatic interaction between an enzyme and electrodes in the electric double layer examined in a view of direct electron transfer-type bioelectrocatalysis. *Biosens. Bioelectron.* **2015**, *63*, 138–144. [CrossRef] [PubMed]
188. Sugimoto, Y.; Kitazumi, Y.; Shirai, O.; Yamamoto, M.; Kano, K. Role of 2-mercaptoethanol in direct electron transfer-type bioelectrocatalysis of fructose dehydrogenase at Au electrodes. *Electrochim. Acta* **2015**, *170*, 242–247. [CrossRef]
189. Lopez, F.; Siepenkoetter, T.; Xiao, X.; Magner, E.; Schuhmann, W.; Salaj-Kosla, U. Potential pulse-assisted immobilization of Myrothecium verrucaria bilirubin oxidase at planar and nanoporous gold electrodes. *J. Electroanal. Chem.* **2018**, *812*, 194–198. [CrossRef]
190. Millo, D.; Ranieri, A.; Gross, P.; Ly, H.K.; Borsari, M.; Hildebrandt, P.; Wuite, G.J.L.; Gooijer, C.; van der Zwan, G. Electrochemical Response of Cytochrome *c* Immobilized on Smooth and Roughened Silver and Gold Surfaces Chemically Modified with 11-Mercaptounodecanoic Acid. *J. Phys. Chem. C* **2009**, *113*, 2861–2866. [CrossRef]
191. Salewski, J.; Batista, A.P.; Sena, F.V.; Millo, D.; Zebger, I.; Pereira, M.M.; Hildebrandt, P. Substrate-Protein Interactions of Type II NADH:Quinone Oxidoreductase from Escherichia coli. *Biochemistry* **2016**, *55*, 2722–2734. [CrossRef] [PubMed]
192. Rivas, L.; Soares, C.M.; Baptista, A.M.; Simaan, J.; Di Paolo, R.E.; Murgida, D.H.; Hildebrandt, P. Electric-field-induced redox potential shifts of tetraheme cytochromes c_3 immobilized on self-assembled monolayers: Surface-enhanced resonance Raman spectroscopy and simulation studies. *Biophys. J.* **2005**, *88*, 4188–4199. [CrossRef] [PubMed]
193. Petrey, D.; Honig, B. Structural bioinformatics of the interactome. *Annu. Rev. Biophys.* **2014**, *43*, 193–210. [CrossRef] [PubMed]

194. Monsalve, K.; Mazurenko, I.; Gutierrez-Sanchez, C.; Ilbert, M.; Infossi, P.; Frielingsdorf, S.; Giudici-Orticoni, M.T.; Lenz, O.; Lojou, E. Impact of Carbon Nanotube Surface Chemistry on Hydrogen Oxidation by Membrane-Bound Oxygen-Tolerant Hydrogenases. *Chemelectrochem* **2016**, *3*, 2179–2188. [CrossRef]
195. Salamon, Z.; Fitch, J.; Cai, M.; Tumati, S.; Navratilova, E.; Tollin, G. Plasmon-waveguide resonance studies of ligand binding to integral proteins in membrane fragments derived from bacterial and mammalian cells. *Anal. Biochem.* **2009**, *387*, 95–101. [CrossRef] [PubMed]
196. Bouffier, L.; Doneux, T. Coupling electrochemistry with in situ fluorescence (confocal) microscopy. *Curr. Opin. Electrochem.* **2017**, *6*, 31–37. [CrossRef]
197. Siepenkoetter, T.; Salaj-Kosla, U.; Xiao, X.X.; Conghaile, P.O.; Pita, M.; Ludwig, R.; Magner, E. Immobilization of Redox Enzymes on Nanoporous Gold Electrodes: Applications in Biofuel Cells. *Chempluschem* **2017**, *82*, 553–560. [CrossRef]
198. Gutierrez-Sanchez, C.; Pita, M.; Vaz-Dominguez, C.; Shleev, S.; De Lacey, A.L. Gold Nanoparticles as Electronic Bridges for Laccase-Based Biocathodes. *J. Am. Chem. Soc.* **2012**, *134*, 17212–17220. [CrossRef] [PubMed]
199. Sugimoto, Y.; Kitazumi, Y.; Shirai, O.; Kano, K. Effects of Mesoporous Structures on Direct Electron Transfer-Type Bioelectrocatalysis: Facts and Simulation on a Three-Dimensional Model of Random Orientation of Enzymes. *Electrochemistry* **2017**, *85*, 82–87. [CrossRef]

© 2018 by the authors. Licensee MDPI, Basel, Switzerland. This article is an open access article distributed under the terms and conditions of the Creative Commons Attribution (CC BY) license (http://creativecommons.org/licenses/by/4.0/).

catalysts

MDPI

Communication

Co-Detection of Dopamine and Glucose with High Temporal Resolution

Jenny Bergman [1], Lisa Mellander [2], Yuanmo Wang [3] and Ann-Sofie Cans [3,*]

[1] Department of Chemistry and Molecular Biology, Gothenburg University, 41296 Gothenburg, Sweden; jenny.bergman@chem.gu.se
[2] Department of Physiology, Institute of Neuroscience and Physiology, University of Gothenburg, 41390 Gothenburg, Sweden; lisa.mellander@gu.se
[3] Department of Chemistry and Chemical Engineering, Chalmers University of Technology, 41296 Gothenburg, Sweden; yuanmo@chalmers.se
* Correspondence: cans@chalmers.se; Tel.: +46-31-772-1000

Received: 6 December 2017; Accepted: 15 January 2018; Published: 19 January 2018

Abstract: Neuronal activity and brain glucose metabolism are tightly coupled, where triggered neurotransmission leads to a higher demand for glucose. To better understand the regulation of neuronal activity and its relation to high-speed metabolism, development of analytical tools that can temporally resolve the transients of vesicular neurotransmitter release and fluctuations of metabolites such as glucose in the local vicinity of the activated neurons is needed. Here we present an amperometric biosensor design for rapid co-detection of glucose and the neurotransmitter dopamine. The sensor is based on the immobilization of an ultra-thin layer of glucose oxidase on to a gold-nanoparticle-covered carbon fiber microelectrode. Our electrode, by altering the potential applied at the sensor surface, allows for the high-speed recording of both glucose and dopamine. We demonstrate that, even though glucose is electrochemically detected indirectly through the enzymatic product and the electroactive dopamine is sensed directly, when exposing the sensor surface to a mixture of the two analytes, fluctuations in glucose and dopamine concentrations can be visualized with similar speed and at a millisecond time scale. Hence, by minimizing the enzyme coating thickness at the sensor surface, dual detection of glucose and dopamine can be realized at the same sensor surface and at time scales necessary for monitoring fast metabolic alterations during neurotransmission.

Keywords: biosensor; glucose; glucose oxidase; amperometry; co-detection; temporal resolution; gold nanoparticles; microelectrode

1. Introduction

Enzymes are highly specific biocatalysts, converting a substrate to a product, making them excellent for incorporation in sensors aimed at selective detection of analytes that are otherwise difficult to detect. The first enzymatic biosensor was developed in the 1960s by Clark and Lyon for the detection of glucose with the use of the enzyme glucose oxidase (GOx) as part of the detection scheme [1]. Since then, there have been a tremendous number of biosensors developed for applications within the food industry, pharmacology, neurochemistry, environmental analysis, and chemistry [2–12]. The field of biosensors has been extensively expanded and a vast array of methods for detection has been explored [13–21]. Electrochemical detection has several advantages, such as fast sample rates, the possibility to miniaturize the sensor by the use of microelectrodes, and high biocompatibility of the electrode material where, e.g., carbon and gold have been successfully used for in vivo applications [22–24]. In addition to its use in biosensor design, electrochemical detection is also frequently employed in the study of electroactive substances, where the analyte undergoes a redox

reaction directly at the electrode surface when a redox potential is applied. The neurotransmitter dopamine is extensively explored by electrochemistry due to its ability to easily oxidize at a positively polarized electrode [25,26]. Dopamine is related to the reward system of the brain, and it has a central role in Parkinson's disease [27,28] as well as in addiction [29]. Glucose is the primary source of energy in the mammalian brain as its metabolism generates ATP, the fuel for cellular maintenance and neurotransmission. It has been shown that an increase in local neuronal activity is associated with a higher glucose concentration in the activated brain area and that glucose-excited neurons sense fluctuations in local glucose levels [30,31]. Therefore, the ability to co-detect rapid local fluctuations of dopamine and glucose has the potential to reveal new insights in how neuronal activity is connected to and regulated by the energy metabolism in the brain [32].

The construction of enzyme-based electrochemical biosensors relies on the immobilization of enzymes at an electrode surface where the enzymatic activity product can be detected [33,34]. Enzymes adsorbing to a flat surface have a tendency to flatten out, which causes an alteration of their protein tertiary structure and often thereby a reduction in enzymatic activity. In order to prevent enzyme denaturation upon adsorption to an electrode surface, several methods for enzyme immobilization have been developed, e.g., enzyme attachment using cross-linkers, enzyme entrapment in polymers, and the incorporation of nanomaterials at the sensor surface as support for enzymes to bind [35–41]. Several studies have shown that immobilizing enzymes on a high curvature surface is beneficial for retaining enzymatic activity by minimizing changes in the tertiary structure of the enzyme [42–45]. Modifying the electrode surface with nanomaterials such as nanotubes and nanoparticles (NPs) introduces a high curvature support for enzyme immobilization. Additionally, the introduction of nanostructures will also increase the electrode surface area, thereby allowing for a higher enzyme loading that increases the sensitivity of the sensor. Gold nanomaterials, such as gold nanoparticles (AuNPs), have been widely used due to their high biocompatibility and increased ability to oxidize/reduce enzymatic electroactive products, e.g., hydrogen peroxide (H_2O_2) [46–49].

Earlier reported glucose biosensors have not focused on applications that demand high temporal resolution. Our aim is to develop novel miniaturized electrochemical biosensors that can be used for analyzing real-time rapid fluctuations of non-electroactive molecules at single secretory cells and locally by groups of cells in brain tissue. We have previously shown that a two-sequential enzyme system, acetylcholine esterase (AChE) and choline oxidase (ChO), immobilized as a monolayer on to an AuNP-coated carbon fiber microelectrode (CFME) can be used to detect the vesicular release of the non-electroactive neurotransmitter acetylcholine with a millisecond temporal resolution [50]. Here, we immobilize a single enzyme system (GOx) to the surface of AuNPs covering a CFME and we investigate the temporal resolution for glucose detection and compare it with that of the electroactive neurotransmitter dopamine. Glucose, a non-electroactive molecule, must undergo an enzymatic catalytic reaction by the immobilized GOx at the electrode surface in order to generate an electroactive product that can be detected by the electrode. Each glucose molecule is enzymatically converted to gluconic acid and H_2O_2, which is then reduced at the AuNP surface of the electrode held at a potential of -0.5 V (vs. Ag/AgCl), where one H_2O_2 molecule generates two electrons according to the following chemical reactions:

$$\text{glucose} + \ O_2 \ \rightarrow \text{gluconic acid} \ + H_2O_2$$

$$H_2O_2 + \ 2H^+ + 2e^- \ \rightarrow \ 2\,H_2O$$

In the sensor schemes used here for the high temporal dual detection of glucose and dopamine, dopamine is oxidized at +0.5 V (vs. Ag/AgCl), a potential sufficient for diffusion limited dopamine oxidation, and a potential where H_2O_2 not is detectable (Figure S1). In order to compare the kinetics for the detection of glucose and dopamine, the two analytes must be selectively detected at the same sensor. Here we monitor the kinetics and selective detection of glucose undergoing a catalytic reaction by the immobilized GOx, resulting in the production of H_2O_2, which diffuses to the electrode surface for electrochemical detection, and compare it to the speed for the detection of dopamine, which,

following diffusion through the thin coating of immobilized enzyme, is directly detected when it is in contact with the electrode surface. The results demonstrate the uniqueness of this sensor, as it allows for the dual detection of a non-electroactive analyte and an electroactive one with the same time resolution.

2. Results and Discussion

2.1. Preparation of the Biosensor

AuNPs were electrodeposited to the electrode surface by placement in a 0.5 mM $HAuCl_4$ solution and subsequent reduction of Au^{3+} to Au^0 through application of a large overpotential (−0.6 V vs. Ag/AgCl) for 24 s, a method originally developed by Finot et al. [51]. The electrodeposition parameters have previously been optimized by our lab for a CFME 33 μm in diameter and provide a coating of AuNPs approximately 20 nm in diameter with a 30% electrode surface coverage [50]. Monolayer enzyme coverage at the surface of nanoparticles has been demonstrated to be beneficial in several aspects, e.g., a greater accessibility of the enzyme active site, a reduction of steric hindrance between enzymes, and a faster diffusion of the enzymatic product to the electrode surface [42–44]. Glucose oxidase is an enzyme unwilling to form multiple layers when it is immobilized upon a surface [52]. We have previously developed a method for quantifying the number of GOx enzymes immobilized onto the surface of AuNPs coating a glassy carbon electrode, resulting in close to a monolayer coverage at an AuNP surface [53]. Based on these previous results, we estimate that the conditions used here for GOx immobilization (2 mg mL^{-1} and an incubation time of 2 h at room temperature) results in approximately monolayer coverage of GOx.

2.2. Biosensor Characterization

The modification of the carbon surface with AuNPs fills two functions in this sensor design. It provides a high curvature surface for enzyme immobilization and provides an electrode surface with an enhanced ability to detect the enzymatic product H_2O_2. The enhanced detection ability is important as H_2O_2 can only be reduced at the Au surface of the electrode—not at the carbon—and at the potential applied in these experiments. As a consequence, since the total deposited Au surface varies between electrodes, all current responses should be normalized to the total AuNP surface area of each electrode in order to compare the response magnitude between electrodes. The AuNP–CFME response to H_2O_2 shows linearity over a large concentration range (10 μM–10 mM) where the response in the lower concentration range (10 μM–1 mM) is shown in Figure 1b. The sensitivity to H_2O_2 at the AuNP–CFME was determined to be 8.4 ± 0.5 pA mM^{-1} μm^{-2} (R-square 0.992) in the linear range of H_2O_2 concentrations tested (Figure S2). The enzymatic sensor was exposed to glucose concentrations between 10 μM and 10 mM (Figure S3) to generate a Michaelis–Menten curve revealing a K_M for the biosensor of 0.07 ± 0.03 mM. Typically, enzymes in solution have K_M values ranging between 10^{-1} M (low affinity) and 10^{-7} M (high affinity) [54]. At lower concentrations of glucose, the sensor demonstrates a linear response between 10 μM and 100 μM, while the current reached a plateau at 1 mM glucose (Figure 1a). The sensitivity of glucose within the linear range was determined to be 1.9 ± 0.04 pA mM^{-1} μm^{-2} (R-square 0.999), which is approximately one quarter the sensitivity of the response towards H_2O_2 by the AuNP–CFME, indicating a highly retained enzymatic activity of the GOx enzyme when immobilized to the sensor surface in this concentration range. The limit of detection for this biosensor was determined to 10 μM (3σ).

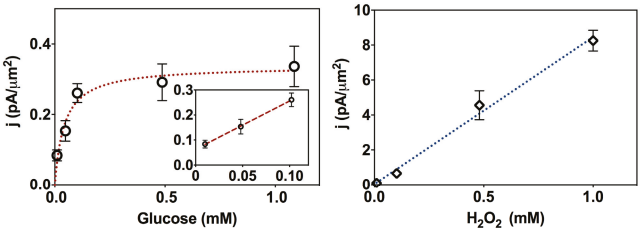

Figure 1. (**a**) A reproducible calibration curve for glucose using the glucose oxidase and gold nanoparticle modified carbon fiber microelectrode (GOx–AuNP–CFME) (n = 7–10) when recording the cathodic current at −0.5 V (vs. an Ag/AgCl reference electrode) and normalized the current response by the total AuNP surface area at each electrode. Inset: the linear detection range of glucose from 10 to 100 μM. (**b**) The linear response towards H_2O_2 by AuNP–CFME (n = 3–6) at the lower concentration range tested and recording the cathodic current at −0.5 V (vs. an Ag/AgCl reference electrode). All errors are shown as standard error of the mean.

Since GOx is an extensively used enzyme in biosensor fabrication with many different approaches for biosensor design, reported values for K_M, sensitivity, linear range, and limit of detection for GOx-based sensors are very heterogeneous, as reviewed by Zaidi and Shin [55], with K_M values ranging between 15 μM and 2 mM, while the sensitivity varies between 10 and 5000 μA mM^{-1} cm^{-2} and the limit of detection between 0.07 μM and 4.8 mM. Hence, the values obtained for our sensor fits well in the range of what has been previously determined for nanostructured glucose sensors.

The specificity of the biosensor for glucose is of importance for possible future in vivo applications for monitoring, e.g., alterations in glucose metabolism in relation to local neuronal activity. To evaluate possible common interferences for the sensor in brain tissue, several biologically relevant substances were tested; the electroactive neurotransmitters dopamine and serotonin, the non-electroactive neurotransmitters glutamate and acetylcholine, and two other commonly interfering molecules, ascorbic acid and lactate. Except for lactate which is present at concentrations of approximately 1 mM, these molecules generally occur in low concentrations in the brain tissue environment, typically in the μM range [56–59], while the average resting concentration of glucose in the human brain during normoglycemia is around 1 mM [60]. As seen in Figure 2, at 1 mM, none of the tested possible interferences gave a response greater than 25% of the glucose signal, indicating that interfering species will not be a limitation for glucose detection during in vivo measurements in the brain.

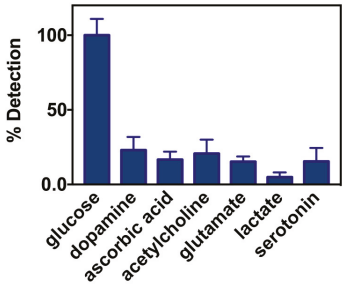

Figure 2. The resulting cathodic current recorded at −0.5 V and illustrating selectivity by the glucose oxidase and gold nanoparticle modified carbon fiber microelectrode (GOx–AuNP–CFME) (n = 3–6) after exposure to different possible interfering analytes in the extracellular brain tissue environment with concentrations of 1 mM and in the presence of 1 mM glucose. Due to the possibility of analyte detection also by the carbon at the electrode surface, the signal is not normalized to total Au surface area. All errors are shown as standard error of the mean.

To investigate and compare the response time for the sensor to fast local alterations in glucose and dopamine concentrations, the kinetics of the sensor was tested by exposing the sensor surface to controlled rapid fluctuations of the two analytes in solution. As schematically displayed in Figure 3, by placing the tip of a glass micropipette filled with 25 mM glucose and 20 μM dopamine solution at approximately 30 μm distance from the sensor surface, 500 ms microinjection puffs were applied toward the electrode surface using a microinjector. Due to the higher sensor sensitivity for dopamine compared to glucose, the analyte concentrations were adjusted to result in similar peak currents.

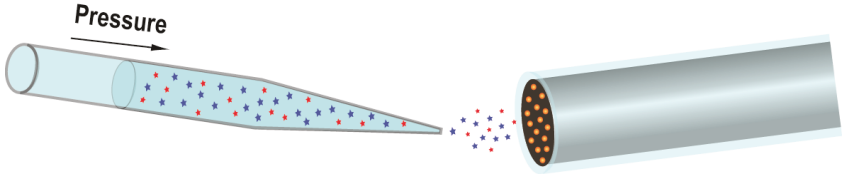

Figure 3. A schematic of the experimental set-up for comparing the kinetic response for detection of glucose (red stars) and dopamine (blue stars) using the glucose oxidase and gold nanoparticle modified carbon fiber microelectrode (GOx–AuNP–CFME). Here a micropipette filled with a solution mixture containing dopamine (20 μM) and glucose (25 mM) is placed approximately 30 μm from the surface of a GOx–AuNP–CFME. Using a microinjector pump, 500 ms puffs of the solution mixture is injected against the sensor surface placed in buffer solution creating a controlled rapid fluctuation of the two analytes towards the electrode. By applying a potential of +0.5 V and −0.5 V to the sensor surface (vs. an Ag/AgCl reference electrode) the dopamine and glucose are amperometrically detected, through a reduction or oxidation reaction, respectively.

When the electrode was held at −0.5 V, a sharp rise in reductive current was observed as the puff of analyte solution reached the sensor surface, followed by a current decline to baseline as the pressure on the micropipette was switched off (Figure 4). The response to dopamine was tested by puffing the dopamine and glucose containing solution towards the same electrode, while instead applying a potential of +0.5 V to the electrode surface. The electrode response to dopamine was used for evaluation of the ability of the sensor to co-detect glucose and dopamine, as well as to compare the kinetic response for the two analytes. The results show that, in the initial rise of the current peak, the enzymatically catalyzed reaction of glucose to H_2O_2, followed by the reduction of H_2O_2 at the electrode, is as fast as the direct oxidation of the electroactive dopamine, with rise times (25–75%) of the peaks of 300 ms for dopamine and 260 ms for glucose. However, the current transient returns to the baseline faster for glucose than for dopamine. A possible explanation for this observation could be the higher sensor detection limit for glucose as compared to dopamine, since the concentration of analyte will quickly decrease as the pressure from the microinjector is switched off, and glucose will more rapidly reach a concentration that is not detected by the electrode.

In summary, the results from these experiments demonstrate that, by altering the potential applied to the sensor surface according to the respective redox potential for glucose-derived H_2O_2 and dopamine, rapid fluctuations of these analytes can be monitored. Even though the sensitivity for detection of glucose versus dopamine at this sensor scheme is significantly reduced, by limiting the coating to an ultra-thin enzyme layer during fabrication, the temporal resolution of glucose concentration fluctuation recordings in solution is comparable to the speed of that for dopamine. Hence, this sensor design provides a tool for correlating dopamine activity with metabolic glucose levels at a time scale relevant for neuronal communication. As development of many enzyme-coated electrochemical biosensors are functionalized with nanomaterials, this methodology can also be applied for construction of biosensors that aim for dual detection of other fast fluctuating non-electroactive and electroactive analytes that are involved in neuronal communication.

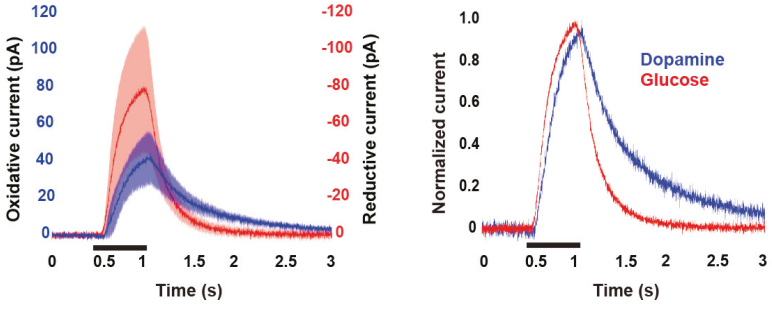

Figure 4. (**a**) The temporal response for detection of puffing a solution containing 20 μM dopamine (blue) and 25 mM glucose (red) against the biosensor surface when applying a potential of +0.5 V and −0.5 V vs. an Ag/AgCl reference electrode, respectively. (**b**) Normalized detection response of the dopamine- and glucose-containing solution. The black band indicates the timing for the 500 ms injection pulse applied to the glass microinjection pipette.

3. Materials and Methods

3.1. Chemical Reagents

Glucose oxidase (type VII) from *Aspergillus niger*, phosphate-buffered saline tablets (10 mM, pH 7.2), sulfuric acid, copper sulfate, tetrachloroaurate, serotonin chloride, dopamine chloride, glucose, lactic acid, monosodium glutamate, acetylcholine chloride, ascorbic acid, ferrocene methanol, tungsten wire, and hydrogen peroxide were purchased from Sigma-Aldrich (St. Louis, MO, USA). All reagents used where of reagent grade and used as received. Deionized water (resistivity $\geq$ 18 MΩ cm) was used in all experiments.

3.2. Electrochemical Set-Up

Electrochemical measurements, cyclic voltammetry, chronoamperometry, and amperometry were performed using a two-electrode system with a computer-controlled 1000C Series Multi-Potentiostat (CH Instruments, Austin, TX, USA) or an Axopatch potentiostat 200B (Axon Instruments, Foster City, CA, USA). For all experiments, a saturated Ag/AgCl was used as a reference electrode and all potentials are reported against this reference electrode unless otherwise stated.

3.3. Preparation of a 33 μm CFME

Carbon fiber microelectrodes were prepared by aspirating single 33-μm diameter carbon fibers (Cytec Engineered Materials, Tempe, AZ, USA) into borosilicate glass capillaries (1.2 mm O.D., 0.69 mm I.D., Sutter Instrument Co., Novato, CA, USA). The filled capillaries were then pulled to a taper using a commercial micropipette puller (P-1000; Sutter Instrument Co., Novato, CA, USA) and epoxy (Epoxy Technology, Billerica, MA, USA) was used to seal the glass-carbon fiber junction of the electrode. The electrode tips were cut using a scalpel and polished at a 45° angle on a diamond dust-embedded micropipette beveling wheel (Narishige, Inc., London, UK). The electrodes were backfilled with silver paint or KCl (3 M) and a metal wire (tungsten and silver, respectively) was inserted and used as the connection to the potentiostat. All electrodes were tested in 1 mM ferrocene methanol by performing cyclic voltammetry between −0.2 and +0.6 V at 0.1 V s^{-1} in order to make sure the electrodes where well-functioning by evaluating their voltammograms prior to each experiment.

3.4. Functionalization with AuNP

Electrodes were functionalized with AuNP by an electrochemical deposition similar to Finot et al. [51] with minor alterations. The CFME and an Ag/AgCl reference electrode were immersed in a 0.5 mM solution of $HAuCl_4$ in 0.5 M H_2SO_4. A potential of +1.2 V was applied for 10 s followed by a potential of −0.6 V for 24 s. The AuNP surface area was then measured electrochemically by performing a linear sweep from +1.4 V (potential held for 5 s) to +0.5 V at a rate of 0.1 V s^{-1} in 0.5 M H_2SO_4. Here a $Cu/CuSO_4$ reference electrode was used to avoid chloride contamination. The resulting peak at approximately +0.8 V was integrated by the inbuilt software in the 1000C Series Multi-Potentiostat (CH Instruments, Austin, TX, USA) and the obtained charge was divided with a factor of 4.89 pC μm^{-2} as used by Finot et al. [51]. The electrodes used for further experiments had a total gold surface area of approximately 2000 μm^2.

3.5. Immobilization of Enzymes

The tip of each electrode was immersed in a solution containing 2 mg mL^{-1}. Glucose oxidase in phosphate-buffered saline, (10 mM, pH 7.2) for 2 h at room temperature. After immersion, the tip of each electrode was washed with deionized water and stored in a solution of phosphate-buffered saline (PBS) (10 mM, pH 7.2) at 4 °C when not used immediately for experiments.

3.6. Characterization of the Glucose Sensor

The detection of glucose was tested using chronoamperometry in PBS. Briefly, a constant potential where no reaction occurs (at 0 V) was held for a certain time (10 s) and then immediately changed to −0.5 V where the reduction of the enzymatic product hydrogen peroxide takes place and held constant until the resulting reduction current had reached a steady state (30 s). A glucose calibration curve was performed from 10 µM to 10 mM using freshly prepared solutions from a 1 M glucose stock solution by adding aliquots of 1, 10, and 100 mM to the bulk PBS solution followed by convection induced by a pipette. The response of the following interferences, acetylcholine, lactate, dopamine, serotonin, ascorbic acid, and glutamate were tested in a 1 mM concentration in the presence of 1 mM glucose with the same chronoamperometry method as described above. The AuNP-modified CFME response to the enzymatic product hydrogen peroxide was performed using the same method and concentrations as for the glucose calibration. Statistical analysis and enzyme kinetic parameters where analyzed using GraphPad Prism 7 (La Jolla, CA, USA).

For the kinetic characterization, a micropipette (o.d. 1 mm, i.d. 0.78 mm, with filament; Harvard Apparatus, Holliston, MA, USA) was pulled on a commercial filament puller (P-1000; Sutter Instrument Co., Novato, CA, USA) and back-filled with a solution containing 20 µM dopamine and 25 mM glucose in PBS. The pipette was placed together with a glucose sensor in a dish containing PBS on an Olympus IX-71 microscope (Olympus, Melville, NY, USA). Hydraulic micromanipulators (MHW-3, Narishige, Tokyo, Japan) were used to position the pipette approximately 30 µm away from the electrode surface. A potential was applied at the electrode vs. a silver/silver chloride reference electrode (World Precision Instruments, Inc., Sarasota, FL, USA) also placed in the dish. A commercial patch-clamp instrument (Axopatch 200B; Axon Instruments, Foster City, CA, USA) was used to control the potential at the working electrode, +0.5 V for the detection of dopamine, while a negative potential of −0.5 V was applied to detect the enzymatic product hydrogen peroxide. Pressure was applied to the back of the pipette (Picospritzer II; General Valve Instruments, Fairfield, NJ, USA) to create a 500 ms puff of solution towards the electrode, resulting in a peak in either reductive or oxidative current depending on the applied potential. The current, digitized at 5 kHz, was displayed in real time (AxoScope 8.1; Axon Instruments, Union City, CA, USA) and stored digitally. The peaks were analyzed in Igor Pro 6 (Version 6.2.2.0; WaveMetrics, Lake Oswego, OR, USA) using an Igor Procedure File designed for analysis of quantal release by the group of David Sulzer [61].

Supplementary Materials: The following are available online at www.mdpi.com/2073-4344/8/1/34/s1, Figure S1: Cyclic voltammetry of a CFME–AuNP in PBS buffer (black) 5 mM H_2O_2 (red) and 10 mM H_2O_2. The voltammogram

shows that H_2O_2 is reduced at potentials below −0.25 V and that no oxidation reaction occurs involving H_2O_2 when potential +0.5 V is applied. Figure S2: The AuNP–CFME response to H_2O_2 shows linearity over a large concentration range (10 μM–10 mM) and display a sensitivity of 8.4 ± 0.5 pA mM^{-1} μm^{-2}. Figure S3: The GOx–AuNP–CFME response to glucose for the whole concentration range tested (10 μM–10 mM).

Acknowledgments: The authors acknowledge the Swedish Research Council for funding.

Author Contributions: J.B., Y.W., and A.-S.C. conceived the project. J.B. designed and performed the experiments for characterization of the sensor, and Y.W. took part in the early development stage for the sensor characterization. J.B. performed the sensor characterization experiments and analyzed the data; J.B. and L.M. designed and performed the experiments for temporal characterization of the sensor, and L.M. analyzed the data. J.B. wrote the paper together with L.M. and A.-S.C.

Conflicts of Interest: The authors declare no conflict of interest. The founding sponsors had no role in the design of the study; in the collection, analyses, or interpretation of data; in the writing of the manuscript; or in the decision to publish the results.

References

1. Clark, L.C.; Lyons, C. Electrode Systems for Continous Monitoring in cardiovascular surgery cardivascular surgery. *Ann. N. Y. Acad. Sci.* **1962**, *102*, 29–45. [CrossRef] [PubMed]
2. Khan, M.S.; Misra, S.K.; Schwartz-Duval, A.S.; Daza, E.; Ostadhossein, F.; Bowman, M.; Jain, A.; Taylor, G.; McDonagh, D.; Labriola, L.T.; et al. Real-Time Monitoring of Post-Surgical and Post-Traumatic Eye Injuries Using Multilayered Electrical Biosensor Chip. *ACS Appl. Mater. Interfaces* **2017**, *9*, 8609–8622. [CrossRef] [PubMed]
3. Monosik, R.; Stredansky, M.; Tkac, J.; Sturdik, E. Application of Enzyme Biosensors in Analysis of Food and Beverages. *Food Anal. Methods* **2012**, *5*, 40–53. [CrossRef]
4. Prodromidis, M.I.; Karayannis, M.I. Enzyme based amperometric biosensors for food analysis. *Electroanalysis* **2002**, *14*, 241–261. [CrossRef]
5. Rocchitta, G.; Spanu, A.; Babudieri, S.; Latte, G.; Madeddu, G.; Galleri, G.; Nuvoli, S.; Bagella, P.; Demartis, M.I.; Fiore, V.; et al. Enzyme Biosensors for Biomedical Applications: Strategies for Safeguarding Analytical Performances in Biological Fluids. *Sensors* **2016**, *16*, 780. [CrossRef] [PubMed]
6. Verma, N.; Bhardwaj, A. Biosensor Technology for Pesticides—A review. *Appl. Biochem. Biotechnol.* **2015**, *175*, 3093–3119. [CrossRef] [PubMed]
7. Dale, N.; Hatz, S.; Tian, F.; Llaudet, E. Listening to the brain: Microelectrode biosensors for neurochemicals. *Trends Biotechnol.* **2005**, *23*, 420–428. [CrossRef] [PubMed]
8. Cordeiro, C.; de Vries, M.G.; Ngabi, W.; Oomen, P.E.; Cremers, T.I.F.H.; Westerink, B.H.C. In vivo continuous and simultaneous monitoring of brain energy substrates with a multiplex amperometric enzyme-based biosensor device. *Biosens. Bioelectron.* **2015**, *67*, 677–686. [CrossRef] [PubMed]
9. Kiyatkin, E.A.; Wakabayashi, K.T. Parsing glucose entry into the brain: Novel findings obtained with enzyme-based glucose biosensors. *ACS Chem. Neurosci.* **2014**, *6*, 108–116. [CrossRef] [PubMed]
10. Lourenço, C.F.; Ledo, A.; Laranjinha, J.; Gerhardt, G.A.; Barbosa, R.M. Microelectrode array biosensor for high-resolution measurements of extracellular glucose in the brain. *Sens. Actuators B Chem.* **2016**, *237*, 298–307. [CrossRef]
11. Santos, R.M.; Laranjinha, J.; Barbosa, R.M.; Sirota, A. Simultaneous measurement of cholinergic tone and neuronal network dynamics in vivo in the rat brain using a novel choline oxidase based electrochemical biosensor. *Biosens. Bioelectron.* **2015**, *69*, 83–94. [CrossRef] [PubMed]
12. Du, Y.; Zhang, W.; Wang, M. Sensing of Salivary Glucose Using Nano-Structured Biosensors. *Biosensors* **2016**, *6*, 10. [CrossRef] [PubMed]
13. Rauf, S.; Hayat Nawaz, M.A.; Badea, M.; Marty, J.L.; Hayat, A. Nano-engineered biomimetic optical sensors for glucose monitoring in diabetes. *Sensors* **2016**, *16*, 1931. [CrossRef] [PubMed]
14. Chen, C.; Xie, Q.; Yang, D.; Xiao, H.; Fu, Y.; Tan, Y.; Yao, S. Recent advances in electrochemical glucose biosensors: A review. *RSC Adv.* **2013**, *3*, 4473–4491. [CrossRef]
15. Devadoss, A.; Sudhagar, P.; Terashima, C.; Nakata, K.; Fujishima, A. Photoelectrochemical biosensors: New insights into promising photoelectrodes and signal amplification strategies. *J. Photochem. Photobiol. C* **2015**, *24*, 43–63. [CrossRef]

16. Papa, H.; Gaillard, M.; Gonzalez, L.; Chatterjee, J. Fabrication of Functionalized Carbon Nanotube Buckypaper Electrodes for Application in Glucose Biosensors. *Biosensors* **2014**, *4*, 449–460. [CrossRef] [PubMed]
17. Kitte, S.A.; Gao, W.; Zholudov, Y.T.; Qi, L.; Nsabimana, A.; Liu, Z.; Xu, G. Stainless Steel Electrode for Sensitive Luminol Electrochemiluminescent Detection of H_2O_2, Glucose, and Glucose Oxidase Activity. *Anal. Chem.* **2017**, *89*, 9864–9869. [CrossRef] [PubMed]
18. Theuer, L.; Lehmann, M.; Junne, S.; Neubauer, P.; Birkholz, M. Micro-Electromechanical Affinity Sensor for the Monitoring of Glucose in Bioprocess Media. *Int. J. Mol. Sci.* **2017**, *18*, 1235. [CrossRef] [PubMed]
19. He, Y.; Zheng, J.; Wang, B.; Ren, H. Double Biocatalysis Signal Amplification Glucose Biosensor Based on Porous Graphene. *Materials* **2017**, *10*, 1139. [CrossRef] [PubMed]
20. Li, C.; Chen, X.; Zhang, F.; He, X.; Fang, G.; Liu, J.; Wang, S. Design of Cyclic Peptide Based Glucose Receptors and Their Application in Glucose Sensing. *Anal. Chem.* **2017**, *89*, 10431–10438. [CrossRef] [PubMed]
21. Bornhoeft, L.; Biswas, A.; McShane, M. Composite Hydrogels with Engineered Microdomains for Optical Glucose Sensing at Low Oxygen Conditions. *Biosensors* **2017**, *7*, 8. [CrossRef] [PubMed]
22. Weltin, A.; Kieninger, J.; Urban, G.A. Microfabricated, amperometric, enzyme-based biosensors for in vivo applications. *Anal. Bioanal. Chem.* **2016**, *408*, 4503–4521. [CrossRef] [PubMed]
23. Xiao, T.; Wu, F.; Hao, J.; Zhang, M.; Yu, P.; Mao, L. In Vivo Analysis with Electrochemical Sensors and Biosensors. *Anal. Chem.* **2017**, *89*, 300–313. [CrossRef] [PubMed]
24. Bucher, E.S.; Wightman, R.M. Electrochemical Analysis of Neurotransmitters. *Annu. Rev. Anal. Chem.* **2015**, *8*, 239–261. [CrossRef] [PubMed]
25. Ferapontova, E.E. Electrochemical Analysis of Dopamine: Perspectives of Specific In Vivo Detection. *Electrochim. Acta* **2017**. [CrossRef]
26. Fox, M.E.; Wightman, R.M. Contrasting Regulation of Catecholamine Neurotransmission in the Behaving Brain: Pharmacological Insights from an Electrochemical Perspective. *Pharmacol. Rev.* **2017**, *69*, 12–32. [CrossRef] [PubMed]
27. Davie, C.A. A review of Parkinson's disease. *Br. Med. Bull.* **2008**, *86*, 109–127. [CrossRef] [PubMed]
28. Kalia, L.V.; Lang, A.E. Parkinson's disease. *Lancet* **2015**, *386*, 896–912. [CrossRef]
29. Nutt, D.J.; Lingford-Hughes, A.; Erritzoe, D.; Stokes, P.R. The dopamine theory of addiction: 40 years of highs and lows. *Nat. Rev. Neurosci.* **2015**, *16*, 305–312. [CrossRef] [PubMed]
30. Mergenthaler, P.; Lindauer, U.; Dienel, G.A.; Meisel, A. Sugar for the brain: The role of glucose in physiological and pathological brain function. *Trends Neurosci.* **2013**, *36*, 587–597. [CrossRef] [PubMed]
31. Zheng, H.; Wang, R.; Qu, J. Effect of different glucose supply conditions on neuronal energy metabolism. *Cogn. Neurodyn.* **2016**, *10*, 563–571. [CrossRef] [PubMed]
32. Smith, S.K.; Lee, C.A.; Dausch, M.E.; Horman, B.M.; Patisaul, H.B.; McCarty, G.S.; Sombers, L.A. Simultaneous Voltammetric Measurements of Glucose and Dopamine Demonstrate the Coupling of Glucose Availability with Increased Metabolic Demand in the Rat Striatum. *ACS Chem. Neurosci.* **2017**, *8*, 272–280. [CrossRef] [PubMed]
33. Grieshaber, D.; MacKenzie, R.; Voeroes, J.; Reimhult, E. Electrochemical Biosensors—Sensor Principles and Architectures. *Sensors* **2008**, *8*, 1400–1458. [CrossRef] [PubMed]
34. Kimmel, D.W.; LeBlanc, G.; Meschievitz, M.E.; Cliffel, D.E. Electrochemical sensors and biosensors. *Anal. Chem.* **2012**, *84*, 685–707. [CrossRef] [PubMed]
35. Bhardwaj, T. A Review on Immobilization Techniques of Biosensors. *Int. J. Eng. Res. Technol.* **2014**, *3*, 294–298.
36. Cosnier, S. Biosensors based on electropolymerized films: New trends. *Anal. Bioanal. Chem.* **2003**, *377*, 507–520. [CrossRef] [PubMed]
37. Homaei, A.A.; Sariri, R.; Vianello, F.; Stevanato, R. Enzyme immobilization: An update. *J. Chem. Biol.* **2013**, *6*, 185–205. [CrossRef] [PubMed]
38. Jesionowski, T.; Zdarta, J.; Krajewska, B. Enzyme immobilization by adsorption: A review. *Adsorption* **2014**, *20*, 801–821. [CrossRef]
39. Noll, T.; Noll, G. Strategies for "wiring" redox-active proteins to electrodes and applications in biosensors, biofuel cells, and nanotechnology. *Chem. Soc. Rev.* **2011**, *40*, 3564–3576. [CrossRef] [PubMed]
40. Putzbach, W.; Ronkainen, N.J. Immobilization Techniques in the Fabrication of Nanomaterial-Based Electrochemical Biosensors: A Review. *Sensors* **2013**, *13*, 4811–4840. [CrossRef] [PubMed]

41. Vasylieva, N.; Maucler, C.; Meiller, A.; Viscogliosi, H.; Lieutaud, T.; Barbier, D.; Marinesco, S. Immobilization method to preserve enzyme specificity in biosensors: Consequences for brain glutamate detection. *Anal. Chem.* **2013**, *85*, 2507–2515. [CrossRef] [PubMed]
42. Asuri, P.; Karajanagi, S.S.; Vertegel, A.A.; Dordick, J.S.; Kane, R.S. Enhanced stability of enzymes adsorbed onto nanoparticles. *J. Nanosci. Nanotechnol.* **2007**, *7*, 1675–1678. [CrossRef] [PubMed]
43. Cans, A.-S.; Dean, S.L.; Reyes, F.E.; Keating, C.D. Synthesis and characterization of enzyme-Au bioconjugates: HRP and fluorescein-labeled HRP. *Nanobiotechnology* **2007**, *3*, 12–22. [CrossRef]
44. Gagner, J.E.; Lopez, M.D.; Dordick, J.S.; Siegel, R.W. Effect of gold nanoparticle morphology on adsorbed protein structure and function. *Biomaterials* **2011**, *32*, 7241–7252. [CrossRef] [PubMed]
45. Keighron, J.D.; Åkesson, S.; Cans, A.-S. Coimmobilization of acetylcholinesterase and choline oxidase on gold nanoparticles: Stoichiometry, activity, and reaction efficiency. *Langmuir* **2014**, *30*, 11348–11355. [CrossRef] [PubMed]
46. Li, Y.; Schluesener, H.J.; Xu, S. Gold nanoparticle-based biosensors. *Gold Bull.* **2010**, *43*, 29–41. [CrossRef]
47. Luo, X.-L.; Xu, J.J.; Du, Y.; Chen, H.Y. A glucose biosensor based on chitosan–glucose oxidase–gold nanoparticles biocomposite formed by one-step electrodeposition. *Anal. Biochem.* **2004**, *334*, 284–289. [CrossRef] [PubMed]
48. Zhang, S.; Wang, N.; Niu, Y.; Sun, C. Immobilization of glucose oxidase on gold nanoparticles modified Au electrode for the construction of biosensor. *Sens. Actuator B Chem.* **2005**, *109*, 367–374. [CrossRef]
49. Zhao, S.; Zhang, K.; Bai, Y.; Yang, W.; Sun, C. Glucose oxidase/colloidal gold nanoparticles immobilized in Nafion film on glassy carbon electrode: Direct electron transfer and electrocatalysis. *Bioelectrochemistry* **2006**, *69*, 158–163. [CrossRef] [PubMed]
50. Keighron, J.D.; Wigström, J.; Kurczy, M.E.; Bergman, J.; Wang, Y.; Cans, A.S. Amperometric detection of single vesicle acetylcholine release events from an artificial cell. *ACS Chem. Neurosci.* **2015**, *6*, 181–188. [CrossRef] [PubMed]
51. Finot, M.O.; Braybrook, G.D.; McDermott, M.T. Characterization of electrochemically deposited gold nanocrystals on glassy carbon electrodes. *J. Electroanal. Chem.* **1999**, *466*, 234–241. [CrossRef]
52. Ferreyra, N.; Coche-Guérente, L.; Labbé, P. Construction of layer-by-layer self-assemblies of glucose oxidase and cationic polyelectrolyte onto glassy carbon electrodes and electrochemical study of the redox-mediated enzymatic activity. *Electrochim. Acta* **2004**, *49*, 477–484. [CrossRef]
53. Bergman, J.; Wang, Y.; Wigström, J.; Cans, A.S. Counting the number of enzymes immobilized onto a nanoparticle-coated electrode. *Anal. Bioanal. Chem.* **2017**. [CrossRef] [PubMed]
54. Berg, J.M.; Tymoczko, J.L.; Stryer, L. *Biochemistry*, 6th ed.; W. H. Freeman and Company: New York, NY, USA, 2007.
55. Zaidi, S.A.; Shin, J.H. Recent developments in nanostructure based electrochemical glucose sensors. *Talanta* **2016**, *149*, 30–42. [CrossRef] [PubMed]
56. Harrison, F.E.; May, J.M. Vitamin C Function in the Brain: Vital Role of the Ascorbate Transporter (SVCT2). *Free Radic. Biol. Med.* **2009**, *46*, 719–730. [CrossRef] [PubMed]
57. Meldrum, B.S. Glutamate as a neurotransmitter in the brain: Review of physiology and pathology. *J. Nutr.* **2000**, *130* (Suppl. 4S), 1007s–1015s. [PubMed]
58. Bruno, J.P.; Gash, C.; Martin, B.; Zmarowski, A.; Pomerleau, F.; Burmeister, J.; Huettl, P.; Gerhardt, G.A. Second-by-second measurement of acetylcholine release in prefrontal cortex. *Eur. J. Neurosci.* **2006**, *24*, 2749–2757. [CrossRef] [PubMed]
59. Gu, H.; Varner, E.L.; Groskreutz, S.R.; Michael, A.C.; Weber, S.G. In Vivo Monitoring of Dopamine by Microdialysis with 1 min Temporal Resolution Using Online Capillary Liquid Chromatography with Electrochemical Detection. *Anal. Chem.* **2015**, *87*, 6088–6094. [CrossRef] [PubMed]
60. Barros, L.F.; Deitmer, J.W. Glucose and lactate supply to the synapse. *Brain Res. Rev.* **2010**, *63*, 149–159. [CrossRef] [PubMed]
61. Mosharov, E.V.; Sulzer, D. Analysis of exocytotic events recorded by amperometry. *Nat. Methods* **2005**, *2*, 651–658. [CrossRef] [PubMed]

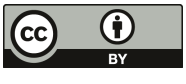

© 2018 by the authors. Licensee MDPI, Basel, Switzerland. This article is an open access article distributed under the terms and conditions of the Creative Commons Attribution (CC BY) license (http://creativecommons.org/licenses/by/4.0/).

catalysts

MDPI

Article

Polyelectrolyte Complex Beads by Novel Two-Step Process for Improved Performance of Viable Whole-Cell Baeyer-Villiger Monoxygenase by Immobilization

Tomáš Krajčovič [1], Marek Bučko [1], Alica Vikartovská [1], Igor Lacík [2], Lucia Uhelská [2], Dušan Chorvát [3], Vilém Neděla [4], Eva Tihlaříková [4], Martin Gericke [5], Thomas Heinze [5] and Peter Gemeiner [1,*]

1 Department of Glycobiotechnology, Institute of Chemistry, Slovak Academy of Sciences, Dúbravská cesta 9, SK-845 38 Bratislava, Slovakia; tomas.krajcovic@savba.sk (T.K.); marek.bucko@savba.sk (M.B.); alica.vikartovska@savba.sk (A.V.)

2 Polymer Institute, Slovak Academy of Sciences, Dúbravská cesta 9, SK-845 41 Bratislava, Slovakia; igor.lacik@savba.sk (I.L.); lucia.ucnova@savba.sk (L.U.)

3 Department of Biophotonics, International Laser Centre, Ilkovičova 3, SK-841 04 Bratislava, Slovakia; dusan.chorvat@ilc.sk

4 Department of Electron Microscopy, Institute of Scientific Instruments of the ASCR v.v.i., Královopolská 147, CZ-612 64 Brno, Czech Republic; vilem@isibrno.cz (V.N.); tihlarik@isibrno.cz (E.T.)

5 Institute of Organic Chemistry and Macromolecular Chemistry, Centre of Excellence for Polysaccharide Research, Friedrich Schiller University of Jena, Humboldtstrasse 10, D-07743 Jena, Germany; martin.gericke@uni-jena.de (M.G.); thomas.heinze@uni-jena.de (T.H.)

* Correspondence: Peter.Gemeiner@savba.sk; Tel.: +421-2-5941-0211

Received: 18 October 2017; Accepted: 13 November 2017; Published: 21 November 2017

Abstract: A novel immobilization matrix for the entrapment of viable whole-cell Baeyer–Villiger monooxygenase was developed. Viable recombinant *Escherichia coli* cells overexpressing cyclohexanone monooxygenase were entrapped in polyelectrolyte complex beads prepared by a two-step reaction of oppositely-charged polymers including highly defined cellulose sulphate. Immobilized cells exhibited higher operational stability than free cells during 10 repeated cycles of Baeyer–Villiger biooxidations of rac-bicyclo[3.2.0]hept-2-en-6-one to the corresponding lactones (1*R*,5*S*)-3-oxabicyclo-[3.3.0]oct-6-en-3-one and (1*S*,5*R*)-2-oxabicyclo-[3.3.0]oct-6-en-3-one. The morphology of polyelectrolyte complex beads was characterised by environmental scanning electron microscopy; the spatial distribution of polymers in the beads and cell viability were examined using confocal laser scanning microscopy, and the texture was characterised by the mechanical resistance measurements.

Keywords: polyelectrolyte complex beads; environmental scanning electron microscopy; confocal laser scanning microscopy; Baeyer-Villiger biooxidation; cyclohexanone monoxygenase; immobilization; viable whole-cell biocatalyst

1. Introduction

The immobilization of viable whole-cell biocatalysts has long been considered an important method for ensuring their recyclability and stabilisation for the development of the industrial production of chemical specialities and chiral drug precursors [1]. In particular, the combination of viable recombinant cells with overproduced enzymes and their immobilization facilitates recyclability and renders possible a continuous bioreactor arrangement with high application potential [2].

One of the validated techniques for immobilizing viable recombinant cells is their encapsulation in polyelectrolyte complex (PEC) capsules, which afforded promising results in the previous development

of encapsulated viable whole-cell biocatalysts [3–5]. PEC capsules have been produced by a single-step polyelectrolyte complexation of oppositely-charged polyanion (PA) aqueous solutions consisting of cellulose sulphate (CS), high-viscosity sodium alginate and living bacterial cells with a polycation solution of poly(methylene-co-guanidine) (PMCG), $CaCl_2$ as gelling and NaCl as antigelling agents [6]. PA microdrops have been air-stripped by a coaxial nozzle into a polycation solution flowing in a multiloop chemical reactor for the preparation of spherical and monodispersed PEC capsules [7]. This encapsulation protocol preserved the high viability of the encapsulated recombinant *Escherichia coli* (*E. coli*) cells with overproduced ezymes from the group of Baeyer–Villiger monooxygenases (BVMOs) as well as their long-term storage and operational stability [4,8–10].

The development of encapsulation techniques, including the PEC capsules, has progressed towards a precise and targeted characterisation of the morphology, physicochemical properties of capsules, biocompatibility and their changes over time, using the latest techniques [11,12] for applications in biotechnology and medicine. Additionally, there is also an increased effort to optimise immobilization by predicting and modelling the bioengineering parameters of potential industrial processes [13]. On the other hand, current practice in industrial applications of immobilized biocatalysts [14] does not entail the consistent characterisation of the immobilization procedure and influence over the geometry, size, stability of composition, mechanical and diffusion properties of immobilized cell particles. This could lead to an incomplete knowledge of the immobilization parameters and methods for their control as well as the unsubstantiated exclusion of promising immobilization techniques for industrial use. The current development and production of tailor-made CS is crucial for further research into innovative and improved PEC capsules [15]. Parameters such as the origin of cellulose, molecular weight (MW), viscosity and degree of substitution (DS) of the CS significantly influence the successful formation of PEC capsules. Hence, the selection of commercial, tailor-made CS by the process described in [15], which, to the best of our knowledge, alone meets the latter scientific requirements, is essential for the encapsulation of cells. Although the production of PEC capsules with semipermeable membranes has been useful for the development of viable whole-cell biocatalysts under laboratory conditions, it entails a relatively complex encapsulation procedure and considerable consumption of PMCG and washing solutions using a continuous, one-step protocol. In addition, for more robust uses, PEC capsules with immobilized whole-cell biocatalysts have proved to be fragile during intensive mixing [10], and it was necessary to use fluidised-bed bioreactors [5] or mini packed-bed reactors with a low flow-rate [9]. Hence, it is desirable to develop protocols for the preparation of PEC beads with enhanced mechanical properties, with a lower consumption of PMCG and washing solutions, and with a simpler cation immobilization procedure.

The present work sought to develop PEC beads with entrapped viable cells complexed in the whole volume of the beads. Another aim was the use of imaging techniques to characterise the morphology of PEC beads and cells in the native state, the spatial distribution of the polymer within PEC beads and the mechanical resistance of the PEC beads. Viable recombinant *E. coli* (*Escherichia coli*) cells overproducing cyklohexanone monooxygenase (CHMO) from the group of BVMOs were used as a model biocatalyst in this study. Currently, there is increased interest in research into novel enzymes and the industrial applications of BVMOs, as they catalyse the enantioselective BV biooxidation of a wide range of cyclic ketones to the corresponding lactones as chiral precursors of natural and bioactive compounds as well as potential drugs [16–19]. The study also sought to determine the operational stability of PEC beads with immobilized recombinant *E. coli* cells with CHMO during repeated Baeyer–Villiger (BV) biooxidations as well as the influence of repeated biotransformations on the viability of cells.

2. Results and Discussion

2.1. Production of PEC Bads with Immobilized E. coli Containing CHMO

The development of PEC beads was performed following a modified protocol originally developed for the one-step encapsulation of viable *E. coli* cells with overproduced BVMO in PEC capsules [4,9]. In the present work, PEC beads were prepared by a two-step procedure. This included the gelation of PA microdrops with cells in a solution of $CaCl_2$ in the first step followed by polyelectrolyte complexation with PMCG in the second step, and finally washing in a physiological saline solution. This immobilization protocol resulted in less stringent and simpler conditions including higher utility and approximately a 2-fold decrease in the consumption of expensive PMCG and washing solutions for the preparation of immobilized viable *E. coli* with CHMO as compared with the PEC capsules previously used [9]. Use of the two-step procedure for the preparation of PEC beads led to an approximately one-third cost reduction as compared with the previous production of PEC capsules. Irrespective of this, a narrow size distribution of PEC beads of 0.64 ± 0.03 mm (Figure 1), high cell viability as well as higher operational stability of immobilized cells than in free cells was achieved, as detailed subsequently.

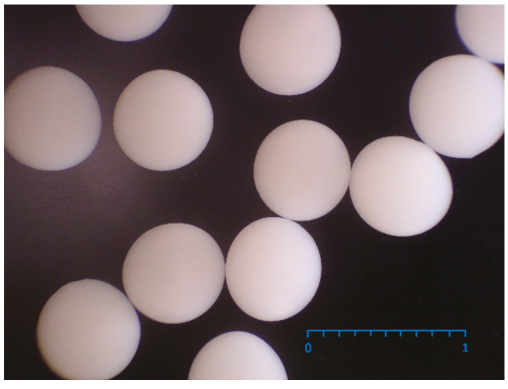

Figure 1. Photomicrography of uniform polyelectrolyte complex (PEC) beads with entrapped recombinant *E. coli* (*Escherichia coli*) cells with overexpressed cyklohexanone monooxygenase (CHMO). The immobilization yield was 100%. The scale bar is 1 mm.

2.2. Suitability of Cellulose Sulphate

The selection of suitable CS as the polyanion component is the key to polyelectrolyte complexation with the PMCG polycation, which is crucial for the integrity, mechanical and chemical resistance and biocompatibility of PEC beads. CS with a DS of 1.45 and a molecular weight of 400,000 g/mol–500,000 g/mol was used for the preparation of the PEC beads using a two-stage procedure including gelation and complexation steps. The substitution did not apparently depolymerise the cellulose, because the DS of 1.45 was in good agreement with the increase in MW of the starting cellulose (254,700 g/mol). The crystallinity index of the bleached kraft pulp (BKP) CrI of 50 ± 3%, determined by the method developed by [20] showed a relatively high proportion of the amorphous phase distorted by the supra-molecular structure of the starting cellulose. If a similar crystallinity is exhibited by the spruce sulphite pulp (SSP) used in this work, a relatively high proportion of the amorphous phase should afford a more homogeneous distribution of substitution in the over-molecular cellulose structure. The amorphous phase also affords the availability of the polycations (PMCG) forming the PEC complex as well as better permeability of substrates and products for a biocatalytic reaction in that part of PEC beads in which the CS is incorporated.

2.3. Repeated Biotransformations Using Immobilized Cells

Stabilisation of the high enzyme activity of cells to achieve the maximum substrate conversion in repeated biotransformation cycles is one of the most important parameters in respect of the profitability of immobilized whole-cell biocatalysts [1]. At the same time, when using live cells, the need to maintain the highest degree of cell viability is also important. Over the course of 10 repeated BV biooxidations of bicyclo[3.2.0]hept-2-ene-6-one to regioisomeric lactones (1*R*,5*S*)-3-oxabicyclo-[3.3.0]oct-6-en-3-one and (1*S*,5*R*)-2-oxabicyclo-[3.3.0]oct-6-en-3-one, a high and stable conversion rate was observed using *E. coli* cells with CHMO immobilized in PEC beads (Figure 2). For up to 8 cycles, conversion rates of 100–93 ± 4% were achieved. After the 9th and 10th cycles, decreases to 85 ± 6% and 65 ± 5%, respectively were observed. In contrast with these findings, unprotected free cells exhibited a distinct decrease of 85 ± 6% in substrate conversion of the BV biooxidation in the 4th cycle, which showed a steady decline to 48 ± 6% in the 10th cycle. Cell stabilization within mild and physiological microenvironment of the PEC beads may contribute to higher stability of immobilized cells and delayed their deactivation compared to free cells (Figure 2).

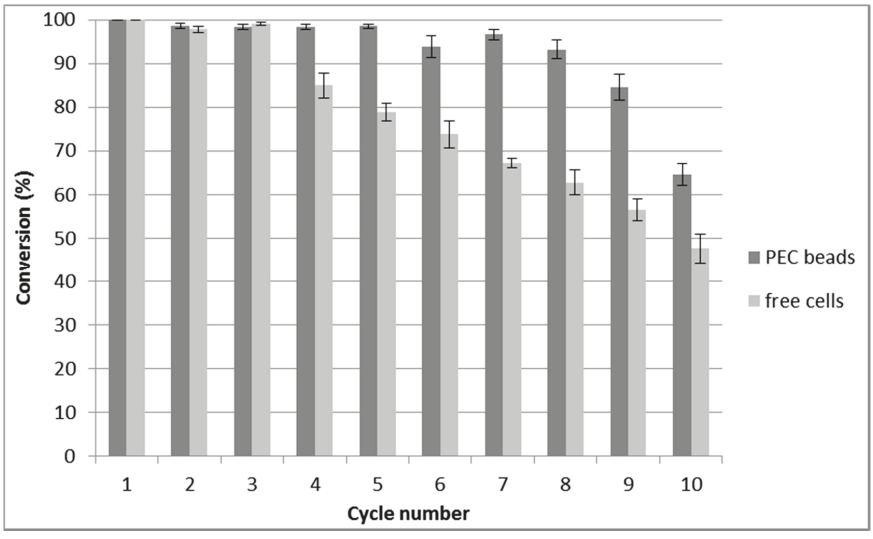

Figure 2. Conversion of bicyclic substrate to enantiomerically pure lactones using free and PEC immobilized *E. coli* cells containing CHMO enzyme catalysing Baeyer–Villger BV biooxidation. The graph shows the conversion rate in reaction time of 120 min. PEC: polyelectrolyte complex; BV: Baeyer–Villiger.

2.4. Morphology of PEC Beads

To investigate the morphology of the PEC beads, the confocal laser scanning microscopy arrangement described in the previous section was used (Figure 3). The beads contained Rhodamine 123 and Eosin Y as fluorescent tracer dyes of a concentration of 10^{-6} mol/L and were incubated for 15−30 min. These two non-covalently bound fluorescent tracer dyes were employed to monitor the distribution of the residual opposite charge within the PEC microcapsule [21]. Anionic Eosin Y (Figure 3A) was predominantly localised in the outer region of the PEC bead, and its concentration dropped sharply towards the bead interior. On the other hand, cationic Rhodamine 123 (Figure 3B) was observed in the entire volume of the PEC bead, with a higher intensity at the outer region and a lower intensity in the centre. Unlike in the previous study on polyelectrolyte capsules [21], no specific layers or internal structures were observed in the present study. It is worth noting that the spatial

distribution of the fluorescence reflects the concentration of the dye molecules, corresponding to the residual free-charged groups of the matrix, rather than the spatial distribution of polymer components in the bead.

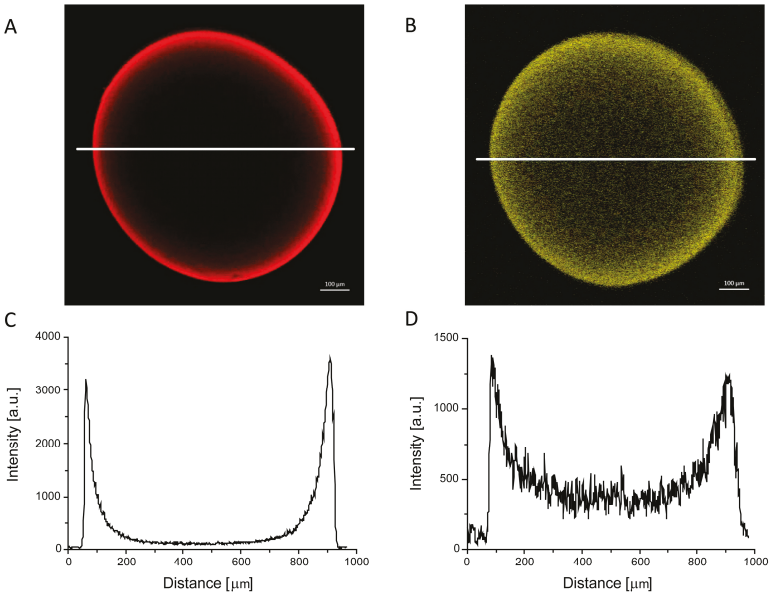

Figure 3. Image of PEC beads obtained by confocal laser scanning microscopy. Visualisation of the spatial distribution of fluorescence of Eosin Y (**A**) and Rhodamine 123 (**B**); Profiles of fluorescence intensity distribution, estimated along the white line for the respective tracer dye (**C**,**D**).

2.5. Cell Viability

Cell viability prior to and after biotransformation was measured by the intake of PI by the necrotic cells [8]. The viability of immobilized cells of *E. coli* with CHMO under different conditions and after 10 repeated biotransformation cycles (Figure 4) was evaluated. The viability in all cases remained within an 85−95% range.

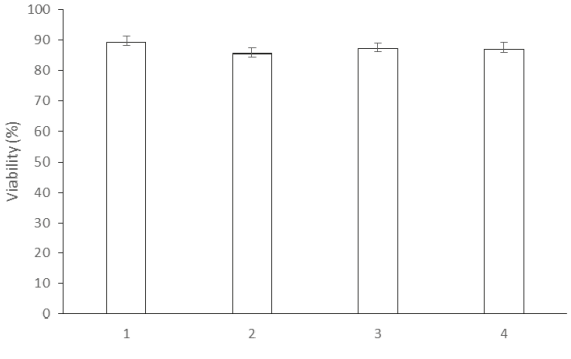

Figure 4. Viability of recombinant *E. coli* cells with CHMO in different preparations. 1: PEC beads after 10 biotransformation cycles; 2: PEC beads prior to biotransformations; 3: free cells after 10 biotransformation·cycles; 4: free cells prior to biotransformations.

The high viability of cells immobilized in PEC beads was identical with that of free cells prior to biotransformations. This demonstrates the excellent biocompatibility of the novel PEC beads and their ability to preserve the physiological microenvironment for immobilized cells. At the same time, the nontoxicity of the PEC complex with CS in capsules [22] was also confirmed in the PEC beads developed in the present work. In addition, the high cell viability which did not vary after 10 biotransformation cycles demonstrates the preservation of the physiological conditions for immobilized cells during biotransformations.

2.6. Environmental Scanning Electron Microscopy (ESEM)

The PEC beads with and without *E. coli* cells showed a very regular spherical shape with a relatively smooth surface free from cracks and corrugations that was maintained after repeated biotransformations (Figure 5A–C). *E. coli* cells in their native state covered with a very thin liquid layer of a solution are shown in Figure 5D. The PEC bead microstructure was significantly improved compared with the microstructure described in a previous study, where the roughness of the PEC capsule surface with *Gluconobacter oxydans* cells was higher [5]. A slight wrinkling of the PEC bead surface without cells is commonly formed during polyelectrolyte complexation (highlighted by white dashed arrows in Figure 5A). In all cases, good roundness and bead regularity as well as low size distribution were demonstrated using ESEM. A slightly blurred image of *E. coli* cells partially covered by a small layer of the solution exhibited the unique possibility to depict fully wet cells in their native state using the ESEM AQUASEM II (Figure 5D) equipped with custom-built detectors of signal electrons with a very high detection efficiency [23]. A lower quality of this image was caused by the unprocessed state of these live cells, depicted without the use of any preparation technique such as chemical fixation, drying or metal coating [24] as well as their imaging under a very low beam current and a relatively high pressure of water vapour in the specimen chamber of the ESEM.

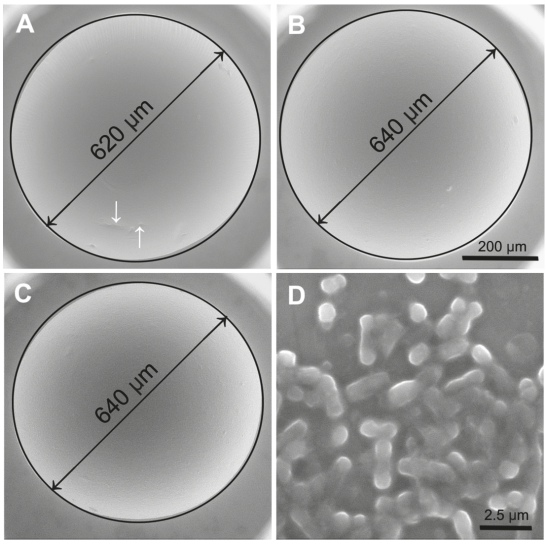

Figure 5. Microstructure of PEC bead surface free from cells (**A**), PEC bead with 10% (*w/v*) of wet *E. coli* cells prior to biotransformations (**B**), PEC bead with 10% (*w/v*) of wet *E. coli* cells after 10 biotransformation cycles (**C**), free live *E. coli* cells (**D**) in aqueous solution of phosphate buffer recorded by environmental scanning electron microscopy (ESEM) AQUASEM II with highlighted circularity and diameter measurement (*black lines*). The surface corrugation is due to cells clustering (**A**, *white dashed arrow*). The scale bar indicates 200 µm in (**A**–**C**) and 2.5 µm in (**D**).

2.7. Mechanical Resistance

Figure 6 depicts a typical course of the force during measurement of the mechanical resistance of PEC beads. The point marked by the arrow represents the bursting force required for mechanical disruption of the PEC bead. The average bursting force of PEC beads with entrapped cells prior to biotransformations was 0.95 ± 0.04 g/bead, which was close to the average bursting force of 1.16 ± 0.26 g/bead obtained for PEC beads after 10 biotransformation cycles. Practically the same mean values of bursting force prior to and after biotransformations showed that the mechanical strength of the PEC complex in the beads was not influenced either by mechanical forces induced by mixing or the sequestering agents such as phosphate buffer present in the reaction media.

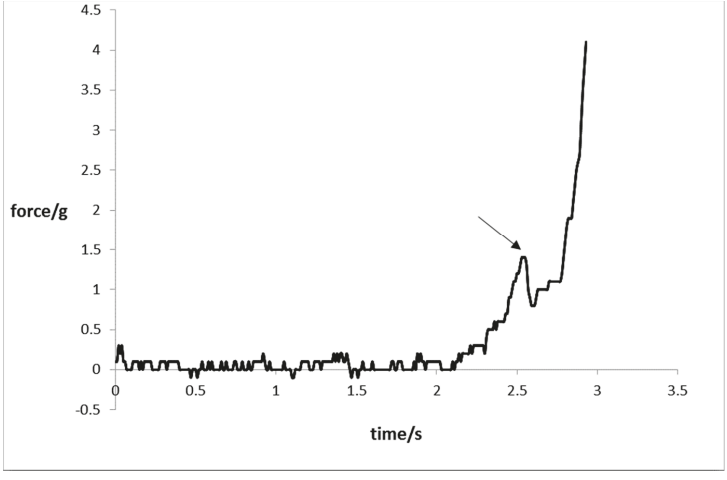

Figure 6. Time evolution of compression force applied onto a single PEC bead with immobilized cells after the 10th biotransformation cycle, measured during mechanical resistance test. The arrow indicates the moment of bead disruption.

It is also important to note that the PEC complex found throughout the volume of PEC beads provides additional mechanical resistance to the cells compared with the previously reported PEC capsule which contains the PEC membrane and the liquid core [25]. This can be seen in the course of the compression force where, after the disruption of a PEC bead at the point indicated by the arrow, a small decrease in the force occurred, followed by an increase in the bead resistance. On the other hand, the bursting of the PEC capsule observed previously [25] was followed by a sharp drop in force caused by the immediate and irreversible PEC capsule collapse.

3. Materials and Methods

3.1. Characterisation Polymers

High-viscosity, high-mannuronic acid sodium alginate from ISP Alginate (Girvan, UK) with the following chemical composition (determined by ^{1}H NMR) was employed: fraction of alginate consisting of guluronic acid $F_G = 0.41$, fraction of alginate consisting of mannuronic acid $F_M = 0.59$; fractions of alginate consisting of dimers and trimers of gluronic acid (G) and mannuronic acid (M): $F_{GG} = 0.21$, $F_{GM} = F_{MG} = 0.20$, $F_{MM} = 0.39$; $F_{GGM} = F_{MGG} = 0.03$, $F_{MGM} = 0.18$, $F_{GGG} = 0.18$, $N_{G>1} = 8$. PMCG from Scientific Polymer Products Inc. (Ontario, NY, USA), supplied as a 35% (*w*/*v*) aqueous solution, was lyophilised prior to use. The fluorescent tracer dyes Rhodamine 123 and Eosin Y were obtained from Acros Organics (Geel, Belgium). Water-soluble CS with the required DS,

dynamic viscosity and MW was provided by Senova Biotechnologieunternehmen (Weimar, Germany). The derivative was prepared in accordance with the literature by the homogeneous conversion of spruce sulphite pulp (MW_{Cuen} 254, 700 g/mol from Borregaard ChemCell, Sarpsborg, Norway) with SO_3-pyridine complex in the ionic liquid 1-butyl-3-methylimidazolium chloride (BMIMCl) with *N*,*N*-dimethylformamide as a dipolar aprotic co-solvent in order to improve the miscibility of the reaction mixture [15]. The final product had a DS of 1.45 and a dynamic viscosity of 15.6 mPa·s in 0.9% NaCl aqueous solution. The viscosity average molecular weight of around 500,000–600,000 g/mol corresponds to the weight average molecular weight of CS in the range from 310,000 to 460,000 g/mol determined by size exclusion chromatography [15]. These values were similar to those of the starting cellulose of 254,700 g/mol [15]. Sharp peaks characteristic of CS originating from sulphate groups were observed at 1256 cm^{-1} (δ SO_2) and 805 cm^{-1} (δ SO).

A Flash 2000 CHNS/O Analyser (Thermo Fisher Scientific, Waltham, MA, USA) was used for elemental analyses. The DS was calculated from the elemental composition as described in the literature [15]. Size exclusion chromatography (SEC) of CS was performed on a JASCO system (PU-980 isocratic pump, RI-930 refractive index detector, Suprema guard column and columns (100 Å, 1000 Å, 3000 Å, in series) with 1 M Na_2HPO_4 (pH = 9, 200 mg/L NaN_3) as eluent (flow-rate: 1 mL/min, sample, concentration: 0.5 mg/mL). A viscometer (Brookfield Programmable DV-II+ Instrument, Middleboro, MA, USA) equipped with Thermostat Julabo F12 (Seelbach, Germany) was employed to determine the dynamic viscosity of CS solutions in an 0.9% NaCl aqueous solution. The viscosity average molecular weight of CS was determined from the intrinsic viscosity in 0.5 M NaCl at 25 °C (Mark Houwink parameters: α = 0.94, K = $6.37 \cdot 10^{-6}$ mL/g) in accordance with the literature [26]. Fourier-transform infra red (FTIR) spectra were measured using a Nicolet 6700 spectrometer (Thermo Fisher Scientific, Waltham, MA, USA) equipped with DTGS detector and Omnic 8.0 software (Thermo Fisher Scientific, Waltham, MA, USA). The spectra were collected in the range from 4000 cm^{-1} to 400 cm^{-1} at a resolution of 4 cm^{-1}; the number of scans was 128. Diamond Smart Orbit ATR accessory was applied to solid-state measurements.

3.2. Cultivation of Cells

Cell stocks of *E. coli* overexpressing CHMO (EC1.14.13.22) from *Acinetobacter calcoaceticus* NCIMB 9871 were stored at −80 °C. The recombinant *E. coli* strain was kindly donated by Prof. Marko D. Mihovilovič (TU Vienna, Austria). Cells, streaked at LB_{amp} agar Petri dish containing 10 g/L of peptone, 5 g/L of yeasts extract, 10 g/L of NaCl, 15 g/L of agar and 0.2 g/L of ampiciline, were cultivated in an incubator at 37 °C to afford colonies of approximately 1 mm size. A single colony from LB_{amp} agar was inoculated to a 10 mL of LB_{amp} medium in an Erlenmayer flask and allowed to grow at 37 °C in an orbital shaker at 150 rpm for 12 h. 1% of the inoculum (*v*/*v*) was pipetted into a TB_{amp} medium and cultivated at 37 °C in an orbital shaker at 150 rpm for 12 h. The addition of isopropyl β-D-1-thiogalactopyranoside (IPTG) to the final concentration of 0.25 mM to the medium, during shaking at 25 °C in an orbital shaker at 200 rpm for 2 h, induced the synthesis of CHMO enzyme. The biomass was separated from the medium by centrifugation at 15 °C and 4000× *g* for 15 min and used for biotransformation experiments and immobilization.

3.3. Preparation of Polyelectrolyte Complex Beads

A suspension of cells was prepared in a solution of 1.8% (*w*/*v*) of PA consisting of 0.9% (*w*/*v*) of sodium alginate and 0.9% of CS in 0.9% (*w*/*v*) NaCl at pH = 7 to the final concentration of 10% of wet cells. The PA solution with the cells was added dropwise into a stirred gelation solution of 1.0% (*w*/*v*) of $CaCl_2$ using a custom-made coaxial air-stripping extrusion device. The time of gelation was 10 min and the collection time was 1 min. Subsequently, the prepared beads were separated from the gelation medium and transferred into a stirred solution containing 1.8% (*w*/*v*) of PMCG and 0.9% (*w*/*v*) of NaCl at pH = 7 for 10 min in order to undergo polyelectrolyte complexation. The polyelectrolyte complex beads were washed with 0.9% (*w*/*v*) of NaCl and used in biotransformation.

3.4. Repeated Biotransformations

PEC beads with immobilized cells (10% *w/w*) and free *E. coli* cells were transferred into a reaction medium containing 50 mM phosphate buffer (pH = 7), 0.2 g/L of ampiciline and 4 g/L of glucose. Model Baeyer–Villiger biooxidation resulting in the production of lactone regioisomers (1*S*,5*R*)-2-oxabicyclo[3.3.0]oct-6-en-3-one and (1*R*,5*S*)-3-oxabicyclo-[3.3.0]-oct-6-en-2-one [27] was initiated by the addition of substrate rac-bicyclo[3.2.0]hept-2-en-6-one in ethanol (volume ratio 1:9) to the reaction medium to a final concentration of 0.5 g/L. The reaction conditions were 25 °C and 150 rpm in an orbital shaker. Substrate and produced lactones in samples were extracted in dichlormethane with methyl benzoate as internal standard (0.5 mg/mL) and analysed using gas chromatography as reported previously [9]. After each biotransformation, the PEC beads containing cells, and the free cells, were separated from the reaction medium by filtration (encapsulated cells) or centrifugation (free cells), washed with a substrate-free medium and subjected to another biotransformation cycle.

3.5. Confocal Laser Scanning Microscopy

The internal structure of the PEC beads was characterised using confocal laser scanning microscopy (CLSM). Images of the PEC beads were recorded simultaneously in transmission, reflection and fluorescence modes using a laser scanning microscope head LSM 510 META on Axiovert 200M stand (both from Carl Zeiss, Jena, Germany). A Zeiss PlanApochromat 10x/0.45 lens was used to visualise the whole beads. Laser lines of 488 nm for Rhodamine 123 and 543 nm for Eosin Y were used for excitation. Two channels with band-pass filter 500–550 nm for detection of the reflected light and a long-pass filter LP 560 nm were used for fluorescence.

3.6. Cell Viability

The CLSM confocal laser scanning microscopy system described for the investigation of the PEC bead structure was also used for cell viability imaging. Cells necrosis was detected using fluorescence of propidium iodide by LSM 510 META NLO microscope (Carl Zeiss, Jena, Germany) equipped with the C-Apochromat 40xW/corr water immersion objective. Viability of the encapsulated cells was determined after mild disruption of the beads in a test tube. The mixture was carefully stirred so as to ensure that the remains of beads did not affect the measurement. The cells were incubated for 10 min with 1 μM of propidium iodide (PI). Fluorescence was initiated by the 543 nm line of HeNe laser and an LP 560 nm long-pass emission filter was used for PI fluorescence detection. The cell viability was evaluated as a ratio of the number of the surviving bacterial cells to the total number of bacterial cells. The number of viable bacterial cells was calculated as the difference between the total number of bacterial cells and the number of necrotic cells identified by propidium iodide fluorescence. The total number of cells was counted from the respective transmission image in accordance with the literature [8].

3.7. Environmental Scanning Electron Microscopy

Due to the very high sensitivity of PEC beads to electron beam irradiation resulting in radiation damage and a high risk of surface dehydration, images of the beads were recorded under conditions of carefully controlled and very slowly reduced relative humidity (from 100% to 90%) in a specimen chamber of the ESEM AQUASEM II developed by the group of Environmental Electron Microscopy (ISI ASCR in Brno, Czech Republic) in cooperation with TESCAN (Brno, Czech Republic). A sophisticated hydration system with heated needle valve (35 °C) was used as an additional water supply in the microscope. PEC beads and *E. coli* cells were observed in a small droplet of aqueous solution of 50 mM phosphate buffer (pH = 7), ampicillin 0.2 g/L and glucose 4 g/L, at a reduced beam accelerating voltage of 10 kV and very low beam current of 30 pA. A specially modified ionisation detector of secondary electrons [28] affording a low beam current observation with a large field of view (up to 850 μm) was used.

3.8. Mechanical Strength

The mechanical properties of the PEC beads were determined in compression mode using a Texture Analyser TA-XT2i (Stable Micro Systems, Godalming, UK) equipped with a mobile probe and Texture Expert Exceed 2.64 software (Stable Micro Systems, Godalming, UK). Compression measurements were conducted at a compression speed of 0.5 mm/s to the point at which 95% of 50 PEC beads per batch were deformed. The bursting force is the result of this compression test.

4. Conclusions

This work focused on the development of an immobilization procedure providing PEC beads for the entrapment of viable recombinant *E. coli* cells with overexpressed cyclohexanone monooxygenase. Uniform and stable PEC beads were successfully produced by a two-step procedure including ionotropic gelation and polyelectrolyte complexation. The PEC beads were prepared under less stringent conditions with a lower consumption of polycation and washing solutions than for the PEC capsules previously used. These characteristics are highly advantageous for a potential production scale-up of Baeyer–Villiger biooxidations using entrapped viable cells. Accordingly, it was important that the performance of cells entrapped in PEC beads for a model Baeyer–Villiger biooxidation, expressed as their operational stability, was enhanced over that of free cells. The PEC beads preserved high cell viability and enabled faster and more precise handling with cells during repeated Baeyer–Villiger biooxidations. Further studies using environmental scanning electron microscopy confirmed the stability of the dimensions and the sphericity of the PEC beads. In addition, both the surface morphology and the mechanical resistance of the PEC beads remained unchanged prior to and after biotransformations.

Acknowledgments: This work was supported by the Slovak Grant Agency for Science VEGA 2/0090/16 and by the Slovak Research and Development Agency under contracts no. APVV-15-0227 and APVV-14-0858. This publication is the result of the project implementation: Applied research in the field of industrial biocatalysis, ITMS code: 26240220079 supported by the Research & Development Operational Programme funded by the ERDF. The authors are indebted to P. Laudeley (Institute of Organic Chemistry and Macromolecular Chemistry, Friedrich Schiller University of Jena) for her assistance with the synthesis of tailored CS.

Author Contributions: Tomáš Krajčovič performed experiments, analyzed data and wrote the paper; Marek Bučko and Peter Gemeiner conceived and designed the experiments, and wrote the paper; Alica Vikartovská contributed reagents/materials/analysis tools; Igor Lacík, Vilém Neděla, Dušan Chorvát and Martin Gericke conceived and designed the experiments, and wrote the paper; Thomas Heinze conceived and designed the experiments and contributed reagents/materials/analysis tools; Lucia Uhelská, Dušan Chorvát, Martin Gericke and Eva Tihlaříková performed experiments and analyzed data.

Conflicts of Interest: The authors declare no conflict of interest.

References

1. Kadisch, M.; Willrodt, C.; Hillen, M.; Bühler, B.; Schmid, A. Maximizing the stability of metabolic engineering-derived whole-cell biocatalysts. *Biotechnol. J.* **2017**, *12*. [CrossRef] [PubMed]
2. Wachtmeister, J.; Rother, D. Recent advances in whole cell biocatalysis techniques bridging from investigative to industrial scale. *Curr. Opin. Biotechnol.* **2016**, *42*, 169–177. [CrossRef] [PubMed]
3. Bučko, M.; Vikartovská, A.; Lacík, I.; Kolláriková, G.; Gemeiner, P.; Pätoprstý, V.; Brygin, M. Immobilization of a whole-cell epoxide-hydrolyzing biocatalyst in sodium alginate-cellulose sulfate-poly(methylene-co-guanidine) capsules using a controlled encapsulation process. *Enzyme Microb. Technol.* **2005**, *36*, 118–126. [CrossRef]
4. Hucík, M.; Bučko, M.; Gemeiner, P.; Štefuca, V.; Vikartovská, A.; Mihovilovic, M.D.; Rudroff, F.; Iqbal, N.; Chorvát, D., Jr.; Lacík, I. Encapsulation of recombinant *E. coli* expressing cyclopentanone monooxygenase in polyelectrolyte complex capsules for Baeyer-Villiger biooxidation of 8-oxabicyclo[3.2.1]oct-6-en-3-one. *Biotechnol. Lett.* **2010**, *32*, 675–680. [CrossRef] [PubMed]
5. Bertóková, A.; Vikartovská, A.; Bučko, M.; Gemeiner, P.; Tkáč, J.; Chorvát, D.; Štefuca, V.; Neděla, V. Biooxidation of 2-phenylethanol to phenylacetic acid by whole-cell *Gluconobacter oxydans* biocatalyst immobilized in polyelectrolyte complex capsules. *Biocatal. Biotransform.* **2015**, *33*, 111–120. [CrossRef]

6. Lacík, I.; Briššová, M.; Anilkumar, A.V.; Powers, A.C.; Wang, T. New capsule with tailored properties for the encapsulation of living cells. *J. Biomed. Mater. Res.* **1998**, *39*, 52–60. [CrossRef]
7. Anilkumar, A.V.; Lacik, I.; Wang, T.G. A novel reactor for making uniform capsules. *Biotechnol. Bioeng.* **2001**, *75*, 581–589. [CrossRef] [PubMed]
8. Schenkmayerová, A.; Bučko, M.; Gemeiner, P.; Chorvát, D., Jr.; Lacík, I. Viability of free and encapsulated *Escherichia coli* overexpressing cyclopentanone monooxygenase monitored during model Baeyer–Villiger biooxidation by confocal laser scanning microscopy. *Biotechnol. Lett.* **2012**, *34*, 309–314. [CrossRef] [PubMed]
9. Bučko, M.; Schenkmayerová, A.; Gemeiner, P.; Vikartovská, A.; Mihovilovič, M.D.; Lacík, I. Continuous testing system for Baeyer-Villiger biooxidation using recombinant *Escherichia coli* expressing cyclohexanone monooxygenase encapsulated in polyelectrolyte complex capsules. *Enzyme Microb. Technol.* **2011**, *49*, 284–288. [CrossRef] [PubMed]
10. Schenkmayerová, A.; Bučko, M.; Gemeiner, P.; Treľová, D.; Lacík, I.; Chorvát, D., Jr.; Ačai, P.; Polakovič, M.; Lipták, L.; Rebroš, M.; et al. Physical and bioengineering properties of polyvinyl alcohol lens-shaped particles versus spherical polyelectrolyte complex microcapsules as immobilization matrices for a whole-cell Baeyer-Villiger monooxygenase. *Appl. Biochem. Biotechnol.* **2014**, *174*, 1834–1849. [CrossRef]
11. De Vos, P.; Bučko, M.; Gemeiner, P.; Navrátil, M.; Švitel, J.; Faas, M.; Strand, B.L.; Skjak-Braek, G.; Morch, Y.A.; Vikartovská, A.; et al. Multiscale requirements for bioencapsulation in medicine and biotechnology. *Biomaterials* **2009**, *30*, 2559–2570. [CrossRef] [PubMed]
12. Rokstad, A.M.A.; Lacík, I.; de Vos, P.; Strand, B.L. Advances in biocompatibility and physico-chemical characterization of micorspheres for cell encapsulation. *Adv. Drug Deliv. Rev.* **2014**, *67–68*, 111–130. [CrossRef] [PubMed]
13. Polakovič, M.; Švitel, J.; Bučko, M.; Filip, J.; Neděla, V.; Ansorge-Schumacher, M.B.; Gemeiner, P. Progress in biocatalysis with immobilized viable whole cells: Systems development, reaction engineering and applications. *Biotechnol. Lett.* **2017**, *39*, 667–683. [CrossRef] [PubMed]
14. Liese, A.; Seelbach, K.; Buchholz, A.; Haberland, J. Processes. In *Industrial Biotransformations*, 2nd ed.; Liese, A., Seelbach, K., Wandrey, C., Eds.; Wiley-VCH Verlag GmbH&Co.: Weinheim, Germany, 2006; pp. 147–513. ISBN 3-527-31001-0.
15. Gericke, M.; Liebert, T.; Heinze, T. Interaction of ionic liquids with polysaccharides, 8–synthesis of cellulose sulfates suitable for polyelectrolyte complex formation. *Macromol. Biosci.* **2009**, *9*, 343–353. [CrossRef] [PubMed]
16. Bučko, M.; Gemeiner, P.; Schenkmayerová, A.; Krajčovič, T.; Rudroff, F.; Mihovilovič, M.D. Baeyer-Villiger oxidations: Biotechnological approach. *Appl. Microbiol. Biotechnol.* **2016**, *100*, 6585–6599. [CrossRef] [PubMed]
17. Leisch, H.; Morley, K.; Lau, C.K. Baeyer-Villiger Monooxygenases: More Than Just Green Chemistry. *Chem. Rev.* **2011**, *111*, 4165–4222. [CrossRef] [PubMed]
18. Balke, K.; Kadow, M.; Mallin, H.; Saß, S.; Bornscheuer, U.T. Discovery, application and protein engineering of Baeyer–Villiger monooxygenases for organic synthesis. *Org. Biomol. Chem.* **2012**, *10*, 6249–6265. [CrossRef] [PubMed]
19. Rudroff, F.; Fink, M.J.; Pydi, R.; Bornscheuer, U.T.; Mihovilovic, M.D. First chemo-enzymatic synthesis of the (*R*)-Taniguchi lactone and substrate profiles of CAMO and OTEMO, two new Baeyer-Villiger monooxygenases. *Monatsh. Chem.* **2017**, *148*, 157–165. [CrossRef] [PubMed]
20. Ju, X.; Bowden, M.; Brown, E.E.; Zhang, X. An improved X-ray diffraction method for cellulose crystallinity measurement. *Carbohyd. Polym.* **2015**, *123*, 476–481. [CrossRef] [PubMed]
21. Podskočová, J.; Chorvát, D., Jr.; Kolláriková, G.; Lacík, I. Characterization of polyelectrolyte microcapsules by confocal laser scanning microscopy and atomic force microscopy. *Laser Phys.* **2005**, *15*, 545–551.
22. Zhang, L.Y.; Yao, S.J.; Guan, Y.X. Effects of poly(methylene-co-guanidine) in microbial growth in an alginate/cellulose sulphate-$CaCl_2$/poly(methylene-co-guanidine) capsule system. *Process Biochem.* **2005**, *40*, 189–193. [CrossRef]
23. Neděla, V.; Tihlaříková, E.; Runštuk, J.; Hudec, J. High-efficiency detector of secondary and backscattered electrons for low-dose imaging in the ESEM. *Ultramicroscopy* **2018**, *184*, 1–11. [CrossRef] [PubMed]
24. Tihlaříková, E.; Neděla, V.; Shiojiri, M. In Situ study of live specimens in an environmental scanning electron microscope. *Microsc. Microanal.* **2013**, *19*, 914–918. [CrossRef] [PubMed]

25. Bučko, M.; Vikartovská, A.; Gemeiner, P.; Lacík, I.; Kolláriková, G.; Marison, I.W. *Nocardia tartaricans* cells immobilized in sodium alginate-cellulose sulfate-poly(methylene-co-guanidine) capsules: Mechanical resistance and operational stability. *J. Chem. Technol. Biotechnol.* **2006**, *81*, 500–504. [CrossRef]
26. Kishino, K.; Kawai, T.; Nose, M.; Saitoh, M.; Kamide, K. Dilute Solution Properties of sodium cellulose disulphate. *Eur. Polym. J.* **1981**, *17*, 623–630. [CrossRef]
27. Mihovilovic, M.D.; Rudroff, F.; Grötzl, B.; Kapitan, P.; Snajdrova, R.; Rydz, J.; Mach, R. Family clustering of Baeyer–Villiger monooxygenases based on protein sequence and stereopreference. *Angew. Chem. Int. Ed.* **2005**, *44*, 3609–3613. [CrossRef] [PubMed]
28. Neděla, V.; Konvalina, I.; Lencová, B.; Zlámal, J. Comparison of calculated, simulated and measured signal amplification in a variable pressure SEM. *Nucl. Instrum. Meth. A* **2011**, *645*, 79–83. [CrossRef]

© 2017 by the authors. Licensee MDPI, Basel, Switzerland. This article is an open access article distributed under the terms and conditions of the Creative Commons Attribution (CC BY) license (http://creativecommons.org/licenses/by/4.0/).

catalysts

MDPI

Article

Immobilization of *Planococcus* sp. S5 Strain on the Loofah Sponge and Its Application in Naproxen Removal

Anna Dzionek [1], Danuta Wojcieszyńska [1], Katarzyna Hupert-Kocurek [1], Małgorzata Adamczyk-Habrajska [2] and Urszula Guzik [1,*]

[1] Department of Biochemistry, Faculty of Biology and Environmental Protection, University of Silesia in Katowice, Jagiellońska 28, 40-032 Katowice, Poland; adzionek@us.edu.pl (A.D.); danuta.wojcieszynska@us.edu.pl (D.W.); katarzyna.hupert-kocurek@us.edu.pl (K.H.-K.)

[2] Institute of Technology and Mechatronics, University of Silesia in Katowice, Żytnia 12, 41-200 Sosnowiec, Poland; malgorzata.adamczyk-habrajska@us.edu.pl

* Correspondence: urszula.guzik@us.edu.pl; Tel.: +32-200-9567

Received: 30 March 2018; Accepted: 23 April 2018; Published: 26 April 2018

Abstract: *Planococcus* sp. S5, a Gram-positive bacterium isolated from the activated sludge is known to degrade naproxen in the presence of an additional carbon source. Due to the possible toxicity of naproxen and intermediates of its degradation, the whole cells of S5 strain were immobilized onto loofah sponge. The immobilized cells degraded 6, 9, 12 or 15 mg/L of naproxen faster than the free cells. *Planococcus* sp. cells immobilized onto the loofah sponge were able to degrade naproxen efficiently for 55 days without significant damage and disintegration of the carrier. Analysis of the activity of enzymes involved in naproxen degradation showed that stabilization of S5 cells in exopolysaccharide (EPS) resulted in a significant increase of their activity. Changes in the structure of biofilm formed on the loofah sponge cubes during degradation of naproxen were observed. Developed biocatalyst system showed high resistance to naproxen and its intermediates and degraded higher concentrations of the drug in comparison to the free cells.

Keywords: whole-cell immobilization; loofah sponge; *Planococcus* sp. S5; naproxen

1. Introduction

In recent years more attention has been paid to the presence of various medicines in the natural environment. One of them is naproxen (2-(6-methoxy-2-naphthyl)propionic acid) which belongs to the group of polycyclic Non-Steroidal Anti-Inflammatory Drugs (NSAIDs). This drug is not metabolized in human body and the sewage treatment plants are not adapted to its utilization. Therefore, naproxen has been releasing into the natural environment in an unchanged form for over 40 years. Due to its continuous accumulation in the environment, naproxen is now one of the most frequently detected drug in surface and drinking water (concentration in the range 0.01–2.6 μg/L) [1–3].

The most efficient methods for naproxen removal from the environment are based on the physicochemical processes. However, the biggest disadvantage of these methods is generation of products with greater toxicity than the drug itself and formation of free radicals that directly damage biological structures [3–6]. The use of microorganisms in naproxen utilization brings many benefits. Bioremediation is based on the capabilities of selected microorganisms for accumulation, transformation, detoxification or degradation of pollutants. This technology is environmentally friendly, cheap and effective [7–9].

During application of microbial cells in bioremediation processes, extremely important is their immobilization. It allows increasing microbial degradation capacity, extends viability and catalytic

activity of cells introduced into bioremediation systems as well as increases the chances of microbial cells survival and adaptation to changing environment. In immobilization process, microbial cells are trapped in polymeric gels (entrapment, encapsulation) or on the surface of various carriers (adsorption, electrostatic or covalent binding on the surface). However, the main disadvantages of immobilization are: limitation of diffusion, leakage of cells into the medium or lowering their catalytic functions depending on the binding compounds used. Recently, immobilization based on the natural ability of some microorganisms to biofilm formation on the surface of various carriers is gaining more attention. Through the existence of many microenvironments in the biofilm, cells are less vulnerable to changing environmental conditions. Created in this way stable matrix is also characterized by a high degree of heterogeneity in which microbial cells are protected against anti-bacterial agents and bacteriophages and are able to degrade contaminants at higher concentrations [8,10,11].

From an economic point of view, the carrier and the procedure for immobilization of microorganisms should be cheap. Therefore, natural and organic carriers are widely used in bioremediation processes [8,12]. These biodegradable and biocompatible supports are characterized by hydrophilic surface on which many functional groups are located. Among these natural carriers, particular attention is paid to the group of lignocellulolistic plant materials. One of them is loofah sponge derived from the dry mature fruit of *Luffa aegyptiaca*, grown in most subtropical and tropical regions. This sponge is composed of an open network of fibres that form the skeleton of the fruit. The main advantages of this material are its high porosity, low price, non-toxicity, simple application and operation technique and high mechanical resistance [13–15].

The present work is a continuation of studies on bacterial degradation of NSAIDs. Our previous study showed the ability of Gram-positive *Planococcus* sp. S5 to catalyse naproxen degradation under cometabolic conditions [2]. The aim of this study was to investigate the effect of immobilization of *Planococcus* sp. S5 cells on the loofah sponge on degradation processes. The degradation capacity of the developed biocatalyst at various concentrations of naproxen and its reusability were examined. To investigate how immobilization affected degradation activity of S5 strain, the activity of enzymes involved in naproxen utilization was examined. Additionally, visualization of biofilm formed on the surface of the carrier and its changes during drug degradation was performed. This is the first report about degradation of naproxen by immobilized bacterial cells. Moreover, the results of these studies enable evaluation of potential application of tested strain in bioremediation systems.

2. Results and Discussion

2.1. Immobilization of Planococcus sp. S5 on Loofah Sponge

The natural ability of some microorganisms to colonize surface of porous materials is a key feature for efficient immobilization. At the beginning, process of cells attachment to the surface is reversible and cells may be easily removed from the carrier by washing. In the second phase, cells which synthesize extracellular polymeric substances bind to the surface of the carrier with such a force that more invasive process is needed to remove them. Taking into consideration stability of the constructed biocatalyst, it is desirable that the formed biofilm should be strongly bound to the carrier. This feature depends on the species of the microorganism and the type of the surface. Additionally, selection of proper conditions of immobilization can improve the quality of biofilm [16–18]. To verify the quality of biofilm formed by S5 strain, which corresponds to its catalytic functions, its physiological state was evaluated by determination of its ability to hydrolyse fluorescein diacetate by non-specific esterases produced by alive bacterial cells (total enzymatic activity). This assay was chosen due to its simplicity, short incubation time (1 h) and possibility of spectrophotometric determination of the data. What is more important, the test used is correlated with other bacterial indicators such as an amount of biomass or adenosine triphosphate (ATP) and the oxygen consumption [19,20].

Selection of the optimal conditions for immobilization of the whole bacterial cells by their adsorption on the surface is an extremely important in designing of biocatalyst systems. Due to

the diversity of bacteria, optimization should be carried out for each immobilized strain. Strain *Planococcus* sp. S5, which was isolated from the activated sludge from a sewage treatment plant in Bytom Miechowice (Poland), was able to degrade aromatic compounds like salicylate, benzoate, hydroxybenzoate and dihydroxybenzoate and phenol [21,22]. However, this is the first report regarding its immobilization and one of a few on the ability of biofilm formation by bacteria from *Planococcus* genus [23].

Procedure of *Planococcus* sp. S5 immobilization on the loofah sponge through its adsorption on the surface was developed by optimizing each parameter to obtain the highest amount and enzymatic activity of immobilized microorganisms. Immobilization of S5 cells on the loofah sponge was the most effective in mineral salts medium (pH 7.2), in the presence of glucose and manganese salt, during bacteria incubation with shaking (90 rpm) at 30 °C. The effect of the growth phase on immobilization process was also observed. The best results were obtained for a culture at stationary phase. Immobilization of S5 strain was also more efficient during the osmotic stress caused by a higher concentration of NaCl (19 g/L) and at high number of cells in the medium (initial OD_{600} equal to 1.2) (Figure S1).

It has been proven that limitation of carbon source in the medium stimulates biofilm formation by *Bacillus subtilis* by activating the Spo0A transcription factor [24]. This mechanism enables survival and proliferation of bacteria during nutrient deficiency at which growth in the form of planktonic cells is impossible. On the other hand, *Staphylococcus aureus* and *Staphylococcus epidermidis* form biofilms only when glucose is present in the medium because it is necessary for the synthesis of adhesins [25]. Therefore, since S5 strain is not spores producing bacterium [21], efficient immobilization in the presence of glucose probably resulted from synthesis of adhesins which are involved in attachment of cells to the carrier. Bacteria of genus *Planococcus* are known to be moderately halophilic [26–28]. Recent research [23] shows that osmotic stress favours the formation of biofilm by *Planococcus rifietoensis* by increasing production of exopolysaccharides (EPS), which additionally improves water holding capacity at higher salt concentrations.

The developed method of S5 strain immobilization on the loofah sponge resulted in 0.0191 ± 0.0022 g of *Planococcus* sp. S5 cells (dry mass) immobilized on each loofah cube, able to hydrolysis of 23.88 ± 1.06 μg of fluorescein diacetate during 1 h (total enzymatic activity) (Figure 1). Results for fluorescein diacetate hydrolysis and fluorescein adsorption by unimmobilized loofah cubes were not statistically significant.

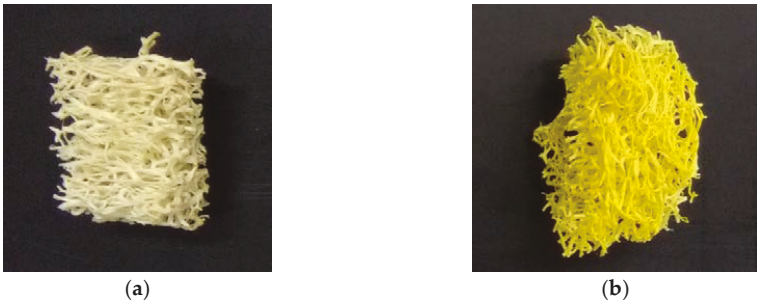

(**a**) (**b**)

Figure 1. Loofah sponges cubes after total enzymatic activity assay; (**a**) unimmobilized carrier (**b**) loofah cubes after incubation with *Planococcus* sp. S5 cells.

2.2. Naproxen Biodegradation

2.2.1. Biodegradation of Different Concentration of Naproxen

Naproxen (2-(6-methoxy-2-naphthyl)propionic acid)) belongs to the propionic acid derivatives family. Due to the presence of two aromatic rings, naproxen biodegradation is more difficult than monocyclic NSAIDs. Only a few strains (mainly white-rot fungi) are known to possess enzymatic systems which enable them to acquire carbon and energy from naproxen [29,30]. Biodegradation of naproxen by bacterial strains is a process that is being explored. However, none of the known bacterial strains—*Planococcus* sp. S5 [2], *Bacillus thuringiensis* B1(2015b) [31], *Stenotrophomonas maltophilia* KB2 [32], *Pseudomonas* sp. CE21 [33]—are able to use naproxen as the sole carbon source. First study about naproxen biodegradation by strain *Planococcus* sp. S5 [2] revealed that the addition of glucose which was readily available source of carbon and energy resulted with complete biodegradation of the drug. However, due to the negative effect of naproxen on the total enzymatic activity of free S5 cells, the degradation of the drug at a concentration of 6 mg/L lasted 38 days (data not published). For this reason it was decided to carry out the immobilization process.

Loofah sponge due to the relatively large surface area and chemical composition (cellulose, hemicellulose, lignin) shows good sorption properties. However, making the loofah sponge capable of sorption of hydrophobic substances (like naproxen) requires subjecting it to a cooking process with NaOH to increase its hydrophobicity and to create available vacant sites [34,35]. For this reason, the loofah sponge in this study has not been subjected to a cooking process with NaOH to limit its sorption capacity. Another important factor that needed to be consider in biodegradation studies with immobilized cells by adsorption of the surface is accumulation of xenobiotics in biofilm. This phenomenon is related to the sorption properties of exopolysaccharides (EPS). While the sorption of positively-charged compounds by EPS is more efficient due to anionic nature of biofilm, sorption of anionic organic molecules is limited due to electrostatic repulsion [36].

There was no changes observed in drug concentration during incubation with sterile non-immobilized carriers, which confirms lack of the naproxen adsorption capacities by prepared in that way loofah sponges. Naproxen was also not detected in the biofilm formed onto the loofah sponges by *Planococcus* sp. S5. Obtained results demonstrated that loss of the drug from the medium during biodegradation experiments was caused only by immobilized cells of *Planococcus* sp. S5.

To investigate whether the immobilization onto the loofah sponges affected the degradation capacity of *Planococcus* sp. S5, biodegradation of various concentrations of naproxen (6, 9, 12 or 15 mg/L) by immobilized cells with respect to non-immobilized cells was tested (Figures 2 and 3).

Observation of the efficiency of the naproxen cometabolic biodegradation conducted by free cells of *Planococcus* sp. S5 showed that they were able to degrade naproxen in concentration 6, 9 and 12 mg/L respectively in 38, 44 and 62 days. Biodegradation of the highest tested concentration of the drug (15 mg/L) stopped after biodegradation of 29% of naproxen (Figure 2a). Obtained results shows that the free cells of S5 strain were able to complete cometabolic naproxen biodegradation at a concentration up to 12 mg/L. Higher drug concentrations showed inhibitory effects on free cells of the S5 strain. Immobilization of *Planococcus* sp. S5 cells onto the loofah sponges resulted in a significant acceleration of the naproxen cometabolic biodegradation. It was observed a complete biodegradation of 6, 9, 12 and 15 mg/L of naproxen respectively after 17, 32, 43 and 53 days (Figure 2b).

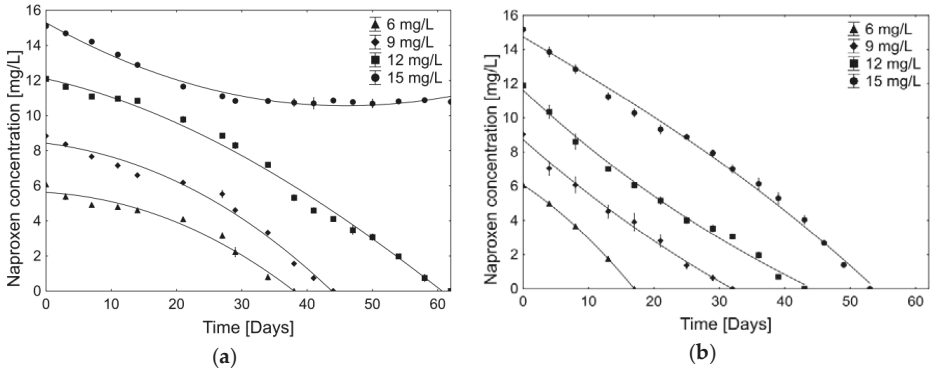

Figure 2. Cometabolic degradation of 6, 9, 12 and 15 mg/L naproxen by (**a**) free cells of *Planococcus* sp. S5; (**b**) cells of *Planococcus* sp. S5 immobilized onto the loofah sponge. Data presented as mean ± standard deviation of three replicates.

In order to evaluate changes in the course of the biodegradation process, the rate of naproxen biodegradation was calculated (Tables 1 and 2). Biodegradation rates by free cells of S5 were statistically different (Test T, $p \geq 0.05$) than by immobilized cells. During the biodegradation of naproxen by free cells, in the initial phase the slower drug degradation was observed, independently of the drug concentration (average 6.3 ± 3.4 μg/h). After 29 days twice faster biodegradation of the drug (12.0 ± 4.5 μg/h) was observed that lasted until the end of biodegradation (Table 1). Designation of the naproxen biodegradation rates by immobilized cells of S5 strain revealed its almost linear and constant course (12.1 ± 4 μg/h) (Table 2). Interestingly, there was no significant difference between naproxen biodegradation rates by the immobilized cells and by free cells during faster drug degradation phase (Test T, $p \geq 0.05$). This situation was most likely caused by the fact that cells in the biofilm exhibit characteristics of the stationary phase (altered genetic expression profile and slower growth) [37]. Confirmation of this hypothesis is the fact that the phase of faster naproxen degradation by free cells of *Planococcus* sp. S5 occurred when cells entry into the stationary phase (data not published).

Table 1. Naproxen degradation rates by free cells of *Planococcus* sp. S5. Data presented as a mean ± standard deviation of three replicates.

Period [Day–Day]	Average Naproxen Degradation Rate [μg/h]			
	6 mg/L	9 mg/L	12 mg/L	15 mg/L
0–3	9.8 ± 2.2	6.6 ± 0.6	6.4 ± 1.1	5.7 ± 0.9
3–7	4.8 ± 2.2	7.3 ± 1.7	5.8 ± 1.0	5.0 ± 1.7
7–11	1.3 ± 0.5	5.3 ± 2.5	1.2 ± 0.5	7.6 ± 0.2
11–14	2.6 ± 1.4	7.7 ± 1.5	1.7 ± 2.6	8.1 ± 1.9
14–21	3.0 ± 0.4	2.5 ± 0.4	6.4 ± 1.5	7.4 ± 0.1
21–27	6.5 ± 1.4	4.5 ± 1.7	6.4 ± 0.5	3.8 ± 0.6
27–29	19.6 ± 3.3	19.2 ± 6.0	11.5 ± 4.6	5.5 ± 1.2
29–34	11.9 ± 0.9	10.6 ± 1.4	9.2 ± 1.5	0.1 ± 1.9
34–38	8.2 ± 1.6	18.4 ± 1.3	19.6 ± 0.6	1.0 ± 3.2
38–41		11.4 ± 0.5	10.1 ± 0.7	0.6 ± 7.3
41–44		10.3 ± 0.6	6.7 ± 1.1	−2.2 ± 4.9
44–47			8.9 ± 5.1	1.3 ± 3.8
47–50			5.5 ± 4.0	1.2 ± 4.0
50–54			11.4 ± 0.9	−1.3 ± 3.7
54–58			12.8 ± 1.1	−0.7 ± 2.4
58–62			7.8 ± 2.0	1.0 ± 1.9

Table 2. Average naproxen degradation rates by immobilized cells of *Planococcus* sp. S5. Data presented as a mean ± standard deviation of three replicates.

Period [Day–Day]	Average Naproxen Degradation Rate [μg/h]			
	6 mg/L	9 mg/L	12 mg/L	15 mg/L
0–4	11.2 ± 1.2	20.7 ± 8.6	16.1 ± 6.7	13.9 ± 0.6
4–8	13.9 ± 0.9	10.1 ± 1.4	18.0 ± 14.6	10.5 ± 2.5
8–13	15.8 ± 1.1	12.9 ± 1.8	13.2 ± 5.4	13.4 ± 4.2
13–17	18.2 ± 1.7	6.4 ± 2.4	10.1 ± 1.2	10.0 ± 1.4
17–21		11.6 ± 3.0	9.4 ± 0.9	10.0 ± 1.0
21–25		15.0 ± 5.8	12.0 ± 4.8	4.6 ± 4.2
25–29		7.6 ± 3.9	5.1 ± 0.6	9.7 ± 5.6
29–32		8.7 ± 4.2	6.4 ± 2.9	13.1 ± 5.6
32–36			11.5 ± 1.7	10.8 ± 6.0
36–39			17.4 ± 4.8	9.4 ± 4.3
39–43			7.3 ± 2.4	13.0 ± 2.5
43–46				19.0 ± 2.8
46–49				17.7 ± 0.6
49–53				14.6 ± 2.2

It is known that one of the most important parameters that can significantly affect the biodegradation process is initial substrate concentration. Analysis of the patterns and correlations between the time of incubation, naproxen concentration and biodegradation rate shows that free cells of *Planococcus* sp. S5 were capable of the fastest biodegradation of naproxen at the lowest dose. With increasing drug concentration the rate of naproxen biodegradation was decreased (Figure 3a). Obtained results indicated that during decomposition of naproxen, accumulation of metabolites occurred, which negatively affect free cells of S5 strain and caused increasing difficulties with its total degradation. Therefore, biodegradation of the highest dose of naproxen (15 mg/L) ended with 29% efficiency most likely due to the critical level of inhibitory or toxic metabolites. Recently, more attention has been focused on the antibacterial activity of certain NSAIDs or their derivatives [38,39]. Although the mechanisms of this process are not known, one study found that vedaprofen, bromfenac and carprofen—by binding to polymerase α subunit—inhibit the proliferation of *E. coli*, *A. baylyi*, *S. aureus* and *B. subtilis* cells [39]. Inhibitory effect of naproxen on the ammonia oxidizing bacterium (AOB) *Nitrosomonas europaea* was observed by Wang et al. [40]. They revealed that naproxen at concentration of 10 μM significantly inhibits nitrile production by AOB by affecting membrane integrity of the cells, while exposure on the drug in concentration of 1 μM did not influences AOB cells. To reveal possibility of antibacterial activity of naproxen or its intermediates on *Planococcus* S5 cells more research should be attempted.

No correlation between analysed variables was observed for the immobilized cells. Degradation proceeded with the same trend regardless of the initial naproxen concentration (Figure 3b). Obtained results indicated good adaptation of immobilized S5 cells to the presence of higher concentrations of naproxen. Lack of the lag phase and concentration-independent drug biodegradation course suggests that formed biofilm reduced the sensitivity of the cells to naproxen and its intermediates. Due to the good sorption properties and the limited diffusion in the extracellular biofilm matrix, immobilized microorganisms have limited contact with xenobiotics, which are transported to the cells at a constant, slower rate. This mechanism allows the immobilized cells to biodegrade higher concentrations of impurities, without causing toxic effects [41]. Thus, the immobilized cells of *Planococcus* sp. S5 onto the loofah sponge have a promising potential to use them for the bioremediation of naproxen-contaminated sites. In addition, lack of the toxic effect of naproxen and its metabolites on immobilized cells allowed them to utilize higher concentrations of the drug compared to the free cells.

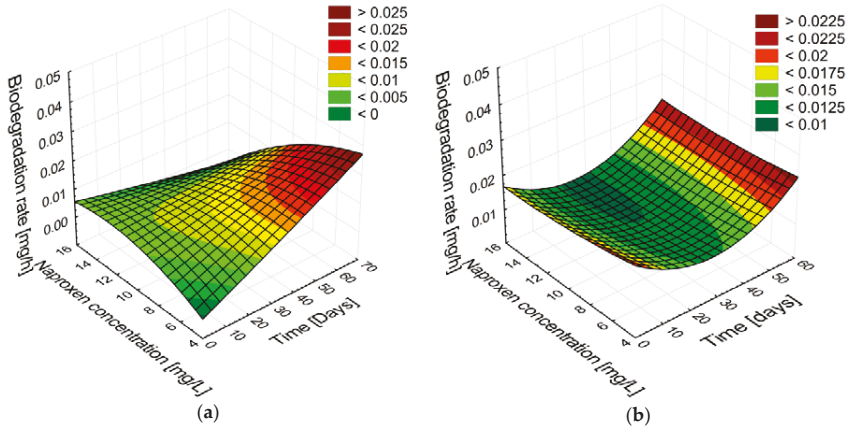

Figure 3. Naproxen (6, 9, 12 and 15 mg/L) biodegradation rate by (**a**) free cells of *Planococcus* sp. S5; and (**b**) immobilized on loofah sponges cells of *Planococcus* sp. S5; presented as patterns and the relationships among the time of incubation, naproxen concentration and biodegradation rate.

2.2.2. Stability and Degradation Capacity of the Developed Whole-Cell Biocatalyst System

The stability during long-term operations is a crucial factor for practical application of immobilized biocatalysts. To test reusability of *Planococcus* sp. S5 cells immobilized on the loofah sponges, the efficiency of naproxen biodegradation in subsequent cycles has been determined. In the presence of fresh sterile mineral salts medium in each cycle, immobilized cells were able to complete drug degradation in 3 repetitions (Figure 4). The first and the second dose of naproxen were utilized within respectively 17 and 15 days. In the next cycle it was observed deceleration of the degradation efficiency (21 days) while in the 4th cycle, the biodegradation ended after decomposition of 27% of the drug. However, cells of *Planococcus* sp. S5 immobilized on loofah sponges demonstrated the ability to efficient naproxen biodegradation for 55 days. After the end of the experiment, no significant damage and disintegration of the loofah sponges was observed, which confirms its high mechanical resistance [14].

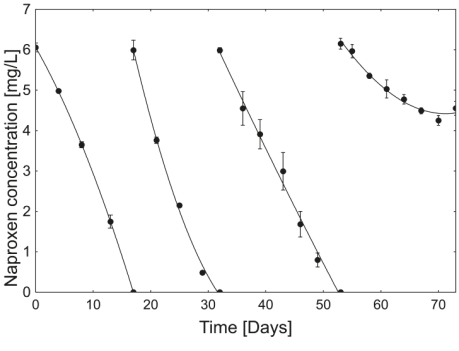

Figure 4. Cycles of 6 mg/L naproxen degradation by immobilized *Planococcus* sp. S5 on the loofah sponge. Data presented as a mean ± standard deviation of three replicates.

Evaluation of the biodegradation rate during each cycle shows not significant differences in the first 3 cycles of naproxen biodegradation amounting 14.8 ± 3.0, 16.0 ± 6.9 and 11.4 ± 3.9 µg/h respectively (Table 3, Figure 5). Only during the first cycle it was observed increasing rate of

drug degradation. The second and third cycle, however, were characterized by slowing down biodegradation rate, while the last one proceeded unstable (Table 3). It is suggested that one of the reasons why immobilization extends the catalytic activity of cells is to ensure the stability of cell membranes and adequate permeability [41].

Table 3. Average biodegradation rate of 6 mg/L naproxen by immobilized cells of *Planococcus* sp. S5 in each cycle. Data presented as a mean ± standard deviation of three replicates. Different letters (a, b, c) indicate a statistically significant difference between biodegradation rates during subsequent cycles ($p \geq 0.05$).

Period [Day–Day]	Average Naproxen Degradation Rate [μg/h]			
	I Cycle	II Cycle	III Cycle	IV Cycle
0–4	11.2 ± 1.2 ^{a}			
4–8	13.9 ± 0.9 ^{b}			
8–13	15.8 ± 1.1 ^{b}			
13–17	18.2 ± 1.7 ^{c}			
17–21		23.2 ± 1.8 ^{a}		
21–25		16.8 ± 0.7 ^{b}		
25–29		17.4 ± 0.2 ^{b}		
29–32		6.7 ± 0.1 ^{c}		
32–36			15.0 ± 3.8 ^{a}	
36–39			8.9 ± 1.4 ^{b}	
39–43			9.6 ± 1.2 ^{b}	
43–46			18.2 ± 2.0 ^{a}	
46–49			12.3 ± 2.4 ^{ab}	
49–53			8.3 ± 1.8 ^{b}	
53–55				3.8 ± 3.5 ^{a}
55–58				8.5 ± 3.2 ^{b}
58–61				6.8 ± 0.1 ^{ab}
61–64				3.5 ± 1.7 ^{a}
64–67				3.9 ± 1.0 ^{a}
67–70				3.3 ± 1.9 ^{a}
70–73				−4.2 ± 2.5 ^{c}

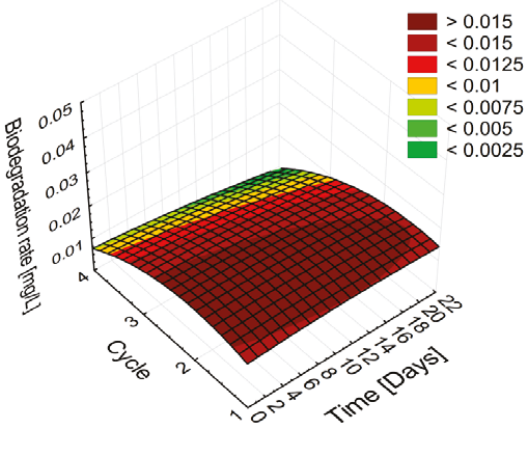

Figure 5. Naproxen (6 mg/L) biodegradation rate during subsequent cycles by immobilized on loofah sponges cells of *Planococcus* sp. S5 presented as patterns and the relationships among the time of incubation, cycle and biodegradation rate.

The ability of immobilized cells of *Planococcus* sp. S5 to carry out the biodegradation of naproxen in several cycles indicates the possibility of their use in bioremediation. However, to study their behaviour in such systems it is necessary to conduct pilot studies.

2.3. The Influence of Immobilization on Enzymes Activity

The process of biodegradation of naproxen by white rot fungi is much better understood than by bacteria [29,42–44]. One of the proposed mechanisms demonstrates naproxen demethylation carried out by cytochrome P-450 [32]. The reaction product, 6-desmethylnaproxen appeared during biodegradation of naproxen by the *Planococcus* sp. S5 strain. Domaradzka et al. [2] showed that some enzymes involved in the degradation of polycyclic aromatic hydrocarbons were active during cometabolic (with glucose) biodegradation of naproxen by free cells of *Planococcus* sp. S5. The activity of phenol monooxygenase, naphthalene dioxygenase, hydroxyquinol 1,2-dioxygenase and gentisate 1,2-dioxygenase was demonstrated.

A typical degradation pathway of aromatic compounds by bacteria is the initial hydroxylation followed by the ring cleavage [45]. The first step in degradation of naphthalene (the derivative of which is naproxen) is the hydroxylation of C1 and C2 catalysed by naphthalene dioxygenase [46]. It was suggested that this enzyme is responsible for hydroxylation of C7 and C8 of naproxen. Moreover, on the base of the activity of phenol monooxygenase additional hydroxylation was proposed. Formed trihydroxylated derivative probably is cleaved by hydroxyquinol 1,2-dioxygenase [2]. One of the most important steps in catabolism of naphthalene is its conversion to salicylate, which bacterial pathway has been well described. The most important part of the catabolism of salicylate is direct ring cleavage by salicylate 1,2-dioxygenase or gentisate 1,2-dioxygenase (in case salicylate transformation to gentisate by monooxygenase). The salicylate transformation products are next introduced into the tricarboxylic acid cycle [47–49].

Because the immobilization of bacterial cells may change the xenobiotic degradation pathway, the activity of enzymes that are involved in naproxen degradation were examined. This phenomenon is related to the change in the gene expression profile that occurs during the formation of the biofilm and can be related to the type of carrier surface [50,51].

The activities of *O*-demethylase, aromatic monooxygenase (with phenol or naproxen as a substrate), naphthalene dioxygenase, gentisate 1,2-dioxygenase and salicylate 1,2-dioxygenase were compared. As is shown in Table 4, the activity of all analysed enzymes was observed, both in free and immobilized cells. Obtained results showed that the naproxen biodegradation pathway in immobilized S5 cells probably did not change markedly. Significant changes, however, were observed in the values of activity (Table 4). As expected, during the slower degradation phase of naproxen (15th day), free S5 cells were characterized by the lowest activity of enzymes associated with drug degradation. At the same time, the enzymatic activity of immobilized cells was about 2 times higher in the case of *O*-demethylase, aromatic monooxygenase (with phenol as a substrate), naphthalene dioxygenase and salicylate 1,2-dioxygenase. Interesting increase in the activity of aromatic monooxygenase (with naproxen as a substrate, 10 times higher) and gentisate 1,2-dioxygenase (4 times higher) was observed in the immobilized cells. However, due to the methodology for determining the activity of aromatic monooxygenase (determination of reduced nicotinamide adenine dinucleotide - NADH oxidation), it is not excluded that more of the enzymes belonging to the class of oxidoreductases are involved in the degradation of naproxen by immobilized cells of *Planococcus* sp. S5. A higher gentisate 1,2-dioxygenase activity may have been caused by the increase of its participation (in relation to salicylate 1,2-dioxygenase) in the drug biodegradation due to immobilization.

Due to the non-statistically different biodegradation rate of naproxen by free cells in the phase of faster drug degradation and immobilized cells, it was suspected that the enzymatic activity of these systems would also not be different. However, according to the analysis (Table 4), the activity of all analysed enzymes was higher in the immobilized cells. Higher activity of enzymes associated with the biodegradation of naproxen in immobilized cells confirms that the sensitivity to the drug of cells in the

developed biocatalyst was reduced. For that reason, the significant acceleration of its biodegradation was observed.

Table 4. Specific activity of enzymes involved in naproxen degradation under cometabolic conditions by immobilized and non-immobilized *Planococcus* sp. S5. Different letters (a, b, c) indicate a statistically significant difference between activity of enzymes from free and immobilized cells ($p \geq 0.05$).

Enzyme	Specific Enzyme Activity (U/mg protein)		
	Free Cells		Immobilized Cells 15th Day
	15th Day	35th Day	
O-demethylase	412.84 ± 48.53 [a]	737.16 ± 55.81 [b]	1051.84 ± 65.57 [c]
Aromatic monooxygenase (Phe)	13.06 ± 0.83 [a]	27.14 ± 2.40 [b]	31.55 ± 1.18 [c]
Aromatic monooxygenase (Npx)	14.78 ± 1.28 [a]	65.17 ± 3.59 [b]	123.71 ± 12.39 [c]
Naphthalene dioxygenase	8.16 ± 0.82 [a]	10.71 ± 2.23 [a]	15.73 ± 1.80 [b]
Gentisate 1,2-dioxygenase	52.95 ± 2.90 [a]	122.26 ± 9.44 [b]	203.03 ± 18.55 [c]
Salicylate 1,2-dioxygenase	388.26 ± 11.12 [a]	520.38 ± 24.60 [b]	714.87 ± 71.58 [c]

2.4. Changes in Biofilm Formed Onto the Loofah Sponge during Naproxen Degradation

Visualization of bacterial biofilm in high resolution using SEM (Scanning Electron Microscopy) is one of the best methods to determine the biofilm structure. Preparation of samples for analysis by SEM involves the fixation of their structures (using glutaraldehyde and osmium tetraoxide), dewatering, drying and covering with a conductive layer. However, due to the fact that the structure of EPS (which stability is dependent on the presence of water) often collapses during dewatering and drying, identifying certain structures in biofilm sometimes is problematic [52]. The procedure of sample preparation very often leads to the creation of artefacts. One of them, especially at higher magnifications, is the appearance of EPS as fibres or granularity and not as a gel structure surrounding the cells [53]. However, the advantage of this visualization method is the possibility of determining the distribution of microorganisms and changes in the biofilm structure caused by specific factors. Considering the identical preparation of samples for analysis, demonstration of changes in the biofilm structure in relation to the state of biofilm before exposure to a specific factor reduces the probability of incorrect image analysis.

Loofah sponge which was used as a carrier for immobilization, observed in SEM revealed its multidirectional highly fibrous network and porous surface with a small protuberances (Figure 6a) which was a suitable place for the attachment of microorganisms.

After immobilization of *Planococcus* sp. S5 cells through the adsorption on the surface (lasting 72 h), accumulation of cells covered with an extracellular matrix (Figure 6b) was observed. Flat biofilm formed on the loofah sponges had the form of irregular rods of different lengths (Figure 6b) and appeared in aggregates.

When the first and the second dose of naproxen (6 mg/L) have been degraded (respectively 17th and 36th day of incubation), immobilized loofah sponges were observed in SEM to reveal changes in biofilm structure during naproxen biodegradation. After complete degradation of the first dose of naproxen, a more diversified and intense colonization of the carrier was observed (Figure 6c). There was present formation of the connections between aggregates (Figure 6c) and new fibrous extracellular matrix-like structures. When the second dose of naproxen was degraded, surface of loofah sponges was completely covered by biofilm formed by *Planococcus* sp. S5 (Figure 6d). A decrease in the amount of aggregates in relation to the newly formed structures was observed.

In the presence of toxic substances bacteria trigger different protective mechanisms. One of them is the secretion of large amounts of EPS, which will create a protective layer for cells. At the same time, by forming clusters, the cells reduce the contact surface with the toxin-containing environment [54]. Due to the problematic utilization of naproxen by free S5 cells (especially in the first phase of degradation), increased tolerance of immobilized cells appears to be the result of the accumulation of large amounts of extracellular substances in the biofilm. The same defence mechanism was observed by Ma et al. [55] against to immobilized bacteria from activated sludge during biodegradation of phenol. They showed that with the increase in the amount of toxic phenol nol photodegradation products, the number of microbial cells in the biofilm decreased. On the other hand, the amount of secreted EPS was increasing, which resulted with a lack of differences in the phenol biodegradation way.

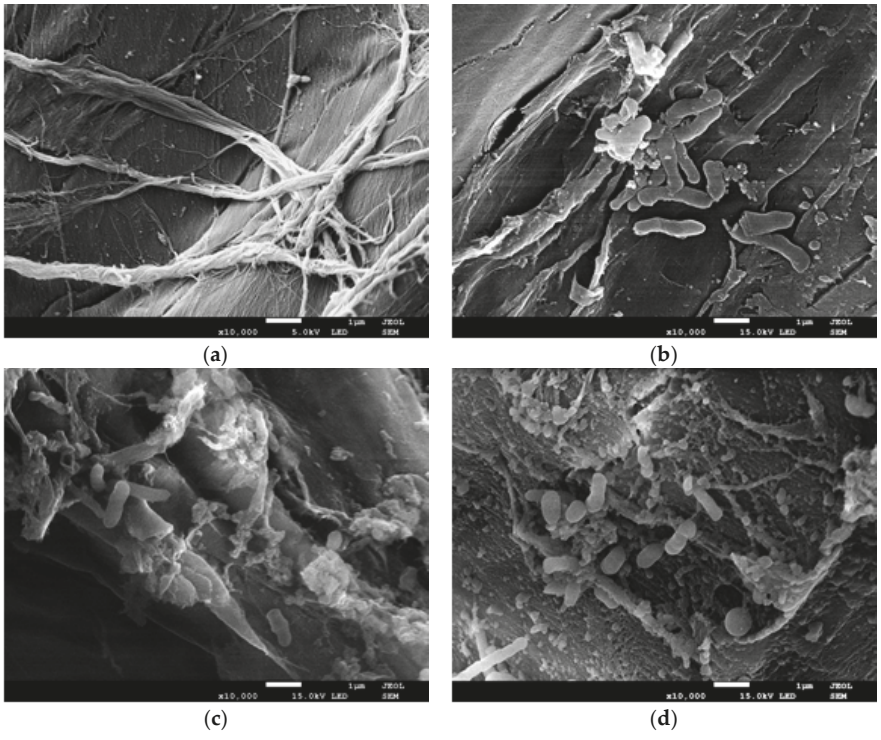

Figure 6. Scanning electron microscopy (SEM) micrographs of unimmobilized loofah sponge (**a**), biofilm formed by *Planococcus* sp. S5 cells onto loofah sponge before naproxen degradation (**b**), after decomposition of the first dose of naproxen (6 mg/L) (**c**) and the second dose of the drug (6 mg/L) (**d**).

3. Materials and Methods

3.1. Bacterial Cultures Cultivation

Isolated from activated sludge Gram-positive strain *Planococcus* sp. S5 described by Łabużek et al. [21] was used. Proliferation of S5 cells was carried out in the nutrient broth (BBL) at 30 °C on a rotary shaker at 130 rpm. After 72 h of incubation bacterial cultures were centrifuged (5000 rpm, 15 min), washed twice with mineral salts medium [56] and resuspended in the same medium. Prepared bacterial suspensions were used as an inoculum for immobilization and control non-immobilized cells experiments.

3.2. Carrier Preparation for Immobilization

The first step in the preparation of the loofah sponges (York, Bolechowo, Poland) for immobilization was drying them in a desiccator to establish constant weight and cutting out fragments weighing 0.15 g. Obtained cubes were washed according to Iqbal et al. [14] and sterilized (121 °C, 1.2 atm) two times at an interval of 24 h.

3.3. Immobilization Procedure

Cells of S5 strain were immobilized through the adsorption on the surface of loofah sponge. Immobilization was conducted in 250 mL Erlenmeyer flasks, which contained 0.75 g of the carrier and 100 mL of the mineral salts medium (pH 7.2) with *Planococcus* sp. S5 cells (optical density at 600 nm equal to 1.2; Genesys 20, Thermo Scientific). Medium was supplemented with glucose (0.5 g/L), NaCl (10 g/L) and $MnSO_4$ (0.01 g/L). Flasks were incubated with shaking (90 rpm), at temperature of 30 °C. After 72 h of incubation, loofah sponges with immobilized bacteria were rinsed with aqueous solution of NaCl (0.9%) to remove unbound microorganisms and used for biodegradation experiments.

3.4. Characterization of Immobilized Loofah Sponges

Dry mass of the immobilized bacteria was obtained by comparing the dried weight of immobilized carrier (105 °C, 2 h and stored in a desiccator) with unimmobilized carriers incubated and dried under the same conditions. Enzymatic activity of biofilm formed onto loofah sponge was measured as follow (modified method proposed by Jiang et al. [19]): immobilized carrier (1 cube) was added to 8 mL of phosphate buffer (pH 7.6) and incubated for 15 min on the orbital shaker (130 rpm, 30 °C). After pre-incubation, 0.1 mL of FDA (Sigma-Aldrich, St. Louis, MO, USA) (4.8 mmol L^{-1}) was slowly injected directly into middle of the carrier and incubated in the dark on the orbital shaker (130 rpm, 30 °C) for 1 h. Fluorescence intensity in the liquid was measured spectrophotometrically at 490 nm (Genesys 20, Thermo Scientific, Waltham, MA, USA). Concentration of fluorescein was calculated on the basis of a standard curve.

3.5. Biodegradation Experiments

Naproxen decomposition was conducted in 500 mL Erlenmeyer flask containing 250 mL of the mineral salts medium [56] and 10 pieces of the loofa sponge colonized by bacteria. Each flash was supplement with naproxen (Sigma-Aldrich, USA) to obtain a final concentration of 6, 9, 12 or 15 mg/L and at every 3 days with glucose (0.5 g/L, POCH, Gliwice, Poland) and incubated with shaking (130 rpm) at 30 °C. The control cultures contained non-immobilized cells of *Planococcus* sp. S5 were also prepared. For estimation of naproxen accumulation in the biofilm the drug extraction with modified Huerta et al. protocol was performed [36]. Loofah sponges with immobilized bacteria were cut into small pieces and placed in 15 mL falcon tube with 10 mL of mixture of citric buffer (pH 4) and acetonitrile (1:1, *v/v*, Sigma-Aldrich, USA). Mixtures were subsequently sonicated 3 times for 10 min and centrifuged (15,000 rpm, 20 min). Obtained supernatants were analysed by HPLC and naproxen concentrations were calculated based on a standard curve prepared with extraction mixture. Determination of naproxen adsorption on the carrier was conducted by incubation sterile loofah sponges (1.5 g) with 250 mL of MSM medium supplemented with naproxen (6 mg/L) and glucose (0.5 g/L) in 500 mL Erlenmeyer flasks. Medium samples were taken every 24 h for 7 days and analysed by HPLC to determine naproxen concentration.

3.6. Determination of Naproxen Concentration

Decomposition of naproxen was monitored by HPLC (Merck HITACHI, Darmstadt, Germany) equipped with a LiChromospher® RP-18 column (4 × 250 mm), liChroCART® 250-4 Nucleosil 5 C18 and a DAD detector (Merck HITACHI). Medium samples from each flask were taken at 3 days period and centrifuged (14,000 rpm, 20 min). Naproxen identification and quantification in the supernatant

was done by following the protocol proposed by Wojcieszyńska et al. [32]. The mobile phase consisted acetonitrile and 1% acetic acid (50:50 v/v) with a flow rate of 1 mL/min and column temperature was 23 °C. The detection wavelength was set at 260 nm. Naproxen was identified by way of comparison of HPLC retention time (2.41 min) and ultraviolet-visible spectra with those of the external standards. To determine the abiotic degradation of naproxen, uninoculated controls were prepared.

3.7. Enzyme Assay

After 15 days of incubation (additionally free cells after 35 days), free and immobilized cells of *Planococcus* sp. S5 were separated from the medium by centrifugation (4500× g for 15 min at 4 °C). The release of immobilized cells from the carrier was carried out by vortexing. The obtained pellet was washed with 50 mM phosphate buffer (pH 7.0), disrupted by sonication (6 times for 15 s) and centrifuged at 9000× g for 30 min at 4 °C. Obtained crude extract was used for the measurement of enzyme activities.

The activity of *O*-demethylase was determined by measuring the loss of vanillic acid (λ = 260 nm) with the use of the HPLC method [57]. In order to determine monooxygenase activity (with phenol or naproxen as a substrate), NADH oxidation (ε_{340} = 6220/M cm) was measured spectrophotometrically [58]. The naphthalene dioxygenase, gentisate 1,2-dioxygenase and salicylate 1,2-dioxygenase activity was measured spectrophotometrically by the formation of *cis*,*cis*-dihydrodiol (ε_{262} = 8230/M cm) [46], maleylpyruvate (ε_{330} = 10,800/M cm) [49] and 2-oxohepta-3,5-dienedioic acid (ε_{283} = 13,600/M cm) [48], respectively. Protein concentration was determined using the Bradford method [59]. One unit of enzyme activity was defined as the amount of enzyme required to generate 1 µmol of product per minute.

3.8. Scanning Electron Microscopy

To observe the structure of biofilm formed onto the loofah sponges and its changes during naproxen biodegradation, samples for Scanning Electron Microscopy were prepared. For this examination, unimmobilized and immobilized loofah sponges before and after naproxen biodegradation were collected from the medium and prepared as follows: fixation in 3% glutaraldehyde (24 h), in 1% osmium tetroxide (3 h), dehydration with ethanol (30, 50, 70, 80, 90, 95 and 100%, each for 10 min), drying by lyophilisation and covering with gold. Samples were observed in high-resolution electron microscope JSM-7100F TTL LV (JEOL, Tokio, Japan).

3.9. Statistical Analysis

All experiments were performed in at least three replicates. The values of the efficiency of naproxen biodegradation and enzymes activities were analysed by STATISTICA 12 PL software package. Statistically significant differences and similarities have been demonstrated by the *t*-test or the Least Significant Differences (LSD) test ($p \geq 0.05$).

4. Conclusions

Ability of some bacterial strains to form a biofilm on the surface of various materials is a key element for efficient immobilization process. By optimizing each parameter of the immobilization procedure, a biocatalyst that is characterized by increased naproxen biodegradation capacities has been developed. Immobilized cells of *Planococcus* sp. S5 strain on the loofah sponge, compared to the free cells, were able to faster biodegradation of naproxen added at higher doses. Additionally, due to the maintenance of full catalytic activity for 3 cycles (55 days), immobilized onto the loofah sponge S5 cells, show promising potential in their application in bioremediation systems. Analysis of the effect of immobilization on the activity of enzymes associated with naproxen biodegradation showed that it caused a significant increase in the activity of all examined enzymes. The significant increase in the efficiency of the naproxen biodegradation by immobilized S5 cells was most probably caused by the synthesis of large amounts of EPS, which by sorption and limitation of the substrates diffusion increased the tolerance of the strain to the drug.

Supplementary Materials: The following are available online at http://www.mdpi.com/2073-4344/8/5/176/s1, Figure S1: Effect of various environmental and physiological factors on the efficiency of *Planococcus* sp. S5 cells immobilization onto the loofah sponge.

Author Contributions: A.D. conceived, designed and performed the experiment, analysed the data and wrote the paper; D.W. analysed the data and wrote the paper; K.H.-K. corrected manuscript, M.A.-H. contribution in analysis of SEM micrographs, U.G. designed the experiment, analysed the data and wrote the paper.

Acknowledgments: This work was financed by the National Science Centre (Poland), granted on the basis of decision DEC-2017/25/N/NZ9/00422. We are grateful to Jolanta Dzik for help with preparing SEM micrographs.

Conflicts of Interest: The authors declare no conflict of interest.

References

1. Wojcieszyńska, D.; Domaradzka, D.; Hupert-Kocurek, K.; Guzik, U. Enzymes Involved in Naproxen Degradation by *Planococcus* sp. S5. *Pol. J. Microbiol.* **2016**, *1*, 177–182. [CrossRef]
2. Domaradzka, D.; Guzik, U.; Hupert-Kocurek, K.; Wojcieszyńska, D. Cometabolic degradation of naproxen by *Planococcus* sp. strain S5. *Water Air Soil Pollut.* **2015**, *226*, 297. [CrossRef] [PubMed]
3. Grenni, P.; Patrolecco, L.; Ademollo, N.; Tolomei, A.; Caracciolo, A.B. Degradation of gemfibrozil and naproxen in a river water ecosystem. *Microchem. J.* **2013**, *107*, 158–164. [CrossRef]
4. Marotta, R.; Spasiano, D.; Di Somma, I.; Andreozzi, R. Photodegradation of naproxen and its photoproducts in aqueous solution at 254 nm: A kinetic investigation. *Water Res.* **2013**, *47*, 373–383. [CrossRef] [PubMed]
5. Musa, K.A.; Eriksson, L.A. Theoretical study of the phototoxicity of naproxen and the active form of nabumetone. *J. Phys. Chem. A* **2008**, *112*, 10921–10930. [CrossRef] [PubMed]
6. Isidori, M.; Lavorgna, M.; Nardelli, A.; Parrella, A.; Previtera, L.; Rubino, M. Ecotoxicity of naproxen and its phototransformation products. *Sci. Total Environ.* **2005**, *348*, 93–101. [CrossRef] [PubMed]
7. Alvarez, A.; Saez, J.M.; Costa, J.S.D.; Colin, V.L.; Fuentes, M.S.; Cuozzo, S.A.; Amoroso, M.J. *Actinobacteria*: Current research and perspectives for bioremediation of pesticides and heavy metals. *Chemosphere* **2017**, *166*, 41–62. [CrossRef] [PubMed]
8. Dzionek, A.; Wojcieszyńska, D.; Guzik, U. Natural carriers in bioremediation: A review. *Electron. J. Biotechnol.* **2016**, *19*, 28–36. [CrossRef]
9. Xu, Y.; Lu, M. Bioremediation of crude oil-contaminated soil: Comparison of different biostimulation and bioaugmentation treatments. *J. Hazard. Mater.* **2010**, *183*, 395–401. [CrossRef] [PubMed]
10. Alessandrello, M.J.; Parellada, E.A.; Tomás, M.S.J.; Neske, A.; Vullo, D.L.; Ferrero, M.A. Polycyclic aromatic hydrocarbons removal by immobilized bacterial cells using annonaceous acetogenins for biofilm formation stimulation on polyurethane foam. *J. Environ. Chem. Eng.* **2017**, *5*, 189–195. [CrossRef]
11. Carpentier, B.; Cerf, O. Biofilms and their consequences, with particular reference to hygiene in the food industry. *J. Appl. Microbiol.* **1993**, *75*, 499–511. [CrossRef]
12. Bayat, Z.; Hassanshahian, M.; Cappello, S. Immobilization of microbes for bioremediation of crude oil polluted environments: A mini review. *Open Microbiol. J.* **2015**, *9*, 48–54. [PubMed]
13. Moreno-Medina, D.A.; Sánchez-Salinas, E.; Ortiz-Hernández, M.L. Removal of methyl parathion and coumaphos pesticides by a bacterial consortium immobilized in *Luffa cylindrica*. *Rev. Int. Contam. Ambient.* **2014**, *30*, 51–63.
14. Iqbal, M.; Saeed, A.; Edyvean, R.G.J.; O'Sullivan, B.; Styring, P. Production of fungal biomass immobilized loofa sponge (FBILS)-discs for the removal of heavy metal ions and chlorinated compounds from aqueous solution. *Biotechnol. Lett.* **2005**, *27*, 1319–1323. [CrossRef] [PubMed]
15. Mazmanci, M.A.; Ünyayar, A. Decolourisation of reactive black 5 by *Funalia trogii* immobilised on *Luffa cylindrica* sponge. *Process Biochem.* **2005**, *40*, 337–342. [CrossRef]
16. Picioreanu, C.; Van Loosdrecht, M.C.; Heijnen, J.J. Two-dimensional model of biofilm detachment caused by internal stress from liquid flow. *Biotechnol. Bioeng.* **2001**, *72*, 205–218. [CrossRef]
17. Ohashi, A.; Harada, H. Adhesion strength of biofilm developed in an attached-growth reactor. *Water Sci. Technol.* **1994**, *29*, 281–288.
18. Stanley, P.M. Factors affecting the irreversible attachment of *Pseudomonas aeruginosa* to stainless steel. *Can. J. Microbiol.* **1983**, *29*, 1493–1499. [CrossRef] [PubMed]

19. Jiang, S.; Huang, J.; Lu, H.; Liu, J.; Yan, C. Optimisation for assay of fluorescein diacetate hydrolytic activity as a sensitive tool to evaluate impacts of pollutants and nutrients on microbial activity in coastal sediments. *Mar. Pollut. Bull.* **2016**, *110*, 424–431. [CrossRef] [PubMed]
20. Fontvieille, D.A.; Outaguerouine, A.; Thevenot, D.R. Fluorescein diacetate hydrolysis as a measure of microbial activity in aquatic systems: Application to activated sludges. *Environ. Technol.* **1992**, *13*, 531–540. [CrossRef]
21. Łabużek, S.; Hupert-Kocurek, K.; Skurnik, M. Isolation and characterisation of new *Planococcus* sp. strain able for aromatic hydrocarbons degradation. *Acta Microbiol. Pol.* **2003**, *52*, 395–404. [PubMed]
22. Hupert-Kocurek, K.; Guzik, U.; Wojcieszynska, D. Characterization of catechol 2,3-dioxygenase from *Planococcus* sp. strain S5 induced by high phenol concentration. *Acta Biochem. Pol.* **2012**, *59*, 345–351.
23. Qurashi, A.W.; Sabri, A.N. Bacterial exopolysaccharide and biofilm formation stimulate chickpea growth and soil aggregation under salt stress. *Braz. J. Microbiol.* **2012**, *43*, 1183–1191. [CrossRef] [PubMed]
24. Sonenshein, A.L. Control of sporulation initiation in *Bacillus subtilis*. *Curr. Opin. Microbiol.* **2000**, *3*, 561–566. [CrossRef]
25. Gotz, F. *Staphylococcus* and biofilms. *Mol. Microbiol.* **2002**, *43*, 1367–1378. [CrossRef] [PubMed]
26. Li, H.; Liu, Y.H.; Luo, N.; Zhang, X.Y.; Luan, T.G.; Hu, J.M.; Wang, Z.Y.; Wu, P.C.; Chen, M.J.; Lu, J.Q. Biodegradation of benzene and its derivatives by a psychrotolerant and moderately haloalkaliphilic *Planococcus* sp. strain ZD22. *Res. Microbiol.* **2006**, *157*, 629–636. [CrossRef] [PubMed]
27. Romano, I.; Giordano, A.; Lama, L.; Nicolaus, B.; Gambacorta, A. *Planococcus rifietensis* sp. nov, Isolated from Algal Mat Collected from a Sulfurous Spring in Campania (Italy). *Syst. Appl. Microbiol.* **2003**, *26*, 357–366. [CrossRef] [PubMed]
28. Sprott, G.D.; Larocque, S.; Cadotte, N.; Dicaire, C.J.; McGee, M.; Brisson, J.R. Novel polar lipids of halophilic eubacterium *Planococcus* H8 and archaeon *Haloferax volcanii*. *Biochim. Biophys. Acta* **2003**, *1633*, 179–188. [CrossRef] [PubMed]
29. Marco-Urrea, E.; Pérez-Trujillo, M.; Blánquez, P.; Vicent, T.; Caminal, G. Biodegradation of the analgesic naproxen by *Trametes versicolor* and identification of intermediates using HPLC-DAD-MS and NMR. *Bioresour. Technol.* **2010**, *101*, 2159–2166. [CrossRef] [PubMed]
30. Rodarte-Morales, A.I.; Feijoo, G.; Moreira, M.T.; Lema, J.M. Degradation of selected pharmaceutical and personal care products (PPCPs) by white-rot fungi. *World J. Microbiol. Biotechnol.* **2011**, *27*, 1839–1846. [CrossRef]
31. Marchlewicz, A.; Domaradzka, D.; Guzik, U.; Wojcieszyńska, D. *Bacillus thuringiensis* B1 (2015b) is a Gram-positive bacteria able to degrade naproxen and ibuprofen. *Water Air Soil Pollut.* **2016**, *227*, 197. [CrossRef] [PubMed]
32. Wojcieszyńska, D.; Domaradzka, D.; Hupert-Kocurek, K.; Guzik, U. Bacterial degradation of naproxen–Undisclosed pollutant in the environment. *J. Environ. Manag.* **2014**, *145*, 157–161. [CrossRef] [PubMed]
33. Lin, B.; Lyu, J.; Lyu, X.J.; Yu, H.Q.; Hu, Z.; Lam, J.C.; Lam, P.K. Characterization of cefalexin degradation capabilities of two *Pseudomonas* strains isolated from activated sludge. *J. Hazard. Mater.* **2015**, *282*, 158–164. [CrossRef] [PubMed]
34. Ye, C.; Hu, N.; Wang, Z. Experimental investigation of *Luffa cylindrica* as a natural sorbent material for the removal of a cationic surfactant. *J. Taiwan Inst. Chem. Eng.* **2013**, *44*, 74–80. [CrossRef]
35. Demir, H.; Top, A.; Balköse, D.; Ülkü, S. Dye adsorption behaviour of *Luffa cylindrica* fibres. *J. Hazard. Mater.* **2008**, *153*, 389–394. [CrossRef] [PubMed]
36. Huerta, B.; Rodriguez-Mozaz, S.; Nannou, C.; Nakis, L.; Ruhi, A.; Acuña, V.; Barcelo, D. Determination of a broad spectrum of pharmaceuticals and endocrine disruptors in biofilm from a waste water treatment plant-impacted river. *Sci. Total Environ.* **2016**, *540*, 241–249. [CrossRef] [PubMed]
37. Flemming, H.C.; Wingender, J.; Szewzyk, U.; Steinberg, P.; Rice, S.A.; Kjelleberg, S. Biofilms: An emergent form of bacterial life. *Nat. Rev. Microbiol.* **2016**, *14*, 563–575. [CrossRef] [PubMed]
38. Neeraja, P.; Srinivas, S.; Mukkanti, K.; Dubey, P.K.; Pal, S. 1H-1, 2, 3-Triazolyl-substituted 1, 3, 4-oxadiazole derivatives containing structural features of ibuprofen/naproxen: Their synthesis and antibacterial evaluation. *Bioorg. Med. Chem. Lett.* **2016**, *26*, 5212–5217. [CrossRef] [PubMed]

39. Yin, Z.; Wang, Y.; Whittell, L.R.; Jergic, S.; Liu, M.; Harry, E.; Oakley, A.J. DNA replication is the target for the antibacterial effects of nonsteroidal anti-inflammatory drugs. *Chem. Biol.* **2014**, *21*, 481–487. [CrossRef] [PubMed]
40. Wang, S.; Gunsch, C.K. Effects of selected pharmaceutically active compounds on the ammonia oxidizing bacterium *Nitrosomonas europaea*. *Chemosphere* **2011**, *82*, 565–572. [CrossRef] [PubMed]
41. Rahman, R.N.Z.A.; Ghazali, F.M.; Salleh, A.B.; Basri, M. Biodegradation of hydrocarbon contamination by immobilized bacterial cells. *J. Microbiol.* **2006**, *44*, 354–359. [PubMed]
42. Lloret, L.; Eibes, G.; Lú-Chau, T.A.; Moreira, M.T.; Feijoo, G.; Lema, J.M. Laccase-catalysed degradation of anti-inflammatories and estrogens. *Biochem. Eng. J.* **2010**, *51*, 124–131. [CrossRef]
43. Rodríguez-Rodríguez, C.E.; Marco-Urrea, E.; Caminal, G. Naproxen degradation test to monitor *Trametes versicolor* activity in solid-state bioremediation processes. *J. Hazard. Mater.* **2010**, *179*, 1152–1155. [CrossRef] [PubMed]
44. Tran, N.H.; Urase, T.; Kusakabe, O. Biodegradation characteristics of pharmaceutical substances by whole fungal culture *Trametes versicolor* and its laccase. *J. Water Environ. Technol.* **2010**, *8*, 125–140. [CrossRef]
45. Guzik, U.; Hupert-Kocurek, K.; Wojcieszyńska, D. Intradiol dioxygenases—The key enzymes in xenobiotics degradation in biodegradation of hazardous and special products. *InTech* **2013**, *7*, 129–153.
46. Cidaria, D.; Deidda, F.; Bosetti, A. A rapid method for naphtalene dioxygenase assay in whole cells of naphtalene cis-dihydrodiol dehydrogenase blocked *Pseudomonas fluoresecens*: Screening of potential inducers of dioxygenase activity. *Appl. Microbiol. Biotechnol.* **1994**, *41*, 689–693. [CrossRef]
47. Jõesaar, M.; Viggor, S.; Heinaru, E.; Naanuri, E.; Mehike, M.; Leito, I.; Heinaru, A. Strategy of *Pseudomonas pseudoalcaligenes* C70 for effective degradation of phenol and salicylate. *PLoS ONE* **2017**, *12*, e0173180. [CrossRef] [PubMed]
48. Hintner, J.P.; Lechner, C.; Riegert, U.; Kuhm, A.E.; Storm, T.; Reemtsma, T.; Stolz, A. Direct ring fission of salicylate by a salicylate 1, 2-dioxygenase activity from *Pseudaminobacter salicylatoxidans*. *J. Bacteriol.* **2001**, *183*, 6936–6942. [CrossRef] [PubMed]
49. Feng, Y.; Khoo, H.E.; Poh, C.L. Purification and characterization of gentisate 1, 2-dioxygenases from *Pseudomonas alcaligenes* NCIB 9867 and *Pseudomonas putida* NCIB 9869. *J. Appl. Environ. Microbiol.* **1999**, *65*, 946–950.
50. Tuson, H.H.; Weibel, D.B. Bacteria–surface interactions. *Soft Matter* **2013**, *9*, 4368–4380. [CrossRef] [PubMed]
51. Mirpuri, R.; Jones, W.; Bryers, J.D. Toluene degradation kinetics for planktonic and biofilm-grown cells of *Pseudomonas putida* 54G. *Biotechnol. Bioeng.* **1997**, *53*, 535–546. [CrossRef]
52. Priester, J.H.; Horst, A.M.; Van De Werfhorst, L.C.; Saleta, J.L.; Mertes, L.A.; Holden, P.A. Enhanced visualization of microbial biofilms by staining and environmental scanning electron microscopy. *J. Microbiol. Methods* **2007**, *68*, 577–587. [CrossRef] [PubMed]
53. Asahi, Y.; Miura, J.; Tsuda, T.; Kuwabata, S.; Tsunashima, K.; Noiri, Y.; Hayashi, M. Simple observation of *Streptococcus* mutans biofilm by scanning electron microscopy using ionic liquids. *AMB Express* **2015**, *5*, 6. [CrossRef] [PubMed]
54. Zhou, D.D.; Dong, S.S.; Gao, L.L.; Liu, M.Y.; Niu, S. Distribution characteristics of extracellular polymeric substances and cells of aerobic granules cultivated in a continuous-flow airlift reactor. *J. Chem. Technol. Biotechnol.* **2013**, *88*, 942–947. [CrossRef]
55. Ma, D.; Zou, D.; Zhou, D.; Li, T.; Dong, S.; Xu, Z.; Dong, S. Phenol removal and biofilm response in coupling of visible-light-driven photocatalysis and biodegradation: Effect of hydrothermal treatment temperature. *Int. Biodeterior. Biodegrad.* **2015**, *104*, 178–185. [CrossRef]
56. Greń, I.; Wojcieszyńska, D.; Guzik, U.; Perkosz, M.; Hupert-Kocurek, K. Enhanced biotransformation of mononitrophenols by *Stenotrophomonas malthophilia* KB2 in the presence of aromatic compounds of plant origin. *World J. Microbiol. Biotechnol.* **2010**, *26*, 289–295. [CrossRef]
57. Abe, T.; Masai, E.; Miyauchi, K.; Katayama, Y.; Fukuda, M. A tetrahydrofolate-dependent O-demethylase, LigM, is crucial for catabolism of vanillate and syringate in *Sphingomonas paucimobilis* SYK-6. *J. Bacteriol.* **2005**, *187*, 2030–2037. [CrossRef] [PubMed]

58. Wojcieszyńska, D.; Greń, I.; Hupert-Kocurek, K.; Guzik, U. Modulation of FAD-dependent monooxygenase activity from aromatic compounds-degrading *Stenotrophomonas maltophilia* strain KB2. *Acta Biochem. Pol.* **2011**, *58*, 421–426.
59. Bradford, M.M. A rapid and sensitive method for the quantitation of microgram quantities of protein utilizing the principle of protein-dye binding. *Anal. Biochem.* **1976**, *72*, 248–254. [CrossRef]

© 2018 by the authors. Licensee MDPI, Basel, Switzerland. This article is an open access article distributed under the terms and conditions of the Creative Commons Attribution (CC BY) license (http://creativecommons.org/licenses/by/4.0/).

catalysts

MDPI

Article

Asymmetric Ketone Reduction by Immobilized *Rhodotorula mucilaginosa*

Hui Liu [1], Wen-Di Duan [2,3], Fayene Zeferino Ribeiro de Souza [4], Lan Liu [1] and Bi-Shuang Chen [1,*]

1 School of Marine Sciences, Sun Yat-Sen University, Guangzhou 510275, China; liuh229@mail2.sysu.edu.cn (H.L.); cesllan@mail.sysu.edu.cn (L.L.)
2 Shanghai Institute of Materia Medica, Chinese Academy of Sciences, Shanghai 210203, China; duanwd@mail2.sysu.edu.cn
3 University of Chinese Academy of Sciences, Beijing 100049, China
4 Departamento de Química, Faculdade de Ciências, UNESP, Bauru 17033-360, Brazil; faylittlefay@yahoo.com.br
* Correspondence: chenbsh23@mail.sysu.edu.cn; Tel.: +86-20-84725459

Received: 29 March 2018; Accepted: 17 April 2018; Published: 19 April 2018

Abstract: In our previous study, *Rhodotorula mucilaginosa* (*R. mucilaginosa*) was selected via high throughput screening as a very active and selective whole-cell biocatalyst for the asymmetric reduction of ketones. In this study, the reduction of ketones to the desired chiral alcohols by immobilized cells of this strain was investigated. Characterization with Fourier-transform infrared (FTIR) spectroscopy and scanning electron microscopy (SEM) showed that whole *R. mucilaginosa* cells were successfully immobilized on support matrices composed of agar, calcium alginate, PVA-alginate and chitosan. The immobilized cells were applied to the enantioselective reduction of fourteen different aromatic ketones. Good to excellent results were achieved with *R. mucilaginosa* cells immobilized on agar and calcium alginate. The immobilized cells on the selected support matrix composed of agar exhibited a significant increase in pH tolerance at pH 3.5–9 and demonstrated highly improved thermal stability compared to free cells. The cells immobilized on agar retained 90% activity after 60 days storage at 4 °C and retained almost 100% activity after 6 reuse cycles. In addition, the immobilization procedures are very simple and cause minimal pollution. These results suggest that the application of immobilized *R. mucilaginosa* can be practical on an industrial scale to produce chiral alcohols.

Keywords: biocatalyst; *Rhodotorula mucilaginosa*; immobilization; asymmetric reduction; stability

1. Introduction

Chiral alcohols are useful intermediates that are applicable for the synthesis of pharmaceuticals, flavors, aromas, agricultural chemicals and specialty materials [1]. Among the methods for their production, enantioselective ketone reduction is generally regarded as a reliable, scalable and straightforward method to obtain optically active alcohols [2,3]. Whereas traditional synthetic methods usually use toxic metals or expensive complex hydrides [4–6], enzymatic enantioselective reductions benefit from high selectivity, environmentally friendly processes and simple operations and are thus of great interest [7]. Nevertheless, biotechnological approaches are still limited in their industrial application due, in most cases, to low volumetric productivity, high cost of catalyst preparation, complex final products, and/or complicated downstream processing [8]. Much attention is needed for the development of robust biocatalysts to facilitate the performance of biocatalytic reduction processes, such as high substrate loads, to obtain industrial feasibility and competitiveness of preparative-scale biotransformations.

Biocatalytic processes can benefit from the habitat-related characteristics of marine enzymes, that is excellent stability and activity under extreme conditions (such as, extreme temperature, pressure, or pH or an organic solvent) and the unique enzyme properties of substrate specificity and affinity [9,10]. In our previous study, after a microbial screen, the marine fungi *R. mucilaginosa* was selected as a very active and selective whole-cell biocatalyst for the asymmetric reduction of ketones [11,12]. Although this strain has promising catalytic properties, several challenges remain before it can be used in industrial applications. In particular, its pH tolerance and thermostability were not perfect yet compared to those of other marine-derived biocatalysts, which limits the utilization of this strain.

To maintain the effectiveness of a biocatalyst in a certain process, it should be protected from interactions with the reaction solvent to avoid inactivation, as inactivation might halt the enzymatic reaction [13]. In this context, a range of immobilization technologies have been introduced to improve the stability of biocatalysts and assist their recovery and reusability [14]. Among the immobilized biocatalysts, purified enzymes are commonly immobilized in/on materials known as matrices, yet the immobilization of marine fungi has rarely been reported. Notably, the immobilization of whole cell biocatalysts is of interest in light of the growing number of industrial applications using biotechnological approaches in the medicinal and food industries, especially the application of methods using filamentous fungi with a large production of enzymes [15].

The present study is a continuation of our work on the use of marine-derived fungi as biocatalysts for the asymmetric reduction of ketones. The conversion of ketones to the corresponding chiral alcohols by immobilized *R. mucilaginosa* cells was investigated. Whole *R. mucilaginosa* cells were immobilized on support matrices composed of agar, calcium alginate, PVA-alginate and chitosan and the synthetic potential of the immobilized cells was evaluated for the enantioselective reduction of fourteen aromatic ketones of various compound classes.

2. Results and Discussion

Marine fungi, which are considered promising biological carriers, have been employed in many industrial sectors [16]. Recently, we investigated the use of marine-derived fungi for the reduction of aromatic ketones [10,11] and *R. mucilaginosa* GIM 2.157 was selected as a very active and selective whole-cell biocatalyst after a microbial screen. Whole-cell immobilization technology has attracted widespread attention for its application in several fields, such as its application for the biodegradation of mixed wastes and drug or fuel biosynthesis [17]. To develop a successful bioprocess, we immobilized *R. mucilaginosa* GIM 2.157 cells on various support matrices for the catalytic reduction of ketones (**1a**–**1n**) and tested the immobilized cells for recyclability and storage stability.

2.1. Characterization of Immobilized Cells

2.1.1. FTIR Spectroscopy

The immobilized and non-immobilized cells were confirmed by FTIR (Fourier transform infrared spectroscopy) and SEM (scanning electron microscopy). FTIR spectra showed the functional group of the immobilized cell matrices [18]. Scans were performed at 4000–400 cm^{-1} using a Hitachi 270–50 IR spectrophotometer with KBr discs. For the immobilization of whole cells on agar, the FTIR spectra of free cells, agar and immobilized cells are shown in Figure 1a [(a) is for free cells; (b) is for agar; (c) is for immobilized cells on agar]. Figure 1a (b) shows characteristic peaks at 3313 cm^{-1} (O–H stretching), 2911 cm^{-1} (C–H stretching) and 1152 cm^{-1} (C–O–C stretching) for the agar. The FTIR results support that the immobilization reaction occurred, as the peaks of the whole cells immobilized on agar show changes relative to the position and intensity of the characteristic peaks for native agar. The presence of additional peaks at 1742 cm^{-1} and 1546 cm^{-1} [Figure 1a (c)] confirms that immobilization reaction occurred.

For the immobilization of whole cells on calcium alginate, the FTIR spectra of free cells, calcium alginate and immobilized cells are shown in Figure 1b [(a) is for free cells; (d) is for calcium alginate;

(e) is for immobilized cells on calcium alginate]. Figure 1b (d) shows characteristic peaks at 3428 cm^{-1} (O–H trenching), 2930 cm^{-1} (C–H stretching), 1032 cm^{-1} (C–O–C stretching), 1623 cm^{-1} and 1419 cm^{-1} (–COO asymmetric and symmetric stretching) for calcium alginate. The FTIR results support that the immobilization reaction occurred, as the peaks for the whole cells immobilized on calcium alginate show changes relative to the position and intensity of the characteristic peaks for native calcium alginate]. The presence of additional peaks at 1743 cm^{-1} and 1548 cm^{-1} [Figure 1b (e)] confirms that the immobilization reaction occurred.

For the immobilization of whole cells on PVA-alginate, the FTIR spectra of free cells, PVA-alginate and immobilized cells are shown in Figure 1c [(a) is for free cells; (f) is for PVA-alginate; (g) is for immobilized cells on PVA-alginate]. Figure 1c (f) shows characteristic peaks at 3417 cm^{-1} (for O–H stretching) and 2941 cm^{-1} (for C–H stretching) in PVA-alginate. The FTIR results support the occurrence of the immobilization reaction, as the peaks for whole cells immobilized on PVA-alginate show changes relative to the position and intensity of the characteristic peaks for native PVA-alginate. The presence of additional peaks at 1547 cm^{-1} [Figure 1c (g)] confirms that the immobilization reaction occurred.

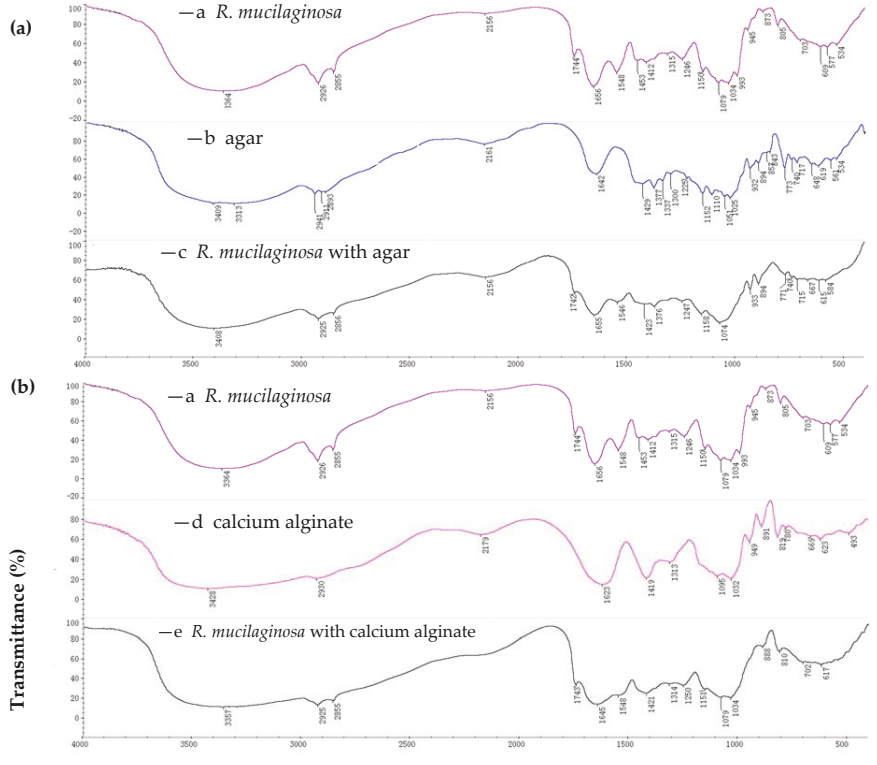

Figure 1. *Cont.*

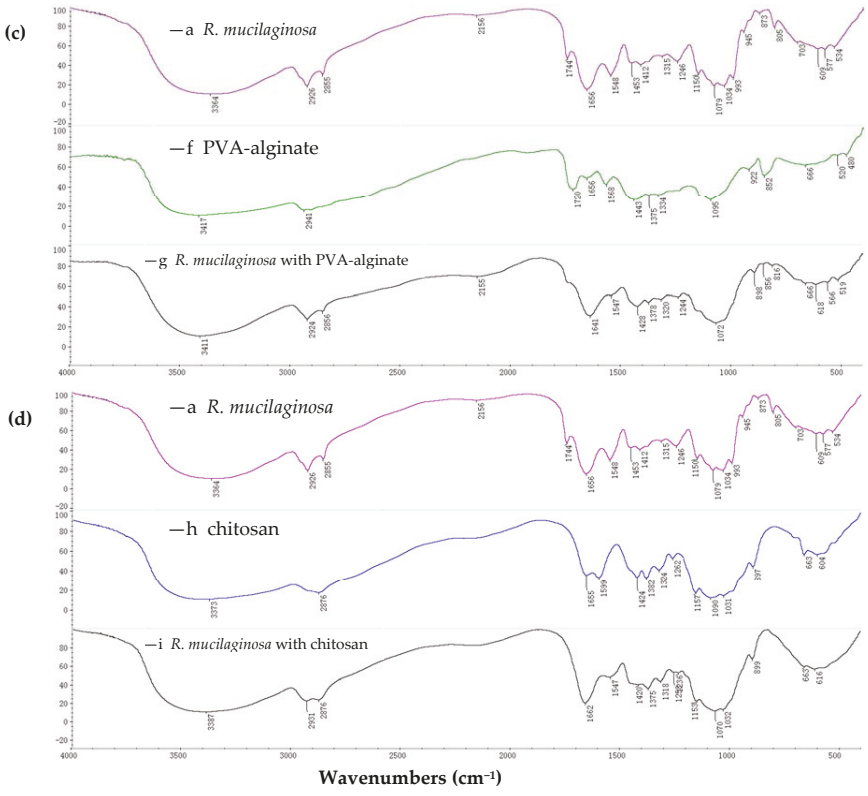

Figure 1. Fourier transform infrared (FTIR) for immobilization of *R. mucilaginosa* GIM 2.157 on agar (**a**), on calcium alginate (**b**), on PVA-alginate (**c**) and on chitosan (**d**): —a *R. mucilaginosa*; —b agar; —c *R. mucilaginosa* with agar; —d calcium alginate; —e *R. mucilaginosa* with calcium alginate; —f PVA-alginate; —g *R. mucilaginosa* with PVA-alginate; —h chitosan; —i *R. mucilaginosa* with chitosan.

For the immobilization of whole cells on chitosan, the FTIR spectra of free cells, chitosan and immobilized cells on chitosan are shown in Figure 1d [(a) is for free cells; (h) is for chitosan; (i) is for immobilized cells on chitosan]. Figure 1d (h) shows characteristic peaks at 3373 cm^{-1} (for O–H stretching), 1157 cm^{-1} (for C–O–C stretching), 1655 cm^{-1} and 2876 cm^{-1} (for C–H stretching) for chitosan. FTIR confirmed the occurrence of the immobilization reaction, as the peaks for whole cells immobilized on calcium alginate show changes relative to the position and intensity of the characteristic peaks of native chitosan. The presence of additional peaks at 1547 cm^{-1} [Figure 1d (i)] confirms that the immobilization reaction occurred.

2.1.2. SEM Spectroscopy

The SEM images of agar, calcium alginate, PVA-alginate and chitosan immobilization are shown in Figure 2. Using simple and easy gelation technology, *R. mucilaginosa* GIM 2.157 cells were captured in agar microspheres and cross-linked with agar using distilled water. The SEM images for the agar immobilization are shown in Figure 2A–C. These images confirmed good immobilization of *R. mucilaginosa* GIM 2.157 cells on the surface due to the agar's flocculating ability and cross-linkability.

R. mucilaginosa GIM 2.157 cells were captured in calcium alginate (one of the most important immobilization matrices) microspheres and cross-linked with calcium alginate using $CaCl_2$. The SEM

images for calcium alginate immobilization are shown in Figure 2A,D,E. These images confirmed good immobilization of *R. mucilaginosa* GIM 2.157 cells on the surface due to calcium alginate's high mechanical strength and cross-linkability. Notably, the gelling characteristic of an alginate highly depend on its monomeric composition and sequential arrangement, which is essential for its use as an immobilization matrix [19]. The electron micrographs revealed that 4% $CaCl_2$ played a vital role in the formation of microspheres and that complex interactions occurred between cells and support materials.

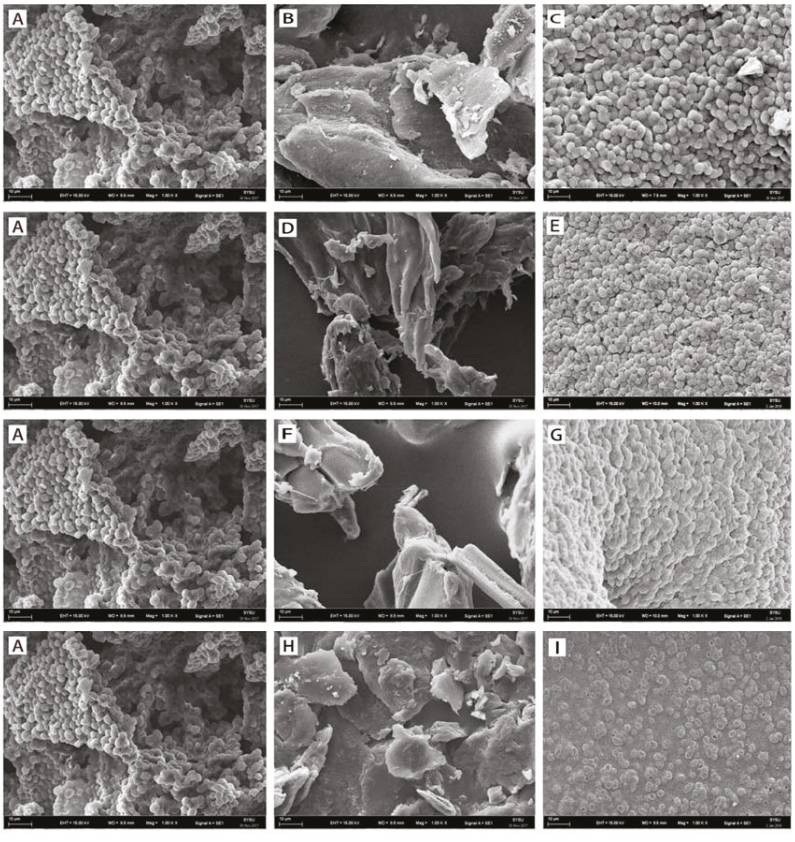

Figure 2. Scanning electron micrographs of agar, calcium alginate, PVA-alginate and chitosan beads containing *R. mucilaginosa* GIM 2.157 cells. (**A**) Free *R. mucilaginosa* GIM 2.157 cells; (**B**) agar; (**C**) *R. mucilaginosa* GIM 2.157 cells immobilized on agar; (**D**) calcium alginate; (**E**) *R. mucilaginosa* GIM 2.157 cells immobilized on calcium alginate; (**F**) PVA-alginate; (**G**) *R. mucilaginosa* GIM 2.157 cells immobilized on PVA-alginate; (**H**) chitosan; and (**I**) *R. mucilaginosa* GIM 2.157 cells immobilized on chitosan.

The addition of calcium alginate to the mixture improved the bead characteristics by reducing the agglomeration problems of the PVA–boric acid method thus enhanced the surface characteristics of the beads [20]. *R. mucilaginosa* GIM 2.157 cells were captured in PVA-alginate microspheres and cross-linked with alginate-polyvinyl alcohol using boric acid. The SEM images for PVA-alginate immobilization were specifically shown in Figure 2A,F,G. These images confirmed good immobilization of *R. mucilaginosa* GIM 2.157 cells on the surface due to alginate-polyvinyl alcohol's covalent

interactions and cross-linkability [21]. The electron micrographs also revealed that pores were made on the outer layer of the beads and the pores were almost evenly distributed and had an average size.

R. mucilaginosa GIM 2.157 cells were entrapped in chitosan surface and cross-linked using glutaraldehyde. The SEM images for chitosan immobilization are shown in Figure 2A,H,I. These images confirmed the effective immobilization of *R. mucilaginosa* GIM 2.157 cells on the surface because of chitosan's flocculating ability and cross-linkability [22]. Moreover, (interconnected) porous structures were observed for chitosan-immobilized *R. mucilaginosa* GIM 2.157 cells, suggesting that the cells have excellent immobilization performance and strong adhesion properties.

2.2. Catalytic Activity of Immobilized Cells for the Reduction of Various Ketones

The biocatalytic reduction of a series of prochiral ketones was attempted with *R. mucilaginosa* GIM 2.157 cells immobilized on the abovementioned support matrices (Table 1). Parallel reactions were conducted with free resting cells without the support matrices. The resting cells were also used for immobilization on agar, calcium alginate, PVA-alginate and chitosan. *R. mucilaginosa* GIM 2.157 cells were cultured for 24 h. The cell mixture was centrifuged at 4000 rpm (4 °C) and washed three times with given buffer and the pellets were collected as resting cells, which were further used for immobilization reactions. All reduction reactions were performed in 10 mL of Na_2HPO_4-KH_2PO_4 buffer (100 mM, pH 7.0) supplemented with glucose (0.5 g), substrates (10 mM) and biocatalysts (3 g resting cells or 4.5 g immobilized cells) at 25 °C for 24 h. Yield and enantioselectivity were measured on a chiral HPLC (Conditions see the Experimental section). The absolute configuration of reduction products was assigned by comparison the optical rotations measured for the isolated products with those reported. The results are shown in Table 1. According to the data displayed in Table 1, the free (not immobilized) resting cells catalyzed Prelog's stereospecific reduction of ketones **1a**–**1h**, **1k** and **1l** into the corresponding chiral alcohols with excellent yield and enantioselectivities. Notably, the immobilized cells showed slightly better activity towards substrates with substituent –Cl (**1d**, **1e** and **1f**) than those with substituent –Br (**1a**, **1b** and **1c**). Regarding the mechanism, although ketone **1c** is closely related to **1f**, the substituent –Br in **1c** is a relatively poor electron-withdrawing group compared to –Cl in substrate **1f**. In our previous study with free resting cells [11,12], we found that substrates with electron-donating substituents inhibited the enzyme activity of *R. mucilageinosa* GIM 2.157, which might be useful to explain why the yield and *ee* value of **2c** was slightly lower than those of **2f**. On the other hand, –Br has larger atomic radius than –Cl, increasing the distances between substrates and immobilized cells and thus resulting in slightly lower activity (*i.e.*, yield and *ee*). When resting cells were immobilized on agar, calcium alginate and PVA-alginate, they could still catalyze the reduction of assayed ketones (**1a**–**1h**, **1k** and **1l**) with excellent activities; however, in some cases, the yields/enantioselectivities were slightly lower. It is possible that the access of the substrate to the carbonyl reductases must have been hindered by partial coverage of the mycelia, preventing the reaction. The *R. mucilaginosa* GIM 2.157 cells immobilized on agar showed slightly better activity (higher yields/*ee*) than those immobilized on calcium alginate and PVA-alginate. The agar bead surface likely had many porous structures, allowing more substrates and carbonyl reductases to freely access to cells inside and outside, maintaining stronger mechanical strength than other support matrices and improving the stability of the entire cellular system [23]. However, when the *R. mucilaginosa* GIM 2.157 cells were immobilized on chitosan, the reduction occurred in only substrates **1l** and **1k**. This might be due to two factors: chitosan adhered strongly to the surface of the whole cells, forming a strong barrier and blocking the access of the substrate to one or more enzymes involved in the reduction [24] and the chitosan matrix completely covered the entire cellular surface so that the ketone reductase cannot be released, halting the reactions [9,25,26]. Interestingly, the reduction of **1l** and **1k** with *R. mucilaginosa* GIM 2.157 cells immobilized on chitosan resulted in total inversion of the configuration compared to the other biocatalysts (free cells and *R. mucilaginosa* GIM 2.157 cells immobilized on agar, calcium alginate and PVA-alginate). This phenomenon might occur because all carbons present in the chitosan itself were chiral, making the reaction environment chiral. In these

chiral conditions, the configurations of the glycosidic bonds could be easily altered, which is likely related to the inversion of the configuration of reduction products **2l** and **2k**. Further experiments regarding the mechanism are currently being implemented in our laboratory. Nevertheless, it can be concluded that agar was a perfect support matrix for the immobilization of *R. mucilaginosa* GIM 2.157 cells, which were used for all further studies.

Table 1. Catalytic activity of immobilized cells in the reduction of various ketones [a]: the numbers indicate chemical yields of desired products, numbers within brackets indicate the enantiomeric excess values of the desired product (%), *S*/*R* within brackets indicate the absolute configuration of the desired products.

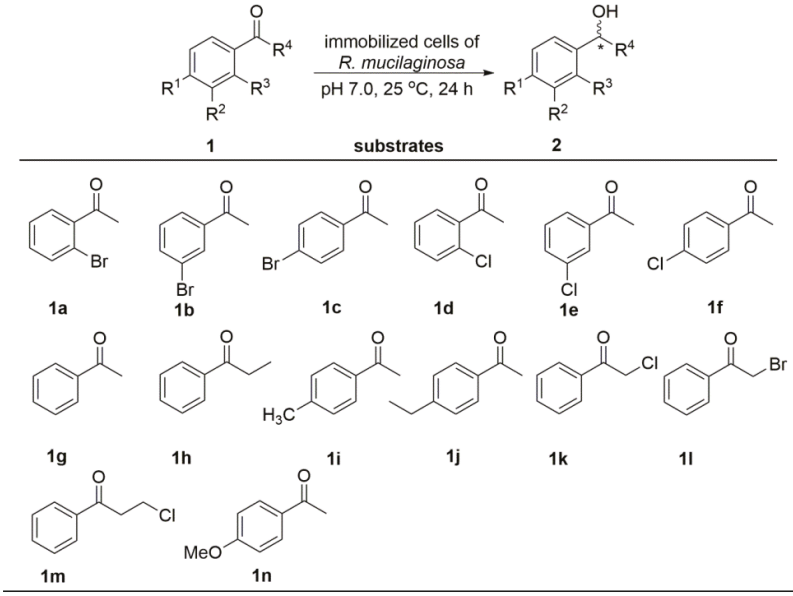

Reduction Products	Biocatalysts				
	Free Cells	*R. mucilaginosa* Cells Immobilized on			
		Agar	Calcium Alginate	PVA-Alginate	Chitosan
2a	99 (99, *S*)	99 (99, *S*)	99 (99, *S*)	99 (99, *S*)	0
2b	99 (99, *S*)	99 (89, *S*)	86 (99, *S*)	89 (94, *S*)	0
2c	99 (99, *S*)	73 (68, *S*)	71 (19, *S*)	51 (54, *S*)	0
2d	99 (99, *S*)	99 (99, *S*)	89 (99, *S*)	97 (99, *S*)	0
2e	99 (99, *S*)	99 (99, *S*)	94 (89, *S*)	99 (99, *S*)	0
2f	99 (99, *S*)	94 (83, *S*)	91 (94, *S*)	59 (77, *S*)	0
2g	99 (99, *S*)	99 (91, *S*)	94 (97, *S*)	75 (66, *S*)	0
2h	99 (99, *S*)	99 (99, *S*)	93 (99, *S*)	94 (99, *S*)	0
2i	0	0	0	0	0
2j	0	0	0	0	0
2k	99 (99, *S*)	99 (89, *S*)	99 (85, *S*)	77 (84, *S*)	88 (91, *R*)
2l	99 (99, *R*)	99 (73, *R*)	99 (82, *R*)	23 (21, *R*)	72 (84, *S*)
2m	0	0	0	0	0
2n	0	0	0	0	0

[a] Reaction conditions: 10 mL Na_2HPO_4-KH_2PO_4 buffer (100 mM, pH 7.0), 3 g resting cells (or 4.5 g immobilized cells), 10 mM substrate, 0.5 g glucose, 25 °C, 24 h; 94 (83, *S*) indicates 94% yield of desired (*S*)-selective reduction product with 83% *ee* for all data listed in the table above; Yield and *ee* were determined by chiral HPLC analysis equipped with a Chiralcel AD-H chiral column; Configuration was assigned by comparing specific signs of rotation measured for isolated products to those reported in the literature.

2.3. Stability of Immobilized Cells on Agar

2.3.1. pH Tolerance

It is commonly known that pH plays an essential role in biocatalytic reactions, that is, pH variation can affect the activity and selectivity of the biocatalyst. In principle, the pH stability of a biocatalyst can be strongly enhanced by immobilization. Thus, the effects of pH on the enzymatic activity of immobilized cells and free cells were both studied. Either free cells or immobilized cells were added to buffer (10 mL) containing 10 mM of 1-(2-bromophenyl)ethanone **1a** and glucose (0.5 g) at a given pH value between 3.5–11 (buffers at pH 3.5 and 4.5 were prepared with citrate buffer; buffers at pH 5.5, 6.5, 7 and 7.5 were prepared with phosphate buffer; buffers at pH 8.5, 9, 10 and 11 were prepared with Tris buffer; 100 mM) at 25 °C for 24 h. As shown in Figure 3, the reaction product yield was kept above 99% within the tested range of pH 3.5–9.0 when substrate **1a** was treated with immobilized cells. As the buffer pH increased from 9.0 to 11.0, the activity of the immobilized cells slightly decreased and approximately 90% of its original activity was maintained. However, the catalytic activity of the free cells was much more sensitive to alkaline/acidic environments. As illustrated in Figure 3, buffer pH showed a significant impact on the product yield of the reaction treated with free cells. The product yield slowly increased with the increase in pH from 3.5 to 7.0. When buffer pH was further increased to alkaline ranges (pH 7.0–11), the activity of the free cells dramatically decreased to 10% of their original activity at pH 11. Notably, within the tested buffer pH ranged from 3.5 to 11.0, there was only a marginal change in the product *ee* (not shown in Figure 3). Obviously, these results suggested that *R. mucilaginosa* GIM 2.157 immobilization on agar beads was much more effective for improving the pH stability of the cells, which might be due to the unique micro-environment induced by the gel networks that may protected cells from the impact of H^+ ions (pH variation).

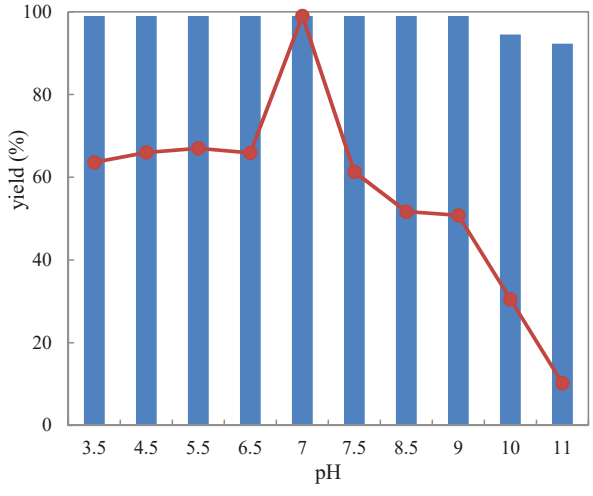

Figure 3. Optimum pH profile of free (represented by the dots) and agar-immobilized (striped bar) *R. mucilaginosa* GIM 2.157 cells for catalyzing the reduction of 1-(2-bromophenyl)ethanone (**1a**).

2.3.2. Thermostability

The immobilized cells are particularly interesting because of their stability with respect to higher temperatures, which makes them superior to the free cells. Hence, the thermostability of the immobilized *R. mucilaginosa* GIM 2.157 cells was characterized compared to that of the free resting cells. The immobilized cells were incubated at various temperatures (30–70 °C) for 1 h, 3 h, 6 h, 12 h

and 15 h. The cells were added to a solution containing 10 mL Na_2HPO_4-KH_2PO_4 buffer (100 mM, pH 7.0) supplemented with substrate **1a** (10 mM) and 0.5 g glucose. The reaction proceeded at 25 °C for 24 h. As shown in Figure 4, the immobilized biocatalyst showed a retention of >99% of its original activity after 15 h of incubation at 30 °C or 40 °C. The immobilized cells maintained approximately 99% of their original activity after 1 h of incubation at 50 °C or 60 °C. However, when the temperature was higher than 60 °C, a significant decrease was observed in the activity of the immobilized cells over a 3-h period. The immobilized cells were completely deactivated after 1 h at 70 °C. Free cells retained >99% of their original activity after incubation for 1 h at 30 °C. When the temperature increasing from 30 to 60 °C led to a clear reduction in the activity (27% of initial activity was lost after 1 h at 40 °C, 40% was lost after 1 h at 50 °C and total deactivation was observed after 1 h at 60 °C). It is clear that the immobilized cells have huge thermal stability advantages compared to the free cells.

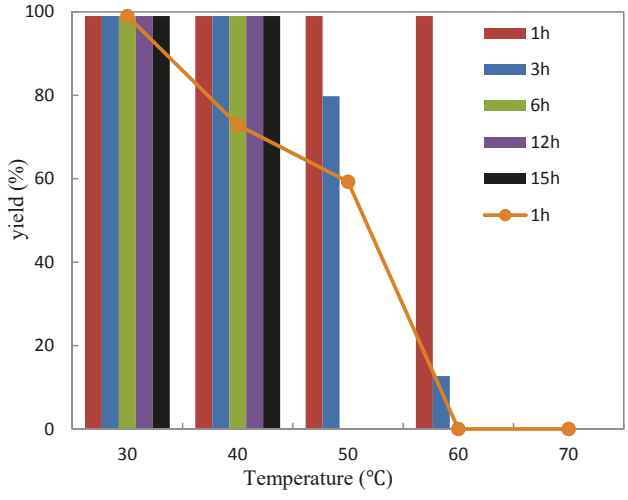

Figure 4. Thermostability of free (represented by the dots) and agar-immobilized (striped bar) *R. mucilaginosa* GIM 2.157 cells for catalyzing the reduction of 1-(2-bromophenyl)ethanone (**1a**). Cells were incubated at various temperatures and times before substrate was added to initiate reactions.

2.3.3. Storage Stability

One essential factor for the practical application of whole cells is their storage stability for an extended period of time. The longer the period that a biocatalyst maintains stable, the more efficient a process is. To estimate the storage stability of *R. mucilaginosa* GIM 2.157, free cells and cells immobilized on agar were stored at 4 °C with physiological saline (0.85% NaCl, *w*/*v*). Samples were withdrawn at various time intervals (5, 10, 20, 25, 30, 60 days) to determine the catalytic activity at 25 °C using 1-(2-bromophenyl)ethanone (**1a**) as the substrate. As shown in Figure 5, the cells immobilized on agar showed a superior retention of activity comparing to free cells after storage for 60 days at 4 °C. The cells immobilized on agar maintained approximately 95% of their original activity after storage for 60 days at 4 °C, while the catalytic activity of free cells decreased to 82% after storage for 20 days at 4 °C and to 7% after storage for 60 days at 4 °C. Hence, we concluded that immobilization of *R. mucilaginosa* GIM 2.157 cells on agar resulted in a biocatalyst with excellent storage properties and essential industrial application potential.

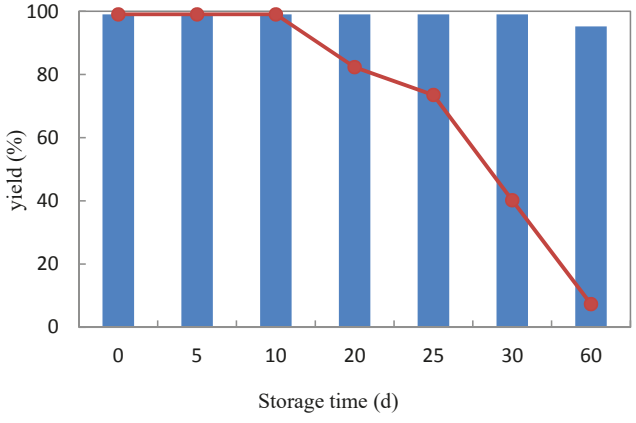

Figure 5. Storage stability of free (represented by the dots) and agar-immobilized (represented by striped bar) *R. mucilaginosa* GIM 2.157 cells for catalyzing the reduction of 1-(2-bromophenyl)ethanone (**1a**) at 4 °C.

2.3.4. Recyclability

Recyclability is a crucial parameter for the practical application of an immobilized cell system. From a process economics point of view, if immobilized cells are stable for a higher number of cycles, then the process can be more efficiently operated. Thus, experiments were conducted to examine the recyclability of the free and agar-immobilized *R. mucilaginosa* GIM 2.157 cells for the reduction of 1-(2-bromophenyl)ethanone (**1a**) as an example. Each reaction was carried out in 10 mL Na_2HPO_4-KH_2PO_4 buffer (100 mM, pH 7.0) with 4.5 g immobilized cells or 3 g free cells, 10 mM substrate and 0.5 g glucose and the reactions were shaken at 25 °C for 23 h. Afterwards, the cells were separated, washed two times with the same buffer [Na_2HPO_4-KH_2PO_4 buffer (100 mM, pH 7.0)] and reused for the next batch under the same reaction conditions. *R. mucilaginosa* GIM 2.157 cells immobilized on agar showed high activity than free cells and completed the reduction of **1a** for six cycles without significant loss of activity and selectivity. A loss of 68% of the initial activity was detected in cycle 7, whereas almost no activity (3.7% yield of alcohol) was retained in cycle 8 (Figure 6). When the free cells were used, the yield dropped to 80% at cycle 4. At cycle 5, the activity of free cells was completely lost (corresponding to the yield of 1.4%). Consequently, the immobilization of the *R. mucilaginosa* GIM 2.157 cells on agar provided a slight advantage for increasing the reusability of the cells, potentially making their implementation in commercial availability simpler and more cost effective.

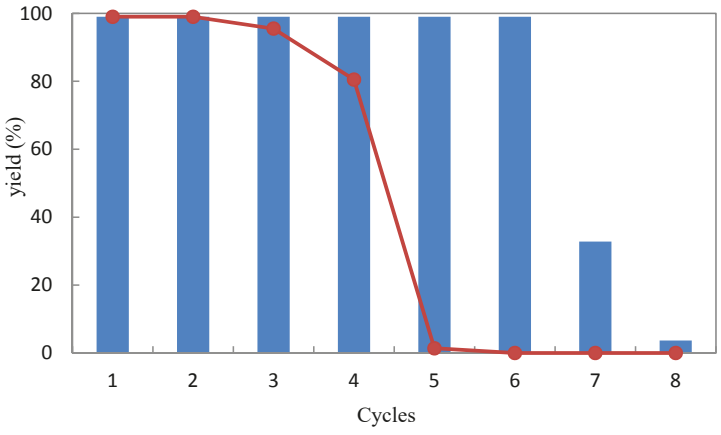

Figure 6. Repeated bioreduction of 1-(2-bromophenyl)ethanone (**1a**) catalyzed by free (dots) and agar-immobilized (striped bar) *R. mucilaginosa* GIM 2.157 cells.

3. Materials and Methods

3.1. General Methods

All substrates used in this study were obtained from Sigma-Aldrich (Schnelldorf, Denmark) and were used directly without any further purification. Fungus culture media components were purchased from Huankai Microbial (Guangzhou, China).

All NMR experiments were recorded with a Bruker Avance 500 instrument (^{1}H 500 MHz and ^{13}C 125 MHz) using $CDCl_3$ as the solvent. Data for ^{1}H NMR are documented in terms of chemical shift (δ ppm), multiplicity (s = singlet, d = doublet, t = triplet, q = quartet, m = multiplet), integration, coupling constant (Hz) and assignment. Data for ^{13}C NMR are recorded as chemical shift. Optical rotations were measured at 20 °C on a MCP 300 (Anton Paar) (sodium D line). Column chromatography (CC) was performed with silica gel (200–300 mesh, Qingdao Marine Chemical Factory) and mixtures of petroleum ether (PE) and ethyl acetate (EtOAc) as solvents. Thin-layer chromatography (TLC) was performed on silica gel plates (Qingdao Huang Hai Chemical Group Co., G60, F-254).

Reduction products were analyzed using High Performance Liquid Chromatography (HPLC) coupled to a UV/Vis detector SPD-M10Avp (190–370 nm, Shimadzu) on a column (Daicel 4.6 × 250 mm 5 m Chiralcel AD-H). The mobile phase: *n*-hexane/*i*-PrOH (95:5, *v*/*v*); flow rate: 0.5 mL/min; column temperature: 25 °C. Retention times: 11.85 min [1-(2-bromophenyl)ethanone (1a)], 12.71 min [(*R*)-1-(2-bromophenyl)ethan-1-ol (*R*-**2a**)], 13.23 min [(*S*)-1-(2-bromophenyl)ethan-1-ol (*S*-**2a**)]; 10.66 min [1-(3-bromophenyl)ethanone (1b)], 16.45 min [(*R*)-1-(3-bromophenyl)ethan-1-ol (*R*-**2b**)], 17.39 min [(*S*)-1-(3-bromophenyl)ethan-1-ol (*S*-**2b**)]; 11.21 min [1-(4-bromophenyl)ethanone (1c)], 16.83 min [(*R*)-1-(4-bromophenyl)ethan-1-ol (*R*-**2c**)], 17.99 min [(*S*)-1-(4-bromophenyl)ethan-1-ol (*S*-**2c**)]; 10.71 min [1-(2-chlorophenyl)ethanone (1d)], 13.32 min [(*R*)-1-(2-chlorophenyl)ethan-1-ol (*R*-**2d**)], 13.98 min [(*S*)-1-(2-chlorophenyl)ethan-1-ol (*S*-**2d**)]; 10.49 min [1-(3-chlorophenyl)ethanone (1e)], 14.60 min [(*R*)-1-(3-chlorophenyl)ethan-1-ol (*R*-**2e**)], 16.35 min [(*S*)-1-(3-chlorophenyl)ethan-1-ol (*S*-**2e**)]; 10.78 min [1-(4-chlorophenyl)ethanone (1f)], 15.09 min [(*R*)-1-(4-chlorophenyl)ethan-1-ol (*R*-**2f**)], 16.09 min [(*S*)-1-(4-chlorophenyl)ethan-1-ol (*S*-**2f**)]; 11.46 min [acetophenone (**1g**)], 15.93 min [(*R*)-1-phenylethan-1-ol (*R*-**2g**)], 17.93 min [(*S*)-1-phenylethan-1-ol (*S*-**2g**)]; 10.94 min [propiophenone (**1h**)], 14.74 min [(*R*)-1-phenylpropan-1-ol (*R*-**2h**)], 16.49 min [(*S*)-1-phenylpropan-1-ol (*S*-**2h**)]; 16.75 min [2-chloro-1-phenylethanone (1k)], 20.98 min [(*R*)-2-chloro-1-phenylethan-1-ol (*R*-**2k**)], 24.71 min [(*S*)-2-chloro-1-phenylethan-1-ol (*S*-**2k**)]; 16.42 min [2-bromo-1-phenylethanone (1l)], 22.33 min [(*R*)-2-bromo-1-phenylethan-1-ol (*R*-**2l**)], 27.39 min [(*S*)-2-bromo-1-phenylethan-1-ol (*S*-**2l**)].

The optical rotations of reduction products were recorded as: (*S*)-**2a**, $[\alpha]_D^{20}$ = −62.4 (*c* 1.00, $CHCl_3$); {Ref. [23] (*S*)-1-(2-bromophenyl)ethanol $[\alpha]_D^{27}$ = −29.8 (*c* 0.68, $CHCl_3$)}; (*S*)-**2b**, $[\alpha]_D^{20}$ = −43.9 (*c* 1.00, $CHCl_3$); {Ref. [24] (*S*)-1-(3-bromophenyl)ethanol $[\alpha]_D^{25}$ = −27.6 (*c* 1.00, $CHCl_3$)}; (*S*)-**2c**, $[\alpha]_D^{20}$ = −17.3 (*c* 1.00, MeOH), {Ref. [25] (*S*)-1-(4-bromophenyl)ethanol $[\alpha]_D^{21}$ = −20.6 (*c* 1.07, MeOH)}; (*S*)-**2d**, $[\alpha]_D^{20}$ = −78.4 (*c* 1.00, MeOH), Ref. [26] (*S*)-1-(2-chlorophenyl)ethanone $[\alpha]_D^{20}$ = −57.75 (*c* 1.46, $CHCl_3$)}; (*S*)-**2e**, $[\alpha]_D^{20}$ = −49.7 (*c* 1.00, MeOH), Ref. [27] (*R*)-1-(3-chlorophenyl)ethanone $[\alpha]_D^{20}$ = +40.4 (*c* 1.00, $CHCl_3$)}; (*S*)-**2f**, $[\alpha]_D^{20}$ = −66.49 (*c* 1.00, MeOH), Ref. [27] (*R*)-1-(4-chlorophenyl)ethanone $[\alpha]_D^{20}$ = +46.1 (*c* 1.70, $CHCl_3$)}; (*S*)-**2h**, $[\alpha]_D^{20}$ = −38.5 (*c* 1.00, MeOH), Ref. [28] (*S*)-1-phenylpropan-1-ol $[\alpha]_D^{20}$ = −45.4 (*c* 1.00, $CHCl_3$)}; (*S*)-**2k**, $[\alpha]_D^{20}$ = +9.68 (*c* 0. 05, MeOH), Ref. [28] (*R*)-2-chloro-1-phenylethanone $[\alpha]_D^{20}$ = −5.5 (*c* 1.00, $CHCl_3$)}; (*R*)-**2l**, $[\alpha]_D^{20}$ = −16.9 (*c* 0.35, MeOH), Ref. [28] (*R*)-2-bromo-1-phenylethanone $[\alpha]_D^{20}$ = −30.9 (*c* 1.00, $CHCl_3$)}.

3.2. Microorganism and Culture Conditions

The marine fungus *R. mucilaginosa* GIM 2.157 was isolated from marine sediments collected in Guangdong Province, China and deposited at the Guangdong Culture Collection Center.

The marine fungus was cultivated on medium containing 15 g glucose, 5 g peptone, 5 g yeast extract, 0.5 g disodium hydrogen phosphate, 0.5 g sodium dihydrogen phosphate, 0.5 g magnesium sulphate and 10 g sodium chloride, in 1 L distilled water, final pH 7.0. The medium was autoclaved at 115 °C for 30 min to get sterilized. A single colony was cut from the agar stock cultures and added to 1 L of medium in a 2-L Erlenmeyer flask. This culture was shaken at 28 °C for about 48 h. Then the cells were harvested by centrifugation at 4000 rpm at 4 °C for 20 min. The supernatant was discard and the cells were rinsed with a Na_2HPO_4-KH_2PO_4 buffer (100 mM, pH 7.0) and centrifuged again. The supernatant was removed and the pellets were stored at −20 °C.

3.3. Immobilization of R. mucilaginosa GIM 2.157 by Various Matrices

3.3.1. On Agar

First, 2.5 g wet cells were suspended in 2 mL distilled water and the suspensions were added to a 10-mL sterilized agar (5% *w*/*v*) solution in a 50-mL screw-capped glass vial and mixed thoroughly for 5 min. Subsequently, the mixture was poured into the plate. The mixture was allowed to solidify and yielded a solid agar layer. The solid layer was divided into blocks ($3 \times 3 \times 3$ mm^3) using a grid-cutter and then washed with distilled water and stored in phosphate buffer (pH 7, 0.1 M) at 4 °C.

3.3.2. On Calcium Alginate

First, 2.5 g wet cells were suspended in 5 mL distilled water and the suspensions were added to a 5-mL sterilized calcium alginate (40 g/L) solution in a 50-mL screw-capped glass vial, stirring thoroughly for 5 min. Subsequently, the mixture was injected dropwise into a sterilized $CaCl_2$ (4% *v*/*v*) solution with a needle. After the formation of stable bead structures, the solid layers were moved to a 20–22 °C water bath for 2 h. The spherical particles were washed thoroughly and stored in $CaCl_2$ (4%) solution at 4 °C.

3.3.3. On PVA-Alginate

First, 2.5 g wet cells were suspended in 5 mL distilled water and the suspensions were added to 5 mL calcium alginate (1% *w*/*v*) in a polyvinyl alcohol (10% *w*/*v*) solution and stirred thoroughly for 5 min in a 50-mL screw-capped glass vial. Subsequently, the mixture was injected dropwise into a sterilized $CaCl_2$ (4% *v*/*v*) solution by a needle. After the formation of stable bead structures, the solid layers were moved to a 20–22 °C water bath for 2 h. These spherical particles were washed thoroughly and stored in saturated boric acid solution at 4 °C.

3.3.4. On Chitosan

First, 2.5 g wet cells were suspended in 5 mL distilled water and the suspensions were added to a 10-mL sterilized chitosan solution (3% *w*/*v*) in acetic acid 3% *v*/*v*, with thorough stirring for 5 min in a 50-mL screw-capped glass vial. Subsequently, this mixture was dropped with the help of a syringe into an NaOH (1 M):MeOH (80:20) solution. After 30 min, the beads were washed thoroughly with distilled water. Thereafter, glutaraldehyde (1% *v*/*v*) was added and stored at 4 °C for further use.

3.4. Scanning Electron Microscopy

For the scanning electron microscopy (SEM) analysis, the surfaces of the immobilized whole cells were washed with water to remove the non-adhering support matrix. Alcohol dehydration was performed using 10%, 30%, 50%, 70%, 90% and 100% ethanol; samples contacted each alcoholic solution for 15 min. The samples were air dried at room temperature and coated with 8–10 nm of gold using argon ion sputtering with a Baltec MCS 010 model sputter. Finally, the metallization of the dehydrated samples was achieved and samples were observed at 15 kV on a Joel JMS 6480 LV computer for Scanning Electron Microscopy.

3.5. Bioconversion of Ketones with Immobilized Cells

The asymmetric catalytic reduction of ketones was performed in a 50-mL screw cap glass vial to prevent spillage of substrate or product. Shaking was performed in a heated ground-top shaker at 25 °C with 240 rpm. Approximately 4.5 g immobilized cells with agar (or with calcium alginate, PVA-alginate, chitosan) were suspended in 10 mL of Na_2HPO_4-KH_2PO_4 buffer (100 mM, pH 7.0) containing 0.5 g glucose and 10 mM of aromatic ketones (**1a**–**1n**). For the control reaction, the setup was the same but with the addition of free cells instead of immobilized cells. Reactions were performed for 24 h. For workup, the cells were discarded by filtration and 1 mL of the supernatant was saturated with NaCl, followed by extraction with 1 × 1 mL of HPLC eluent (*n*-hexane/*i*-PrOH = 95/5, *v*/*v*) with shaking for 5 min. The organic layer was combined, dried over Na_2SO_4 and measured by HPLC for yield and *ee*.

3.6. pH Profile

Reactions were performed in 10 mL buffer (100 mM) containing 10 mM 1-(2-bromophenyl) ethanone (**1a**), 4.5 g immobilized cells on agar and glucose (0.5 g) at pH values of 3.5–11 (buffers at pH 3.5 and 4.5 were prepared with citrate buffer; buffers at pH 5.5, 6.5, 7 and 7.5 were prepared with phosphate buffer; and buffers at pH 8.5, 9, 10 and 11 were prepared with Tris buffer) at 25 °C for 24 h. Afterwards, the cells were removed by filtration and 1 mL of the supernatant was saturated with NaCl, followed by extraction with 1 × 1 mL of HPLC eluent (*n*-hexane/*i*-PrOH = 95/5, *v*/*v*) with shaking for 5 min. The organic layer was combined, dried over Na_2SO_4 and measured using an HPLC to determine the yield and *ee*.

3.7. Thermostability

For thermostability studies, the immobilized cells (physiological saline) or free cells were incubated at various temperatures (30–70 °C) for 1 h, 3 h, 6 h, 12 h and 15 h before being added to the reaction. The cells were recovered, washed thoroughly with distilled water and used for the reduction of 1-(2-bromophenyl)ethanone (**1a**). Reactions were performed in 10 mL of Na_2HPO_4-KH_2PO_4 buffer (100 mM, pH 7.0) containing 10 mM of 1-(2-bromophenyl)ethanone (**1a**), 4.5 g cells immobilized on agar and glucose (0.5 g) at 25 °C for 24 h. Then, the cells were discarded by filtration and 1 mL of supernatant was saturated with NaCl, followed by extraction with 1 × 1 mL of HPLC eluent (*n*-hexane/*i*-PrOH = 95/5, *v*/*v*) with shaking for 5 min. The organic layer was combined, dried over Na_2SO_4 and measured using an HPLC to determine the yield and *ee*.

3.8. Storage Stability

To estimate their storage stability, both free and immobilized cells were stored in 100 mL physiological saline (0.85% NaCl, *w*/*v*) at 4 °C for 5, 10, 20, 25, 30 or 60 days. The cells were used to reduce 1-(2-bromophenyl)ethanone (**1a**). The reactions were performed in 10 mL of Na_2HPO_4-KH_2PO_4 buffer (100 mM, pH 7.0) containing 10 mM of 1-(2-bromophenyl)ethanone (**1a**), 4.5 g cells immobilized on agar and glucose (0.5 g) at 25 °C for 24 h. Then, the cells were discarded by filtration and 1 mL of the supernatant was saturated with NaCl followed by extraction with 1 × 1 mL of HPLC eluent (*n*-hexane/*i*-PrOH = 95/5, *v*/*v*) with shaking for 5 min. The organic layer was combined, dried over Na_2SO_4 and measured using an HPLC to determine the yield and *ee*.

3.9. Reusability

For recyclability studies, reactions were performed with substrate **1a** (10 mM) in 10 mL of Na_2HPO_4-KH_2PO_4 buffer (100 mM, pH 7.0) and 4.5 g *R. mucilaginosa* GIM 2.157 cells immobilized on agar at 25 °C for 23 h. At the end of the reaction, the cells were centrifuged at 4000 rpm for 20 min to separate them from the reaction mixture, washed with Na_2HPO_4-KH_2PO_4 buffer (100 mM, pH 7.0) and suspended in 10 mL of the same buffer containing the same substrate. The reaction mixture (1 mL of supernatant separated from cells) was saturated with NaCl and extracted with 1 mL (×2) of HPLC eluents (*n*-hexane/*i*-PrOH = 95/5, *v*/*v*) while being shaken for 5 min. The organic phases were combined, dried over Na_2SO_4 and crude samples were analyzed using HPLC to determine the yield and *ee*.

4. Conclusions

In this study, we reported the immobilization of whole mycelia of a selected strain of marine-derived *R. mucilaginosa* GIM 2.157 on agar, calcium alginate, PVA-alginate and chitosan as support matrices. The successful immobilization was confirmed by FTIR and SEM. The immobilized cells showed a potential for the asymmetric reduction of various ketones, depending on the support matrix. It was shown that agar is a highly effective material for the entrapment of *R. mucilaginosa* GIM 2.157 cells in terms of the catalytic activity of the cells for the asymmetric reduction of ketones. The cells immobilized on agar maintained activities and selectivities comparable to those of free cells. The free cells exhibited an optimum activity at pH of 7.0 and were very sensitive to alkaline or acidic environments. The cells immobilized on agar retained approximately 99% of their initial activity in the pH range 3.5–9, with a slight decrease at pH 10 and 11. The cells immobilized on agar retained >99% of their original activity after incubation for 1 h at 60 °C, while the activity of the free cells decreased to 70% after incubation for 1 h at 40 °C. The storage stability of the *R. mucilaginosa* GIM 2.157 strain was greatly enhance by immobilization on agar. The agar-immobilized cells maintained approximately 95% of their original activity after storage at 4 °C for 60 days, while the catalytic activity of free cells decreased to 82% after storage at 4 °C for 20 days and to 7% after storage at 4 °C for 60 days. The immobilized cells on agar could be reused for 6 cycles without significant loss of activity, while free cells began to lose their activity at cycle 4. As a result, the *R. mucilaginosa* GIM 2.157 cells immobilized on agar are highly practical for the enantioselective preparation of chiral alcohols.

Acknowledgments: This study was funded by the Natural Science Foundation of Guangdong Province (Grant No. 2017A030310232), the National Natural Science Foundation of China (Grant No. 41706148), the Basic Research Program of Sun Yat-Sen University (Grant No. 17lgpy58) and the National Science and Technology Major Project of the Ministry of Science and Technology of China (2018ZX09735010).

Author Contributions: Bi-Shuang Chen and Fayene Zeferino Ribeiro de Souza designed the study. Bi-Shuang Chen wrote the paper. Hui Liu and Wen-Di Duan performed the experiments. Bi-Shuang Chen and Lan Liu supervised the study. All authors made substantial contributions to the discussion of data and approved the final manuscript.

Conflicts of Interest: The authors declare no conflict of interest.

References

1. Kataoka, M.; Kita, K.; Wada, M.; Yasohara, Y.; Hasegawa, J.; Shimizu, S. Novel bioreduction system for the production of chiral alcohols. *Appl. Microbiol. Biotechnol.* **2003**, *62*, 437–445. [CrossRef] [PubMed]
2. Nealon, C.M.; Musa, M.M.; Patel, J.M.; Phillips, R.S. Controlling substrate specificity and stereospecificity of alcohol dehydrogenases. *ACS Catal.* **2015**, *2*, 2100–2114. [CrossRef]
3. Zhang, R.; Xu, Y.; Xiao, R. Redesigning alcohol dehydrogenases/reductases for more efficient biosynthesis of enantiopure isomers. *Biotechnol. Adv.* **2015**, *33*, 1671–1684. [CrossRef] [PubMed]
4. Gyarmati, J.; Hajdu, C.; Dinya, Z.; Micskei, K.; Pályi, G. Asymmetric induction by amino acid ligands in chromium(II)-assisted reduction of ketones. *J. Organomet. Chem.* **1999**, *586*, 106–109. [CrossRef]
5. Micskei, K.; Holczknecht, O.; Hajdu, C.; Patonay, T.; Marchis, V.; Meo, M.; Zucchi, C.; Pályi, G. Asymmetric synthesis of amino acids by Cr(II) complexes of natural amino acids. *J. Organomet. Chem.* **2003**, *682*, 143–148. [CrossRef]
6. Micskei, K.; Patonay, T.; Caglioti, L.; Pályi, G. Amino acid ligand chirality for enantioselective syntheses. *Chem. Biodivers.* **2010**, *7*, 1660–1669. [CrossRef] [PubMed]
7. Kroutil, W.; Mang, H.; Edegger, K.; Faber, K. Recent advances in the biocatalytic reduction of ketones and oxidation of sec-alcohols. *Curr. Opin. Chem. Biol.* **2004**, *8*, 120–126. [CrossRef] [PubMed]
8. Stefaan, M.A.; De, W.; Theo, S.; Hans, E.S.; Oliver, M. Biocatalytic reductions: From lab curiosity to "first choice". *Acc. Chem. Res.* **2007**, *40*, 1260–1266.
9. Rocha, L.C.; de Souza, A.L.; Filho, U.P.R.; Filho, S.P.C.; Sette, L.D.; Porto, A.L.M. Immobilization of marine fungi on silica gel, silica xerogel and chitosan for biocatalytic reduction of ketones. *J. Mol. Catal. B Enzym.* **2012**, *84*, 160–165. [CrossRef]
10. Chen, B.-S.; Liu, H.; de Souza, F.Z.R.; Liu, L. Organic solvent-tolerant marine microorganisms as catalysts for kinetic resolution of cyclic β-hydroxy ketones. *Mar. Biotechnol.* **2017**, *19*, 351–360. [CrossRef] [PubMed]
11. Liu, H.; de Souza, F.Z.R.; Liu, L.; Chen, B.-S. The use of marine-derived fungi for preparation of enantiomerically pure alcohols. *Appl. Microbiol. Biotechnol.* **2018**, *102*, 1317–1330. [CrossRef] [PubMed]
12. Liu, H.; Chen, B.-S.; de Souza, F.Z.R.; Liu, L. A comparative study on asymmetric reduction of ketones using the growing and resting cells of marine-derived fungi. *Mar. Drugs* **2018**, *16*, 62. [CrossRef] [PubMed]
13. Chen, X.-H.; Wang, X.-T.; Lou, W.-Y.; Li, Y.; Wu, H.; Zong, M.-H.; Smith, T.J.; Chen, X.-D. Immobilization of *Acetobacter* sp. CCTCC M209061 for efficient asymmetric reduction of ketones and biocatalyst recycling. *Microb. Cell Fact.* **2012**, *11*, 119. [CrossRef] [PubMed]
14. Lusta, K.A.; Chung, I.K.; Sul, I.W.; Park, H.S.; Shin, D.I. Immobilization of fungus *Aspergillus* sp. by a novel cryogel technique for production of extracellular hydrolytic enzymes. *Process Biochem.* **2000**, *35*, 1177–1182. [CrossRef]
15. Sanchez, S.; Demain, A.L. Enzymes and bioconversions of industrial, pharmaceutical, and biotechnological significance. *Org. Process Res.* **2011**, *15*, 224–230. [CrossRef]
16. Rocha, L.C.; Seleghim, M.H.R.; Comasseto, J.V.; Sette, L.D.; Porto, A.L.M. Stereoselective bioreduction of α-azido ketones by whole cells of marine-derived fungi. *Mar. Biotechnol.* **2015**, *17*, 736–742. [CrossRef] [PubMed]
17. Zhang, Y.W.; Prabhu, P.; Lee, J.K. Alginate immobilization of recombinant *Escherichia coli* whole cells harboring L-arabinose isomerase for L-ribulose production. *Bioprocess. Biosyst. Eng.* **2010**, *33*, 741–748. [CrossRef] [PubMed]
18. Li, G.Y.; Huang, K.L.; Jiang, Y.R.; Ding, P. Production of (*R*)-mandelic acid by immobilized cells of *Saccharomyces cerevisiae* on chitosan carrier. *Process Biochem.* **2007**, *42*, 1465–1469. [CrossRef]
19. Idris, A.; Suzana, W. Effect of calcium alginate concentration, bead diameter, initial pH and temperature on lactic acid production from pineapple waste using immobilized *Lactobacillus delbrueckii*. *Process Biochem.* **2006**, *41*, 1117–1123. [CrossRef]
20. Wang, W.; Huang, X.J.; Cao, J.D.; Lan, P.; Wu, W. Immobilization of calcium alginate sulfates on polysulfone ultrafiltration membranes for selective adsorption of low-density lipoprotein. *Acta Biomater.* **2014**, *10*, 234–243. [CrossRef] [PubMed]
21. Cheng, Y.; Lin, H.Y.; Chen, Z.; Megharaj, M.; Naidu, R. Biodegradation of crystal violet using *Burkholderia vietnamiensis* C09V immobilized on PVA–calcium alginate–kaolin gel beads. *Ecotoxiol. Environ. Saf.* **2012**, *83*, 108–114. [CrossRef] [PubMed]

22. Krajewska, B. Application of chitin- and chitosan-based materials for enzyme immobilizations: A review. *Enzyme Microb. Technol.* **2004**, *35*, 126–139. [CrossRef]
23. Nunes, M.A.P.; Vila-Real, H.; Fernandes, P.C.B.; Ribeiro, M.H.L. Immobilization of naringinase in PVA–alginate matrix using an innovative technique. *Appl. Biochem. Biotechnol.* **2010**, *160*, 2129–2147. [CrossRef] [PubMed]
24. Wu, H.; Wang, J.; Kang, X.; Wang, C.; Wang, D.; Liu, J.; Aksay, I.A.; Lin, Y. Glucose biosensor based on immobilization of glucose oxidase in platinum nanoparticles/graphene/chitosan nanocomposite film. *Talanta* **2009**, *80*, 403–406. [CrossRef] [PubMed]
25. Wu, F.C.; Tseng, R.L.; Juang, R.S. Enhanced abilities of highly swollen chitosan beads for color removal and tyrosinase immobilization. *J. Hazard. Mater.* **2001**, *81*, 167–177. [CrossRef]
26. Kumirska, J.; Czerwicka, M.; Kaczyński, Z.; Bychowska, A.; Brzozowski, K.; Thöming, J.; Stepnowski, P. Application of spectroscopic methods for structural analysis of chitin and chitosan. *Mar. Drugs* **2010**, *8*, 1567–1636. [CrossRef] [PubMed]
27. Martins, J.E.D.; Morris, D.J.; Wills, M. Asymmetric hydrogenation of ketones using Ir(III) complexes of *N*-alkyl-*N*′-tosyl-1,2-ethanediamine ligands. *Tetrahedron Lett.* **2009**, *50*, 688–692. [CrossRef]
28. Yearick, K.; Wolf, C. Catalytic enantioselective addition of diethylzinc to trifluoromethyl ketones. *Org. Lett.* **2008**, *10*, 4391.

© 2018 by the authors. Licensee MDPI, Basel, Switzerland. This article is an open access article distributed under the terms and conditions of the Creative Commons Attribution (CC BY) license (http://creativecommons.org/licenses/by/4.0/).

catalysts

MDPI

Article

Immobilization of *Enterobacter aerogenes* by a Trimeric Autotransporter Adhesin, AtaA, and Its Application to Biohydrogen Production

Hajime Nakatani †, Nan Ding †, Yuki Ohara and Katsutoshi Hori *

Department of Biomolecular Engineering, Graduate School of Engineering, Nagoya University, Furo-cho, Chikusa-ku, Nagoya 464-8603, Japan; nakatanih@chembio.nagoya-u.ac.jp (H.N.); dingnaner@aliyun.com (N.D.); ohara.yuuki@g.mbox.nagoya-u.ac.jp (Y.O.)

* Correspondence: khori@chembio.nagoya-u.ac.jp; Tel.: +81-52-789-3339

† These authors contributed equally to this work.

Received: 30 March 2018; Accepted: 13 April 2018; Published: 16 April 2018

Abstract: Biological hydrogen production by microbial cells has been extensively researched as an energy-efficient and environmentally-friendly process. In this study, we propose a fast, easy method for immobilizing *Enterobacter aerogenes* by expressing *ataA*, which encodes the adhesive protein of *Acinetobacter* sp. Tol 5. AtaA protein on the *E. aerogenes* cells carrying the *ataA* gene was demonstrated by immunoblotting and flow cytometry. The AtaA-producing cells exhibited stronger adherence and auto-agglutination characteristics than wild-type cells, and were successfully immobilized (at approximately 2.5 mg/cm^3) on polyurethane foam. Hydrogen production from the cell-immobilized polyurethane foams was monitored in repetitive batch reactions and flow reactor studies. The total hydrogen production in triple-repetitive batch reactions reached 0.6 mol/mol glucose, and the hydrogen production rate in the flow reactor was 42 mL·h^{-1}·L^{-1}. The AtaA production achieved simple and immediate immobilization of *E. aerogenes* on the foam, enabling repetitive and continuous hydrogen production. This report newly demonstrates the production of AtaA on the cell surfaces of bacterial genera other than *Acinetobacter*, and can simplify and accelerate the immobilization of whole-cell catalysts.

Keywords: hydrogen production; *Enterobacter*; immobilization; trimeric autotransporter adhesin; cell surface engineering; whole-cell catalyst; surface display

1. Introduction

Biological hydrogen production promises a less energy intensive and more environmentally friendly process than traditional processes [1,2]. Most bioprocesses occur at ambient temperatures and pressures. More importantly, they generate hydrogen from various waste biomasses, such as industrial and agricultural organic wastes and wastewaters [2–6]. Hydrogen conversion bioprocesses by heterotrophic bacteria can be classified into two types: light-dependent and light-independent. Light-dependent processes include biophotolysis by cyanobacteria and photo-fermentation by photosynthetic bacteria, which need light energy for hydrogen production [7]. These bioprocesses are disadvantaged by the requirement for lighting throughout the process and the low efficiency of the light-energy conversion. Light-independent hydrogen-production processes include microbial electrolysis [8] and dark fermentation under anaerobic conditions [9]. Dark-fermentation is the most promising of these two approaches, and has been well studied. Although several bacterial species reportedly produce hydrogen via dark-fermentation in pure culture [9], the facultative anaerobes belonging to genus *Enterobacter* are often exploited for this purpose, because they are easily grown and completely consume the residuary oxygen in the reactor before starting the hydrogen

production [10]. Mutant strains of *E. aerogenes* isolated in previous research have demonstrated high hydrogen productivity via fermentation on several substrates [5,10–12].

In most exploratory studies, bio-hydrogen production under dark fermentative conditions has been implemented by the batch-reactor method, which is simply operated and efficiently controlled. However, the development of continuous production processes is recommended for large-scale industrial operations, which must be practically and economically viable [13]. To achieve effective continuous hydrogen production, many studies have developed the cell immobilization method. Cells affixed by various immobilization strategies have been evaluated for their performance as biohydrogen producers [4,14–19]. Unlike planktonic cells, immobilized cells can be repeatedly used in continuous hydrogen production, because the stability and durability of them during the process is enhanced by the immobilization. However, conventional immobilization methods are hindered by complex processes or long startup periods, which increase the manufacturing costs of the immobilized whole-cell catalysts.

Previously, we discovered a bacterial nanofiber protein, *Acinetobacter* trimeric autotransporter adhesin (AtaA), which plays a vital role in cell adhesion and auto-agglutination of its natural producer, *Acinetobacter* sp. Tol 5 [20–25]. AtaA belongs to the protein family of trimeric autotransporter adhesins (TAAs), which participate in cell adhesion of Gram-negative pathogens to biotic materials in their host tissues [26,27]. Unlike other TAAs, AtaA mediates adhesion to various abiotic materials such as plastics, glass, and stainless steel [20,24]. Importantly, introducing the *ataA* gene induces these features in non-adhesive and non-agglutinating *Acinetobacter* species. We developed a new immobilization method for bacterial cells on the basis of a kind of physical adsorption mechanism through AtaA [28,29]. However, the immobilization of bacterial species other than *Acinetobacter* has not been reported. In this study, we demonstrate the first evidence that *E. aerogenes* beyond the *Acinetobacter* genus can be immobilized by expressing *ataA*, and that the immobilized cells can be utilized in repetitive and continuous hydrogen production. We chose polyurethane foam as a typical carrier material for microbial cells. It is light, durable, inexpensive, and easy to handle material, and is practically used for wastewater treatment [30–32].

2. Results

2.1. Production of AtaA on the Cell Surface of E. aerogenes

The *E. aerogenes* cells were transformed by conjugal transfer from *Escherichia coli* harboring pAtaA, and the transformant was analyzed for AtaA production by sodium dodecyl sulfate-polyacrylamide gel electrophoresis (SDS–PAGE) followed by immunoblotting (Figure 1A). The AtaA protein band (~300 kDa) was detected in the outer membrane fraction prepared from the transformant by immunoblotting with anti-AtaA antibody (Figure 1A). This result confirmed AtaA production by the transformant cells. Surface display of AtaA on the cell was then confirmed by immunocytostaining of the transformant cells. In the flow cytometry analysis, the fluorescent signal for AtaA on the cell surface of the transformant was clearly more positive than that of wild-type cells (Figure 1B). These data demonstrate the surface display of AtaA on *E. aerogenes*.

2.2. AtaA-Mediated Immobilization of E. aerogenes

The cell adhesion, auto-agglutination, and immobilization of the transformant were analyzed. Crystal Violet staining of the adherent cells on polystyrene (PS) plates revealed a clearly greater adhesion of the *E. aerogenes* transformant than the wild-type (photographs in Figure 2A, inset). Quantitatively, the cell adhesion was 19 times higher in the transformant than the wild-type cells (Figure 2A). Auto-agglutination of the transformant cells was then observed by tube-settling assay. The transformant sank faster than the wild-type cells, and approximately 40–50% of the transformant cells were sedimented in 3 h (Figure 2B). These data demonstrate that *E. aerogenes* acquired adhesive and auto-agglutinative properties by expressing *ataA*.

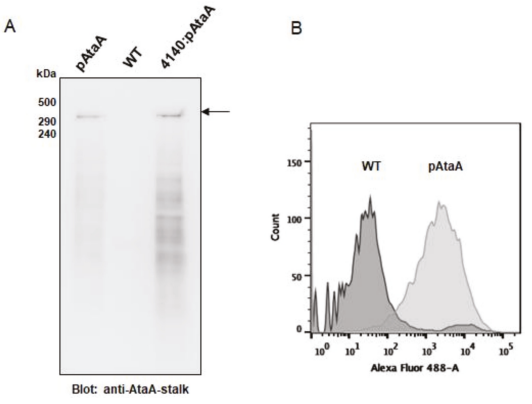

Figure 1. Expression and production of AtaA in *Enterobacter aerogenes* IAM1183. (**A**) Immunoblotting of outer membrane proteins prepared from the wild-type *E. aerogenes* IAM1183 (middle lane) and the cells transformed with the pAtaA construct (left lane) or Tol 5 4140::pAtaA (positive control, right lane). Arrow points to the detected band of the full-length AtaA protein. (**B**) Flow cytometry analysis for confirming surface display of AtaA on the transformant.

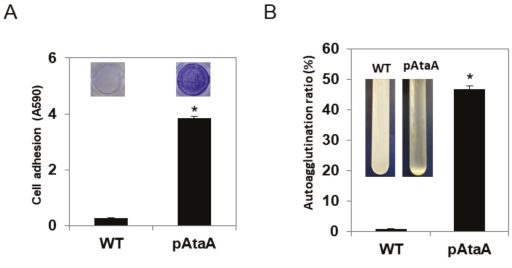

Figure 2. Adherence and auto-agglutination assay of *Enterobacter aerogenes*-expressing *ataA*. (**A**) A cell suspension was placed on the polystyrene plate, and the cells adhering to the bottom of a 48-well were stained with Crystal Violet (photographs, inset). Adherent cells were quantified by measuring the Crystal Violet absorbance at 590 nm. (**B**) The sediment of the transformant at the bottom of the test tube was observed after settling for 3 h (photographs, inset), and the auto-agglutination ratio was calculated from the OD_{600} decrease in the upper segment of the cell suspension. Data are the mean ± SD of three independent measurements. Significant differences between the data (student *t*-test, $p < 0.01$) are marked with asterisk (*).

We next attempted instant and direct immobilization of *ataA*-expressing *E. aerogenes* on polyurethane foams, as previously demonstrated by *ataA*-expressing *Acinetobacter* [28]. We first optimized conditions for AtaA-mediated immobilization of *E. aerogenes* cells onto the polyurethane foam, and found the suitable conditions; the cells were suspended in BS-N medium to 4.0 of OD_{600}, shaken in the presence of polyurethane foams at 115 rpm at 30 °C for 2 h. After merely shaking the polyurethane foams and a cell suspension of the transformant cells in a flask for 2 h, the turbidity was decreased (Figure 3A), and the immobilized cell density on polyurethane foams was approximately 5 times higher than that of the planktonic cells (Figure 3B). The immobilized cell concentration in the polyurethane foams reached 2.5 g-dry cell weight (DCW)/L-medium. The loading capacity of the polyurethane foams was calculated to be 80 mg-DCW/g-foam. In contrast, the wild-type cells were not immobilized by shaking with polyurethane foams in a flask; after 2 h, the cell density on polyurethane foams was lower than that of the cells that remained in the planktonic state (Figure 3B).

The result clearly showed that *ataA* expression enhances the immobilization of *E. aerogenes* on the polyurethane foam.

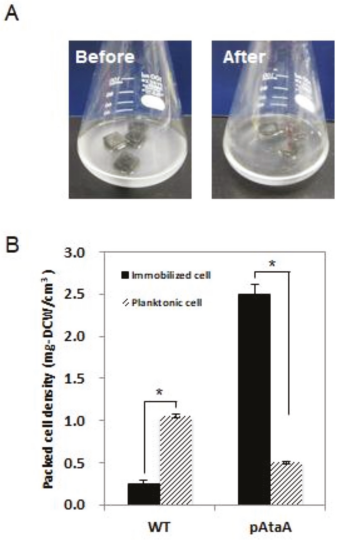

Figure 3. Immobilization of *ataA*-expressing *E. aerogenes* on polyurethane foams. A cell suspension of the transformant was shaken with polyurethane foams in the flask. (**A**) A clear suspension was observed after 2 h of shaking. (**B**) Immobilized cells were detached from the 4 pieces of polyurethane foams, and the cells were freeze-dried for dry cell weight (DCW) measurements. The DCW of the remaining cells in the 20 mL of suspension was also measured. Dry cell densities packed in the unit volume were calculated. Data are the mean ± SD of three independent studies. Significant differences between the data (student *t*-test, $p < 0.01$) are marked with an asterisk (*).

2.3. Repetitive and Continuous Hydrogen Production by Immobilized E. aerogenes

Figure 4A describes batch-mode repetitive hydrogen production utilizing immobilized *E. aerogenes* on polyurethane foams. The processes was performed under the restriction of a nitrogen source (0.02 g/L $(NH_4)_2SO_4$) to prevent cell growth during the reaction. The glucose consumption and hydrogen production in the batch reactor were measured during each reaction (Figure 4B).

When most of the glucose was consumed, the cell-immobilized polyurethane foams were transferred to new reaction medium for the next hydrogen production. At least three batch reactions were completed by the cell-immobilized polyurethane foams, whereas the polyurethane foams shaken with wild-type cells were unavailable for repetitive hydrogen production because an insufficient quantity of the cells was immobilized on the carrier (Figures 3B and 4B). Batches 1, 2, and 3 of the transformant-adhered foams yielded approximately 0.4, 0.6, and 0.4 mol/mol glucose of hydrogen, respectively.

Finally, we constructed a flow reactor for hydrogen production (Figure 5A) and measured the hydrogen production during continuous culture. The transformants immobilized on the polyurethane foams or cultured under planktonic conditions (without polyurethane foams) were loaded into the reactor. These processes were also performed under the restriction of a nitrogen source. Hydrogen production by the immobilized cells continued for at least 30 h, and the hydrogen production rate from 5 to 30 h was 42 $mL \cdot h^{-1} \cdot L^{-1}$. In contrast, hydrogen was hardly produced in the planktonic condition, because the cells were washed out (Figure 5B). These data suggest that AtaA-mediated immobilization is tenacious enough to enable continuous hydrogen production in the flow reactor.

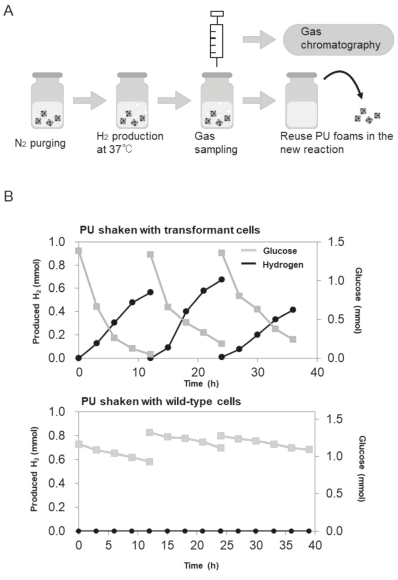

Figure 4. Repetitive hydrogen production by immobilized *E. aerogenes* in batch reactions. (**A**) Repetitive batch reactions utilizing polyurethane foams shaken with the transformant or wild-type cells; (**B**) hydrogen yields (black) and glucose consumptions (gray) measured during the three repetitive batches.

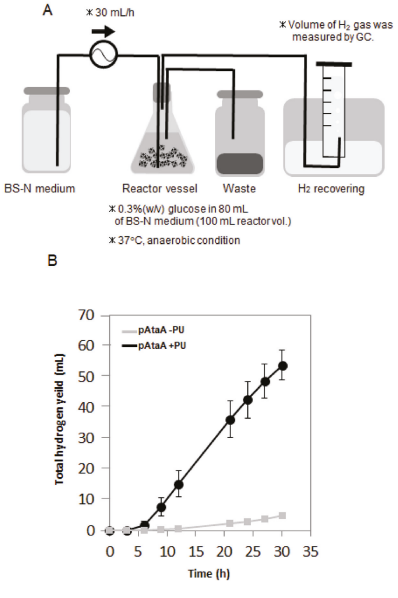

Figure 5. Continuous hydrogen production by immobilized *E. aerogenes* in a flow reactor. The flow reactor was inoculated with immobilized or planktonic cells. (**A**) Measurement procedure of hydrogen yields during the reactions. (**B**) Hydrogen yield versus time in the flow reactor with immobilized-cells on polyurethane (pAtaA +PU: black) and with the planktonic-cell (pAtaA -U: gray). Data are the mean ± SD of three independent studies.

3. Discussion

We achieved simple and immediate immobilization of *E. aerogenes* cells by introducing *ataA* gene. The immobilized bacterial cells were successfully applied in repetitive and continuous hydrogen production.

In previous studies, we demonstrated the heterologous cell-surface production of AtaA in *Acinetobacter baylyi* ADP1 and sp. ST550 [28,29], but whether heterologous hosts outside the genus *Acinetobacter* can produce AtaA was not investigated. In this report, we newly demonstrate that AtaA can be produced on the surface of another genus, *Enterobacter*. This implies that AtaA-mediated bacterial cell immobilization [28,29] is achievable in broader hosts.

To realize large-scale hydrogen production, continuous/repetitive production processes are recommended [13]. Immobilized whole-cell catalysts enable continuous and efficient bioprocessing by maintaining a sufficient cell density in the reactor. Hydrogen-producing microbes are usually immobilized by the gel or resin embedding method using alginate or polyvinyl alcohol (PVA) [14,18]. However, this method requires additional gelling and molding processes after mixing the bacteria and gelling agent. Direct immobilization through bacterial biofilm formation has also been reported in previous *Enterobacter* studies, but these approaches require a long startup period; biofilm formation on a support ranges from 20 h to over 14 days [4,17]. For hydrogen production, AtaA-mediated immobilization offers several advantages over conventional immobilization methods: (1) wide-variety of carrier availability, (2) rapid and tenacious immobilization, and (3) direct immobilization on the surfaces of materials [24,28,29]. Moreover, we recently showed that whole-cell catalysts expressing AtaA can be reversibly immobilized on a carrier, enabling the reuse of bacterial cells and supports [33]. This feature is hardly realized in direct immobilization through biofilm formation. The immobilized-cells by AtaA are hardly detached in buffer solution, while they are easily detached in pure water [33]. In this study, the results shown in Figure 5 suggest that the cells on polyurethane were maintained during the continuous reaction over 30 h without leaching, because the reaction rate did not reduce. Taken together, these considerations imply that the AtaA-based method can improve the cell immobilization process for whole-cell catalyst production, and would likely reduce the production cost of biohydrogen.

We demonstrated that the transformant cells maintained their hydrogen-production ability after displaying AtaA on their surfaces; moreover, the immobilized cells were sufficiently robust to withstand several repeats of the reaction, as well as continuous reaction (Figures 4 and 5). Our results suggest that AtaA-mediated immobilization of *E. aerogenes* caused no serious damage to the cell. *E. aerogenes* produces hydrogen from glucose through several metabolic pathways [9], which can be circulated only if the immobilized cells remain viable. Overexpression of membrane proteins such as AtaA is commonly considered to become toxic, because the excessively produced proteins disrupt the bacterial membrane structures [34–36]. In our previous report, we unexpectedly found that immobilization of bacteria by surface production of AtaA causes no damage to the cells [33]. Moreover, the over expression of *ataA* did not seem to affect severely on *E. aerogenes*'s growth. In fact, we could prepare the cells producing AtaA at a high cell density (OD_{600} = 4.0) for immobilization. These features are useful for immobilizing *E. aerogenes* and other hydrogen-producing Gram-negative bacteria. In the third batch reaction with cell-immobilized polyurethane, however, slight reduction of hydrogen production was observed (Figure 4). Because we restricted a nitrogen source during hydrogen production to prevent cell growth, the resting cells immobilized might gradually have lost their activities during the repetitive reaction.

The hydrogen production in each batch of the triple batch reactions was 0.4–0.6 mol/mol glucose, and the hydrogen production rate in the flow reactor was 42 $mL \cdot h^{-1} \cdot L^{-1}$. These values are unremarkable when compared with those of pure *Enterobacter* spp. cultures in previous laboratory studies [4,17,37–39]. Table 1 summarizes our results with previously reported studies utilizing immobilized *Enterobacter* for hydrogen production. However, a proper comparison between the present and previous results is difficult, because the experimental conditions such as reactor types, bacterial

strains used, and operation systems are different among the studies. To further increase the hydrogen yield in our system, it is necessary to increase the immobilized-cell mass by examining carriers, design a sophisticated reactor, and optimize operating conditions for hydrogen production. The selection of bacterial strain and implement metabolic engineering of the cells is also important [40–42]. Combining our new simple method for microbial immobilization with knowledge from previous studies would develop a practical biohydrogen production process with high performance.

Table 1. Comparison of hydrogen production with immobilized *Enterobacter* spp.

Biocatalyst	Immobilization Method	Reactor Type	Feed Stock	Production Rate	Conversion Rate	Advantage/ Disadvantage	Reference
Enterobacter aerogenes IAM1183	Adhesion of AtaA protein on polyurethane foam	CSTR in Erlenmeyer flask	Glucose	42 mL·h^{-1}·L^{-1} (1.87 mmol·h^{-1}·L^{-1})	0.6 mol/mol glucose (Batch)	Immediate and direct immobilization (2–3 h)/ Low production rate	This study
Enterobacter aerogenes ATCC 13048	Gel entrupment in alginate gel	Packed-bed tubular column reactor	Glucose	n/d	9.44 mmol/g glucose (1.7 mol/mol glucose)	High conversion rate/ Complex immobilization processes	[37]
Enterobacter aerogenes HO-39	Adsorptionon porous glass beads	Packed-bed column reactor	Glucose	850 mL·h^{-1}·L^{-1} (37 mmol·h^{-1}·L^{-1})	0.73 mol/mol glucose	High production rate/ complex immobilization processes	[38]
Enterobacter cloacae IIT-BT 08	Biofilm formation on Lignocellulosic agroresidues	Packed-bed reactor	Glucose	75.6 mmol·h^{-1}·L^{-1}	n/d	High production rate/ Long setup time (20 h)	[4]
Enterobacter aerogenes NCIMB 10102	Biofilm formation on synthetic sponge	Packed-bed column reactor	Glucose	10.2 mmol·h^{-1}·L^{-1}	1.36 to 3.02 mmol/mmol glucose	High production and conversion rate/ Long setup time	[39]
Enterobacter aerogenes E.82005	Biofilm formation on polyurethane foam	Hand-made fermenter	Molasses from a sugar refinery	13 mmol·h^{-1}·L-culture^{-1}	1.5–3.5 mol/mol sugar	High production and conversion rate/ Long setup time (14 days)	[17]

n/d: Not determined.

4. Materials and Methods

4.1. Materials

Luria-Bertani (LB) medium was purchased from Nakarai Tesque (Kyoto, Japan). Glucose, anmonium sulfate, ampicillin, and gentamicin were purchased from Fujifilm Wako Pure Chemical Corp. (Osaka, Japan). Polyurethane foam (CFH-40) was given from Inoac Corp. (Nagoya, Japan). N_2 gas and argon gas were purchased from Sogo Kariya Sanso (Nagoya, Japan).

4.2. Plasmid Construct, Bacterial Strains, and Culture Conditions

The plasmid construct, pAtaA [19], was used for *ataA* gene expression in *E. aerogenes*.

The bacterial strains used were *E. aerogenes* IAM1183, its transformant harboring pAtaA, and a ΔAtaA mutant of *Acinetobacter* sp. Tol 5 harboring pAtaA (Tol 5 4140::pAtaA) [43]. Cells of all strains were grown aerobically in New Brunswick Scientific (NBS) mineral salts medium or Luria-Bertani (LB) medium at 30 °C with shaking. To cultivate the transformant cells, the antibiotics ampicillin (100 μg/mL) and gentamicin (10 μg/mL) were added to the growth media. To induce *ataA* expression on the plasmid construct, 0.5% (*w*/*v*) arabinose was added to the NBS medium. After transferring the seed culture to the induction medium, AtaA production on the cells was promoted by incubation for 12 h at 30 °C.

4.3. Transformation of E. aerogenes and Isolation of the Transformants

Enterobacter aerogenes was transformed by conjugal transfer as previously described [20], with slight modification of the transformant selection processes. The chemically competent cells of *Escherichi coli* S17-1 strain [44] were transformed with pAtaA, which was passed by conjugal transfer to *E. aerogenes*. The transformants obtained by conjugal transfer were selected by the color change of the medium on Shimon's citrate agar plates [45] supplemented with ampicillin and gentamicin.

4.4. Analysis of AtaA Production by E. aerogenes Transformants

To confirm AtaA production on the outer membranes of the transformants, the bacterial cells were collected from liquid culture, and the proteins on their outer membranes were extracted, separated by SDS–PAGE, and immunoblotted with anti-$AtaA_{699\text{-}1014}$ antibody [20]. The production of AtaA on the cells was then confirmed by flow cytometry. The extraction, immunoblotting, and flow cytometry procedures were described previously [20]. The data were obtained by a FACSCanto II flow cytometer (BD biosciences, San Jose, CA, USA), and were further analyzed by comparing their fluorescence intensities using FlowJo software (TOMY digital biology, Tokyo, Japan).

Adherence and tube-settling assays of the transformant were performed as previously described [24], with slight modifications. Bacterial cell suspensions in BS-N medium (prepared at OD_{600} = 4.0) were injected into the wells of a 48-well PS plate or test tubes as described previously [24].

4.5. Cell Immobilization on Polyurethane

To check the immobilization of resting cells, *E. aerogenes* and its transformant were prepared as previously described [28]. A bacterial cell suspension (grown to OD_{600} = 4.0) was transferred to a 100-mL Erlenmeyer flask containing polyurethane foams with a specific surface area of 50 cm^2/cm^3 (1 cm^3 cubes). The cells were immobilized on the polyurethane foams by incubating the flask at 30 °C with shaking at 115 rpm for 2 h in 20 mL of BS-N medium as previously described [28].

The DCW of the immobilized cell mass was quantified as described previously [28]. The packed cell density was calculated by dividing the immobilized cell mass (i.e., the DCW) by the immobilzation support volume, which was calculated as described previously [28].

4.6. Hydrogen Production by the Immobilized Cells

Repetitive hydrogen production in the batch reactor was started by adding 20 pieces of the polyurethane foams holding the immobilized cells to 30 mL of BS-N medium supplemented with 0.5% glucose and 0.02 g/L $(NH_4)_2SO_4$ in a sealed vial. The head-space gas was switched to N_2, and the vial was incubated at 37 °C. During the incubation, the gases produced were collected by a gass-tight syringe, and their hydrogen content was measured by gas chromatography at designated time intervals (0, 3, 6, 8, 12, 15, 18, 21, 27, 30, 33, and 36 h). The glucose concentration in the reaction medium was measured by a Glucose CII-Test Wako kit (Wako, Osaka, Japan) following the manufacturer's instructions. At the end of every batch reaction (i.e., after 12 and 24 h operation), carrier pieces were collected from the vial, washed in 300 mL BS-N medium for 5 min, dewatered on a paper towel for 2 min, and transferred to the new reaction medium in the new vial for the next reaction.

Hydrogen production by the *ataA*-expressing cells in the flow reactor was started by loading the immobilized cells (50 pieces of polyurethane foam) or planktonic cells into a 100 mL Erlenmeyer flask containing 80 mL of BS-N medium was supplemented with 0.3% (*w*/*v*) glucose and 0.02 g/L $(NH_4)_2SO_4$. The air in the head space of the flask was purged by filling with N_2 gas. Fresh medium was supplied through an inlet line in the flask at a flow rate of 30 mL/h. At the same time, the spent medium in the flask was expelled through an outlet line at the same flow rate. The gas produced was collected by the downward displacement of water through the sampling line.

4.7. Quantification of H_2 Production by Gas Chromatography Coupled to a Thermal Conductivity Detector (GC–TCD)

The produced H_2 was quantified by gas chromatography (CG) (GC-2014; Shimadzu, Kyoto, Japan) equipped with a thermal conductivity detector (TCD) and a SHINCARBON-ST packed column (4.0 m × 3.0 mm ϕ, Shinwakako; Kyoto, Japan). The TCD was set to 150 °C. The recovered gas was injected into the GC–TCD. The carrier gas was argon flowing at 25 mL/min. The GC operating program was run in isocratic mode at 40 °C for 12 min. The H_2 peak was detected at a retention time of 3.3 min. The H_2 production was calculated from the peak area.

Acknowledgments: This work was supported by a Strategic International Research Cooperative Program from JST. We thank Leonie Pipe, PhD, from Edanz Group (www.edanzediting.com/ac) for editing a draft of this manuscript.

Author Contributions: K.H., H.N., and Y.O. designed the study, and H.N. and K.H. wrote the paper. N.D. obtained the transformant cells, analyzed the cells by flow cytometry, and measured the hydrogen production. Y.O. conducted the SDS–PAGE and immunoblotting. N.D., H.N., and Y.O. analyzed the data. All authors reviewed the manuscript.

Conflicts of Interest: The authors declare that they have no conflicts of interest with the contents of this article.

References

1. Mudhoo, A.; Forster-Carneiro, T.; Sánchez, A. Biohydrogen production and bioprocess enhancement: A review. *Crit. Rev. Biotechnol.* **2011**, *31*, 250–263. [CrossRef] [PubMed]
2. Kalinci, Y.; Hepbasli, A.; Dincer, I. Biomass-based hydrogen production: A review and analysis. *Int. J. Hydrog. Energy* **2009**, *34*, 8799–8817. [CrossRef]
3. Fang, H.H.P.; Liu, H.; Zhang, T. Bio-hydrogen production from wastewater. *Water Sci. Technol. Water Supply* **2004**, *4*, 77–85.
4. Kumar, N.; Das, D. Continuous hydrogen production by immobilized *Enterobacter cloacae* IIT-BT 08 using lignocellulosic materials as solid matrices. *Enzyme Microb. Technol.* **2001**, *29*, 280–287. [CrossRef]
5. Tanisho, S.; Ishiwata, Y. Continuous hydrogen production from molasses by the bacterium *Enterobacter aerogenes*. *Int. J. Hydrog. Energy* **1994**, *19*, 807–812. [CrossRef]
6. Xu, Y.; Jiang, Y.; Chen, Y.; Zhu, S.; Shen, S. Hydrogen production and wastewater treatment in a microbial electrolysis cell with a biocathode. *Water Environ. Res.* **2014**, *86*, 649–653. [CrossRef] [PubMed]
7. Miyake, J. Hydrogen Production Using Photosynthetic Bacteria. In *Microbial Production*; Anazawa, H., Shimizu, S., Eds.; Springer: Tokyo, Japan, 2014; pp. 263–281, ISBN 978-4-431-54606-1.
8. Logan, B.E.; Call, D.; Cheng, S.; Hamelers, H.V.; Sleutels, T.H.; Jeremiasse, A.W.; Rozendal, R.A. Microbial electrolysis cells for high yield hydrogen gas production from organic matter. *Environ. Sci. Technol.* **2008**, *42*, 8630–8640. [CrossRef] [PubMed]
9. Lee, D.-J.; Show, K.-Y.; Su, A. Dark fermentation on biohydrogen production: Pure culture. *Bioresour. Technol.* **2011**, *102*, 8393–8402. [CrossRef] [PubMed]
10. Tanisho, S.; Wakao, N.; Kosako, Y. Biological hydrogen production by *Enterobacter aerogenes*. *J. Chem. Eng. Jpn.* **1983**, *16*, 529–530. [CrossRef]
11. Ito, T.; Nakashimada, Y.; Kakizono, T.; Nishio, N. High-yield production of hydrogen by *Enterobacter aerogenes* mutants with decreased a-acetolactate synthase activity. *J. Biosci. Bioeng.* **2004**, *97*, 227–232. [CrossRef]
12. Ren, Y.; Wang, J.; Liu, Z.; Ren, Y.; Li, G. Hydrogen production from the monomeric sugars hydrolyzed from hemicellulose by *Enterobacter aerogenes*. *Renew. Energy* **2009**, *34*, 2774–2779. [CrossRef]
13. Argun, H.; Kargi, F. Bio-hydrogen production by different operational modes of dark and photo-fermentation: An overview. *Int. J. Hydrog. Energy* **2011**, *36*, 7443–7459. [CrossRef]
14. Bagai, R.; Madamwar, D. Prolonged evolution of photohydrogen by intermittent supply of nitrogen using a combined system of *Phormidium valderianum*, *Halobacterium halobium*, and *Escherichia coli*. *Int. J. Hydrog. Energy* **1998**, *23*, 545–550. [CrossRef]
15. Chang, J.-S.; Lee, K.-S.; Lin, P.-J. Biohydrogen production with fixed-bed bioreactors. *Int. J. Hydrog. Energy* **2002**, *27*, 1167–1174. [CrossRef]

16. Liu, Z.D.; Lv, F.X.; Zheng, H.; Zhang, C.; Wei, F.; Xing, X.H. Enhanced hydrogen production in a UASB reactor by retaining microbial consortium onto carbon nanotubes (CNTs). *Int. J. Hydrog. Energy* **2012**, *37*, 10619–10626. [CrossRef]
17. Tanisho, S.; Ishiwata, Y. Continuous hydrogen production from molasses by fermentation using urethane foam as a support of flocks. *Int. J. Hydrog. Energy* **1995**, *20*, 541–545. [CrossRef]
18. Wu, S.-Y.; Lin, C.-N.; Chang, J.-S.; Lee, K.-S.; Lin, P.-J. Microbial hydrogen production with immobilized sewage sludge. *Biotechnol. Prog.* **2002**, *18*, 921–926. [CrossRef] [PubMed]
19. Yokoi, H.; Maeda, Y.; Hirose, J.; Hayashi, S.; Takasaki, Y. H_2 production by immobilized cells of *Clostridium butyricum* on porous glass beads. *Biotechnol. Tech.* **1997**, *11*, 431–433. [CrossRef]
20. Ishikawa, M.; Nakatani, H.; Hori, K. AtaA, a new member of the trimeric autotransporter adhesins from *Acinetobacter* sp. Tol 5 mediating high adhesiveness to various abiotic surfaces. *PLoS ONE* **2012**, *7*, e48830. [CrossRef] [PubMed]
21. Hori, K.; Yamashita, S.; Ishii, S.; Kitagawa, M.; Tanji, Y.; Unno, H. Isolation, characterization and application to off-gas treatment of toluene-degrading bacteria. *J. Chem. Eng. Jpn.* **2001**, *34*, 1120–1126. [CrossRef]
22. Hori, K.; Ishikawa, M.; Yamada, M.; Higuchi, A.; Ishikawa, Y.; Ebi, H. Production of peritrichate bacterionanofibers and their proteinaceous components by *Acinetobacter* sp. Tol 5 cells affected by growth substrates. *J. Biosci. Bioeng.* **2011**, *111*, 31–36. [CrossRef] [PubMed]
23. Ishii, S.; Unno, H.; Miyata, S.; Hori, K. Effect of cell appendages on the adhesion properties of a highly adhesive bacterium, *Acinetobacter* sp. Tol 5. *Biosci. Biotechnol. Biochem.* **2006**, *70*, 2635–2640. [CrossRef] [PubMed]
24. Ishikawa, M.; Shigemori, K.; Suzuki, A.; Hori, K. Evaluation of adhesiveness of *Acinetobacter* sp. Tol 5 to abiotic surfaces. *J. Biosci. Bioeng.* **2012**, *113*, 719–725. [CrossRef] [PubMed]
25. Ishii, S.; Koki, J.; Unno, H.; Hori, K. Two morphological types of cell appendages on a strongly adhesive bacterium, *Acinetobacter* sp. Strain Tol 5. *Appl. Environ. Microbiol.* **2004**, *70*, 5026–5029. [CrossRef] [PubMed]
26. Hoiczyk, E.; Roggenkamp, A.; Reichenbecher, M.; Lupas, A.; Heesemann, J. Structure and sequence analysis of *Yersinia* YadA and *Moraxella* UspAs reveal a novel class of adhesins. *EMBO J.* **2000**, *19*, 5989–5999. [CrossRef] [PubMed]
27. Linke, D.; Riess, T.; Autenrieth, I.B.; Lupas, A.; Kempf, V.A.J. Trimeric autotransporter adhesins: Variable structure, common function. *Trends Microbiol.* **2006**, *14*, 264–270. [CrossRef] [PubMed]
28. Hori, K.; Ohara, Y.; Ishikawa, M.; Nakatani, H. Effectiveness of direct immobilization of bacterial cells onto material surfaces using the bacterionanofiber protein AtaA. *Appl. Microbiol. Biotechnol.* **2015**, *99*, 5025–5032. [CrossRef] [PubMed]
29. Ishikawa, M.; Shigemori, K.; Hori, K. Application of the adhesive bacterionanofiber AtaA to a novel microbial immobilization method for the production of indigo as a model chemical. *Biotechnol. Bioeng.* **2014**, *111*, 16–24. [CrossRef] [PubMed]
30. Xing, X.H.; Jun, B.H.; Yanagida, M.; Tanji, Y.; Unno, H. Effect of C/N values on microbial simultaneous removal of carbonaceous and nitrogenous substances in wastewater by single continuous-flow fluidized-bed bioreactor containing porous carrier particles. *Biochem. Eng. J.* **2000**, *5*, 29–37. [CrossRef]
31. Guo, W.; Ngo, H.-H.; Dharmawan, F.; Palmer, C.G. Roles of polyurethane foam in aerobic moving and fixed bed bioreactors. *Bioresour. Technol.* **2010**, *101*, 1435–1439. [CrossRef] [PubMed]
32. Feng, Q.; Wang, Y.; Wang, T.; Zheng, H.; Chu, L.; Zhang, C.; Chen, H.; Kong, X.; Xing, X.-H. Effects of packing rates of cubic-shaped polyurethane foam carriers on the microbial community and the removal of organics and nitrogen in moving bed biofilm reactors. *Bioresour. Technol.* **2012**, *117*, 201–207. [CrossRef] [PubMed]
33. Yoshimoto, S.; Ohara, Y.; Nakatani, H.; Hori, K. Reversible bacterial immobilization based on the salt-dependent adhesion of the bacterionanofiber protein AtaA. *Microb. Cell Fact.* **2017**, *16*. [CrossRef] [PubMed]
34. Thai, K.; Choi, J.; Franzin, C.M.; Marassi, F.M. Bcl-xl as a fusion protein for the high-level expression of membrane-associated proteins. *Protein Sci.* **2005**, *14*, 948–955. [CrossRef] [PubMed]
35. Diefenderfer, C.; Lee, J.; Mlyanarski, S.; Guo, Y.; Glover, K.J. Reliable expression and purification of highly insoluble transmembrane domains. *Anal. Biochem.* **2009**, *384*, 274–278. [CrossRef] [PubMed]
36. Laage, R.; Langosch, D. Strategies for prokaryotic expression of eukaryotic membrane proteins. *Traffic* **2001**, *2*, 99–104. [CrossRef] [PubMed]

37. Satar, I.; Ghasemi, M.; Aljlil, S.A.; Isahak, W.N.R.W.; Abdalla, A.M.; Alam, J.; Daud, W.R.W.; Yarmo, M.A.; Akbarzadeh, O. Production of hydrogen by *Enterobacter aerogenes* in an immobilized cell reactor. *Int. J. Hydrog. Energy* **2017**, *42*, 9024–9030. [CrossRef]
38. Yokoi, H.; Tokushige, T.; Hirose, J.; Hayashi, S.; Takasaki, Y. Hydrogen production by immobilized cells of aciduric *Enterobacter aerogenes* strain HO-39. *J. Ferment. Bioeng.* **1997**, *83*, 481–484. [CrossRef]
39. Palazzi, E.; Fabiano, B.; Perego, P. Process development of continuous hydrogen production by *Enterobacter aerogenes* in a packed column reactor. *Bioprocess Eng.* **2000**, *22*, 205–213. [CrossRef]
40. Lu, Y.; Lai, Q.; Zhang, C.; Zhao, H.; Xing, X.-H. Alteration of energy metabolism in *Enterobacter aerogenes* by external addition of pyrophosphates and overexpression of polyphosphate kinase for enhanced hydrogen production. *J. Chem. Technol. Biotechnol.* **2012**, *87*, 996–1003. [CrossRef]
41. Zhang, C.; Lv, F.-X.; Xing, X.-H. Bioengineering of the *Enterobacter aerogenes* strain for biohydrogen production. *Bioresour. Technol.* **2011**, *102*, 8344–8349. [CrossRef] [PubMed]
42. Goyal, Y.; Kumar, M.; Gayen, K. Metabolic engineering for enhanced hydrogen production: A review. *Can. J. Microbiol.* **2012**, *59*, 59–78. [CrossRef] [PubMed]
43. Ishikawa, M.; Hori, K. A new simple method for introducing an unmarked mutation into a large gene of non-competent gram-negative bacteria by FLP/FRT recombination. *BMC Microbiol.* **2013**, *13*, 86. [CrossRef] [PubMed]
44. Simon, R.; Priefer, U.; Pühler, A. A broad host range mobilization system for in vivo genetic engineering: Transposon mutagenesis in gram negative bacteria. *Nat. Biotechnol.* **1983**, *1*, 784–791. [CrossRef]
45. Simmons, J.S. A culture medium for differentiating organisms of typhoid-colon aerogenes groups and for isolation of certain fungi. *J. Infect. Dis.* **1926**, *39*, 209–214. [CrossRef]

© 2018 by the authors. Licensee MDPI, Basel, Switzerland. This article is an open access article distributed under the terms and conditions of the Creative Commons Attribution (CC BY) license (http://creativecommons.org/licenses/by/4.0/).

catalysts

MDPI

Article

Co-Immobilization of Ketoreductase and Glucose Dehydrogenase

Tatiana Petrovičová [1], Kristína Markošová [1], Zuzana Hegyi [1], Ioulia Smonou [2], Michal Rosenberg [1] and Martin Rebroš [1,*]

[1] Institute of Biotechnology, Faculty of Chemical and Food Technology, Slovak University of Technology, Radlinského 9, 812 37 Bratislava, Slovakia; tatiana.petrovicova@stuba.sk (T.P.); xmarkosova@stuba.sk (K.M.); zuzana.hegyi@stuba.sk (Z.H.); michal.rosenberg@stuba.sk (M.R.)

[2] Department of Chemistry, University of Crete, Heraklion 71003, Greece; smonou@uoc.gr

* Correspondence: martin.rebros@stuba.sk; Tel.: +421-2-59-325-480

Received: 29 March 2018; Accepted: 18 April 2018; Published: 20 April 2018

Abstract: A two-enzyme system composed of immobilized ketoreductase (*Hansenula polymorpha*) and glucose dehydrogenase (*Bacillus megaterium*) was developed for the asymmetric reduction of keto esters to optically active hydroxy esters via immobilization in polyvinyl alcohol (PVA) gel particles. The concentration of enzymes was optimized, and the final particles were used 18 times in a row in a batch mode to achieve minimal loss of activity and complete conversion of the model substrate, β-ketoester ethyl-2-methylacetoacetate. Excellent stability was also achieved using new storage conditions of PVA particles, with 80% of activity being retained after almost 10 months.

Keywords: ketoreductase; co-immobilization; PVA gel

1. Introduction

Ketoreductases (KREDs) are powerful tools for the asymmetric reduction of ketone substrates to optically active alcohols, which are useful chiral building blocks in chemical and pharmaceutical industries [1]. Numerous potentially interesting substrates were tested, including aryl γ,δ-unsaturated-β-ketoesters [2], various substituted β-ketoesters [3–6], diaryl ketones [7], and bicyclic ketones [8]. All KREDs require a reduced cofactor NAD(P)H, which increases the cost of their application. Therefore, cofactor recycling systems were applied to overcome this problem [9]. One of the well-established systems consists of glucose dehydrogenase (GDH)/glucose.

Despite the many advantages of and recent successes in biocatalysis, the use of enzymes is often hampered by a lack of long-term operational stability due to low-substrate solubility in the aqueous reaction system, poor enzyme stability in commonly-used organic solvents, and difficulties in recovering and reusing the enzyme. Enzyme immobilization provides an attractive approach to overcoming these drawbacks [1]; however, the immobilization of KREDs remains challenging and only a few examples have been reported. For example, one system used nonporous glass as a support for the KRED and was used in a continuous gas-phase reactor [10]. Another system used covalent binding of KRED on resin EC-HFA, which was applied in both batch mode and flow reactor mode [1]. KRED and GDH were also separately immobilized on aldehyde-activated agarose and used in a flow reactor to perform stereoselective ketone reduction [11]. Combined cross-linked enzyme aggregates (combi-CLEAs) of KRED and GDH were used for repeated conversions of ethyl 4-chloro-3-oxobutanoate (COBE). The system retained 70% of its activity after 10 cycles in aqueous system probably because of relatively weaker bond between enzyme molecules [12].

LentiKats® is an entrapment technology that has been applied for the immobilization of whole cells and enzymes [13–21]. Its lens-shaped capsules are made of polyvinyl alcohol gel which offers several advantages such as low matrix costs, inexpensive and simple gel preparation, low diffusion

limits, etc. [13]; however, the co-immobilization of redox enzymes linked with cofactor regeneration have not been studied to date. Scale-up process of immobilization into PVA gel is also possible and was reviewed recently [22].

This article reports the optimization and application of co-entrapped KRED and GDH in a PVA gel.

2. Results and Discussion

2.1. KRED and GDH Expression and Purification

The KRED gene from *H. polymorpha* was first sequenced and cloned by Hanson et al. and the enzyme was used to prepare (*S*)-2-chloro-1-(3-chloro-4-fluorophenyl)-ethanol with 81% yield and excellent optical purity >99% ee [23]. GDH (EC. 1.1.1.47) from *B. megaterium* was chosen for effective NADPH regeneration.

Enzymes were expressed in *E. coli* BL21(DE3) with a combined *lac* and T7 promoter. The presence of enzymes (Supplementary Material Figure S1, (a) KRED: 32 kDa, (b) GDH: 35 kDa) was checked by SDS-PAGE. Enzymes were further purified, concentrated, and desalted, which was verified by protein electrophoresis (Supplementary Material Figure S2).

The activity of purified enzymes was determined spectrophotometrically by cofactor utilization separately for each enzyme. The initial specific activity of GDH was 45.7 U·mg^{-1}, which was 3.5-fold higher than the initial specific activity of KRED (13.06 U·mg^{-1}). Based on the pH and temperature profiles of KRED and GDH (Figure 1), pH 6.5 and 37 °C were chosen as the conditions for all experiments. According to spectrophotometric measurements of enzyme temperature profiles, the optimal temperatures were 25–35 °C; however, in combined cascade reaction with both enzymes, 37 °C was observed as the optimum for product formation. For the same type of KRED, pH 7 and 30 °C were used as the optimal conditions [23], while pH 6.9–7 and 32–37 °C were used for commercial KREDs [2,3,8].

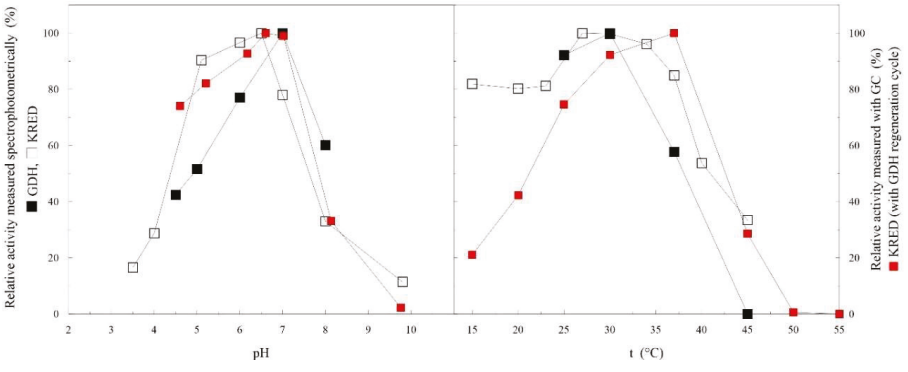

Figure 1. pH and temperature profile of KRED and GDH.

2.2. Free-Enzyme Biotransformations

Biotransformations were performed to verify the activity of purified KRED in combination with NADPH regeneration with GDH (Section 3.6). Ethyl-2-methylacetoacetate, which is an α-alkyl-β-keto ester, was selected as a model substrate for these purposes. This group of substrates are used in relatively low concentrations (25–50 mM) due to their low solubility in water and their potential ability to inhibit enzymes [3].

Free enzymes were used at different ratios for the complete conversion of the substrate (Supplementary Material, Figures S3 and S4). According to the results summarized in Table 1, a five-fold higher concentration of KRED increased the initial activity approximately five and half times and

total conversion of the substrate was achieved within 90 min. In contrast, a four-fold increase in the GDH concentration had no significant effect on initial activity. As expected, KRED was the rate-limiting enzyme and GDH was added in excess in biotransformations. GDH was previously used at concentrations equal to [3] or three-quarters lower than KRED [23], which is similar to the experiments reported above. One study reported the effect of GDH concentration on reaction rate in the kinetic resolution of 11-oxo-5,6,7,8,9,10-hexahydro-6,9-methanobenzocyclooctene and an increasing rate was only observed until 0.15 $g \cdot dm^{-3}$, while the KRED concentration was 0.2 $g \cdot dm^{-3}$ [8]. This represents a KRED:GDH ratio of 1.33:1. In general, to overcome the limitation of NADPH access in the reaction, GDH should always be in excess and the enzyme ratio should be optimized.

Table 1. Biotransformations with free enzymes.

KRED:GDH	c_{KRED} ($\mu g \cdot mL^{-1}$)	c_{GDH} ($\mu g \cdot mL^{-1}$)	Initial Activity (U)	Final Conversion (%)
1:1.7	9.21	15.79	0.27	84
5:1.7	46.04	15.79	1.51	>99
5:6.9	46.04	63.16	1.85	>99

2.3. Optimization of Co-Immobilization

Various factors of LentiKats® need to be verified as the co-immobilization of two or more enzymes using this technology has not been described to date. As for the free enzymes, the most important factor is determining the optimal concentration and ratio of both enzymes to achieve total substrate conversion in a reasonable time. Five different ratios and concentrations of KRED and GDH were used for co-immobilizations (Table 2). Based on the free-enzyme experiments described above, KRED was added in excess as it is rate limiting enzyme.

The graph in Figure 2 displays the dependence of initial specific activity on the concentrations of enzymes entrapped in particles. A four-fold lower amount of KRED and a constant concentration of GDH led to a three-fold decrease in activity while only a 50% conversion rate was achieved. Half of the amount of KRED had no influence on initial specific activity. The concentration of GDH in batch four was limiting and caused a significant decrease in activity, while a two-fold higher amount made no additional improvements. Therefore, 0.19 $mg \cdot g^{-1}_{LKs}$ of GDH was optimum. The major impact of KRED concentration within particles was proven in the free-enzyme reactions. To prevent the possible inactivation of KRED during co-immobilization and the repetitive use of particles for all further experiments, a KRED:GDH weight ratio of 25:1 was applied (batch number 1, Table 2). The ratio depends on the enzyme activities; for example, in previously reported immobilized KRED and GDH cascades, the optimal KRED:GDH ratio was 1:25 [11], which is opposite to the results reported here. Furthermore, the concentrations of KRED (Table 2) used were very low in comparison with the 100 $g \cdot dm^{-3}$ of KRED used in the immobilization on EC-HFA resin [1].

Table 2. Concentration of enzymes loaded into particles.

Batch Nr.	KRED:GDH	c_{KRED} ($mg\ g^{-1}_{LKs}$)	c_{GDH} ($mg\ g^{-1}_{LKs}$)	Initial Specific Activity ($U\ g^{-1}_{LKs}$)	Conversion [a] (%)
1	25:1	4.84	0.19	3.63	>99
2	12.5:1	2.42	0.19	3.62	92
3	6.25:1	1.21	0.19	1.29	50
4	12.5:0.5	2.42	0.1	2.74	92
5	12.5:2	2.42	0.39	3.69	95

LKs—LentiKats® particles. [a] after 90 min.

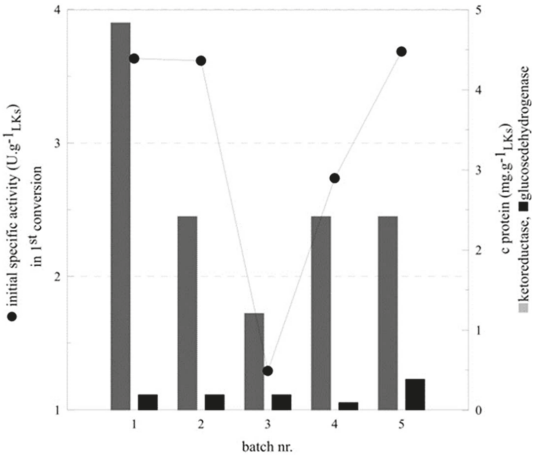

Figure 2. Influence of KRED and GDH concentrations in co-immobilization on the initial specific activity in biotransformations.

2.4. Repeated Biotransformations

To verify the stability of selected co-immobilized KRED and GDH (Table 2, batch number 1), particles were used for 18 repeated batch bioconversions in nonstop mode. Three parallel reactions were stopped at different stages of the conversion (50, 60, and 90 min) to see how the presence of the product could influence the level of bioconversion and the initial specific activity (Figure 3). The non-constant trend of activity during repeated bioconversions can be caused by different residual reaction components after each washing of particles. There were observed similar effect in work with PVA particles before [19]. The activity of the 90-min reaction dropped at the same speed as the others despite particles being exposed to the highest product concentrations, therefore inhibition was excluded. The level of total conversion was still >95%, which is an advantage for product separation and downstream processing.

Conversely, the 50-min reaction had the highest activity decline (36%), which may have been caused by the substrate remaining in the particles after each round. The total level of conversion decreased faster than in the other reactions, which also signifies possible inhibition by the accumulated substrate.

The 60-min biotransformations achieved the most consistent results. The overall activity decline was only 16% after 18 biotransformations, while the total conversion reached 90% for all rounds. Termination of the biotransformation at the exact moment of substrate utilization seemed to be optimal for stability of the co-immobilized enzymes' activity.

Despite the least activity decrease being achieved with the 60-min reaction, a better method would be to let the reaction run to the total conversion as product inhibition was not observed and the subsequent product separation is easier without any residual substrate.

In comparison, only a few KRED immobilizations have been described; for example, covalent binding of KRED on EC-HFA resin with a self-isopropanol regeneration cycle showed no activity decrease during 10 repetitions [1], and covalent binding of KRED on aldehyde-activated agarose together with immobilized GDH in a flow reactor for 15 days also showed no activity decrease [11].

Co-immobilized enzymes demonstrated possible reusability with 80% retained activity and >95% conversion, which is an enormous advantage and yield increasing mainly in biotransformations with small concentrations of inhibiting ketone substrates (25–100 mM). Enantiomeric ratio of chiral products was not changed after co-immobilization of enzymes (Supplementary Material Figures S11 and S12). Complete time graphs of the bioconversions are provided in the Supplementary Material, Figures S8–S10.

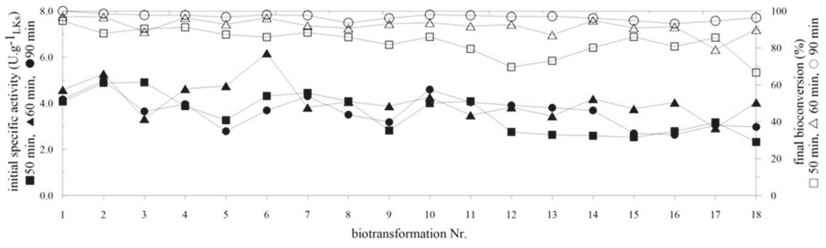

Figure 3. Initial specific activity and final bioconversion in repeated biotransformations of three parallel reactions of co-immobilized KRED and GDH.

2.5. Storage of Particles

The storage of immobilized enzymes is one of the crucial parameters in applied immobilized biocatalysis. Samples from batch number 1 (Table 2) were stored at 4 °C in 0.1 M potassium phosphate buffer (pH 6.5) or at −80 °C without any buffer or solvent. After each biotransformation, particles were washed twice with buffer and stored. Storage at 4 °C caused a significant decrease in relative activity after 90 h (Figure 4) and is therefore not suitable for these co-immobilized enzymes. Storage at 4 °C was chosen based on the previously reported application for immobilized invertase [19]. The particles retained 78% of activity after eight months. Complete time graphs of the bioconversions are provided in the Supplementary Material, Figures S5–S7).

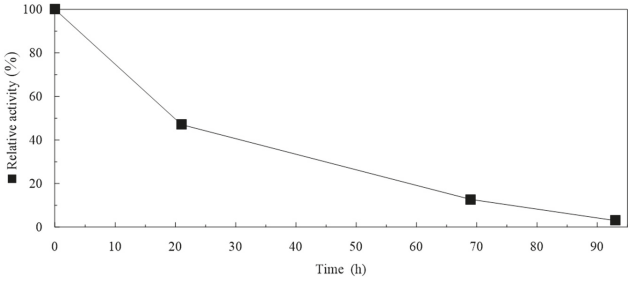

Figure 4. Relative activity of co-immobilized KRED and GDH during storage at 4 °C.

The particles stored at −80 °C surprisingly retained 87% of their relative activity after nine-and-a-half months (Figure 5). This was the first-time the storage conditions of PVA particles had been reported and it showed a huge improvement compared with storage at 4 °C where particles lost their entire activity after four days. Moreover, the properties of the PVA particles remained unchanged.

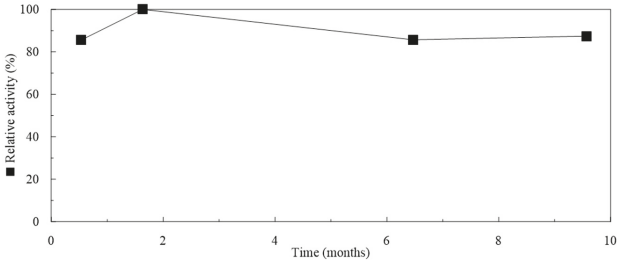

Figure 5. Relative activity of co-immobilized KRED and GDH during storage at −80 °C.

3. Materials and Methods

3.1. Chemicals and Media

Kanamycin was purchased from Gibco® (Life Technologies, Glasgow, UK), ethyl-2-methylacetoacetate was purchased from Sigma-Aldrich (St. Louis, MO, USA) and $NADP^+$ and NADPH were purchased from Prozomix (Haltwhistle, UK). All other chemicals were of analytical grade and were commercially available. Luria-Bertani (LB) medium contained 1% (*w*/*v*) NaCl, 1% (*w*/*v*) tryptone, and 0.5% (*w*/*v*) yeast extract, and plates additionally contained 2% (*w*/*v*) agar. Kanamycin was used at a concentration of 30 $\mu g \cdot mL^{-1}$.

3.2. Cloning

Codon-optimized genes encoding KRED from *Hansenula polymorpha* [23] and GDH from *Bacillus megaterium* were obtained from Generay Biotech Co., Ltd. (Shanghai, China). Genes were inserted into a pET28b vector system, and these plasmids were transformed into *Escherichia coli* BL21(DE3) cells.

3.3. Preparation and Purification of KRED and GDH

An inoculum of *E. coli* BL21(DE3) expressing KRED or GDH was prepared from a single colony. Glass tubes containing 3 mL of LB medium were incubated overnight at 37 °C and 200 rpm. After approximately 12 h, a 500 mL flask containing 100 mL of LB medium was inoculated with 1% (*v*/*v*) inoculation culture and cultivated at 37 °C and 200 rpm. Isopropyl β-D-thiogalactopyranosid was added at a final concentration 0.5 mM when the cell density at OD600 reached 0.5–0.6.

After cultivation at 30 °C for 3 h, the induced cells were harvested by centrifugation (7197× *g*, 15 min, 4 °C). The sediment was subsequently resuspended in 20 mL of 0.1 M potassium phosphate buffer (KRED: pH 6.5; GDH: pH 7). The cell suspension was disrupted in a continual cell disruptor (CF Range, Constant Systems Ltd., Daventry, UK) in two cycles at 4 °C and 20 kPSI. After disruption, 70 µL of protease inhibitor (Complete EDTA-free, Roche, Berlin, Germany) per 20 mL of cell lysate was added. The cell debris was removed by centrifugation (7197× *g*, 30 min, 4 °C).

The cell extract was filtered (Filtropur S, 0.2 µm; Sarstedt, Germany) and loaded onto 5 mL HisTrapTM FF columns (GE Healthcare, Chicago, IL, USA) equilibrated with binding buffer (pH 5.8, 300 mM sodium phosphate, 300 mM NaCl and 10 mM imidazole). Enzymes were eluted with 80% (KRED) or 75% (GDH) elution buffer (pH 7.4, 300 mM sodium phosphate, 300 mM NaCl, and 500 mM imidazole) using an ÄKTA purifier system (GE Healthcare, Chicago, IL, USA). The presence of expressed proteins in eluted fractions was determined by sodium dodecyl sulfate polyacrylamide gel electrophoresis (SDS-PAGE) (Mini PROTEAN® Tetra Cell, Bio-Rad, Hercules, CA, USA). Fractions showing a band of the expected size (GDH: 35 kDa; KRED: 32 kDa) were pooled, concentrated either 180 (KRED) or 40 times (GDH) and desalted using 3 × 14.5 mL of 0.1 M potassium phosphate buffer (pH 6.5) using an Amicon® Ultra centrifugation membrane (15 mL, 30 kDa; Merck, Kenilworth, NJ, USA).

3.4. Enzyme Assays

KRED assays (1 mL) contained 0.1 M potassium phosphate buffer (pH 6.5), 35 mM ethyl 2-methylacetoacetate and 16.53 $\mu g \cdot mL^{-1}$ of purified enzyme. The reaction was started with 0.5 mM NADPH and its decrease was measured spectrophotometrically at 340 nm. GDH assays (1 mL) contained 0.1 M potassium phosphate buffer (pH 7), 100 mM glucose, and 3.72 $\mu g \cdot mL^{-1}$ of purified enzyme. The reaction was started with 0.5 mM NADP+. One unit of an enzyme was defined as the amount of KRED catalyzing the oxidation of 1 µmol NADPH/min or the amount of GDH catalyzing the reduction of 1 µmol $NADP^+$/min at a pH of 6.5 (KRED) or 7 (GDH) and 25 °C. Experiments were duplicated.

The concentrations of purified enzymes were measured spectrophotometrically at 280 nm using an Eppendorf µCuvette® G1.0 (Eppendorf, Hauppauge, NY, USA). The initial specific activity was expressed in units/mg of protein used in the reaction.

3.5. Co-Immobilization

LentiKats® technology was used for co-immobilization. The PVA gel was composed of polyvinyl alcohol (PVA, 10% *w*/*v*), polyethylene glycol (6% *w*/*v*), and water. The amount of water varied according to the concentration of the added enzyme (Table 2). This mixture was heated at 90 °C for 30 min before being cooled at 40 °C under continuous stirring. Enzymes were added to the mixture in a dropwise manner and, after approximately 5 min, the particles were prepared by dripping onto a polyethylene plate using a syringe. The PVA drops were subsequently dried in an air flow cabinet at 35–40 °C for 45 min and hardened in 0.1 M sodium sulfate. The prepared particles were washed with a sterile 0.1 M potassium phosphate buffer (pH 6.5) and used directly for biocatalysis.

3.6. Biotransformation

Ethyl 2-methylacetoacetate, was used as a β-keto ester substrate for the KRED biotransformations. The GDH regeneration system (Figure 6) was used to regenerate NADPH. The reaction mixture contained 0.1 M potassium phosphate buffer (pH 6.5), 35 mM ethyl 2-methylacetoacetate, 100 mM glucose, 1 mM $NADP^+$, and free or 20% (*w*/*v*) co-immobilized enzyme. Free enzymes were used in different concentrations and ratios as reported in Table 1. The amount of buffer added depended on the volume of enzyme used. In repeated batch biotransformations, the particles were washed twice in 0.1 M potassium phosphate buffer (pH 6.5) after each biotransformation. Reactions were carried out in Eppendorf tubes in a total volume of 1 mL at 37 °C with shaking at 550 (free enzymes) or 700 rpm (co-immobilized enzymes). Experiments were duplicated.

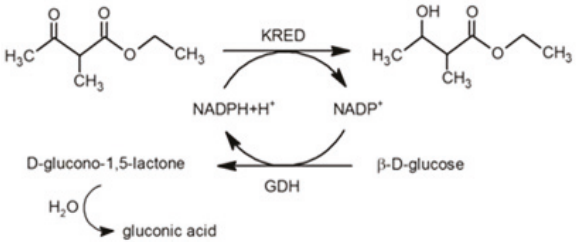

Figure 6. Reduction of ethyl 2-methylacetoacetate to ethyl 3-hydroxy-2-methylbutanoate by NADPH-dependent KRED combined with cofactor regeneration system using GDH.

3.7. Analytics

During the biotransformations, 10 µL of sample was taken at regular intervals and 0.5 mL of ethyl acetate was added to the extract substrate and product. After vortexing, the sample was centrifuged (13,300× *g*, 1 min) to facilitate phase separation. The organic phase was transferred to a glass vial for analysis. The bioconversion of keto ester to hydroxy ester was monitored by gas chromatography-flame ionization detector (GC-FID) (Agilent 6890N, Santa Clara, CA, USA) with a DB-5 capillary column (Agilent J&W, 30 m × 0.25 mm × 0.25 µm) and H_2 as the carrier gas with a flow of 1 mL·min^{-1}. The volume of injection was 1 µL with split 50:1. The oven temperature was initially 90 °C for 5.5 min, but increased to 280 °C with a gradient of 30 °C/min and was held for 3 min.

The percentage conversion was evaluated as the peak area of alcohol product/(peak area of ketone substrate + peak area of alcohol product) × 100. One unit of KRED was the amount of enzyme that catalyzed the production of 1 µmol·min^{-1} of hydroxy ester (Figure 6). The middle volume of the reaction mixture was included in the calculation of co-immobilized KRED activity. The initial specific activity of free (or co-immobilized) KRED was defined as µmol of hydroxy ester (Figure 6) produced/min by 1 mg of KRED (or 1 g of particles).

The activity decline during repeated biotransformations with co-immobilized KRED and GDH was evaluated as the difference between the average first five and last five activities and was expressed as a percentage.

4. Conclusions

KRED and GDH were successfully produced, purified and co-immobilized using PVA entrapment technology and applied in a cascade reaction with NADPH regeneration. This immobilization method was used for the first time for a two-enzyme cascade. The ratio of enzymes entrapped in particles was optimized, and the best option (KRED:GDH = 25:1) was employed in 18 repeated batch conversions of ethyl-2-methylacetoacetate. Particles retained approximately 80% of their activity, which is the highest stability of co-immobilized KRED reported to date. Furthermore, the storage of co-immobilized redox enzymes was found to be effective when particles were stored without any buffer or solvent at −80 °C. Particles lost 20% of their initial activity after almost 10 months of storage and their mechanical properties remained unchanged. This storage technique may also be applied to other immobilized unstable oxidoreductases.

Supplementary Materials: The following are available online at http://www.mdpi.com/2073-4344/8/4/168/s1. Figure S1 (a) expression of KRED (32 kDa); column 1—molecular standard, 2—start of induction, 3—after 2h, 4—after 3h, 5—cell extract (b) expression of GDH (35 kDa); 1—molecular standard, 2—start of induction, 3—after 1h, 4—after 2 h, 5—after 3 h, 6—cell extract. Conditions of induction for both KRED and GDH: 30 °C, 0.5 mM IPTG, Figure S2 Purification of (a) KRED (1—molecular standard, 2–3—flow through, 4—unspecific proteins eluted with 25% elution buffer, 5—KRED eluted with 80% elution buffer) and (b) GDH (1—molecular standard, 2–3—flow through, 4—unspecific proteins eluted with 20% elution buffer, 5–6—GDH eluted with 75% elution buffer). Figure S3 Product conversion in biotransformations with free ketoreductase (KRED) and glucosedehydrogenase (GDH) with three different ratios (KRED:GDH) of enzymes: nr. 1—1:1.7; nr. 2—5:1.7; nr. 3—5:6.9. Figure S4 Influence of KRED:GDH ratio and enzyme concentration on initial activity in biotransformation with free enzymes. Figure S5 Product conversion in biotransformations with co-immobilzed enzymes nr. 1 during six biotransformations with 12-h storage at 4 °C in potassium phosphate buffer (0.1 M; pH = 6.5) after 3rd, 4th and 5th batch. Figure S6 Product conversion in biotransformations with co-immobilzed enzymes nr. 2 during five biotransformations with 12-h storage at 4 °C in potassium phosphate buffer (0.1 M; pH = 6.5) after 3rd and 4th batch. Figure S7 Product conversion in biotransformations with co-immobilzed enzymes nr. 5 during five biotransformations with 12-h storage at 4 °C in potassium phosphate buffer (0.1 M; pH = 6.5) after 3rd and 4th batch. Figure S8 Product conversion in 18 batches of 50-min reactions. Figure S9 Product conversion in 18 batches of 60-min reactions. Figure S10 Product conversion in 18 batches of 90-min reactions. Figure S11 Chromatogram of hydroxy ester product after biotransformation with free enzymes. Figure S12 Chromatogram of hydroxy ester product after biotransformation with co-immobilized enzymes. Figure S13 Bioconversions after 45 h and relative activity of free and co-immobilized enzymes with different substrate concentrations.

Acknowledgments: This work was done during implementation of the project Establishment of Competence center for research and development in the field of molecular medicine, ITMS code 26240220071, supported by the Research and Development Operational Program funded by ERDF.

Author Contributions: Tatiana Petrovičová and Kristína Markošová performed immobilized and free enzyme experiments; Martin Rebroš and Zuzana Hegyi performed the cloning experiments; Tatiana Petrovičová, Martin Rebroš and Ioulia Smonou analyzed the data, wrote the manuscript; Michal Rosenberg and Martin Rebroš contributed funding of the research, immobilization set up.

Conflicts of Interest: The authors declare no conflict of interest.

References

1. Li, H.M.; Moncecchi, J.; Truppo, M.D. Development of an immobilized ketoreductase for enzymatic (r)-1-(3,5-bis(trifluoromethyl)phenyl)ethanol production. *Organ. Process Res. Dev.* **2015**, *19*, 695–700. [CrossRef]
2. Dai, Z.; Guillemette, K.; Green, T.K. Stereoselective synthesis of aryl γ,δ-unsaturated β-hydroxyesters by ketoreductases. *J. Mol. Catal. B Enzym.* **2013**, *97*, 264–269. [CrossRef]
3. Kalaitzakis, D.; David Rozzell, J.; Kambourakis, S.; Smonou, I. Highly stereoselective reductions of α-alkyl-1,3-diketones and α-alkyl-β-keto esters catalyzed by isolated nadph-dependent ketoreductases. *Org. Lett.* **2005**, *7*, 4799–4801. [CrossRef] [PubMed]

4. Guo, Z.; Chen, Y.; Goswami, A.; Hanson, R.L.; Patel, R.N. Synthesis of ethyl and t-butyl (3r,5s)-dihydroxy-6-benzyloxy hexanoates via diastereo- and enantioselective microbial reduction. *Tetrahedron Asymmetry* **2006**, *17*, 1589–1602. [CrossRef]
5. Zhu, D.; Mukherjee, C.; Rozzell, J.D.; Kambourakis, S.; Hua, L. A recombinant ketoreductase tool-box. Assessing the substrate selectivity and stereoselectivity toward the reduction of β-ketoesters. *Tetrahedron* **2006**, *62*, 901–905. [CrossRef]
6. Kaluzna, I.A.; David Rozzell, J.; Kambourakis, S. Ketoreductases: Stereoselective catalysts for the facile synthesis of chiral alcohols. *Tetrahedron Asymmetry* **2005**, *16*, 3682–3689. [CrossRef]
7. Li, H.; Zhu, D.; Hua, L.; Biehl, E.R. Enantioselective reduction of diaryl ketones catalyzed by a carbonyl reductase from sporobolomyces salmonicolor and its mutant enzymes. *Adv. Synth. Catal.* **2009**, *351*, 583–588. [CrossRef]
8. Truppo, M.D.; Kim, J.; Brower, M.; Madin, A.; Sturr, M.G.; Moore, J.C. A novel resolution of a pharmaceutically important bridged bicyclic ketone intermediate via selective enzymatic reduction with a commercially available ketoreductase. *J. Mol. Catal. B Enzym.* **2006**, *38*, 158–162. [CrossRef]
9. Milner, S.E.; Maguire, A.R. Recent trends in whole cell and isolated enzymes in enantioselective synthesis. *Arkivoc* **2012**, *2012*, 321–382.
10. Nagayama, K.; Spiess, A.C.; Büchs, J. Gas phase enantioselective reduction catalyzed by immobilized ketoreductase: Effects of water activity and reaction temperature. *Biochem. Eng. J.* **2010**, *52*, 301–303. [CrossRef]
11. Dall'Oglio, F.; Contente, M.L.; Conti, P.; Molinari, F.; Monfredi, D.; Pinto, A.; Romano, D.; Ubiali, D.; Tamborini, L.; Serra, I. Flow-based stereoselective reduction of ketones using an immobilized ketoreductase/glucose dehydrogenase mixed bed system. *Catal. Commun.* **2017**, *93*, 29–32. [CrossRef]
12. Ning, C.; Su, E.; Tian, Y.; Wei, D. Combined cross-linked enzyme aggregates (combi-cleas) for efficient integration of a ketoreductase and a cofactor regeneration system. *J. Biotechnol.* **2014**, *184*, 7–10. [CrossRef] [PubMed]
13. Rebroš, M.; Rosenberg, M.; Mlichová, Z.; Krištofíková, L.; Paluch, M. A simple entrapment of glucoamylase into lentikats®as an efficient catalyst for maltodextrin hydrolysis. *Enzym. Microb. Technol.* **2006**, *39*, 800–804. [CrossRef]
14. Rebroš, M.; Rosenberg, M.; Stloukal, R.; Krištofíková, L. High efficiency ethanol fermentation by entrapment of zymomonas mobilis into lentikats®. *Lett. Appl. Microbiol.* **2005**, *41*, 412–416. [CrossRef] [PubMed]
15. Rosenberg, M.; Rebroš, M.; Krištofíková, L.; Malátová, K. High temperature lactic acid production by bacillus coagulans immobilized in lentikats. *Biotechnol. Lett.* **2005**, *27*, 1943–1947. [CrossRef] [PubMed]
16. Dolejš, I.; Krasňan, V.; Stloukal, R.; Rosenberg, M.; Rebroš, M. Butanol production by immobilised clostridium acetobutylicum in repeated batch, fed-batch, and continuous modes of fermentation. *Bioresour. Technol.* **2014**, *169*, 723–730. [CrossRef] [PubMed]
17. Rebroš, M.; Dolejš, I.; Stloukal, R.; Rosenberg, M. Butyric acid production with clostridium tyrobutyricum immobilised to pva gel. *Process Biochem.* **2015**, *51*, 704–708. [CrossRef]
18. Cerreti, M.; Markošová, K.; Esti, M.; Rosenberg, M.; Rebroš, M. Immobilisation of pectinases into pva gel for fruit juice application. *Int. J. Food Sci. Technol.* **2017**, *52*, 531–539. [CrossRef]
19. Rebroš, M.; Rosenberg, M.; Mlichová, Z.; Krištofíková, L. Hydrolysis of sucrose by invertase entrapped in polyvinyl alcohol hydrogel capsules. *Food Chem.* **2007**, *102*, 784–787. [CrossRef]
20. Grosová, Z.; Rosenberg, M.; Rebroš, M.; Šipocz, M.; Sedláčková, B. Entrapment of β-galactosidase in polyvinylalcohol hydrogel. *Biotechnol. Lett.* **2008**, *30*, 763–767. [CrossRef] [PubMed]
21. Grosová, Z.; Rosenberg, M.; Gdovin, M.; Sláviková, L.; Rebroš, M. Production of d-galactose using β-galactosidase and saccharomyces cerevisiae entrapped in poly(vinylalcohol) hydrogel. *Food Chem.* **2009**, *116*, 96–100. [CrossRef]
22. Krasnan, V.; Stloukal, R.; Rosenberg, M.; Rebros, M. Immobilization of cells and enzymes to lentikats(r). *Appl. Microbiol. Biotechnol.* **2016**, *100*, 2535–2553. [CrossRef] [PubMed]
23. Hanson, R.L.; Goldberg, S.; Goswami, A.; Tully, T.P.; Patel, R.N. Purification and cloning of a ketoreductase used for the preparation of chiral alcohols. *Adv. Synth. Catal.* **2005**, *347*, 1073–1080. [CrossRef]

© 2018 by the authors. Licensee MDPI, Basel, Switzerland. This article is an open access article distributed under the terms and conditions of the Creative Commons Attribution (CC BY) license (http://creativecommons.org/licenses/by/4.0/).

catalysts

MDPI

Article

Approaching Immobilization of Enzymes onto Open Porous Basotect®

Peter J. Allertz [1,†], Steffen Berger [1,†], Grit Sellenk [1], Christin Dittmer [1], Marco Dietze [1], Klaus-Peter Stahmann [2] and Katrin Salchert [1,*]

[1] Laboratory for Biopolymers, Institute of Applied Chemistry, Brandenburg University of Technology Cottbus-Senftenberg, Universitätsplatz1, 01968 Senftenberg, Germany
[2] Laboratory for Technical Microbiology, Institute of Biotechnology, Brandenburg University of Technology Cottbus-Senftenberg, Universitätsplatz1, 01968 Senftenberg, Germany
* Correspondence: Katrin.Salchert@b-tu.de; Tel.: +49-3573-85811
† These authors contributed equally to this work.

Academic Editor: Peter Grunwald
Received: 17 October 2017; Accepted: 16 November 2017; Published: 27 November 2017

Abstract: For the first time, commercial macroporous melamine formaldehyde foam Basotect® (BT) was used as a basic carrier material for both adsorptive and covalent enzyme immobilization. In order to access inherent amino groups, the Basotect® surface was pretreated with hydrochloric acid. The resulting material revealed 6 nmol of superficial amino groups per milligram Basotect®. Different optimized strategies for tethering the laccase from *Trametes versicolor* and the lipase from *Thermomyces lanuginosus* onto the pre-treated Basotect® surface were studied. Particularly, for covalent immobilization, two different strategies were pursued: lipase was tethered via a cross-linking method using 1-ethyl-3-(3-dimethylaminopropyl)carbodiimide, and laccase was bound after functionalizing Basotect® with hydrophilic copolymer poly(ethylene-*alt*-maleic anhydride) (PEMA). Prior to laccase immobilization, the PEMA coating of Basotect® was verified by ATR-FTIR analysis. Subsequent quantification of available high-reactive PEMA anhydride moieties revealed an amount of 1028 ± 73 nmol per mg Basotect®. The surface-bound enzyme amounts were quantified as 4.1–5.8 µg per mg Basotect®. A theoretical surface-covered enzyme mass for the ideal case that an enzyme monolayer was immobilized onto the Basotect® surface was calculated and compared to the amount of adsorptive and covalently bound enzymes before and after treatment with SDS. Furthermore, the enzyme activities were determined for the different immobilization approaches, and the stability during storage over time and against sodium dodecyl sulfate treatment was monitored. Additionally, PEMA-BT-bound laccase was tested for the elimination of anthropogenic micropollutant bisphenol A from contaminated water in a cost-effective and environmentally-friendly way and resulted in a degradation rate higher than 80%.

Keywords: Basotect®; enzyme immobilization; laccase; lipase; PEMA; EDC; bisphenol A

1. Introduction

Industrially-produced duroplastic Basotect® (BT) is a white slabstock foam with recent applications in lightweight constructions, as well as for acoustic and thermal insulation. BT polymer consists of highly cross-linked melamine and formaldehyde monomers, leading to high mechanical stability and hardness. In addition, BT reveals high chemical stability and is non-soluble in any organic solvent. Due to its chemical structure, amino and hydroxyl functionalities are buried within the framework, making this material a promising candidate for covalent enzyme immobilization approaches. Since enzyme immobilization is preliminary performed using films and beads [1,2],

BT's open porous morphology is favorable for enzyme immobilization and its application as a compact block under flow conditions, as well.

In general, the immobilization of enzymes strongly enhances the usability of biocatalysts for industrial or catalytic purposes [1,3,4]. Therefore, not only high loadings of enzymes on carrier materials are favorable, but also the carrier material characteristics play an important role in how effective the enzyme-modified material will be. It often depends on the carrier material whether the transport of substrates to and products from an enzyme is ensured. Key factors in enzyme immobilization, besides the reaction medium and diffusion limitations, are the precipitation of products, the viscosity of the mixture and reaction thermodynamics [5]. These requirements have to be considered when choosing the carrier material for any special application. In cases where low flow rates or highly viscous fluids have to be used, an open porous carrier with bigger pores is necessary. BT provides excellent preconditions as a carrier with respect to flow-through processes.

There are many different techniques available to immobilize enzymes, which are continuously enhanced [1,5–7], resulting in heterogeneous catalysts with advantageous properties over homogeneous catalyst. In particular, re-use or continuous operation of the biocatalyst, as well as enhancement of stability [8] against thermal influences or organic solvents [9] are of interest. Due to its simplicity, physical adsorption is a very common approach to immobilize enzymes, although issues with enzyme desorption over time exist [10]. Covalent immobilization, as well as cross-linking of enzymes are also widely-used alternatives for tethering enzymes on surfaces [7]. Enzymes can be linked directly to the carrier surface, in case it is providing suitable functional groups, like the herein studied Basotect®. The water-soluble 1-ethyl-3-(3-dimethylaminopropyl)carbodiimide (EDC) [11] is an extensively-used coupling agent, which increases the reactivity of carboxylic groups as an active ester. However, activating enzyme carboxylic groups can lead to enzyme-enzyme cross-linking since activated enzyme molecules may react with nucleophiles, e.g., amino groups, of other enzymes [12]. As an alternative, if the carrier surface does not provide enough or suitable functional groups, surface modification with highly functional polymers is often applied [13]. The latter is an easy possibility for changing the surface chemistry of carrier materials to get optimized conditions for enzymes and thus improve immobilization rates and increase enzyme activity. Poly(ethylene-*alt*-maleic anhydride) (PEMA) is one example for this purpose and has been used by our group and others for several years to bind enzymes [14,15]. Due to the high density of anhydride moieties in PEMA, there is an increased amount of binding sites for protein immobilization along the polymer chain. Additionally, the functional groups for covalent tethering are well accessible because of the atactic configuration of the anhydride moieties and the short sidechain of the comonomer. Furthermore, the good solubility of the polymer in aqueous solution results in a hydrogel-like 3D swelling behavior of surface-bound PEMA and thus provides an optimal environment for hydrophilic enzymes [16]. Lipase and laccase immobilization have been extensively studied, particularly either for applications in the dairy industry, oil and fat processing and for producing fine chemicals or even biofuels [11,17–19], or in case of laccase, in the pulp and paper industry, cosmetics or for dye synthesis and biosensors, as well as wastewater treatment [20–23]. Different carrier materials, e.g., zeolites, silica gel, polypropylene, polyethylene, octyl-agarose and cellulose ester, as well as silica-based mesoporous cements and fibers, ceramic membranes or polyacrylonitrile beads, and immobilization techniques were applied [24–32]. Immobilized laccase is also a promising candidate for wastewater treatment to remove anthropogenic pollutants [33–37].

In the present study, we primarily aim at the evaluation of the industrial melamine formaldehyde foam Basotect® as a new and suitable carrier for the immobilization of enzymes using common and established adsorptive and covalent immobilization techniques. To our knowledge, the use of a melamine formaldehyde foam for enzyme immobilization has not been studied before. A few working groups [38] applied melamine-based resins in pyrolysis to form templates for mostly non-enzymatic catalysts. Furthermore, BT was used as the moving bed for fungal lipase producers [39]. Using BT as a carrier material for catalytically-active enzymes, either adsorptively or covalently bound,

is a completely new approach. Based on BT's chemical structure, inherent amino groups might be favorable for covalent immobilization approaches. Thus, we intended to develop a method to expose amino groups, followed by suitable characterization of the resulting material. Utilizing EDC-mediated cross-linking of lipase and modified BT, as well as laccase tethering on PEMA-functionalized BT, two different covalent immobilization approaches were pursued. Aiming at an implementation of a particularly reactive BT surface for covalent immobilization, an intermediate PEMA layer providing highly reactive anhydride functional groups should be proven. Utilizing a theoretical model, the limits of loading the BT with an enzyme monolayer should be calculated. The comparison of these theoretical values with the actually measured degree of immobilization of the respective enzyme should make it possible to evaluate the utilization of the available BT surface for enzyme attachment. In addition, further evaluations of the enzyme activity after binding to BT and the stability of the adsorptively- and covalently-bound enzymes against SDS treatment, as well as enzyme stability during storage, should allow a distinct assessment of the suitability of BT as a new carrier material for enzyme immobilization. Finally, laccase-BT should be applied exemplarily to degrade bisphenol A in wastewater, to demonstrate the functionality of enzyme-loaded BT.

2. Results

2.1. Characterization of Basotect®

In order to evaluate the accessibility of BT's inner surface and to obtain information about flow-through conditions, pore diameter and fillet widths were determined by SEM. The analyzed BT was a white open porous foam. Its macro-porous morphology was characterized by a set of three to five slight fillets, connected in a coupling point. By these interconnections, a highly branched three-dimensional network was formed, as shown in Figure 1a. Furthermore, BET characterization of the surface area was performed, and additional micropore analysis (de Boer and Saito-Foley method) showed an absence of any micro-pores on the BT surface. Results are shown in Table 1.

Table 1. Characteristics of Basotect®.

Pore diameter	30–240 µm
Fillet width	4–7 µm
BET surface	5.91 $m^2 \cdot g^{-1}$

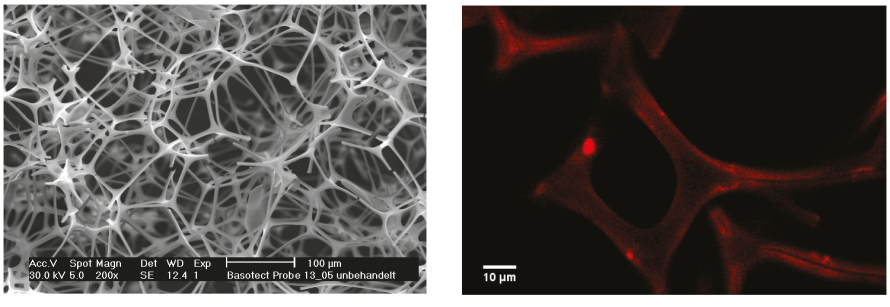

(**a**) (**b**)

Figure 1. (**a**) Scanning electron microscopy view of pure Basotect®; (**b**) fluorescence microscopy of ATTO-TAG™ labeled amino functionalities on the Basotect® surface after partial hydrolysis with concentrated HCl. The labeled sample was excited at 488 nm, and the emission was detected at 590 nm.

Initial investigations of the BT solubility showed a distinct non-solubility in all organic solvents, as this is typical for duroplastics. In contrast, applying hydrolysis conditions using concentrated hydrochloric acid at 55 °C resulted in a cleavage of chemical bonds and a total dissolution after 4 h. A reduction of hydrolysis time made the decomposition incomplete, which resulted only in a slight shrinkage of the foam framework. This process led to an exposure of primary amino functionalities, suitable for covalent enzyme immobilization.

The potential exposition of primary amino groups by a slight HCl-induced etch of the BT surface was analyzed by the specific fluorescence marker ATTO-TAG^{TM} FQ (3-2-(furoyl quinoline-2-carboxaldehyde). Its special performance is based on the non-fluorescent status of the non-reacted aldehyde form, whereas after reacting with a primary amino group, the resulting isoindole product reveals a distinct red fluorescent emission. After treatment of BT with concentrated HCl for 20 min, ATTO-TAG^{TM} FQ indicated the availability of primary amino groups, as shown in Figure 1b, whereas for non-treated samples, no reaction with the dye was observed.

The amount of amino groups on the polymer surface was quantified by a photometric assay with the azo dye Orange II (β-naphthol orange). The assay was used as previously described by Noel et al. [40] with some modifications. It is based on ionic interactions between the sulfonate group of the dye and the protonated amino groups in an acidic milieu. If the pH value rises, the interactions get weaker, and the dye is released in solution where it is measured at a 484-nm wavelength. For acid pretreated BT, the amount of amino groups was characterized by the Orange II assay, and a degree of amination of 6.0 ± 0.7 nmol·mg^{-1} was determined for pieces of the typical size of $10 \times 3 \times 3$ mm^3.

2.2. PEMA Functionalization of Basotect® and Characterization

The coating of BT with PEMA was shown by ATR-FTIR. Acid pre-treated BT was treated with PEMA and compared to PEMA-free samples. As shown in Figure 2, the PEMA-BT samples show distinctive signals of carboxylic acid anhydride groups at 1775 cm^{-1} and 1850 cm^{-1}, which proves the tethering of PEMA to the BT surface. As PEMA provides cyclic anhydride moieties, the signal at 1775 cm^{-1} is larger than the other one at 1850 cm^{-1}.

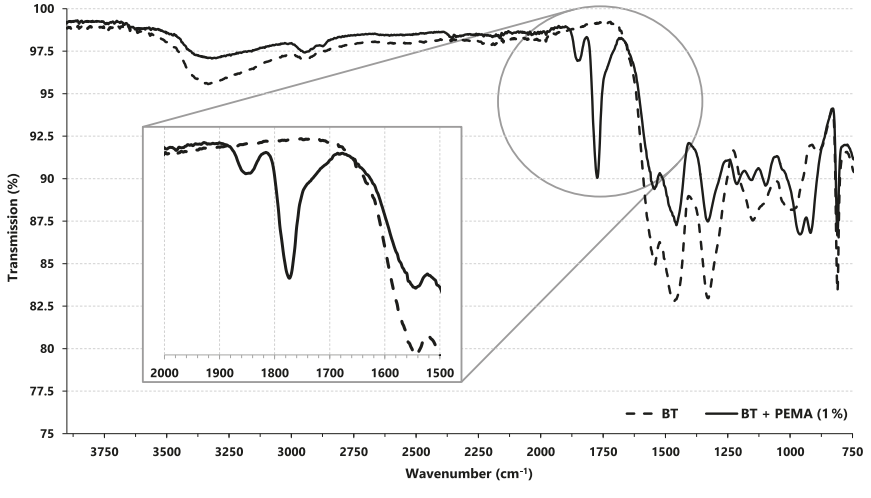

Figure 2. Comparison of ATR transmission spectra of plain Basotect® (BT) and PEMA functionalized BT (not normalized). The figure shows untreated and PEMA functionalized BT for comparison. The signals at 1775 cm^{-1} and 1850 cm^{-1} account for tethering of PEMA to the BT surface.

The amount of free surface bound carboxyl groups (degree of carboxylation, DoC) on the BT surface after functionalization with PEMA was additionally quantified via a photometric assay using toluidine blue O. On average, 1028 ± 73 nmol·mg^{-1} carboxyl moieties on PEMA-coated BT surfaces were detected.

2.3. Enzyme Immobilization

2.3.1. Adsorptive and Covalent Immobilization

This study aimed at the evaluation of a melamine formaldehyde slabstock foam as a suitable carrier material for the immobilization of the enzymes lipase and laccase. Thus, the immobilized enzyme quantities and activities were analyzed after adsorptive immobilization on acid-treated BT samples, as well as after covalent immobilization using two different approaches. Lipase was bound by the EDC-induced linkage. Covalent laccase immobilization was performed after linkage of PEMA on the BT surface, creating multiple attachment points.

Immobilization methods varied in immobilization time, as well as in concentration and pH value of the enzyme solution. Details are described in Section 4.5. In initial experiments, the optimum lipase and laccase concentrations in solution were stated for achieving the highest amount of immobilized enzyme quantities on the BT surface. Furthermore, the composition of enzyme solution and its pH value was ascertained for the best maintenance of the enzyme stability. To evaluate the differences in the amount of adsorptively- and covalently-immobilized enzyme, the immobilization conditions were selected identically within a certain enzymes. As shown in Table 2, the adsorptive immobilization of laccase and lipase resulted in an immobilized mass of just under 6 µg protein per mg of BT, respectively. Covalently-bound enzymes were treated with SDS, additionally, to desorb non-bound enzymes. Thus, the residual lipase and laccase amount decreased slightly, in contrast to the adsorptive immobilization method.

Verification of enzyme activity after immobilization is essential for further applications of the enzyme-BT assemblies. Specific activity assays, as described in the literature [39,41], were utilized. For lipase activity measurements, the hydrolysis of the fatty acid derivative *p*-nitrophenyl palmitate was used, and laccase activity was detected by transformation of ABTS. In addition to the activity of immobilized enzymes, the activities of dissolved enzymes were determined. Compared to the free enzyme, a general decrease of activity after enzyme immobilization was determined and is shown in Table 2. After adsorptive immobilization, lipase activity decreased to eight-fold less than free lipase activity, whereas after EDC induced covalent immobilization, the activity was a quarter compared to free lipase. In contrast, laccase activity after adsorptive and covalent immobilization was decreased to about a quarter of the free laccase value, and no distinct difference in remaining activity due to the immobilization method was detected.

Table 2. Protein quantity and laccase- or lipase-specific activity, respectively, after adsorptive or covalent immobilization on BT. Covalent lipase immobilization was performed on acid pre-treated BT using EDC, whereas laccase was tethered on PEMA-BT. Further immobilization conditions were described in Table 4. $n = 6$.

	Adsorptive		**Covalent**		
	Quantity on BT (µg·mg^{-1})	**Activity (U·mg^{-1}$_{enzyme}$)**	**Quantity on BT (µg·mg^{-1})**	**Activity (U·mg^{-1}$_{enzyme}$)**	**Activity of Free Enzyme (U·mg^{-1}$_{enzyme}$)**
Lipase	5.8 ± 1.2	0.3 ± 0.1	4.3 ± 0.4	0.5 ± 0.1	2.2 ± 0.1
Laccase	5.8 ± 1.6	4.5 ± 0.8	4.1 ± 1.2	4.2 ± 0.7	18.5 ± 3.6

2.3.2. Surface Coverage with Enzyme

For further estimation of the ability of BT binding enzymes, the coverage of available BT surface with immobilized enzyme was analyzed. Aiming at this, the theoretical minimum and maximum

enzyme quantities that cover a specific BT surface were calculated (see Section 4.9) and compared to the actual immobilized enzyme quantity for lipase, as well as laccase.

For comparison, the calculated theoretical surface coverage and the experimental data for lipase and laccase immobilization according to the adsorptive or covalent immobilization technique, as well as the effect of SDS treatment are shown in Table 3. In particular, for covalent enzyme immobilization, SDS was used to remove non-covalently bound enzyme molecules.

Table 3. Determined surface coverage of lipase and laccase after adsorptive and covalent immobilization and calculated theoretical minimum and maximum coverages of the enzymes on the BT surface. Additionally, the effect of SDS treatment after enzyme immobilization for each immobilization technique on surface coverage is presented. Immobilization conditions were described in Table 4. $n = 6$.

Surface Coverage		**Lipase**	**Laccase**
Theoretical ($ng \cdot cm^{-2}$)	min	25	114
	max	44	125
After adsorptive immobilization ($ng \cdot cm^{-2}$)	without SDS treatment	98 ± 20	98 ± 37
	after SDS treatment	17 ± 15	63 ± 19
After covalent immobilization ($ng \cdot cm^{-2}$)	without SDS treatment	113 ± 14	126 ± 36
	after SDS treatment	73 ± 7	69 ± 20

Analyzing lipase surface concentration, the measured value exceeded the theoretical maximum after adsorptive immobilization. SDS treatment after immobilization resulted in a distinct decrease of bound enzyme amount (83%) associated with the fall of the indicated value below the theoretical minimum surface coverage. In contrast, after covalent lipase immobilization and SDS treatment, the remaining lipase concentration decreased by 35%, but continued to exceed the theoretical maximum surface concentration. After adsorptive immobilization, laccase surface coverage was slightly below the theoretical minimum, indicating an almost complete coverage of the BT surface. A subsequent SDS treatment resulted in a slight decrease of surface concentration (36%). However, SDS treatment after adsorptive laccase immobilization did not lead to the same extent of laccase molecule detachment from the BT surface that was observed after adsorptive lipase immobilization. As a result, the same surface coverage was obtained after adsorptive and covalent laccase immobilization followed by SDS treatment. As detected with lipase, the laccase surface coverage after covalent immobilization and SDS treatment was lower, compared to covalent (45%) and adsorptive immobilized laccase without SDS treatment.

Since adsorptive immobilization of lipase and laccase was performed using uniformly acid-pretreated BT, a consideration of the molar surface concentration of both enzymes on BT after using the same molar enzyme solution concentrations allows a comparison of the ability of the BT to bind the respective enzyme. With the respective enzyme mass concentration shown in Table 4, a molar surface concentration of $1.8\,pmol \cdot cm^{-2}$ for laccase and $3.4\,pmol \cdot cm^{-2}$ for lipase on the BT surface was achieved. In contrast, the use of the same molar enzyme solution concentrations of approximately $9\,nmol \cdot mL^{-1}$ (corresponding to $0.25\,mg \cdot mL^{-1}$ of lipase solution and $0.5\,mg \cdot mL^{-1}$ of laccase solution, respectively) resulted in an almost similar molar surface coverage of $1.6\,pmol \cdot cm^{-2}$ for lipase and $1.8\,pmol \cdot cm^{-2}$ for laccase on the BT surface. Additionally, in the case of a lower lipase solution concentration, a lipase surface concentration of $47 \pm 3\,ng \cdot cm^{-2}$ was almost similar to the theoretical maximum concentration.

2.4. Storage Stability of Enzyme-Basotect® Interactions

The stability of immobilized enzymes was estimated after tethering on BT and subsequent storage for one or seven days at two different conditions. After adsorptive and covalent immobilization, the lipase-BT specimens were frozen at −18 °C, whereas covalent fixed laccase on PEMA-BT was stored at 4 °C. Results in Figure 3 show a decrease of laccase activity to 60% relative to initial activity after one day. However, remaining activity was constant during the next six days. The activity of adsorptive immobilized lipase decreased stepwise after freezing. After one day, activity decreased by about one-fourth, and further storage led to a remaining activity of 12%. A similar trend of activity decrease was determined analyzing covalently-bound lipase on BT, but remaining activity after seven days freezing was at about 40%.

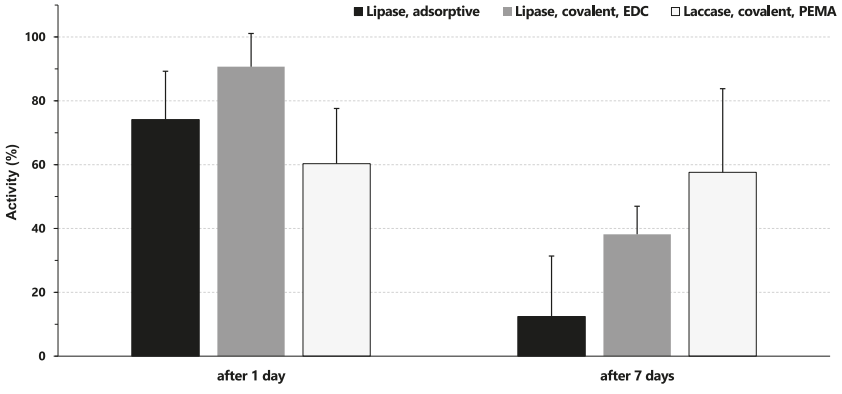

Figure 3. Remaining relative activity of lipase and laccase on BT after storage for one or seven days, respectively. Lipase-loaded BT was stored at −18 °C and laccase-loaded PEMA-BT at 4 °C.

2.5. Application of Immobilized Laccase for the Elimination of Bisphenol A

To demonstrate the function of immobilized laccase, we applied a laccase from *Trametes versicolor* for the degradation of several anthropogenic organic micropollutants in surface water and wastewater effluent. Among others, bisphenol A (BPA) was tested in degradation experiments. Results are shown exemplarily in Figure 4. It was possible to degrade the pollutant BPA almost completely within one week, or by nearly 90% within 48 h. After one week of experiments, the same functionalized BT pieces were placed in another mixture of the same micropollutant mix again, and the degradation was monitored for a second time (second curve in Figure 4).

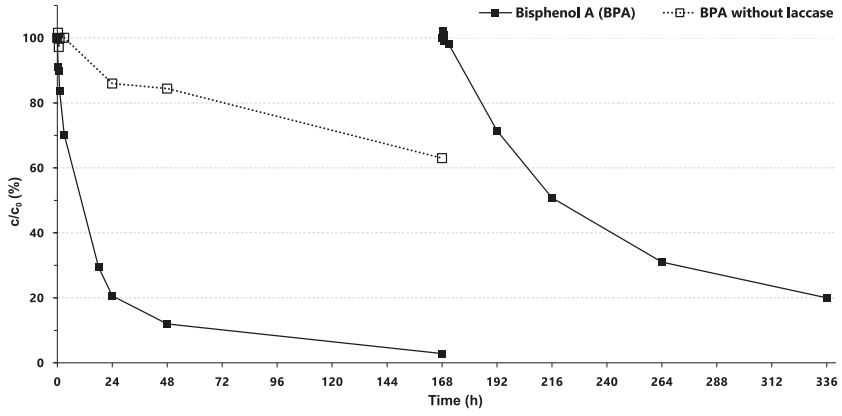

Figure 4. Oxidative elimination of BPA with BT-PEMA bound laccase from *Trametes versicolor* over two periods of one week. After the first week, the same amount of pollutants was added again (second cycle). Dotted curves represent the same setup with BT pieces without laccase. $n = 3$.

3. Discussion

3.1. Characterization and Functionalization of Basotect®

Due to its open porous structure, BT is characterized by its favorable flow performance and, consequently, its ability for easy mass transport through the pore network. Furthermore, a suitable specific surface and a useful surface chemistry are important for successful application as an enzyme carrier material. Despite large pores, BT offers a good mechanical stability and hence can be used for further functionalization. Enzymes and other proteins can be tethered to the inner surface either adsorptively or via covalent immobilization. The chemical structure of BT is very stable and resistant, but can also easily be functionalized by partly breaking chemical bonds between melamine and formaldehyde with strong acids. We used concentrated HCl to uncover amino moieties onto the surface of BT in a quick and easy way. These amino groups can be used for further functionalization. However, with increasing HCl treatment time, the BT becomes less stable. We optimized the exposure process of amino groups to balance out both mechanical stability and preferably the degree of amination (DoA).

DoA was measured with a photometric assay using the Orange II azo dye. A mean amount of 6.0 nmol·mg^{-1} for DoA was found. Since the application of BT for enzyme immobilization is a completely new approach, comparison with likewise findings or similar materials is limited. Leirião et al. [42] reported a value of 3.3 ± 0.95 µmol of NH_2 groups per mg material for a polyacrylonitrile membrane enzyme support material. Due to different densities and unknown BET surface areas for these materials, a direct comparison is not possible. Others report NH_2 group amounts only per particle [43] or as the concentration of nitrogen [44]. Additionally, every quantification method provides deviating results and hence is inappropriate for exact comparability.

HCl-treated BT was further functionalized with the copolymer PEMA, to attach anhydride moieties to the carriers inner surface as an additional option for optimized covalent enzyme tethering. PEMA was successfully linked to BT, and remaining maleic carboxylic groups were identified by ATR-FTIR and quantified using the TBO assay. A mean amount of 1027 nmol·mg^{-1} of available carboxylic groups was found. This is more than 170-fold of the identified amount of amino groups, so it can be assumed that the introduction of a PEMA interlayer increases the capability of BT to bind enzymes. Although the inner surface of BT might not get fully covered with a PEMA coating

during the functionalization process, the long polymer chains can be tethered to a few amino groups. Thus, a significant increase of binding possibilities seems reasonable.

3.2. Enzyme Immobilization

For the selected enzymes lipase and laccase, adsorptive and covalent immobilization to the BT surface was the aim. Exclusively considering one enzyme, the results of achieved surface amounts were compared. The generation of an enzyme-carrier interaction depends significantly on the spatial presentation of suitable functional groups or binding domains of the enzyme, as well as the surface chemistry of the carrier material. Prior to its application for enzyme immobilization, the surveyed BT was treated with HCl, leading to superficial hydrolysis. Polymer inherent amino groups were thereby exposed, which were not available for the raw material. This generated BT surface served as a basis for adsorptive immobilization of the enzymes or was used either directly for covalent attachment or after implementation of a reactive PEMA layer on BT surface. Lipase was fixed directly on the BT surface by EDC activation of carboxyl functions of the enzyme, and covalent laccase tethering was performed onto PEMA-modified BT. The advantage of the additional PEMA hydrogel layer is based on the introduction of highly reactive anhydride moieties to the surface. These moieties ensure, on the one hand, the linkage of the interlayer to the amine-containing carrier, creating stable imide bonds. On the other hand, unused anhydride groups enable covalent fixation of enzymes. However, the enzyme might also adsorb additionally onto the surface and thus add to the final amount of immobilized enzymes. Compared to the use of EDC for the activation of carboxyl functions on the enzymes' surface, PEMA provides reactive groups located on the BT surface. The latter allows for specific covalent bonds to be formed only between enzyme and carrier and prevents the uncontrolled additional linkage of enzyme molecules to each other, thus preventing loss of enzyme activity.

After adsorptive lipase and laccase immobilization, a higher amount of immobilized enzymes was determined, as after covalent fixation, since SDS treatment was applied afterwards. It can therefore be assumed that the covalent type of immobilization includes also a portion of adsorptive immobilization, as well, because the covalent immobilization cannot occur independently of the adsorptive one. The hypothesis can be proposed that this portion of non-covalent-bound enzyme molecules has been desorbed, leading to a decline of immobilized enzyme amount. As SDS treatment is a very rough approach for detaching enzymes from surfaces, the remaining amounts can be seen as firmly attached to the BT surface. For enzyme-BT samples after adsorptive tethering, no SDS treatment was performed so that a high number of non-covalent interactions can persist. This interplay may occur between enzyme and carrier and, particularly, between enzyme molecules themselves, but does not allow for permanent anchoring of the enzyme molecules to the carrier surface.

Figure 5 shows a comparison of the used immobilization techniques for both chosen enzymes. Based on the theoretical assumptions made in section 2.3.2, immobilization results are compared to a theoretical ideal monolayer of immobilized enzymes. Therefore, the amount of immobilized enzymes, as well as the enzyme activity of the samples were considered. Adsorptively-bound lipase showed the highest amounts of immobilized enzymes. As it was significantly higher than for an expected monolayer, it can be assumed that multilayer immobilization occurred. However, it did not result in higher amounts of enzyme activity. For laccase, adsorptively-bound enzyme resulted in slightly better enzyme activity compared to the covalent binding method, which is also the case when comparing the immobilized enzyme amounts. The difference between the immobilization results of adsorptively-bound lipase and laccase can partly be explained by taking the concept of 'hard' and 'soft' proteins into account, which was introduced by Norde and Anusiem in 1992 [45]. While 'soft' proteins, with their lower internal structural stability, can be adsorbed better onto surfaces, 'hard' proteins, in contrast, have stronger inner connections and hence a higher stability of their native structure.

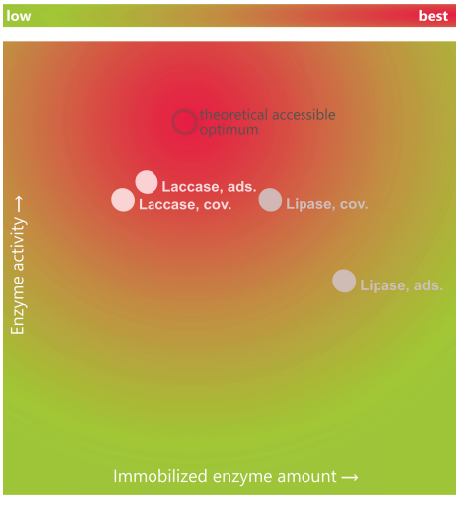

Figure 5. Classification of used immobilization strategies for laccase and lipase compared to a theoretically-accessible optimum of enzyme immobilization. Red shading represents better results, while green shading otherwise symbolizes lower immobilization rates and/or lower enzyme activity. The figure compares the respective optimal conditions of enzyme immobilization for adsorptive (ads.) immobilization without SDS treatment and for covalent (cov.) immobilization results after washing with SDS solution. Activity values were compared to the free enzymes as given in Table 2.

In comparison to the dissolved enzymes, the immobilization leads to an activity decrease for both biocatalysts. Nonetheless, the respective best activity results reached a comparable level for both enzymes. The used immobilization methods tether the enzyme molecules to the BT surface, but it cannot be excluded that access to the active side is hindered by the spatial orientation of the enzymes on the BT surface. Furthermore, there is a probability that during covalent immobilization, on the one hand, functional groups of the active site or some close to it are linked to the BT surface or to other functionalities of further lipase molecules during the lipase immobilization. On the other hand, besides the linkage of nucleophilic groups on the surface of the laccase molecule with the anhydride moieties on the BT-PEMA surface, a covalent bond between anhydride groups and amino acid sidechains of the active side of laccase can occur. Moreover, structural changes in the secondary and tertiary structure of the enzyme molecules caused by the immobilization processes are possible. All these factors would explain a decrease in enzyme activity.

3.3. Analysis of Basotect® Surface Coverage with Enzyme

Determination of the theoretical surface coverage and its comparison with the BT surface actually covered by enzyme molecules allows for the evaluation of the BT surface to be available for immobilization. It was assumed that the enzyme molecules' spheres are rectangular cuboid-shaped and the surface is coated with an enzyme monolayer. For its formation, a theoretical coverage area is edged by the two extreme states of enzyme molecule orientation on the BT surface. These boundaries represent the minimum or maximum surface-specific enzyme mass and frame a permitted surface coverage range (see Figure 6). For this purpose, it was assumed that all enzyme cuboids are bound exclusively to the BT with their smallest (maximum surface-specific enzyme mass) or exclusively with their largest contact surface (minimum surface-specific enzyme mass). All values below the minimum surface-specific enzyme mass indicate that the surface is not completely covered by enzyme molecules and free space is present. In contrast, measured surface-specific enzyme masses above the maximum limit allow the assumption that enzyme aggregates or multilayers were formed. For the range between

the two limits, it can be assumed that an enzyme monolayer was formed. However, local enzyme aggregations associated with uncovered regions cannot be excluded, although the surface-specific enzyme mass is within the permissible range.

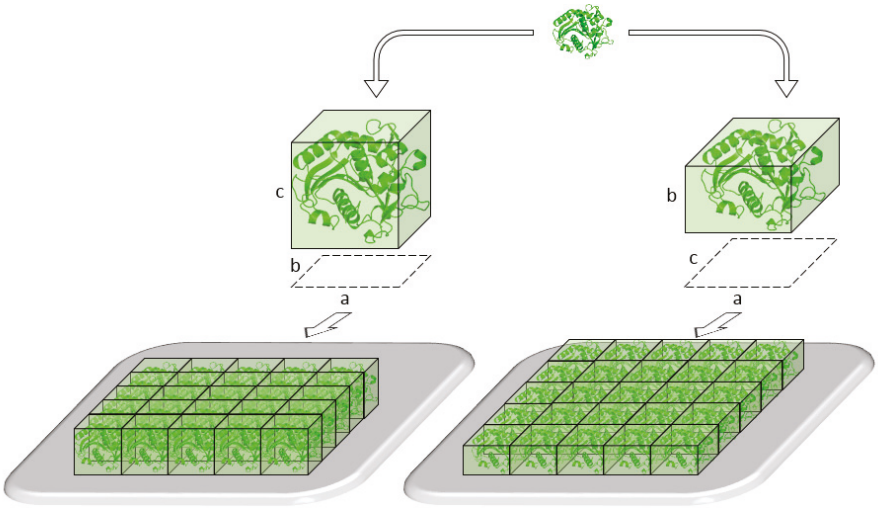

Figure 6. Visualization of the theoretical orientation and distribution of a lipase molecule on the BT surface. Assuming a cuboid morphology, lipase can theoretically attach to the BT surface with its smallest (area a × b) or largest (area a × c) cuboid area. After complete coverage of the carrier surface with enzyme, a minimum and maximum of lipase molecules per BT surface can be calculated and represent a range of theoretical surface-specific enzyme mass. In comparison, the real orientation of the lipase molecules on the BT surface is assumed as a random process. Furthermore, real coverage can take place in three states: (I) below the theoretical minimum, representing incomplete BT surface coverage, (II) above the theoretical maximum, representing an enzyme multilayer or enzyme aggregate formation, and (III) within the theoretical minimum and maximum, when immobilized enzyme mass is in this range, but enzyme aggregates exist with free space between. However, comparing the theoretical and measured states allows an assessment of utilizing the available BT surface for enzyme immobilization. The 3D model of lipase was taken from the RCSB Protein Data Base (ID code: 1DT3).

After adsorptive immobilization of lipase, the determined surface concentration indicates a multilayer composition or aggregation of enzyme molecules on the surface, since the maximum theoretical surface concentration has been exceeded. A subsequent SDS treatment also showed inadequate interactions between enzyme aggregates and the BT surface. The lipase molecules could be detached from the surface so much that an incompletely covered surface remained. For covalent lipase immobilization utilizing EDC, exceeding of the maximum theoretical surface coverage was found to be positive in regard to the amount of fixed lipase. It has been suggested that during this immobilization, two processes run in parallel: lipase molecules bind to the BT surface adsorptively and other lipase molecules aggregate to the existing enzyme layer. At the same time, EDC induces the covalent linkage of lipase and BT, as well as the cross-linking of lipase molecules among themselves. However, this non-directed immobilization must be regarded as critical, since the chemical bond can also be generated with amino acids of the active side and thus lead to enzyme inactivation. The fact that the lipase molecules in the aggregates are not completely interconnected with each other or with the BT surface is suggested by SDS treatment. Nevertheless, in comparison to adsorptive immobilization, a higher amount of lipase could be stably bound to the BT, which has not been detached from the surface by SDS. Furthermore, in comparison to adsorptive lipase immobilization,

the higher surface concentration of the enzyme automatically leads to a higher BT-specific activity after covalent immobilization.

Considering the range of theoretical surface coverage of the BT with laccase, the measured surface concentrations indicate that after adsorptive and covalent immobilization and without SDS treatment, almost the entire surface is covered. After covalent immobilization and SDS treatment, however, slightly more than half of the surface was occupied with laccase. This is a clear difference to lipase immobilization, in which the theoretically maximum surface concentration was consistently exceeded. Furthermore, the additional detachment of enzyme molecules by SDS treatment indicates that parts of the covalently-immobilized laccase have not formed a sufficiently strong bond to the BT surface. Furthermore, the almost equal surface concentrations after adsorptive immobilization at BT and covalent immobilization at PEMA-BT with subsequent SDS treatment indicate that the covalent technique does not lead to an enhancement of the binding stability between enzyme and BT in laccase immobilization. It can be assumed that adsorptive interactions between laccase and BT are beneficially developed such that no desorption from the BT surface can be initiated by SDS treatment. The lack of formation of the covalent bond between laccase and PEMA-BT is also conceivable.

Since BT was pretreated in the same way for the adsorptive immobilization without subsequent SDS treatment for both enzymes, a comparison of the immobilization ability of the BT can be carried out. For this purpose equal molar enzyme solution concentrations of about 9 $nmol \cdot mL^{-1}$ were used for the immobilization. If the obtained surface coverage of both enzymes is compared, regardless of the pH of immobilization solution (see Table 4) and the isoelectric point of the enzymes (pI_{lipase} = 4.4, $pI_{laccase}$ = 5.8), almost the same molar surface concentration at the BT could be achieved after adsorptive lipase and laccase immobilization when using the same molar enzyme solution concentrations. This suggests that the immobilization process with the acid pretreated BT surface is primarily independent of the polarity of the binding partners. Despite having the same molar concentrations in the immobilization solution, the BT surface could not be fully occupied when using laccase compared to lipase. This is due to the smaller size of a laccase molecule in comparison with lipase (for sizes of the enzymes, see Section 4.9).

3.4. Stability of Immobilized Enzymes

Immobilization of enzymes on solid support materials can fix their geometrical structure and increase stability. This enables, i.a., an increase of operating time, the application in enzyme hostile reaction systems and the more economical application of these biocatalysts. Furthermore, the immobilization of enzymes enables the preservation of activity during storage periods, while the activity of free enzymes frequently decreases. According to the immobilization method and storage conditions, immobilization of the enzymes on BT preserve the activity. Lipase was bound adsorptively and covalently via EDC activation to the BT and frozen at −18 °C. The results indicate that the freeze and thaw process changes the tertiary structure of the lipase and thus continuously reduces the activity after seven days. However, it was found that the decline of activity after adsorptive lipase tethering was significantly higher than after covalent linkage, possibly caused by additional desorption processes. This suggests that the generation of covalent cross-links between BT and lipase and between lipase molecules themselves better preserves the enzyme structure than adsorptive fixation. In contrast, the activity of immobilized laccase could be maintained at a constant level during storage at 4 °C. Accordingly, it can be concluded that the cooled and non-frozen storage of immobilized enzymes on BT carrier is advantageous.

3.5. Prospect and Applications

Due to its porous structure, functionalized Basotect® can be easily applied as a catalyst for utilization in fluid media. A possible application for immobilized enzymes is the elimination of hazardous trace substances from wastewater or drinking water [46,47]. The oxidoreductase laccase was immobilized on PEMA-functionalized BT and tested in an application in order to demonstrate

an alternative possibility to reduce water pollution of anthropogenic contaminants. Often, many of these substances cannot be removed from urban wastewater by conventional wastewater treatment plants mainly due to their polarity and toxicity and thus become persistent in the environment over time [48]. In recent years, alternative methods were developed, to get rid of such pollutants mainly by oxidizing them with UV radiation or ozonation [49]. Other alternatives like the Fenton process and sonification were also considered [50]. All these new approaches can be summarized by the term advanced oxidation processes (AOPs) [51] and are mostly still under development for technical use. Using oxidizing enzymes for a similar approach is, therefore, also a promising option. The persistent water pollutant bisphenol A was chosen to show that immobilized laccase can be utilized to eliminate organic micropollutants. Immobilized laccase on BT carrier was applied to eliminate bisphenol A out of a mix of water pollutants. A reduction of initial BPA amount by 90% within 48 h was figured out. A higher result could be achieved by a longer reaction time. To examine multiple uses of immobilized laccase in a second attempt, the same pieces of BT were used again to reduce the amount of bisphenol A, and a reduction of the initial BPA content by 80% within the first two days was shown. Degradation efficiency and rate can be adjusted by the amount of applied laccase-functionalized BT pieces. As aging of the immobilized enzyme and maybe also desorption of adsorptively-bound laccase occur, the degradation rate becomes lesser when immobilized laccase was applied repeatedly. For a technical application of this first approach, a scale up is necessary. Furthermore, reaction times may also decrease, if immobilized oxidoreductases are applied in a flow-through reactor. Basotect® analyzed in this study provides an excellent carrier material for such an application, especially because it can be easy flowed through due to its wide open porous structure. Additionally, it is easy to functionalize with several biocatalysts and ensures their multiple and long-term usability. Particularly for such use cases, we can recommend this carrier material, which supplies a highly customizable surface and allows also an easy exchange between the biocatalysts and their substrates.

4. Materials and Methods

The melamine formaldehyde resin Basotect® was provided by BASF Schwarzheide GmbH as white slabstock foam. The copolymer PEMA with a molecular weight of 100 to 500 $kg \cdot mol^{-1}$ was obtained from Sigma Aldrich (Taufkirchen, Germany). Lipase from *Thermomyces lanuginosus* was acquired as type "NOVAREKO" solution from NovaBiotech Dr. Fechter GmbH. Laccase was used from the white rot fungus *Trametes versicolor* and purchased from Sigma Aldrich (#51639 with 10 $kU \cdot g^{-1}$).

4.1. Size and HCl Treatment of Basotect® Samples

BT was cut into pieces having a final size of $10 \times 3 \times 3\,mm^3$ (each with a weight of about 500 µg), predominantly, to generate samples for the analyses.

For all enzyme immobilization experiments, BT was pretreated with hydrochloric acid. In detail, BT samples were immersed in concentrated HCl solution for 20 min at 24 °C without previous cleaning of the raw material. Afterwards, the samples were rinsed with ultrapure water and incubated in 1 mL 0.1 M phosphate buffer pH = 8.0 for 15 min. Finally, the water-rinsed samples were dried at 60 °C for 4 h.

4.2. Scanning Electron Microscopy of Basotect®

Morphological analysis of BT was performed using a Philips XL 30 scanning electron microscope. Samples were examined in native form and after incubation in concentrated hydrochloric acid at 24 °C for 90 min, respectively. Subsequently, acid-treated samples were rinsed with ultrapure water intensively and dried at 60 °C for 4 h. After mounting on an aluminum specimen holder, the samples were coated with gold utilizing an Emitech K550 sputter-coater to create a layer of approximately 20 nm.

4.3. Amino Group Detection

4.3.1. ATTO-TAG FQ Fluorescence Labeling

Primary amino groups on the BT surface were identified by derivatization with the ATTO-TAG™ FQ Amine-Derivatization Kit (Molecular Probes, Eugene, OR, USA) with subsequent fluorescence microscopy. For fluorescence labeling, the manufacturer's protocol was modified to perform the reaction with superficially available amino groups. In detail, 2.5 mg·mL^{-1} ATTO-TAG™ FQ solution in methanol, 0.01 M KCN solution and a 0.1 M borate buffer pH = 9.5 were mixed at a volume ratio of 1:2:2.5. BT samples were immersed in 0.3 mL of these solution and incubated at room temperature for 1 h. Subsequently, samples were rinsed intensively with ultrapure water and analyzed using a Leica TCP SP laser scanning microscope (excitation 488 nm, emission 590 nm).

For the positive control, glass slides were cleaned as described elsewhere [52], subsequently placed in a Petri dish (diameter 150 mm), and 100 µL of 3-aminopropyltriethoxysilane were added on a small watch-glass. The Petri dish was sealed with parafilm, and gas phase silanization was carried out at room temperature overnight. The resulting amino silanized glass slides were rinsed with toluene and dried with nitrogen. ATTO-TAG™ FQ treatment of the glass slides was carried out as described for BT.

4.3.2. Orange II Assay

The assay, which had been previously described by Noel et al. [40], is based on the pH-driven ionic interaction between a negatively-charged dye and the positively-charged surface and was modified for use with BT. A piece of foam was incubated in 1.5 mL Orange II solution (0.5 mM, in water at pH = 3 adjusted with hydrochloric acid; Orange II was obtained from Sigma Aldrich, Taufkirchen, Germany) at 40 °C for two hours and shaken vigorously at 750 rpm. Afterwards, the pieces were washed with at least 4 mL of HCl (pH = 3) four times. Desorption of bound dye was carried out by incubation of washed and dried BT pieces in 1 mL NaOH (pH = 12) for ten minutes. Finally, one-hundredth fuming HCl (37%) was added to the solution and its absorption in a 10-mm cuvette was measured at 484 nm. DoA was determined from absorption ΔE by the following formula using the Orange II molar attenuation coefficient ε of 18.1 mL·µmol^{-1}·cm^{-1}, the volume V of the assay solution, the mass of BT (m_{BT}) and the layer thickness d (length of the light path in the cuvette):

$$\mathrm{DoA} = \frac{\Delta \mathrm{E} \cdot V}{m_{\mathrm{BT}} \cdot d \cdot \varepsilon}.$$

4.4. PEMA Functionalization

To obtain a homogeneous coating of the inner surface of BT with the copolymer PEMA, HCl-pretreated pieces were submerged in a solution of 1 wt% PEMA in acetone and THF (volume ratio 1:2) and shaken firmly at 150 rpm for 24 h. The small pieces were removed from solution, and the remaining solvent was withdrawn by using a pipette until dry. Afterwards, the BT foam was tempered at 120 °C for at least two hours. In a final step, the cooled functionalized pieces were flushed with acetone at 120 rpm twice for 15 min and subsequently tempered again at 120 °C for two hours. The functionalized carrier was used immediately or stored dry and in the dark.

4.4.1. ATR-FTIR Analysis

The surface modification of PEMA-functionalized Basotect® was analyzed with a Nicolet™ iS™10 FTIR spectrometer (Thermo Scientific, Dreieich, Germany) equipped with a diamond crystal.

4.4.2. TBO Assay

Toluidine blue O (TBO), a blue cationic dye, was purchased from Sigma Aldrich and used as an easy photometric assay to quantify free carboxylic moieties onto PEMA-functionalized BT surfaces.

This application was earlier specified by Sano et al. [53] and is based on pH shifting. At basic conditions carboxylic groups exist as carboxylate anion, so cationic TBO is able to bind via ionic interactions [43]. At first, all carboxylic groups were hydrolyzed by immersing BT pieces in water twice for 30 min at 40 °C and shaken at 750 rpm. Dyeing of BT was performed afterwards by incubation of one BT piece in 1 mL 0.25 M TBO solution in 0.1 M NaOH for two hours at 40 °C and 1000 rpm. The unbound dye was subsequently removed by washing BT pieces repeatedly with 10 mL 0.1 M NaOH until the washing solution appeared clear, or at least five times for 10 min each. Attached TBO dye was then dissolved by washing in 1 mL 50 vol% acetic acid for 30 min at 40 °C and 1000 rpm. Absorption (ΔE) of this solution was measured at 633 nm, and the degree of carboxylation (DoC) in nmol·mg^{-1} was calculated with a molar attenuation coefficient (ε) of 54.8 mL·µmol^{-1}·cm^{-1} and by assuming that 3.4 mole carboxylic groups bind one TBO molecule according to Henning et al. [54].

$$\mathrm{DoC} = 3.4 \cdot \frac{\Delta \mathrm{E} \cdot V}{m_{\mathrm{BT}} \cdot d \cdot \varepsilon},$$

where V is the volume of the assay solution, m_{BT} is the mass of applied BT and d the layer thickness (length of the light path in the cuvette).

4.5. Enzyme Immobilization

Detailed conditions for adsorptive and covalent enzyme immobilization are summarized in Table 4.

Table 4. Conditions for adsorptive and covalent immobilization of laccase and lipase on acid-pretreated BT or PEMA-BT, respectively.

	Enzyme Concentration in Solution (mg·mL^{-1})	Immobilization Time (h)	Composition of Immobilization Solution	Wash Procedure
Lipase	3.0	0.5 (adsorptive) 2.0 (covalent)	1% Propylene glycol, 1.6% PEG400, 0.01% $CaCl_2$, pH = 6.1	Five-times dipping into 30 mL ultrapure water, three wash cycles
Laccase	0.5	4.0	0.2 M sodium citrate buffer, pH = 4.5	Incubation in 5 mL 0.2 M sodium citrate buffer (pH = 4.5) on orbital shaker at 110 rpm for 15 min, three wash cycles

4.5.1. Adsorptive Immobilization

The acid-pretreated slabstocks were incubated on a horizontal shaker at 100 rpm and at room temperature in 1 mL laccase or lipase solution, respectively, and washed subsequently.

4.5.2. Covalent Immobilization

For lipase immobilization, one piece of HCl-treated (see Section 4.1) and non-dried BT was immersed in 1 mL lipase solution containing 0.1 M EDC (Sigma Aldrich, Taufkirchen, Germany) at room temperature. For laccase immobilization, 1 mL of laccase solution was added to three PEMA functionalized BT pieces (see Section 4.4) and incubated on an orbital shaker at 90 rpm and room temperature. Afterwards, all samples were washed (see Table 4) and treated with SDS solution (see Section 4.5.3).

4.5.3. SDS Treatment

After covalent immobilization, enzyme-functionalized BT or PEMA-BT pieces, respectively, were treated with SDS solution. Lipase-BT samples were treated with 2 wt% SDS solution at 25 °C for 30 min. Laccase-PEMA-BT samples were treated with 1 wt% SDS solution at 25 °C while vigorously shaking at 800 rpm for 24 h and, subsequently, washed in Millipore water again for 24 h under the same conditions.

4.6. Storage Conditions

4.6.1. Laccase on PEMA-BT

Laccase functionalized PEMA-BT pieces were stored in citrate buffer solution (pH = 4.5) at 4 °C until the next measurement of laccase activity, as described in Section 4.8.

4.6.2. Lipase on BT

Lipase-loaded BT samples were stored in 0.1 M phosphate buffer (pH = 7.4) at −18 °C, and lipase activity was determined (see Section 4.8) after several periods.

4.7. Protein Quantification

The amount of surface-bound protein was analyzed using a micro-bicinchoninic acid (BCA) protein quantification assay (Pierce, Thermo Scientific, Waltham, MA, USA). BCA working reagent was prepared following the manufacturer's protocol. To one moist protein-loaded BT or PEMA-BT sample, ultrapure water was added to a final liquid volume of 500 µL. Subsequently, the sample solution was mixed with 500 µL of BCA working reagent and incubated on a Thermomixer (Eppendorf AG, Hamburg, Germany) at 60 °C and 750 rpm for 1 h. After cooling to room temperature, the resulting solution was transferred to polystyrene cuvettes, and absorption at 562 nm was analyzed. For the generation of blanks, immobilization procedures onto acid-pretreated BT and PEMA-BT were performed without enzyme, and BCA assay was applied.

4.8. Enzyme Activity

4.8.1. Lipase

For activity measurement, the lipase-catalyzed hydrolysis of *p*-nitrophenyl palmitate to palmitate and the chromatic *p*-nitrophenolate was followed spectrophotometrically. In detail, 9 mL of 0.1 M TRIS buffer pH = 8.0, containing 1.0 $mg \cdot mL^{-1}$ gum arabic (Sigma Aldrich, Taufkirchen, Germany) and 8 $mg \cdot mL^{-1}$ Triton X-100 (AppliChem GmbH, Darmstadt, Germany), was blended with 1.0 mL of 3.0 $mg \cdot mL^{-1}$ *p*-nitrophenyl palmitate (Sigma Aldrich, Taufkirchen, Germany) in 2-propanol in a beaker equipped with a magnetic stir bar. The temperature of the resulting solution was adjusted to 45 °C. Subsequently, one piece of lipase-loaded BT was added and stirred at 500 rpm. After 1 min and 5 min, respectively, 1 mL of solution was removed, and absorption was measured at 405 nm.

4.8.2. Laccase

Laccase activity was determined via the ABTS assay (ABTS = 2,2′-azino-bis(3-ethylbenzthiazoline-6-sulfonic acid; Sigma Aldrich, Taufkirchen, Germany). A sodium citrate buffer (0.5 M, pH = 5.3) was used, and a 207 µM ABTS solution was prepared and tempered at 37 °C. Eight hundred fifty two microliters of ABTS solution and 648 µL buffer were mixed together with one piece of laccase-functionalized BT in a cuvette, and absorption at 420 nm was recorded for 30 min to 120 min every 30 s, while tempered at 37 °C. Every ten minutes, the porous BT was squeezed in order to get a homogeneous mixture. The slope of the linear front part of the curve (absorption vs. time) was used to calculate laccase enzyme units assuming that 1 µmol ABTS was oxidized per minute

To calculate the enzyme activity (EA) for the respective assay, the difference in absorption (ΔE) corrected by the blank was inserted in the equation:

$$\mathrm{EA} = \frac{\Delta \mathrm{E}}{\Delta t} \cdot \frac{V}{\varepsilon \cdot d},$$

where V is the total volume of the assay solution, $\Delta t$is the time difference, ε is the molar attenuation coefficient (18.3 mL·µmol^{-1}·cm^{-1} (for *p*-nitrophenolate) and 36.0 mL·µmol^{-1}·cm^{-1} (for ABTS)) and d is the path length of the beam of light through the solution.

4.9. Calculation of Theoretical and Actual Enzyme Surface Concentration

The sizes of a laccase molecule (RCSB PDB ID code: 1GYC) is $9.2 \times 8.5 \times 8.4\,\mathrm{nm}^3$ and of a lipase molecule (RCSB PDB ID code: 1DT3) is $13.9 \times 13.9 \times 8.1\,\mathrm{nm}^3$. Values were taken from the RCSB protein database. Assuming a rectangular cuboid morphology of the enzymes as shown in Figure 6, the minimum and maximum rectangular planar surface area of a laccase molecule are 71.4 nm^2 and 78.2 nm^2, respectively, and for lipase are 112.6 nm^2 and 193.2 nm^2, respectively. The theoretical minimum and maximum of enzyme surface coverage was calculated, assuming the creation of enzyme monolayers in a compact side-on configuration. The quantity of enzyme molecules was identified, when a specific BT surface is fully covered either with all molecules in contact with the smallest or the largest contact surface of the enzyme cuboid, respectively. The theoretical surface coverage Γ is calculated using the equation:

$$\Gamma = \frac{M}{A_1 \cdot N_A},$$

where M is the molar mass of the enzyme, N_A is the Avogadro constant and A_1 is the respective smallest or largest contact area of one enzyme molecule cuboid.

For the calculation of actual enzyme surface concentration, the detected enzyme mass per mass of BT (see Table 2) was divided by the specific surface of BT.

4.10. Degradation of Bisphenol A Utilizing Laccase on PEMA-BT

4.10.1. Experimental Setup

Degradation, more precisely an oxidative removal, of anthropogenic micropollutants was done by treating a solution of organic micropollutants with laccase-functionalized pieces of PEMA-BT. The design of the experiment was established as follows: PEMA-coated BT foam pieces were functionalized with laccase as described above (see Section 4.5.2). Around twenty of them (which together carried ~1 U of laccase activity) were placed in a reaction tube, and a 10-mL mix of anthropogenic micropollutants was added (the final concentration of each pollutant was 1.4 nM). The mixture was then shaken vigorously for several days. The amount of micropollutants was monitored by LC-MS/MS at reasonable periods.

4.10.2. LC-MS/MS Detection of BPA

For quantification of bisphenol A (BPA; Sigma Aldrich, Taufkirchen, Germany), an Agilent Triple Quadrupole LC-MS/MS 6400 system was used. BPA was separated with a Phenomenex reversed phase column (Gemini-NX 3 µm; C_{18}; 110 Å; 100 × 2 mm) and a mobile phase mixture of acetonitrile (A) and 0.05 vol% NH_3 (B) from 67% A to 97% B within two minutes and back to 33% B (stop time: 4 min) with a retention time of 2.4 min and identified after ESI ionization in negative ion mode by its specific fragments at m/z 212 (quantifier) and m/z 195, 133 and 117 as qualifiers (see Tables 5 and 6 for detailed LC and MS parameters). BPA-16d was used as the internal standard for quantification. Calibration was established from 0.1 and 75 µM with 12 levels and a coefficient of determination of 99.8%.

Table 5. MS parameters for quantification of BPA.

	Precursor Ion	Product Ion	Frag-Mentor (V)	Collision Energy (V)	CAV (V)
BPA-16d	241	223	140	17	4
	241	142	140	23	3
BPA	227	212	140	17	4
	227	195	140	42	5
	227	133	140	23	3
	227	117	140	57	4

Table 6. LC parameters for quantification of BPA.

Parameter	Value
Temperature	35 °C
Flow	0.4 mL·min^{-1}
Injection volume	15 µL
Source	300 °C
Gas flow (N_2)	11 L·min^{-1}
Capillary	4000 V

5. Conclusions

This study has found that the applied macroporous BT is generally suitable for enzyme immobilization. The developed enzyme-BT assemblies were active in reactions with model substrates, but the immobilization reduces the enzyme activity. Due to the uncovering of amino groups on its surface, BT represents a favorable framework for covalent enzyme immobilization. Existing amino groups on the BT surface can be presumably used to achieve a stable covalent attachment of lipase molecules by an EDC-mediated reaction. Furthermore, PEMA modification of the BT surface leads to high-reactive anhydride moieties that increase the number of functionalities for covalent tethering compared to amino moieties and are more suitable for enzyme immobilization than EDC. The assessment of BT surface coverage with enzyme molecules suggests that lipase not only interacts with the BT surface, but also forms appropriate interactions within lipase molecules. It is assumed that aggregations or multilayers are formed on the BT surface. This intermolecular interaction probably does not exist between laccase molecules. Consequently, interactions between BT and laccase molecules lead to the almost complete coverage of the BT surface by the formation of an enzyme monolayer. Although the immobilized enzyme amount is low, compared to other carrier materials, due to its open porous structure and resultant favorable flow conditions, as well as its chemical resistance, the potential as an enzyme carrier for technical and industrial application is ascribed to BT.

Acknowledgments: The authors thank the BASF Schwarzheide GmbH for allocation of Basotect® and for financial support. Parts of this work were funded by the German Federal Ministry of Economics Affairs and Energy (Grant No. KF2088012RH1: "Biokatalytische Entfernung von persistenten synthetischen organischen Kohlenwasserstoffen (SOC) aus (Ab-)wässern"). We thank Victoria Albrecht (Leibniz Institute of Polymer Research Dresden) for the determination of BT surface area and Bernhard Glück (BTUCottbus-Senftenberg) for support with the scanning electron microscopy. The technical assistance of Peter Kermer is gratefully acknowledged.

Author Contributions: P.J.A., S.B. and K.S. conceived of and designed the experiments. S.B., G.S., C.D. and M.D. performed the experiments. P.J.A. and S.B. analyzed the data. BASF Schwarzheide GmbH contributed Basotect®. P.J.A. and S.B. wrote the paper and K.S., K.-P.S. contributed to the paper.

Conflicts of Interest: The authors declare no conflict of interest. The founding sponsors had no role in the design of the study; in the collection, analyses or interpretation of data; in the writing of the manuscript; nor in the decision to publish the results.

References

1. Cantone, S.; Ferrario, V.; Corici, L.; Ebert, C.; Fattor, D.; Spizzo, P.; Gardossi, L. Efficient immobilisation of industrial biocatalysts: criteria and constraints for the selection of organic polymeric carriers and immobilisation methods. *Chem. Soc. Rev.* **2013**, *42*, 6262–6276.
2. Garcia-Galan, C.; Berenguer-Murcia, N.; Fernandez-Lafuente, R.; Rodrigues, R.C. Potential of different enzyme immobilization strategies to improve enzyme performance. *Adv. Synth. Catal.* **2011**, *353*, 2885–2904.
3. DiCosimo, R.; McAuliffe, J.; Poulose, A.J.; Bohlmann, G. Industrial use of immobilized enzymes. *Chem. Soc. Rev.* **2013**, *42*, 6437–6474.
4. Liese, A.; Hilterhaus, L. Evaluation of immobilized enzymes for industrial applications. *Chem. Soc. Rev.* **2013**, *42*, 6236–6249.
5. Hanefeld, U.; Gardossi, L.; Magner, E. Understanding enzyme immobilisation. *Chem. Soc. Rev.* **2009**, *38*, 453–468.
6. Tischer, W.; Wedekind, F. Immobilized Enzymes: Methods and Applications. In *Biocatalysis—From Discovery to Application*; Springer: Berlin/Heidelberg, Germany, 1999; pp. 95–126.
7. Rodrigues, R.C.; Berenguer-Murcia, N.; Fernandez-Lafuente, R. Coupling chemical modification and immobilization to improve the catalytic performance of enzymes. *Adv. Synth. Catal.* **2011**, *353*, 2216–2238.
8. Balcão, V.M.; Vila, M.M. Structural and functional stabilization of protein entities: State-of-the-art. *Adv. Drug Deliv. Rev.* **2015**, *93*, 25–41.
9. Stepankova, V.; Bidmanova, S.; Koudelakova, T.; Prokop, Z.; Chaloupkova, R.; Damborsky, J. Strategies for stabilization of enzymes in organic solvents. *ACS Catal.* **2013**, *3*, 2823–2836.
10. Brady, D.; Jordaan, J. Advances in enzyme immobilisation. *Biotechnol. Lett.* **2009**, *31*, 1639–1650.
11. Bayramoglu, G.; Kacar, Y.; Denizli, A.; Yakup Arica, M. Covalent immobilization of lipase onto hydrophobic group incorporated poly(2-hydroxyethyl methacrylate) based hydrophilic membrane matrix. *J. Food Eng.* **2002**, *52*, 367–374.
12. Min, K.; Yoo, Y.J. Recent progress in nanobiocatalysis for enzyme immobilization and its application. *Biotechnol. Bioprocess Eng.* **2014**, *19*, 553–567.
13. Rodrigues, R.C.; Ortiz, C.; Berenguer-Murcia, A.; Torres, R.; Fernandez-Lafuente, R. Modifying enzyme activity and selectivity by immobilization. *Chem. Soc. Rev.* **2013**, *42*, 6290–6307.
14. Pompe, T.; Zschoche, S.; Herold, N.; Salchert, K.; Gouzy, M.F.; Sperling, C.; Werner, C. Maleic anhydride copolymersa versatile platform for molecular biosurface engineering. *Biomacromolecules* **2003**, *4*, 1072–1079.
15. Wetzel, S.; Allertz, P.J.; Koschnicke, S.; Tasso, M.; Salchert, K. Immobilized enzymes—Valuable tools for the indication of temperature events. *Biocatal. Biotransform.* **2013**, *31*, 100–113.
16. Pompe, T.; Renner, L.; Grimmer, M.; Herold, N.; Werner, C. Functional films of maleic anhydride copolymers under physiological conditions. *Macromol. Biosci.* **2005**, *5*, 890–895.
17. Fernandez-Lafuente, R. Lipase from Thermomyces lanuginosus: Uses and prospects as an industrial biocatalyst. *J. Mol. Catal. B Enzym.* **2010**, *62*, 197–212.
18. Bezerra, R.M.; Neto, D.M.A.; GalvÃ£o, W.S.; Rios, N.S.; de Carvalho, A.C.L.M.; Correa, M.A.; Bohn, F.; Fernandez-Lafuente, R.; Fechine, P.B.; de Mattos, M.C.; et al. Design of a lipase-nano particle biocatalysts and its use in the kinetic resolution of medicament precursors. *Biochem. Eng. J.* **2017**, *125*, 104–115.
19. Tacias-Pascacio, V.G.; Virgen-OrtÃz, J.J.; Jiménez-Pérez, M.; Yates, M.; Torrestiana-Sanchez, B.; Rosales-Quintero, A.; Fernandez-Lafuente, R. Evaluation of different lipase biocatalysts in the production of biodiesel from used cooking oil: Critical role of the immobilization support. *Fuel* **2017**, *200*, 1–10.
20. Rodríguez Couto, S.; Toca Herrera, J.L. Industrial and biotechnological applications of laccases: A review. *Biotechnol. Adv.* **2006**, *24*, 500–513.
21. Gamallo, M.; Moldes-Diz, Y.; Eibes, G.; Feijoo, G.; Lema, J.M.; Moreira, M.T. Sequential reactors for the removal of endocrine disrupting chemicals by laccase immobilized onto fumed silica microparticles. *Biocatal. Biotransform.* **2017**, 1–11, doi:10.1080/10242422.2017.1316489.
22. Dai, Y.; Yao, J.; Song, Y.; Liu, X.; Wang, S.; Yuan, Y. Enhanced performance of immobilized laccase in electrospun fibrous membranes by carbon nanotubes modification and its application for bisphenol A removal from water. *J. Hazard. Mater.* **2016**, *317*, 485–493.

23. Torrinha, L.; Montenegro, M.C.B.S.M.; AraÃjo, A.N. Implementation of a simple nanostructured bio-electrode with immobilized *Rhus vernicifera* laccase for oxygen sensing applications. *Electroanalysis* **2017**, *29*, 1566–1572.
24. Fernandez-Lafuente, R.; Armisen, P.; Sabuquillo, P.; Fernandez-Lorente, G.; Guisan, J.M. Immobilization of lipases by selective adsorption on hydrophobic supports. *Chem. Phys. Lipids* **1998**, *93*, 185–197.
25. Minovska, V.; Winkelhausen, E.; Kuzmanova, S. Lipase immobilized by different techniques on various support materials applied in oil hydrolysis. *J. Serbian Chem. Soc.* **2005**, *70*, 609–624.
26. Kosaka, P.M.; Kawano, Y.; El Seoud, O.A.; Petri, D.F.S. Catalytic Activity of Lipase Immobilized onto Ultrathin Films of Cellulose Esters. *Langmuir* **2007**, *23*, 12167–12173.
27. Xu, R.; Si, Y.; Wu, X.; Li, F.; Zhang, B. Triclosan removal by laccase immobilized on mesoporous nanofibers: Strong adsorption and efficient degradation. *Chem. Eng. J.* **2014**, *255*, 63–70.
28. De Cazes, M.; Belleville, M.P.; Mougel, M.; Kellner, H.; Sanchez-Marcano, J. Characterization of laccase-grafted ceramic membranes for pharmaceuticals degradation. *J. Membr. Sci.* **2015**, *476*, 384–393.
29. Bautista, L.F.; Morales, G.; Sanz, R. Immobilization strategies for laccase from *Trametes versicolor* on mesostructured silica materials and the application to the degradation of naphthalene. *Bioresour. Technol.* **2010**, *101*, 8541–8548.
30. Nicolucci, C.; Rossi, S.; Menale, C.; Godjevargova, T.; Ivanov, Y.; Bianco, M.; Mita, L.; Bencivenga, U.; Mita, D.; Diano, N. Biodegradation of bisphenols with immobilized laccase or tyrosinase on polyacrylonitrile beads. *Biodegradation* **2011**, *22*, 673–683.
31. Lloret, L.; Hollmann, F.; Eibes, G.; Feijoo, G.; Moreira, M.; Lema, J.M. Immobilisation of laccase on Eupergit supports and its application for the removal of endocrine disrupting chemicals in a packed-bed reactor. *Biodegradation* **2012**, *23*, 373–386.
32. Touahar, I.E.; Haroune, L.; Ba, S.; Bellenger, J.P.; Cabana, H. Characterization of combined cross-linked enzyme aggregates from laccase, versatile peroxidase and glucose oxidase, and their utilization for the elimination of pharmaceuticals. *Sci. Total Environ.* **2014**, *481*, 90–99.
33. Wong, K.S.; Huang, Q.; Au, C.H.; Wang, J.; Kwan, H.S. Biodegradation of dyes and polyaromatic hydrocarbons by two allelic forms of *Lentinula edodes* laccase expressed from *Pichia pastoris*. *Bioresour. Technol.* **2012**, *104*, 157–164.
34. Demarche, P.; Junghanns, C.; Nair, R.R.; Agathos, S.N. Harnessing the power of enzymes for environmental stewardship. *Biotechnol. Adv.* **2012**, *30*, 933–953.
35. Cardinal-Watkins, C.; Nicell, J.A. Enzyme-catalyzed oxidation of 17Î²-Estradiol using immobilized laccase from *Trametes versicolor*. *Enzym. Res.* **2011**, *2011*, 11.
36. Macellaro, G.; Pezzella, C.; Cicatiello, P.; Sannia, G.; Piscitelli, A. Fungal laccases degradation of endocrine disrupting compounds. *BioMed Res. Int.* **2014**, *2014*, 1–8.
37. Nguyen, L.N.; Hai, F.I.; Price, W.E.; Kang, J.; Leusch, F.D.; Roddick, F.; van de Merwe, J.P.; Magram, S.F.; Nghiem, L.D. Degradation of a broad spectrum of trace organic contaminants by an enzymatic membrane reactor: Complementary role of membrane retention and enzymatic degradation. *Int. Biodeterior. Biodegrad.* **2015**, *99*, 115–122.
38. Pham, T.N.; Samikannu, A.; Rautio, A.R.; Juhasz, K.L.; Konya, Z.; Wärnå, J.; Kordas, K.; Mikkola, J.P. Catalytic hydrogenation of D-xylose over Ru decorated carbon foam catalyst in a SpinChem® rotating bed reactor. *Top. Catal.* **2016**, *59*, 1165–1177.
39. Barig, S.; Alisch, R.; Nieland, S.; Wuttke, A.; Gräser, Y.; Huddar, M.; Schnitzlein, K.; Stahmann, K.P. Monoseptic growth of fungal lipase producers under minimized sterile conditions: Cultivation of Phialemonium curvatum in 350 L scale. *Eng. Life Sci.* **2011**, *11*, 387–394.
40. Noel, S.; Liberelle, B.; Robitaille, L.; de Crescenzo, G. Quantification of primary amine groups available for subsequent biofunctionalization of polymer surfaces. *Bioconjug. Chem.* **2011**, *22*, 1690–1699.
41. Bourbonnais, R.; Paice, M.G.; Reid, I.D.; Lanthier, P.; Yaguchi, M. Lignin oxidation by laccase isozymes from *Trametes versicolor* and role of the mediator 2,2′-azinobis(3-ethylbenzthiazoline-6-sulfonate) in kraft lignin depolymerization. *Appl. Environ. Microbiol.* **1995**, *61*, 1876–1880.
42. Leirião, P.; Fonseca, L.; Taipa, M.; Cabral, J.; Mateus, M. Horseradish peroxidase immobilized through its carboxylic groups onto a polyacrylonitrile membrane. *Appl. Biochem. Biotechnol.* **2003**, *110*, 1–10.
43. Chen, Y.; Zhang, Y. Fluorescent quantification of amino groups on silica nanoparticle surfaces. *Anal. Bioanal. Chem.* **2011**, *399*, 2503–2509.

44. Ramanathan, T.; Fisher, F.T.; Ruoff, R.S.; Brinson, L.C. Amino-functionalized carbon nanotubes for binding to polymers and biological systems. *Chem. Mater.* **2005**, *17*, 1290–1295.
45. Norde, W.; Anusiem, A.C. Adsorption, desorption and re-adsorption of proteins on solid surfaces. *Colloids Surf.* **1992**, *66*, 73–80.
46. Durán, N.; Esposito, E. Potential applications of oxidative enzymes and phenoloxidase-like compounds in wastewater and soil treatment: A review. *Appl. Catal. B Environ.* **2000**, *28*, 83–99.
47. Becker, D.; Rodriguez-Mozaz, S.; Insa, S.; Schoevaart, R.; Barceló, D.; de Cazes, M.; Belleville, M.P.; Sanchez-Marcano, J.; Misovic, A.; Oehlmann, J.; et al. Removal of endocrine disrupting chemicals in wastewater by enzymatic treatment with fungal laccases. *Org. Process Res. Dev.* **2017**, *21*, 480–491.
48. Daughton, C.G.; Ternes, T.A. Pharmaceuticals and personal care products in the environment: Agents of subtle change? *Environ. Health Perspect.* **1999**, *107*, 907–938.
49. Basile, T.; Petrella, A.; Petrella, M.; Boghetich, G.; Petruzzelli, V.; Colasuonno, S.; Petruzzelli, D. Review of endocrine-disrupting-compound removal technologies in water and wastewater treatment plants: An EU perspective. *Ind. Eng. Chem. Res.* **2011**, *50*, 8389–8401.
50. Rodriguez, S.; Santos, A.; Romero, A. Effectiveness of AOP's on abatement of emerging pollutants and their oxidation intermediates: Nicotine removal with Fenton's Reagent. *Desalination* **2011**, *280*, 108–113.
51. Savchuk, N.; Krizova, P. Membrane and AOP processes—Their application and comparison in treatment of wastewater with high organics content. *Desalin. Water Treat.* **2015**, *56*, 3247–3251.
52. Pompe, T.; Salchert, K.; Alberti, K.; Zandstra, P.; Werner, C. Immobilization of growth factors on solid supports for the modulation of stem cell fate. *Nat. Protoc.* **2010**, *5*, 1042–1050.
53. Sano, S.; Kato, K.; Ikada, Y. Introduction of functional groups onto the surface of polyethylene for protein immobilization. *Biomaterials* **1993**, *14*, 817–822.
54. Hennig, A.; Borcherding, H.; Jaeger, C.; Hatami, S.; Würth, C.; Hoffmann, A.; Hoffmann, K.; Thiele, T.; Schedler, U.; Resch-Genger, U. Scope and limitations of surface functional group quantification methods: Exploratory study with poly(acrylic acid)-grafted micro- and nanoparticles. *J. Am. Chem. Soc.* **2012**, *134*, 8268–8276.

© 2017 by the authors. Licensee MDPI, Basel, Switzerland. This article is an open access article distributed under the terms and conditions of the Creative Commons Attribution (CC BY) license (http://creativecommons.org/licenses/by/4.0/).

catalysts

MDPI

Article

One-Pot, One-Step Production of Dietary Nucleotides by Magnetic Biocatalysts

Jon del Arco [1], Sara Martínez-Pascual [1], Vicente Javier Clemente-Suárez [2], Octavio Jorge Corral [3], Justin Jordaan [4,5], Daniel Hormigo [1], Almudena Perona [1] and Jesús Fernández-Lucas [1,6,*]

1 Applied Biotechnology Group, Universidad Europea de Madrid, c/ Tajo s/n, Villaviciosa de Odón, Madrid 28670, Spain; jondelarco@gmail.com (J.d.A.); sara.mp.94@gmail.com (S.M.-P.); daniel.hormigo@universidadeuropea.es (D.H.); almudena.perona@universidadeuropea.es (A.P.)
2 Applied Psychophysiological Research Group, Universidad Europea de Madrid, c/ Tajo s/n, Villaviciosa de Odón, Madrid 28670, Spain; vicentejavier.clemente@universidadeuropea.es
3 Facultad Ciencias de la Salud, Universidad Internacional de la Rioja, c/ Almansa 101, Madrid 28040, Spain; octavio.corral@unir.net
4 Biotechnology Innovation Centre, Rhodes University, Grahamstown 6140, South Africa; jjordaan@resynbio.com
5 ReSyn Biosciences, Meiring Naudé Road, Brummeria, Pretoria 0184, South Africa
6 Grupo de Investigación en Desarrollo Agroindustrial Sostenible, Universidad de la Costa, CUC, Calle 58 # 55-66, Barranquilla 080002, Colombia
* Correspondence: jesus.fernandez2@universidadeuropea.es; Tel.: +34-91-2115147

Received: 6 April 2018; Accepted: 27 April 2018; Published: 30 April 2018

Abstract: The enzymatic synthesis of nucleotides offers several advantages over traditional multistep chemical methods, such as stereoselectivity, regioselectivity, enantioselectivity, simple downstream processing, and the use of mild reaction conditions. However, in order to scale up these bioprocesses, several drawbacks, such as the low enzyme stability and recycling, must be considered. Enzyme immobilization may overcome these cost-related problems by enhancing protein stability and facilitating the separation of products. In this regard, tetrameric hypoxanthine–guanine–xanthine phosphoribosyltransferase (HGXPRT) from *Thermus thermophilus* HB8 was covalently immobilized onto glutaraldehyde-activated MagReSyn®Amine magnetic iron oxide porous microparticles (M*Tt*HGXPRT). In this context, two different strategies were followed: (a) an enzyme immobilization through its N-terminus residues at pH 8.5 (derivatives M*Tt*HGXPRT1-3); and (b) a multipoint covalent immobilization through the surface lysine residues at pH 10 (derivatives M*Tt*HGXPRT4-5). The immobilized derivatives of M*Tt*HGXPRT3 (activity 1581 international units per gram of support, IU/g; retained activity 29%) and M*Tt*HGXPRT5 (activity 1108 IU/g; retained activity 23%) displayed the best wet biocatalyst activity, and retained activity values in the enzymatic synthesis of inosine-5′-monophosphate (IMP). In addition, the dependence of the activities and stabilities of both derivatives on pH and temperature was tested, as well as their reusability potential. Taking these results into account, M*Tt*HGXPRT3 was chosen as the best biocatalyst (negligible loss of activity at 60 °C during 24 h; reusable up to seven cycles). Finally, as proof of concept, the enzymatic production of dietary nucleotides from high concentrations of low soluble bases was achieved.

Keywords: phosphoribosyltransferases; enzyme immobilization; green process; dietary nucleotides

1. Introduction

Nucleoside-5′-monophosphates (NMPs) are often used as additives in food. For example, some dietary nucleotides, such as inosinic acid (inosine-5′-monophosphate, or IMP) or guanosinic acid (guanosine-5′-monophosphate, GMP), are common additives that are used as flavor enhancers in

foods, since they induce an umami taste sensation [1]. In addition, the effect of some dietary nucleotide supplementation on growth and immune function in term infants has been extensively reported [2]. For this reason, nowadays, the demand for nucleotides in the food additives market is increasing, and the production of NMPs has been well studied.

These molecules have been traditionally synthesized by different chemical methods through multistep processes requiring the protection and de-protection of labile groups from precursor nucleosides, as well as the isolation of intermediates [3–5]. In addition, chemical strategies usually require the use of chemical reagents (phosphoryl chloride, $POCl_3$, or phosphorus pentoxide, P_2O_5), acidic conditions, and organic solvents, which are expensive and environmentally harmful [6,7]. These synthetic routes usually provide poor or moderate global yields and low product purity, and are also associated with harsh reaction conditions and waste disposal issues. On the contrary, the enzymatic synthesis of NMPs shows many advantages, such as one-pot reactions under mild conditions, high stereoselectivity and regioselectivity, and an environmentally-friendly technology [1,8–16]. However, despite the advantages of the bioprocesses, their industrial application is often hampered by several factors, such as: (i) the high cost of the production of recombinant enzymes; (ii) a low stability of biocatalysts under the drastic conditions that are often needed in some industrial processes; (iii) the difficulty of separating the biocatalyst from the reaction medium; and (iv) the reuse of the biocatalyst.

Enzyme immobilization can circumvent these drawbacks by facilitating the separation of products and allowing biocatalyst reutilization in various reactor configurations. This enhances some enzyme features, such as protein stability, but also activity, selectivity, specificity, and resistance to inhibitors or chemical reagents, even purity [17–21]. Since the covalent immobilization of proteins is usually achieved via the nucleophilic attack of primary amino groups (especially the ε-NH_2 of lysine residues) on electrophile groups from the support, covalent immobilization methodologies usually employ long reaction times (2−10 h) and alkaline conditions (pH 8−10) in order to avoid the protonation of amino groups. In this context, the activation of primary amino groups in the support by reaction with glutaraldehyde is one of the most versatile methods for support activation.

However, since different reactive species of glutaraldehyde (monomeric and polymeric forms) are found in equilibrium, the coupling mechanism between protein and glutaraldehyde is not well defined yet, and it seems that it is not limited to just one mechanism [22,23]. Moreover, it is proposed that glutaraldehyde suffers from intramolecular aldolic condensations, leading to an α,β-unsaturated aldehyde under alkaline conditions. These glutaraldehyde molecules can react with protein amino groups by means of two different mechanisms—Schiff base and Michael-type additions—but the formation of Schiff bases between internal aldehyde groups from the polymeric form of glutaraldehyde and primary amino groups from the protein leads to a more stable product.

During the last decade, the immobilization of enzymes onto magnetic supports has appeared as an alternative immobilization methodology that enables an easy recovery of the biocatalyst by applying a magnetic field [24,25]. Among various supports, porous magnetic materials have attracted much attention, due to their excellent magnetic responsibility, high specific surface area, good biocompatibility, chemically modifiable surface, and good reusability [26]. In this regard, glutaraldehyde-activated magnetic supports are suitable matrices for the development of bioprocesses catalyzed by immobilized enzymes.

Hypoxanthine–guanine–xanthine phosphoribosyltransferase (HGXPRT, EC 2.4.2.8) catalyzes the reversible transfer of the 5-phosphoribosyl group from 5-phospho-α-D-ribosyl-1-pyrophosphate (PRPP) to N9 on the 6-oxopurine bases hypoxanthine (1), guanine (2), or xanthine (3) to form IMP (4), GMP (5), or xanthosine-5′-monophosphate (XMP) (6), respectively, in the presence of Mg^{2+} (Figure 1). In a previous work, our research group has shown the potential of HGXPRT from *Thermus themophilus* HB8, *Tt*HGXPRT, as an industrial biocatalyst in the monoenzymatic and multienzymatic synthesis of dietary nucleotides [8,11,27]. However, this enzymatic approach has significant limitations to its practical application as an industrial biocatalyst, such as the high cost and instability of PRPP or the high cost of the production of the recombinant enzyme. In this context, the immobilization of the

enzyme onto magnetic microbeads would offer several advantages, such as an easy recovery and the possibility of being successfully reused in batch reactions.

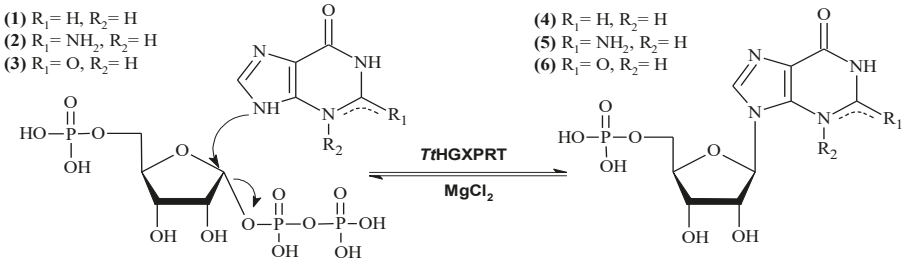

Figure 1. Enzymatic synthesis of nucleoside-5′-monophosphates (NMPs) catalyzed by *Thermus themophilus* HB8 (*Tt*HGXPRT).

Within this field, the present work describes—for the first time, to the best of our knowledge—the covalent immobilization of *Tt*HGXPRT onto glutaraldehyde-activated magnetic iron oxide porous microspheres (M*Tt*HGXPRT). The efficiency of these immobilization processes was tested at several pH values, temperatures, and protein loadings, leading to the selection of M*Tt*HGXPRT3 as the best derivative (in terms of stability, activity, and reusability). Finally, M*Tt*HGXPRT3 was employed in the enzymatic production of valuable nucleoside-5′-monophosphates (NMPs) that are commercially available as food additives (IMP or GMP).

The only precedent in the literature for the immobilization of a 6-oxopurine phosphoribosyltransferase was the development of a covalently linked enzyme aggregate (CLEA) multienzyme system, which contains an engineered 6-oxopurine phosphoribosyltransferase combined with several adenosine triphosphate (ATP) regeneration enzymes [28]. In this regard, the M*Tt*HGXPRT3 derivative represents the first strict characterization and application of an immobilized pure purine phosphoribosyltransferase.

2. Results and Discussion

2.1. Covalent Immobilization of TtHGXPRT

According to results reported by the H++ protonation predictor program (Table S1, Supplemental Material), the N-terminus of His_6-tagged *Tt*HGXPRT is deprotonated at pH 8.5, and can perform a nucleophilic attack on aldehyde groups, leading to a covalent linkage. Accordingly, *Tt*HGXPRT should be immobilized through its *N*-terminus at pH 8.5, and since *Tt*HGXPRT has been reported as a homotetramer, four potential interaction sites are possible (one of each N-terminal group). Unfortunately, since the only available structure of *Tt*HGXPRT deposited in the Protein Data Bank (PDB) shows monomers in the crystal lattice (PDB code 3ACD), we cannot confirm if all of the N-termini are located on the same plane. *Tt*HGXPRT also contains seven lysine residues, all of which are fairly exposed and scattered around the protein surface. However, program H++ predicts that only five of them are deprotonated, with apparent pK_a values lower than 10.0 (Lys18, Lys36, Lys37, Lys94, and Lys138) (Table S1). The calculated electrostatic potential surface of *Tt*HGXPRT at pH values of 8.5 and 10 is shown in Figure S1. Lys94 and Lys138 are highlighted to show how the titration state changes with pH. These theoretical results suggest that *Tt*HGXPRT could be immobilized through surface lysine residues when it is incubated at pH 10. However, due to the tetrameric nature of *Tt*HGXPRT, the orientation of Lys residues on the monomer surface is unlikely to play a very important role. In addition, since the only available structure of *Tt*HGXPRT deposited in the PDB is the monomer (PDB 3ACD), we cannot predict how the immobilization process will be conducted at pH 10.

The recombinant N-terminus His_6-tagged *Tt*HGXPRT was covalently immobilized onto glutaraldehyde-activated MagReSyn®Amine microspheres. In this regard, different immobilized

biocatalysts were prepared by the immobilization of *Tt*HGXPRT in 50 mM of potassium phosphate, pH 8.5 (M*Tt*HGXPRT1–M*Tt*HGXPRT3), and 50 mM of sodium borate, pH 10.0 (M*Tt*HGXPRT4–M*Tt*HGXPRT5). Magnetic biocatalysts were prepared by increasing the amount of enzyme in contact with the support in order to obtain a high load of the enzyme attached to the carrier (Table 1). In view of the experimental results, M*Tt*HGXPRT3 and MTtHGXPRT5 were chosen as the best derivatives for further biochemical studies. M*Tt*HGXPRT3 displayed an activity of 1581 IU/g of wet biocatalyst, and a retained activity of approximately 29% compared with the soluble enzyme. Similarly, the M*Tt*HGXPRT5 derivative showed an activity of 1108 IU/g of wet biocatalyst, and an activity recovery of 23%.

Table 1. Effect of enzyme/support mass ratio on the immobilization of *Tt*HGXPRT on MagReSyn® aldehyde microspheres. M*Tt*HGXPRT: MagReSyn® Amine magnetic iron oxide porous microparticles of hypoxanthine–guanine–xanthine phosphoribosyltransferase.

Derivative	Biocatalyst Loading (Mgenz/$g_{support}$)	Immobilization Yield (%)	Activity (IU/$g_{support}$)	Recovery(%)
M*Tt*HGXPRT pH 8.5				
M*Tt*HGXPRT1	102	84 ± 1	800 ± 33	25 ± 2
M*Tt*HGXPRT2	226	88 ± 4	802 ± 29	21 ± 1
M*Tt*HGXPRT3	322	85 ± 3	1581 ± 27	29 ± 2
M*Tt*HGXPRT pH 10.0				
M*Tt*HGXPRT4	226	67 ± 2	783 ± 26	21 ± 4
M*Tt*HGXPRT5	322	71 ± 3	1108 ± 21	23 ± 1

Reaction conditions: 6 μg of immobilized *Tt*HGXPRT, [Hyp] = [PRPP] = 10 mM, [$MgCl_2$] = 12 mM, in 12 mM of Tris-HCl buffer, pH 8.0 at 60 °C, 10 min, 300 r.p.m. Vr = 80 μL.

According to our previous work, *Tt*HGXPRT works as a homotetramer [11], and its oligomeric state may not only contribute to the high thermal stability exhibited by this protein: it also plays an essential role in the catalysis and stabilization of the active conformation [11]. Since M*Tt*HGXPRT derivatives displayed a significant loss of activity (only 25–30% of retained activity), we think that the immobilization process could affect the oligomeric assembly of the enzyme, leading to a lack of reactivity.

Moreover, as reported in the literature, three different types of interactions between the support and the protein may take place when using a support that is highly activated with glutaraldehyde: covalent, hydrophobic, and anionic exchange interactions [29]. Even if all of the enzyme molecules are immediately incorporated into the support, it is not certain that the enzyme is covalently attached to the support. In fact, when a highly activated support is used, in most cases, an ionic exchange reaction among the enzyme and amino groups in the support takes place at the beginning [29–35]. In order to discard that the immobilization takes place through ionic exchange, the derivatives were washed four times with 1 M of NaCl solution to promote protein relase, but the presence of *Tt*HGXPRT in the solution was not detected in the solution. Moreover, the sodium dodecyl sulfate polyacrylamide gel electrophoresis (SDS-PAGE) analysis of M*Tt*HGXPRT derivatives was performed to detect any non-covalently attached subunits. As shown in Figure S2, the presence of monomeric subunits of *Tt*HGXPRT was observed after boiling the immobilized preparations in the presence of SDS and mercaptoethanol. These results suggest to us that not all of the subunits are covalently bonded, and this could be another reason for the significant loss of activity.

2.2. Biochemical Characterization of MTtHGXPRT Derivatives

The dependence of the stability and activity of M*Tt*HGXPRT3 and M*Tt*HGXPRT5 on temperature and pH was studied to determine the optimal operating conditions of the enzyme (Figure 2).

The temperature profile revealed that M*Tt*HGXPRT3 displayed high activity (more than 80%) across a broad temperature range (from 50 °C to 90 °C), with a maximum of activity at 60–90 °C (Figure 2a). In a similar way, M*Tt*HGXPRT5 displayed high activity in the 60–90 °C temperature range (more than 90%), with the maximum activity being observed at 60–70 °C (Figure 2b). In this regard,

both derivatives, M*Tt*HGXPRT3 and M*Tt*HGXPRT5, displayed higher activity than soluble *Tt*HGXPRT at high temperatures (relative activity <70% at 90 °C) (Figure 2a,b) [11].

Nonetheless, the pH profile revealed significant differences between both derivatives. M*Tt*HGXPRT3 displayed high activity (relative activity >80%) in the pH 7–9 range, and there were no substantial differences depending on the nature of the buffer solution (similar activity at pH 7 in sodium phosphate buffer and Tris-HCl; similar activity at pH 8 in sodium phosphate buffer, Tris-HCl, and sodium borate). On the contrary, the relative activity of M*Tt*HGXPRT5 was also high (>80%) in the pH 7–8 range, but was strongly affected by the nature of the solution and only displayed high activity values when it was incubated in 50 mM of sodium phosphate buffer. Since soluble *Tt*HGXPRT has excellent activity (more than 80% of retained activity) in the pH 8–11 range, the results displayed in Figure 2 (Figure 2a,b) demonstrate that the pH dependence is affected by the immobilization process.

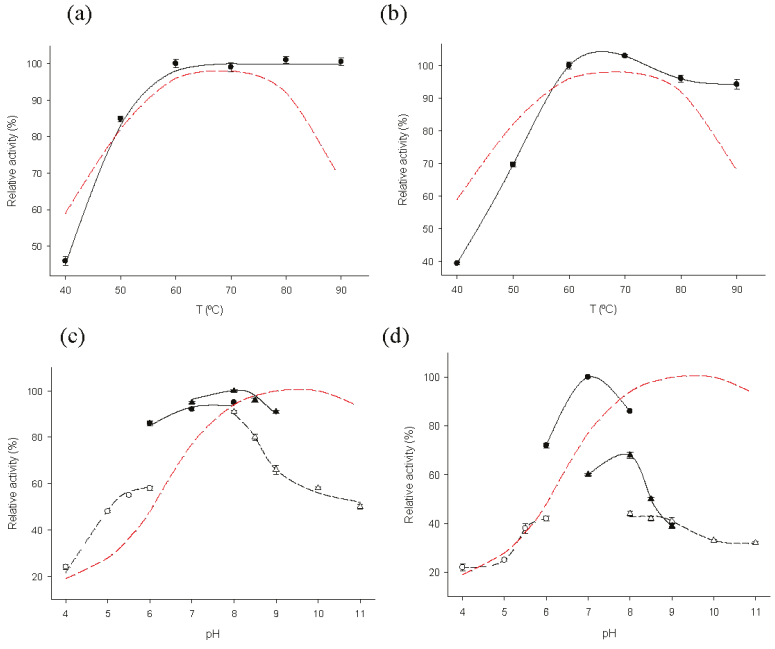

Figure 2. Temperature and pH dependence on the activity of M*Tt*HGXPRT derivatives. (**a**) Effect of temperature on the activity of (●) M*Tt*HGXPRT3 and (—) *Tt*HGXPRT; (**b**) Effect of temperature on the activity of (●) M*Tt*HGXPRT5 and (—) *Tt*HGXPRT; (**c**) Effect of pH on M*Tt*HGXPRT3 activity, (○) 50 mM sodium citrate (pH 4–6), (●) 50 mM sodium phosphate (pH 6–8), (▲) 50 mM Tris-HCl (pH 7–9), (Δ) 50 mM sodium borate (pH 8–11), (—) effect of pH on *Tt*HGXPRT activity; (**d**) Effect of pH on M*Tt*HGXPRT5 activity, (○) 50 mM sodium citrate (pH 4–6), (●) 50 mM sodium phosphate (pH 6–8), (▲) 50 mM Tris-HCl (pH 7–9), (Δ) 50 mM sodium borate (pH 8–11), (—) effect of pH on *Tt*HGXPRT activity.

2.3. Thermal Stability of MTtHGXPRT Derivatives

The effect of the storage of M*Tt*HGXPRT derivatives at 4 °C was analyzed in order to ensure biocatalyst stability, and both derivatives, M*Tt*HGXPRT3 and M*Tt*HGXPRT5, retained their activity for more than 100 days (85% relative activity) (data not shown). In addition, the effect of temperature on the stability of M*Tt*HGXPRT derivatives was evaluated by incubating both derivatives for 24 h in 50 mM sodium phosphate pH 8, at 60 °C. Interestingly, there was a negligible loss of activity under any of these experimental conditions (Figure 3). On the contrary, we can observe that the stability

of soluble *Tt*HGXPRT is affected for storage periods longer than 4 h. Therefore, the immobilization process clearly increases the thermal stability of *Tt*HGXPRT.

It is extensively reported that a multimeric state leads to a more functional and stable immobilized enzyme due to multipoint interactions [35,36]. In this regard, enzyme immobilization by surface lysine residues involves the largest surface of the protein, meaning that most of the subunits participate in the process. This fact may explain the good stabilization results achieved when immobilizing *Tt*HGXPRT at pH 10 (M*Tt*HGXPRT5) (no loss of activity when it is incubated at 60 °C during 24 h), but we have evidence that not all of the subunits are covalently attached to the support (Figure S2). Moreover, unexpectedly high thermal stability is also observed when immobilizing *Tt*HGXPRT at pH 8.5 (immobilization through the *N*-terminus; M*Tt*HGXPRT3). In this case, the oligomeric state of *Tt*HGXPRT could lead to an immobilization process involving several N-terminal residues, thereby increasing the thermal stability of the protein. In addition, after the first immobilization, other lysine residues can react because of the proximity of the support.

Experimental results display a similar thermal stability in both derivatives. Since surface lysine residues reactivity is around 50% at pH 10 and not all of the subunits are covalently bonded, it seems that the protein would be preferably immobilized by N-terminal amino groups in both cases (pH 8.5 and pH 10). However, we cannot discard the possibility of an additional multipoint covalent immobilization at pH 10.

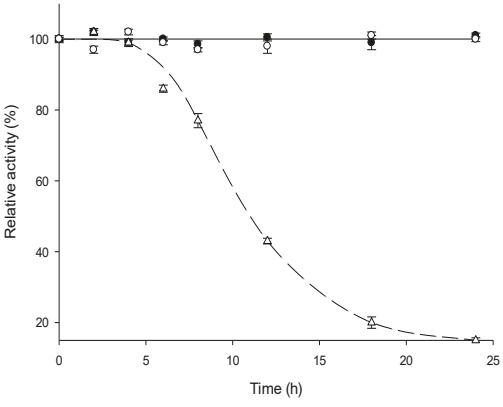

Figure 3. Thermal inactivation at 60 °C and pH 8 of (Δ) soluble *Tt*HGXPRT, (●) M*Tt*HGXPRT3, and (○) M*Tt*HGXPRT5.

2.4. Recycling of MTtHGXPRT Derivatives

The recycling of enzymes is an essential requisite for their industrial application, so once the optimal operating conditions were established, the next step was to evaluate the reusability of the immobilized enzyme. To this end, M*Tt*HGXPRT derivatives were employed in eight consecutive batch reactions (Figure 4).

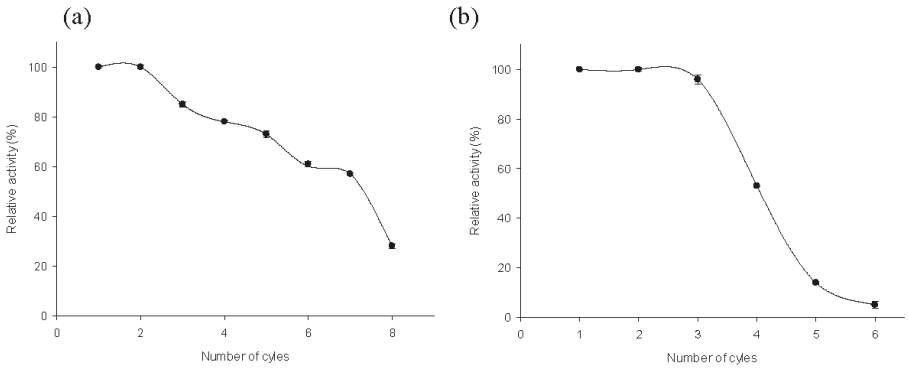

Figure 4. Recycling of M*Tt*HGXPRT derivatives in the enzymatic production of inosine-5′-monophosphate (IMP). (**a**) M*Tt*HGXPRT3; (**b**) M*Tt*HGXPRT5.

As shown in Figure 4, M*Tt*HGXPRT3 and M*Tt*HGXPRT5 suffered a progressive loss of activity as the reuse number increased. M*Tt*HGXPRT3 could be efficiently reused for at least seven cycles (>60% of retained activity) in the enzymatic synthesis of IMP, whereas M*Tt*HGXPRT5 suffered a drastic activity decrease after three cycles (<60% of retained activity after four cycles). These results suggest that multipoint covalent immobilization could also be happening at pH 10, and it may lead to the rigidification of *Tt*HGXPRT, thus altering the enzyme conformation and distorting its active site. Nevertheless, both derivatives display a similar trend.

Taking into account all of the experimental results (catalyst loading, retained activity, temperature and pH dependence on enzymatic activity, and thermal stability), M*Tt*HGXPRT3 was chosen as the best derivative for synthetic applications.

2.5. Effect of Molar Ratio

To avoid the reverse reaction, different initial ratios of hypoxanthine (Hyp) and $MgCl_2$ were analyzed. As shown in Table 2, an excess of Hyp leads to an increase of conversion (≈2-fold greater enzymatic activity). Thus, it seems that an excess of Hyp partially shifts the reaction equilibrium. In addition, an excess of $MgCl_2$ is clearly harmful for the enzymatic process (Table 2). According to our experimental results, the ratio 2/1/1 (Hyp/PRPP/$MgCl_2$) appears to be the optimal molar ratio.

Table 2. Effect of substrate ratio in M*Tt*HGXPRT3 activity.

PRPP (mM)	Hypoxanthine (mM)	$MgCl_2$ (mM)	IMP (mM)	Activity (IU/$g_{support}$)
10	10	12	2.1 ± 0.1	1830 ± 24
	10	24	1.1 ± 0.2	962 ± 32
	20	12	3.0 ± 0.1	2400 ± 57
	20	24	1.4 ± 0.1	1060 ± 35

Reaction conditions: 6 μg of immobilized *Tt*HGXPRT, [Hyp] = 10–20 mM, [PRPP] = 10 mM, [$MgCl_2$] = 12–24 mM in 12 mM Tris-HCl buffer, pH 8.0 at 60 °C, 10 min, 300 r.p.m. Vr = 80 μL.

Moreover, in order to know whether the presence of phosphate buffers affects the reaction (a high concentration of phosphate ions can chelate Mg^{2+} and decrease the concentration of such cations in the reaction medium), we tested the transferase reaction in the presence of phosphate buffer, Tris-HCl, and sodium borate buffer at pH 8. Our results show that 50 mM of sodium phosphate does not affect protein activity (Figure 3c,d).

2.6. Enzymatic Production of IMP and GMP

To explore the potential of M*Tt*HGXPRT3 as an industrial biocatalyst, the enzymatic production of several dietary nucleotides (IMP and GMP) was carried out using high concentrations of low soluble nucleobases (guanine and hypoxanthine) (Table 3).

Table 3. Enzymatic production of dietary nucleotides catalyzed by M*Tt*HGXPRT3.

	PRPP (mM)	Base (mM)	$MgCl_2$ (mM)	Derivative (μg)	IMP (mM)	Activity (IU/$g_{support}$)
IMP synthesis						
	10	20	12	12	2.9 ± 0.1	2200 ± 24
	20	40	24	12	2.4 ± 0.2	1654 ± 29
	40	80	48	12	4.8 ± 0.2	3365 ± 45
	10	20	12	30	3.8 ± 0.1	2800 ± 69
	20	40	24	30	5.6 ± 0.1	4400 ± 100
	40	80	48	30	7.5 ± 0.1	5600 ± 49
GMP synthesis						
	10	20	12	12	1.6 ± 0.1	1149 ± 120
	20	40	24	12	3.7 ± 0.1	2722 ± 80
	40	80	48	12	1.4 ± 0.2	1000 ± 70
	10	20	12	30	3.8 ± 0.1	2835 ± 87
	20	40	24	30	3.2 ± 0.1	2335 ± 90
	40	80	48	30	2.4 ± 0.2	1790 ± 56

Reaction conditions: 12–30 μg of immobilized *Tt*HGXPRT, [Hyp] = 20–80 mM, [PRPP] = 10–40 mM, [$MgCl_2$] = 12–48 mM in 12 mM Tris-HCl buffer, pH 8.0 at 60 °C, 10 min, 300 r.p.m. Vr = 80 μL.

3. Materials and Methods

3.1. Chemicals

Cell culture medium reagents were purchased from Difco (St. Louis, MO, USA). Trimethyl ammonium acetate buffer was acquired from Sigma-Aldrich (Madrid, Spain). All of the other reagents and organic solvents were purchased from Scharlab (Barcelona, Spain) and Symta (Madrid, Spain). All of the nucleoside-5′-monophosphates and bases used in this work were provided by Carbosynth Ltd. (Compton, United Kingdom).

3.2. Production TtHGXPRT

Recombinant His_6-tagged *Tt*HGXPRT was produced and purified as previously described [11]. In brief, *Tt*HGXPRT was overexpressed by adding 0.5 mM isopropyl β-D-1-thiogalactopyranoside, and the cells were grown for a further 5 h. Cells were harvested using centrifugation (3500× *g*), and the resulting pellet was resuspended in Tris buffer (20 mM Tris-HCl, pH 8.0) containing 100 mM NaCl. Crude extracts were prepared by the ultrasonic cell disruption of whole cells. The lysate was centrifuged at 17,000× *g* for 35 min, and the cell pellet was removed. The lysate was then heated at 70 °C for 20 min. Insoluble material was removed by centrifugation (17,000× *g*, 15 min, 4 °C), and the supernatant was passed through a 0.22-μm filter (Merck Millipore, Madrid, Spain). Clear lysate was loaded onto a 5-mL HisTrap FF column (GE Healthcare, Madrid, Spain) that was pre-equilibrated in binding buffer (20 mM of Tris-HCl buffer, pH 8.0, with 100 mM NaCl and 10 mM imidazole). Bound proteins were eluted using a linear gradient of imidazole (from 10 mM to 500 mM). Fractions containing recombinant *Tt*HGXPRT were identified by SDS-PAGE, pooled, and concentrated before being loaded onto a HiLoad 16/60 Superdex 200 prep grade column (GE Healthcare) pre-equilibrated in 20 mM Tris-HCl, pH 8.0. Fractions with the protein of interest identified by SDS-PAGE were pooled, and the protein was concentrated and stored at 4 °C until use. The standard activity assay for soluble enzyme was achieved by incubating 3 μg of pure enzyme with 10 mM PRPP, 10 mM Hyp, and 12 mM $MgCl_2$ in 12 mM Tris pH 8 for a final volume of 40 μL. The reaction mixture was incubated at 40 °C for 10 min (300 rpm). The enzyme was inactivated by adding 40 μL of cold methanol in an ice bath and heating for 5 min at 100 °C. After centrifugation at 9000× *g* for 5 min, samples were half-diluted

with water, and NMP production was analysed using HPLC to quantitatively measure the reaction products, as described below [11].

All of the determinations were carried out in triplicate, and the maximum error was less than 5%. Under such conditions, specific activity was defined as the amount of enzyme (mg) producing 1 μmol/min (IU) of IMP under the assay conditions.

3.3. Enzyme Immobilization

*Tt*HGXPRT immobilization was carried out by covalent attachment of the enzyme to glutaraldehyde-activated MagReSyn®Amine porous microspheres (from ReSyn Biosciences, Pretoria, South Africa), according to the recommendations of the manufacturer. These iron-oxide containing porous microparticles consist of a loosely linked interpenetrating network of polymer, which is more fully described by Jordaan et al. in patent number WO2009057049 [37].

First, 25 μL of the bead suspension (20 mg mL^{-1}) were washed and equilibrated in binding buffer (M*Tt*HGXPRT 1–3 in 50 mM potassium phosphate buffer, pH 8.5; M*Tt*HGXPRT 4–5 in 50 mM sodium borate buffer, pH 10) during 4 h at 25 °C. After the equilibration procedure, the beads were collected by a magnetic separator, and the supernatant was discarded. Activation of the support was accomplished by contacting MagReSyn®Amine microspheres with 200.0 μL of 50 mM sodium phosphate buffer pH 8.5 containing 5% (*w*/*v*) glutaraldehyde during 3 h at 25 °C, and then they were washed extensively with distilled water to remove the excess of the activating agent. Finally, activated microspheres were washed and equilibrated in binding buffer (50 mM potassium phosphate buffer, pH 8.5, or 50 mM sodium borate buffer, pH 10) shortly prior to use.

Subsequently, different amounts of enzyme (75–225 μg) were mixed with activated MagReSyn®Amine microspheres. The enzyme solution with the binding buffer was adjusted to 10× the volume of the initial beads suspension. The enzyme and bead suspensions were mixed thoroughly and incubated at room temperature under orbital shaking using a Sunflower 3D Mini–Shaker (BioSan, Latvia) for 4 h. After the binding procedure, the beads were collected by a magnetic separator and the supernatant was discarded. The beads were washed three times with washing buffer (50 mM of potassium phosphate buffer, pH 8.5, or 50 mM of sodium borate buffer, pH 10) to remove the non-covalently bound enzyme. After this, the beads were also treated with Glycine 3 N for 3 h at room temperature to quench any remaining amine reactive residues on the microparticles. The beads were washed with 50 mM of potassium phosphate buffer (pH 8.5) three times, and then stored at 4 °C.

3.4. Enzyme Activity Assay for Immobilized TtHGXPRT

As performed with the soluble enzyme, the enzymatic production of IMP from Hyp and PRPP was established as the standard reaction. The enzymatic activity of the immobilized enzyme was measured using 9–30 μg of different M*Tt*HGXPRT derivatives (containing 6 μg of immobilized M*Tt*HGXPRT), which was added to a 80-μL solution containing 10 mM 5-PRPP, 10 mM hypoxanthine, and 12 mM $MgCl_2$ in 12 mM Tris-HCl pH 8.0 in a final volume of 80 μL. The reaction mixture was incubated at 60 °C for 10 min (300 rpm). The reaction was stopped by collecting the beads with a magnetic separator, and the supernatant was treated following the general procedure that was previously described [11]. NMP production was analysed using HPLC to quantitatively measure the reaction products, as described below. Biocatalyst activity was defined as the amount of derivative (g) producing 1 μmol/min (IU) of IMP under the assay conditions. All of the determinations were carried out in triplicate, and the maximum error was less than 5%.

3.5. Biochemical Characterization of Immobilized Biocatalysts

The pH profile of purified recombinant enzyme was initially determined using the standard assay described for immobilized *Tt*HGXPRT with sodium citrate (pH 4–6), sodium phosphate (pH 6–8), Tris-HCl (pH 7–9), or sodium borate (pH 8–10) as reaction buffers (50 mM). The optimum temperature was determined using the standard assay across a 40–90 °C temperature range.

3.6. Thermal Stability and Reusability of MTtHGXPRT

M*Tt*HGXPRT derivatives were stored at 4 °C in 50 mM sodium phosphate, pH 8.5, for 100 days. Samples were taken periodically, and enzymatic activity was evaluated. Storage stability was defined as the relative activity between the first and successive reactions. Moreover, the thermal stability of M*Tt*HGXPRT3 and M*Tt*HGXPRT5 was assessed by incubating 6 μg of derivative in 50 mM Tris-HCl buffer pH 8.0, at 60 °C for a period of 1–24 h. After this, the derivative was incubated during 15 min at 4 °C, and then, the activity was measured using the standard assay.

In addition, the reusability of M*Tt*HGXPRT3 and M*Tt*HGXPRT5 was evaluated by employing both derivatives in consecutive reactions. After each use, magnetic derivatives were recovered by an imposed magnetic field, and washed with 50 mM Tris-HCl buffer, pH 8.0. Then, the recovered derivatives were introduced into a fresh reaction medium and reused again.

3.7. Enzymatic Production of Dietary Nucleotides

The enzymatic production of IMP and GMP was carried out by incubating 12–30 μg of immobilized enzyme with 10–40 mM 5-PRPP, 20–80 mM purine base, and 12–48 mM $MgCl_2$ in 12 mM Tris-HCl buffer pH 8.0, at 60 °C with 300 rpm orbital shaking at 10 min, in a final volume of 80 μL. Biocatalyst activity was evaluated as described in the Analytical methods section (see below).

3.8. Analytical Methods

The production of NMPs was followed and quantitatively measured with an ACE EXCEL 5 μm CN-ES column 250 mm × 4.6 mm (Advanced Chromatography Technologies) equilibrated with 100% trimethyl ammonium acetate at a flow rate of 0.8 mL/min. The NMP was eluted into the diode array detector for quantification at 254 nm.

Retention times for the bases and NMPs (hereafter abbreviated according to the recommendations of the IUPAC-IUB Commission on Biochemical Nomenclature) were as follows: guanine (Gua), 5.8 min; hypoxanthine (Hyp), 5.3 min; guanosine-5′-monophosphate (GMP), 3.1 min; inosine-5′-monophosphate (IMP), 3.4 min. The identification and quantification of most of the reaction substrates and products was performed in relation to the external standard calibration curve using the above, well-characterized commercial products (IMP or GMP).

3.9. Molecular Docking and Surface Analysis of TtHGXPRT

Recombinant N-terminus His_6-tagged *Tt*HGXPRT was modeled using the crystal structure of *Tt*HGXPRT in complex with IMP (PDB code 3ACD) as a template [38]. This structure was improved by refining the loop conformations through assessing the compatibility of an amino acid sequence to known PDB structures, and the geometry of loop region was corrected as previously described [11]. PyMOL 2.1 [39] was used for building the *Tt*HGXPRT structure, and for molecular illustration. The predicted titratable residues in the protein were studied at pH 8.5 and 10.0 using the H++ web server. (http://biophysics.cs.vt.edu/H++). The electrostatic potential on the surface of *Tt*HGXPRT was computed using the APBS program [40].

4. Conclusions

Herein, we report for the first time the covalent immobilization of a purine phosphoribosyltransferase onto magnetic glutaraldehyde-activated microbeads, as well as its characterization and application in the enzymatic production of dietary nucleotides. Among all of the magnetic derivatives produced, M*Tt*HGXPRT3 was selected as the optimum biocatalyst, displaying an activity of 1581 IU/g of wet biocatalyst and a retained activity of 29%. In addition, M*Tt*HGXPRT3 outperformed soluble *Tt*HGXPRT in thermal stability and could be reused for up to seven cycles.

Notwithstanding that several drawbacks still need to be overcome, such as the high price of PRPP and shifting the reaction equilibrium in a desired way, the reusability of this biocatalyst and the sustainability of this process are good reasons to further investigate this novel bioprocess.

Supplementary Materials: The following are available online at http://www.mdpi.com/2073-4344/8/5/184/s1, Table S1: Computed theoretical pKa values of the lysine residues in *Tt*HGXPRT using the server H++ (http://biophysics.cs.vt.edu/H++), Figure S1: APBS-generated electrostatic surface of TtHGXPRT. (a) Titrable state of the protein at pH 8.5 ; (b) Titrable state of the protein at pH 10.5. Figure S2. SDS-PAGE analysis of soluble and immobilized *Tt*HGXPRT, Lane 1. Prestained standard proteins from BioRad used as molecular weight markers. Lane 2. Supernatant obtained after boiling the soluble *Tt*HGXPRT in the presence of SDS and mercaptoethanol. Lane 3. Supernatant obtained after boiling the M*Tt*HGXPRT3 in the presence of SDS and mercaptoethanol. Lane 4. Supernatant obtained after boiling the M*Tt*HGXPRT5 in the presence of SDS and mercaptoethanol.

Author Contributions: J.F.-L. and A.P., conceived and designed the experiments. J.d.A., S.M.-P., V.J.C.-S., O.J.C., D.H., A.P. and J.F.-L. contributed to the development and analysis of experimental data. J.J. provided magnetic MagReSyn®Amine magnetic iron oxide porous microparticles and advised on immobilization strategies.

Acknowledgments: This work was supported by grant SAN151610 from the Santander Foundation. Grant 2016/UEM08 from Universidad Europea de Madrid is also acknowledged.

Conflicts of Interest: Justin Jordaan has an interest in ReSyn Biosciences. For the purpose of this study he advised on immobilization strategy but did not directly participate in the experimentation and did not generate any data.

References

1. Behrens, M.; Meyerhof, W.; Hellfritsch, C.; Hofmann, T. Sweet and umami taste: Natural products, their chemosensory targets, and beyond. *Angew. Chem. Int. Ed.* **2011**, *50*, 2220–2242. [CrossRef] [PubMed]
2. Hawkes, J.S.; Gibson, R.A.; Roberton, D.; Makrides, M. Effect of dietary nucleotide supplementation on growth and immune function in term infants: A randomized controlled trial. *Eur. J. Clin. Nutr.* **2006**, *60*, 254–264. [CrossRef] [PubMed]
3. Lapponi, M.J.; Rivero, C.W.; Zinni, M.A.; Britos, C.N.; Trelles, J.A. New developments in nucleoside analogues biosynthesis: A review. *J. Mol. Catal. B Enzym.* **2016**, *133*, 218–233. [CrossRef]
4. Mikhailopulo, I.A. Biotechnology of nucleic acid constituents—State of the art and perspectives. *Curr. Org. Chem.* **2007**, *11*, 317–333. [CrossRef]
5. Fresco-Taboada, A.; de la Mata, I.; Arroyo, M.; Fernández-Lucas, J. New insights on nucleoside 2′-deoxyribosyltransferases: A versatile biocatalyst for one-pot one-step synthesis of nucleoside analogs. *Appl. Microbiol. Biotechnol.* **2013**, *97*, 3773–3785. [CrossRef] [PubMed]
6. Yoshikawa, M.; Kato, T.; Takenishi, T. A novel method for phosphorylation of nucleosides to 5′-nucleotides. *Tetrahedron Lett.* **1967**, *8*, 5065–5068. [CrossRef]
7. Yoshikawa, M.; Kato, T.; Takenishi, T. Studies of phosphorylation. III. Selective phosphorylation of unprotected nucleosides. *Bull. Chem. Soc. Jpn.* **1969**, *42*, 3505–3508. [CrossRef]
8. Del Arco, J.; Fernández-Lucas, J. Purine and Pyrimidine Phosphoribosytransferases: A versatile tool for enzymatic synthesis of nucleoside-5′-monophosphates. *Curr. Pharm. Des.* **2015**, *23*, 6898–6912. [CrossRef] [PubMed]
9. Del Arco, J.; Acosta, J.; Pereira, H.M.; Perona, A.; Lokanath, N.K.; Kunishima, N.; Fernández-Lucas, J. Enzymatic production of non-natural nucleoside-5′-monophosphates by a novel thermostable uracil phosphoribosyltransferase. *ChemCatChem* **2018**, *10*, 439–448. [CrossRef]
10. Del Arco, J.; Martinez, M.; Donday, M.; Clemente-Suarez, V.J.; Fernández-Lucas, J. Cloning, expression and biochemical characterization of xanthine and adenine phosphoribosyltransferases from *Thermus thermophilus* HB8. *Biocatal. Biotransform.* **2017**, 1–8. [CrossRef]
11. Del Arco, J.; Cejudo-Sanches, J.; Esteban, I.; Clemente-Suarez, V.J.; Hormigo-Cisneros, D.; Perona, A.; Fernández-Lucas, J. Enzymatic production of dietary nucleotides from low-soluble purine bases by an efficient, thermostable and alkali-tolerant biocatalyst. *Food Chem.* **2017**, *237*, 605–611. [CrossRef] [PubMed]
12. Serra, I.; Conti, S.; Piškur, J.; Clausen, A.R.; Munch-Petersen, B.; Terreni, M.; Ubiali, D. Immobilized *Drosophila melanogaster* deoxyribonucleoside kinase (*Dm*dNK) as a high performing biocatalyst for the synthesis of purine arabinonucleotides. *Adv. Synth. Catal.* **2014**, *356*, 563–570. [CrossRef]
13. Fernández-Lucas, J. Multienzymatic synthesis of nucleic acid derivatives: A general perspective. *Appl. Microbiol. Biotechnol.* **2015**, *99*, 4615–4627. [CrossRef] [PubMed]

14. Zou, Z.; Ding, Q.; Ou, L.; Yan, B. Efficient production of deoxynucleoside-5′-monophosphates using deoxynucleoside kinase coupled with a GTP-regeneration system. *Appl. Microbiol. Biotechnol.* **2013**, *97*, 9389–9395. [CrossRef] [PubMed]
15. Mori, H.; Iida, A.; Fujio, T.; Teshiba, S. A novel process of inosine 5′-monophosphate production using overexpressed guanosine/inosine kinase. *Appl. Microbiol. Biotechnol.* **1997**, *48*, 693–698. [CrossRef] [PubMed]
16. Gudiño, E.D.; Santillán, J.Y.; Iglesias, L.E.; Iribarren, A.M. An enzymatic alternative for the synthesis of nucleoside 5′-monophosphates. *Enzyme Microb. Technol.* **2018**, *111*, 1–6. [CrossRef] [PubMed]
17. Mateo, C.; Palomo, J.M.; Fernandez-Lorente, G.; Guisan, J.M.; Fernandez-Lafuente, R. Improvement of enzyme activity, stability and selectivity via immobilization techniques. *Enzyme Microb. Technol.* **2007**, *40*, 1451–1463. [CrossRef]
18. Sheldon, R.A.; van Pelt, S. Enzyme immobilisation in biocatalysis: Why, what and how. *Chem. Soc. Rev.* **2013**, *42*, 6223–6235. [CrossRef] [PubMed]
19. Rodrigues, R.C.; Ortiz, C.; Berenguer-Murcia, A.; Torres, R.; Fernández-Lafuente, R. Modifying enzyme activity and selectivity by immobilization. *Chem. Soc. Rev.* **2013**, *42*, 6290–6307. [CrossRef] [PubMed]
20. Secundo, F. Conformational changes of enzymes upon immobilization. *Chem. Soc. Rev.* **2013**, *42*, 6250–6261. [CrossRef] [PubMed]
21. Barbosa, O.; Ortiz, C.; Berenguer-Murcia, Á.; Torres, R.; Rodrigues, R.C.; Fernandez-Lafuente, R. Strategies for the one-step immobilization-purification of enzymes as industrial biocatalysts. *Biotechnol. Adv.* **2015**, *33*, 435–456. [CrossRef] [PubMed]
22. Barbosa, O.; Ortiz, C.; Berenguer-Murcia, Á.; Torres, R.; Rodrigues, R.C.; Fernandez-Lafuente, R. Glutaraldehyde in bio-catalysts design: A useful crosslinker and a versatile tool in enzyme immobilization. *RSC Adv.* **2014**, *4*, 1583–1600. [CrossRef]
23. Zucca, P.; Sanjust, E. Inorganic materials as supports for covalent enzyme immobilization: Methods and mechanisms. *Molecules* **2014**, *19*, 14139–14194. [CrossRef] [PubMed]
24. Fernández-Lucas, J.; Harris, R.; Mata-Casar, I.; Heras, A.; de la Mata, I.; Arroyo, M. Magnetic chitosan beads for covalent immobilization of nucleoside 2′-deoxyribosyltransferase: Application in nucleoside analogues synthesis. *J. Ind. Microbiol. Biotechnol.* **2013**, *40*, 955–966. [CrossRef] [PubMed]
25. Bayramoglu, G.; Yilmaz, M.; Arica, M.Y. Preparation and characterization of epoxy-functionalized magnetic chitosan beads: Laccase immobilized for degradation of reactive dyes. *Bioprocess Biosyst. Eng.* **2010**, *33*, 439–448. [CrossRef] [PubMed]
26. Sheng, W.; Xi, Y.; Zhang, L.; Ye, T.; Zhao, X. Enhanced activity and stability of papain by covalent immobilization on porous magnetic nanoparticles. *Int. J. Biol. Macromol.* **2018**, *114*, 143–148. [CrossRef] [PubMed]
27. Acosta, J.; Arco, J.D.; Martinez-Pascual, S.; Clemente-Suárez, V.J.; Fernández-Lucas, J. One-Pot Multi-Enzymatic Production of Purine Derivatives with Application in Pharmaceutical and Food Industry. *Catalysts* **2018**, *8*, 9. [CrossRef]
28. Scism, R.A.; Bachmann, B.O. Five-component cascade synthesis of nucleotide analogues in an engineered self-immobilized enzyme aggregate. *ChemBioChem* **2010**, *11*, 67–70. [CrossRef] [PubMed]
29. Barbosa, O.; Torres, R.; Ortiz, C.; Fernandez-Lafuente, R. Modulation of the properties of immobilized CALB by chemical modification with 2, 3, 4-trinitrobenzenesulfonate or ethylendiamine. Advantages of using adsorbed lipases on hydrophobic supports. *Process. Biochem.* **2012**, *47*, 1220–1227. [CrossRef]
30. Hernandez, K.; Fernandez-Lafuente, R. Control of protein immobilization: coupling immobilization and site-directed mutagenesis to improve biocatalyst or biosensor performance. *Enzyme Microb. Technol.* **2011**, *48*, 107–122. [CrossRef] [PubMed]
31. Betancor, L.; López-Gallego, F.; Hidalgo, A.; Alonso-Morales, N.; Dellamora-Ortiz, G.; Mateo, C.; Fernández-Lafuente, R.; Guisán, J.M. Different mechanisms of protein immobilization on glutaraldehyde activated supports: Effect of support activation and immobilization conditions. *Enzyme Microb. Technol.* **2006**, *39*, 877–882. [CrossRef]
32. Adriano, W.S.; Filho, E.H.C.; Silva, J.A.; Giordano, R.L.C.; Gonçalves, L.R.B. Stabilization of penicillin G acylase by immobilization on glutaraldehyde-activated chitosan. *Braz. J. Chem. Eng.* **2005**, *22*, 529–538. [CrossRef]

33. Adriano, W.S.; Filho, E.H.C.; Silva, J.A.; Gonçalves, L.R.B. Optimization of penicillin G acylase multipoint immobilization on to glutaraldehyde–chitosan beads. *Biotechnol. Appl. Biochem.* **2005**, *41*, 201–207. [CrossRef] [PubMed]
34. Adriano, W.S.; Mendonça, D.B.; Rodrigues, D.S.; Mammarella, E.J.; Giordano, R.L.C. Improving the properties of chitosan as support for the covalent multipoint immobilization of chymotrypsin. *Biomacromolecules* **2008**, *9*, 2170–2179. [CrossRef] [PubMed]
35. Barbosa, O.; Torres, R.; Ortiz, C.; Berenguer-Murcia, Á.; Rodrigues, R.C.; Fernandez-Lafuente, R. Heterofunctional supports in enzyme immobilization: From traditional immobilization protocols to opportunities in tuning enzyme properties. *Biomacromolecules* **2013**, *14*, 2433–2462. [CrossRef] [PubMed]
36. Fernandez-Lafuente, R. Stabilization of multimeric enzymes: Strategies to prevent subunit dissociation. *Enzyme Microb. Technol.* **2009**, *45*, 405–418. [CrossRef]
37. Jordaan, J.; Simpson, C.; Brady, D.; Gardiner, N.S.; Gerber, I.B. Emulsion-derived particles. U.S. Patent No. 9,574,054, 2017.
38. Kanagawa, M.; Baba, S.; Ebihara, A.; Shinkai, A.; Hirotsu, K.; Mega, R.; Kim, K.; Kuramitsu, S.; Sampei, G.; Kawai, G. Structures of hypoxanthine-guanine phosphoribosyltransferase (TTHA0220) from Thermus thermophilus HB8. *Acta Crystallogr. Sect. F Struct. Biol. Cryst. Commun.* **2010**, *66*, 893–898. [CrossRef] [PubMed]
39. DeLano, W.L. The PyMOL molecular graphics system. 2002. Available online: http://www.pymol.org (accessed on 20 April 2018).
40. Baker, N.A.; Sept, D.; Joseph, S.; Holst, M.J.; McCammon, J.A. Electrostatics of nanosystems: Application to microtubules and the ribosome. *Proc. Natl. Acad. Sci. USA* **2001**, *98*, 10037–10041. [CrossRef] [PubMed]

© 2018 by the authors. Licensee MDPI, Basel, Switzerland. This article is an open access article distributed under the terms and conditions of the Creative Commons Attribution (CC BY) license (http://creativecommons.org/licenses/by/4.0/).

catalysts

MDPI

Article

Maltose Production Using Starch from Cassava Bagasse Catalyzed by Cross-Linked β-Amylase Aggregates

Rafael Araujo-Silva [1], Agnes Cristina Oliveira Mafra [1,†], Mayerlenis Jimenez Rojas [1], Willian Kopp [2], Roberto de Campos Giordano [1], Roberto Fernandez-Lafuente [3,*] and Paulo Waldir Tardioli [1,*]

1 Graduate Program in Chemical Engineering, Department of Chemical Engineering, Federal University of São Carlos, Rod. Washington Luiz, São Carlos 13565-905, Brazil; rafa.araujo.silva@outlook.com (R.A.-S.); agnesmafra@ufmt.br (A.C.O.M.); mayerlenis@gmail.com (M.J.R.); roberto@ufscar.br (R.d.C.G.)

2 Kopp Technologies, Rua Alfredo Lopes, 1717, São Carlos 13560-460, Brazil; willkopp@gmail.com

3 Departamento de Biocatálisis, ICP-CSIC, Campus UAM-CSIC Madrid, Madrid 28049, Spain

* Correspondence: rfl@icp.csic.es (R.F.-L.); pwtardioli@ufscar.br (P.W.T.); Tel.:+34-915954941 (R.F.-L.); +55-16-3351-9362 (P.W.T.)

† Present address: Instituto de Engenharia de Várzea Grande, Universidade Federal de Mato Grosso, Av. Fernando Corrêa da Costa, 2367, Cuiabá 78060-900, Brazil.

Received: 20 March 2018; Accepted: 19 April 2018; Published: 21 April 2018

Abstract: Barley β-amylase was immobilized using different techniques. The highest global yield was obtained using the cross-linked enzyme aggregates (CLEA) technique, employing bovine serum albumin (BSA) or soy protein isolate (SPI) as feeder proteins to reduce diffusion problems. The CLEAs produced using BSA or SPI showed 82.7 ± 5.8 and 53.3 ± 2.4% global yield, respectively, and a stabilization effect was observed upon immobilization at neutral pH value, e.g., after 12 h at 55 °C, the free β-amylase is fully inactivated, while CLEAs retained 25 and 15% of activity (using BSA and SPI, respectively). CLEA using SPI was selected because of its easier recovery, being chosen to convert the residual starch contained in cassava bagasse into maltose. This biocatalyst permitted to reach almost 70% of maltose conversion in 4 h using 30.0 g/L bagasse starch solution (Dextrose Equivalent of 15.88) and 1.2 U of biocatalyst per gram of starch at pH 7.0 and 40 °C. After 4 reuses (batches of 12 h) the CLEA using SPI maintained 25.50 ± 0.01% of conversion due to the difficulty of recovering.

Keywords: barley β-amylase; cross-linked enzyme aggregates (CLEA); cofeeders; enzyme immobilization; cassava bagasse

1. Introduction

Cassava (*Manihot esculenta* Cranz) is produced worldwide and plays an important role in food security in tropical areas [1]. One of the most important cassava industrial products is starch [2], which is usually extracted by a mechanical shear. The mechanical extraction of starch from 1 ton of cassava roots results in 254.7 kg of starch (~10% moisture) and 928.6 kg bagasse (85% moisture) [3]. Sriroth et al. [4] reported that the mechanical extraction of starch from cassava is limited, removing only partially the starch existing in the root fibers. The bagasse waste can contain up to 60 wt % of starch (dried basis) and is usually considered as a residue and disposed to the environment as landfill without any treatment [2], although in some instances it is used in animal feed mixtures or as additive to enrich fertilizers [2,4,5]. An alternative application of the residual starch from cassava waste could be the conversion into added-value products such as maltodextrins, glucose and maltose syrups using amylolytic enzymes. Maltose is widely used in the food industry, particularly in the brewing industry [6].

The starch chain can be hydrolyzed into dextrins by several groups of amylases [7,8]. α-Amylases cleave the starch molecule into smaller oligosaccharides, being used to improve the gelatinization process, in enzymatic starch extraction, to decrease medium viscosity and in saccharification processes (combined or not with other amylases) [7,8]; β-amylases (EC 3.2.1.2) are responsible for partial hydrolysis of starch non-reducing ends into maltose molecules [7–9]. There are several different sources of β-amylase, i.e., *Bacillus* spp, *Bacillus cereus*, soybean, sweet potato and barley [7,8]. A commercial β-amylase used for maltose production is that from barley [7]. Barley β-amylase has a monomeric structure with a molecular mass of 56–60 kDa [10], high activity in a pH ranging from 4.0 to 7.0 (optimum pH of 4.35 [11]). However, it is unstable at temperatures over 55 °C [12,13]. The use of a high temperature is desirable in maltose syrup production to improve operational aspects like viscosity of gelatinized starch solutions and highly concentrated sugar solutions and to avoid microbial growth [7]. Moreover, it looks convenient for the economy of the process to develop strategies that may permit the easy reuse of the barley β-amylase in several reactions cycles.

The enzyme immobilization may be a solution for these enzyme problems and even other enzyme limitations [14–17]: it allows a simple biocatalysts recovery and reuse [18], and becomes a powerful tool to improve enzyme features [19,20], such as stability [21,22], selectivity, specificity [23] or even purity [24]. These advantages have, as main costs, the immobilization process and immobilization carrier prices.

Chitosan is a prominent and versatile support, allowing different immobilization strategies [25–28]. It is obtained by deacetylation of chitin, a component of the exoskeleton of crustaceans and other arthropods [26]. That way, a support containing primary amino groups is easily obtained from a residue. This support may be used to directly ionically exchange enzymes [29], enabling a reversible immobilization that may not have high stabilizing effects on the protein [30]. The reversibility of the immobilization enables the reuse of the support, but may also raise a problem: the release of the enzyme during operation. To solve this, covalent glutaraldehyde immobilization may be a good alternative, this is a very used reactive even though the exact mechanism is unknown [31–33]. Amino-glutaraldehyde supports are heterofunctional ones [34] and they are very versatile for enzyme immobilization [35], enabling the use of glutaraldehyde preactivated supports [36] or the treatment of the previously adsorbed enzymes to obtain enzyme-support bonds [37]. Recently, the effect of the pH on the first immobilization step has been also showed [38,39]. Chitosan may be also utilized to encapsulate the enzyme [40,41]. Encapsulation has always the risks of enzyme release, as the pores need to be very small to relay trap the enzyme [42–44], but using chitosan some ion exchange of the enzyme on the polymer may be expected to reduce the enzyme release and crosslinking with glutaraldehyde may further reduce this enzyme leakage.

Professor Sheldon's group proposed a strategy that avoided the use of supports to immobilize enzymes: the cross-linked enzyme aggregates (CLEAs) [45–47]. The preparation of CLEAs is a very simple method that consists of two steps: (i) aggregation/precipitation of proteins induced by precipitant agents (salts, water-miscible organic solvents, non-ionic polymers, etc.); and (ii) chemical crosslinking of the formed aggregates with a bifunctional reagent (e.g., glutaraldehyde) via reaction with amino groups of the lysine residues that are presented on the surface of the enzyme [48,49]. However, if the enzyme has low surface density of amino groups, the immobilization could be inefficient, due to the low cross-linking bonds. Some authors suggest the amination of the enzyme (genetically or chemically) [50,51], or the coaggregation of enzyme and aminated polymers [52,53]. Yet, the first solution is complex and the second one produces a highly hydrophilic and cationic micro-environment around the enzyme that may be undesired. An alternative with a great success is the use of a feeder protein rich in lysine residues, such as bovine serum albumin (BSA), which can contribute to the formation of CLEAs with high global yield and excellent operational stability [48,49,54–60]. A cheaper alternative to BSA is soy protein isolate (SPI). This is an industrial residue from extraction of soybean oil [61], which has about 90% of heterogenic protein content, mainly composed by 7S (β-conglycinin) and 11S (glycinin) storage proteins [62], of molecular sizes

of 150–175 kDa [63] and 340–375 kDa [64], respectively. SPI is about 250 times cheaper than BSA (R$34.90/kg and R$9803.00/kg, respectively; values from Estação dos Grãos Ltd. (Perdizes, Brazil) and Sigma-Aldrich (St. Louis, MO, USA) in March 2018), what could turn CLEA technology economically viable when a feeder protein is necessary. The feeder could also reduce other CLEAs problems, due to the high volumetric activity in many instances diffusion limitations become very high and the feeder protein will "dilute" the enzyme [18].

Several researchers immobilized β-amylases from different sources using carrier-bound methods, stabilizing the enzyme [65–67] but recovering low activity [65–69], attributed mainly to substrate diffusional problems. As far as we know, there are no reports about the immobilization of β-amylase by the CLEA technique.

This study shows an option for the use of cassava bagasse as starch source for maltose production and explores the barley β-amylase immobilization by different techniques, including the CLEA methodology using two different feeder proteins, bovine serum albumin (BSA), which is used as feeder protein in many other studies [48,54–60], and soy protein isolate (SPI). The best biocatalyst obtained in this study will be tested in the maltose production using commercial and residual cassava starch.

2. Results and Discussion

2.1. β-Amylase Immobilization

The enzyme was first immobilized using chitosan as a carrier using the different strategies described in the Methods section. Immobilization via ion exchange presented low immobilization and global yields (less than 25%, Table 1); however, high expressed activity was achieved (around 100%). The treatment of the already ionically exchanged enzyme with glutaraldehyde drives to full enzyme inactivation. Immobilization on glutaraldehyde activated chitosan permitted the full enzyme immobilization, but the expressed activity and global yield were very low (just over 6%). Thus, these strategies seem unsuitable to immobilize this enzyme; as an alternative, we tried to trap the enzyme on chitosan beads at a lower concentration, to have larger pores. The immobilization is not really a trapping, as the polymer will ionically immobilize the enzyme and we treat the immobilized enzyme with glutaraldehyde; in any case the expressed activity was even lower than in the other cases, perhaps the enzyme may be released, perhaps the polymer may block the active center of the enzyme, or the glutaraldehyde inactive the enzyme.

Table 1. Carrier-bond immobilization using chitosan 2% (for adsorption and covalent attachment), 1% (for encapsulation) and free-carrier immobilization (CLEA) without feeder protein. It was supplied 0.53 mg of protein per gram of carrier in each immobilization method using chitosan.

Immobilization Method	Immobilization Yield (%)	Expressed Activity (%)	Global Yield (%)
Adsorption	21.4 ± 3.4	108.9 ± 17.6	23.3 ± 3.8
Adsorption followed by crosslinking [1]	21.4 ± 3.4	0.0 ± 0.0	0.0 ± 0.0
Covalent attachment [2]	100.0 ± 0.0	6.7 ± 0.8	6.7 ± 0.8
Encapsulation [3]	–	–	1.1 ± 0.5
CLEA [4]	–	–	34.2 ± 3.3
CLEA [5]	–	–	25.8 ± 1.2

[1] Using 0.15% glutaraldehyde solution as crosslinker; [2] activated with 0.80% glutaraldehyde solution; [3] using 0.10% glutaraldehyde solution as crosslinker; [4] using 0.30% glutaraldehyde solution as crosslinker; [5] using 0.60% glutaraldehyde solution as crosslinker.

For this reason we tried the immobilization of β-amylase using CLEA technology. The results (Table 1) were better than when using chitosan (near to 30% of global yield). Thus, CLEAs technology appeared to be more suitable to immobilize this β-amylase, with the advantage of saving the support.

Aiming to improve the CLEA global yield, we tried to optimize some immobilization aspects of this biocatalyst.

2.2. Optimization of β-Amylase Immobilization Using CLEAs Technology

To optimize the CLEA, we decided to use feeder proteins. As explained in introduction, this may have a double positive effect: to improve the crosslinking step and to reduce the diffusion problems by diluting the enzyme into inert protein [46,48,49]. Thus, the effects of the feeder proteins (BSA or SPI) and glutaraldehyde concentrations for the same β-amylase concentration on the global yield were studied (Section 3.4). More than 80% of global yield was achieved using BSA as feeder at condition 5 (CLEA-β-BSA-5) and more than 50% using SPI as feeder at condition 12 (CLEA-β-SPI-12), as presented in Table 2. Using a feeder protein, the final activity of the biocatalyst was higher than using just the enzyme.

Table 2. Global yields for CLEAs of β-amylase prepared with different concentrations of feeder protein and glutaraldehyde.

Assay	Feeder Protein	Global Yield (%)
1	None	34.2 ± 3.3
2		25.8 ± 1.2
3	BSA	54.5 ± 0.9
4		43.2 ± 0.4
5		82.7 ± 5.8
6		53.1 ± 0.1
7		33.6 ± 0.5
8		0
9		0
10		0
11	SPI	45.2 ± 2.1
12		53.3 ± 2.4
13		48.0 ± 2.3
14		47.5 ± 1.5
15		38.2 ± 5.2
16		31.0 ± 1.8
17		28.4 ± 2.9
18		24.4 ± 0.5
19		28.6 ± 0.0

The CLEAs obtained using SPI (CLEA-β-SPI) were noticeably larger than the CLEAs produced using BSA or without feeder protein, helping in the separation of the biocatalyst from the viscous medium when submitted to centrifugation. This larger size may be the cause of the lower expressed activity of CLEA-β-SPI-12 compared to CLEA-β-BSA-5.

Figure 1 shows images of CLEA-β-SPI-12 using scanning electron microscopy, where it is possible to see the heterogeneity in the particle size (lower than 70 μm) of the prepared biocatalyst.

The activities obtained using both feeder proteins in the CLEA preparation were better than those reported in several studies employing β-amylases from different sources immobilized on preexisting supports. Vretblad and Axen [66] reported a global yield of 35% for barley β-amylase covalently attached on Sepharose activated with 4,4′-methylene dianiline. Tavano et al. [69] reported global yield of 21% for sweet potato β-amylase immobilized on glyoxyl-agarose support. These results are much closer to those obtained in our work for barley β-amylase ionically adsorbed on chitosan (Table 1).

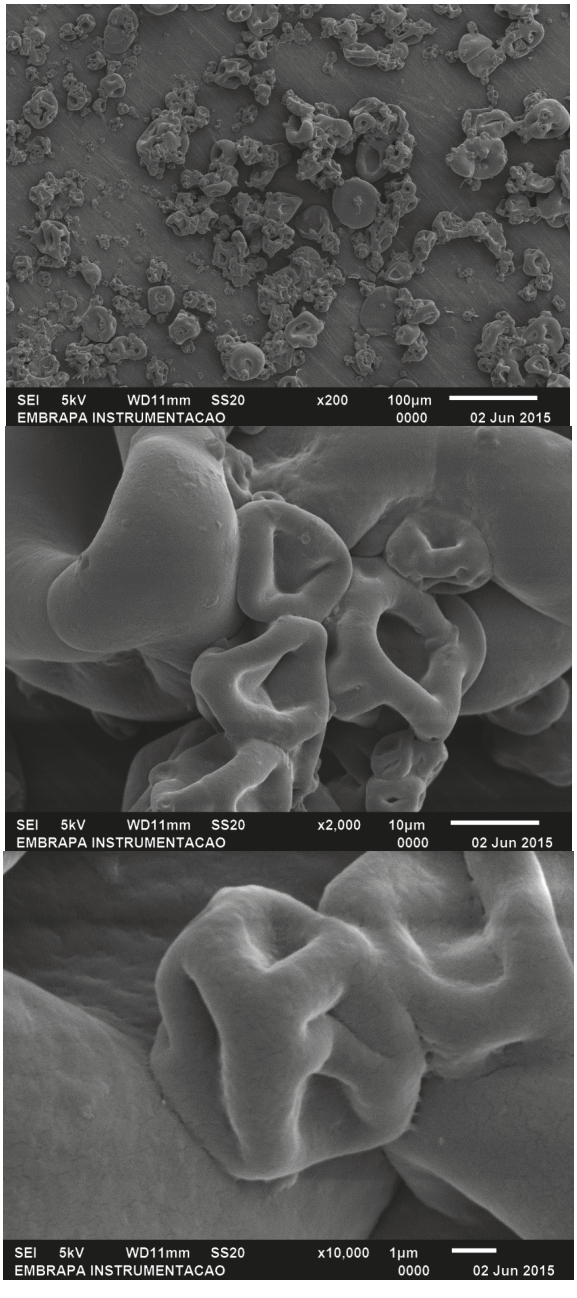

Figure 1. Images of CLEA-β-SPI-12 using scanning electron microscopy at different amplifications.

2.3. Effects of pH and Temperature on the Activity and the Stability of β-Amylase Preparations

The study of the effect of the reaction pH and temperature on the enzyme activity of β-amylase was performed using free enzyme, CLEA-β-BSA-5 and CLEA-β-SPI-12 to investigate the influence of the enzyme immobilization technique on enzyme response to the medium [68–71] (Figure 2).

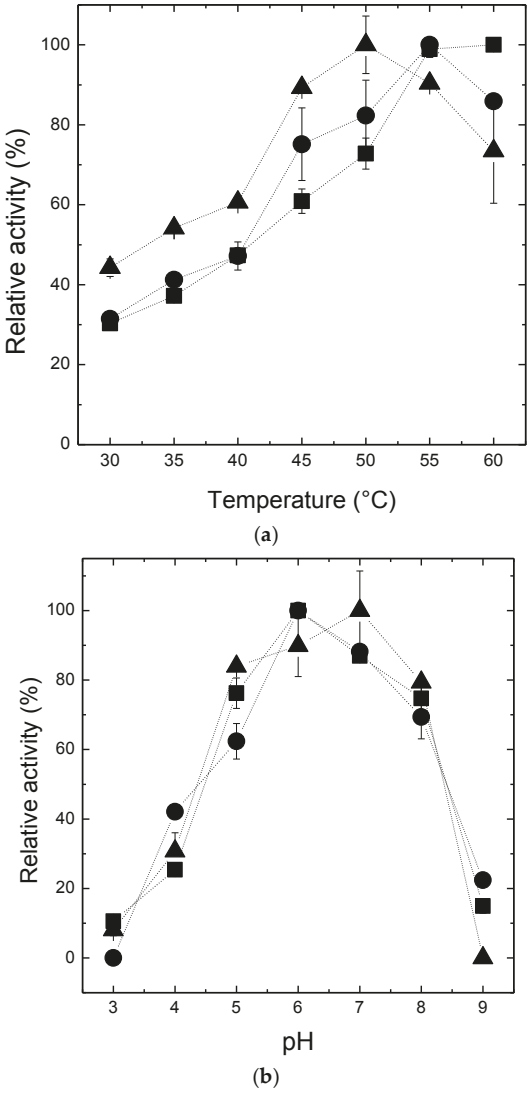

Figure 2. Temperature activity profile (**a**), using 1% (*w*/*v*) soluble starch solution at pH 4.8 (standard condition for enzymatic assay as described in the Section 3.2) and pH activity profile (**b**), using 1% (*w*/*v*) soluble starch solution at 20 °C, for free β-amylase (squares), CLEA-β-BSA-5 (circles) and CLEA-β-SPI-12 (triangles). The maximum activities were taken as 100%.

The effect of the temperature on the enzyme activity was similar for all β-amylase preparations (Figure 2a), expressing maximum activities in the range 50–55 °C. In the case of CLEA-β-SPI-12,

a small shift to lower temperature (approximately 5 °C) of the maximum activity temperature was observed. It was expected that optimal pH and temperature of enzymes immobilized as CLEAs were shifted because covalent bonds established between amino groups of the enzyme and glutaraldehyde, changing the microenvironment and the conformational flexibility of the enzyme [49]. Talekar et al. [72] reported a shift to higher temperature (around 15 °C) for β-amylase from *Bacillus amyloliquefaciens* after immobilization by CLEA technique. However, Mafra et al. [58] reported the same maximum activity temperature for soluble and CLEAs of catalase. The effect of the pH on enzyme activity (Figure 2b) was similar for all enzymes, expressing maximum activity in the pH range 6.0–7.0. Talekar et al. [72] reported a pH shift from 6.0 to 7.0 for α-amylase from *B. amyloliquefaciens* immobilized as CLEA, while Mafra et al. (2016) also reported a pH shift from 7.0 to 7.4 for catalase immobilized as CLEA with BSA as feeder protein. In our work, the pH shift from 6.0 to 7.0 for β-amylase immobilized as CLEA with SPI as feeder protein was not different statistically, considering the standard deviations (as provided by the F test).

Figure 3a shows the residual activity after 12 h incubation at different pH values and 25 °C of free β-amylase, CLEA-β-BSA-5 and CLEA-β-SPI-12. In almost all cases, the free enzyme exhibited a slightly higher residual activity, followed by CLEA-β-BSA-5. The highest activity retained for each sample was observed at pH 7.0 (96.0 ± 0.6%), 6.0 (88.2 ± 3.5%) and 7.0 (64.2 ± 22.9%), for free β-amylase, CLEA-β-BSA-5 and CLEA-β-SPI-12, respectively. Figure 3a shows that at pH 5.0 (very similar to pH 4.8 used in optimal temperature assay), the stability of free β-amylase is higher than those of CLEA-β-BSA-5 and CLEA-β-SPI-12 (residual activities of 94.2 ± 0.0, 75.7 ± 3.2 and 45.1 ± 2.2% respectively). This enzyme inactivation (especially high for CLEA-β-SPI-12) at acid pH value can explain the results observed in the effect of temperature on enzyme activity.

The temperature stability test was performed at the optimal pH for the stability of each β-amylase, pH 6.0 for CLEA-β-BSA-5 and pH 7.0 for free β-amylase and CLEA-β-SPI-12. Figure 3b shows that at 40 °C free β-amylase and CLEA-β-SPI-12 did not present significant thermal deactivation after 12 h (109. 2 ± 3.2 and 96.1 ± 5.5% of residual activity respectively). At 55 °C the CLEAs retained some activity when the free enzyme was fully inactivated. The thermal stabilization observed at 55 °C was reported for several enzymes immobilized as CLEAs by Sheldon [48] and Talekar et al. [49].

Although CLEA-β-BSA-5 presented higher global yield and pH stability than CLEA-β-SPI-12, its stability at high temperatures was high. Also, the CLEA-β-BSA-5 was more difficult to manipulate and separate from the very viscous reactional medium, containing a high sugar concentration. Thus, the CLEA-β-SPI-12 was chosen to be compared with free β-amylase on the maltose production assay.

2.4. Maltose Production

Maltose production was performed using soluble and residual cassava bagasse (enzymatically extracted) starches with free and CLEA-β-SPI-12 under the respective pH and temperature conditions where the biocatalysts exhibited optimal stabilities.

The residual starch solution was obtained via enzymatic extraction of cassava bagasse with starch content of 45.7 ± 0.8% (d.m.). The high starch content in cassava bagasse from industrial mechanical extraction can be related, as explained in introduction, to the limitations of shear and broke the cassava root fibers to extract the starch [4] and this content can vary depending on cassava crop and processing conditions [2].

The maltose conversion by free β-amylase and CLEA-β-SPI-12 were compared using soluble starch solution containing 30.0 g/L of commercial starch (dextrose equivalent, DE ≈ 0) and 36.0 U/L, the equivalent of 1.2 U/g (enzymatic unit per gram of starch), for each enzyme preparation. Figure 4a shows that maltose conversion using free enzyme was faster than using CLEA-β-SPI-12. After 45 min, the free enzyme achieved 44.5% of conversion, while CLEA-β-SPI-12 presented the same conversion after 9 h. The maximum conversions were 52.3 ± 2.3 (after 6 h) and 46.4 ± 5.4% (after 12 h) for free β-amylase and CLEA-β-SPI-12, respectively. The productivities and specific productivities of both soluble starch conversions were 2.7 ± 0.1 and 1.2 ± 0.1 kg/m^3 h, and 75.9 ± 3.3 and 33.7 ± 3.9 mg/Uh

using free β-amylase and CLEA-β-SPI-12, respectively. Yoshigi et al. [73] reported 57.7% of starch conversion using free barley β-amylase and 5.0 g/L soluble starch solution (50 mM acetate buffer, pH 5.5) incubated at temperature of 37 °C. This could be due to the high size of the starch used, as well as the low DE, probably causing diffusional limitations in the CLEA-β-SPI-12.

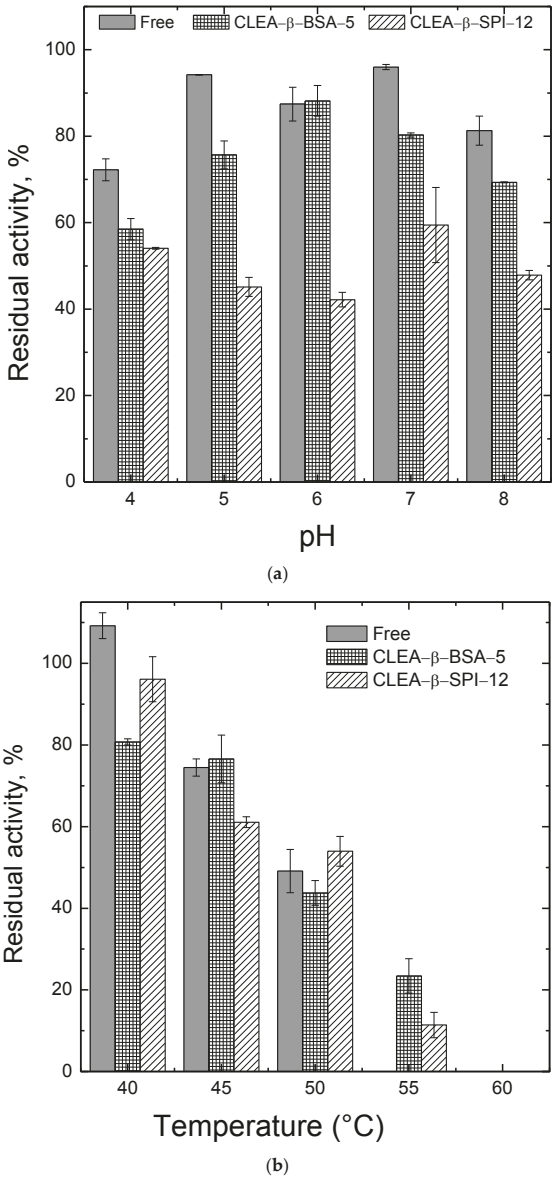

Figure 3. Residual activities of free β-amylase, CLEA-β-BSA-5 and CLEA-β-SPI-12 for pH stability (**a**) after 12 h of incubation at 25 °C and temperature stability and, (**b**) after 12 h of incubation at pH 6.0 (CLEA-β-BSA-5) and pH 7.0 (free β-amylase and CLEA-β-SPI-12). 100% is the initial activity.

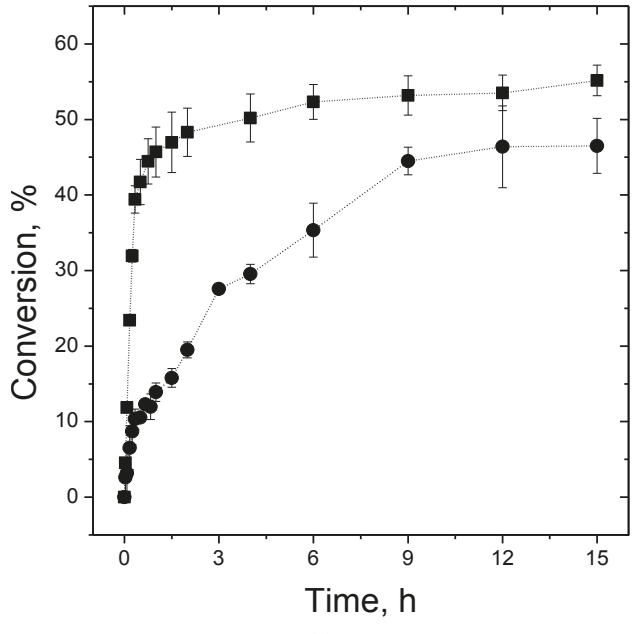

(**a**)

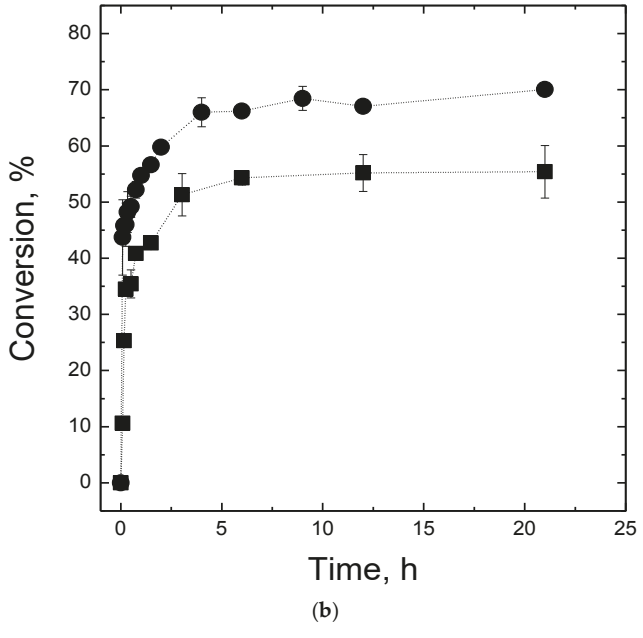

(**b**)

Figure 4. Comparative soluble starch (30 g/L) conversion using free β-amylase (squares) and CLEA-β-PS-12 (circles) at pH 7.0 and 40 °C; (**a**) comparative starch conversion using cassava bagasse starch solutions with free β-amylase (squares) and CLEA-β-PS-12 (circles), using 1.2 U/g of starch, pH 7.0 and 40 °C (**b**).

The assay using cassava bagasse starch solutions 30.0 g/L (DE of 7.95 and 15.88) with free enzyme and CLEA-β-PS-12 (using 36 U/L) reached maximum conversion of 54.3 ± 1.2% and 66.0 ± 2.6% at 6 h and 4 h, respectively (Figure 4b). With both catalyst a higher maltose yield and activity was detected using this product (starch partially hydrolyzed extracted by α-amylase action), very likely due to the very low DE using the commercial starch (near 0) compared to the high one of these home-obtained products (DE 8-16), offering more non-reducing ends to the enzyme action. Moreover, the lower size of the starch extracted from bagasse can reduce the diffusion limitations found using commercial starch, greatly improving the performance of the immobilized enzyme, that now overpass the free enzyme. The productivity and specific productivity of cassava bagasse starch conversions using free β-amylase and CLEA-β-PS-12 were 2.8 ± 0.1 and 5.2 ± 0.2 kg/m3h, and 78.8 ± 1.8 and 143.7 ± 5.6 mg/Uh, respectively. The CLEA-β-PS-12 productivity and specific productivity using cassava bagasse starch solution with DE of 15.88 was 4.3 times higher than using soluble starch (DE near 0).

Gaouar et al. [74] used in this reaction a highly concentrated liquefied starch, 340 ± 25 g/L (DE unknown) and free Maltogenase 4000 L (from *Bacillus subtilis*) as biocatalyst, at pH values between 5.0 to 5.5 in a 1.0 L jacketed Pyrex cell with magnetic stirring, achieving 65.4% of maltose production, practically the same as using cassava bagasse residual starch with DE of 15.88 and CLEA-β-SPI-12. Shiraishi et al. [75] also achieved comparable starch conversion, using 150, 200 and 300 g/L of liquefied white potato starch (DE = 5.6) with 1.59 g/L of free soybean β-amylase in a baffled flask with magnetic stirring at temperature of 40 °C and pH 4.8, achieving a value of maltose content of 58.2% for all the tests.

CLEA-β-SPI-12 was utilized for four successive cycles of reaction (12 h reaction for each cycle) (Figure 5); the continuous decrease on yields becomes evident. The reasons for this may be the difficulty to capture the CLEAs in this very viscous media, even though the size of the biocatalyst was quite large, as enzyme inactivation under these conditions may be discarded in these very short reaction courses. The breakage of the CLEA particles during use will further increase this difficulty in the recovery, and that occurs even using a vortex reactor. In fact, Talekar et al. [72] also reported a reduction in the activity of CLEA of α-amylase to around 65% of its original activity after four cycles of 30 min reaction at 60 °C. They attributed the loss of activity to the substantial change in the CLEA morphology after four batches as shown by SEM images. In fact, in our work, the weight of CLEA obtained after the four reuses almost fit with the decreased activity. An alternative to improve the CLEA recovery may be to use magnetic nanoparticles trapped in the CLEAs to facilitate the capture [71,76–80]. Another possibility may be the trapping of the CLEAs in some larger and more rigid solids, e.g., lentikats [81,82] or silica [83,84].

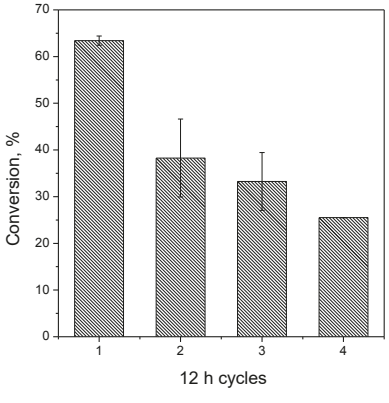

Figure 5. Reuse assays converting starch to maltose at 40 °C, pH 7.0 in a vortex flow reactor stirred at 900 rpm, using cassava bagasse starch solution (8.2 g/L) and CLEA-β-PS-12 (36.0 U/L).

3. Materials and Methods

3.1. Materials

Cassava bagasse was supplied by Tereos Syral (Palmital, Brazil), soluble starch was purchased from Sigma-Aldrich (St. Louis, MO, USA). The α-amylases Termamyl 120 L from *Bacillus licheniformis* and BAN 480 LS from *Bacillus amyloliquefaciens* were supplied by LNF Latino Americana (Bento Gonçalves, Brazil). Crude extract of barley β-amylase (type II-B) and bovine serum albumin (BSA, 96% purity) were purchased from Sigma-Aldrich (St. Louis, MO, USA). Soy protein isolate (SPI, 90% purity) was purchased from Doremus Ingredientes (Guarulhos, Brazil). Other reagents were of analytical grade.

3.2. Enzymatic Activity Assay

The activity of β-amylase was determinate according to Bernfeld [85] by measuring the initial velocity of maltose production. A solution of 1% (*w*/*v*) soluble starch in 16 mM sodium acetate buffer (pH 4.8) was used as substrate. Free or immobilized β-amylase was added to the reaction medium, which was thermostatically equilibrated at 20 °C in a batch reactor. Periodically, sample aliquots were withdrawn until 12 min and the maltose content was quantified by the dinitrosalicylic acid method [86] using pure commercial maltose as standard. An enzymatic unit of β-amylase (U) was defined as the amount of enzyme required to release 1.0 mg of maltose per minute under the assay conditions.

3.3. β-Amylase Immobilization Using CLEA Technique

A set of experiments were carried out using 0.5 mL of BSA or SPI solution (feeder protein), with concentrations values described in Table 3, and 0.5 mL of 100 mM sodium phosphate buffer at pH 7.0 containing 2.0 mg of protein/mL of β-amylase. Then, 1.0 mL of 5.0 M ammonium sulfate solution was added to precipitate the proteins; after 5 min stirring 24.0 or 48.0 μL of 25% (*w*/*w*) glutaraldehyde aqueous solution were added, reaching a glutaraldehyde final concentration of 30.0 or 60.0 mM, respectively. The protein suspension was kept under 200 rpm stirring at 4 °C for 3 h. Finally, the CLEA of β-amylase was separated from the supernatant by centrifugation at 21,000× g and 4 °C, washed with 100 mM sodium phosphate buffer pH 7.0, centrifuged again and resuspended in 1.0 mL of 100 mM sodium phosphate buffer pH 7.0 for β-amylase activity measurement.

The global yield was calculated according to Equation (1):

$$\text{Global yeld } (\%) = \frac{\text{CLEA activity}}{\text{Initial activity}} \times 100, \quad (1)$$

where the CLEA activity is the observed activity in the CLEA after centrifugation, washing (2 times with 1.0 mL of 100 mM phosphate buffer pH 7.0) and resuspension in the same washing buffer; initial activity is the total activity offered to the immobilization.

3.4. Immobilizations on Chitosan Based Supports by Adsorption, Covalent Attachment and Encapsulation

β-amylase was immobilized on chitosan according to Vieira et al. [87], with chitosan-based matrices of 2.0% (for adsorption and covalent attachment) and 1.0% (for encapsulation) (*w*/*w*), aiming to achieve bigger pore sizes. The amount of enzyme supplied for immobilization was 0.53 mg of protein per gram of chitosan. Table 4 shows the conditions for chitosan-based immobilizations.

Chitosan powder was solubilized in 2.0% (*v*/*v*) acetic acid solution and coagulated using 0.5 M potassium hydroxide solution (volume ratio chitosan:KOH solutions of 2:3). The suspension was stirred at 50 °C for 30 min to form flakes. The flakes were filtrated and washed with Milli-Q water and 5 mM sodium phosphate buffer pH 7.0.

Table 3. Conditions of preparation of CLEAs of β-amylase using bovine serum albumin (BSA) and soy protein isolate (SPI) as cofeeder and glutaraldehyde as crosslinker.

Assay [1]	Feeder Protein	Cofeeder Concentration [2] (mg/mL)	Glutaraldehyde Concentration [3] (mM)	Glutaraldehyde/Total Protein [4] Ratio (mM/mg)
1	None	0	30	60.0
2		0	60	120.0
3	BSA	160	30	0.74
4		120	30	0.98
5		80	30	1.46
6		60	30	1.93
7		40	30	2.86
8		120	60	1.97
9		80	60	2.93
10		40	60	5.71
11	SPI	80	30	1.46
12		60	30	1.93
13		40	30	2.86
14		30	30	3.75
15		20	30	5.45
16		60	60	3.87
17		40	60	5.71
18		30	60	7.50
19		20	60	10.91

[1] All assays were carried out at 4 °C and amonium sulfate solution (5 M) was used to precipitate the proteins. [2] Feeder protein concentration in water solution; [3] Glutaraldehyde concentration in protein solution (2 mg/mL), prepared in 100 mM sodium phosphate buffer pH 7.0.; [4] Total amount of enzyme and cofeeder (BSA or SPI).

Table 4. Conditions for adsorption, covalent attachment and encapsulation in chitosan using 0.53 mg of protein (crude enzyme) per gram of chitosan.

Immobilization Method	Adsorption	Adsorption Followed by Crosslinking	Covalent Attachment	Encapsulation
Carrier	Chitosan 2 wt %	Chitosan 2 wt %	Chitosan 2 wt %	Chitosan 1 wt %
Glutaraldehyde concentration	0	0.15%	0.80%	0.10%
Temperature (°C)	25	25	25	0 (Ice bath)
Stirring	100 rpm	100 rpm	100 rpm	50 rpm

The β-amylase adsorption was performed in a shaker at 25 °C and 100 rpm, suspending 1 g of chitosan flakes in 5 mL of enzyme solution (0.53 mg of β-amylase/g of chitosan), prepared in 5 mM sodium phosphate buffer pH 7.0. The immobilization was monitored by measuring the enzyme activity in the supernatant and suspension, using an identical enzyme solution without chitosan as blank reference. At the end, the immobilization yield was determined (Equation (2)), then the flakes were filtrated, washed with distilled water and the expressed activity (Equation (3)) and the global yield (Equation (4)) were calculated. We also determined the global yield of the adsorbed enzyme after treatment with 0.15% (*v*/*v*) glutaraldehyde solution under mild stirring, at room temperature for 1 h at pH 7.0.

For covalent immobilization, firstly the chitosan flakes were activated with 0.8% (*v*/*v*) glutaraldehyde solution at pH 7.0 under mild stirring for 30 min, followed by washing with Milli-Q water and 100 mM sodium phosphate buffer at pH 7.0. The immobilization of β-amylase on activated chitosan was carried out in 100 mM sodium phosphate buffer pH 7.0 (1:5 solid/liquid ratio, 0.53 mg of β-amylase/g of chitosan, as in the adsorption method) at 25 °C and 100 rpm stirring, monitoring the supernatant, suspension and blank reference. The immobilization yield, expressed activity and the global yield were calculated as described above.

For the encapsulation into chitosan, chitosan powder was solubilized in 2.0% (*v*/*v*) acetic acid solution and homogenized under stirring at room temperature for 1 h. Then the pH was adjusted

to 4.35 using sodium hydroxide solution and the β-amylase was added. This solution was added dropwise into a 100 mM Tris-HCl buffer pH 8.0 (in ice bath) in a volume ratio chitosan solution:buffer of 1:10, under mild stirring for 30 min. After, glutaraldehyde 25% (*w*/*w*) was added to achieve a final concentration of 0.1% (*v*/*v*) and the reaction occurred under mild stirring at room temperature for 2 h. The chitosan gels were filtrated, washed with distilled water and 100 mM sodium phosphate buffer pH 7.0, and the global yield was calculated by Equation (4).

The immobilization yield and expressed activity for adsorption and covalent attachment on chitosan were calculated according to Equations (2) and (3), respectively:

$$\text{Immobilization yield } (\%) = \frac{\text{Immobilized activity}}{\text{Initial activity}} \times 100, \quad (2)$$

$$\text{Expressed activity } (\%) = \frac{\text{Derivative activity}}{\text{Immobilized activity}} \times 100, \quad (3)$$

where the immobilized activity is the initial activity offered to the immobilization minus the activity in the final supernatant. Derivative activity is the activity measured in the immobilized enzyme.

The global yield was calculated according Equation (4):

$$\text{Global yield } (\%) = \frac{\text{Derivative activity}}{\text{Initial activity}} \times 100, \quad (4)$$

3.5. Effect of pH and Temperature on Activity and Stability of β-Amylase Preparations

The enzymatic activity of immobilized or free enzyme was determined at different pH values and 20 °C as described in the Section 3.2, using different buffers (16 mM): sodium acetate buffer at pH values from 3.0 to 5.0, sodium phosphate buffer at pH values from 6.0 to 8.0 or sodium carbonate buffer at pH 9.0.

To determinate the optimum activity temperature of free or immobilized β-amylase, the enzymatic activity was measured using 16 mM sodium acetate buffer at pH 4.8 in a temperature range from 30 to 60 °C.

For the stability assays, free and CLEAs of β-amylase samples were incubated at the indicated temperature and pH values for 12 h under 200 rpm stirring. The pH stability assay was studied at 25 °C and pH values from 4.0 to 8.0, using the same buffers of the pH effect on activity assay. The temperature stability assay was performed incubating the samples in the buffer of highest stability for each sample (free or CLEAs β-amylase) and temperatures from 40 to 60 °C. The relative residual activity was calculated as the ratio between the activity after the incubation and the initial activity.

3.6. Cassava Bagasse Compositional Analysis

Starch was extracted from cassava bagasse using 0.625 mL of α-amylase (Termamyl 120 L) per g of bagasse (dry mass) in 50.0 mL of water, at 90 °C, with 540 rpm mechanic stirring for 2 h [88]. Then, the reactional medium was filtrated to remove the solid fraction. The liquid fraction, containing mainly maltodextrins, was submitted to acid hydrolysis (1.0 mL of 72% (*v*/*v*) sulfuric acid to 22.5 mL of maltodextrin solution) in an autoclave for 30 min to produce glucose monomers [89]. The acid hydrolysis in an autoclave can also generate a small amount of hydroxymethylfurfural (HMF) molecules. Glucose was quantified by liquid chromatography in a Shimadzu chromatograph equipped with a refractive index detector (RID) at 50 °C, using a BioRad Aminex HPX-87H column (300 × 7.8 mm) set to 65 °C and 5 mM sulfuric acid solution as eluent with a flow of 0.6 mL/min. HMF was quantified in a Shimadzu Chromatograph equipped with a UV-Visible detector (set to 274 nm) using a SunFire C18 column (4.6 × 150 mm) at 40 °C and acetonitrile-water solution (1:8 *v*/*v*), containing 1% (*v*/*v*) acetic acid, as mobile phase at 0.8 mL/min flow rate. The amount of glucose and HMF was used to calculate the total amount of extractable starch from cassava bagasse.

3.7. Residual Starch Extraction

The residual starch contained in cassava bagasse was gelatinized in 50 mM sodium phosphate buffer pH 7.0 (28.0 g of starch/L) under stirring in boiling water bath for 10 min. The bagasse suspension was cooled to 60 °C and the pH was adjusted to 6.0 using diluted HCl solution. Then 12.6 mL of α-amylase (BAN 480 LS) per kg of starch was added to the bagasse suspension, the medium was stirred for 5 min, and the reaction was stopped by adding a 50% (*v*/*v*) HCl solution to the reactional medium (1:333 volume ratio). The medium was filtrated at 60 °C, the starch concentration and dextrose equivalent (DE = 100 × amount of reducing sugar expressed as glucose/solid dry mass) were quantified and, if necessary, the soluble starch was diluted or concentrated. DE is a measure of polymerization degree of the starch chains, using glucose as pattern. When the DE value is near to zero the polymerization degree is very high, the starch molecules have high molecular weight. When the DE value is near to 100 the polymerization degree is very low, the starch molecules were practically converted into glucose [7].

The amount of reducing sugar was determinate by DNS method [86] using glucose as standard.

3.8. Maltose Production

The enzymatic maltose production was performed in a batch Taylor vortex flow reactor (VFR) [90] with radius ratio (η = Ri/Re) of 0.24, aspect ratio (Γ = L/d) of 6.32 and inner cylinder rotation rate (ω) of 900 rpm, using 50.0 mL of commercial starch solution or residual starch solution extracted from cassava bagasse and 36.0 U/L of free or CLEA of β-amylase, at pH and temperature values of maximum stability (determined as described before). The starch conversion was followed by the increase of maltose concentration during the reaction time. Samples of the reactional medium were treated with 1.0 M HCl (50:3 *v*/*v*) to inactivate the enzymes in the sample, the maltose concentrations were determinate by HPLC (Shimadzu Chromatograph, using a BioRad Aminex HPX-87H column and 5 mM sulfuric acid solution at 0.6 mL/min as eluent, as described above for glucose quantification) and the starch conversion was calculated using 0.957 g of starch/g of maltose as conversion factor.

3.9. Reuse Assays

The reuse assays were performed using the same conditions for maltose production catalyzed by CLEA of β-amylase. Each batch was carried out for 12 h reaction, being the maltose conversion determined in the end of each batch. Between each reactional cycle the biocatalyst was separated by centrifugation (15,370× *g* at 4 °C for 10 min) and washed with distilled water.

3.10. Protein Assay

The protein concentrations of β-amylase extracts were determined according to the Bradford's method [91] using BSA as the standard protein.

4. Conclusions

This study showed that barley β-amylase can be immobilized by CLEA technology and can achieve a higher global yield than other strategies used to immobilize this β-amylases. Soy protein isolated could be used as feeder protein for barley β-amylase CLEA, creating an immobilized enzyme cheaper and easier to manipulate than using bovine serum albumin as feeder protein. The use of soy protein isolated as an alternative as feeder protein could reduce the cost of the CLEAs biocatalyst production when a feeder is required. The bagasse-starch conversion using CLEA-β-SPI-12 reached maximum starch conversion even slightly better that that obtained by using free β-amylase, and achieved high starch conversion similar to the best results reported in the literature in a short period of time. This study also shows that the cassava bagasse could be used as starch source for maltose production, giving this residue a new and more profitable use. CLEAs recovering in this viscous medium become a problem that should be attacked using different strategies, e.g., use of magnetic

nanoparticles, trapping of the CLEAs in larger and more rigid solids, easier to recover in this very viscous medium.

Acknowledgments: The authors thank Tereos Syral (Palmital, Brazil) for the donation of cassava bagasse and LNF Latino Americana (Bento Gonçalves, Brazil) for the donation of α-amylases (Termamyl 120 L and BAN 480 LS). We gratefully recognize the support from the São Paulo Foundation (FAPESP), National Council for Scientific and Technology Development (CNPq) and Coordination for the Improvement of Higher Level or Education Personnel (CAPES, doctorate fellowship of R. A. Silva) from Brazilian Government, and MINECO from Spanish Government, (project number CTQ2017-86170-R). Ángel Berenguer's (Instituto Universitario de Materiales, Universidad de Alicante) help and suggestions during the writing of this paper are gratefully recognized.

Author Contributions: Rafael Araujo-Silva performed all experimental assays; Agnes Cristina Oliveira Mafra and Willian Kopp help to prepare the CLEAs; Mayerlenis Jimenez Rojas helped in the starch extraction and its characterization; Roberto de Campos Giordano, Roberto Fernandez-Lafuente and Paulo Waldir Tardioli designed and supervised all experiments, as well as wrote/reviewed the manuscript with help of Rafael Araujo-Silva as part of his Masters of Science in Chemical Engineering. All authors have given approval to the final version of the manuscript.

Conflicts of Interest: The authors declare no conflicts of interest.

References

1. Food and Agriculture Organization (FAO). *Food Outlook—Biannual Report on Global Food Markets*; FAO: Rome, Italy, 2017; Volume November.
2. Pandey, A.; Soccol, C.R.; Nigam, P.; Soccol, V.T.; Vanderberghe, L.P.S.; Mohan, R. Biotechnological potential of agro-industrial residues: II cassava bagasse. *Bioresour. Technol.* **2000**, *74*, 81–87. [CrossRef]
3. Leonel, M.; Cereda, M.P. Starch extration from cassava fibrous residue. *Ciência e Tecnol. Aliment.* **2000**, *20*, 122–127. [CrossRef]
4. Sriroth, K.; Chollakup, R.; Chotineeranat, S.; Piyachomkwan, K.; Oates, C.G. Processing of cassava waste for improved biomass utilization. *Bioresour. Technol.* **2000**, *71*, 63–69. [CrossRef]
5. Prado, I.N.; Martins, A.D.S.; Alcalde, C.R.; Zeoula, L.M.; Marques, J.D.A. Performance of heifers fed diets containing corn or cassava hull as energy source and cottonseed meal or yeast as protein source. *Rev. Bras. Zootec.* **2000**, *29*, 278–287. [CrossRef]
6. Piddocke, M.P.; Kreisz, S.; Heldt-Hansen, H.P.; Nielsen, K.F.; Olsson, L. Physiological characterization of brewer's yeast in high-gravity beer fermentations with glucose or maltose syrups as adjuncts. *Appl. Microbiol. Biotechnol.* **2009**, *84*, 453–464. [CrossRef] [PubMed]
7. BeMiller, J.N.; Huber, K.C. Carbohydrates. In *Fennema's Food Chemistry*; Damodaran, S., Parkin, K.L., Fennema, O.R., Eds.; CRC Press: Boca Raton, FL, USA, 2007; pp. 83–151.
8. Synowiecki, J. The use of starch processing enzymes in the food industry. In *Industrial Enzymes*; Polaina, J., MacCabe, A.P., Eds.; Springer: Dordrecht, The Netherlands, 2007; ISBN 9781402053764.
9. Das, R.; Mishra, H.; Srivastava, A.; Kayastha, A.M. Covalent immobilization of beta-amylase onto functionalized molybdenum sulfide nanosheets, its kinetics and stability studies: A gateway to boost enzyme application. *Chem. Eng. J.* **2017**, *328*, 215–227. [CrossRef]
10. Ma, Y.; Stewart, D.C.; Eglinton, J.K.; Logue, S.J.; Langridge, P.; Evans, D.E. Comparative Enzyme Kinetics of Two Allelic Forms of Barley (*Hordeum vulgare* L.) Beta -amylase. *J. Cereal Sci.* **2000**, *31*, 335–344. [CrossRef]
11. Baker, W.L.; Smiley, K.L. Beta-amylase sulphydryl and disulphide group reactions. Additional aspects on enzyme inhibition by ascorbic acid. *J. Inst. Brew.* **1985**, *91*, 25–30. [CrossRef]
12. Mikami, B.; Yoon, H.; Yoshigi, N. The Crystal Structure of the Sevenfold Mutant of Barley β-Amylase with Increased Thermostability at 2.5 Å Resolution. *J. Mol. Biol.* **1999**, *285*, 1235–1243. [CrossRef] [PubMed]
13. Yoshigi, N.; Okada, Y.; Maeba, H.; Sahara, H.; Tamaki, T. Construction of a Plasmid Used for the Expression of a Sevenfold-Mutant Barley β-Amylase with Increased Thermostability in Escherichia coli and Properties of the Sevenfold-Mutant β-Amylase. *J. Biochem.* **1995**, *118*, 562–567. [CrossRef] [PubMed]
14. Brady, D.; Jordaan, J. Advances in enzyme immobilisation. *Biotechnol. Lett.* **2009**, *31*, 1639–1650. [CrossRef] [PubMed]
15. Cantone, S.; Ferrario, V.; Corici, L.; Ebert, C.; Fattor, D.; Spizzo, P.; Gardossi, L. Efficient immobilisation of industrial biocatalysts: Criteria and constraints for the selection of organic polymeric carriers and immobilisation methods. *Chem. Soc. Rev.* **2013**, *42*, 6262–6276. [CrossRef] [PubMed]

16. DiCosimo, R.; McAuliffe, J.; Poulose, A.J.; Bohlmann, G. Industrial use of immobilized enzymes. *Chem. Soc. Rev.* **2013**, *42*, 6437–6474. [CrossRef] [PubMed]
17. Sheldon, R.A.; van Pelt, S. Enzyme immobilisation in biocatalysis: Why, what and how. *Chem. Soc. Rev.* **2013**, *42*, 6223–6235. [CrossRef] [PubMed]
18. Garcia-Galan, C.; Berenguer-Murcia, Á.; Fernandez-Lafuente, R.; Rodrigues, R.C. Potential of different enzyme immobilization strategies to improve enzyme performance. *Adv. Synth. Catal.* **2011**, *353*, 2885–2904. [CrossRef]
19. Guzik, U.; Hupert-Kocurek, K.; Wojcieszyńska, D. Immobilization as a Strategy for Improving Enzyme Properties-Application to Oxidoreductases. *Molecules* **2014**, *19*, 8995–9018. [CrossRef] [PubMed]
20. Mateo, C.; Palomo, J.M.; Fernandez-Lorente, G.; Guisan, J.M.; Fernandez-Lafuente, R. Improvement of enzyme activity, stability and selectivity via immobilization techniques. *Enzyme Microb. Technol.* **2007**, *40*, 1451–1463. [CrossRef]
21. Balcão, V.M.; Vila, M.M.D.C. Structural and functional stabilization of protein entities: State-of-the-art. *Adv. Drug Deliv. Rev.* **2015**, *93*, 25–41. [CrossRef] [PubMed]
22. Iyer, P.V.; Ananthanarayan, L. Enzyme stability and stabilization—Aqueous and non-aqueous environment. *Process Biochem.* **2008**, *43*, 1019–1032. [CrossRef]
23. Rodrigues, R.C.; Ortiz, C.; Berenguer-Murcia, A.; Torres, R.; Fernández-Lafuente, R.; Berenguer-Murcia, Á.; Torres, R.; Fernández-Lafuente, R. Modifying enzyme activity and selectivity by immobilization. *Chem. Soc. Rev.* **2013**, *42*, 6290–6307. [CrossRef] [PubMed]
24. Barbosa, O.; Ortiz, C.; Berenguer-Murcia, Á.; Torres, R.; Rodrigues, R.C.; Fernandez-Lafuente, R. Strategies for the one-step immobilization–purification of enzymes as industrial biocatalysts. *Biotechnol. Adv.* **2015**, *33*, 435–456. [CrossRef] [PubMed]
25. Biró, E.; Németh, Á.S.; Sisak, C.; Feczkó, T.; Gyenis, J. Preparation of chitosan particles suitable for enzyme immobilization. *J. Biochem. Biophys. Methods* **2008**, *70*, 1240–1246. [CrossRef] [PubMed]
26. Krajewska, B. Application of chitin- and chitosan-based materials for enzyme immobilizations: A review. *Enzyme Microb. Technol.* **2004**, *35*, 126–139. [CrossRef]
27. Malmiri, H.J.; Jahanian, M.A.G.; Berenjian, A. Potential applications of chitosan nanoparticles as novel support in enzyme immobilization. *Am. J. Biochem. Biotechnol.* **2012**, *8*, 203–219. [CrossRef]
28. Sjoholm, K.H.; Cooney, M.; Minteer, S.D. Effects of degree of deacetylation on enzyme immobilization in hydrophobically modified chitosan. *Carbohydr. Polym.* **2009**, *77*, 420–424. [CrossRef]
29. Jesionowski, T.; Zdarta, J.; Krajewska, B. Enzyme immobilization by adsorption: A review. *Adsorption* **2014**, *20*, 801–821. [CrossRef]
30. Santos, J.C.S.; Barbosa, O.; Ortiz, C.; Berenguer-Murcia, A.; Rodrigues, R.C.; Fernandez-Lafuente, R. Importance of the support properties for immobilization or purification of enzymes. *ChemCatChem* **2015**, *7*, 2413–2432. [CrossRef]
31. Barbosa, O.; Ortiz, C.; Berenguer-Murcia, Á.; Torres, R.; Rodrigues, R.C.; Fernandez-Lafuente, R. Glutaraldehyde in bio-catalysts design: A useful crosslinker and a versatile tool in enzyme immobilization. *RSC Adv.* **2014**, *4*, 1583–1600. [CrossRef]
32. Migneault, I.; Dartiguenave, C.; Bertrand, M.J.; Waldron, K.C. Glutaraldehyde: Behavior in aqueous solution, reaction with proteins, and application to enzyme crosslinking. *Biotechniques* **2004**, *37*, 790–802. [PubMed]
33. Wine, Y.; Cohen-Hadar, N.; Freeman, A.; Frolow, F. Elucidation of the mechanism and end products of glutaraldehyde crosslinking reaction by X-ray structure analysis. *Biotechnol. Bioeng.* **2007**, *98*, 711–718. [CrossRef] [PubMed]
34. Barbosa, O.; Torres, R.; Ortiz, C.; Berenguer-Murcia, Á.; Rodrigues, R.C.; Fernandez-Lafuente, R. Heterofunctional supports in enzyme immobilization: From traditional immobilization protocols to opportunities in tuning enzyme properties. *Biomacromolecules* **2013**, *14*, 2433–2462. [CrossRef] [PubMed]
35. Barbosa, O.; Torres, R.; Ortiz, C.; Fernandez-Lafuente, R. Versatility of glutaraldehyde to immobilize lipases: Effect of the immobilization protocol on the properties of lipase B from Candida antarctica. *Process Biochem.* **2012**, *47*, 1220–1227. [CrossRef]
36. Betancor, L.; López-Gallego, F.; Hidalgo, A.; Alonso-Morales, N.; Mateo, G.D.-O.C.; Fernández-Lafuente, R.; Guisán, J.M. Different mechanisms of protein immobilization on glutaraldehyde activated supports: Effect of support activation and immobilization conditions. *Enzyme Microb. Technol.* **2006**, *39*, 877–882. [CrossRef]

37. López-Gallego, F.; Betancor, L.; Mateo, C.; Hidalgo, A.; Alonso-Morales, N.; Dellamora-Ortiz, G.; Guisán, J.M.; Fernández-Lafuente, R. Enzyme stabilization by glutaraldehyde crosslinking of adsorbed proteins on aminated supports. *J. Biotechnol.* **2005**, *119*, 70–75. [CrossRef] [PubMed]
38. Zaak, H.; Peirce, S.; de Albuquerque, T.; Sassi, M.; Fernandez-Lafuente, R. Exploiting the Versatility of Aminated Supports Activated with Glutaraldehyde to Immobilize β-galactosidase from Aspergillus oryzae. *Catalysts* **2017**, *7*, 250. [CrossRef]
39. Vazquez-Ortega, P.G.; Alcaraz-Fructuoso, M.T.; Rojas-Contreras, J.A.; López-Miranda, J.; Fernandez-Lafuente, R. Stabilization of dimeric β-glucosidase from Aspergillus niger via glutaraldehyde immobilization under different conditions. *Enzyme Microb. Technol.* **2018**, *110*, 38–45. [CrossRef] [PubMed]
40. Peniche, C.; Argüelles-Monal, W.; Peniche, H.; Acosta, N. Chitosan: An Attractive Biocompatible Polymer for Microencapsulation. *Macromol. Biosci.* **2003**, *3*, 511–520. [CrossRef]
41. Zhang, Y.; Tao, L.; Li, S.; Wei, Y. Synthesis of Multiresponsive and Dynamic Chitosan-Based Hydrogels for Controlled Release of Bioactive Molecules. *Biomacromolecules* **2011**, *12*, 2894–2901. [CrossRef] [PubMed]
42. Betancor, L.; Luckarift, H.R. Bioinspired enzyme encapsulation for biocatalysis. *Trends Biotechnol.* **2008**, *26*, 566–572. [CrossRef] [PubMed]
43. Chakraborty, S. Carrageenan for encapsulation and immobilization of flavor, fragrance, probiotics, and enzymes: A review. *J. Carbohydr. Chem.* **2017**, *36*, 1–19. [CrossRef]
44. Pierre, A.C. The sol-gel encapsulation of enzymes. *Biocatal. Biotransformation* **2004**, *22*, 145–170. [CrossRef]
45. Cao, L.; van Rantwijk, F.; Sheldon, R.A. Cross-Linked Enzyme Aggregates: A Simple and Effective Method for the Immobilization of Penicillin Acylase. *Org. Lett.* **2000**, *2*, 1361–1364. [CrossRef] [PubMed]
46. Schoevaart, R.; Wolbers, M.W.; Golubovic, M.; Ottens, M.; Kieboom, A.P.G.; van Rantwijk, F.; van der Wielen, L.A.M.; Sheldon, R.A. Preparation, optimization, and structures of cross-linked enzyme aggregates (CLEAs). *Biotechnol. Bioeng.* **2004**, *87*, 754–762. [CrossRef] [PubMed]
47. Sheldon, R.A. Cross-linked enzyme aggregates (CLEA®s): Stable and recyclable biocatalysts. *Biochem. Soc. Trans.* **2007**, *35*, 1583–1587. [CrossRef] [PubMed]
48. Sheldon, R.A. Cross-linked enzyme aggregates as industrial biocatalysts. *Org. Process Res. Dev.* **2011**, *15*, 213–223. [CrossRef]
49. Talekar, S.; Joshi, A.; Joshi, G.; Kamat, P.; Haripurkar, R.; Kambale, S. Parameters in preparation and characterization of cross linked enzyme aggregates (CLEAs). *RSC Adv.* **2013**, *3*, 12485–12511. [CrossRef]
50. Galvis, M.; Barbosa, O.; Ruiz, M.; Cruz, J.; Ortiz, C.; Torres, R.; Fernandez-Lafuente, R. Chemical amination of lipase B from Candida antarctica is an efficient solution for the preparation of crosslinked enzyme aggregates. *Process Biochem.* **2012**, *47*, 2373–2378. [CrossRef]
51. Rodrigues, R.C.; Barbosa, O.; Ortiz, C.; Berenguer-Murcia, Á.; Torres, R.; Fernandez-Lafuente, R. Amination of enzymes to improve biocatalyst performance: Coupling genetic modification and physicochemical tools. *RSC Adv.* **2014**, *4*, 38350–38374. [CrossRef]
52. López-Gallego, F.; Betancor, L.; Hidalgo, A.; Alonso, N.; Fernández-Lafuente, R.; Guisán, J.M. Co-aggregation of Enzymes and Polyethyleneimine: A Simple Method To Prepare Stable and Immobilized Derivatives of Glutaryl Acylase. *Biomacromolecules* **2005**, *6*, 1839–1842. [CrossRef] [PubMed]
53. Wilson, L.; Fernández-Lorente, G.; Fernández-Lafuente, R.; Illanes, A.; Guisán, J.M.; Palomo, J.M. CLEAs of lipases and poly-ionic polymers: A simple way of preparing stable biocatalysts with improved properties. *Enzyme Microb. Technol.* **2006**, *39*, 750–755. [CrossRef]
54. Ahumada, K.; Urrutia, P.; Illanes, A.; Wilson, L. Production of combi-CLEAs of glycosidases utilized for aroma enhancement in wine. *Food Bioprod. Process.* **2015**, *94*, 555–560. [CrossRef]
55. Cruz, J.; Barbosa, O.; Rodrigues, R.C.; Fernandez-Lafuente, R.; Torres, R.; Ortiz, C. Optimized preparation of CALB-CLEAs by response surface methodology: The necessity to employ a feeder to have an effective crosslinking. *J. Mol. Catal. B Enzym.* **2012**, *80*, 7–14. [CrossRef]
56. Cui, J.D.; Sun, L.M.; Li, L.L. A simple technique of preparing stable CLEAs of Phenylalanine ammonia lyase using co-aggregation with starch and bovine serum albumin. *Appl. Biochem. Biotechnol.* **2013**, *170*, 1827–1837. [CrossRef] [PubMed]
57. Dal Magro, L.; Hertz, P.F.; Fernandez-Lafuente, R.; Klein, M.P.; Rodrigues, R.C. Preparation and characterization of a Combi-CLEAs from pectinases and cellulases: A potential biocatalyst for grape juice clarification. *RSC Adv.* **2016**, *6*, 27242–27251. [CrossRef]

58. Mafra, A.C.O.; Kopp, W.; Beltrame, M.B.; Giordano, R.L.C.; Ribeiro, M.P.A.; Tardioli, P.W. Diffusion effects of bovine serum albumin on cross-linked aggregates of catalase. *J. Mol. Catal. B Enzym.* **2016**, *133*, 107–116. [CrossRef]
59. Shah, S.; Sharma, A.; Gupta, M.N. Preparation of cross-linked enzyme aggregates by using bovine serum albumin as a proteic feeder. *Anal. Biochem.* **2006**, *351*, 207–213. [CrossRef] [PubMed]
60. Torabizadeh, H.; Tavakoli, M.; Safari, M. Immobilization of thermostable α-amylase from Bacillus licheniformis by cross-linked enzyme aggregates method using calcium and sodium ions as additives. *J. Mol. Catal. B Enzym.* **2014**, *108*, 13–20. [CrossRef]
61. Perkins, E.G. Composition of soybean and soybean products. In *Practical Handbook of Soybean Processing and Utilization*; Erickson, D.R., Ed.; AOCS Press: St. Louis, France, 1995; ISBN 978-0-935315-63-9.
62. Iwabuchi, S.; Yamauchi, F. Determination of glycinin and β-conglycinin in soybean proteins by immunological methods. *J. Agric. Food Chem.* **1987**, *35*, 200–205. [CrossRef]
63. Thanh, V.H.; Shibasaki, K. Major proteins of soybean seeds. subunit structure of β-conglycinin. *J. Agric. Food Chem.* **1978**, *26*, 692–695. [CrossRef]
64. Utsumi, S.; Inaba, H.; Mori, T. Heterogeneity of soybean glycinin. *Phytochemistry* **1981**, *20*, 585–589. [CrossRef]
65. Noda, T.; Furuta, S.; Suda, I. Sweet potato beta-amylase immobilized on chitosan beads and its application in the semi-continuous production of maltose. *Carbohydr. Polym.* **2001**, *44*, 189–195. [CrossRef]
66. Vretblad, P.; Axen, R. Preparation and properties of an immobilized Barley β-amylase. *Biotechnol. Bioeng.* **1973**, *15*, 783–794. [CrossRef]
67. Martensson, K.A.J. Preparation of an immobilized two-enzyme system, beta-amylase-Pullulanase, to an acrylic copolymer for the conversion of starch to maltose. I. Preparation and stability of immobilized beta-amylase. *Biotechnol. Bioeng.* **1974**, *XVI*, 579–591. [CrossRef] [PubMed]
68. Khan, M.J.; Khan, F.H.; Husain, Q. Application of immobilized Ipomoea batata beta amylase in the saccharification of starch. *J. Appl. Biol. Sci.* **2011**, *5*, 33–39.
69. Tavano, O.L.; Fernandez-Lafuente, R.; Goulart, A.J.; Monti, R. Optimization of the immobilization of sweet potato amylase using glutaraldehyde-agarose support. Characterization of the immobilized enzyme. *Process Biochem.* **2013**, *48*, 1054–1058. [CrossRef]
70. Talekar, S.; Desai, S.; Pillai, M.; Nagavekar, N.; Ambarkar, S.; Surnis, S.; Ladole, M.; Nadar, S.; Mulla, M. Carrier free co-immobilization of glucoamylase and pullulanase as combi-cross linked enzyme aggregates (combi-CLEAs). *RSC Adv.* **2013**, *3*, 2265–2271. [CrossRef]
71. Talekar, S.; Ghodake, V.; Ghotage, T.; Rathod, P.; Deshmukh, P.; Nadar, S.; Mulla, M.; Ladole, M. Novel magnetic cross-linked enzyme aggregates (magnetic CLEAs) of alpha amylase. *Bioresour. Technol.* **2012**, *123*, 542–547. [CrossRef] [PubMed]
72. Talekar, S.; Waingade, S.; Gaikwad, V.; Patil, S.; Nagavekar, N. Preparation and characterization of cross linked enzyme aggregates (CLEAs) of Bacillus amyloliquefaciens alpha amylase. *J. Biochem. Technol.* **2012**, *3*, 349–353.
73. Yoshigi, N.; Okada, Y.; Sahara, H.; Koshino, S. Expression in Escherichia coli of cDNA encoding barley beta-amylase and properties of recombinant beta-amylase. *Biosci. Biotechnol. Biochem.* **1994**, *58*, 1080–1086. [CrossRef] [PubMed]
74. Gaouar, O.; Zakhia, N.; Aymard, C.; Rios, G.M. Production of maltose syrup by bioconversion of cassava starch in an ultrafiltration reactor. *Ind. Crops Prod.* **1998**, *7*, 159–167. [CrossRef]
75. Shiraishi, F.; Kawakami, K.; Yuasa, A.; Kojima, T.; Kusunoki, K. Kinetic expression for maltose production from soluble starch by simultaneous use of beta-amylase and debranching enzymes. *Biotechnol. Bioeng.* **1987**, *30*, 374–380. [CrossRef] [PubMed]
76. Bhattacharya, A.; Pletschke, B.I. Magnetic cross-linked enzyme aggregates (CLEAs): A novel concept towards carrier free immobilization of lignocellulolytic enzymes. *Enzyme Microb. Technol.* **2014**, *61*, 17–27. [CrossRef] [PubMed]
77. Kopp, W.; Da Costa, T.P.; Pereira, S.C.; Jafelicci, M.; Giordano, R.C.; Marques, R.F.C.; Araújo-Moreira, F.M.; Giordano, R.L.C. Easily handling penicillin G acylase magnetic cross-linked enzymes aggregates: Catalytic and morphological studies. *Process Biochem.* **2014**, *49*, 38–46. [CrossRef]
78. Kumar, V.V.; Sivanesan, S.; Cabana, H. Magnetic cross-linked laccase aggregates—Bioremediation tool for decolorization of distinct classes of recalcitrant dyes. *Sci. Total Environ.* **2014**, *487*, 830–839. [CrossRef] [PubMed]

79. Nadar, S.S.; Rathod, V.K. Magnetic macromolecular cross linked enzyme aggregates (CLEAs) of glucoamylase. *Enzyme Microb. Technol.* **2016**, *83*, 78–87. [CrossRef] [PubMed]
80. Park, J.-M.; Kim, M.; Park, J.-Y.; Lee, D.-H.; Lee, K.-H.; Min, J.; Kim, Y.-H. Immobilization of the cross-linked para-nitrobenzyl esterase of Bacillus subtilis aggregates onto magnetic beads. *Process Biochem.* **2010**, *45*, 259–263. [CrossRef]
81. Wilson, L.; Illanes, A.; Pessela, B.C.C.; Abian, O.; Fernández-Lafuente, R.; Guisán, J.M. Encapsulation of crosslinked penicillin G acylase aggregates in lentikats: Evaluation of a novel biocatalyst in organic media. *Biotechnol. Bioeng.* **2004**, *86*, 558–562. [CrossRef] [PubMed]
82. Molawa, L.; Jordaan, J.; Limson, J.; Brady, D. Modification of Alcalase SphereZyme™ by entrapment in LentiKats® to impart improved particle stability. *Biocatal. Biotransformation* **2013**, *31*, 71–78. [CrossRef]
83. Cui, J.D.; Li, L.L.; Bian, H.J. Immobilization of Cross-Linked Phenylalanine Ammonia Lyase Aggregates in Microporous Silica Gel. *PLoS ONE* **2013**, *8*, e80581. [CrossRef] [PubMed]
84. Jiang, Y.; Wang, Q.; Wang, W.; Zhou, L.; Gao, J. Preparation of immobilized lipase through combination of cross-linked enzyme aggregates and biomimetic silicification. *Chin. J. Catal.* **2012**, *33*, 857–862. [CrossRef]
85. Bernfeld, P. Amylases, alpha and beta. In *Methods in Enzymology*; Colowick, S.P., Kaplan, N.O., Eds.; Academic Press: New York, NY, USA, 1955; pp. 149–158.
86. Miller, G.L. Use of DinitrosaIicyIic Acid Reagent for Determination of Reducing Sugar. *Anal. Chem.* **1959**, *31*, 426–428. [CrossRef]
87. Vieira, D.C.; Lima, L.N.; Mendes, A.A.; Adriano, W.S.; Giordano, R.C.; Giordano, R.L.C.; Tardioli, P.W. Hydrolysis of lactose in whole milk catalyzed by β-galactosidase from Kluyveromyces fragilis immobilized on chitosan-based matrix. *Biochem. Eng. J.* **2013**, *81*. [CrossRef]
88. Lacerda, L.G.; Almeida, R.R.; Demiate, I.M.; Carvalho Filho, M.A.S.; Vasconcelos, E.C.; Woiciechowski, A.L.; Bannach, G.; Schnitzler, E.; Soccol, C.R. Thermoanalytical and starch content evaluation of cassava bagasse as agro-industrial residue. *Brazilian Arch. Biol. Technol.* **2009**, *52*, 143–150. [CrossRef]
89. Gouveia, E.R.; Nascimento, R.T.D.; Souto-Maior, A.M.; Rocha, G.J.D.M. Validation of methodology for the chemical characterization of sugar cane bagasse. *Quim. Nova* **2009**, *32*, 1500–1503. [CrossRef]
90. Giordano, R.C.; Giordano, R.L.C. Taylor-Couette vortex flow in enzymatic reactors. In *Immobilization of enzymes and cells*; Guisan, J.M., Ed.; Humana Press: Totowa, NJ, USA, 2006; pp. 321–332.
91. Bradford, M.M. A rapid and sensitive method for the quantitation of microgram quantities of protein utilizing the principle of protein-dye binding. *Anal. Biochem.* **1976**, *72*, 248–254. [CrossRef]

© 2018 by the authors. Licensee MDPI, Basel, Switzerland. This article is an open access article distributed under the terms and conditions of the Creative Commons Attribution (CC BY) license (http://creativecommons.org/licenses/by/4.0/).

catalysts

MDPI

Article

X-Shaped ZIF-8 for Immobilization *Rhizomucor miehei* Lipase via Encapsulation and Its Application toward Biodiesel Production

Miaad Adnan [1,2], Kai Li [1], Li Xu [1] and Yunjun Yan [1,*]

[1] Key Laboratory of Molecular Biophysics of the Ministry of Education, College of Life Science and Technology, Huazhong University of Science and Technology, Wuhan 430074, China; miaadadnan14@gmail.com (M.A.); D201577434@hust.edu.cn (K.L.); xuli@hust.edu.cn (L.X.)

[2] Ministry of Science and Technology, Baghdad 10001, Iraq

* Correspondence: yanyunjun@mail.hust.edu.cn; Tel.: +86-27-8779-2213

Received: 25 January 2018; Accepted: 26 February 2018; Published: 28 February 2018

Abstract: This study presents a one-step encapsulation method for synthesizing X-shaped zeolitic imidazolate frameworks (ZIF-8) and immobilizing *Rhizomucor miehei* lipase (RML). We proved that the morphological structure of ZIF-8 had changed after immobilization with enhanced characterization using a field-emission scanning electron microscope, an energy-dispersive spectrometer, a transmission electron microscope, a Fourier transform infrared spectrometer, and powder X-ray diffraction. The surface area and pore size of the carrier were investigated before and after immobilization using Brunauer–Emmett–Teller and Barrett–Joyner–Halenda methods, respectively. RML@ZIF-8 exhibited high recovery activity of up to 2632%, representing a 26-fold increase in its free lipase. Encapsulated RML was used for biodiesel production from soybean oil in an isooctane system with a conversion yield of 95.6% under optimum conditions. The resulting reusability of the immobilized enzyme indicated no substantial decline in the conversion yield, which remained at 84.7% of the initial activity after 10 cycles. The stability and high performance of the immobilized enzyme are attributed to the harmony between RML and ZIF-8 based on the easy synthesis of ZIF-8 and the short time required to immobilize RML.

Keywords: X-shape ZIF-8; *Rhizomucor miehei* lipase (RML); encapsulation technique; biodiesel yield; soybean oil

1. Introduction

The depletion of fossil fuel resources and the environmental impacts of fossil fuel use are the main motives for investigating and developing renewable fuel sources. The term biodiesel implies a fuel that is biodegradable, and such fuels are being increasingly used in compression-combustion engines [1]. Biodiesel consists of oxoalkyl esters that include ethyl and methyl esters that originate from animal fats or vegetable oils as renewable feedstock [2]. However, the applicability of the chemical processes used to create biodiesel has been restricted due to substantial energy requirements, challenges in retrieving catalyzers, and various environmental barriers [3]. Enzymatic methods, including lipase catalysis, are more advantageous than chemical processes due to their lower energy consumption, easier product retrieval, environmentally friendly means, and adaptability to a broad range of crude substances, particularly those with large free fatty acid content [4]. Despite the multiple advantages of lipases, the high price of enzyme catalysts is a significant barrier in biodiesel manufacturing. Immobilization is a possible solution to this problem, because immobilized lipases are repeatable and tolerate a wide range of pH values, temperatures, and organic solvents and more stable than the free counterparts [5].

In-depth studies have explored immobilization enzymes and their applications to various fields. The literature describes conventional methods used in immobilization, adsorption, covalent bond

cross-linking, and entrapping [6,7]. The adsorption technique is easy to complete, but the bonding of enzymes is frequently weak, resulting in the leaching of biocatalysts [8]. Conversely, covalent techniques prevent leaching, but the processes are lengthy and require several chemical steps that lead to the loss of enzyme activity [9]. The entrapment technique has attracted considerable interest because of its numerous advantages, including its speed, stability, simple treatment process, low cost, and requirement of mild conditions [10]. Macario et al. [11] investigated the sol-gel for entrapped lipase, obtaining the highest yield of fatty acid methyl esters at 77% and retaining 60% of the original activity after five batches. For biodiesel synthesis, lipase from *Pseudomonas cepacia* was encapsulated into hydrophobic sol-gel, yielding nearly 67% [4]. Calcium alginates were used as substrates for providing beads; the obtained biocatalysts were reused for four cycles with minimal leakage [12]. These materials that use gel structures for entrapment, such as calcium alginate or sol-gel, suffer from mass transfer limitation; thus, the biocatalyst performance is slightly restricted, which is another disadvantage in addition to the leaching of enzymes and loss of activity [13,14]. To overcome this problem, coordinated matrices of carriers are needed with a pore size that allows the flow of substrates and other materials, but is sufficiently small to prevent the rinsing of encapsulated enzymes.

To this end, we have been investigating the potential of metal-organic frameworks (MOFs). MOFs are hybrid materials with both organic and inorganic components that acts a host and protective shield for enzymes subjected to harsh environmental conditions [15].

The zeolitic imidazolate framework (ZIF-8), an MOF subdivision, is a novel type of microporous material formed by the coordination between zinc (Zn^{2+}) ions and 2-methylimidazole. It is the branch of the ZIF subclass of MOFs that has attracted significant research attention due to its high porosity, tunable surface properties, negligible cytotoxicity, exceptional thermal and chemical stability, and ease of synthesis under mild biocompatible conditions [16,17]. These properties allow ZIF-8 to be used for a variety of applications, such as adsorption, separation, [18,19], gas storage [20], drug delivery [21], and catalysis [22].

In the present work, we used X-shaped ZIF-8 as a carrier to immobilize *Rhizomucor miehei* lipase (RML) via the encapsulation method in a single step from synthesis and immobilization in an aqueous solution. We also investigated the optimum conditions for immobilizing lipases. Several specific characteristics of the encapsulated RML@ZIF-8 and its morphological properties were studied to prove the ability of the lipase to directly regulate the morphology of ZIF-8 and ensure successful immobilization. Eventually, experiments were performed with the encapsulated lipase by stimulating transesterification in biodiesel production from soybean oil.

2. Results and Discussion

2.1. Synthesis and Characterization of ZIF-8 and Lipase@ZIF-8

The lipase was entrapped within ZIF-8 using the encapsulation method (Figure 1), dried in a vacuum dryer, and characterized by scanning electron microscope (SEM), the morphology of ZIF-8 changed after RML encapsulation, as shown in Figure 2a,b. The same morphology was identified by TEM (Figure 2c,d), but it did not match the morphology obtained by Cui et al. [23], who reported that the shape of ZIF-8 did not change with the macromolecule protein (lipase). EDS analysis demonstrated differences between ZIF-8 and RML@ZIF-8 (Figure 2e,f). The immobilized lipase consisted of sodium (Na) due to the presence of RML. However, we did not find Na in ZIF-8, confirming the success of the immobilization.

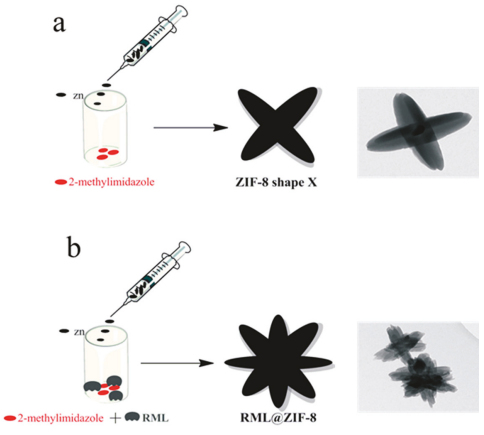

Figure 1. Schematic illustration of (**a**) the synthesis of zeolitic imidazolate frameworks (ZIF-8) and (**b**) the immobilization of *Rhizomucor miehei* lipase (RML)@ZIF-8.

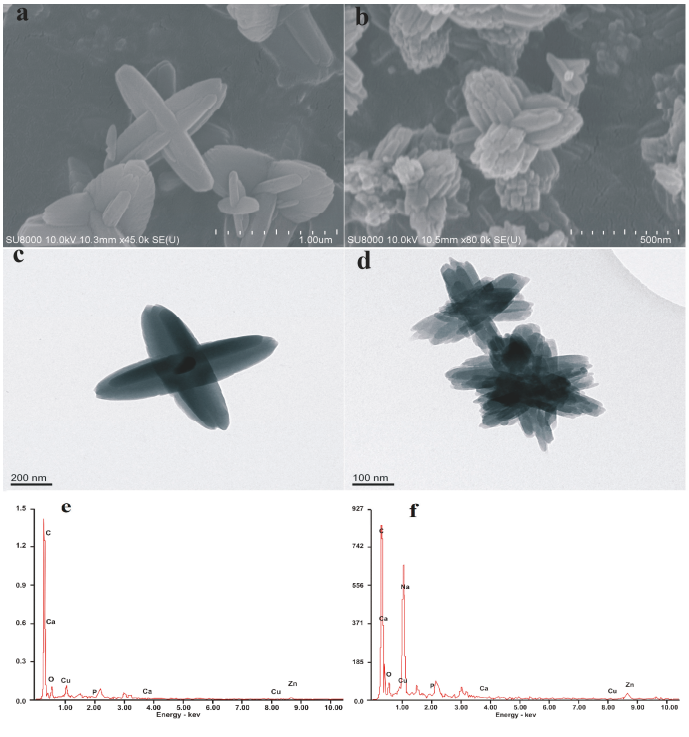

Figure 2. SEM images (**a**) ZIF-8 and (**b**) ZIF-8@RML; TEM images of (**c**) ZIF-8 and (**d**) ZIF-8@RML; EDS patterns of (**e**) ZIF-8 and (**f**) RML@ZIF-8.

Figure 3 presents additional evidence for RML encapsulation in ZIF-8. The FTIR spectra exhibited ZIF-8, RML@ZIF-8, and absolute RML. A notable characteristic peak of Zn–N stretched at 434 cm^{-1}. The strong bending vibrations at 756 and 1424 cm^{-1} were due to the Hmim ring. Simultaneously,

the feeble peaks at 2922–3200 cm^{-1} were due to the aliphatic and aromatic stretching of the C–H bond of Hmim [24]. The aforementioned bands in the spectrum included ZIF-8 and RML@ZIF-8. The spectrum (RML) displayed characteristic bands of the free RML protein. Two bands were observed at 1640–1660 and 3370–3380 cm^{-1}, which align with the amide I band of the enzyme, corresponding to C=O and N–H stretching, respectively. After the immobilization of RML in ZIF-8, the same characteristic peaks of RML were retained.

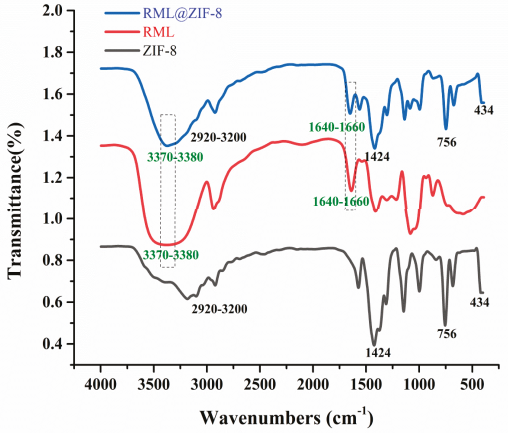

Figure 3. Fourier transform infrared (FT-IR) spectra of samples of ZIF-8, RML, and ZIF-8@RML.

Powder X-ray diffraction (PXRD) further confirmed our findings by demonstrating the differences in the peak intensities of ZIF-8 and lipase@ZIF-8. The main summits denoted the increase in intensity for pure ZIF-8 at 2θ = 10.98°, 15.11°, 17.04°, 18.01°, 21.76°, 27.78°, and 29.05°, which corresponded to the 1833, 1840, 2800, 3710, 1388, 1504, and 2245 plates of the crystal face structure. In contrast, the intensity of lipase@ZIF-8 decreased due to the diminished distance between the atomic layers in the crystalline material and the decrease in crystallinity of RML@ZIF-8 after modification [25,26]. This result shows that the modification of the morphological properties of ZIF-8 resulted from the encapsulation of biomacromolecules (RML) (Figure 4).

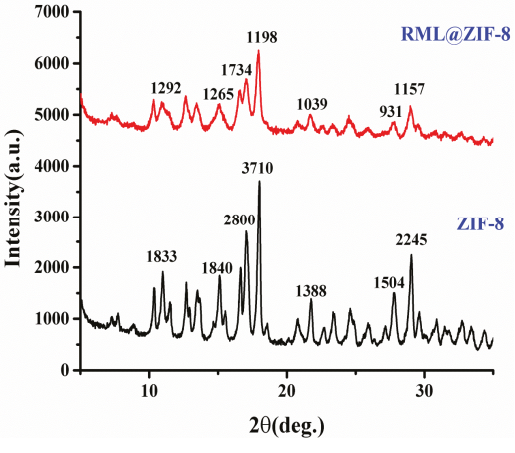

Figure 4. PXRD patterns of ZIF-8 of ZIF-8@RML.

For ZIF-8 and RML@ZIF-8, Figure 5 shows the N_2 adsorption–desorption isotherm test results, which were between Types I and IV, correlating to the International Union of Pure and Applied Chemistry (IUPAC), which suggests that this nanocomposite contains micro- and mesopores due to the gas adsorption at low relative pressure and increased uptake at pressures higher than 0.6 P/P0 [27]. The BET-based specific surface area for ZIF-8 before lipase immobilization was 697.51 m^2/g, but this value decreased to 593.36 m^2/g after immobilization. The average pore diameter of RML@ZIF-8 was 4.65 nm after immobilization and 9.67 nm before immobilization. This is a 5.11 nm reduction in diameter. These results were due to the role of the enzyme in modulating the morphological properties of ZIF-8 during the immobilization process. In this case, RML occupied some of the pores and destroyed other pores, creating new pores with different sizes and unusual shapes. Consequently, the surface area and diameter of the pores reduced.

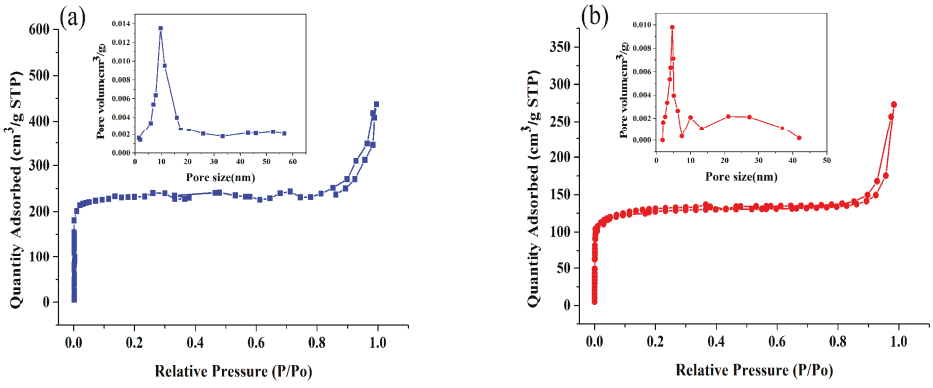

Figure 5. Nitrogen adsorption–desorption isotherms and pore size distributions (insert figures) for (**a**) ZIF-8 and (**b**) RML@ZIF-8.

2.2. Impacts of Immobilization Parameters

During lipase immobilization, we observed the effects of enzyme loading, encapsulation time, and immobilization temperature on the efficiency of immobilization and activity recovery. For lipase loading, the amount of lipase ranged from 15 to 27 mg and was increased by 2 mg after each run. Maximum activity recovery was 2426% when RML loading was 25 mg, whereas the immobilization efficiency exhibited a consistent decline whenever loading increased (Figure 6a). Therefore, we chose 25 mg as the suitable lipase amount for the immobilization of RML. A large quantity of lipase loading can reduce activity recovery, as the enzyme particles interred in the inner pore of ZIF-8 cannot be reached by the substrate [28].

Duration time did not significantly affect the efficiency of immobilization. The activity recovery increased with increasing encapsulation time, reaching the highest value of 2528% at 20 min and then decreasing when the encapsulation time exceeded 20 min. Consequently, 20 min was chosen as the best encapsulation period (Figure 6b). The enzyme activity in the aqueous phase decreased as encapsulation time increased [29].

For the immobilization temperature, immobilization efficiency increased gradually. Activity recovery increased despite the elevated temperature, reaching a maximum value of 2632% at 30 °C. Thereafter, activity recovery began to decline due to the thermal inactivation of the lipase (Figure 6c). Thus, 30 °C was chosen as the most suitable immobilization temperature.

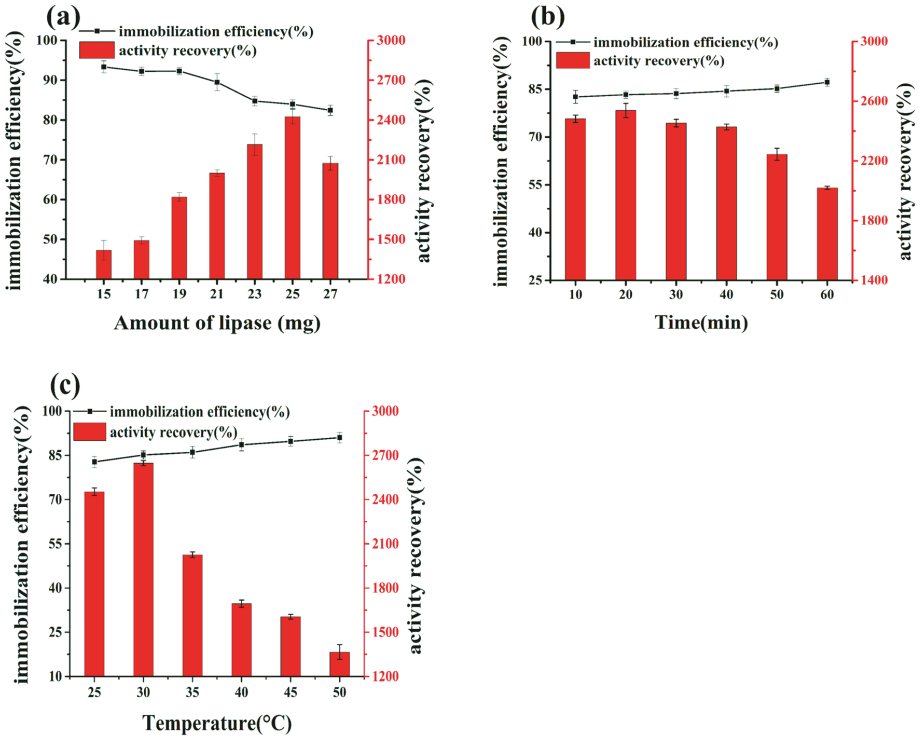

Figure 6. Impacts of three variables on the immobilization efficiency and activity recovery of the enzyme. (**a**) Amounts of lipase, (**b**) encapsulation time and (**c**) reaction temperature.

Under these optimal conditions, enzyme loading, encapsulation time, and immobilization temperature led to a 26-fold increase in the activity recovery of the enzyme relative to the free enzyme. This result is attributed to the features of the carrier and to the immobilization method and unique characteristics of the lipase. To improve the activity and stability of the immobilized enzyme caused by the complicated process, the following factors were considered. The first factor is related to the immobilization method. The encapsulation method was found to be better than other conventional methods because it protects the enzyme upon encapsulation and prevents direct contact between the enzyme and the substrate, which can influence enzyme activity. The other methods used for immobilization occasionally couple the active site of the enzyme with the substrate, leading to an expected loss in enzyme activity due to direct contact [30,31]. Second, immobilization carriers, and particularly ZIF-8, can significantly affect enzyme activity by creating microenvironments that are suitable for enzyme catalysis through ZIF-8 for a limited time in mild biocompatible conditions that allow for the preservation of enzymatic activity [32,33]. In addition, MOF biomimetic mineralization is aided by the attraction of biomacromolecules (lipase) to imidazole, which is a component that emerges from intermolecular hydrogen bonding and hydrophobic interactions. Simultaneously, RML affects the morphology, crystal dimension, and crystallinity when it is encapsulated within the porous crystal, leading to the formation of different holes that firmly envelope the lipase [34]. Finally, the active catalytic center of the lipase is closed by the mobile element called the "lid" configuration, which regulates the passage of substrates to active enzymatic sites. The secondary structure related to RML can be altered by the conformation of lipase@ZIF-8. The lid opens to the substrate for a long period, which causes an increase in lipase activity due to the ease of access [35].

2.3. Influence of Transesterification Parameters on the Biodiesel Yield

Many previous reports explored the effects of kinetic parameters on transesterification reactions in biodiesel production. We conducted a string of investigations to identify the ideal conditions to production (FAAE) using the biocatalysis of lipase@ZIF-8 with soybean oil.

As shown in Figure 7a, the biodiesel product considerably increased to 84.7% with the addition of 20% isooctane to the reaction system. Above 20% isooctane, the biodiesel yield gradually decreased. An explanation for this phenomenon is that the residual amino acids in the lid react with the isooctane molecules, so the immobilized enzyme remains in the open conformation, reaching higher catalytic activity [36]. We ascribe the decrease in biodiesel yield to the ethanol and the by-product, glycerol, exhibiting poor solubility in isooctane when the concentration and deposit of ethanol and glycerol layering on RML occur with an isooctane concentration above 20% [37].

Water is fundamental to the reaction mixture in ester production because it retains and enhances enzyme activity in organic solvents [38]. Furthermore, water significantly influences the reaction equilibrium. The transesterification reaction involves aqueous and organic phases that enable the lipase to work at water–oil interfaces; thus, performance is appreciably influenced by the interfacial region [39]. As shown in Figure 7b, RML@ZIF activity significantly increased when 3% water was added to the reaction mixture, therefore proving that activating the enzyme requires a small amount of moisture content. The highest biodiesel yield of 87.1% was obtained with 9 wt % water. The conversion yield decreased to 83.1%, 81.5%, and 72.8% yield with a water content of 12%, 15%, and 18%, respectively. Nevertheless, the moisture concentration in a transesterification reaction mixture can positively or negatively affect the lipase catalytic activity. Excess moisture in the reaction mixture provides the lipase with additional flexibility and can lead to undesirable reactions, such as hydrolysis. For example, the highest catalytic activity in the transesterification of commercial Novozym 435 lipase was achieved without adding water to the batch system [40]. Thus, the best moisturizing content is the lowest value in hydrolysis and the highest enzyme activity for the transesterification reaction, depending on the oil of the feedstock, the organic solvent, lipase type, and the immobilized carrier [28].

The catalytic activity of each enzyme at the optimum temperature directly influences the rate and velocity of the reaction. Hence, the impact of temperature on enzymatic reactions should not be neglected. According to Figure 7c, the maximum conversion yield of RML@ZIF-8 transesterification was 88.8% at a temperature of 45 °C. A further increase in temperature to 55 °C induced a notable drop in biodiesel product. As reported, the optimal temperature for enzymatic transesterification results from the interaction between the transesterification rate and operational stability of the biocatalyst [41,42].

Alcohols have two roles in transesterification reactions. First, the surplus of alcohols in transesterification reactions increases the reaction rate and drives the high yield of FAEEs [43]. Second, a high concentration of alcohol negatively affects enzymes, which typically become unstable in alcohols, such as ethanol and methanol, enabling the deactivation of RML@ZIF-8 through its contact with insoluble ethanol that exists in a reaction system and results from decreases in ethyl ester production [44]. Accordingly, we determined the optimum volume of ethanol added to the system that causes the least harm to the lipase and leads to an increase in maximal conversion value (Figure 7d). The highest conversion yield for biodiesel was 91.2% at a molar ratio of 1:4, declining gradually when the molar ratio increased from 1:5 to 1:6.

Yan et al. [45] reported that an equivalent of alcohols higher than 1/2 M added to the mixture at onset interplay disrupt the enzyme activity. To prevent the inactivation of the enzyme caused by alcohol, we applied a stepwise addition of EtOH to the system. Thus, the interval time between alcohol addition and the reaction positively affected the reaction system. Fan et al. [46] obtained a 93.1% biodiesel yield when they used a three-step approach with a time interval of 10 h. Therefore, we studied the effects of the interval time of ethanol addition on biodiesel product. We improved biodiesel yield from 73.8 to 92.3% when we increased the interval time from 4 to 8 h (Figure 7e). Although the interval time was extended to 12 h, this level of transmutation did not significantly increase biodiesel yield

due to the dynamic equilibrium in the reaction components. Therefore, the optimal biodiesel yield required an 8 h interval. Based on that, 8 h were regarded as the best interval at which ethanol is added, and a maximum biodiesel yield of 92.3% was obtained within a 24 h reaction time.

To reduce the cost of biodiesel production and obtain maximum yield, we optimized the measure of immobilized RML added to the reaction mixture. Biodiesel product increased as the quantity of immobilized enzyme was increased from 4 to 14 wt %, and the highest output of 95.6% was found at 8 wt % (Figure 7f). No considerable improvement in the conversion yield was observed when the lipase dosage was increased from 8 to 14%. Therefore, 8 wt % RML@ZIF-8 was considered the best dosage.

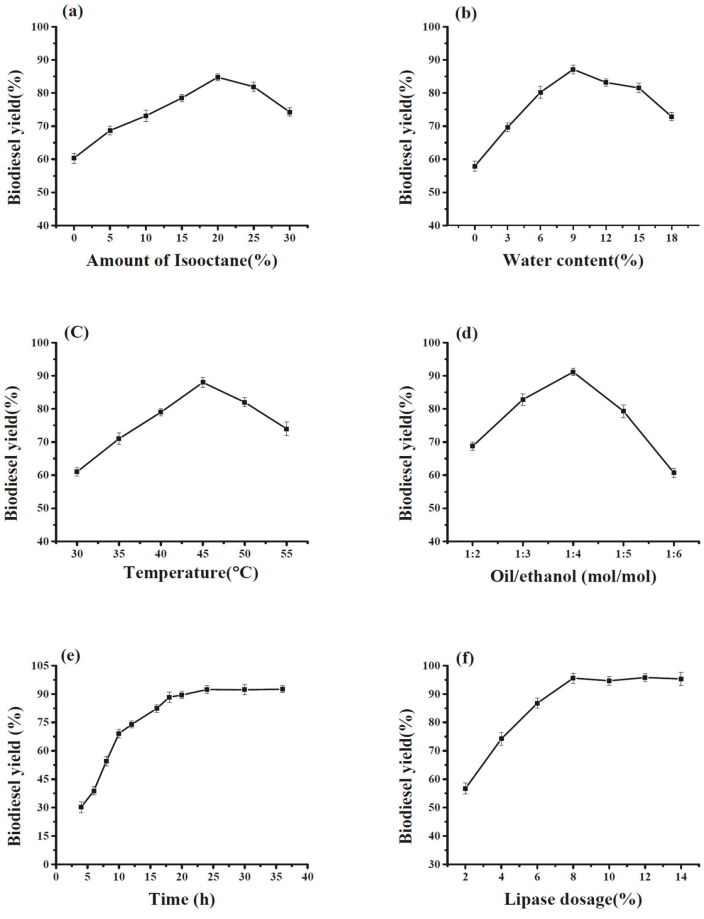

Figure 7. Impacts of reaction parameters on biodiesel production catalyzed by RML@ZIF-8. (**a**) The amount of isooctane; (**b**) Water content; (**c**) Reaction temperature; (**d**) Molar ratio oil to ethanol; (**e**) Reaction time; (**f**) The dosage of lipase.

2.4. Reusability of the Immobilized RML@ZIF-8

The purpose of using immobilize lipase in industrial applications is to achieve reusability, reducing the cost of the process. The reusability of RML@ZIF-8 in an isooctane medium was investigated, and the results are presented in Figure 8. We noted that the encapsulation of ZIF-8 to RML maintained an

84.7% yield after a continuous run of 10 cycles. The immobilized RML in the X-shaped ZIF-8 carrier had good operational stability. The lipase immobilized by the encapsulation method was more stable than it was under physical adsorption and was different from the covalent bonding that used a complex and time-consuming mechanism to connect the enzyme to the carrier. The proposed method specifically uses a relatively simple design and procedure. The decrease in biodiesel yield production with an increasing number of cycles was attributed to the excess ethanol and the glycerol by-product being adsorbed onto the surface of RML@ZIF-8. The poor solubility of these alcohols in feedstock oil decreases the biodiesel yield, which results from the gradual inactivation of the enzyme. Breaking the carrier apart by mechanical force results in a continuous reaction and leads to lipase leakage, reducing the effect of the immobilized lipase.

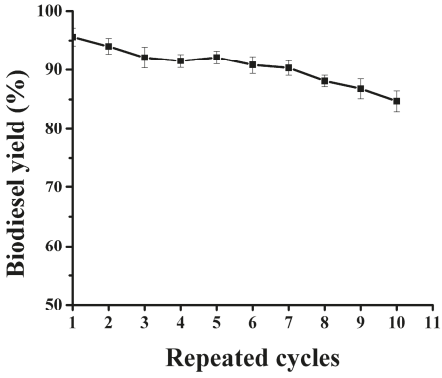

Figure 8. Reuse of RML@ZIF-8 for biodiesel production.

3. Materials and Methods

3.1. Materials

Lipase from *Rhizomucor miehei* (RML) was purchased from Sigma Aldrich (Copenhagen, Denmark). 2-Methylimidazole (HMeIM) and fatty acid methyl and ethyl ester standards were purchased from Aladdin Industrial Corporation (Shanghai, China). Bovine serum albumin (BSA) was procured from Shenshi Chemical Industry (Wuhan, China). Soybean oil with nearly 99% purity was brought from local markets. Other reagents of analytical grade were purchased from Sinopharm Chemical Reagent Co., Ltd. (Shanghai, China). These reagents included Zn $(NO_3)_2 \cdot 6H_2O$, lauric acid, acetone, 1-dodecanol, ethanol, isooctane, hexane, phenolphthalein, and sodium hydroxide (NaOH). They were used without any further purification. For all the experiments, purified water was used in the water refining system, with a resistance exceeding 18.2 MΩ cm.

3.2. Lipase Immobilization

Zif-8 encapsulated lipases were prepared according to a modified method [23]. Zn $(NO3)_2$ (0.148 g, 0.5 M) had been disbanding in 1 mL deionized (DI) water and dripped through a syringe into mixture solution of 25 mg of lipase and 2-methylimidazole (0.656 g, 0.8 M, 10 mL) under stirring at 200 rpm at 30 °C for 20 min. The nanoparticles that formed were gathered by centrifuging at 8000 rpm for 6 min and washed twice with DI water to remove excess unbound lipase. RML@ZIF-8 was vacuum dried and stored at 4 °C until further use. The remaining protein content in the supernatant was measured to determine the amount of immobilized enzyme using the Bradford protein assay with bovine serum albumin (BSA) as the standard protein. Within the immobilization procedure, the impacts of enzyme loading, period immobilization, and temperature on specific activity, immobilization efficiency, and lipase activity recovery were examined.

3.3. Measurement Activity for Immobilization Enzyme

The activity of RML@ZIF-8 and free lipases was examined with the esterification process previously explained [47]. A specific amount of the free and immobilized enzyme was added to 10 mL of a combination containing 1-dodecanol (0.2 M) and lauric acid (0.2 M) in isooctane with the addition of 0.01 mL water. The reactions occurred at 40 °C for 30 min with persistent agitation at 200 rpm. Afterward, the reactions were stopped by adding 1 mL of the samples to 5 mL of the stop solution consisting of acetone-ethanol 1:1, v/v. NaOH (0.05 M) was used in a titration to determine residual acid in the sample. Phenolphthalein solution (0.05%, w/v) was used as a pH indicator. One unit of RML activity (U) was expressed as the quantity of lipase required to liberate 1 µmol of lauric acid per 1 min under the assay conditions. The specific activity (U/g protein), activity recovery (%), and immobilization efficiency (%) were determined using Equations (1)–(3) [29].

$$\text{Specific activity (U/g protein)} = \frac{\text{initial activity}}{\text{protein content of immobilized lipase}} \quad (1)$$

$$\text{Immobilization efficiency (\%)} = \frac{\text{immobilized protein}}{\text{total loading protein}} \times 100\% \quad (2)$$

$$\text{Activity recovery (\%)} = \frac{\text{activity of immobilized lipase}}{\text{total activity of free lipase}} \times 100\% \quad (3)$$

3.4. Characterization

The detailed morphological structure was visualized using a field emission-scanning electron microscope (FE-SEM) SU-8010 equipped with a Hitachi energy-dispersive spectrometer (EDS) for elemental analysis. Transmission electron microscopy (TEM) images were obtained with an H-7000FA (Hitachi, Tokyo, Japan). Fourier-transform infrared spectrometer (FT-IR) images were obtained on a Bruker, VERTEX 70 using the KBr pellet system, in the range of 400–4000 cm^{-1}. Powder X-ray diffraction (PXRD) (Empyrean PANanalytical Company, Almelo, The Netherlands) patterns were conducted using copper and potassium radiation (40 kV, 40 mA) to study the crystal structures of ZIF-8 and RML@ZIF-8. The nitrogen gas adsorption and desorption isotherms at 77 K were applied to Micromeritics ASAP 2420 (Norcross, GA, USA). The surface area was measured using the Brunauer–Emmett–Teller (BET) method. Pore size was measured using the Barrett–Joyner–Halenda design.

3.5. Lipase@ZIF-8 for Biodiesel Production

Lipase@ZIF-8 was used as a catalyst for real world applications, such as biodiesel production for soybean oil. Transesterification reactions were performed in 50 mL capped flasks with a shaking speed of 200 rpm. The mixed reaction included 2.19 g soybean oil, RML@ZIF-8 lipase, isooctane, ethanol, and water. Ethanol was added in three steps to avoid its inhibitory influence on the immobilized RML during the same period. The effects of biodiesel production conditions, including isooctane amount, immobilized RML amount, water content, alcohol-to-oil molar ratio, reaction temperature, and reaction duration, were methodically determined. After a specified reaction time, the supernatant was collected through centrifugal separation at 12,000 rpm for 5 min. Thereafter, 10 µL supernatant was withdrawn and mixed with 290 µL n-hexane and 300 µL of 1.0 mg/mL heptadecanoic acid methyl ester as the interior standard. The mixture was then completely agitated for gas chromatography (GC) to determination biodiesel yield.

3.6. GC Analysis of Biodiesel Yield

The fatty acid ethyl esters (FAEEs) content was analyzed via GC using a previously reported method [48]. We used heptadecanoic acid methyl ester as the interior standard for defining biodiesel products. The GC-9790 gas chromatography system included an Agilent HP-INNOWAX capillary

column (30 m × 0.25 i.d. mm × 0.25 μm, Scientific, Folsom, CA, USA). The initial column temperature was 180 °C and was then increased to 230 °C at a rate of 3 °C/min and maintained at 230 °C for 3 min. The injector and detector temperatures were fixed at 230 °C and 280 °C, respectively. The biodiesel yield (%) was specified as the gross quantity of FAAE content in the diversion oil. The output was computed using Equations (4)–(6) [49,50]:

$$\text{Weight of FAAE} = \frac{Asample f_0}{AinternalWinternal} \quad (4)$$

$$f_0 = \frac{WsampleAinternl}{WinternalAsample} \quad (5)$$

$$\text{Biodiesel yield } (\%) = \frac{We}{Wt} \times 100\% \quad (6)$$

where A_{sample} is the peak region of FAAE in specimen, f_0 is the response agent, $A_{internal}$ is the peak region of the interior standard, $W_{internal}$ is the weight (g) of the interior standard, W_{sample} is the weight (g) of the sample, W_e is the experimental value of FAAE tested with GC, and W_t is the theoretical value of FAAE.

4. Conclusions

We successfully immobilized lipase in X-shaped ZIF-8 for the first time using the encapsulation method within a short time period under mild conditions. In addition, we enhanced the esterification activity 26-fold by optimizing the immobilization conditions. The immobilized RML was applied to catalyze biodiesel production with a high diversion average and excellent operational stabilization. Moreover, the SEM and TEM analyses indicated a change in the morphology of ZIF-8 after immobilizing the lipase. This X-shaped RML@ZIF-8 nanobiocatalyst is promising not only for biofuel production but also for other industrial applications, such as biosensors, the food industry, and biopharmaceuticals.

Acknowledgments: This work was financially supported by the National Natural Science Foundation of China (grant Nos. 31070089, 31170078 and J1103514), the National High Technology Research and Development Program of China (grant Nos. 2013AA065805 and 2014AA093510), the National Natural Science Foundation of Hubei Province (grant No. 2015CFA085), and the Fundamental Research Funds for HUST (grant Nos. 2014NY007, 2017KFYXJJ212, 2017KFXKJC010, 2017KFTSZZ001). The authors thank Chen Hong from Analytical and Testing Centre of HUST for her valuable assistance in XRD, FT-IR, EDS, TEM, and FE-SEM measurement and Li Na from the key laboratory of material chemistry for energy conversion and storage (HUST) for help in BET test. Many thanks are indebted to the Analytical and Testing Center of Huazhong University of Science and Technology for the measurements of water quality.

Author Contributions: Miaad Adnan and Yunjun Yan conceived and designed the experiments; Miaad Adnan and Kai Li performed the experiments and wrote the paper; Li Xu analyzed the data; Miaad Adnan and Yunjun Yan contributed to the revision and proofreading of the manuscript.

Conflicts of Interest: The authors declare no conflict of interest.

References

1. Guldhe, A.; Singh, B.; Mutanda, T.; Permaul, K.; Bux, F. Advances in synthesis of biodiesel via enzyme catalysis: Novel and sustainable approaches. *Renew. Sustain. Energy Rev.* **2015**, *41*, 1447–1464. [CrossRef]
2. Mehrasbi, M.R.; Mohammadi, J.; Peyda, M.; Mohammadi, M. Covalent immobilization of *Candida antarctica* lipase on core-shell magnetic nanoparticles for production of biodiesel from waste cooking oil. *Renew. Energy* **2017**, *101*, 593–602. [CrossRef]
3. Fan, Y.; Wu, G.; Su, F.; Li, K.; Xu, L.; Han, X.; Yan, Y. Lipase oriented-immobilized on dendrimer-coated magnetic multi-walled carbon nanotubes toward catalyzing biodiesel production from waste vegetable oil. *Fuel* **2016**, *178*, 172–178. [CrossRef]
4. Zhang, B.; Weng, Y.; Xu, H.; Mao, Z. Enzyme immobilization for biodiesel production. *Appl. Microbiol. Biotechnol.* **2012**, *93*, 61–70. [CrossRef] [PubMed]

5. Abdulla, R.; Ravindra, P. *Cross-Linked Lipase in Hybrid Matrix for Biodiesel Production from Crude Jatropha Curcas Oil*; Springer: Boston, MA, USA, 2013; pp. 197–202.
6. Garmroodi, M.; Mohammadi, M.; Ramazani, A.; Ashjari, M.; Mohammadi, J.; Sabour, B.; Yousefi, M. Covalent binding of hyper-activated *Rhizomucor miehei* lipase (RML) on hetero-functionalized siliceous supports. *Int. J. Biol. Macromol.* **2016**, *86*, 208–215. [CrossRef] [PubMed]
7. Mohammadi, M.; Ashjari, M.; Dezvarei, S.; Yousefi, M.; Babaki, M.; Mohammadi, J. Rapid and high-density covalent immobilization of *Rhizomucor miehei* lipase using a multi component reaction: Application in biodiesel production. *RSC Adv.* **2015**, *5*, 32698–32705. [CrossRef]
8. Luna, D.; Calero, J.; Sancho, E.D.; Luna, C.; Posadillo, A.; Bautista, F.M.; Romero, A.A.; Berbel, J.; Verdugo, C. Technological challenges for the production of biodiesel in arid lands. *J. Arid Environ.* **2014**, *102*, 127–138. [CrossRef]
9. Zubiolo, C.; Santos, R.C.; Carvalho, N.B.; Soares, C.M.; Lima, A.S.; de Aquino Santana, L.C. Encapsulation in a sol-gel matrix of lipase from aspergillus niger obtained by bioconversion of a novel agricultural residue. *Bioprocess Biosyst. Eng.* **2014**, *37*, 1781–1788. [CrossRef] [PubMed]
10. Su, F.; Li, G.; Fan, Y.; Yan, Y. Enhanced performance of lipase via microcapsulation and its application in biodiesel preparation. *Sci. Rep.* **2016**, *6*, 29670. [CrossRef] [PubMed]
11. Macario, A.; Moliner, M.; Corma, A.; Giordano, G. Increasing stability and productivity of lipase enzyme by encapsulation in a porous organic–inorganic system. *Microporous Mesoporous Mater.* **2009**, *118*, 334–340. [CrossRef]
12. Yadav, G.D.; Jadhav, S.R. Synthesis of reusable lipases by immobilization on hexagonal mesoporous silica and encapsulation in calcium alginate: Transesterification in non-aqueous medium. *Microporous Mesoporous Mater.* **2005**, *86*, 215–222. [CrossRef]
13. Zhao, Z.Y.; Liu, J.; Hahn, M.; Qiao, S.; Middelberg, A.P.J.; He, L. Encapsulation of lipase in mesoporous silica yolk–shell spheres with enhanced enzyme stability. *RSC Adv.* **2013**, *3*, 22008. [CrossRef]
14. Betancor, L.; Luckarift, H.R. Bioinspired enzyme encapsulation for biocatalysis. *Trends Biotechnol.* **2008**, *26*, 566–572. [CrossRef] [PubMed]
15. Liang, K.; Coghlan, C.J.; Bell, S.G.; Doonan, C.; Falcaro, P. Enzyme encapsulation in zeolitic imidazolate frameworks: A comparison between controlled co-precipitation and biomimetic mineralisation. *Chem. Commun.* **2016**, *52*, 473–476. [CrossRef] [PubMed]
16. Zhang, C.; Dai, Y.; Johnson, J.R.; Karvan, O.; Koros, W.J. High performance zif-8/6fda-dam mixed matrix membrane for propylene/propane separations. *J. Membr. Sci.* **2012**, *389*, 34–42. [CrossRef]
17. Yim, C.; Lee, H.; Lee, S.; Jeon, S. One-step immobilization of antibodies on zif-8/fe3o4 hybrid nanoparticles for the immunoassay of staphylococcus aureus. *RSC Adv.* **2017**, *7*, 1418–1422. [CrossRef]
18. Khan, N.A.; Jung, B.K.; Hasan, Z.; Jhung, S.H. Adsorption and removal of phthalic acid and diethyl phthalate from water with zeolitic imidazolate and metal-organic frameworks. *J. Hazard. Mater.* **2015**, *282*, 194–200. [CrossRef] [PubMed]
19. Lin, K.-Y.A.; Chang, H.-A. Efficient adsorptive removal of humic acid from water using zeolitic imidazole framework-8 (zif-8). *Water Air Soil Pollut.* **2015**, *226*. [CrossRef]
20. Wu, H.; Zhou, W.; Yildirim, T. Hydrogen storage in a prototypical zeolitic imidazolate framework-8. *J. Am. Chem. Soc.* **2007**, *129*, 5314–5315. [CrossRef] [PubMed]
21. Sun, C.Y.; Qin, C.; Wang, X.L.; Yang, G.S.; Shao, K.Z.; Lan, Y.Q.; Su, Z.M.; Huang, P.; Wang, C.G.; Wang, E.B. Zeolitic imidazolate framework-8 as efficient PH-sensitive drug delivery vehicle. *Dalton Trans.* **2012**, *41*, 6906–6909. [CrossRef] [PubMed]
22. Zhou, X.; Zhang, H.P.; Wang, G.Y.; Yao, Z.G.; Tang, Y.R.; Zheng, S.S. Zeolitic imidazolate framework as efficient heterogeneous catalyst for the synthesis of ethyl methyl carbonate. *J. Mol. Catal. A Chem.* **2013**, *366*, 43–47. [CrossRef]
23. Cui, J.; Feng, Y.; Lin, T.; Tan, Z.; Zhong, C.; Jia, S. Mesoporous metal-organic framework with well-defined cruciate flower-like morphology for enzyme immobilization. *ACS Appl. Mater. Interfaces* **2017**, *9*, 10587–10594. [CrossRef] [PubMed]
24. Kida, K.; Okita, M.; Fujita, K.; Tanaka, S.; Miyake, Y. Formation of high crystalline zif-8 in an aqueous solution. *CrystEngComm* **2013**, *15*, 1794. [CrossRef]
25. Amedi, H.R.; Aghajani, M. Aminosilane-functionalized zif-8/peba mixed matrix membrane for gas separation application. *Microporous Mesoporous Mater.* **2017**, *247*, 124–135. [CrossRef]

26. Liang, K.; Ricco, R.; Doherty, C.M.; Styles, M.J.; Bell, S.; Kirby, N.; Mudie, S.; Haylock, D.; Hill, A.J.; Doonan, C.J.; et al. Biomimetic mineralization of metal-organic frameworks as protective coatings for biomacromolecules. *Nat. Commun.* **2015**, *6*, 7240. [CrossRef] [PubMed]
27. Ramimoghadam, D.; Hussein, M.Z.; Taufiq-Yap, Y.H. The effect of sodium dodecyl sulfate (SDS) and cetyltrimethylammonium bromide (CTAB) on the properties of Zno synthesized by hydrothermal method. *Int. J. Mol. Sci.* **2012**, *13*, 13275–13293. [CrossRef] [PubMed]
28. Kuan, I.C.; Lee, C.-C.; Tsai, B.-H.; Lee, S.-L.; Lee, W.-T.; Yu, C.-Y. Optimizing the production of biodiesel using lipase entrapped in biomimetic silica. *Energies* **2013**, *6*, 2052–2064. [CrossRef]
29. Su, F.; Li, G.; Zhang, H.; Yan, Y. Enhanced performance of rhizopus oryzae lipase immobilized on hydrophobic carriers and its application in biorefinery of rapeseed oil deodorizer distillate. *BioEnergy Res.* **2014**, *7*, 935–945. [CrossRef]
30. Jin, W.; Brennan, J.D. Properties and applications of proteins encapsulated within sol-gel derived materials. *Anal. Chim. Acta* **2002**, *461*, 1–36. [CrossRef]
31. Tsai, H.C.; Doong, R.A. Preparation and characterization of urease-encapsulated biosensors in poly(vinyl alcohol)-modified silica sol-gel materials. *Biosens. Bioelectron.* **2007**, *23*, 66–73. [CrossRef] [PubMed]
32. Mateo, C.; Palomo, J.M.; Fernandez-Lorente, G.; Guisan, J.M.; Fernandez-Lafuente, R. Improvement of enzyme activity, stability and selectivity via immobilization techniques. *Enzyme Microb. Technol.* **2007**, *40*, 1451–1463. [CrossRef]
33. Kim, J.; Grate, J.W.; Wang, P. Nanobiocatalysis and its potential applications. *Trends Biotechnol.* **2008**, *26*, 639–646. [CrossRef] [PubMed]
34. Cauet, E.; Rooman, M.; Wintjens, R.; Lievin, J.; Biot, C. Histidine-aromatic interactions in proteins and protein-ligand complexes: Quantum chemical study of X-ray and model structures. *J. Chem. Theory Comput.* **2005**, *1*, 472–483. [CrossRef] [PubMed]
35. Khan, F.I.; Lan, D.; Durrani, R.; Huan, W.; Zhao, Z.; Wang, Y. The lid domain in lipases: Structural and functional determinant of enzymatic properties. *Front. Bioeng. Biotechnol.* **2017**, *5*, 16. [CrossRef] [PubMed]
36. Ji, Q.; Xiao, S.; He, B.; Liu, X. Purification and characterization of an organic solvent-tolerant lipase from *Pseudomonas aeruginosa* LX1 and its application for biodiesel production. *J. Mol. Catal. B Enzym.* **2010**, *66*, 264–269. [CrossRef]
37. Liu, Y.; Liu, T.; Wang, X.; Xu, L.; Yan, Y. Biodiesel synthesis catalyzed byburkholderia cenocepacialipase supported on macroporous resin nka in solvent-free and isooctane systems. *Energy Fuels* **2011**, *25*, 1206–1212. [CrossRef]
38. Lu, J.; Chen, Y.; Wang, F.; Tan, T. Effect of water on methanolysis of glycerol trioleate catalyzed by immobilized lipase *Candida* sp. 99–125 in organic solvent system. *J. Mol. Catal. B Enzym.* **2009**, *56*, 122–125. [CrossRef]
39. Li, Q.; Yan, Y. Production of biodiesel catalyzed by immobilized *Pseudomonas cepacia* lipase from sapium sebiferum oil in micro-aqueous phase. *Appl. Energy* **2010**, *87*, 3148–3154. [CrossRef]
40. Royon, D.; Daz, M.; Ellenrieder, G.; Locatelli, S. Enzymatic production of biodiesel from cotton seed oil using t-butanol as a solvent. *Bioresour. Technol.* **2007**, *98*, 648–653. [CrossRef] [PubMed]
41. Szczęsna Antczak, M.; Kubiak, A.; Antczak, T.; Bielecki, S. Enzymatic biodiesel synthesis—Key factors affecting efficiency of the process. *Renew. Energy* **2009**, *34*, 1185–1194. [CrossRef]
42. Kumari, A.; Mahapatra, P.; Garlapati, V.K.; Banerjee, R. Enzymatic transesterification of jatropha oil. *Biotechnol. Biofuels* **2009**, *2*, 1. [CrossRef] [PubMed]
43. Fan, Y.; Su, F.; Li, K.; Ke, C.; Yan, Y. Carbon nanotube filled with magnetic iron oxide and modified with polyamidoamine dendrimers for immobilizing lipase toward application in biodiesel production. *Sci. Rep.* **2017**, *7*, 45643. [CrossRef] [PubMed]
44. Andrade, T.A.; Errico, M.; Christensen, K.V. Influence of the reaction conditions on the enzyme catalyzed transesterification of castor oil: A possible step in biodiesel production. *Bioresour. Technol.* **2017**, *243*, 366–374. [CrossRef] [PubMed]
45. Yan, Y.; Li, X.; Wang, G.; Gui, X.; Li, G.; Su, F.; Wang, X.; Liu, T. Biotechnological preparation of biodiesel and its high-valued derivatives: A review. *Appl. Energy* **2014**, *113*, 1614–1631. [CrossRef]
46. Fan, Y.; Ke, C.; Su, F.; Li, K.; Yan, Y. Various types of lipases immobilized on dendrimer-functionalized magnetic nanocomposite and application in biodiesel preparation. *Energy Fuels* **2017**, *31*, 4372–4381. [CrossRef]

47. Pan, S.; Liu, X.; Xie, Y.; Yi, Y.; Li, C.; Yan, Y.; Liu, Y. Esterification activity and conformation studies of *Burkholderia cepacia* lipase in conventional organic solvents, ionic liquids and their co-solvent mixture media. *Bioresour. Technol.* **2010**, *101*, 9822–9824. [CrossRef] [PubMed]
48. Liu, Y.; Chen, D.; Yan, Y.; Peng, C.; Xu, L. Biodiesel synthesis and conformation of lipase from *Burkholderia cepacia* in room temperature ionic liquids and organic solvents. *Bioresour. Technol.* **2011**, *102*, 10414–10418. [CrossRef] [PubMed]
49. Li, K.; Fan, Y.; He, Y.; Zeng, L.; Han, X.; Yan, Y. *Burkholderia cepacia* lipase immobilized on heterofunctional magnetic nanoparticles and its application in biodiesel synthesis. *Sci. Rep.* **2017**, *7*, 16473. [CrossRef] [PubMed]
50. Su, F.; Li, G.-L.; Fan, Y.-L.; Yan, Y.-J. Enhancing biodiesel production via a synergic effect between immobilized *Rhizopus oryzae* lipase and novozym 435. *Fuel Process. Technol.* **2015**, *137*, 298–304. [CrossRef]

© 2018 by the authors. Licensee MDPI, Basel, Switzerland. This article is an open access article distributed under the terms and conditions of the Creative Commons Attribution (CC BY) license (http://creativecommons.org/licenses/by/4.0/).

catalysts

MDPI

Article

Immobilization Effects on the Catalytic Properties of Two *Fusarium Verticillioides* Lipases: Stability, Hydrolysis, Transesterification and Enantioselectivity Improvement

Fernanda Dell Antonio Facchini [1], Marita Gimenez Pereira [2], Ana Claudia Vici [2], Marco Filice [3], Benevides Costa Pessela [4], Jose Manuel Guisan [5], Glória Fernandez-Lorente [4] and Maria de Lourdes Teixeira de Moraes Polizeli [2,*]

1 Departamento de Medicina, Faculdade de Medicina de Ribeirão Preto, Universidade de São Paulo, 14040-900 Sao Paulo, Brazil; fda.facchini@gmail.com
2 Departamento de Biologia, Faculdade de Filosofia, Ciências e Letras de Ribeirão Preto, Universidade de São Paulo, 14040-901 Sao Paulo, Brazil; maritagimenez@hotmail.com (M.G.P.); acvici@gmail.com (A.C.V.); polizeli@ffclrp.usp.br (M.L.T.M.P.)
3 Nanobiotechnology, Molecular Imaging and Metabolomics Group, Spanish National Centre for Cardiovascular Research–CNIC, 28029 Madrid, Spain; marco.filice1@gmail.com
4 Departamento de Biotecnología y Microbiologia de los Alimentos, Instituto de Ciencias de la Alimentación, CIAL-CSIC, Calle Nicolás Cabrera 9, CampusUAM, 28049 Cantoblanco, Spain; b.pessela@csic.es (B.C.P.); gflorente@ifi.csic.es (G.F.-L.)
5 Departamento de Biocatálisis, Instituto de Catálisis y Petroleoquímica—CSIC, Campus UAM, Cantoblanco, 28049 Madrid, Spain; jmguisan@icp.csic.es
* Correspondence: polizeli@ffclrp.usp.br; Tel.: +55-16-3602-4680; Fax: +55-16-3602-4886

Received: 15 December 2017; Accepted: 2 February 2018; Published: 16 February 2018

Abstract: *Fusarium verticillioides* lipases were purified in a "cascade" method using octadecyl Sepabeads and octyl Sepharose resins, which led to the isolation of two proteins with lipolytic activities. Lip 1 was purified after octyl Sepharose adsorption presenting 30.3 kDa and, Lip 2 presented 68.0 kDa after octadecyl adsorption. These immobilization processes resulted in an increase of 3-fold in activity of each immobilized enzyme. These enzymes presented optima of pH of 5.0 and 6.0, respectively and temperature at 40 °C. They were thermostable at 40 °C and both remained more than 50% of its activity at the pH range of 5.0 to 7.0, with 180 min of incubation. The sardine oil hydrolysis showed higher EPA/DHA ratio. Concerning the ethanolysis reaction, Lip 2 showed higher conversion (5.5%) and both lipases showed activity in the release of the S enantiomers from 2-*O*-butyryl-2-phenylacetic acid (mandelic butyrate acid) and HPBE hydrolysis. Lip 2 also demonstrated capacity of transesterification. These applications made these enzymes attractive for industrial application.

Keywords: immobilization; purification; lipase; *Fusarium verticillioides*; EPA; DHA

1. Introduction

Lipases are very interesting enzymes due to their ability to catalyze a wide range of reactions, such as synthesis, transesterification and ester hydrolysis in aqueous or organic media, accompanied with a high regio- or enantioselectivity. The interest in this class of enzymes essentially increased due to their industrial and biotechnological applications in oil and fat hydrolysis and also because of their capacity to recognize different synthetic or natural substrates. Additionally, the increasing interest in the kinetic resolution of racemic mixtures with high regio- and stereo-specificities producing intermediates for

pharmaceutical industries as well as the use of fatty acid esters synthesis as cosmetic ingredients or surfactants, pesticides and agro-chemistry synthesis are also interesting [1–5]. Currently, due to these broad uses, they are attractive in biotechnological application and there is an increasing search for new microorganisms able to produce these enzymes with different specificities and stabilities.

Aiming their biotechnological applications, lipases should be stable enough to be reused for several reaction cycles. Consequently, immobilization techniques can improve this stability and catalytic properties leading to higher catalyst efficiencies [3,6–9]. Another advantage is the enzyme purification which minimizes or eliminates the contamination of other proteins, as shown in this work. Lipase adsorption on a cascade of hydrophobic supports at low ionic strength is a new purification strategy, capable to separate two or more enzymes with different hydrophobicity at low cost, fast procedure and high yield [1,10].

The selectivity of these enzymes is another attractive feature that enables their use in a large number of applications, which includes the resolution of racemic mixtures. Consequently, the enantioselectivity is gaining more and more space in industrial processes and in fine chemistry biocatalysts due to its importance in the preparation of pure enantiomers of chiral intermediates, which have been widely applied in synthetic purposes as well as stereochemical investigations. [4,11–13].

Besides, the use of lipases on fish oil reactions has increased in the last years. The release of omega-3 fatty acids [e.g. eicosapentaenoic acid (EPA) and decosahexaenoic acid (DHA)] from this oil have encouraged many studies involving health and food professionals, once these acids are able to improve the learning ability, mental development and visual perception in the early stages of life as well as prevent cardiovascular diseases in adults [3,14].

Fusarium verticillioides is among the most common *Fusarium* spp. infecting maize in most areas of the world and they are also famous in the production of fumonisin. *Fusarium* sp. has recently been described as a remarkable lipase producer [15–17], however no publication was found describing lipases from *Fusarium verticillioides*.

In this context, this study aims a high selective purification of two lipases from *Fusarium verticillioides* by their immobilization in hydrophobic supports, in which the stability of lipases was increased and the catalytic properties were improved through modulation of the enzyme properties with immobilization procedures.

2. Results and Discussion

2.1. Hydrophobic Immobilization

It was important to test the behavior of *F. verticillioides* crude extract on different supports with increasing levels of hydrophobicity. The crude extract containing lipases was adsorbed on all supports tested at different adsorption rates (Table 1). Except by Butyl Sepharose, lipases were efficiently immobilized in all the other supports, which showed more than 100% of residual activity presenting an activation above 2-fold. Phenyl Toyopearl derivative was the one with the highest activation, despite having only 50% immobilization. Other lipases of fungi described in the literature also presented activation when immobilized [1,18,19].

Table 1. Lipase immobilization on hydrophobic supports at pH 7.0.

Derivatives	Immobilization (%)	Fold *
Butyl Sepharose	28.2 ± 2.0	0.1
Phenyl Toyopearl	50.0 ± 2.0	3.7
Hexyl Toyopearl	59.6 ± 0.8	2.6
Octyl Sepharose	74.3 ± 1.0	2.4
Octadecyl Sepabeads	89.3 ± 0.5	2.6

* Fold-degree of activation and/or inhibition of the lipases when immobilized on hydrophobic supports, compared to their free form.

The phenomenon of hyper-activation could occur possibly due to the fact that when lipases are immobilized on hydrophobic supports, they keep the lid open, exposing the active site, which facilitates substrate input resulting in an easier hydrolysis [20].

2.2. Cascade Purification of Two Lipases

Possibly, in the enzymatic crude extracts, more than one type of lipase could be present and in order to verify this possibility in *F. verticillioides* crude extract, a SDS-PAGE analysis was performed. Notably, the presence of two lipases were suggested: one totally adsorbed octyl derivative and the other adsorbed in octadecyl derivative.

In order to separate these possible lipase isoforms from this crude extract a cascade purification strategy using two hydrophobic supports was performed. Initially, 70% of the active lipase (confirmed by *p*NPB assay) was adsorbed on octyl Sepharose (Lip1) after 3 h (Supplementary Figure S1A) and the supernatant containing the remaining lipase activity (Lip2) was further incorporated to octadecyl Sepabeads, which resulted in a total lipase adsorption (Supplementary Figure S1B). No lipase activity was observed in the supernatant after octadecyl immobilization. A single band in each support corresponding to Lip1 and Lip2 could be observed by this cascade technique. Afterwards, both pure lipases were fully desorbed from each support by incubating 1 g of the derivatives with 10 mL crescent Triton X-100 solution (1%, *v*/*v*) (Figure 1). At 0.3% Triton-X100 was sufficient to desorb 100% of Lip1 and the same concentration desorbed 80% of Lip2. Purified Lip1 and Lip2 presented 30.3 and 68 kDa, respectively. Table 2 summarizes the purification steps of the lipases from *F. verticillioides*. The immobilization on Octyl provided a purification factor of 2.14-fold with 44.5% protein recovery and the immobilization on octadecyl resulted in a purification factor of 4.1-fold and 25.7% protein recovery. The total recuperation was 70.2%.

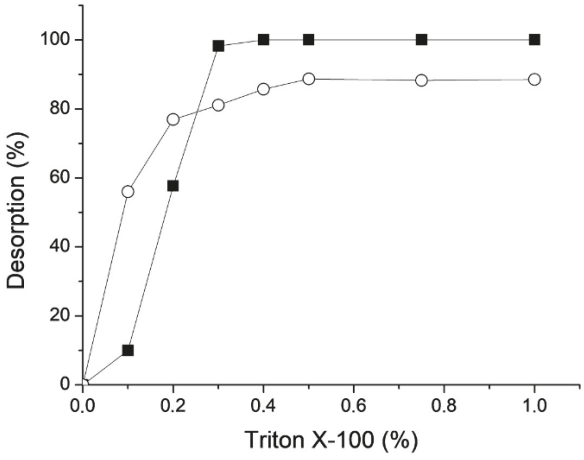

Figure 1. Desorption of the immobilized lipases on octyl and octadecyl supports. Full squares: octyl derivatives (Lip1); empty circles: octadecyl derivatives (Lip2).

Table 2. Purification of two lipases from *F. verticillioides*.

Enzyme	Volume (mL)	Mass (g)	Total Activity (U)	Immobilization (%)	SA * (U/mg)	Recuperation (%)	PF **
Crude extract	10	-	21.8	-	90.8	100	1
Octyl	-	1.0	9.7	70	194.0	44.5	2.14
Octadecyl	-	1.0	5.6	100 [a]	373.3	25.7	4.11

* SA = specific activity; ** PF = purification factor ($SA/SA_{crude\ extract}$); [a] lipase immobilized from octyl supernatant.

2.3. Thermal Stability of Derivatives

After the cascade purification, both lipases were desorbed from the supports where they were previously immobilized. Further, both lipases were immobilized on CNBr-activated supports (Table 3). FVL1 exhibited 53.5% of immobilization while FVL2 presented 38.3%. The uni-punctual immobilization on CNBr support was used as control in the characterization experiments, because, as this linkage does not modify the enzyme characteristics, this type of immobilization simulates the activity of the enzyme in its free form.

Table 3. *F. verticillioides* lipases immobilization at uni-punctual support.

Lipase	Time (min)	Immobilization (%)
FVL1	30	53.5
FVL2	30	38.3

Therefore, lipase thermal stability of soluble and immobilized lipase on different supports was compared at 40 °C and 50 °C. At 50 °C, after 24 h, all derivatives presented residual activity of less than 40% (Figure 2). This may have occurred because, at these temperatures, the enzyme could possibly be desorbed and may have aggregated, reducing the stability. At 40 °C, in 24 h, the uni-punctual immobilized Lip1 and Lip2 on CNBr lost about 35% and 85% of their residual activities, respectively. Therefore, at this temperature, the immobilization on octyl Sepharose and octadecyl Sepabeads supports contributed to increase Lip1 and Lip2 stabilities when compared to the CNBr-activated supports, thereby extending their application range.

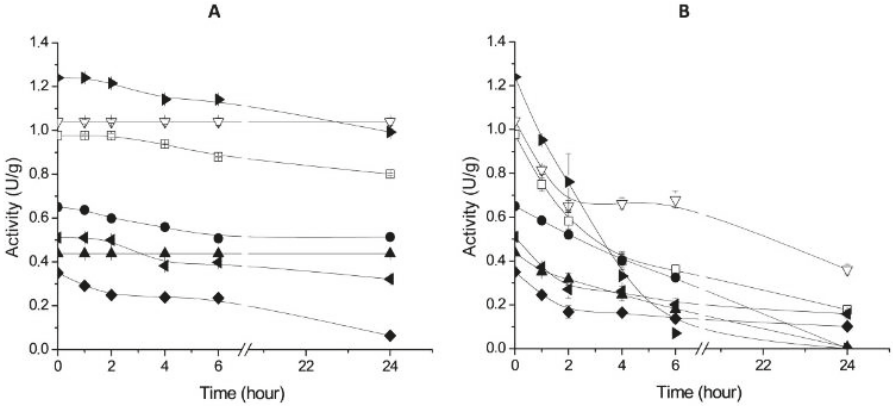

Figure 2. Thermal stability of *F. verticillioides* lipases (**A**) 40 °C (**B**) 50 °C. Symbols: -□- Butyl Sepharose; -●- Hexyl Toyopearl; -▲- Phenyl Toyopearl; -▽- Octyl Sepharose; -►-Octadecyl Sepabeads -◄- CNBr-activated Lip1 and -♦- CNBr-activated Lip2.

Increased thermal stability of derivatives was also observed by Cunha et al. the stability of butyl and octyl derivatives increased as the pH decreased, at 30 °C, retaining 78% to 100% of the lipolytic activity after 48 h [1]. Lipase from *Thermomyces lanuginosa* presented a more stable derivative obtained from hexyl Toyopearl than the others studied, whereas octyl agarose showed an intermediate stability [21].

2.4. Biochemical Characterization of Purified and Free Lipases

2.4.1. pH and Temperature Effects

The optimum pH values obtained for both free lipases showed a slightly acidic character (Figure 3A). The optima pH observed were 6.0 and 5.5, respectively to Lip1 and Lip2. The optimum temperature for both lipases studied was 40 °C; however, Lip1 presented activity higher than 50% in a range of 25 °C to 55 °C (Figure 3B). The same optimum temperature was observed to *Pseudomonas monteilii* [22] and the optimum pH of 8.0.

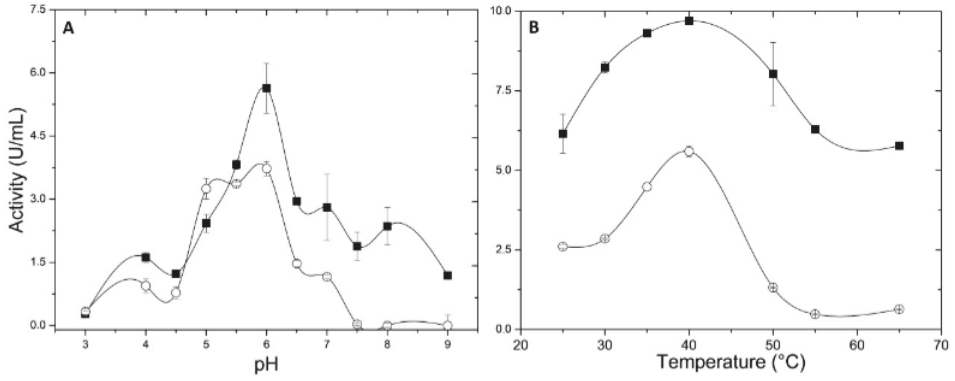

Figure 3. *Fusarium verticillioides* free lipases characterization. (**A**) pH effect in enzymatic activity; (**B**) temperature effect in enzymatic activity. Symbols: -■- Lip1; -○- Lip2.

Regarding pH stabilities (Figure 4), both lipases maintained more than 50% of their residual activity in a pH range of 5.0–7.0, with 180 min. Lip 1 presented better pH stability than Lip 2, at non-suitable pH (4, 5, 9 and 10) maintaining at least 20% of its activity. Concerning the thermal stability, Lip1 also presented better stability than Lip2 at temperatures of 40, 50 and 60 °C (Figure 5A). Both lipases are 60% stable at 30 °C with 180 min.

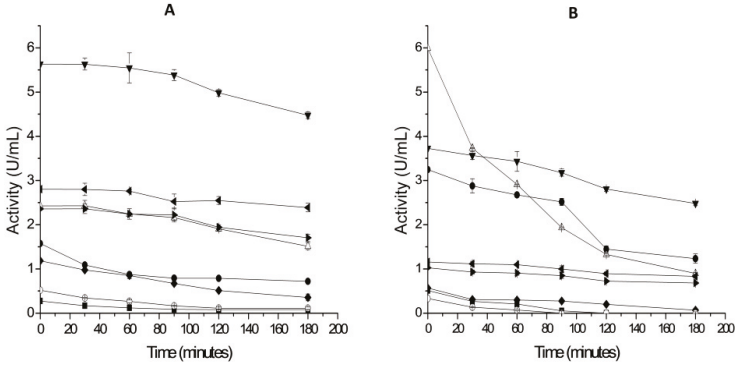

Figure 4. pH stability of pure lipases (**A**) Lip1 (**B**) Lip2. pH symbols: -■- 3.0; -●- 4.0; -△- 5.0; -▼- 6.0; -◄- 7.0; -►- 8.0; -♦- 9.0; -○- 10.0.

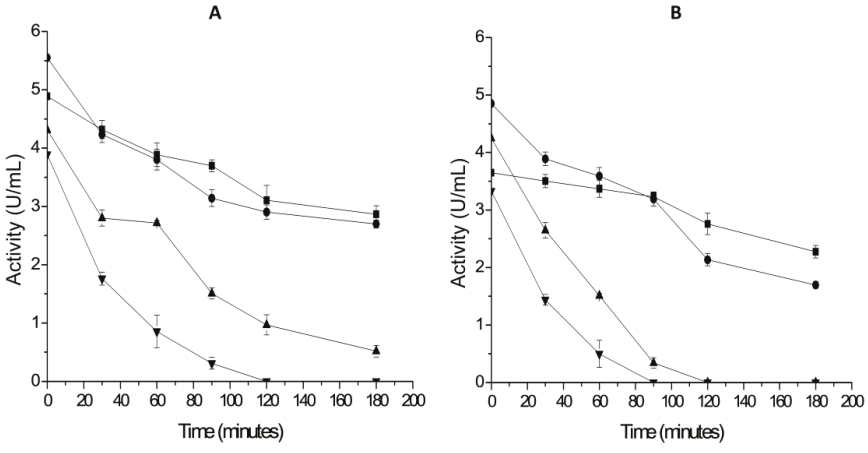

Figure 5. Thermal stability of pure lipases (**A**) Lip1 (**B**) Lip2. pH symbols: -■- 30 °C; -●- 40 °C; -▲- 50 °C; -▼- 60 °C.

Generally, free lipases from mesophilic fungi are active and stable at temperatures between 25 and 40 °C [23]. *F. solani* lipase was stable up to 45 °C and in a range of pH 5–10. Above this temperature, the stability decreased [15]. The lipase obtained from *Aspergillus niger* was stable at 40 °C for 3 h but it sharply decreased when the temperature was increased, losing 52% of its original activity at 50 °C after 1 h. However, in alkaline pH, the residual activity remained 100% after 24 h [24].

2.4.2. Effect of Metallic Ions

In this experiment, Ca^{2+} and Ba^{2+} ions increased the activity of both lipases (Figure 6). Barium had a better effect on Lip1, increasing activity by 20% and 60% using the final concentrations of 5 mM and 10 mM, respectively. However, Ba^{2+} decreased Lip2 activity by 30% when 5 mM of this ion was used. On the other hand, Ba^{2+} increased the activity of the same enzyme by 45% when 10 mM (final concentration) was added. Calcium had no effect on Lip1 at the final concentration of 5 mM but at 10 mM Ca^{2+} was able to activate the enzyme in 20%. In contrast, Ca^{2+} activated Lip2 in about 45% in both concentrations. Calcium activation corroborates with literature results, since it is well-known that some lipases described are positively influenced by this ion, for the reason that in a calcium-free system, lipases are not able to adsorb at the water-fat interface and no lipolytic activity occurs [22,25,26]. On the other hand, it is known that heavy metals inhibit lipase activity as copper, aluminum and zinc ions. Consequently, in this study $Co^{2+,}$ Al^{3+} and Cu^{2+} ions and EDTA decreased Lip1 activity around 40% and Pb^{+} and Zn^{2+} decreased approximately 60% Lip2 activity, while other ions did not affect them significantly. The inhibition by Zn^{2+} and Hg^{2+} ions was observed for the lipase from *Mortierela alliacea* [26].

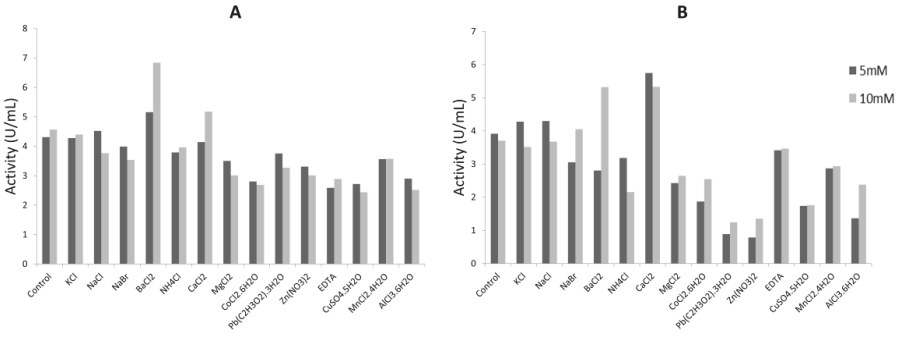

Figure 6. Effect of ions on lipases activity (**A**) Lip1 e (**B**) Lip2.

2.4.3. Isoelectric Point and Kinetic Parameters

The kinetic parameters of *F. verticillioides* purified lipases were calculated using *p*-nitrophenylpalmitate synthetic substrate (pNPP). The purified lipases had their kinetic parameters (K_M and V_{max}) calculated by SigrafW software and they were described in Table 4. The value of K_M and V_{max} obtained for Lip1 were 0.16 mM and 47.71 U/mg protein, respectively (n = 1.78). Lip2 K_M and V_{max} values were 0.26 mM and 37.4 U/mg, respectively. The values of the isoelectric points for Lip1 were 5.2 and for Lip 2 were around 4.2–5.0.

Table 4. Kinetic parameters of *F. verticillioides* purified lipases

Enzyme	K_M (mM)	V_{max} (U·mg·protein^{-1})	kcat (s^{-1})	kcat/K_M (M^{-1}·s^{-1})
Lip1	0.16	47.71	2.00×10^9	1.25×10^{13}
Lip2	0.26	37.4	3.53×10^9	1.35×10^{13}

Lipase from *Aspergillus fumigatus* presented K_M of 14 mM and V_{max} of 1.37 mM·mg^{-1}·min^{-1} with *p*-nitrophenyl acetate [27]; even lower values were found to *Aspergillus japonicus* lipase, for which K_M and V_{max} were 0.64×10^{-3} mmol and 0.25 µmol·min^{-1}·mL^{-1} [28]. Vici et al. [29] obtained from a recombinant lipase from *Beauveria bassiana* a K_M and V_{max} value of 0.5546 µM and 85.67 µmol·min^{-1}·mg^{-1} respectively, against *p*NPB, pH 6.0 at 50 °C.

2.5. Lip1 and Lip 2 Biotechnological Applications

2.5.1. Transesterification Reaction Applications

Both purified lipases adsorbed on octadecyl supports were submitted to this transesterification reaction. A control sample was performed using the same assay conditions without enzyme to each oil tested (Figure 7). Ethanol was used in all reactions.

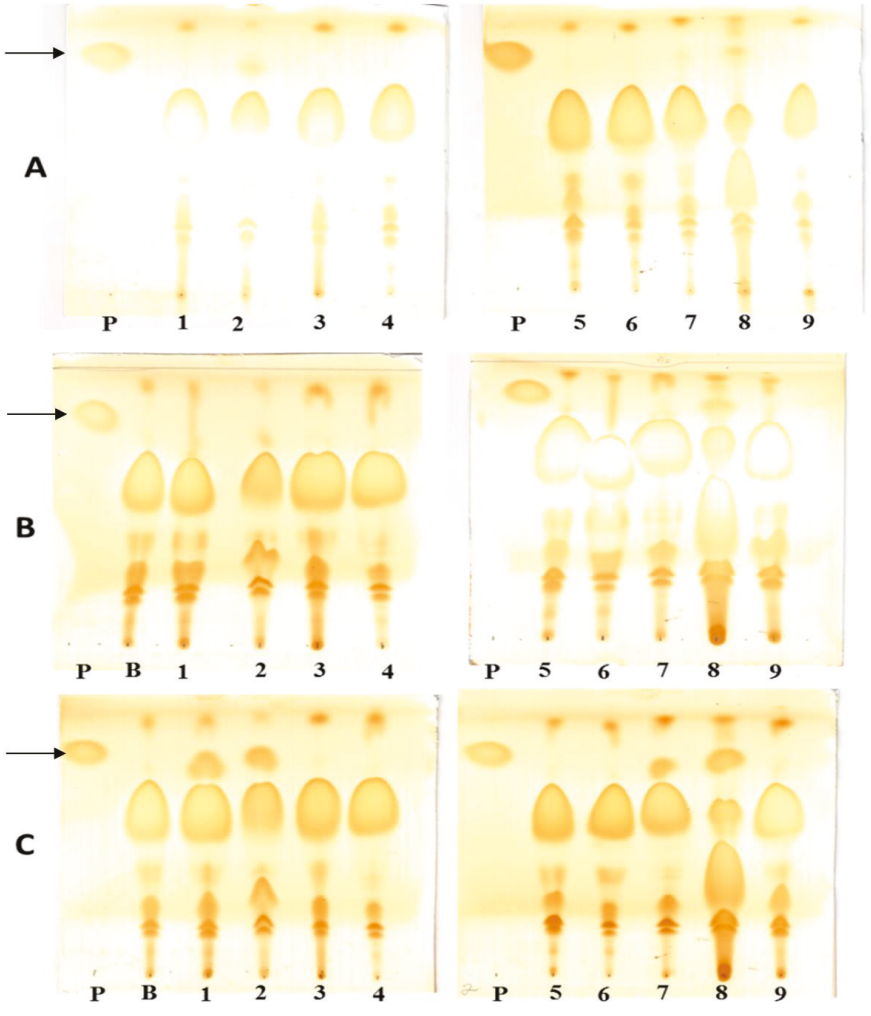

Figure 7. Transesterification assay with ethanol in different oils (black arrow). (**A**) Control (**B**) Lip1 adsorbed in octadecyl (**C**) Lip2 adsorbed on octadecyl. P = ethyl oleate 1%, B = soy oil control, 1 = soy oil, 2 = macaúba almond oil, 3 = canola oil, 4 = corn oil, 5 = pequi oil, 6 = sunflower oil, 7 = olive oil, 8 = macaúba pulp oil, 9 = sesame oil.

Macaúba pulp oil and macaúba almond oil controls presented bands which corresponded to the expected ethyl ester, possibly due to the presence of free fatty acids in these oils. However, the derivatives were able to react and release ester (Figure 7). Lip1 showed lower ability than Lip2, which showed a notable transesterification capacity with soybean oil, almond and macaúba pulp as well as olive oil, producing esters. It could make these enzymes attractive for industrial and biodiesel applications.

The conversion rate of the transesterification reaction was also checked by gas chromatography coupled to a mass spectrometer (Table 5). The highest conversion was observed on macaúba pulp, about 4%. Several authors studied the immobilization of lipases from different sources in biodiesel production [30–32].

Table 5. Conversion rate of the transesterification reaction to Lip2 derivative.

Samples	Oils	Conversion (%)
Ethyl oleate 1%		100
Controls	Soy oil	0.0
	Macaúba pulp oil	0.29
	Macaúba almond oil	0.13
	Olive oil	0.0
Octadecyl Sepabeads (Lip2)	Soy oil	1.71
	Macaúba pulp oil	3.62
	Macaúba almond oil	1.28
	Olive oil	1.18

2.5.2. Ethanolysis of Sardine Oil

Both free and pure lipases were first adsorbed on octadecyl supports in order to be used in ethanolysis reaction and presented activities around 0.3–0.5 U/mL. Lip2 derivatives presented a conversion rate about 2-fold higher than Lip1 (Table 6). This result was significant to demonstrate the ability to synthesize esters from oils (important feature for biodiesel production). However, it was lower when compared to the selectivity of commercial lipase from *Thermomuyces lanuginosus*, *Candida albicans* B and *Rhizomucor miehei* (Novo Nordish, Denmark) [33].

Table 6. Ethanolysis of sardine oil catalyzed by *F. verticillioides* lipases adsorbed to octadecyl Sepabeads in cyclohexane.

Derivative	Ester	Conversion (%)	Selectivity (EPA/DHA)
Control	EPA	nd *	nd *
	DHA	nd *	
Lip1	EPA	2.1	1.25
	DHA	1.7	
Lip2	EPA	5.5	1.15
	DHA	4.8	

* Non-detected.

2.5.3. Sardine Oil Hydrolysis

The main purpose of this experiment was to examine the specificity of lipases by EPA/DHA ratio, as well as check the lipases behavior on hydrolysis reaction, to confirm the enzyme activity as lipases. Both lipases could hydrolyze the sardine oil. Lip1 immobilized on octyl Sepharose support, presented the best conversion (6% EPA and 2.4% DHA) and a great ratio between both omega 3 released, EPA/DHA 14.72 (Table 7). Lip2 presented a better conversion rate in EPA. Results published by Pereira et al. [20] showed a ratio of 3.0 with glyoxyl-immobilized lipase from *Trichoderma pseudokoningii*.

Table 7. Sardine oil hydrolysis catalyzed by *F. verticillioides* lipase immobilized on hydrophobic support.

Enzyme	Derivative	Selectivity (EPA/DHA)	EPA (%)	DHA (%)	Total Conversion (%)
Lip1	Octyl	14.72	6.00	2.40	8.40
	CNBr-activated	19.57	1.50	0.40	1.90
Lip2	Octadecyl	13.89	1.80	0.80	2.60
	CNBr-activated	2.84	1.00	0.60	1.60
	Control	-	0.08	0.06	0.07

In general, *F. verticillioides* lipases proved to be very selective and released EPA better than DHA. Similar results were obtained by Fernandez-Lorente et al. [14], where the release of DHA was lower than EPA. *F. verticillioides* lipases also showed 4-fold higher selectivity compared to EPA released from *Rhizomucor miehei* lipase immobilized on octyl support [7]. Pizarro et al. [8] after 48 h hydrolysis reached maximum conversion of EPA and DHA of 8.7% and 6.1% respectively.

2.5.4. Hydrolysis of Racemic Mixtures

In this application, Lip1 and Lip2 were used immobilized on octyl and octadecyl supports, respectively. Moreover, they were necessary to compare these results with CNBr-activated derivatives.

2-*O*-butyryl-2-phenylacetic

Lip2 showed better conversion rates in a shorter period of time, 10.3%; while Lip1 reached half of this value. Both CNBr-activated derivatives required longer periods to achieve some conversion rate (Table 8).

Table 8. 2-*O*-butyryl-2-phenylacetic hydrolysis by Lip1 and Lip2.

Lipase	Derivatives	Time (h)	Conversion (%)	SA * (U/mg)	Selectivity E	*ee*	Isomer
Lip1	CNBr-activated	240	1.7	0.25	1.0	21.2	S
	Octyl	144	4.8	1.15	3.4	54.5	S
Lip2	CNBr-activated	336	2.0	0.28	1.3	13.6	S
	Octadecyl	144	10.3	4.51	2.6	44.3	S

* SA = Specific Activity.

The second analysis refers to selectivity (E) and enantiomeric excess (*ee*) coefficients evaluated by HPLC analysis using a chiral column. Lip1 presented the best E and *ee* results; however, both lipases indicated a high isomer S purity. This result corroborates with Fernandez-Lorente et al. [34] which reported the enzyme preparation of *Aspergillus niger* lipases, immobilized on DEAE-Sepharose, that showed different E values but preferred enantiomer S. However, not all authors reported S as the preferred isomer, as the reported for *Mucor miehei* lipase that the conversion of the R isomer by octadecyl derivative, with a value of E equal to 5.0 and *ee* around 51.0 [12].

HPBE Hydrolysis

HPBE hydrolysis presented excellent conversion rates by both lipases in a shorter time than 2-O-butyryl-2-phenylacetic acid, probably indicating preference by this substrate (Table 9). Octyl derivative obtained the best conversion rate reaction in just 1.5 h and therefore its specific activity increased by about 400 times when compared with other derivatives (after 96 h). Higher specificity, around 3.5, was reached by both lipases. However, excellent E and *ee* values have been reported by Fernandez-Lorente et al. [35], in which *Pseudomonas fluorescens* lipase reached 86 and 92.5, respectively.

Table 9. HPBE hydrolysis by Lip1 and Lip2.

Lipase	Derivatives	Time (h)	Conversion (%)	SA * (U/mg)	Selectivity E	*ee*	Isomer
Lip1	CNBr-activated	96	18	6.51	2.1	35.7	S
	Octyl	1.5	6.9	159.7	3.7	57.6	S
Lip2	CNBr-activated	96	10.8	5.4	1.4	17.8	R
	Octadecyl	96	10.8	7.13	3.6	56.2	S

* SA = Specific Activity.

3. Materials and Methods

3.1. Microorganism and Culture Maintenance

Fusarium verticillioides stock culture was maintained on oatmeal agar medium, at 4 °C and in silica gel at −20 °C.

3.2. Lipase Production

Lipase production was carried out in 125 mL Erlenmeyers flasks under 100 rpm, at 30 °C, for 4 days. The liquid culture medium was composed by 0.2% peptone, 0.05% $MgSO_4$, 0.1% monobasic sodium phosphate and 1% sunflower oil. The filtrate named FVL (*Fusarium verticillioides* lipase) was collected by vacuum filtration and stored at 4 °C [36].

3.3. Measurement of Lipase Activity

3.3.1. *p*-Nitrophenyl Butyrate (*p*NPB)

Lipolytic activity was measured by the increase in absorbance at 348 nm produced by the release of *p*NPB hydrolysis, using a spectrophotometer equipped with a thermostatized chamber and continuous magnetic stirring, which kept the immobilized enzyme homogenously suspended. Standard assay conditions were 50 µL of enzymatic sample (or suspension), 2.5 mL of 25 mM sodium phosphate buffer, pH 7.0 containing 20 µL of 50 mM p-nitrophenylbutyrate diluted in pure acetonitrile. The mixture was incubated at 25 °C for different periods. One unit (U) of enzyme activity was defined as that catalyzing the conversion of 1µmol of substrate (or the formation of 1 µmol of product) in 1 min in the assay conditions.

3.3.2. *p*-Nitrophenyl Palmitate (*p*NPP)

Lipase activities were determined using *p*NPP according to Pencreach and Baratti (1996) [37]. The reaction was carried out using McIlvaine buffer (pH 5.5 or 6.0), at 40 °C [38]. One unit (U) of enzyme activity was defined as that catalyzing the conversion of 1 µmol of substrate (or the formation of 1 µmol of product) in 1 min in the assay conditions.

3.4. Lipase Hydrophobic Immobilization

The adsorption of enzyme was analyzed in hydrophobic supports: Butyl Sepharose, Hexyl Toyopearl, Phenyl Toyopearl, Octyl Sepharose and Octadecyl Sepabeads. One gram of each support was added to 5 mL of 10 mM sodium phosphate buffer, at pH 7 and to 5 mL of the crude extract. All suspensions were incubated at 25 °C with constant stirring. Periodically, suspension and supernatant activities were assayed by using the *p*NPB assay. Once adsorbed, the immobilized preparations (derivatives) were thoroughly washed with distilled water, filtered and stored at 4 °C. A blank suspension was prepared by adding 1 g of Sepharose 4 BCL. The initial protein offered was specified by Bradford's method [39].

3.5. Hydrophobic Derivatives Thermal Stability

In order to determine the thermal stability, the derivatives were incubated in 25 mM sodium phosphate buffer (pH 7.0) at different temperatures (40 °C to 70 °C). Samples were withdrawn at different times using a pipette with a cut-tip and under strong stirring aiming a homogeneous biocatalyst suspension. The activity, measured immediately after withdrawn, was determined by the *p*NPB assay. The experiments were carried out in triplicates.

3.6. Cascade Purification

It was performed a sequential immobilization with adsorption of *F. verticillioides* crude extract in octyl followed by octadecyl supports at a low ionic strength. Previously, the crude enzymatic extract was diluted in 10 mM sodium phosphate buffer at pH 7 (1:2 *v*/*v*) and sequentially, 1 g of octyl support was added. After adsorption, the supernatant was added to 1 g of octadecyl support until complete adsorption. After immobilization, both derivatives were thoroughly washed with distilled water and with increasing concentrations of Triton X-100 until the complete desorption.

The analysis of the adsorbed lipases on supports was performed using SDS-PAGE. Aiming to verify the lipases purity in both supports, 0.1 g of each derivative was suspended in 0.5 mL of rupture buffer, containing bromophenol, 10% (*v*/*v*) mercaptoethanol, 40% glycerol and 4% (*w*/*v*) SDS. After boiling for 5 min, the supernatant of the derivatives was quickly withdrawn and analyzed by SDS–PAGE. The gel was stained using silver nitrate or Coomassie method. Molecular weight markers were from a Pharmacia LMW kit (14,400–94,000 Da).

After purification, the enzyme recuperation, specific activity (SA) and the purification factor (PF) were calculated. The purification factor shows how much the specific activity increased compared to the crude preparation ($PF = SA/SA_{\text{crude extract}}$).

3.7. Enzyme Desorption

In order to analyze the mechanism of lipase desorption, 250 mg of derivatives were diluted to 2.5 mL of 25 mM sodium phosphate buffer at pH 7 and were sequentially washed with different concentrations of Triton X-100.

3.8. Immobilization of the Lipase on CNBr-Activated Support

Immobilization of both desorbed lipases on CNBr-activated support was prepared by Pharmacia protocol, at pH 7. The immobilization occurred through the lipase amino terminal group [35]. One gram of CNBr-activated support was added to a solution of 10 mL of purified lipase in 25 mM sodium phosphate buffer, at pH 7.0. After 30 min, the enzyme immobilization was ended by blocking the amine reactive groups with 1 M ethanolamine, at pH 8. After 2 h, the immobilized preparation was washed with abundant distilled water.

3.9. Biochemical Characterization of Lipases

3.9.1. Temperature and pH Influence

The optima of temperature and pH were determined to each lipase. In order to determine the thermal stability, both derivatives were incubated in 25 mM sodium phosphate, pH 7.0 at different temperatures. The residual activity was measured after incubation. As the same, the pH stability was carried out in a range of pH 3.0–10.0, the enzymes were pre-incubated in citrate phosphate buffer (range 3.0–7.0), sodium phosphate 0.1 mol·L^{-1} (pH 7.0), Tris-HCl (range, 8.0–9.0) and glycine (pH 10.0) at 25 °C, for 24 h. Samples were withdrawn at different times using a pipette with a cut-tip and under strong stirring aiming a homogeneous biocatalyst suspension. The activity, measured immediately after withdrawn, was determined by the *p*NPB assay, as described above. The experiments were carried out in triplicates.

3.9.2. Effect of Metallic Ions

In order to determine the effect of metallic ions on lipases activity, assays were performed at the final concentrations of 5 and 10 mM of $Zn(NO_3)_2{\cdot}6H_2O$; NaCl, NH_4Cl, $BaCl_2$, $MnCl_2{\cdot}4H_2O$, $CoCl_2{\cdot}6\ H_2O$, $MgCl_2$, $AlCl_3{\cdot}6H_2O$, $CuSO_4{\cdot}5H_2O$, $CaCl_2$, $Pb(C_2H_30_2){\cdot}3H_2O$, NaBr, KCl and EDTA. The activity in the absence of these components was defined as the control.

3.9.3. Isoelectric Point and Kinetic Parameters

Isoelectric focusing was carried out according to O'Farrel et al. [40], using Pharmalyte Ampholyte (pH range 3.0–10.0). The apparent kinetic parameters K_M, V_{max} and kcat of the FVLs were determined and calculated by SigrafW software [41,42].

3.10. Hydrolysis of Sardine Oil

The sardine oil composition has been previously reported by Fernandez-Lorente et al. [2,6] and the main fat acids present are eicosapentaenoic acid (EPA, 18.6%), docosahexaenoic acid (DHA, 12.7%), palmitic acid (16.1%) and oleic acid (11.7%). The release of EPA and DHA was analyzed. The hydrolysis was performed in an organic-aqueous system, in which 4.5 mL of cyclohexane, 5 mL of Tris–HCl buffer (0.01 M) pH 6.0, 0.5 mL of sardine oil and 0.5 U/g of each lipase derivative were incubated at 25 °C and stirred at 150 rpm. The control samples did not have derivatives. Aliquots were withdrawn after 7 and 14 days. The concentration of free fatty acids was determined by the HPLC-UV method. The chromatograms of the aliquots from the organic phase obtained from UV–HPLC were compared to the corresponding calibration curves to facilitate the calculation of the rates of hydrolysis (EPA + DHA) and the EPA/DHA ratios. Aliquots of 0.1 mL from organic phase were withdrawn and dissolved in 0.4 mL of acetonitrile. The organic phase was easily separated from the aqueous phase after stopping stirring. The unsaturated fatty acids produced were analyzed by RP-HPLC [Spectra Physic SP 100 coupled with an UV detector Spectra Physic SP 8450 (Spectra Physics, Santa Clara, CA, USA)] using a Kromasil C8 (5 μm, 15 cm × 0.4 cm) column. Products were eluted at a flow rate of 1.0 mL/min using acetonitrile-milli-Q water- acetic acid, pH 3.0 (70:30:1, *v*/*v*) and UV detection performed at 215 nm. The retention times for the unsaturated fatty acids were 9.4 min (EPA) and 13.5 min (DHA). These produced fat acids were compared to their corresponding pure commercial standards.

3.11. Ethanolysis of Sardine Oil

The enzymatic ethanolysis was investigated to octadecyl Sepabeads derivatives for both lipases (Lip1 and Lip2), at 0.5 U/g. The procedure was performed in an organic solvent system containing 0.5 g of molecular sieves to guarantee total water absorption. First, 1.77 mL of sardine oil, 0.9 mL of ethanol and 0.5 U/g of lipase preparation were intensely mixed and incubated at 25 °C, 150 rpm. The control samples did not have derivatives. After 7 and 14 days, aliquots of 8 μL were diluted in 992 μL of acetonitrile and the concentration of free fatty acids esters was determined by RP-HPLC [Spectra Physic SP 100 coupled with an UV detector Spectra Physic SP 8450 (Spectra Physics, Santa Clara, CA. USA)] using an Ultrabase C18 (5 μm, 150 × 4.6 mm) column. The flow rate elution was 1.0 mL/min with acetonitrile-milli-Q water- acetic acid, pH 3.0 (80:20:0.1, *v*/*v*) and UV detection performed at 215 nm. The retention times were 20 min (EPA) and 26 min (DHA). The area of EPA and DHA chromatograms were compared to their corresponding pure commercial standards.

3.12. Hydrolysis of Racemic Mixtures

The different immobilized derivatives were assayed by adding 0.3 g of wet immobilized preparations (0.3–0.6 U/g) to the (*R*,*S*)-2-Hydroxy-4-phenylbutanoic acid ethyl ester (HPBE) (2 mM, 20 mL) or (*R*,*S*)-2-*O*-butyryl-2-phenylacetic acid solutions (10 mM, 10 mL), prepared in 25 mM sodium phosphate buffer, pH 5 (2.5 mL), at 25 °C, under mechanical stirring. The control experiments were performed using the support without enzymes. The mobile phases were: (1) for mandelic acid an isocratic mixture of acetonitrile (35%) and 10 mM ammonium phosphate buffer (65%) at pH 3.0; (2) for HPBE an isocratic mixture of acetonitrile (40%) and 10 mM ammonium phosphate buffer (60%) at pH 2.9. The detection was at 220 nm and 1.0 mL/min flow rate.

The optical purity of the hydrolyzed product as enantiomeric excess of the chiral product (*ee*), the extent of conversion of the racemic mixture and the enantiomeric ratio or enantioselectivity (E) were important parameters to be analyzed. At different conversion degrees, the enantiomeric excesses

of the released acid were analyzed by HPLC using a Chiracel OD-R column [43]. The mobile phase was an isocratic mixture of acetonitrile/$NaClO_4$/$HClO_4$ 0.5 M (5:95), pH 2.3. The analyzes were performed at a flow rate of 0.5 mL/min and at 225 nm. Enantioselectivity value and the conversion degree were calculated [10,12].

3.13. Transesterification Reaction

The pure Lip1 was desorbed from octyl support and adsorbed on octadecyl Sepabeads. The enzymatic transesterification was carried out in a non-aqueous medium, with a molar ratio of 1:9 (oil:ethanol), 20 mL, including 6% n-hexane and lipases derivatives. Ethanol was added in two steps to prevent any interference in the enzyme activity. All experiments were performed at 40 °C, 150 rpm for 24 h.

3.14. Thin Layer Chromatography Analysis (TLC)

The preliminary transesterification results were obtained by analyzing the ester released by TLC. The reaction carried out on silica gel G-60 plates (Merk®). The migration solvent consisted in a mixture of hexane: ethyl acetate: acetic acid (90:10:1). Chromatograms were revealed in an iodine vapor atmosphere [44].

3.15. Transesterification Assay by Gas Chromatography (CG-MS)

The product of enzymatic transesterification samples was diluted in 1% methanol and the samples were analyzed using an HP gas chromatograph (model GC-2012 5890) with a BP column (1.30 m length and 0.25 mm internal diameter). The mobile phase consisted of helium gas flow of 1.47 mL/minute. The analysis was accomplished by using a temperature ramp from 80 to 200 °C with an injector at temperature of 200 °C. The mass spectra of the main chromatographic peaks were monitored in a mass spectrometer model GCMS-QP 2010 Plus, which was coupled to the chromatograph. Standard curves were performed using ethyl oleate with 23 min of retention time. All esters produced between 23 and 26 min were considered as lipase product.

4. Conclusions

Cascade purification was a simple and rapid method to isolate and purify two lipases from the same crude extract with differences in hydrophobicity. The lipase adsorption, at low ionic strength, increased lipase activity and stability. The characterization and application demonstrated two different enzymes with distinct properties, mainly in their transesterification capacity. Moreover, the results indicated a slightly enantioselectivity improvement; the transesterification reactions showed excellent capacity of Lip2 to be used in biodiesel production and hydrolysis of sardine oil, releasing omega 3, suggesting the enzyme applicability in industrial food processes. Improvements using genetic engineering are been studied.

Supplementary Materials: The following are available online at www.mdpi.com/2073-4344/8/2/84/s1, Figure S1: SDS-PAGE analysis. (A) pure Lip1 adsorbed on octyl Sepharose (B) pure Lip2 adsorbed on octadecyl Sepabeads. M: molecular marker; 1: crude extract before immobilization; 2: octyl supernatant; 3: octyl derivative; 4: octadecyl derivative.

Acknowledgments: This work was supported by grants from Fundação de Amparo à Pesquisa do Estado de São Paulo (FAPESP, n° 2013/50892-5) and Conselho Nacional de Desenvolvimento Científico e Tecnológico (CNPq, n° 406838/2013-5). This project is also part of the National Institute of Science and Technology of the Bioethanol (FAPESP, n° 2010/52322-3). MLTMP is Research Fellow of CNPq. FDAF was recipient of a FAPESP fellowship (n° 2012/14615-4). MGP and ACV are supported by CNPq. We thank Ricardo F. Alarcon, Mariana Cereia and Mauricio de Oliveira for the technical assistance.

Author Contributions: This work is part of the Ph.D of F.D.A.F. and she is the main author. M.G.P. and M.F. partially collaborated in the experiments with chemical synthesis reaction. A.C.V. assisted in enzyme reaction and the discussion of experiments. B.C.P. and G.F.-L. were responsible for designing the experiments. J.M.G. and M.L.T.M.P. contributed to the experimental design and the final manuscript.

Conflicts of Interest: The authors declare no conflict of interest.

References

1. Cunha, A.G.; Fernandez-Lorente, G.; Gutarra, M.L.E.; Bevilaqua, J.V.; Almeida, R.V.; Paiva, L.M.C.; Fernandez-Lafuente, R.; Guisan, J.M.; Freire, D.M.G. Separation and immobilization of lipase from *Penicillium simplicissimum* by selective adsorption on hydrophobic supports. *Appl. Biochem. Biotechnol.* **2009**, *156*, 563–575. [CrossRef] [PubMed]
2. Fernandez-Lorente, G.; Pizarro, C.; Lopez-Vela, D.; Betancor, L.; Carrascosa, A.V.; Pessela, B.; Guisan, J.M. Hydrolysis of fish oil by lipases immobilized inside porous supports. *J. Am. Oil Chem. Soc.* **2011**, *88*, 819–826. [CrossRef]
3. Fernandez-Lorente, G.; Betancor, L.; Carrascosa, A.V.; Palomo, J.M.; Guisan, J.M. Modulation of the selectivity of immobilized lipases by chemical and physical modifications: Release of Omega-3 fatty acids from fish oil. *J. Am. Oil Chem. Soc.* **2012**, *89*, 97–102. [CrossRef]
4. Cabrera, Z.; Palomo, J.M. Enantioselective desymmetrization of prochiral diesters catalyzed by immobilized *Rhizopus oryzae* lipase. *Tetrahedron Asymmetry* **2011**, *22*, 2080–2084. [CrossRef]
5. Acosta, A.; Filice, M.; Fernandez-Lorente, G.; Palomo, J.M.; Guisan, J.M. Kinetically controlled synthesis of monoglyceryl esters from chiral and prochiral acids methyl esters catalyzed by immobilized *Rhizomucor miehei* lipase. *Bioresour. Technol.* **2011**, *102*, 507–512. [CrossRef] [PubMed]
6. Fernandez-Lorente, G.; Filice, M.; Lopez-Vela, D.; Pizarro, C.; Wilson, L.; Betancor, L.; Avila, Y.; Guisan, J.M. Cross-Linking of lipases adsorbed on hydrophobic supports: Highly selective hydrolysis of fish oil catalyzed by RML. *J. Am. Oil Chem. Soc.* **2011**, *88*, 801–807. [CrossRef]
7. Filice, M.; Marciello, M.; Betancor, L.; Carrascosa, A.V.; Guisan, J.M.; Fernandez-Lorente, G. Hydrolysis of fish oil by hyperactivated *Rhizomucor miehei* lipase immobilized by multipoint anion exchange. *Biotechnol. Prog.* **2011**, *27*, 961–968. [CrossRef] [PubMed]
8. Pizarro, C.; Branes, M.C.; Markovits, A.; Fernandez-Lorente, G.; Guisan, J.M.; Chamy, R.; Wilson, L. Influence of different immobilization techniques for *Candida cylindracea* lipase on its stability and fish oil hydrolysis. *J. Mol. Catal. B Enzym.* **2012**, *78*, 111–118. [CrossRef]
9. Rodrigues, R.C.; Bolivar, J.M.; Palau-Ors, A.; Volpato, G.; Ayub, M.A.Z.; Fernandez-Lafuente, R.; Guisan, J.M. Positive effects of the multipoint covalent immobilization in the reactivation of partially inactivated derivatives of lipase from *Thermomyces lanuginosus*. *Enzym. Microb. Technol.* **2009**, *44*, 386–393. [CrossRef]
10. Brabcova, J.; Demianova, Z.; Vondrasek, J.; Jagr, M.; Zarevucka, M.; Palomo, J.M. Highly selective purification of three lipases from *Geotrichum candidum* 4013 and their characterization and biotechnological applications. *J. Mol. Catal. B Enzym.* **2013**, *98*, 62–72. [CrossRef]
11. Palomo, J.M.; Fernandez-Lorente, G.; Mateo, C.; Ortiz, C.; Fernandez-Lafuente, R.; Guisan, J.M. Modulation of the enantioselectivity of lipases via controlled immobilization and medium engineering: Hydrolytic resolution of mandelic acid esters. *Enzym. Microb. Technol.* **2002**, *31*, 775–783. [CrossRef]
12. Palomo, J.M.; Munoz, G.; Fernandez-Lorente, G.; Mateo, C.; Fuentes, M.; Guisan, J.M.; Fernandez-Lafuente, R. Modulation of *Mucor miehei* lipase properties via directed immobilization on different hetero-functional epoxy resins—Hydrolytic resolution of (*R*,*S*)-2-butyroyl-2-phenylacetic acid. *J. Mol. Catal. B Enzym.* **2003**, *21*, 201–210. [CrossRef]
13. Velasco-Lozano, S.; Rodriguez-Gonzalez, J.A.; Mateos-Diaz, J.C.; Reyes-Duarte, D.; Favela-Torres, E. Catalytic profiles of lipolytic biocatalysts produced by filamentous fungi. *Biocatal. Biotransform.* **2012**, *30*, 459–468. [CrossRef]
14. Fernandez-Lorente, G.; Betancor, L.; Carrascosa, A.V.; Guisan, J.M. Release of Omega-3 fatty acids by the hydrolysis of fish oil catalyzed by lipases immobilized on hydrophobic supports. *J. Am. Oil Chem. Soc.* **2011**, *88*, 1173–1178. [CrossRef]
15. Jallouli, R.; Khrouf, F.; Fendri, A.; Mechichi, T.; Gargouri, Y.; Bezzine, S. Purification and biochemical characterization of a novel alkaline (phospho)lipase from a newly isolated *Fusarium solani* strain. *Appl. Biochem. Biotechnol.* **2012**, *168*, 2330–2343. [CrossRef] [PubMed]
16. Jallouli, R.; Fendri, A.; Mechichi, T.; Gargouri, Y.T.; Bezzine, S. Kinetic properties of a novel *Fusarium solani* (phospho)lipase: A monolayer study. *Chirality* **2013**, *25*, 35–38. [CrossRef] [PubMed]

17. Tehreema, L. Process optimization for extracellular lipase production from *Fusarium oxysporum* (mbl21) through solid state fermentation technique. *Clin. Biochem.* **2011**, *44*, S243. [CrossRef]
18. Bastida, A.; Sabuquillo, P.; Armisen, P.; Fernandez-Lafuente, R.; Huguet, J.; Guisan, J.M. Single step purification, immobilization and hyperactivation of lipases via interfacial adsorption on strongly hydrophobic supports. *Biotechnol. Bioeng.* **1998**, *58*, 486–493. [CrossRef]
19. Palomo, J.M.; Munoz, G.; Fernandez-Lorente, G.; Mateo, C.; Fernandez-Lafuente, R.; Guisan, J.M. Interfacial adsorption of lipases on very hydrophobic support (octadecyl-Sepabeads): Immobilization, hyperactivation and stabilization of the open form of lipases. *J. Mol. Catal. B Enzym.* **2002**, *19*, 279–286. [CrossRef]
20. Pereira, M.G.; Facchini, F.D.A.; Polizeli, A.M.; Vici, A.C.; Guisan, J.M.; Jorge, J.A.; Pessela, B.C.; Fernandez-Lorente, G.; Polizeli, M.L.T.M. Stabilization of the lipase of *Hypocrea pseudokoningii* by multipoint covalent immobilization after chemical modification and application of the biocatalyst in oil hydrolysis. *J. Mol. Catal. B Enzym.* **2015**, *121*, 82–89. [CrossRef]
21. Fernandez-Lorente, G.; Cabrera, Z.; Godoy, C.; Fernandez-Lafuente, R.; Palomo, J.M.; Guisan, J.M. Interfacially activated lipases against hydrophobic supports: Effect of the support nature on the biocatalytic properties. *Process Biochem.* **2008**, *43*, 1061–1067. [CrossRef]
22. Adan Gokbulut, A.; Arslanoglu, A. Purification and biochemical characterization of an extracellular lipase from psychrotolerant *Pseudomonas fluorescens* KE38. *Turk. J. Biol.* **2013**, *37*, 538–546. [CrossRef]
23. Pereira, M.G.; Vici, A.C.; Facchini, F.D.A.; Tristão, A.P.; Cursino-Santos, J.R.; Sanches, P.R.; Jorge, J.A.; Polizeli, M.L.T.M. Screening of filamentous fungi for lipase production: *Hypocrea pseudokoningii* a new producer with a high biotechnological potential. *Biocatal. Biotransform.* **2014**, *32*, 74–83. [CrossRef]
24. Mhetras, N.C.; Bastawde, K.B.; Gokhale, D.V. Purification and characterization of acidic lipase from *Aspergillus niger* NCIM 1207. *Bioresour. Technol.* **2009**, *100*, 1486–1490. [CrossRef] [PubMed]
25. Polizelli, P.P.; Antonio Facchini, F.D.; Cabral, H.; Bonilla-Rodriguez, G.O. A new lipase isolated from oleaginous seeds from *Pachira aquatica* (Bombacaceae). *Appl. Biochem. Biotechnol.* **2008**, *150*, 233–242. [CrossRef] [PubMed]
26. Jermsuntiea, W.; Aki, T.; Toyoura, R.; Iwashita, K.; Kawamoto, S.; Ono, K. Purification and characterization of intracellular lipase from the polyunsaturated fatty acid-producing fungus *Mortierella alliacea*. *New Biotechnol.* **2011**, *28*, 158–164. [CrossRef] [PubMed]
27. Shangguan, J.J.; Liu, Y.Q.; Wang, F.J.; Zhao, J.; Fan, L.Q.; Li, S.X.; Xu, J.H. Expression and Characterization of a novel lipase from *Aspergillus fumigatus* with high specific activity. *Appl. Biochem. Biotechnol.* **2011**, *165*, 949–962. [CrossRef] [PubMed]
28. Bharti, M.K.; Khokhar, D.; Pandey, A.K.; Gaur, A.K. Purification and characterization of lipase from *Aspergillus japonicus*: A potent enzyme for biodiesel production. *Natl. Acad. Sci. Lett.* **2013**, *36*, 151–156. [CrossRef]
29. Vici, A.C.; Cruz, A.F.; Facchini, F.D.A.; Carvalho, C.C.; Pereira, M.G.; Fonseca-Maldonado, R.; Ward, R.J.; Pessela, B.C.; Fernandez-Lorente, G.; Torres, F.A.G.; et al. *Beauveria bassiana* Lipase A expressed in *Komagataella* (*Pichia*) *pastoris* with potential for biodiesel catalysis. *Front. Microbiol.* **2015**, *6*. [CrossRef] [PubMed]
30. Abdulla, R.; Ravindra, P. Immobilized *Burkholderia cepacia* lipase for biodiesel production from crude *Jatropha curcas* L. oil. *Biomass Bioenergy* **2013**, *56*, 8–13. [CrossRef]
31. Salis, A.; Pinna, M.; Monduzzi, M.; Solinas, V. Biodiesel production from triolein and short chain alcohols through biocatalysis. *J. Biotechnol.* **2005**, *119*, 291–299. [CrossRef] [PubMed]
32. Shao, P.; Meng, X.H.; He, J.Z.; Sun, P.L. Analysis of immobilized *Candida rugosa* lipase catalyzed preparation of biodiesel from rapeseed soapstock. *Food Bioprod. Process.* **2008**, *86*, 283–289. [CrossRef]
33. Moreno-Perez, S.; Guisan, J.M.; Fernandez-Lorente, G. Selective ethanolysis of fish oil catalyzed by immobilized lipases. *J. Am. Oil Chem. Soc.* **2014**, *91*, 63–69. [CrossRef]
34. Fernandez-Lorente, G.; Ortiz, C.; Segura, R.L.; Fernandez-Lafuente, R.; Guisan, J.M.; Palomo, J.M. Purification of different lipases from *Aspergillus niger* by using a highly selective adsorption on hydrophobic supports. *Biotechnol. Bioeng.* **2005**, *92*, 773–779. [CrossRef] [PubMed]
35. Fernandez-Lorente, G.; Palomo, J.M.; Cabrera, Z.; Fernandez-Lafuente, R.; Guisan, J.M. Improved catalytic properties of immobilized lipases by the presence of very low concentrations of detergents in the reaction medium. *Biotechnol. Bioeng.* **2007**, *97*, 242–250. [CrossRef] [PubMed]

36. Facchini, F.D.A.; Vici, A.C.; Pereira, M.G.; Jorge, J.A.; Polizeli, M.L.T.M. Enhanced lipase production of *Fusarium verticillioides* by using response surface methodology and wastewater pretreatment application. *J. Biochem. Technol.* **2015**, *6*, 996–1002.
37. Pencreach, G.; Baratti, J.C. Hydrolysis of p-nitrophenyl palmitate in n-heptane by the *Pseudomonas cepacia* lipase: A simple test for the determination of lipase activity in organic media. *Enzym. Microb. Technol.* **1996**, *18*, 417–422. [CrossRef]
38. McIlvaine, T.C. A buffer solution for colorimetric comparison. *J. Biolog. Chem.* **1921**, *49*, 183–186.
39. Bradford, M.M. Rapid and sensitive method for quantitation of microgram quantities of protein utilizing principle of protein-dye binding. *Anal. Biochem.* **1976**, *72*, 248–254. [CrossRef]
40. O'Farrel, P.Z.; Goodman, H.M.; O'Farrel, P.H. High resolution two dimensional electrophoresis of basic as acidic proteins. *Cell* **1977**, *12*, 1133–1142. [CrossRef]
41. Leone, F.A.; Degreve, L.; Baranauskas, J.A. SIGRAF: A versatile computer program for fitting enzyme kinetics data. *Biochemistry* **1992**, *20*, 94–96. [CrossRef]
42. Leone, F.A.; Baranauskas, J.A.; Furriel, R.P.M.; Borin, I.A. SIGRAFW: An easy-to-use program for fitting enzyme kinetic data. *Biochem. Mol. Biol. Educ.* **2005**, *33*, 399–403. [CrossRef] [PubMed]
43. Fernandez-Lorente, G.; Terreni, M.; Mateo, C.; Bastida, A.; Fernandez-Lafuente, R.; Dalmases, P.; Huguet, J.; Guisan, J.M. Modulation of lipase properties in macro-aqueous systems by controlled enzyme immobilization: Enantioselective hydrolysis of a chiral ester by immobilized Pseudomonas lipase. *Enzym. Microb. Technol.* **2001**, *28*, 389–396. [CrossRef]
44. Shah, S.; Sharma, S.; Gupta, M.N. Biodiesel preparation by lipase-catalyzed transesterification of *Jatropha* oil. *Energy Fuels* **2004**, *18*, 154–159. [CrossRef]

© 2018 by the authors. Licensee MDPI, Basel, Switzerland. This article is an open access article distributed under the terms and conditions of the Creative Commons Attribution (CC BY) license (http://creativecommons.org/licenses/by/4.0/).

catalysts

MDPI

Article

Immobilization of an Antarctic *Pseudomonas* AMS8 Lipase for Low Temperature Ethyl Hexanoate Synthesis

Nurshakila Musa [1], Wahhida Latip [1], Raja Noor Zaliha Abd Rahman [1,2], Abu Bakar Salleh [1] and Mohd Shukuri Mohamad Ali [1,3,*]

[1] Enzyme and Microbial Technology Research Center, Universiti Putra Malaysia, Serdang 43400, Selangor, Malaysia; nurshakilamusa@gmail.com (N.M.); wahhidalatip@gmail.com (W.L.); rnzaliha@upm.edu.my (R.N.Z.A.R); abubakar@upm.edu.my (A.B.S.)
[2] Department of Microbiology, Universiti Putra Malaysia, Serdang 43400, Selangor, Malaysia
[3] Department of Biochemistry, Universiti Putra Malaysia, Serdang 43400, Selangor, Malaysia
* Correspondence: mshukuri@upm.edu.my; Tel.: +60-38946-6721

Received: 31 March 2018; Accepted: 2 May 2018; Published: 4 June 2018

Abstract: The demand for synthetic flavor ester is high, especially in the food, beverage, and cosmetic and pharmaceutical industries. It is derived from the reaction between a short-chain fatty acid and alcohol. Lipases from Antarctic bacteria have gained huge interest in the industry due to its ability react at low temperatures. The use of immobilization enzymes is one of the methods that can improve the stability of the enzyme. The current work encompasses the low temperature enzymatic synthesis of ethyl hexanoate by direct esterification of ethanol with hexanoic acid in a toluene and solvent-free system. The effects of various reaction parameters such as the organic solvent, temperature, time, substrate, substrate ratio and concentration, enzyme concentration on ethyl hexanoate synthesis were tested. Several matrices were used for immobilization and comparisons of the efficiency of immobilized enzyme with free enzyme in the synthesis of flavor ester were conducted. Ester production was optimally synthesized at 20 °C in both systems—immobilized and free enzyme. A 69% ester conversion rate was achieved after a two-hour incubation in toluene, compared to 47% in a solvent-free system for free enzyme. Immobilized AMS8 lipase showed a higher conversion of ester in toluene with respect to free-solvents, from 80% to 59%, respectively. Immobilized enzymes showed enhancement to the stability of the enzyme in the presence of the organic solvent. The development of AMS8 lipase as an immobilized biocatalyst demonstrates great potential as a cost-effective enzyme for biocatalysis and biotransformation in the food industry.

Keywords: cold adapted lipase; immobilization; esterification

1. Introduction

Flavor esters are short chain esters that are widely distributed in nature. These compounds are also known as carboxylic acid esters, which are largely used in the food, beverage, cosmetic and pharmaceutical industries. Flavor esters are fine organic compounds that form a part of the natural aromas in fruits and flowers [1]. In addition, low molecular weight flavor esters are the most important and versatile components of flavors and fragrances [2]. Currently, there is an increasing commercial demand for natural flavors. These compounds are typically isolated from natural sources such as plants, fruits, and flowers or are produced by chemical synthesis. However, the commercial use of natural extracts is hindered by limited supply and high production costs [3]. In addition, flavors produced by chemical synthesis cause negative side effects due to the use of dangerous chemicals instead of flammable and highly toxic hazardous chemicals [4]. Recently, the enzymatic

production of flavor esters has received increasing attention because of the inherent catalytic selectivity of enzymes, enhanced product purity and mild reaction conditions [5].

Lipases catalyze the hydrolysis of triacylglycerol into free fatty acids and glycerol. These enzymes can catalyze many types of reactions such as hydrolysis, esterification and transesterification. Lipases are uniquely able to function at the interface between an aqueous and a nonaqueous phase. Moreover, lipases have been used to synthesize esters of short chain carboxylic acids and alcohols in the food industry [2]. The production of flavor ester by lipases is well-known. However, until recently, almost all of these reactions were performed by commercial lipases, as well as mesophilic lipases such as *Candida rugosa*, *Candida antarctica* and *Mucor miehei*, whereas the synthesis of esters by psychrophilic lipases has rarely been studied [6]. Lipases or the other enzymes used in industry facing many problems generally with regard to stability and productivity [7].

Isolated enzymes in biocatalytic processes lack long-term stability under operational condition and limit reusability cycles [8]. Lipases are not used as much as other enzymes in industrial applications because of their high cost of production and their relatively unstable nature. Due to these reasons, immobilization methods have been developed [9]. Immobilization is one of the useful techniques to improve the application of enzymes in the industry [10]. The advantages of using immobilized enzyme systems compared to free enzyme systems are their reusability, lower cost, easily controlled product formation, rapid termination rate, and ease in separating from reactants and product [9]. The effectiveness of an immobilization process depends much depends on the support used. Comparative studies indicated that dramatic differences existed in the activity of lipases supported on different materials [11]. The cold-active AMS8 lipase is secreted by a psychrophilic microorganism, *Pseudomonas* sp. strain AMS8. This strain was isolated from Antarctic soil, and the AMS8 gene has been cloned and expressed in *Escherichia coli* [12]. The cold-active lipase AMS8 exhibits unique properties such as a faster reaction time in comparison to mesophilic and thermophilic enzymes, as well as increased flexibility, stability and low activation energy at low temperatures. In addition, this enzyme demonstrates high specific activity, as well as high catalytic activity between 0 °C to 20 °C. Thus, the aim of this study was to investigate the capacity of the novel psychrophilic lipase, cold-active AMS8 lipase, to synthesize ethyl hexanoate by direct esterification and to compare the ability of immobilize and free enzyme in the ester conversion.

2. Results

2.1. Effect of Organic Solvents on the Esterification Reaction

Other than lipase used as a biocatalyst in the synthesis of flavour ester, organic solvent is also needed in enhancing the reaction organic solvents often to catalyze reverse reactions where water should be minimal [13]. The effect of organic solvents was studied in order to obtain the esters of good quality and high percentage of yield. The favoured organic solvent is depending on the polarity of the enzyme. The production of ethyl hexanoate by AMS8 lipase was studied in the presence and absence of various organic solvents. Figure 1 shows that the maximum yield for ester conversion obtained in the presence of toluene was 62%. This value is higher than that obtained in the absence of any organic solvents (35%). Thus, the conversion percentage was improved in the presence of toluene, compared to a solvent-free system. The use of hydrophobic solvents such as toluene, hexane and heptane preserve catalytic activity without disturbing the micro-aqueous layer of enzyme [5]. The presence of solvent can shift the equilibrium towards the synthesis of esters, most likely due to the total transfer of the esters into the organic phase [14]. In addition, the use of organic solvents provides high enzyme thermostability. Enzymes have been reported to be stable and flexible within organic solvents but tend to exhibit low specific activity [15].

In contrast with polar organic solvent, it has been reported that polar solvent can distort the water layer around the enzyme which make the enzyme less stable and lead to deactivation of the enzyme [16]. AMS8 lipase showed the maximum ester conversion was only at 36% in 1-butanol, a polar

organic solvent which was 1-butanol. A polar organic solvent was reported make low conversion of ester for *R. miehei* lipase similarly with AMS8 lipase [17]. In such a medium, the solvent may alter the native conformation of the enzyme by disrupting hydrogen bonding and hydrophobic interaction, thereby leading to very low alcoholysis rate [18]. Normally, the ester synthesis by the esterification, transesterification or interesterification required a suitable mixture of the nonpolar solvents, but in the food application process, solvent-free systems are preferred [19]. Besides that, solvent-free systems are preferable due to the absence of any toxicity resulting from the synthesized flavor esters [2].

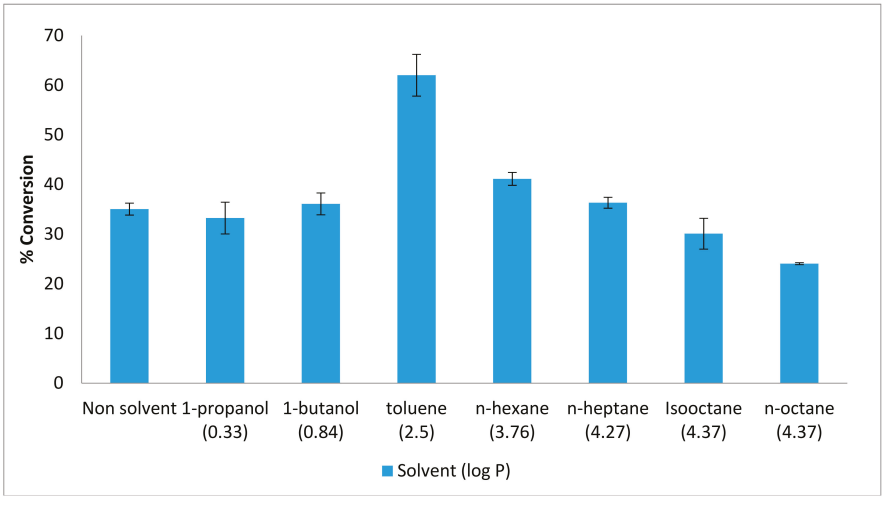

Figure 1. Effect of various organic solvents on lipAMS8 lipase. Percentage conversion of ethyl hexanoate catalysed by native AMS8 lipase as affected by various organic solvents in different polarity (log *p* value) and solvent-free system. Reactions were performed at 20 °C for two hours with 1:1 molar ratio of hexanoic acid to ethanol.

2.2. Effect of Temperature on the Esterification Reaction

The changes in the reaction temperature can affect the activity and stability of the enzyme and thus the rate of reaction. Besides that, the effect of temperature can be apportioned to its direct influences on esterification reaction and the enzyme as well as effect on substrate solubility. The effect of varying reaction temperatures on the enzymatic synthesis of ethyl hexanoate is shown in Figure 2. The reaction was optimized at 20 °C, with a high percentage of ester conversion (approximately 68.3%) in toluene, compared to a solvent-free system which was about 45.4%. The ester conversion rate began to decrease at 25 °C. An esterification yield of 75% was reported for the same optimal temperature of 20 °C for butyl-caprylate in n-heptane with an organic phase water concentration 0.25% (*v*/*v*) using *Pseudomonas* P38 lipase. It shows that the psychrotroph-derived lipase had stable structural flexibility and enzyme activity within a nearly anhydrous organic solvent phase [20].

The decrease in flavor ester synthesis observed above 20 °C was due to the inactivation of the enzyme at high temperatures. Environmental factors such as low water activity prohibits enzyme flexibility if thermo stability within an organic solvent is achieved [21]. The optimum temperature for an enzyme depends on its source, the solvent, the pH, the substrate and the nature of the immobilization or chemical modification of the reaction medium.

Selvam (2013) had reported that lipase from *Rhizopus arrhizus* showed that, the percentage of ester conversion was high at 30 °C and started to decrease slowly after 35 °C and decreased drastically above 50 °C [22]. Besides, in the other work, the percentage conversion for ethyl valerate increased with increasing temperature from 30 °C (73.29%) to 40 °C (77.39%) due to energy received from the

higher temperature heat used to increase the frequency of collision between the molecules. However, the percentage conversion of ester was slightly decreased at range of 45 °C to 55 °C and decreased sharply at 70 °C to 80 °C. An increment in the reaction of temperature had improved the substrates solubility and dissociation lead to unfavourable esterification conditions [10].

In addition, the cold active lipases from cold adapted microorganisms and their potential applications have been examined [23]. The 'low activity' meaning that high catalytic activity at low temperature and flexible as well as stable at low temperature are some of special features of psychrophilic microorganism thus these features might be the key to success in some of their applications. These applications include their use as catalyst for organic synthesis of unstable compounds at low temperature [24].

Cold active lipases having low thermal stability were shown to be favorable for some purposes. For instance, heat labile lipase can be inactivated by treatment for short periods of time at relatively low temperatures after being used for the processing of food and other materials. Thus, during heat activation, materials can be prevented from damage [25]. Ethyl esterification of docosahexaenoic acid (DHA) in an organic solvent-free system using *C. Antarctica* lipase has been reported [26], which acts strongly on DHA and ethanol. Eighty-eight percent of ester product was produced by shaking the mixture of DHA/ethanol with ratio (1:1, mol/mol) and 2 % (*w*/*v*) immobilized *C. Antarctica* lipase B at 30 °C for 24 h. In addition, the use of lipase B from *C. antarctica* for the preparation of optically active alcohol was reported in previous study [27]. The ability of psychrophilic lipases to catalyse reactions at low or moderate temperature offers novel opportunities for industrial and biotechnological potential [22]. The effect of reaction temperature can be distributed to its effect on substrate solubility as well as its direct influences on the enzyme and the esterification reaction.

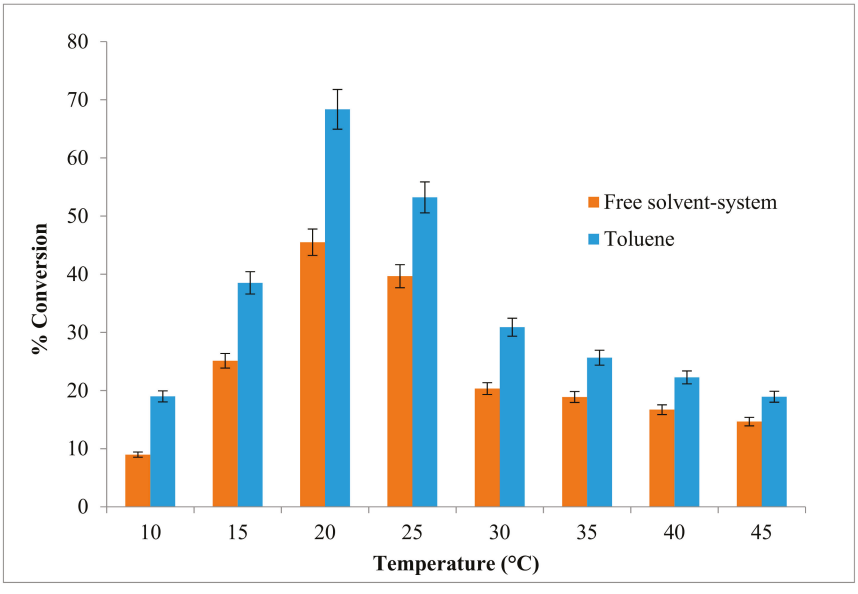

Figure 2. Effect of various reaction temperatures on AMS8 lipase in toluene and free-solvent-system. Percentage conversion of ethyl hexanoate catalysed by native AMS8 lipase as affected different reaction of temperature in toluene and free-solvent system. Reactions were performed for two hours with 1:1 molar ratio of hexanoic acid to ethanol.

2.3. *Effect of Time on the Esterification Reaction*

The reaction time for an enzyme provides an insight into its performance. As the reaction progresses, a determination of the shortest time required to obtain a suitable yield is helpful and enhances the cost-effectiveness of the process. The lipase-catalyzed reaction reached equilibrium after two hours at 20 °C, with a conversion yield of 69% in toluene while in free solvent-system about 47% of ester conversion was achieved (Figure 3). After more than two hours of incubation, the ester yield began to decrease. This was due to production of water molecule, which had achieved the equilibrium state. As the reaction proceeded, the substrates concentration decreased which led to a fall in the degree of substrate saturation of the enzyme [28].

In this study, the AMS8 lipase acts as catalyst to speed up the reaction. The best ester conversion of AMS8 was achieved at 2 h. Ester production declines after prolonged incubation. The instability of the psychrophilic lipases over longer time periods is one of the factors contributing to the favorable results obtained for a short AMS8 lipase reaction time. As the reaction proceeds, the substrate concentration decreases, which reduces the degree of enzyme substrate saturation. The best production of ethyl hexanoate in 2 h using cold active AMS8 lipase was considered to be a rapid conversion. In contrast with *Pseudomonas* P38 lipase catalyzed reaction which reached equilibrium state after 96 h at 20 °C [20]. The lipase from *Aspergillus terreus* was reported to catalyze the esterification of stearic acid with sorbitol and the ester conversion of 65% was achieved after 48 h at 37 °C. The percentage of ester conversion keeps increasing from 12 h to 24 h; however, the conversion of ester was found to remain constant after 24 h to 48 h and slightly decrease after prolonged reaction times [29].

The reaction time and the product yield are two important process endpoints in this study. A short reaction time reduces overall process cost, reduces the requirement for energy and decreases substrate inventory. Therefore, it has been proven that AMS8 used as a catalyst had speed up esterification reaction between hexanoic acid and ethanol within two hours incubation time. The time of reaction is dependent on kinetic factors such as choice of organic solvent, reaction temperature, amount of biocatalyst used, specific enzyme activity, concentration of cosubstrates, shaking or sonication that affects mass transfer limitations and reaction rate and also the degree of stirring [30].

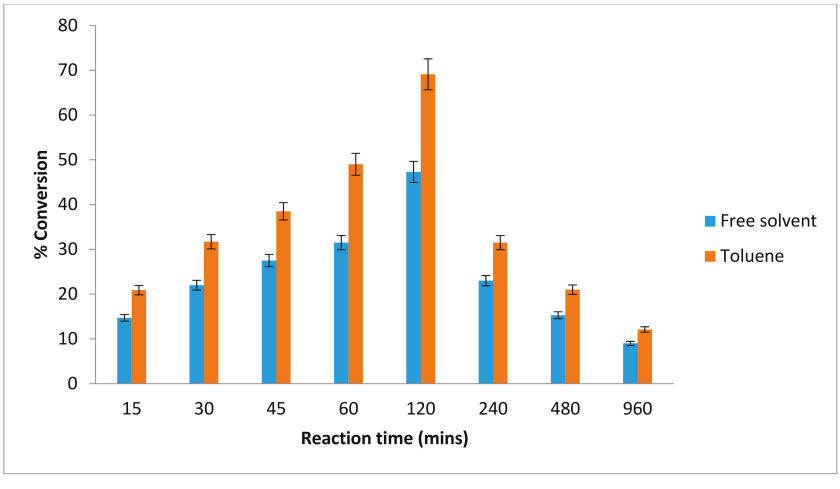

Figure 3. Effect of various reaction times on lipAMS8 lipase in toluene and free-solvent-system. Percentage conversion of ethyl hexanoate catalysed by native lipAMS8 lipase as affected different reaction of time in toluene and free-solvent system. Reactions were performed at 20 °C with 1:1 molar ratio of hexanoic acid to ethanol.

2.4. Effect of the Substrate Molar Ratio on the Esterification Reaction

The effect of the substrate (acid to alcohol) molar ratio was investigated using freeze-dried AMS8 lipase. Figure 4 shows that the ester conversion rate in toluene increased from 15.4% to 71% as the alcohol-to-acid molar ratio was decreased from 4 to 1, respectively, while an increase in the acid-to-alcohol molar ratio also contributed to a lower ester yield. However, in free solvent-system, the ester conversion shows about 48.6% in 1:1 molar ratio acid-to-alcohol. In this study, the substrate concentration was constant at 25 mM for both acid and alcohol.

The synthesis of ethyl hexanoate increased with an increase in the acyl donor concentration, and a high percentage of ester formation (70%) was obtained with a 0.025 M substrate mixture (hexanoic acid and alcohol) after two-hour incubation at 20 °C. However, at substrate concentrations greater than 0.025 M, a decrease in the ester yield was observed. This result could have occurred because polar substrates might have accumulated in the aqueous microenvironment of the enzyme, reaching a concentration level sufficient to cause protein denaturation [31]. Moreover, high concentration of alcohols is reported to be terminal inhibitors of lipases [32]. This inhibition may result from substrate inhibition, enzyme dehydration and pH reduction in the aqueous microenvironment of the enzyme. This phenomenon is described with lipases with the exception of the esterification rate of *C. cylindracea* lipase [33] which was not inhibited even at butyric acid concentration as high as 1 M. However, most of enzymes are inhibited by low concentration of acid and alcohol. For instance, the *Mucor miehei* lipase was inhibited by 0.05 M of acetic acid [34].

A previous study reported that a high concentration of alcohol might impair the reaction rate [35]. Therefore, it is necessary to optimize the actual excess nucleophile concentration to be employed in a given reaction. Several observations on alcohol inhibition have been reported for lipase catalysis. For instance, in a previous study, synthesis of ethyl ester has been affected by increasing ethanol concentration [36].

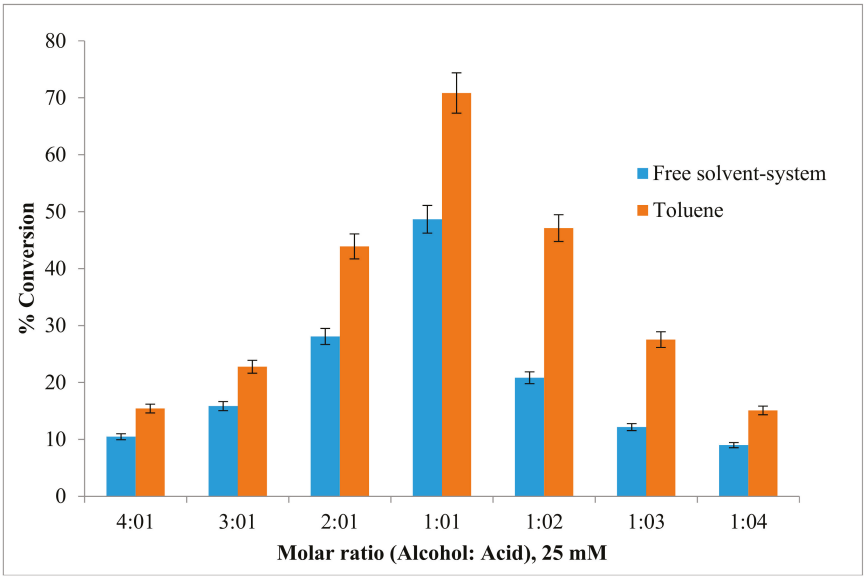

Figure 4. Effect of different ratio concentration of substrate on lipAMS8 lipase in toluene and free-solvent-system. Percentage conversion of ethyl hexanoate catalysed by AMS8 lipase is affected at different substrate molar ratio in toluene and free-solvent system. Reactions were performed at 20 °C for 2 h.

In addition, an increase in the fatty acid concentration can affect enzyme activation and also decreases the pH, which can contribute to the hydrolysis of the esters formed [37]. Furthermore, an increase in either acid or alcohol concentration affects the polarity of the medium, thus altering the affinity of the organic solvent and reducing the ester conversion rate [38]. Thus, the use of an equimolar acid-to-alcohol ratio was recommended to achieve an optimal ester conversion rate [37]. However, the ideal substrate molar ratio required to produce a high ester conversion rate depends on an enzyme's properties because every enzyme exhibits its own unique characteristics [39].

2.5. Effect of the Enzyme Concentration on the Esterification Reaction

Amount of enzyme plays a crucial role in any biocatalytic process especially in large scale production. Its influence on the reaction was assessed to facilitate determination of the minimal amount necessary for achieving good yield. The reaction in this study was carried out using equimolar concentration of alcohol and acid substrates (0.025 M), and different enzyme amount (1% to 10%) (*w*/*v*) (mg/mL). The system used for ester synthesis was biphasic with the solid enzyme powder in suspension in the liquid phase in toluene as well as the free solvent-system. The enzyme AMS8 lipase was lyophilized and dried for 48 h before use. The initial rate of ethyl hexanoate synthesis was proportional to the amount of enzyme added to the reaction mixture. Figure 5 shows that the ester conversion rate in toluene increased from 1% (24%) to 5% (68%) of enzyme concentration in (*w*/*v*) and started to decrease when added 7% to 10% of enzyme concentration, whereas only 48% of ester conversion was seen when 5% of enzyme concentration was added in free solvent-system.

The result shows an excess of enzyme concentration did not contribute to the increase in the percentage conversion. The previous study shows that the percentage of ester conversion for ethyl valerate was 75.3% in 5% (*w*/*w*) to 80.0% (15%) (*w*/*w*) and slightly decreased at 20% of enzyme concentration and sharply dropped when more than 30% of the enzyme amount was added [1]. As the enzyme concentration was increased above this point, the reaction will slightly decline due to the steric hindrance produce by excessive enzyme. The amount of enzyme will influence the total reaction times in esterification reaction, which are required to achieve desired conversion. The most significant main effect in enzymatic esterification reaction is the initial catalyst concentration [40]. The use of a large amount of enzyme could significantly increase the fraction of acyl donor molecules to form acyl–enzyme complexes was indicated in the previous study [41]. Moreover, their active sites were not exposed to the substrate and remained inside the bulk of enzyme particles without contributing significantly to the reaction. According to a study, not all active sites are exposed to the substrates in the presence of high amount of lipase, and resulted molecules of the enzyme tend to aggregate together [42]. However, small amounts of enzymes may have been insufficient for complete substrate conversion within the specified reaction period [43].

The percentage yield of ester product from *S. acrimycini* NGP 1, *S. albogriseolus* NGP 2 and *S. variabilis* NGP 3 were found to be 40.1%, 48.8% and 63.3% from the previous study. It shows that the percentage of ester conversion was found reach its maximum at 5% to 15% of the enzyme concentration and decreased when 20% and 25% of the enzyme amount were added in the reaction mixture [44]. A simple kinetic model derived from a ping pong mechanism was proposed to describe the mono-esterification of glucose with stearic acid catalysed by immobilized lipases from *Candida* sp. When the concentration of the enzyme increased, the percentage yield of ester product was decreased [27].

The observation the silica immobilized lipase, (SIL) showed that the percentage of ester conversion were 50% and 56% for n-butyl acetate and n-propyl acetate synthesis respectively after 24 h of incubation time at an enzyme concentration of 25% (15/mL). Upon an increase of the enzyme amount, the yield did not increase significantly due to the lack of substrate to access the active site of enzyme and difficulty in maintaining the uniformity of the biocatalyst at a higher enzyme concentration [45]. In addition, synthesis of isoamyl acetate using the immobilized lipase as a biocatalyst studied the effect of enzyme concentration in the range of 4 to 20% (by mass per volume) at 40 °C [3].

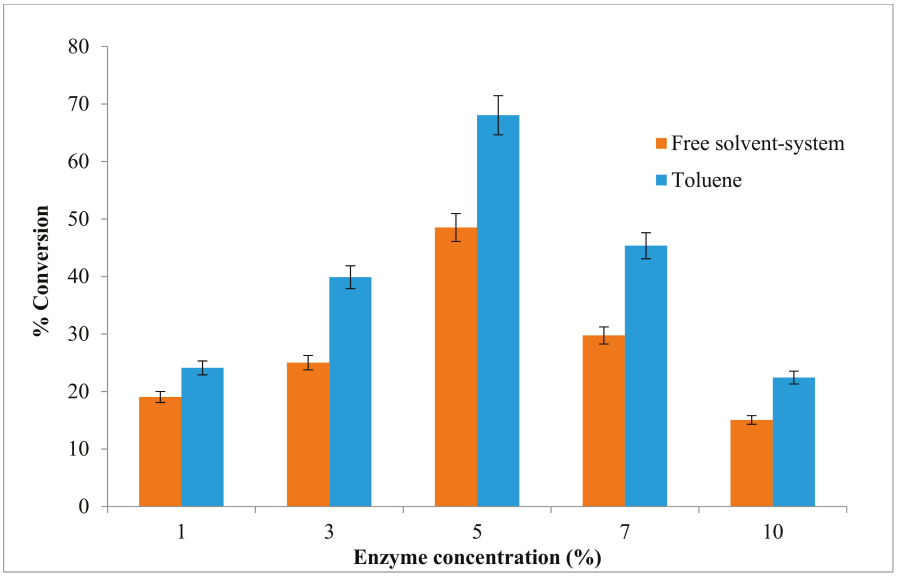

Figure 5. Effect of different concentration of enzyme on AMS8 lipase in toluene and free-solvent-system. Percentage conversion of ethyl hexanoate catalysed by native AMS8 lipase as affected different of enzyme concentration in toluene and free-solvent system. Reactions were performed at 20 °C for two hours 25 mM of substrate concentration (1:1 molar ratio ethanol to hexanoic acid).

2.6. Immobilization of Lipase

In this study, the AMS8 lipase was immobilized using physical adsorption method. The percentage of immobilization of AMS8 lipase on four types of matrices is investigated. Among the matrices or supports used, chitosan shows highest percentage of lipase immobilization (76.2%) while, kaolin showed low percentage of lipases immobilization at 31.2% (Figure 6). It shows that the difference in percentage values of immobilization as well as protein loadings were in accordance to the physicochemical properties.

The lipase activity in native and immobilized forms was measured. The lipase activity of native AMS8 lipase was about 30.5 U/mL, whereas the lipase activity of immobilized enzyme in chitosan, celite, Amberlite XAD7 and kaolin were 37.2, 33.5, 28.1 and 15 U/mL, respectively.

The differences in percentage of immobilization appeared to be influenced by support pore size and adsorption capacities. The great value of immobilization onto chitosan could be due to its particle size and diameter. Previous study shows that chitosan has been shown to be a versatile nontoxic material with some effects like it controls pathogenic microorganisms and activates several defence responses including and inhibiting different biochemical activities during the plant-pathogen interaction. The advantages of chitosan might be extended from the field through to the storage of numerous horticultural commodities [46].

Bansal, (2011) reported that chitosan can be tailored to produce different forms for use in different biotechnological industrial applications such as cosmetic fields [47]. It is an essential component in skin care creams, shampoo, and hairsprays due to its antibacterial properties. Chitosan forms a moisturizing, protective, and elastic film on the surface of the skin that has the ability to bind other ingredients that act on the skin. It can be concluded that chitosan is an important support, natural polymer and versatile, which successfully used in pharmaceutical industries. Therefore, from this experiment, chitosan was selected to other supports for immobilization of lipase to synthesize ethyl hexanoate.

The particle size of support material also influences the coupling effect during immobilization [48]. The forces between a support and the enzymes include hydrogen bonding, Van der Waals forces and electrostatic interaction. Furthermore, the smaller pore size may restrict mass transfer and pore penetration of the protein which is limited the protein interaction with the total surface area of supports. Hence, intraparticle diffusion effect of substrates was reduce and helping to interact between enzyme and substrates [49].

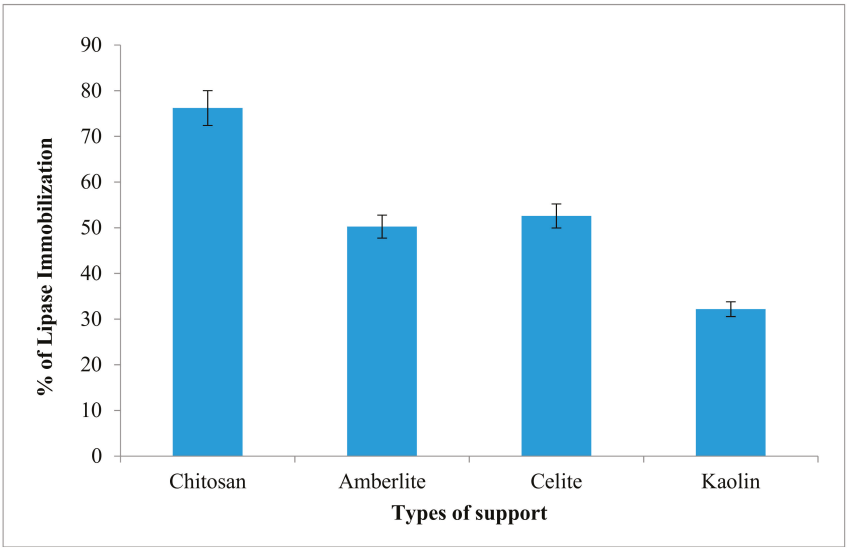

Figure 6. Percentage of AMS8 lipase immobilization on various matrices. Protein content was determined using Bradford (1976) method and percentage of immobilization was calculated using formula described in earlier section.

Comparison between native AMS8 lipase and immobilized lipases towards the synthesis of ethyl hexanoate was done. As shown in Figure 7, the lipase immobilized with chitosan showed higher relative conversion as compared with control with 125.7% and 115.6% in the free-solvent system and toluene, respectively. Similarly with the previous study reported the activity and stability of the lipase after immobilization on both LDHs were found to be increased in ester conversion compared to in native lipase [50]. Similar trend was also reported on Zn/Al-diocytyl sodium sulfosuccinate (DSS) nanocomposite (NAZAD) which has higher porosity and able to adsorb higher protein and subsequently increase the ester production. The obtained immobilized lipase was applied for the synthesis of ethyl butyrate and resulted an ester conversion of 89% compared to native lipase 65% [51].

From the previous study, a method of immobilization of *Candida rugosa* was investigated where, the immobilization procedure was improved by addition of calcium alginate to polymer of polyvinyl alcohol (PVA) to improve the surface area properties and reduce the tendency to agglomerate [52]. On the other hand, the lipase isolated from *Bacillus* sp. was immobilized on different supports and the results shows the activity and stability of immobilized lipase were much better compared to native lipase [53]. Similarly with immobilized lipase from *Candida rugosa* showed and increment in thermal stability where the enzyme shifted the temperature from 37 °C to 45 °C [54]. It shows that the thermal stability of the immobilized lipase was higher than that the native lipase thus, making immobilized lipase more stable and more preferable for use in the synthesis of ester [54]. The effectiveness of an immobilization process depends much on the support used. Comparative studies indicated that dramatic differences exist in the activity of lipases supported on different materials [11]. Similarly with

Candida rugose lipase where the enzyme shown high activity or ester conversion when immobilize with chitosan [55].

In contrast with kaolin, this support showed decrement of synthesize ethyl hexanoate ester compare with control which are 40.4% and 41% in free solvent and toluene. The unsuitability of this support also has been reported by a few enzymes such as porcine pancreatic lipase and acid phosphatase [56–58]. The decrement of ester conversion might be due to electrostatic forces that play an important role in the adsorption of enzyme where the kaolin was reported to have the negative charge [58,59].

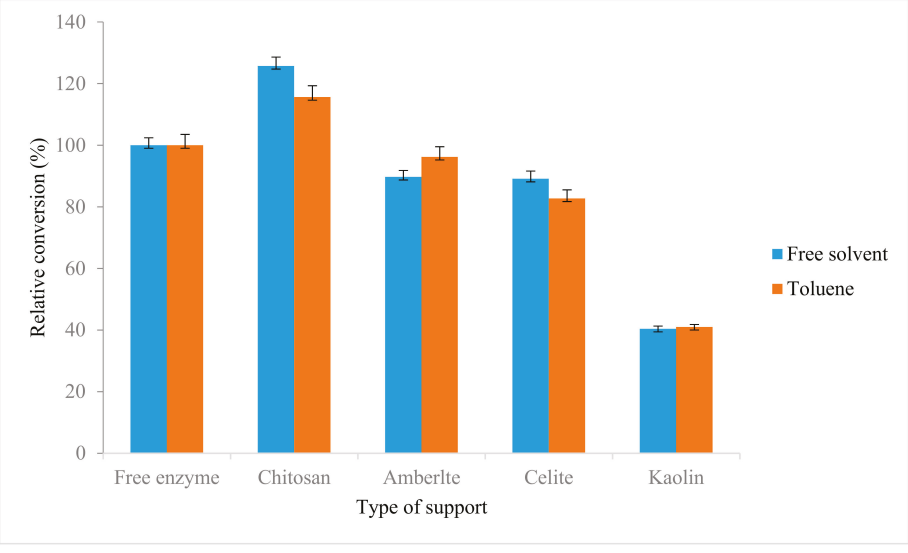

Figure 7. Synthesis of ethyl hexanoate using native AMS8 lipase and immobilized lipases. The ethyl hexanoate was synthesis relative to the control (free enzyme) in toluene and free-solvent system. The reactions were performed at 20 °C for two hours 25 mM of substrate concentration (1:1 molar ratio ethanol to hexanoic acid).

2.7. Morphology Analysis of Chitosan Using Scanning Electron Microscopy (SEM)

A suitable support material that can function effectively in immobilization generally requires the following characteristics. Among those, it should ease enzyme immobilization without any significant loss of enzyme activity and it must not contain extractable materials which it may contaminate the product stream. A support or matrix should also have suitable mechanical properties for the desired process and should have appropriate pores and particle sizes as well as the surface area, so as not to limit diffusion of substrates and therefore reaction rates and it should be less expensive [59]. Chitosan showed the highest ester conversion among others support or matrices. High exchange rates indicate matrix compatibility. In order to support the data, morphology analysis has been done using scanning electron microscopy (SEM). Figure 8a,b shows that the structure of the chitosan-lipase is more compact compared the support only. The existence in compactness could indicate the presence of lipase. The pores or holes of chitosan powder can also be clearly seen under 500× and 1000× magnification. The pore diameter should be four- to fivefold of the protein diameter in order to prevent restrictions to the access of the enzymes [59,60]. Pore sizes of the support also contribute to the suitability of the support with the enzyme leading to increase enzyme activity. Previous study reported that supports with smaller pore sizes can result in restricting mass transfer and the penetration of the enzyme molecules, thus limiting protein interaction with the total surface area of the support particles [61].

The pore size might be useful to explain the adsorption capacity of chitosan. Similarly, a commercial crude lipase and lyophilized *Candida antarctica* lipase was not easily dispersed and formed aggregates due to incompatibility of support [62]. The aggregation of freeze-dried lipase as well as lipase crude powder is the cause of decrease in their specific activities. This phenomenon could be due to the removal of essential water surrounding lipase during lyophilization.

Lipase is a hydrophobic enzyme, which explained how a strong hydrophobic or electrostatic interaction was needed between enzyme and support in an immobilization process in order for the adsorption to be successful. Strong hydrophobic interactions can be achieved by using hydrophobic supports or enzymes [10]. Moreover, hydrophobicity of lipase plays an important role in increasing the amount of immobilized activity due to the stronger preferential binding of the more hydrophobic lipase on the supports. To show how important physical factors influenced the rate of absorption of the enzyme, lipase from *Candida rugosa* has been immobilized using chitosan flakes and porous chitosan beads (PCB). The result showed that PCB has higher recovery compared to flakes, and internal mass transfer occurred during the process [61]. Thus, selections of supports have a biggest influence in the successful immobilization of enzymes.

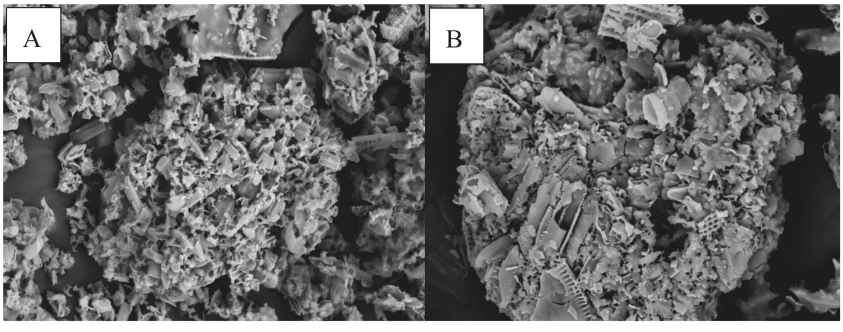

Figure 8. Scanning electron micrographs of chitosan and chitosan with AMS8 lipase. (**A**) Chitosan (500× magnification); (**B**) chitosan-lipase (1000× magnification).

2.8. Fourier Transform Infrared (FTIR) and Gas Chromatography–Mass Spectrometry (GC–MS) Analyses of Flavor Ester

Product of the reaction was ascertained using FTIR and GC–MS. The aim of these analyses is to identify those functional groups in each of samples and specifically is the presence of ethyl hexanoate ester. The infrared result for ethyl hexanoate is tabulated in Table 1.

Figure 9 show that the sharp peaks at 1704.30 cm^{-1} that indicated the presence of functional group carbonyl include esters, aldehydes and ketone group which is more specific for ester within the samples. The free carbonyl stretching frequency ester in pyrrolic ester is in range of 1701–1711 cm^{-1} [63] Then, the ester structures were followed by the presence of v(C-O) in 1257.22 cm^{-1}. This characteristic differentiates between esters and ketones. The band of ester is doublet at 1717–1723 cm^{-1} for v(C=O) and 1266–1257 cm^{-1} for v(C-O) in acetyl ester bonds [64]. Based on the figure also, it showed the infrared at 2935.11 cm^{-1} that indicated the stretching v(C-H) functional group while the infrared at 1423.00 cm^{-1} showed the bending v(C-H) functional group. The stretching v(C-H) functional group showed the presence of C-H aromatic group. The infrared spectrum in range around 2800–3000 cm^{-1} indicated the C-H stretching [64].

Table 1. Infrared spectrum of ethyl hexanoate.

Compound	Frequencies of Absorption (cm^{-1})				
	v(C=O)	v(C-H) stretch	v(O-H)	v(C-O)	v(C-H) bend
Ethyl hexanoate	1704.30	2935.11	-	1257.22	1423.00

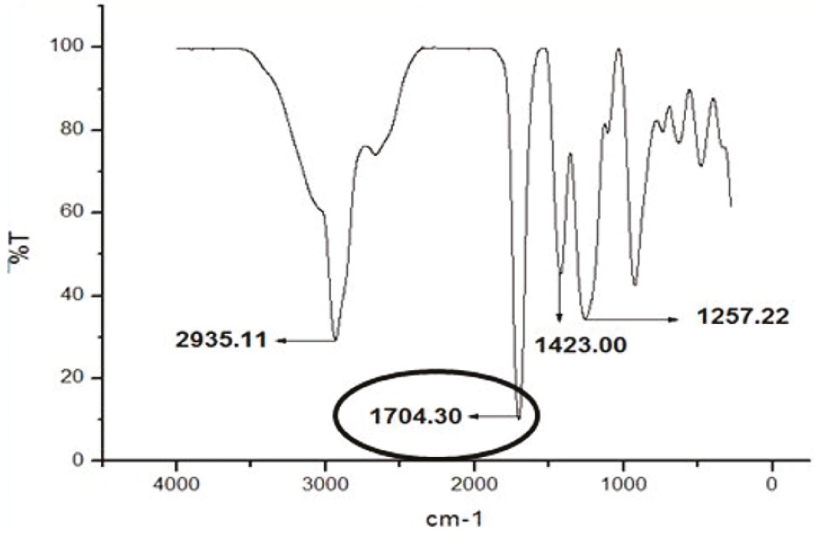

Figure 9. IR spectrum of ethyl hexanoate. Spectrum indicating the presence of ester is shown in circle area.

The total molecular ion of ester mixtures is represented in Table 2. The molecular ion of 144 m/z indicated the presence of ethyl hexanoate molecules with molecular weight of 144.21 g/mol. The corresponding ester compound of ethyl hexanoate ($C_8H_{16}O_2$) can be recognized by mass spectra. The highest peak at 43 m/z indicates the hexane substituent fragmented from the ethyl hexanoate ester while at 60 m/z, the peak showed the presence of ethoxide structure, which is a product of fragmentation of hydrogen from ethanol. At 88 m/z, the peak indicates presence of hexanoic acid in the sample whereas the peak for ethyl ester appeared at 73 m/z. Thus, it has proven that the existence of ester group in the sample. The presence of suitable organic solvent in esterification reaction has helped to minimize the water content and lead to maximize the yield ester production due to the thermodynamic equilibrium shifting to forward reaction (synthesis) instead of reverse (hydrolysis) reaction of esterification.

Table 2. Molecular ion fragments of ethyl hexanoate mixtures. The mass spectrum showed the presence of ethyl hexanoate (144 m/z) in the sample with the compound structure and fragment molecular ions.

m/z	Fragment Ion
43	$CH_3CH_2CH_2+$
60	CH_2COOH
73	$+COOCH_2CH_3$
88	$CH_3COOCH_2CH_3$
99	$CH_3CH_2CH_2CH_2CH_2CO+$
115	$CH_3CH_2CH_2CH_2CH_2COO+$
144	$CH_2CH_2CH_2CH_2COOCH_2CH_3$

3. Materials and Methods

3.1. Materials

Hexanoic acid (95%) and toluene (95%) were purchased from Merck KGaA (Darmstadt, Germany). Acetone and absolute ethanol were obtained from Sigma-Aldrich Co. Ltd. (Poole, UK). Sodium hydroxide was supplied by Merck. Molecular sieve dehydrate 3A, with indicator, for drying solvents was purchased from Fluka (Buchs, Switzerland). All other chemicals and solvents used in this study were of analytical grade.

3.2. Preparation of Crude Freeze-Dried AMS8 Lipase

Recombinant *E. coli* containing a pET32/*LipAMS8* gene vector was obtained from the Laboratory of Enzyme and Microbial Technology, Faculty of Biotechnology and Biomolecular Sciences, Universiti Putra Malaysia, Selangor, Malaysia The stock culture was maintained in a sterile microcentrifuge tube containing 0.2 mL of glycerol and 0.8 mL of Luria-Bertani (LB) medium in a deep freezer at −80 °C prior to use. For the production of lipase, the culture was incubated in a 500 mL conical flask containing 100 mL of production medium (LB medium with 1% (*v*/*v*) culture, 0.1 mL ampicillin and 0.1 mL IPTG) for 12 h with reciprocal shaking at 20 °C and 200 rpm. After incubation, the culture was centrifuged at 4 °C, and the supernatant was discarded. The pellet was resuspended in 30 mL of 0.05 M Tris-HCl buffer (pH 8) and was sonicated for six minutes at 30-second intervals. Then, the enzyme was centrifuged at 4 °C, and the supernatant was collected. The AMS8 lipase was freeze-dried overnight. The dried crude AMS8 lipase sample was stored at 4 °C prior to use.

3.3. Lipase Hydrolytic Activity

The activity of the freeze-dried AMS8 lipase was measured under the standard assay conditions described previously [10] using an olive oil emulsion as a substrate. AMS8 lipase activity is expressed as unit per milliliter of enzymatic solution. One unit (IU) of lipase activity was defined as the amount of enzyme that catalyzed the liberation of 1 μmol of free fatty acid from olive oil per minute at 20 °C under optimized conditions.

3.4. Synthesis of Ethyl Hexanoate

3.4.1. In Solvent-Free System

The reactions were carried out in screw-capped bottles containing 5 mL of the substrate mixture (hexanoic acid and ethanol), which consisted of a 1:1 molar ratio of acid to alcohol, at 20 °C in the presence of 5% freeze-dried AMS8 lipase with shaking (200 rpm). A reaction under the same conditions without added enzyme was performed in parallel and used as a control.

3.4.2. In Toluene

The reactions were performed in 5-mL screw-capped bottles with a substrate concentration of 0.025 M each. Afterwards, 10 mL of toluene was added to the mixture. The reaction mixture was incubated at 20 °C in the presence of 5% freeze-dried AMS8 lipase with shaking (200 rpm).

3.5. Reaction Analysis

Aliquots of the reaction mixture were withdrawn periodically, and the residual acid content was assayed by titration with 0.5 M sodium hydroxide using phenolphthalein as an indicator and 3 mL of ethanol as a quenching agent. The ester synthesis rate was calculated based on the conversion of the acid to an ester. The ethyl hexanoate yield is expressed as a percentage (%) of converted hexanoic acid compared to the total initial fatty acid content in the reaction mixture.

The conversion of ester was expressed as percentage conversion (%) under various reaction conditions according to the following formula:

$$\text{Conversion of ester } (\%) = \frac{[\text{ volume of NaOH (control} - \text{with enzyme) }] \times 100}{\text{volume NaOH (control)}}$$

3.6. Effect of Reaction Temperature

The reaction mixture was incubated at various temperatures (10, 15, 20, 25, 30, 35, 40, 45, 50) °C using a horizontal water bath shaker with a continuous shaking speed of 200 rpm. The conversion percentage was determined as described above.

3.7. Effect of Reaction Time

The reaction mixture was incubated for various reaction time intervals (15, 30 45, 60, 120, 240, 480, and 960 min) using a horizontal water bath shaker with a continuous shaking speed of 200 rpm. The conversion percentage was determined as described above.

3.8. Effect of Substrate Concentration

The reaction mixture was incubated at various substrate molar ratios (1:1, 1:2, 1:3, 1:4, 1:1, 2:1, 3:1, and 4:1) and different substrate concentrations (5, 10, 25, 50, 75, and 100) mM using a horizontal water bath shaker with a continuous shaking speed of 200 rpm. The conversion percentage was determined as described above.

3.9. Effect of Enzyme Concentration

The reaction mixture was incubated at various enzyme concentrations (w/v) in percentage (%) which are (1%, 3%, 5%, 7% and 10%) using a horizontal water bath shaker with a continuous shaking speed of 200 rpm. The conversion percentage was determined as described above.

3.10. Immobilization of AMS8 Using Commercial Supports

10 mL of AMS8 lipase and 1.0 g of commercial supports (celite, chitosan, amberlite and kaolin) were chosen to immobilize the AMS8 lipase. The mixture was incubated for two hours at 25 °C with 100 rpm in a water bath shaker. The enzyme-loaded supports were separated from the supernatant by filtering through Whatmann No. 1 filter paper using vacuum pump. Then, two to three times of washing of the enzyme-loaded supports were carried out using distilled water (10 mL) to remove the unabsorbed enzyme. The immobilized AMS8 lipases were then lyophilized in the freeze drier for 24 h.

The lipase activity of immobilized AMS8 lipases were determined using colorimetric method (Kwon and Rhee, 1986) while the protein content was determined by Coomassie dye binding (Bradford, 1976). The amount of bound protein was indirectly determined by comparing the difference between the amounts of protein introduced into the support (before immobilization) and the amount of protein both in filtrate and in the washing solutions after immobilization.

The protein immobilization was calculated using the following formula:

$$\%\ \text{Immobilization} = \frac{(\text{Protein A } - \text{Protein B}) \times 100\%}{\text{Protein A}}$$

whereby, Protein A is total amount of protein in supernatant before immobilization and Protein B is total amount of protein in supernatant after immobilization.

Esterification Reaction Using the Immobilized Lipase

The enzymatic esterification reactions for immobilized AMS8 lipase was conducted using optimum parameters at optimized reaction conditions using native AMS8 lipase. They consisted of

substrates (3.12 mL of 25 mM of hexanoic acid and 1.46 mL of 25 mM of ethanol) were mixed in 10 mL of toluene, 0.15 g of molecular sieves and various immobilized lipase derivatives (containing 10 mg protein). The mixture was incubated with shaking speed of 200 rpm in water bath shaker at 20 °C for two hours. The mixture without lipase acted as the control of the process. After incubation, the mixtures were terminated using mixture of acetone and ethanol, ratio (1:1). The mixtures then were filtered by Whatman No. 1 filter paper and followed by titration with NaOH. This reaction was done in triplicate.

3.11. Fourier Transform Infra-Red Spectroscopy (FTIR) and Gas Chromatography—Mass Spectrometry (GC–MS) Analysis

FTIR and GC–MS (Shimadzu, Japan) were used to identify the functional groups present in the sample by utilizing a universal attenuated total reflectance sensor and the wavenumbers ranging from 280–4000 cm^{-1}. At the end of the reaction of two hours, enzyme (native lipase and immobilized lipases) and molecular sieve were filtered, while the solvent (toluene) from the reaction mixture was removed by rotary evaporation at 40 °C. Product and substrate were identified using FTIR spectroscopy (Shimadzu, Japan). A semi-solid sample was dissolved in a defined amount of methanol/acetonitrile (70:30). Through this solution, the FTIR spectra of reaction mixtures were analyzed on a spectrophotometer (Secomam, France).

GC–MS analysis of product from the reaction mixtures before incubation (absence of lipase) and after incubation in the presence of lipase were performed on a Shimadzu (model GC-17 A., model MS QP5050A; Shimadzu, Tokyo, Japan) instrument using a nonpolar column (column SGE BPXS, 30 m, 0.25 mm ID, 0.25 μm thickness). The carrier gas was helium at a flow rate of 2.0 mL/min with injection volume of 0.5 μL. The column temperature was programmed at 50 °C.

4. Conclusions

The AMS8 lipase can act as a catalyst to speed up the esterification reaction between hexanoic acid and ethanol. AMS8 lipase has an ester conversion rate of 70%, which was obtained at 20 °C in the presence of toluene. Immobilization of the enzymes has proven that the enzyme is more stable compared with the native enzyme during esterification process. Matrices enhance and decrease the process of ester conversion. Comparison between the native AMS8 lipase and the immobilized lipases revealed that immobilized lipases with suitable matrices (chitosan) showed a higher production of ethyl hexanoate than native lipase. Thus, the ability of psychrophilic lipase, AMS8 lipaseto catalyze reactions at a low temperature offers novel opportunities for industrial and biotechnological applications.

Author Contributions: N.M. conceived and designed the experiment, performed the experiments, and analyzed the data. W.L. wrote the paper and reviewed drafts of the paper. R.N.Z.A.R., A.B.S., and M.S.M.A. conceived and designed the experiment, analyzed the data, contributed to reagent/material/analysis tools, and reviewed drafts of the paper.

Acknowledgments: The research was supported by the Ministry of Higher Education Malaysia (MOHE) under FRGS research funding (Project number: 02-01-14-1403FR).

Conflicts of Interest: The authors declare no conflicts of interest.

References

1. Muhamad, S.K.; Radzi, S.M.; Othman, S.S.; Basyaruddin, M.; Rahman, A.; Noor, H.M. Optimization of lipase-catalyzed synthesis of flavor esters in solvent free system. *J. Fundam. Sci.* **2010**, *6*, 31–36.
2. Joseph, B.; Ramteke, P.W.; Thomas, G. Cold active microbial lipases: Some hot issues and recent developments. *Biotechnol. Adv.* **2008**, *26*, 457–470. [CrossRef] [PubMed]
3. Mahapatra, P.; Kumari, A.; Kumar Garlapati, V.; Banerjee, R.; Nag, A. Enzymatic synthesis of fruit flavor esters by immobilized lipase from Rhizopus oligosporus optimized with response surface methodology. *J. Mol. Catal. B Enzym.* **2009**, *60*, 57–63. [CrossRef]

4. Ghamgui, H.; Karra-Chaâbouni, M.; Bezzine, S.; Miled, N.; Gargouri, Y. Production of isoamyl acetate with immobilized Staphylococcus simulans lipase in a solvent-free system. *Enzym. Microb. Technol.* **2006**, *38*, 788–794. [CrossRef]
5. Liaquat, M.; Apenten, R.K.O. Synthesis of Low Molecular Weight Flavor Esters Using Plant Seedling Lipases in Organic Media. *J. Food Sci.* **2000**, *65*, 295–299. [CrossRef]
6. Abbas, H.; Hiol, A.; Deyris, V.; Comeau, L. Isolation and characterization of an extracellular lipase from *Mucor* sp strain isolated from palm fruit. *Enzyme Microb. Technol.* **2002**, *31*, 968–975. [CrossRef]
7. Bisswanger, H. *Practical Enzymology*; John Wiley & Sons: Hoboken, NJ, USA, 2013.
8. Zhang, X.; Guan, R.-F.; Wu, D.-Q.; Chan, K.-Y. Enzyme immobilization on amino-functionalized mesostructured cellular foam surfaces, characterization and catalytic properties. *J. Mol. Catal. B Enzym.* **2005**, *33*, 43–50. [CrossRef]
9. Jaeger, K.E.; Reetz, M.T. Microbial lipases form versatile tools for biotechnology. *Trends Biotechnol.* **1998**, *16*, 396–403. [CrossRef]
10. Abdul Rahman, M.B.; Tajudin, S.M.; Hussein, M.Z.; Abdul Rahman, R.N.Z.R.; Salleh, A.B.; Basri, M. Application of natural kaolin as support for the immobilization of lipase from *Candida rugosa* as biocatalsyt for effective esterification. *Appl. Clay Sci.* **2005**, *29*, 111–116. [CrossRef]
11. Reslow, M.; Adlercreutz, P.; Mattiasson, B. On the importance of the support material for bioorganic synthesis. Influence of water partition between solvent, enzyme and solid support in water-poor reaction media. *Eur. J. Biochem.* **1988**, *172*, 573–578. [CrossRef] [PubMed]
12. Ali, M.S.; Ganasen, M.; Rahman, R.N.; Chor, A.L.; Salleh, A.B.; Basri, M. Cold-adapted RTX lipase from *Antarctic Pseudomonas* sp. strain AMS8: Isolation, molecular modeling and heterologous expression. *Protein J.* **2013**, *32*, 317–325. [CrossRef] [PubMed]
13. Klibanov, A. Improving Enzymes by Using Them in Organic Solvents. *Nature* **2001**, *409*, 241–247. [CrossRef] [PubMed]
14. Ghamgui, H.; Karra-Chaâbouni, M.; Gargouri, Y. 1-Butyl oleate synthesis by immobilized lipase from Rhizopus oryzae: A comparative study between n-hexane and solvent-free system. *Enzym. Microb. Technol.* **2004**, *35*, 355–363. [CrossRef]
15. Torres, S.; Baigorí, M.D.; Swathy, S.L.; Pandey, A.; Castro, G.R. Enzymatic synthesis of banana flavour (isoamyl acetate) by Bacillus licheniformis S-86 esterase. *Food Res. Int.* **2009**, *42*, 454–460. [CrossRef]
16. Latip, W.; Raja Abd Rahman, R.N.Z.; Leow, A.T.C.; Mohd Shariff, F.; Kamarudin, N.H.A.; Mohamad Ali, M.S. The Effect of N-Terminal Domain Removal towards the Biochemical and Structural Features of a Thermotolerant Lipase from an *Antarctic Pseudomonas* sp. strain AMS3. *Int. J. Mol. Sci.* **2018**, *19*, 560. [CrossRef] [PubMed]
17. Sharma, S.; Kanwar, S.S. Organic solvent tolerant lipases and applications. *Sci. World J.* **2014**, *2014*, 625258. [CrossRef] [PubMed]
18. Kazandjian, R.Z.; Dordick, J.S.; Klibanov, A.M. Enzymatic analyses in organic solvents. *Biotechnol. Bioeng.* **1986**, *28*, 417–421. [CrossRef] [PubMed]
19. Pinyaphong, P.; Phutrakul, S. Synthesis of cocoa butter equivalent from palm oil by Carica papaya lipase-catalyzed interesterification. *Chiang Mai J. Sci.* **2009**, *36*, 359–368.
20. Tan, S.; Apenten, R.K.O.; Knapp, J. Low temperature organic phase biocatalysis using cold-adapted lipase from psychrotrophic *Pseudomonas* P38. *Food Chem.* **1996**, *57*, 415–418. [CrossRef]
21. Gupta, A.; Khare, S.K. Enzymes from solvent-tolerant microbes: Useful biocatalysts for non-aqueous enzymology. *Crit. Rev. Biotechnol.* **2009**, *29*, 44–54. [CrossRef] [PubMed]
22. Selvam, K.; Vishnupriya, B.; Maanvizhi, M. Enzymatic Synthesis of Fragrance Ester by Lipase from Marine Actinomycetes for Textile Industry. *Int. J. Eng. Adv. Technol.* **2013**, *3*, 91–96.
23. Choo, D.; Kurihara, T.; Suzuki, T.; Soda, K. A Cold-Adapted Lipase of an Alaskan Gene Cloning and Enzyme Purification and Characterization A Cold-Adapted Lipase of an Alaskan Psychrotroph, *Pseudomonas* sp. Strain B11-1: Gene Cloning and Enzyme Purification and Characterization. *Appl. Environ. Microbiol.* **1998**, *64*, 486–491. [PubMed]
24. Siddiqui, K.S.; Cavicchioli, R. Cold-adapted enzymes. *Annu. Rev. Biochem.* **2006**, *75*, 403–433. [CrossRef] [PubMed]

25. Margesin, R.; Feller, G.; Gerday, C.; Russell, N. Cold-adapted microorganisms: Adaptation strategies and biotechnological potential. In *Encyclopedia of Environmental Microbiology*; John Wiley & Sons, Inc.: New York, NY, USA, 2003.
26. Shimada, Y.; Watanabe, Y.; Sugihara, A.; Baba, T.; Ooguri, T.; Moriyama, S.; Terai, T.; Tominaga, Y. Ethyl esterification of docosahexaenoic acid in an organic solvent-free system with immobilized *Candida antarctica* lipase. *J. Biosci. Bioeng.* **2001**, *92*, 19–23. [CrossRef]
27. Yu, J.; Zhang, J.; Zhao, A.; Ma, X. Study of glucose ester synthesis by immobilized lipase from *Candida* sp. *Catal. Commun.* **2008**, *9*, 1369–1374. [CrossRef]
28. Aracil, J.; Martinez, M.; Sa'nchez, N.; Corma, A. Formation of a jojoba oil analog by esterification of oleic acid using zeolites as catalyst. *Zeolites* **1992**, *12*, 233–236. [CrossRef]
29. Gulati, R.; Arya, P.; Malhotra, B.; Prasad, A.K.; Saxena, R.K.; Kumar, J.; Watterson, A.C.; Parmar, V.S. Novel biocatalytic esterification reactions on fatty acids: Synthesis of sorbitol 1(6)-monostearate. *Arch. Org. Chem.* **2003**, *2003*, 159–170.
30. Halling, P.J. Thermodynamic predictions for biocatalysis in nonconventional media: Theory, tests, and recommendations for experimental design and analysis. *Enzyme Microb. Technol.* **1994**, *16*, 178–206. [CrossRef]
31. Laane, C.; Boeren, S.; Vos, K.; Veeger, C. Rules for optimization of biocatalysis in organic solvents. *Biotechnol. Bioeng.* **1987**, *30*, 81–87. [CrossRef] [PubMed]
32. Alvarez-Macarie, E.; Baratti, J. Short chain flavour ester synthesis by a new esterase from Bacillus licheniformis. *J. Mol. Catal. B Enzym.* **2000**, *10*, 377–383. [CrossRef]
33. Gillies, B.; Yamazaki, H.; Armstrong, D.W. Production of flavor esters by immobilized lipase. *Biotechnol. Lett.* **1987**, *9*, 709–714. [CrossRef]
34. Welsh, F.W.; Williams, R.E.; Dawson, K.H. Lipase Mediated Synthesis of Low Molecular Weight Flavor Esters. *J. Food Sci.* **1990**, *55*, 1679–1682. [CrossRef]
35. Chowdary, G.V.; Ramesh, M.N.; Prapulla, S.G. Enzymic synthesis of isoamyl isovalerate using immobilized lipase from *Rhizomucor miehei*: A multivariate analysis. *Process Biochem.* **2000**, *36*, 331–339. [CrossRef]
36. Marty, A.; Chulalaksananukul, W.; Willemot, R.M.; Condoret, J.S. Kinetics of lipase-catalyzed esterification in supercritical CO_2. *Biotechnol. Bioeng.* **1992**, *39*, 273–280. [CrossRef] [PubMed]
37. Hari Krishna, S.; Divakar, S.; Prapulla, S.G.; Karanth, N.G. Enzymatic synthesis of isoamyl acetate using immobilized lipase from *Rhizomucor miehei*. *J. Biotechnol.* **2001**, *87*, 193–201. [CrossRef]
38. Romero, M.D.; Calvo, L.; Alba, C.; Habulin, M.; Primožič, M.; Knez, Ž. Enzymatic synthesis of isoamyl acetate with immobilized *Candida antarctica* lipase in supercritical carbon dioxide. *J. Supercrit. Fluids* **2005**, *33*, 77–84. [CrossRef]
39. Bezbradica, D.; Mijin, D.; Šiler-Marinković, S.; Knežević, Z. The effect of substrate polarity on the lipase-catalyzed synthesis of aroma esters in solvent-free systems. *J. Mol. Catal. B Enzym.* **2007**, *45*, 97–101. [CrossRef]
40. Sánchez, N.; Martinez, M.; Aracil, J.; Corma, A. Synthesis of oleyl oleate as a jojoba oil analog. *J. Am. Oil Chem. Soc.* **1992**, *69*, 1150–1153. [CrossRef]
41. Xin, J.Y.; Li, S.B.; Xu, Y.; Wang, L.L. Enzymatic resolution of (S)-(+)-naproxen in a trapped aqueous-organic solvent biphase continuous reactor. *Biotechnol. Bioeng.* **2000**, *68*, 78–83. [CrossRef]
42. Karra-Châabouni, M.; Ghamgui, H.; Bezzine, S.; Rekik, A.; Gargouri, Y. Production of flavour esters by immobilized Staphylococcus simulans lipase in a solvent-free system. *Process Biochem.* **2006**, *41*, 1692–1698. [CrossRef]
43. Liaquat, M.; Khan, S.; Aslam, S.; Khan, A.; Khan, H.; Khan, S.M.; Ali, S.; Wahab, S.; Bhatti, H.N. Rape Seedling Lipase Catalyzed Synthesis of Flavor Esters Through Transesterification in Hexane. *J. Chem. Soc. Pakistan* **2012**, *34*, 144–150.
44. Alves Macedo, G.; Soberón Lozano, M.M.; Pastore, G.M. Enzymatic synthesis of short chain citronellyl esters by a new lipase from *Rhizopus* sp. *Electron. J. Biotechnol.* **2003**, *9*, 72–75. [CrossRef]
45. Zulkeflee, S.A.; Sata, S.A.; Aziz, N. Kinetic Model of Batch Lipase-Catalyzed Esterification Process with Function of Temperature and Water Content. *Appl. Mech. Mater.* **2013**, *284–287*, 423–428. [CrossRef]
46. Bautista-Baños, S.; Hernández-Lauzardo, A.N.; Velázquez-del Valle, M.G.; Hernández-López, M.; Ait Barka, E.; Bosquez-Molina, E.; Wilson, C.L. Chitosan as a potential natural compound to control pre and postharvest diseases of horticultural commodities. *Crop Prot.* **2006**, *25*, 108–118. [CrossRef]

47. Bansal, V.; Sharma, P.K.; Sharma, N.; Pal, O.P.; Malviya, R. Applications of Chitosan and Chitosan Derivatives in Drug Delivery. *Biol. Res.* **2011**, *5*, 28–37.
48. Othman, S.S.; Basri, M.; Hussein, M.Z.; Abdul Rahman, M.B.; Rahman, R.N.Z.A.; Salleh, A.B.; Jasmani, H. Production of highly enantioselective (−)-menthyl butyrate using *Candida rugosa* lipase immobilized on epoxy-activated supports. *Food Chem.* **2008**, *106*, 437–443. [CrossRef]
49. Gao, Y.; Tan, T.; Nie, K.; Wang, F. Immobilization of Lipase on Macroporous Resin and Its Application in Synthesis of Biodiesel in Low Aqueous Media. *Chin. J. Biotechnol.* **2006**, *22*, 114–118. [CrossRef]
50. Rahman, M.B.A.; Basri, M.; Hussein, M.Z.; Rahman, R.N.Z.A.; Zainol, D.H.; Salleh, A.B. Immobilization of lipase from *Candida rugosa* on layered double hydroxides for esterification reaction. *Appl. Biochem. Biotechnol.* **2004**, *118*, 313–320. [CrossRef]
51. Shu, C.; Cai, J.; Huang, L.; Zhu, X.; Xu, Z. Biocatalytic production of ethyl butyrate from butyric acid with immobilized *Candida rugosa* lipase on cotton cloth. *J. Mol. Catal. B Enzym.* **2011**, *72*, 139–144. [CrossRef]
52. Dave, R.; Madamwar, D. Esterification in organic solvents by lipase immobilized in polymer of PVA–alginate–boric acid. *Process Biochem.* **2006**, *41*, 951–955. [CrossRef]
53. Nawani, N.; Singh, R.; Kaur, J. Immobilization and stability studies of a lipase from thermophilic Bacillus sp: The effect of process parameters on immobilization of enzyme. *Electron. J. Biotechnol.* **2006**, *9*, 559–565. [CrossRef]
54. Pereira, E.B.; Zanin, G.M.; Castro, H.F. Immobilization and catalytic properties of lipase on chitosan for hydrolysis and esterification reactions. *Braz. J. Chem. Eng.* **2003**, *20*, 343–355. [CrossRef]
55. Lau, S.C.; Lim, H.N.; Basri, M.; Masoumi, H.R.F.; Tajudin, A.A.; Huang, N.M.; Andou, Y. Enhanced biocatalytic esterification with lipase-immobilized chitosan/graphene oxide beads. *PLoS ONE* **2014**, *9*, e104695. [CrossRef] [PubMed]
56. Scherer, R.; Oliveira, J.V.; Pergher, S.; Oliveira, D.D. Screening of supports for immobilization of commercial porcine pancreatic lipase. *Mater. Res.* **2011**, *14*, 483–492. [CrossRef]
57. Shindo, H.; Watanabe, D.; Onaga, T.; Urakawa, M.; Nakahara, O.; Huang, Q. Adsorption, activity, and kinetics of acid phosphatase as influenced by selected oxides and clay minerals. *Soil Sci. Plant Nutr.* **2002**, *48*, 763–767. [CrossRef]
58. Huang, Q.; Liang, W.; Cai, P. Adsorption, desorption and activities of acid phosphatase on various colloidal particles from an Ultisol. *Colloids Surf. B Biointerfaces* **2005**, *45*, 209–214. [CrossRef] [PubMed]
59. Bosley, J.A.; Clayton, J.C. Blueprint for a lipase support: Use of hydrophobic controlled-pore glasses as model systems. *Biotechnol. Bioeng.* **1994**, *43*, 934–938. [CrossRef] [PubMed]
60. Bosley, J. Turning lipases into industrial biocatalysts. *Biochem. Soc. Trans.* **1997**, *25*, 174–178. [CrossRef] [PubMed]
61. Pereira, E.B.; De Castro, H.F.; De Moraes, F.F.; Zanin, G.M. Kinetic studies of lipase from *Candida rugosa*. In *Twenty-Second Symposium on Biotechnology for Fuels and Chemicals*; Humana Press: Totowa, NJ, USA, 2001; pp. 739–752.
62. Persson, M.; Wehtje, E.; Adlercreutz, P. Factors governing the activity of lyophilised and immobilised lipase preparations in organic solvents. *ChemBioChem* **2002**, *3*, 566–571. [CrossRef]
63. Prabu, K.; Natarajan, E. Isolation and FTIR spectroscopy characterization of chitin from local sources. *Adv. Appl. Sci. Res.* **2012**, *3*, 1870–1875.
64. Tai, H.-S.; Lee, J.-Y. Changes in the C-H stretching region of infrared spectra at the cholesteric phase transition. *J. Phys. D Appl. Phys.* **1990**, *23*, 940–944. [CrossRef]

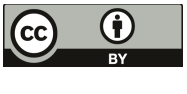

© 2018 by the authors. Licensee MDPI, Basel, Switzerland. This article is an open access article distributed under the terms and conditions of the Creative Commons Attribution (CC BY) license (http://creativecommons.org/licenses/by/4.0/).

catalysts

MDPI

Article

Heterogeneous Biocatalysts Prepared by Immuring Enzymatic Active Components inside Silica Xerogel and Nanocarbons-In-Silica Composites

Galina A. Kovalenko [1,2,*], Larisa V. Perminova [1], Anatoly B. Beklemishev [1] and Valentin N. Parmon [1,2]

[1] Institute of Catalysis, 630090 Novosibirsk, Russia; perminova@catalysis.ru (L.V.P.); beklem@niibch.ru (A.B.B.); parmon@catalysis.ru (V.N.P.)
[2] Department of Chemistry, Novosibirsk State University, 630090 Novosibirsk, Russia
* Correspondence: galina@catalysis.ru; Tel.: +7-383-32-69-743

Received: 22 March 2018; Accepted: 20 April 2018; Published: 26 April 2018

Abstract: Proprietary results on preparation and studies of whole-cell and lysates-based heterogeneous biocatalysts with different enzymatic activity were reviewed. A peculiar method was developed for preparing these biocatalysts by immuring (entrapping) enzymatic active components (EAC) inside silica (SiO_2) xerogel and nanocarbons-in-silica composites. Properties of the multi-component composite biocatalysts such as enzymatic activity and operational stability were compared. The effect of the inclusion of nanocarbons such as nanotubes, nanofibers, and onion-like nanospheres with various texture, nanostructure and dispersion were thoroughly studied. With invertase-active biocatalysts, the direct correlation between an increase in the enzymatic activity of the nanocarbons-in-silica biocatalyst and efficiency of EAC adhesion on nanocarbons was observed. The steady-state invertase activity of the baker yeast lysates-based biocatalysts was determined to increase by a factor of 5–6 after inclusion of the multi-walled carbon nanotubes inside SiO_2-xerogel. With lipase-active biocatalysts, the effect of the included nanocarbons on the biocatalytic properties depended significantly on the reaction type. In interesterification of oil-fat blends, the biocatalysts without any included nanocarbons demonstrated the maximal lipase activity. In esterification of fatty acids with aliphatic alcohols, the activity of the biocatalysts increased by a factor of 1.5–2 after inclusion of the aggregated multi-walled carbon nanotubes (CNTs) inside SiO_2-xerogel. In the low-temperature synthesis of isopentyl esters of butyric (C4:0), capric (C10:0), and srearic (C18:0) fatty acids, the lipase-active composite CNTs-in-silica biocatalysts operated without loss of activity for more than thousand hours.

Keywords: heterogeneous biocatalysts; immuring enzymatic active components; nanocarbons-in-silica composites

1. Introduction

Biocatalysis is of great practical importance and used for deliberate conversion of the one target substrate (S) into a commercially important valuable product (P) through a single enzymatic reaction, with the high chemo-, regio- and enantio-selectivity. Biocatalysis is an interdisciplinary field of knowledge; and many disciplines are needed for its successful implementation: enzymology and biochemistry; molecular biology and gene engineering; industrial microbiology; kinetics and catalysis; transport phenomena (diffusion kinetics); engineering and design of high-capacity reactors. Areas of application of biocatalysis are mainly the food and pharmaceutical industry, less the manufacture of fine and basic chemicals. More than hundred industrial-scale biocatalytic processes using enzymes or whole non-growing microorganisms, of more than 100 kg capacities were described elsewhere [1–5]. Biocatalytic

processes penetrated the large-tonnage food industry, including the production of glucose-fructose syrups and interesterified oil-fat blends.

Heterogeneous biocatalysts prepared by immobilizing enzymatic active substances such as enzymes or whole microorganisms are in the heart of modern biotech processes of "green" chemistry. The main advantage of the immobilization is a combination of the activity and unique selectivity of enzymes, as well as enhancement of their operational stability with the heterogeneity of the biocatalysts applied in the continuous or periodic bioprocesses.

Heterogeneous biocatalytical processes are considered more commercially attractive for large-scale implementation than homogeneous technologies due to considerable simplification and reduction (1.2–1.4 times) of the total production cost. In order to reduce the cost of the heterogeneous biocatalysts and the contribution of this cost into the final product, not purified enzymes isolated from microbial strain-producers but the whole non-growing microbial cells, as well as partially or fully disrupted microorganisms (lysates or sonicates) can be used. Such approach allows the multi-stage enzyme purification to be avoided; this is especially labor- and time-consuming process if the enzyme is intracellular and not extracted during bacteria growth in the nutrient media. In most cases, whole-cell or lysates-based biocatalyst are highly active and stable, probably, due to more friendly environment in the vicinity of native enzyme. The drawback is the relatively low specific enzymatic activity normalized to 1 mg of dry-weight substances; in some cases, it is 1–2 orders of magnitude lower than that per 1 mg of immobilized purified enzyme. However, in majority cases there may take place diffusion limitations to mass transfer of the substrate toward individual enzyme immobilized usually on mesoporous supports, and no more than 10–20% of activity of soluble enzyme is determined after immobilization. Meanwhile, the enzymatic activity of whole or fully disrupted microorganisms is almost completely retained after immobilization; and the whole-cell and lysates-based biocatalysts operate in the kinetic (not diffusion) regime. Therefore, despite significant differences in the initial enzymatic activity, the final activities of the biocatalysts prepared by immobilization of either enzymes or whole microorganisms are of the same order. Indeed, the commercial biocatalyst for glucose isomerization prepared using the purified glucose isomerase are only 2–3 times more active than the biocatalysts prepared using substantially less active (by orders of magnitude) whole *Streptomyces* sp. cells [3].

Inorganic silica-based supports often are used for immobilization of enzymatic active substances; and some commercially available heterogeneous biocatalysts are prepared using silica or silicates. For example, the glucose isomerase-active biocatalyst Optisweet® is prepared by cross-linking of *S. rubiginosus* adsorbed on the commercial silica. Another example is the lipase-active biocatalyst Lipozyme® TL IM prepared by immobilization of recombinant *Thermomyces lanuginosus* lipase on aerosil. Silica-based supports may be divided into the following groups: (i) commercial granulated mesoporous silica and glasses; (ii) natural minerals—clay, diatomite, zeolites; and (iii) modern silica material synthesized using various silanes and sol-gel techniques. Many recent scientific publications are devoted to encapsulation (entrapment) of enzymes into synthetic silica-based supports (iii) [6].

Obviously, the inorganic supports are selected for the heterogeneous biocatalyst preparation due to their availability and relatively low cost as well as high mechanical strength and durability of biocatalysts granules in the reaction media. The main role is to improve noticeably the operating parameters both of down-stream processes using the traditional continuous packed-bed reactors and periodic processes using the batch stirred-tank reactors [7]. Novel types of reactors—a rotor inertial reactor and an immersed vortex reactor, were specially designed for the heterogeneous biocatalysts in order to enhance of the process productivity [8,9].

Immobilization by adsorption/adhesion of enzymatic active substances on inorganic supports has a high commercial potential but some enzymes and microorganisms are poorly fixed on solid surfaces because of their natural peculiarities. For example, *Arthrobacter nicotianae* cells producing glucose isomerase did not adhere on the surfaces of the majority of macroporous inorganic supports such as foam-like ceramics, foamed carbon, vermiculite, corundum, CNFs- or coke-coated minerals; the observed adhesion was less than 0.1 mg of dry-weight cells per 1 g of adsorbent [10]. The maximal

adhesion of *A. nicotianae*, 1.6 mg/g, was observed on the *Sapropel* type macroporous carbon-mineral supports [11]. Thus, the immobilization by adhesion of whole non-growing *A. nicotianae* cells is not suitable for preparing GI-active biocatalysts. Thus, research and development of a universal, simple and inexpensive method of immobilization of various enzymatic active substances, including microorganisms of different taxonomy, was in demand. Entrapping (or immuring, or embedding) inside silica-based matrices seemed the most appropriate and attractive method for preparing highly active and stable heterogeneous biocatalysts. A peculiar universal method of immobilization was first developed for the non-adhered *A. nicotianae* cells and described in papers published in 2009–2010 [12–14].

In this authors' report, the results on study of multi-component heterogeneous biocatalysts prepared by immuring enzymatic active substances inside silica xerogel and nanocarbons-in-silica composites were summarized. Whole non-growing microorganisms, as well as fully disrupted bacteria and yeast cells (named lysates) were used as an active component for preparing biocatalysts with the desired enzyme activity. Advanced carbonic materials such as nanotubes, nanofibers, and nanospheres were examined for inclusion inside SiO_2-based biocatalysts. The properties of whole-cell and lysates-based heterogeneous biocatalysts such as enzymatic activity and operational stability, were systematically and thoroughly investigated as dependent on their compositions, in particular on texture and nanostructure of the nanocarbons included. Multi-component composition of the biocatalysts was optimized individually for the each enzymatic active substance and type of reaction. Biocatalysts with the highest activity and stability were investigated in the corresponding biotransformation processes such as hydrolysis, isomerization, interesterification and esterification.

2. Results and Discussion

2.1. Procedure for Immuring Enzymatic Active Substances Inside Silica Xerogel and Nanocarbons-In-Silica Composites

A peculiar method of preparing whole-cell biocatalysts was first developed for the non-adhered *A. nicotianae* cells in 2008–2009, as mentioned above. The main stages were following: (I) thorough mixing of all components including EAC with silica hydrogel; (II) drying of the mixture; (III) crushing of the dried mixture and fractionation to 0.4–4 mm sized granules of biocatalysts.

Stage I—mixing. Silica hydrogel was prepared by the sol-gel method via slow precipitation of sodium silicate (liquid glass, Na_2SiO_3) with ammonium nitrate at pH 7.5 and 70 °C; the precipitation rate was 300 g $(SiO_2)\cdot L^{-1}\cdot h^{-1}$ [15]. The precipitated SiO_2-hydrogel was washed to neutral pH, pressed and squeezed, then stored as a gelatinous mass in a dense polyethylene bag for several years. The SiO_2-hydrogel humidity was 80–90%. Microbial biomass as EAC for preparing whole-cell biocatalysts was the non-growing microorganisms such as *A. nicotianae*, baker yeasts *Saccharomyces cerevisiae* and recombinant *E. coli* strains producing glucose isomerase or lipase. Biomass as EAC for preparing lysates-based biocatalysts was fully disrupted cells of *S. cerevisiae* and recombinant *E. coli* strain via enzymatic lysis. The biomass humidity was 75–95%. Additional functional components such as activator of enzyme, or moister-holder, or nanocarbons, were mixed with SiO_2-hydrogel in order to improve properties of the final biocatalysts. In the case of GI-active biocatalysts, insoluble cobalt(II) hydroxides were included in order to increase the stability of the biocatalysts. In the case of LIP-active biocatalysts, the maltodextrin was added to prevent quick dehydration of the biocatalysts during operation in anhydrous reaction media. Carbonic material such as nanotubes, nanofibers, onion-like nanospheres, or nanodiamonds were added into SiO_2-hydrogel for possible additional binding EAC by adsorption/adhesion on nanocarbons to decrease their leakage into reaction media and enhance operational stability of the biocatalysts.

Stage II—drying. After stage I, drying of the wet multi-component biocatalyst in a stationary thin bed under ambient conditions (room temperature, air humidity 40–60%) for 1–3 days was carried out. The humidity of dried biocatalysts was 5–15%. Variations in the drying conditions, for example in flowing dry nitrogen at 20–40 °C, did not affect the properties of the biocatalysts. During drying silica hydrogel transformed into SiO_2-xerogel with specific surface area of 200–250 m^2/g.

Stage III—granulation. In the case of GI-active biocatalysts operated in aqueous buffer media, pH 7–8, and at elevated temperature, 60–70 °C, the mixture dried at stage II was pre-ground into a fine powder, then compressed at 50–150 bars and, finally, fractionated for obtaining solid granules 1–4 mm in size suitable for filling into a packed-bed reactor. In the case of LIP-active biocatalysts operated in anhydrous reaction media of oil-fat blends or organic solvents, the mixture dried at stage II was carefully mechanically crushed and fractionated as granules 1–2 mm in size

Accomplishment and finish of I–III stages resulted in the preparation of the multi-component heterogeneous biocatalysts. One can see from the above description that the developed method of immobilization of various EAC was simple in implementation, did not require expensive equipment and aggressive reagents (e.g., silanes). Toxic pollutants and corrosive wastewater was not formed. This method was universal with respect to taxonomy of microorganisms and the chemical nature of the functional components added to the silica hydrogel at stage I. The general regularities for the biocatalysts granules with high mechanical strength were as follows: (1) the content of silica as the main binder was no less than 20 *w*/*w* %; (2) the content of the nanocarbons was no more than 15 *w*/*w* %.

2.2. Selection of the Optimal Compositions of the Biocatalysts

Properties of the prepared multi-component biocatalysts depending on the ratio of all components in SiO_2-xerogel were thoroughly studied. The biocatalysts' composition was optimized by the simultaneous satisfaction of two parameters, namely, (1) the maximal enzymatic activity; and (2) high stability of granules due to its mechanical strength and durability in the reaction media. Durability of the biocatalysts' granules in the aqueous media was estimated visually. For instance, after several hours of periodic operation in hydrolysis, the not optimized whole-cell biocatalysts were converted into an amorphous formless mass; the granules were destroyed. Such simultaneous satisfaction ensured the high operational stability of the biocatalysts in continuous and periodic processes, and, as a result, the high productivity. Optimal compositions of the whole-cell biocatalysts are shown in Table 1. Referring to this Table, the optimal content of microbial biomass depended upon the taxonomy of microorganisms. For example, the optimal contents of *A. nicotianae* and r*E. coli*/xyl biomass inside GI-active biocatalysts were 10–15 *w*/*w* % and 35–40 *w*/*w* %, respectively (Table 1).

Table 1. Optimal compositions of the whole-cell biocatalysts prepared by immuring non-growing microorganisms inside silica xerogel and nanocarbons-in-silica composites.

Microorganism	Biocatalytical Process	Optimal Composition, *w*/*w* %				
		Microbial Biomass	Co_xO_y	Maltodextrin	Carbon Nanotubes	SiO_2
S. cerevisiae	Sucrose inversion	60–80	0	0	5–10	20–30
A. nicotianae	Glucose/fructose isomerization	10–15	20–40	0	0	45–70
r*E. coli*/xyl		35–40	10–40	0	0–5	20–40
r*E. coli*/lip	Tributyrin hydrolysis	35–40	0	0	5–10	50–55
	Interesterification	35–40	0	10–20	0	40–55

The optimal content of included nanocarbons (carbon nanotubes) depended both on the taxonomy of microorganisms and on the type of the enzymatic reaction (Table 1). For example, the properties of GI-active biocatalysts depended slightly upon the presence of included nanocarbons because of weak adhesion of *A. nicotianae* cells as mentioned above. The activity of LIP-active whole-cells biocatalysts in hydrolysis of triglyceride was twice as high when the CNTs were included [16]. On the other hand, in interesterification the activity of nanocarbons-free (without included CNTs) biocatalysts was maximal [17]. It was of interest to elucidate the function of nanocarbons included into the composite biocatalysts. It was first assumed that the main role of nanocarbons was to hold enzymatic active substances inside biocatalysts due to adsorption/adhesion in order to ensure high biocatalytic activity and stability as mentioned above. Indeed, the direct proportion between the adhesion of yeast autolysates and steady-state invertase activity of the biocatalysts was found [18]. The further study of LIP-active composite biocatalysts revealed that hydrophobic substrates such as triglycerides were

adsorbed tightly onto highly hydrophobic nanocarbons and, as a result, essential water was displaced from the vicinity of immobilized lipase; and the activity of the composite biocatalysts decreased. Thus, different functional roles are characteristic of included nanocarbons.

3. Texture of the Biocatalysts

The texture of the whole-cell biocatalysts was studied. The specific surface area ($S_{sp.BET}$) depended both on the taxonomy of the microorganisms and the composition of the multi-component biocatalysts (Table 2). When the content of the microbial biomass was less than 15 *w*/*w* %, the specific surface area of the biocatalysts was 250 m^2/g that was close to $S_{sp.BET}$ of the parent SiO_2-xerogel (without biomass), 260 m^2/g. When the content of the baker yeast biomass increased up to 80 *w*/*w* %, the surface area of these biocatalysts decreased from 250 to 35 m^2/g (Table 2).

Table 2. Textural characteristics of the whole-cell biocatalysts depending on taxonomy of immobilized microorganisms and composition of the prepared multi-component biocatalysts.

Microorganism	Biocatalyst Composition, *w*/*w* % of Dry Substances				$S_{sp.BET}$, m^2/g	V, cm^3/g	D_{pore}, nm
	Biomass	SiO_2	$CoSO_4$	Co_xO_y			
S. cerevisiae	15	85			250	0.6	22
	20	80			220	0.9	15
	60	40			100	0.6	22
	80	20			35	0.4	36
A. nicotianae	15	85	0.06		230	0.9	15
	10	50		40	175	0.6	13
r*E. coli*/xyl	40	40		20	75	0.35	19
r*E. coli*/lip	40	60			90	0.6	25

The porosity of the dried biocatalysts was studied mainly by Hg-intrusion method; and pore size distribution curves were analyzed. Mesopores with diameter 2–50 nm were estimated to occupy more than 50–80% of the total pore volume ($V_{\sum}$), and macropores with diameter more than 50 nm less than 20% of $V_{\sum}$. The absence of micropores smaller than 2–3 nm was indicated by N_2 porosimetry as well. In the whole-cell biocatalysts with low biomass content (10–15 *w*/*w* %), the pore distribution was similar to the pure mesoporous SiO_2-xerogel. It was found that the higher content of baker yeast biomass, the wider distribution of pore sizes and the larger average diameter of pores (Table 2, Figure 1a). SEM-images in Figure 1a (right) demonstrated that macropores could be formed by "shadow" defects of the dried cells entrapped inside SiO_2-xerogel. Almost identical pore size distribution was observed for the glucose isomerase-active biocatalysts prepared by entrapment of *A. nicotianae* and r*E. coli*/xyl cells (Figure 1b). Thus, mesoporous texture was characteristic of the whole-cell biocatalysts (Table 2, Figure 1).

Mesoporous textures were characteristic of the lysate-based biocatalysts as well. Comparative consideration of Figures 1 and 2 led to conclusions about predomination of mesopores, but neither macropores nor microporesare in the pore structure of both biocatalysts. The mesopore diameter distribution was wider in the r*E. coli*/lip lysate-based than in yeast lysates-based biocatalysts (Figure 2). The average pore diameter of the former was about two times as large as that of the latter (Table 3).

The texture of the composite nanocarbons-in-silica biocatalysts was also examined. $S_{sp.BET}$ of the composite lysate-based biocatalysts decreased by a factor of 1.1–1.8 against that of the biocatalysts without nanocarbons (Table 3). For example, after inclusion CNT1s inside yeast autolysate-based biocatalysts $S_{sp.BET}$ decreased insignificantly, whereas pore volume and average diameter increased as follows: $V_{\sum}$ from 0.3 to 0.5 cm^3/g, D_{pore} from 11 to 19 nm. It was shown that the higher specific surface area of included nanocarbon, the greater specific surface area of the composite biocatalyst (Table 3). Hence, the mesoporous texture was characteristic of the lysates-based biocatalysts and their nanocarbons-in-silica composites (Table 3, Figure 2).

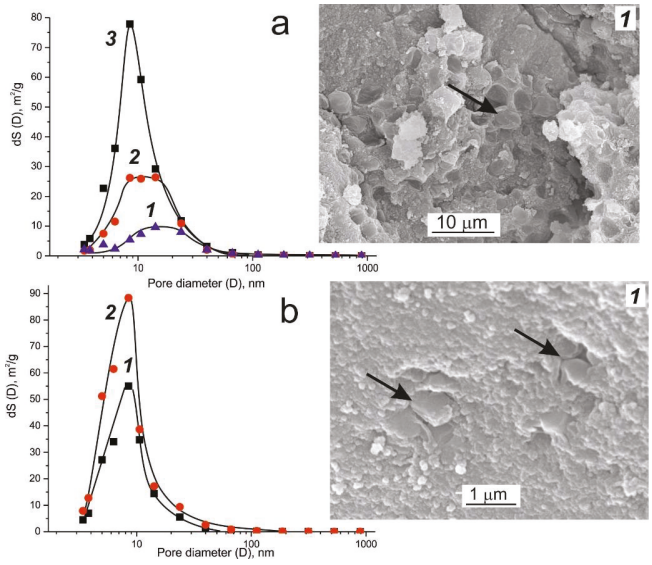

Figure 1. (**Left**) Pore size distributions: (**a**) entrapped *S. cerevisiae* biomass in contents of 20 *w*/*w* % (*1*), 60 *w*/*w* % (2) and 80 *w*/*w* % (*3*); (**b**) entrapped *A. nicotianae* (*1*) and r*E. coli*/xyl (2) biomass in content of 15 *w*/*w* %. (**Right**) SEM images of cleavages of the whole-cell biocatalysts. Arrows indicate microbial whole cells entrapped inside SiO_2-xerogel.

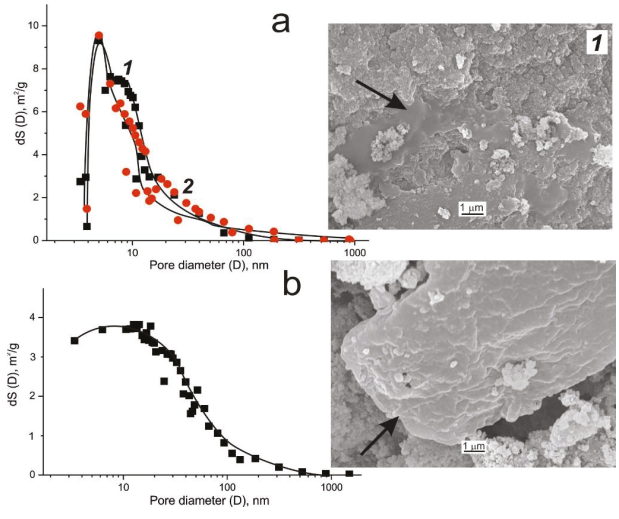

Figure 2. (**Left**) Pore size distribution: (**a**) baker yeast autolysates entrapped inside SiO_2-xerogel without nanocarbon (*1*, ■) and with CNT1s (*2*, ●), (**b**) r*E. coli*/lip lysates entrapped inside SiO_2-xerogel without nanocarbon. (**Right**) SEM images of cleavages of the lysate-based biocatalysts. Arrows indicate the smooth area corresponding to lysates entrapped in SiO_2-xerogel.

Table 3. Textural characteristic of composite lysate-based biocatalysts depending on the type of included nanocarbons and enzymatic activity of prepared biocatalyst.

Type of Included Nanocarbon * ($S_{sp.BET}$ of Nanocarbons)	Baker Yeast Autolysate-Based Biocatalysts		r*E. coli*/lip Lysate-Based Biocatalysts	
	$S_{sp.BET}$, m^2/g	D_{pore}, nm	$S_{sp.BET}$, m^2/g	D_{pore}, nm
Without nanocarbons	110	11	105	31
Carbon nanotubes CNT1 (320 m^2/g)	105	19	90	25
Carbon nanofibers CNF (160 m^2/g)	60	12		
Carbon nanospheres CNS1 (485 m^2/g)	95	11	110	22
Nanodiamond ND (325 m^2/g)	80	14		

* Content of nanocarbons inside biocatalysts was 15 *w*/*w* %.

The results obtained lead to conclude about mesoporous texture of all the prepared biocatalysts. Particular attention was paid to the macrokinetics of biocatalytic heterogeneous processes under study. The conditions for biocatalyst operation in the kinetic (not diffusion) regime were chosen experimentally. The mesoporous texture of the biocatalysts makes the mass transfer of substrates toward entrapped enzymatic active component free of internal diffusion limitations [12,13,18,19].

The single-enzymatic activity and operational stability of the prepared multi-component biocatalysts and their properties for the process of substrate conversion into valuable product are discussed below.

4. Heterogeneous Whole-Cell and Lysates-Based Biocatalysts

4.1. Glucose Isomerase-Active Biocatalyst

The whole-cell biocatalysts were prepared by immuring native *A. nicotianae* and recombinant r*E. coli*/xyl non-growing bacteria cells producing thermostable glucose isomerase intracellularly. The high thermostability of microbial GI provided a linear increase in the enzymatic activity of the biocatalysts with temperature (T) in the range of 55 to 85 °C with the T-coefficient equal to 1.3–1.5; the inactivation half-life time ($t_{\frac{1}{2}}$) of the biocatalysts heated at 80 °C in the buffer solution, pH 7.8, was equal to 6–7 h [12].

As mentioned above, the optimization of composition of the GI-active biocatalyst has to provide the highest enzymatic activity along with the high mechanical strength and durability of the granules during operation in buffer, pH 7–8, at 60–75 °C in a flow packed-bed reactor. Referring to Table 1, the optimal content of *A. nicotianae* biomass varied only in a relatively narrow range from 10 to 15 *w*/*w* %. When the biomass content was more than 15 *w*/*w* %, the mechanical strength of the biocatalyst fell down quickly; and the granules were destructed and transformed into an amorphous paste within 1–2 h of the operation.

It is of common knowledge that Mg(II) and Co(II) ions activate glucose isomerase and enhance the stability of this enzyme. Various Co(II)-containing component were included into whole-cell biocatalysts. With a soluble Co(II) component, e.g., $CoSO_4$, the biocatalysts' granules had relatively low durability, and the half-life times ($t_{\frac{1}{2}}$) of the biocatalysts were no longer than 20–24 h in buffer at 75 °C. Therefore, insoluble Co(II) compounds were studied as a functional component of the GI-active biocatalysts. Freshly prepared Co(II) hydroxide was precipitated by adding gradually ammonia solution (NH_4OH) to cobalt nitrate ($Co(NO_3)_2$). The intensely blue colored precipitate identified as unstable β-$Co(OH)_2$ was dried and transformed to grey-green $Co_3O_4 \cdot nH_2O$ and then to $CoO/Co_3O_4(Co_xO_y)$. Granules of the dried biocatalysts containing insoluble Co_xO_y turned color from grey-green to pink during operation under the reaction conditions (pH 7.8, 70–75 °C). The pink color indicated predomination of stable cobalt hydroxide α-$Co(OH)_2$ species inside the biocatalysts. Inclusion of insoluble Co_xO_y (not soluble $CoSO_4$) resulted in 1.5–1.6 times increase in the glucose isomerase activity of the biocatalysts, as well as in an increase in durability of the granules in the

reaction medium and, therefore, in enhancement of the operational stability under studied conditions. The optimal content of Co_xO_y was 20–40 *w*/*v* % (Table 2); the composition of GI-active whole-cell biocatalysts was covered by a patent [20].

The commercial technology of glucose isomerization (but not the process using the prepared here biocatalysts containing insoluble Co_xO_y) needs addition of Co^{2+} ions (1 mM) to the glucose solution. We analyzed the samples of the produced glucose-fructose syrup at the outlet of packed-bed reactor to show that the Co and Si concentrations in the product (syrup) were practically constant during 816 h operation at 65 ± 5 °C and equal to 1–2 μg·mL^{-1} (max. 0.03 mM Co^{2+}) and 16–36 μg·mL^{-1}, respectively. Thus, the usage of the prepared GI-active biocatalyst for monosaccharide isomerization allowed us to decrease the Co^{2+} concentration in the final product by a factor of 30–70.

The glucose isomerase activity of the biocatalysts prepared by immuring recombinant strain-producer r*E. coli*/xyl was ten times as high as that for entrapped *A. nicotianae*(100–500 U·g^{-1} vs. 10–30 U·g^{-1}) [21]. Referring to Figure 3, the stability of the r*E. coli*/xyl whole-cell biocatalysts was two-fold higher than for entrapped *A. nicotianae*; the half-life time was found to be more than 1200 h under studied conditions [13,21].

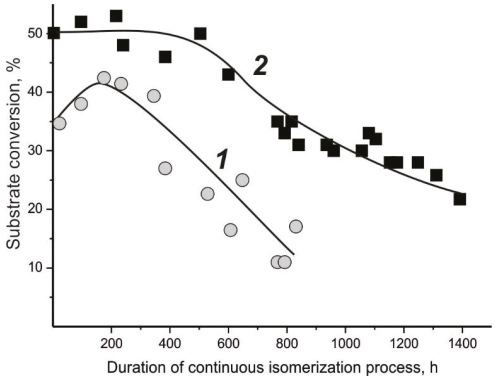

Figure 3. Dependence of substrate conversion at the outlet of column packed-bed reactor on the duration of continuous isomerization of fructose by the *A. nicotianae* (*1*) and r*E. coli*/xyl (*2*) whole-cell biocatalyst. Reaction conditions: 65 °C, 3 M fructose, 0.02 M phosphate buffer pH 7.8 and 7.0 for *A. nicotianae* and r*E. coli*/xyl respectively, 1 mM Mg^{2+}. Contact time was 5.5 h.

The composite nanocarbons-in-silica whole-cell biocatalysts were prepared using r*E. coli*/xyl cells, Co_xO_y component and various types of nanocarbons such as CNTs, CNFs, CNSs and nanodiamond. The bulk morphology of these biocatalysts was examined with a scanning electron microscope (Figure 4).

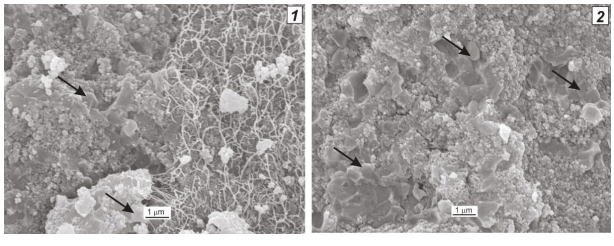

Figure 4. SEM images of cleavages of the whole-cell biocatalysts prepared by immuring r*E. coli*/xyl cells inside SiO_2-xerogel with included CNTs (*1*) and CNFs (*2*). Arrows indicate entrapped bacteria.

An inconsiderable effect of inclusions of nanocarbons on the activity and stability of the GI-active biocatalysts was observed and described in [18]. The steady-state glucose isomerase activity was ~100 $U \cdot g^{-1}$ for the biocatalysts except nanocarbons-containing composite biocatalysts which were only 10–15% more active. The main reason was found to be the weak adhesion of GI-active substances on nanocarbons and leakage of enzymatic active component from biocatalysts [18]. The dried biocatalysts were cross-linked with glutaric dialdehyde (less than 1 v/v%); the steady-state activity increased by a factor 1.5 in comparison with the non-crosslinked biocatalysts, and the enhanced stability was determined. These biocatalysts retained fully their initial activity during 28 periodic reaction cycles under the reaction conditions (pH 7.0, 70 °C) [18].

4.2. Invertase-Active Biocatalyst

Analysis of the literature showed that more than a quarter of studies on immobilization of non-growing *S. cerevisiae (*baker yeasts) cells were devoted to only single, namely invertase activity for hydrolysis of disaccharide (sucrose) to equimolar mixture of monosaccharides (glucose and fructose), the so-called invert syrup. The invert syrup as a sweetener is valuable and marketable product of food industry. A majority of INV-active heterogeneous biocatalysts were prepared by immobilization of whole cells of baker yeasts [22–26]; the yeast autolysates and purified intracellular invertase as an EAC were described rarely. For example, the baker yeasts were immobilized by adhesion to a composite material, jute fabric coated by polyethyleneimine; and this biocatalyst operated in a column reactor without loss in efficiency to hydrolyze concentrated (60–80%) sucrose syrups for 45 days at 45 °C [22]. The most active and stable biocatalyst described in literature [24] was prepared by mutual bonding of native baker yeasts with polyethyleneimine and glutaraldehyde. The specific invertase activity of this biocatalyst was 300–1500 $U \cdot g^{-1}$; the half-life of the biocatalyst was 500–1000 h (pH 4.6, 60–75 °C). The total biocatalyst productivity over the period of its lifetime was 2–10 tons of hydrolyzed sucrose per 1 kg of the biocatalyst [24].

Silica gel was first described for encapsulation (inclusion) of *S. cerevisiae* cells into thin SiO_2-layers deposited on glass sheets [26]. The precursors of silica gel were various silanes (not liquid glass, as described here); the hydrolysis and polycondensation of silanes occurred after addition of aqueous solution of enzymatic active substances. In most cases silanes and products of their hydrolysis were toxic reagents and inhibited enzymes. For example, the specific invertase activity was 3.6 times decreased after inclusion of *S. cerevisiae* cells into SiO_2-gel formed during polycondensation of tetra-ethoxysilane [26].

In this report, neutral and inert SiO_2-xerogel obtained without any toxic reagents was found to be friendlier matrix for preparing highly active biocatalysts; the invertase activity reached 500–700 $U \cdot g^{-1}$ that was comparable in magnitude with the best results described in [24]. It was found that the invertase activity of the whole-cell biocatalysts depended linearly on the baker yeast content from 5 to 80 w/w %. Exactly, due to high content of non-growing *S. cerevisiae* cells inside biocatalysts their activities were high. The process of sucrose inversion was carried out both in periodic and continuous mode in stirred-tank and packed-bed reactors respectively. The full conversion of 50 w/v % sucrose into invert syrup was reached for less than 7 h at 50 °C; the biocatalyst operated without loss of activity during 25–30 reaction cycles. In the continuous process of sucrose inversion, the half-life time of the whole-cell biocatalyst was more than 200 h (pH 4.6, 50 °C) [27].

Yeast autolysates are fully disrupted cells via lysis by own intracellular enzymes such as lysozyme, and this EAC were used for preparing invertase-active biocatalysts. Earlier the biocatalysts were prepared by adhesion of baker yeast autolysates on natural materials such as expanded clay, Sapropels, and lignin [28]. It was found that macroporous Sapropels were the most efficient supports for adhesion of yeast autolysates, but the steady-state activity of such biocatalysts was comparatively small (avg. 60 $U \cdot g^{-1}$) [11,28]. Here, the baker yeast autolysates were used as an active component of the biocatalysts prepared by immuring inside silica xerogel and nanocarbons-in-silica composites. It was shown that the invertase activity of these lysate-based biocatalysts was 2–3 times higher than for the whole-cells

biocatalysts with similar compositions. The interior morphology of the composite nanocarbons-in-silica lysate-based biocatalysts examined with a scanning electron microscope is shown in Figure 5.

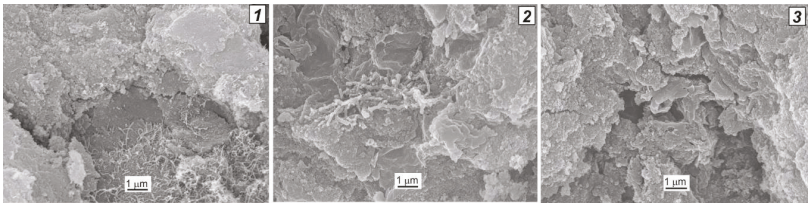

Figure 5. SEM images of cleavages of the biocatalysts prepared by immuring baker yeast autolysates inside nanocarbons-in-silica composites: *1*—CNT1s, *2*—CNFs, *3*—CNSs. Smooth areas corresponded to entrapped autolysates.

Pronounced positive effect on the properties of autolysate-based biocatalyst was observed with all types of nanocarbon included inside SiO_2-xerogel (Figure 6); the maximal steady-state invertase activity was more than 3000 $U \cdot g^{-1}$ (vs. 60 $U \cdot g^{-1}$ for adhered autolysates). A correlation between adhesion ability of yeast autolysates on nanocarbons and properties of composite biocatalysts was found: the more efficient adhesion of autolysates, the higher was steady-state activity [18]. For example, an increase in the content of included CNFs up to five-fold (from 5% to 25%) provided an increase in the steady-state activity of the biocatalysts by a factor of 1.8. The values of tight adhesion of yeast autolysates on CNTs and CNFs were determined as 5 and 2 mg/g respectively. As one can see in Figure 6, the steady-state activities of composite biocatalysts such as CNTs-in-silica and CNFs-in-silica were proportional to their capability of adhering autolysates. The values of steady-state activities of composite lysate-based biocatalysts were 2–6 times higher than that of nanocarbons-free biocatalysts based on SiO_2–xerogel (Figure 6). With the composite biocatalysts, $t_{1/2}$ in continuous sucrose inversion process was 200–500 h (pH 4.6, 50 °C).

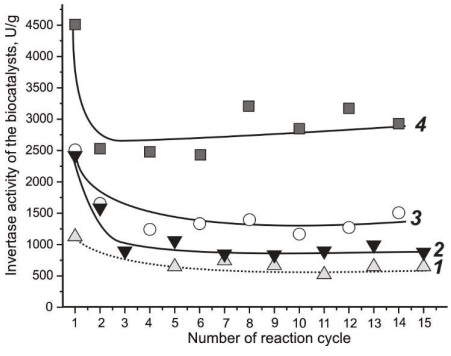

Figure 6. The invertase activity of lysate-based biocatalyst in dependence of type of nanocarbon included and numbers of reaction cycles of sucrose inversion: ***1***—without nanocarbon (dotted line), ***2***—CNFs, ***3***—CNS1s, ***4***—CNT1s. Reaction conditions: 50 °C, 2 M sucrose, 0.02 M acetate buffer pH 4.6.

4.3. Lipase-Active Biocatalyst

Much attention is given now to the application of lipases in industry. Microbial lipases are a powerful tool for catalytic hydrolytic breakdown of fats and oils followed by the formation of free fatty acids, diglycerides, monoglycerides, and glycerol. The reverse synthetic reactions such as esterification, acidolysis, alcoholysis, and aminolysis of fatty acids, as well as triglyceride interesterification are of the most interest [1–5]. The development of the commercially attractive inexpensive, highly active

and stable heterogeneous biocatalysts is still an exciting goal. A number of reviews [29–35] deal with methods for immobilization of lipases, as well as properties of the prepared lipase-active biocatalysts, such as enzyme activity, stability, regio- and enantio-selectivity.

Extracellular production of lipases is characteristic of a majority of native microorganisms but recombinant *E. coli* strains usually synthesize lipase intracellularly. The authoring constructed r*E. coli*/lip strain was found to produce recombinant *T. lanuginosus* lipase in the amount of ~30–40% of the total cell protein [36]. The study of recombinant lipase localization inside r*E. coli*/lip cells showed that more than 70% of the lipase activity was localized in the intracellular cytoplasm, and only small values of activity in debris and inclusion bodies [36]. The specific lipase activity of suspended r*E. coli*/lip whole cells was rather low (2.5 U per 1 mg of dry substances). Partial disruption of cells via drying and thawing led to ~20-fold increase in the observed activity (45 U·mg^{-1}), whereas the full disruption of cells via enzymatic lysis and sonification increased the lipase activity by two orders of magnitude (210 U·mg^{-1}) [19,36].

The partially disrupted r*E. coli*/lip cells, and r*E. coli*/lip lysates, and recombinant $His_6\times$lipase purified by affinity chromatography were studied as EAC for preparing lipase-active heterogeneous biocatalysts based on SiO_2-xerogel and nanocarbon-in-silica composites. Interior morphology of the composite lysate-based biocatalysts was examined with electron-scanning microscope (Figure 7).

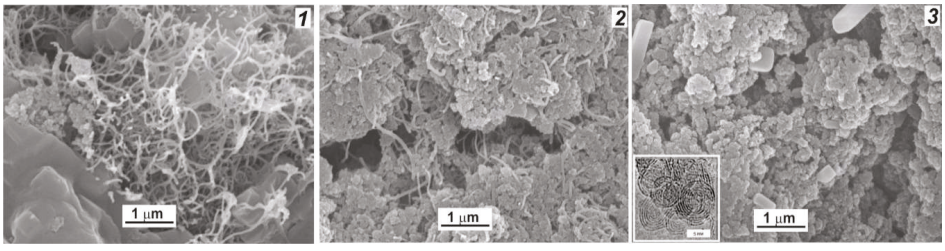

Figure 7. SEM images of cleavages of the biocatalysts prepared by immuring r*E. coli*/lip lysates inside nanocarbons-in-silica composites: *1*—CNT1s, *2*—CNT2s, *3*—CNSs. Smooth areas correspond to entrapped lysates. The nanostructure of CNSs (in insert *3*) was examined with high-resolution transmission microscope.

The lysate-based biocatalysts were found to be the most active, they being 4–8 and 2–16 times more active than the whole-cell biocatalysts and the immobilized recombinant lipase, respectively (Table 4). Referring to this Table, the hydrolytic activity decreased to one fifth upon supersonic dispersion of 100–150 μm nanocarbon aggregates into separate primary nanotubes distributed more uniformly inside SiO_2-xerogel. This phenomenon was described elsewhere [16]. In addition, the reasons for decrease in activity of immobilized lipase associated with peculiarities of lipase molecular structure and high hydrophobicity of nanocarbons were discussed. As illustrated in the scheme [16], the active site of adsorbed lipase may be blocked by hydrophobic surface of nanotubes or nanospheres; the apparent inactivation of the biocatalysts was observed, especially pronounced for uniformly distributed nanotubes. The important role of mutual correspondence of the hydrophobic-hydrophilic natures of immobilized enzyme and immobilizing support was discussed firstly in 1988 [37] and confirmed in previous [38,39] and current studies. As a result of tuning properties of inorganic supports including surface morphology toward immobilized enzymes (alcohol dehydrogenase, glucoamylase and invertase), it was found that the synthesis of CNFs on the surface of the aluminosilicate honeycomb monolith and ceramic foam allowed preparing the highly active and stable biocatalysts due to mesoporous texture and optimal hydrophilic-hydrophobic properties of the surface carbons [39].

Table 4. Hydrolytic activities (in $U \cdot g^{-1}$) of prepared lipase-active biocatalysts depending on the origin of enzymatic active component and nanocarbons included inside silica xerogel.

Type of Nanocarbon Included in Content of 10 *w/v* %	Enzymatic Active Component		
	Partially Disrupted r*E. coli*/lip Cells	Lysates of r*E. coli*/lip Cells	$His_6 \times$ Lipase Purified *
Without nanocarbons	210	870	510
Multi-walled CNT1s (5–11 nm in diameter) *aggregated*	220	1050	120
Multi-walled CNT1s (5–11 nm in diameter) *dispergated*	50	400	25
Multi-walled CNT2s (20–22 nm in diameter) *aggregated*	250	870	260
Carbon onion-like nanospheres (5–6 nm in diameter) *aggregated*	105	710	

* Recombinant lipase was purified by affinity chromatography on Ni-NTA Sepharose.

Below is authors' report of the most effective r*E. coli*/lip lysate-based biocatalysts prepared and studied in the following reactions: (1) hydrolysis of tributyrin [16,19]; (2) interesterification of oil-fat blends [16,19,36,40]; (3) interesterification of sun flower oil with ethyl acetate [40,41]; (4) esterification of fatty acid with aliphatic alcohols [36,42]. It was found that the rates of reactions were considerably in more than 500 times higher in aqueous buffered media (hydrolysis) than in anhydrous organic solvents (esterification). However, low-temperature enzymatic synthesis of esters is of increasing importance as an alternative to organic synthesis of these valuable products to be applied in perfume and cosmetic industries as odorants, emollients, and inert surfactants.

The effect of inclusion of nanocarbons into lysate-based LIP-active biocatalysts depended on the type of catalyzed reaction. The rates of reactions with participation/formation of water (hydrolysis/esterification, respectively) were maximal when r*E. coli*/lip lysates were entrapped inside CNTs-in-silica composites (Table 5). The rates of reactions with triglycerides (interesterification in anhydrous media) were maximal when r*E. coli*/lip lysates were entrapped inside nanocarbons-free SiO_2-xerogel (Table 5).

Table 5. Relative activity * of r*E. coli*/lip lysate-based biocatalysts in various reactions.

Type of Aggregated Nanocarbon Included **	The Type of Reaction (Reaction Media)			
	Hydrolysis of Emulsified Tributyrin (Aqueous)	Interesterification in Oil-Fat Blends (Anhydrous)	Interesterification of Oil with Ethyl Acetate (in Hexane)	Esterification of Capric Acid with Isopentanol (in Hexane with Diethyl Ether)
Without nanocarbons	0.9	1.0	1.0	0.3
CNT1	1.0	0.9	0.8	
CNT2	0.8	0.9	1.0	1.0
CNS1	0.7	0.5	0.4	
CNS2	0.9		0.8	0.5

* The maximum activity was taken as 1.0; ** content of nanocarbons inside biocatalysts was 10 *w/w* %.

Operational stability of the lipase-active biocatalysts also depended on the type of catalyzed reaction. In periodic interesterification of oil-fat blends in a stirred-tank reactor, the stability of all lysates-based biocatalysts was low enough; the half-life time was no longer than 10–15 h at 70 °C [19]. In continuous/periodic interesterification of oil-fat blends in a lab-scale packed-bed reactor, the stability of the lysates-based biocatalysts was higher at the half-life time longer than 70 h at 70–75 °C (Figure 8a). In periodic interesterification of sunflower or linseed oils with methyl- or ethyl acetate in a stirred-tank reactor, the stability of the biocatalysts was even higher at the half-life time longer than 600–700 h at 40 °C (Figure 8b). Generally, the highest operational stability of the composite biocatalysts was

observed when aggregated CNT2s (but not dispersed CNTs and CNSs) were used for the biocatalyst preparation (Figure 8b).

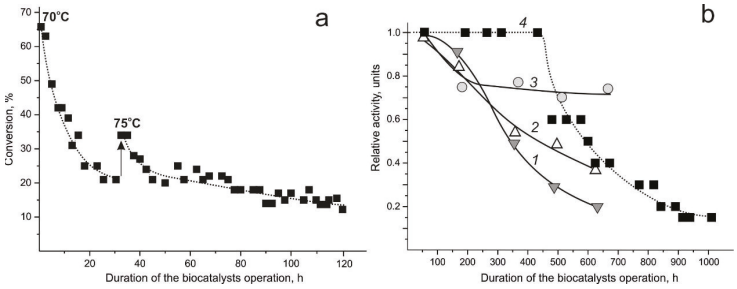

Figure 8. Operational stability of r*E. coli*/lip lysate-based biocatalysts in the processes: (**a**) Continuous/periodic interesterification of oil-fat blends at 70–75 °C; the biocatalyst composition, in *w*/*w* %: r*E. coli*/lip lysate—37–38, maltodextrin—10, SiO_2—till 100. (**b**) Periodic interesterification of sunflower oils with ethyl acetate at 40 °C; the biocatalyst composition, in *w*/*w* %: r*E. coli*/lip lysate—25–28, maltodextrin—10, nanocabons—10, ***1***—CNSs, ***2***—CNT1s, ***3***—CNT2s, ***4***—without nanocarbon (dotted line), SiO_2—till 100.

One of the reasons for inactivation of the lipase-active biocatalysts during long-term interesterification in anhydrous media was the dehydration of biocatalysts because of replacement of essential water from the vicinity of immobilized lipase by highly hydrophobic substrate—oil triglycerides. In periodic esterification of fatty acids with isopentanol, the stability of all prepared biocatalysts was extremely high; the biocatalysts operated without the activity loss longer than several hundred hours at 40 °C [36,42] due to accumulation of essential water as a product of this reaction inside biocatalysts.

The study of selectivity of the lipase-active heterogeneous biocatalysts in esterification toward the structure of substrates—acid and alcohol—was started by the authors; the initial results were described in [36,43]. The rate of esterificarion was higher for fatty acids with 10 and 18 carbon atoms in the molecule than for butyric acid with 4 carbon atoms (Figure 9), whereas cyclic and aromatic acids reacted at the lowest rates close to zero. Inclusion of carbon nanotubes provided the two-fold increase in activity of the biocatalysts and some changes of selectivity (Figure 9). The systematic study on selective esterification by immobilized recombinant lipase is in progress now, and possible modulation of the selectivity via biocatalysts engineering is of great interest.

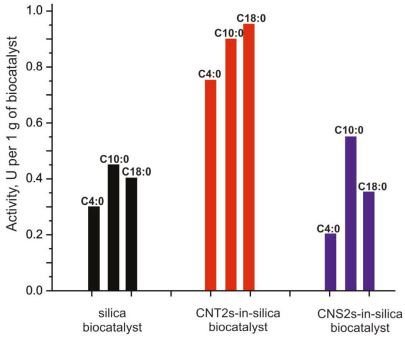

Figure 9. Activity of r*E. coli*/lip lysate-based biocatalysts and the nanocarbons-in-silica composites in reaction of esterification of fatty acids such as butyric C4:0, capric C10:0 and stearic C18:0 with isopentanol. Reaction conditions: 20 °C, 0.1 M fatty acid, 0.2 M isopentanol, hexane and diethyl ether in ratio 1:1. Reactions were performed in six replicates.

5. Materials and Methods

5.1. Enzymatic Active Substances

5.1.1. Glucose Isomerase Active Component of the Biocatalysts

Bacteria strains producing glucose isomerase such as *Arthrobacter nicotianae* deposited in the collection of non-pathogenic microorganisms and recombinant strain-producer *E. coli* BL21(DE3)/pET24bxylA (designated as r*E. coli*/xyl) were provided by colleagues from the Institute of Microbiology (Minsk, Belarus) and described in a number of papers [12,13,20,21]. *A. nicotianae* biomass was harvested by centrifugation at 10,000 g for 15 min. The r*E. coli*/xyl biomass was collected at the end of the late logarithmic phase or at the beginning of the steady-state phase by centrifugation at 5000 rpm for 15 min. The humidity of the biomass was 75–80 *w*/*w* %.

The specific activities of *A. nicotianae* cells in buffered suspension, pH 7.8 were avg. 150 and 550 U·per 1 g of dry cells at 60 and 75 °C, respectively. The glucose isomerase activity in r*E. coli*/xyl cell suspension was avg. 3000 U per 1 g of dry cells at 70 °C.

The glucose isomerase activity were measured in the medium of 0.02 M phosphate buffer pH 7.0 (for r*E. coli*/xyl) and 7.8 (for *A. nicotianae*) at 60–75 °C. Fructose in concentration of 2–3 M was used as a substrate. In order to determine the enzymatic activity in cell suspensions, ions of Mg^{2+} and Co^{2+} as 1 mM sulfate salt solutions were added to the reaction medium. No Co^{2+} ions were added to the reaction medium for measuring the activity of heterogeneous biocatalysts containing insoluble Co_xO_y. The concentration of glucose produced via fructose isomerization was determined using HPLC [13] and spectrophotometric techniques with glucose oxidase (GO) as a selective reagent for glucose, for example, using procedure described in [44] with GO, KJ and $NaMoO_4$.

5.1.2. Invertase Active Component of the Biocatalysts

Commercial *Saccharomyces cerevisiae* baker yeasts was suspended in 0.02 M acetate buffer pH 4.6 and used for preparing whole-cell biocatalysts. The invertase activity in cell suspension was avg. 6000 U per 1 g of dry cells at 50 °C.

Yeast autolysates were obtained by autolysis of commercial baker yeast under continuous stirring at 50 ± 1 °C for 18–22 h. The autolyzed biomass was collected by centrifugation at 5000 rpm for 30 min, the supernatant was withdrawn, and the sediment was then re-suspended in 0.15 M KCl and washed. This procedure was three or four times repeated until the supernatant became transparent and colorless. The beige-colored paste-like sediment of yeast autolysates contained 20–22 *w*/*w* % of dry substances (the humidity was 78–80 *w*/*w* %) was used for biocatalysts preparation.

The invertase activity was measured in 0.02 M acetate buffer pH 4.6 at 50 °C using 0.6 M sucrose as a substrate. The analysis of glucose as a product of sucrose inversion was done with glucose oxidase [44]. The invertase activity in suspension was avg. 30,000 U per 1 g of dry autolysates at 50 °C.

5.1.3. Lipase Active Component of the Biocatalysts

The recombinant *E. coli* BL21(DE3) strain producing thermostable lipase (denoted as r*E. coli*/lip) was constructed by cloning chemically synthesized gene of mature *Thermomyces lanuginosus* lipase in the pJExpress 401 expression vector under the control of the bacteriophage T5 promoter as described in [16,19,36]. When the cultivation of the recombinant strain-producer was completed, the r*E. coli*/lip biomass was harvested by centrifugation at 3000 g for 20 min. The sediment was re-suspended in 10 mM phosphate-buffered saline pH 8.0. The lipase activity was measured in the reaction of hydrolysis of 0.2 M tributyrin in 0.02 M phosphate buffer pH 7.0 at 20 °C. Glycerol (1.2 M) and Gum arabic (0.6 *w*/*v* %) were added to reaction medium for emulsifying tributyrin. The lipase activity of suspended r*E. coli*/lip cells was avg. 50 U per 1 g of dry cells.

Lysates of r*E. coli*/lip cells were obtained as follows. The harvested recombinant cells were suspended and incubated with 1–2 mg·mL^{-1} lysozyme in ice for 30 min, then sonicated in an ultrasonic

disintegrator at the maximum power of 300 W for 20–30 s. Then, $MgCl_2$, DNAase and RNAase A solutions were added to sonicated cells at the final concentrations of 5 mM, 10 μg·mL^{-1} and 50 μg·mL^{-1}, respectively. This mixture was placed in a water bath and incubated at 20 °C for 10 min, then sonicated again seven times for 15–20 s in ice in the ultrasonic disintegrator at the maximum power. The suspension of twice sonicated cells was centrifuged, and the supernatant (named r*E. coli*/lip lysates) was collected and used for preparation of LIP-active biocatalysts. The hydrolytic lipase activity of r*E. coli*/lip lysates in suspension was avg. 150 U per 1 g of dry lysates.

The relative experimental error of measuring enzymatic activity was no more than 15%.

5.2. Silica Hydrogel and Nanocarbon Materials

Silica hydrogel was obtained via coagel formation in continuous sol–gel procedure using sodium silicate (liquid glass, Na_2SiO_3) reacting with ammonium nitrate at pH 7.5 and 70 °C [15]. The hydrogel humidity was 80–90 *w*/*w* %. Drying of silica hydrogel at 105–120 °C resulted in the formation of mesoporous silica xerogel (SiO_2–xerogel) with the specific surface area ($S_{sp.BET}$) equal to 260 m^2/g, total pore volume (V_Σ) 0.5–0.6 cm^3/g and average pore diameter (D_{pore}) 20–22 nm.

Fine powders of nanostructured carbons were used for preparing multi-component composite biocatalysts. Texture characteristic of the nanocarbons are listed in Table 6. Multi-walled carbon nanotubes (CNTs) were synthesized by CVD ethylene decomposition over supported Fe,Co-catalyst at 670 °C [45]. Carbon nanospheres with onion-like structure (CNSs) were synthesized by high temperature annealing of nanodiamonds in vacuum at 1600 °C [46,47]. Nanodiamonds (NDs) of 4–6 nm in size were produced in Biysk, Russia and contained 85–91 *w*/*w* % of carbon. The primary particles of CNTs, CNSs and NDs were associated to 100–200 nm aggregates; these aggregates were dispersed using an ultrasonic disintegrator as follows. The aggregated nanocarbons, in particular CNTs, were mixed with SiO_2-hydrogel and distilled water, then treated with ultrasound at 22 kHz-frequency and 300 W power for 30 min in a water-cooled vessel.

Table 6. Texture characteristic of nanocarbons.

Type of Nanocarbon	Diameter of Primary Particle, nm	$S_{sp.BET}$, m^2/g
CNT1	9–11	320
CNT2	20–22	140
CNF	20–60	160
CNS1	5–6	485
CNS2	8–10	250
ND	4–6	325

Carbon nanofibers (CNFs) with the "fishbone" structure were synthesized by methane pyrolysis over supported Ni-catalysts [48,49]. Bulk CNFs granules were grinded to fine powder in a mortar prior to the preparation of biocatalysts.

5.3. Biocatalytic Processes of Substrate Conversion

5.3.1. Substrates and Reagents

Tributyrin and butyric acid were purchased from MP Biomedicals, LLC. Gum Arabic was purchased from Fluka. Sucrose, fructose and vegetable oils such as sunflower and linseed oils were purchase in a local food-shop. Hexane, diethyl ether, methyl and ethyl acetate, isopentanol, glycerol, and organic acids including saturated fatty acids (capric C10:0 and stearic C18:0) were produced in Russia. All the reagents and solvents used were of analytical grade.

5.3.2. Monosaccharide (Glucose, Fructose) Isomerization

The continuous process of isomerization of monosaccharides (glucose and fructose) was carried out in a plug flow packed-bed reactor. The reactor was filled with the prepared GI-active biocatalyst granules of 1–4 mm in size and inert filler, such as glass balls of 2 mm in diameter, their volume ratio being 1:1. The use of the filler reduced significantly the pressure drop of the bed. The reactor was placed into a thermostat at 65 ± 5 °C, and 3 M monosaccharide solution was run through the bed downward at the flow rate of 0.02 mL·min^{-1}. Aliquots were taken at the reactor outlet in regular intervals (once per day) and glucose concentrations were analyzed. The conversion (in %) of the substrate was calculated, and half-life time ($t_{\frac{1}{2}}$) was determined.

5.3.3. Sucrose Inversion

The activity of the invertase-active biocatalysts was measured using a circulation set-up consisting of a differential gradientless column reactor with a thin bed of the prepared biocatalyst (0.1–0.5 g). The thermostat was maintained at given temperature (50–60 °C) of the reaction medium and in the biocatalyst bed. A peristaltic pump provided circulation of the substrate solution through the biocatalyst bed at the flow rate 1–35 mL·min^{-1}. The duration of one reaction cycle ranged from 2 to 8 h. After finishing the reaction cycle, the reaction medium was removed, and the biocatalyst was rinsed with distilled water and buffer. The steady-state activity of the biocatalyst was determined after conditioning biocatalysts as described elsewhere [18].

5.3.4. Interesterification of Oil-Fat Blends

The interesterification of oil-fat blend was carried out in periodic mode in a stirred-tank reactor and in a lab-scale set-up comprising a flow packed-bed bioreactor at 60–75 °C [16,17]. Initial blends and interesterified (final) products were analyzed using a pulsed NMR spectrometer. The conversion (x, %) was calculated from the decrease in the solid fat content measured at 35 °C in final products in comparison with initial oil-fat blends. The initial blends were prepared by mixing vegetable (soybean, sunflower or oleic) oils with heated fully hydrogenated one in proportion of 2–3 parts of oil to 1 part of hydrogenate. The interesterification in the lab-scale set-up was performed as follows. A stainless still column reactor was filled with 0.5–2 mm granules of the r*E. coli*/lip lysate-based biocatalyst of mixing uniformly with the inert filler such as 1–2 mm granules of commercial silica at the volume ratio of 3:1. Samples for analysis were collected every 3 h. The temperature in the reservoir with substrate and in reactor was kept at 70–75 °C. Initial oil-fat blends were pumped through the fixed bed at the flow rate of 0.12 mL·min^{-1} for 8–10 h. Then the flow of blends was stopped and the reactor was cooled down to 20–22 °C. After 14–15 h storage, the next reaction cycle was started by heating the reservoir and the reactor up to 70–75 °C. The biocatalyst was tested in this regime for 120 h.

5.3.5. Interesterification of Vegetable Oil with Ethyl Acetate

The interesterification of vegetable oil with methyl- or ethyl acetate was carried out in periodic mode in a stirred-tank reactor on a shaker at 120–150 rpm and 40 °C. The reaction medium had the following composition: 0.1 M oil, 2.3–2.5 M ethyl acetate, solvent—*n*-hexane. Depending on the activity of the prepared biocatalyst, the duration of one reaction cycle ranged from 5 to 144 h. The products—ethyl esters of fatty acids—were analyzed using gas (GC) and thin-layer chromatography (TLC) under the conditions described elsewhere [41].

5.3.6. Esterification of Fatty Acids with Aliphatic Alcohols

Esterification was carried out in periodic mode in a stirred-tank reactor on a shaker at 70 rpm and 40 °C. Two substrates (S) used for esterification were following: substrate S_1—butyric C4:0, capric C10:0, and stearic C18:0 fatty acids, as well as benzoic and phenoxyacetic acids; substrate S_2—isoamyl alcohol (isopentanol). The reaction medium had the following composition:0.1 M acid (S_1)

and 0.2 M alcohol (S_2) in solvent—mixture of hexane and diethyl ether in a 1:1 ratio. The duration of one reaction cycle was 24 h. The esterification rate was determined from the consumption of the organic acid involved in the synthesis of the ester. The concentration of S_1 was determined titrimetrically with water-ethanol solution of NaOH with known concentration. The conversion (x, in %) of the S_1 was calculated.

6. Main Equipment

The texture parameters of the heterogeneous biocatalysts were examined by both the nitrogen adsorption/desorption and mercury intrusion porosimetry using ASAP 2400 V3.07 and AUTO-PORE IV 9500 V1.09 devices (Micromeritics Instrument Corporation, Norcross, GA, USA), respectively. The specific surface areas ($S_{sp.BET}$) were measured by thermal desorption of argon using a SORBI-M instrument (ZAO Meta, Novosibirsk, Russia). The content of nanocarbons was determined gravimetrically and by thermal analysis using a STA-449 C Jupiter instrument (Netzsch, Selb, Germany).The morphology of the cleavages of the biocatalysts was examined with a scanning electron microscope (SEM) JSM 6460 LV (JEOL Ltd., Tokyo, Japan). Marks in the SEM images corresponded to the distance in μm. A pulsed NMR spectrophotometer (ZAO Chromatek, Yoshkar-Ola, Russia) was used for measuring the solid fat contents in oil-fat blends and interesterified products.

7. Conclusions

Multi-component heterogeneous biocatalysts were prepared using a peculiar method developed for immobilization both of whole non-growing microorganisms and fully disrupted microbial cells (lysates) by immuring inside silica xerogel and nanocarbons-in-silica composites. Properties of these whole-cell and lysate-based biocatalysts such as single-enzymatic activity and operational stability were investigated systematically. The effect of the included nanocarbons such as nanotubes, nanofibers, onion-like nanospheres on the activity and stability of composite biocatalysts was studied.

With glucose isomerase-active whole-cell biocatalysts, only inconsiderable effect after inclusion of nanocarbons on the properties of the composite nanocarbons-in-silica biocatalysts was established. The glucose isomerase activity was only 1.1–1.15 times as high as that of the nanocarbons-free SiO_2-xerogel because of weak adhesion of *A. nicotianae* and recombinant r*E. coli*/xyl bacteria on nanocarbons. The cross-linking of the dried biocatalysts by 0.1–1% glutaric dialdehyde led to increase in one and half times biocatalytic activity; the maximal steady-state activity was 160 $U \cdot g^{-1}$ at 70 °C. The operational stability was enhanced as well; $t_{1/2}$ > 1200 h under continuous glucose/fructose isomerization.

With invertase-active biocatalysts, there was significant positive effect after inclusion of nanocarbons inside silica xerogel. The maximal effect on properties of the composite lysate-based biocatalysts was observed upon inclusion of CNTs, the invertase activity being as high as 2–6 times of that of the nanocarbons-free biocatalysts. The highest steady-state activity, 3000 $U \cdot g^{-1}$ at 50 °C, was determined for the composite CNTs-in-silica lysate-based biocatalysts; $t_{1/2}$ > 200 h under continuous sucrose inversion at 50 °C. Correlation between the adhesion ability of yeast lysates on nanocarbons and the steady-state activity of the biocatalysts was found.

The lipase-active biocatalysts prepared by immuring r*E. coli*/lip lysates inside silica xerogel and nanocarbons-in-silica composites, the effect of the included nanocarbons on biocatalytic activity and stability depended significantly on the reaction type. In interesterification of oil-fat blends, the biocatalysts prepared without nanocarbons and with inclusion of maltodextrin demonstrated the highest activity and stability. The half-life time was ~70 h at 70–75 °C. In interesterification of sunflower oil with ethyl acetate, the most active and stable biocatalysts were prepared both without nanocarbons and with included CNT2s. The half-life time was ~720 h at 40 °C. In low-temperature esterification of fatty acid with aliphatic alcohols in organic solvents, the lipase activity was 5–6 times increased after inclusion of carbon nanotubes (CNT2s) and nanospheres (CNS2s) inside silica xerogel.

The composite nanocarbons-in-silica biocatalysts for synthesis of isopentyl esters of capric (C10:0) and srearic (C18:0) acids operated for more than 1000 h at 40 °C without loss of activity.

Author Contributions: G.A.K. conceived and designed the experiments, and wrote the paper; L.V.P. and A.B.B. performed the experiments and analyzed the experimental data; V.N. Parmon provided acquisition of the financial support for the project leading to this publication.

Acknowledgments: The authors are grateful to Sapunova L.I. and co-workers from the Institute of Microbiology (Minsk, Belarus) who provided bacteria strains producing glucose isomerase, as well as to Mamaev A.L. and all co-workers from the Institute of Biochemistry (Novosibirsk, Russia) for constructing and growing the recombinant strains-producer in order to obtain lipase-active lysates. The authors are also grateful Kuznetsov V.L. and co-workers from the Boreskov Institute of Catalysis (Novosibirsk, Russia) who produced nanocarbons and provided the CNTs, CNSs and ND for the studies. The work was conducted under the budget Project of the Boreskov Institute of Catalysis.

Conflicts of Interest: The authors declare no conflict of interest.

Abbreviations

CNT	carbon nanotube, multi-walled
CNF	carbon nanofiber
CNS	carbon nanosphere, onion-like
EAC	enzymatic active component of the heterogeneous biocatalyst
GI	glucose isomerase
INV	invertase
LIP	lipase
U	Unit of enzyme activity defined as μmols of conversed substrate per minute under the conditions described

References

1. Bommarius, A.S.; Reidel, B.R. *Biocatalysis*; WILEY-VCH Veglar GmbH& Co. RGaA: Weiheim, Germany, 2004; pp. 2–611. ISBN 3-527-30344-8.
2. Grunwald, P. *Biocatalysis*; Imperial College Press: London, UK, 2009; pp. 2–1035. ISBN 10-1-86094-744-1.
3. Buchholz, K.; Kasche, V.; Bornscheuer, U.T. *Biocatalysts and Enzyme Technology*; WILEY-VCH Veglar GmbH& Co. RGaA: Weiheim, Germany, 2005; pp. 2–431. ISBN 10-3-527-30497-5.
4. Hou, C.H. *Handbook of Industrial Biocatalysis*; Tailor & Francis Group, LLC: Abingdon, UK, 2005; pp. 2–900. ISBN 0-8247-2423-2.
5. Tao, J.; Kazlauskas, R. (Eds.) *Biocatalysis for Green Chemistry and Chemical Process Development*; WILEY, John Wiley & Sons, Inc.: Hoboken, NJ, USA, 2011; pp. 1–479. ISBN 978-0-470-43778-0.
6. Rodgers, L.E.; Holden, P.J.; Hanna, J.V.; Foster, L.J.R.; Knott, R.B.; Pike, K.J.; Bartlett, J.R. Structural evolution and stability of sol–gel biocatalysts. *Physica B* **2006**, *385–386*, 508–510. [CrossRef]
7. Illanes, A.; Wilson, L.; Vera, C. *Problem Solving in Enzyme Biocatalysis*; WILEY, John Wiley & Sons, Inc.: Hoboken, NJ, USA, 2014; pp. 141–180. ISBN 978-1-118-34171-1.
8. Kovalenko, G.A.; Sukhinin, S.V.; Perminova, L.V. Vortex Reactors for Heterogeneous Biocatalytical Processes. In *Industrial Application of Biotechnology*; Krylov, I.A., Zaikov, G.E., Eds.; NOVA Science Publisher, Inc.: New York, NY, USA, 2006; pp. 45–53.
9. Kovalenko, G.A.; Perminova, L.V. Immobilization of glucoamylase by adsorption on carbon supports and its application for heterogeneous hydrolysis of dextrin. *Carbohydr. Res.* **2008**, *343*, 1202–1211. [CrossRef] [PubMed]
10. Kovalenko, G.A.; Perminova, L.V.; Terentyeva, T.G.; Sapunova, L.I.; Lobanok, A.G.; Chuenko, T.V.; Rudina, N.A.; Cherhyak, E.I. Glucose isomerase activity in suspensions of *Arthrobacter nicotianae* cells and adsorption immobilization of the microorganisms on inorganic carriers. *Appl. Biochem. Microbiol.* **2008**, *44*, 174–181. [CrossRef]
11. Kovalenko, G.A.; Perminova, L.V.; Rudina, N.A.; Maksimova, Y.G.; Maksimov, A.Y. Sapropel-based supports as novel macroporous carbon-mineral adsorbents for enzymatic active substances. *Resour. Effic. Technol.* **2016**, *2*, 159–167. [CrossRef]

12. Perminova, L.V.; Kovalenko, G.A.; Rudina, N.A.; Sapunova, L.I.; Tamkovic, I.O.; Lobanok, A.G. Catalytical properties of *Arthrobacter nicotianae* cells, a producer of glucose isomerase, immobilized inside xerogel of silicium dioxide. *Appl. Biochem. Microbiol.* **2009**, *45*, 389–394. [CrossRef]
13. Kovalenko, G.A.; Perminova, L.V.; Chernyak, E.I.; Sapunova, L.I. Investigation on macrokinetics of heterogeneous process of monosaccharide isomerization using non-growing cells of a glucose isomerase producer *Arthrobacter nicotianae* immobilized inside SiO_2-xerogel. *Appl. Biochem. Microbiol.* **2010**, *46*, 697–705. [CrossRef]
14. Kovalenko, G.A.; Perminova, L.V.; Sapunova, L.I. A peculiar method for immobilization of non-growing microbial cells by entrapment into silica xerogel. In *Biotechnology in Medicine, Foodstuffs, Biocatalysis, Environment and Biogeotechnology*; Varfolomeev, S.D., Zaikov, G.E., Krylova, L.P., Eds.; NOVA Science Publisher, Inc.: New York, NY, USA, 2010; pp. 41–49.
15. Kovalenko, G.A.; Simonova, L.G.; Perminova, L.V.; Yakushko, R.I. Biocatalyst, Method of Its Preparation and Method of Production of Glucose-Fructose Syrups. Patent RU 2341560 C1, 10 June 2008.
16. Kovalenko, G.A.; Beklemishev, A.B.; Perminova, L.V.; Mamaev, A.L.; Rudina, N.A.; Moseenkov, S.I.; Kuznetsov, V.L. Immobilization of recombinant *E. coli* thermostable lipase by entrapment inside silica xerogel and nanocarbon-in-silica composites. *J. Mol. Catal. B Enzym.* **2013**, *98*, 78–86. [CrossRef]
17. Kovalenko, G.A.; Perminova, L.V.; Beklemishev, A.B.; Tkachenko, V.I. Study on physicochemical properties of biocatalysts with thermostable lipase activity and final products of triglycerides' interesterification. *Appl. Biochem. Microbiol.* **2014**, *50*, 709–721. [CrossRef]
18. Kovalenko, G.A.; Perminova, L.V.; Rudina, N.A.; Mazov, I.N.; Moseenkov, S.I.; Kuznetsov, V.L. Immobilization of enzymatic active substances by immuring inside nanocarbon-in-silica composites. *J. Mol. Catal. B Enzym.* **2012**, *76*, 116–124. [CrossRef]
19. Kovalenko, G.A.; Beklemishev, A.B.; Perminova, L.V.; Chuenko, T.V.; Mamaev, A.L.; Ivanov, I.D.; Moseenkov, S.I.; Kuznetsov, V.L. Recombinant strain producing thermostable lipase from *Thermomyces lanuginosus* immobilized into nanocarbon-in-silica matrixes and properties of prepared biocatalysts. *Appl. Biochem. Microbiol.* **2013**, *49*, 296–305. [CrossRef]
20. Kovalenko, G.A.; Perminova, L.V.; Lenskaya, V.M.; Sapunova, L.I.; Tamkovich, I.O.; Lobanok, A.G. Biocatalyst, Method of Its Preparation and Method of Production of Glucose-Fructose Syrups. Patent Eurasia 01766 B1, 30 November 2012.
21. Kovalenko, G.A.; Perminova, L.V.; Chuenko, T.V.; Sapunova, L.I.; Shlyakhotko, E.A.; Lobanok, A.G. Immobilization of a recombinant strain producing glucose isomerase inside SiO_2-xerogel and properties of prepared biocatalysts. *Appl. Biochem. Microbiol.* **2011**, *47*, 151–157. [CrossRef]
22. D'Souza, S.F.; Melo, J.S. Immobilization of bakers yeast on jute fabric through adhesion using polyethyleneimine: Application in an annular column reactor for the inversion of sucrose. *Process. Biochem.* **2001**, *36*, 677–681. [CrossRef]
23. Sungur, S.; Al-Taweel, R.; Yildirim, O.; Logoglu, E. Immobilization of *Saccharomyces cerevisiae* in gelatin cross-linked with chromium ions for conversion of sucrose by intracellular invertase. *Polym. Plast. Technol. Eng.* **2006**, *45*, 929–934. [CrossRef]
24. Hasal, P.; Vojtisek, V.; Lejkova, A.; Kleczek, P.; Kofronova, O. An immobilized whole yeast cell biocatalyst for enzymatic sucrose hydrolysis. *Enzym. Microb. Technol.* **1992**, *14*, 221–229. [CrossRef]
25. Nassif, N.; Bouvet, O.; Rager, M.N.; Roux, C.; Coradin, T.; Livage, J. Living bacteria in silica gels. *Nat. Mater.* **2002**, *1*, 42–44. [CrossRef] [PubMed]
26. Carturan, G.; Campostrini, R.; Dir, S.; Scardi, V.; De Alteriis, E. Inorganic gels for immobilization of biocatalysts: Inclusion of invertase-active whole cells of yeast *(Saccharomyces cerevisiae)* into thin layers of SiO_2 gel deposited on glass sheets. *J. Mol. Catal.* **1989**, *57*, L13–L16. [CrossRef]
27. Kovalenko, G.A.; Perminova, L.V. Biocatalyst, Method of Its Preparation and Method of Production of Invert Syrup Using This Biocatalyst. Patent RU 2372403 C1, 10 November 2009.
28. Kovalenko, G.A.; Perminova, L.V.; Plaksin, G.V.; Komova, O.V.; Chuenko, T.V.; Rudina, N.A. Immobilized yeast membranes as biocatalysts for sucrose inversion. *Appl. Biochem. Microbiol.* **2005**, *41*, 399–403. [CrossRef]
29. Mateo, C.; Palomo, J.M.; Lorente, G.; Guisan, J.M.; Fernandez-Lafuente, R. Improvement of enzyme activity, stability and selectivity via immobilization techniques. *Enzym. Microb. Technol.* **2007**, *40*, 1451–1463. [CrossRef]

30. Rodrigues, R.C.; Fernandez-Lafuente, R. Lipase from *Rhizomucor miehei* as an industrial biocatalyst in chemical process. *J. Mol. Catal. B Enzym.* **2010**, *64*, 1–22. [CrossRef]
31. Rodrigues, R.C.; Fernandez-Lafuente, R. Lipase from *Rhizomucor miehei* as a biocatalyst in fats and oils modification. *J. Mol. Catal. B Enzym.* **2010**, *66*, 15–32. [CrossRef]
32. Contesini, F.J.; Lopes, D.B.; Macedo, G.A.; da G. Nascimento, M.; de O. Carvalho, P. *Aspergillus* sp. lipase: Potential biocatalyst for industrial use. *J. Mol. Catal. B Enzym.* **2010**, *67*, 163–171. [CrossRef]
33. Fernandez-Lafuente, R. Lipase from *Thermomyces lanuginosus*: Uses and prospects as an industrial biocatalyst. *J. Mol. Catal. B Enzym.* **2010**, *62*, 197–212. [CrossRef]
34. Itabaiana, I., Jr.; Miranda, L.S.M.; Mendon, R.O.; de Souza, R.O.M.A. Towards a continuous flow environment for lipase-catalyzed reactions. *J. Mol. Catal. B Enzym.* **2013**, *85–86*, 1–9. [CrossRef]
35. Bezborodov, A.M.; Zagustina, N.A. Lipases in catalytic reactions of organic synthesis (review). *Appl. Biochem. Microbiol.* **2014**, *50*, 313–337. [CrossRef]
36. Perminova, L.V.; Kovalenko, G.A.; Beklemishev, A.B.; Mamaev, A.L.; Pykhtina, M.B.; Rudina, N.A. Catalytic properties of lipase entrapped as lysates of recombinant strain-producer r*Escherichia coli*/lip into nanocarbon-in-silica composites in the bioconversion of triglycerides and fatty acids. *Appl. Biochem. Microbiol.* **2018**, *54*, 38–44. [CrossRef]
37. Sokolovskii, V.D.; Kovalenko, G.A. Immobilization of oxydoreductases on inorganic supports based on alumina: The role of mutual correspondence of enzyme-support hydrophobic-hydrophilic characters. *Biotechnol. Bioeng.* **1988**, *32*, 916–919. [CrossRef] [PubMed]
38. Kovalenko, G.A.; Sokolovskii, V.D. Immobilization of oxydoreductases on inorganic supports based on alumina: Immobilization of alcohol dehydrogenase on nonmodified and modified alumina. *Biotechnol. Bioeng.* **1983**, *25*, 3177–3184. [CrossRef] [PubMed]
39. Kovalenko, G.A.; Perminova, L.V.; Chuenko, T.V.; Rudina, N.A. Tuning surface morphology of inorganic supports for adsorptive immobilization of enzymatic active substances. *Compos. Interfaces* **2009**, *16*, 293–305. [CrossRef]
40. Kovalenko, G.A.; Beklemishev, A.B.; Perminova, L.V.; Mamaev, A.L.; Chuenko, T.V.; Kuznetsov, V.L. Biocatalyst, Method of Its Preparation and Method of Interesterification of Vegetable Oils Using This Biocatalyst. Patent RU 2539101 C2, 10 January 2014.
41. Kovalenko, G.A.; Perminova, L.V.; Beklemishev, A.B.; Yakovleva, E.Y.; Pykhtina, M.B. Heterogeneous biocatalytic processes of vegetable oil interesterification to biodiesel. *Catal. Ind.* **2015**, *7*, 73–81. [CrossRef]
42. Kovalenko, G.A.; Perminova, L.V.; Beklemishev, A.B.; Mamaev, A.L.; Patrushev, Y.V. Heterogeneous biocatalytic processes of esterification of saturated fatty acids with aliphatic alcohols. *Catal. Ind.* **2018**, *10*, 68–74. [CrossRef]
43. Perminova, L.V.; Kovalenko, G.A.; Chukanov, N.V.; Patrushev, Y.V. Enzymatic esterification of saturated fatty acids with aliphatic alcohols as an alternative method of a low-temperature synthesis of esters. *Russ. Chem. Bull.* **2017**, *66*, 2194–2197. [CrossRef]
44. Joseph, M.D.; Kasprzak, D.J.; Crouch, S.R. A stopped-flow clinical analyzer in which immobilized-enzyme reaction loops are used. *Clin. Chem.* **1977**, *23*, 1033–1036. [PubMed]
45. Usoltseva, A.N.; Kuznetsov, V.L.; Rudina, N.A.; Moroz, E.M.; Haluska, M.; Roth, S. Influence of catalysts activation on their activity and selectivity in carbon nanotubes synthesis. *Phys. Status Solidi* **2007**, *244*, 3920–3924. [CrossRef]
46. Kuznetsov, V.L.; Chuvilin, A.L.; Moroz, E.M.; Kolomiichuk, V.N.; Shaichutdinov, S.K.; Butenko, Y.V.; Malkov, I.Y. Effect of explosion conditions on the structure of detonation soot: Ultra disperse diamond and onion carbon. *Carbon* **1994**, *32*, 873–882. [CrossRef]
47. Kuznetsov, V.L.; Chuvilin, A.L.; Butenko, Y.V.; Malkov, I.Y.; Titov, V.M. Onion-like carbon from ultra disperse diamond. *Chem. Phys. Lett.* **1994**, *222*, 343–348. [CrossRef]

48. Kuvshinov, G.G.; Mogilnykh, Y.I.; Kuvshinov, D.G.; Zaikovskii, V.I.; Avdeeva, L.B. Pecularities of filamentous carbon formation in metane decomposition in Ni-containing catalysts. *Carbon* **1998**, *36*, 87–97. [CrossRef]
49. Kuvshinov, G.G.; Mogilnykh, Y.I.; Kuvshinov, D.G. Kinetics of carbon formation from CH_4-H_2 mixtures over a nickel containing catalyst. *Catal. Today.* **1998**, *42*, 357–360. [CrossRef]

© 2018 by the authors. Licensee MDPI, Basel, Switzerland. This article is an open access article distributed under the terms and conditions of the Creative Commons Attribution (CC BY) license (http://creativecommons.org/licenses/by/4.0/).

catalysts

MDPI

Article

Preparation of Stable Cross-Linked Enzyme Aggregates (CLEAs) of a *Ureibacillus thermosphaericus* Esterase for Application in Malathion Removal from Wastewater

Yuliya V. Samoylova [1], Ksenia N. Sorokina [1,2,*], Alexander V. Piligaev [1] and Valentin N. Parmon [1,2]

[1] Boreskov Institute of Catalysis (BIC), Lavrentieva ave. 5, 630090 Novosibirsk, Russia; samoylova.jv@catalysis.ru (Y.V.S.); piligaev@catalysis.ru (A.V.P.); parmon@catalysis.ru (V.N.P.)
[2] Novosibirsk State University (NSU), Pirogova str. 2, 630090 Novosibirsk, Russia
* Correspondence: sorokina@catalysis.ru; Tel.: +7-383-326-95-86

Received: 26 March 2018; Accepted: 8 April 2018; Published: 11 April 2018

Abstract: In this study, the active and stable cross-linked enzyme aggregates (CLEAs) of the thermostable esterase estUT1 of the bacterium *Ureibacillus thermosphaericus* were prepared for application in malathion removal from municipal wastewater. Co-expression of esterase with an *E. coli* chaperone team (KJE, ClpB, and ELS) increased the activity of the soluble enzyme fraction up to 200.7 ± 15.5 U mg^{-1}. Response surface methodology (RSM) was used to optimize the preparation of the CLEA-estUT1 biocatalyst to maximize its activity and minimize enzyme loss. CLEA-estUT1 with the highest activity of 29.4 ± 0.5 U mg^{-1} (90.6 ± 2.7% of the recovered activity) was prepared with 65.1% (*w*/*v*) ammonium sulfate, 120.6 mM glutaraldehyde, and 0.2 mM bovine serum albumin at 5.1 h of cross-linking. The biocatalyst has maximal activity at 80 °C and pH 8.0. Analysis of the properties of CLEA-estUT1 and free enzyme at 50–80 °C and pH 5.0–10.0 showed higher stability of the biocatalyst. CLEA-estUT1 showed marked tolerance against a number of chemicals and high operational stability and activity in the reaction of malathion hydrolysis in wastewater (up to 99.5 ± 1.4%). After 25 cycles of malathion hydrolysis at 37 °C, it retained 55.2 ± 1.1% of the initial activity. The high stability and reusability of CLEA-estUT1 make it applicable for the degradation of insecticides.

Keywords: molecular chaperones; esterase; *Ureibacillus thermosphaericus*; cross-linked enzyme aggregates; response surface methodology; malathion hydrolysis

1. Introduction

Malathion (*S*-(1,2-dicarbethoxyethyl)-*O*,*O*-dimethyldithiophosphate) is a broad-spectrum insecticide which is widely used due to its efficiency for pest and insect control and low price. However, malathion and its derivates are highly toxic for living organisms, including humans. Malathion mainly targets the central nervous and immune systems and causes various symptoms including dizziness, nausea, and attention disorder [1]. Therefore, it is important to prevent the pollution of air and soil and especially water with this insecticide [2,3]. There are several approaches to degrading malathion in wastewater, including chemical oxidation [3], ultraviolet irradiation [4], nanofiltration [3], and biological treatment (with bacteria [5], fungi [6], and algae [7]). Currently, biological treatment is considered as a preferred method for malathion removal from aqueous solutions, since it is inexpensive, less time-consuming, and in most cases, provides complete degradation of this insecticide. A wide range of bacteria, including *Bacillus licheniformis* [8], *Pseudomonas putida*, *Pseudomonas* sp. [9], *Rhodoccocus rhodochrous*, and *Sphingomonas* sp. [5], have been

successfully applied in malathion biodegradation due to their ability to produce hydrolytic enzymes (hydrolases and carboxylesterases). Application of purified microbial hydrolytic enzymes is an alternative way to degrade malathion as they have higher activity and specificity as compared to the microbial strains [10,11]. Their immobilization allows their activity and stability to be increased and promotes their separation from the reaction medium, along with repeated use [12–14]. Currently, the hydrolytic immobilized enzymes are not applied for malathion removal from municipal wastewater, but Adhikari et al. [15] applied immobilized cells of *Bacillus* sp. S14 for its hydrolysis in aqueous solutions.

The widespread application of hydrolytic enzymes (lipases and esterases) in industry and for the biodegradation of insecticides is still limited by their high production costs. One of the problems is the low protein expression in common host systems. This may be the result of the toxicity of the expressed proteins [16], presence of disulfide bonds [17], or inactivation of the protein and formation of inclusion bodies after intracellular aggregation of proteins [18,19]. Expression of molecular chaperones and chaperonins with enzymes can decrease the formation of protein aggregates. It was shown that the co-expression of the *E. coli* DnaK and GroEL chaperone team proved to be most effective for increasing the expression of lipase from *Psychrobacter* sp. in a soluble form, as compared to expression with each chaperone alone [20]. Application of this approach allows the yield of protein to be increased, thereby reducing the cost of its production.

In addition to high protein activity, the stability in a wide range of pH and temperature, along with superior tolerance to solvents and chemicals [21], are required for the successful application of enzymes in various processes, including malathion removal from municipal wastewater. Immobilization prolongs protein operation and can be performed by physical adsorption, entrapment, covalent bonding, and cross-linking (carrier free) [22]. Among these methods, the application of cross-linked enzyme aggregates (CLEAs) is a prospective immobilization approach that combines all steps of preparation (purification, precipitation, and immobilization) in one, making the process simple, time-saving, and low-cost. CLEAs biocatalysts have high activity and stability over a wide range of pH (4.0–11.0) [23], temperature (10–90 °C) [24,25], and a high tolerance to chemical reagents including phenylmethylsulfonyl fluoride (PMSF), sodium dodecyl sulfate (SDS), ethanol, and phenol [26]. Such biocatalysts were previously successfully applied for the production of biodiesel [27,28] and chemicals [29], but not for insecticide degradation.

In this study, we report the preparation of a highly active CLEAs biocatalyst from the novel thermostable esterase estUT1 of the bacterium *Ureibacillus thermosphaericus* for application in malathion removal from real wastewater. Co-expression of the *E. coli* chaperone team of KJE, ClpB, and ELS with the esterase led to an increase in the production of soluble and active enzyme. Optimization of the biocatalyst preparation was performed with response surface methodology (RSM) using face-centered central composite design (FCCCD) for the following parameters: cross-linking time and concentrations of precipitating reagent, glutaraldehyde, and chemical additives. The biocatalyst was stable in a wide range of pH and temperature and in the presence of various chemicals, and was further tested in the reaction of malathion hydrolysis in municipal wastewater. Therefore, this approach allowed the yield of soluble estUT1 in *E. coli* to be increased and enzyme loss to be reduced during the preparation of a highly active and stable biocatalyst for application in the degradation of organophosphorus insecticide during wastewater treatment.

2. Results and Discussion

2.1. Chaperone Co-Expression with estUT1

Recently, we have cloned and studied properties of the new thermostable esterase estUT1 from the bacterium *U. thermosphaericus* [30]. EstUT1 is stable at pH 5.0–9.0, at temperature 50–70 °C, and is tolerant to various chemicals and organic solvents, which makes it promising for application as a catalyst in wastewater treatment for malathion removal. The esterase estUT1 is expressed in

E. coli BL21(DE3) as inclusion bodies that need to be further refolded in vitro [30]. In this respect, the co-expression of a combination of molecular chaperones and chaperonins with the recombinant proteins is the one of the strategies to solve this problem. The DnaK system (DnaK with its co-chaperones DnaJ and GrpE; KJE) prevents formation of the inclusion bodies by reducing aggregation and stimulating the proteolysis of misfolded proteins [31]. The bi-chaperone system comprised by KJE and ClpB promotes solubilization and disaggregation of proteins [32,33]. The GroEL system (GroEL with its co-chaperonin GroES; ELS) promotes protein transit between the soluble and insoluble protein fractions [34]. Therefore, to study the influence of chaperones on the expression of estUT1, a combination of KJE, ClpB, and ELS chaperones was used as one of the most effective folding systems. Previously, it was shown that a chaperone team (KJE, ClpB, and ELS) improves the yield of soluble fraction of proteins expressed in *E. coli* by 2.5–3.5 times [35].

In this study, the estUT1 gene was expressed in *E. coli* BL21(DE3) as a His-tagged fusion protein. The esterase estUT1 alone was produced as inclusion bodies in the insoluble fraction (Figure 1, line 2) [30]. Its co-expression with the chaperone team (KJE, ClpB, and ELS) resulted in a higher yield of active estUT1 in a soluble fraction of cell lysate (Figure 1, line 4). The specific activity of purified esterase in a soluble fraction after its co-expression with chaperones increased up to 200.7 ± 15.5 U mg^{-1}, as compared to esterase expressed without chaperones (22.6 ± 1.7 U mg^{-1}). These results correlate with the data on the expression of other lipolytic enzymes; for example, co-expression of the molecular chaperone team KJE and ELS with the lipase from *Psychrobacter* sp. resulted in an increase in its specific activity from 66.51 ± 3.84 to 108.77 ± 4.62 U mg^{-1} in *E. coli* [20]. These results confirm that the expression of *E. coli* molecular chaperones (KJE, ClpB, and ELS) has a positive effect on the yield of the soluble esterase estUT1. The resulting highly active purified protein from *E. coli* co-expressing chaperones and estUT1 was further used to prepare CLEAs biocatalyst.

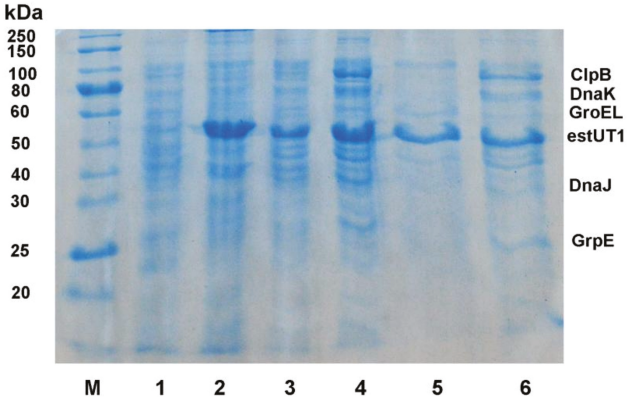

Figure 1. Co-expression of the molecular chaperone team (KJE, ClpB, and ELS) and the esterase estUT1 in *E. coli* BL21(DE3). M: protein molecular weight marker; 1: *E. coli* BL21(DE3) transformed with pET32b vector (soluble fraction); 2: *E. coli* BL21(DE3) transformed with pET32b-UT1 plasmid (insoluble fraction); 3: *E. coli* BL21(DE3) transformed with pET32b-UT1 plasmid (soluble fraction); 4: *E. coli* BL21(DE3) transformed with pET32b-UT1 co-expressed with chaperones (soluble fraction); 5: estUT1 (Ni-NTA purification); 6: estUT1 co-expressed with chaperones (Ni-NTA purification).

2.2. Preparation of CLEA-estUT1

In this study, the CLEAs approach was used for the preparation of biocatalyst from the esterase estUT1 for application in malathion hydrolysis. The procedure involves the aggregation of free enzyme from the aqueous solution with a precipitation agent (ammonium sulfate, ethanol, acetone), followed

by cross-linking of aggregates by a bifunctional agent (glutaraldehyde) [36]. This approach does not require the use of a carrier [22], therefore resulting in an improvement of biocatalyst activity.

2.2.1. Selection of Precipitant

Various chemicals including acetone, *tert*-butanol, isopropanol, ethanol, and ammonium sulfate (50%, *w*/*v*) were tested using the precipitant–protein ratio of 3:1 (*v*/*v*) to select the optimal precipitant for the preparation of CLEAs from the purified esterase estUT1. Results are shown in Table 1.

Table 1. Effect of various precipitants on the activity of CLEAs biocatalyst.

Precipitant Type	Recovered Activity, %
Acetone	30.3 ± 2.8
tert-Butanol	34.5 ± 4.7
Isopropanol	8.7 ± 1.1
Ethanol	6.2 ± 0.4
Ammonium sulfate (50%, *w*/*v*)	58.4 ± 4.1

Preparation of biocatalyst: 0.5 mL of the enzyme solution (1 mg mL^{-1}), precipitant–protein ratio 3:1 (*v*/*v*), 75 mM glutaraldehyde, 4 h of cross-linking.

Ammonium sulfate is a widely used precipitant for preparation of CLEAs from various enzymes including lipases [37], esterases [38], amylases [39], and proteases [40]. In this study, ammonium sulfate was also found as the most suitable precipitant and used for further studies on biocatalyst preparation.

2.2.2. Selection of Additives

In this study, two additives were tested in order to elucidate their effect on the activity of CLEAs (Table 2): bovine serum albumin (BSA) as a protein feeder [41] and SDS as a surfactant that facilitates the precipitation of aggregates in a stable conformation and increases the interfacial surface of the enzyme [42]. In this study, BSA increased the CLEAs activity up to 154.2 ± 16.5%. This may be due to the presence of free amino groups on the surface of the protein, for example, lysine, which reacts with glutaraldehyde, thereby preventing the denaturation of protein [43]. If SDS was used as an additive, CLEA-estUT1 showed only a slight increase in its activity (up to 109.7 ± 8.4%), which correlates with the data of Gupta et al. [42]. They reported an efficient cross-linking of the enzyme after precipitation with ammonium sulfate, along with an increase in the activity of CLEAs in the presence of SDS by two-fold. According to these data, BSA was selected as the most effective additive for CLEAs preparation.

Table 2. Effect of additives on the activity of CLEAs.

Additives	Relative Activity, %
Control [1]	100.0 ± 4.7
BSA	154.2 ± 16.5
SDS	109.7 ± 8.4

[1] Biocatalyst activity without additives was considered as 100% of the relative activity. Preparation of biocatalyst: 0.5 mL of the enzyme solution (1 mg mL^{-1}), 60% (*w*/*v*) ammonium sulfate, 75 mM glutaraldehyde, 4 h of cross-linking.

2.2.3. Optimization of CLEA-estUT1 Preparation

In this study, the RSM with FCCCD was used to optimize conditions for preparation of the CLEA-estUT1 biocatalyst (Table 3). The highest recovered CLEA-estUT1 activity was found to be 85.4% in run 7, at 55% (*w*/*v*), 87.5 mM, and 0.2 mM of ammonium sulfate, glutaraldehyde, and BSA, respectively, after 4.5 h of cross-linking. The coefficients of the equation of the complete regression model and their statistical significance were determined and evaluated after processing of

the experimental data. A second-order polynomial model was built with the regression analysis and is represented by the following equation:

$$\begin{aligned}\text{Recovered activity of CLEA-estUT1 (\%)} = {} & 66.18 + 4.74A + 6.70B + 7.78C + 13.84D + 3.28AB + \\ & 2.12AC + 0.50AD + 0.45BC + 1.13BD - 0.47CD - 23.67A^2 - 10.69B^2 - 7.42C^2 + 7.32D^2\end{aligned} \quad (1)$$

where A: cross-linking time, B: concentration of ammonium sulfate, C: concentration of glutaraldehyde, and D: concentration of BSA.

Table 3. Experimental design for optimization of CLEA-estUT1 preparation.

Run	Time, h	Ammonium Sulfate, % (*w*/*v*)	Glutaraldehyde, mM	BSA, mM	Recovered Activity, %
1	4.5	55	25	0.105	45.1
2	1	80	25	0.2	42.0
3	8	30	25	0.01	7.5
4	4.5	55	87.5	0.105	72.4
5	1	80	25	0.01	9.7
6	4.5	55	87.5	0.105	71.4
7	4.5	55	87.5	0.2	85.4
8	8	80	25	0.01	19.8
9	1	30	150	0.01	21.8
10	4.5	55	87.5	0.105	74.1
11	1	30	150	0.2	38.7
12	1	80	150	0.2	50.4
13	4.5	55	87.5	0.105	65.1
14	8	55	87.5	0.105	40.4
15	1	30	25	0.2	29.6
16	1	80	150	0.01	18.9
17	4.5	30	87.5	0.105	43.2
18	4.5	80	87.5	0.105	60.3
19	8	30	150	0.01	18.2
20	8	80	150	0.01	47.2
21	1	30	25	0.01	5.3
22	4.5	55	87.5	0.105	65.7
23	8	30	25	0.2	32.1
24	1	55	87.5	0.105	37.2
25	4.5	55	87.5	0.01	54.2
26	8	30	150	0.2	52.4
27	4.5	55	87.5	0.105	70.6
28	8	80	25	0.2	51.3
29	8	80	150	0.2	70.0
30	4.5	55	150	0.105	65.0

Table 4 shows the result of analysis of variance (ANOVA),which verifies the significance of the model as well as the effect of individual independent variables and their interaction on the response. The efficiency of the resulting model was indicated by the high value of R^2 (0.97) and adjusted R^2 (0.94), and the model equation accounts for 97 or 94% variation. The F-value (33.36) and p-value (<0.0001) of this model confirm that the model is significant. The p-values presented in Table 4 show that the most significant factors in the CLEA-estUT1 preparation are the concentrations of BSA and glutaraldehyde ($p < 0.0001$). The time of cross-linking (0.0021) and the concentration of ammonium sulfate (0.0001) have a less pronounced effect on CLEA-estUT1 activity.

Table 4. ANOVA for CLEA-estUT1 preparation.

Source	Sum of Squares	*F*-Value	*p*-Value
Model	13,771.01	33.36	<0.0001
Time, A	403.56	13.69	0.0021
Ammonium sulfate, B	808.96	27.44	0.0001
Glutaraldehyde, C	1090.45	36.98	<0.0001
BSA, D	3449.76	117.00	<0.0001
AB	172.27	5.84	0.0288
AC	71.83	2.44	0.1394
AD	4.00	0.14	0.7178
BC	3.28	0.11	0.7435
BD	20.48	0.69	0.4177
CD	3.59	0.12	0.7319
A^2	1451.57	49.23	<0.0001
B^2	296.06	10.04	0.0064
C^2	142.83	4.84	0.0438
D^2	138.84	4.71	0.0465
Lack of fit	375.04	2.79	0.1345

The three-dimensional (3D) response surface (Figure 2) represents the regression equation used for the analysis of the interaction between variables and determination of the optimum concentration of each factor for maximizing biocatalyst activity. The 3D plot shows the concentration functions of two variables at a fixed value at the central point of the remaining factors.

The time of cross-linking is an important parameter for CLEAs preparation, and for different enzymes, may vary from 1 h [44] to 20 h [23]. In this study, this parameter was 1–8 h. Figure 2a–c shows the effect of cross-linking time on the activity of CLEAs, depending on the concentration of ammonium sulfate, glutaraldehyde, and BSA, respectively. The highest activity of CLEAs was observed at 4.5–5.5 h.

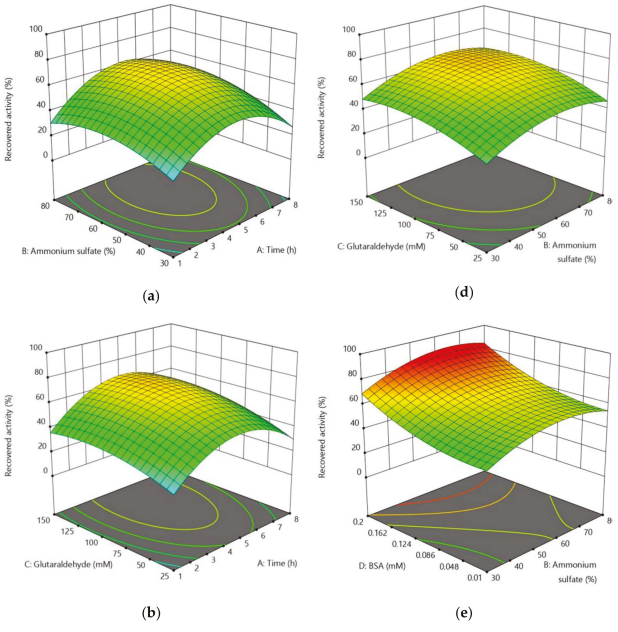

Figure 2. *Cont.*

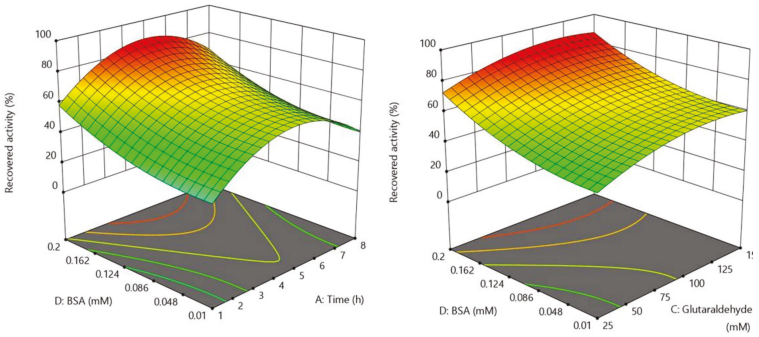

Figure 2. Response surface plots representing the dependence of the CLEA-estUT1 activity on the parameters of biocatalyst preparation: (**a**) concentration of ammonium sulfate and cross-linking time; (**b**) concentration of glutaraldehyde and cross-linking time; (**c**) concentration of BSA and cross-linking time; (**d**) concentration of glutaraldehyde and ammonium sulfate; (**e**) concentration of BSA and ammonium sulfate; (**f**) concentration of BSA and glutaraldehyde.

The amount of precipitant (ammonium sulfate) plays an important role in CLEAs preparation, thereby affecting the size of the protein aggregates. It was found that a low concentration of precipitant results in its inability to form protein aggregates. On the contrary, a high precipitant concentration can inhibit the enzyme activity [37]. According to the model from this study, the protein is preferably precipitated from the solution at 60–70% saturation with ammonium sulfate (Figure 2a,d,e). This range of concentrations is widely used for the precipitation of enzymes. For example, CLEAs of lipase M37 from *Photobacterium lipolyticum* [23] and α-amylase from *Bacillus amyloliquefaciens* [45] were prepared with 70% saturated ammonium sulfate.

The concentration of glutaraldehyde strongly affects the activity of the enzyme. If a low concentration of a cross-linker is used, the enzyme molecule may remain flexible and unstable, which will lead to protein leaching in solution. Excessive use of glutaraldehyde can cause loss of the minimum flexibility of the enzyme due to the formation of protein aggregates with a strong diffusion resistance [41]. Therefore, the concentration of glutaraldehyde should be optimized in order to obtain active CLEAs. As shown in Figure 2b,d,f, the highest activity of CLEAs was observed when 115–125 mM of glutaraldehyde was used for biocatalyst preparation. Previously, 75 and 60 mM glutaraldehyde was applied for the preparation of CLEAs of lipase from *Rhizopus oryzae* [44] and esterase from *Bacillus subtilis* [38], respectively. However, higher concentrations of the cross-linking agent have also been used for CLEAs preparation. For example, 140 mM glutaraldehyde has been used to immobilize catalase from the bovine liver [24].

In this study, the effect of the BSA concentration on the activity of CLEAs was evaluated. Figure 2c,e,f shows that its effect on the activity of CLEAs depends on the time of cross-linking and concentrations of ammonium sulfate and glutaraldehyde, respectively. The highest recovered activity of CLEA-estUT1 was at 0.2 mM BSA, which correlates with the study of Khanahmadi et al. [37], where 0.17 mM BSA was used as a co-feeder for the preparation of CLEAs of lipase isolated from cocoa pods.

The model obtained in this study was validated as shown in Table 5, and the experimental values were compared with those predicted by the model. Thus, the model based on RSM with FCCCD showed a high correlation with the experimental data and can be used for modeling of the CLEA-estUT1 preparation. The optimal conditions for the preparation of CLEAs biocatalyst from the esterase estUT1 were 65.1% ammonium sulfate, 120.6 mM glutaraldehyde, and 0.2 mM BSA at 5.1 h of cross-linking.

Table 5. Validation of the experimental model.

Time, h	Ammonium Sulfate, % (*w*/*v*)	Glutaraldehyde, mM	BSA, mM	Recovered Activity, %	
				Experimental	Predicted
5.1	65.1	120.6	0.2	90.6 ± 2.7	91.3

2.3. Study of CLEA-estUT1 Properties

Biocatalysts for industrial applications including wastewater treatment must be stable in a broad range of conditions. Therefore, a comparative analysis of the stability of free and immobilized esterase estUT1 is performed here in order to evaluate the biocatalyst's effectiveness in the application of malathion hydrolysis in municipal wastewater.

2.3.1. Effect of pH and Temperature on the Activity and Stability of Free estUT1 and CLEA-estUT1

The catalytic activity of free and immobilized estUT1 esterase was evaluated at pH 5.0–10.0. As shown in Figure 3a, the optimum pH for both forms of enzyme was 8.0, but CLEA-estUT1 had higher activity at pH 7.0 and 9.0, which was 92.4 ± 7.6% and 90.3 ± 4.7%, respectively. The higher pH stability of CLEAs (Figure 3b) is due to the covalent cross-linking between enzyme aggregates that increases the rigidity of the enzyme structure [46].

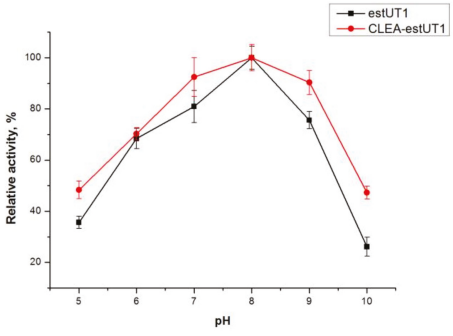

(**a**)

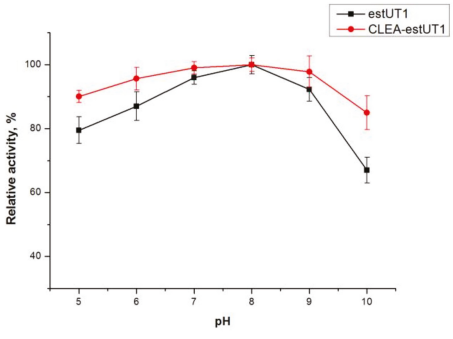

(**b**)

Figure 3. Effect of pH on the activity and stability of free and immobilized estUT1. (**a**) The activity of estUT1 and CLEA-estUT1 in buffers with different pH values was assayed with *p*-nitrophenyl acetate (*p*NPC2) as a substrate at 50 °C. (**b**) The pH stability of estUT1 and CLEA-estUT1 was examined in different buffers at 50 °C after 1 h of incubation.

As shown in Figure 4, enzyme immobilization does not affect the temperature optimum of estUT1 esterase (80 °C). However, CLEA-estUT1 has higher activity at all temperatures. Higher temperature tolerance of the immobilized enzyme is due to the decrease of the conformational flexibility of the protein.

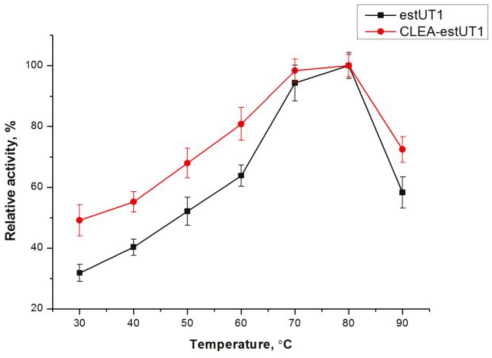

Figure 4. Effect of temperature on the activity of free and immobilized estUT1. The activity of estUT1 and CLEA-estUT1 at temperature range of 30–90 °C was assayed in 50 mM of Tris–HCl buffer (pH 8.0) using *p*NPC2 as a substrate.

Comparative study of the thermostability of free and immobilized enzyme was performed at 50–80 °C for 1–8 h (Figure 5). The inactivation rate constants (k_i) and the half-life ($t_{1/2}$) values of free and immobilized enzyme were determined according to Equations (3) and (4), respectively (Table 6). The k_i and $t_{1/2}$ values suggest that the thermostability of the esterase is considerably enhanced after immobilization. In fact, the $t_{1/2}$ of free estUT1 increased 1.9- and 1.5-fold after CLEAs preparation at 50 and 60 °C, respectively. The higher thermostability of the immobilized enzymes is due to additional covalent bonding in the tertiary and secondary structure that prevents their denaturation at the high temperatures [37,40,46].

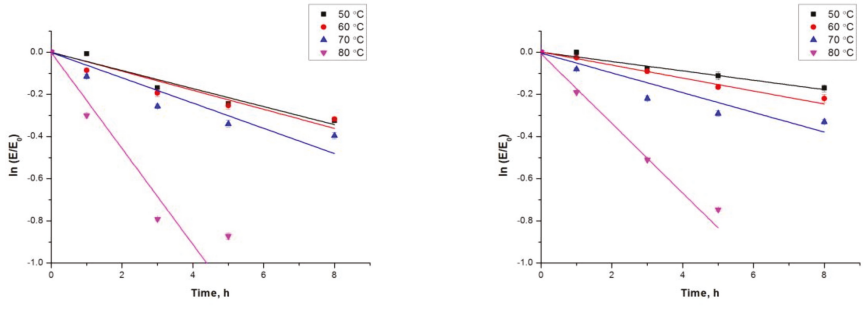

(**a**) (**b**)

Figure 5. Thermal inactivation of free (**a**) and immobilized (**b**) estUT1 at 50–80 °C. The thermostability of estUT1 and CLEA-estUT1 was assayed by incubating the enzyme in 50 mM of Tris–HCl buffer (pH 8.0) at 50–80 °C for 1–8 h.

Table 6. Comparison of the inactivation constants (k_i) and half-life ($t_{1/2}$) values of free estUT1 and CLEA-estUT1 at 50–80 °C.

Temperature, °C	k_i, h^{-1}		$t_{1/2}$, h	
	estUT1	CLEA-estUT1	estUT1	CLEA-estUT1
50	4.3×10^{-2}	2.2×10^{-2}	16.1	31.3
60	4.5×10^{-2}	3.1×10^{-2}	15.4	22.5
70	6.0×10^{-2}	4.7×10^{-2}	11.5	14.8
80	22.7×10^{-2}	16.5×10^{-2}	3.1	4.2

2.3.2. Effect of Chemicals on the Activity of Free estUT1 and CLEA-estUT1

The effects of various chemicals on the activity of free and immobilized estUT1 were observed after 1 h of incubation at 50 °C (Figure 6). The immobilized enzyme showed higher tolerance against these reagents than the enzyme in free form, which is consistent with the data of [26,47]. The activity of immobilized esterase as compared to free enzyme after incubation with 10 mM PMSF, dithiothreitol (DTT), β-mercaptoethanol (BME), 1% SDS, and Tween 20 was increased by 1.9, 1.2, 1.2, 1.5, and 1.6 times, respectively. Therefore, the immobilization of estUT1 by the cross-linking method can effectively protect the enzyme from thermal inactivation and increase tolerance to chemicals including water pollutants (surfactants, detergents [48], heavy metals, organic contaminants [49], etc.).

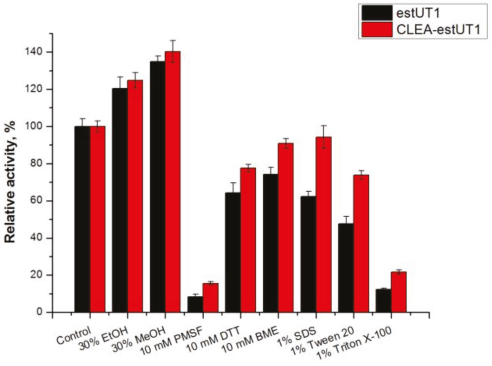

Figure 6. Effect of various chemicals on the activity of free and immobilized estUT1. EstUT1 and CLEA-estUT1 were incubated with different chemicals in 50 mM of Tris–HCl buffer (pH 8.0) at 50 °C for 1 h.

2.3.3. Kinetic Studies of Free and Immobilized estUT1

Kinetic parameters of the free estUT1 and CLEA-estUT1 were assayed with commonly used substrates including *p*NPC2, *p*-nitrophenyl butyrate (*p*NPC4), *p*-nitrophenyl octanoate (*p*NPC8), and malathion in order to study the effect of immobilization on the catalytic efficiency of the esterase estUT1. The results are summarized in Table 7. Free estUT1 is more selective towards short-chain fatty acids (C2 > C4 > C8), revealing the smallest K_m value for *p*NPC2 among the *p*-nitrophenyl esters examined. After enzyme immobilization, the K_m value of CLEA-estUT1 becomes higher than that of free esterase for all substrates, including *p*-nitrophenyl esters and malathion. This effect might be due to the changes in protein structure during cross-linking that results in a reduced accessibility of the substrate to the active site of the enzyme [41,50]. The higher K_m for immobilized enzyme as compared to free enzyme was also observed for CLEAs of protease [51], lipase [37], and esterase [38]. The catalytic efficiency (k_{cat}/K_m) of CLEA-estUT1 was lower as compared to free enzyme, which correlates with other studies [37,38]. The kinetic studies revealed a high catalytic efficiency of the enzyme toward

malathion. The k_{cat}/K_m value for estUT1 (835.5 ± 58.7 s^{-1} mM^{-1}) was higher than that of other known hydrolytic enzymes. For example, the k_{cat}/K_m value for the organophosphorus hydrolase mutant from *Flavobacterium* spp. was 154.91 s^{-1} mM^{-1} [10], and for a hydrolase from *Aspergillus niger* ZD11 was 55 s^{-1} mM^{-1} [52].

Thus, the CLEA-estUT1 biocatalyst, which is stable to various inhibitory conditions (pH, temperature, different chemicals) and shows a high catalytic efficiency against malathion, can be used as an effective biocatalyst in the reaction of malathion hydrolysis.

Table 7. Comparison of kinetic parameters of free estUT1 and CLEA-estUT1.

Substrate	K_m, μM		k_{cat}, s^{-1}		k_{cat}/K_m, s^{-1} mM^{-1}	
	estUT1	CLEA-estUT1	estUT1	CLEA-estUT1	estUT1	CLEA-estUT1
*p*NPC2	96.0 ± 5.3	176.7 ± 8.5	27.0 ± 0.7	31.1 ± 1.2	281.3 ± 8.7	176.1 ± 2.2
*p*NPC4	550.0 ± 78.1	710.7 ± 64.7	39.2 ± 1.2	41.8 ± 0.4	72.1 ± 8.8	59.1 ± 5.6
*p*NPC8	2113.3 ± 180.4	2490.0 ± 141.8	54.1 ± 2.0	56.9 ± 1.2	25.2 ± 1.3	22.9 ± 1.1
Malathion	19.5 ± 1.1	29.6 ± 3.3	16.3 ± 0.3	15.2 ± 1.0	835.5 ± 58.7	515.4 ± 22.8

2.3.4. Malathion Hydrolysis with CLEA-estUT1

The stability of a biocatalyst during operation is an important criterion for its industrial application. The reusability of CLEA-estUT1 biocatalyst produced in optimal conditions (Table 5) was studied in the reaction of malathion hydrolysis at its concentration of 27.5 mg L^{-1} at 37 °C in different media (Figure 7): buffer comprising 50 mM Tris–HCl (pH 7.0), synthetic wastewater medium according to Organization of Economic Co-operation and Development (OECD), and autoclaved real municipal wastewater (MWW). In all studied media, a high percentage of malathion removal was observed: after the first cycle, the percent of malathion degradation was 99.4 ± 2.8%, 99.2 ± 2.4%, and 99.5 ± 1.4% in 50 mM Tris–HCl (pH 7.0), OECD, and MWW, respectively. During the operation, the activity of the biocatalyst decreased gradually during all cycles of malathion hydrolysis. However, the catalyst showed high stability in all studied media, providing a percent of malathion degradation above 55% after 25 cycles of reaction (350 h).

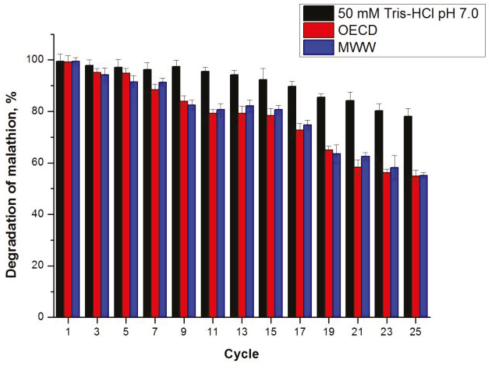

Figure 7. Operational stability of CLEA-estUT1 during cycles of malathion hydrolysis in various media. Reactions were performed at initial malathion concentration of 27.5 mg L^{-1} at 37 °C. After each cycle, biocatalyst was centrifuged and washed three times with 50 mM Tris–HCl (pH 7.0), and then resuspended in a fresh reaction mixture. OECD: synthetic wastewater; MWW: autoclaved real municipal wastewater.

2.3.5. Comparison of Microbial Biodegradation and CLEA-estUT1 Hydrolysis of Malathion

Typically, the microbial biodegradation of malathion (up to 50–80%) takes from a few hours up to a few days (Table 8) if the liquid culture is used. For example, *B. licheniformis* strain ML-1 provided about 78% malathion removal from liquid media within five days [8]. Carboxylesterase D1CarE5 from the bacterium *Alicyclobacillus tengchongensis*, which was cloned in pET28a (+) and expressed in *E. coli* BL21(DE3), revealed the high capability to hydrolyze malathion: the removal of malathion was 89% within 100 min at its initial concentration of 5 mg L^{-1} [11]. However, such a high activity of the carboxylesterase D1CarE5 may be due to a low initial concentration of malathion in the solution. *Bacillus* sp. S14 immobilized in 3% calcium alginate is the only biocatalyst that has been applied in malathion removal from aqueous solutions (64.4% under optimal conditions) [15]. The CLEA-estUT1 biocatalyst in this study not only exceeds the activity of the last microbial biocatalyst (Table 8) [15], but also remains stable (malathion removal > 78.1 ± 3.1%) within 25 cycles of hydrolysis in 50 mM Tris–HCl (pH 7.0). In this study, the real municipal wastewater (MWW) supplemented with malathion was successfully used for the evaluation of the ability of CLEA-estUT1 to hydrolyse insecticide. Under these conditions, the percentage of malathion removal was above 55.2 ± 1.1% for 25 cycles. Application of immobilized esterase estUT1 allowed the effective hydrolysis of malathion and repeated use of the biocatalyst, which make it promising for application in processes of insecticide biodegradation, including wastewater treatment.

Table 8. Comparison of malathion biodegradation with microbial biocatalysts.

Biocatalyst	Experimental Condition	Removal of Malathion, %	Reference
CLEA-estUT1 (*U. thermosphaericus*)	Malathion concentration = 27.5 mg L^{-1} Temperature = 37 °C Time = 14 h pH = 7.0 rpm = 250	99.4 ± 2.8	This study
CLEA-estUT1 (*U. thermosphaericus*)	Malathion concentration = 27.5 mg L^{-1} Temperature = 37 °C Time = 14 h Municipal wastewater (MWW) rpm = 250	99.5 ± 1.4	This study
Bacillus sp. S14 immobilized in 3% calcium alginate	Malathion concentration = 50 mg L^{-1} Temperature = 25 °C Time = 8 h pH = 7.0 rpm = 120	64.4	[15]
B. licheniformis strain ML-1	Malathion concentration = 25 mg L^{-1} Temperature = 32 °C Time = 5 days pH = 7.5 rpm = 250	78	[8]
Carboxylesterase D1CarE5 (*A. tengchongensis*)	Malathion concentration = 5 mg L^{-1} Temperature = 37 °C Time = 100 min pH = 7.0	89	[11]
Bacillus thuringiensis	Malathion concentration = 250 mg L^{-1} Temperature = 30 °C Time = 3 days	50	[53]
Bacillus cereus strain PU	Malathion concentration = 72.5 mg L^{-1} Temperature = 30 °C Time = 7 days pH = 7.0	49.31	[54]
P. putida	Malathion concentration = 125 mg L^{-1} Temperature = 30 °C Time = 7 days pH = 7.0 rpm = 150	72	[5]

3. Materials and Methods

3.1. Materials

Plasmid pET32b-UT1 containing the esterase gene estUT1 (Genbank accession number MF156209) was constructed in our laboratory [30]; *E. coli* strain BL21(DE3) (Thermo Fisher Scientific, Waltham, MA, USA) was used for the enzyme expression; plasmids pBB540 and pBB542 were a gift from Bernd Bukau (Addgene plasmids #27393 and #27395, respectively, Cambridge, MA, USA) [35]; *p*-nitrophenyl esters and SDS were purchased from Sigma-Aldrich (St. Louis, MO, USA). All other chemicals were of analytical grade (Merck, Darmstadt, Germany).

3.2. Expression of Esterase estUT1

Overnight culture of *E. coli* BL21(DE3) cells transformed with plasmid pET32b-UT1 was inoculated into 250 mL of LB and cultivated at 32 °C until OD_{600} of 0.6. Protein synthesis was induced with 0.5 mM IPTG at 16 °C for 20 h. Cells were harvested by centrifugation (3000× *g*, 4 °C for 10 min), washed twice by 50 mM Tris–HCl pH 7.0, and disrupted by sonication (5 cycles, 40 s pulse, 20 s pause) at 0 °C. The cell-free protein extract was prepared by centrifugation at 5500× *g* and 4 °C for 20 min. The supernatant and the precipitate were collected as soluble and insoluble fractions, respectively. The supernatant containing the recombinant esterase was purified by ion metal affinity chromatography using a Ni-NTA (Ni-nitrilotriacetic acid) agarose; the enzyme was eluted using an increasing concentration gradient of imidazole (0–300 mM) in 50 mM Tris–HCl pH 8.0, 0.5 M NaCl.

3.3. Co-Expression of Chaperones

For co-expression of esterase with chaperones, *E. coli* BL21(DE3) cells were first transformed with plasmids pBB540 (GrpE, ClpB) and pBB542 (DnaK, DnaJ, GroEL, and GroES) [35]. Then, the chaperone-overexpressing cells were transformed with plasmid pET32b-UT1. EstUT1 was expressed as described above, and after cell lysis, the supernatant was collected as a soluble fraction. This fraction was purified with Ni-NTA agarose as described above.

The molecular mass of proteins was examined with 12% sodium dodecyl sulfate-polyacrylamide gel electrophoresis (SDS-PAGE) according to the standard procedures [55]. Protein concentration was determined by the Bradford method [56] with bovine serum albumin as a standard.

3.4. Enzyme Activity Assay

Esterase activity was determined by measuring the amount of *p*-nitrophenol released after hydrolysis of *p*NPC2 [57]. The *p*NPC2 was dissolved in acetonitrile at a concentration of 100 mM. Ethanol and 50 mM Tris–HCl (pH 8.0) buffer were subsequently added to this solution, in which the final ratio of acetonitrile to ethanol to Tris–HCl buffer was 1:4:95 ($v/v/v$). The reaction was initiated by adding 20 µL of the enzyme solution (0.05 mg mL^{-1}) to 150 µL of substrate mixture and incubated for 15 min at 50 °C, followed by analysis of absorbance at 405 nm. One unit (U) of esterase activity was defined as the amount of enzyme that released 1 µmol of *p*-nitrophenol per minute.

Recovered activity of CLEA-estUT1 biocatalyst was calculated by the following equation [58]:

$$\text{Recovered activity (\%)} = (\text{total activity of CLEAs})/(\text{total activity of free enzyme for CLEAs preparation}) \times 100 \quad (2)$$

Malathion hydrolysis was assayed according to the method of Liang et al. [52], with minor modifications. 5 µL of malathion solution in ethanol (10 mM) was added to 515 µL of 50 mM Tris–HCl pH 7.0 and 80 µL of enzyme (0.05 mg mL^{-1}) for incubation at 37 °C and 250 rpm for 30 min. Residual malathion was extracted with *n*-hexane and analyzed by gas chromatography mass spectrometry (GC/MS). GC/MS quantitative analysis was performed by using an Agilent 7000B GC/MS (Agilent Technologies, Santa Clara, CA, USA) system equipped with a HP-5ms fused silica

capillary column (30 m × 0.25 mm × 0.25 μm). Temperature was programmed from 200 °C (3 min) to 250 °C at 5 °C min^{-1}. Helium was used as a carrier gas (1.2 mL min^{-1}) and injector temperature was 250 °C. The mass spectrometer was operated in electron ionization (EI) mode at 70 eV; selected ion monitoring (SIM) mode with m/z 125 (the major fragment of malathion parent ion (m/z 330) after EI); m/z 154 (diphenyl as an internal standard). Malathion amount was calculated as malathion/diphenyl peak ratio. Malathion solution without enzyme was used as a control.

3.5. Preparation of CLEA-estUT1

Preparation of CLEAs from the estUT1 after its co-expression with the chaperone team of KJE, ClpB, and ELS was performed as follows: 0.5 mL of the enzyme solution (1 mg mL^{-1} in 50 mM Tris–HCl pH 8.0) was mixed with the varying concentrations of precipitant, water solution of glutaraldehyde, and additives to the final volume of 2 mL. The solution was agitated at 200 rpm and 4 °C for a required period. Samples were collected and centrifuged at 4000× *g* and 4 °C for 15 min, then washed two times with 50 mM Tris–HCl pH 8.0. The biocatalyst was stored in 50 mM Tris–HCl pH 8.0 at 4 °C.

3.6. Selection of Precipitant

The effect of different precipitants including acetone, *tert*-butanol, isopropanol, ethanol, and ammonium sulfate 50% (*w*/*v*) was assayed in this study. The precipitant–enzyme ratio was 2:1 (*v*/*v*). Biocatalyst was prepared as described in Section 3.5. 75 mM glutaraldehyde was used as cross-linker; time of cross-linking was 4 h.

3.7. Selection of Various Additives

BSA (10 mg) and SDS (10 mg) as additives were used in this study. Biocatalyst was prepared as described in Section 3.5. The concentrations of ammonium sulfate and glutaraldehyde were 60% (*w*/*v*) and 75 mM, respectively. The cross-linking time was 4 h.

3.8. Optimization of CLEA-estUT1 Preparation

The process for preparation of CLEA-estUT1 biocatalyst was optimized with RSM based on FCCCD. Four factors were selected: cross-linking time (1, 4.5, and 8 h), concentration of ammonium sulfate (30, 55, and 80%, *w*/*v*), glutaraldehyde (25, 87.5, and 150 mM) and BSA (0.01, 0.105, and 0.2 mM). The design consisted of 30 runs with six replicates at the central point and provided enough information to establish a second-order polynomial model for the response surface. Regression analysis and regression equation (ANOVA) was performed using Design-Expert software v. 10 (Stat-Ease Inc., Minneapolis, MN, USA).

3.9. Properties of CLEA-estUT1 Biocatalyst

3.9.1. Effect of pH and Temperature

The effect of pH was examined by assaying enzyme activity of free and immobilized estUT1 at pH 5.0–10.0 in different 50 mM buffers: citrate phosphate (pH 5.0–6.0), sodium phosphate (pH 6.0–8.0), Tris–HCl (pH 8.0–9.0), and glycine–NaOH (pH 9.0–10.0). Reactions were performed using *p*NPC2 as a substrate in buffer at 50 °C. The pH stability of estUT1 and CLEA-estUT1 was examined in different buffers at 50 °C after 1 h of incubation.

The temperature optimum of free and immobilized estUT1 was determined in the range of 30–90 °C in 50 mM of Tris–HCl buffer (pH 8.0) with *p*NPC2 as a substrate. The thermostability of estUT1 and CLEA-estUT1 was examined by incubating the enzyme in 50 mM of Tris–HCl buffer (pH 8.0) at 50–80 °C for 1–8 h. The inactivation rate constant (k_i) was determined from the slope of the inactivation time using equation [59]:

$$\ln(E/E_0) = -k_i t \quad (3)$$

where E: the residual enzyme activity after heat treatment for time t and E_0: the initial activity before the heat treatment.

The half-life of thermal inactivation ($t_{1/2}$) was determined according to equation [60]:

$$t_{1/2} = \ln(2)/k_i \quad (4)$$

3.9.2. Effect of Chemicals

The effect of various reagents (30% ethanol and methanol, v/v; 10 mM PMSF, BME, and DTT; 1% SDS, Tween 20, and Triton X-100, w/v) on the activity of free and immobilized estUT1 was determined by adding these chemicals to the enzyme or biocatalyst solution and assayed after preincubation for 1 h at 50 °C. Esterase activity without addition of reagents was defined as 100%.

3.9.3. Kinetic Parameters

Kinetic parameters (K_m, k_{cat}) of free and immobilized estUT1 were determined by nonlinear regression using the Michaelis–Menten equation. The kinetic assay was performed with different concentrations (0.003–10 mM) of *p*NPC2, *p*NPC4, *p*NPC8, and malathion as substrates with the standard procedure as described above (Section 3.4).

3.9.4. Operational Stability of CLEA-estUT1 during Hydrolysis of Malathion

The operational stability of CLEA-estUT1 was determined by repeated use of CLEA-estUT1 in hydrolysis of malathion in three different media: autoclaved wastewater after the primary settler from the Novosibirsk municipal wastewater treatment facility (MWW), autoclaved synthetic wastewater (OECD) [61], and 50 mM Tris–HCl pH 7.0. 0.1 g CLEA-estUT1 in 495.8 µL of the medium was incubated with 4.2 µL malathion solution in EtOH (10 mM) at 37 °C at 250 rpm for 14 h. Residual malathion was determined as described in Section 3.4. Between cycles, CLEAs were recovered by centrifugation (4000× *g*, 4 °C, 5 min) and washed three times with 50 mM Tris–HCl pH 7.0.

MWW had the following composition [62]: COD 161.0 ± 5.0 mg L^{-1}, 27.7 ± 1.3 mg L^{-1} N-NH_4, 0.2 ± 0.0 mg L^{-1} N-NO_3, 1.8 ± 0.1 mg L^{-1} P-PO_4, 10.7 ± 1.0 mg L^{-1} S-SO_4, and 139.0 ± 5.0 mg L^{-1} Cl.

3.10. Statistical Analysis

Data on the experiments of the central compositional plan (RSM with FCCCD) were used to determine the regression coefficients of the quadratic polynomial model and the *F*-test analysis. Dispersion analysis (ANOVA), regression analysis, and surface plotting were used to optimize the CLEAs preparation. The accuracy of the resulting polynomial model was estimated using the determination coefficient R^2. All experiments in this work, with the exception of the FCCCD experiments, were performed in triplicate, and the results are presented as the arithmetic mean ± standard deviation.

4. Conclusions

In this study, the CLEAs biocatalyst was used for the first time for the hydrolysis of malathion in municipal wastewater. A complex approach involving the improved expression of a new thermostable esterase estUT1 in a soluble form and optimization of CLEAs preparation was applied to maximize biocatalyst activity. In particular, the intracellular aggregation of the esterase estUT1 from *U. thermosphaericus* in *E. coli* BL21(DE3) was partially resolved by its co-expression with molecular chaperones (KJE, ClpB, and ELS), and a stable CLEA-estUT1 biocatalyst was prepared after purification of estUT1 from the soluble fraction of cell protein. Optimization of the CLEAs preparation was performed with RSM using FCCCD. Immobilization by the cross-linking method allowed the stability of the esterase estUT1 at high temperatures (50–80 °C) to be increased, in a wide range of pH (5.0–10.0). Immobilization improved enzyme tolerance against various chemicals, especially PMSF, DTT, BME, 1% SDS, and Tween 20. CLEA-estUT1 showed high activity in the reaction of malathion hydrolysis

in wastewater (the removal of malathion was 99.5 ± 1.4%) and reusability, maintaining 55.2 ± 1.1% of its activity after 25 cycles of malathion hydrolysis at 37 °C. A novel CLEA-estUT1 biocatalyst can be effectively applied for the removal of malathion from wastewaters from municipal wastewater treatment facilities and in clean-out procedures of malathion storage tanks.

Acknowledgments: The reported study was funded by Russian Foundation for Basic Research according to the research project no. 18-38-00386.

Author Contributions: Yuliya V. Samoylova, Ksenia N. Sorokina, and Valentin N. Parmon designed the experiments; Yuliya V. Samoylova and Alexander V. Piligaev performed the experiments; Yuliya V. Samoylova, Alexander V. Piligaev, and Ksenia N. Sorokina analyzed the data; Yuliya V. Samoylova and Ksenia N. Sorokina wrote the paper.

Conflicts of Interest: The authors declare no conflict of interest.

References

1. Firestone, J.A.; Smith-Weller, T.; Franklin, G.; Swanson, P.; Longstreth, W.T., Jr.; Checkoway, H. Pesticides and risk of parkinson disease: A population-based case-control study. *Arch. Neurol.* **2005**, *62*, 91–95. [CrossRef] [PubMed]
2. Alavanja, M.C.R.; Hoppin, J.A.; Kamel, F. Health effects of chronic pesticide exposure: Cancer and neurotoxicity. *Ann. Rev. Public Health* **2004**, *25*, 155–197. [CrossRef] [PubMed]
3. Zhang, Y.; Pagilla, K. Treatment of malathion pesticide wastewater with nanofiltration and photo-fenton oxidation. *Desalination* **2010**, *263*, 36–44. [CrossRef]
4. Shayeghi, M.; Dehghani, M.H.; Alimohammadi, M.; Goodini, K. Using ultraviolet irradiation for removal of malathion pesticide in water. *J. Arthropod-Borne Dis.* **2012**, *6*, 45–53. [PubMed]
5. Geed, S.R.; Kureel, M.K.; Shukla, A.K.; Singh, R.S.; Rai, B.N. Biodegradation of malathion and evaluation of kinetic parameters using three bacterial species. *Resour. Effic. Technol.* **2016**, *2*, S3–S11. [CrossRef]
6. Kim, Y.-H.; Ahn, J.-Y.; Moon, S.-H.; Lee, J. Biodegradation and detoxification of organophosphate insecticide, malathion by *Fusarium oxysporum* f. sp. *pisi* cutinase. *Chemosphere* **2005**, *60*, 1349–1355. [CrossRef] [PubMed]
7. Ibrahim, W.M.; Karam, M.A.; El-Shahat, R.M.; Adway, A.A. Biodegradation and utilization of organophosphorus pesticide malathion by cyanobacteria. *BioMed Res. Int.* **2014**, *2014*, 392682. [CrossRef] [PubMed]
8. Khan, S.; Zaffar, H.; Irshad, U.; Ahmad, R.; Khan, A.R.; Shah, M.M.; Bilal, M.; Iqbal, M.; Naqvi, T. Biodegradation of malathion by *Bacillus licheniformis* strain ML-1. *Arch. Biol. Sci.* **2016**, *68*, 9. [CrossRef]
9. Goda, S.K.; Elsayed, I.E.; Khodair, T.A.; El-Sayed, W.; Mohamed, M.E. Screening for and isolation and identification of malathion-degrading bacteria: Cloning and sequencing a gene that potentially encodes the malathion-degrading enzyme, carboxylestrase in soil bacteria. *Biodegradation* **2010**, *21*, 903–913. [CrossRef] [PubMed]
10. Schofield, D.A.; DiNovo, A.A. Generation of a mutagenized organophosphorus hydrolase for the biodegradation of the organophosphate pesticides malathion and demeton-s. *J. Appl. Microbiol.* **2010**, *109*, 548–557. [CrossRef] [PubMed]
11. Xie, Z.; Xu, B.; Ding, J.; Liu, L.; Zhang, X.; Li, J.; Huang, Z. Heterologous expression and characterization of a malathion-hydrolyzing carboxylesterase from a thermophilic bacterium, *Alicyclobacillus tengchongensis*. *Biotechnol. Lett.* **2013**, *35*, 1283–1289. [CrossRef] [PubMed]
12. Sheldon, R.A.; van Pelt, S. Enzyme immobilisation in biocatalysis: Why, what and how. *Chem. Soc. Rev.* **2013**, *42*, 6223–6235. [CrossRef] [PubMed]
13. Samoylova, Y.V.; Piligaev, A.V.; Sorokina, K.N.; Rozanov, A.S.; Peltek, S.E.; Novikov, A.A.; Almyasheva, N.R.; Parmon, V.N. Application of the immobilized bacterial recombinant lipase from *Geobacillus stearothermophilus* G3 for the production of fatty acid methyl esters. *Catal. Ind.* **2016**, *8*, 187–193. [CrossRef]
14. Samoylova, Y.V.; Piligaev, A.V.; Sorokina, K.N.; Parmon, V.N. Enzymatic interesterification of sunflower oil and hydrogenated soybean oil with the immobilized bacterial recombinant lipase from *Geobacillus stearothermophilus* G3. *Catal. Ind.* **2017**, *9*, 62–70. [CrossRef]
15. Adhikari, S.; Chattopadhyay, P.; Ray, L. Biosorption of malathion by immobilized cells of *Bacillus* sp. S14. *Chem. Spec. Bioavailabil.* **2010**, *22*, 271–276. [CrossRef]

16. Saida, F.; Uzan, M.; Odaert, B.; Bontems, F. Expression of highly toxic genes in *E. coli*: Special strategies and genetic tools. *Curr. Protein Pept. Sci.* **2006**, *7*, 47–56. [CrossRef] [PubMed]
17. De Marco, A. Strategies for successful recombinant expression of disulfide bond-dependent proteins in *Escherichia coli*. *Microb. Cell Fact.* **2009**, *8*, 26. [CrossRef] [PubMed]
18. Rosano, G.L.; Ceccarelli, E.A. Recombinant protein expression in Escherichia coli: Advances and challenges. *Front. Microbiol.* **2014**, *5*, 172. [CrossRef] [PubMed]
19. Valero, F. Heterologous expression systems for lipases: A review. In *Lipases and Phospholipases: Methods and Protocols*; Sandoval, G., Ed.; Humana Press: Totowa, NJ, USA, 2012; pp. 161–178.
20. Shuo-shuo, C.; Xue-zheng, L.; Ji-hong, S. Effects of co-expression of molecular chaperones on heterologous soluble expression of the cold-active lipase lip-948. *Protein Expr. Purif.* **2011**, *77*, 166–172. [CrossRef] [PubMed]
21. Singh, R.K.; Tiwari, M.K.; Singh, R.; Lee, J.-K. From protein engineering to immobilization: Promising strategies for the upgrade of industrial enzymes. *Int. J. Mol. Sci.* **2013**, *14*, 1232–1277. [CrossRef] [PubMed]
22. Mohamad, N.R.; Marzuki, N.H.C.; Buang, N.A.; Huyop, F.; Wahab, R.A. An overview of technologies for immobilization of enzymes and surface analysis techniques for immobilized enzymes. *Biotechnol. Biotechnol. Equip.* **2015**, *29*, 205–220. [CrossRef] [PubMed]
23. Han, J.Y.; Kim, H. Transesterification using the cross-linked enzyme aggregate of *Photobacterium lipolyticum* lipase M37. *J. Microbiol. Biotechnol.* **2011**, *21*, 1159–1165. [CrossRef] [PubMed]
24. Tükel, S.S.; Hürrem, F.; Yildirim, D.; Alptekin, Ö. Preparation of crosslinked enzyme aggregates (CLEA) of catalase and its characterization. *J. Mol. Catal. B Enzym.* **2013**, *97*, 252–257. [CrossRef]
25. Morales, A.; Barbosa, O.; Rueda, N.; Fonseca, Z.; Torres, R.; Rodrigues, R.C.; Ortiz, C.; Fernandez-Lafuente, R. Optimization and characterization of CLEAs of the very thermostable dimeric peroxidase from *Roystonea regia*. *RSC Adv.* **2015**, *5*, 53047–53053. [CrossRef]
26. Jang, E.; Ryu, B.; Kim, T. Identification, characterization, and immobilization of an organic solvent-stable alkaline hydrolase (PA27) from *Pseudomonas aeruginosa* MH38. *Molecules* **2014**, *19*, 14396. [CrossRef] [PubMed]
27. Kumari, V.; Shah, S.; Gupta, M.N. Preparation of biodiesel by lipase-catalyzed transesterification of high free fatty acid containing oil from *Madhuca indica*. *Energy Fuels* **2007**, *21*, 368–372. [CrossRef]
28. Piligaev, A.V.; Sorokina, K.N.; Samoylova, Y.V.; Parmon, V.N. Lipid production by microalga *Micractinium* sp. IC-76 in a flat panel photobioreactor and its transesterification with cross-linked enzyme aggregates of *Burkholderia cepacia* lipase. *Energy Convers. Manag.* **2018**, *156*, 1–9. [CrossRef]
29. Shah, S.; Gupta, M.N. Kinetic resolution of (±)-1-phenylethanol in [Bmim][PF6] using high activity preparations of lipases. *Bioorgan. Med. Chem. Lett.* **2007**, *17*, 921–924. [CrossRef] [PubMed]
30. Samoylova, Y.V.; Sorokina, K.N.; Romanenko, M.V.; Parmon, V.N. Cloning, expression and characterization of the esterase estUT1 from *Ureibacillus thermosphaericus* which belongs to a new lipase family XVIII. *Extremophiles* **2018**, *22*, 271–285. [CrossRef] [PubMed]
31. Mogk, A.; Mayer, M.P.; Deuerling, E. Mechanisms of Protein Folding: Molecular Chaperones and Their Application in Biotechnology. *Chembiochem* **2002**, *3*, 807–814. [CrossRef]
32. Schlieker, C.; Bukau, B.; Mogk, A. Prevention and reversion of protein aggregation by molecular chaperones in the *E. coli* cytosol: Implications for their applicability in biotechnology. *J. Biotechnol.* **2002**, *96*, 13–21. [CrossRef]
33. Mogk, A.; Tomoyasu, T.; Goloubinoff, P.; Rüdiger, S.; Röder, D.; Langen, H.; Bukau, B. Identification of thermolabile *Escherichia coli* proteins: Prevention and reversion of aggregation by DnaK and ClpB. *EMBO J.* **1999**, *18*, 6934–6949. [CrossRef] [PubMed]
34. Sørensen, H.P.; Mortensen, K.K. Soluble expression of recombinant proteins in the cytoplasm of *Escherichia coli*. *Microb. Cell Fact.* **2005**, *4*, 1. [CrossRef] [PubMed]
35. De Marco, A.; Deuerling, E.; Mogk, A.; Tomoyasu, T.; Bukau, B. Chaperone-based procedure to increase yields of soluble recombinant proteins produced in *E. coli*. *BMC Biotechnol.* **2007**, *7*, 32. [CrossRef] [PubMed]
36. Hanefeld, U.; Gardossi, L.; Magner, E. Understanding enzyme immobilisation. *Chem. Soc. Rev.* **2009**, *38*, 453–468. [CrossRef] [PubMed]
37. Khanahmadi, S.; Yusof, F.; Amid, A.; Mahmod, S.S.; Mahat, M.K. Optimized preparation and characterization of CLEA-lipase from cocoa pod husk. *J. Biotechnol.* **2015**, *202*, 153–161. [CrossRef] [PubMed]

38. Zheng, G.-W.; Yu, H.-L.; Li, C.-X.; Pan, J.; Xu, J.-H. Immobilization of *Bacillus subtilis* esterase by simple cross-linking for enzymatic resolution of dl-menthyl acetate. *J. Mol. Catal. B Enzym.* **2011**, *70*, 138–143. [CrossRef]
39. Nadar, S.S.; Muley, A.B.; Ladole, M.R.; Joshi, P.U. Macromolecular cross-linked enzyme aggregates (M-CLEAs) of α-amylase. *Int. J. Biol. Macromol.* **2016**, *84*, 69–78. [CrossRef] [PubMed]
40. Mahmod, S.S.; Yusof, F.; Jami, M.S.; Khanahmadi, S.; Shah, H. Development of an immobilized biocatalyst with lipase and protease activities as a multipurpose cross-linked enzyme aggregate (multi-CLEA). *Process Biochem.* **2015**, *50*, 2144–2157. [CrossRef]
41. Dong, T.; Zhao, L.; Huang, Y.; Tan, X. Preparation of cross-linked aggregates of aminoacylase from *Aspergillus melleus* by using bovine serum albumin as an inert additive. *Bioresour. Technol.* **2010**, *101*, 6569–6571. [CrossRef] [PubMed]
42. Gupta, R.; Beg, Q.; Lorenz, P. Bacterial alkaline proteases: Molecular approaches and industrial applications. *Appl. Microbiol. Biotechnol.* **2002**, *59*, 15–32. [PubMed]
43. Torres, M.P.G.; Foresti, M.L.; Ferreira, M.L. Effect of different parameters on the hydrolytic activity of cross-linked enzyme aggregates (CLEAs) of lipase from *Thermomyces lanuginosa*. *Biochem. Eng. J.* **2013**, *72*, 18–23. [CrossRef]
44. Kartal, F.; Kilinc, A. Crosslinked aggregates of *Rhizopus oryzae* lipase as industrial biocatalysts: Preparation, optimization, characterization, and application for enantioselective resolution reactions. *Biotechnol. Prog.* **2012**, *28*, 937–945. [CrossRef] [PubMed]
45. Talekar, S.; Waingade, S.; Gaikwad, V.; Patil, S.; Nagavekar, N. Preparation and characterization of cross linked enzyme aggregates (CLEAs) of *Bacillus amyloliquefaciens* alpha amylase. *J. Biochem. Technol.* **2012**, *3*, 349–353.
46. Yu, C.-Y.; Li, X.-F.; Lou, W.-Y.; Zong, M.-H. Cross-linked enzyme aggregates of mung bean epoxide hydrolases: A highly active, stable and recyclable biocatalyst for asymmetric hydrolysis of epoxides. *J. Biotechnol.* **2013**, *166*, 12–19. [CrossRef] [PubMed]
47. Ju, H.; Ryu, B.H.; Doohun Kim, T. Identification, characterization, immobilization of a novel type hydrolase (LmH) from *Listeria monocytogenes*. *Int. J. Biol. Macromol.* **2015**, *72*, 63–70. [CrossRef] [PubMed]
48. Scott, M.J.; Jones, M.N. The biodegradation of surfactants in the environment. *Biochim. Biophys. Acta (BBA) Biomembr.* **2000**, *1508*, 235–251. [CrossRef]
49. Amin, M.T.; Alazba, A.A.; Manzoor, U. A review of removal of pollutants from water/wastewater using different types of nanomaterials. *Adv. Mater. Sci. Eng.* **2014**, *2014*, 825910. [CrossRef]
50. Xu, D.-Y.; Yang, Y.; Yang, Z. Activity and stability of cross-linked tyrosinase aggregates in aqueous and nonaqueous media. *J. Biotechnol.* **2011**, *152*, 30–36. [CrossRef] [PubMed]
51. Mahmod, S.S.; Yusof, F.; Jami, M.S.; Khanahmadi, S. Optimizing the preparation conditions and characterization of a stable and recyclable cross-linked enzyme aggregate (CLEA)-protease. *Bioresour. Bioprocess.* **2016**, *3*, 3. [CrossRef]
52. Liang, W.Q.; Wang, Z.Y.; Li, H.; Wu, P.C.; Hu, J.M.; Luo, N.; Cao, L.X.; Liu, Y.H. Purification and characterization of a novel pyrethroid hydrolase from *Aspergillus niger* ZD11. *J. Agric. Food Chem.* **2005**, *53*, 7415–7420. [CrossRef] [PubMed]
53. Mohamed, Z.K.; Ahmed, M.A.; Fetyan, N.A.; Elnagdy, S.M. Isolation and molecular characterisation of malathion-degrading bacterial strains from waste water in Egypt. *J. Adv. Res.* **2010**, *1*, 145–149. [CrossRef]
54. Singh, B.; Kaur, J.; Singh, K. Biodegradation of malathion by *Brevibacillus* sp. strain KB2 and *Bacillus cereus* strain PU. *World J. Microbiol. Biotechnol.* **2012**, *28*, 1133–1141. [CrossRef] [PubMed]
55. Laemmli, U.K. Cleavage of structural proteins during the assembly of the head of bacteriophage T4. *Nature* **1970**, *227*, 680. [CrossRef] [PubMed]
56. Bradford, M.M. A rapid and sensitive method for the quantitation of microgram quantities of protein utilizing the principle of protein-dye binding. *Anal. Biochem.* **1976**, *72*, 248–254. [CrossRef]
57. Eom, G.T.; Song, J.K.; Ahn, J.H.; Seo, Y.S.; Rhee, J.S. Enhancement of the efficiency of secretion of heterologous lipase in *Escherichia coli* by directed evolution of the abc transporter system. *Appl. Environ. Microbiol.* **2005**, *71*, 3468–3474. [CrossRef] [PubMed]
58. Kim, M.H.; Park, S.; Kim, Y.H.; Won, K.; Lee, S.H. Immobilization of formate dehydrogenase from *Candida boidinii* through cross-linked enzyme aggregates. *J. Mol. Catal. B Enzym.* **2013**, *97*, 209–214. [CrossRef]

59. Lawton, J.M.; Doonan, S. Thermal inactivation and chaperonin-mediated renaturation of mitochondrial aspartate aminotransferase. *Biochem. J.* **1998**, *334*, 219. [CrossRef] [PubMed]
60. Xu, Z.; Liu, S.; Lu, X.; Rao, S.; Kang, Z.; Li, J.; Wang, M.; Chen, J. Thermal inactivation of a recombinant lipoxygenase from *Pseudomonas aeruginosa* BBE in the absence and presence of additives. *J. Sci. Food Agric.* **2014**, *94*, 1753–1757. [CrossRef] [PubMed]
61. OECD. *Guidelines for Testing of Chemicals Simulation Tests-Aerobic Sewage Treatment*; Technical Report; Organisation for Economic Co-Operation and Development (OECD): Paris, France, 1996; pp. 19–142.
62. Piligaev, A.V.; Sorokina, K.N.; Shashkov, M.V.; Parmon, V.N. Screening and comparative metabolic profiling of high lipid content microalgae strains for application in wastewater treatment. *Bioresour. Technol.* **2018**, *250*, 538–547. [CrossRef] [PubMed]

© 2018 by the authors. Licensee MDPI, Basel, Switzerland. This article is an open access article distributed under the terms and conditions of the Creative Commons Attribution (CC BY) license (http://creativecommons.org/licenses/by/4.0/).

catalysts

MDPI

Article

Genetically Fused T4L Acts as a Shield in Covalent Enzyme Immobilisation Enhancing the Rescued Activity

Matteo Planchestainer, David Roura Padrosa, Martina Letizia Contente and Francesca Paradisi *

School of Chemistry, University of Nottingham, University Park, Nottingham NG7 2RD, UK; matteo.planchestainer@nottingham.ac.uk (M.P.); pcxdr1@exmail.nottingham.ac.uk (D.R.P.); martina.contente@nottingham.ac.uk (M.L.C.)

* Correspondence: francesca.paradisi@nottingham.ac.uk; Tel.: +44-(0)115-74-86267

Received: 3 January 2018; Accepted: 16 January 2018; Published: 20 January 2018

Abstract: Enzyme immobilisation is a common strategy to increase enzymes resistance and reusability in a variety of excellent 'green' applications. However, the interaction with the solid support often leads to diminished specific activity, especially when non-specific covalent binding to the carrier takes place which affects the delicate architecture of the enzyme. Here we developed a broadly applicable strategy where the T4-lysozyme (T4L) is genetically fused at the N-terminus of different enzymes and used as inert protein spacer which directly attaches to the carrier preventing shape distortion of the catalyst. *Halomonas elongata* aminotransferase (HEWT), *Bacillus subtilis* engineered esterase (BS2m), and horse liver alcohol dehydrogenase (HLADH) were used as model enzymes to elucidate the benefits of the spacer. While HEWT and HLADH activity and expression were diminished by the fused T4L, both enzymes retained almost quantitative activity after immobilisation. In the case of BS2m, the protective effect of the T4L effectively was important and led to up to 10-fold improvement in the rescued activity.

Keywords: aminotransferase; esterase; alcohol dehydrogenases; biocatalysis; enzyme immobilisation

1. Introduction

With the current expansion of biocatalysis and the consequent extensive application of enzymes to chemistry manufacturing, solutions have been introduced to overcome the issues caused by the low stability of these natural catalysts [1,2]. In this panorama, immobilisation offers the significant advantage of rendering enzymes robust and reusable 'green' tools, which allow for the development of efficient biotransformations [3,4]. Enzyme immobilisation is indeed a very common solution to improve enzymatic stability and to make it less sensible to harsh environments (temperature, solvents, different pH) typical of synthetic reaction conditions [5].

Immobilisation techniques involve the interaction between a solid support, the carrier, and the enzyme. An essential requirement for any carrier is a large surface area which can be obtained using small porous beads. The physical characteristics of the matrices, the material (natural or synthetic, organic or inorganic), and the surface properties play an important role in the efficient binding of the enzymes [6] and the catalytic features of the immobilised catalyst. Although the immobilised enzymes show generally a satisfactory improvement in their stability, the loss of performance is significant compared to the free protein [7,8]. This effect is almost universally observed, especially among covalently immobilised enzymes, and it is mainly attributed to a severe protein shape distortion that develops during the process [9]. Several strategies have been described in the literature to overcome these limitations, however, they often shy away from covalent linking and are directed to non-covalent immobilisation strategies and interactions [6,10].

Despite the loss of catalytic efficiency, covalent immobilisation is still often a method of choice as it prevents leaching of the enzyme in the reaction. Molecular spacers, such as glutaraldehyde, have been satisfactorily applied in minimising enzyme deactivation [11]. Interestingly, in literature there are no examples where a second protein is used as a spacer for covalent immobilisation.

Chimeric structures where a second protein is fused to a target macromolecule (i.e., enzymes, receptors, etc.) have been successfully reported for a variety of applications such as increasing protein solubility, purification strategies, labelling, and crystallization [12]. An excellent example was the use of the lysozyme from the bacteriophage T4 (T4L), a small (160 amino acids), globular, highly soluble, protein which was exploited as fused chimeric system in several remarkable experiments of X-ray crystallography as a crystallization promoting agent, and it allowed for the first time to elucidate the structure of G-protein coupled receptors (GPCRs) [13]. In the context of enzyme immobilisation, a protein linker has been described for a non-covalent attachment driven by the insertion of a cationic binding module ($Z_{basic}2$) as an additional domain. However, in this case the fused protein was mainly exploited to promote the interaction towards an anionic carrier (CPG-sulfonate) [14,15].

In this work, we investigated the use of a protein linker in covalent enzyme immobilisation with the scope of maximising the rescued activity. The one-pot strategy developed for covalent immobilisation by Guisan et al. [16] exploits a polyhistidine tag, commonly used for ion metal affinity chromatography (IMAC) purification, to selectively direct the enzyme on metal-activated supports thus allowing for a faster reaction between the reactive matrix moieties (i.e., epoxy groups) and the nucleophilic lysine of the protein. This technique is reliable and broadly applied, however the random distribution of lysines on the enzymatic surface prevents rational attachment, and the rescued activity, while commonly expected to be lower than the free enzyme, is unpredictable. The genetic insertion of T4L, naturally rich in lysines, between the His-tag and the target enzyme would more favourably form covalent bonding, possibly preventing any direct cross-linking between the target enzyme and the carrier, leaving the enzyme solvent exposed.

The strategy was initially tested on the well characterised *Halomonas elongata* aminotransferase (HEWT) [17] which we have used covalently immobilised for biotransfomations in continuo; however, upon direct cross-linking to the carrier, the recovered activity reached about 30% when compared to the free enzyme [18,19]. T4L mediated immobilisation was then extended to horse liver alcohol dehydrogenase (HLADH) [20] and to a *Bacillus subtilis* esterase (BS2m) engineered (I270F/F314Y) to enhance its amidase activity [21].

2. Results

2.1. Construction of the Chimeras

A plasmid harbouring the T4L gene was exploited as vector backbone for the sub-cloning of the three target enzymes. The T4L was engineered by point mutation to render it catalytically inactive (E11Q mutation) in order to prevent any possible interference with the enzymatic activity of the selected catalysts. Kobilka and co-workers demonstrated that a relatively flexible linker may be necessary to allow the receptor and the T4L to fold correctly [22]. Therefore, a first construct was designed to incorporate a linker of nine amino acids between the T4L and the protein exploiting the existing amino acid sequence already present in the pRSET-b plasmid between the His-tag and the multi-cloning site (MCS). Furthermore, to evaluate the effect of the rigidity induced by the peptide loop between the two proteins, a second construct was created, reducing the existing spacer from nine to three amino acids (Figure 1).

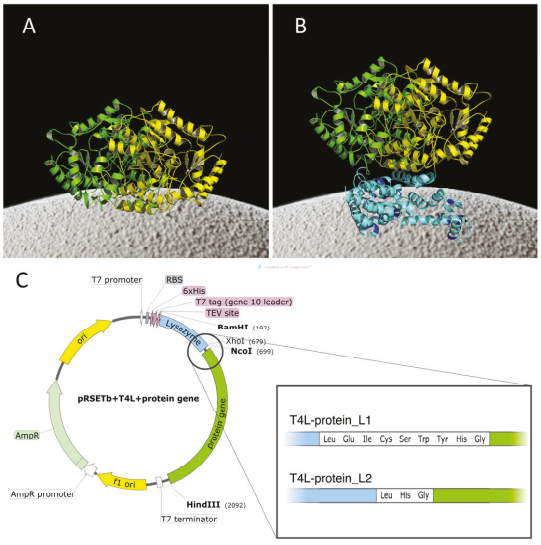

Figure 1. Proposed architecture of HEWT (green and yellow represent the two enzyme subunits) in covalent bonding directly on the solid support surface (**A**) or mediated by a linker protein (light blue, in dark blue the reactive lysines) (**B**). pRSET-b construct map outlining T4L (blue) and the protein gene (green). The inset shows the sequences of the two aminoacidic linkers separating the lysozyme and the target protein (**C**).

2.2. Halomonas elongata Aminotransferase

HEWT gene (*spuC*) was trialled first in both constructs (T4L-HEWT_L1 and T4L-HEWT_L2, nine and three amino acid long spacers, respectively). The expression level of both chimeras was lower than what obtained for HEWT, resulting in 12 and 20 mg of protein per litre of media, after IMAC purification, for T4L-HEWT_L1 and L2, respectively (Table 1). The proteins analysed by SDS-page electrophoresis did not show formation of any inclusion bodies caused by incorrect folding, and the decrease expression might simply be attributed to physiological limitation of the *E. coli* host in translating a longer gene. Although fusion tags have been reported to have a positive influence on protein solubility and expression, they do not function equally well with all target proteins [12]. Furthermore, analysis of the purified fractions confirmed the integrity of the constructs showing a molecular weight in the correct range of expected mass (Figure S1). HEWT specific activity was also affected by the presence of the lysozyme, with values of 1.37 and 0.50 U/mg for the two T4L-HEWT (Table 1). Such an effect could be explained with the fact that the N-term is a delicate structural domain which forms part of the active site; an exogenous module linked to it has a direct influence on its position and consequently on its catalytic efficiency. Indeed, with the longer linker the effect on activity was less severe, while with only three amino acids separating the lysozyme from HEWT the activity dropped 10 times with respect to the control. The proximity of the T4L can also hinder the substrate accessibility to the active site further influencing the reactivity.

The immobilisation of the chimeric constructs was carried out on two supports: Sepabeads EC-EP/S are described to have an average pore diameter of 10–20 nm, and ReliZyme EP403/S with a larger pore size (20–40 nm) which should favour better protein distribution and prevent 'caging' of the enzymes into narrow pores. In fact, the additional bulk of the T4L makes the chimeric construct significantly larger and this could potentially lead to immobilisation difficulties when the pore size of the resin is small. Immobilisation of the constructs followed the same procedure described

previously [18], maintaining cobalt(II) as the coordinating metal. Initially, 5 mg of enzyme per gram of resin were used, allowing the protein to react with the epoxy groups on the carrier for 24 h (Table 1).

Table 1. Comparison of specific activities and expression levels of the original *Halomonas elongata* aminotransferases (HEWT) and the two chimeric proteins in the free enzyme form. Specific activities of the resin following immobilisation of enzymes (5 mg_{enzyme}/g_{resin}), and percentage of residual activity after immobilisation (24 h, room temperature, in 50 mM phosphate buffer pH 8) with respect to the free protein.

	Free Enzyme		Immobilised Enzyme onto Sepabeads EC-EP/S (Pore ø 10–20 nm)		Immobilised Enzyme onto ReliZyme EP403/S (Pore ø 20–40 nm)	
	Specific Activity (U/mg)	Expression (mg/L)	Specific Activity (U/g)	Rescued Activity (%)	Specific Activity (U/g)	Rescued Activity (%)
HEWT	4.51 ± 0.05	40	5.1 ± 0.8	22.3	5.8 ± 0.6	26.1
T4L-HEWT_L1	1.37 ± 0.08	12	5.5 ± 0.5	80.4	6.0 ± 0.4	89.1
T4L-HEWT_L2	0.50 ± 0.07	20	1.5 ± 0.3	59.8	2.1 ± 0.1	84.1

On Sepabeads EC-EP/S, the control HEWT sample yielded 22% of recovered activity, while both T4L-HEWTs showed a marked improvement in the retention of activity with 80.4% and 59.8%, for the nine- and three-amino acid linker, respectively. These results confirm that the TL4 prevents direct attachment of the enzyme to the resin and this effect is enhanced by a longer spacer. On ReliZyme EP403/S the smaller wild type HEWT behaved virtually in the same manner, and likewise T4L-HEWT_L1 for which the rescued activity was already very high and the benefits of larger pores were not particularly significant. However, for the T4L-HEWT_L2 construct, the change observed in recovered activity was important, with almost a 30% improvement. Larger pores in this case may impact the number or covalent bonding with the surrounding surface leading to a reduced rigidity and distortion of the protein as well as generally increasing the substrate diffusion rate.

A range of concentrations for HEWT and T4L-HEWTs were then screened to assess the loading capacity of the resin, and whether the specific activity as well as the rescued activity could be further improved. The behaviour of HEWT and T4L + HEWT_L2 did not change significantly between 1 and 5 mg. At 10 mg of enzyme, the rescued activity decreased presumably due to surface overloading. On the other hand, the T4L + HEWT_L1 presents a bell-shape behaviour with a peak at 3 mg_{enzyme}/g_{resin} (Figure 2); it is plausible that the T4L coats the surface of the resin further protecting the enzyme from any binding to the resin yielding to almost equal activity as recorded for the free enzyme and a specific activity of the imm-T4L-HEWT_L1 of 1.28 U/mg versus 1.38 U/mg of the free T4L-HEWT_L1.

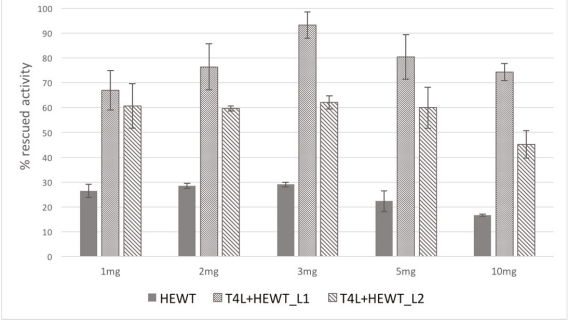

Figure 2. HEWT, T4L + HEWT_L1 and T4L + HEWT_L2 immobilisation (24 h, room temperature, in 50 mM phosphate buffer pH 8) at different enzyme loading per gram of resin Sepabeads EC-EP/S (pore ø 10–20 nm).

The incubation time to facilitate enzyme binding was investigated. It was postulated that the high distribution of lysines on the T4L surface could promote a faster immobilisation, and shorter incubation time may result in higher rescued activity. The immobilisation was thus carried out by leaving the enzymes to react with the resin between 1 and 24 h. Wild-type HEWT rescued activity was unaffected by the incubation time and consistent around 25–30%, while T4L + HEWT_L1 showed an unexpected behaviour with optimal value of rescued activity only after 24 h (Figure S2). 24 h was therefore selected as the ideal incubation time for further assays for all the HEWT variants.

Since the T4L chimeric proteins showed greater retained activities, they were further analysed to investigate the effect of the linker protein on the stability of the enzyme. Under standard storage conditions (4 °C, buffer phosphate pH 8, 0.1 mM PLP), the immobilised T4L-HEWTs showed unchanged specific activity for over a month. When the stability was evaluated by incubating the resin at 37 °C and 45 °C, no significant differences were observed with respect of the control HEWT immobilisation. On the other hand, the stability under working conditions (consecutive cycles of bioconversion), showed a slight negative trend in performance for the T4L-HEWT_L1 (Figure S3—circle), while the T4L-HEWT_L2 (Figure S3—square) was more stable with a virtually unchanged activity after 10 cycles, similarly to the imm-HEWT behaviour [18].

A significant feature of the imm-HEWT was the improved ability to withstand the presence of organic co-solvent in the reaction media with respect to the free enzyme. The construct harbouring the lysozyme spaced by the longer linker showed a similar behaviour to the free enzyme (Figure S4). This is not unexpected since the rationale of the protein linker was to prevent a direct bonding of the enzyme to the resin allowing a greater degree of freedom to the catalyst, which in this way no longer benefits from the imposed rigidity of the multi-point attachment to the carrier. However, when the shorter linker construct was assessed, the catalyst performed marginally better than the imm-HEWT (Figure S4), which is indicative of an enhanced stability induced by the close proximity of T4L to protein, similarly to the effect that BSA may have on pure proteins [23].

2.3. Bacillus subtilis Esterase

To validate the approach of the protein linker as a beneficial addition in enzymatic immobilisation, the strategy was extended to a second enzyme: *Bacillus subtilis* esterase, specifically a mutant variant (BS2m) engineered to augment its amidase activity [21]. Immobilisation of the purified enzyme via covalent attachment proved to be virtually impossible with almost complete loss of activity yielding negligible nominal activity of the support (1.3 U/g) when 5 mg_{enzyme}/g_{resin} were applied, equal to a rescued activity of 0.4% (Table 2). Such inability to retain activity upon covalent immobilisation is characteristic of many esterases [24,25]. Gross and co-workers speculated that this class of proteins tend to create a superficial layer preventing an efficient substrate diffusion [26]. As an example, the commercial catalyst NovoZyme 435 (*Candida antarctica* lipase-B, CAL-B) is immobilised at 82 mg_{enzyme}/g_{resin} but yields only 7.5% recovery activity, highlighting how this class of enzyme is particularly affected by immobilisation [27]. In addition, in the case of the BS2m variant, the superficial lysines, are concentrated in proximity to the active site which could drive the orientation of the enzyme in such a way that the catalytic pocket faces the support limiting its accessibility.

The same strategy applied for the HEWT was thus evolved towards the BS2m creating two chimeric constructs harbouring the 9- and 3-amino acid linkers. In this particular case, both longer and shorter linkers (T4L-BS2m_L1 and T4L-BS2m_L2, respectively) showed a less severe reduction in expression levels when compared to the original BS2m (Table 2, Figure S5) and an activity of 31 and 35 U/mg, respectively (Table 2). Covalent immobilisation onto the Sepabeads EC-EP/S epoxy-resin of the T4L-BS2m_L1 yielded an active resin with 5.5 U/g equal to 3.6% recovery activity, a notable 10-fold improvement on the original BS2m (Table 2). T4L-BS2m_L2, as observed for HEWT, did not perform as well as the L1 linker, with lower, yet still improved, immobilisation qualities (2.9 U/g and a 1.7% recovery activity). The co-immobilisation of T4L and BS2m, separately expressed and purified, was also tested to exclude a possible non-specific effect of the T4L but no enhancement of the

recovered activity was noted in this case (data not shown). This further confirmed that the fused T4L physically shields the enzyme from covalent attachment and does not directly affect enzyme activity.

Table 2. Comparison of specific activities and expression levels of the original *Bacillus subtilis* esterase (BS2m) and the two chimeric proteins in the free enzyme form. Specific activities of the resin following immobilisation of enzymes (5 mg_{enzyme}/g_{resin}), and percentage of residual activity after immobilisation (2 h, room temperature, in 50 mM phosphate buffer pH 8) with respect to the free protein.

	Free Enzyme		Immobilised Enzyme onto Sepabeads EC-EP/S (Pore ø 10–20 nm)		Immobilised Enzyme onto ReliZyme EP403/S (Pore ø 20–40 nm)	
	Specific Activity (U/mg)	Expression (mg/L)	Specific Activity (U/g)	Rescued Activity (%)	Specific Activity (U/g)	Rescued Activity (%)
BS2m	61 ± 4	30	1.3 ± 0.1	0.4	1.6 ± 0.3	0.5
T4L-BS2m_L1	31 ± 3	15	5.5 ± 0.8	3.6	6.2 ± 0.8	3.9
T4L-BS2m_L2	35 ± 2	13	2.9 ± 0.6	1.7	3.7 ± 0.4	2.1

Immobilisation of BS2m, T4L-BS2m_L1, and L2 was also tested on the ReliZyme (EP403/S). Interestingly, the new support offered better performance than the Sepabeads, allowing for a more efficient immobilisation for all variants (though still lower for the BS2m control). The recovered specific activity of T4L-BS2m_L1 reached 6.2 U/g (3.9%) and 3.7 U/g (2.1%) for the construct with the shorter link, confirming the benefits of a facilitated diffusion inside the solid support. This strategy therefore allowed to prepare an immobilised esterase with an activity considerably higher than the commercial NovoZyme 435 (4.5 U/g, tested under the same condition) using 16-fold less enzyme. Furthermore, the immobilised enzyme exhibited a great stability retaining 87% of its initial activity after five reaction cycles, comparable to the commercial CAL-B (83%) [27].

2.4. Horse Liver Alcohol Dehydrogenase

Finally, horse liver alcohol dehydrogenase (HLADH) was selected as an additional test enzyme, since its immobilisation had already been carried out on the same epoxy resin, providing a good reference for the experiment [28]. This enzyme presents additional challenges to general immobilisation strategies since its cofactor is not tightly bound and the cofactor binding domain needs to be accessible during the catalytic cycle [29]. For these reasons, structural alterations may have a major impact on the reactivity, unlike in the case of the aminotransferase where the PLP cofactor is permanently buried inside the active site.

The *adh* gene was subcloned into both vectors similarly to the other two genes. However, for both constructs, expression level and specific activity dropped dramatically with an activity 10 times lower, and yielding less than 1 mg of protein per litre of culture media after IMAC purification (Figure S6). Nevertheless, immobilisation of both chimeras and wild type HLADH was performed. The specific activity of the resin following immobilisation of the T4L-HLADHs (1 mg_{enzyme}/g_{resin}) was very low overall compared to the native imm-HLADH (Table 3). However, similarly to what observed for the HEWT, the T4L-shielded enzymes showed an improvement in the recovered activity although the overall nominal activity remained rather low. Immobilisation of the enzymes on Relizyme EP403/S in this case did not offer any appreciable improvement.

Table 3. Comparison of specific activities and expression levels of the original horse liver alcohol dehydrogenases (HLADH) and the two chimeric proteins in the free enzyme form. Specific activities of the resin following immobilisation of enzymes (1 mg_{enzyme}/g_{resin}) and percentage of residual activity after immobilisation (24 h, room temperature, in 50 mM phosphate buffer pH 8) with respect to the free protein.

	Free Enzyme		Immobilised Enzyme onto Sepabeads EC-EP/S (Pore ø 10–20 nm)		Immobilised Enzyme onto ReliZyme EP403/S (Pore ø 20–40 nm)	
	Specific Activity (U/mg)	Expression (mg/L)	Specific Activity (U/g)	Rescued Activity (%)	Specific Activity (U/g)	Rescued Activity (%)
HLADH	2.6 ± 0.3	20	0.80 ± 0.08	30.8	1.11 ± 0.05	32.4
T4L-HLADH_L1	0.18 ± 0.01	>1	0.08 ± 0.01	48.1	0.07 ± 0.02	38.9
T4L-HLADH_L2	0.15 ± 0.01	>1	0.07 ± 0.02	45.7	0.06 ± 0.01	39.9

The original HLADH lost about two-thirds of the activity, while the two chimeric enzymes responded better to the immobilisation, reaching around 50% of recovered activity. The stability of the immobilised enzymes was excellent for all the constructs under storage condition (4 °C in Tris-HCl buffer pH 8), with almost unchanged activity for over a month.

3. Discussion

This novel strategy of immobilisation, developed by introducing an inert protein linker, resulted in significantly enhanced recovered activity of the anchored enzymes. All the cases studied—HEWT, BS2m, and HLADH—when immobilised via T4L linking, showed an improvement in their retained activity, with a maximum of 90% displayed by the HEWT with the longer peptide linker. The most impressive result was achieved with the most challenging enzyme, BS2m esterase, which reached the performance of a competitive solid catalyst, with a maximum activity of 6.2 U/g when immobilised on Relizyme EP403/S. These results are superior to any other covalent method reported in the literature to date and might give an indication of the protective action that the protein spacer exercises by preventing direct bonding to the carrier. However, the expression levels and activity of the chimeras are not easily predictable and the immobilised enzymes may become more sensible to the reaction environment, partially diminishing the benefits of the immobilisation. Again, this was not observed for the chimeric BS2m which showed operational stability comparable to the commercial NovoZyme 435 and a recovered activity 8-to-10-fold higher than achievable with the BS2m control enzyme. While additional research will still have to be carried out to develop a universal method for successful immobilisation, this work shows that protein linkers should be considered in covalent strategies to maximise the activity of the solid catalyst. Further investigation of the composition and length of the peptide linker may also lead to more active constructs and, likewise, positioning of the T4L and His-tag at the C-terminus may be beneficial for enzymes where the active site is structurally affected by the N-terminus region.

4. Materials and Methods

4.1. T4L- HEWT, T4L-BS2m, and T4L-HLADH Constructs Generation

The pVL1392 vectors harbouring the T4-Lysozyme (T4L) was first used as templates for PCR amplification. The genes were amplified by PCR using Q5 High-Fidelity DNA Polymerase (New England Biolab). The primers FWD-T4L (5′-AAAAGGATCCGAACATCTTCGAGATGCTGCGCAT CGACGAAG-3′) and RVS-T4L (5′-AAAACTCGAGGTAAGCGTCCCAAGTTCCAGTACGGAAG GTAGTG-3′) were designed to incorporate *Bam*HI and *Xho*I restriction sites, respectively (underlined). The gel-purified PCR products were digested with *Bam*HI and *Xho*I and the genes were cloned into a *Bam*HI/*Xho*I digested pRSETb vector and ligated overnight with T4 ligase at 16 °C. The resulting clone, named pRSETb-T4L, was propagated in electrocompetent *E. coli* XL10-Gold cells and the construct was confirmed by sequencing analysis. The pRSETb-T4L D11N mutation was performed using the QuikChange Lightning Multi single point mutation kit (Agilent Technologies®,

Santa Clara, CA, USA) (primer: 5′-GCTGCGCATCGACCAGGGCCTGCGTCTCA-3′). The results were confirmed by DNA sequencing.

The pHESPUC plasmid was used as template for the HEWT cloning. The genes were amplified by PCR using Q5 High-Fidelity DNA Polymerase (New England Biolab, Ipswich, MA, USA). The oligonucleotide primers FWD-HEWT (5′-AAAACCATGGGATGCAAACCCAAGACTATCAGG CCCTGGACCGC-3′) and RVS-HEWT (5′-AAAAAAGCTTTCATGCGGTTGGCTCCTCTTGCGTGT GC-3′) were designed to incorporate *Nco*I and *Hind*III restriction sites, respectively (underlined). The gel-purified PCR products were digested with *Nco*I and *Hind*III and the genes were cloned into a *Nco*I/*Hind*III digested pRSETb-T4L vector and ligated overnight with T4 ligase at 16 °C. The resulting clone, named pRSETb-T4L-HEWT_L1 (link one), was propagated in electrocompetent *E. coli* XL10-Gold cells and the construct was confirmed by sequencing analysis.

In order to change the linker length, the XhoI restriction site after the T4L gene was mutated and substituted with a second NcoI site by directed mutagenesis with QuikChange Lightning Multi single point mutation kit (Agilent Technologies®) exploiting an oligonucleotide (5′-AACTTGGGACGCTT ACCTCCATGGCTGCAGCTGGTACCATGGG-3′) synthesised from Eurofins Genomics®. The construct pRSETb-T4L-HEWT_L1 was digested with NcoI, purified from agarose gel, and self-ligated overnight with T4 ligase at 16 °C. The resulting clone, named pRSETb-T4L-HEWT_L2 (link two), was propagated in electrocompetent *E. coli* XL10-Gold cells and the construct was confirmed by sequencing analysis.

The pET28b_BS2m and pEqADH plasmid were used as template for the BS2m and HLADH cloning. The genes were amplified by PCR using Q5 High-Fidelity DNA Polymerase (New England Biolab). The oligonucleotide primers FWD-BS2m (5′-GAAAACCATGGATGACTCATCAAATA GTAACGACTCA-3′), RVS-BS2m (5′-GAAAAAAGCTTTCAGGATCCTTCTCCTTTTGAAGGG AATAGCT-3′), FWD-HLADH (5′-GAAAACCATGGGATGAGCACAGCAGGAAAAGTAATA AAATG-3′), and RVS-HLADH (5′-GAAAAAAGCTTTTCAAAACGTCAGGATGGTACGGATAC-3′) were designed to incorporate *Nco*I and *Hind*III restriction sites, respectively (underlined). The gel-purified PCR products were digested with *Nco*I and *Hind*III and the genes were cloned into a *Nco*I/*Hind*III digested and gel-purified pRSETb-T4L-HEWT_L1 or pRSETb-T4L-HEWT_L2 vectors and ligated overnight with T4 ligase at 16 °C. The resulting clones, named pRSETb-T4L-BS2m_L1 and pRSETb-T4L-HLADH_L1 (link one), and pRSETb-T4L-BS2m_L2 and pRSETb-T4L-HLADH_L2 (link two), were propagated in electrocompetent *E. coli* XL10-Gold cells and the construct was confirmed by sequencing analysis.

4.2. Expression, Purification, and Characterization of the HEWT, BS2m, HLADH, and T4L Proteins in E. coli

Protein expression, purification, characterization of the original HEWT, BS2m, and HLADH, and their T4L constructs was performed following previously reported protocols [17,20,21]. The assay for the BS2m esterase (and NovoZyme 435) was adapted using the para-nitrophenyl acetate (PNPA) as standard substrate.

Protein quantification was determined by UV reading (280 nm) considering for each enzyme the calculated molar extinction coefficient (Table S1).

4.3. Immobilisation of HEWT, BS2m, and HLADH

The immobilisation of HEWT and HLADH were performed following the published procedures [18,28] originally developed by Guisan and co-workers [16]. For the BS2m immobilisation, 1 g of resin (Sepabeads® EC-EP/S or ReliZyme EP403/S from Resindion S.r.l., Milan, Italy) immobilisation support was treated with 2 mL of modification buffer (0.1 M of sodium borate and 2 M of iminodiacetic acid in phosphate buffer 50 mM pH 8.5) under gentle shaking for two hours at room temperature. The sample was then filtered and washed with distilled water and incubated with a metal containing solution (1 M of sodium chloride and 5 mg/mL of metal cation in phosphate buffer 50 mM pH 6) for two hours. 2 mL of enzyme solution, suitably prepared to provide a ratio

of 5 mg of enzyme per 1 g of beads, were added to the resin and kept under gentle agitation (2–24 h, 200 rpm orbital shaking, at room temperature). The beads were filtered and washed thoroughly with desorption buffer (0.05 M of EDTA and 0.5 M of sodium chloride in phosphate buffer pH 7.4 20 mM) and distilled water, 4 mL of blocking buffer (3 M of glycine in phosphate buffer pH 8.5 50 mM) were added and the suspension left under agitation for 20 h. Finally, the beads were washed, collected, and conserved in 2 mL of storage buffer (50 mM phosphate pH 8.0). The imm-BS2m was routinely stored at 4 °C. The activity of immobilised BS2m was determined by weighing an appropriate amount of resin (5–50 mg) into a 25 mL reaction tube with cap, followed by the addition of 10 mL reaction mixture (50 mM phosphate pH 8.0, containing 0.5 mM PNPA). The immobilised enzyme reaction mixture was shaken at 25 °C, 250 rpm and the absorbance at 410 nm was recorded every minute as single readings using Brand UV-cuvettes. The imm-BS2m specific activity (U/g) is defined as µmol of *para*-nitrophenol formed (ε = 15 mM^{-1} cm^{-1}) *per* minute *per* gram of immobilised enzyme.

Unless differently stated, chemicals were purchased from Sigma Aldrich Merck (St. Louis, MO, USA).

Supplementary Materials: The following are available online at www.mdpi.com/2073-4344/8/1/40/s1, Figure S1: SDS-gel (12%) electrophoresis of T4L-HEWTs, Figure S2: HEWTs immobilisation at different incubation times, Figure S3: Reusability profile of the immobilised T4L-HEWT_L1 (circle) and T4L-HEWT_L2 (square) after 10 reaction cycles, Figure S4: Stability of HEWTs in different organic co-solvent, Table S1: computed molecular weight (MW) and molar extinction coefficients (ε), Figure S5: SDS-gel (12%) electrophoresis of T4L-BS2ms, Figure S6: SDS-gel (12%) electrophoresis of T4L-HLADHs.

Acknowledgments: The authors wish to thank Resindion S.R.L. for donating the Sepabeads® EC-EP/S and RelyZime® EP403/S, Brian Kobilka (Stanford University, CA, USA) for donating the plasmid encoding the T4-lysozyme, and UK Biotechnology and Biological Sciences Research Council (BBSRC; BB/P002536/1) for general financial support.

Author Contributions: M.P. and F.P. designed the study. M.P. cloned, immobilised, and evaluated the HEWT and HLADH originals enzyme and T4L-variants. D.R.P. and M.L.C. cloned, immobilised, and evaluated the BS2m original enzyme and T4L-variants. M.P. and F.P. wrote the paper. All authors discussed the results and commented on the manuscript.

Conflicts of Interest: The authors declare no conflict of interest.

References

1. Wenda, S.; Illner, S.; Mell, A.; Kragl, U. Industrial biotechnology—The future of green chemistry? *Green Chem.* **2011**, *13*, 3007. [CrossRef]
2. Nestl, B.M.; Hammer, S.C.; Nebel, B.A.; Hauer, B. New generation of biocatalysts for organic synthesis. *Angew. Chem. Int. Ed.* **2014**, *53*, 3070–3095. [CrossRef] [PubMed]
3. Hanefeld, U.; Gardossi, L.; Magner, E. Understanding enzyme immobilisation. *Chem. Soc. Rev.* **2009**, *38*, 453–468. [CrossRef] [PubMed]
4. Hanefeld, U.; Cao, L.; Magner, E. Enzyme immobilisation: Fundamentals and application. *Chem. Soc. Rev.* **2013**, *42*, 6211–6212. [CrossRef] [PubMed]
5. Garcia-Galan, C.; Berenguer-Murcia, A.; Fernandez-Lafuente, R.; Rodrigues, R.C. Potential of different enzyme immobilization strategies to improve enzyme performance. *Adv. Synth. Catal.* **2011**, *353*, 2885–2904. [CrossRef]
6. Sheldon, R.A.; Van Pelt, S. Enzyme immobilisation in biocatalysis: Why, what and how. *Chem. Soc. Rev.* **2013**, *42*, 6223–6235. [CrossRef] [PubMed]
7. Yi, S.S.; Lee, C.; Kim, J.; Kyung, D.; Kim, B.G.; Lee, Y.S. Covalent immobilization of ω-transaminase from Vibrio fluvialis JS17 on chitosan beads. *Process Biochem.* **2007**, *42*, 895–898. [CrossRef]
8. Guisan, J.M. *Immobilization of Enzymes and Cells IN Series Editor. Immobilization of Enzymes and Cells*; Humana Press Inc.: New York, NY, USA, 2013; Volume 1051.
9. Shuai, W.; Das, R.K.; Naghdi, M.; Brar, S.K.; Verma, M. A review on the important aspects of lipase immobilization on nanomaterials. *Biotechnol. Appl. Biochem.* **2017**, *64*, 496–508. [CrossRef] [PubMed]
10. Barbosa, O.; Ortiz, C.; Berenguer-Murcia, Á.; Torres, R.; Rodrigues, R.C.; Fernandez-Lafuente, R. Strategies for the one-step immobilization-purification of enzymes as industrial biocatalysts. *Biotechnol. Adv.* **2015**, *33*, 435–456. [CrossRef] [PubMed]

11. Datta, S.; Christena, L.R.; Rajaram, Y.R.S. Enzyme immobilization: An overview on techniques and support materials. *3 Biotech* **2013**, *3*, 1–9. [CrossRef] [PubMed]
12. Jia, B.; Jeon, C.O. High-throughput recombinant protein expression in *Escherichia coli*: Current status and future perspectives. *Open Biol.* **2016**, *6*, 1–17. [CrossRef] [PubMed]
13. Thorsen, T.S.; Matt, R.; Weis, W.I.; Kobilka, B.K. Modified T4 Lysozyme Fusion Proteins Facilitate G Protein-Coupled Receptor Crystallogenesis. *Structure* **2014**, *22*, 1657–1664. [CrossRef] [PubMed]
14. Wiesbauer, J.; Bolivar, J.M.; Mueller, M.; Schiller, M.; Nidetzky, B. Oriented Immobilization of Enzymes Made Fit for Applied Biocatalysis: Non-Covalent Attachment to Anionic Supports using Zbasic2 Module. *ChemCatChem* **2011**, *3*, 1299–1303. [CrossRef]
15. Bolivar, J.M.; Nidetzky, B. Oriented and selective enzyme immobilization on functionalized silica carrier using the cationic binding module Z-basic2: Design of a heterogeneous D-amino acid oxidase catalyst on porous glass. *Biotechnol. Bioeng.* **2012**, *109*, 1490–1498. [CrossRef] [PubMed]
16. Mateo, C.; Fernandez-Lorente, G.; Cortes, E.; Garcia, J.L.; Fernandez-Lafuente, R.; Guisan, J.M. One-step purification, covalent immobilization, and additional stabilization of poly-his-tagged proteins using novel heterofunctional chelate-epoxy supports. *Biotechnol. Bioeng.* **2001**, *76*, 269–276. [CrossRef] [PubMed]
17. Cerioli, L.; Planchestainer, M.; Cassidy, J.; Tessaro, D.; Paradisi, F. Characterization of a novel amine transaminase from *Halomonas elongata*. *J. Mol. Catal. B Enzym.* **2015**, *120*, 141–150. [CrossRef]
18. Planchestainer, M.; Contente, M.L.; Cassidy, J.; Molinari, F.; Tamborini, L.; Paradisi, F. Continuous flow biocatalysis: Production and in-line purification of amines by immobilised transaminase from *Halomonas elongata*. *Green Chem* **2017**, *53*, 3007–3048. [CrossRef]
19. Contente, M.L.; Dall'Oglio, F.; Tamborini, L.; Molinari, F.; Paradisi, F. Highly Efficient Oxidation of Amines to Aldehydes with Flow-based Biocatalysis. *ChemCatChem* **2017**, *9*, 3843–3848. [CrossRef]
20. Quaglia, D.; Irwin, J.A.; Paradisi, F. Horse liver alcohol dehydrogenase: New perspectives for an old enzyme. *Mol. Biotechnol.* **2012**, *52*, 244–250. [CrossRef] [PubMed]
21. Hackenschmidt, S.; Moldenhauer, E.J.; Behrens, G.A.; Gand, M.; Pavlidis, I.V.; Bornscheuer, U.T. Enhancement of promiscuous amidase activity of a Bacillus subtilis esterase by formation of a π-π Network. *ChemCatChem* **2014**, *6*, 1015–1020. [CrossRef]
22. Zou, Y.; Weis, W.I.; Kobilka, B.K. N-Terminal T4 Lysozyme Fusion Facilitates Crystallization of a G Protein Coupled Receptor. *PLoS ONE* **2012**, *7*. [CrossRef] [PubMed]
23. Chang, B.S.; Mahoney, R.R. Enzyme thermostabilization by bovine serum albumin and other proteins: Evidence for hydrophobic interactions. *Biotechnol. Appl. Biochem.* **1995**, *22*, 203–214. [CrossRef] [PubMed]
24. Ren, H.; Xing, Z.; Yang, J.; Jiang, W.; Zhang, G.; Tang, J.; Li, Q. Construction of an Immobilized Thermophilic Esterase on Epoxy Support for Poly(ε-caprolactone) Synthesis. *Molecules* **2016**, *21*, 796. [CrossRef] [PubMed]
25. Sousa, H.A.; Rodrigues, C.; Klein, E.; Afonso, C.A.M.; Crespo, J.G. Immobilisation of pig liver esterase in hollow fibre membranes. *Enzyme Microb. Technol.* **2001**, *29*, 625–634. [CrossRef]
26. Mei, Y.; Kumar, A.; Gross, R.A. Probing water-temperature relationships for Lipase-catalyzed lactone ring-opening polymerizations. *Macromolecules* **2002**, *35*, 5444–5448. [CrossRef]
27. Pierre, S.J.; Thies, J.C.; Dureault, A.; Cameron, N.R.; Van Hest, J.C.M.; Carette, N.; Weberskirch, R. Covalent enzyme immobilization onto photopolymerized highly porous monoliths. *Adv. Mater.* **2006**, *18*, 1822–1826. [CrossRef]
28. Quaglia, D.; Pori, M.; Galletti, P.; Emer, E.; Paradisi, F.; Giacomini, D. His-tagged Horse Liver Alcohol Dehydrogenase: Immobilization and application in the bio-based enantioselective synthesis of (S)-arylpropanols. *Process Biochem.* **2013**, *48*, 810–818. [CrossRef]
29. Hammes-Schiffer, S.; Benkovic, S.J. Relating protein motion to catalysis. *Annu. Rev. Biochem.* **2006**, *75*, 519–541. [CrossRef] [PubMed]

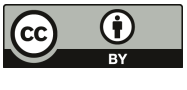

© 2018 by the authors. Licensee MDPI, Basel, Switzerland. This article is an open access article distributed under the terms and conditions of the Creative Commons Attribution (CC BY) license (http://creativecommons.org/licenses/by/4.0/).

catalysts

MDPI

Article

Immobilization of an Endo-β-*N*-acetylglucosaminidase for the Release of Bioactive *N*-glycans

Joshua L. Cohen [1], Sercan Karav [2], Daniela Barile [1,3] and Juliana M. L. N. de Moura Bell [1,4,*]

[1] Department of Food Science and Technology, University of California, One Shields Avenue, Davis, CA 95616, USA; jlcohen@ucdavis.edu (J.L.C.); dbarile@ucdavis.edu (D.B.)
[2] Department of Molecular Biology and Genetics, Canakkale Onsekiz Mart University, 17100 Canakkale, Turkey; sercankarav@comu.edu.tr
[3] Foods for Health Institute, University of California, One Shields Avenue, Davis, CA 95616, USA
[4] Department of Biological and Agricultural Engineering, University of California, One Shields Avenue, Davis, CA 95616, USA
* Correspondence: jdemourabell@ucdavis.edu; Tel.: +1-530-752-5007

Received: 1 June 2018; Accepted: 5 July 2018; Published: 10 July 2018

Abstract: As more is learned about glycoproteins' roles in human health and disease, the biological functionalities of *N*-linked glycans are becoming more relevant. Protein deglycosylation allows for the selective release of *N*-glycans and facilitates glycoproteomic investigation into their roles as prebiotics or anti-pathogenic factors. To increase throughput and enzyme reusability, this work evaluated several immobilization methods for an endo-β-*N*-acetylglucosaminidase recently discovered from the commensal *Bifidobacterium infantis*. Ribonuclease B was used as a model glycoprotein to compare *N*-glycans released by the free and immobilized enzyme. Amino-based covalent method showed the highest enzyme immobilization. Relative abundance of *N*-glycans and enzyme activity were determined using matrix-assisted laser desorption/ionization time-of-flight mass spectrometry. Kinetic evaluation demonstrated that upon immobilization, both V_{max} and the K_m decreased. Optimal pH values of 5 and 7 were identified for the free and immobilized enzyme, respectively. Although a higher temperature (65 vs. 45 °C) favored rapid glycan release, the immobilized enzyme retained over 50% of its original activity after seven use cycles at 45 °C. In view of future applications in the dairy industry, we investigated the ability of this enzyme to deglycosylate whey proteins. The immobilized enzyme released a higher abundance of neutral glycans from whey proteins, while the free enzyme released more sialylated glycans, determined by nano-LC Chip Q-ToF MS.

Keywords: *N*-glycans; mass spectrometry; immobilization; prebiotic; glycosidase; recombinant; kinetic; nano-LC Chip Q-ToF MS

1. Introduction

Glycoproteins are a biologically important class of components with modulatory roles in signaling and cell adhesion. *N*-linked glycans are covalently bound to an asparagine residue with the consensus sequence on the primary structure of asparagine-X-serine/threonine (with X representing any amino acid besides proline) [1]. The attachment is mediated by the reducing end *N*-acetylglucosamine moiety of the glycan onto the asparagine residue [2]. All *N*-glycans share a common trimannosyl, chitobiose (two β-1,4 linked *N*-acetylglucosamine residues) core and are classified based on how the core is elongated with various monosaccharides. *N*-glycans can be decorated with *N*-acetylneuraminic acid or *N*-glycolylneuraminic acid (sialylated) and/or fucose (fucosylated) in various antennary combinations to give rise to a heterogeneity of combinations, even on a single glycosylation site. Glycans can

be classified based on their antennary decorations, with neutral, fucosylated, sialylated, and both fucosylated and sialylated being the primary non-plant glycans.

As a model for understanding the interplay of indigestible carbohydrates and beneficial gut bacteria, human milk oligosaccharides (HMOs) have been widely studied and found to exhibit uniquely effective prebiotic functionalities [3]. While HMOs are quite abundant in human milk (up to 15 g/L in colostrum), their commercial-scale isolation from human milk is not feasible [4]. The activities and roles of intact and released *N*-linked glycans upon human consumption are not well understood due, in part, to the lack of adequate deglycosylation and analytic methods to release, identify, and quantity the released glycans [5]. *N*-glycans can be released from the protein moiety using harsh chemical treatments or enzymatic methods, the latter allowing for the recovery of intact protein and glycans. Deglycosylating enzymes include peptide-*N*-glycosidases and endo-β-*N*-acetylglucosaminidases, which differ in cleavage points of the core of *N*-glycans [6].

Due to striking similarities in structures and functions, released *N*-linked glycans from bovine milk glycoproteins have been studied for their ability to promote the growth of commensal bacteria in vitro [7,8]. A recently discovered endo-β-*N*-acetylglucosaminidase (Endo-BI-1), isolated from *B. infantis*, was shown to deglycosylate human milk glycoproteins more effectively than other endo-β-*N*-acetylglucosaminidase isolated from several commensal *Bifidobacterium* species [9]. More importantly, released *N*-glycans by this novel enzyme from bovine milk proteins displayed a remarkable selective prebiotic activity on *Bifidobacterium longum* subsp. *infantis* in vitro, and may promote the growth of other beneficial bacteria while inhibiting pathogens [7,8,10]. However, to establish *N*-glycans as an alternative source of prebiotic carbohydrates to human milk, further research into the selectivity of bovine *N*-glycans and their functional similarity with HMOs with respect to commensal, beneficial, and pathogenic gut organisms is necessary.

Whey, the co-product of cheese manufacture, is a potential commercially available source of underutilized glycoproteins. The concentration of proteins in bovine cheese whey ranges from 1 to 2%, wherein approximately 4–9% of those proteins are *N*-glycosylated immunoglobulins, lactoferrin, and transferrin [11,12]. Lactoferrin, while found in substantial quantities in human milk and bovine colostrum, is present in bovine milk and cheese whey at the trace level.

Yet, the nearly 200 million tonnes of whey produced each year globally [13] conservatively translates to 2 million tonnes of whey proteins, corresponding to approximately 100,000 tonnes of bovine milk glycoproteins available for subsequent processing. With such a large availability of glycoproteins, the development of large-scale processing strategies to release and isolate *N*-glycans for further characterization and elucidation of their biological functionalities becomes a key step for further commercialization of these compounds.

Indeed, enzyme immobilization may facilitate reaction scale-up considering the possibility for broad reactor systems and catalyst reusability. Enzyme immobilization is the process wherein a soluble enzyme is attached or adsorbed onto a solid support, entrapped within a matrix, or otherwise aggregated enabling enzyme reuse during production [14]. However, widespread industrial use of immobilized enzyme remains limited due to a perceived loss of enzyme activity, lack of universal immobilization techniques, and cost implications [15,16]. In general, enzyme immobilization facilitates the separation of products and catalyst where removal from the final product to terminate the reaction and to reuse the catalyst is important in producing pure bioactive molecules. Covalent, adsorption, entrapment, and aggregation methods of immobilization have their inherent advantages and disadvantages in a reactor system. These factors are based on substrate size and ability to access the enzyme active site, physicochemical stability, and applicability in industrial processes [15]. Although the use of immobilized enzymes has been validated by the food industry to a limited extent [17], the use of glycosidases has been restricted to lab-scale [6].

The overall goal of this study was to evaluate several types of immobilization methods and resins for a novel endo-β-*N*-acetylglucosaminidase (Endo-BI-1) isolated from *B. infantis*. In addition to the development of an immobilization method based on protein immobilization yield and enzyme activity, the effects of the immobilization method on pH and temperature sensitivity of the immobilized enzyme

were evaluated. Enzyme reusability was also evaluated. Significant efforts were directed towards the development of sensitive and high-throughput analytical methods: in particular, MALDI-ToF MS was used to study the rate and specificity of the deglycosylation reaction kinetics on RNase B, and nano-LC-Chip Q-ToF MS was used to characterize the diverse pool of *N*-glycans released from bovine colostrum whey proteins using free and immobilized enzyme.

2. Results and Discussion

2.1. Protein Immobilization Yield

Enzyme immobilization yield of amino-, epoxy- and adsorption-immobilized Endo BI-1 was evaluated by quantifying the unbound protein remaining in the supernatant and resin washing buffer post-immobilization. The fluorescence method employed herein (Qubit Protein Assay Kit) demonstrated the high immobilization yield (>98%) of the amino-based resin, whereas divinylbenzene (DVB)-based hydrophobic interaction adsorption immobilized 70% of the enzyme (Figure 1). Epoxy-based covalent binding yielded the lowest immobilization yield at 12%. These results were corroborated by SDS-PAGE, where denser Endo BI-1 bands in the supernatants were present in epoxy and adsorption methods, while amino-based immobilization had no visible band (Figure S1). Differences between immobilization yields for covalent and adsorption immobilization methods have been observed previously and can possibly be attributed to the strength of interaction between hydrophobic interactions and covalent bonds [18]. However, low binding using epoxide-activated resin may be due to non-optimal methods to identify the ideal pH, time, and temperature for increased binding [19]. Further investigation into those conditions may improve protein immobilization yield for the epoxide-activated resin.

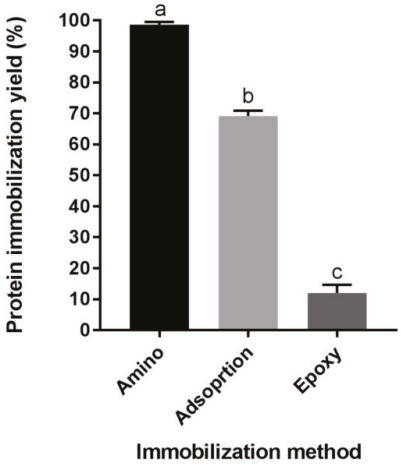

Figure 1. Protein immobilization yield for amino, adsorption, and epoxy immobilization methods, measured fluorometrically by Qubit Protein Assay Kit. Error bars represent one standard deviation and means followed by different letters (a, b, and c) are statistically different at $p < 0.05$.

2.2. Relative Quantification of N-glycans by MALDI-ToF MS

An additional goal of this research was to identify a sensitive, specific, and rapid method to determine relative quantities of *N*-glycans to facilitate assessment of enzyme activity. Spectrophotometric methods involving phenol-sulfuric acid have been used, but lack selectivity for certain saccharide types and tend to be affected by other compounds present in the sample, not only the *N*-glycan products of this reaction [20–22]. Additionally, the diverse array of monosaccharides present in *N*-glycans adds a layer

of complexity leading to inconsistent responses in these assays [21]. As an alternative, matrix-assisted laser desorption/ionization time-of-flight mass spectrometry MALDI-ToF MS has been used for relative quantification of various carbohydrates [23,24]. It is known that MALDI-ToF, albeit rapid and effective in providing results, may suffer from low reproducibility due to inconsistent crystallization of the samples on the target plate, leading to shot-to-shot variation. These disadvantages can be overcome by using an internal standard [25]. Additionally, MALDI has been used to study enzymatic reactions including both large and small substrates/products [26–28].

Linearity of the 3-FL (3'-fucosyllactose)-spiked released *N*-glycan system was evaluated. An example of a typical annotated mass spectrum of *N*-glycans can be seen in Figure 2. The theoretical *m/z* for sodiated 3-FL, Man 5, Man 6, Man 7, and Man 8 are 511.16, 1054.34, 1216.40, 1378.45, and 1540.50 respectively, accounting for one fewer *N*-acetylglucosamine residue according to cleavage by Endo BI-1. The most abundant glycan released from RNase B was Man5 (*m/z* 1054), with larger glycans being less abundant, which was consistent with previous literature [29]. Bovine RNase B was chosen as a model glycoprotein due to its single *N*-glycosylation site and straightforward glycan composition.

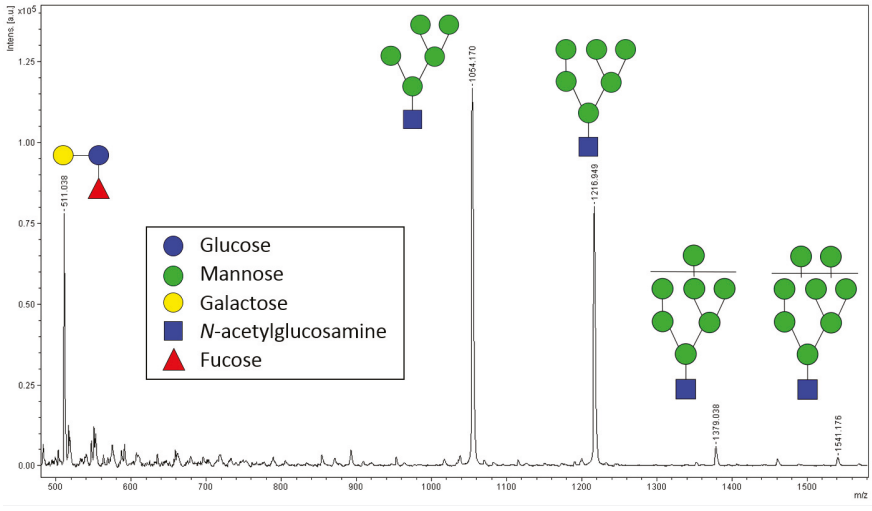

Figure 2. MALDI-ToF mass spectrum for 3-FL (*m/z* 511)-spiked *N*-glycans released from RNase B using Endo BI-1.

Over the examined order of magnitude range, the normalized response plotted against *N*-glycan/I.S. (internal standard) ratio was linear ($R^2 = 0.995$, Figure S2). A high R^2 value indicates that analysis of released *N*-glycans in presence of I.S. analyzed by MALDI-ToF MS is a suitable tool for rapid relative quantification of *N*-glycans needed for evaluating kinetic parameters over a substantial range of concentrations and amounts of reactant.

2.3. Comparing Immobilized Enzyme Activities

The activity of the enzyme immobilized by each method (amino, epoxy, and adsorption) was evaluated on RNase B, and reacted for 90 min at 45 °C and pH 5.0. The normalized relative abundance of released *N*-glycans was determined by MALDI-ToF MS, with activity based on the amount of glycans released by the free enzyme (Figure 3). Free enzyme had the highest activity, with amino, epoxy, and adsorption methods retaining 73, 51, and 57% activity, respectively. Diminished activity upon immobilization is common, and has been reported previously with glutaraldehyde-mediated binding and hydrophobic adsorption [30]. A combination of diffusional/steric hindrances and possible binding

and occlusion of enzyme active sites may explain the reduction in enzyme activity [16]. Additionally, heterogeneous catalysis impacts enzyme activity. The amino-based immobilization was selected for all subsequent experiments due to its higher activity compared with epoxy and adsorption methods, as well as its improved catalyst density on the resin.

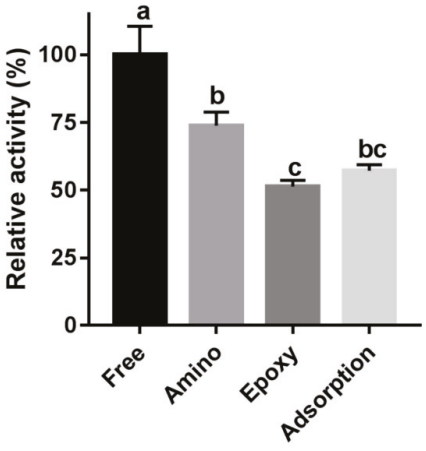

Figure 3. Relative activity of free or immobilized Endo BI-1 (on amino, epoxy, and adsorption resins) on the glycoprotein RNase B. Error bars represent one standard deviation. Means followed by different letters (a, b, and c) are statistically different at $p < 0.05$.

2.4. Temperature and pH Sensitivity of Immobilized Enzyme Using RNase B

Enzyme properties can change with respect to pH and temperature sensitivity when immobilized [31,32]. Temperature sensitivity was evaluated at pH 5 with 20 mM Na_2HPO_4 buffer at temperatures from 45 to 85 °C (Figure 4a). The optimal temperature for both free and immobilized Endo BI-1 was 65 °C. These results differ from what was previously reported by Karav et al. [33], in which a lower optimum temperature of 52 °C was identified for the free enzyme. This discrepancy could be attributed to different reaction conditions used in both studies. While RNase B and a short reaction time (20 min) were used in the present work, bovine colostrum whey protein and longer reaction times (15–475 min) were evaluated in the previous study. At the optimum temperature identified (65 °C), the immobilized enzyme retained 63% of the activity compared with the free enzyme. In each experimental condition of both temperature and pH, the activity of immobilized Endo BI-1 was lower than that of the free enzyme, at all conditions. For both free and immobilized enzymes, activities decreased at temperatures above 65 °C.

To evaluate pH sensitivity, 20 mM Na_2HPO_4 buffer was adjusted to pH 3, 5, 7, and 9. Reactions with free and immobilized Endo BI-1 and RNase B were carried out at 45 °C for 20 min, and the normalized activity can be seen in Figure 4b. The optimal pH for free Endo BI-1 was 5, in agreement with previous reports [9], while for the immobilized enzyme a shift to a neutral pH (7.0) was observed. At the optimal pH for the free (pH 5) and immobilized enzyme (pH 7), the immobilized enzyme retained approximately 62% of the activity of the free enzyme at 20 min of reaction. However, the immobilized enzyme was more resilient in the range of pH 7 to 9, where reduced differences in the activities of the free and immobilized enzyme were observed. Indeed, at pH 9, the activities of free and immobilized Endo BI-1 were not statistically different (Figure 4a). Our results are in agreement with several reports in the literature where a shift on the working pH of the immobilized enzyme to a neutral or more alkaline pH was observed, with the same being attributed to changes in the amine group during the covalent binding [31,34]. In the context of scaling up *N*-glycan release using bovine

milk proteins, the optimum pH of the immobilized enzyme (pH 7), presents a clear advantage over the free enzyme, considering that milk and dairy streams naturally have a pH close to neutral and would not necessitate the use of buffers for pH adjustment, which can become problematic and costly at large scale. Literature suggests that immobilization alters temperature and pH sensitivity by stabilizing the enzyme conformation and creating stable microenvironments around the enzyme or close to its active site [35]. The data here presented provides valuable information for future scale-up of the process and testing other substrates for glycan release.

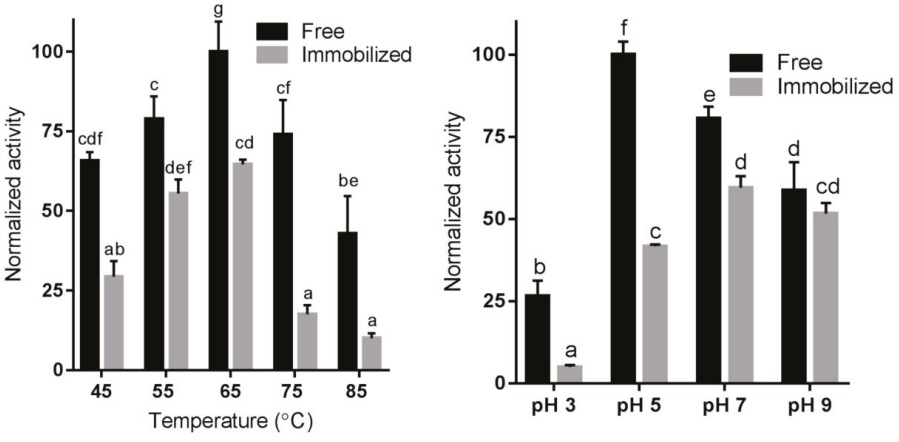

Figure 4. Mean relative activity of free and immobilized enzyme at different (**a**) temperature and (**b**) pH values using RNase B. Error bars represent one standard deviation and means, within the same chart, followed by different letters (a, b, c, d, e, and f) are statistically different at $p < 0.05$.

2.5. Enzyme Kinetics Using RNase B

To gain more quantitative insight into the mechanistic changes of the enzymatic deglycosylation upon immobilization, the kinetic parameters (V_{max}, K_m) were estimated using linearized plotting techniques (Lineweaver-Burk and Hanes Woolf) to reduce the error of non-linear estimation (Figure 5). V_{max}, the maximum forward velocity of the reaction, decreased from 0.551 glycan/min to 0.076 glycan/min (Lineweaver Burk estimation) upon immobilization of Endo BI-1 as calculated on RNase B (Figure 6). The Michaelis constant (K_m, a measure of substrate affinity) also decreased upon immobilization from 2.27 mg/mL for the free enzyme to 0.299 mg/mL once Endo BI-1 was immobilized on the amino-activated methacrylate resin. The goodness-of-fit for the Lineweaver Burk linear model (R^2) for free and immobilized enzyme was 0.89 and 0.96 respectively. Hanes Woolf linear estimation revealed similar trends (0.333 and 0.081 V_{max} values, 1.17 and 0.345 K_m values for free and immobilized enzymes, respectively) to Lineweaver Burk. Decreased V_{max} is typical of enzyme immobilization [32,36], wherein lower maximum velocity is likely due to limited access of the large, macromolecular substrate to the active site of the immobilized enzyme. The immobilized enzyme is on a molecular tether, and steric hindrances limit access to more occluded glycan sites on the substrate with respect to the three-dimensional structure. As a point of comparison, β-1,4-galactosidase, with a molecular weight of approximately 465 kDa in its tetrameric form, with lactose as substrate at 360 Da has an overall substrate/enzyme size ratio of 0.0008:1, whereas for RNase B and Endo BI-1, the substrate/enzyme size ratio is approximately 0.32:1. This suggests a more limited diffusion and increased steric challenge with respect to active site availability.

Increased apparent affinity accompanied by decreased V_{max} is consistent with uncompetitive inhibition. Possible explanations of this phenomenon are the formation of a more stable enzyme-substrate complex between Endo BI-1 and RNase B upon immobilization, or simply deglycosylated RNase B may have difficulty diffusing away from immobilized Endo BI-1 upon interaction with the active site. Both stable enzyme-substrate complexes and diffusional challenges would increase apparent affinity and inhibit forward reaction progress and are documented phenomena [36,37].

Enzymes with diverse, macromolecular substrates may exhibit substrate-dependent kinetic behavior. For example, when Endo BI-1 was tested on different glycoproteins, V_{max} and K_m also varied. The Michaelis constants for RNase B, lactoferrin, and concentrated whey proteins were 0.25, 0.43, and 0.90 mg/mL respectively, potentially due to different sizes, purities, and physicochemical properties of the glycoproteins [20]. The overall increase in K_m for Endo BI-1 in this study (0.33 vs. 025 mg/mL) is likely related to differences in reaction conditions and analytical methods used in both studies. While this study utilized MALDI-ToF MS to measure the hydrolytic efficiency of Endo BI-1, previous studies utilized a spectrophotometric phenol-sulfuric assay, wherein the diverse array of monosaccharides present in *N*-glycans from lactoferrin and other whey proteins could have yielded different responses.

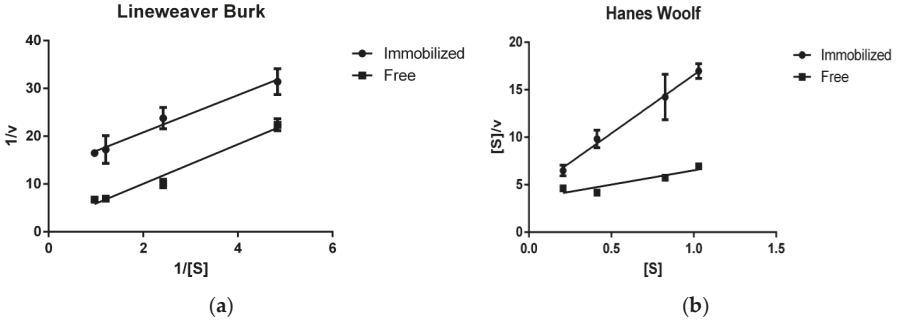

Figure 5. Lineweaver Burk ($1/[S]$ (mL/mg) vs. $1/v$ (mL × min/mg)) (**a**) and Hanes–Woolf ($[S]$ (mg/mL) vs. s/v (min)) (**b**) linearized plotting techniques for the estimation of kinetic parameters of free and immobilized EndoBI-1 on RNase B.

2.6. Immobilized Enzyme Reusability with RNase B

A substantial advantage of enzyme immobilization is the potential reusability of the catalyst. Amino-mediated immobilized Endo BI-1 was subjected to ten 20-min reuse cycles at 45 and 65 °C to determine the effects of different temperatures on the activity and reusability of the immobilized enzyme (Figure 6). Enzyme activity was higher at 65 °C compared with 45 °C. At 45 °C, the immobilized enzyme activity corresponded to approximately 65% of the enzyme activity at 65 °C. Despite higher enzyme activity at 65 °C, a higher decrease in the enzyme activity was observed after each reuse cycle. At 65 °C, enzyme activity was reduced to 63% of its original value after one cycle of reuse, and by the sixth use cycle, it had been reduced to and stabilized at 10 to 15% of its original activity. Conversely, at 45 °C, the enzyme activity remained consistent up to three reuse cycles. Despite the initial higher enzyme activity at 65 °C, from the third cycle onward reactions at 45 °C had greater residual enzyme activity than reactions performed at 65 °C. These results indicate that although 65 °C is optimal for initial glycan release, it does not favor repeated enzyme use for longer reaction times. It is possible to reuse the immobilized enzyme up to seven cycles at 45 °C with significant retention of its activity (50% from the initial activity). Our results are in agreement with several reports in the literature, where the use of lower temperatures (e.g., 37 °C) has favored high reusability, even though higher temperatures may favor more rapid catalysis [38,39]. Regarding an industrially-relevant enzyme with macromolecular substrates, Chauhan reported a loss

of over 85% of polygalacturonase activity after 6 cycles using adsorption onto celite [40]. Additionally, reaction time and temperature affect the selective release of *N*-glycans from more complex and diverse glycoproteins, which may determine the choice of the reaction temperature thus affecting reusability of the immobilized enzyme [41]. Importantly, fouling with a protein-based substrate may also impact reusability [42].

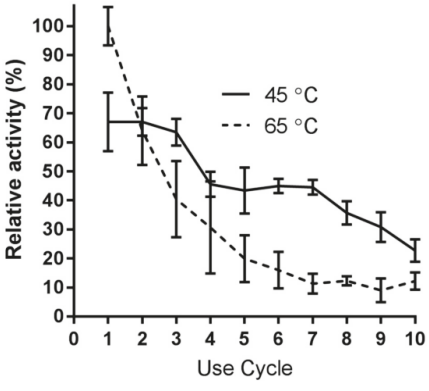

Figure 6. Mean relative activity of immobilized Endo BI-1 on RNase B following several reuse cycles. Error bars represent one standard deviation.

2.7. Release of N-glycans from Bovine whey Proteins

Cheese whey, a co-product of the dairy industry, is a source of *N*-linked glycoproteins including lactoferrin, lactoperoxidase, transferrin, and various immunoglobulins [12]. Free and immobilized Endo BI-1 was incubated with whey proteins purified from bovine colostrum at pH 7 at 45 °C for 1 h. The glycans were purified and characterized by nano LC-Chip Q-ToF mass spectrometry and each compound's relative abundance was determined and further classified based on the class of glycan to which each compound belongs (Figure 7).

Overall, twenty-six unique *N*-glycan structures were identified and confirmed by tandem mass spectra. The *N*-glycans were characterized based on their monosaccharide composition, which included neutral (containing only hexose and *N*-acetylhexosamine residues), sialylated, fucosylated, and fucosylated and sialylated. For neutral glycans the immobilized enzyme released eight times higher relative amounts than free Endo BI-1. For the class fucosylated and sialylated, the free enzyme released significantly higher amount of glycans (approximately double) compared with the free enzyme. Free enzyme released 50% more of each fucosylated and sialylated glycan class. For glycans with both sialylation and fucosylation, the free enzyme released nearly double the relative amount of glycans compared with immobilization. It is worth mentioning that fucosylated and sialylated glycans were present in lowest amounts. Both sialylated and neutral glycans represented the most abundant glycan types released from colostrum whey proteins. Importantly, unique glycan compositions should only be compared between samples, and not among the various *N*-glycan structures themselves. In fact, differences in ionization efficiency due to diverse monosaccharide composition hinder direct comparisons in the absence of identical pure standards.

The *N*-glycan structures released by Endo BI-1 were tabulated according to the glycan composition notation Hex_HexNAc_Fuc_NeuAc_NeuGc, which correspond with the number of hexose, *N*-acetylhexosamine, fucose, *N*-acetylneuraminic acid, and *N*-glycolylneuraminic acid residues respectively (Table S1). The most abundant glycans released from colostrum whey proteins by free Endo BI-1 were 4_3_0_1_0 and 3_3_0_1_0 while the most abundant glycan structures released by immobilized Endo BI-1 were 3_3_0_0_0 and 5_1_0_0_0 (Man5). The relative abundance for released

3_3_0_0_0 and 5_1_0_0_0 for immobilized enzyme compared with free enzyme were 27 and 14 times higher, respectively. These large differences are the main drivers of the substantial differences in relative abundance of neutral glycans. Both 3_3_0_0_0 and 4_3_0_1_0 were identified as the most abundant glycans released from a similar protein source using Endo BI-1 [41]. Although high mannose compounds like 5_1_0_0_0 and 6_1_0_0_0 were previously found in the bovine and human milk *N*-glycome, likely deriving from bovine lactoferrin, they were not previously described as being released from bovine colostrum whey proteins with free Endo BI-1 [41,43].

Despite the many technological breakthroughs, deglycosylation is still not a well-characterized process. Recently, the kinetics of the commercial enzyme peptide-*N*-glycosidase F (PNGase F) were investigated to understand the impact of sialylation on the release of *N*-glycans [44]. Presence of sialic acid slowed glycan release, while fucosylation also affected the deglycosylation rate. Because RNase B contains a single glycosylation site and high mannose type glycans, these differences would not be observed. However, when using a different enzyme (Endo BI-1) and complex substrates like bovine colostrum whey proteins under different conditions, kinetics and deglycosylation behavior would likely be substantially different. Additionally, the presence of methacrylate resin with pore diameters within the range of 300 to 600 Å may facilitate binding of small, neutral glycans such as 3_3_0_0_0 and 5_1_0_0_0 or the protein regions containing them, favoring their release compared with free Endo BI-1. Antennary moieties such as fucose or sialic acid could also change physicochemical interactions between the glycan and the methacrylate supports as well as the glycan with the immobilized enzyme itself. The ability to modulate glycan release based on reaction conditions has been previously described by Le Parc et al. [41]. Additional changes on the glycan release resulting from the immobilization method used suggests a high degree of complexity concerning enzymatic deglycosylation.

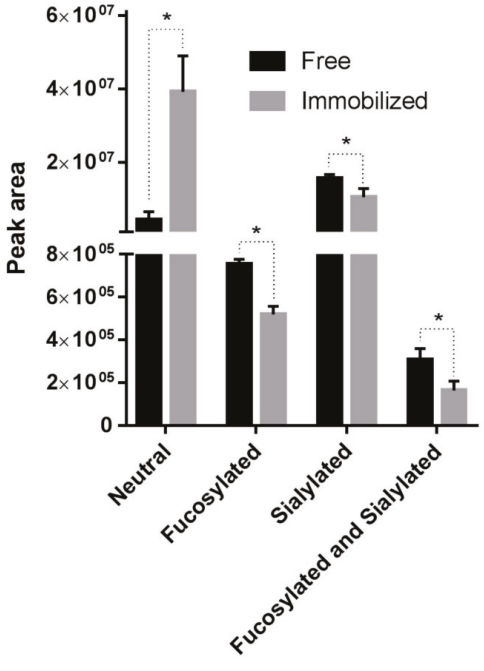

Figure 7. Mean relative quantities of various classes of released *N*-glycans from bovine colostrum whey proteins determined by nano-LC Chip Q-ToF MS/MS by free and immobilized Endo BI-1. Error bars represent one standard deviation. * Represents significant differences within the same class of *N*-glycans at $p < 0.05$.

3. Materials and Methods

3.1. Enzyme Production

Recombinant endo-β-(1,4)-*N*-acetylglucosaminidase (Endo BI-1) from *Bifidobacterium longum* subsp. *infantis* ATCC 15697 from the University of California Davis Viticulture and Enology Culture Collection (Davis, CA, USA) was cloned into *E. coli* using a pEcoTM-T7-cHis cloning kit (GeneTarget Inc, San Diego, CA, USA). Endo BI-1 was expressed and isolated in a stock containing 65 mg/mL enzymebased upon previous literature [33].

3.2. Enzyme Immobilization

Endo BI-1 was immobilized onto methacrylate resin according to manufacturer's directions (Purolite, Llantrisant, Wales, UK). Epoxide-activated (Lifetech ECR8204F), amino-activated (Lifetech ECR8309F), and divinylbenzene (DVB, Lifetech ECR1030M) adsorption resins were used in this study. Covalent (epoxide- and amino-activated resins) and adsorption (divinylbenzene resin) immobilization techniques were selected in this study due to limited macromolecular substrate diffusion through entrapment matrices [45].

To activate the amino resin, 2% glutaraldehyde in 1X PBS as a crosslinking agent was added to the resin prior to enzyme addition and incubated for 1 h, after which it was washed with 0.1X phosphate-buffered saline (PBS) to remove excess glutaraldehyde. Endo BI-1 enzyme stock was added to each activated resin (50 mg enzyme per gram activated resin, wet basis) in buffer mass equal to four times the mass of the resin. For epoxide-activated immobilization, resin was incubated with enzyme in 10X PBS buffer for 42 h. For adsorption-based immobilization, DVB resin was incubated with enzyme for 18 h in 0.1X PBS buffer. Amino-based immobilization was incubated with enzyme in 0.1X PBS for 24 h, based on the manufacturers' recommendations. Enzyme incubation took place at 25 °C and 100 rpm and each immobilization method was performed in triplicate. Following incubation, resins were washed with four volumes of 0.1X PBS buffer. The wash buffer was collected and further analyzed to determine the protein immobilization yield.

3.3. Evaluating Protein Immobilization Yield

Wash buffers from enzyme immobilization were treated with four volumes of −20 °C ethanol and held at −30 °C for 60 min to precipitate proteins, after which the samples were centrifuged at 4000× *g* for 30 min at 4 °C. The supernatant was discarded, and the pellet was resuspended in nanopure water. The total protein was loaded to the immobilization resin and the protein remaining in the wash buffer was measured. The protein immobilization yield was determined by the following equation:

$$\text{Protein immobilization yield } (\%) = \frac{P_L - P_w}{P_L} \times 100\%$$

where P_L is the mass of protein loaded and P_w is the mass of protein in the resin washing buffer after immobilization [46]. Total protein was measured fluorometrically in triplicate using the Qubit Protein Assay Kit (Life Technologies, Grand Island, NY, USA). Purified protein samples were also analyzed by sodium dodecyl sulfate polyacrylamide gel electrophoresis (SDS-PAGE) on 4–15% precast polyacrylamide gels to visualize amount of protein not bound to immobilization resin [9].

3.4. N-glycan Analysis by MALDI-ToF Mass Spectrometry

A microflex MALDI-ToF mass spectrometer (Bruker Daltonics GmbH, Bremen, Germany) was used. Ten μL of purified *N*-glycan samples were spiked with five μL 100 mg/L of the human milk oligosaccharide 3'-fucosyllactose (3-FL, Dextra Laboratories Inc., Reading, UK) as an internal standard. A one μL aliquot of spiked sample was combined with an equal volume of 2,5-dihydroxybenzoic acid matrix (20 mg/mL in 30% acetonitrile, 0.1% trifluoroacetic acid) and 0.4 μL 1 mM NaCl was added

to achieve ionization in positive mode. 0.5 μL spiked sample with matrix and NaCl was spotted in duplicate onto a ground steel target plate and dried under vacuum. Mass calibration was conducted using a polysaccharide ladder extracted from beer [47].

Ionization was carried out using a 337.1 nm laser, and detected in reflectron positive mode with a reflector voltage of 20.02 kV in the mass range of 300 to 2500 *m/z*. The final spectra were the sum of 2000 laser shots. MS intensities of four glycans (namely Man 5, Man 6, Man 7, Man 8) released from bovine ribonuclease B (RNase B, Sigma Aldrich, St. Louis, MO, USA) were normalized to the MS intensity of 3-FL internal standard, summed, and considered the normalized relative abundance of glycan.

Linearity of the MALDI-ToF method was determined by preparing a stock of glycans released from RNase B using free Endo BI-1. Following purification as described above, varying amounts of released *N*-glycan was added to a constant amount of 3-FL internal standard and analyzed by MALDI-ToF MS as described above. The summed, normalized intensity was plotted against the volume of *N*-glycans added and a linear regression was fit to the data.

3.5. Preliminary Comparison of Immobilization Methods Efficiency Using Ribonuclease (RNase) B

Accounting for varying immobilization yields of the enzyme onto the beads, resin containing 40 μg immobilized Endo BI-1 or 40 μg free enzyme was reacted with 600 μg in 20 mM Na_2HPO_4 buffer for 90 min at 45 °C at pH 5. The reaction was terminated with ethanol at −30 °C and glycans were purified and characterized as described in the MALDI-ToF MS analysis section. Summed, normalized MS intensities for the four most abundant glycans were normalized to 100% activity for the free enzyme. One-way analysis of variance (ANOVA) was used along with Tukey's multiple comparisons test with GraphPad Prism 7 (Graphpad, La Jolla, CA, USA) to determine the statistical significance of the data at $p < 0.05$.

3.6. Effect of Immobilization on Enzyme Resilience to pH and Thermal Changes

To identify the optimum temperature for the immobilized enzyme, RNase B was incubated in pH 5 buffer as described previously and free or immobilized enzyme was added [9]. The reaction mixture (enzyme + substrate) was incubated for 20 min at temperatures ranging from 45 to 85 °C. Their respective deglycosylating activities were normalized and compared.

The pH of 20 mM Na_2HPO_4 buffer was adjusted to 3, 5, 7, and 9 using 1 N HCl or NaOH. Free and immobilized Endo BI-1 was reacted with RNase B at 45 °C at each pH for 20 min and the relative activity, measured as the enzyme ability to deglycosylate RNase B, was measured by MALDI-ToF MS. Experiments were conducted in triplicate and a two-way ANOVA was used along with Tukey's multiple comparisons in GraphPad Prism 7 to determine statistical significance of the data at $p < 0.05$.

3.7. Determination of Kinetic Parameters of Enzyme Using RNase B

Relevant kinetic parameters relating to maximum reaction velocity (V_{max}) and the Michaelis-Menten constant (k_m) were determined by measuring the normalized glycan intensity at varying substrate concentrations (0.1 to 1.1 g/L) in 20 mM Na_2HPO_4 buffer under optimal pH and temperature conditions for the free and immobilized enzyme. Aliquots were taken in four-minute intervals up to 20 min. Linearized plotting (Lineweaver Burk and Hanes Woolf) were utilized to calculate K_m and V_{max} [48,49].

3.8. Evaluating Reusability of Immobilized Endo BI-1 Using RNase B

Reusability of immobilized Endo BI-1 was evaluated for ten cycles of 20 min at both 65 °C and 45 °C in presence of RNase B. Between each cycle, the supernatant from the reaction was removed and subsequently treated with cold ethanol for protein precipitation and glycan isolation. After each reaction cycle, the remaining resin containing the immobilized enzyme was washed with a 20 mM Na_2HPO_4 buffer at a 4:1 ratio (buffer/reaction volume) and fresh substrate-containing buffer was

added for the next reaction cycle. Enzyme activity after the first reaction was considered as 100%. Experiments were conducted in triplicate.

3.9. Release of N-glycans from Bovine Colostrum whey Proteins by Free and Immobilized Endo BI-1

Bovine colostrum whey proteins were isolated from bovine colostrum whey kindly provided by La Belle (Bellingham, WA, USA). Bovine colostrum whey proteins were isolated and purified using a 10 kDa molecular weight cut-off ultrafiltration as described previosly by Karav et al. [33] and were deglycosylated by free and immobilized Endo BI-1 in triplicate. Bovine colostrum whey protein concentration was determined by Qubit fluorometric kit according to manufacturer's instructions as described previously. Briefly, Endo BI-1 (free or immobilized) was added to purified colostrum whey proteins at a ratio of 1:75 in 20 mM Na_2HPO_4 buffer at pH 7 and reacted for 1 h at 45 °C based on previous reports [33]. The reaction was terminated, and proteins were precipitated using cold ethanol. The supernatant was dried by vacuum centrifuge and subsequently resuspended, whereupon glycans were purified from contaminants using C18 cartridges (Glygen, Columbia, MD, USA) and desalted by porous graphitized carbon (PGC, Glygen) solid phase extraction as described previously [7,50]. Eluate from PGC was dried, resuspended in nanopure water for subsequent nano-LC-Chip Q ToF analysis.

3.10. N-glycan Analysis by Mass Spectrometry Nano-LC-Chip Q ToF

Samples were transferred to polypropylene vials and 6 µL were injected into an Agilent 6520 nano-LC-Chip quadrupole time-of-flight mass spectrometer (Q-ToF MS, Agilent Technologies, Santa Clara, CA, USA). Glycans were further purified on a 9 mm × 75 µm PGC enrichment column and then separated on a 43 mm × 75 µm PGC analytical column with binary solvents, gradient, and data collection based on Karav et al. [7]. The following minor modifications were applied: scan range for MS was 450 to 2500 *m/z*, and for MS/MS was 100 to 3200 *m/z*. Spectra in both MS and MS/MS modes were collected at a rate of 0.63 spectra/s. The collision energy in the collision cell corresponded to a slope of 1.8/100 Da.

Chromatograms from the nano-LC-Chip Q ToF were curated and compounds identified in Masshunter Qualitative Analysis software (version B.07.00 Agilent Technologies) using a previously described bovine milk *N*-glycan bioinformatic library adjusted for one fewer *N*-acetylglucosamine in the chitobiose core. The library assumed compositions including hexose (Hex), *N*-acetylhexosamine (HexNAc), fucose (Fuc), *N*-acetylneuraminic acid (NeuAc), and *N*-glycolylneuraminic acid (NeuGc) [43]. Additionally, structures included a tetrasaccharide core containing three hexose (e.g., mannose) moieties and one HexNAc (*N*-acetylglucosamine) moiety. Structures were confirmed using MS/MS fragmentation patterns and isotopic distribution. A library of glycan structures specific to the sample set was assembled based on retention time, molecular formula and confirmed *m/z*. Relative abundances of *N*-glycans were obtained using Masshunter Profinder software (version B.06.00, Agilent Technologies). The batch targeted feature extraction algorithm with the following parameters was applied using the generated database: minimum abundance of 750 counts, charge state up to +3, retention time window of 2 min, and a glycan isotope model. Peak areas were verified for accurate integration and isotopic distribution.

4. Conclusions

These findings highlight the advantages and limitations of different enzyme immobilization strategies, in particular when considering an enzyme targeting the release of glycans from macromolecular substrates such as glycoproteins. The immobilization process shifted the optimum pH of the enzyme to a neutral pH, which is of relevance when considering the immobilization of this enzyme for industrial applications, such as in dairy products or other food products having a pH close to neutral. The use of moderate temperatures favored the reuse of the immobilized enzyme. Immobilized enzyme reusability may compensate for its initial reduced activity. When using a complex and diverse source of glycoproteins as bovine colostrum, the immobilized enzyme released a higher abundance of neutral *N*-glycans than the free

enzyme, which yielded a different overall composition of glycans by class. This difference suggests that specific glycan release can be achieved by potentially tailoring immobilized enzyme reactions conditions in future studies.

Further investigation of the different rates of glycan release, possibly due to limited enzyme accessibility to specific glycan sites on glycoproteins, may enhance our understanding of the role of certain glycosylation sites and structures on their function, in particular for therapeutic glycoproteins such as monoclonal antibodies. Investigation on alternative glycoprotein substrates of plant origin is warranted to understand substrate specificity. This study presents a scalable technique for enzymatic deglycosylation of industrially relevant glycoproteins. Optimized reactor configurations, including flow-through column reactors and fluidized beds, could favor glycan release and subsequent isolation from deglycosylated proteins in downstream isolation, enabling future processing scale-up and commercialization of bioactive glycans and novel therapeutics.

Supplementary Materials: The following are available online at http://www.mdpi.com/2073-4344/8/7/278/s1, Figure S1: Sodium dodecyl sulfate polyacrylamide gel electrophoresis of immobilization washings from amino, adsorption, and epoxy methods on a 4–15% acrylamide gel. Endo BI-1 weighs approximately 53 kDa, Figure S2: Normalized MALDI-ToF MS intensity vs. N glycan: I.S. ratio for glycans released from RNase B, Table S1: Mean relative quantities (±S.D.) of *N*-glycans released by free and immobilized Endo BI-1 from bovine colostrum whey proteins as determined by nano-LC Chip Q-ToF MS/MS Compound formula is signified by the number of residues of each monosaccharide in the following order: Hex_HexNAc_Fuc_NeuAc_NeuGc.

Author Contributions: D.B. and J.M.L.N.de.M.B. came up with the original idea. J.L.C. and J.M.L.N.de.M.B. designed the experiments. S.K. expressed and isolated the enzyme. J.L.C. performed the experiments and analyzed the data. J.L.C., S.K., D.B., and J.M.L.N.de.M.B. wrote the paper.

Acknowledgments: This research was supported by the Center for Advanced Processing and Packaging Studies (CAPPS), the National Institutes of Health awards R01AT007079 and R01AT008759, the USDA:NIFA Hatch project 232719, and was partially supported by an industry/campus supported fellowship under the Training Program in Biomolecular Technology (T32-GM008799) at the University of California, Davis. The authors would like to thank David Mills for providing the endo- β-*N*-acetylglucosaminidase enzyme and Nannan Tao from Bruker Daltonics for assistance with MALDI-ToF MS applications.

Conflicts of Interest: D.B. is a cofounder of Evolve Biosystems, a company focused on diet-based manipulation of the gut microbiota. Evolve Biosystems played no role in the funding, design, execution, interpretation, or publication of this work. The other authors declare no conflict of interest.

References

1. Lafite, P.; Daniellou, R. Rare and unusual glycosylation of peptides and proteins. *Nat. Prod. Rep.* **2012**, *29*, 729–738. [CrossRef] [PubMed]
2. Montreuil, J. Primary Structure of Glycoprotein Glycans Basis for the Molecular Biology of Glycoproteins. In *Advances in Carbohydrate Chemistry and Biochemistry*; Elsevier: Cambridge, MA, USA, 1980; Volume 37, pp. 157–223, ISBN 978-0-12-007237-8.
3. Zivkovic, A.M.; German, J.B.; Lebrilla, C.B.; Mills, D.A. Human milk glycobiome and its impact on the infant gastrointestinal microbiota. *Proc. Natl. Acad. Sci. USA* **2011**, *108*, 4653–4658. [CrossRef] [PubMed]
4. Thurl, S.; Munzert, M.; Henker, J.; Boehm, G.; Müller-Werner, B.; Jelinek, J.; Stahl, B. Variation of human milk oligosaccharides in relation to milk groups and lactational periods. *Br. J. Nutr.* **2010**, *104*, 1261–1271. [CrossRef] [PubMed]
5. Helenius, A.; Aebi, M. Intracellular Functions of N-Linked Glycans. *Science* **2001**, *291*, 2364–2369. [CrossRef] [PubMed]
6. Karav, S.; Cohen, J.L.; Barile, D.; de Moura Bell, J.M.L.N. Recent advances in immobilization strategies for glycosidases. *Biotechnol. Prog.* **2017**, *33*, 104–112. [CrossRef] [PubMed]
7. Karav, S.; Parc, A.L.; de Moura Bell, J.M.L.N; Frese, S.A.; Kirmiz, N.; Block, D.E.; Barile, D.; Mills, D.A. Oligosaccharides Released from Milk Glycoproteins Are Selective Growth Substrates for Infant-Associated Bifidobacteria. *Appl. Environ. Microbiol.* **2016**, *82*, 3622–3630. [CrossRef] [PubMed]
8. Wang, W.L.; Du, Y.M.; Wang, W.; Conway, L.P.; Cai, Z.P.; Voglmeir, J.; Liu, L. Comparison of the bifidogenic activity of human and bovine milk *N*-glycome. *J. Funct. Foods* **2017**, *33*, 40–51. [CrossRef]

9. Garrido, D.; Nwosu, C.; Ruiz-Moyano, S.; Aldredge, D.; German, J.B.; Lebrilla, C.B.; Mills, D.A. Endo-β-*N*-acetylglucosaminidases from Infant Gut-associated Bifidobacteria Release Complex *N*-glycans from Human Milk Glycoproteins. *Mol. Cell. Proteom.* **2012**, *11*, 775–785. [CrossRef] [PubMed]
10. Wang, W.-L.; Wang, W.; Du, Y.-M.; Wu, H.; Yu, X.-B.; Ye, K.-P.; Li, C.-B.; Jung, Y.-S.; Qian, Y.-J.; Voglmeir, J.; et al. Comparison of anti-pathogenic activities of the human and bovine milk *N*-glycome: Fucosylation is a key factor. *Food Chem.* **2017**, *235*, 167–174. [CrossRef] [PubMed]
11. Blaschek, K.M.; Wendorff, W.L.; Rankin, S.A. Survey of Salty and Sweet Whey Composition from Various Cheese Plants in Wisconsin. *J. Dairy Sci.* **2007**, *90*, 2029–2034. [CrossRef] [PubMed]
12. Walstra, P.; Walstra, P.; Wouters, J.T.M.; Geurts, T.J. *Dairy Science and Technology*, 2nd ed.; CRC Press: Boca Raton, Fl, USA, 2010; ISBN 978-1-4200-2801-0.
13. USDA. *Dairy Products 2016 Summary*; USDA National Agricultural Statistics Service, United States Department of Agriculture: Washington, DC, USA, 2017.
14. Cao, L.; van Langen, L.; Sheldon, R.A. Immobilised enzymes: Carrier-bound or carrier-free? *Curr. Opin. Biotechnol.* **2003**, *14*, 387–394. [CrossRef]
15. Cao, L. Immobilised enzymes: science or art? *Curr. Opin. Chem. Biol.* **2005**, *9*, 217–226. [CrossRef] [PubMed]
16. DiCosimo, R.; McAuliffe, J.; Poulose, A.J.; Bohlmann, G. Industrial use of immobilized enzymes. *Chem. Soc. Rev.* **2013**, *42*, 6437–6474. [CrossRef] [PubMed]
17. Fernandes, P. Enzymes in Food Processing: A Condensed Overview on Strategies for Better Biocatalysts. *Enzyme Res.* **2010**, *2010*, 862537. [CrossRef] [PubMed]
18. Alloue, W.A.M.; Destain, J.; Medjoub, T.E.; Ghalfi, H.; Kabran, P.; Thonart, P. Comparison of Yarrowia lipolytica Lipase Immobilization Yield of Entrapment, Adsorption, and Covalent Bond Techniques. *Appl. Biochem. Biotechnol.* **2008**, *150*, 51–63. [CrossRef] [PubMed]
19. Mateo, C.; Grazú, V.; Pessela, B.C.C.; Montes, T.; Palomo, J.M.; Torres, R.; López-Gallego, F.; Fernández-Lafuente, R.; Guisán, J.M. Advances in the design of new epoxy supports for enzyme immobilization–stabilization. *Biochem. Soc. Trans.* **2007**, *35*, 1593–1601. [CrossRef] [PubMed]
20. Karav, S.; Le Parc, A.; de Moura Bell, J.M.L.N.; Rouquié, C.; Mills, D.A.; Barile, D.; Block, D.E. Others Kinetic characterization of a novel endo-β-*N*-acetylglucosaminidase on concentrated bovine colostrum whey to release bioactive glycans. *Enzyme Microb. Technol.* **2015**, *77*, 46–53. [CrossRef] [PubMed]
21. Masuko, T.; Minami, A.; Iwasaki, N.; Majima, T.; Nishimura, S.-I.; Lee, Y.C. Carbohydrate analysis by a phenol–sulfuric acid method in microplate format. *Anal. Biochem.* **2005**, *339*, 69–72. [CrossRef] [PubMed]
22. Scott, T.A., Jr.; Melvin, E.H. Determination of dextran with anthrone. *Anal. Chem.* **1953**, *25*, 1656–1661. [CrossRef]
23. Pfenninger, A.; Karas, M.; Finke, B.; Stahl, B.; Sawatzki, G. Mass Spectrometric Investigations of Human Milk Oligosaccharides. In *Bioactive Components of Human Milk*; Advances in Experimental Medicine and Biology; Springer: Boston, MA, USA, 2001; pp. 279–284. ISBN 978-1-4613-5521-2.
24. Nishimura, S.-I.; Niikura, K.; Kurogochi, M.; Matsushita, T.; Fumoto, M.; Hinou, H.; Kamitani, R.; Nakagawa, H.; Deguchi, K.; Miura, N.; et al. High-Throughput Protein Glycomics: Combined Use of Chemoselective Glycoblotting and MALDI-TOF/TOF Mass Spectrometry. *Angew. Chem. Int. Ed.* **2005**, *44*, 91–96. [CrossRef] [PubMed]
25. Bucknall, M.; Fung, K.Y.C.; Duncan, M.W. Practical quantitative biomedical applications of MALDI-TOF mass spectrometry. *J. Am. Soc. Mass Spectrom.* **2002**, *13*, 1015–1027. [CrossRef]
26. Bothner, B.; Chavez, R.; Wei, J.; Strupp, C.; Phung, Q.; Schneemann, A.; Siuzdak, G. Monitoring Enzyme Catalysis with Mass Spectrometry. *J. Biol. Chem.* **2000**, *275*, 13455–13459. [CrossRef] [PubMed]
27. Leboeuf, E.; Immerzeel, P.; Gibon, Y.; Steup, M.; Pauly, M. High-throughput functional assessment of polysaccharide-active enzymes using matrix-assisted laser desorption/ionization–time-of-flight mass spectrometry as exemplified on plant cell wall polysaccharides. *Anal. Biochem.* **2008**, *373*, 9–17. [CrossRef] [PubMed]
28. Kang, M.-J.; Tholey, A.; Heinzle, E. Application of automated matrix-assisted laser desorption/ionization time-of-flight mass spectrometry for the measurement of enzyme activities. *Rapid Commun. Mass Spectrom.* **2001**, *15*, 1327–1333. [CrossRef] [PubMed]
29. Mechref, Y.; Novotny, M.V.; Krishnan, C. Structural Characterization of Oligosaccharides Using Maldi-TOF/TOF Tandem Mass Spectrometry. *Anal. Chem.* **2003**, *75*, 4895–4903. [CrossRef] [PubMed]

30. Gaur, R.; Pant, H.; Jain, R.; Khare, S.K. Galacto-oligosaccharide synthesis by immobilized Aspergillus oryzae β-galactosidase. *Food Chem.* **2006**, *97*, 426–430. [CrossRef]
31. Wong, D.E.; Senecal, K.J.; Goddard, J.M. Immobilization of chymotrypsin on hierarchical nylon 6,6 nanofiber improves enzyme performance. *Colloids Surf. B Biointerfaces* **2017**, *154*, 270–278. [CrossRef] [PubMed]
32. Rehman, H.U.; Aman, A.; Silipo, A.; Qader, S.A.U.; Molinaro, A.; Ansari, A. Degradation of complex carbohydrate: Immobilization of pectinase from Bacillus licheniformis KIBGE-IB21 using calcium alginate as a support. *Food Chem.* **2013**, *139*, 1081–1086. [CrossRef] [PubMed]
33. Karav, S.; de Moura Bell, J.M.L.N.; Parc, A.L.; Liu, Y.; Mills, D.A.; Block, D.E.; Barile, D. Characterizing the release of bioactive *N*-glycans from dairy products by a novel endo-β-*N*-acetylglucosaminidase. *Biotechnol. Prog.* **2015**, *31*, 1331–1339. [CrossRef] [PubMed]
34. Li, D.; Teoh, W.Y.; Gooding, J.J.; Selomulya, C.; Amal, R. Functionalization Strategies for Protease Immobilization on Magnetic Nanoparticles. *Adv. Funct. Mater.* **2010**, *20*, 1767–1777. [CrossRef]
35. Iyer, P.V.; Ananthanarayan, L. Enzyme stability and stabilization—Aqueous and non-aqueous environment. *Process Biochem.* **2008**, *43*, 1019–1032. [CrossRef]
36. Busto, M.D.; García-Tramontín, K.E.; Ortega, N.; Perez-Mateos, M. Preparation and properties of an immobilized pectinlyase for the treatment of fruit juices. *Bioresour. Technol.* **2006**, *97*, 1477–1483. [CrossRef] [PubMed]
37. Demirel, G.; Özçetin, G.; Şahin, F.; Tümtürk, H.; Aksoy, S.; Hasirci, N. Semi-interpenetrating polymer networks (IPNs) for entrapment of glucose isomerase. *React. Funct. Polym.* **2006**, *66*, 389–394. [CrossRef]
38. Wei, L.; Zhang, W.; Lu, H.; Yang, P. Immobilization of enzyme on detonation nanodiamond for highly efficient proteolysis. *Talanta* **2010**, *80*, 1298–1304. [CrossRef] [PubMed]
39. Klein, M.P.; Nunes, M.R.; Rodrigues, R.C.; Benvenutti, E.V.; Costa, T.M.H.; Hertz, P.F.; Ninow, J.L. Effect of the Support Size on the Properties of β-Galactosidase Immobilized on Chitosan: Advantages and Disadvantages of Macro and Nanoparticles. *Biomacromolecules* **2012**, *13*, 2456–2464. [CrossRef] [PubMed]
40. Chauhan, S.; Vohra, A.; Lakhanpal, A.; Gupta, R. Immobilization of Commercial Pectinase (Polygalacturonase) on Celite and Its Application in Juice Clarification. *J. Food Process. Preserv.* **2015**, *6*, 2135–2141. [CrossRef]
41. Parc, A.L.; Karav, S.; de Moura Bell, J.M.L.N.; Frese, S.A.; Liu, Y.; Mills, D.A.; Block, D.E.; Barile, D. A novel endo-β-*N*-acetylglucosaminidase releases specific *N*-glycans depending on different reaction conditions. *Biotechnol. Prog.* **2015**, *31*, 1323–1330. [CrossRef] [PubMed]
42. Axelsson, A.; Zacchi, G. Economic evaluation of the hydrolysis of lactose using immobilized β-galactosidase. *Appl. Biochem. Biotechnol.* **1990**, *24*, 679–693. [CrossRef]
43. Nwosu, C.C.; Aldredge, D.L.; Lee, H.; Lerno, L.A.; Zivkovic, A.M.; German, J.B.; Lebrilla, C.B. Comparison of the Human and Bovine Milk *N*-glycome via High-Performance Microfluidic Chip Liquid Chromatography and Tandem Mass Spectrometry. *J. Proteome Res.* **2012**, *11*, 2912–2924. [CrossRef] [PubMed]
44. Huang, Y.; Orlando, R. Kinetics of *N*-Glycan Release from Human Immunoglobulin G (IgG) by PNGase F: All Glycans Are Not Created Equal. *J. Biomol. Tech. JBT* **2017**. [CrossRef] [PubMed]
45. Tanaka, H.; Matsumura, M.; Veliky, I.A. Diffusion characteristics of substrates in Ca-alginate gel beads. *Biotechnol. Bioeng.* **1984**, *26*, 53–58. [CrossRef] [PubMed]
46. Manjon, A.; Iborra, J.L.; Lozano, P.; Canovas, M. A practical experiment on enzyme immobilization and characterization of the immobilized derivatives. *Biochem. Mol. Biol. Educ.* **1995**, *23*, 213–216. [CrossRef]
47. Park, E.; Yang, H.; Kim, Y.; Kim, J. Analysis of oligosaccharides in beer using MALDI-TOF-MS. *Food Chem.* **2012**, *134*, 1658–1664. [CrossRef] [PubMed]
48. Lineweaver, H.; Burk, D. The determination of enzyme dissociation constants. *J. Am. Chem. Soc.* **1934**, *56*, 658–666. [CrossRef]
49. Hanes, C.S. Studies on plant amylases: The effect of starch concentration upon the velocity of hydrolysis by the amylase of germinated barley. *Biochem. J.* **1932**, *26*, 1406–1421. [CrossRef] [PubMed]
50. Cohen, J.L.; Barile, D.; Liu, Y.; de Moura Bell, J.M.L.N. Role of pH in the recovery of bovine milk oligosaccharides from colostrum whey permeate by nanofiltration. *Int. Dairy J.* **2017**, *66*, 68–75. [CrossRef] [PubMed]

© 2018 by the authors. Licensee MDPI, Basel, Switzerland. This article is an open access article distributed under the terms and conditions of the Creative Commons Attribution (CC BY) license (http://creativecommons.org/licenses/by/4.0/).

catalysts

MDPI

Article

Immobilization of the β-fructofuranosidase from *Xanthophyllomyces dendrorhous* by Entrapment in Polyvinyl Alcohol and Its Application to Neo-Fructooligosaccharides Production

Noa Míguez [1], María Gimeno-Pérez [2], David Fernández-Polo [1], Fadia V. Cervantes [1], Antonio O. Ballesteros [1], María Fernández-Lobato [2], María H. Ribeiro [3] and Francisco J. Plou [1,*]

1 Instituto de Catálisis y Petroleoquímica, CSIC, 28049 Madrid, Spain; noa.miguez@csic.es (N.M.); david.fernandezpolo@estudiante.uam.es (D.F.-P.); fadiacervantes@gmail.com (F.V.C.); a.ballesteros@icp.csic.es (A.O.B.)

2 Centro de Biología Molecular Severo Ochoa, CSIC-UAM, 28049 Madrid, Spain; mgimeno@cbm.csic.es (M.G.-P.); mfernandez@cbm.csic.es (M.F.-L.)

3 Research Institute for Medicines (iMed.ULisboa), Faculdade de Farmácia, Universidade Lisboa, 1649-003 Lisboa, Portugal; mhribeiro@ff.ulisboa.pt

* Correspondence: fplou@icp.csic.es; Tel.: +34-91-585-4869

Received: 21 April 2018; Accepted: 9 May 2018; Published: 11 May 2018

Abstract: The β-fructofuranosidase (Xd-INV) from the basidiomycota yeast *Xanthophyllomyces dendrorhous* (formerly *Phaffia rhodozyma*) is unique in its ability to synthesize neo- fructooligosaccharides (neo-FOS). In order to facilitate its industrial application, the recombinant enzyme expressed in *Pichia pastoris* (pXd-INV) was immobilized by entrapment in polyvinyl alcohol (PVA) hydrogels. The encapsulation efficiency exceeded 80%. The PVA lenticular particles of immobilized pXd-INV were stable up to approximately 40 °C. Using 600 g/L sucrose, the immobilized biocatalyst synthesized 18.9% (*w*/*w*) FOS (59.1 g/L of neokestose, 30.2 g/L of 1-kestose, 11.6 g/L of neonystose and 12.6 g/L of blastose). The operational stability of PVA-immobilized biocatalyst was assayed in a batch reactor at 30 °C. The enzyme preserved its initial activity during at least 7 cycles of 26 h.

Keywords: glycosidases; fructooligosaccharides; prebiotics; enzyme entrapment; immobilization; bioreactors; hydrogels; neokestose

1. Introduction

Fructooligosaccharides (FOS) are fructose oligomers linked to a sucrose skeleton by different β(2→1) or β(2→6) glycosidic bonds [1]. In addition to their prebiotic properties—which promote the development of bifidobacteria and lactobacillus in the gastrointestinal tract [2]—and their low glycemic index, FOS may exert other benefits in human health, including a better gut absorption of Ca^{2+} and Mg^{2+}, a reduction of blood lipid levels and a reduced risk of suffering colon cancer [3,4]. FOS can be synthesized from sucrose by a transfructosylation reaction [5]. Commercial FOS possess an inulin-type structure containing β(2→1) linked fructose units [6]. However, it has been reported that neo-FOS, in which one fructosyl moiety is β(2→6) linked to the glucose unit of sucrose, could display improved prebiotic and physicochemical properties with regard to inulin-type FOS [7,8].

The β-fructofuranosidase Xd-INV from the yeast *Xanthophyllomyces dendrorhous* (formerly *Phaffia rhodozyma*) is a dimeric glycoprotein with a molecular mass of 320–380 kDa, which belongs to the glycoside hydrolase (GH) family 32 [9,10]. Like other β-fructofuranosidases, Xd-INV catalyzes both the hydrolysis of sucrose and the synthesis of FOS [11,12]. However, Xd-INV is unique in its ability to catalyze the transfer a fructosyl moiety to the 6-OH hydroxyl of glucose unit in sucrose.

In fact, this is the most efficient enzyme reported for the production of neo-FOS (basically neokestose and neonystose) [11,13]. Xd-INV is an attractive enzyme not only for the production of neo-FOS, but also for the preparation of novel fructosylated derivatives [13]. Recently we successfully expressed this enzyme in *Pichia pastoris* (pXd-INV) yielding a significant volumetric activity [12].

Despite the enormous potential of biocatalytic processes [14], the industrial application of enzymes is often hampered by a lack of long-term operational stability and the difficulties to recover and reuse the biocatalysts [15]. Enzyme immobilization can help to overcome these drawbacks, since it allows the easy separation of the biocatalyst facilitating product recovery, which is commonly accompanied by the stabilization effect towards denaturation by high temperatures, extreme pHs or organic cosolvents [16,17].

Immobilization methodologies for industrial biotransformations should be relatively simple, inexpensive and provide active biocatalysts with substantial stability [15]. The strategies for enzyme immobilization are commonly classified into three groups [18]: support binding (by adsorption or covalent linkages), entrapment and cross-linking. For reactions involving the transformation of carbohydrates, covalent binding is preferred over adsorption to avoid enzyme leakage [19], but most of the commercial activated carriers are expensive [20–22]. Cross-linking gives rise to biocatalysts with highly concentrated enzyme activity, significant stability and low production costs due to the absence of carrier, although the recovery of activity is commonly low [14,15]. Entrapment is an efficient and inexpensive technique, which is very useful when substrates and products have low molecular sizes and high diffusion rates, as occurs with simple sugars [14,23,24]. The entrapment in hydrogels can be combined with cross-linking in order to provide more resistant biocatalysts [25,26].

In this work, we have investigated the immobilization of recombinant pXd-INV to facilitate its industrial application in the production of neo-FOS and other fructosylated derivatives. Considering that the size of Xd-INV is significantly large (it is a dimeric enzyme with an average molecular mass of 360 kDa and dimensions 135 × 75 × 45 Å [10]), we believed that entrapment methodologies could be appropriate for this enzyme as the leakage through pores should be restricted Our focus was to evaluate polyvinyl alcohol (PVA) entrapment as an immobilization strategy. PVA is cheap, mechanically robust and nontoxic to organisms [27]. The efficiency of this methodology was assessed in terms of the recovered activity and operational stability. The resulting biocatalysts were applied to the production of neo-FOS.

2. Results and Discussion

2.1. Immobilization of pXd-INV in PVA Hydrogels

The recombinant β-fructofuranosidase pXd-INV from *X. dendrorhous* was immobilized by entrapment in lenses of polyvinyl alcohol (PVA), as represented in Figure 1. The enzyme was mixed with a solution of PVA, and the gelification was accomplished by dripping the mixture onto a surface (96-well microplate) followed by partial drying at 50 °C [28]. The gelification can be also promoted by freezing and thawing [29,30] or by UV radiation [31]. The entrapment in highly elastic and stable hydrogels formed by PVA has given excellent results with glycosidic enzymes [26,30,32]. The gelation takes place by the formation of hydrogen bonds between the hydroxyl groups of the PVA, resulting in a noncovalent spatial network [33]. These hydrogels are also very useful in controlled drug release, artificial tissues, bioseparations or biosensors [34,35]. PVA-based biocatalysts have proven remarkable operational and mechanical stability in different types of bioreactors, including shaken microtiter plates, batch stirred tanks and packed-bed reactors [32].

Table 1 summarizes the main immobilization parameters using 10% (*w*/*v*) PVA in 100 mM sodium acetate (pH 5.0), the optimum buffer for this enzyme. Two different enzyme loadings were assayed. Lens volume ranged 52–56 μL. An increment of the initial enzyme activity did not result in a significant increase of the volumetric activity of the biocatalyst. In contrast, the recovered activity was substantially diminished compared with lower enzyme loadings. We checked by successive washings that pXd-INV was not released from the PVA hydrogels. Considering that this enzyme is quite stable under the immobilization conditions, we believe that a high enzyme concentration inside the PVA lenses may cause some diffusional limitations, thus explaining the results obtained when increasing the enzyme loading. Starting from 35.5 enzyme units (measured in the DNS assay) and 5 mL PVA solution, the encapsulation efficiency was satisfactory (>80%).

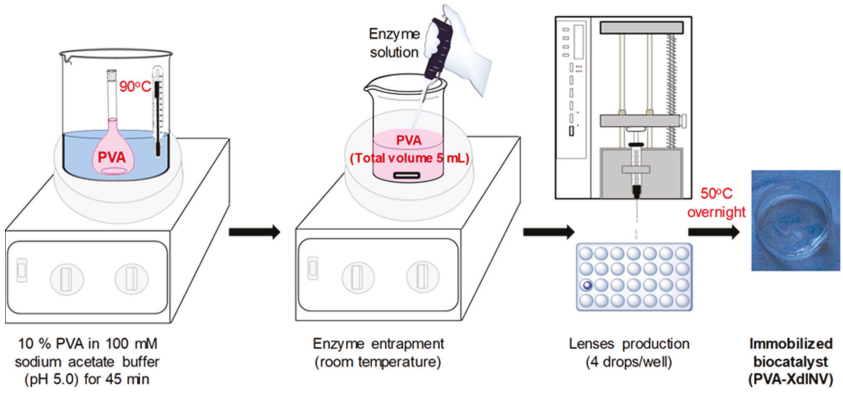

Figure 1. Immobilization of pXd-INV by entrapment in polyvinyl alcohol (PVA).

Table 1. Effect of pXd-INV enzyme loading on the activity and recovery upon immobilization by entrapment in PVA hydrogels.

Total Initial Activity (U) [a]	Volume of Biocatalyst (mL)	Lens Volume (μL) [b]	Activity of the Biocatalyst (U/lens) [a]	Activity of the Biocatalyst (U/ml) [a]	Recovered Activity (%) [c]
35.5	4.8	56.3	0.34	5.96	80.6
84.5	4.7	52.6	0.33	6.20	34.5

[a] Measured by the DNS assay; [b] Lens volume = (volume dispensed/number of drops dispensed) × number of drops in each lens; [c] (Activity of the biocatalyst × Volume of biocatalyst obtained × 100)/Total activity introduced.

The operational stability of the biocatalyst obtained with the lowest enzyme loading (35.5 U) was assayed following a micro-scale procedure previously described by our group [36]. We performed 10 reaction cycles of 20 min with 100 mg/mL sucrose as substrate at 50 °C, measuring the amount of reducing sugars by the DNS method (Figure 2). Between cycles, the biocatalyst was thoroughly washed with 100 mM sodium acetate buffer (pH 5.0). As shown, the operational stability of PVA-lens shaped particles was very satisfactory during at least 10 short cycles.

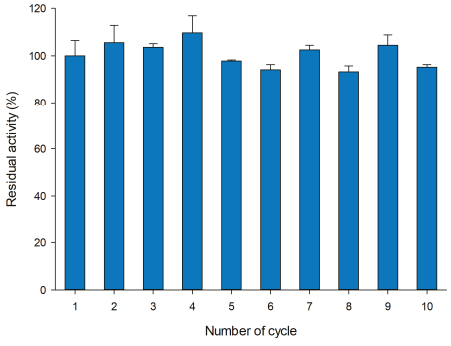

Figure 2. Operational stability of entrapped pXd-INV in PVA. Conditions for each cycle: 100 mg/mL sucrose, 50 °C, 20 min reaction.

2.2. Production of FOS by Entrapped pXd-INV

Using 600 g/L substrate, we analyzed the production of fructooligosaccharides catalyzed by immobilized pXd-INV. A high concentration of sucrose favours transglycosylation reaction in detriment of hydrolysis of the disaccharide [37]. The profile of the reaction products was characterized by High Performance Anion-Exchange Chromatography with Pulsed Amperometric Detection (HPAEC-PAD) (Figure 3). The products pattern correlated well with that obtained using the soluble enzyme expressed in *P. pastoris* [12]. Using neo-FOS standards purified and characterized as described in previous works [11,38], we were able to identify neokestose (the major product), 1-kestose and neonystose. Peak 5 was blastose [Fru-β-(2→6)-Glc], a sucrose isomer member of the neo-FOS series, which is produced by the hydrolysis of neokestose. We demonstrated in previous publications that Xd-INV was unable to transfer the fructosyl moiety to free glucose [11,12]. The structure of the FOS synthesized by immobilized pXd-INV is depicted in Figure 4.

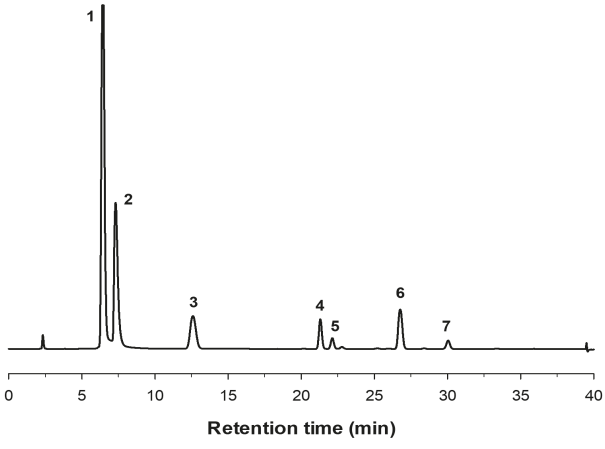

Figure 3. HPAEC-PAD chromatogram of the reaction of 600 g/L sucrose at 50 °C with pXd-INV entrapped in PVA. (1) Glucose; (2) Fructose; (3) Sucrose; (4) 1-Kestose; (5) Blastose; (6) Neokestose; (7) Neonystose.

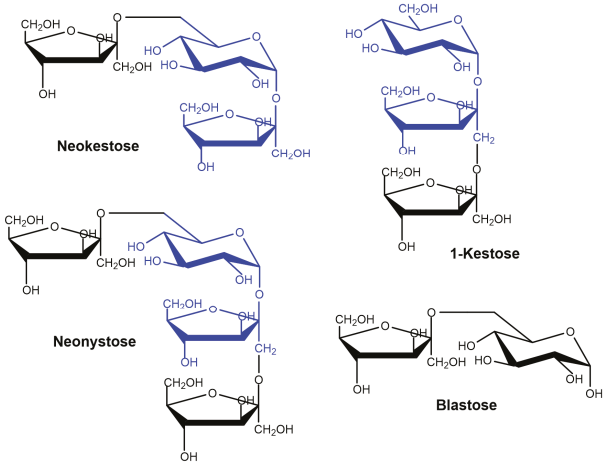

Figure 4. Structure of the FOS synthesized by immobilized pXd-INV. The sucrose skeleton is represented in blue.

2.3. Thermal Stability of PVA Lens-Shaped Particles

The operational stability represented in Figure 2 corresponded to short reaction cycles (20 min) at 50 °C. The optimum temperature for both native and recombinant Xd-INV is in the range 50–60 °C [11,12]. However, in order to assess the potential of the immobilized pXd-INV biocatalysts for the synthesis of neo-FOS, we should consider the thermostability of the PVA lens-shaped particles in long-term operation. Thus, the immobilized biocatalyst was incubated at different temperatures (4–60 °C) for 24 h at pH 5.0, and the residual activity was measured by the DNS assay (Figure 5). As shown, the activity of the PVA-lens shaped particles was maintained up to approximately 40 °C. At higher temperatures, more than half of the activity was lost in one cycle. However, the soluble enzyme is very stable up to 60 °C during at least 24 h (data not shown). In this context, it is well reported that PVA hydrogels become unstable at temperatures above 50 °C [39,40]. The loss of 3D structure of the lenses may facilitate enzyme leakage thus resulting in a decrease of the activity. Based on the above data, we selected 30 °C to assess the operational stability of the biocatalyst for neo-FOS synthesis, as a compromise between enzyme activity and stability.

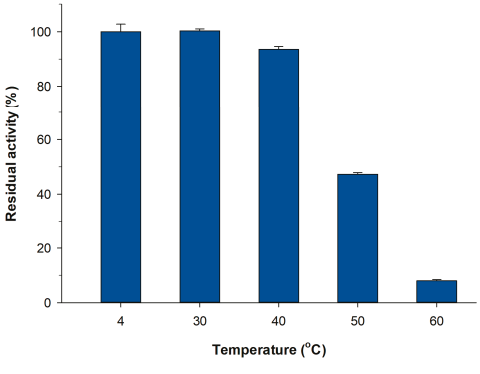

Figure 5. Thermostability of immobilized pXd-INV in PVA. Incubation conditions: 100 mM sodium acetate buffer (pH 5.0), 24 h.

2.4. Kinetics of Neo-FOS Formation by Entrapped pXd-INV

The kinetics of FOS formation with the PVA-entrapped enzyme was analyzed using 600 g/L sucrose as substrate at 30 °C. Figure 6 represents the formation of the different products as a function of sucrose consumption. Maximum FOS production was reached when approximately 86% of the initial sucrose had disappeared, as occurred with the soluble enzyme [12]. At this point, the immobilized pXd-INV yielded 18.9% (*w*/*w*) FOS (113.5 g/L), of which 59.1 g/L corresponded to neokestose, 30.2 g/L to 1-kestose, 11.6 g/L to neonystose, and 12.6 g/L to blastose.

We confirmed that blastose was formed by hydrolysis of neokestose, as the concentration of this disaccharide increased up to 30.5 g/L concomitant with the sharp decrease of neokestose at the end of the reaction. This value represents a notable concentration of blastose considering that by now the largest production reported of this disaccharide was 34 g/L using the *Cladosporium cladosporioides* mycelium-bound transfructosylation activity [38]. The sharp decrease of FOS concentration observed after 85–90% consumption of sucrose was also observed with the soluble native enzyme [12] and is typical in the preparation of FOS with other β-fructofuranosidases [41].

It is worth noting that the maximum FOS concentration (18.9%) was significantly lower than the obtained with the soluble enzyme (29%) [42]. This fact might be related with the hydrophilic microenvironment of the PVA lenses, which could favour the hydrolysis in detriment of the transfructosylation. The effect of the microenvironment of the carrier on the transferase to hydrolysis ratio has been also reported in previous works [30,43–46]. In this context, the amount of blastose synthesized by the immobilized pXd-INV was higher than the reported with the recombinant soluble enzyme (30 g/L vs. 8 g/L), which is in accordance as it is obtained in a hydrolytic process.

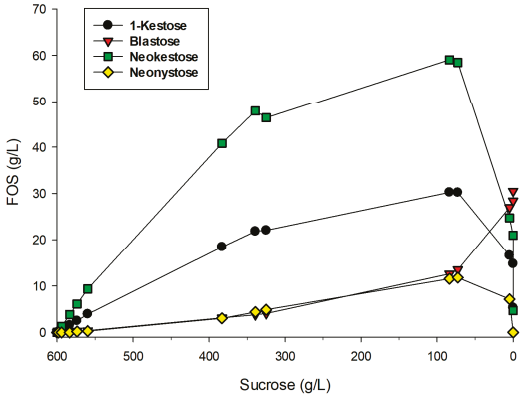

Figure 6. Kinetics of FOS formation with entrapped pXd-INV in PVA. Reaction conditions: 600 g/L sucrose, 100 mM sodium acetate buffer (pH 5.0), 30 °C.

2.5. Operational Stability of Immobilized pXd-INV for Neo-FOS Production

We performed seven cycles of 26 h at 30 °C using 600 g/L as substrate in a batch reactor. Between cycles, the lenses were thoroughly washed with the reaction buffer to remove any remaining sugars. The production of the different FOS is represented in Figure 7. Under the assayed conditions, the conversion of sucrose was approximately 23%, which implies that it was a bit far from the optimum FOS yield (Figure 6). However, the present study was very valuable to determine if these PVA biocatalysts could be reused for the industrial production of neo-FOS a. As shown in Figure 7, the concentration of the main reaction products was maintained nearly constant during the seven reaction cycles.

The excellent operational stability of the lens-shaped PVA biocatalysts seems to be related with the fact that the lenses apparently maintained their original shape during the study. The operational stability of immobilized enzymes for FOS synthesis has been studied by different groups [47]. Satisfactory results have been obtained, among other methods, by entrapment in alginate followed by a drying process [48], cross-linking in presence of chitosan [49], glutaraldehyde-activated chitosan [50] or adsorption onto niobium ore [51].

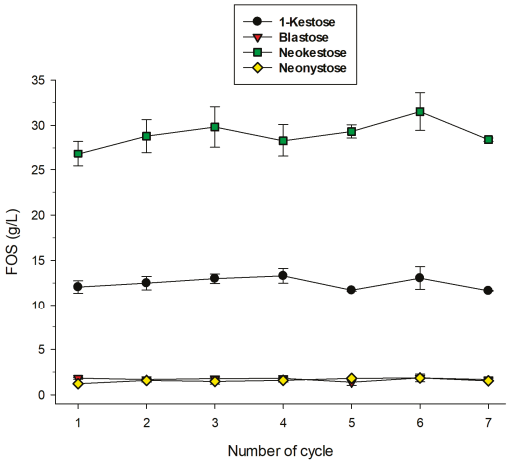

Figure 7. Operational stability of immobilized biocatalyst. Reaction conditions per cycle: 600 g/L sucrose in 100 mM sodium acetate buffer (pH 5.0), 26 h, 30 °C.

3. Materials and Methods

3.1. Materials

Sucrose was from Scharlau. Polyvinyl alcohol (PVA) (99% hydrolyzed, average MW 130,000) was purchased from Sigma Aldrich (Madrid, Spain). Fructose was from Merck and 1-kestose was from TCI. Neokestose, 6-kestose, neonystose and blastose were synthesized according to previous works [9,38,52]. All other reagents and solvents were of the highest purity available.

3.2. β-Fructofuranosidase Activity Source

The β-fructofuranosidase from *Xanthophyllomyces dendrorhous* ATCC MYA-131 (Xd-INV) was expressed in *Pichia pastoris* as previously reported [12]. Basically, the gene *Xd-INV* (GenBank accession no. FJ539193.2) fused to the *Saccharomyces cerevisiae* MFα secretion signal sequence was cloned in plasmid pIB4 (construction QDNS-pIB4) and included in *P. pastoris*. Transformants were grown in 50 mL of Buffered Minimal Glycerol (BMG), yeast nitrogen base w/o amino acids 1.34%, biotin 4 × 10^{-5}%, glycerol 1%, 50 mM potassium phosphate buffer, pH 6.0) during 24 h and then in 400 mL of Buffered Minimal Methanol (BMM) the same as BMG but containing 0.5% methanol instead of glycerol) for 35 h, giving approximately 21 U/mL of β-fructofuranosidase activity per mL of culture. The extracellular β-fructofuranosidase activity (pXd-INV) was purified by tangential concentration followed by DEAE-Sephacel chromatography. Active fractions were concentrated using Microcon YM-10 (Amicon) filters (0.7 mL; 4220 U/mL; 5.8 mg/mL) and stored at −70 °C.

3.3. Entrapment of β-Fructofuranosidase in PVA Lenses

The PVA solution (10% *w*/*v*) was prepared in 100 mM sodium acetate buffer (pH 5.0) at 90 °C under magnetic stirring for 45 min [53]. Enzyme entrapment was carried out at room temperature

by directly adding the enzyme to the PVA solution under magnetic stirring. Two different enzyme loadings were assayed (7.1 and 16.9 enzyme units per mL of PVA solution). The amount of enzyme was adjusted by diluting the enzyme stock solution (in 20 mM Tris-HCl pH 7.0) with 100 mM sodium acetate buffer (pH 5.0) and measuring the activity by the 3,5-dinitrosalicylic acid (DNS) assay. Lenses were produced by pumping the mixture through a syringe pump volume dispenser (NewERA model NE-300) into a 96-well microplate. Lenses were made by dripping 4 drops of the PVA solution in each well and then dried overnight at 50 °C. After that, lenses were hydrated in 100 mM sodium acetate buffer (pH 5.0) until constant weight. The average volume of each lens was calculated according to the total number of drops dispensed, the drops used for the production of each lens and the total volume of solution dispensed. Lens volume was determined using the following equation:

$$\textit{Lens volume } (\mu L) = (\textit{volume dispensed/number of drops dispensed}) \times \textit{number of drops in each lens}$$

3.4. Enzyme Activity Assay

β-Fructofuranosidase activity was determined by detection of reducing sugars with a modified 3,5-dinitrosalicylic acid (DNS) method adapted to a 96-well microplate scale [37]. The reaction mixture contained 45 μL of a 100 mg/mL sucrose solution in 100 mM sodium acetate buffer (pH 5.0) and 5 μL of a conveniently diluted enzyme solution. The reaction was incubated at 50 °C for 20 min, and then stopped by adding 50 μL of 3,5-dinitrosalicylic acid (DNS). The quantification of reducing sugars was carried out with a calibration curve of D-glucose, and one unit of activity (U) corresponded to the release of one μmol of reducing sugars per minute. The apparent activity of the immobilized biocatalysts was determined using a methodology developed in our group [36]. Basically, the lens-shaped PVA particles was incubated with 500 μL of 100 g/L sucrose solution in a micro-centrifuge filter tube (Spin-X®, 0.45 μm, Costar, Corning Inc., Corning, NY, USA) at the desired temperature for 60 min under vigorous agitation (900 rpm). The reaction mixture was separated from the biocatalyst by centrifugation at 2000× *g*. Inactivation of the possible lixiviated enzyme was carried out by adding 500 μL of 0.4 M sodium carbonate. Finally, reducing sugars were measured by the DNS assay as described above.

3.5. Microscale Assay for the Operational Stability of Immobilized pXd-INV

The operational stability of the immobilized biocatalysts was assayed following a previously described microscale assay [36]. One PVA lens was placed in a filtered micro-centrifuge tube (Spin-X®, 0.45 μm, Costar, Corning Inc., Corning, NY, USA) with 500 μL of a 100 mg/mL sucrose solution. Reactions were carried out at 50 °C and pH 5.0 for 20 min. Centrifugation was carried out at 2000× *g* to separate the lens from the reaction medium. The amount of reducing sugars was measured by the DNS method, as described before. The biocatalysts were washed three times with 100 mM sodium acetate buffer (pH 5.0) between cycles. Experiments were performed in triplicate to calculate the standard deviations.

3.6. Thermostability of the Immobilized PVA Particles

The thermostability of the lens-shaped PVA particles was analyzed by incubating the immobilized biocatalyst at different temperatures (4–60 °C) for 24 h in 100 mM sodium acetate buffer (pH 5.0). Residual activity was measured using the DNS assay under standard conditions (50 °C, pH 5.0). Experiments were performed in triplicate to calculate the standard deviations.

3.7. Analysis of Fructooligosacharides by HPAEC-PAD

The identification and quantification of FOS was carried out by High Performance Anion-Exchange Chromatography with Pulsed Amperometric Detection (HPAEC-PAD, Dionex ICS3000 system, Sunnyvale, CA, USA) and a CarboPack PA-1 column (4 × 250 mm) connected to a PA-1 guard column. The method was adapted from Campbell et al. [54]. Initial mobile phase was 100 mM NaOH at 1 mL/min and it was maintained for 8 min. Then, a gradient from 100

to 88% 100 mM NaOH and from 0 to 12% 100 mM NaOH/600 mM sodium acetate was performed in 22 min. These conditions were kept for 6 min and then the eluents concentration was changed to 50% 100 mM NaOH and 50% 100 mM NaOH/600 mM sodium acetate. Eluents were degassed by flushing with helium and peaks were analyzed using Chromeleon software.

3.8. Production of Fructooligosacharides by Immobilized pXd-INV

Lenses of immobilized pXd-INV were added to a 600 mg/mL sucrose solution in 100 mM sodium acetate buffer, pH 5.0, until reaching a final activity of 1 U/mL. The reaction mixture was incubated at 30 °C in an orbital stirrer, and aliquots (100 μL) were taken out at different times and inactivated with 0.4 M Na_2CO_3. The formation of the different FOS was analyzed by HPAEC-PAD.

3.9. Operational Stability of Immobilized pXd-INV for Neo-FOS Production

The operational stability of the immobilized biocatalysts was assayed following neo-FOS production. One lens-shaped PVA particle (0.3 U) was placed in a filtered micro-centrifuge tube (Spin-X®, 0.45 μm, Costar, Corning Inc, Corning, NY, USA) with 340 μL of a 600 mg/mL sucrose solution in 100 mM sodium acetate buffer (pH 5.0). The mixture was incubated at 30 °C for 26 h in a Thermoshaker (model TS-100, bioSan, Nebikon, Switzerland) at 900 rpm. The tube was then centrifuged at 2000× *g* for 2 min to separate the supernatant. To inactivate any possible lixiviated enzyme, the supernatant was diluted with 340 μL of 0.4 M sodium carbonate solution. Samples were diluted 1:500 before analyzing the FOS composition by HPAEC-PAD as described before. Experiments were performed in triplicate to calculate the standard deviations. Between cycles, the lens-shaped biocatalysts were washed three times with 100 mM sodium acetate buffer (pH 5.0) followed by centrifugation at 2000× *g* for 2 min.

4. Conclusions

The PVA-entrapped biocatalysts of pXd-INV displayed a notable recovery of activity and excellent operational stability at 30 °C during at least 180 h. These immobilized biocatalystscould be employed for the high-scale production of neo-FOS as well as for the fructosylation of different bioactive compounds.

Author Contributions: M.H.R. and F.J.P. conceived and designed the experiments; N.M. performed most of the experiments; D.F.-P. contributed operational stability of biocatalysts; F.V.C. contributed HPAEC-PAD analysis; M.G.-P. and M.F.-L. contributed preparation and characterization of pXd-INV; A.O.B. contributed discussion of results; F.J.P. wrote the paper.

Acknowledgments: This work was supported by grants from the Spanish Ministry of Economy, Industry and Competitiveness (Grants BIO2016-76601-C3-1-R and BIO2016-76601-C3-3-R). We thank the support of COST-Action CM1303 on Systems Biocatalysis. M.G.-P. thanks the Spanish Ministry of Education for FPU Grant. We acknowledge support of the publication fee by the CSIC Open Access Publication Support Initiative through its Unit of Information Resources for Research (URICI).

Conflicts of Interest: The authors declare no conflict of interest.

References

1. Plou, F.J.; Gómez de Segura, A.; Ballesteros, A. Application of glycosidases and transglycosidases for the synthesis of oligosaccharides. In *Industrial Enzymes: Structure, Function and Application*; Polaina, J., MacCabe, A.P., Eds.; Springer: New York, NY, USA, 2007; pp. 141–157.
2. Gibson, G.R.; Probert, H.M.; Van Loo, J.; Rastall, R.A.; Roberfroid, M.B. Dietary modulation of the human colonic microbiota: Updating the concept of prebiotics. *Nutr. Res. Rev.* **2004**, *17*, 259–275. [CrossRef] [PubMed]
3. Singh, S.P.; Jadaun, J.S.; Narnoliya, L.K.; Pandey, A. Prebiotic oligosaccharides: Special focus on fructooligosaccharides, its biosynthesis and bioactivity. *Appl. Biochem. Biotech.* **2017**, *183*, 613–635. [CrossRef] [PubMed]

4. Hidaka, H.; Eida, T.; Takizawa, T.; Tokunaga, T.; Tashiro, Y. Effects of fructooligosaccharides on intestinal flora and human health. *Bifidobact. Microflora* **1986**, *5*, 37–50. [CrossRef]
5. Cruz, R.; Cruz, V.D.; Belini, M.Z.; Belote, J.G.; Vieira, C.R. Production of fructooligosaccharides by the mycelia of *Aspergillus japonicus* immobilized in calcium alginate. *Biores. Technol.* **1998**, *65*, 139–143. [CrossRef]
6. Flores-Maltos, D.A.; Mussatto, S.I.; Contreras-Esquivel, J.C.; Rodríguez-Herrera, R.; Teixeira, J.A.; Aguilar, C.N. Biotechnological production and application of fructooligosaccharides. *Crit. Rev. Biotechnol.* **2016**, *36*, 259–267. [CrossRef] [PubMed]
7. Kilian, S.; Kritzinger, S.; Rycroft, C.; Gibson, G.; du Preez, J. The effects of the novel bifidogenic trisaccharide, neokestose, on the human colonic microbiota. *World J. Microb. Biot.* **2002**, *18*, 637–644. [CrossRef]
8. Lim, J.S.; Lee, J.H.; Kang, S.W.; Park, S.W.; Kim, S.W. Studies on production and physical properties of neo-FOS produced by co-immobilized *Penicillium citrinum* and neo-fructosyltransferase. *Eur. Food Res. Technol.* **2007**, *225*, 457–462. [CrossRef]
9. Linde, D.; Macias, I.; Fernández-Arrojo, L.; Plou, F.J.; Jiménez, A.; Fernández-Lobato, M. Molecular and biochemical characterization of a β-fructofuranosidase from *Xanthophyllomyces dendrorhous*. *Appl. Environ. Microbiol.* **2009**, *75*, 1065–1073. [CrossRef] [PubMed]
10. Ramirez-Escudero, M.; Gimeno-Perez, M.; Gonzalez, B.; Linde, D.; Merzdo, Z.; Fernandez-Lobato, M.; Sanz-Aparicio, J. Structural analysis of β-fructofuranosidase from *Xanthophyllomyces dendrorhous* reveals unique features and the crucial role of n-glycosylation in oligomerization and activity. *J. Biol. Chem.* **2016**, *291*, 6843–6857. [CrossRef] [PubMed]
11. Linde, D.; Rodríguez-Colinas, B.; Estévez, M.; Poveda, A.; Plou, F.J.; Fernández Lobato, M. Analysis of neofructooligosaccharides production mediated by the extracellular β-fructofuranosidase from *Xanthophyllomyces dendrorhous*. *Biores. Technol.* **2012**, *109*, 123–130. [CrossRef] [PubMed]
12. Gimeno-Pérez, M.; Linde, D.; Fernández-Arrojo, L.; Plou, F.J.; Fernández-Lobato, M. Heterologous overproduction of β-fructofuranosidase from yeast *Xanthophyllomyces dendrorhous*, an enzyme producing prebiotic sugars. *Appl. Microbiol. Biotechnol.* **2015**, *99*, 3459–3467. [CrossRef] [PubMed]
13. Gimeno-Perez, M.; Santos-Moriano, P.; Fernandez-Arrojo, L.; Poveda, A.; Jimenez-Barbero, J.; Ballesteros, A.O.; Fernandez-Lobato, M.; Plou, F.J. Regioselective synthesis of neo-erlose by the β-fructofuranosidase from *Xanthophyllomyces dendrorhous*. *Process Biochem.* **2014**, *49*, 423–429. [CrossRef]
14. Madhavan, A.; Sindhu, R.; Binod, P.; Sukumaran, R.K.; Pandey, A. Strategies for design of improved biocatalysts for industrial applications. *Biores. Technol.* **2017**, *245*, 1304–1313. [CrossRef] [PubMed]
15. Sheldon, R.A. Enzyme immobilization: The quest for optimum performance. *Adv. Synth. Catal.* **2007**, *349*, 1289–1307. [CrossRef]
16. Torres-Salas, P.; Del Monte-Martinez, A.; Cutiño-Avila, B.; Rodriguez-Colinas, B.; Alcalde, M.; Ballesteros, A.O.; Plou, F.J. Immobilized biocatalysts: Novel approaches and tools for binding enzymes to supports. *Adv. Mater.* **2011**, *23*, 5275–5282. [CrossRef] [PubMed]
17. Torres, P.; Reyes-Duarte, D.; Lopez-Cortes, N.; Ferrer, M.; Ballesteros, A.; Plou, F.J. Acetylation of vitamin E by *Candida antarctica* lipase B immobilized on different carriers. *Process Biochem.* **2008**, *43*, 145–153. [CrossRef]
18. Datta, S.; Christena, L.R.; Rajaram, Y.R.S. Enzyme immobilization: An overview on techniques and support materials. *3 Biotech* **2013**, *3*, 1–9. [CrossRef] [PubMed]
19. Santos-Moriano, P.; Monsalve-Ledesma, L.; Ortega-Munoz, M.; Fernandez-Arrojo, L.; Ballesteros, A.O.; Santoyo-Gonzalez, F.; Plou, F.J. Vinyl sulfone-activated silica for efficient covalent immobilization of alkaline unstable enzymes: Application to levansucrase for fructooligosaccharide synthesis. *RSC Adv.* **2016**, *6*, 64175–64181. [CrossRef]
20. Santos-Moriano, P.; Woodley, J.M.; Plou, F.J. Continuous production of chitooligosaccharides by an immobilized enzyme in a dual-reactor system. *J. Mol. Catal. B Enzym.* **2016**, *133*, 211–217. [CrossRef]
21. Kahar, U.M.; Sani, M.H.; Chan, K.G.; Goh, K.M. Immobilization of α-amylase from *Anoxybacillus* sp. SK3-4 on ReliZyme and Immobead supports. *Molecules* **2016**, *21*, 1196. [CrossRef] [PubMed]
22. Carević, M.; Ćorović, M.; Mihailović, M.; Banjanac, K.; Milisavljević, A.; Veličković, D.; Bezbradica, D. Galacto-oligosaccharide synthesis using chemically modified β-galactosidase from *Aspergillus oryzae* immobilised onto macroporous amino resin. *Int. Dairy J.* **2016**, *54*, 50–57. [CrossRef]
23. Gomez de Segura, A.; Alcalde, M.; Bernabe, M.; Ballesteros, A.; Plou, F.J. Synthesis of methyl α-D-glucooligosaccharides by entrapped dextransucrase from *Leuconostoc mesenteroides* B-1299. *J. Biotechnol.* **2006**, *124*, 439–445. [CrossRef] [PubMed]

24. Alcalde, M.; Plou, F.J.; de Segura, A.G.; Remaud-Simeon, M.; Willemot, R.M.; Monsan, P.; Ballesteros, A. Immobilization of native and dextran-free dextransucrases from *Leuconostoc mesenteroides* NRRL B-512F for the synthesis of glucooligosaccharides. *Biotechnol. Tech.* **1999**, *13*, 749–755. [CrossRef]
25. Gadea, J.L.; Cesteros, L.C.; Katime, I. Chemical-physical behavior of hydrogels of poly(vinyl alcohol) and poly(ethylene glycol). *Eur. Polym. J.* **2013**, *49*, 3582–3589. [CrossRef]
26. Nuneslentik, M.A.P.; Gois, P.M.P.; Rosa, M.E.; Martins, S.; Fernandes, P.C.B.; Ribeiro, M.H.L. Boronic acids as efficient cross linkers for PVA: Synthesis and application of tunable hollow microspheres in biocatalysis. *Tetrahedron* **2016**, *72*, 7293–7305.
27. Durieux, A.; Nicolay, X.; Simon, J.P. Continuous malolactic fermentation by *Oenococcus oeni* entrapped in LentiKats. *Biotechnol. Lett.* **2000**, *22*, 1679–1684. [CrossRef]
28. Schlieker, M.; Vorlop, K.-D. A novel immobilization method for entrapment: LentiKats. In *Immobilization of Enzymes and Cells*; Guisan, J.M., Ed.; Springer: Heidelberg, Germany, 2006; pp. 333–343.
29. Ariga, O.; Kubo, T.; Sano, Y. Effective diffusivity of glucose in PVA hydrogel. *J. Ferment. Bioeng.* **1994**, *78*, 200–201. [CrossRef]
30. Gómez de Segura, A.; Alcalde, M.; Plou, F.J.; Remaud-Simeon, M.; Monsan, P.; Ballesteros, A. Encapsulation in LentiKats of dextransucrase from *Leuconostoc mesenteroides* NRRL B-1299, and its effect on product selectivity. *Biocatal. Biotransform.* **2003**, *21*, 325–331. [CrossRef]
31. Imai, K.; Shiomi, T.; Uchida, K.; Miya, M. Immobilization of enzyme into poly(vinyl alcohol) membrane. *Biotechnol. Bioeng.* **1986**, *28*, 1721–1726. [CrossRef] [PubMed]
32. Nunes, M.A.P.; Rosa, M.E.; Fernandes, P.C.B.; Ribeiro, M.H.L. Operational stability of naringinase PVA lens-shaped microparticles in batch stirred reactors and mini packed bed reactors-one step closer to industry. *Biores. Technol.* **2014**, *164*, 362–370. [CrossRef] [PubMed]
33. Lozinsky, V.I.; Plieva, F.M. Poly(vinyl alcohol) cryogels employed as matrices for cell immobilization. 3. Overview of recent research and developments. *Enzyme Microb. Tech.* **1998**, *23*, 227–242. [CrossRef]
34. Luo, M.; Wang, W.; Zhao, Q.; Li, M.; Chen, Y.; Lu, Z.; Liu, K.; Wang, D. Chemiluminescence biosensor for hydrogen peroxide determination by immobilizing horseradish peroxidase onto PVA-CO-PE nanofiber membrane. *Eur. Polym. J.* **2017**, *91*, 307–314. [CrossRef]
35. Cao, Y.; Liu, F.; Chen, Y.; Yu, T.; Lou, D.; Guo, Y.; Li, P.; Wang, Z.; Ran, H. Drug release from core-shell PVA/silk fibroin nanoparticles fabricated by one-step electrospraying. *Sci. Rep.* **2017**, *7*, 11913. [CrossRef] [PubMed]
36. Fernandez-Arrojo, L.; Santos-Moriano, P.; Rodriguez-Colinas, B.; Ballesteros, A.O.; Plou, F.J. Micro-scale procedure for enzyme immobilization screening and operational stability assays. *Biotechnol. Lett.* **2015**, *37*, 1593–1600. [CrossRef] [PubMed]
37. Ghazi, I.; Fernandez-Arrojo, L.; Garcia-Arellano, H.; Ferrer, M.; Ballesteros, A.; Plou, F.J. Purification and kinetic characterization of a fructosyltransferase from *Aspergillus aculeatus*. *J. Biotechnol.* **2007**, *128*, 204–211. [CrossRef] [PubMed]
38. Zambelli, P.; Fernandez-Arrojo, L.; Romano, D.; Santos-Moriano, P.; Gimeno-Perez, M.; Poveda, A.; Gandolfi, R.; Fernandez-Lobato, M.; Molinari, F.; Plou, F.J. Production of fructooligosaccharides by mycelium-bound transfructosylation activity present in *Cladosporium cladosporioides* and *Penicilium sizovae*. *Process Biochem.* **2014**, *49*, 2174–2180. [CrossRef]
39. Alves, M.H.; Jensen, B.E.B.; Smith, A.A.A.; Zelikin, A.N. Poly(vinyl alcohol) physical hydrogels: New vista on a long serving biomaterial. *Macromol. Biosci.* **2011**, *11*, 1293–1313. [CrossRef] [PubMed]
40. Rescignano, N.; Fortunati, E.; Montesano, S.; Emiliani, C.; Kenny, J.M.; Martino, S.; Armentano, I. PVA bio-nanocomposites: A new take-off using cellulose nanocrystals and PLGA nanoparticles. *Carbohydr. Polym.* **2014**, *99*, 47–58. [CrossRef] [PubMed]
41. Gutierrez-Alonso, P.; Fernandez-Arrojo, L.; Plou, F.J.; Fernandez-Lobato, M. Biochemical characterization of a β-fructofuranosidase from *Rhodotorula dairenensis* with transfructosylating activity. *FEMS Yeast Res.* **2009**, *9*, 768–773. [CrossRef] [PubMed]
42. Gutierrez-Alonso, P.; Gimeno-Perez, M.; Ramirez-Escudero, M.; Plou, F.J.; Sanz-Aparicio, J.; Fernandez-Lobato, M. Molecular characterization and heterologous expression of a *Xanthophyllomyces dendrorhous* α-glucosidase with potential for prebiotics production. *Appl. Microbiol. Biot.* **2016**, *100*, 3125–3135. [CrossRef] [PubMed]

43. Ghazi, I.; de Segura, A.G.; Fernandez-Arrojo, L.; Alcalde, M.; Yates, M.; Rojas-Cervantes, M.L.; Plou, F.J.; Ballesteros, A. Immobilisation of fructosyltransferase from *Aspergillus aculeatus* on epoxy-activated Sepabeads EC for the synthesis of fructo-oligosaccharides. *J. Mol. Catal. B Enzym.* **2005**, *35*, 19–27. [CrossRef]
44. Rodrigues, R.C.; Ortiz, C.; Berenguer-Murcia, A.; Torres, R.; Fernández-Lafuente, R. Modifying enzyme activity and selectivity by immobilization. *Chem. Soc. Rev.* **2013**, *42*, 6290–6307. [CrossRef] [PubMed]
45. Hill, A.; Karboune, S.; Mateo, C. Immobilization and stabilization of levansucrase biocatalyst of high interest for the production of fructooligosaccharides and levan. *J. Chem. Technol. Biot.* **2016**, *91*, 2440–2448. [CrossRef]
46. Palomo, J.M. Modulation of enzymes selectivity via immobilization. *Curr. Org. Synth.* **2009**, *6*, 1–14. [CrossRef]
47. Plou, F.J.; Fernandez-Arrojo, L.; Santos-Moriano, P.; Ballesteros, A.O. Application of immobilized enzymes for the synthesis of bioactive fructooligosaccharides. In *Food Oligosaccharides: Production, Analysis and Bioactivity*; Moreno, F.J., Sanz, M.L., Eds.; Wiley Blackwell: Hoboken, NJ, USA, 2014; pp. 200–216.
48. Fernandez-Arrojo, L.; Rodriguez-Colinas, B.; Gutierrez-Alonso, P.; Fernandez-Lobato, M.; Alcalde, M.; Ballesteros, A.O.; Plou, F.J. Dried alginate-entrapped enzymes (DALGEEs) and their application to the production of fructooligosaccharides. *Process Biochem.* **2013**, *48*, 677–682. [CrossRef]
49. Mouelhi, R.; Abidi, F.; Marzouki, M.N. An improved method for the production of fructooligosaccharides by immobilized β-fructofuranosidase from *Sclerotinia sclerotiorum*. *Biotechnol. Appl. Biochem.* **2016**, *63*, 281–291. [CrossRef] [PubMed]
50. Lorenzoni, A.S.G.; Aydos, L.F.; Klein, M.P.; Rodrigues, R.C.; Hertz, P.F. Fructooligosaccharides synthesis by highly stable immobilized β-fructofuranosidase from *Aspergillus aculeatus*. *Carbohydr. Polym.* **2014**, *103*, 193–197. [CrossRef] [PubMed]
51. Aguiar-Oliveira, E.; Maugeri, F. Characterization of the immobilized fructosyltranferase from *Rhodotorula* sp. *Int. J. Food Eng.* **2010**, *6*. [CrossRef]
52. Alvaro-Benito, M.; de Abreu, M.; Fernandez-Arrojo, L.; Plou, F.J.; Jimenez-Barbero, J.; Ballesteros, A.; Polaina, J.; Fernandez-Lobato, M. Characterization of a β-fructofuranosidase from *Schwanniomyces occidentalis* with transfructosylating activity yielding the prebiotic 6-kestose. *J. Biotechnol.* **2007**, *132*, 75–81. [CrossRef] [PubMed]
53. Nunes, M.A.P.; Vila-Real, H.; Fernandes, P.C.B.; Ribeiro, M.H.L. Immobilization of naringinase in PVA-alginate matrix using an innovative technique. *Appl. Biochem. Biotech.* **2010**, *160*, 2129–2147. [CrossRef] [PubMed]
54. Campbell, J.M.; Bauer, L.L.; Fahey, G.C.; Hogarth, A.J.C.L.; Wolf, B.W.; Hunter, D.E. Selected fructooligosaccharide (1-kestose, nystose, and 1F-β-fructofuranosylnystose) composition of foods and feeds. *J. Agric. Food Chem.* **1997**, *45*, 3076–3082. [CrossRef]

© 2018 by the authors. Licensee MDPI, Basel, Switzerland. This article is an open access article distributed under the terms and conditions of the Creative Commons Attribution (CC BY) license (http://creativecommons.org/licenses/by/4.0/).

catalysts

MDPI

Article

Immobilization/Stabilization of Ficin Extract on Glutaraldehyde-Activated Agarose Beads. Variables That Control the Final Stability and Activity in Protein Hydrolyses

El-Hocine Siar [1,2,†], Sara Arana-Peña [1,†], Oveimar Barbosa [3], Mohammed Nasreddine Zidoune [2] and Roberto Fernandez-Lafuente [1,*]

1 Departamento de Biocatálisis, Instituto de Catálisis-CSIC, Campus UAM-CSIC, 28049 Madrid, Spain; hocines1@hotmail.fr (E.-H.S.); sara_arana@hotmail.com (S.A.-P.)
2 Equipe TEPA, Laboratoire LNTA, INATAA, Université des Frères Mentouri Constantine 1, 25000 Constantine, Algeria; zidounem@yahoo.fr
3 Departamento de Química, Facultad de Ciencias, Universidad del Tolima, 730006299 Ibagué, Colombia; oveimar@gmail.com
* Correspondence: rfl@icp.csic.es; Tel.: +34-915-854-941
† Both authors have evenly contributed to this paper.

Received: 12 March 2018; Accepted: 2 April 2018; Published: 6 April 2018

Abstract: Ficin extract has been immobilized on different 4% aminated-agarose beads. Using just ion exchange, immobilization yield was poor and expressed activity did not surpass 10% of the offered enzyme, with no significant effects on enzyme stability. The treatment with glutaraldehyde of this ionically exchanged enzyme produced an almost full enzyme inactivation. Using aminated supports activated with glutaraldehyde, immobilization was optimal at pH 7 (at pH 5 immobilization yield was 80%, while at pH 9, the immobilized enzyme became inactivated). At pH 7, full immobilization was accomplished maintaining 40% activity versus a small synthetic substrate and 30% versus casein. Ficin stabilization upon immobilization could be observed but it depended on the inactivation pH and the substrate employed, suggesting the complexity of the mechanism of inactivation of the immobilized enzyme. The maximum enzyme loading on the support was determined to be around 70 mg/g. The loading has no significant effect on the enzyme stability or enzyme activity using the synthetic substrate but it had a significant effect on the activity using casein; the biocatalysts activity greatly decreased using more than 30 mg/g, suggesting that the near presence of other immobilized enzyme molecules may generate some steric hindrances for the casein hydrolysis.

Keywords: immobilization using glutaraldehyde; versatility of glutaraldehyde; steric problems in enzyme activity; effect of loading on enzyme activity

1. Introduction

Proteases are among the first enzymes used by humans in biotechnological food processing [1,2]. Nowadays, proteases are used in many different areas, for example in the production of active peptides from inexpensive proteins, to improve the organoleptic or functional properties of foods [3], although perhaps its main use is as detergent components [4–7]. In some instances, a chemical alternative exists [8] but proteases have clear advantages, as the process will be more specific, avoiding the production of by-products or destruction of some amino acids [9]. Among the most used proteases of vegetal origin, the latex of the fig tree (based in ficin) should be mentioned. It has been employed in the brewing [9], pharmaceutical [10] and in cheese making [11,12] industries. It has also been used for bioactive peptides production [13,14] and meat tenderization [15,16]. Ficin is considered to give

a more reproducible hydrolysis map and it has been employed in the generation of antibodies via specific hydrolysis of some peptide bonds, [17–19]. Four isoforms of ficin have been described (A, B, C and D) and crystallized, resolving their structure [20,21]. Ficin isoforms are glycoproteins and present a high sequence similarity with bromelaine [22].

The immobilization of an enzyme may facilitate enzyme reuse and that way, the economic feasibility of the process [23–26]. Moreover, immobilization may be used to improve other enzyme limitations, like stability, activity, resistance to chemicals or inhibitors, even purity [27–29]. In the case of proteases to be used in protein hydrolysis, there are specific problems that must be considered: the enzyme must have the active centre properly oriented; otherwise the enzyme will be inactive [1]. Only when the active centre is fully oriented to the medium, the protease will be active under any loading; if the active centre is not "perfectly" oriented, the fully loaded biocatalyst may become fully inactive versus proteins larger than the immobilized protease molecule [30]. This steric problem will be coupled to the standard diffusional limitations, even if the active centre is fully intact [31] or a non-porous nanoparticle is utilized [32]. However, due to the multiple uses of proteases, this should not discard the biocatalysts for other uses, for example synthesis of peptide bonds [33–35]. Ficin has been immobilized in just some few examples [36–40].

In this sense, immobilization of ficin using the glutaraldehyde chemistry may benefit from the versatility of the system [41]. In most cases, glutaraldehyde is used to activate supports containing primary amino groups. This way, the glutaraldehyde activated support becomes a heterofunctional one, with the range of opportunities that this may open. Thus, the enzyme may be directly immobilized at high ionic strength via a covalent reaction using glutaraldehyde pre-activated supports, or may be first ionically exchanged [42–44]. That way, using a support with the amino groups modified with glutaraldehyde, the enzymes may be ionically exchanged at low ionic strength and later a covalent reaction between the immobilized enzyme molecules and the nearby glutaraldehyde groups may take place, or using high ionic strength, the ionic adsorption will be prevented, forcing the covalent attachment as first event of the immobilization. Using just the aminated support, the ionic exchange will permit to immobilize the enzyme, later the treatment with glutaraldehyde may permit to establish support-enzyme bonds. In this case, together with enzyme-support reactions, modification of the overall enzyme surface occurs (one point modification, inter or intramolecular crosslinking) and this may have positive, negative or neutral effects on enzyme performance [41]. The possibilities of altering the enzyme orientation regarding the support surface and that way, of increasing the possibility of yielding immobilized enzyme preparations with different properties, may be enlarged considering that the conditions where the ion exchange is performed, for example the pH value, may also alter the orientation of the enzyme regarding the support surface [45–47].

Previously, our research group has immobilized ficin extract in glyoxyl activated support, focused only on the stability of lowly loaded enzyme immobilized preparations [40]. In this new research effort, ficin extract has been immobilized on amino and amino glutaraldehyde agarose beads, trying to explore the versatility of glutaraldehyde to get a biocatalyst with high activity and stability. In this new paper, the effect of the protein loading on enzyme activity versus small synthetic substrate (benzoyl-arginine-*p*-nitroanilide (BANA)) and large casein was analysed [1,30,31], as well as the likely effects on enzyme stability, as the loading may affect the distance between different immobilized enzyme molecules and that, in turn, enzyme stability [48,49].

2. Results and Discussion

2.1. Immobilization of Ficin Extract in MANAE-Agarose

Figure 1 shows the immobilization courses at pH 5, 7 and 9 of ficin on aminated supports. Immobilization was very slow at all studied pH values, with a significant decrease in enzyme activity, although the free enzyme maintained full activity. Yields were higher at pH 9 than at pH 5 or 7, although expressed activity (the observed activity of the immobilized enzyme compared to the expected one

from the immobilization yields data) was always very low (just near to 10%). To check of the yield was determined by the full loading of the support, the supernatant was used in a new immobilization cycle (at pH 7) and a similar immobilization yield was observed (results not shown). This suggest that the yield was not caused by the overloading of the support or by the presence of some enzyme isoforms that cannot be immobilized on the support, suggesting that was due to some kind of adsorption equilibrium. The activity was determined with casein and the small synthetic substrate (BANA), with scarce differences. These facts suggested two contradictory ideas: the ion exchange was so mild that it was unable to fully adsorb the enzyme but the immobilization produces very negative effects on enzyme structure that yielded a decrease versus small and large substrates. Figures 2–5 show the distribution of anionic and main cationic residues on the 4 isoforms of ficin component. In most cases, there is not an area clearly richer in anionic residues than in cationic ones; this may explain why immobilization via ionic exchange is so slow and ineffective. However, in all sides of the proteins there are some Lys groups that could give at least one covalent attachment after ion exchange if treated with glutaraldehyde.

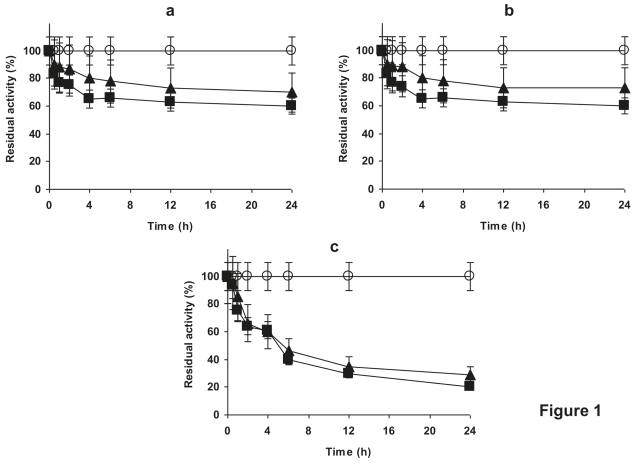

Figure 1. Immobilization of ficin extract on MANAE-agarose beads at pH 5 (**a**), 7 (**b**) or 9 (**c**). Immobilization was performed as described in methods. Activity was followed using BANA as substrate. Circles: reference; Triangles: suspension, Squares: supernatant.

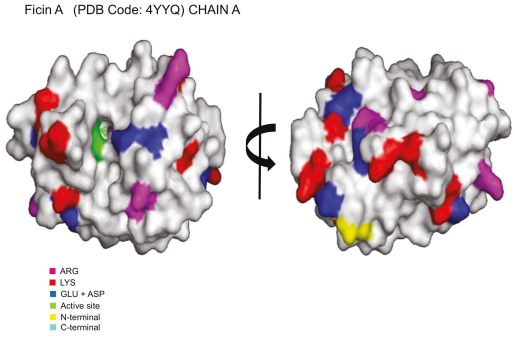

Figure 2. 3D surface structure model of Ficin A obtained from the Protein Data Bank (PDB) and displayed using PyMol versus 0.99. Arg, Lys, Glu+Asp, -NH_2 terminal and -COOH terminal residues are indicated.

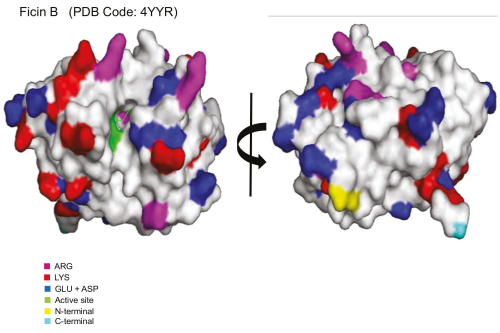

Figure 3. 3D surface structure model of Ficin B obtained from the PDB and displayed using PyMol versus 0.99. Arg, Lys, Glu+Asp, -NH_2 terminal and -COOH terminal residues are indicated.

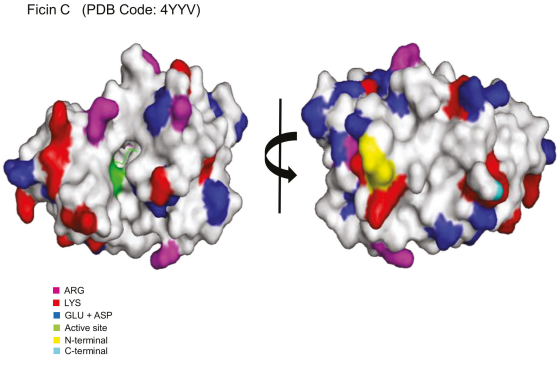

Figure 4. 3D surface structure model of Ficin C obtained from the PDB and displayed using PyMol versus 0.99. Arg, Lys, Glu+Asp, -NH_2 terminal and -COOH terminal residues are indicated.

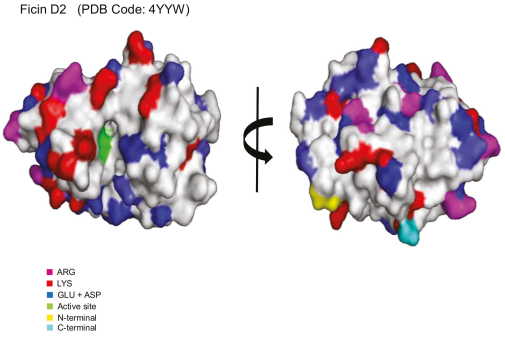

Figure 5. 3D surface structure model of Ficin D_2 obtained from the PDB and displayed using PyMol versus 0.99. Arg, Lys, Glu+Asp, -NH_2 terminal and -COOH terminal residues are indicated.

Figure 6 shows the inactivation of the ionically exchanged proteins at pH 7 when inactivated at pH 5, pH 7 and pH 9. A slight stabilization may be found at pH 5 and 9, while a slight destabilization may be found at pH 7. These differences may be based in the way the free enzyme is inactivated. The free enzyme may suffer enzyme autolysis, that way reducing the enzyme stability/activity.

Moreover, the free enzyme may experience protein aggregation (mainly near to the isoelectric point). These two inactivations are not possible using an immobilized enzyme form [30]. In fact, under conditions where aggregation is quite unlikely, stability of the enzyme decreased after immobilization. This may be caused by undesired enzyme-support interactions where inactivation that can stabilize incorrect enzyme structures [29,50,51].

These results were not very positive and anion exchange was discarded as a likely one to immobilize ficin.

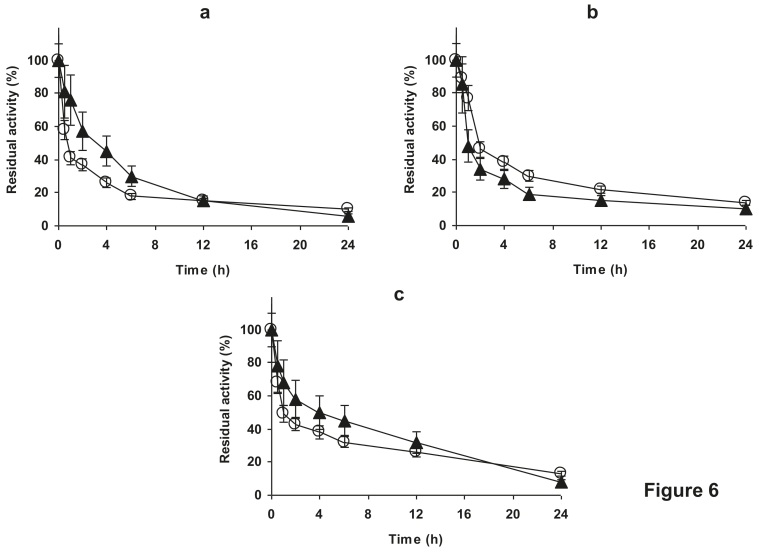

Figure 6. Inactivation courses of the ionically exchanged ficin extract on MANAE-agarose beads at pH 7. The inactivation studies were performed as indicated in Methods section at pH 5, (**a**), 7 (**b**) or 9 (**c**) at 55 °C, using BANA as substrate. Circles: Free enzyme. Triangles: immobilized enzyme.

2.2. Modification of the Ionically Exchanged Enzyme with Glutaraldehyde

In a trial to improve the stability of the ionically exchanged enzyme, the immobilized enzyme was treated with glutaraldehyde, even although the expressed activity of this preparation was already quite low. When the ionically exchanged enzyme was modified with glutaraldehyde, most of the remaining activity was lost, making unsuitable this strategy to improve the enzyme stability.

To check if the problem was a consequence of a too intense support-enzyme reaction or the chemical modification of the enzymes with glutaraldehyde, the enzyme immobilized on glyoxyl agarose was modified with glutaraldehyde under the conditions used to modify the adsorbed enzyme. Figure 7 shows how the modification of the glyoxyl-ficin biocatalyst with glutaraldehyde produces some enzyme inactivation, suggesting that the direct modification of the enzyme with this chemical reagent could be partially responsible of the enzyme inactivation. As this preparation was more stable than the free enzyme [40], it may be expected that the enzyme may be also more stable versus chemical modification [52]. However, using the aminated support the residual activity was under 10% after 1 h (Figure 7), suggesting that an inactivation caused by the activated support and enzyme reaction cannot be discarded.

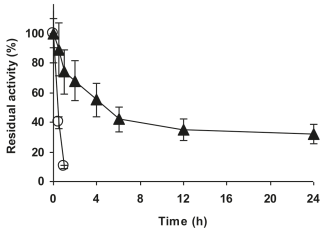

Figure 7. Modification of glyoxyl (triangles) or MANAE agarose (circles) immobilized ficin extract when incubated in 1% glutaraldehyde at pH 7. Experiments were performed as described in Methods using BANA as substrate.

2.3. Immobilization of the Enzyme in Glutaraldehyde Pre-Activated MANAE Agarose Beads

Figure 8 shows the immobilization course at pH 5, 7 and 9 of ficin extract on glutaraldehyde pre-activated agarose beads. At pH 5 immobilization yield was 80% after 24 h and only 20% of the initial activity was present in the immobilized biocatalyst. Thus, this preparation was discarded. At pH 9 the enzyme was almost fully immobilized after 6 h but the enzyme was almost fully inactivated (16% after 24 h). That way, this preparation was also discarded. However, when the enzyme was immobilized at pH 7, full immobilization was obtained after 4 h and the expressed activity was around 40% versus BANA. When the activity was followed versus casein, initially both lines were almost identical, suggesting that immobilized ficin molecules had no reduced accessibility to the casein substrate (that is, the active centre is not oriented towards the support surface). When 24 h of enzyme-support interaction were permitted, the activity versus casein was a 25% lower than versus BANA (about 40% versus about 30%), suggesting that the changes of the enzyme structure during support-enzyme interactions may affect more to the activity versus casein that versus BANA.

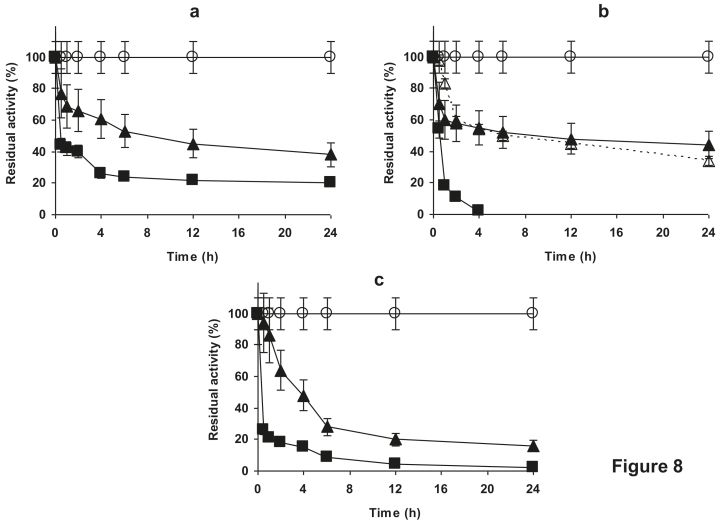

Figure 8. Immobilization of ficin extract on MANAE-agarose beads activated with glutaraldehyde. Experiments were performed as described in the Section 3 using 25 mM of buffer, at pH 5 (**a**), 7 (**b**) or 9 (**c**). Open circles, solid lines: reference; Using BANA as substrate (solid lines, solid symbols): Triangles: suspension, Squares: supernatant. Using casein as substrate (only at pH 7): dotted line, empty triangles.

Many reports stated that covalent glutaraldehyde immobilization is so slow that, if ion exchange was permitted, immobilization proceeded via a first ion exchange, followed by the covalent reaction. Figure 9 shows the immobilization of ficin extract at pH 7 and 200 mM sodium phosphate, where ion exchange was prevented. The immobilization course is pretty similar to the use of 25 mM, suggesting that in both cases the immobilization mainly proceeded via a first covalent attachment. After 4 h, the enzyme could not be desorbed from the support by incubating the biocatalysts in 500 mM NaCl. We analysed the results obtained when immobilizing at pH from 6.5 to 8.5 and the results in terms of activity and stability were optimal at pH 7–8, with a slight advantage at pH 7 (results not shown). Thus, pH 7 was selected as optimal pH for the enzyme immobilization on this support.

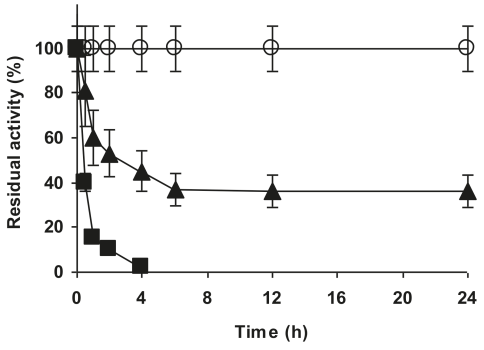

Figure 9. Immobilization of ficin extract on MANAE-agarose beads activated with glutaraldehyde at pH 7 and 200 mM sodium phosphate using BANA as substrate. Experiments were performed as described in Methods, using BANA as substrate. Circles: reference; Triangles: suspension, Squares: supernatant.

2.4. Stability of the Enzyme Immobilized at pH 7 on Glutaraldehyde Pre-Activated MANAE Agarose Beads

The enzyme immobilized at pH 7 at low and high ionic strength presented a very similar behaviour, thus we have just shown the results obtained with the enzyme immobilized at 25 mM sodium phosphate. Figure 10 shows the inactivation courses at pH 5, 7 and 9, of the free and immobilized enzymes, followed with BANA and casein hydrolyses. Results suggested that a certain stabilization has been achieved using this support but stabilization was clearer at pH 7 than at pH 5 or 9. These differences in stabilization may be due to different interactions of the enzyme and the support—as the support remained as an ion exchanger—or to the fact the enzyme may follow different pathways in the inactivations, that way the immobilization by a specific area may affect enzyme stability in different ways [53]. Using BANA, the immobilized enzyme always seemed to be slightly more stable than when using casein, suggesting that the activity versus the casein is lost before the activity versus BANA. This was more evident at pH 7 than at the other pH values. The situation was not so evident using the free enzyme, where inactivations were very similar with both substrates at pH 5, while at pH 7 and 9 higher stability using casein as substrate was observed. In fact, stabilization at pH 5 and 7 caused by the enzyme immobilization was smaller using casein as substrate than using BANA. This finding may be related to different changes on the enzyme structure that may affect more significantly to the hydrolysis of one substrate or other one.

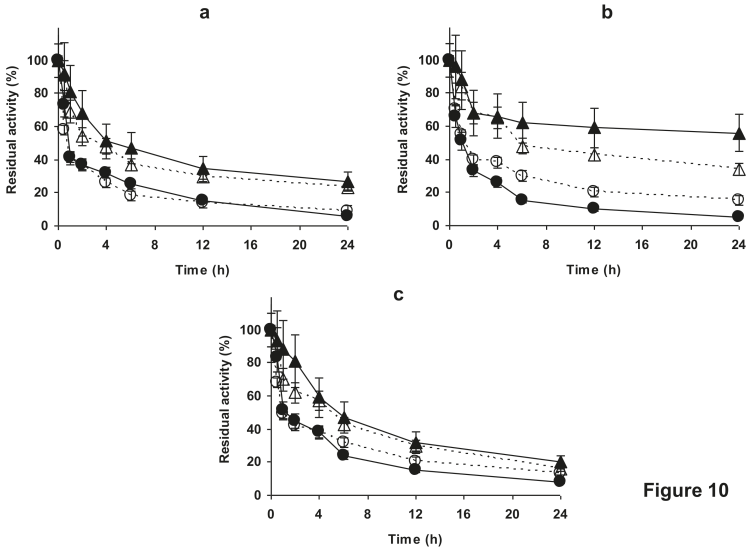

Figure 10. Inactivation of ficin immobilized at pH 7 using 25 mM sodium phosphate. Experiments were performed as described in Section 3, at pH 5 (**a**), 7 (**b**) or 9 (**c**) and 55 °C. Solid lines and solid circles: inactivation was followed using BANA, Dotted line and empty symbols: inactivation was followed with casein. Circles: free enzyme; Triangles: immobilized enzyme.

2.5. Determination of Loading Capacity

Figure 11 shows the immobilization yields when the amount of enzyme was increased using BANA and casein. From these experiments, maximum loading was established in the range 68–72 mg ficin/g of support. Expressed activity per mg of enzyme versus the small synthetic substrate was slightly lower when using higher enzyme loadings, although the values were pretty similar. The small differences may be attributed to an increment of the diffusion limitations.

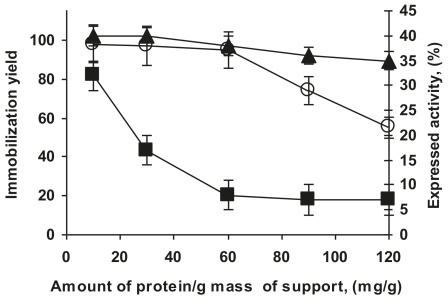

Figure 11. Immobilization yield and expressed activity when growing the amount of offered ficin extract per g of MANAE activate with glutaraldehyde support. Experiments were carried out as described in Methods section. Triangles: immobilization yield; Circles: expressed activity versus BANA, Squares: expressed activity versus casein.

One critical point using proteases to hydrolyse proteins, as stated in the introduction, is that the loading of the support with the enzyme may generate some steric hindrances that prevent the accessibility of the large substrate to the enzyme if the orientation is not perfect towards the reaction medium [1]. Figure 11 shows that using casein the specific activity of the immobilized ficin

extract rapidly decreased with increasing loading, going from slightly more than 30% of the activity immobilized at 10 mg/g to around 15% using 30 mg/g and only 7–8% using maximum loading or overloading. In fact, the observed activity per gram of biocatalyst was maximal using 30 mg/g, using higher enzyme loading the biocatalyst mass activity decreased by 30–35%. This suggested that the enzyme active centre was not perfectly looking toward the opposite side of the support surface and that way the nearby enzyme molecules may cause steric hindrances to the entry of the large substrate casein when the support was fully loaded. However, this limitation only affected the use of the biocatalyst in the hydrolysis of proteins, not in the other applications that the enzyme may have and that involve small substrates (see Section 1).

Another point that may have interest was to determine if the loading may somehow affect the immobilized ficin enzyme molecule stability. If the immobilization rate is high enough, it is likely that some molecules may be packed together and near enough to interact with each other, altering the final stability properties in a positive or a negative way, depending on the enzyme and inactivation conditions [48,49]. However, when we analysed this effect, we did not find any significant difference among the different preparations, just a very slight higher stability of the more loaded preparations; differences are scarce and may be attributed to diffusional limitations (e.g., after 6 h, the biocatalyst having 1 mg/g retained a 55 $\pm$ 2% of the initial activity, while the one prepared using 12 mg retained 60 $\pm$ 2%).

Using the preparation with 1 mg/g in hydrolysis of casein, we have reused the biocatalyst in 6 consecutive cycles of casein hydrolysis at 50 °C and pH 7 for 2 h without detecting any significant change in the biocatalyst performance (not shown results).

3. Materials and Methods

3.1. Materials

Glycidol, 25% (*v*/*v*) glutaraldehyde solution, sodium borohydride, sodium periodate, ethylenediamine, benzoyl-arginine-p-nitroanilide (BANA), cysteine, bovine serum albumin (BSA) and casein were purchased from Sigma-Aldrich (St. Louis, MO, USA). Agarose beads 4 BCL support was purchased from Agarose Bead Technologies (ABT), Madrid, Spain. All other reagents were of analytical grade. All experiments were performed by triplicate and the reported values the mean of the results of this set of experiments with their standard deviation. Glyoxyl agarose beads were prepared as previously described [54,55]. MANAE- supports was prepared from glyoxyl supports with a modification of the protocol previously described [56,57], ethylenediamine/glyoxyl agarose beads reaction time was 24 h before reduction. Glyoxyl-ficin was prepared using 1 mg ficin/g of support as previously described [40].

3.2. Preparation of Glutaraldehyde Agarose Beads

50 grams of MANAE agarose beads was suspended in 100 mL of 15% (*v*/*v*) glutaraldehyde in 200 mM phosphate buffer pH 7.0. The suspension was gently stirred 14–16 h at 4 °C. After that, the activated support was washed with distilled water. The activated support was used immediately after preparation. This protocol guarantees that each primary amino in the support has been modified with two glutaraldehyde molecules [44,58,59].

3.3. Preparation of Ficin Extract

Fresh fig latex was obtained breaking fresh immature green fruits and leaves of *Ficus carica* L. The samples were picked in Kabylia, north of Algeria (Adekar, Bejaia). The fluid was collected in a clean flask at 4 °C. The latex was centrifuged at 3200× *g* for 15 min at 4 °C [60] to eliminate debris (e.g., gums). The supernatant was used as "crude extract of ficin" (with a concentration of 98.5 mg protein/mL). The extract contains the four protease isoforms and it is similar to the usually utilized in ficin applications. A SDS-PAGE may be observed in support ting information. It was stored at −20 °C

until use. The protein concentration was quantified by Bradford's method [61]. BSA was used as the standard protein. The activity of the free enzyme versus casein (see below) was 5 ± 0.7 units/mg of protein.

3.4. Enzymatic Assays

Activity of immobilized and free ficin extract was determined using casein and benzoyl-D, L-arginine *p*-nitroanilide hydrochloride (BANA) as enzyme substrates.

The enzyme activity determination using BANA was performed as previously described [29], BANA solution was prepared by dissolving 43.5 mg of BANA in 1.0 mL of dimethyl sulfoxide and diluting to 100 mL in 0.1 M sodium phosphate pH 7, containing 5 mM EDTA. The enzyme activity was assessed by measuring the *p*-nitroaniline released at 405 nm (under these conditions, the ε for *p*-nitroaniline was 8800). Activity of ficin was expressed as μmols of *p*-nitroaniline released per mg of extract and min.

The enzyme activity using casein was determined as described by Kunitz, with some modifications [62]. A solution of 1% (*w*/*v*) casein was prepared in 100 mM sodium phosphate at pH 7.0 containing 5 mM cysteine hydrochloride and 5 mM EDTA at 55 °C. To 1 mL of this substrate solution, 100 μL of ficin (enzyme extract solution or immobilized ficin suspension) was added and the reaction mixture was incubated at the desired temperature for 20 min. The reaction was stopped by the addition of 1 mL of 10% trichloroacetic acid (TCA), incubated for 10 min at room temperature and centrifuged at 10,000 rpm. This treatment produces the precipitation of the remaining protein but the peptides remained in solution. The absorbance of soluble peptides in the supernatant was measured at 280 nm. In the case of the reference, substrate was added after the enzyme was first inactivated by incubation in TCA. One unit of activity is defined as increment in absorbance of 0.001 per mg of ficin and min under the given assay conditions.

3.5. Immobilization of Ficin Extract

Ten grams (10 g) of the corresponding support (MANAE-agarose or glutaraldehyde-agarose) were added to 100 mL of ficin extract (containing 1 mg protein/mL) in 25 mM sodium acetate at pH 5, 25 mM sodium phosphate at pH 6.5–8.5 or 25 mM sodium carbonate at pH 9, in all cases the temperature was 25 °C. In some instances, the enzyme concentration was increased to increase the amount of offered enzyme (a maximum of 12 mg/mL was employed). Samples from suspensions and supernatants were periodically withdrawn and their catalytic activity determined using BANA and casein. After 24 h, the biocatalysts were vacuum filtered and washed thoroughly with distilled water.

3.6. Enzyme Inactivation Studies

1 g of immobilized enzyme was suspended in 10 mL of 50 mM in the corresponding buffer at 55 °C (sodium acetate at pH 5, sodium phosphate at pH 7 or 50 mM sodium carbonate at pH 9). For the free enzyme extract, 1 mg/mL of ficin solution was prepared in the same buffer and temperature. Samples were periodically withdrawn and the activity determined using the BANA and casein assay described above.

3.7. Reuse of the Immobilized Ficin in the Hydrolysis of Casein

Six cycles of casein hydrolysis (2 h each) were performed at 50 °C and pH 7. After 2 h of casein proteolysis, the peptide production was checked as described above and the immobilized enzyme was washed 5 times with 10 volumes of distilled water and employed in a new reaction cycle.

4. Conclusions

Ficin extract may be immobilized on glutaraldehyde activated supports, best results in terms of immobilization yield and expressed activity are achieved when the enzyme is immobilized at pH 7.

Immobilization at 25 or 200 mM sodium phosphate is relatively similar, while the aminated support is unable to immobilize more than 30–40% of the enzyme. This suggested that the first immobilization step is in both cases the covalent attachment of the enzyme. Immobilization at pH 5 failed in permitting full enzyme immobilization, while at pH 9 the enzyme become inactivated. Stabilization depended on the pH and the substrate used to determine the residual activity, being larger when using BANA and shorter using casein. Results suggest a complex net of interactions between enzyme and support that differently affect the activity versus the different substrates. For the hydrolysis of casein, enzyme specific activity drops rapidly using high loadings, while it is almost identical using BANA. Enzyme loading has not a significant effect on immobilized enzyme stability.

Supplementary Materials: The following are available online at http://www.mdpi.com/2073-4344/8/4/149/s1, Figure S1: SDS PAGE of ficin extract (1 mg/ml). Lane 1 Molecular weight markers, Lane 2, 3, 4 different ficin extracts used in this paper.

Acknowledgments: We gratefully recognize the support from the MINECO from Spanish Government, (project number CTQ2017-86170-R). El-Hocine Siar thanks the Algerian Ministry of Higher Education and Scientific Research for his fellowship. The help and suggestions of Ángel Berenguer (Instituto de Materiales, Universidad de Alicante) are gratefully recognized.

Author Contributions: R.F.-L. and M.N.Z. conceived the experiments; R.F.-L. designed and supervised the experiments, E.-H.A., S.A.-P. and O.B. performed the experiments, E.-H.A., S.A.-P. and R.F.-L. wrote the paper.

Conflicts of Interest: The authors declare no conflict of interest. The founding sponsors had no role in the design of the study; in the collection, analyses, or interpretation of data; in the writing of the manuscript and in the decision to publish the results.

References

1. Tavano, O.L.; Berenguer-Murcia, A.; Secundo, F.; Fernandez-Lafuente, R. Biotechnological Applications of Proteases in Food Technology. *Compr. Rev. Food Sci. Food Saf.* **2018**, *17*, 412–436. [CrossRef]
2. Tavano, O.L. Protein hydrolysis using proteases: An important tool for food biotechnology. *J. Mol. Catal. B Enzym.* **2013**, *90*, 1–11. [CrossRef]
3. Clemente, A. Enzymatic protein hydrolysates in human nutrition. *Trends Food Sci. Technol.* **2000**, *11*, 254–262. [CrossRef]
4. Maurer, K.H. Detergent proteases. *Curr. Opin. Biotechnol.* **2004**, *15*, 330–334. [CrossRef] [PubMed]
5. Banerjee, U.C.; Sani, R.K.; Azmi, W.; Soni, R. Thermostable alkaline protease from *Bacillus brevis* and its characterization as a laundry detergent additive. *Process Biochem.* **1999**, *35*, 213–219. [CrossRef]
6. Phadatare, S.U.; Deshpande, V.V.; Srinivasan, M.C. High activity alkaline protease from Conidiobolus coronatus (NCL 86.8.20): Enzyme production and compatibility with commercial detergents. *Enzyme Microb. Technol.* **1993**, *15*, 72–76. [CrossRef]
7. David, A.; Singh, C.P.; Kumar, A.; Angural, S.; Kumar, D.; Puri, N.; Gupta, N. Coproduction of protease and mannanase from Bacillus nealsonii PN-11 in solid state fermentation and their combined application as detergent additives. *Int. J. Biol. Macromol.* **2018**, *108*, 1176–1184. [CrossRef] [PubMed]
8. Cuq, J.C.; Vi, M.; Cheftel, J.C. Tryptophan degradation during heat treatments: Part 2—Degradation of protein-bound tryptophan. *Food Chem.* **1983**, *12*, 73–88. [CrossRef]
9. Masuda, A.; Dohmae, N. Automated protein hydrolysis delivering sample to a solid acid catalyst for amino acid analysis. *Anal. Chem.* **2010**, *82*, 8939–8945. [CrossRef] [PubMed]
10. Feijoo-Siota, L.; Villa, T.G. Native and Biotechnologically Engineered Plant Proteases with Industrial Applications. *Food Bioprocess Technol.* **2011**, *4*, 1066–1088. [CrossRef]
11. Shah, M.A.; Mir, S.A.; Paray, M.A. Plant proteases as milk-clotting enzymes in cheesemaking: A review. *Dairy Sci. Technol.* **2014**, *94*, 5–16. [CrossRef]
12. Faccia, M.; Picariello, G.; Trani, A.; Loizzo, P.; Gambacorta, G.; Lamacchia, C.; Di Luccia, A. Proteolysis of Cacioricotta cheese made from goat milk coagulated with caprifig (*Ficus carica sylvestris*) or calf rennet. *Eur. Food Res. Technol.* **2012**, *234*, 527–533. [CrossRef]
13. Esmaeilpour, M.; Ehsani, M.R.; Aminlari, M.; Shekarforoush, S.; Hoseini, E. Antimicrobial activity of peptides derived from enzymatic hydrolysis of goat milk caseins. *Comp. Clin. Pathol.* **2016**, *25*, 599–605. [CrossRef]

14. Di Pierro, G.; O'Keeffe, M.B.; Poyarkov, A.; Lomolino, G.; Fitzgerald, R.J. Antioxidant activity of bovine casein hydrolysates produced by *Ficus carica* L.-derived proteinase. *Food Chem.* **2014**, *156*, 305–311. [CrossRef] [PubMed]
15. Bekhit, A.A.; Hopkins, D.L.; Geesink, G.; Bekhit, A.A.; Franks, P. Exogenous Proteases for Meat Tenderization. *Crit. Rev. Food Sci. Nutr.* **2014**, *54*, 1012–1031. [CrossRef] [PubMed]
16. Sullivan, G.A.; Calkins, C.R. Application of exogenous enzymes to beef muscle of high and low-connective tissue. *Meat Sci.* **2010**, *85*, 730–734. [CrossRef] [PubMed]
17. Mariant, M.; Camagna, M.; Tarditi, L.; Seccamani, E. A new enzymatic method to obtain high-yield F(ab)2 suitable for clinical use from mouse IgGl. *Mol. Immunol.* **1991**, *28*, 69–77. [CrossRef]
18. Sham, J.G.; Kievit, F.M.; Grierson, J.R.; Chiarelli, P.A.; Miyaoka, R.S.; Zhang, M.; Yeung, R.S.; Minoshima, S.; Park, J.O. Glypican-3-targeting F(ab′)2 for 89Zr PET of hepatocellular carcinoma. *J. Nucl. Med.* **2014**, *55*, 2032–2037. [CrossRef] [PubMed]
19. Saczyńska, V.; Bierczyńska-Krzysik, A.; Cecuda-Adamczewska, V.; Baran, P.; Porębska, A.; Florys, K.; Zieliński, M.; Płucienniczak, G. Production of highly and broad-range specific monoclonal antibodies against hemagglutinin of H5-subtype avian influenza viruses and their differentiation by mass spectrometry. *Virol. J.* **2018**, *15*, 13. [CrossRef] [PubMed]
20. Haesaerts, S.; Rodriguez Buitrago, J.A.; Loris, R.; Baeyens-Volant, D.; Azarkan, M. Crystallization and preliminary X-ray analysis of four cysteine proteases from *Ficus carica* latex. *Acta Crystallogr. Sect. F Struct. Biol. Cryst. Commun.* **2015**, *71*, 459–465. [CrossRef] [PubMed]
21. Zare, H.; Moosavi-Movahedi, A.A.; Salami, M.; Mirzaei, M.; Saboury, A.A.; Sheibani, N. Purification and autolysis of the ficin isoforms from fig (*Ficus carica cv. Sabz*) latex. *Phytochemistry* **2013**, *87*, 16–22. [CrossRef] [PubMed]
22. Devaraj, K.B.; Kumar, P.R.; Prakash, V. Purification, characterization, and solvent-induced thermal stabilization of ficin from *Ficus carica*. *J. Agric. Food Chem.* **2008**, *56*, 11417–11423. [CrossRef] [PubMed]
23. Di Cosimo, R.; McAuliffe, J.; Poulose, A.J.; Bohlmann, G. Industrial use of immobilized enzymes. *Chem. Soc. Rev.* **2013**, *42*, 6437–6474. [CrossRef]
24. Cantone, S.; Ferrario, V.; Corici, L.; Ebert, C.; Fattor, D.; Spizzo, P.; Gardossi, L. Efficient immobilisation of industrial biocatalysts: Criteria and constraints for the selection of organic polymeric carriers and immobilisation methods. *Chem. Soc. Rev.* **2013**, *42*, 6262–6276. [CrossRef] [PubMed]
25. Sheldon, R.A.; van Pelt, S. Enzyme immobilisation in biocatalysis: Why, what and how. *Chem. Soc. Rev.* **2013**, *42*, 6223–6235. [CrossRef] [PubMed]
26. Liese, A.; Hilterhaus, L. Evaluation of immobilized enzymes for industrial applications. *Chem. Soc. Rev.* **2013**, *42*, 6236–6249. [CrossRef] [PubMed]
27. Mateo, C.; Palomo, J.M.; Fernandez-Lorente, G.; Guisan, J.M.; Fernandez-Lafuente, R. Improvement of enzyme activity, stability and selectivity via immobilization techniques. *Enzyme Microb. Technol.* **2007**, *40*, 1451–1463. [CrossRef]
28. Barbosa, O.; Ortiz, C.; Berenguer-Murcia, Á.; Torres, R.; Rodrigues, R.C.; Fernandez-Lafuente, R. Strategies for the one-step immobilization-purification of enzymes as industrial biocatalysts. *Biotechnol. Adv.* **2015**, *33*, 435–456. [CrossRef] [PubMed]
29. Santos, J.C.S.D.; Barbosa, O.; Ortiz, C.; Berenguer-Murcia, A.; Rodrigues, R.C.; Fernandez-Lafuente, R. Importance of the Support Properties for Immobilization or Purification of Enzymes. *ChemCatChem* **2015**, *7*, 2413–2432. [CrossRef]
30. Garcia-Galan, C.; Berenguer-Murcia, A.; Fernandez-Lafuente, R.; Rodrigues, R.C. Potential of different enzyme immobilization strategies to improve enzyme performance. *Adv. Synth. Catal.* **2011**, *35*, 2885–2904. [CrossRef]
31. Rodrigues, R.C.; Ortiz, C.; Berenguer-Murcia, A.; Torres, R.; Fernández-Lafuente, R. Modifying enzyme activity and selectivity by immobilization. *Chem. Soc. Rev.* **2013**, *42*, 6290–6307. [CrossRef] [PubMed]
32. Cipolatti, E.P.; Valério, A.; Henriques, R.O.; Moritz, D.E.; Ninow, J.L.; Freire, D.M.G.; Manoel, E.A.; Fernandez-Lafuente, R.; De Oliveira, D. Nanomaterials for biocatalyst immobilization-state of the art and future trends. *RSC Adv.* **2016**, *6*, 104675–104692. [CrossRef]
33. Wang, M.; Qi, W.; Yu, Q.; Su, R.; He, Z. Kinetically controlled enzymatic synthesis of dipeptide precursor of L-alanyl-L-glutamine. *Biotechnol. Appl. Biochem.* **2011**, *58*, 449–455. [CrossRef] [PubMed]

34. Kumar, D.; Bhalla, T.C. Microbial proteases in peptide synthesis: Approaches and applications. *Appl. Microbiol. Biotechnol.* **2015**, *68*, 726–736. [CrossRef] [PubMed]
35. Lombard, C.; Saulnier, J.; Wallach, J.M. Recent trends in protease-catalyzed peptide synthesis. *Protein Pept. Lett.* **2005**, *12*, 621–629. [CrossRef] [PubMed]
36. Hayashi, T.; Ikada, Y. Protease immobilization onto porous chitosan beads. *J. Appl. Polym. Sci.* **1991**, *42*, 85–92. [CrossRef]
37. Hayashi, T.; Hyon, S.-H.; Cha, W.; Ikada, Y. Immobilization of thiol proteases onto porous poly(vinyl alcohol) beads. *Polym. J.* **1993**, *25*, 489–497. [CrossRef]
38. Tai, D.F.; Huang, H.Y.; Huang, C.C. Immobilized ficin catalyzed synthesis of peptides in organic solvent. *Bioorg. Med. Chem. Lett.* **1995**, *5*, 1475–1478. [CrossRef]
39. Jasim, M.A.; Hall, G.M.; Mann, J.; Taylor, K.D.A. A comparison of immobilised protease activities. *J. Chem. Technol. Biotechnol.* **1987**, *40*, 251–258. [CrossRef]
40. Siar, E.-H.; Zaak, H.; Kornecki, J.F.; Zidoune, M.N.; Barbosa, O.; Fernandez-Lafuente, R. Stabilization of ficin extract by immobilization on glyoxyl agarose. Preliminary characterization of the biocatalyst performance in hydrolysis of proteins. *Process Biochem.* **2017**, *58*, 98–104. [CrossRef]
41. Barbosa, O.; Ortiz, C.; Berenguer-Murcia, A.; Torres, R.; Rodrigues, R.C.; Fernandez-Lafuente, R. Glutaraldehyde in bio-catalysts design: A useful crosslinker and a versatile tool in enzyme immobilization. *RSC Adv.* **2014**, *4*, 1583–1600. [CrossRef]
42. Betancor, L.; López-Gallego, F.; Hidalgo, A.; Alonso-Morales, N.; Dellamora-Ortiz, G.; Mateo, C.; Fernández-Lafuente, R.; Guisán, J.M. Different mechanisms of protein immobilization on glutaraldehyde activated supports: Effect of support activation and immobilization conditions. *Enzyme Microb. Technol.* **2006**, *39*, 877–882. [CrossRef]
43. López-Gallego, F.; Betancor, L.; Mateo, C.; Hidalgo, A.; Alonso-Morales, N.; Dellamora-Ortiz, G.; Guisán, J.M.; Fernández-Lafuente, R. Enzyme stabilization by glutaraldehyde crosslinking of adsorbed proteins on aminated supports. *J. Biotechnol.* **2005**, *119*, 70–75. [CrossRef] [PubMed]
44. Barbosa, O.; Torres, R.; Ortiz, C.; Fernandez-Lafuente, R. Versatility of glutaraldehyde to immobilize lipases: Effect of the immobilization protocol on the properties of lipase B from *Candida antárctica*. *Process Biochem.* **2012**, *47*, 1220–1227. [CrossRef]
45. Zaak, H.; Peirce, S.; de Albuquerque, T.L.; Sassi, M.; Fernandez-Lafuente, R. Exploiting the versatility of aminated supports activated with glutaraldehyde to immobilize β-galactosidase from *Aspergillus oryzae*. *Catalysts* **2017**, *7*, 250. [CrossRef]
46. Vazquez-Ortega, P.G.; Alcaraz-Fructuoso, M.T.; Rojas-Contreras, J.A.; López-Miranda, J.; Fernandez-Lafuente, R. Stabilization of dimeric β-glucosidase from *Aspergillus niger* via glutaraldehyde immobilization under different conditions. *Enzyme Microb. Technol.* **2018**, *110*, 38–45. [CrossRef] [PubMed]
47. De Albuquerque, T.L.; Peirce, S.; Rueda, N.; Marzocchella, A.; Gonçalves, L.R.B.; Rocha, M.V.P.; Fernandez-Lafuente, R. Ion exchange of β-galactosidase: The effect of the immobilization pH on enzyme stability. *Process Biochem.* **2016**, *51*, 875–880. [CrossRef]
48. Fernandez-Lopez, L.; Pedrero, S.G.; Lopez-Carrobles, N.; Gorines, B.C.; Virgen-Ortíz, J.J.; Fernandez-Lafuente, R. Effect of protein load on stability of immobilized enzymes. *Enzyme Microb. Technol.* **2017**, *98*, 18–25. [CrossRef] [PubMed]
49. Zaak, H.; Siar, E.H.; Kornecki, J.F.; Fernandez-Lopez, L.; Pedrero, S.G.; Virgen-Ortíz, J.J.; Fernandez-Lafuente, R. Effect of immobilization rate and enzyme crowding on enzyme stability under different conditions. The case of lipase from *Thermomyces lanuginosus* immobilized on octyl agarose beads. *Process Biochem.* **2017**, *56*, 117–123. [CrossRef]
50. Virgen-Ortíz, J.J.; Pedrero, S.G.; Fernandez-Lopez, L.; Lopez-Carrobles, N.; Gorines, B.C.; Otero, C.; Fernandez-Lafuente, R. Desorption of lipases immobilized on octyl-agarose beads and coated with ionic polymers after thermal inactivation. Stronger adsorption of polymers/unfolded protein composites. *Molecules* **2017**, *22*, 91. [CrossRef]
51. Virgen-Ortíz, J.J.; Peirce, S.; Tacias-Pascacio, V.G.; Cortes-Corberan, V.; Marzocchella, A.; Russo, M.E.; Fernandez-Lafuente, R. Reuse of anion exchangers as supports for enzyme immobilization: Reinforcement of the enzyme-support multiinteraction after enzyme inactivation. *Process Biochem.* **2016**, *51*, 1391–1396. [CrossRef]

52. Fernandez-Lafuente, R.; Rosell, C.M.; Rodriguez, V.; Guisan, J.M. Strategies for enzyme stabilization by intramolecular crosslinking with bifunctional reagents. *Enzyme Microb. Technol.* **1995**, *17*, 517–523. [CrossRef]
53. Sanchez, A.; Cruz, J.; Rueda, N.; Dos Santos, J.C.S.; Torres, R.; Ortiz, C.; Villalonga, R.; Fernandez-Lafuente, R. Inactivation of immobilized trypsin under dissimilar conditions produces trypsin molecules with different structures. *RSC Adv.* **2016**, *6*, 27329–27334. [CrossRef]
54. Mateo, C.; Abian, O.; Bernedo, M.; Cuenca, E.; Fuentes, M.; Fernandez-Lorente, G.; Palomo, J.M.; Grazu, V.; Pessela, B.C.C.; Giacomini, C.; et al. Some special features of glyoxyl supports to immobilize proteins. *Enzyme Microb. Technol.* **2005**, *37*, 456–462. [CrossRef]
55. Grazu, V.; Betancor, L.; Montes, T.; Lopez-Gallego, F.; Guisan, J.M.; Fernandez-Lafuente, R. Glyoxyl agarose as a new chromatographic matrix. *Enzyme Microb. Technol.* **2006**, *38*, 960–966. [CrossRef]
56. Mateo, C.; Palomo, J.M.; Fuentes, M.; Betancor, L.; Grazú, V.; Lopez-Gallego, F.; Pessela, B.C.C.; Hidalgo, A.; Fernández-Lorente, G.; Fernández-Lafuente, R. Glyoxyl agarose: A fully inert and hydrophilic support for immobilization and high stabilization of proteins. *Enzyme Microb. Technol.* **2006**, *39*, 274–280. [CrossRef]
57. Fernández-Lafuente, R.; Rosell, C.M.; Rodriguez, V.; Santana, C.; Soler, G.; Bastida, A.; Guisán, J.M. Preparation of activated supports containing low pK amino groups. A new tool for protein immobilization via the carboxyl coupling method. *Enzyme Microb. Technol.* **1993**, *15*, 546–550. [CrossRef]
58. Corma, A.; Fornés, V.; Jordá, J.L.; Rey, F.; Fernandez-Lafuente, R.; Guisan, J.M.; Mateo, C. Electrostatic and covalent immobilisation of enzymes on ITQ-6 delaminated zeolitic materials. *Chem. Commun.* **2001**, *5*, 419–420. [CrossRef]
59. Betancor, L.; López-Gallego, F.; Alonso-Morales, N.; Dellamora, G.; Mateo, C.; Fernandez-Lafuente, R.; Guisan, J.M. Glutaraldehyde in Protein Immobilization. A Versatile Reagent. In *Immobilization of Enzymes and Cells*, 2nd ed.; Guisan, J.M., Ed.; Humana Press Inc.: New York, NY, USA, 2006; pp. 57–64, ISBN 1-58829-290-8.
60. Nouani, A.; Dako, E.; Morsli, A.; Belhamiche, N.; Belbraouet, S.; Bellal, M.M.; Dadie, A. Characterization of the purified coagulant extracts derived from artichoke flowers (*Cynaras scolymus*) and from the fig tree latex (*Ficus carica*) in light of their use in the manufacture of traditional cheeses in Algeria. *J. Food Technol.* **2009**, *7*, 20–29.
61. Bradford, M.M. A rapid and sensitive method for the quantitation of microgram quantities of protein utilizing the principle of protein-dye binding. *Anal. Biochem.* **1976**, *72*, 248–254. [CrossRef]
62. Kunitz, M.J. Crystalline soybean trypsin inhibitor: II. General properties. *J. Gen. Physiol.* **1947**, *30*, 291–310. [CrossRef] [PubMed]

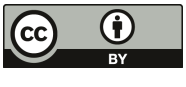

© 2018 by the authors. Licensee MDPI, Basel, Switzerland. This article is an open access article distributed under the terms and conditions of the Creative Commons Attribution (CC BY) license (http://creativecommons.org/licenses/by/4.0/).

catalysts

MDPI

Review

Techniques for Preparation of Cross-Linked Enzyme Aggregates and Their Applications in Bioconversions

Hiroshi Yamaguchi [1], Yuhei Kiyota [2] and Masaya Miyazaki [2,3,*]

[1] Liberal Arts Education Center, Tokai University, Kumamoto 862-8652, Japan; yamahiro@tokai-u.jp
[2] Department of Applied Chemistry, Graduate School of Engineering, Hokkaido University, Sapporo, Hokkaido 060-8628, Japan; kiyota.y@eng.hokudai.ac.jp
[3] Advanced Manufacture Research Institute, National Institute of Advanced Industrial Science and Technology, Tosu, Saga 841-0052, Japan
* Correspondence: m.miyazaki@aist.go.jp or m.miyazaki@eng.hokudai.ac.jp; Tel.: +81-11-706-8188

Received: 27 March 2018; Accepted: 20 April 2018; Published: 24 April 2018

Abstract: Enzymes are biocatalysts. They are useful in environmentally friendly production processes and have high potential for industrial applications. However, because of problems with operational stability, cost, and catalytic efficiency, many enzymatic processes have limited applications. The use of cross-linked enzyme aggregates (CLEAs) has been introduced as an effective carrier-free immobilization method. This immobilization method is attractive because it is simple and robust, and unpurified enzymes can be used. Coimmobilization of different enzymes can be achieved. CLEAs generally show high catalytic activities, good storage and operational stabilities, and good reusability. In this review, we summarize techniques for the preparation of CLEAs for use as biocatalysts. Some important applications of these techniques in chemical synthesis and environmental applications are also included. CLEAs provide feasible and efficient techniques for improving the properties of immobilized enzymes for use in industrial applications.

Keywords: enzyme; immobilization; cross-linked enzyme aggregates

1. Introduction

Enzymes have high catalytic activities and substrate specificities. One single substrate is usually converted to one product. Enzymes are active at modest reaction temperatures, mainly in the range 20–80 °C. These features can reduce the cost per unit of manufactured products. In addition, enzymatic conversions generate less waste than conventional chemical synthetic processes. Synthesis by enzymatic conversion is therefore more energy efficient than chemical synthetic processes. In the last two decades, the use of enzymes in various industries has been continuously increasing. The catalytic and biophysical properties of enzymes, such as catalytic efficiency, substrate specificity, and stability, need to be improved for industrial applications [1,2]. A variety of approaches such as the screening of enzymes from natural sources or random mutations have been used for these purposes [3].

Despite their advantages, several limitations prevent the use of enzymes in industrial applications. Enzymes are proteins with unique three-dimensional structures that are essential for their catalytic activity. Because they often have low operational stability, exposure to high temperatures or organic solvents can denature enzymes, leading to loss of catalytic activity. Modern protein engineering techniques can improve the catalytic and biophysical properties of some, but not all, enzymes with potential industrial uses. Immobilized enzymes provide one solution to these difficulties. They have several advantages [2,4–6]. An enzyme can be immobilized at high concentrations on the carrier material, resulting in a high concentration of catalyst in the reaction system. Consequently, catalytic reactions can be performed rapidly. The operational stability and reusability of immobilized enzymes

are reported to be higher than those of free enzymes. Furthermore, because enzymes immobilized on carrier materials are insoluble catalysts, they can be easily separated and removed from reaction vessels.

Recently, various enzymes immobilized on carrier materials such as modified glass or polymethyl methacrylate have been developed for industrial use [7,8]. Enzyme immobilization is usually achieved by chemical covalent linking, affinity labeling, physical adsorption, or entrapment. These immobilization methods have been described in recent reviews [5–8]. Adsorption is a simple and low-cost method. Enzyme immobilization by this method can provide high retention of enzymatic activity. However, adsorbed enzymes are likely to leak gradually from the carrier materials, therefore the operational stability is lower than that provided by covalent linking. For covalent or noncovalent linking methods, surface modification of the carrier materials is generally necessary to improve the operational stability. Noncovalent binding is often achieved by affinity interactions such as that between a histidine-tagged enzyme and metal-ion-chelated beads [9,10]. Although the interaction is specific, it requires the use of recombinant tagged enzymes. This method is therefore unsuitable for routine immobilization of all other enzymes. In contrast, covalent linking methods involve chemical reactions between the side-chains in enzymes and surface-modified carrier materials. These methods do not require any modification of the target enzymes. However, it requires expensive surface-modified carrier materials. Furthermore, multiple reaction points often alter the three-dimensional structure of the enzyme, leading to loss of activity and operational stability [11,12]. In addition, the reported procedures for preparing immobilized enzymes are usually multistep procedures. Facile techniques for routine immobilization of enzymes are therefore needed.

Enzyme cross-linking, in which enzymes are covalently connected to each other by cross-linkers, can be partly categorized as covalent linking. This method enables the formation of miniature structures that consist of polymerized enzymes. Cross-linked enzyme aggregates (CLEAs) have recently been prepared for use in carrier-free enzyme-immobilization methods [2,4]. They are easily prepared, and carrier costs are circumvented. The prepared CLEAs showed good retention of catalytic activity, high operational stability, and reusability [4]. Improvement of the biophysical properties can significantly reduce the cost of enzymes and this makes industrial applications economically feasible. In this review, we specifically introduce recent advances in CLEA techniques for industrial applications. Typical and modified methods for CLEA preparation are summarized. The coimmobilization of two or more enzymes is also covered. Finally, the use of CLEA reactors for chemical synthesis and environmental applications is introduced.

2. Cross-Linking Enzyme Immobilization

Cross-linked enzymes were first reported in the 1960s [13], but were never popular because they were generally difficult to handle. In addition, they showed low catalytic activities and low operational stabilities. In the 1990s, cross-linked enzyme crystals were prepared for use as biocatalysts [14, 15]. Although the method was applicable to a wide variety of enzymes and cross-linked enzyme crystals showed excellent operational stabilities, highly purified enzymes were needed for protein crystallization. In contrast, CLEA preparation involves simple precipitation (physical aggregation) of the enzymes from an aqueous buffer with a precipitant (a salt, an ionic/nonionic polymer, or an organic solvent) instead of crystallization. Aggregation (precipitation) of enzymes induced by addition of a precipitant to an aqueous solution of enzymes is commonly used in traditional protein purification. Physical aggregation of enzyme molecules into microstructures can be induced without denaturation of the enzyme's three-dimensional structure by addition of a precipitant. Chemical cross-linking of the aggregated enzymes produces CLEAs. This improved enzyme immobilization method is simple and does not require highly purified enzymes.

2.1. General Preparation of CLEAs

A typical procedure for the preparation of CLEAs is shown in Figure 1a. CLEAs are generally prepared by aggregating an enzyme by addition of a precipitant such as $(NH_4)_2SO_4$ or *t*-butanol,

and then cross-linking with a cross-linker such as glutaraldehyde [16]. Cross-linking occurs between lysine (Lys) residues on the surfaces of neighboring enzyme molecules and glutaraldehyde via a Schiff's base reaction. This procedure is simple and can be widely applied. Every enzyme has a unique primary structure (amino acid sequence) and surface structure (the number of accessible Lys residues), therefore the preparation of CLEAs can be optimized, as described below.

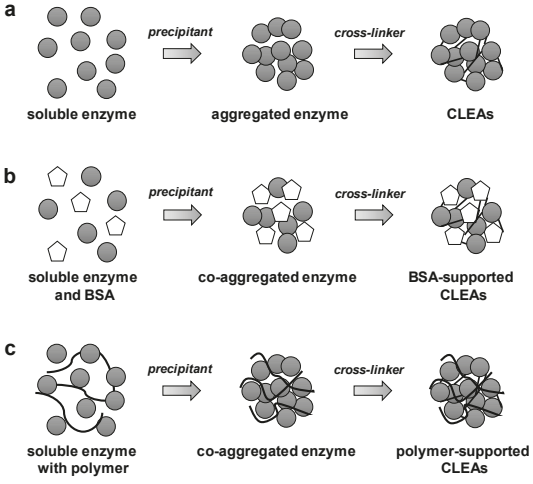

Figure 1. Preparation of CLEAs. (**a**) General cross-linking method [4]; (**b**) bovine serum albumin (BSA)-supported CLEA cross-linking method. Combined (combi)-CLEAs are prepared by similar processes (see Section 3); (**c**) ionic-polymer-supported CLEA cross-linking method.

2.2. Optimization by Additives

2.2.1. Bovine Serum Albumin (BSA)

Shah et al. reported that addition of BSA facilitates CLEA preparation when the enzyme concentration is low and/or the enzymatic activity is affected by the high concentration of glutaraldehyde that is required to obtain aggregation [17]. The preparation of CLEAs with BSA is shown in Figure 1b. In this study, lipase-CLEAs and penicillin acylase-CLEAs were prepared. The lipase-CLEAs that were prepared with BSA showed 100% activity, whereas CLEAs without BSA did not retain their activity because little insoluble aggregate was obtained at low enzyme concentrations. Similar results were observed in the case of penicillin acylase-CLEAs. Scanning electron microscopy showed that the CLEAs that were prepared with BSA were less amorphous and had a similar morphology to those of other reported CLEAs [18]. Recently, it was reported that lipase-CLEAs prepared optimally with BSA resisted lipase deactivation by acetaldehyde, which occurs by transacetylation between benzyl alcohols and vinyl acetate [19]. The CLEA structure consists of networks of cross-linked lipase and BSA, and this prevents access of acetaldehyde to the important amino acid residues of lipase.

2.2.2. Ionic Polymer

As described above, cross-linking typically requires activation of a Lys residue on the enzyme surface with the aldehyde groups of a cross-linker that can react readily with other Lys residues of the enzyme. The cross-linking efficiency depends on the number of surface Lys residues. An acidic or neutral enzyme with a low content of Lys residues therefore cannot be cross-linked efficiently merely

by using a cross-linker. Although a high concentration of cross-linker can increase the cross-linking efficiency, this often causes a conformational change, leading to loss of enzymatic activity [20].

To overcome this problem, coaggregation of enzymes and ionic polymers (Figure 1c) was investigated [21–23]. López-Gallego et al. reported that glutaryl acylase, with a low content of Lys residues, was efficiently cross-linked by coaggregation with the aminated polymer polyethylenimine (PEI) [21]. Glutaryl acylase-CLEAs retained more than 60% of their initial activity, and the thermal stability of the immobilized enzyme was improved. The same research group also prepared penicillin acylase-CLEAs by coaggregation with PEI. The stability of these CLEAs in organic media was high [22]. Enzymatic reactions in organic media are important in industry. Zhang et al. prepared trehalose synthase-CLEAs by coaggregation with PEI [23]. They showed that coimmobilization with PEI enhanced the cross-linking efficiency even at low concentrations of the enzyme. Recently, metal-ion-chelated PEI was used for immobilization of a multimeric oxidoreductase (glycerol dehydrogenase). The CLEAs formed were stabilized by hydrogen bonding, electrostatic forces, and coordination bonding [24]. Although a cross-linker was not used to immobilize the enzyme in this study, nanoparticles of diameter 250–650 nm were obtained. The operational stability and catalytic activity were enhanced. This strategy of cross-linking enzymes with modified PEI has potential applications in the immobilization of multimeric enzymes.

Our group developed a facile and inexpensive method for preparing an enzyme-immobilized reactor via an enzyme cross-linking reaction. Enzyme immobilization was achieved by the formation of a polymeric membrane of enzyme molecules on the inner wall of a polytetrafluoroethylene tube through cross-linking aggregation under laminar flow [25] (Figure 2a). The aggregated enzyme membrane was based on CLEAs prepared with glutaraldehyde as a cross-linker. This method for the preparation of a CLEA-based enzyme microreactor (CEM) is unsuitable for electronegative enzymes because the relative paucity of amino groups results in inefficient CLEA formation. To extend the generality of CEM preparation, we developed an improved method with poly-Lys as an aggregation booster to achieve effective aggregation of acidic enzymes [26] (Figure 2b). CEM preparation can be used for immobilization of a broad range of functional enzymes. These methods have been used to develop several enzymatic microfluidic systems [27–30]. In addition, the operational stability of enzymes in CLEAs formed by coaggregation with poly-Lys was examined [31]. Two proteases (chymotrypsin and subtilisin), an oxidase (laccase), and a multimeric enzyme (citrate synthase), which have diverse three-dimensional structures and catalytic activities, were used as model enzymes. Compared with the free enzymes, these four CLEAs were more stable at high temperatures, in the presence of a chemical denaturant, or in an organic solvent. They were recycled without appreciable loss of activity. As in the case of coaggregation with PEI, poly-Lys-supported immobilization is also applicable to multimeric enzymes [31].

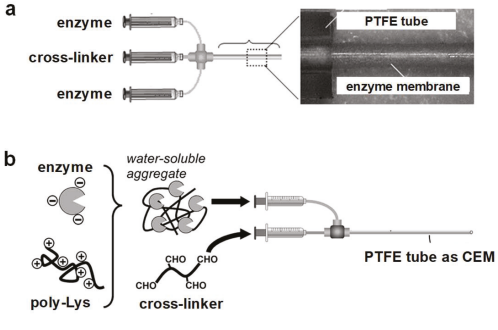

Figure 2. Preparation of CLEAs on inner wall of polytetrafluoroethylene (PTFE) tube by cross-linking aggregation under laminar flow: (**a**) general cross-linking method [25] and (**b**) poly-Lys-supported cross-linking method [26]. CEM: CLEA-based enzyme microreactor.

2.2.3. Surfactants

The activation of enzymes with additives such as surfactants or amines is well known [32]. On the basis of this property of enzymes, a surfactant (SDS, Triton X-100, or Tween 80) was added during the preparation of lipase-CLEAs [33–35]. The CLEAs showed a two-fold or greater increase in catalytic activity when SDS was present during CLEA preparation [33]. Such enhanced activity of lipase-CLEAs by other surfactants has been reported [34]. These surfactants were added at the aggregation step and initiated binding to the hydrophobic active sites of the enzyme. It has been proposed that the enzyme forms open active sites by interactions with the surfactant. The open active sites can produce hyperactive CLEAs. It is assumed that the surfactants can be washed out of the active sites after the cross-linking reaction [35].

2.2.4. Cations

Amylase is a metal-ion-dependent enzyme. Calcium and sodium ions are reported to increase the activity of α-amylase [36]. Thermostable α-amylase-CLEA preparation by a cation-assisted strategy was recently reported [37]. The aggregation and cross-linking of α-amylase were performed in a cation-enriched nonaqueous environment. The addition of calcium and sodium ions at the optimum ratio gave α-amylase-CLEAs with increased activity and operational stability [37].

2.3. Optimization by Precipitant Selection

Because aggregation and precipitation of enzymes are induced by addition of a precipitant, precipitant selection is important for optimization [18]. The type of precipitant used to prepare CLEAs varied and the operational stabilities of the CLEAs differed, but the same enzyme was used in the studies described. Khorshidi et al. reported that cellulase-CLEAs produced using saturated $(NH_4)_2SO_4$ lost 70% of their activity after one cycle [38]. Several cellulase-CLEAs produced using organic solvents showed better activities and reusability [39,40]. Recently, a systematic study of the effects of different precipitants and various cross-linking parameters was reported [41]. The effects of different precipitants, namely $(NH_4)_2SO_4$, poly(ethylene glycol) (PEG), and *t*-butanol, on the resolubilized enzyme activity and final CLEA activity were examined. Cellulase-CLEAs prepared with PEG retained high activity. The activity of cellulase-CLEAs prepared with $(NH_4)_2SO_4$ was lower than that of cellulase-CLEAs produced with PEG. The CLEAs prepared with *t*-butanol were inactive [41]. Similar results were reported in the case of lipase-CLEAs. Lipase-CLEAs were prepared with four types of precipitant, namely acetone, PEG 200 and 600, and $(NH_4)_2SO_4$. The CLEAs precipitated with PEG and saturated $(NH_4)_2SO_4$ had superior catalytic activities [42]. Enzymes precipitated with water-miscible and water-immiscible solvents showed decreased activities [18]. The yield of CLEAs greatly depends on the type of precipitant and microbial source. It is hypothesized that lipases from different sources have different glycosylated surfaces, and this may result in different biophysical properties. The aggregation and packing of the enzyme molecules may be affected by the precipitant.

2.4. Optimization by Cross-Linker

The cross-linker forms covalent bonds between Lys residues on the enzyme surface, and the CLEAs formed are permanently insoluble. Glutaraldehyde is commonly used as a cross-linker. Excess glutaraldehyde can bind to amino acid residues during cross-link formation. If the catalytically essential residues react with glutaraldehyde, the catalytic activity of the CLEAs will be reduced. The use of mild cross-linkers instead of glutaraldehyde is therefore essential to overcome the drawbacks associated with traditional cross-linking reactions.

Based on this idea, ethylene glycol *bis*(succinimidylsuccinate) (EG-NHS) was proposed as an alternative cross-linker for the preparation of lipase-CLEAs (EGS-CLEAs). The operational stability and reusability of EGS-CLEAs were compared with those of lipase-CLEAs formed using glutaraldehyde [43]. The hydrolytic and esterification activities of the EGS-CLEAs were better than

those of the glutaraldehyde aggregates. Both CLEAs showed similar thermal and operational stabilities. These results indicate that EG-NHS could be used as a mild cross-linker in the preparation of CLEAs instead of glutaraldehyde. This strategy can be extended to the preparation of CLEAs of other enzymes.

2.5. Novel Method for Preparation of CLEAs

2.5.1. CLEA Particle Size

Because most CLEAs are prepared in solution, the particle size and cross-linking efficiency may not be uniform. Large particles may result in diffusion constraints and low catalytic efficiency, and tiny clusters have poor recoverability [18]. CLEAs that consist of small particles cannot be filtered off or recycled. Control of the CLEA particle size and a uniform size distribution are therefore essential to overcome these drawbacks. To address these problems, a new method for preparing trehalose synthase-CLEAs in a water-in-oil emulsion instead of in solution was developed [44]. This method involves precipitation of an enzyme in solution, and then mixing the aqueous phase with an oil phase to form a water-in-oil emulsion. Cross-linking was performed within the emulsion droplets. CLEAs prepared by this emulsion-based method rather than the conventional method were spherical. The CLEAs had a ball-like structure and were of diameter 20–60 μm. These CLEAs were easily separated from the reaction mixture. As expected, the operational stability of the spherical CLEAs was higher than that of the free enzyme.

Nguyen et al. reported the preparation of uniform cellulase-CLEAs by using a millifluidic reactor. The reactor had two inlets and a Y-junction that can control the mixing pattern of the enzyme and precipitant solutions [40]. The particle size of the cellulase-CLEAs can be strictly controlled between 200 and 400 nm by controlling the concentrations of the precipitant and cross-linker and the flow rates. The activity of the cellulase-CLEAs was more stable than that of the free enzyme at high temperatures.

2.5.2. Molecular-Imprinted CLEAs

Molecular imprinting enhances the catalytic activity by increasing electrostatic interactions and hydrogen bonding between the surface residues on enzymes [45,46]. It has been suggested that the lid that covers the active site of an enzyme can be opened at the interface in the presence of imprinting molecules [45]. This mechanism resembles the concept of the approach that uses additives to improve the CLEA properties, as described in Section 2.2.3. Recently, the advantages of molecular imprinting of CLEAs were investigated. Hydroxynitrile lyase-CLEAs prepared with 2-butanone as a molecular-imprinting additive showed improved activity [47]. Winter et al. used α-glucosylglycerol to prepare sucrose phosphorylase-CLEAs and reported that the enzymatic performance was better than those of nonimprinted CLEAs and the free enzyme in solution [48]. Similarly, lipase-CLEAs immobilized by molecular imprinting showed improved thermal stability, hydrolytic efficiency, and reusability [49].

2.6. Carrier-Bound CLEAs

The particle sizes of the majority of reported CLEAs are less than 10 μm [50]. As described in Section 2.5.1, CLEAs of small particle size are difficult to separate and recover from the reaction system. This can result in problems in the continuous use of CLEAs. To overcome this problem, some researchers recently investigated carrier-bound CLEAs to develop biocatalysts with good mechanical stabilities.

2.6.1. CLEAs in Silica Material

α-Chymotrypsin-CLEAs and lipase-CLEAs formed by cross-linking into hierarchically ordered mesoporous silica have been reported [51]. α-Chymotrypsin-CLEAs showed high enzyme immobilization efficiency and significantly increased enzyme stability. However, the mesoporous silica pore size was small, which limited the maximum immobilization of CLEAs. To improve the

immobilization yield, a simple strategy for preparation of CLEAs by one-step cross-linking into the pores of macroporous silica gel was developed [52]. Macroporous silica gel is usually used as a carrier material because it has controlled porosity and a high surface area. Papain-CLEAs in macroporous silica gel showed good storage and thermal stabilities. Moreover, papain-CLEAs showed good reusability because the CLEAs were of appropriate size. Cui et al. reported that the formation of phenylalanine ammonia lyase-CLEAs in the pores of mesoporous materials also gave a high loading yield of the enzyme, and good operational stability and activity retention [53]. Recently, lipase-CLEAs in three-dimensionally ordered macroporous silica materials (3DOM SiO_2) were developed [54]. Lipase was precipitated in the pores of 3DOM SiO_2 before cross-linking with glutaraldehyde. Compared with free lipase, lipase-CLEAs in 3DOM SiO_2 showed excellent thermal and mechanical stability. Improved activity and reusability were also achieved.

2.6.2. Magnetic CLEAs

Use of a magnetic field is a simple method for the separation and recovery of magnetic materials. Magnetic α-amylase-CLEAs were prepared by addition of magnetite nanoparticles (MNPs) with NH_2-functionalized surfaces to an enzyme solution [55]. In the case of magnetic CLEAs, 100% of the α-amylase activity was recovered, whereas only 45% recovery was achieved in the case of nonmagnetic CLEAs because of the low content of Lys residues of amylase. The optimum operating temperature of the magnetic CLEAs was better than those of the free enzyme and nonmagnetic CLEAs. The magnetic CLEAs also had enhanced thermal and storage stabilities. Furthermore, because of the magnetic properties of the nanoparticles, magnetic α-amylase-CLEAs can be easily separated from the reaction mixture without centrifugation or filtration [55]. Sekhon et al. prepared magnetic cutinase-CLEAs for degradation of polycaprolactone (PCL) [56]. The CLEAs retained 55% activity after 50 cycles; therefore, enzymatic degradation of PCL with CLEAs is a good strategy.

In most cases, modification of the MPN surfaces is required, both for stabilization of the magnetic fluid and for introduction of functional groups. Cellulase-CLEAs on NH_2-functionalized Fe_3O_4@silica core–shell MNPs have been reported [38]. Separation of the magnetic cellulase-CLEAs from the reaction system was simple, and their thermal and operational stabilities were better than those of the free enzyme. Liu et al. prepared magnetic lipase-CLEAs by immobilization of lipase-CLEAs on magnetic particles. To improve immobilization, a large number of amino terminal groups were introduced by using *p*-benzoquinone as the cross-linker [57]. *p*-Benzoquinone reacts with the amino or hydroxyl groups of the enzyme and NH_2-groups on the MNPs, to form stable magnetic CLEAs by formation of C–O and C–N bonds. It is suggested that this improved immobilization method could prevent gradual release of the enzyme from CLEAs and/or MNPs. As expected, the magnetic lipase-CLEAs showed improved immobilization efficiency, activity, and reusability, compared with nonmagnetic CLEAs. The magnetic CLEAs efficiently resolved (*R*,*S*)-2-octanol and retained 100% activity with 100% enantioselectivity [57].

2.6.3. Entrapment CLEAs in Alginate Beads

Enzyme entrapment in alginate beads is a popular immobilization method. However, the enzyme often leaks from the alginate beads during enzymatic reactions because enzymes are usually smaller than the pore size of alginate beads (~200 nm). Because the CLEA size is generally 1–10 μm, entrapment of CLEAs in alginate beads can solve leakage problems [4,16]. In addition, the alginate beads can be easily separated by simple filtration. Xu and Yang reported the entrapment of tyrosinase-CLEAs. The CLEAs in alginate beads retained 100% activity after six cycles [58]. Nguyen et al. reported that cellulase-CLEAs in alginate beads had good operational stability and leakage of cellulase was prevented [59].

3. Coimmobilization of Two or More Enzymes in CLEAs

A new concept, that is, CLEAs with various catalytic activities within a single CLEA particle, has been developed. In this section, combined CLEAs (combi-CLEAs) and multipurpose CLEAs (multi-CLEAs) are introduced.

3.1. Combi-CLEAs

Multistep chemical syntheses usually require several procedures such as the separation of intermediates. Combined CLEAs (combi-CLEAs) were introduced for one-pot chemical synthesis [2,4]. Combi-CLEAs with (*S*)-hydroxynitrile lyase, nitrilase, and penicillin G amidase were prepared and used to catalyze one-pot synthesis of (*S*)-mandelic acid from benzaldehyde. A good yield (90%) and enantiomeric excess (99%) were achieved, with complete benzaldehyde conversion [60]. Combi-CLEAs consisting of α-amylase, glucoamylase, and pullulanase were prepared and used to catalyze one-pot starch hydrolysis [61]. Combi-CLEAs, a separate CLEA mixture, and a free enzyme mixture gave 100%, 60%, and 40% conversions, respectively, in one-pot starch hydrolysis. The enzymes in combi-CLEAs were reported to be thermally stable. In addition, the combi-CLEAs retained 100% catalytic activity after five cycles.

Combi-CLEAs have also been used in bioethanol production from lignocellulosic biomass. Periyasamy et al. prepared combi-CLEAs of xylanase, cellulase, and β-1,3-glucanase for this purpose [62]. The thermal and storage stabilities of the CLEAs were better than those of the free enzymes. The recovered combi-CLEAs retained 90% activity for six cycles. Combi-CLEAs hydrolyzed about 84% of ammonia-cooked sugarcane bagasse (SCB) in 48 h, whereas the free enzymes gave a maximum hydrolysis of 73%,

Combi-CLEAs of ketoreductase and D-glucose dehydrogenase were used for the regeneration of dihydropyridine nucleotide cofactors in the synthesis of valuable chiral alcohols [63]. The CLEAs showed high activity, long-term operational stability, and reusability. A prochiral keto ester was used in the synthesis of a key atorvastatin intermediate. Combi-CLEAs catalyzed the enantioselective reduction of the prochiral keto ester with high activity and selectivity. More recently, magnetic combi-CLEAs containing ketoreductase and D-glucose dehydrogenase were developed [64]. Magnetic combi-CLEAs showed an optimum temperature, thermal stability, and optimum pH similar to those of combi-CLEAs. Magnetic combi-CLEAs also showed more efficient activity and better operational stability in both aqueous and biphasic systems than did nonmagnetic combi-CLEAs. Furthermore, the magnetic CLEAs can be recovered with a magnetic field during multiple use.

Cascade reactions that involve unstable intermediates are often found in biological systems. Nguyen et al. prepared combi-CLEAs of glucose oxidase and horseradish peroxidase (HRP) and used them to catalyze a cascade reaction in which hydrogen peroxide is formed as an unstable intermediate [65]. The CLEAs were effective even in the presence of catalase, which rapidly catalyzes the decomposition of hydrogen peroxide. Because of the short diffusion distance between glucose oxidase and peroxidase in the combi-CLEAs, the intermediate hydrogen peroxide was not efficiently decomposed by catalase [65].

Recent studies have investigated pharmaceutical applications of combi-CLEAs. Trehalose has many applications in the food, pharmaceutical, and cosmetic industries. Park et al. reported the production of trehalose from sucrose in a one-pot synthesis using combi-CLEAs of sucrase, trehalose synthase, and trehalose hydrolase [66]. Scism and Bachmann reported five-enzyme combi-CLEAs of ribokinase, phosphoribosyl pyrophosphate synthetase, engineered hypoxanthine phosphoribosyl transferase, adenylate kinase, and pyruvate kinase for use in the cascade synthesis of nucleotide analogs [67].

3.2. Multi-CLEAs

Dalal et al. developed a single multipurpose biocatalyst that was based on multi-CLEAs containing pectinase, xylanase, and cellulase [39]. These CLEAs were designed to catalyze three different and independent reactions. The obtained multi-CLEAs were more thermostable than the free enzymes. All three enzymes in the multi-CLEA were reusable and showed no loss of activity after three cycles. Mahmod et al. prepared multi-CLEAs containing lipase and protease from fish viscera [68]. The multi-CLEAs were used to catalyze two reactions. The stain-removing ability of commercial detergents during washing was improved by 68% by addition of multi-CLEAs. Protease in multi-CLEAs was used to catalyze biodiesel production from vegetable oil. These results indicate that the use of multi-CLEAs is a promising technique for biotechnological applications. Neutrase and papain were coimmobilized in CLEAs and their properties were investigated [69]. The thermal and pH stabilities of the multi-CLEAs were clearly better than those of the free enzymes. In addition, the multi-CLEAs retained relatively high activities in nonpolar and hydrophilic solvents, and no loss of activity occurred during storage at 4 °C for more than six months. The activities of multi-CLEAs in bean protein and zein hydrolysis were better than those of the free enzymes. These results show that multi-CLEAs have a wide range of industrial uses as a multifunctional catalyst.

4. Application for Processing by CLEAs

As described above, enzyme immobilization by CLEA formation is a simple and useful technique. The three-dimensional structure of the enzyme in CLEAs is conserved, therefore its catalytic activity is retained. Moreover, CLEAs have several advantages such as insolubility and superior operational stability. The use of CLEAs as biocatalysts in various industries is therefore continuously increasing. In this section, we introduce recent applications of CLEA techniques, especially in chemical synthesis and environmental applications.

4.1. Chemical Synthesis

4.1.1. Pharmaceutical Chemicals

(−)-γ-Lactam is an essential building block in the synthesis of carbocyclic nucleosides, which have potent antiviral activities because of their inhibitory activity against viral reverse transcriptase. (+)-γ-Lactamase can catalyze the conversion of only (+)-γ-lactam in a racemic mixture, suggesting that (−)-γ-lactam can be recovered from the reaction mixture by a simple reaction. Modified CEMs packed with γ-lactamase-CLEAs combined with pore-glass particles have been reported [70]. The thermophilic γ-lactamase-CLEAs retained 100% of their initial activity and retained 52% activity after 10 h.

α-Cyanohydrins are key building blocks in the pharmaceutical and agrochemical industries. Hydroxynitrile lyase from Davallia tyermannii (DtHNL) catalyzes the enantioselective synthesis of α-cyanohydrins. DtHNL-CLEAs were prepared [71] and showed enhanced stability under acidic conditions. The DtHNL-CLEAs were used for (*R*)-mandelonitrile synthesis (99% conversion, 98% ee) in a biphasic system, and evaluated for use in the synthesis of (*R*)-hydroxypivaldehyde cyanohydrin.

We developed a microreaction system for the optical resolution of racemic amino acids [27]. This system was based on a continuous microfluidic system consisting of acylase-CEM (see Section 2.2.2) and a microextractor. Acylase-CEM showed high enantioselectivity for racemic amino acids or amino acid derivatives. The microextractor supplied a laminar flow of two immiscible solutions and selectively extracted (separated) the products. This microfluidic system could be used for efficient continuous production of optically pure chemical compounds.

L-3,4-Dihydroxyphenylalanine (L-DOPA) is used to treat Parkinson's disease. Tyrosinase-CLEAs catalyzed the conversion of tyrosine to L-DOPA [72]. A conversion yield of 53% was obtained in 2 h, with a productivity of 209 mg L^{-1} h^{-1}. This result is much better than those reported for batch processes that used tyrosinase immobilized on carrier materials. The operational stability of the CLEAs was improved by entrapment in alginate beads. A continuous stirred-tank reactor with

entrapped CLEAs in alginate beads achieved good mechanical stability (a long lifetime of >104 h) and a productivity of 57 mg L^{-1} h^{-1}.

Peptide synthesis with enzymes is a potentially cost-efficient technique. However, there are some limitations to the synthesis of peptides with sterically hindered structures or noncoded amino acids. Lipase-CLEA- and alcalase-CLEA-mediated peptide syntheses have been reported [73]. To enable specific recognition by the enzymes, special ester moieties, that is, guanidinophenyl, carboxamidomethyl (Cam), and trifluoroethyl (Tfe) esters have been used. The Cam and Tfe esters enable alcalase-CLEA-catalyzed synthesis of peptides with sterically hindered structures and noncoded acyl donors. Although chemical synthesis of these special esters is usually difficult, they can be efficiently synthesized by using lipase-CLEAs or alcalase-CLEAs. These results suggest that ester synthesis by lipase-CLEAs and subsequent peptide synthesis by alcalase-CLEAs can be performed simultaneously in a one-pot approach.

4.1.2. Polymers

Synthetic polyamides have high mechanical strength and good thermal resistance and are widely used in industrial applications. The industrial synthesis of these polymers usually involves a melting process. Because of the high melting temperatures and relatively low decomposition temperatures of polyamides with aliphatic–aromatic structures, the synthesis of polyamides by melting processes is usually difficult. Cutinase-CLEA-catalyzed synthesis of oligoamides with aliphatic–aromatic structures overcomes this difficulty [74]. Although a commercially available immobilized lipase gave a higher conversion efficiency than cutinase-CLEAs, the CLEAs achieved the highest degree of polymerization in the one-step or two-step synthesis of oligo(*p*-xylylene sebacamide).

4.1.3. Nanoparticles

Silver nanoparticles are the focus of much research because of their catalytic, antimicrobial, and optical properties. The synthesis of silver nanoparticles by conventional methods is energy- and capital-intensive and is environmentally unfriendly because of the use of toxic solvents or additives that are difficult to dispose of and degrade on industrial scales. Moreover, silver nanoparticles synthesized by these conventional methods cannot be used for in vivo biomedical applications because the toxic chemicals from the synthetic process are incompatible with biological systems. To overcome these problems, nicotinamide adenine dinucleotide (NADH)-dependent nitrate reductase-CLEAs were developed for the synthesis of silver nanoparticles from silver nitrate [75]. The CLEAs catalyzed reduction of silver ions to silver nanoparticles at neutral pH. NADH and 8-hydroxyquinoline were used as an electron source and an electron shuttle, respectively. The size of the obtained silver nanoparticles was strictly controlled between 5 and 7 nm. In addition, these CLEAs showed 80% catalytic recovery after five cycles, indicating that they have good operational stability.

4.2. Environmental Purposes

4.2.1. Decolorization and Detoxification of Dyes

For environmental protection, the textile, dyeing, printing, and related industries should dispose of or treat synthetic dye-contaminating wastewater. The use of enzymes potentially enables the efficient and low-cost degradation of pollutants and has therefore been investigated for the treatment of wastewater. One of the examined enzymes, laccase, is widely used for catalytic degradation in the treatment of industrial wastewater [76]. Kumar et al. reported the degradation and detoxification of synthetic dyes by magnetic laccase-CLEAs [77]. The magnetic laccase-CLEAs showed good thermal and operational stabilities. Laccase-CLEAs (0.2 U mL^{-1}) rapidly degraded 61–96% of synthetic dyes (initial concentration of 50 mg L^{-1}) such as Remazol brilliant blue R, malachite green, and Reactive Black 5 at 20 °C and pH 7.0.

HRP-CLEAs were prepared and their biocatalytic efficacy in biodegradation was investigated [78]. The immobilization efficiency was improved by cross-linking HRP with EG-NHS (see Section 2.4). Dye degradations were performed in a CLEA-packed reactor. Methyl orange degradation of 94% was observed within the shortest treatment time. The CLEA reactor system was also used to treat other dyes (92% of Basic red 9, 84% of indigo, 82% of rhodamine B, and 74% of rhodamine 6G). The toxicities of these CLEA-treated dye samples were significantly reduced. The HRP-CLEAs retained 60% of catalytic activity after seven cycles of methyl orange degradation.

Hollow CLEAs of laccase (h-CLEA laccase) were developed by using a millifluidic reactor [79]. Control of the solution flow rates in laminar flow enabled h-CLEA laccase particles of size 220 ± 10 nm to be obtained. The activity of h-CLEA laccase was comparable to that of the free enzyme at neutral pH, indicating that the laccase in the hollow structures had the same three-dimensional structure as free laccase. Uniformly sized h-CLEA laccase was trapped inside a disposable polyether sulfone membrane and continuously used for degradation of trypan blue for up to 96 h without loss of catalytic activity.

These studies indicate that improved CLEA techniques have great potential for industrial applications.

4.2.2. Elimination of Endocrine-Disrupting Chemicals

Endocrine-disrupting chemicals (EDCs) are defined as "exogenous chemical substances or mixtures that alter the structure or function(s) of the endocrine system and cause adverse effects at the level of the organism, its progeny, populations, or subpopulations of organisms, based on scientific principles, data, weight-of-evidence, and the precautionary principle" [80]. EDCs are often detected in industrial wastewaters. Oxidases such as laccase and peroxidase have been widely used for EDC degradation.

We developed a novel continuous-flow laccase-CEM for the degradation of EDCs [30]. Estrogens (E1, E2, and EE2) and anti-inflammatories (naproxen and diclofenac) were used as model EDCs for degradation studies. The degradation efficiency of our microreaction system was better than those of conventional bioreactors. Furthermore, it enabled two-step degradation in laccase-mediated reactions, thereby avoiding inactivation of laccase-CLEAs. Taboada-Puig et al. used combi-CLEAs containing peroxidase and glucose oxidase for degradation reactions [81]. The degradation of bisphenol A, nonylphenol, triclosan, EE2, and E2 by combi-CLEAs and their residual estrogenic activities were studied. Within 10 min, the combi-CLEAs degraded almost all the EDCs except triclosan. The residual estrogenic activity was lower than 45% for all compounds, except triclosan. In addition, a continuous membrane reactor with combi-CLEAs almost completely removed bisphenol A (10 mg L^{-1}) in 43 h. These reports indicate that a CLEA-based continuous degradation system provides a simple catalytic system that can eliminate EDCs effectively.

4.2.3. Bioconversion of Agroindustrial Waste

The immobilized enzymatic bioconversion of lignocellulosic biomass such as SCB to biofuels is an important technology in the production of clean energy. Xylanase-CLEAs were prepared and used for SCB bioconversion [82]. The CLEAs produced xylo-oligosaccharides from SCB, whereas the free enzyme produced xylose as the main product from the same SCB. This indicates that immobilization modified the catalytic properties. Bhattacharya and Pletschke prepared magnetic xylanase-CLEAs for bioconversion of SCB to sugar [83]. They reported that the activity and stability of the magnetite-CLEAs and reusability of the CLEAs were enhanced; a higher hydrolysis yield was obtained from SCB.

5. Conclusions

Immobilized enzymes retain their catalytic activity and are more robust to environmental changes compared with free enzymes. The operational stability depends on the immobilization method. CLEAs were developed for carrier-free immobilization as an alternative to conventional immobilization on solid carriers and cross-linked enzyme crystals. CLEAs have several advantages over conventional

methods, for example, simple preparation, high catalytic activity, high operational stability, and low production costs. Applications of CLEAs have therefore been widely investigated in various industries. There are still obstacles to the development of immobilized enzymes as biocatalysts for practical applications. As noted in this review, improved CLEA techniques will enable the development of novel enzymatic reaction systems. The development of new techniques will enable expansion of the industrial use of enzyme immobilization.

Author Contributions: Hiroshi Yamaguchi researched the literature and wrote the manuscript; Yuhei Kiyota and Masaya Miyazaki discussed ideas and edited the manuscript.

Funding: This research received no external funding.

Acknowledgments: Part of this work was supported by a Grant-in-Aid for Basic Scientific Research (C: 15K04639) from JSPS (H.Y.) and the Research and Study Program/Project of Tokai University Education System General Research Organization (H.Y.). We thank Helen McPherson, from Liwen Bianji, Edanz Editing China (www.liwenbianji.cn/ac), for editing the English text of a draft of this manuscript.

Conflicts of Interest: The authors declare no conflict of interest.

References

1. Madhavan, A.; Sindhu, R.; Binod, P.; Sukumaran, R.K.; Pandey, A. Strategies for design of improved biocatalysts for industrial applications. *Bioresour. Technol.* **2017**, *245*, 1304–1313. [CrossRef] [PubMed]
2. Sheldon, R.A.; Woodley, J.M. Role of biocatalysis in sustainable chemistry. *Chem. Rev.* **2018**, *118*, 801–838. [CrossRef] [PubMed]
3. Elleuche, S.; Schröder, C.; Sahm, K.; Antranikian, G. Extremozymes—Biocatalysts with unique properties from extremophilic microorganisms. *Curr. Opin. Biotechnol.* **2014**, *29*, 116–123. [CrossRef] [PubMed]
4. Sheldon, R.A. Characteristic features and biotechnological applications of cross-linked enzyme aggregates (CLEAs). *Appl. Microbiol. Biotechnol.* **2011**, *92*, 467–477. [CrossRef] [PubMed]
5. Franssen, M.C.; Steunenberg, P.; Scott, E.L.; Zuilhof, H.; Sanders, J.P. Immobilised enzymes in biorenewables production. *Chem. Soc. Rev.* **2013**, *42*, 6491–6533. [CrossRef] [PubMed]
6. Bilal, M.; Iqbal, H.M.N.; Guo, S.; Hu, H.; Wang, W.; Zhang, X. State-of-the-art protein engineering approaches using biological macromolecules: A review from immobilization to implementation view point. *Int. J. Biol. Macromol.* **2018**, *108*, 893–901. [CrossRef] [PubMed]
7. Miyazaki, M.; Portia Nagata, M.; Honda, T.; Yamaguchi, H. Bioorganic and biocatalytic reactions. In *Microreactors in Organic Synthesis and Catalysis*, 2nd ed.; Wiley-VCH: Hoboken, NJ, USA, 2013; Chapter 10.
8. Honda, T.; Yamaguchi, H.; Miyazaki, M. Development of enzymatic reactions in miniaturized reactors. In *Innovations and Future Directions Applied Bioengineering*; Wiley-VCH: Hoboken, NJ, USA, 2017; pp. 99–166.
9. Wang, L.S.; Khan, F.; Micklefield, J. Selective covalent protein immobilization: Strategies and applications. *Chem. Rev.* **2009**, *109*, 4025–4053. [CrossRef] [PubMed]
10. Asanomi, Y.; Yamaguchi, H.; Miyazaki, M.; Maeda, H. Enzyme-immobilized microfluidic process reactors. *Molecules* **2011**, *16*, 6041–6059. [CrossRef] [PubMed]
11. Yiu, H.H.P.; Wright, P.A. Enzymes supported on ordered mesoporous solids: A special case of an inorganic–organic hybrid. *J. Mater. Chem.* **2005**, *15*, 3690–3700. [CrossRef]
12. Cha, T.W.; Guo, A.; Zhu, X.Y. Enzymatic activity on a chip: The critical role of protein orientation. *Proteomics* **2005**, *5*, 416–419. [CrossRef] [PubMed]
13. Zaborsky, O.R. *Immobilized Enzymes*; CRC Press: Cleveland, OH, USA, 1973.
14. St. Clair, N.L.; Navia, M.A. Cross-linked enzyme crystals as robust biocatalysts. *J. Am. Chem. Soc.* **1992**, *114*, 7314–7316. [CrossRef]
15. Roy, J.J.; Abraham, T.E. Strategies in making cross-linked enzyme crystals. *Chem. Rev.* **2004**, *104*, 3705–3722. [CrossRef]
16. Cao, L.; van Langen, L.; Sheldon, R.A. Immobilised enzymes: Carrier-bound or carrier-free? *Curr. Opin. Biotechnol.* **2003**, *14*, 387–394. [CrossRef]
17. Shah, S.; Sharma, A.; Gupta, M.N. Preparation of cross-linked enzyme aggregates by using bovine serum albumin as a proteic feeder. *Anal. Biochem.* **2006**, *351*, 207–213. [CrossRef] [PubMed]

18. Schoevaart, R.; Wolbers, M.W.; Golubovic, M.; Ottens, M.; Kieboom, A.P.; van Rantwijk, F.; van der Wielen, L.A.; Sheldon, R.A. Preparation, optimization, and structures of cross-linked enzyme aggregates (CLEAs). *Biotechnol. Bioeng.* **2004**, *87*, 754–762. [CrossRef] [PubMed]
19. Majumder, A.B.; Gupta, M.N. Stabilization of *Candida rugosa* lipase during transacetylation with vinyl acetate. *Bioresour. Technol.* **2010**, *101*, 2877–2879. [CrossRef] [PubMed]
20. Mateo, C.; Palomo, J.M.; van Langen, L.M.; van Rantwijk, F.; Sheldon, R.A. A new, mild cross-linking methodology to prepare cross-linked enzyme aggregates. *Biotechnol. Bioeng.* **2004**, *86*, 273–276. [CrossRef] [PubMed]
21. López-Gallego, F.; Betancor, L.; Hidalgo, A.; Alonso, N.; Fernández-Lafuente, R.; Guisán, J.M. Coaggregation of enzymes and polyethyleneimine: A simple method to prepare stable and immobilized derivatives of glutaryl acylase. *Biomacromolecules* **2005**, *6*, 1839–1842. [CrossRef] [PubMed]
22. Wilson, L.; Illanes, A.; Abián, O.; Pessela, B.C.; Fernández-Lafuente, R.; Guisán, J.M. Coaggregation of penicillin g acylase and polyionic polymers: An easy methodology to prepare enzyme biocatalysts stable in organic media. *Biomacromolecules* **2004**, *5*, 852–857. [CrossRef] [PubMed]
23. Zheng, J.; Chen, Y.; Yang, L.; Li, M.; Zhang, J. Preparation of cross-linked enzyme aggregates of trehalose synthase via coaggregation with polyethyleneimine. *Appl. Biochem. Biotechnol.* **2014**, *174*, 2067–2078. [CrossRef] [PubMed]
24. Zhang, Y.; Ren, H.; Wang, Y.; Chen, K.; Fang, B.; Wang, S. Bioinspired immobilization of glycerol dehydrogenase by metal ion-chelated polyethyleneimines as artificial polypeptides. *Sci. Rep.* **2016**, *6*, 24163. [CrossRef] [PubMed]
25. Honda, T.; Miyazaki, M.; Nakamura, H.; Maeda, H. Immobilization of enzymes on a microchannel surface through cross-linking polymerization. *Chem. Commun.* **2005**, *40*, 5062–5064. [CrossRef] [PubMed]
26. Honda, T.; Miyazaki, M.; Nakamura, H.; Maeda, H. Facile preparation of an enzyme-immobilized microreactor using a cross-linking enzyme membrane on a microchannel surface. *Adv. Synth. Catal.* **2006**, *348*, 2163–2171. [CrossRef]
27. Honda, T.; Miyazaki, M.; Yamaguchi, Y.; Nakamura, H.; Maeda, H. Integrated microreaction system for optical resolution of racemic amino acids. *Lab Chip* **2007**, *7*, 366–372. [CrossRef] [PubMed]
28. Yamaguchi, H.; Miyazaki, M.; Maeda, H. Proteolysis approach without chemical modification for a simple and rapid analysis of disulfide bonds using thermostable protease-immobilized microreactors. *Proteomics* **2010**, *10*, 2942–2949. [CrossRef] [PubMed]
29. Yamaguchi, H.; Miyazaki, M.; Kawazumi, H.; Maeda, H. Multidigestion in continuous flow tandem protease-immobilized microreactors for proteomic analysis. *Anal. Biochem.* **2010**, *407*, 12–18. [CrossRef] [PubMed]
30. Lloret, L.; Eibes, G.; Moreira, M.T.; Feijoo, G.; Lema, J.M.; Miyazaki, M. Improving the catalytic performance of laccase using a novel continuous-flow microreactor. *Chem. Eng. J.* **2013**, *223*, 497–506. [CrossRef]
31. Yamaguchi, H.; Miyazaki, M.; Asanomi, Y.; Maeda, H. Poly-lysine supported cross-linked enzyme aggregates with efficient enzymatic activity and high operational stability. *Catal. Sci. Technol.* **2011**, *1*, 1256–1261. [CrossRef]
32. Theil, F. Enhancement of selectivity and reactivity of lipases by additives. *Tetrahedron* **2000**, *56*, 2905–3076. [CrossRef]
33. Gupta, P.; Dutt, K.; Misra, S.; Raghuwanshi, S.; Saxena, R.K. Characterization of cross-linked immobilized lipase from thermophilic mould *Thermomyces lanuginosa* using glutaraldehyde. *Bioresour. Technol.* **2009**, *100*, 4074–4076. [CrossRef] [PubMed]
34. Fernández-Lorente, G.; Palomo, J.M.; Mateo, C.; Munilla, R.; Ortiz, C.; Cabrera, Z.; Guisán, J.M.; Fernandez-Lafuente, R. Glutaraldehyde cross-linking of lipases adsorbed on aminated supports in the presence of detergents leads to improved performance. *Biomacromolecules* **2006**, *7*, 2610–2615. [CrossRef] [PubMed]
35. De Rose, S.A.; Novak, H.; Dowd, A.; Singh, S.; Lang, D.A.; Littlechild, J. Stabilization of a lipolytic enzyme for commercial application. *Catalysts* **2017**, *7*, 91. [CrossRef]
36. Burhan, A.; Nisa, U.; Gökhan, C.; Ömer, C.; Ashabil, A.; Osman, G. Enzymatic properties of a novel thermostable, thermophilic, alkaline and chelator resistant amylase from an alkaliphilic *Bacillus* sp. isolate ANT-6. *Process Biochem.* **2003**, *38*, 1397–1403. [CrossRef]

37. Torabizadeh, H.; Tavakoli, M.; Safari, M. Immobilization of thermostable α-amylase from *Bacillus licheniformis* by cross-linked enzyme aggregates method using calcium and sodium ions as additives. *J. Mol. Catal. B: Enzym.* **2014**, *108*, 13–20. [CrossRef]
38. Khorshidi, K.J.; Lenjannezhadian, H.; Jamalan, M.; Zeinali, M. Preparation and characterization of nanomagnetic cross-linked cellulase aggregates for cellulose bioconversion. *J. Chem. Technol. Biotechnol.* **2016**, *91*, 539–546. [CrossRef]
39. Dalal, S.; Sharma, A.; Gupta, M.N. A multipurpose immobilized biocatalyst with pectinase, xylanase and cellulase activities. *Chem. Cent. J.* **2007**, *1*, 16. [CrossRef] [PubMed]
40. Nguyen, L.T.; Yang, K.L. Uniform cross-linked cellulase aggregates prepared in millifluidic reactors. *J. Colloid Interface Sci.* **2014**, *428*, 146–151. [CrossRef] [PubMed]
41. Perzon, A.; Dicko, C.; Çobanoğlu, Ö.; Yükselen, O.; Eryilmaz, J.; Dey, E.S. Cellulase cross-linked enzyme aggregates (CLEA) activities can be modulated and enhanced by precipitant selection. *J. Chem. Technol. Biotechnol.* **2017**, *92*, 1645–1649. [CrossRef]
42. Devi, B.L.A.P.; Guo, Z.; Xu, X. Characterization of cross-linked lipase aggregates. *J. Am. Oil Chem. Soc.* **2009**, *86*, 637–642. [CrossRef]
43. Rehman, S.; Bhatti, H.N.; Bilal, M.; Asgher, M. Cross-linked enzyme aggregates (CLEAs) of *Pencilluim notatum* lipase enzyme with improved activity, stability and reusability characteristics. *Int. J. Biol. Macromol.* **2016**, *91*, 1161–1169. [CrossRef] [PubMed]
44. Chen, Y.; Xiao, C.; Chen, X.; Yang, L.; Qi, X.; Zheng, J.; Li, M.; Zhang, J. Preparation of cross-linked enzyme aggregates in water-in-oil emulsion: Application to trehalose synthase. *J. Mol. Catal. B: Enzym.* **2014**, *100*, 84–90. [CrossRef]
45. Verheyen, E.; Schillemans, J.P.; van Wijk, M.; Demeniex, M.A.; Hennink, W.E.; van Nostrum, C.F. Challenges for the effective molecular imprinting of proteins. *Biomaterials* **2011**, *32*, 3008–3020. [CrossRef] [PubMed]
46. Fishman, A.; Coganb, U. Bio-imprinting of lipases with fatty acids. *J. Mol. Catal. B: Enzym.* **2003**, *22*, 193–202. [CrossRef]
47. Cabirol, F.L.; Tan, P.L.; Tay, B.; Cheng, S.; Hanefeld, U.; Sheldon, R.A. *Linum usitatissimum* Hydroxynitrile lyase cross-linked enzyme aggregates: A recyclable enantioselective catalyst. *Adv. Synth. Catal.* **2008**, *350*, 2329–2338. [CrossRef]
48. De Winter, K.; Soetaert, W.; Desmet, T. An imprinted cross-linked enzyme aggregate (iCLEA) of sucrose phosphorylase: Combining improved stability with altered specificity. *Int. J. Mol. Sci.* **2012**, *13*, 11333–11342. [CrossRef] [PubMed]
49. Sampath, C.; Belur, P.D.; Iyyasami, R. Enhancement of n-3 polyunsaturated fatty acid glycerides in Sardine oil by a bioimprinted cross-linked *Candida rugosa* lipase. *Enzyme Microb. Technol.* **2018**, *110*, 20–29. [CrossRef] [PubMed]
50. Cao, L. Immobilised enzymes: Science or art? *Curr. Opin. Chem. Biol.* **2005**, *9*, 217–226. [CrossRef] [PubMed]
51. Kim, M.I.; Kim, J.; Lee, J.; Jia, H.; Na, H.B.; Youn, J.K.; Kwak, J.H.; Dohnalkova, A.; Grate, J.W.; Wang, P.; et al. Crosslinked enzyme aggregates in hierarchically-ordered mesoporous silica: A simple and effective method for enzyme stabilization. *Biotechnol. Bioeng.* **2007**, *96*, 210–218. [CrossRef] [PubMed]
52. Wang, M.; Qi, W.; Yu, Q.; Su, R.; He, S. Cross-linking enzyme aggregates in the macropores of silica gel: A practical and efficient method for enzyme stabilization. *Biochem. Eng. J.* **2010**, *52*, 168–174. [CrossRef]
53. Cui, J.D.; Li, L.L.; Bian, H.J. Immobilization of cross-linked phenylalanine ammonia lyase aggregates in microporous silica gel. *PLoS ONE* **2013**, *8*, e80581. [CrossRef] [PubMed]
54. Jiang, Y.; Shi, L.; Huang, Y.; Gao, J.; Zhang, X.; Zhou, L. Preparation of robust biocatalyst based on cross-linked enzyme aggregates entrapped in three-dimensionally ordered macroporous silica. *ACS Appl. Mater. Interfaces* **2014**, *6*, 2622–2628. [CrossRef] [PubMed]
55. Talekar, S.; Ghodake, V.; Ghotage, T.; Rathod, P.; Deshmukh, P.; Nadar, S.; Mulla, M.; Ladole, M. Novel magnetic cross-linked enzyme aggregates (magnetic CLEAs) of alpha amylase. *Bioresour. Technol.* **2012**, *123*, 542–547. [CrossRef] [PubMed]
56. Sekhon, S.S.; Ahn, J.-Y.; Shin, W.-R.; Ko, J.H.; Lee, L.; Dawes, M.; Tyler, J.; Han, J.; Kim, S.Y.; Min, J.; Kim, Y.-H. Immobilization of cross-linked cutinase aggregates onto magnetic beads for degradation of polycaprolactone. *J. Nanosci. Nanotechnol.* **2017**, *17*, 9306–9311. [CrossRef]
57. Liu, Y.; Guo, C.; Liu, C.-Z. Novel magnetic cross-linked lipase aggregates for improving the resolution of (*R*, *S*)-2-octanol. *Chirality* **2015**, *27*, 199–204. [CrossRef] [PubMed]

58. Xu, D.-Y.; Yang, Z. Cross-linked tyrosinase aggregates for elimination of phenolic compounds from wastewater. *Chemosphere* **2013**, *92*, 391–398. [CrossRef] [PubMed]
59. Nguyen, L.T.; Lau, Y.S.; Yang, K.L. Entrapment of cross-linked cellulase colloids in alginate beads for hydrolysis of cellulose. *Colloids Surf. B Biointerfaces.* **2016**, *145*, 862–869. [CrossRef] [PubMed]
60. Mateo, C.; Chmura, A.; Rustler, S.; van Rantwijk, F.; Stolz, A.; Sheldon, R.A. Synthesis of enantiomerically pure (*S*)-mandelic acid using an oxynitrilase-nitrilase bienzymatic cascade: A nitrilase surprisingly shows nitrile hydratase activity. *Tetrahedron Asymm.* **2006**, *17*, 320–323. [CrossRef]
61. Talekar, S.; Pandharbale, A.; Ladole, M.; Nadar, S.; Mulla, M.; Japhalekar, K.; Pattankude, K.; Arage, D. Carrier free coimmobilization of alpha amylase, glucoamylase and pullulanase as combined cross-linked enzyme aggregates (combi-CLEAs): A tri-enzyme biocatalyst with one pot starch hydrolytic activity. *Bioresour. Technol.* **2013**, *147*, 269–275. [CrossRef] [PubMed]
62. Periyasamy, K.; Santhalembi, L.; Mortha, G.; Aurousseau, M.; Subramanian, S. Carrier-free coimmobilization of xylanase, cellulase and β-1,3-glucanase as combined crosslinked enzyme aggregates (combi-CLEAs) for one-pot saccharification of sugarcane bagasse. *RSC Adv.* **2016**, *6*, 32849–32857. [CrossRef]
63. Ning, C.; Su, E.; Tian, Y.; Wei, D. Combined cross-linked enzyme aggregates (combi-CLEAs) for efficient integration of a ketoreductase and a cofactor regeneration system. *J. Biotechnol.* **2014**, *184*, 7–10. [CrossRef] [PubMed]
64. Su, E.; Meng, Y.; Ning, C.; Ma, X.; Deng, S. Magnetic combined cross-linked enzyme aggregates (combi-CLEAs) for cofactor regeneration in the synthesis of chiral alcohol. *J. Biotechnol.* **2018**, *271*, 1–7. [CrossRef] [PubMed]
65. Nguyen, L.T.; Yang, K.L. Combined cross-linked enzyme aggregates of horseradish peroxidase and glucose oxidase for catalyzing cascade chemical reactions. *Enzyme Microb. Technol.* **2017**, *100*, 52–59. [CrossRef] [PubMed]
66. Jung, D.-H.; Jung, J.-H.; Seo, D.-H.; Ha, S.-J.; Kweon, D.-K.; Park, C.-S. One-pot bioconversion of sucrose to trehalose using enzymatic sequential reactions in combined cross-linked enzyme aggregates. *Bioresour. Technol.* **2013**, *130*, 801–804. [CrossRef] [PubMed]
67. Scism, R.A.; Bachmann, B.O. Five-component cascade synthesis of nucleotide analogues in an engineered self-immobilized enzyme aggregate. *ChemBioChem* **2010**, *11*, 67–70. [CrossRef] [PubMed]
68. Mahmod, S.S.; Yusof, F.; Jami, M.S.; Khanahmadi, S.; Shah, H. Development of an immobilized biocatalyst with lipase and protease activities as a multipurpose cross-linked enzyme aggregate (multi-CLEA). *Process Biochem.* **2015**, *50*, 2144–2157. [CrossRef]
69. Chen, Z.; Wang, Y.; Liu, W.; Wang, J.; Chen, H. A novel cross-linked enzyme aggregates (CLEAs) of papain and neutrase-production, partial characterization and application. *Int. J. Biol. Macromol.* **2017**, *95*, 650–657. [CrossRef] [PubMed]
70. Hickey, A.M.; Ngamsom, B.; Wiles, C.; Greenway, G.M.; Watts, P.; Littlechild, J.A. A microreactor for the study of biotransformations by a cross-linked γ-lactamase enzyme. *Biotechnol. J.* **2009**, *4*, 510–516. [CrossRef] [PubMed]
71. Lanfranchi, E.; Grill, B.; Raghoebar, Z.; Van Pelt, S.; Sheldon, R.A.; Steiner, K.; Glieder, A.; Winkler, M. Production of hydroxynitrile lyase from *D. tyermannii* (*Dt*HNL) in *Komagataella phaffii* and its immobilization as a CLEA to generate a robust biocatalyst. *ChemBioChem* **2018**, *19*, 312–316. [CrossRef] [PubMed]
72. Xu, D.-Y.; Chen, J.-Y.; Yang, Z. Use of cross-linked tyrosinase aggregates as catalyst for synthesis of L-DOPA. *Biochem. Eng. J.* **2012**, *63*, 88–94. [CrossRef]
73. Nuijens, T.; Cusan, C.; Schepers, A.C.H.M.; Kruijtzer, J.A.W.; Quaedflieg, P.J.L.M. Enzymatic synthesis of activated esters and their subsequent use in enzyme-based peptide synthesis. *J. Mol. Catal. B: Enzym.* **2011**, *71*, 79–84. [CrossRef]
74. Stavila, E.; Alberda van Ekenstein, G.R.O.; Loos, K. Enzyme-catalyzed synthesis of aliphatic–aromatic oligoamides. *Biomacromolecules* **2013**, *14*, 1600–1606. [CrossRef] [PubMed]
75. Talekar, S.; Joshi, A.; Chougle, R.; Nakhe, A.; Bhojwani, R. Immobilized enzyme mediated synthesis of silver nanoparticles using cross-linked enzyme aggregates (CLEAs) of NADH-dependent nitrate reductase. *Nano-Struct. Nano-Objects.* **2016**, *6*, 23–33. [CrossRef]
76. Forootanfar, H.; Faramarzi, M.A. Insights into laccase producing organisms, fermentation states, purification strategies, and biotechnological applications. *Biotechnol. Prog.* **2015**, *31*, 1443–1463. [CrossRef] [PubMed]

77. Kumar, V.V.; Sivanesan, S.; Cabana, H. Magnetic cross-linked laccase aggregates—Bioremediation tool for decolorization of distinct classes of recalcitrant dyes. *Sci. Total Environ.* **2014**, *487*, 830–839. [CrossRef] [PubMed]
78. Bilal, M.; Iqbal, H.M.N.; Hu, H.; Wang, W.; Zhang, X. Development of horseradish peroxidase-based cross-linked enzyme aggregates and their environmental exploitation for bioremediation purposes. *J. Environ. Manag.* **2017**, *188*, 137–143. [CrossRef] [PubMed]
79. Nguyen, L.T.; Seow, N.; Yang, K.-L. Hollow cross-linked enzyme aggregates (h-CLEA) of laccase with high uniformity and activity. *Colloids Surf. B Biointerfaces.* **2017**, *151*, 88–94. [CrossRef] [PubMed]
80. Special Report on Environmental Endocrine Disruption: An Effects Assessment and Analysis. 1997. Available online: https://archive.epa.gov/raf/web/html/special-rpt-endocrine-disruption.html (accessed on 8 February 2018).
81. Taboada-Puig, R.; Junghanns, C.; Demarche, P.; Moreira, M.T.; Feijoo, G.; Lema, J.M.; Agathos, S.N. Combined cross-linked enzyme aggregates from versatile peroxidase and glucose oxidase: Production, partial characterization and application for the elimination of endocrine disruptors. *Bioresour. Technol.* **2011**, *102*, 6593–6599. [CrossRef] [PubMed]
82. Hero, J.S.; Romero, C.M.; Pisa, J.H.; Perotti, N.I.; Olivaro, C.; Martinez, M.A. Designing cross-linked xylanase aggregates for bioconversion of agroindustrial waste biomass towards potential production of nutraceuticals. *Int. J. Biol. Macromol.* **2018**, *111*, 229–236. [CrossRef] [PubMed]
83. Bhattacharya, A.; Pletschke, B.I. Magnetic cross-linked enzyme aggregates (CLEAs): A novel concepttowards carrier free immobilization of lignocellulolytic enzymes. *Enzyme Microb. Technol.* **2014**, *61–62*, 17–27. [CrossRef] [PubMed]

© 2018 by the authors. Licensee MDPI, Basel, Switzerland. This article is an open access article distributed under the terms and conditions of the Creative Commons Attribution (CC BY) license (http://creativecommons.org/licenses/by/4.0/).

catalysts

MDPI

Article

Rapid Immobilization of Cellulase onto Graphene Oxide with a Hydrophobic Spacer

Jian Gao [1], Chun-Liu Lu [2], Yue Wang [3], Shuang-Shuang Wang [1], Jia-Jia Shen [2], Jiu-Xun Zhang [2] and Ye-Wang Zhang [1,2,*]

1 College of Petroleum and Chemical Engineering, Qinzhou University, Qinzhou 535011, China; jgao12@163.com (J.G.); doublewang123@163.com (S.-S.W.)
2 School of Pharmacy, United Pharmaceutical Institute of Jiangsu University and Shandong Tianzhilvye Biotechnology Co. Ltd., Jiangsu University, Zhenjiang 212013, China; luchunliu@outlook.com (C.L.L.); shenjiajia20@163.com (J.-J.S.); zhongshixun661@163.com (J.-X.Z.)
3 School of Pharmacy, Guangxi Medical University, Nanning 530021, China; wyjs69@outlook.com
* Correspondence: zhangyewang@ujs.edu.cn; Tel.: +86-511-8503-8201

Received: 29 March 2018; Accepted: 25 April 2018; Published: 28 April 2018

Abstract: A rapid immobilization method for cellulase was developed. Functional graphene oxide was synthesized and grafted with hydrophobic spacer P-β-sulfuric acid ester ethyl sulfone aniline (SESA) though etherification and diazotization. The functionalized graphene oxide was characterized by Fourier-transform infrared spectroscopy and was used as the carrier for the immobilization of cellulase via covalent binding. The immobilization of cellulase was finished in a very short time (10 min) and very high immobilization yield and efficiency of above 90% were achieved after optimization. When compared with the free cellulase, thermal and operational stabilities of the immobilized cellulase were improved significantly. At 50 °C, the half-life of the immobilized cellulase (533 min) was six-fold higher than that of the free cellulase (89 min). Additionally, the affinity between immobilized cellulase (Km = 2.19 $g \cdot L^{-1}$) and substrate was more favorable than that of free cellulase (Km = 3.84 $g \cdot L^{-1}$), suggesting the immobilized cellulase has higher catalytic efficiency. The possible immobilization mechanism was proposed. The results strongly indicate that the immobilization is highly efficient and has great potential for the immobilization of other enzymes.

Keywords: Graphene hybrid; Surface modification; Cellulase; Immobilization; Stability

1. Introduction

Cellulase (E.C 3.2.14) is widely used in the detergent, food, textile, and animal husbandry industries. It can catalyze hydrolyzing β-1,4-glycosidic bonds of the cellulosic materials to produce glucose that could be further bioconverted into bioethanol [1]. Because cellulosic materials are the most abundant materials and renewable resource in the world, the enzymatic conversion process for biofuels has enormous potential and it been received increasing attentions. However, free cellulase is inevitable to have some drawbacks such as instability, difficult separation from the reaction solution, and low reuse possibility [2]. In order to overcome these shortcomings, immobilization was introduced to improve the performance of cellulase in the biocatalysis, finally to lower the cost to meet the industrial requirements.

In the past few years, cellulase has been immobilized with various methods. Mabarak et al. [3] immobilized cellulase onto multiwall carbon nanotubes with adsorption, and the immobilized enzyme retained 52% initial activity after six cycles. When compared with the adsorption, covalent binding is more attractive because of the stable covalent bonds formed during the immobilization. Cellulase was covalently immobilized onto magnetic chitosan nanoparticles [4] and polyaniline coated

polymer microspheres [5], Au-nanoparticles [6], pH-sensitive copolymer [7], and the high stability and reusability of the immobilized enzyme were achieved in these research works.

Immobilization of an enzyme involves the interactions between the enzyme and the carrier [8–12]. The properties of the carrier play an important role and normally the carrier should have large surface area [13–15]. Graphene with a lamellar structure has many industrial applications due to its unique physical and electronic properties [16]. Graphene oxide (GO), as an oxygenated of graphene, has gained increasing attention for its application in biotechnology because it contains oxygen-containing functional groups such as epoxide, hydroxyl, and carboxylic acids [17]. In addition, GO has some significant advantages, including easy processing, simple production from graphite, and available sites for functionalization [18]. Particularly, GO is afforded an ideal carrier for enzyme immobilization after functionalization, and it has been used as the carrier for immobilization of enzymes [2,19–22].

Appropriate spacer between the enzyme and carrier has been proved to improve the activity of the immobilized enzyme [23]. In the immobilization of trypsin, PEG-diamine, aldehyde dextran, amino dextran, and bovine serum albumin (BSA) spacers were investigated. It is indicated that longer spacers are required for the efficient immobilization of enzymes onto solid carriers because they will minimize steric hindrance and environmental effects that are imposed by the surface properties of the matrices [24]. However, when poly glycine linker was used as the spacer for immobilization of α-chymotrypsin onto controlled pore glass and polyethylene glycol copolymer cross-linked with polyacrylamide, it was found that 2 glycines were the optimal linker length [25]. Introducing of appropriate spacer will change the unfavorable surface polarity of the carrier, causing the enzymatic denaturation and preventing the steric hindrance [26].

In the present work, we prepared graphene oxide as carrier for immobilization of cellulase with covalent binding (shown in Scheme 1). The prepared graphene oxide was activated by etherification with p-β-sulfuric acid ester ethyl sulfone aniline (SESA) as a hydrophobic spacer. The obtained SESA-GO was modified by diazotization, and then cellulase was rapidly covalently immobilized onto the activated functional GO. Characterization of the prepared carrier and the final immobilized cellulase were also performed.

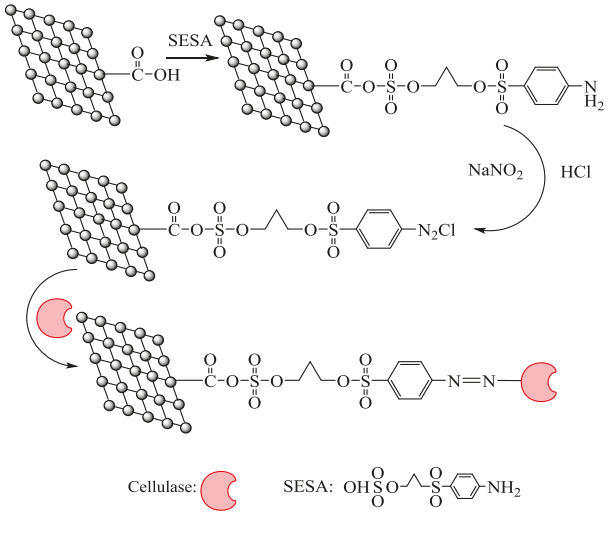

Scheme 1. Schematic description of preparation of functionalized graphene oxide (GO) and immobilization of cellulase.

2. Results

2.1. Characterization of Activated Graphene Oxide

The Fourier transform infrared (FTIR) spectra of GO and SESA-GO were presented in Figure 1. As shown in Figure 1a, the characteristic band of carbonyl groups at ~1710 cm^{-1} corresponding to v (C=O) of –COOH on the GO, and the C–O vibration of epoxy groups appeared at ~1052 cm^{-1} before activation. The peak at ~3383 cm^{-1} and ~1618 cm^{-1} corresponded to the O–H and C=C vibration, respectively. The peak at ~1710 cm^{-1} in Figure 1b disappeared which indicated that –COOH was modified obviously.

The morphologies of GO and immobilized cellulase were observed by TEM. Figure 2a shows that irregular sheets of GO with some wrinkles which presented a larger surface area. Cellulase molecular were not observed clearly in Figure 2b. There is not much difference between Figure 2a,b, indicating that immobilization of cellulase onto the surface of GO did not change the morphology of GO significantly.

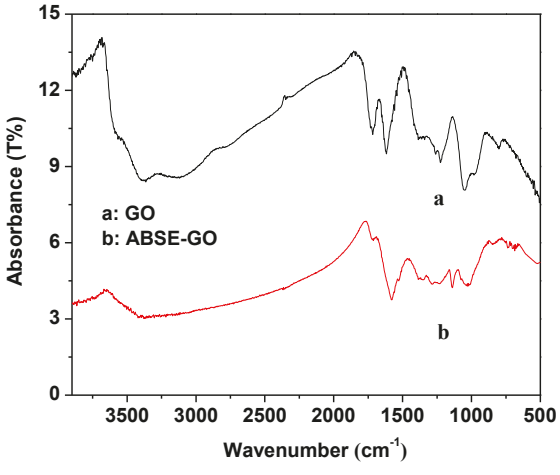

Figure 1. Fourier transform infrared (FTIR) spectra of (**a**) graphene oxide (GO); and, (**b**) SESA-GO.

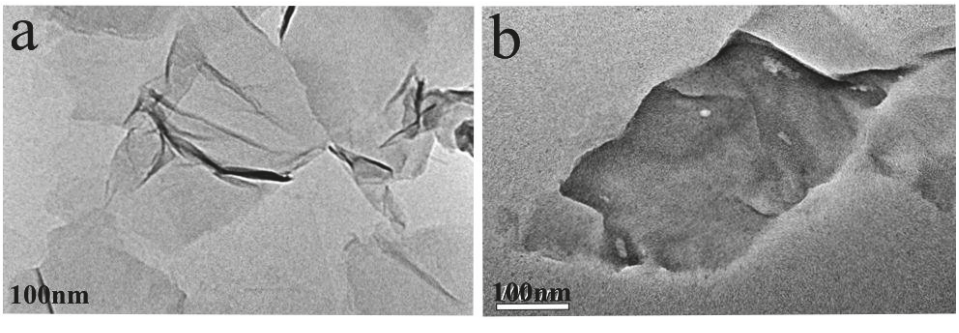

Figure 2. TEM images of (**a**) GO; (**b**) immobilized cellulase.

2.2. Optimization of the Immobilization Conditions

As shown in Figure 3, the activity of the immobilized enzyme was increased with the increasing pH in the reactions. The maximum enzyme activity could be obtained when couple pH was 5.0,

which is the isoelectronic point of cellulase. If the pH was further increased, the activity of immobilized cellulase would be decreased. The immobilization process time course was checked from 1 min to 60 min. As shown in Figure 4, immobilization yield and efficiency were increased rapidly when immobilization time was prolonged from 1 to 10 min. After 10 min, the yield and efficiency reached a plateau, and as time was continued to increase to 60 min, the immobilization yield and the activity recovery changed only a little. Obviously, this reaction was finished within 10 min and the optimal immobilization time was determined as 10 min. The immobilization yield and activity recovery for carrier incubated with cellulase solution of different concentrations were shown in Figure 5. With rising enzyme/support ratio until it reached 4.9 mg·g^{-1}, the yield and efficiency were increased gradually. The maximum yield along with the highest efficiency were achieved at 4.9 mg·g^{-1} and the values were 94% and 91%, respectively. However, further increasing in ratio decreased the immobilization yield and activity recovery linearly, with a similar tendency.

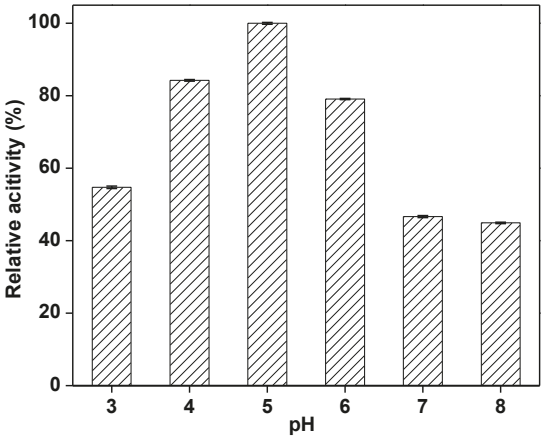

Figure 3. Effect of immobilization pH value on the immobilization of cellulase.

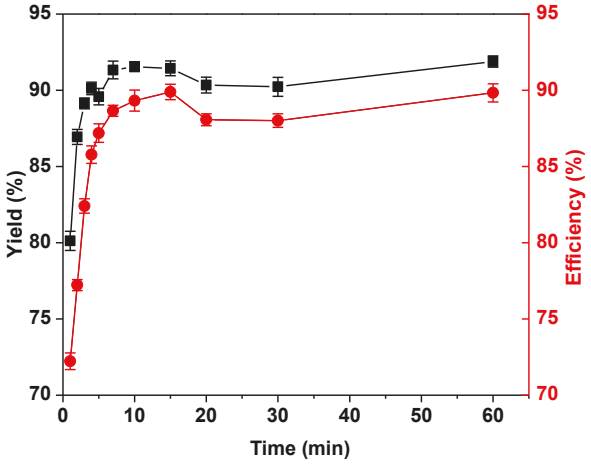

Figure 4. Time course of the immobilization of cellulase onto the functionalized graphene oxide composites.

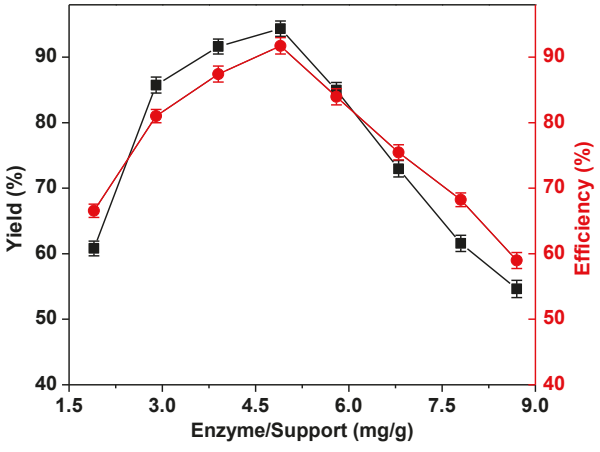

Figure 5. Effect of enzyme/support ratio on the immobilization of cellulase.

2.3. Characterization of the Immobilized Cellulase

The relative activity of free and immobilized cellulase were evaluated in the pH range from 3.0 to 8.0 and 30 to 80 °C (Figure 6). The maximal activities of the free and immobilized cellulase were observed at pH 5.0, as shown in Figure 6a. The immobilized cellulase showed a significant higher relative activity than that of free cellulase at pH from 3.0 to 6.0. It is noted that the relative activity of immobilized cellulase was approximately two-fold higher than those of free cellulase at pH 3.0~4.0. Figure 6b shows the effect of temperature on the activity of immobilized and free cellulase. The optimal temperature (50 °C) of the immobilized enzyme was the same as the free cellulase. The immobilized cellulase displayed relative higher activities at the temperature range from 30 to 80 °C when compared with the free cellulase. The kinetic parameters K_m of the immobilized and free cellulase were calculated with nonlinear regression as shown in Figure 7, and they were 2.19 $g{\cdot}L^{-1}$ and 3.84 $g{\cdot}L^{-1}$, while V_{max} were 0.27 $g{\cdot}L^{-1}$ min^{-1} and 0.23 $g{\cdot}L^{-1}$ min^{-1}, respectively. The thermal stability and reusability as important parameters for immobilized cellulase were investigated at 50 °C within 3 h, and the results were shown in Figures 8 and 9. As shown in Figure 8, the relative activity of free and immobilized decreased with the increase of incubation time, the activity of free cellulase decreased sharply than that of the immobilized cellulase. When the incubation time was raised to 3 h, the immobilized cellulase remained above 85% of its original activity, while the free cellulase was only 67% of its original activity. The thermal deactivation constant (kd) of the immobilized cellulase (0.013) was six-fold lower than that of the free enzyme (0.078). The values of half-lives for the free and immobilized cellulase were 533 min and 89 min, respectively. There is a five-fold improvement than that of the free cellulase. The reusability of the immobilized enzyme was checked, as shown in Figure 9. It still had 90% and 80% residual activities after four and nine reaction cycles, respectively.

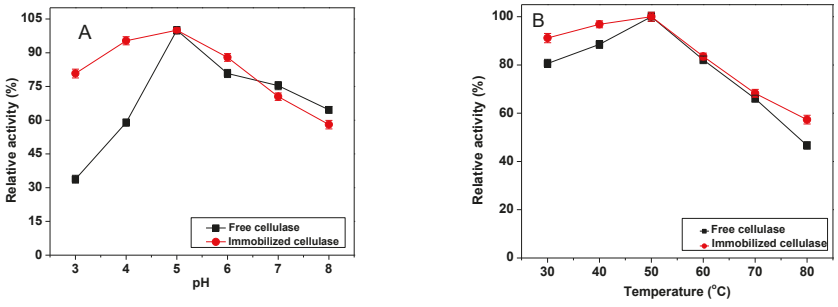

Figure 6. Effects of pH value (**A**) and temperature (**B**) on the activity of free (square) and immobilized cellulase (circle).

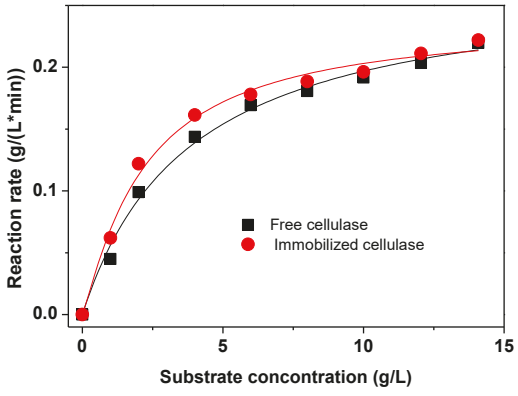

Figure 7. Effect of reaction rate on the substrate concentration of free cellulase (square) and immobilized cellulase (circle).

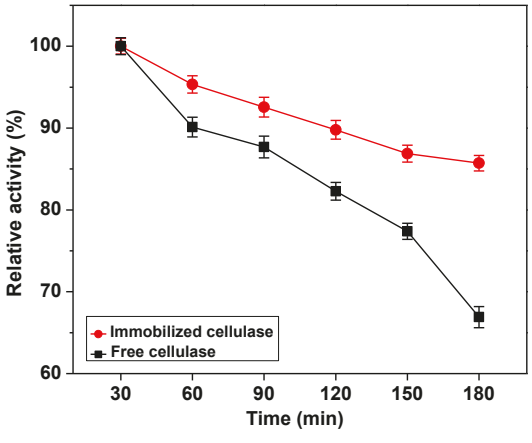

Figure 8. The thermal stability of free cellulase (square) and immobilized (circle) at 50 °C.

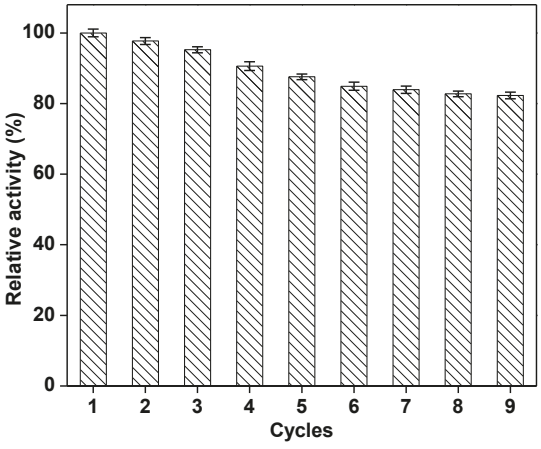

Figure 9. The reusability of the immobilized cellulase.

3. Discussion

Immobilization of enzymes has received wide attention because of the high cost of enzymes. It is well known that GO contained epoxy, carbonyl, and hydroxyl groups [27] and the modification is easier than other nanoparticles [28–33]. In our previous work, GO derivatives were used as the carrier for immobilization of cellulose [2] and NADH oxidase [22], and the immobilized enzyme retain higher stability and good reusability. In the present work, functionalized GO was prepared by etherification and diazotization (Scheme 1). The changes of FTIR peaks indicated that GO was successful prepared and activated. Subsequently, cellulase was covalently coupled onto the functionalized GO, and the factors, including pH, initial concentration of protein and immobilization time were optimized. A high immobilization yield and activity recovery of above 90% were achieved. When compared with the free enzyme, the immobilized cellulase displayed high relative activity in a wide range of pH, especially pH 3–5. It might be induced by covalent immobilization that fixed the configuration of enzyme on the surface of supports, resulting in the tolerability of cellulase to pH in surroundings increased [34]. In addition, owing to the unique properties of functionalized GO, such as high surface area and more binding-sites, the microenvironment of the immobilization process could have been buffered [35]. When compared with free enzyme, the lower K_m and the higher V_{max} demonstrated the high binding affinity to substrates. The higher relative enzyme activity for immobilized cellulase would be due to the hydrophobic spacer SESA. The proper length and hydrophobic property of the spacer would restrict the immobilized enzyme mobile range and improve the mobile frequency, and thus the immobilized showed higher substrate binding affinity. Another reason for this phenomenon probably is that the activated GO has many hydrophilic groups on the surface that could enrich substrates nearby, and this will present more chances for substrate to bind enzymes.

The immobilized cellulase showed higher relative activity at higher temperatures. It is possible because the functional GO has high special surface area, thermal tolerance, and mechanical hardness. These properties would increase the stabilization of cellulase and could keep its active structure even at a higher temperature [36]. The very good reusability of immobilized cellulase makes the process catalyzed by cellulase much economic. A higher residual activity after reusing was because of the strong covalent bonds between the enzyme molecules and the prepared carrier. The decrease in immobilized enzyme activity was possibly caused by several reasons including unavoidable enzyme deactivation during repeated operation and batch separation.

As an important factor affected the productivity and the economic benefit in the industrial production, the immobilization time was investigated. It is interesting that the immobilization yield

reached 90% within 10 min. Comparison with the previous reports [7,37–39] (as shown in Table 1), the immobilization of cellulase is in this work is quite quick and efficient. The reason might be the contribution of hydrophilic groups of GO and the hydrophobic spacer.

Table 1. Comparison of different carrier for covalent immobilization of cellulase.

Carrier	Spacer	Km ($g \cdot L^{-1}$)	Stability [1]	Immobilization Time	Reference
Clay composite materials	-	-	1.4	8 h	[39]
polyacrylate amphiphilic copolymer	carbodiimide	120.89	1.2	4 h	[7]
polyamidoamine dendrimer-grafted silica	glutaraldehyde	0.33	2.2	2 h	[37]
PVA membrane	-	-	-	1 h	[38]
Graphene oxide	SESA	2.17	2.1	10 min	This work

[1] Folds compared to the free counterpart.

In summary, graphene oxide was prepared and modified with SESA for immobilization for cellulase. The immobilization of cellulase was very fast and finished in 10 min. The preparation process is simple and a high activity recovery (above 90%) was obtained. In comparison with the free cellulase, the immobilized enzyme showed higher affinity to substrate. Furthermore, the good reusability and high thermal stability of immobilized cellulase make them rather charming for industrial applications.

4. Materials and Methods

4.1. Materials

Cellulase was obtained from Runyang Co. Ltd. (Wuxi, China). P-β-sulfuric acid ester ethyl sulfone aniline (SESA) was purchased from Sigma-aldrich (St. Louis, MO, USA). Bovine serum albumin from Bio-Rad (Hercules, CA, USA) was used as the standard protein. Carboxyl methyl cellulose (CMC) salt (medium viscosity), graphite powder, sodium nitrite, and the other chemicals were biotechnological or analytical reagents from Sinopharm (Shanghai, China).

4.2. Preparation of Functional Graphene Oxide

The synthesis of graphene oxide (GO) via a slight modified method developed by Hummers and Offerman [40]. Briefly, suspended 1 g of graphite powder in 25 mL sulfuric acid (98%) under ice bath, and then added $NaNO_3$ (1 g) and $KMnO_4$ (3 g), respectively. The resultant suspension was vigorous stirred and cooled, so as to maintain the temperature of the mixture under 20 °C. Then, the mixture was heated to 35 °C and was stirred 30 min. The reaction temperature was increased to 90 °C and followed by slowly adding 50 mL of distilled water and stirred 1 h. To stop the oxidation reaction, 40 mL of distilled water and 3 mL of 30% hydrogen peroxide solution were added sequentially. Then, the mixture was filtered, and washed with double-distilled water. The product was then resuspended in double-distilled water, and ultrasonicated 5 min. The resultant nanoparticles were collected by centrifugation and drying 24 h at 40 °C under vacuum.

To successfully obtain the immobilized enzyme via covalent immobilization, the carrier was activated primarily via etherification and diazotization. In brief, dissolve 0.5 g SESA in 6 mL deionized water. The pH was adjusted to 7.0 at 40 °C using 1.0 M Na_2CO_3. Added 0.5 g of GO into the above solution with stirring, and adjusted the pH to 13.0 with 0.5 M NaOH solution. In order to obtain the SESA-GO, the mixture was subjected to heat 30 min at 100 °C and then washed twice with 0.05 M NaOH solution and deionized water, respectively. Subsequently, SESA-GO was suspended in 5 mL distilled water, and then 2.5 mL HCl (1 M) and 2.5 mL $NaNO_2$ (5%) were added simultaneously. The reaction was sustained 30 min under ice bath for finishing the diazotization. The resultant was washed three times with 0.05 M HCl and dried 12 h with vacuum drier.

Characterization of the prepared particles with Fourier transform infrared (FTIR) spectra was performed with a spectrometer (FT-IR, Thermo NicoletAVATAR-370, Waltham, MA, USA) using

the KBr pellet technique. The morphology of materials was observed with Transmission electron microscopy (TEM, Philips Tecnai 12, Holland).

4.3. Immobilization of Cellulase

Dispersed 50 mg modified carrier in 0.7 mL citrate buffer (0.1 M, pH 5.0), and added 0.3 mL buffers containing cellulase to start the immobilization. After 1 h reaction at room temperature, the immobilized cellulase was collected by centrifugation and washed three times with citrate buffer (0.1 M pH 5.0). The protein concentration of the supernatant was measured by the Bradford method [41] and the activity of immobilized cellulase was determined. The immobilization yield and activity recovery were calculated, as the follows:

$$\text{Immobilization yield} = 100 \times [(\varrho i - \varrho w - \varrho s)/\varrho i]; \text{Activity recovery} = 100 \times (\alpha i/\alpha f) \quad (1)$$

where ϱi is the total protein of the crude enzyme preparation; ϱw and ϱs are the protein content of wash solution and supernatant after immobilization, respectively; αi is the total activity of the immobilized cellulase; and, αf is the total activity of the free cellulase. All of the assays were performed in triplicate.

4.4. Enzyme Assay

The activity of cellulase was detected based on the amount of released glucose from CMC solution under the catalysis of cellulase. For free enzyme, 0.25 mL enzyme was pre-incubated 10 min at 50 °C. Then, the mixture of 0.25 mL enzyme that was dissolved in acetate buffer (pH 5.0) and 0.5 mL substrate (*w*/*v* = 2%) were incubated at 50 °C for 10 min. Then, added 3 mL DNS to the mixture and terminated the reaction by heating the mixture 5 min in boiled water. The produced reducing sugar was measured with a UV detector (UV-1800, Mapada instrument, Shanghai, China) at 540 nm. For immobilized enzyme, 50 mg of immobilized enzyme was pre-incubated 10 min at 50 °C. Then, 0.5 mL of substrate was added into to react 10 min. The reaction was terminated by adding 3 mL DNS and put into boiled water bath for 5 min. After separation, the supernatant was subjected to determine the concentration of glucose to calculate the activity. One unit (U) of cellulase is defined as the amount of enzyme that hydrolyzes CMC in order to produce 1 mg equivalent of glucose per minute under the assay conditions.

4.5. Optimization of Immobilization Conditions

The effect of pH on the immobilization was assessed over the range of pH (3.0–8.0). Similarly, the mixture of varying enzyme/support ratios from 1.9 to 8.7 mg/g in the pH range of 3.0 to 8.0 was reacted in the various time periods ranging from 1 min to 60 min. After certain time intervals, the mixture was separated by centrifugation of 5 min at 12,000 rpm. Subsequently, the amount of the protein in the supernatant was determined. Each experiment was performed in triplicate. The optimization data are presented as the averages of statistically relevant measurements with their associated standard deviation.

4.6. Characterization of the Immobilized Cellulase

The effect of temperature on the activities of free and immobilized cellulase was evaluated by assaying the enzyme samples over the range of 30–80 °C for 10 min. To check the effect of pH, activities of immobilized and free cellulase were determined using the standard assay conditions with two buffer systems, citrate buffer (0.1 M, pH 3.0, 4.0, 5.0) and phosphate buffer (0.1 M, pH 6.0, 7.0, 8.0). To determine maximum reaction rates (V_{max}) and kinetic parameters (K_m) of free and immobilized cellulase, the activity assays were performed in different CMC concentrations. Vmax and Km of cellulase was obtained by nonlinear regression.

The thermal stability of cellulase was investigated by incubating the free and immobilized enzyme from 30 to 180 min at optimal pH and at 50 °C. At certain time intervals, samples were withdrawn,

and residual activity was measured under standard assay conditions. The half-life ($t_{1/2}$) of cellulase at 50 °C was determined using the following equation:

$$t1/2 = 0.693/kd; kd*t = \ln(E_0/E) \quad (2)$$

where E_0 is the initial cellulase activity, E is the residual cellulase activity after t min, and kd is the attenuation constant.

The reusability of immobilized cellulase was investigated at the optimal pH and temperature. Each sample was performed in triplicate. The characterization data are presented as the averages of statistically relevant measurements with their associated standard deviation.

Author Contributions: J.G. and Y.-W.Z. conceived and designed the experiments; J.G., C.-L.L., Y.W., S.-S.W. and J.-J.S. performed the experiments; J.G., C.-L.L. and Y.W. analyzed the data; J.G. and Y.-W.Z. wrote the paper. J.-X.Z. instructed experiments design.

Acknowledgments: The authors appreciate the financial support from National Natural Science Foundation of China (No. 21376110) and Guangxi Natural Science Foundation (2016GXNSFCA380011).

Conflicts of Interest: The authors declare no conflict of interest.

References

1. Hamid, S.B.A.; Islam, M.M.; Das, R. Cellulase biocatalysis: Key influencing factors and mode of action. *Cellulose* **2015**, *22*, 2157–2182. [CrossRef]
2. Li, Y.; Wang, X.-Y.; Jiang, X.-P.; Ye, J.-J.; Zhang, Y.-W.; Zhang, X.-Y. Fabrication of graphene oxide decorated with Fe_3O_4@SiO_2 for immobilization of cellulase. *J. Nanopart. Res.* **2015**, *17*, 1–12. [CrossRef]
3. Mubarak, N.M.; Wong, J.R.; Tan, K.W.; Sahu, J.N.; Abdullah, E.C.; Jayakumar, N.S.; Ganesan, P. Immobilization of cellulase enzyme on functionalized multiwall carbon nanotubes. *J. Mol. Catal. B Enzym.* **2014**, *107*, 124–131. [CrossRef]
4. Zang, L.; Qiu, J.; Wu, X.; Zhang, W.; Sakai, E.; Wei, Y. Preparation of magnetic chitosan nanoparticles as support for cellulase immobilization. *Ind. Eng. Chem. Res.* **2014**, *53*, 3448–3454. [CrossRef]
5. Ince, A.; Bayramoglu, G.; Karagoz, B.; Altintas, B.; Bicak, N.; Arica, M.Y. A method for fabrication of polyaniline coated polymer microspheres and its application for cellulase immobilization. *Chem. Eng. J.* **2012**, *189–190*, 404–412. [CrossRef]
6. Cho, E.J.; Jung, S.; Kim, H.J.; Lee, Y.G.; Nam, K.C.; Lee, H.-J.; Bae, H.-J. Co-immobilization of three cellulases on Au-doped magnetic silica nanoparticles for the degradation of cellulose. *Chem. Commun.* **2011**, *48*, 886–888. [CrossRef] [PubMed]
7. Liang, W.; Cao, X. Preparation of a pH-sensitive polyacrylate amphiphilic copolymer and its application in cellulase immobilization. *Bioresour. Technol.* **2012**, *116*, 140–146. [CrossRef] [PubMed]
8. Li, Y.; Wang, X.-Y.; Zhang, R.-Z.; Zhang, X.-Y.; Liu, W.; Xu, X.-M.; Zhang, Y.-W. Molecular Imprinting and Immobilization of Cellulase onto Magnetic Fe3O4@SiO2 Nanoparticles. *J. Nanosci. Nanotechnol.* **2014**, *14*, 2931–2936. [CrossRef] [PubMed]
9. Ling, X.-M.; Wang, X.-Y.; Ma, P.; Yang, Y.; Qin, J.-M.; Zhang, X.-J.; Zhang, Y.-W. Covalent immobilization of penicillin G acylase onto Fe_3O_4@Chitosan magnetic nanoparticles. *J. Microbiol. Biotechnol.* **2016**, *26*, 829–836. [CrossRef] [PubMed]
10. Tao, Q.-L.; Li, Y.; Shi, Y.; Liu, R.-J.; Zhang, Y.-W.; Guo, J. Application of molecular imprinted magnetic Fe_3O_4@SiO_2 nanoparticles for selective immobilization of cellulase. *J. Nanosci. Nanotechnol.* **2016**, *16*, 6055–6060. [CrossRef] [PubMed]
11. Zhuang, M.-Y.; Zhou, Q.-L.; Wang, X.-Y.; Zhang, J.-X.; Xue, L.; Wang, R.; Zhang, J.-X.; Zhang, Y.-W. Immobilization of lipase onto dopamine functionalized magnetic nanoparticles. *Nanosci. Nanotechnol. Lett.* **2016**, *8*, 251–254. [CrossRef]
12. Zhuang, M.-Y.; Jiang, X.-P.; Ling, X.-M.; Xu, M.-Q.; Zhu, Y.-H.; Zhang, Y.-W. Immobilization of glycerol dehydrogenase and NADH oxidase for enzymatic synthesis of 1,3-dihydroxyacetone with in situ cofactor regeneration. *J. Chem. Technol. Biotechnol.* **2018**, *93*. [CrossRef]

13. Wang, X.-Y.; Jiang, X.-P.; Li, Y.; Zeng, S.; Zhang, Y.-W. Preparation Fe_3O_4@chitosan magnetic particles for covalent immobilization of lipase from *Thermomyces lanuginosus*. *Int. J. Biol. Macromol.* **2015**, *75*, 44–50. [CrossRef] [PubMed]
14. Zhuang, M.-Y.; Wang, C.; Xu, M.-Q.; Ling, X.-M.; Shen, J.-J.; Zhang, Y.-W. Using concanavalinA as a spacer for immobilization of *E. coli* onto magnetic nanoparticles. *Int. J. Biol. Macromol.* **2017**, *104*, 63–69. [CrossRef] [PubMed]
15. Liu, W.; Zhou, F.; Zhang, X.-Y.; Li, Y.; Wang, X.-Y.; Xu, X.-M.; Zhang, Y.-W. Preparation of magnetic Fe_3O_4@SiO_2 nanoparticles for immobilization of lipase. *J. Nanosci. Nanotechnol.* **2014**, *14*, 3068–3072. [CrossRef] [PubMed]
16. Chowdhury, S.; Balasubramanian, R. Graphene/semiconductor nanocomposites (GSNs) for heterogeneous photocatalytic decolorization of wastewaters contaminated with synthetic dyes: A review. *Appl. Catal. B Environ.* **2014**, *160–161*, 307–324. [CrossRef]
17. Lee, H.; Jeong, H.K.; Han, J.; Chung, H.-S.; Jang, S.-H.; Lee, C. Increased thermal stability of cold-adapted esterase at ambient temperatures by immobilization on graphene oxide. *Bioresour. Technol.* **2013**, *148*, 620–623. [CrossRef] [PubMed]
18. Mani, V.; Devasenathipathy, R.; Chen, S.-M.; Huang, S.-T.; Vasantha, V.S. Immobilization of glucose oxidase on graphene and cobalt phthalocyanine composite and its application for the determination of glucose. *Enzyme Microb. Technol.* **2014**, *66*, 60–66. [CrossRef] [PubMed]
19. Gokhale, A.A.; Lu, J.; Lee, I. Immobilization of cellulase on magnetoresponsive graphene nano-supports. *J. Mol. Catal. B Enzym.* **2013**, *90*, 76–86. [CrossRef]
20. Liu, J.; Wang, T.; Wang, J.; Wang, E. Mussel-inspired biopolymer modified 3D graphene foam for enzyme immobilization and high performance biosensor. *Electrochim. Acta* **2015**, *161*, 17–22. [CrossRef]
21. Wang, J.; Zhao, G.; Jing, L.; Peng, X.; Li, Y. Facile self-assembly of magnetite nanoparticles on three-dimensional graphene oxide-chitosan composite for lipase immobilization. *Biochem. Eng. J.* **2015**, *98*, 75–83. [CrossRef]
22. Liu, C.-H.; Li, X.-Q.; Jiang, X.-P.; Zhuang, M.-Y.; Zhang, J.-X.; Bao, C.-H.; Zhang, Y.-W. Preparation of functionalized graphene oxide nanocomposites for covalent immobilization of NADH oxidase. *Nanosci. Nanotechnol. Lett.* **2016**, *8*, 164–167. [CrossRef]
23. Andre, J.; Saleh, D.; Syldatk, C.; Hausmann, R. Effect of spacer modification on enzymatic synthetic and hydrolytic activities of immobilized trypsin. *J. Mol. Catal. B Enzym.* **2016**, *125*, 88–96. [CrossRef]
24. Nouaimi, M.; Moschel, K.; Bisswanger, H. Immobilization of trypsin on polyester fleece via different spacers. *Enzyme Microb. Technol.* **2001**, *29*, 567–574. [CrossRef]
25. Deere, J.; De Oliveira, R.F.; Tomaszewski, B.; Millar, S.; Lalaouni, A.; Solares, L.F.; Flitsch, S.L.; Halling, P.J. Kinetics of enzyme attack on substrates covalently attached to solid surfaces: Influence of spacer chain length, immobilized substrate surface concentration and surface charge. *Langmuir* **2008**, *24*, 11762–11769. [CrossRef] [PubMed]
26. Du, T.; Liu, B.; Hou, X.; Zhang, B.; Du, C. Covalent immobilization of glucose oxidase onto Poly(St-GMA-NaSS) monodisperse microspheres via BSA as spacer arm. *Appl. Surf. Sci.* **2009**, *255*, 7937–7941. [CrossRef]
27. Hu, Y.; Wang, K.; Zhang, Q.; Li, F.; Wu, T.; Niu, L. Decorated graphene sheets for label-free DNA impedance biosensing. *Biomaterials* **2012**, *33*, 1097–1106. [CrossRef] [PubMed]
28. Xiong, F.; Hu, K.; Yu, H.; Zhou, L.; Song, L.; Zhang, Y.; Shan, X.; Liu, J.; Gu, N. A functional iron oxide nanoparticles modified with PLA-PEG-DG as tumor-targeted MRI contrast agent. *Pharm. Res.* **2017**, *34*, 1683–1692. [CrossRef] [PubMed]
29. Xie, M.; Xu, Y.; Shen, H.; Shen, S.; Ge, Y.; Xie, J. Negative-charge-functionalized mesoporous silica nanoparticles as drug vehicles targeting hepatocellular carcinoma. *Int. J. Pharmaceut.* **2014**, *474*, 223–231. [CrossRef] [PubMed]
30. Shen, S.; Wu, L.; Liu, J.; Xie, M.; Shen, H.; Qi, X.; Yan, Y.; Ge, Y.; Jin, Y. Core–shell structured Fe_3O_4@TiO_2-doxorubicin nanoparticles for targeted chemo-sonodynamic therapy of cancer. *Int. J. Pharmaceut.* **2015**, *486*, 380–388. [CrossRef] [PubMed]
31. Zhu, T.; Tao, Z.; Jia, L.; Luo, Y.-F.; Xu, J.; Chen, R.-H.; Ge, Z.-J.; Ma, T.-L.; Chen, H. Multifunctional nanocomposite based on halloysite nanotubes for efficient luminescent bioimaging and magnetic resonance imaging. *Int. J. Nanomed.* **2016**, *11*, 4765–4776. [CrossRef] [PubMed]

32. Ali, S.; Morsy, R.; El-Zawawy, N.; Fareed, M.; Bedaiwy, M. Synthesized zinc peroxide nanoparticles (ZnO2-NPs): a novel antimicrobial, anti-elastase, anti-keratinase, and anti-inflammatory approach toward polymicrobial burn wounds. *Int. J. Nanomed.* **2017**, *12*, 6059–6073. [CrossRef] [PubMed]
33. Liu, H.; Shi, S.; Cao, J.; Ji, L.; He, Y.; Xi, J. Preparation and evaluation of a novel bioactive glass/lysozyme/PLGA composite microsphere. *Drug Dev. Ind. Pharm.* **2015**, *41*, 458–463. [CrossRef] [PubMed]
34. Mateo, C.; Palomo, J.M.; Fernandez-Lorente, G.; Guisan, J.M.; Fernandez-Lafuente, R. Improvement of enzyme activity, stability and selectivity via immobilization techniques. *Enzyme Microb. Technol.* **2007**, *40*, 1451–1463. [CrossRef]
35. Li, T.; Li, S.; Wang, N.; Tain, L. Immobilization and stabilization of pectinase by multipoint attachment onto an activated agar-gel support. *Food Chem.* **2008**, *109*, 703–708. [CrossRef] [PubMed]
36. Tang, T.; Fan, H.; Ai, S.; Han, R.; Qiu, Y. Hemoglobin (Hb) immobilized on amino-modified magnetic nanoparticles for the catalytic removal of bisphenol A. *Chemosphere* **2011**, *83*, 255–264. [CrossRef] [PubMed]
37. Wang, S.; Su, P.; Ding, F.; Yang, Y. Immobilization of cellulase on polyamidoamine dendrimer-grafted silica. *J. Mol. Catal. B-Enzym.* **2013**, *89*, 35–40. [CrossRef]
38. Wu, L.L.; Yuan, X.Y.; Sheng, J. Immobilization of cellulase in nanofibrous PVA membranes by electrospinning. *J. Membr. Sci.* **2005**, *250*, 167–173. [CrossRef]
39. Bayramoglu, G.; Senkal, B.F.; Arica, M.Y. Preparation of clay–poly(glycidyl methacrylate) composite support for immobilization of cellulase. *Appl. Clay Sci.* **2013**, *85*, 88–95. [CrossRef]
40. Hummers, W.S., Jr.; Offeman, R.E. Preparation of graphitic oxide. *J. Am. Chem. Soc.* **1958**, *80*, 1339. [CrossRef]
41. Bradford, M.M. A rapid and sensitive method for the quantitation of microgram quantities of protein utilizing the principle of protein-dye binding. *Anal. Biochem.* **1976**, *72*, 248–254. [CrossRef]

© 2018 by the authors. Licensee MDPI, Basel, Switzerland. This article is an open access article distributed under the terms and conditions of the Creative Commons Attribution (CC BY) license (http://creativecommons.org/licenses/by/4.0/).

catalysts

MDPI

Article

Immobilization of Cellulase on a Functional Inorganic–Organic Hybrid Support: Stability and Kinetic Study

Jakub Zdarta *, Artur Jędrzak, Łukasz Klapiszewski and Teofil Jesionowski *

Institute of Chemical Technology and Engineering, Faculty of Chemical Technology, Poznan University of Technology, Berdychowo 4, PL-60965 Poznan, Poland; artur.jedrzak@gmail.com (A.J.); lukasz.klapiszeswki@put.poznan.pl (Ł.K.)

* Correspondence: jakub.zdarta@put.poznan.pl (J.Z.); teofil.jesionowski@put.poznan.pl (T.J.); Tel.: +48-616-65-3747 (J.Z.); +48-616-65-3720 (T.J.)

Received: 7 November 2017; Accepted: 29 November 2017; Published: 1 December 2017

Abstract: Cellulase from *Aspergillus niger* was immobilized on a synthesized TiO_2–lignin hybrid support. The enzyme was effectively deposited on the inorganic–organic hybrid matrix, mainly via physical interactions. The optimal initial immobilization parameters, selected for the highest relative activity, were pH 5.0, 6 h process duration, and an enzyme solution concentration of 5 mg/mL. Moreover, the effects of pH, temperature, and number of consecutive catalytic cycles and the storage stability of free and immobilized cellulase were evaluated and compared. Thermal and chemical stability were significantly improved, while after 3 h at a temperature of 50 °C and pH 6.0, the immobilized cellulase retained over 80% of its initial activity. In addition, the half-life of the immobilized cellulase (307 min) was five times that of the free enzyme (63 min). After ten repeated catalytic cycles, the immobilized biocatalyst retained over 90% of its initial catalytic properties. This study presents a protocol for the production of highly stable and reusable biocatalytic systems for practical application in the hydrolysis of cellulose.

Keywords: enzyme immobilization; cellulases; titania-lignin hybrid; immobilized cellulase stability; cellulose hydrolysis

1. Introduction

Cellulases are classified as hydrolytic enzymes [1] and include at least three types of biocatalysts: endo-(1,4)-β-D-glucanase (EC 3.2.1.4), exo-(1,4)-β-D-glucanase (EC 3.2.1.91), and β-glucosidases (EC 3.2.1.21) [2–4]. They are produced by bacteria and microbes; however, the main enzyme acquisition process is based on fungi, which provide the highest production index [1,5,6]. The most frequently used for the production of cellulases are strains of cellulolytic fungi such as *Aspergillus*, *Humicola*, *Penicillium*, and *Trichoderma* [7,8]. Cellulases are responsible for the process of depolymerization of cellulose by delamination of the cell walls, which is a consequence of cellulose hydrolysis [1,6]. These biocatalysts have numerous practical applications in many fields of industry and agriculture. Commercial cellulases have been available for several decades, and have found applications in several important branches of industry, particularly in the wood and cellulose-paper industries, as well as in other branches including the conservation of thermoplastic polymers and plastics, bioconversion of cellulosic materials to organic solvents, fermentation processes, detergents, textiles, laundry, and the food and feed industries [9]. In view of the broad application of these enzymes, it is necessary to develop novel and more stable materials to enable the aforementioned processes to be carried out more efficiently.

Immobilization is a technique of confining cells or enzymes on organic, inorganic, or hybrid carriers [10]. Depending on the method of immobilization, the binding of the biocatalyst may occur

more or less permanently. This technique is intended to increase the efficiency of catalytic processes, reduce the associated costs, and improve the properties of enzymes [10], mainly its stability at harsh reaction conditions, as variable reaction parameters might affect enzymes' properties. Among others, the most important properties are pH and temperature, as protein denaturation is caused mainly by abovementioned parameters [11]. Immobilization of enzymes enables the retention of catalytic activity, which results in the possibility of reusing the biocatalytic system. Moreover, easier and faster separation of immobilized enzymes from the reaction mixture makes them more attractive for industrial applications [11,12]. The immobilization of biocatalysts also prevents protein from entering the process in a mobile phase reactor containing the reagents, resulting in cleaner products [13].

As has already been noted, immobilization processes are of great importance and are used in many branches of industry, mainly in the pharmaceutical, food, chemical, and biological industries, but also in research and implementation of new technological solutions. The use of immobilized enzymes might result in greater process efficiency compared with the use of free biocatalysts, by better utilizing the potential of raw materials [11–14]. Various enzyme immobilization methods have enabled the development of industrial technology on a larger scale, reducing the costs of production. At present, there are several well-known techniques that rely on physical or chemical interactions [11,14]. Immobilized enzymes are a subject of great interest, which will certainly grow, as the properties of many of the biocatalysts are not yet fully known. Furthermore, the possibility of their immobilization may contribute to a steady progress in their development and use in bioprocesses and in the field of biosensing [15,16].

The continuous development of technology helps obtain more effective and stable materials with targeted industrial applications. Nowadays, novel hybrid or composite material with immobilized enzymes, achieved by creating an innovative biocatalytic system, are increasingly used in many fields of industry, like pharmaceutical, chemical, and food industries. A combination of inorganic and organic components can provide advanced features such as better thermal and chemical resistance or electrokinetic and biological stability. For instance, Tao et al., used magnetic Fe_3O_4–SiO_2 nanoparticles for the selective immobilization of cellulase [17]. The novel hybrid material, due to the influence of the metallic oxides, exhibited enhanced adsorption parameters as well as biocompatibility and bioactivity. Similar findings are reported by Velmurugan et al., who confirmed that a newly developed MgO–Fe_3O_4 material was suitable for cellulose immobilization [18]. Furthermore, Hong et al., obtained a polyhedral oligomeric silsesquioxane-silica-titania (POSS–SiO_2–TiO_2) hybrid material for cellulase immobilization for biocatalytic applications [19]. In other studies laccase was successfully immobilized on TiO_2 nanoparticles and TiO_2 nanoparticle functionalized polyethersulfone (PES) membranes. The results revealed that both the immobilization procedures and the properties of the immobilization supports have significant impacts on the biocatalyst performance [20]. In addition, Hou et al. showed in [21] great potential for the application of the TiO_2 based biocatalytic nanoparticles and membranes for CO_2 conversion in a gas–liquid membrane contactor. These examples show that it is extremely important to continue research into the development of novel support materials for enzyme immobilization, which will lead to the creation of more effective and stable biocatalytic systems.

The main research goal of the present study was to evaluate a functional hybrid titanium dioxide–lignin hybrid material in terms of its suitability for the immobilization of cellulase, and to use the resulting biocatalytic system in the hydrolysis process of cellulose. The synthesized hybrid support was concisely characterized, immobilization of the enzyme was confirmed, and the effect of various operational conditions on the enzyme's stability and activity, as well as its reusability and storage stability, were examined.

2. Results

2.1. Synthesis of Titania–Lignin Hybrid Material and Cellulase Immobilization

The thermal stability of the TiO_2 modified by poly-L-lisine (PLL), lignin activated by sodium (meta)periodate and the synthesized TiO_2–lignin hybrid material was determined using thermogravimetric analysis (TGA) (Figure 1). Commercial titanium dioxide after surface modification exhibited extremely high thermal stability, losing only about 2% of its mass in the analyzed temperature range, which might be explained by the evaporation of physically bound water. The thermogravimetric curve of the activated lignin showed a significant decrease in mass of the activated biopolymer consisted in three mass loss stages, at temperatures up to 200 °C (marked in yellow) and in the temperature ranges 200–600 °C (marked in blue) and 650–1000 °C (marked in red), linked respectively to the removal of physically bound water, decomposition of the lignin structure, and elimination of carbon and hydrogen atoms [22]. The synthesized TiO_2–lignin hybrid showed relatively good thermal stability: up to a temperature of 1000 °C it lost about 10% of its mass. The high thermal stability (characteristic for TiO_2) and the shape of the TGA curve for the obtained material, similar to that recorded for lignin, also proved the effective connection of TiO_2 and lignin.

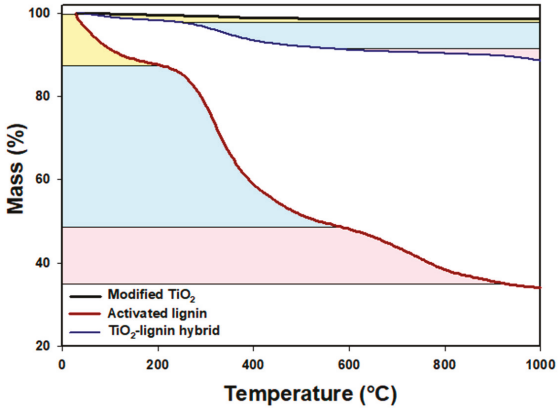

Figure 1. Results of thermogravimetric analysis of modified TiO_2, activated lignin and TiO_2–lignin hybrid.

The Fourier-transform infrared (FTIR) spectrum of the TiO_2–lignin hybrid (Figure 2) contained many signals characteristic for functional groups of both modified precursors, which indirectly confirmed the effective synthesis of the hybrid support. Among these signals, the most important are those at wavenumbers 3450 cm^{-1}, 2940 cm^{-1}, 1680 cm^{-1}, and around 1100 cm^{-1}, attributed respectively to stretching vibrations of –OH groups, C–H bonds, C=O groups, and C–O and C–O–C bonds in the lignin structure [23]. Signals were also observed in the wavenumber range 1600–1450 cm^{-1} and at 720 cm^{-1}, representing, respectively, stretching vibrations of C_{Ar}–C_{Ar} bonds in the structure of the biopolymer, and Ti–O–Ti bonds.

In the FTIR spectrum of free cellulase from *Aspergillus niger*, the most important signal is that at 3430 cm^{-1}, characteristic for amine groups, which are mainly responsible for attachment of the enzyme to the solid support, as well as peaks around 1665 cm^{-1} and 1530 cm^{-1}, generated by stretching vibrations of amide I and amide II bands. The FTIR spectrum of the produced biocatalytic system contains signals characteristic for cellulase as well as for the hybrid matrix. This suggested that the biocatalyst was successfully deposited on the surface of the support material. This is proven by the presence of a peak at 1090 cm^{-1} (C–N stretching vibrations) and changes in the intensity of signals generated by amine groups (3430 cm^{-1}), C–H bonds (2930 cm^{-1}), and amide bands, in comparison with the FTIR spectrum of the TiO_2–lignin hybrid before enzyme binding.

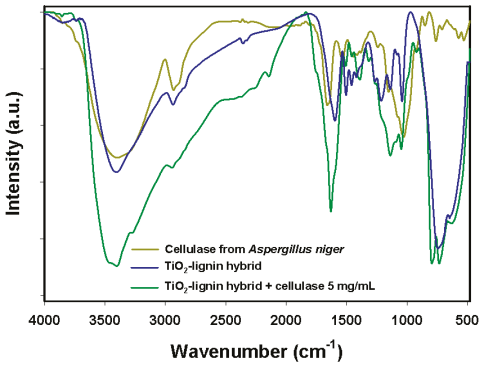

Figure 2. Results of Fourier-transform infrared (FTIR) analysis of cellulase from *Aspergillus niger*, TiO_2–lignin hybrid and the product after enzyme immobilization (immobilization conditions: pH = 7.0, T = 4 °C, t = 6 h, C_{enz} = 5 mg/mL).

Based also on the results of the analysis of the porous structure parameters of the TiO_2–lignin support material before and after immobilization, some additional conclusions can be drawn. The synthesized TiO_2–lignin hybrid before enzyme attachment had a relatively low surface area of around 10 m^2/g, while for the matrix after cellulase immobilization, this parameter decreased to about 8 m^2/g. This might suggest that effective enzyme attachment was achieved. Moreover, a decrease was recorded in the pores diameter and pores volume in the samples after immobilization. The hybrid biocomposite had pores with a mean diameter of 3.3 nm and a volume of 0.005 cm^3/g, while after cellulase immobilization these parameters fell to 1.7 nm and 0.003 cm^3/g.

2.2. Cellulase Immobilization

Besides confirmation of effective cellulase binding, the effect of initial immobilization parameters (process time and concentration of enzyme solution) on the quantity of immobilized enzyme and its relative activity was also evaluated (Figure 3).

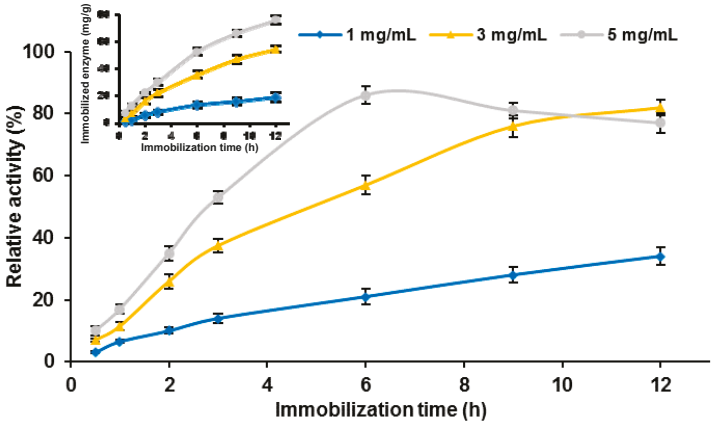

Figure 3. Effect of immobilization time on the relative activity of the immobilized cellulase. Inset: effect of immobilization time on the amount of the enzyme immobilized on the TiO_2–lignin hybrid.

As Figure 3 shows, the products after immobilization exhibited lower catalytic activity than free cellulase (relative activity up to 85%). When solution concentrations of 1 and 3 mg/mL were used, the highest relative activities, of around 30% and 80% respectively, were recorded after 12 h of the process. The amount of immobilized cellulase increased with process duration, irrespective of the concentration of the initial enzyme solution (Figure 3 inset). After 12 h of immobilization, 19, 55, and 76 mg of the biocatalyst per 1 g of the support material was deposited from solutions of 1, 3, and 5 mg/mL respectively. The results indicated that with increasing process time, the relative activity of the immobilized enzyme increased along with the amount of bounded cellulase, except in the case of the 5 mg/mL solution. When cellulase solution at this concentration was employed, the highest relative activity, about 85%, was obtained after 6 h of immobilization. Further increase in the immobilization time caused the relative activity of the bound cellulase to decrease.

As has already been mentioned, the immobilization technique used led to the attachment of cellulase molecules mainly via physical and ionic interactions, but the formation of covalent bonds cannot be excluded. Electrokinetic measurements showed that the zeta potential of the titania–lignin hybrid matrix took negative values over the whole of the analyzed pH range, which indicates that the surface of the support material was negatively charged during immobilization. Under the immobilization conditions (acetate buffer at pH 4.8), the enzyme molecules were positively charged (the IEP of cellulase is around 5). These facts imply that effective biocatalyst immobilization occurred mainly via electrostatic and ionic interactions. To verify this statement, solutions of sodium chloride at various ionic strengths were applied in cellulase desorption tests, because this salt might elute the enzyme by way of ionic exchange (Figure 4) [24].

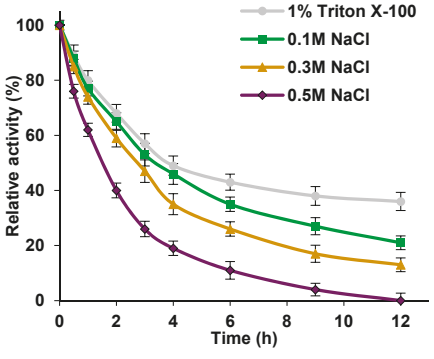

Figure 4. Effect of Triton X-100 and NaCl solution on the relative activity of free and immobilized onto TiO_2–lignin hybrid cellulase from *Aspergillus niger*.

Figure 4 shows that the relative activity of the immobilized cellulase treated with 1% Triton X-100 and NaCl solutions at various molar concentrations declined gradually during the first 6 h of treatment, which suggests elution of the enzyme from the matrix. The further decrease in relative activity is insignificant (less than 10% in all cases), which indicates that desorption occurred in the initial stages of the test and is limited in its later stages. After treatment with 1% Triton X-100 for 12 h, the immobilized cellulase retained over 40% of its relative activity. When the immobilized biocatalyst was incubated in sodium chloride solutions at molarities of 0.1; 0.3, and 0.5 M, a more significant drop in the relative activity was observed. The produced systems finally exhibited 25%, 18%, and 0% of its relative activity, respectively. Additionally, to verify if the immobilized enzyme was eluted from the support material following the treatments or was deactivated by such treatments, amount of the immobilized enzyme retained on the matrix, after 6 and 12 h of desorption process was evaluated (Table 1).

Table 1. Amount of the immobilized cellulase remained after desorption process, at different conditions.

Type of Eluent	Amount of Immobilized Enzyme (mg/g)	
	Desorption Time	
	6 h	12 h
1% Triton X-100	25.8 ± 1.3	22.4 ± 1.6
0.1 M NaCl	20.3 ± 1.5	12.6 ± 1.2
0.3 M NaCl	16.8 ± 0.6	6.9 ± 0.9
0.5 M NaCl	9.7 ± 1.0	5.1 ± 1.1

It can be seen from Table 2, that amount of the immobilized enzyme that remained on the surface of the hybrid material after desorption, irrespectively of the type and ionic strength of the eluent, is about 10–20% higher than amount of the immobilized cellulase, which corresponds to the evaluated relative activity of the biocatalytic system after desorption. The biggest differences were noticed for 0.5 M NaCl solution. After 6 and 12 h of the process, the surface of the titania–lignin hybrid retained 9.7 and 5.1 mg of the enzyme per 1 g of the support. These values corresponded to the relative activity of 18.3% and 9.7%, meanwhile, the noticed values of relative activity were 11.2% and 0%.

2.3. Stability Study of Immobilized Cellulase

Various process parameters such as pH and temperature might affect the ability of the immobilized cellulase to degrade cellulosic material. Thus, in this study, the effect of the aforementioned parameters, as well as the chemical and thermal stability of the free and immobilized enzyme, were examined and compared. Moreover, the reusability and storage stability of the free and immobilized enzyme under different conditions were tested. Kinetic parameters for both forms of the enzyme were evaluated to verify how immobilization affected the affinity of the enzyme to the substrate molecules and its catalytic efficiency.

2.3.1. Effect of pH

The effect of pH on the relative activity of free and immobilized cellulase was studied over a broad range of pH values, from 3.0 to 9.0 (Figure 5a).

The maximum relative activity was recorded at pH 5.5 for the free enzyme, and at pH 6.0 for the immobilized enzyme, as expected, since acidic cellulase was used in this study. Although the graph showed similar trends for the free and immobilized biocatalyst over the whole of the analyzed pH range, the immobilized biomolecules have higher relative activity than the free ones in the same pH conditions. The immobilized cellulase exhibited over 80% of its relative activity at pH values from 4.5 to 6.0, as the free catalyst did so only at pH values from 5.0 to 6.0. The bound enzyme also exhibited about 20% higher relative activity (76%) than the free enzyme (54%) at pH 3.0. The results also indicated a significant decrease in cellulase activity when the pH is above or below its optimum value. This was especially visible in alkaline conditions: at pH 9.0, both biocatalysts retained less than 40% of their activity. To test the chemical stability of the free and immobilized cellulase, both enzymes were incubated for 3 h under their optimal reaction conditions (Figure 5b). After 3 h, the free cellulase retained about 20% of its initial activity, as the immobilized enzymes incubated at pH 5.0 and 6.0 retained over 75% of their activity, which proved that cellulase attached to a TiO_2–lignin hybrid support has higher thermal stability than the free enzyme.

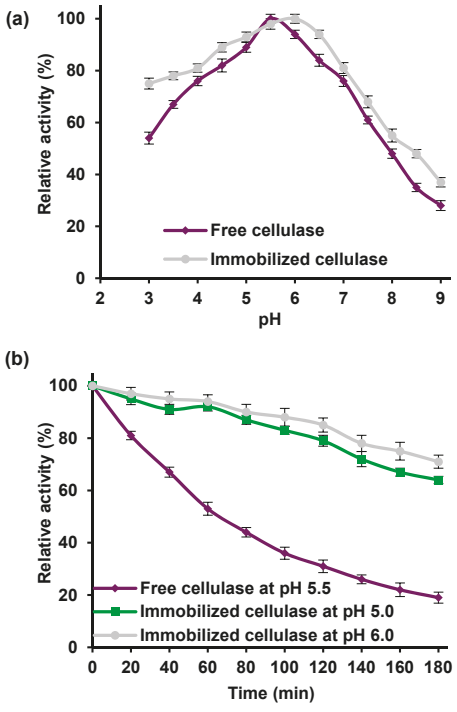

Figure 5. (**a**) Effect of pH on the relative activity of free and immobilized cellulose; (**b**) Chemical stability of free and immobilized enzyme after incubation for 3 h under optimal pH and temperature conditions.

2.3.2. Effect of Temperature

The effect of temperature on the relative activity of free and immobilized cellulase from *Aspergillus niger* was studied between 30 and 80 °C, under optimal pH conditions for free and immobilized cellulase (Figure 6a).

The free enzyme exhibited its maximum activity at 50 °C and retained 80% of its activity in a temperature range from 45 to 60 °C. At temperatures below 50 and above 60 °C the catalytic activity of the free biocatalyst significantly decreased, suggesting that the free enzyme is unstable in these conditions due to denaturation of the peptide structure [25]. By comparison, the immobilized cellulase exhibited its highest activity at temperatures of 55 and 60 °C, and retained over 80% of its maximum activity over a wide temperature range from 40 to 70 °C. In addition, the drop in relative activity above 70 °C is less significant that in the case of the free enzyme, while at 80 °C the bound cellulase exhibited over 60% of its relative activity. To determine the thermal stability of the immobilized cellulase, the free enzyme was incubated for 3 h at 50 °C and the immobilized cellulase at 50 and 60 °C (Figure 6b). After 3 h, the relative activity of the immobilized cellulase remained at a high level (over 75% and 80%, at temperatures of 50 and 60 °C, respectively). Meanwhile, there was more significant decline in the catalytic properties of the free enzyme, which after 3 h of incubation had lost almost 80% of its activity.

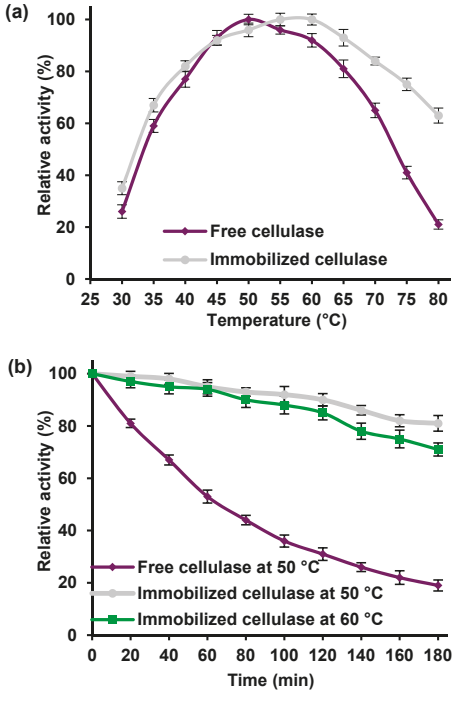

Figure 6. (**a**) Effect of temperature on the relative activity of free and immobilized cellulose; (**b**) Thermal stability of free and immobilized enzyme after incubation for 3 h under optimal temperature and pH conditions.

2.3.3. Storage Stability and Reusability

The storage stability of free and immobilized cellulase at 4 and 25 °C was evaluated by measuring the enzyme's relative activity every 5 days for 30 days (Figure 7a).

It can be seen that, irrespective of the storage temperature, the immobilized enzyme was characterized by higher activity than the free cellulase: after 30 days of storage at 4 and 25 °C, it retained over 95% and 85% of its initial activity, compared with less than 75% and less than 40% in the case of the free enzyme. These results indicated that the immobilization strategy used in this study improved the storage stability of the cellulase.

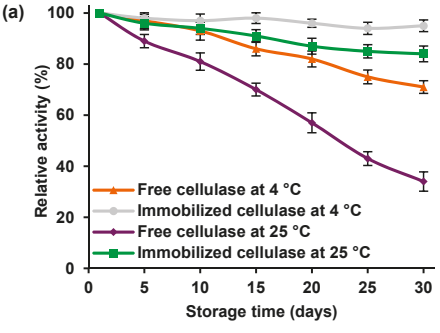

Figure 7. *Cont.*

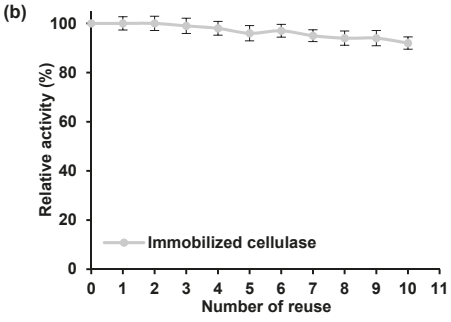

Figure 7. (**a**) Relative activity of free and immobilized cellulase stored for 30 days at 4 °C and 25 °C; (**b**) Reusability of the immobilized cellulase.

In this study, reusability of the bounded enzyme was evaluated over ten consecutive cycles of cellulose hydrolysis (Figure 7b). As can be seen, the relative activity of the immobilized cellulase remained almost unaltered during repeated catalytic cycles, and after ten cycles it retained 93% of its initial activity.

2.4. Kinetic Parameters of Free and Immobilized Cellulase

It is clear that, with changes in the three-dimensional structure of the enzyme, and its pH and temperature profiles as a result of immobilization, its kinetic parameters might also be affected. Kinetic parameters, including K_m, V_{max}, and turnover number (k_{cat}), were determined for both free and immobilized cellulase by measuring the initial reaction rates during the hydrolysis of cellulose with various initial concentrations of substrate, under optimal process conditions (Table 2).

Table 2. Kinetic parameters of cellulase from *Aspergillus niger*, free and immobilized on TiO_2–lignin hybrid.

Kinetic Parameters	Free Cellulase	Immobilized Cellulase
K_m (mM)	2.06 ± 0.85	2.63 ± 0.96
V_{max} (U/mg)	159 ± 11	125 ± 19
k_{cat} (s^{-1})	145 ± 19	114 ± 15
k_{cat}/K_m (s^{-1}·mM^{-1})	70.5 ± 3.5	43.6 ± 3.2
$t_{1/2}$ (min)	63 ± 13	307 ± 21

It can be seen that for the immobilized cellulase the value of K_m reached 2.63 mM, which is higher in comparison with free enzyme (2.06 mM), while the V_{max} value recorded for the immobilized enzyme (159 U/mg) was lower than for free cellulase. Nevertheless, higher values of the Michaelis–Menten constant and lower values of V_{max} after immobilization are typical for immobilized biocatalysts. A similar pattern was observed for turnover number (k_{cat}), which after immobilization took a value of 114 s^{-1}, and is lower than noticed for the free enzyme (145 s^{-1}). In consequence, the value of catalytic efficiency (k_{cat}/K_m) recorded for the immobilized cellulase (43.6 s^{-1}·mM^{-1}) is also significantly lower than that of the free biocatalyst (70.5 s^{-1}·mM^{-1}). This can be explained by the decrease in the affinity of the immobilized biomolecules to the substrate molecules. Nevertheless, it should be emphasized that the half-life ($t_{1/2}$) calculated for the immobilized cellulase (307 min) is almost five times as long as that of the free enzyme (63 min).

3. Discussion

3.1. Synthesis of Titania-Lignin Hybrid Material and Cellulase Immobilization

The synthesized TiO_2–lignin hybrid support was found to have relatively high thermal stability, significantly higher than that of activated kraft lignin. The improvement in thermal stability was a direct result of the incorporation of titanium dioxide particles, known to be highly thermo-resistant, into the hybrid material. The presence of various chemical moieties, such as –OH, C=O, and C–O, in the structure of the synthesized material facilitated the attachment of the cellulase molecules and the formation of relatively stable interactions. From the FTIR spectrum of the free enzyme, it can be concluded that the biocatalyst was attached mainly through the amine groups (–NH_2) present in its structure. However, particular attention should be paid to the shifts in the signals attributed to amide I bands from 1665 cm^{-1} (free enzyme) to 1645 cm^{-1} (immobilized cellulase), which suggests a mixed mechanism of interaction based mainly on the formation of physical and ionic interactions as well as covalent bonds between the enzyme and support [26]. By contrast, Tao et al. used a magnetite–silica hybrid support modified by arginine for the immobilization of cellulase. They observed that at pH above 5.0, the enzyme is negatively charged while arginine is positively charged, and in consequence, the formation of electrostatic interactions was strongly favored [17]. Moreover, after immobilization, the values of BET (Brunauer–Emmett–Teller) surface area, mean pores size, and pores volume were reduced, which suggests that the enzyme particles may be immobilized in the pores of the support as well as on its surface [27].

3.2. Cellulase Immobilization

During the study, it was also investigated how the catalytic activity of the immobilized enzyme depends on the initial immobilization parameters, namely the concentration of enzyme solution and immobilization time. The best catalytic properties were recorded for the system obtained after 6 h of immobilization from a cellulase solution with a concentration of 5 mg/mL, even though a greater amount of the enzyme was immobilized after a longer process time. This fact might be explained by the overloading of enzyme particles on the surface of the hybrid support, causing steric hindrances and diffusional limitations in transport of the reaction mixture components to the active sites of the enzyme [28]. In consequence, the relative activity of the immobilized enzyme decreased. Thus, the above parameter values were determined as the optimal immobilization conditions.

To confirm the type of interactions formed between the cellulase and hybrid support, solutions of Triton X-100 and sodium chloride at various concentrations were used to determine their effect on the activity of the immobilized enzyme. A significant decrease in relative activity might suggest that the cellulase is linked to the hybrid support mainly via hydrogen bonds and ionic interactions. The formation of these types of interactions is related to the presence of negative and positive charges on the surface of the matrix and in the structure of the enzyme, respectively in the conditions of the immobilization process. However, such interactions are unstable under the conditions of the desorption tests. In fact, the immobilized enzyme retained its catalytic properties, which indicates that covalent bonds are also present between the biomolecules and support material [29]. This is confirmed by the findings of Hirsh et al., who used polystyrene film after surface activation by plasma immersion ion implantation. They reported that, when cellulase was immobilized via covalent bonds, desorption was strongly reduced and the enzyme retained its catalytic properties [30]. Moreover, changes in the relative activity of immobilized cellulase after treatment with NaCl solutions at various concentrations indicated that the ionic strength of the solutions affected the catalytic activity of the immobilized cellulase. It also should be added that this statement is confirmed by the results of the immobilized enzyme retained on the surface of the support after desorption, which is higher than the amount of the enzyme corresponding to the measured relative activity. This could suggest that the enzyme is not only desorbed by the eluent, but partially might be also deactivated by the treatment, which is particularly noticeable in the presence of 0.5 M NaCl.

3.3. Stability Study of Immobilized Cellulase

During the immobilization process, the structure of biocatalysts may be altered, causing changes in their activity and stability. It has been shown that immobilized cellulase exhibited higher stability than the free enzyme over the analyzed pH range; however, the catalytic properties are significantly better in acidic than in alkaline conditions. This might be explained by the fact that in a basic environment, ionic groups present in the cellulase molecules form an electrostatic repulsion which influences the three-dimensional structure of the enzyme, leading to disruption and destruction of the active sites of the cellulase, and thus impairing its catalytic properties [31]. Similar observations were reported by Khorshidi et al., who cross-linked cellulase aggregates on amine-functionalized Fe_3O_4–silica core–shell magnetic nanoparticles. They recorded a large decrease in the enzyme's catalytic properties at pH values above 5.0 [32]. By comparison, in this study, the relative activity of immobilized cellulase measured at pH 7.0 was around 80%, proving that application of the titania–lignin hybrid as a support significantly improved the pH resistance of the cellulase. This may be explained by the protective effect of the hybrid support against conformational changes caused by harsh pH conditions [33] and by the fact that after immobilization, interactions between the biocatalyst and carrier are formed which stabilize the entire structure of the enzyme [34]. Results relate to the thermal stability clearly show that the stability of the cellulase was improved after immobilization on the TiO_2–lignin hybrid. This was probably because the immobilization process provided an additional external backbone and stabilization for the molecules of cellulase, as a result of the formation of interactions between the enzyme and support [35]. Moreover, as an effect of immobilization, thermal vibrations of cellulase biomolecules were reduced, which limited conformational changes caused by heat and helped to maintain the proper globular structure of the entire biomolecule [36,37]. Similar findings to those presented in this study were reported by Sanchez-Ramirez et al., who used another inorganic–organic hybrid support (chitosan-coated magnetic nanoparticles) for covalent immobilization of *Trichoderma reesei* cellulase, and found that the resulting biocatalytic system exhibited its maximum activity at 60 °C. In addition, after 3 h of incubation at that temperature, it retained about 60% of its initial activity; however, an increase in the temperature by 10 °C caused the relative activity to drop significantly, to below 40% [38]. By contrast, cellulase immobilized on the titania–lignin support retained over 80% of its activity after 3 h of incubation at 70 °C.

The storage stability of cellulase from *Aspergillus niger* was found to be significantly improved following immobilization. This can probably be attributed to a reduction in the dissociation of peptide subunits and in the enzyme denaturation rate [39]. A significant increase in the storage stability of immobilized cellulase was also reported when graphene oxide supplemented by magnesium oxide nanoparticles was used as a support. In that study, after 30 days of storage the free enzyme retained less than 20% of its initial catalytic activity, compared with over 80% for the immobilized biocatalyst [40]. It was also found that the immobilized cellulase can be used in as many as ten reaction cycles without significant loss of activity. The observed slight decrease in catalytic properties is probably related to the relatively weak strength of the interactions (mainly ionic interactions and van der Waals forces) between the enzyme and support, which causes partial leakage of the catalyst from the support. Moreover, the immobilized cellulase may undergo partial inactivation as a result of its repeated use [41]. Nevertheless, the results clearly show that immobilization is an effective tool to ensure the reusability of cellulase in the hydrolysis of cellulose. Earlier studies of cellulase immobilization have reported the retention of about 40% and 70% of initial activity after eight biocatalytic cycles, when the enzyme was attached to, respectively, magnetic nanoparticles consisting of hematite and ferrite activated by glutaraldehyde, and magnetic nanoparticles encapsulated in polymer nanospheres [34,42]. Such improvement in the operational stability and reusability of cellulase makes it more suitable for large-scale processes and greatly increases its economic viability.

3.4. Kinetic Parameters of Free and Immobilized Cellulase

The observed increase in the value of K_m and simultaneous decrease in V_{max} reflect a lower affinity to the substrate, and consequently a lower maximum reaction rate, in the case of the immobilized enzyme. These changes are probably related to the creation of diffusional limitations and changes in the structure of the enzyme caused by its attachment to the solid support, which blocks active sites of the enzyme and restricts transport of the substrates [43]. In addition, the decrease in the turnover number after immobilization suggests that the binding process has a negative effect on substrate conversion by the immobilized cellulase. However, a significant (fivefold) increase in the enzyme's half-life was recorded, indicating that cellulase attached to the TiO_2–lignin hybrid support retains its catalytic properties for a longer time than the free enzyme. These findings are in agreement with the data on thermal and chemical stability, which show a significant improvement in the stability of the cellulase after immobilization. The foregoing observations are in agreement with data published by Senyay-Oncel and Yesil-Celiktas, which showed that after the immobilization of cellulase on commercially available NaY zeolite, its substrate affinity and reaction rate also decreased [44]. Nonetheless, their study found much more significant changes in K_m (a 100% rise), V_{max} (a 30% drop), and k_{cat} (a 50% drop) than in the present study.

4. Materials and Methods

4.1. Materials

Cellulase from *Aspergillus niger* (EC 3.2.1.4, product number 22178), poly-L-lisine (PLL), kraft lignin, sodium (meta)periodate, cellulose, glucose, Whatman® qualitative filter paper (Grade 1 circles, diam. 15 mm), 3,5-dinitrosalicylic acid (3,5-DNS), sodium chloride, Triton X-100, phosphate buffer (PBS) at pH 7, acetate buffer at pH 4.8, Coomassie Brilliant Blue G-250 (CBB G-250), and bovine serum albumin (BSA) were delivered by Sigma-Aldrich (St. Louis, MO, USA). Commercially available titanium dioxide (product name Tytanpol® R-001) was supplied by Grupa Azoty SA (Tarnów, Poland). Sodium hydroxide, hydrochloric acid, dioxane, 96% ethyl alcohol, and 85% phosphoric acid were delivered by Chempur (Katowice, Poland).

4.2. Synthesis of TiO_2–Lignin Hybrid Support Material

The synthesis of a titania–lignin hybrid support was carried out in three steps, using the method described in our previous work [45,46] with some modifications. In this study, the titanium dioxide was modified with poly-L-lysine (PLL), in view of its peptide nature and to increase the amount of reactive chemical groups for the effective binding of lignin. For surface functionalization of TiO_2, it was suspended in PBS at pH 7, then a 10% (w/w) solution of PLL was added. The mixture was shaken for 12 h (KS260 Basic, IKA Werke GmbH, Staufen im Breisgau, Germany) at 4 °C and centrifuged (Eppendorf Centrifuge 5810 R, Hamburg, Germany), and washed with deionized water to remove unbound PLL and PBS. In the next step, kraft lignin was activated by sodium (meta)periodate. Finally, the activated lignin and modified titanium dioxide were linked at a mass ratio of 1:1.

4.3. Immobilization of Cellulase from Aspergillus niger

Immobilization was carried out using 0.25 g of the previously obtained TiO_2–lignin hybrid support, to which 10 mL of a solution of cellulase from *Aspergillus niger*, at concentrations of 1.0, 3.0, and 5.0 mg/mL in acetate buffer at pH 4.8, was added. The mixture was shaken for a specified period of time (1, 2, 3, 6, 9, or 12 h) in a KS 4000i Control incubator (IKA Werke GmbH, Staufen im Breisgau, Germany) at a temperature of 4 °C. Finally, the products were centrifuged (Eppendorf Centrifuge 5810 R, Hamburg, Germany) and washed several times with the acetate buffer to remove unbound enzyme.

4.4. Characterization of the Hybrid Support and Product after Immobilization

Thermogravimetric curves for the modified TiO_2, activated lignin, and synthesized TiO_2–lignin hybrid material (sample weight approximately 10 mg) were obtained using a Jupiter STA449F3 apparatus (Netzsch, Selb, Germany). Measurements were made at a heating rate of 10 °C/min over the temperature range 25–1000 °C under nitrogen flow (10 mL/min).

Porous structure parameters (BET surface area, pores diameter and pores volume) were determined using an ASAP 2020 instrument (Micromeritics Instrument Co., Norcross, GA, USA). The surface area was evaluated based on the multipoint BET (Brunauer–Emmett–Teller) method using data for nitrogen adsorption under relative pressure (p/p_0). The BJH (Barrett–Joyner–Halenda) algorithm was applied to examine the mean size and total volume of pores.

Zeta potential measurements were made on a Zetasizer Nano ZS instrument (Malvern Instruments Ltd., Malvern, UK) equipped with an autotitrator. The measurements were performed in a 0.001 M NaCl solution over the pH range 2.0–11.0. The zeta potential was computed using Henry's equation.

Fourier transform infrared (FTIR) spectra were obtained using a Vertex 70 spectrophotometer (Bruker, Billerica, MA, USA), analyzing samples in the form of KBr pellets at a resolution of 0.1 cm^{-1} over a wavenumber range of 4000–400 cm^{-1}. Pellets were made by mixing 200 mg of anhydrous potassium bromide and 2 mg of the sample.

The amount of cellulase immobilized on the hybrid support was evaluated based on the Bradford method [47]. Briefly, amount of the cellulase was measured before and after immobilization at wavelength 595 nm, using a calibration curve based on BSA solutions at known concentrations to calculate the quantity of immobilized enzyme present, in mg of cellulase per gram of support.

4.5. Activity and Stability of Free and Immobilized Cellulase

The catalytic activity of free and immobilized cellulase was evaluated by measuring the quantity of reducing sugars (glucose) during hydrolysis of the cellulose substrate. The concentration of glucose was quantified using the previously described DNS method [48]. The activity measurements were carried out as follows: 50 mg of cellulosic substrate (Whatman® paper) was placed in acetate buffer at pH 4.8, and 10 mg of free or immobilized cellulase was added to the reactor. The mixture was incubated for 60 min at 50 °C. The reaction was terminated by the addition of 2 mL of 3,5-DNS. The resulting solution was then incubated at 100 °C for 5 min in an oil bath, and after that time was immediately cooled in ice. Samples were then diluted with distilled water and centrifuged (Eppendorf Centrifuge 5810 R, Hamburg, Germany) to remove solid particles, and were subjected to spectrophotometric measurements at 540 nm using a Jasco V-750 UV–Vis spectrophotometer (Jasco, Tokyo, Japan). The calibration curve of glucose was used to determine the relation between absorbance and the quantity of reducing sugars. All measurements were made in triplicate. One enzyme activity unit (U) of free and immobilized cellulase was defined as the amount of enzyme that produced 1 μmol of glucose per minute.

The relative activity (A_R) (Equation (1)) was defined as the percentage ratio of the activity of cellulase at a specific value (A_i) to the enzyme's maximum activity (A_{max}). A_{max} is the highest activity among all values of enzymatic activity recorded in this study.

$$A_R = \frac{A_i}{A_{max}} \times 100\% \quad (1)$$

Also based on the above-mentioned reaction, the effect of pH and temperature on the activity of immobilized cellulase, as well as its thermal and chemical stability, storage stability, and reusability, were evaluated. The effect of pH was studied by incubating the reaction mixture with free or immobilized cellulase at pH values ranging from 3 to 9 (pH was adjusted by the addition of 0.1 M HCl or NaOH). The effect of temperature was evaluated over the temperature range 30–80 °C by incubating the reaction mixture under the desired temperature conditions. pH and thermal inactivation curves for free cellulase were examined after incubation of the free enzyme at pH 5.5 and a temperature

of 50 °C for 3 h. Thermal inactivation curves of immobilized cellulase were evaluated after 3 h of incubation at pH 6 at temperatures of 50 and 60 °C, while pH inactivation curves were examined after 3 h of incubation at 60 °C, at pH 5 and 6. The reusability of the immobilized cellulase was examined by measuring enzymatic activity in ten consecutive reaction cycles. After each hydrolysis cycle, the immobilized cellulase was separated from the reaction mixture by centrifugation and washed with buffer solution before the next cycle. The enzymatic activity in the first cycle was defined as 100%, and relative activity was calculated for the following cycles. Storage stability was evaluated every 5 days under optimum reaction conditions for free and immobilized cellulase stored at 4 and 25 °C, in phosphate buffer at pH 7. The initial activity was defined as 100%.

The effect of 1% Triton X-100 and sodium chloride solutions at various concentrations (0.1–0.5 M) on the relative activity of immobilized cellulase from *Aspergillus niger* was evaluated over a time of 12 h. For this purpose, the immobilized enzyme was dispersed in sodium chloride or Triton X-100 solution. After the specified period of time, the relative activity of the immobilized enzyme was evaluated based on the hydrolysis reaction of the cellulosic substrate.

4.6. Kinetic Parameters of Free and Immobilized Enzyme

The Lineweaver–Burk plots were used to evaluate the kinetic parameters: the Michaelis–Menten constant (K_m), maximum reaction rate (V_{max}), specificity constant (k_{cat}/K_m), and turnover number (k_{cat}) of free and immobilized cellulase. These parameters were evaluated based on the hydrolysis reaction of cellulose substrate at different concentrations. Initial reaction rates were evaluated under optimum reaction conditions.

5. Conclusions

The results presented in this study clearly demonstrate that cellulase, an industrially relevant enzyme, was successfully immobilized on a hybrid TiO_2–lignin support material. The immobilized cellulase exhibited significant improvement in thermal and chemical stability (with relative activity above 80% after 3 h of incubation). Furthermore, after 10 consecutive hydrolysis cycles the immobilized cellulase retained over 90% of its initial activity, which confirms its operational stability, a relevant feature for industrial applications. The approach described here provides an efficient and simple method for the synthesis of a hybrid titanium dioxide–lignin material and its application as a support material for the immobilization of cellulase. The produced biocatalytic system may be employed in industrial applications without significant loss of its properties over several cycles. Moreover, the synthesized hybrid material and the applied immobilization methodology might easily be used for the immobilization of other biocatalysts.

Acknowledgments: The scientific work was financed from budgetary resources for science in the years 2016–2019, project number IP2015 032574 (Iuventus Plus).

Author Contributions: J.Z. planned the studies, evaluated the enzyme immobilization efficiency and the immobilized enzyme's activity and stability, as well as developed results. A.J. prepared the functional hybrid material and carried out the immobilization experiments. Ł.K. interpreted the data and wrote up the results. T.J. coordinated all project tasks, planned the studies, developed the results, and participated in discussions.

Conflicts of Interest: The authors declare no conflict of interest. The funding sponsors had no role in the design of the study; in the collection, analysis, or interpretation of data; in the writing of the manuscript; or in the decision to publish the results.

References

1. Gupta, C.; Jain, P.; Kumar, D.; Dixit, A.K.; Jain, R.K. Production of cellulase enzyme from isolated fungus and its application as efficient refining aid for production of security paper. *Int. J. Appl. Microbiol. Biotechnol. Res.* **2015**, *3*, 11–19.
2. Zhang, Y.H.P.; Himmel, M.E.; Mielenz, J.R. Outlook for cellulase improvement: Screening and selection strategies. *Biotechnol. Adv.* **2006**, *24*, 452–481. [CrossRef] [PubMed]

3. Kuhad, R.C.; Singh, A.; Eriksson, K.E. Microorganisms and enzymes involved in the degradation of plant fiber cell walls. *Adv. Biochem. Eng. Biotechnol.* **1997**, *57*, 45–125. [PubMed]
4. Deswal, D.; Khasa, Y.P.; Kuhad, R.C. Optimization of cellulase production by a brown rot fungus *Fomitopsis* sp. *Bioresour. Technol.* **2011**, *102*, 6065–6072. [CrossRef] [PubMed]
5. Rana, S.; Kaur, M. Isolation and screening of cellulase-producing microorganisms from degraded wood. *Int. J. Pharm. Biol. Sci. Fundam.* **2012**, *2*, 10–15.
6. Kuhad, R.C.; Gupta, R.; Singh, A. Microbial cellulases and their industrial applications. *Enzyme Res.* **2011**, *2011*, 280696. [CrossRef] [PubMed]
7. Sun, Y.; Cheng, J. Hydrolysis of lignocellulosic materials for ethanol production: A review. *Bioresour. Technol.* **2002**, *83*, 1–11. [CrossRef]
8. Sukumaran, R.K.; Singhania, R.R.; Pandey, A. Microbial cellulases—Production, applications and challenges. *J. Sci. Ind. Res.* **2005**, *64*, 832–844.
9. Cao, L. *Carrier-Bound Immobilized Enzymes: Principles, Application and Design*; Wiley-VCh: Weinheim, Germany, 2005.
10. Rodrigues, R.C.; Ortiz, C.; Berenguer-Murcia, A.; Torres, R.; Fernandez-Lafuente, R. Modifying enzyme activity and selectivity by immobilization. *Chem. Soc. Rev.* **2013**, *42*, 6290–6307. [CrossRef] [PubMed]
11. Tischer, W.; Wedekind, F. Immobilized enzymes: Methods and applications. *Top. Curr. Chem.* **1999**, *200*, 96–126.
12. Barbosa, O.; Ortiz, C.; Berenguer-Murcia, A.; Torres, R.; Rodrigues, R.C.; Fernandez-Lafuente, R. Strategies for the one-step immobilization-purification of enzymes as industrial biocatalysts. *Biotechnol. Adv.* **2015**, *33*, 435–456. [CrossRef] [PubMed]
13. Brena, B.; González-Pombo, P.; Batista-Viera, F. Immobilization of enzymes and cells. *Methods Mol. Biol.* **2013**, *1051*, 5–31.
14. Mateo, C.; Abian, O.; Fernandez-Lorente, G.; Pedroche, J.; Fernandez-Lafuente, R.; Guisan, J.M. Epoxy sepabeads: A novel epoxy support for stabilization of industrial enzymes via very intense multipoint covalent attachment. *Biotechnol. Prog.* **2002**, *18*, 629–634. [CrossRef] [PubMed]
15. Hernandez, K.; Fernandez-Lafuente, R. Control of protein immobilization: Coupling immobilization and site-directed mutagenesis to improve biocatalyst or biosensor performance. *Enzyme Microb. Technol.* **2011**, *48*, 107–122. [CrossRef] [PubMed]
16. Jędrzak, A.; Rębiś, T.; Klapiszewski, Ł.; Zdarta, J.; Milczarek, G.; Jesionowski, T. Carbon paste electrode based on functional GOx/silica-lignin system to prepare an amperometric glucose biosensor. *Sens. Actuators B Chem.* **2018**, *256*, 176–185. [CrossRef]
17. Tao, Q.L.; Li, Y.; Shi, Y.; Liu, R.J.; Zhang, Y.W.; Guo, J. Application of molecular imprinted magnetic Fe_3O_4@SiO_2 nanoparticles for selective immobilization of cellulase. *J. Nanosci. Nanotechnol.* **2016**, *16*, 6055–6060. [CrossRef] [PubMed]
18. Velmurugan, R.; Incharoensakdi, A. MgO-Fe_3O_4 linked cellulase enzyme complex improves the hydrolysis of cellulose from *Chlorella* sp. CYB2. *Biochem. Eng. J.* **2017**, *122*, 22–30. [CrossRef]
19. Hong, G.W.; Ramesh, S.; Kim, J.H.; Kim, H.J.; Lee, H.S. Synthesis and properties of cellulose-functionalized POSS-SiO_2/TiO_2hybrid composites. *J. Nanosci. Nanotechnol.* **2015**, *15*, 8048–8054. [CrossRef] [PubMed]
20. Hou, J.; Dong, G.; Ye, Y.; Chen, V. Laccase immobilization on titania nanoparticles and titania-functionalized membranes. *J. Membr. Sci.* **2014**, *452*, 229–240. [CrossRef]
21. Hou, J.; Dong, G.; Xiao, B.; Malassigne, C.; Chen, V. Preparation of titania based biocatalytic nanoparticles and membranes for CO_2 conversion. *J. Mater. Chem. A* **2015**, *3*, 3332–3342. [CrossRef]
22. Klapiszewski, Ł.; Zdarta, J.; Antecka, K.; Synoradzki, K.; Siwińska-Stefańska, K.; Moszyński, D.; Jesionowski, T. Magnetite nanoparticles conjugated with lignin: A physicochemical and magnetic study. *Appl. Surf. Sci.* **2017**, *422*, 94–103. [CrossRef]
23. Zdarta, J.; Klapiszewski, Ł.; Jędrzak, A.; Nowicki, M.; Moszyński, D.; Jesionowski, T. Lipase B from *Candida antarctica* immobilized on a silica-lignin matrix as a stable and reusable biocatalytic system. *Catalysts* **2017**, *7*, 14. [CrossRef]
24. Hanefeld, U.; Gardossi, L.; Magner, E. Understanding enzyme immobilization. *Chem. Soc. Rev.* **2009**, *38*, 453–468. [CrossRef] [PubMed]
25. Magri, M.L.; Miranda, M.V.; Cascone, O. Immobilization of soybean seed coat peroxidase on polyaniline: Synthesis optimization and catalytic properties. *Biocatal. Biotransform.* **2005**, *22*, 339–346. [CrossRef]

26. Eslamipour, F.; Hejazi, P. Evaluating effective factors on activity and loading of immobilized α-amylase onto magnetic nanoparticles using response surface desirability approach. *RSC Adv.* **2016**, *6*, 20187–20197. [CrossRef]
27. Hou, J.; Dong, G.; Ye, Y.; Chen, V. Enzymatic degradation of bisphenol-A with immobilized laccase on TiO_2 sol–gel coated PVDF membrane. *J. Membr. Sci.* **2014**, *469*, 19–30. [CrossRef]
28. Zhang, D.H.; Zhang, Y.F.; Zhi, G.Y.; Xie, Y.L. Effect of hydrophobic/hydrophilic characteristics of magnetic microspheres on the immobilization of BSA. *Colloids Surf. B* **2011**, *82*, 302–306. [CrossRef] [PubMed]
29. Straksys, A.; Kochane, T.; Budriene, S. Catalytic properties of maltogenic α-amylase from *Bacillus stearothermophilus* immobilized onto poly(urethane urea) microparticles. *Food Chem.* **2016**, *211*, 294–299. [CrossRef] [PubMed]
30. Hirsh, S.L.; Bilek, M.M.M.; Nosworthy, N.J.; Kondyurin, A.; dos Remedios, C.G.; McKenzie, D.R. A comparison of covalent immobilization and physical adsorption of a cellulase enzyme mixture. *Langmuir* **2010**, *26*, 14380–14388. [CrossRef] [PubMed]
31. Mubarak, N.N.; Wong, J.R.; Tan, K.W.; Sahu, J.N.; Abdullah, E.C.; Jayakumar, N.S.; Ganesan, P. Immobilization of cellulase enzyme on functionalized multiwall carbon nanotubes. *J. Mol. Catal. B Enzym.* **2014**, *107*, 124–131. [CrossRef]
32. Khorshidi, K.J.; Lenjannezhadian, H.; Jamalan, M.; Zeinali, M. Preparation and characterization of nanomagnetic cross-linked cellulase aggregates for cellulose bioconversion. *J. Chem. Technol. Biotechnol.* **2016**, *91*, 539–546. [CrossRef]
33. Bohara, R.A.; Thorat, N.D.; Pawar, S.H. Immobilization of cellulase on functionalized cobalt ferrite nanoparticles. *Korean J. Chem. Eng.* **2016**, *33*, 216–222. [CrossRef]
34. Abraham, R.E.; Verma, M.L.; Barrow, C.J.; Puri, M. Suitability of magnetic nanoparticle immobilised cellulases in enhancing enzymatic saccharification of pretreated hemp biomass. *Biotechnol. Biofuels* **2014**, *7*, 1–12. [CrossRef] [PubMed]
35. Zhang, W.; Qiu, J.; Feng, H.; Zang, L.; Sakai, E. Increase in stability of cellulase immobilized on functionalized magnetic nanospheres. *J. Magn. Magn. Mater.* **2015**, *375*, 117–123. [CrossRef]
36. Sharma, S.; Kaur, P.; Jain, A.; Rajeswari, M.R.; Gupta, M.N. A smart bioconjugate of chymotrypsin. *Biomacromolecules* **2003**, *4*, 330–336. [CrossRef] [PubMed]
37. Li, Y.; Wang, X.Y.; Zhang, R.Z.; Zhang, X.Y.; Liu, W.; Xu, X.M.; Zhang, Y.W. Molecular imprinting and immobilization of cellulase onto magnetic Fe_3O_4@SiO_2 nanoparticles. *J. Nanosci. Nanotechnol.* **2014**, *14*, 2931–2936. [CrossRef] [PubMed]
38. Sanchez-Ramirez, J.; Martinez-Hernandez, J.L.; Segura-Ceniceros, P.; Lopez, G.; Saade, H.; Medina-Morales, M.A.; Ramos-Gonzalez, R.; Aguilar, C.N.; Ilyina, A. Cellulases immobilization on chitosan-coated magnetic nanoparticles: Application for *Agave atrovirens* lignocellulosic biomass hydrolysis. *Bioprocess. Biosyst. Eng.* **2017**, *40*, 9–22. [CrossRef] [PubMed]
39. Zhang, D.; Hegab, H.E.; Lvov, Y.; Snow, L.D.; Palmer, J. Immobilization of cellulase on a silica gel substrate modified using a 3-APTES self-assembled monolayer. *SpringerPlus* **2016**, *5*, 1–20. [CrossRef] [PubMed]
40. Dutta, N.; Biswas, S.; Saha, M.K. Biophysical characterization and activity analysis of nano-magnesium supplemented cellulase obtained from a psychrobacterium following graphene oxide immobilization. *Enzym. Microb. Technol.* **2016**, *95*, 248–258. [CrossRef] [PubMed]
41. Swarnalatha, V.; Esther, R.A.; Dhamodharan, R. Immobilization of α-amylase on gum acacia stabilized magnetite nanoparticles, an easily recoverable and reusable support. *J. Mol. Catal. B Enzym.* **2013**, *96*, 6–13. [CrossRef]
42. Lima, J.S.; Araujo, P.H.H.; Sayer, C.; Viegas, A.C.; de Oliveira, D. Cellulase immobilization on magnetic nanoparticles encapsulated in polymer nanospheres. *Bioprocess. Biosyst. Eng.* **2017**, *40*, 511–518. [CrossRef] [PubMed]
43. Bayramoglu, S.G.; Kiralp, S.; Yilmaz, M.; Toppare, L.; Arica, M.Y. Covalent immobilization of chloroperoxidase onto magnetic beads: Catalytic properties and stability. *Biochem. Eng. J.* **2008**, *38*, 180–188. [CrossRef]
44. Senyay-Oncel, D.; Yesil-Celiktas, O. Characterization, immobilization, and activity enhancement of cellulase treated with supercritical CO_2. *Cellulose* **2015**, *22*, 3619–3631. [CrossRef]

45. Klapiszewski, Ł.; Siwińska-Stefańska, K.; Kołodyńska, D. Preparation and characterization of novel TiO_2/lignin and TiO_2-SiO_2/lignin hybrids and their use as functional biosorbents for Pb(II). *Chem. Eng. J.* **2017**, *314*, 169–171. [CrossRef]
46. Klapiszewski, Ł.; Siwińska-Stefańska, K.; Kołodyńska, D. Development of lignin based multifunctional hybrid materials for Cu(II) and Cd(II) removal from the aqueous system. *Chem. Eng. J.* **2017**, *330*, 518–530. [CrossRef]
47. Bradford, M.M. A rapid and sensitive method for the quantitation of microgram quantities of protein utilizing the principle of protein-dye binding. *Anal. Biochem.* **1976**, *72*, 248–254. [CrossRef]
48. Miller, G.L. Use of dinitrosalicylic acid reagent for determination of reducing sugar. *Anal. Chem.* **1959**, *31*, 426–428. [CrossRef]

© 2017 by the authors. Licensee MDPI, Basel, Switzerland. This article is an open access article distributed under the terms and conditions of the Creative Commons Attribution (CC BY) license (http://creativecommons.org/licenses/by/4.0/).

catalysts

MDPI

Article

"Deceived" Concentrated Immobilized Cells as Biocatalyst for Intensive Bacterial Cellulose Production from Various Sources

Nikolay Stepanov and Elena Efremenko *

Faculty of Chemistry, Lomonosov Moscow State University, Moscow 119991, Russia; na.stepanov@gmail.com
* Correspondence: elena_efremenko@list.ru; Tel.: +7-495-939-3170

Received: 21 December 2017; Accepted: 15 January 2018; Published: 18 January 2018

Abstract: A new biocatalyst in the form of *Komagataeibacter xylinum* B-12429 cells immobilized in poly(vinyl alcohol) cryogel for production of bacterial cellulose was demonstrated. Normally, the increased bacteria concentration causes an enlarged bacterial cellulose synthesis while cells push the polysaccharide out to pack themselves into this polymer and go into a stasis. Immobilization of cells into the poly(vinyl alcohol) cryogel allowed "deceiving" them: bacteria producing cellulose pushed it out, which further passed through the pores of cryogel matrix and was accumulated in the medium while not covering the cells; hence, the latter were deprived of a possible transition to inactivity and worked on the synthesis of bacterial cellulose even more actively. The repeated use of immobilized cells retaining 100% of their metabolic activity for at least 10 working cycles (60 days) was performed. The immobilized cells produce bacterial cellulose with crystallinity and porosity similar to polysaccharide of free cells, but having improved stiffness and tensile strength. Various media containing sugars and glycerol, based on hydrolysates of renewable biomass sources (aspen, Jerusalem artichoke, rice straw, microalgae) were successfully applied for bacterial cellulose production by immobilized cells, and the level of polysaccharide accumulation was 1.3–1.8-times greater than suspended cells could produce.

Keywords: bacterial cellulose; poly(vinyl alcohol); cell immobilization; hydrolysates of renewable biomass

1. Introduction

Currently, the interest in bacterial cellulose (BC) is increasing because of its possible use in such areas as medicine, food and textile industries, the production of new nanocomposite materials based on it and the solution of environmental problems [1–4]. First of all, this is due to the fact that BC is nontoxic and biocompatible material with an increased water-holding capacity, high tensile strength, as well as elasticity and porosity [5,6]. Unlike plant cellulose, BC does not require isolation and purification of lignin and hemicellulose, so the processes of producing BC are much less costly and energy-consuming [7].

Broadening of the scope and applications of BC is directly dependent on the availability of productive processes that provide high yields of this valuable biotechnological product [8]. Acetic acid bacteria in a static culture are mainly used to produce BC [9,10]. Analysis of known results enables determination of several main problems of BC production in general. It is a rather long process (up to 336 h), and the final product yield is influenced by many factors (type and concentration of the carbon source in the medium, composition and pH of the nutrient medium) [11]. Various carbon sources were examined for the purpose of BC synthesis, while glucose appeared to be the high-usage carbon source for the synthesis of BC [12]. However, when bacterial cells are grown, gluconic acid accumulates in a glucose-containing medium, which lowers the pH of the medium and reduces the level of BC

synthesis [10]. The adjustment of pH with $CaCO_3$ results in inhibition of several main enzymes participating in the BC production since they contain bivalent metal ions in their active sites. In order to avoid this, researchers attempt to replace glucose as a major carbon source completely or partially with other substrates as the productivity of cells producing BC is often higher when using these substrates than in a medium with glucose [13–15], The possible use of non-food substrates (renewable biomass sources, in particular) in the form of hydrolysates of various wastes is extremely attractive for scalable BC biosynthesis [16–19]. However, such raw materials and wastes often require preliminary physicochemical pretreatment for sugar releasing, and the obtained media may contain substances inhibiting the metabolic activity of cells [20]. Moreover, variations in chemical composition are inherent to natural biomass sources, requiring an increased cell capability to adapt to changing cultivation conditions and to keep the process productivity at a desired level. In this regard, the efficient approach to BC production enabling cells to improve their resistance to varying conditions of BC accumulation when the media discussed are employed should be offered.

Another problem associated with obtaining BC is the accumulation of polysaccharide in the process of cell growth and an increase in their concentration in the medium, that is cells partly spend the consumed substrate on the accumulation of their biomass, rather than on the synthesis of the target polymer [21]. The problem can be solved by the use of highly concentrated slowly-growing/non-growing cell populations, which are maintained in a membrane reactor to produce BC [22]. The problem is that cells synthesizing BC happen to be "included" in the polymer matrix that forms and accumulates around them. Since BC usually has a structure with nanoscale pores [12], the mass transfer of substances through them turns out to be rather hindered; the cells simply cease to function, and BC synthesis stops [23]. As a result, the obtained polymer has to be further processed and treated with alkaline agents in order to hydrolyze a significant biomass of cells that are "self-immured" in the BC so that a pure polymer could be obtained [10,24]. Thus, BC synthesis proves self-regulating.

Many researchers are trying to increase the level of BC synthesis by using traditional biotechnological approaches, namely by introducing into the nutrient medium some regulators of bacterial metabolism. For example, ethanol or organic acids (succinic, lactic, etc.) being cellular metabolites are applied to inhibit the basic metabolic processes in order to enhance the synthesis of by-products or substances necessary for the cell stabilization, in particular BC [25,26]. However, these measures appear not very successful, because the BC biosynthesis is "outside the main" metabolic processes in cells (Figure 1), with bacterial cellulose synthase (BC-synthase) (guanosine diphosphate-forming (GDP-glucose-beta-D-glucan glucosyltransferase, EC 2.4.1.29)), which is typically activated in the presence of cyclic diguanidine monophosphate (c-di-GMP) playing a major role in the BC biosynthesis [27]. The key idea of this activation is that the entry into the active center of BC-synthase is usually closed by an amino acid sequence loop held by the arginine R580 residue [28]. The c-di-GMP molecule appearing next to the active site of BC synthetase is coordinated with the R580 residue and enables it to weaken and lose its links to the functional residues of the loop, shielding the entrance to the active site. As a result, the entire loop that blocks the entrance to the catalytic center of the enzyme shifts to the side, making BC synthetase available for the substrate. Consequently, BC synthesis is predetermined by the molecule c-di-GMP appearing in the medium. As a rule, an artificial introduction of this substance into the medium leads to the activation of phosphodiesterases in the cells catalyzing decomposition of the substance. Therefore, the impact of the substance depends on whether it was synthesized by the cells themselves [28]. Therefore, in order to increase the synthesis of BC, it is necessary to foster the cell production of the substance. However, as is known, c-di-GMP is a "quorum factor," that is a substance that is synthesized by cells and is indispensable for their transition to a quorum state (when highly concentrated populations are formed, whose functioning is stabilized by the expression of "silent genes" and the synthesis of exopolysaccharides with a simultaneous decrease in the rate of active cell growth). Therefore, cells that produce BC should be stimulated to come into a quorum state, that is into a programmed genetic response of cells to their increased concentration per

unit volume. The rectitude of these arguments is confirmed by recently published results, according to which BC synthesis is activated when cell concentration notably increases [29].

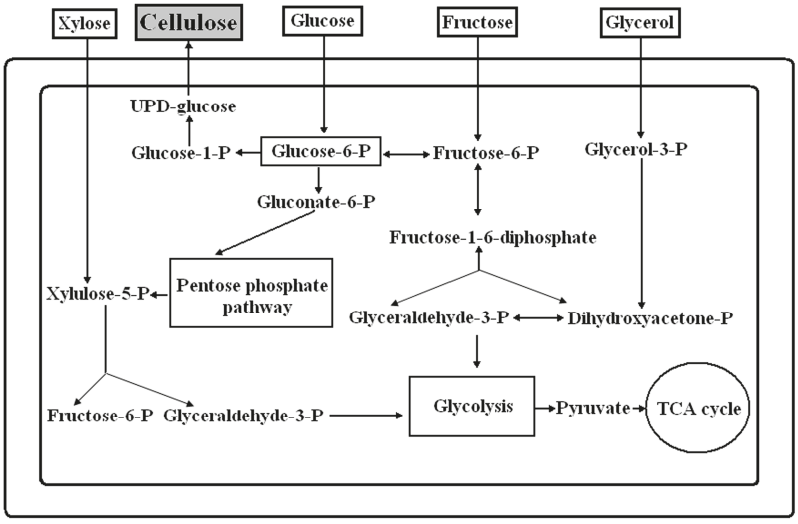

Figure 1. General scheme of sugars' conversion and bacterial cellulose synthesis by *Komagataeibacter xylinum* bacterial cells. TCA (tricarboxylic acid cycle).

Theoretically, in the case of BC producers, the immobilization of cells could allow one to obtain highly concentrated populations of cells where BC biosynthesis is regulated by such phenomena as quorum sensing [30]. Therefore, application of cell immobilization looks like a way to improve cell stabilization and increase process productivity. Despite the mentioned advantages of immobilization, currently examples of using immobilized producer cells of BC are rare. For example, to increase the synthesis of BC, a bioreactor was used with *Acetobacter xylinum* ATCC 700178 cells immobilized on a plastic composite support (PCS) produced on the basis of polypropylene. The synthesis of BC has been shown to increase 2.5-times as compared with free cells. The obtained BC samples had a higher degree of crystallinity (93%) with a crystal size of 5.2 nm. Such cellulose samples had improved tensile properties [22]. However, the researchers emphasized that the support used and the method of immobilization applied (cell adsorption on the surface of the carrier) did not enable long-term application of the immobilized cells in BC production.

The possibility and effectiveness of the application of immobilization methods differed from cell adsorption for BC producers, namely inclusion of bacterial cells into the gel matrices, under question, since according to the basic ideas with regard to the immobilization of microorganism cells, it is considered expedient to include cells in gel carriers only if the substrate and product for these cells are low molecular substances [31,32]. The highly molecular weight polysaccharide like BC is synthesized by cells being inside of the carrier, while BC should accumulate in the medium.

This situation seems nonsensical. However, having extensive and successful experience in applying poly(vinyl alcohol) (PVA) cryogels, which ensure favorable conditions for mass transfer processes for immobilized cells of various microorganisms [33,34], it was decided to try this medium to immobilize BC producers. The idea of such an investigation initially seemed ineffective, but the prospect of looking at the final result was encouraging (namely, at the BC cell synthesis and the polymer yield out of the carrier). Since PVA cryogel has a macroporous structure with a variable pore size, it is a stable in chemically different media and has high mechanical and thermal resistance while being inexpensive and generally recognized as safe [35], so its use seemed very attractive.

Thus, the purpose of this study was to investigate the possibility and effectiveness of employing *Komagataeibacter xylinum* bacterial cells in an immobilized form with the use of a highly porous support (PVA cryogel) for cell inclusion in the process of BC biosynthesis while different culture media prepared using hydrolysates of various renewable sources of biomass (aspen, Jerusalem artichokes, wheat and rice straw) were applied. The comparison analysis of BC production by the same free and immobilized cells as biocatalysts was also very interesting.

2. Results

2.1. Conditions Influencing BC Production by Immobilized Cells

Initially, the samples of immobilized biocatalysts based on *Komagataeibacter xylinum* B-12429 cells were produced by using PVA cryogel in the form of granules and sheets (Figure 2).

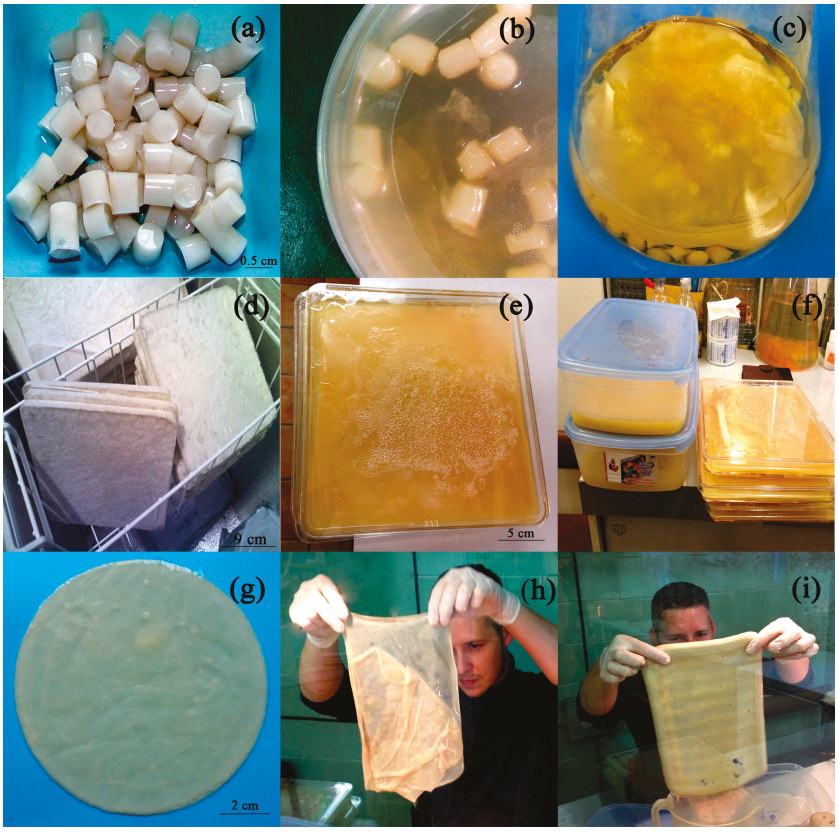

Figure 2. Bacterial cellulose (BC) production by immobilized *Komagataeibacter xylinum* cells. Images of immobilized biocatalysts based on poly(vinyl alcohol) (PVA) cryogel in the form of granules (**a**–**c**) or sheets (**d**–**f**); beginning of BC appearance from the granules with immobilized cells (**b**); PVA cryogel sheet with immobilized cells after biocatalyst obtaining and its placing into the nutritional medium (**e**,**f**); flask with granules containing immobilized cells and accumulated layer of BC (**c**); boxes with biocatalyst sheets for BC obtaining (**f**); BC formed in the flask (**g**) and box with cells immobilized in cryogel sheet (**h**); PVA cryogel sheet with immobilized cells after its use in the first cycle of BC production (**i**).

Firstly, the immobilized biocatalyst shaped like granules was used for BC accumulation in the Hestrin–Schramm (HS) medium (pH 5.6) with 20 g/L glucose. To better visualize the appearance of BC from granules with immobilized cells, the sample of the biocatalyst was placed into a Petri dish (Figure 2b). It became clear that immobilized cells weaved and push out the pieces of BC from the volume of polymeric granules (Figure 2b) that further combine into the joint BC slice. Further, a portion of granules was inoculated into HS-medium for accumulation of BC in flask (Figure 2c) to evaluate the efficacy of producing BC by using immobilized cells (Figure 3). A process using immobilized and free cells concurrently conducted during 190 h at a temperature of 28 °C. The initial concentrations of cells in the medium were the same and equaled 0.03 g cell dry weight (CDW)/L.

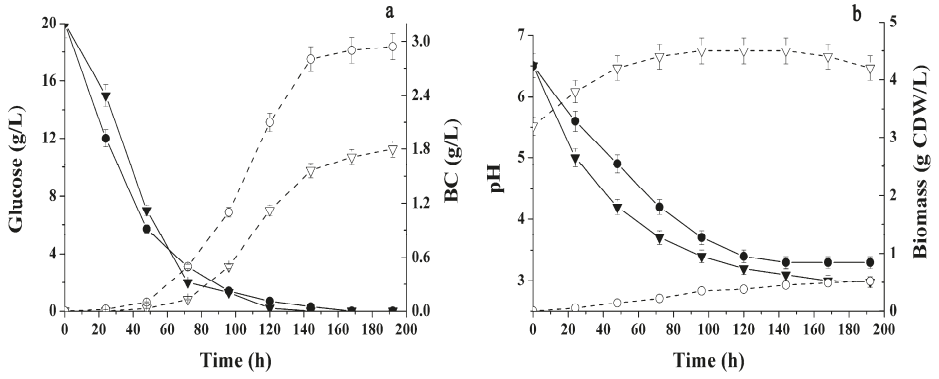

Figure 3. The kinetics of glucose consumption (black symbols) and BC production (white symbols) (**a**); pH changes (black symbols) and accumulation of free cell biomass (white symbols) (**b**) in the Hestrin–Schramm (HS)-medium with *Komagataeibacter xylinum* B-12429 cells taken in free (triangles) and immobilized (circles) forms. CDW (cell dry weight).

It was shown that almost all the glucose amount initially introduced into the medium was consumed by the cells by 120 h (Figure 3a). Accumulation of BC was 1.6-times higher with immobilized cells employed in comparison with free producers. The accumulation of free cells in the medium was negligible in the case of immobilized biocatalyst and maximally amounted to 0.05 g CDW/L, which was six-times less in comparison with suspended cells used as BC producers (Figure 3b). Obviously, this process was followed by the decrease in pH of culture medium owing to accumulation of acidic metabolites, and in the case of immobilized cells it was notably less intensive especially for the first 70 h of cultivation.

The effect of varying the shape of immobilized biocatalyst (granules or sheets), as well as the concentration of cells initially introduced into the PVA cryogel on the process of BC producing by immobilized biocatalyst was investigated (Table 1). It was demonstrated that the rate of BC accumulation in the medium slightly increases as the concentration of immobilized cells rises from 20–60 g CDW/kg in granules, whereas the general amount of PVA cryogel with entrapped cells was the same in all samples. There was no difference between concentrations of BC accumulated by cells immobilized in polymer matrix shaped like granules or sheets.

The use of increased concentration of immobilized cells in the PVA cryogel allows one to enlarge the cell concentration in the medium without changing the total amounts of biocatalysts implemented in the process. The introduction of cell biomass in the range 3.2–9.5 g CDW/L into immobilized biocatalyst did not result in the significant improvement of the process productivity, which was probably due to the limitation of immobilized cells along the substrate in the polymer support. Nevertheless, the presence of macroporous matrix such as PVA cryogel spatially dividing the cells between each other and concurrently allowing retaining a high volumetric concentration of cells

appeared to change by a little bit the mentioned conception related to cell inoculum concentrations useful for BC production.

Table 1. The result of the application of immobilized biocatalyst of different shapes containing different concentrations of bacterial cell biomass in the synthesis of BC in an Hestrin–Schramm -medium with 20 g/L of glucose. CDW, cell dry weight. BC, bacterial cellulose.

Shape of Immobilized Biocatalyst	Dry Cell Biomass Concentration in Immobilized Biocatalyst (g/kg)	BC (g/L)	Biomass of Free Cells Accumulated in the Medium (g CDW/L)
Granules	20	2.9 ± 0.1	0.50 ± 0.03
	40	3.4 ± 0.2	0.53 ± 0.04
	60	3.6 ± 0.2	0.57 ± 0.05
Sheets	20	2.8 ± 0.1	0.75 ± 0.05
	40	3.2 ± 0.2	0.88 ± 0.04
	60	3.4 ± 0.2	0.98 ± 0.07

2.2. Different Sugars and Glycerol as Sources for BC Synthesis

Then, it was further investigated what the impact of the glucose concentration introduced into the medium on the yield of BC produced by immobilized biocatalyst in the same concentration of 9.5 g CDW/L was. For this purpose, the glucose concentration ranging from 30–100 g/L was further applied (Figure 4). It was demonstrated that when the original concentration of glucose in the medium was 30 g/L, there was an increase in BC accumulation, and the BC productivity of the process was 1.25-time higher.

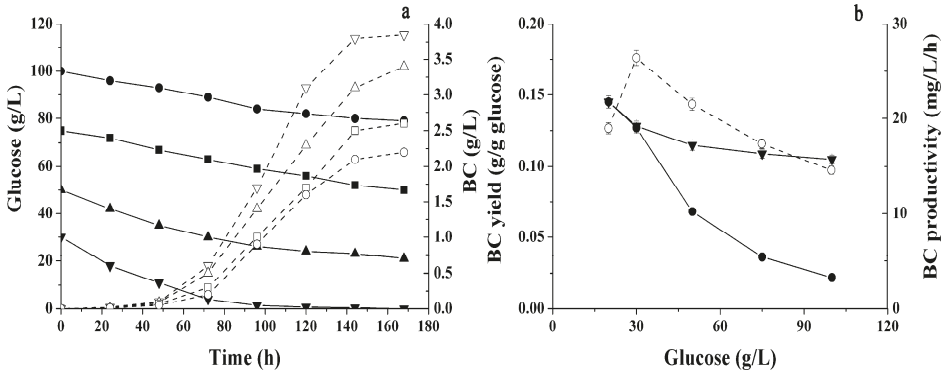

Figure 4. The kinetics of glucose consumption and BC production by immobilized *Komagataeibacter xylinum* B-12429 cells in the HS-medium with different glucose concentrations (g/L): ▼ −30, ▲ −50, ■ −75, ●−100 (**a**). The BC output depending on the concentration of glucose consumed (■), the BC output depending on the initial glucose concentration (●) and the rate of BC accumulation (○) by immobilized cells depending on the initial glucose concentration in the medium (**b**).

The optimal initial concentration of glucose in the medium appeared to be 30 g/L (Figure 4), and when it was over this level, both parameters such as process productivity and the target product yield decreased with the consumed substrate taken into account. When the initial concentration of glucose in the medium was more than 50 g/L, immobilized cells produced BC 1.3-times less than during the same time period compared to the concentration of glucose at 30 g/L, while the glucose consumption rate decreased. Accumulation of free cells in the culture liquid was more pronounced at higher concentrations of glucose in the medium. Therefore, a part of the consumed substrate was

obviously used by immobilized cells for free biomass accumulation instead of BC synthesis, since then, the use of glucose concentration over 30 g/L appeared to be unreasonable.

The study was focused on the potential of using not only glucose, but other sugars as sources of carbon for BC obtaining (Table 2). To this end, various mono- and di-saccharides (as well as their mixtures at a concentration of 20 g/L) were introduced into the HS-medium instead of glucose; a parallel assessment of the level of BC was performed that was produced in these media by free and immobilized cells used in the same concentrations. The process was conducted over seven days at 28 °C. Once again, immobilized cells provided the best indicators for the process, but both them and free cells showed a low BC yield in media with maltose and galactose taken as the main carbon source; xylose and arabinose happened to be almost non-convertible into BC by the bacterial strain used. In general, the experiment confirmed that the cells investigated can synthesize BC in media with mixtures of different sugars, and this created the grounds for further study of possibilities for producing BC in media with hydrolysates of various renewable raw materials, in which such mixtures of sugars are present.

Table 2. Concentration of BC produced by free and immobilized cells of *Komagataeibacter xylinum* B-12429 in the media with different sugars.

Sugar	Concentration (g/L)	BC (g/L)	
		Free Cells	Immobilized Cells
Arabinose	20	0.03 ± 0.01	0.07 ± 0.01
Galactose	20	0.08 ± 0.01	0.12 ± 0.02
Glucose	20	1.8 ± 0.10	3.6 ± 0.20
Xylose	20	0.19 ± 0.02	0.24 ± 0.03
Maltose	20	0.04 ± 0.01	0.08 ± 0.01
Sucrose	20	1.9 ± 0.20	2.8 ± 0.20
Fructose	20	2.1 ± 0.20	3.1 ± 0.20
Glucose/Fructose	10/10	1.9 ± 0.10	3.2 ± 0.20
Glucose/Sucrose	10/10	1.8 ± 0.20	2.4 ± 0.20
Glucose/Xylose	10/10	0.8 ± 0.10	1.3 ± 0.10
Glucose/Fructose	15/5	1.8 ± 0.10	2.8 ± 0.20
Glucose/Fructose	5/15	2.1 ± 0.10	3.5 ± 0.20

According to the literature data [14], glycerol may be a promising substrate for BC synthesis, which is a large-tonnage waste product of biodiesel production. In this connection, there has been a study of BC synthesis by immobilized cells in a medium with glycerol in various concentrations (Figure 5). It was found that an increase in the initial concentration of glycerol in the medium to 20 g/L triggered an increase in the concentration of the BC accumulating. However, a subsequent increase in the concentration of glycerol did not lead to increased levels in BC synthesis. Thus, it was first shown that glycerol can be successfully applied as the main source of carbon for the BC production with immobilized cells, with the level of BC synthesis using 20 g/L of glycerol comparable to the level of BC synthesis in media with 20 g/L of glucose (Table 2).

2.3. Various Hydrolysates of Renewable Raw Materials as Media for BC Obtaining

To assess the range of the substrates spectrum employed to obtain BC produced by immobilized cells, a process was conducted during six days under static conditions using enzymatic hydrolysates of plant materials (aspen, rice straw, wheat straw and Jerusalem artichoke) (Table 3). The concentration of immobilized and free cells was identical (9.5 g CDW/L). The initial concentration of reducing sugars (RS) in hydrolysates was analyzed (Table 3). It should be noted that the main sugar in the aspen, rice and wheat straw hydrolysates was glucose, and in the artichoke hydrolysate, there were two main sugars: fructose (36 g/L) and glucose (17 g/L). It was found that the concentration of BC produced by immobilized cells in the artichoke enzymatic hydrolysate was 1.25-time higher than it was in the

enzymatic hydrolysates of aspen, wheat and rice straw. The advantages of immobilized cells were also obvious in this process.

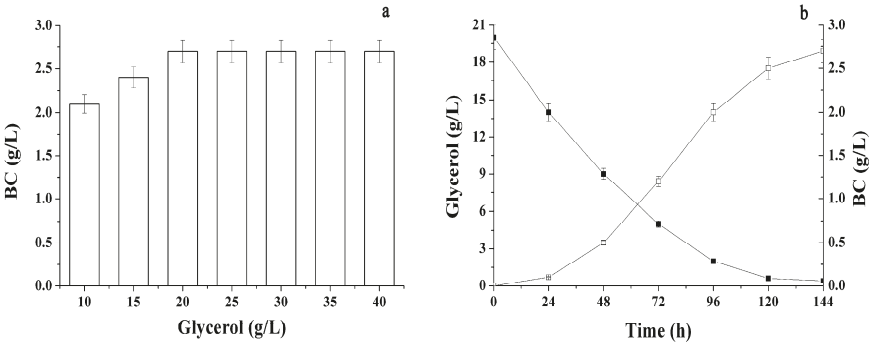

Figure 5. Influence of glycerol concentration in medium as a single carbon source on the synthesis of BC by immobilized *Komagataeibacter xylinum* cells (**a**) and the kinetics of glycerol consumption (■) and BC production (□) in a medium with 20 g/L glycerol (**b**).

Table 3. The production of BC by free and immobilized cells in media with hydrolysates of renewable raw materials. RS, reducing sugars.

Parameters	Cells	Hydrolysate			
		Aspen	*Jerusalem artichoke*	Rice Straw	Wheat Straw
The residual concentration of RS (g/L)	Free	11.0 ± 0.5	17.0 ± 0.4	7.8 ± 0.2	4.6 ± 0.3
	Immobilized	12.8 ± 0.5	22.7 ± 0.4	9.8 ± 0.4	7.8 ± 0.3
BC (g/L)	Free	2.2 ± 0.2	2.5 ± 0.2	2.4 ± 0.2	2.4 ± 0.3
	Immobilized	2.9 ± 0.1	4.5 ± 0.2	3.5 ± 0.3	3.6 ± 0.2
BC (g/g RS)	Free	0.07 ± 0.01	0.07 ± 0.01	0.08 ± 0.01	0.07 ± 0.01
	Immobilized	0.1 ± 0.01	0.15 ± 0.02	0.12 ± 0.01	0.12 ± 0.01
BC productivity (g/L/day)	Free	0.37 ± 0.2	0.42 ± 0.3	0.40 ± 0.3	0.40 ± 0.3
	Immobilized	0.48 ± 0.2	0.75 ± 0.3	0.60 ± 0.3	0.60 ± 0.3

The process of the transformation of sugars present in biomass hydrolysates of micro- and macro-algae in BC was carried out (Table 4). The conditions of the process were identical to the previous experiment. The best indicators for BC synthesis were achieved in a medium with hydrolysates of *Chlorella vulgaris* biomass. However, for hydrolysates of macroalgae in general compared to hydrolysates of other renewable raw materials (Table 3), BC synthesis was lower, which may be explained by the high viscosity of the medium itself, which was caused by strongly swelling substrates, which prevented a highly effective mass transfer in the cells.

Table 4. Characteristics of the BC production by immobilized *Komagataeibacter xylinum* B-12429 cells in the media based on hydrolysates of biomass of micro- and macro-algae. RS, reducing sugars.

Hydrolysates	Initial RS (g/L)	Initial Glucose (g/L)	Accumulated BC (g/L)	BC Productivity (g/L/day)
Chlorella vulgaris C1	45.1 ± 1.6	29.0 ± 0.8	2.62 ± 0.12	0.440 ± 0.020
Laminaria saccharina (brown)	36.6 ± 1.1	5.1 ± 0.1	0.07 ± 0.01	0.012 ± 0.001
Acanthophora muscoides (red)	56.0 ± 1.4	13.2 ± 0.3	0.42 ± 0.01	0.070 ± 0.010
Ulva lactuca (green)	24.1 ± 0.7	7.3 ± 0.2	0.08 ± 0.02	0.013 ± 0.002

In this regard, cells immobilized in PVA cryogel were reused multiple times under static conditions of BC production. For this purpose, the culture broth was replaced with a fresh medium (artichoke hydrolysate) after each working cycle in the reactor with immobilized cells (Figure 6). It was shown that immobilized cells maintain 100% metabolic activity after 10 cycles under static conditions (60 days). The BC yield in this case amounted to 4.5 ± 0.1 g/L, and the process productivity was 0.75 ± 0.2 g/L/day.

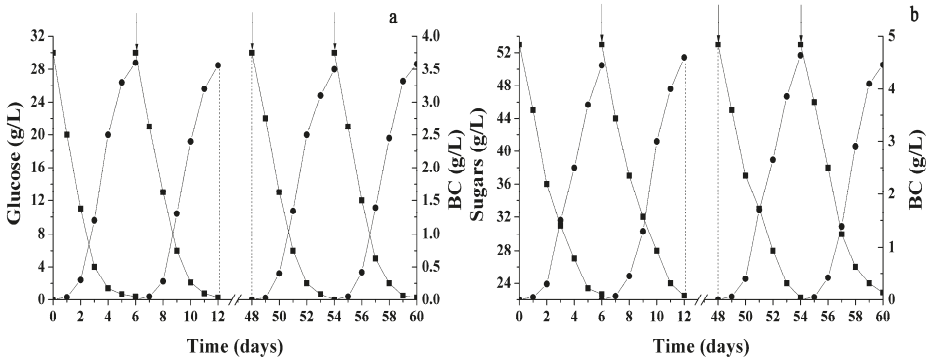

Figure 6. The sugars consumption (■) and BC accumulation (●) during the repeated use of *Komagataeibacter xylinum* B-12429 immobilized cells (9.5 CDW g/L) under static conditions. The broken lines and the arrows indicate the time when the culture broth was substituted with a fresh medium: containing glucose (**a**) or hydrolysate of Jerusalem artichoke (**b**).

One of the known advantages of immobilized cells is in the fact that they can be re-used many times in biotechnological procedures, and in this work, immobilized cells demonstrated a high metabolic activity after 10 working cycles under batch static conditions when the artichoke enzymatic hydrolysate was used as a carbon source (Figure 6).

At the next stage, the obtained BC samples' characteristics were investigated (Table 5). As it turned out, BC produced with immobilized cells under the same conditions with free cells had higher tear resistance, a 30% greater thickness and a higher degree of polymerization. An even thicker and more durable BC film was formed by culturing immobilized cells on the hydrolysate of Jerusalem artichoke. As for the other properties, the resulting films were virtually identical.

Table 5. Properties of the BC produced by *Komagataeibacter xylinum* B-12429 cells in free and immobilized forms under identical conditions.

Parameters	BC Free Cells	BC Immobilized Cells				
				Hydrolysates of		
	Glucose	Glucose	Glycerol	*Jerusalem artichoke*	Rice Straw	Biomass of *Chlorella. vulgaris*
Humidity (%)	97.5 ± 0.3	97.2 ± 0.2	97.1 ± 0.2	97.0 ± 0.2	97.3 ± 0.2	98.2 ± 0.2
Thickness (microns)	35 ± 5	45 ± 5	65 ± 3	70 ± 5	40 ± 2	40 ± 3
Tensile strength (MPa)	50 ± 10	70 ± 10	75 ± 15	80 ± 15	65 ± 10	55 ± 10
Young's modulus (GPa)	1.2 ± 0.2	1.6 ± 0.2	1.5 ± 0.2	1.8 ± 0.2	1.4 ± 0.2	1.3 ± 0.2
Crystallinity (%)	81 ± 1	82 ± 1	78 ± 1	79 ± 1	79 ± 1	77 ± 1

3. Discussion

The formation of BC three-dimensional interconnected reticular pellicle was previously reported for free cells cultivated under static conditions [10]. According to the results of Borzani and Desouza [36], the process of cellulose formation under static conditions is regulated by the concentration of free cells in the medium, and BC synthesis usually reaches its limit when the pellicle growth is downward, since BC entraps all bacteria, and bacterial cells become inactive due to insufficient oxygen supply through the BC-cover with nanosized pores. The process of BC formation under static condition is regulated by air supply from the medium surface [37]. All these facts were generated in the following existing paradigm: when the bacterial cells are entrapped by adsorption into BC matrix, they are metabolically inactive, so the immobilization of BC producers is not a good means for successful production of the polysaccharide.

This work demonstrated the opposite results to this paradigm since the immobilization of BC-producing cells into PVA cryogel appeared to be efficient. Obviously, the effect was obtained owing to the difference between the porous characteristics of the specially-used PVA cryogel and naturally-forming BC that have micro- and nano-porous structures, correspondently.

An advantage of applying immobilized cells is the possibility of their repeated use, which can be quite beneficial in BC production, since it is known that during BC formation, free bacterial cells are adsorbed on its surface [10], making it necessary to constantly re-grow a fresh biomass of cells for BC producing, and the process of accumulation of BC producer biomass takes about 24 h [38,39]. This means that with immobilized cells, it is possible to overcome this problem (loss of time for biomass accumulation de novo) in BC production.

The use of HS-medium for genus *Komagataeibacter* cells usually provides low enough levels of accumulated BC. For example, it was shown for *K. hansenii* cells that application of HS-medium results in production of BC in concentration of 0.422 ± 0.007 g dry weight (DW)/L for 14 days under static conditions [40]. In another publication, one can see that it possible to reach the BC accumulation by free cells in a concentration of 1.15 ± 0.03 g DW/L by using HS-medium for seven days [41]. In this work, the BC was obtained under the same conditions (HS-medium, seven days and static cultivation) in concentrations of 1.74 ± 0.03 g DW/L and 2.9 ± 0.1 g DW/L when the free and immobilized *Komagataeibacter xylinum* cells were used, correspondently. Therefore, it appeared that production of BC depends not only on the medium used, but is influenced by both species of bacterial genus *Komagataeibacter* and the state of cells (suspended or immobilized) used in the process.

Medium pH was found to be critical for high BC productivity in many studies [10,11]. Obviously, gluconic acid reduces the pH of the medium down to 3.0, which can result in inhibition of BC accumulation. It is worth noting that in the medium with immobilized cells, there was also a notable decrease in pH of the medium (Figure 3) already after the first day of cultivation, but it was less than in samples with free cells, probably due to less formation of metabolites (of gluconic acid lowering the pH, in particular) and more accumulation of BC.

The main purpose of this work was to develop and use a biocatalyst in the form of PVA cryogel-immobilized *Komagataeibacter xylinum* cells that can more efficiently produce BC in the batch static mode of cultivation as compared to free cells and to demonstrate that immobilization of bacteria is not a barrier for BC production.

The increased BC accumulation by immobilized *Acetobacter xylinum* ATCC 700178 cells as compared to their suspended form was previously published by Cheng et al. [22]. These experimental data were obtained with cells adsorbed on PCS, so the conditions of the immobilizing procedure were very friendly for cell survival. The results of the present investigation also demonstrated that the BC-producing cells were rather successful at surviving within the immobilization procedure consisting of freezing a cell suspension in a PVA solution with simultaneous formation of a cryogel matrix around the cells.

The concentration of BC-producing cells initially introduced into the process plays an important role in cellulose production. For instance, it was revealed that the increase in cell inoculum

concentration over 5% (*v*/*v*) lowers the BC yield [42]. A similar conclusion done by other researches experimentally revealed how the amount of cell inoculum influences the BC production [43]. It appeared that when the inoculum concentration was decreased from 6–4% (*v*/*v*), the BC accumulation was increased, and further increasing or decreasing the inoculum from 4%, a decline in BC production was observed. Hornung et al. reported that for maximum BC production, the total cell count is not important, and the really significant quantity is the number of cells in the aerobic zone that are producing BC [23]. In this work, it was clearly shown that the initial concentration of cells in the medium can affect the BC production efficiency (Table 1), and an increase in cell concentration can be positive if the cells are in immobilized form, allowing one to separate them from each other in the frame of the porous matrix.

It is known then that a higher concentration of glucose is initially used for BC production, then lower BC yield can be observed, since the accumulation of cell-inhibiting concentrations of gluconic acid is occurring [10,44]. However, it was shown that BC production can be enhanced with increased glucose concentration up to 4% (*w*/*v*), but decreased above 4% along with the decline of pH-medium to below 2.58 [25].

In is known from previous publications that replacement of glucose-containing HS-medium for suspended cells by glucose-containing hydrolysates obtained on the basis of different wastes usually resulted in increased BC yield. For instance, the use of wheat straw hydrolysates provided 15.4 g/L BC, and the level of BC accumulation was 50% higher as compared to the same parameter obtained using routine carbon sources [45]. BC from cotton cloth hydrolysate was obtained at a yield of 10.8 g/L, which was 83% higher than that from the culture grown on glucose-based medium [16]. A low-cost medium based on soya bean whey (SBW) was used for the production by *Komagataeibacter* sp. PAP1 [41]. The use of SBW medium increased BC production 3.6-fold compared to standard HS-medium. The use of corncob acid hydrolysate as a substrate for BC production by *Gluconacetobacter xylinus* cells provided a BC yield of 4 g/L after 14 days of static cultivation. [44]. This investigation of the possible use of agricultural waste hydrolysates for BC production by immobilized cells demonstrated both productivity and BC yield at a high level in the medium containing artichoke enzymatic hydrolysate (Table 3). Most likely, this was due to the fact that the artichoke hydrolysate included a mixture of sugars (glucose and fructose). Zeng et al. noted that BC production with maple syrup was almost as high as when using pure fructose and much higher than when using glucose [46], and this fact is consistent with the viewpoint that the composition of sugars does not affect BC production if fructose exists in the medium, possibly because fructose activates a phosphoenolpyruvate-dependent phosphotransferase system in *A. xylinum* [47]. In addition, it is worth noting that all the glucose was fully utilized by cells, and the residual concentration of fructose was 22.7 g/L. In other hydrolysates, there was only glucose present.

The results obtained during multiple use of immobilized cells for BC production were very good and show promise to be used in practice, since Cheng et al. previously used PCS as a support for cell immobilization by adsorption of bacteria on the surface of the carrier and reported that this matrix and method did not contribute to a long period of employing the immobilized cells to produce BC [22].

The characteristics of BC samples produced by *Komagataeibacter xylinum* in both free and immobilized form under identical conditions demonstrated higher tear resistance and greater thickness, as well as a higher degree of polymerization of BC produced by immobilized cells. These results correlate with the data of other researches. For example, Suwanposri et al. noted that mechanical properties of BC accumulated in the medium based on the use of SBW had a 108% increase in tensile strength and an 841% rise in Young's modulus over those of the HS medium [41]. However, the elongation at break of SBW film (3.28%) was 3.4-time less than that of HS film (11.17%). Huang et al. showed that BC produced from corncob acid hydrolysate had relatively high crystallinity and a high crystallinity index value (95.2% and 93.8%, respectively) [44]. The mechanical strength analysis done by Cheng et al. demonstrated that BC produced by being immobilized on PCS cells, similar to the pellicle form, improved its tensile strength to a point comparable to that observed in pellicle form [22].

4. Materials and Methods

4.1. Microbial Strains and Culture Media

A strain of *Komagataeibacter xylinum* B-12429 bacteria that derived from the Russian National Collection of Industrial Microorganisms (Moscow, Russia) was used in the study. The cell culture was carried out under aerobic conditions using the thermostatically-controlled shaker Adolf Kuhner AG (Basel, Switzerland) and BioSan ES-20 (Riga, Lithuania), which enabled continuous agitation of the culture liquid (150 rpm). To accumulate bacterial biomass at a temperature of 29 ± 1 °C, a culture medium, Hestrin–Schramm (HS), was used that had the following composition (g/L): glucose: 20; yeast extract: 5; peptone: 5; $K_2HPO_4 \cdot 3H_2O$: 2.7; $MgSO_4 \cdot 7H_2O$: 0.5; citric acid: 1.15, pH: 5.6 ± 0.2.

4.2. Cells' Immobilization

Immobilized cells were produced using a patented procedure [48] by adding to a poly(vinyl alcohol) (PVA) aqueous solution (12%) the biomass of bacteria cells previously separated from the culture medium by centrifugation with a Avanti J 25 (Beckman Coulter, Brea, CA, USA) at 8000 rpm during 15 min. The final concentration of cell biomass in the obtained suspension was 20–60 g cell dry weight (CDW)/kg (Table 1). The mixture of polymer solution and cells was stirred to obtain a homogeneous mass, which was afterwards used to form granules by dispensing the cell suspension into the PVA aqueous solution per 0.5 mL into each well of 96-well plates or the suspension was poured in an even layer (0.5 cm) into a flat bottom tank (30 × 30 cm) to form a single layer of PVA cryogel with cells included in it. All plates were further frozen at −20 °C, then kept in the frozen state for 24 h and later thawed at 8 °C during 8–12 h to obtain immobilized biocatalysts in the form of granules or sheets (Figure 2a–f).

4.3. Analytical Methods

The growth of the biomass of free cells was monitored by spectrophotometry. The degree of optical absorption of samples of the culture liquid at 540 nm was monitored using the spectrophotometer Agilent UV-853 (Agilent Technologies, Waldbronn, Germany), and the exact concentration of the cells was determined by calibration curves that establish the dependence of the optical absorption on the precisely known concentration of cells in a sample to be analyzed. Glucose concentration was determined by the enzymatic technique using a standard Impact reagent kit ("OOO Impact", Moscow, Russia). The Shomody–Nelson method was applied to determine the concentration of reducing sugars (RS) [49]. The concentration of fructose was determined by liquid chromatography under high pressure using a 1100 Agilent chromatograph with an amperometric detector (Agilent Technologies, Waldbronn, Germany) and a Dionex Carbopak PA-20 anion exchange column (Thermo Fisher Scientific, Waltham, MA, USA). A solution of 7.5 mM NaOH was used as the eluent.

Potentiometric measurements were conducted to control pH values of the media prepared and of samples selected in the experiments (a Corning Pinnacle 530 pH-meter (Corning Incorporated, New York, NY, USA) was used).

To determine cell dry weight (CDW), we used a sample of the biomass separated from the culture liquid by centrifugation (8000 rpm, 10 min, Avanti J 25 centrifuge (Beckman Coulter, Brea, CA, USA)) that was brought to constant weight by drying at +80 °C. A granule of the immobilized biocatalyst was also dried to constant weight. Knowing the initial concentrations of cells and the weight of the polymer when forming the granules, we calculated the concentrations of cells in the immobilized biocatalyst using the dry weight parameters.

4.4. BC Production

The following variant of HS-medium (g/L) was used to produce BC (Figure 2g,h): peptone: 5; yeast extract, 5; K_2HPO_4, 2.7; $MgSO_4$, 0.5; citric acid, 1.15; but its pH value was adjusted to 7.0 ± 0.1 with 2 M KOH. The concentration of glucose was varied (20–100 g/L) in the medium. The process

was conducted at 28 °C during 6–7 days under static conditions in a 500-mL Erlenmeyer flask (Purex, Corning Incorporated, New York, NY, USA) with 100 mL of medium.

Free cells and biocatalysts shaped like granules or sheets (Figure 2c,i) with immobilized cells were used multiple times under the same conditions to produce BC. In some experiments, the glucose was replaced in HS-medium by glycerol. In experiments with hydrolysates of renewable sources, the HS-medium was completely replaced by them.

We purified the BC film by placing it into a 0.5% NaOH solution for 24 h at a temperature of 25–27 °C and stirring it periodically. After the BC-film was washed in distilled water, its properties were investigated.

4.5. Pretreatment and Fermentative Hydrolysis of Biomass

Samples of aspen, rice and wheat straw were pre-dried to a residual humidity of 7–10% and milled to a particle size of 100–300 microns using an impeller mill Mikrosilema IM-450 (Techpribor, Schekino, Russia). Physicochemical pretreatment of the renewable biomass was carried out in the presence of 1.5% H_2SO_4 at 150 °C during 1 h. A mixture of commercial preparations of cellulases such as Spezyme CP (Dupont, Ney York, NY, USA) and Novozyme-188 (Novozymes Corp., Copenhagen, Denmark) was used for the enzymatic hydrolysis of renewable raw materials (the ratio between preparations in the mixture was 3:1). Enzyme preparations were introduced into the reaction medium (10 mg of protein per 1 g of the substrate dry matter). Hydrolysis was carried out in the medium based on 0.05 M citrate buffer (pH 5.0) at 50 °C and with constant stirring at 250 rpm during 24 h.

Jerusalem artichoke tubers (humidity: 0%) were hydrolyzed by introducing into the crushed mass of enzyme preparations of inulinases from *Aspergillus niger* (Novozymes Corp., Copenhagen, Denmark), cellulases (2 mg of total protein/g of the dry substrate) and β-glucosidase (40 units of cellobiase activity/g of the dry substrate). The hydrolysis was carried out without addition of water at 50 °C, pH 6.5 and constant stirring at 250 rpm for 6 h. At the end of the process, the hydrolysate was separated from the non-hydrolyzed biomass by centrifuge (Beckman Coulter, Brea, CA, USA) at 6000 rpm during 10 min.

In all samples of obtained hydrolysates, the pH value was adjusted with 2 M KOH up to 7.0 ± 0.1 before their application in BC production.

4.6. Characterization of BC Samples

The tensile strength and Young's modulus of the BC pellicles were analyzed through tensile tests, using a testing machine BP DLC 1 (Tochpribor, Moscow, Russia). The specimens were cut in a rectangular shape using a paper cutting machine, producing samples with dimensions of 1 cm × 7 cm individual sample thickness. Three samples were cut per pellicle and used in each experimental session. The BC samples were stretched at a constant speed of 5 mm/min until the failure of the sample occurred. A Mitutoyo digital thickness indicator was used to measure the thickness of each specimen (Mitutoyo Corp., Kanagawa, Japan).

The crystallinity index of BC was measured using X-ray diffractometric analysis as described by Mohammadkazemi et al. [50]. A multi-purpose diffractometer Philips PW3040/60 (Philips, Amsterdam, The Netherlands) was used in this work. Analysis of polymerization degree and purity of BC was done as described by Lu et al. [5]. Dried BC samples were soaked in deionized water during 12 h at room temperature, and the weight in water was measured by harnessing the sample in a device, which suspended the sample in water. The porosity was calculated using the following formula: porosity (%) = (wet weight − dry weight)/(wet weight − weight in water) × 100.

All experiments were carried out in triplicate. The microbiological purity of cultures used in this work was monitored by microscopy using an Axio Imager Z2m microscope (Carl Zeiss MicroImaging GmbH, Jena, Germany).

5. Conclusions

In summary, these studies revealed the high efficacy of a new biocatalytic system in the form of bacterial cells immobilized in PVA cryogel for BC production. By using the porous support as the matrix for the cell immobilization, it becomes possible to deceive cells, and we did not allow them to cover themselves with the BC layer, which normally stops the cell functioning. Immobilized cells in a state of highly concentrated populations have substantially higher rates of metabolic processes and a higher yield of the target product when compared with free cells, resulting in increased efficiency of the overall process of BC production. Furthermore, these studies demonstrated the possibility of repeated use of immobilized cells retaining 100% of their metabolic activity for at least 10 working cycles (60 days). The approach based on the application of immobilized cells enables obtaining BC possessing the same crystallinity and porosity as in the process with free cells, but having improved stiffness and tensile strength. Various media containing sugars and glycerol, based on hydrolysates of agricultural materials and biomass of microalgae, were successfully applied as effective sources for BC production by immobilized cells.

Acknowledgments: This work was financially supported by the Russian Foundation for Basic Research (Grant No. 16-08-00457).

Author Contributions: E.E. conceived of and designed the experiments. N.S. performed the experiments. N.S. and E.E. analyzed the data and wrote the paper.

Conflicts of Interest: The authors declare no conflict of interest.

References

1. Ullah, H.; Santos, H.A.; Khan, T. Applications of bacterial cellulose in food, cosmetics and drug delivery. *Cellulose* **2016**, *23*, 2291–2314. [CrossRef]
2. Sulaeva, I.; Henniges, U.; Rosenau, T.; Potthast, A. Bacterial cellulose as a material for wound treatment: Properties and modifications. A review. *Biotechnol. Adv.* **2015**, *33*, 1547–1571. [CrossRef] [PubMed]
3. Rajwade, J.M.; Paknikar, K.M.; Kumbhar, J.V. Applications of bacterial cellulose and its composites in biomedicine. *Appl. Microbiol. Biotechnol.* **2015**, *99*, 2491–2511. [CrossRef] [PubMed]
4. Mohite, B.V.; Patil, S.V. A novel biomaterial: Bacterial cellulose and its new era applications. *Biotechnol. Appl. Biochem.* **2014**, *61*, 101–110. [CrossRef] [PubMed]
5. Lu, H.; Jiang, X. Structure and properties of bacterial cellulose produced using a trickling bed reactor. *Appl. Biochem. Biotechnol.* **2014**, *172*, 3844–3861. [CrossRef] [PubMed]
6. Gayathry, G.; Gopalaswamy, G. Production and characterization of bacterial cellulose fibre from *Acetobacter xylinum*. *Indian J. Fibre Text. Res.* **2014**, *39*, 93–96.
7. Keshk, S.M.A.S. Bacterial cellulose production and its industrial applications. *J. Bioprocess Biotech.* **2014**, *4*, 150. [CrossRef]
8. Huang, Y.; Chen, Y. An overview of fermentation production and application of bacterial cellulose. *Adv. Mater. Res.* **2013**, *627*, 878–884. [CrossRef]
9. Kongruang, S. Bacterial cellulose production by *Acetobacter xylinum* strains from agricultural waste products. *Appl. Biochem. Biotechnol.* **2008**, *148*, 245–256. [CrossRef] [PubMed]
10. Chawla, P.R.; Ishwar, B.B.; Shrikant, A.S.; Rekha, S.S. Microbial cellulose: Fermentative production and applications. *Food Technol. Biotechnol.* **2009**, *47*, 107–124.
11. Lin, S.P.; Calvar, I.L.; Catchmark, J.M.; Liu, J.-R.; Demirci, A.; Cheng, K.-C. Biosynthesis, production and applications of bacterial cellulose. *Cellulose* **2013**, *20*, 2191–2219. [CrossRef]
12. Huang, Y.; Zhu, C.; Yang, J.; Nie, Y.; Chen, C.; Sun, D. Recent advances in bacterial cellulose. *Cellulose* **2014**, *21*, 1–30. [CrossRef]
13. Pourramezan, G.Z.; Roayaei, A.M.; Qezelbash, Q.R. Optimization of culture conditions for bacterial cellulose production by *Acetobacter* sp. 4B-2. *Biotechnology* **2009**, *8*, 150–154. [CrossRef]
14. Tsouko, E.; Kourmentza, C.; Ladakis, D.; Kopsahelis, N.; Mandala, I.; Papanikolaou, S.; Paloukis, F.; Alves, V.; Koutinas, A. Bacterial cellulose production from industrial waste and by-product streams. *Int. J. Mol. Sci.* **2015**, *16*, 14832–14849. [CrossRef] [PubMed]

15. Jalili Tabaii, M.; Emtiazi, G. Comparison of bacterial cellulose production among different strains and fermented media. *Appl. Food Biotechnol.* **2016**, *3*, 35–41.
16. Hong, F.; Guo, X.; Zhang, S.; Han, S.F.; Yang, G.; Jönsson, L.J. Bacterial cellulose production from cotton-based waste textiles: Enzymatic saccharification enhanced by ionic liquid pretreatment. *Bioresour. Technol.* **2012**, *104*, 503–508. [CrossRef] [PubMed]
17. Chen, L.; Hong, F.; Yang, X.-X.; Han, S.-F. Biotransformation of wheat straw to bacterial cellulose and its mechanism. *Bioresour. Technol.* **2013**, *135*, 464–468. [CrossRef] [PubMed]
18. Cheng, Z.; Yang, R.; Liu, X. Production of bacterial cellulose by *Acetobacter xylinum* through utilizing acetic acid hydrolysate of bagasse as low-cost carbon source. *BioResources* **2017**, *12*, 1190–1200. [CrossRef]
19. Cheng, Z.; Yang, R.; Liu, X.; Liu, X.; Chen, H. Green synthesis of bacterial cellulose via acetic acid pre-hydrolysis liquor of agricultural corn stalk used as carbon source. *Bioresour. Technol.* **2017**, *234*, 8–14. [CrossRef] [PubMed]
20. Jönsson, L.J.; Martín, C. Pretreatment of lignocellulose: Formation of inhibitory by-products and strategies for minimizing their effects. *Bioresour. Technol.* **2016**, *199*, 103–112. [CrossRef] [PubMed]
21. Campano, C.; Balea, A.; Blanco, A.; Negro, C. Enhancement of the fermentation process and properties of bacterial cellulose: A review. *Cellulose* **2016**, *23*, 57–91. [CrossRef]
22. Cheng, K.C.; Catchmark, J.M.; Demirci, A. Enhanced production of bacterial cellulose by using a biofilm reactor and its material property analysis. *J. Biol. Eng.* **2009**, *3*, 12. [CrossRef] [PubMed]
23. Hornung, M.; Ludwig, M.; Gerrard, A.M.; Schmauder, H.-P. Optimizing the production of bacterial cellulose in surface culture: Evaluation of substrate mass transfer influences on the bioreaction (Part 1). *Eng. Life Sci.* **2006**, *6*, 537–545. [CrossRef]
24. Meftahi, A.; Khajavi, R.; Rashidi, A.; Rahimi, M.K.; Bahador, A. Effect of purification on nano microbial cellulose pellicle properties. *Proced. Mater. Sci.* **2015**, *11*, 206–211. [CrossRef]
25. Usha Rani, M.; Anu Appaiah, K.A. Production of bacterial cellulose by *Gluconacetobacter hansenii* UAC09 using coffee cherry husk. *J. Food Sci. Technol.* **2013**, *50*, 755–762. [CrossRef] [PubMed]
26. Lu, H.; Jia, Q.; Chen, L.; Zhang, L. Effect of organic acids on bacterial cellulose produced by *Acetobacter xylinum*. *RRJMB* **2016**, *5*, 1–6.
27. Römling, U.; Galperin, M.Y.; Gomelsky, M. Cyclic di-GMP: The first 25 years of a universal bacterial second messenger. *Microbiol. Mol. Biol. Rev.* **2013**, *77*, 1–52. [CrossRef] [PubMed]
28. Morgan, J.L.W.; McNamara, J.T.; Zimmer, J. Mechanism of activation of bacterial cellulose synthase by cyclic-di-GMP. *Nat. Struct. Mol. Biol.* **2014**, *21*, 489–496. [CrossRef] [PubMed]
29. Römling, U.; Galperin, M.Y. Bacterial cellulose biosynthesis: Diversity of operons, subunits, products, and functions. *Trends Microbiol.* **2015**, *23*, 545–557. [CrossRef] [PubMed]
30. Srivastava, D.; Waters, C.M. A tangled web: Regulatory connections between quorum sensing and cyclic di-GMP. *J. Bacteriol.* **2012**, *194*, 4485–4493. [CrossRef] [PubMed]
31. Lebrun, L.; Junter, G.-A.; Jouenne, T.; Mignot, L. Exopolysaccharide production by free and immobilized microbial cultures. *Enzyme Microb. Technol.* **1994**, *16*, 1048–1054. [CrossRef]
32. Santos, E.L.I.; Rostro-Alanís, M.; Parra-Saldívar, R.; Alvarez, A.J. A novel method for bioethanol production using immobilized yeast cells in calcium-alginate films and hybrid composite pervaporation membrane. *Bioresour. Technol.* **2018**, *247*, 165–173. [CrossRef] [PubMed]
33. Efremenko, E.N.; Nikolskaya, A.B.; Lyagin, I.V.; Senko, O.V.; Stepanov, N.A.; Maslova, O.V.; Mamedova, F.; Varfolomeyev, S.D. Production of biofuels from pretreated microalgae biomass by anaerobic fermentation with immobilized *Clostridium acetobutylicum* cells. *Bioresour. Technol.* **2012**, *114*, 342–348. [CrossRef] [PubMed]
34. Efremenko, E.N.; Senko, O.V.; Aleskerova, L.E.; Alenina, K.A.; Mazhul, M.M.; Ismailov, A.D. Biosensors based on the luminous bacteria photobaterium phosphoreum immobilized in polyvinyl alcohol cryogel for the monitoring of ecotoxicants. *Appl. Biochem. Microbiol.* **2014**, *50*, 477–482. [CrossRef]
35. Kumar, A. *Supermacroporous Cryogels: Biomedical and Biotechnological Applications*, 1st ed.; CRC Press: Boca Raton, FL, USA, 2016; p. 496; ISBN 978-1482228816.
36. Borzani, W.; Souza, S.J. Mechanism of the film thickness increasing during the bacterial production of cellulose on non-agitated liquid media. *Biotechnol. Lett.* **1995**, *17*, 1271–1272. [CrossRef]
37. Budhiono, A.; Rosidi, B.; Taher, H.; Iguchi, M. Kinetic aspects of bacterial BC formation in nata-de-coco culture system. *Carbohydr. Polym.* **1999**, *40*, 137–143. [CrossRef]

38. Ha, J.H.; Shehzad, O.; Khan, S.; Lee, S.Y.; Park, J.W.; Khan, T.; Park, J.K. Production of bacterial cellulose by a static cultivation using the waste from beer culture broth. *Korean J. Chem. Eng.* **2008**, *25*, 812–815. [CrossRef]
39. Hsieha, J.-T.; Wang, M.-J.; Lai, J.-T.; Liu, H.-S. A novel static cultivation of bacterial cellulose production by intermittent feeding strategy. *J. Taiwan Inst. Chem. Eng.* **2016**, *63*, 46–51. [CrossRef]
40. Uzyol, H.K.; Saçan, M.T. Bacterial cellulose production by *Komagataeibacter hansenii* using algae-based glucose. *Environ. Sci. Pollut. Res.* **2017**, *24*, 11154–11162. [CrossRef] [PubMed]
41. Suwanposri, A.; Yukphan, P.; Yamada, Y.; Ochaikul, D. Statistical optimisation of culture conditions for biocellulose production by *Komagataeibacter* sp. PAP1 using soya bean whey. *Maejo Int. J. Sci. Technol.* **2014**, *8*, 1–14. [CrossRef]
42. Rangaswamy, B.E.; Vanitha, K.P.; Hungund, B.S. Microbial cellulose production from bacteria isolated from rotten fruit. *Int. J. Polym. Sci.* **2015**, *2015*, 8. [CrossRef]
43. Jahan, F.; Kumar, V.; Rawat, G.; Saxena, R.K. Production of microbial cellulose by a bacterium isolated from fruit. *Appl. Biochem. Biotechnol.* **2012**, *167*, 1157–1171. [CrossRef] [PubMed]
44. Huang, C.; Yang, X.A.; Xiong, L.; Guo, H.-J.; Luo, J.; Wang, B.; Zhang, H.-R.; Lin, X.-Q.; Chen, X.-D. Utilization of corncob acid hydrolysate for bacterial cellulose production by *Gluconacetobacter xylinus*. *Appl. Biochem. Biotechnol.* **2015**, *175*, 1678–1688. [CrossRef] [PubMed]
45. Hong, F.; Zhu, Y.X.; Yang, G.; Yang, X.X. Wheat straw acid hydrolysate as a potential cost-effective feedstock for production of bacterial cellulose. *J. Chem. Technol. Biotechnol.* **2011**, *86*, 675–680. [CrossRef]
46. Zeng, X.; Small, D.P.; Wan, W. Statistical optimization of culture conditions for bacterial cellulose production by *Acetobacter xylinum* BPR 2001 from maple syrup. *Carbohydr. Polym.* **2011**, *85*, 506–513. [CrossRef]
47. Tonouchi, N.; Tsuchida, T.; Yoshinaga, F.; Beppu, T.; Horinouchi, S. Characterization of the biosynthetic pathway of cellulose from glucose and fructose in *Acetobacter xylinum*. *Biosci. Biotechnol. Biochem.* **1996**, *60*, 1377–1379. [CrossRef]
48. Efremenko, E.N.; Stepanov, N.A.; Senko, O.V.; Maslova, O.V. Immobilized Biocatalysts for Bacterial Cellulose Production. U.S. Patent 2,636,041, 11 November 2017.
49. Vincenta, M.; Anthony, L.; Pometto, A.L.; van Leeuwen, J.H. Ethanol production via simultaneous saccharification and fermentation of sodium hydroxide treated corn stover using *Phanerochaete chrysosporium* and *Gloeophyllum trabeum*. *Bioresour. Technol.* **2014**, *158*, 1–6. [CrossRef] [PubMed]
50. Mohammadkazemi, F.; Azin, M.; Ashori, A. Production of bacterial cellulose using different carbon sources and culture media. *Carbohydr. Polym.* **2015**, *117*, 518–523. [CrossRef] [PubMed]

© 2018 by the authors. Licensee MDPI, Basel, Switzerland. This article is an open access article distributed under the terms and conditions of the Creative Commons Attribution (CC BY) license (http://creativecommons.org/licenses/by/4.0/).

catalysts

MDPI

Review

The Role of Yeast-Surface-Display Techniques in Creating Biocatalysts for Consolidated BioProcessing

Ian Dominic Flormata Tabañag [1], I-Ming Chu [2], Yu-Hong Wei [3] and Shen-Long Tsai [1,*]

[1] Department of Chemical Engineering, National Taiwan University of Science and Technology, Taipei 10607, Taiwan; d10406801@mail.ntust.edu.tw
[2] Department of Chemical Engineering, National Tsing Hua University, Hsinchu 30013, Taiwan; imchu@che.nthu.edu.tw
[3] Graduate School of Biotechnology and Bioengineering, Yuan Ze University, Taoyuan 32003, Taiwan; yhwei@saturn.yzu.edu.tw
* Correspondence: stsai@mail.ntust.edu.tw; Tel.: +886-22737-6628; Fax: +886-22737-6644

Received: 31 January 2018; Accepted: 21 February 2018; Published: 25 February 2018

Abstract: Climate change is directly linked to the rapid depletion of our non-renewable fossil resources and has posed concerns on sustainability. Thus, imploring the need for us to shift from our fossil based economy to a sustainable bioeconomy centered on biomass utilization. The efficient bioconversion of lignocellulosic biomass (an ideal feedstock) to a platform chemical, such as bioethanol, can be achieved via the consolidated bioprocessing technology, termed yeast surface engineering, to produce yeasts that are capable of this feat. This approach has various strategies that involve the display of enzymes on the surface of yeast to degrade the lignocellulosic biomass, then metabolically convert the degraded sugars directly into ethanol, thus elevating the status of yeast from an immobilization material to a whole-cell biocatalyst. The performance of the engineered strains developed from these strategies are presented, visualized, and compared in this article to highlight the role of this technology in moving forward to our quest against climate change. Furthermore, the qualitative assessment synthesized in this work can serve as a reference material on addressing the areas of improvement of the field and on assessing the capability and potential of the different yeast surface display strategies on the efficient degradation, utilization, and ethanol production from lignocellulosic biomass.

Keywords: consolidated bioprocessing; yeast surface display; bioethanol; lignocellulosic biomass; fermentation; immobilized biocatalyst; whole-cell biocatalyst; DYSD; JANNASEY

1. Introduction

1.1. Climate Change and the Bio-Based Economy

One of the most pressing problems that the world is facing is climate change. Driven by our escalated demand of fossil-based products due to a growing population, vast amounts of greenhouse gases are released into the atmosphere; thus, inducing the greenhouse effect, which leads to global warming. The adverse effects of global warming include: long droughts, severe flooding, and even the melting of our polar ice caps. These severe changes lead to the loss of our biodiversity due to the pressure they impose on our ecosystems [1–3].

From the given scenario above, there is a need for us to shift our dependence on the current fossil-based (non-renewable) economy into a more sustainable one. This is where the bio-based economy comes in; where a lot of the energy, fuels, and products that are conventionally derived from fossil resources are produced from renewable and sustainable alternatives. The bio-based economy or bioeconomy is defined by the European Commission as "the sustainable production

of renewable resources from land, fisheries and aquaculture environments and their conversion into food, feed, fiber bio-based products and bio-energy as well as the related public goods [2,4]". Thus, from a range of sustainable alternatives (e.g., wind, solar, geothermal, biomass, etc.) that are available, only biomass can provide us for the source of carbon that is essential for the production of tangible goods. Thus, biomass, as a sustainable resource, is the feedstock from which platform chemicals (i.e., ethanol, glycerol, butanol, propanediol, etc.) are derived and serve as a pre-cursors for the production of bio-based products (non-food products derived from biomass, such as plants, algae, crops, trees, marine organisms, and biological waste from households, animals, and food production) [3,5]. In addition, of the platform chemicals mentioned, bioethanol is easily obtained at high yields from pre-treated biomass via fermentation by certain yeasts.

1.2. Lignocellulosic Biomass and Consolidated Bio-Processing

The most abundant biomass (which are usually plants) found in nature, which can be used in bioethanol production via fermentation is lignocellulose, and because of its abundance, this raw material can be obtained in fact at a very low cost; it may be the best substrate with the highest potential in bioprocessing. Lignocellulose comprises 50–90% of all plant matter and it is composed of three major components, which are: cellulose, hemicellulose (which is composed mainly of xylan), and lignin. These major components of lignocellulose are in their polysaccharide forms and hydrolysis of these polysaccharides yield fermentable sugars, except for lignin (which produces phenolic compounds that actively inhibit fermentation). The major fermentable sugars produced from lignocellulose are glucose (abundant in cellulose), and xylose (abundant in hemicellulose) [6,7]. The relative concentrations of each major component is different when the plant type varies and their average concentrations are shown in Table 1.

Table 1. Components of plant lignocellulosic biomass and their typical compositions.

Lignocellulose Component	Composition (%)	Fermentable Sugars
Cellulose	~35–50	Glucose
Hemicellulose	~20–35	Xylose, Arabinose, Mannose, Galactose
Lignin	~15–30	-

Direct fermentation of lignocellulosic biomass for bioethanol production is not feasible since the biomass itself is not readily fermentable by ethanol-producing microorganisms thus, expensive pre-treatment processes such as milling or steam explosion, and acid or alkaline hydrolysis are required. In the past few decades, several different strategies have been developed to produce ethanol from this kind of biomass. These strategies consists of four biologically mediated process steps, namely: (i) cellulase production, (ii) cellulose hydrolysis, (iii) hexose fermentation, and (iv) pentose fermentation. These strategies, however, require the biomass to undergo a mild pre-treatment step to disrupt its crystalline structure for the hydrolysis to proceed efficiently. In this pre-treatment step, most of the components of hemicellulose in the biomass are hydrolyzed into fermentable sugars, leaving behind cellulose in its slightly crystalline form (amorphous). Throughout the years, different processing strategies have been developed and these strategies can be categorized based on the degree to which the biologically mediated processes are consolidated. As depicted in where each process is represented as a bioreactor along with the time period when each processing strategy was developed, separate hydrolysis and fermentation (SHF) involves all the four mentioned processes discretely. Simultaneous saccharification and fermentation (SSF) consolidates cellulose hydrolysis and hexose fermentation into one step, which results in a three-step strategy. Simultaneous saccharification and co-fermentation consolidates cellulase hydrolysis and hexose-pentose fermentation which results in a two-step strategy. Finally, consolidated bioprocessing (CBP), which consolidates all process steps into a one-step bioreactor conversion strategy and schematically illustrated in Figure 1 along with the time periods where each strategy was developed [6,8–10].

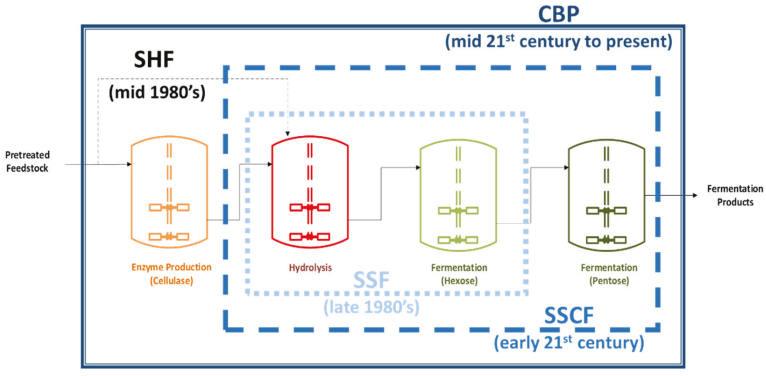

Figure 1. Schematic representation of the consolidated bioprocessing strategy.

The aim of the consolidated bioprocessing strategy is to engineer a microbial strain that is capable of producing the desired product yield by utilizing directly the pre-treated lignocellulosic biomass as a substrate via metabolic engineering (native strategy) and recombinant DNA engineering. The CBP-strategy has the potential to lower the cost of biomass processing, while producing a high-value product; this makes this strategy highly attractive and economical. The CBP-compatible microorganism of interest that has been studied extensively is the ethanologenic yeast *Saccharomyces cerevisiae* (which will referred as "yeast" in the following sections). However, the said yeast does not have the ability to directly use lignocellulosic biomass, although it has can produce ethanol in high yields from simple hexose sugars [6,8–10].

So, there is a need to increase the substrate utilization range of yeast for it to be able to degrade and utilize lignocellulosic biomass. This is achieved by expressing cellulose and hemicellulose degrading enzymes (cellulases, and hemicellulases, respectively) from lignocellulose degrading microorganisms in yeast and along with other metabolic pathway enzymes for the utilization of other fermentable sugars aside from glucose. The heterologous expression of the cellulases and hemicellulases in yeast will enable it to degrade these polysaccharides into fermentable sugars; then, these fermentable sugars are further converted to ethanol via the native and heterologous (for sugars other than hexoses) metabolic pathway enzymes. The following sections describe the heterologous expression of these cellulases and hemicellulases on the surface of yeast on how they improve ethanol production on lignocellulosic substrates.

2. The Development of Yeast Cell Surface Display

2.1. Development of the Surface Display Technology

Surface display systems were developed as a means to exploit the translocation of proteins on the cell surface along with their anchoring regions and apply it to heterologous proteins. In other words, this provides the idea that the cell surface is an avenue for protein immobilization, which makes it a "whole-cell biocatalyst". This system was initially demonstrated by fusing peptides to docking proteins of filamentous phage and then assembled on to the phage particle which led to the development of the "phage display system"; where it was mainly applied in high throughput screening systems using phage libraries for isolation of ligands, antibodies, etc. [11,12]. However, the limitation of the phage display system lies in the display of larger sized peptides and proteins, due to the fact the size of the fusion protein induces steric effects to the assembly of the phage particle. This limitation was then addressed by expressing the heterologous proteins fused to the surface-exposed regions of membrane proteins on the bacterial surface [13–15]. Since then, various proteins were heterologously expressed

and localized on the bacterial surface for a wide range of applications (e.g., biosensing, bioremediation, high throughput screening, protein engineering, etc.) [16–22].

However, some heterologously expressed proteins on the bacterial surface have some limitations in expressing proteins that require post-translational modification of eukaryotic pathways, especially high molecular weight proteins from eukaryotes. Thus, the field of cell surface display was extended in yeasts (especially *S. cerevisiae*), which is then termed as "yeast surface display" or "yeast surface engineering". In the following sections, the term "yeast surface display" is adapted for convenience.

2.2. Yeast Surface Display

The potential of yeast surface display was first highlighted in the idea of an "arming technology" and its developed strains have been termed "arming yeasts" [23,24]. Furthermore, this field has elevated the status of *S. cerevisiae* as a novel and attractive microorganism to be a platform for enzyme immobilization, which enables it to target non-conventional substrates and at the same time, renewable self-immobilized biocatalysts (also known as "whole-cell biocatalysts") [24]. Its history, development, and mechanisms have been extensively discussed in the reviews of Ueda, and colleagues [25–31]. Thus, this section intends to provide a brief description on how heterologous proteins are expressed on the yeast surface in relation to CBP.

The successful expression of the heterologous proteins onto the yeast surface requires fusion to a good yeast anchor protein. An ideal anchor protein contains two essential genetic elements are required for the successful surface display of the protein of interest (POI) and these are: (i) a secretion signal sequence that mediates the transport of the POI to the cell surface where it strongly immobilizes the fused POI without interfering the activity and stability of the POI, and (ii) the glycosylphosphatidylinositol (GPI) anchor attachment signal sequence for the transient anchoring in the plasma membrane. Furthermore, a wide variety of anchor proteins are present in yeast and it is extensively described by Tanaka et al. [27,30]. Therefore, the choice of the anchor protein is thus dependent upon the characteristics of POI (e.g., location of active site, application, complex formation, etc.). In consideration of the inherent properties of the POI, the anchor protein can either be fused to either the N or C termini of the POI and Figure 2 shows on how the POI-anchor fusion is localized on the yeast surface based on the commonly utilized anchor protein systems and Table 2 shows the characteristics of the yeast anchor protein systems presented in the following sections.

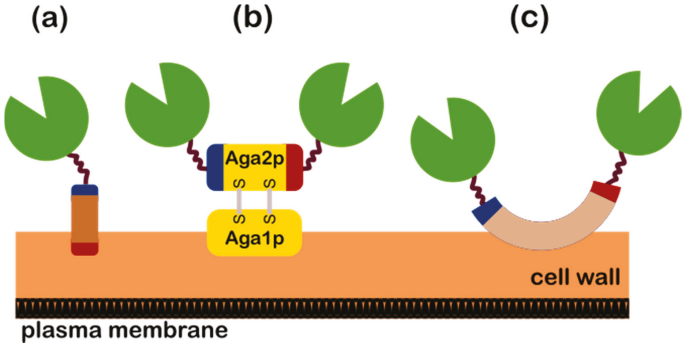

Figure 2. Common anchor protein systems used in yeast surface display: (**a**) N-terminal fused anchor proteins (SAG1, SED1, or CWP2); (**b**) the a-agglutinin display system; and, (**c**) the Flo1p-based display system. Anchor proteins: N-Terminal depicted in blue, and C-terminal depicted in red.

Hence, from the descriptions reported in Table 2, the anchor proteins that are mostly used for N-terminal fusions (where the POI is fused at the N-terminal of the anchor protein as depicted in Figure 2a) are the SAG1, SED1, and CWP2 while the a-agglutinin system is mostly used for C-terminal

fusions (where the POI is fused at the C-terminal of the secreted AGA2 subunit as depicted in Figure 2b). In addition, several proteins have also been fused to the N-terminal (as depicted in Figure 2b) of the AGA2 subunit, which makes this system flexible in terms of the N or C terminal fusion [33]. Furthermore, the protein FLO1 (as depicted in Figure 2c) is also a flexible anchoring system where the POI can either be fused to its N or C terminal. The various truncated forms of FLO1 where its domains contain high level of N-and O-glycosylations provides the platform of options onto which terminal can the POI be fused [34,35]. The details of the anchor proteins utilized by the presented studies in the next sections are detailed in Table A1.

Table 2. Typical yeast anchor proteins used for surface display.

Yeast Anchor Protein	Standard Name	Description
α-agglutinin	SAG1	Alpha-agglutinin of alpha-cells; binds to Aga1p during agglutination, N-terminal half is homologous to the immunoglobulin superfamily and contains binding site for a-agglutinin, C-terminal half is highly glycosylated and contains GPI anchor
SED	SED1	Major stress-induced structural GPI-cell wall glycoprotein; associates with translating ribosomes, possible role in mitochondrial genome maintenance
Cwp2	CWP2	Covalently linked cell wall mannoprotein; major constituent of the cell wall; plays a role in stabilizing the cell wall; involved in low pH resistance; precursor is GPI-anchored
Flo428p	FLO1	Lectin-like protein involved in flocculation; cell wall protein that binds mannose chains on the surface of other cells, confers floc-forming ability that is chymotrypsin sensitive and heat resistant; important for co-flocculation with other yeasts, mediating interaction with specific species
a-agglutinin system	AGA1	Anchorage subunit of a-agglutinin of a-cells; highly O-glycosylated protein with N-terminal secretion signal and C-terminal signal for addition of GPI anchor to cell wall, linked to adhesion subunit Aga2p via two disulfide bonds
	AGA2	Adhesion subunit of a-agglutinin of a-cells; C-terminal sequence acts as a ligand for alpha-agglutinin (Sag1p) during agglutination, modified with O-linked oligomannosyl chains, linked to anchorage subunit Aga1p via two disulfide bonds

Data obtained from SGD Project. http://www.yeastgenome.org [32].

2.3. Strategies for the Yeast Surface Display of CBP-Related Enzymes

The different strategies for the immobilization of cellulases and hemicellulases utilized in the studies presented in the next section are shown in Figure 3.

Due to the complex structure of lignocellulose in lignocellulosic biomass, it is a given that different types of enzymes are required to break down the polysaccharides into the fermentable monosaccharide sugars that the yeast can transport and utilize. Thus, these different types of enzymes are to be displayed on the yeast surface to provide a synergistic effect when it comes to the degradation of lignocellulose. The advantage of expressing multiple-enzymes on the surface of yeast is that the yeast cells are capable of direct degradation and utilization of lignocellulosic substrates in situ. In other words, it combines the enzyme production, immobilization, and metabolic degradation steps in a one-pot setting; a fitting platform for CBP. The description and classification of the strategies shown in Figure 3 are as follows:

1. Direct Yeast Surface Display (DYSD)—this strategy directly involves the fusion of the enzyme of interest/s to the yeast anchor protein for it to be expressed and localize on its surface and is further classified into the following:

    a. Single enzyme display consortium (SEDC)—a mixed culture (a.k.a synthetic consortium) strategy of different strains with each displaying one type of enzyme. The utilization of the mixed culture technique is adapted as a means to control the multi-enzyme composition or ratios via the culture inoculation ratios.
    b. Co-display (CD)—the direct display of more than one enzymes on yeast that is achieved by directly cloning the enzyme/s fused with anchor protein into one yeast strain. The control of the displayed enzyme ratios

2. Juxtaposed Assembly of Non-Native Adaptors and Secreted Enzymes on Yeast (JANNASEY)—this strategy is developed based on the biomimicry of the "cellulosome" machinery of several anaerobic cellulose-consuming microorganisms (e.g., clostridia, ruminal bacteria) [36,37]. In addition, exploiting the cellulosome's nature as a reconfigurable platform for immobilization of multiple enzymes including an enzyme cascade configuration, along with the advancement of molecular biology and conjugation techniques, led to the creation of "designer cellulosomes". These designer cellulosomes typically consists of the cell wall anchoring subunit (or sometimes directly fused to the adaptor subunit) for cell wall attachment, the adaptor subunit (a.k.a. scaffoldin or miniscaffoldin), which consists of the configurable multi-cohesin along with the cellulose binding domains that either bind to the anchoring subunit or onto another adaptor subunit, and finally the secreted enzyme subunit which consists of enzyme/s each fused to a specific dockerin domain that corresponds to the cohesin/s in the adaptor subunit [38]. The term "minicellulosomes" is often used to distinguish the designer cellulosomes that contain engineered adaptor subunits (a.k.a. miniscaffoldin to be consistent with the minicellulosome) with non-native cohesin and cellulose-binding domains. Other researchers' even use the term "truncated cellulosome" that is synonymous to the minicellulosome to even give it a clearer distinction with the cellulosome [37,39]. In order to prevent the inappropriate use of the terms related to cellulosomes in this article, this yeast display strategy is generally classified as the juxtaposed assembly of non-native adaptors and secretion enzymes on yeast in reference to its structured and precise self-assembly on yeast. Furthermore, the various assembly techniques of the cellulosome components are classified as follows:

    a. Single multi-functional adaptor assembly (SMFAA)—this strategy typically involves the consortium of two sets of strains wherein one strain displays the chimeric adaptor subunit on its surface, and another set of strains that secrete the dockerin fused enzymes that assemble in situ onto the displayed adaptor subunit of another strain. The multi-functionality this system is derived from the fact that the adaptor subunit it contains varying cohesin domains from different microorganisms for specificity.
    b. Complex adaptor assembly (CAA)—this is a direct biomimicry of the native bacterial cellulosome assembly where one or more adaptor subunits are assembled on the bacterial surface. When applied to yeast surface display, it involves a consortium of at least three sets of strains where one strain displays the anchoring subunit, another set of strains that secrete one or more adaptor subunits (one of which binds to the anchoring subunit and another type of binds to the cell-surface-anchored adaptor), and finally the strains that secrete the dockerin fused enzymes, which assemble onto the adaptors. The complex assembly is regulated by the valence (monovalent if it contains a single cohesin and polyvalent if it contains more than one) of the adaptor subunit. Adaptor polyvalence can also be achieved by specifically engineering the adaptor to contain multiple cohesin types from different microorganisms for regulating the enzyme loading via cohesin-dockerin specificity.

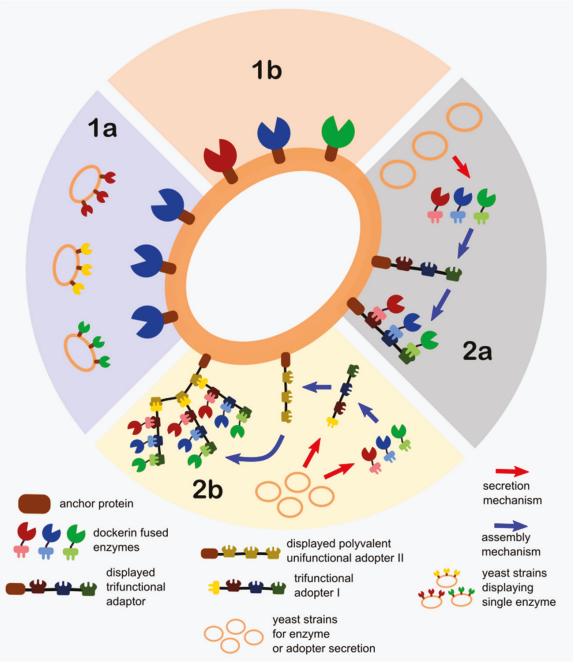

Figure 3. Cellulase and Hemicellulase Surface display strategies for Consolidated BioProcessing. (1a) DYSD-SEDC, (1b) DYSD-CD, (2a) JANNASEY-SMFAA, (2b) JANNASEY-CAA.

3. Yeast Surface Display Studies for Bioethanol Production from Lignocellulosic Biomass

The selected studies presented in this section are those that have applied the yeast surface display system in ethanol fermentation from lignocellulosic substrates. These studies are classified into the ethanol fermentation of: pure cellulose, pure hemicellulose, and pre-treated lignocellulosic biomass substrates. The purpose of this is to differentiate between the systems that utilize pure polysaccharide substrates from actual pre-treated plant substrates. Furthermore, these studies are compared with each other based on the following fermentation parameters: (i) Ethanol titer, (ii) Substrate type, and (iii) Ethanol substrate conversion yield. The ethanol substrate conversion yield (ESCY, %) is defined as the amount of ethanol titer obtained with respect to theoretical ethanol produced from the total fermentable sugars in the substrate and is operationally defined in Equation (1).

$$\text{ESCY}\ (\%) = \frac{C_{\text{EtOH}}^{\text{titer}}}{C_{\text{substrate}} \times X_{\text{TFS}} \times Y_{\text{PS}}^{\text{theo}}} \times 100 \quad (1)$$

where: ESCY—Ethanol Substrate Conversion Yield; $C_{\text{EtOH}}^{\text{titer}}$—ethanol titer; $C_{\text{substrate}}$—substrate concentration; X_{TFS}—composition of total fermentable sugars in the substrate; $Y_{\text{PS}}^{\text{theo}}$—theoretical ethanol yield from monosaccharides (typically ~0.51 g ethanol per g sugar).

Prior to looking into the ethanol performance of yeast surface display in the following sections, it should be noted that the advantage of employing the yeast surface display system lies in the fact that it either retains or increases the overall enzymatic activity upon the immobilization of the enzyme/s of interest on its surface when compared to its free enzyme (enzyme in solution) counterpart. This is discussed in the following paragraph.

In most of the cases, yeast surface display performance can be assessed by comparing the normalized enzymatic activities (expressed in terms of activity units with respect to the amount

of cells secreting/displaying the said enzymes) for both the secreted and displayed configuration of the enzyme of interest. Specifically in the context of this review, the enzymatic activity refers to the rate release of sugars (e.g., total reducing sugars (TRS), or a specific sugar being assayed). Additionally, for the cases when multiple enzymes are employed, the parameter utilized for the assessment of the multi-enzymatic performance would be the "degree of synergy". The degree of synergy is defined as "the ratio of the rate or yield of product released by enzymes when used together to the sum of the rate or yield of these products when the enzymes are used separately in the same amounts as they were employed in the mixture [40,41]". In other words, this refers to the ratio of the mixture activity to its theoretical mixture activity (sum of individual mixture activities). In the context of lignocellulosic bioethanol production, this refers to the amount of fermentable sugars hydrolyzed by an enzyme mixture with respect to its theoretical mixture hydrolysis activity.

It has been demonstrated that the application of yeast surface display to the enzymes (i.e., cellulases, hemicellulases) relevant to lignocellulosic bioethanol production has exhibited improved hydrolytic activities with respect to their free enzyme counterparts. In addition, enhancement in the degree of synergy was observed when mixtures of the said surface displayed enzymes (i.e., cellulases, hemicellulases) were utilized for substrate hydrolysis [42–46].

Thus, in terms of industrial relevance, yeast surface display provides a platform where enzyme/s are both produced and self-immobilized on its surface (creating a whole-cell biocatalyst platform) in a manner where the activities of the enzyme/s are retained as long as there is continuous growth of yeast in the fermentation process. Another feature of this system lies in the ease of separation of the whole-cell biocatalyst from the fermentation media, which enables the reusability of yeast cells. The reusability of the yeast cells as whole cell biocatalysts takes advantage of the fact that the enzymes displayed on its surface are active upon reuse; this translate to cost reduction for yeast propagation or enzyme addition [24,47].

3.1. Pure Cellulose Substrates

The predominant component of lignocellulosic biomass is cellulose and it serves as its main structural component. It consists of glucose chains linked via β-1,4 linkages and this chains are linked together by strong hydrogen bonding that forms the cellulose chains into microfibrils making it crystalline in nature, and thus recalcitrant to degradation; although some parts of the cellulose structure are easier to degrade due to its amorphous configuration. These structural variabilities (crystalline and variable regions) in the cellulose structure make it at least partially hydrated by water when immersed in aqueous media and along with some micropores and capillaries, it provides enough space for some enzymes, such as cellulases to penetrate. Cellulose is produced mainly by delignification of wood or other plant biomass materials. The pure celluloses utilized for hydrolysis studies vary considerably in fine structural features and the choice of substrate can affect the hydrolysis itself. Microcrystalline celluloses are nearly pure cellulose and a dilute-acid treatment step is typically utilized in their preparation, which results in the removal of hemicelluloses and amorphous regions of the cellulose fibers. Furthermore, commercial microcrystalline cellulose differ primarily on size distribution has significant implications for the rate of hydrolysis and utilization, as discussed in the studies presented in this subsection. In addition, the varying structural complexity (in terms of crystallinity) of pure cellulose and the difficulty of its insolubility has led to the wide use of a highly soluble cellulose ether, carboxymethylcellulose (CMC), which is chemically synthesized by the alkali-catalyzed reaction of cellulose with chloroacetic acid [6,8,48–50].

In general, the degradation of cellulose into glucose requires at least three types of enzymes (cellulases). These are typically: endocellulases (randomly cleave internal bonds at amorphous sites that create new chain ends), exocellulases (which includes cellobiohydrolases (CBH) and cleave two to four units from the ends of the exposed chains produced by endocellulase, resulting in tetrasaccharides or disaccharides, such as cellobiose), and cellobioases (a.k.a β-glucosidases, hydrolyse the exocellulase product into individual monosaccharides; specifically cellobiose) [6,7]. The action

of these cellulases on cellulose are schematically illustrated in Figure 4. Basically, the cellulose chains are efficiently degraded into soluble cellooligosaccharides and cellobiose by the endo and exocellulases, and then further hydrolyzed into glucose by the β-glucosidase. The studies presented in this subsection have exploited the different yeast surface display strategies for cellulases, which created recombinant yeasts that produce cellulosic ethanol. Furthermore, synergistic interactions between cellulases have been reported to occur between: different exocellulases (with specificity for reducing and non-reducing ends), endo, and exocellulases, between different endocellulases, and between endocellulases and β-glucosidases [51–56]. Additionally, high cellulase synergy has been observed on the hydrolysis of highly crystalline cellulose substrates when compared to the more amorphous cellulose [53,57].

In conjunction with the different cellulases utilized along with the yeast surface display system, the commonly exploited synergistic interactions for cellulosic bioethanol production are the interactions between endo and exocellulases, and endocellulases and β-glucosidases; as these two synergistic interactions are significant to the efficient glucose release from the cellulose structure. This configuration can produce whole-cell biocatalysts that can directly degrade cellulose and potentially produce high ethanol yields from the glucose released from the cellulose structure.

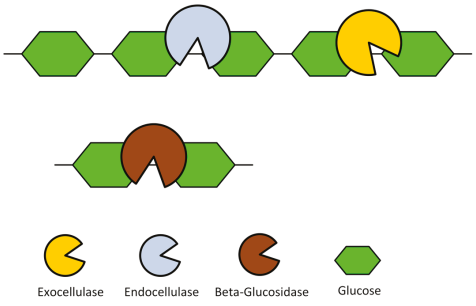

Figure 4. Basic structural component of cellulose and the cellulases responsible for its degradation.

3.1.1. DYSD Strategy for Cellulosic Bioethanol Fermentation

The first reported attempt to convert the cellulosic barley β-glucan into ethanol was described by Fujita, et al. [58]; where the *Trichoderma reesei* endoglucanase II (EGII) and *Aspergillus aculeatus* β-glucosidase (BGL1) were co-displayed on the yeast surface. The resulting strain has performed efficient simultaneous saccharification and fermentation of cellulose to ethanol by producing ~17 g/L ethanol in 48 h from 45 g/L β-glucan with an ethanol substrate conversion yield (ESCY) of ~74%. Then, this yeast strain was further modified by adding the *T. reesei* cellobiohydrolase II (an exoglucanase, CBHII) and tested on phosphoric acid cellulose (PASC). This modified strain has produced 3 g/L of ethanol in 40 h with an ESCY of ~61% from 10 g/L PASC [59]. Furthermore, Kotaka, et al. [60] have co-displayed both an endoglucanase (CelB) and a β-glucosidase (BGL-B7) from *Aspergillus oryzae* on the cell surface of an industrial sake yeast and successfully produced ethanol ~8 g/L ethanol in 24 h with an ESCY of ~70% from 20 g/L β-glucan. Interestingly, Liu, et al. [61] has demonstrated different combined approaches of yeast surface-display and secretion strategies. With the main premise that the β-glucosidase is displayed on the yeast surface to facilitate in the efficient transport of glucose upon the degradation of cellobiose. Their findings suggest that placing endoglucanase (EG) and cellobiohydrolase (CBHI) in the same space (on the cell surface or in the medium) was favorable for amorphous cellulose-based (PASC) ethanol fermentation; while the cellulolytic yeast strain that produced enzymes by the cell-surface display strategy performed better in cell-recycle batch fermentation compared to strains producing enzymes via the secretion strategy. Based on the highest obtained parameters, the system has produced ~3 g/L ethanol in 96 h with an ESCY of ~60% from

10 g/L PASC [61]. In another study by the same research group [62], two exoglucanases from *Talaromyces emersonii* and *Chrysosporium lucknowense*, a *T. reesei* endoglucanase (EG2), and an *A. aculeatus* β-glucosidase (BGL1) were co-displayed on the yeast surface to create a novel cellulose adherent yeast strain. When assessed on the non-treated (Avicel) and acid-treated (PASC) cellulose, the strain exhibited clear cell to cellulose adhesion and a tearing (almost ubiquitous pattern when compared to the layer by layer action by free cellulases) cellulose degradation pattern; adhesion ability correlated with enhance surface area and roughness of cellulose fibers resulting in higher hydrolysis efficiency. The obtained parameters from both substrates are: ~2 g/L ethanol in 96 h with an ESCY of ~30%, and ~7 g/L ethanol in 96 h with an ESCY of ~68%, from 10 g/L Avicel and 20 g/L PASC, respectively [63].

In the degradation of lignocellulosic substrates, the biochemical composition of the substrate dictates the cocktail of enzymes that is required for its efficient hydrolysis. Because of this, one of the major limitations of the direct surface display strategies is the control of the ratio or the composition of the different enzymes being displayed on the yeast surface However, this limitation was overcome through controlling the expression levels of the different enzymes using the novel cocktail delta-integration approach introduced by Yamada, et al. [64,65]. The expression levels of the different enzymes was directly controlled by the gene copy numbers of the different enzymes when integrated into the multiple delta-sites (a long-term terminal repeat, LTR, component of the retrotransposable Ty elements) that are present in the yeast genome. Then this enzyme expression control strategy was applied by Yamada, et al. [66], in the co-display of the *T.reesei* endoglucanase II (EGII) and cellobiohydrolase II (CBHII), along with the *A. aculeatus* β-glucosidase (BGL1) on the yeast cell surface and have successfully obtained ~3 g/L ethanol in 72 h with and ESCY of ~31% from 20 g/L PASC. When the same co-display system was introduced into a diploid yeast strain, the parameters obtained were improved (almost thrice as much) when compared to the co-display system of the haploid yeast strain; specifically ~8 g/L ethanol in 72 h with an ESCY of ~77%. This was a first demonstration that the utilization of a recombinant diploid strain is an improvement to the ethanol fermentation capacity from cellulosic biomass when compared to its haploid counterpart [66]. A similar control strategy was adapted by Apiwatanapiwat, et al. [67] in the co-display of five (5) different (two amylases, two cellulases, and one β-glucosidase) enzymes on the yeast surface. The resulting strain was designed for the ethanol fermentation from cassava pulp (which mainly contains starch and cellulosic fibre). When tested with the cellulosic substrates PASC (~9 g/L, total sugar), and β-glucan (~10 g/L, total sugar), the obtained fermentation parameters ethanol titer, fermentation time, and ESCY were 1.1 g/L, within 24 h, ~25%, and 5.3 g/L, 36 h, 97%, respectively [67]. In an attempt to improve the efficient utilization of cellulose hydrolysis products, Yamada, et al. [68] adapted the same control strategy and cellulase co-display system, while in this case, the β-glucosidase was expressed intracellularly along with the *Neurospora crassa* cellodextrin transporter (cdt1) The expression of the cellodextrin transporter along with the intracellular β-glucosidase will enable the resulting yeast strain to efficiently transport the cellobiose produced during cellulose hydrolysis into the cell and intracellularly degrade it into glucose then convert it to ethanol. When the resulting strain was assessed by ethanol fermentation from 20 g/L PASC, it has successfully obtained 4.3 g/L ethanol in 72 h with an ESCY of ~44% where the titer was about 1.7 times higher when compared to the strain not expressing the cellodextrin utilization pathway [68]. Another case where two exoglucanases from *T. emersonii* and *C. lucknowense*, a *T. reesei* endoglucanase (EG2), and an *A. aculeatus* β-glucosidase (BGL1) were co-displayed using the cocktail delta-integration strategy on the yeast surface by Liu, et al. [69] in the attempt to obtain a highly cellulolytic strain. The transformants were then subjected to a high-throughput screening (HTS) methodology for the selection of the strain that exhibits high cellulolytic activity. The resulting strain that exhibits the highest cellulolytic activity was subjected to ethanol fermentation from Avicel (non-treated crystalline cellulose) and it obtained ~3 g/L of ethanol within 96 h with an ESCY of ~60% (highest reported ethanol yield for from avicel) [69].

An alternative technique of controlling the ratio or the composition of surface displayed enzymes in a mixture for cellulose degradation and utilization was to utilize a consortium of strains where

different types of strains display one type of cellulase per strain was introduced by Baek, et al. [45]. Control was achieved by adjusting the inoculation ratios of each strain displaying the *T. reesei* cellobiohydrolase II (CBHII), *Thermoascus aurantiacus* endoglucanase I (EGI), and the *A. aculeatus* β-glucosidase (BGLI). Different inoculation ratios were investigated and the resulting formulation that exhibits the highest cellulolytic activities were assessed for ethanol fermentation from 10 g/L PASC and obtained ~2.1 g/L ethanol in 85 h with an ESCY of ~43% [45].

3.1.2. JANNASEY Strategy for Cellulosic Bioethanol Fermentation

The successful assembly of multi-functional cellulosomes on the yeast surface were described by Ito, et al. [70] and Lilly, et al. [71]. Tsai, et al. [46] then assessed the ethanol fermentation from 10 g/L PASC of a yeast strain with a pre-assembled minicellulosome (the dockerin-fused enzyme subunits were expressed and purified in *E. coli* before its assembly on the yeast strain displaying the configurable adaptor/miniscaffoldin subunit) that displays *Clostridium cellulolyticum* exoglucanase (CelE), both *Clostridium thermocellum* endoglucanase (CelA) and β-glucosidase (BglA). The pre-assembled minicellulosome-displaying strain has produced ~4 g/L ethanol in 50 h, with an ESCY of ~71% from PASC [46]. In the endeavor to assemble the minicellulosome in situ, the same research group of Tsai, et al. [72] adapted a yeast consortium strategy, which consists of two sets of yeast strains where minicellulosome assembly is achieved via intracellular complementation (i.e., one set of strains displaying adaptor subunit, while another set of strains secretes the three cellulases, CelE, CelA, and BglA onto the adaptor-displaying strains). Different inoculation ratios of the two sets of strains were investigated and the resulting consortium were screened based on their overall cellulolytic activities and ethanol production from PASC. The optimized consortium produced ~2 g/L ethanol in 70 h with an ESCY of ~40% [72]. Another case of utilizing a multi-functional cellulosome system was demonstrated by Wen, et al. [73], where the native adaptor/scaffoldin subunits derived from *C. thermocellum* (CipA1, for the co-display of three uni-functional minicellulosomes and CipA3, for the co-display of a tri-functional minicellulosome) were exploited to produce two minicellulosome display schemes. The cellulases displayed on these minicellulosome schemes were both the *T. reesei* endoglucanase II (EGII), and cellobiohydrolase II (CBHII), along with the *A. aculeatus* β-glucosidase (BGLI). The resulting display scheme that exhibited the highest parameters among them was the one displaying the tri-functional minicellulosome. The obtained parameters were 1.8 g/L ethanol in 70 h with an ESCY of ~37% from 10 g/L PASC [73]. In another endeavor to achieve efficient cellulose hydrolysis using by exploiting the native adaptor subunit of *C. thermocellum* (mini-CipA), Kim, et al. [74] designed a yeast consortium strategy that consists of three sets of strains where two of which is involved in the intracellular complementation minicellulosome assembly (one strain set displays the mini-CipA adaptor subunit while another set secretes the dockerin-fused enzyme subunits), and the third set directly displays the *A. aculeatus* β-glucosidase (BGLI). The resulting consortium is a combination of the minicellulosome assembled *C. thermocellum* endoglucanase (CelA), and the *T. reesei* cellobiohydrolase II (CBHII), along with the strain displaying the BGL1. The inoculation ratios of the four different yeast populations were optimized based on the rational design and screening methods adapted from Baek, et al. [45]; where ethanol production optimization was directly based on changing the population inoculation ratios of the different strain sets. The resulting optimized inoculation ratio did produce ~2 g/L ethanol in 94 h with an ESCY of ~38% from 10 g/L PASC where the titer was 1.2 times higher when compared to an 1:1 (equal) ratio of the three strain sets [74].

One of the limitations of the single multi-functional adaptor cellulosome assembly is on limited number of enzymes (enzyme loading) displayed on the single adaptor platform. This limitation can be overcome by using multiple adaptors that mimic the native bacterial (e.g., *Ruminococcus flavefaciens*) complex cellulosome machinery where it involves the utilization of polyvalent adaptors (either with multiple cohesin domains from one strain, or from multiple strains) [38]. Fan, et al. [75] demonstrated this complex assembly using two different adaptor subunits. Specifically, these adaptor subunits are: (i) the tri-functional chimeric (which contains three cohesin domains from different species and a

dockerin domain for binding on to the adaptor subunit II) trivalent adaptor subunit I that displays the *C. cellulolyticum* endoglucanase(CelCCA), cellobiohydrolase (CelCCE), and β-glucosidase (Ccel_2454) fused to different dockerin domains, (ii) the polyvalent adaptor subunit II that contains more than one cohesin domains that bind to the corresponding dockerin domain on the adaptor subunit I and at the same time displayed on the yeast surface. This complex assembly permits the display of more than one adaptor subunit I with the displayed cellulases on the adaptor subunit II thus increases the amount of cellulases displayed (enhanced enzyme loading) on the yeast surface. In addition, the adaptor subunit I and the cellulases were expressed and purified in *Escherichia coli,* and then assembled on the yeast displaying the adaptor subunit II. The resulting complex cellulosome assembly was then tested for ethanol production from non-treated (Avicel) and acid-treated (PASC) cellulose. Obtained fermentation parameters are ~1.4 g/L ethanol in 96 h with an ESCY of ~29%, and ~1.1 g/L ethanol in 96 h with and ESCY of ~22%, from 10 g/L of Avicel and PASC respectively. The difference in fermentation performance between Avicel and PASC substrate systems was attributed to the enhanced accessibility that is offered by the Avicel structure to the complex cellulosome assembly. In other words, the complex cellulosome prefers being bound to the non-treated substrate [75]. A similar approach in the complex cellulosome assembly was also demonstrated by Tsai, et al. [76]. In this case however, the adaptor subunits are specifically designed to contain chimeric cohesins which leads to a tetravalent designer cellulosome assembly. The adaptor subunits designed are as follows: (i) a bivalent bifunctional adaptor subunit I which contains two chimeric scaffoldins and at the same time displayed on the yeast surface, (ii) two variants of the bivalent bifunctional adaptor subunit II (due to the two different dockerin domains fused to each of the adaptor subunits that bind to the corresponding cohesins on the adaptor subunit I) which displays the *C. cellulolyticum* endoglucanase (CelG), and the *C. thermocellum* β-glucosidase (BGL1), fused with two different chimeric dockerin domains that bind on the respective chimeric cohesins. Similarly, the two variants of the adaptor subunit II along with the cellulases were expressed and purified in *E. coli* and then assembled on the yeast displaying the adaptor subunit I and the resulting assembly was tested for ethanol fermentation from PASC. The system has produced ~2 g/L ethanol in 72 h with an ESCY of ~40%. This tetravalent assembly exhibited a ~2-fold higher ethanol production when compared to the bivalent assembly system. This result indicates a direct relationship between enzyme loading and ethanol production capacity [76]. In an endeavor to enhance cellulose hydrolysis and utilization, Fan, et al. [77] has integrated their complex cellulosome assembly strategy [75], along with the cellodextrin utilization pathway. In this case, the adaptor subunit I in this case was bi-functional and at the same time displays the *T. reesei* cellobiohydrolase II (CBHII), and the *C. cellulolyticum* endoglucanase (EGII) The tetravalent adaptor subunit II, which contains four cohesin domains, was displayed on the surface of yeast. The *N. crassa* cellodextrin transporter (cdt1) along a β-glucosidase (gh1-1) were expressed intracellularly. Furthermore, the cellodextrin utilization pathway and the adaptor subunits were co-expressed in yeast, thus enabling the resulting strain for the co-fermentation of cellulose and galactose (the purpose of galactose is for the co-induction and expression of the adaptor subunits); and the complex cellulosome assembles in situ. The strain was then tested for its ability to produce ethanol acid treated cellulose (PASC) and the soluble carboxymethylcellulose (CMC). The obtained fermentation parameters are ~1.1 g/L ethanol in 60 h with an ESCY of ~22%, and ~3.3 g/L ethanol in 60 h with an ESCY of ~66%, for 10 g/L PASC and 10 g/L CMC, respectively (both are mixed with 20 g/L galactose). Moreover, the advantage of this co-expression system is that the resulting fermentation setup only requires a small inoculation of the non-induced yeast cells to efficiently convert both cellulose and galactose to ethanol in a single-step co-fermentation process [77].

3.2. Pure Hemicellulose Substrates

As the second most abundant polysaccharide in lignocellulosic biomass, efficient enzymatic degradation of hemicellulose is quite challenging due to its complex biochemical structure. In general, hemicellulose is a hetero-polysaccharide that is composed of different sugar units

(the commercially important sugar units are: xylose, mannose, galactose, arabinose, and rhamnose). As a hetero-polysaccharide, it has various polysaccharide forms depending on the biomass feedstock (i.e., wood, plants and plant gum, and agricultural waste), the major hemicelluloses being xylans, mannans, arabinans, and galactans [78]. The most common hemicellulose that is found in lignocellulosic biomass from agricultural waste (e.g., sugar cane bagasse, sugar beet pulp, rice and wheat straw, cornstalk, and cobs) is xylan [79]. The xylan structure relevant enzymes for its degradation are illustrated in Figure 5 [80]. In other words, the xylan side-chains are removed via the action of the accessory enzymes to produce linear xylose chains then cleaved into soluble xylooligosaccharides and xylobiose via the action of the endoxylanase and finally releasing xylose via the action of β-xylosidase. These hemicellulases can be then exploited along with yeast surface display to produce whole-cell biocatalysts for xylan degradation. Also, it was generally reported that accessory enzymes, such as xylan esterases, arabinofuranosidases, glucuronidases, and mannases synergistically enhances the main-chain cleaving enzymes (i.e., xylanases, xylosidases) in the release of xylose from pure hemicellulose substrates, such as wheat arabinoxylan, oat-spelt, beechwood, and birchwood xylans [81–85]. Though it should be noted that not all hemicellulase combinations would lead to a positive synergism between them. Some exhibit negative synergism (also referred as anti-synergism) in cases when one of the enzymes in the mixture inhibits the action of its other constituents [86]. Furthermore, some cases show that some accessory enzymes exhibit no synergy with respect to the main-chain cleaving enzymes; in other words, the addition of the accessory enzyme did not even improve the xylose, arabinose, mannose, or ferulic acid release, either due to the nature of the enzyme (e.g., substrate specificity, reaction conditions, etc.) or the complexity of the substrate [82,87–89].

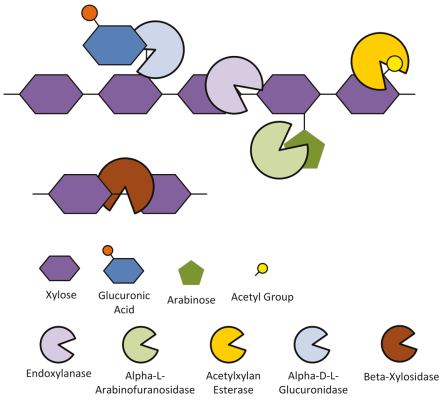

Figure 5. Basic structural component of xylan and the hemicellulases required for the efficient release of xylose from its structure.

On the other hand, another of the most challenging conundrums to use *S. cerevisiae* in CBP is the inability of *S. cerevisiae* to completely break down hemicellulose due to its structural complexity and to utilize the pentose sugars (e.g., xylose) released upon hemicellulose degradation. This drawback is especially relevant for ethanol fermentation from hemicellulosic feedstock. The efforts in metabolic engineering of *S. cerevisiae* has enabled this yeast to utilize xylose and convert to ethanol via two heterologous metabolic pathways. The first developed xylose utilization pathway in yeast (termed XR-XDH pathway) involves the conversion of xylose to xylitol by a xylose reductase (XR), xylitol is then converted into xylulose by a xylose dehydrogenase (XDH), then xylulose is further processed via the pentose-phosphate (PP), and the glycolysis (Embden-Meyerhoff-Parnas, EMP) pathways to produce ethanol [90]. The second developed xylose utilization pathway (termed as the XI or XI-XK pathway) in yeast completely bypasses the xylitol formation by directly converting xylose into xylulose

by a xylose isomerase (XI) enzyme, then further converted to ethanol; a novel pathway derived from anaerobic ruminant bacteria [91–94].

Therefore, the combination of the hemicellulase expression, xylose utilization pathways, has generated recombinant yeast strains that directly produce ethanol from xylan substrates. So far, only a few studies regarding hemicellulosic ethanol production via yeast surface display technologies have been performed. Nonetheless, the studies in this subsection have extended the yeast surface display technologies motivated by the developments in cellulosic ethanol production.

3.2.1. DYSD Strategy for Hemicellulosic Bioethanol Fermentation

Katahira, et al. [95] first demonstrated the construction of a recombinant yeast strain that is capable of producing ethanol from xylan. The heterologous XR-XDH pathway derived from *P. stipitis* was expressed in their previously developed yeast strain that co-displays the *T. reesei* xylanase II (XYNII) and the *A. oryzae* a β-xylosidase (XylA) [96]. The resulting strain was then assessed for its ability to produce ethanol from 100 g/L of birchwood xylan and has obtained ~7 g/L ethanol in 62 h with an ESCY of ~16%.

The endeavor to utilize five *T. reesei* hemicellulases, namely xylanase II (Xyn2), β-xylosidase (Bxl1), arabinofuranosidase (Abf1), α-D-glucurunidase (Glr1), and acetylxylan esterase (Axe1); that efficiently release xylose from the basic xylan structure described in Figure 5 and convert it to ethanol was explored by Tabañag and Tsai [42] upon investigating the synergistic interactions between the five hemicellulases during xylan hydrolysis. These five hemicellulases were then individually displayed on the yeast surface co-expressed along with the XI-XK pathway xylose utilization enzymes derived from *Prevotella ruminicola* where each resulting strain can utilize xylose and display one hemicellulase on its surface. The optimum hemicellulase formulations were obtained from the hemicellulase synergy experiments for xylan hydrolysis using the mixture experimental design methodology. The xylan fermentation setup involves a synthetic consortium of these five stains and hemicellulase formulation was controlled by setting up the inoculation ratios/compositions of each strain adapted from Baek, et al. [45,74]. This synthetic consortium system was assessed for its ethanol production from two xylan substrates and the obtained fermentation parameters are, ~1 g/L ethanol in 168 h with an ESCY of ~23%, and ~0.8 g/L ethanol in 168 h with an ESCY of ~30%, from 10 g/L of beechwood xylan, and wheat arabinoxylan, respectively [42]. This was a demonstration that the xylose released by the synthetic consortium–surface display system was utilized and converted to ethanol via the application of a minimal metabolic engineering approach for xylose utilization.

In another case of hemicellulose degradation, Ishii, et al. [43] focused on the degradation and utilization of mannan using the surface display technology. Mannan, a type of hemicellulose where at its basic structure consists of mannose linked together in a linear fashion (similar to cellulose in both polysaccharide structure and insolubility in water). Furthermore, the mannanases responsible for mannan degradation have similar functions with their cellulase counterparts. Specifically, β-mannanases are the pivotal enzymes that initiate mannan degradation by randomly cleaving the mannan backbone to liberate short manno-oligomers and produce new chain ends, the β-mannosidases which are exo-acting enzymes responsible for the hydrolysis of non-reducing terminal ends and mano-oligomers thus liberating mannose [97]. Unlike xylose, which requires a heterologous metabolic pathway utilization, mannose is inherently utilized by yeast and directly converted to ethanol, thus requiring no further metabolic engineering for mannose utilization. Thus, by co-displaying the *A. aculeatus* β-mannanase (Man5A) and β-mannosidase (Mnd2A), the resulting yeast strain was able to directly convert mannan to ethanol. The obtained fermentation parameters are ~10 g/L of ethanol in 312 h with an ESCY of ~23% from 100 g/L of β-D-mannan.

3.2.2. JANNASEY Strategy for Hemicellulosic Bioethanol Fermentation

Though the application of the surface display adaptor assembly for hemicellulosic ethanol is limited, it is quite relevant that this type of surface display strategy was explored for this type of

substrate. Srikrishnan, et al. [44] demonstrated the assembly of a minixylanosome (a counterpart of the minicellulosome) on yeast. This assembly consists of a trivalent tri-functional adaptor subunit that is attached on the surface of yeast where three hemicellulases fused with different dockerin domains: the *Thermomyces lanuginosus* endoxylanases (XynA), *Aspergillus niger* β-xylosidase (XylA), and the *Aspergillus awamori* acetylxylan esterase (AXE) assemble and display onto. The resulting minixylanosome assembly performed ~3.3 times better (with respect to the degree of synergy) in the hydrolysis of birchwood xylan when compared to their free hemicellulase mixture counterpart. Moreover, their results highlighted the significance of hemicellulase positioning in the minixylanosome assembly in relation to the substrate channeling phenomenon (defined as the coupling of two or more enzymatic reactions, in which the common intermediate is transferred in between the enzymes without escaping to the bulk phase that avoids side reactions or protects the unstable intermediate [98]) [44].

In terms of direct xylan utilization in yeast, Sun, et al. [99] demonstrated the assembly of a single bifunctional minixylanosome in combination with the heterologous XR-XDH xylose utilization pathway derived from *P. stipitis*. The assembly consists of a bivalent adaptor subunit (CipA3) from *C. thermocellum* attached to the yeast surface that displays the *T. reesei* endoxylanase II (Xyn2) and *A. niger* β-xylosidase (XylA) fused with the corresponding dockerin domains. Both the adaptor subunit and the secreted subunits were co-expressed along with the XR-XDH pathway enzymes in one yeast strain and the minixylanosome assembly occurred in situ. The resulting strain that displays the bifunctional minixylanosome assembly was able to directly produce ethanol from xylan. The obtained fermentation parameters are ~1 g/L ethanol in 80 h with an ESCY of ~21%. In addition, the repeated batch fermentation of the mannanase displaying yeast showed ability to produce ethanol in three cycles. Furthermore, recovered yeast after the 1st batch fermentation exhibited high manannase activities from the early fermentation stages of the succeeding cycles, which supports the hypothesis that high activities were due to the relevantly expressed mannanases on the yeast surface [99].

3.3. Pre-Treated Lignocellulosic Substrates

Lignocellulosic biomass is considered as a second generation feedstock; given the conditions that it does not compete with the food supply, has a low-value (or no value), and in abundant supply. The feedstock that fulfills these conditions involve inedible plant materials. This involves agricultural waste (e.g., rice straw, corn stover and cob, bagasse, molasses), forestry wastes (e.g., wood chips), municipal and industrial waste (e.g., used paper), and fast growing energy crops (e.g., switch grass, miscanthus) [100]. Due to its complex lignocellulosic biomass structure, a certain degree of pre-treatment is involved to liberate its polysaccharide components (i.e., cellulose, hemicellulose, and lignin) prior to the bioprocessing steps. In addition, it should be noted that during the pre-treatment process, a certain extent of fermentable sugars are already released from its polysaccharide structure, depending on the severity of the pre-treatment step. Furthermore, the most common substrate that is presented in this subsection is rice straw, which has undergone liquid hot water pre-treatment (a.k.a. autohydrolysis or hydrothermolesis). For this type of pre-treatment, ~50% of the total biomass is dissolved in the process, with 6–22% of cellulose, 30–60% of the lignin, and the removal of all hemicelluloses. More than ~90% of the hemicelluloses are degraded into its monomeric sugars when an acid is utilized to hydrolyze the resulting liquid. Though the results of this pre-treatment step vary with the biomass type due to the high lignin solubilization that impedes the recovery of hemicellulose sugars [78,100–102]. Moreover, for the direct utilization of pre-treated lignocellulosic substrates, the presented studies in this subsection so far have reported the application of the direct yeast surface display strategy (DYSD).

DYSD Strategy for Bioethanol Fermentation from Pre-Treated Lignocellulosic Biomass

Yamada, et al. [66] has first demonstrated the ethanol production from agricultural waste biomass using the engineered cellulase co-displaying diploid yeast without the addition of exogenous enzymes, as presented in Section 3.1.1. When assessed for its ethanol production from pre-treated

rice straw, the engineered yeast has obtained ~8 g/L ethanol in 72 h with an ESCY of ~36.47% from 100 g/L of pre-treated rice straw [66]. In an attempt to improve the ethanol substrate conversion yield from pre-treated rice straw, Matano, et al. [103] has investigated the supplementation of exogenous commercial cellulases (Cellulase SS) to yeast co-displaying the *T. reesei* endoglucanase (EGII) and cellobiohydrolase (CBHII), along with the *A. aculeatus* β-glucosidase (BGL1). This strategy successfully reduced the amount of commercial enzyme required for the fermentation of cellulose as the ethanol production performance of the cellulase co-displaying yeast supplemented with 10 FPU/g biomass .cellulases was comparable to the system that consists of a control yeast strain (no display) supplemented with 100 FPU/g biomass cellulase. These results demonstrate that cellulases displayed on the yeast cell surface are capable of hydrolyzing cellulose that was not hydrolyzed by commercial cellulases, leading to increased sugar utilization for improved ethanol production. The obtained fermentation parameters for the system consisting the cellulase co-displaying yeast supplemented with 10 FPU/g biomass of cellulase are ~43 g/L ethanol in 72 h with an ESCY of ~90% [103]. Then this engineered strain was tested for its performance in a cell batch recycle fermentation (CRBF) setup [104]. For five (5) repeated fermentation cycles, the cells displaying cellulases [103] were recycled and assessed using the same pre-treated rice straw substrate. With five consecutive recycling cycles, ethanol fermentation parameters was maintained all throughout and obtained ~42 g/L ethanol in the total 360 h (five cycles) with an ESCY of ~86%. This was a first demonstration of the utilization of CRBF with cellulase displaying cells. Indeed, the results suggest that the these cells retained their hydrolysis and ethanol production activities when exposed to five consecutive fermentation cycles [104]. In a succeeding study by Sakamoto, et al. [105], the xylose utilization from the pre-treated rice straw was investigated. The XR-XDH pathway xylose utilization enzymes from P. stipitis were co-expressed with the two hemicellulases and one cellulase, *T. reesei* endoxylanase II (Xyn2), *A. oryzae* β-xylosidase (XylA), and *A. aculeatus* β-glucosidase (BGL1), co-displayed on the yeast surface. When assessed for ethanol production from pre-treated rice straw, the obtained fermentation parameters are ~8 g/L ethanol in 72 h with a reported ethanol yield of ~82% (based from the sugars consumed) [105]. Another study by Liu, et al. [62], as described and presented in Section 3.1.1, have assessed the performance of their novel adherent yeast strain co-displaying four cellulases on pre-treated rice straw. The obtained fermentation parameters are ~1.3 g/L of ethanol in 96 h with an ESCY of ~7% from 100 g/L of rice straw hydrolysate. The fermentation performance was then improved by supplementing 1 FPU/g biomass of commercial cellulase (Ctec2) to the novel adherent yeast strain and the system has produced ~18 g/L of ethanol in 96 h with an ESCY of ~91% from 100 g/L of the same substrate. This cellulase supplemented system has the achieved the same ethanol fermentation performance when compared to the control system (non-cellulase displaying yeast with cellulase addition) provided the 40% decrease in commercial cellulase dosage [62]. In another study of the same research group, Liu, et al. [69], which has combined the cellulase ratio optimization with novel high throughput screening (HTS) methodology (as described and presented in Section 3.1.1), have assessed the ethanol fermentation performance of resulting strain from pre-treated rice straw. The fermentation parameters obtained by this strain are ~1 g/L ethanol in 96 h with an ESCY of ~17%. This strain has performed ~2.5 times better than the one previously reported [62] in terms of ethanol substrate conversion. These results demonstrated the potential of the novel high-throughput screening methodology in improving the performance of the engineered strain via tuning the cellulase ratios in the yeast co-display strategy [69]. From another perspective, Guirimand, et al. [106] have explored the direct utilization of pre-treated rice straw and convert it to xylitol. By co-expressing the *P. stipitis* xylose reductase (XR) enzyme along with the *T. reesei* endoxylanase II (Xyn2), *A. oryzae* β-xylosidase (XylA), and *A. aculeatus* β-glucosidase (BGL1), co-displayed on the yeast surface. They have assessed the ethanol performance of this strain on pre-treated rice straw. The resulting strain has produced ~6 g/L xylitol in 96 h with a xylitol substrate conversion yield (XSCY) of ~47% from the total xylose present in the 500 g/L of rice straw hydrolysate. In an effort to increase xylitol yield by increasing the xylose or xylose oligomer concentration in the hydrolysate, an additional membrane filtration step was introduced and this step

significantly concentrated the sugars in the hydrolysate, while drastically reducing the fermentation inhibitor concentrations. The obtained xylitol performance parameters of the developed strain on this substrate are ~38 g/L xylitol in 96 h with a XSCY of ~65% from the total xylose present in 500 g/L filtered hydrolysate. These results demonstrate that the additional filtration step has enabled the strain to perform ~1.4 times better in the filtered hydrolysate when compared to the unfiltered one; showing that increased xylose utilization was attributed to the removal of fermentation inhibitors after filtration [106].

Bioethanol production from other pre-treated lignocellulosic substrates, such as wood chips, cassava pulp, and ivory nut were also explored and presented in the next paragraph.

Katahira, et al. [107] have investigated the xylose and cellobiose utilization in acid-treated wood chips. The XR-XDH xylose utilization pathway enzymes from *P. stipitis* were co-expressed with the *A. aculeatus* β-glucosidase (BGL1) displayed on the yeast surface. This resulting strain was then assed for its ethanol production from wood chip hydrolysate (with ~72 g/L total sugar concentration) and has produced ~30.3 g/L ethanol in 36 h with an ESCY of ~82%. Furthermore, the fermentation of the wood chip hydrolysate was similar to the mixed sugar fermentation model system, which suggests that the inhibitory effects of some of the hydrolysate components does not exhibit significant inhibition to the engineered strain [107]. Apiwatanapiwat, et al. [67] has tested their amylase-cellulase co-displaying yeast strain, as described and presented in Section 3.1.1 in liquid hot water pre-treated cassava pulp. The fermentation parameters obtained by this strain are ~10 g/L ethanol in 48 h with an ESCY of ~80% from 50 g/L pre-treated cassava pulp; demonstrating the ability of the strain to directly utilize starch and cellulose present in the medium [67]. Ishii, et al. [43], whose research group has explored on the direct mannan degradation by mannanase displaying yeast strains, as described and presented in Section 3.1.1, have extended the scope of lignocellulosic biomass utilization to mannan derived from ivory nuts. The ivory nut mannan was subjected to alkaline hydrolysis prior to fermentation. When the engineered strain displaying mannanases were assessed for their ethanol fermentation performance from this substrate, it has obtained ~10 g/L ethanol in 216 h with an ESCY of ~20% from 100 g/L of ivory nut mannan [43].

3.4. Comparing the Various Yeast Surface Display Strategies for Bioethanol Fermentation from Lignocellulosic Biomass Substrates

The fermentation parameters from the different studies presented in this subsection were compared with respect to their different display strategies, and substrate types. These different data types are incorporated and then visualized via bubble charts. By no means does the comparison presented in the bubble charts for the following sub-subsections imply the suitability of a certain surface display strategy to ethanol conversion yield for that type of substrate. It is just a means to visualize the state and progress of yeast surface display technology in bioethanol production from lignocellulosic substrates. In other words, these charts serve as an aid in comparing the performances of the cell-surface engineered strains provided the type of surface display strategy being adapted, and the type of substrate being utilized since the superiority of the different yeast surface technologies were by far already demonstrated in comparison to their free enzyme counterparts.

The data visualized in the bubble charts are presented in a way that the ethanol substrate conversion yield (ESCY) values are plotted in a chronological order such that the progress and development of yeast surface display for lignocellulosic bioethanol production can be directly seen. The ESCY vs time series is then augmented by the ethanol titer as represented by the bubble sizes or circle areas to show how much ethanol was produced from the given substrate that corresponds to its ESCY. The corresponding data labels basically provides the information on the substrate types and their corresponding concentrations in the fermentation media.

3.4.1. Cellulosic Bioethanol Fermentation

In terms of bioethanol production from lignocellulosic biomass, the widely utilized and tested substrate is the pure cellulose substrates since the yeast *S. cerevisiae* is an ethanologenic yeast strain that can produce high amounts of ethanol from glucose, once liberated from the cellulose structure. Thus, in most cases, the various yeast surface display strategies that are presented throughout this article were first explored in the direct utilization of pure cellulose substrates, and then extended to pre-treated lignocellulosic biomass, prior to its application to direct hemicellulose utilization.

The comparison of the different studies presented in Section 3.1 are visualized in Figure 6. Looking at the capability to convert half of the expected ethanol from the substrate (ESCY of >50%), it can be generalized that direct co-display (DSYD-CD) of cellulases performed well given that the substrates are acid (PASC) and alkali (BBglucan) pre-treated, and solubilized (CMC). Furthermore, using the delta-integration strategy to control the cellulase co-display ratio has provided an insight to the importance of cellulase display optimization and strain improvement by diploidization [66,67,69]. It can also be observed that the ESCY performance on the utilization of glucan is better than that of cellulose (either treated or non-treated) substrates, and this can be attributed to their structures where cellulose has a more rigid structure (more crystalline) than glucan. One can also notice that most non-treated cellulose (Avicel) were utilized as substrates for the complex adaptor assembly systems (JANNASEY-CAA), which address the enzyme loading limitation of DSYD systems though the obtained conversion yields were mostly <50%.

3.4.2. Hemicelllulosic Bioethanol Fermentation

The application of yeast surface display technology in hemicellulosic ethanol production demonstrates its potential for efficient lignocellulosic biomass utilization. Though the presented studies report ethanol substrate conversion yields of ~16–30%, as visualized in Figure 7, it has shown that direct conversion of pure hemicellulose substrates like xylan and mannan to ethanol is achievable. These reported studies have gradually filled the gap in the field of hemicellulosic bioethanol fermentation. In terms of efficient xylan hydrolysis by hemicellulases, the direct yeast surface display system (DYSD-SEDC) by Tabañag and Tsai [42] achieved ~23–30% ethanol substrate conversion yields from different xylan substrates, which highlights the significance of different hemicellulase synergistic interactions for the efficient xylose release from the xylan structure. In addition, the utilization of surface display strategies also exhibited superior performance in terms of xylan hydrolysis with respect to their free hemicellulase counterparts.

So far, the attempt to assess the efficiency of these surface display strategies remain a challenge since this field is not that elaborate when compared to the advances in cellulosic bioethanol production. At least it can be stressed out that for xylan degradation and utilization, the combination of the efficient xylan degradation by hemicellulases and the improved xylose utilization are both avenues that warrant further investigation.

3.4.3. Bioethanol Fermentation from Pre-Treated Lignocellulosic Biomass

From the description presented in Section 3.3 that upon pre-treatment, a certain extent of fermentable sugars are already being released to the medium, thus, in principle these sugars are readily available for direct utilization by the yeast cells. As visualized in Figure 8, this explains the high amounts of ethanol titer (in reference to the large circle areas) that are obtained from pre-treated lignocellulosic biomass substrates. The low yields, however, are related to the high substrate loadings (~100 g/L) that directly correspond to the amount of oligosaccharides present in the medium along that require hydrolysis by the engineered yeast strain displaying the necessary enzymes or to the action of exogenous commercial enzymes added to supplement the hydrolysis process prior to the release of fermentable sugars [43,62,66,69]; or to the presence of fermentation inhibitors that can be removed via an additional process step (i.e., membrane filtration) [106].

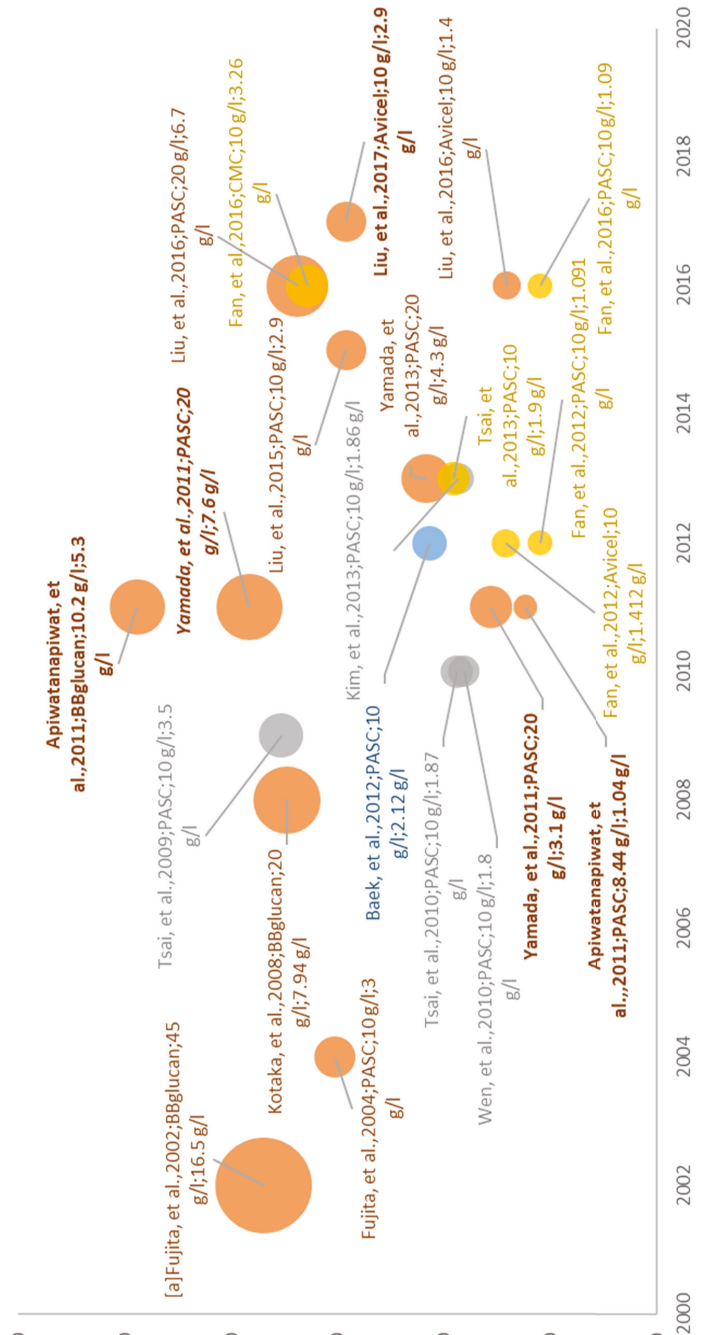

Figure 6. Visualization of the status and development of yeast surface display for Cellulosic Bioethanol Production. Bubble sizes represent ethanol titer. Data labels are formatted as follows: (Reference (author-date); Substrate; Substrate Concentration; Ethanol Titer). For the DSYD-CD data set: labels in boldface represent cellulase ratio control via delta-integration; labels in *italic* represent utilization of diploid host strains.

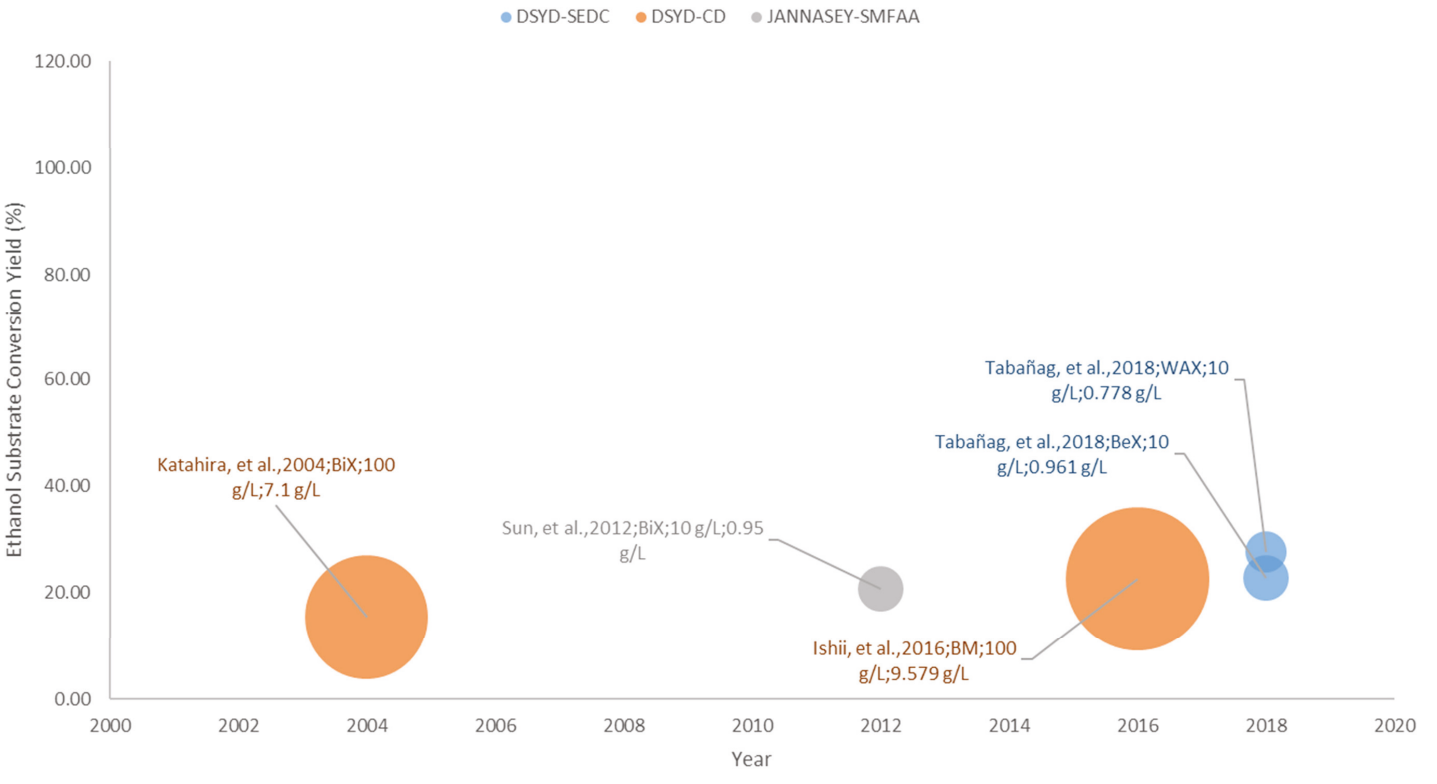

Figure 7. Visualization of the status and development of yeast surface display for Hemicellulosic Bioethanol Production. Bubble sizes represent ethanol titer. Data labels are formatted as follows: (Reference (author-date); Substrate; Substrate Concentration; Ethanol Titer).

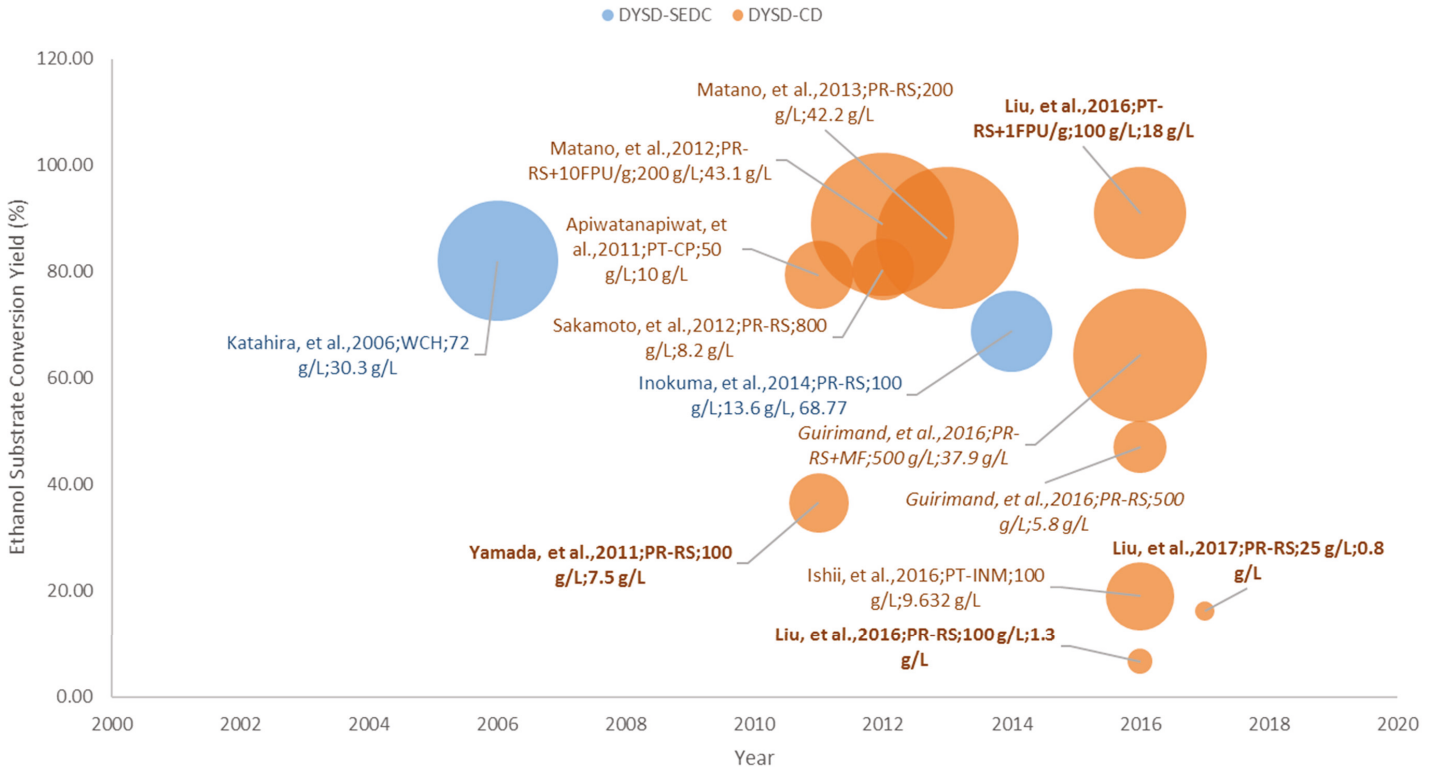

Figure 8. Visualization of the status and development of yeast surface display for Bioethanol Production from Pre-Treated Lignocellulosic Biomass. Bubble sizes represent ethanol titer. Data labels are formatted as follows: (Reference (author-date); Substrate; Substrate Concentration; Ethanol Titer). For DSYD-CD data sets: labels in boldface represent cellulase ratio control via delta-integration; labels in *italic* represent the xylitol fermentation parameters instead of ethanol.

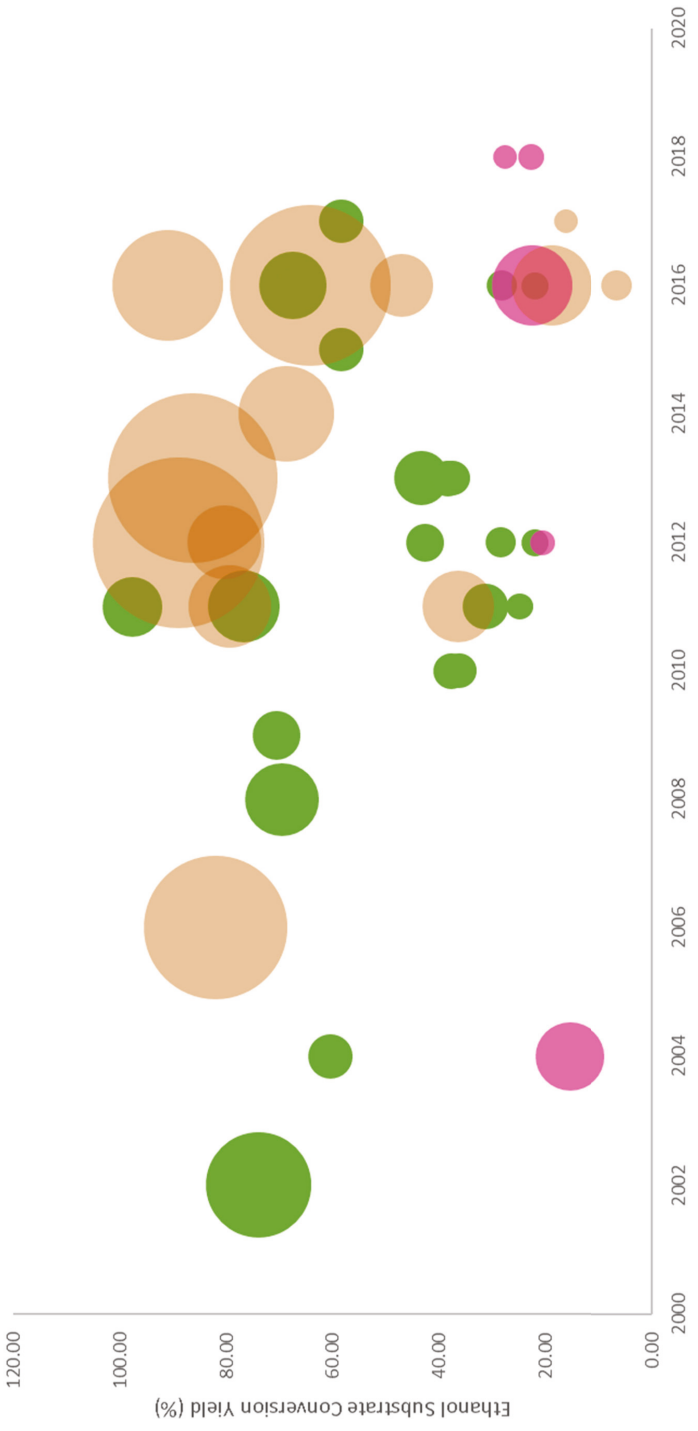

Figure 9. Visualization of the status and development of yeast surface display for Bioethanol Production categorized for the substrate types presented in this article. Bubble sizes represent ethanol titer.

4. Avenues of Improvement for Bioethanol Production Using Yeast Surface Display

As discussed in Section 3.4, the comparative data analysis that are visualized and provided in the bubble charts do not imply the efficiency of a particular surface display strategy to a particular substrate. It just gives an idea on the performance of the engineered strains applying those strategies for the target substrate that it was assessed on. Figure 9 illustrates the impact of yeast surface display to the bioethanol production between the pure polysaccharide and the actual pre-treated lignocellulosic biomass substrates. Moreover, yeast surface display has played an important role in creating engineered strains that obtain high ethanol titers from pre-treated lignocellulosic substrates.

Using the visualized data sets as a guide, we can synthesize from those various techniques on improving the design of the engineered yeast tailored for the efficient degradation and utilization of a target substrate. These techniques are schematically illustrated in Figure 10.

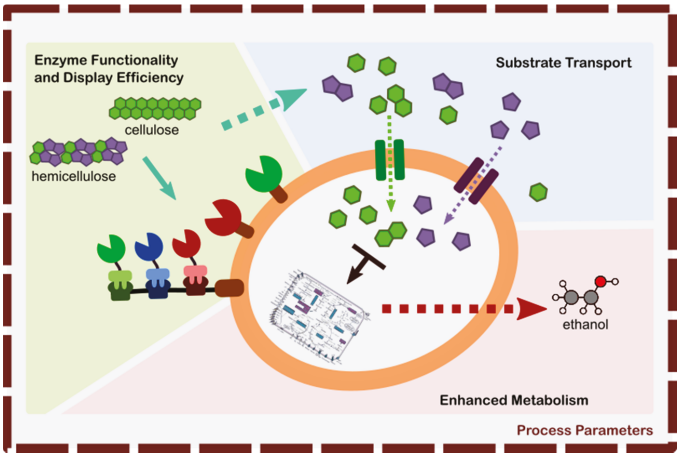

Figure 10. Schematic illustration for the different avenues of improvement for yeast surface display in bioethanol fermentation from lignocellulosic biomass.

These avenues of improvement are categorized into:

1. Enhancement of Enzyme Functionality, and Display Efficiency—this area involves the following: nature of the enzyme being expressed in yeast that it may either retain or increase its activity upon heterologous expression (functionality), enhanced surface display efficiency for DYSD strategy, and adaptor assembly for JANNASEY strategy. The main goal of this area is to increase the hydrolysis efficiency of the resulting strain to optimally liberate the fermentable sugars from their lignocellulosic structure.
2. Substrate Transport into the Yeast Cell—this area involves the efficient transport of the fermentable sugars into the cell. The goal is to provide efficient means transport for the different sugars (e.g., hexose, pentose, cellobiose) where the route is either specific to one type of sugar or a ubiquitous type for generic sugar transport.
3. Metabolic Engineering for Efficient Ethanol Conversion—involves in the rewiring of the yeast itself to convert the sugars efficiently into ethanol by minimizing the generation of by-products.
4. Optimization of Process Conditions for Enhanced Hydrolysis and Ethanol Production—optimization of the process conditions can either have an effect all the areas 1 to 3 or to one of them. This involves varying the process conditions (i.e., temperature, pH, media composition, induction) to achieve efficient enzymatic hydrolysis and cellular metabolism.

4.1. On the Enzyme Functionality and Display Efficiency

Enzyme functionality refers to the retention or improvement of the enzyme activity once heterologously expressed in yeast. This is mainly achieved by a combination of high throughput screening and protein engineering methodologies where the enzymes are tailored for functional expression in yeast that they synergistically interact with other enzymes expressed when it comes to the efficient hydrolysis of lignocellulosic substrates [81,100,108]. Likewise, the functional expression and display of novel enzymes derived from other microorganisms that has undergone some evolution (be it natural or engineered) contributes to the enhancement of hydrolysis activities once they act in concert with other novel enzymes [109–111].

On the other hand, enhancing the display efficiency of enzymes can be achieved by several approaches. In reference to the review of Tanaka, et al. [27], these approaches are classified as the traditional, semi-rational, and combinatorial approaches. The traditional approach targets the yeast secretion pathway itself and the detailed knowledge on yeast secretion has enabled increased secretion efficiency and protein yields. This was achieved through the utilization of various molecular techniques that lead to the optimization of signal sequences, upregulation of ER folding, modification of vesicle transport, and deletion of host proteinases as discussed in detail by Haan, et al. [112]. A recent example of this in relation to the role of surface display for efficient lignocellulose utilization has been demonstrated by Tang, et al. [113]. Where the localization and co-display of the *C. thermocellum* endoglucanase (CelA) along with a *S. fibuligera* β-glucosidase (BGL) was improved by the over-expression of various vesicle trafficking components. Furthermore, their results have shown that there is a protein-specific effect, which limit the vesicle trafficking pathway with respect to the heterologous protein being localized; this provides an insight on how to improve surface display efficiency tailored to the protein of interest [113]. In the semi-rational approach, the genes in the cell wall environment are targeted instead of those in the secretory pathway. These target proteins at the cell wall niche are either deleted or over-expressed. Kotaka, et al. [114] have demonstrated that by deleting the SED1 in the sake yeast displaying the *A. oryzae* β-glucosidase (BGL) anchored via the truncated α-agglutinin anchor protein (SAG1, C-terminal half), the activity of BGL on the yeast surface was enhanced by ~1.6 fold when compared to the wild type; which can be attributed to the increased number of BGL displayed on the yeast surface [114]. In addition, Matsuoka, et al. [115], using a high throughput screening methodology, have identified the potential genes for deletion to enhance surface display efficiency. Screening results indicated that the deletion of the Mnn2 facilitated in the binding of high-molecular weight substrates to the active sites of the displayed enzymes thus improved the cellulase activities each displayed on the yeast surface by ~1.6, and ~2-fold for BGL and endoglucanase, respectively, with respect to their wild-type counterparts [115]. Lastly, the combinatorial approach which combines the high throughput screening methodology with a yeast overexpression library and yeast surface display. This novel screening approach described by Wentz and Shusta [116], has enabled rapid flow cytometric screening of engineered yeast for gene products that improve the display of heterologous proteins. Screening results have identified the ribosomal subunit protein (RPP0, for the overexpression of translational components), an endoplasmic reticulum resident protein (ER01, a folding assistant), and cell-wall related proteins (e.g., SED1, CCW12, CWP2) as general enhancers in target protein secretion; where secretion levels of the target protein was increased by ~2-fold to ~8-fold with ER01 and CCW12 being the notable enhancers. Their results further suggest that display efficiency is dependent on the characteristics of both the target and anchor proteins [116].

4.2. On Substrate Transport

It can be said that substrate transport is what dictates how efficient the substrate can be converted into the desired product via metabolism. Since metabolism occurs in such a short period of time due to their low local concentration inside the cell, it results to a short passage time of molecules inside the cell; where the cell is in somewhat a pseudo-steady state. Thus, because of this transient residence time inside the cell, substrate conversion is dependent on the uptake rate and this is under the

direct control of the substrate transporter [117]. The ideal substrate transporter should be ubiquitous and has no preference such that various substrates can be transported into the cell at almost equal uptake rates which lead to efficient and simultaneous conversion of multiple substrates into desired products. However in yeast, sugar transporters exhibit substrate preference or selectivity; meaning that it has high transport rates for its preferred sugars and low or blocked transport for its non-preferred sugars [118–120]. The quest to tailor or improve the substrate uptake of a specific transporter in yeast is explored in the field of "yeast transporter engineering". One of the major milestones of this field (during the investigation and characterization of the sugar transport mechanism in yeast) is the creation of a yeast strain (named EB.VW4000 [121]) that is devoid of ~20 hexose transporter genes, which resulted in the inability of the strain to take up glucose and also fructose, galactose, and mannose. This strain has been an essential tool for the elucidation of transporter function; for engineering and screening either native or heterologous sugar transporters [122].

A good discussion on the role of yeast transformer engineering in the utilization of various sugars released from lignocellulosic biomass hydrolysis is reviewed by Hara, et al. [123]. The sugar transporters that have been engineered and expressed for consolidated bioprocessing (CBP) are those specific for the sugars derived from lignocellulosic biomass hydrolysates. These sugar transporters are designed and are currently developed specifically for the transport of: (i) cellobiose or cellodextrin from cellulose, (ii) xylose, arabinose, and galactose from hemicellulose, and (iii) sucrose and fructose from starchy plant materials. The details on the identity and the protein engineering methods for the transporters of the said sugars are as provided in the reference material [123].

In the studies presented in Section 3, so far only the combination of the cellobiose transport and utilization pathway with yeast surface display been explored for the direct co-display (DYSD) [68], and complex adaptor assembly strategies (JANNASEY) [77]. Thus, the integration of enhanced substrate uptake with yeast surface display is a challenging area that is not yet fully explored and could provide insights on the substrate channeling phenomenon from the displayed enzymes into the cell via the substrate transporter of interest.

4.3. On Metabolic Engineering for Improved Ethanol Prodution

The inherent ability of the yeast *S. cerevisiae* to produce ethanol has been its major industrial selling point for many years. It is considered as a natural ethanologen (ethanol-producing microbe) that can produce high amounts of ethanol titer from hexose sugars, especially glucose. This capability of yeast is what made it the ideal host microorganism for consolidated bioprocessing (CBP). When the CBP strategy was first introduced, the ideal target substrate for direct ethanol conversion was cellulose (since it mainly consists of linked glucose monomers); this was termed as microbial cellulose utilization [6,8–10]. Thus, it can be observed from Figure 9 that cellulose was the first substrate type that was explored by the yeast surface display strategies for CBP. In contrast to hemicellulose (which is pre-dominantly composed of xylan from plant-based/agricultural waste biomass) where its major fermentable sugar is xylose, where extra efforts to confer a xylose utilization pathway are needed prior to ethanol production.

In terms of the combined xylose utilization from hemicellulosic substrates and yeast surface display strategies, combining the XR-XDH xylose utilization pathway with direct co-display (DSYD-CD) and with single multi-functional adaptor assembly (JANNASEY-SMFAA) has been reported by Katahira, et al. [95] and Sun, et al. [99], respectively, while combining the XI-XK xylose utilization pathway with the single enzyme display consortium (DYSD-SEDC) has been reported by Tabañag and Tsai [42]. Though the reported ESCY's of these studies mentioned are quite low (<30%), these could be improved by the combination of metabolic and evolutionary engineering methodologies. As the xylose conversion to ethanol occurs via the pentose-phosphate pathway (PPP), the metabolic engineering of the downstream PPP genes has been reported to have high specific rates of anaerobic xylose consumption and ethanol production [124,125]. Moreover, combining this metabolic engineering strategy to overexpress xylose-utilization pathway and downstream PPP genes

with systematic evolutionary engineering techniques can further improve xylose utilization, ethanol production, and even inhibitor tolerance [126–130].

4.4. On Process Parameters

In a fermentation system, the conditions of the area surrounding the cell constitute the process parameters. This involves the physiological conditions surrounding the cell (e.g., temperature, pH, media, inhibitors), the type of yeast utilized in the process, and mode of cultivation. Furthermore, when target enzymes are displayed on the yeast surface, it exhibits enhancements on their relative activities and stability; and to some degree that these enhancements especially on a physiological level where there is increased tolerance to some medium components. This two-way enhancement is one of the attractive features that elevate the status of yeast from an immobilization platform to a whole-cell biocatalyst.

4.4.1. Cultivation Conditions

The feature of yeast surface display systems once they are in the fermentation environment is that continuous enzyme regeneration (induction) and display on the surface of yeast is coupled with cell growth. Thus, a properly formulated medium can provide an avenue for optimized enzyme expression. From the presented studies in Section 3, Fan, et al. [77] supplemented their fermentation media with galactose for the continuous expression of their adaptor protein vital for the cellulosome assembly. Since other surface display systems are designed with the constitutive (always on) enzyme expression condition kept in mind, then it is the fermentation medium composition (given that one component is a limiting substrate) that directs enzyme expression and display, along with the substrate utilization and conversion.

In terms of hydrolytic activity, most of the enzymes that are heterologously expressed in yeast exhibit optimum activities at high temperatures (typically 50–60 °C), while the optimal growth conditions for *S. cerevisiae* is at a significantly lower temperature (25–35 °C). Thus, there should be a compromise between the hydrolysis activity and yeast growth, and in most cases yeast growth is always favored at 30 °C, which results in a 2–3-fold decrease in the hydrolytic activity of the said enzymes. Thus, for yeast display systems, the temperature can be optimized to achieve the optimum hydrolytic activity and ethanol conversion. Khatun, et al. [131] have demonstrated that at an elevated temperature of 40 °C, ethanol production of an inulinase displaying industrial yeast strain has enhanced when fermented on inulin and Jerusalem artichoke tubers (a starchy substrate) [131].

4.4.2. Host Strain Type

The use of industrial ethanol yeast strains as a host for the yeast surface display technology can enhance ethanol production from pre-treated substrates as these strains are naturally being exposed in a constant selective pressure (continuous utilization in an industrial setting), which can give rise to high ethanol producing mutants. The utilization of an industrial sake yeast displaying cellulases has produced a high amount of ethanol from a pure cellulosic substrate, as demonstrated by Kotaka, et al. [60]. Furthermore, the same effect can be observed in some extent when the engineered yeast strains displaying cellulases undergo diploidization by mating and assessed on their ethanol fermentation performance, around a 2.5-fold increase in ESCY was observed when comparing the diploid strain with the haploid one, as reported by Yamada, et al. [66]. This strategy is based on the fact that polyploid (including diploid) strains have higher cell growth rates, cell yields, and tolerances to various stresses when compared with haploid strains; wild type industrial yeast strains are diploid (which has both the a, and α mating types).

4.4.3. Inhibitor Removal by Additional Process Treatment Steps

The presence of inhibitors decrease the expected ethanol yield in during the fermentation. The presence of these inhibitors adversely affect the cell growth and metabolism. Thus, their removal

presents another round of pre-treatment step/s. Guirimand, et al. [106] have removed these inhibitors from rice straw hydrolysate by membrane filtration and at the same time concentrated the fermentable sugars. Obtained xylitol yield (XSCY) from the membrane-filtered hydrolysate is 1.4-times higher than the non-filtered, with an approximately 10-fold difference in xylitol titer obtained with respect to the non-filtered hydrolysate.

Another treatment step is by enzymatic degradation of these inhibitors. Nakanishi, et al. [132] have utilized yeast displaying the white rot fungus *Trametes sp*. Ha1 laccase I (LacI) on its surface in the pre-treatment of hydrothermally processed rice straw. Another strain that co-displays three cellulases was used to assess the efficiency of pre-treatment and it was found out that the ethanol productivity from the laccase pre-treatment of rice straw was ~1.2-times higher than the one with no treatment

5. Conclusions

The construction of recombinant yeast strains that display different enzymes via different surface display strategies have played a significant role in the quest of finding the ideal CBP strain. In most of the studies that are presented in this article, the performance of the displayed enzymes on yeast was deemed superior in contrast to their free enzyme counterparts. Furthermore, the different strategies for yeast surface display and their features were discussed and their performance on bioethanol production from lignocellulosic biomass substrates were assessed. The trends and progress in lignocellulosic bioethanol production using the surface-engineered yeasts were evaluated using comparative data analysis and visualization techniques. The resulting data visualization charts serve as a reference material on the status on how the different surface display strategies have affected the ethanol substrate conversion yields between pure polysaccharide and pre-treated lignocellulosic biomass substrates. On the other hand, a discussion on the strategic areas of development for tailoring yeast with surface display technology for lignocellulosic bioethanol production was synthesized to serve as a reference on as to how this field of study will advance.

Acknowledgments: We are grateful to Peter Grunwald (the Guest Editor of Catalysts) and Adela Liao (the Managing Editor of MDPI) for inviting us to submit this review. We would like to acknowledge the jointed financial support from Chang Chun Group and the Ministry of Science and Technology, Taiwan. (MOST 105-2622-8-007-009).

Author Contributions: Ian Dominic Flormata Tabañag and Shen-Long Tsai defined the scope and structure of the paper. Ian Dominic Flormata Tabañag, I-Ming Chu, Yu-Hong Wei and Shen-Long Tsai all participated in the discussion, writing and revision of the paper.

Conflicts of Interest: The authors declare no conflict of interest.

Appendix

Table A1. List of references collated with respect to the substrate types targeted by the different yeast surface display technologies.

Authors	Year	Refs.	Yeast Surface Display Strategy	Anchoring Protein	Subst. Abbrv	Substrate Conc. (g/L)	Ethanol Titer (g/L)	Ferm. Time. (h)	ESCY (%) [i]
PURE CELLULOSE SUBSTRATES									
[a] Fujita, et al.	2002	[58]	DYSD-CD	SAG1 (3′-half)	BBglucan	45	16.5	48	73.97
Fujita, et al.	2004	[59]	DYSD-CD	SAG1 (3′-half)	PASC	10	3	40	60.52
Kotaka, et al.	2008	[60]	DYSD-CD	SAG1 (3′-half)	BBglucan	20	7.94	24	69.60
Tsai, et al.	2009	[46]	JANNASEY-SMFAA	AGA1::AGA2	PASC	10	3.5	50	70.61
Tsai, et al.	2010	[72]	JANNASEY-SMFAA	AGA1::AGA2	PASC	10	1.87	70	37.73
Wen, et al.	2010	[73]	JANNASEY-SMFAA	AGA1::AGA2	PASC	10	1.8	70	36.31
Apiwatanapiwat, et al.	2011	[67]	DYSD-CD	SAG1 (3′-half)	BBglucan	10.2	5.3	36	97.70
Apiwatanapiwat, et al.	2011		DYSD-CD	SAG1 (3′-half)	PASC	8.44	1.04	n.r.	24.86
Yamada, et al.	2011	[66]	DYSD-CD	SAG1 (3′-half)	PASC	20	3.1	72	31.27
Yamada, et al.	2011		DYSD-CD	SAG1 (3′-half)	PASC	20	7.6	72	76.66
Baek, et al.	2012	[45]	DYSD-SEDC	SAG1 (3′-half)	PASC	10	2.12	85	42.77
Fan, et al.	2012	[75]	JANNASEY-CAA	AGA1::AGA2	PASC	10	1.091	96	22.01
Fan, et al.	2012		JANNASEY-CAA	AGA1::AGA2	Avicel	10	1.412	96	28.49
Tsai, et al.	2013	[76]	JANNASEY-CAA	AGA1::AGA2	PASC	10	1.9	72	38.33
Yamada, et al.	2013	[68]	DYSD-CD	SAG1 (3′-half)	PASC	20	4.3	72	43.38
Kim, et al.	2013	[74]	JANNASEY-SMFAA	AGA1::AGA2	PASC	10	1.86	94	37.52
Liu, et al.	2015	[61]	DYSD-CD	SED1	PASC	10	2.9	96	58.51
Fan, et al.	2016	[77]	JANNASEY-CAA	AGA1::AGA2	CMC	10	3.26	60	65.77
Fan, et al.	2016		JANNASEY-CAA	AGA1::AGA2	PASC	10	1.09	60	21.99
Liu, et al.	2016	[62]	DYSD-CD	SED1	PASC	20	6.7	96	67.59
Liu, et al.	2016		DYSD-CD	SED1	Avicel	10	1.4	96	28.24
Liu, et al.	2017	[69]	DYSD-CD	SED1	Avicel	10	2.9	96	58.51
PURE HEMICELLULOSE SUBSTRATES									
Fujita, et al.	2002	[96]	DYSD-CD	SAG1 (3′-half)	BiX	10	n.r.	n.r.	n.r.
Katahira, et al.	2004	[95]	DYSD-CD	SAG1 (3′-half)	BiX	100	7.1	62	15.44
Sun et al.	2012	[99]	JANNASEY-SMFAA	AGA1::AGA2	BiX	10	0.95	80	20.66
Ishii, et al.	2016	[43]	DYSD-CD	Flo428p	BM	100	9.579	312	22.59
Tabañag, et al.	2018	[42]	DYSD-SEDC	SAG1 (3′-half)	BeX	10	0.961	168	22.77
Tabañag, et al.	2018		DYSD-SEDC	SAG1 (3′-half)	WAX	10	0.778	168	27.66

Table A1. *Cont.*

Authors	Year	Refs.	Yeast Surface Display Strategy	Anchoring Protein	Subst. Abbrv	Substrate Conc. (g/L)	Ethanol Titer (g/L)	Ferm. Time. (h)	ESCY (%) [i]
PRE-TREATED LIGNOCELLULOSIC BIOMASS SUBSTRATES									
Murai, et al.	1998	[133]	DYSD-SEDC	SAG1 (3′-half)	RCS[ii]	625	23.25	168	n.r.
Murai, et al.	1998	[134]	DYSD-SEDC	SAG1 (3′-half)	RCS+Term.[ii]	626	53	169	n.r.
Katahira, et al.	2006	[107]	DYSD-CD	SAG1 (3′-half)	WCH	72	30.3	36	80.39
Kotaka, et al.	2008	[135]	DYSD-CD	SAG1 (3′-half)	LCS[ii]	50	20	48	n.r.
Apiwatanapiwat, et al.	2011	[67]	DYSD-CD	SAG1 (3′-half)	PT-CP	50	10	48	79.40
Sakamoto, et al.	2012	[105]	DYSD-CD	SAG1 (3′-half)	PT-RS	800	8.2	72	80.39
Matano, et al.	2012	[103]	DYSD-CD	SAG1 (3′-half)	PT-RS	200	43.1	72	89.00
Matano, et al.	2013	[104]	DYSD-CD	SAG1 (3′-half)	PT-RS	200	42.2	360	86.30
Yamada, et al.	2011	[66]	DYSD-CD	SAG1 (3′-half)	PT-RS	100	7.5	72	33.00
Inokuma, et al.	2014	[136]	DYSD-SEDC	SED1	PT-RS-SF+CTec2	100	13.6	96	68.77
Guirimand, et al.	2016	[106]	DYSD-CD	SED1	PT-RSH	500	5.8	96	79.48
Guirimand, et al.	2016		DYSD-CD	SED1	PT-RSH	500	37.9	96	63.38
Ishii, et al.	2016	[43]	DYSD-CD	Flo428p	PT-INM	100	9.632	216	18.89
Liu, et al.	2016	[62]	DYSD-CD	SED1	PT-RS-SF	100	1.3	96	7.00
Liu, et al.	2016		DYSD-CD	SED1	PT-RS-SF+CTec2	100	18	96	80.00
Liu, et al.	2017	[69]	DYSD-CD	SED1	PT-RS	25	0.8	96	n.r.
Other Studies									
Murai, et al.	1997	[137]	DYSD-CD	SAG1 (3′-half)	n.r.	n.r.	n.r.	n.r.	n.r.
Fukuda, et al.	2007	[111]	DYSD-SEDC	SAG1 (3′-half)	n.r.	n.r.	n.r.	n.r.	n.r.
Lilly, et al.	2009	[71]	JANNASEY-SMFAA	Cwp2	n.r.	n.r.	n.r.	n.r.	n.r.
Kotaka, et al.	2010	[114]	DYSD-SEDC	SAG1 (3′-half)	n.r.	n.r.	n.r.	n.r.	n.r.
Yeasmin, et al.	2011	[110]	DYSD-SEDC	AGA1::AGA2	n.r.	n.r.	n.r.	n.r.	n.r.
Gao, et al.	2017	[109]	DYSD-SEDC	AGA1::AGA2	n.r.	n.r.	n.r.	n.r.	n.r.
Tang, et al.	2017	[113]	DYSD-CD	AGA1::AGA2	n.r.	n.r.	n.r.	n.r.	n.r.

[i] mostly recalculated from the data of the presented studies using Equation (1); [ii] though classified in Pre-Treated lignocellulosic biomass, these feedstock are considered as "first generation" which means that these compete with the food supply thus were not considered during the presentation and visualization of data., [a] distinction from ref. [96]; n.r.-not reported

References

1. Stocker, T.F.; Qin, D.; Plattner, G.-K.; Tignor, M.M.B.; Allen, S.K.; Boschung, J.; Nauels, A.; Xia, Y.; Bex, V.; Midgley, P.M. *Climate Change 2013: The Physical Science Basis: Working Group 1 Contribution to the Fifth Assessment Report of the Intergovernmental Panel on Climate Change*; Cambridge University Press: Cambridge, UK, 2014.
2. Ronzon, T.; Lusser, M.; Klinkenberg, M.; Landa, L.; Lopez, J.S.; M'Barek, R.; Hadjamu, G.; Belward, A.; Camia, A.; Giuntoli, J.; et al. *Bioeconomy Report 2016*; European Commission: Brussels, Belgium, 2017.
3. Langeveld, H.; Sanders, J.; Meeusen, M. *The Biobased Economy: Biofuels, Materials and Chemicals in the Post-Oil Era*; Earthscan LLC: London, UK, 2012.
4. Commission, E. *Innovating for Sustainable Growth: A Bioeconomy for Europe*; European Commission: Brussels, Belgium, 2012.
5. De Jong, E. *Bio-Based Chemicals Value Added Products from Biorefineries*; IEA Bioenergy—Task 42 Biorefinery: Wageningen, The Netherlands, 2012.
6. Lynd, L.R.; Weimer, P.J.; van Zyl, W.H.; Pretorius, I.S. Microbial cellulose utilization: Fundamentals and biotechnology. *Microbiol. Mol. Biol. Rev.* **2002**, *66*, 506–577. [CrossRef] [PubMed]
7. Kricka, W.; Fitzpatrick, J.; Bond, U. Metabolic engineering of yeasts by heterologous enzyme production for degradation of cellulose and hemicellulose from biomass: A perspective. *Front. Microbiol.* **2014**, *5*, 174. [CrossRef] [PubMed]
8. Lynd, L.R.; van Zyl, W.H.; McBride, J.E.; Laser, M. Consolidated bioprocessing of cellulosic biomass: An update. *Curr. Opin. Biotechnol.* **2005**, *16*, 577–583. [CrossRef] [PubMed]
9. Olson, D.G.; McBride, J.E.; Shaw, A.J.; Lynd, L.R. Recent progress in consolidated bioprocessing. *Curr. Opin. Biotechnol.* **2012**, *23*, 396–405. [CrossRef] [PubMed]
10. Van Zyl, W.; Lynd, L.; den Haan, R.; McBride, J. Consolidated bioprocessing for bioethanol production using *Saccharomyces cerevisiae*. In *Biofuels*; Olsson, L., Ed.; Springer: Berlin/Heidelberg, Germany, 2007; Volume 108, pp. 205–235.
11. Chiswell, D.J.; McCaffery, J. Phage antibodies: Will new 'coliclonal' antibodies replace monoclonal antibodies? *Trends Biotechnol.* **1992**, *10*, 80–84. [CrossRef]
12. Scott, J.K.; Smith, G.P. Searching for peptide ligands with an epitope library. *Science* **1990**, *249*, 386–390. [CrossRef] [PubMed]
13. Georgiou, G.; Stathopoulos, C.; Daugherty, P.S.; Nayak, A.R.; Iverson, B.L.; Iii, R.C. Display of heterologous proteins on the surface of microorganisms: From the screening of combinatorial libraries to live recombinant vaccines. *Nat. Biotechnol.* **1997**, *15*, 29. [CrossRef] [PubMed]
14. Little, M.; Fuchs, P.; Breitling, F.; Dübel, S. Bacterial surface presentation of proteins and peptides: An alternative to phage technology? *Trends Biotechnol.* **1993**, *11*, 3–5. [CrossRef]
15. Georgiou, G.; Poetschke, H.L.; Stathopoulos, C.; Francisco, J.A. Practical applications of engineering gram-negative bacterial cell surfaces. *Trends Biotechnol.* **1993**, *11*, 6–10. [CrossRef]
16. Michon, C.; Langella, P.; Eijsink, V.G.H.; Mathiesen, G.; Chatel, J.M. Display of recombinant proteins at the surface of lactic acid bacteria: Strategies and applications. *Microb. Cell Fact.* **2016**, *15*, 70. [CrossRef] [PubMed]
17. Schüürmann, J.; Quehl, P.; Festel, G.; Jose, J. Bacterial whole-cell biocatalysts by surface display of enzymes: Toward industrial application. *Appl. Microbiol. Biotechnol.* **2014**, *98*, 8031–8046. [CrossRef] [PubMed]
18. Desvaux, M.; Dumas, E.; Chafsey, I.; Hébraud, M. Protein cell surface display in gram-positive bacteria: From single protein to macromolecular protein structure. *FEMS Microbiol. Lett.* **2006**, *256*, 1–15. [CrossRef] [PubMed]
19. Lee, S.Y.; Choi, J.H.; Xu, Z. Microbial cell-surface display. *Trends Biotechnol.* **2003**, *21*, 45–52. [CrossRef]
20. Ståhl, S.; Uhlén, M. Bacterial surface display: Trends and progress. *Trends Biotechnol.* **1997**, *15*, 185–192. [CrossRef]
21. Van Bloois, E.; Winter, R.T.; Kolmar, H.; Fraaije, M.W. Decorating microbes: Surface display of proteins on escherichia coli. *Trends Biotechnol.* **2011**, *29*, 79–86. [CrossRef] [PubMed]
22. Wittrup, K.D. Protein engineering by cell-surface display. *Curr. Opin. Biotechnol.* **2001**, *12*, 395–399. [CrossRef]
23. Murai, T.; Ueda, M.; Shibasaki, Y.; Kamasawa, N.; Osumi, M.; Imanaka, T.; Tanaka, A. Development of an arming yeast strain for efficient utilization of starch by co-display of sequential amylolytic enzymes on the cell surface. *Appl. Microbiol. Biotechnol.* **1999**, *51*, 65–70. [CrossRef] [PubMed]

24. Ueda, M.; Tanaka, A. Cell surface engineering of yeast: Construction of arming yeast with biocatalyst. *J. Biosci. Bioeng.* **2000**, *90*, 125–136. [CrossRef]
25. Ueda, M.; Tanaka, A. Genetic immobilization of proteins on the yeast cell surface. *Biotechnol. Adv.* **2000**, *18*, 121–140. [CrossRef]
26. Kondo, A.; Ueda, M. Yeast cell-surface display—Applications of molecular display. *Appl. Microbiol. Biotechnol.* **2004**, *64*, 28–40. [CrossRef] [PubMed]
27. Tanaka, T.; Yamada, R.; Ogino, C.; Kondo, A. Recent developments in yeast cell surface display toward extended applications in biotechnology. *Appl. Microbiol. Biotechnol.* **2012**, *95*, 577–591. [CrossRef] [PubMed]
28. Hasunuma, T.; Kondo, A. Development of yeast cell factories for consolidated bioprocessing of lignocellulose to bioethanol through cell surface engineering. *Biotechnol. Adv.* **2012**, *30*, 1207–1218. [CrossRef] [PubMed]
29. Kuroda, K.; Ueda, M. Arming technology in yeast—Novel strategy for whole-cell biocatalyst and protein engineering. *Biomolecules* **2013**, *3*, 632–650. [CrossRef] [PubMed]
30. Tanaka, T.; Kondo, A. Cell-surface display of enzymes by the yeast *Saccharomyces cerevisiae* for synthetic biology. *FEMS Yeast Res.* **2015**, *15*, 1–9. [PubMed]
31. Ueda, M. Establishment of cell surface engineering and its development. *Biosci. Biotechnol. Biochem.* **2016**, *80*, 1243–1253. [CrossRef] [PubMed]
32. Cherry, J.M.; Hong, E.L.; Amundsen, C.; Balakrishnan, R.; Binkley, G.; Chan, E.T.; Christie, K.R.; Costanzo, M.C.; Dwight, S.S.; Engel, S.R.; et al. Saccharomyces genome database: The genomics resource of budding yeast. *Nucleic Acids Res.* **2012**, *40*, D700–D705. [CrossRef] [PubMed]
33. Wang, Z.; Mathias, A.; Stavrou, S.; Neville, J.D.M. A new yeast display vector permitting free SCFV amino termini can augment ligand binding affinities. *Protein Eng. Des. Sel.* **2005**, *18*, 337–343. [CrossRef] [PubMed]
34. Sato, N.; Matsumoto, T.; Ueda, M.; Tanaka, A.; Fukuda, H.; Kondo, A. Long anchor using Flo1 protein enhances reactivity of cell surface-displayed glucoamylase to polymer substrates. *Appl. Microbiol. Biotechnol.* **2002**, *60*, 469–474. [PubMed]
35. Matsumoto, T.; Fukuda, H.; Ueda, M.; Tanaka, A.; Kondo, A. Construction of yeast strains with high cell surface lipase activity by using novel display systems based on the Flo1p flocculation functional domain. *Appl. Environ. Microbiol.* **2002**, *68*, 4517–4522. [CrossRef] [PubMed]
36. Lamed, R.; Setter, E.; Bayer, E.A. Characterization of a cellulose-binding, cellulase-containing complex in clostridium thermocellum. *J. Bacteriol.* **1983**, *156*, 828–836. [PubMed]
37. Doi, R.H.; Kosugi, A. Cellulosomes: Plant-cell-wall-degrading enzyme complexes. *Nat. Rev. Microbiol.* **2004**, *2*, 541–551. [CrossRef] [PubMed]
38. Artzi, L.; Bayer, E.A.; Morais, S. Cellulosomes: Bacterial nanomachines for dismantling plant polysaccharides. *Nat. Rev. Microbiol.* **2017**, *15*, 83–95. [CrossRef] [PubMed]
39. Mitsuzawa, S.; Kagawa, H.; Li, Y.; Chan, S.L.; Paavola, C.D.; Trent, J.D. The rosettazyme: A synthetic cellulosome. *J. Biotechnol.* **2009**, *143*, 139–144. [CrossRef] [PubMed]
40. Nidetzky, B.; Steiner, W.; Hayn, M.; Claeyssens, M. Cellulose hydrolysis by the cellulases from trichoderma reesei: A new model for synergistic interaction. *Biochem. J.* **1994**, *298*, 705–710. [CrossRef] [PubMed]
41. Kumar, R.; Wyman, C.E. Effects of cellulase and xylanase enzymes on the deconstruction of solids from pretreatment of poplar by leading technologies. *Biotechnol. Prog.* **2009**, *25*, 302–314. [CrossRef] [PubMed]
42. Tabañag, I.D.; Tsai, S.-L. Hemicellulose degradation and utilization by a synthetic *Saccharomyces cerevisiae* consortium. *bioRxiv* **2018**. [CrossRef]
43. Ishii, J.; Okazaki, F.; Djohan, A.C.; Hara, K.Y.; Asai-Nakashima, N.; Teramura, H.; Andriani, A.; Tominaga, M.; Wakai, S.; Kahar, P.; et al. From mannan to bioethanol: Cell surface co-display of β-mannanase and β-mannosidase on yeast *Saccharomyces cerevisiae*. *Biotechnol. Biofuels* **2016**, *9*, 188. [CrossRef] [PubMed]
44. Srikrishnan, S.; Chen, W.; Da Silva, N.A. Functional assembly and characterization of a modular xylanosome for hemicellulose hydrolysis in yeast. *Biotechnol. Bioeng.* **2013**, *110*, 275–285. [CrossRef] [PubMed]
45. Baek, S.-H.; Kim, S.; Lee, K.; Lee, J.-K.; Hahn, J.-S. Cellulosic ethanol production by combination of cellulase-displaying yeast cells. *Enzyme Microb. Technol.* **2012**, *51*, 366–372. [CrossRef] [PubMed]
46. Tsai, S.-L.; Oh, J.; Singh, S.; Chen, R.; Chen, W. Functional assembly of minicellulosomes on the *Saccharomyces cerevisiae* cell surface for cellulose hydrolysis and ethanol production. *Appl. Environ. Microbiol.* **2009**, *75*, 6087–6093. [CrossRef] [PubMed]

47. Kondo, A.; Shigechi, H.; Abe, M.; Uyama, K.; Matsumoto, T.; Takahashi, S.; Ueda, M.; Tanaka, A.; Kishimoto, M.; Fukuda, H. High-level ethanol production from starch by a flocculent *Saccharomyces cerevisiae* strain displaying cell-surface glucoamylase. *Appl. Microbiol. Biotechnol.* **2002**, *58*, 291–296. [CrossRef] [PubMed]
48. Lin, L.; Yan, R.; Liu, Y.; Jiang, W. In-depth investigation of enzymatic hydrolysis of biomass wastes based on three major components: Cellulose, hemicellulose and lignin. *Bioresour. Technol.* **2010**, *101*, 8217–8223. [CrossRef] [PubMed]
49. Carere, C.R.; Sparling, R.; Cicek, N.; Levin, D.B. Third generation biofuels via direct cellulose fermentation. *Int. J. Mol. Sci.* **2008**, *9*, 1342–1360. [CrossRef] [PubMed]
50. Pérez, J.; Muñoz-Dorado, J.; de la Rubia, T.; Martínez, J. Biodegradation and biological treatments of cellulose, hemicellulose and lignin: An overview. *Int. Microbiol.* **2002**, *5*, 53–63. [CrossRef] [PubMed]
51. Zhang, X.-Z.; Sathitsuksanoh, N.; Zhang, Y.H.P. Glycoside hydrolase family 9 processive endoglucanase from clostridium phytofermentans: Heterologous expression, characterization, and synergy with family 48 cellobiohydrolase. *Bioresour. Technol.* **2010**, *101*, 5534–5538. [CrossRef] [PubMed]
52. Qi, M.; Jun, H.-S.; Forsberg, C.W. Characterization and synergistic interactions of fibrobacter succinogenes glycoside hydrolases. *Appl. Environ. Microbiol.* **2007**, *73*, 6098–6105. [CrossRef] [PubMed]
53. Zhang, Y.-H.P.; Lynd, L.R. Toward an aggregated understanding of enzymatic hydrolysis of cellulose: Noncomplexed cellulase systems. *Biotechnol. Bioeng.* **2004**, *88*, 797–824. [CrossRef] [PubMed]
54. Boisset, C.; Pétrequin, C.; Chanzy, H.; Henrissat, B.; Schülein, M. Optimized mixtures of recombinant humicola insolens cellulases for the biodegradation of crystalline cellulose. *Biotechnol. Bioeng.* **2001**, *72*, 339–345. [CrossRef]
55. Zhou, S.; Ingram, L.O. Synergistic hydrolysis of carboxymethyl cellulose and acid-swollen cellulose by two endoglucanases (celz and cely) fromerwinia chrysanthemi. *J. Bacteriol.* **2000**, *182*, 5676–5682. [CrossRef] [PubMed]
56. Boisset, C.; Fraschini, C.; Schülein, M.; Henrissat, B.; Chanzy, H. Imaging the enzymatic digestion of bacterial cellulose ribbons reveals the endo character of the cellobiohydrolase Cel6A from humicola insolens and its mode of synergy with cellobiohydrolase Cel7A. *Appl. Environ. Microbiol.* **2000**, *66*, 1444–1452. [CrossRef] [PubMed]
57. Väljamäe, P.; Sild, V.; Nutt, A.; Pettersson, G.; Johansson, G. Acid hydrolysis of bacterial cellulose reveals different modes of synergistic action between cellobiohydrolase I and endoglucanase I. *Eur. J. Biochem.* **1999**, *266*, 327–334. [CrossRef] [PubMed]
58. Fujita, Y.; Takahashi, S.; Ueda, M.; Tanaka, A.; Okada, H.; Morikawa, Y.; Kawaguchi, T.; Arai, M.; Fukuda, H.; Kondo, A. Direct and efficient production of ethanol from cellulosic material with a yeast strain displaying cellulolytic enzymes. *Appl. Environ. Microbiol.* **2002**, *68*, 5136–5141. [CrossRef] [PubMed]
59. Fujita, Y.; Ito, J.; Ueda, M.; Fukuda, H.; Kondo, A. Synergistic saccharification, and direct fermentation to ethanol, of amorphous cellulose by use of an engineered yeast strain codisplaying three types of cellulolytic enzyme. *Appl. Environ. Microbiol.* **2004**, *70*, 1207–1212. [CrossRef] [PubMed]
60. Kotaka, A.; Bando, H.; Kaya, M.; Kato-Murai, M.; Kuroda, K.; Sahara, H.; Hata, Y.; Kondo, A.; Ueda, M. Direct ethanol production from barley β-glucan by sake yeast displaying aspergillus oryzae β-glucosidase and endoglucanase. *J. Biosci. Bioeng.* **2008**, *105*, 622–627. [CrossRef] [PubMed]
61. Liu, Z.; Inokuma, K.; Ho, S.-H.; Haan, R.d.; Hasunuma, T.; Zyl, W.H.; Kondo, A. Combined cell-surface display- and secretion-based strategies for production of cellulosic ethanol with *Saccharomyces cerevisiae*. *Biotechnol. Biofuels* **2015**, *8*, 1–12. [CrossRef] [PubMed]
62. Liu, Z.; Ho, S.-H.; Sasaki, K.; den Haan, R.; Inokuma, K.; Ogino, C.; van Zyl, W.H.; Hasunuma, T.; Kondo, A. Engineering of a novel cellulose-adherent cellulolytic *Saccharomyces cerevisiae* for cellulosic biofuel production. *Sci. Rep.* **2016**, *6*, 24550. [CrossRef] [PubMed]
63. Liu, Z.; Ho, S.-H.; Hasunuma, T.; Chang, J.-S.; Ren, N.-Q.; Kondo, A. Recent advances in yeast cell-surface display technologies for waste biorefineries. *Bioresour. Technol.* **2016**, *215*, 324–333. [CrossRef] [PubMed]
64. Yamada, R.; Taniguchi, N.; Tanaka, T.; Ogino, C.; Fukuda, H.; Kondo, A. Cocktail delta-integration: A novel method to construct cellulolytic enzyme expression ratio-optimized yeast strains. *Microb. Cell Fact.* **2010**, *9*, 32. [CrossRef] [PubMed]

65. Yamada, R.; Tanaka, T.; Ogino, C.; Fukuda, H.; Kondo, A. Novel strategy for yeast construction using δ-integration and cell fusion to efficiently produce ethanol from raw starch. *Appl. Microbiol. Biotechnol.* **2010**, *85*, 1491–1498. [CrossRef] [PubMed]
66. Yamada, R.; Taniguchi, N.; Tanaka, T.; Ogino, C.; Fukuda, H.; Kondo, A. Direct ethanol production from cellulosic materials using a diploid strain of *Saccharomyces cerevisiae* with optimized cellulase expression. *Biotechnol. Biofuels* **2011**, *4*, 8. [CrossRef] [PubMed]
67. Apiwatanapiwat, W.; Murata, Y.; Kosugi, A.; Yamada, R.; Kondo, A.; Arai, T.; Rugthaworn, P.; Mori, Y. Direct ethanol production from cassava pulp using a surface-engineered yeast strain co-displaying two amylases, two cellulases, and β-glucosidase. *Appl. Microbiol. Biotechnol.* **2011**, *90*, 377–384. [CrossRef] [PubMed]
68. Yamada, R.; Nakatani, Y.; Ogino, C.; Kondo, A. Efficient direct ethanol production from cellulose by cellulase-and cellodextrin transporter-co-expressing *Saccharomyces cerevisiae*. *AMB Express* **2013**, *3*, 34. [CrossRef] [PubMed]
69. Liu, Z.; Inokuma, K.; Ho, S.-H.; den Haan, R.; van Zyl, W.H.; Hasunuma, T.; Kondo, A. Improvement of ethanol production from crystalline cellulose via optimizing cellulase ratios in cellulolytic *Saccharomyces cerevisiae*. *Biotechnol. Bioeng.* **2017**, *114*, 1201–1207. [CrossRef] [PubMed]
70. Ito, J.; Kosugi, A.; Tanaka, T.; Kuroda, K.; Shibasaki, S.; Ogino, C.; Ueda, M.; Fukuda, H.; Doi, R.H.; Kondo, A. Regulation of the display ratio of enzymes on the *Saccharomyces cerevisiae* cell surface by the immunoglobulin g and cellulosomal enzyme binding domains. *Appl. Environ. Microbiol.* **2009**, *75*, 4149–4154. [CrossRef] [PubMed]
71. Lilly, M.; Fierobe, H.-P.; Van Zyl, W.H.; Volschenk, H. Heterologous expression of a clostridium minicellulosome in *Saccharomyces cerevisiae*. *FEMS Yeast Res.* **2009**, *9*, 1236–1249. [CrossRef] [PubMed]
72. Tsai, S.-L.; Goyal, G.; Chen, W. Surface display of a functional minicellulosome by intracellular complementation using a synthetic yeast consortium and its application to cellulose hydrolysis and ethanol production. *Appl. Environ. Microbiol.* **2010**, *76*, 7514–7520. [CrossRef] [PubMed]
73. Wen, F.; Sun, J.; Zhao, H. Yeast surface display of trifunctional minicellulosomes for simultaneous saccharification and fermentation of cellulose to ethanol. *Appl. Environ. Microbiol.* **2010**, *76*, 1251–1260. [CrossRef] [PubMed]
74. Kim, S.; Baek, S.-H.; Lee, K.; Hahn, J.-S. Cellulosic ethanol production using a yeast consortium displaying a minicellulosome and β-glucosidase. *Microb. Cell Fact.* **2013**, *12*, 1–8. [CrossRef] [PubMed]
75. Fan, L.H.; Zhang, Z.J.; Yu, X.Y.; Xue, Y.X.; Tan, T.W. Self-surface assembly of cellulosomes with two miniscaffoldins on *Saccharomyces cerevisiae* for cellulosic ethanol production. *Proc. Natl. Acad. Sci. USA* **2012**, *109*, 13260–13265. [CrossRef] [PubMed]
76. Tsai, S.L.; DaSilva, N.A.; Chen, W. Functional display of complex cellulosomes on the yeast surface via adaptive assembly. *ACS Synth. Biol.* **2013**, *2*, 14–21. [CrossRef] [PubMed]
77. Fan, L.-H.; Zhang, Z.-J.; Mei, S.; Lu, Y.-Y.; Li, M.; Wang, Z.-Y.; Yang, J.-G.; Yang, S.-T.; Tan, T.-W. Engineering yeast with bifunctional minicellulosome and cellodextrin pathway for co-utilization of cellulose-mixed sugars. *Biotechnol. Biofuels* **2016**, *9*, 137. [CrossRef] [PubMed]
78. Belgacem, M.N.; Gandini, A. *Monomers, Polymers and Composites from Renewable Resources*; Elsevier Science: Amsterdam, The Netherlands, 2011.
79. Akpinar, O.; Erdogan, K.; Bostanci, S. Production of xylooligosaccharides by controlled acid hydrolysis of lignocellulosic materials. *Carbohydr. Res.* **2009**, *344*, 660–666. [CrossRef] [PubMed]
80. Moreira, L.R.S.; Filho, E.X.F. Insights into the mechanism of enzymatic hydrolysis of xylan. *Appl. Microbiol. Biotechnol.* **2016**, *100*, 5205–5214. [CrossRef] [PubMed]
81. Van Dyk, J.S.; Pletschke, B.I. Enzyme synergy for enhanced degradation of lignocellulosic waste. In *Advances in Enzyme Biotechnology*; Shukla, P., Pletschke, I.B., Eds.; Springer: New Delhi, India, 2013; pp. 57–65.
82. Vardakou, M.; Katapodis, P.; Topakas, E.; Kekos, D.; Macris, B.J.; Christakopoulos, P. Synergy between enzymes involved in the degradation of insoluble wheat flour arabinoxylan. *Innov. Food Sci. Emerg. Technol.* **2004**, *5*, 107–112. [CrossRef]
83. Sørensen, H.R.; Meyer, A.S.; Pedersen, S. Enzymatic hydrolysis of water-soluble wheat arabinoxylan. 1. Synergy between α-L-arabinofuranosidases, endo-1,4-β-xylanases, and β-xylosidase activities. *Biotechnol. Bioeng.* **2003**, *81*, 726–731. [CrossRef] [PubMed]

84. Sørensen, H.R.; Pedersen, S.; Viksø-Nielsen, A.; Meyer, A.S. Efficiencies of designed enzyme combinations in releasing arabinose and xylose from wheat arabinoxylan in an industrial ethanol fermentation residue. *Enzyme Microb. Technol.* **2005**, *36*, 773–784. [CrossRef]
85. Sørensen, H.R.; Pedersen, S.; Meyer, A.S. Synergistic enzyme mechanisms and effects of sequential enzyme additions on degradation of water insoluble wheat arabinoxylan. *Enzyme Microb. Technol.* **2007**, *40*, 908–918. [CrossRef]
86. Kovacs, K. *Production of Cellulolytic Enzymes with Trichoderma Atroviride Mutants for the Biomass-to-Bioethanol Process*; Lund University: Lund, Sweden, 2009.
87. Adelsberger, H.; Hertel, C.; Glawischnig, E.; Zverlov, V.V.; Schwarz, W.H. Enzyme system of clostridium stercorarium for hydrolysis of arabinoxylan: Reconstitution of the in vivo system from recombinant enzymes. *Microbiology* **2004**, *150*, 2257–2266. [CrossRef] [PubMed]
88. Selig, M.J.; Adney, W.S.; Himmel, M.E.; Decker, S.R. The impact of cell wall acetylation on corn stover hydrolysis by cellulolytic and xylanolytic enzymes. *Cellulose* **2009**, *16*, 711–722. [CrossRef]
89. De Vries, R.P.; Kester, H.C.M.; Poulsen, C.H.; Benen, J.A.E.; Visser, J. Synergy between enzymes from aspergillus involved in the degradation of plant cell wall polysaccharides. *Carbohydr. Res.* **2000**, *327*, 401–410. [CrossRef]
90. Ho, N.W.; Chen, Z.; Brainard, A.P. Genetically engineered saccharomyces yeast capable of effective cofermentation of glucose and xylose. *Appl. Environ. Microbiol.* **1998**, *64*, 1852–1859. [PubMed]
91. Kuyper, M.; Winkler, A.A.; van Dijken, J.P.; Pronk, J.T. Minimal metabolic engineering of *Saccharomyces cerevisiae* for efficient anaerobic xylose fermentation: A proof of principle. *FEMS Yeast Res.* **2004**, *4*, 655–664. [CrossRef] [PubMed]
92. Kuyper, M.; Harhangi, H.; Stave, A.; Winkler, A.; Jetten, M.; De-Laat, W.; Den-Ridder, J.; Op den Camp, H.; van Dijken, J.; Pronk, J. High-level functional expression of a fungal xylose isomerase: The key to efficient ethanolic fermentation of xylose by *Saccharomyces cerevisiae*? *FEMS Yeast Res.* **2003**, *4*, 69–78. [CrossRef]
93. Harhangi, H.; Akhmanova, A.; Emmens, R.; van der-Drift, C.; De-Laat, W.; Van-Dijken, J.; Jetten, M.; Pronk, J.; Op den Camp, H. Xylose metabolism in the anaerobic fungus *Piromyces* sp. Strain E2 follows the bacterial pathway. *Arch. Microbiol.* **2003**, *180*, 134–141. [CrossRef] [PubMed]
94. Karhumaa, K.; Garcia Sanchez, R.; Hahn-Hagerdal, B.; Gorwa-Grauslund, M. Comparison of the xylose reductase-xylitol dehydrogenase and the xylose isomerase pathways for xylose fermentation by recombinant *Saccharomyces cerevisiae*. *Microb. Cell Fact.* **2007**, *6*, 5. [CrossRef] [PubMed]
95. Katahira, S.; Fujita, Y.; Mizuike, A.; Fukuda, H.; Kondo, A. Construction of a xylan-fermenting yeast strain through codisplay of xylanolytic enzymes on the surface of xylose-utilizing *Saccharomyces cerevisiae* cells. *Appl. Environ. Microbiol.* **2004**, *70*, 5407–5414. [CrossRef] [PubMed]
96. Fujita, Y.; Katahira, S.; Ueda, M.; Tanaka, A.; Okada, H.; Morikawa, Y.; Fukuda, H.; Kondo, A. Construction of whole-cell biocatalyst for xylan degradation through cell-surface xylanase display in *Saccharomyces cerevisiae*. *J. Mol. Catal. B Enzym.* **2002**, *17*, 189–195. [CrossRef]
97. Malgas, S.; van Dyk, J.S.; Pletschke, B.I. A review of the enzymatic hydrolysis of mannans and synergistic interactions between β-mannanase, β-mannosidase and α-galactosidase. *World J. Microbiol. Biotechnol.* **2015**, *31*, 1167–1175. [CrossRef] [PubMed]
98. Spivey, H.O.; Ovadi, J. Substrate channeling. *Methods* **1999**, *19*, 306–321. [CrossRef] [PubMed]
99. Sun, J.; Wen, F.; Si, T.; Xu, J.-H.; Zhao, H. Direct conversion of xylan to ethanol by recombinant *Saccharomyces cerevisiae* strains displaying an engineered minihemicellulosome. *Appl. Environ. Microbiol.* **2012**, *78*, 3837–3845. [CrossRef] [PubMed]
100. Wertz, J.L.; Bédué, O. *Lignocellulosic Biorefineries*; EFPL Press: Lausanne, Switzerland, 2013.
101. Harmsen, P.; Huijgen, W.; Bermudez, L.; Bakker, R. *Literature Review of Physical and Chemical Pretreatment Processes for Lignocellulosic Biomass*; 9085857570; Wageningen UR Food & Biobased Research: Wageningen, The Netherlands, 2010.
102. Mosier, N.; Wyman, C.; Dale, B.; Elander, R.; Lee, Y.Y.; Holtzapple, M.; Ladisch, M. Features of promising technologies for pretreatment of lignocellulosic biomass. *Bioresour. Technol.* **2005**, *96*, 673–686. [CrossRef] [PubMed]
103. Matano, Y.; Hasunuma, T.; Kondo, A. Display of cellulases on the cell surface of *Saccharomyces cerevisiae* for high yield ethanol production from high-solid lignocellulosic biomass. *Bioresour. Technol.* **2012**, *108*, 128–133. [CrossRef] [PubMed]

104. Matano, Y.; Hasunuma, T.; Kondo, A. Cell recycle batch fermentation of high-solid lignocellulose using a recombinant cellulase-displaying yeast strain for high yield ethanol production in consolidated bioprocessing. *Bioresour. Technol.* **2013**, *135*, 403–409. [CrossRef] [PubMed]
105. Sakamoto, T.; Hasunuma, T.; Hori, Y.; Yamada, R.; Kondo, A. Direct ethanol production from hemicellulosic materials of rice straw by use of an engineered yeast strain codisplaying three types of hemicellulolytic enzymes on the surface of xylose-utilizing *Saccharomyces cerevisiae* cells. *J. Biotechnol.* **2012**, *158*, 203–210. [CrossRef] [PubMed]
106. Guirimand, G.; Sasaki, K.; Inokuma, K.; Bamba, T.; Hasunuma, T.; Kondo, A. Cell surface engineering of *Saccharomyces cerevisiae* combined with membrane separation technology for xylitol production from rice straw hydrolysate. *Appl. Microbiol. Biotechnol.* **2016**, *100*, 3477–3487. [CrossRef] [PubMed]
107. Katahira, S.; Mizuike, A.; Fukuda, H.; Kondo, A. Ethanol fermentation from lignocellulosic hydrolysate by a recombinant xylose- and cellooligosaccharide-assimilating yeast strain. *Appl. Microbiol. Biotechnol.* **2006**, *72*, 1136–1143. [CrossRef] [PubMed]
108. Haan, R.; Rensburg, E.; Rose, S.H.; Görgens, J.F.; Zyl, W.H. Progress and challenges in the engineering of non-cellulolytic microorganisms for consolidated bioprocessing. *Curr. Opin. Biotechnol.* **2015**, *33*, 32–38. [CrossRef] [PubMed]
109. Gao, G.; Mao, R.-Q.; Xiao, Y.; Zhou, J.; Liu, Y.-H.; Li, G. Efficient yeast cell-surface display of an endoglucanase of aspergillus flavus and functional characterization of the whole-cell enzyme. *World J. Microbiol. Biotechnol.* **2017**, *33*, 114. [CrossRef] [PubMed]
110. Yeasmin, S.; Kim, C.; Park, H.; Sheikh, M.; Lee, J.; Kim, J.; Back, K.; Kim, S. Cell surface display of cellulase activity–free xylanase enzyme on *Saccharomyces cerevisiae* EBY100. *Appl. Biochem. Biotechnol.* **2011**, *164*, 294–304. [CrossRef] [PubMed]
111. Fukuda, T.; Kato-Murai, M.; Kadonosono, T.; Sahara, H.; Hata, Y.; Suye, S.; Ueda, M. Enhancement of substrate recognition ability by combinatorial mutation of β-glucosidase displayed on the yeast cell surface. *Appl. Microbiol. Biotechnol.* **2007**, *76*, 1027–1033. [CrossRef] [PubMed]
112. Haan, R.; Kroukamp, H.; Zyl, J.H.-D.; Zyl, W.H. Cellobiohydrolase secretion by yeast: Current state and prospects for improvement. *Process Biochem.* **2013**, *48*, 1–12. [CrossRef]
113. Tang, H.; Song, M.; He, Y.; Wang, J.; Wang, S.; Shen, Y.; Hou, J.; Bao, X. Engineering vesicle trafficking improves the extracellular activity and surface display efficiency of cellulases in *Saccharomyces cerevisiae*. *Biotechnol. Biofuels* **2017**, *10*, 53. [CrossRef] [PubMed]
114. Kotaka, A.; Sahara, H.; Kuroda, K.; Kondo, A.; Ueda, M.; Hata, Y. Enhancement of β-glucosidase activity on the cell-surface of sake yeast by disruption of SED1. *J. Biosci. Bioeng.* **2010**, *109*, 442–446. [CrossRef] [PubMed]
115. Matsuoka, H.; Hashimoto, K.; Saijo, A.; Takada, Y.; Kondo, A.; Ueda, M.; Ooshima, H.; Tachibana, T.; Azuma, M. Cell wall structure suitable for surface display of proteins in *Saccharomyces cerevisiae*. *Yeast* **2014**, *31*, 67–76. [CrossRef] [PubMed]
116. Wentz, A.E.; Shusta, E.V. A novel high-throughput screen reveals yeast genes that increase secretion of heterologous proteins. *Appl. Environ. Microbiol.* **2007**, *73*, 1189–1198. [CrossRef] [PubMed]
117. Shuler, M.L.; Kargi, F. *Bioprocess Engineering: Basic Concepts*; Prentice Hall: Upper Saddle River, NJ, USA, 2002.
118. Özcan, S.; Johnston, M. Function and regulation of yeast hexose transporters. *Microbiol. Mol. Biol. Rev.* **1999**, *63*, 554–569. [PubMed]
119. André, B. An overview of membrane transport proteins in *Saccharomyces cerevisiae*. *Yeast* **1995**, *11*, 1575–1611. [CrossRef] [PubMed]
120. Bisson, L.F.; Coons, D.M.; Kruckeberg, A.L.; Lewis, D.A. Yeast sugar transporters. *Crit. Rev. Biochem. Mol. Biol.* **1993**, *28*, 259–308. [CrossRef] [PubMed]
121. Wieczorke, R.; Krampe, S.; Weierstall, T.; Freidel, K.; Hollenberg, C.P.; Boles, E. Concurrent knock-out of at least 20 transporter genes is required to block uptake of hexoses in *Saccharomyces cerevisiae*. *FEBS Lett.* **1999**, *464*, 123–128. [CrossRef]
122. Solis-Escalante, D.; van den Broek, M.; Kuijpers, N.G.A.; Pronk, J.T.; Boles, E.; Daran, J.-M.; Daran-Lapujade, P. The genome sequence of the popular hexose-transport-deficient *Saccharomyces cerevisiae* strain EBY.Vw4000 reveals LoxP/Cre-induced translocations and gene loss. *FEMS Yeast Res.* **2015**, *15*. [CrossRef] [PubMed]
123. Hara, K.Y.; Kobayashi, J.; Yamada, R.; Sasaki, D.; Kuriya, Y.; Hirono-Hara, Y.; Ishii, J.; Araki, M.; Kondo, A. Transporter engineering in biomass utilization by yeast. *FEMS Yeast Res.* **2017**, *17*. [CrossRef] [PubMed]

124. Kuijper, S.M. *Engineering of Saccharomyces Cerevisiae for the Production of Fuel Ethanol from Xylose*; Delft University of Technology: Delft, The Netherlands, 2006.
125. Kuyper, M.; Hartog, M.; Toirkens, M.; Almering, M.; Winkler, A.; Van-Dijken, J.; Pronk, J. Metabolic engineering of a xylose-isomerase-expressing *Saccharomyces cerevisiae* strain for rapid anaerobic xylose fermentation. *FEMS Yeast Res.* **2005**, *5*, 399–409. [CrossRef] [PubMed]
126. Lee, S.-M.; Jellison, T.; Alper, H. Systematic and evolutionary engineering of a xylose isomerase-based pathway in *Saccharomyces cerevisiae* for efficient conversion yields. *Biotechnol. Biofuels* **2014**, *7*, 1–8. [CrossRef] [PubMed]
127. Kim, S.R.; Skerker, J.M.; Kang, W.; Lesmana, A.; Wei, N.; Arkin, A.P.; Jin, Y.-S. Rational and evolutionary engineering approaches uncover a small set of genetic changes efficient for rapid xylose fermentation in *Saccharomyces cerevisiae*. *PLoS ONE* **2013**, *8*, e57048. [CrossRef] [PubMed]
128. Demeke, M.; Dietz, H.; Li, Y.; Foulquie-Moreno, M.; Mutturi, S.; Deprez, S.; Den Abt, T.; Bonini, B.; Liden, G.; Dumortier, F.; et al. Development of a D-xylose fermenting and inhibitor tolerant industrial *Saccharomyces cerevisiae* strain with high performance in lignocellulose hydrolysates using metabolic and evolutionary engineering. *Biotechnol. Biofuels* **2013**, *6*, 89. [CrossRef] [PubMed]
129. Zhou, H.; Cheng, J.; Wang, B.; Fink, G.; Stephanopoulos, G. Xylose isomerase overexpression along with engineering of the pentose phosphate pathway and evolutionary engineering enable rapid xylose utilization and ethanol production by *Saccharomyces cerevisiae*. *Metab. Eng.* **2012**, *14*, 611–622. [CrossRef] [PubMed]
130. Lee, S.-M.; Jellison, T.; Alper, H.S. Directed evolution of xylose isomerase for improved xylose catabolism and fermentation in the yeast *Saccharomyces cerevisiae*. *Appl. Environ. Microbiol.* **2012**, *78*, 5708–5716. [CrossRef] [PubMed]
131. Khatun, M.M.; Liu, C.-G.; Zhao, X.-Q.; Yuan, W.-J.; Bai, F.-W. Consolidated ethanol production from jerusalem artichoke tubers at elevated temperature by *Saccharomyces cerevisiae* engineered with inulinase expression through cell surface display. *J. Ind. Microbiol. Biotechnol.* **2017**, *44*, 295–301. [CrossRef] [PubMed]
132. Nakanishi, A.; Bae, J.G.; Fukai, K.; Tokumoto, N.; Kuroda, K.; Ogawa, J.; Nakatani, M.; Shimizu, S.; Ueda, M. Effect of pretreatment of hydrothermally processed rice straw with laccase-displaying yeast on ethanol fermentation. *Appl. Microbiol. Biotechnol.* **2012**, *94*, 939–948. [CrossRef] [PubMed]
133. Murai, T.; Ueda, M.; Kawaguchi, T.; Arai, M.; Tanaka, A. Assimilation of cellooligosaccharides by a cell surface-engineered yeast expressing β-glucosidase and carboxymethylcellulase from aspergillus aculeatus. *Appl. Environ. Microbiol.* **1998**, *64*, 4857–4861. [PubMed]
134. Murai, T.; Yoshino, T.; Ueda, M.; Haranoya, I.; Ashikari, T.; Yoshizumi, H.; Tanaka, A. Evaluation of the function of arming yeast displaying glucoamylase on its cell surface by direct fermentation of corn to ethanol. *J. Ferment. Bioeng.* **1998**, *86*, 569–572. [CrossRef]
135. Kotaka, A.; Sahara, H.; Hata, Y.; Abe, Y.; Kondo, A.; Kato-Murai, M.; Kuroda, K.; Ueda, M. Efficient and direct fermentation of starch to ethanol by sake yeast strains displaying fungal glucoamylases. *Biosci. Biotechnol. Biochem.* **2008**, *72*, 1376–1379. [CrossRef] [PubMed]
136. Inokuma, K.; Hasunuma, T.; Kondo, A. Efficient yeast cell-surface display of exo- and endo-cellulase using the SED1 anchoring region and its original promoter. *Biotechnol. Biofuels* **2014**, *7*, 1–11. [CrossRef] [PubMed]
137. Murai, T.; Ueda, M.; Yamamura, M.; Atomi, H.; Shibasaki, Y.; Kamasawa, N.; Osumi, M.; Amachi, T.; Tanaka, A. Construction of a starch-utilizing yeast by cell surface engineering. *Appl. Environ. Microbiol.* **1997**, *63*, 1362–1366. [PubMed]

© 2018 by the authors. Licensee MDPI, Basel, Switzerland. This article is an open access article distributed under the terms and conditions of the Creative Commons Attribution (CC BY) license (http://creativecommons.org/licenses/by/4.0/).

catalysts

MDPI

Article

Immobilization of *Prunus amygdalus* Hydroxynitrile Lyase on Celite

Paula Bracco, Guzman Torrelo, Sander Noordam, Glenn de Jong and Ulf Hanefeld *

Biokatalyse, Afdeling Biotechnologie, Technische Universiteit Delft, Van der Maasweg 9, 2629 HZ Delft, The Netherlands; paulabracco@gmail.com (P.B.); guzman.torrelo@hotmail.com (G.T.); S.J.Noordam@student.tudelft.nl (S.N.); glenn_de_jong@hotmail.com (G.d.J.)

* Correspondence: u.hanefeld@tudelft.nl; Tel.: +31-15-278-9304

Received: 29 June 2018; Accepted: 13 July 2018; Published: 17 July 2018

Abstract: The hydroxynitrile lyase from *Prunus amygdalus* was immobilized on Celite R-633. The immobilized enzyme could successfully be utilized in buffer saturated MTBE and excellent conversions of benzaldehyde to *R*-mandelonitrile were observed. No leaching occurred. To achieve high enantioselectivities, the suppression of the undesired background reaction was essential. This could be achieved by high enzyme loadings and the tight packing of the immobilized enzymes. When the immobilized enzyme is loosely packed, both the enzyme catalysis and the background reaction accelerates and only a modest enantioselectivity is observed. The enzyme was recycled for up to ten times, with some loss of activity and also enantioselectivity after 5 cycles, independent of packing.

Keywords: biocatalysis; hydroxynitrile lyase; Oxynitrilase; immobilization; Celite; diffusion; cyanohydrin

1. Introduction

In 1837, the first application of a Hydroxynitrile lyase (HNL), namely *Prunus amygdalus* HNL (*Pa*HNL), was reported. In nature, HNLs are an essential part of chemical warfare to defend plants and animals by the release of toxic HCN [1–3]. They achieve this by catalyzing the release of HCN from natural cyanohydrins. Ever since the first report of the reverse reaction, the stereoselective synthesis catalyzed again by *Pa*HNL in 1908, HNLs are the catalyst of choice for the enantioselective synthesis of cyanohydrins. Their use in the laboratory and factory is well established [1–5]. While industrially relevant, the enzyme-catalyzed reaction has two drawbacks, the competing racemic, base-catalyzed chemical reaction and the difficulties with the recycling of the enzyme. Here we describe the immobilization of *Pa*HNL on Celite to address both problems. In this context, we also look at the density of packing the immobilized enzyme.

HNLs and enzymes, in general, have often been immobilized [3,6]. While many successful immobilizations have been described and are applied industrially, a good understanding is still lacking. In comparative studies on the immobilization of HNLs, it was found that Celite as an environmentally benign and food grade carrier is often the carrier of choice. Indeed, Celite is broadly used for the immobilization of many enzymes and successful applications have been described [7–10]. Earlier studies describe many different HNLs on Celite, normally with good success both for stability as well as enantioselectivity [3,11–16]. *Pa*HNL on Celite, however, seems to be the exception. This FAD-containing HNL was immobilized on Celite for the production of pantolactone and even acid resistant mutants did not yield the desirable enantioselectivity of *ee* > 97% [11–13]. This is surprising as a study from 1990 demonstrated excellent stability and also enantioselectivity for *Pa*HNL on Celite in mandelonitrile synthesis [14]. At that stage, enantioselectivity was, however, only determined by optical rotation and not with the more sensitive chromatographic techniques that are currently applied. As it is known that Celite can catalyze the racemic cyanohydrin synthesis, albeit slowly [14,15,17], we set out to carefully evaluate

all parameters that influence the *Pa*HNL on the Celite catalyzed reaction with mandelonitrile as the target molecule (Scheme 1).

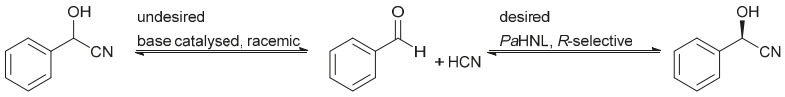

Scheme 1. The *Pa*HNL catalyzes the *R*-selective addition of HCN to benzaldehyde, yielding (*R*)-mandelonitrile; the base catalyzed and racemic reaction needs to be suppressed to achieve high enantiopurity.

2. Results

Celite as a carrier material is versatile and environmentally benign. It is a natural material and exists in countless variations [18]. Unfortunately, the exact Celite type employed for the previous *Pa*HNL immobilization studies was not described [11–14,17]. In this study, Celite R-633 was utilized to ensure comparability with other HNL immobilization studies that described the nature of the carrier [15,16]. Commercial *Pa*HNL was employed, lyophilized and then re-dissolved in a citrate/phosphate buffer at a low pH of 5.4 to suppress the undesired chemical and racemic background reaction. A third of the protein in these samples was estimated to be the desired enzyme, as can be seen in the SDS-PAGE (Figure 1). The same buffer was used to wash the Celite R-633. Reactions were performed in methyl tert. Butyl ether (MTBE). Due to its logP of 1.4, water-immiscible MTBE is particularly suitable for HNL catalysis and thus, is the chosen reaction media [19]. However, it is known that HNLs lose their activity in this dry solvent and for this reason, we usually employ it saturated with buffer [14,20]. Moreover, MTBE dissolves HCN well and a 1.5 M HCN solution in MTBE is used as it is easy-to-handle and thus a safe source of cyanide [15,16].

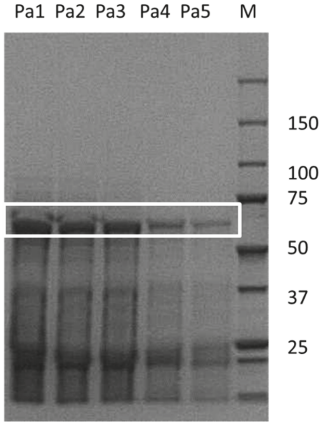

Figure 1. The purity determination was performed with Genetool software according to manufactures instruction of *Pa*HNL on a sodium dodecyl sulfate–polyacrylamide gel electrophoresis (SDS-PAGE) gel. The white box indicates the enzyme. Sample M is the marker, Pa1 to Pa5 are different concentrations of commercial samples of *Pa*HNL utilized in this study.

As the reaction system, the immobilized *Pa*HNL on Celite R-633 was utilized in a teabag to ensure straightforward recycling. The teabag was a standard paper teabag, any brand can be used. Buffer saturated MTBE with HCN was the solvent, with this single phase system the chemical background reaction is essentially suppressed in the solvent. Moreover, MTBE is much safer than the commonly

used diisopropyl ether since it forms essentially no explosive peroxides [21,22]. Additionally, the enzyme is insoluble in water immiscible organic solvents and thus, the leaching of the catalysts is highly unlikely. Indeed, a leaching study revealed that no activity could be detected after the teabag with the immobilized enzyme was removed from the reaction mixture halfway through the reaction (Figure 2). Deliberately, a very high enzyme loading was used in the experiment to ease the detection of leaching. Additionally, the carrier material was evaluated for its catalytic activity in the racemic reaction. As reported earlier [14,15,17], in this case, a slow reaction catalyzed by the buffer washed Celite R-633 tightly packed in a teabag was observed, approximately 5% in 5 h. This implies that the desired enantiopurities of *ee* > 97% can only be obtained if the *Pa*HNL catalyzed reaction clearly outperforms the background reaction.

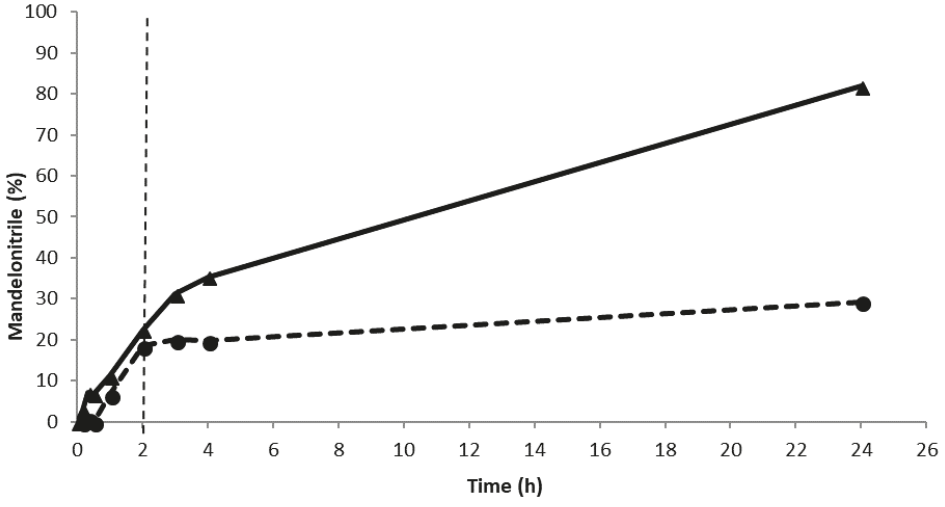

Figure 2. The leaching assays for *Pa*HNL. Conditions: benzaldehyde (±106 mg, 1 mmol), 2 ml HCN solution in methyl tert. Butyl ether (MTBE) (1.5 M), 1,3,5-triisopropylbenzene (±25 mg, internal standard) and a small, tightly packed teabag filled with *Pa*HNL immobilized on 50 mg Celite R-633 (9.2 U/mg). The reaction was stirred at 900 rpm at room temperature. ▲ and the solid line is the continuous reaction, ● and the dashed line is the reaction where the teabag with an immobilized enzyme was removed after 2 h.

Careful examination of the literature reveals that similar background reactions have been reported for Celite before [14,15,17] and that the best enantiopurity (*ee* ~97, albeit at only 37% conversion) was achieved when a high enzyme loading of 0.86 U *Pa*HNL per mg of Celite was utilized [13]. In the other studies, the lower enzyme loadings were used because higher loadings yielded no advantage [14]. This indicates that different types of Celite were used in these studies. If the surface area of the carrier is smaller, full coverage will already occur at lower loading. In the initial study [14], only 0.65 U/mg of Celite was used, which represents an overload for the particular Celite used in that study. Already, at a ratio of 0.25 U/mg of Celite, no improvements in the rate were noticed, at 1 U/mg of Celite, a loss of the rate was reported, signifying the diffusional limitations in that case [14]. The experiments described here were performed with Celite R-633 that had been used successfully for the immobilization of other HNLs [16]. Preliminary experiments with Celite R-633 revealed that above 2.6 U/mg, no significant improvements in the rate were observed and that at 6.5 U/mg, the same rate and enantioselectivity (*ee* = 89%) were measured (Figure 3). Clearly, the type of Celite presented in this study is favorable for *Pa*HNL immobilization, enabling good conditions to suppress the background reaction. To ensure this even further, the Celite R-633 was washed with

50 mM pH 5.4 citrate/phosphate buffer prior to immobilization. Furthermore, the *Pa*HNL was either desalted prior to the lyophilization and immobilization, or the immobilized enzyme on Celite was washed extensively in buffer saturated MTBE.

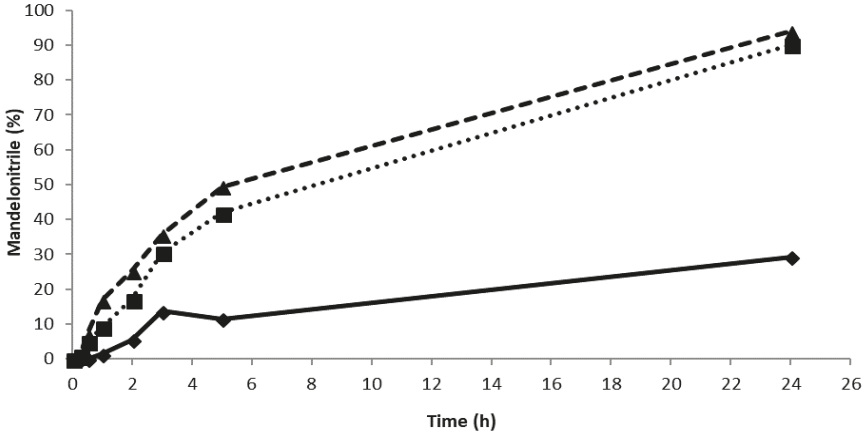

Figure 3. The synthesis of mandelonitrile using *Pa*HNL with different enzyme/support ratios. Conditions: benzaldehyde (±106 mg, 1 mmol), 2 mL HCN solution in MTBE (1.5 M), 1,3,5-triisopropylbenzene (±25 mg, internal standard) and a small, tightly packed teabag filled with *Pa*HNL-immobilized on Celite R-633. The teabags contained 50 mg of Celite with an enzyme/support ratio of 1 U/mg (◆ and solid line; final *ee* = 81%), 2.6 U/mg (■ and dotted line; final *ee* = 89%) and 6.5 U/mg (▲ and dashed line; final *ee* = 89%). The solution was stirred at 900 rpm at room temperature.

The *Pa*HNL was immobilized on Celite R-633 and then packed into teabags and a magnetic stirrer bar was attached [16]. As the catalyst recycling studies can easily lead to misinterpretations if the reactions are left too long [23], the conversion and *ee* were determined both after 5 and 24 h (Figure 4). This is based on the observation that after 5 h, no complete conversion was reached while it was achieved after 24 h. If a loss of activity is observed, this should be immediately visible at the shorter reaction time. In both cases, enantioselectivities of *ee* = 94–95% were observed. However, to our surprise, we noticed an increase in the reaction rate over the first five cycles at the short reaction times and only then observed a slow decrease (Figure 4a). Commonly a decrease in activity is observed due to a deactivation of the enzyme. Earlier the treatment of the immobilized enzymes between cycles had been shown to cause changes in activity, in particular, deactivation [16]. Here the *Pa*HNL was always in a buffer saturated MTBE, ruling out any influence of the steps between cycles. It was, however, noticed that the tight packing of the Celite immobilized enzyme became looser during the progress of the recycling study. This could induce an improved accessibility of the enzyme in the center of the initially tightly packed bag. After 24 h of reaction time, no loss of activity was observed over ten cycles, albeit a decrease of enantioselectivity from an *ee* = 94–95% during the first 6 cycles to 84% in the 10th cycle took place. This might again point to a better accessibility of all of the particles in the bag as the Celite is then also more accessible, catalyzing the undesired, racemic background reaction (Scheme 1). To maintain activity throughout the cycles it was essential to keep the immobilized enzyme in the buffer saturated solvent and never allow it to dry.

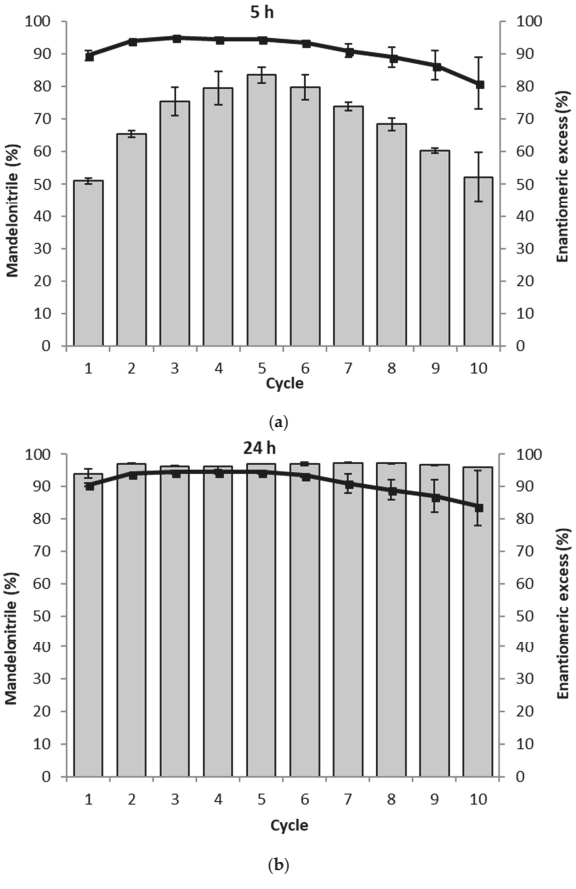

Figure 4. The recycling of the *Pa*HNL immobilized on Celite in ten successive mandelonitrile synthesis reactions. The assay was performed in duplo and the average of both results is shown. The gray bars represent the conversion to mandelonitrile (%) and ■ and the solid line represent the enantiomeric excess (%). Conditions: benzaldehyde (±106 mg, 1 mmol), 2 mL·HCN solution in MTBE (1.5 M), 1,3,5-triisopropylbenzene (±25 mg, internal standard) and a small, tightly packed teabag filled with the *Pa*HNL immobilized on Celite R-633 (6.5 U/mg; 50 mg), stirred at 900 rpm at room temperature. Remarks: before the reaction of cycle 6, the teabag was stored in the fridge over the weekend. (**a**) Results after 5 h; (**b**) Results after 24 h.

To probe the influence of the packing of the *Pa*HNL immobilized on Celite R-633 the study was repeated with loosely packed particles. As in the earlier experiments, 6.5 U/mg were utilized, however, the particles could now freely move in the teabag and consequently, any diffusional effect between the particles could be ruled out. Indeed, this clearly was the case (Figure 5). The reaction proceeded much faster. After 2 h, a high conversion of >80% was observed. From the third cycle onwards, this slowly decreased to approximately 50% in the 10th cycle. This trend can be explained by the gradual deactivation of the enzyme. After 5 h, essentially the full conversion was observed and this remained for 5 cycles and then gradually declined. Diffusion as a factor of influence on the reaction was removed and the conversion was improved a lot. Examining the enantiomeric purity of the products, these experiments do, however, also reveal a downside: throughout the recycling experiments, the *ee* was ~75%, independent of the cycle or reaction time. Not only was the *Pa*HNL

catalyzed formation of *R*-mandelonitrile much faster, the racemic background reaction catalyzed by the Celite was possibly accelerated as well. Background reactions performed with loosely packed Celite supported this observation. Instead of a 5% conversion in 5 h with tightly packed Celite, a conversion of more than 13% was observed.

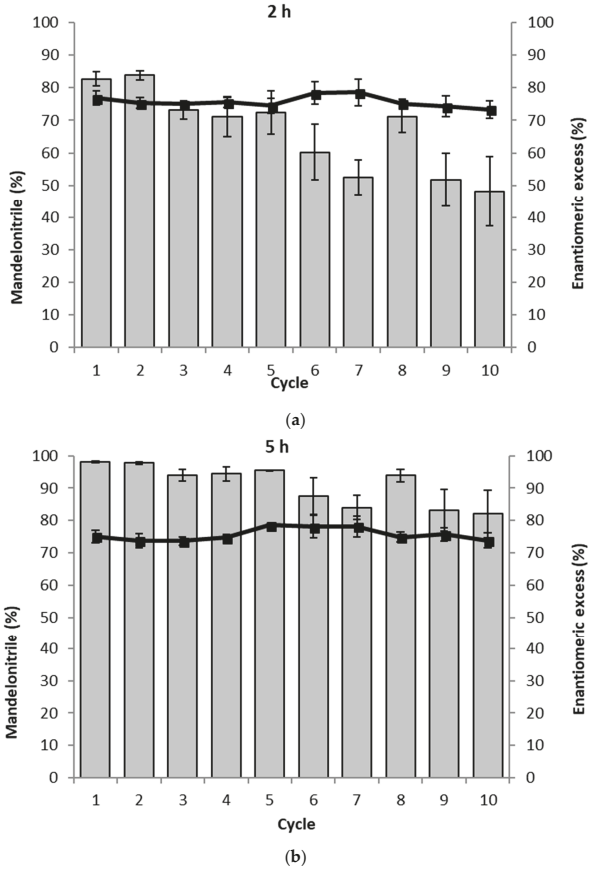

Figure 5. The recycling of the loosely packed *Pa*HNL immobilized on Celite in ten successive mandelonitrile synthesis reactions. The assay was performed in duplo and the average of both results is shown. The gray bars represent the conversion to mandelonitrile (%) and ■ and the solid line represent the enantiomeric excess (%). Conditions: benzaldehyde (±106 mg, 1 mmol), 2 mL·HCN solution in MTBE (1.5 M), 1,3,5-triisopropylbenzene (±25 mg, internal standard) and a small, loosely packed teabag filled with the *Pa*HNL immobilized on Celite R-633 (6.5 U/mg; 50 mg), stirred at 900 rpm at room temperature. (**a**) Results after 2 h; (**b**) Results after 5 h.

3. Discussion

Celite as a carrier material is safe and straightforward to use. Many HNLs have successfully been immobilized on Celite. Additionally, *Pa*HNL is readily immobilized on Celite and stable to use. Earlier work and our current study clearly demonstrate that *Pa*HNL can be used repeatedly and quickly. Furthermore, good conversions are observed even under stringent test conditions, i.e., short reaction times. When it comes to enantioselectivity, a remarkable deviation from the behavior of other HNLs that were immobilized on Celite was noted. *Pa*HNL clearly has difficulties in competing with the

undesired background reaction. Here it is in particular noteworthy that this is greatly influenced by the packing of the Celite. Tight packing that hinders diffusion also suppresses the undesired background reaction. Under these conditions, the overall reaction is slowed but the *ee* of 95% is close to the desired enantiopurity of the product. This bodes well for continuous reactions, as the materials will be tightly packed and might explain the very good optical purities reported earlier [14].

4. Materials and Methods

4.1. Chemicals and Enzymes

All chemicals were bought from Sigma Aldrich (Schnelldorf, Germany). Benzaldehyde was distilled under nitrogen before use. *rac*-Mandelonitrile was purified with flash column chromatography. Commercial *Pa*HNL was purchased from Jülich Fine Chemicals (Jülich, Germany). The enzyme activity was determined according to a previously described assay based on the decomposition of *rac*-Mandelonitrile [24]. An HCN-solution in MTBE was prepared as previously described [16]. The HCN solution was titrated to determine the concentration of HCN. This was done by adding 1 mL of the HCN solution to 5 mL of 2 M NaOH in a 25 mL Erlenmeyer. The mixture was stirred for 2 min. Then a small amount of potassium chromate was added as an indicator. The solution was titrated with 0.1 M silver nitrate. The cyanide will react 1:1 with the silver and will precipitate. If there are no cyanide ions left in the mixture, the mixture will change color [25]. The HCN solution was found to be 1.5–2.0 M and will be referred to as 1.5 M.

4.2. Immobilization

A total of 2 g of Celite R-633 was washed on a Büchner funnel with 15 mL 50 mM pH 5.4 citrate/phosphate buffer. Next, the Celite R-633 was dried overnight over molecular sieves in a desiccator under vacuum. Commercial *Pa*HNL was either lyophilized or desalted (to remove buffer) and then lyophilized. A given number of U *Pa*HNL were redissolved in 600 µL 50 mM pH 5.4 citrate/phosphate buffer. This solution was added to 250 mg Celite R-633 and was dried over molecular sieves in a desiccator under vacuum.

Packing the *Pa*HNL: Two methods were used for packing the *Pa*HNL, utilizing paper teabags. Any paper or nylon teabag can be used, but it was noticed that those paper teabags which contain nylon can be sealed easily and are more robust. Alternatively, the nylon bags as described in Reference [16] can be employed. All teabags were washed with MilliQ and acetone and dried in a desiccator under vacuum overnight. Both methods used a small bag which entrapped the 50 mg celite with an enzyme/support ratio of 6.5 U/mg or as shown in Figures 2 and 3. A magnetic stirring bar was packed into a small but separate bag. Next, the bag containing the enzyme was attached to the bag with the magnetic stirring bar. If *Pa*HNL was not desalted prior to lyophilization, the enzyme packages were placed in a vial containing a buffer saturated MTBE (50 mM pH 5.4 citrate/phosphate buffer) for 4 d, while stirring 900 rpm to equilibrate. The buffer saturated MTBE was refreshed 8 times during these 4 d to ensure a stable pH value.

Method A (Figure 6a): a teabag for the entrapment of the enzyme and magnetic stirring bar was utilized. A small piece of string was used to tie the bags together. The enzyme on the carrier was tightly packed allowing for no movements of the particles.

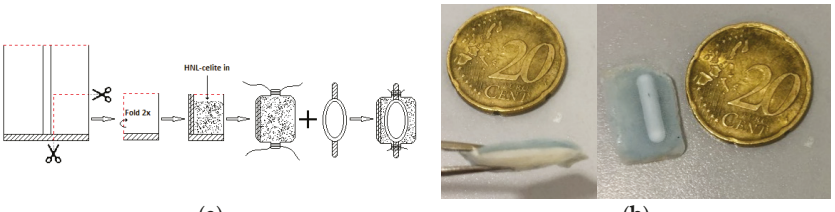

Figure 6. (**a**) the packing of Celite immobilized *Pa*HNL in a tightly packed bag; (**b**) Loosely packed Celite immobilized *Pa*HNL; two bags (one with the enzyme, the other with the stirrer bar) are attached to each other.

Method b (Figure 6b): as above, a teabag for the entrapment of the immobilized enzyme was utilized. Celite particles were loosely packed, allowing movement of the particles. This bag with the enzyme was sealed together with a blue nylon bag containing the magnetic stirring bar. With both methods, no leaking of the solid material was observed.

4.3. Leaching Assay

To check for possible leaching of the enzyme out of the enzyme package, 2 mandelonitrile synthesis reactions were performed in parallel. The only difference between the two reactions is that the enzyme package was removed from the reaction mixture after 2 h at approximately 20% conversion, whereas the enzyme package in the other reaction mixture remained present. The reaction conditions were *Pa*HNL immobilized on 50 mg Celite R-633 (9.2 U/mg) packed according to method A, benzaldehyde (±106 mg, 1 mmol), HCN solution in MTBE (1.5 M), 1,3,5-triisopropylbenzene (±25 mg, internal standard), the stirring speed was 900 rpm, and the reaction was performed at room temperature. Small samples (10 µL) were taken at regular intervals and were analyzed as described below in the Section 4.6 analysis. For results, see Figure 2.

4.4. Enzyme/Support Ratio Assay

Three mandelonitrile synthesis reactions were performed to determine the best enzyme/support ratio. The reaction conditions were benzaldehyde (±106 mg, 1 mmol), the HCN solution in MTBE (1.5 M), 1,3,5-triisopropylbenzene (±25 mg, internal standard) and a small, tightly packed teabag filled with *Pa*HNL-immobilized on Celite R-633 packed according to method A, at 900 rpm, at room temperature. The three reactions used different enzyme/support ratios, namely 1 U/mg, 2.6 U/mg and 6.5 U/mg. Small samples (10 µL) were taken at regular intervals and were analyzed as described below in the Section 4.6 analysis. For results, see Figure 3.

4.5. Recyclability Assay

To determine the recyclability of *Pa*HNL on Celite, 10 reaction cycles of mandelonitrile synthesis were performed in duplicate for both the method A and method B packing. In between the cycles, the enzyme packages were washed for 10 s in 2 mL buffer saturated MTBE (50 mM pH 5.4 citrate/phosphate buffer). After washing, the packages are either directly reused or stored in a clean vial with 2.1 mL buffer saturated MTBE (50 mM pH 5.4 citrate/phosphate buffer) if necessary in a fridge at 4 °C overnight. The reaction conditions were benzaldehyde (±106 mg, 1 mmol), a HCN solution in MTBE (1.5 M), 1,3,5-triisopropylbenzene (±25 mg, internal standard), a packed teabag filled with *Pa*HNL-immobilized on Celite R-633 with enzyme/carrier ratio 6.5 U/mg, packed according to method A or B, and stirred at 900 rpm at room temperature. Small samples (10 µL) were taken at regular intervals and were analyzed as described below in the Section 4.6 analysis. For results, see Figures 4 and 5.

4.6. Analysis

The 10 µL sample was added to 990 µL heptane:2-propanol 95:5 in an Eppendorf tube of 1.5 mL. A small amount of 97% pure anhydrous $MgSO_4$ was added to the 1.5 mL Eppendorf tube to remove the water from the solution. This Eppendorf tube was then centrifuged for a short period. The supernatant was transferred into a glass HPLC vial and 10 µL was injected into the HPLC (LC-20AD (Shimadzu, Kyoto, Japan) liquid chromatograph and a SPD-20A UV-VIS detector (Shimadzu, Kyoto, Japan). The HPLC had an auto-sampler (SIL-20AC (Shimadzu, Kyoto, Japan)) HT auto-sampler (Shimadzu, Kyoto, Japan) at 4 °C and a column (Chiralpak AD-H (Daicel, Osaka, Japan) column). The column oven of the HPLC (CTO-20AC) (Shimadzu, Kyoto, Japan) was set at 40 °C and the UV detection was set at 216 nm and the flow rate was 1 mL/min with the heptane:2-propanol as the mobile phase.

5. Conclusions

*Pa*HNL was successfully immobilized on Celite R-633. The immobilized enzyme can be recycled and it was found that dense packing was essential to achieve good enantioselectivities. This is necessary to suppress the undesired Celite catalyzed background reaction. When the teabag with immobilized enzyme was tightly packed the enzyme could be used 6 times with excellent yields and high enantioselectivity; then a slow decrease of enantioselectivity was observed.

6. Patents

There are no patents resulting from the work reported in this manuscript.

Author Contributions: U.H. conceived the overall study. Together with G.T. and G.d.J. the first series of experiments were conceived and designed; G.d.J. performed them. The second series was conceived by P.B. and designed together with S.N. S.N. then performed them and added control experiments. All authors analyzed the data; with a special emphasis on P.B. for the final analysis; additionally, S.N wrote the experimental part; U.H. wrote the overall paper.

Funding: BE-BASIC; grant number FES-0905 to P.B. and G.T.

Acknowledgments: Generous financial support from BE-BASIC; grant number FES-0905 to P.B. and also G.T. is gratefully acknowledged.

Conflicts of Interest: The authors declare no conflict of interest. The founding sponsors had no role in the design of the study; in the collection, analyses, or interpretation of data; in the writing of the manuscript, and in the decision to publish the results.

References

1. Dadashipour, M.; Asano, Y. Hydroxynitrile Lyases: Insights into Biochemistry, Discovery, and Engineering. *ACS Catal.* **2011**, *1*, 1121–1149. [CrossRef]
2. Steiner, K.; Glieder, A.; Gruber-Khadjawi, M. Cyanohydrin Formation/Henry Reaction. In *Biocatalysis in Organic Synthesis 2*; Faber, K., Fessner, W.-D., Turner, N.J., Eds.; Thieme: Stuttgart, Germany, 2015; Chapter 2.1.1; pp. 1–30. ISBN 9783131741714.
3. Hanefeld, U. Immobilisation of hydroxynitrile lyases. *Chem. Soc. Rev.* **2013**, *42*, 6308–6321. [CrossRef] [PubMed]
4. Holt, J.; Hanefeld, U. Enantioselective Enzyme-Catalysed Synthesis of Cyanohydrins. *Curr. Org. Synth.* **2009**, *6*, 15–37. [CrossRef]
5. Bracco, P.; Busch, H.; von Langermann, J.; Hanefeld, U. Enantioselective synthesis of cyanohydrins catalysed by hydroxynitrile lyases—A review. *Org. Biomol. Chem.* **2016**, *14*, 6375–6389. [CrossRef] [PubMed]
6. DiCosimo, R.; McAuliffe, J.; Poulose, A.J.; Bohlmann, G. Industrial use of immobilized enzymes. *Chem. Soc. Rev.* **2013**, *42*, 6437–6474. [CrossRef] [PubMed]
7. Mendiola, J.; García-Cerrada, S.; de Frutos, Ó.; Luz de la Puente, M. Robust Enzymatic Resolution of 3-Fluoromandelic Acid with Lipase PS Supported on Celite. *Org. Process Res. Dev.* **2012**, *16*, 1312–1316. [CrossRef]

8. Imanparast, S.; Hamedi, J.; Faramarzi, M.A. Enzymatic esterification of acylglycerols rich in omega-3 from flaxseed oil by an immobilized solvent-tolerant lipase from *Actinomadura sediminis* UTMC 2870 isolated from oil-contaminated soil. *Food Chem.* **2018**, *245*, 934–942. [CrossRef] [PubMed]
9. Basso, A.; Ducret, A.; Gardossi, L.; Lortie, R. Synthesis of octyl glucopyranoside by almond-glucosidase adsorbed onto Celite R-640®. *Tetrahedron Lett.* **2002**, *43*, 2005–2008. [CrossRef]
10. Basso, A.; Spizzo, P.; Toniutti, M.; Ebert, C.; Linda, P.; Gardossi, L. Kinetically controlled synthesis of ampicillin and cephalexin in highly condensed systems in the absence of a liquid aqueous phase. *J. Mol. Catal. B Enzym.* **2006**, *39*, 105–111. [CrossRef]
11. Synoradzki, L.; Rowicki, T.; Włostowski, M. Calcium Pantothenate. Part 2.1 Optimisation of Oxynitrilase-Catalysed Asymmetric Hydrocyanation of 3-Hydroxy-2,2-dimethylaldehyde: Synthesis of (*R*)-Pantolactone. *Org. Process Res. Dev.* **2006**, *10*, 103–108. [CrossRef]
12. Effenberger, F.; Eichhorn, J.; Roos, J. Enzyme catalyzed addition of hydrocyanic acid to substituted pivalaldehydes—A novel synthesis of (*R*)-pantolactone. *Tetrahedron Asymmetry* **1995**, *6*, 271–282. [CrossRef]
13. Pscheidt, B.; Liu, Z.; Gaisberger, R.; Avi, M.; Skranc, W.; Gruber, K.; Griengl, H.; Glieder, A. Efficient Biocatalytic Synthesis of (*R*)-Pantolactone. *Adv. Synth. Catal.* **2008**, *350*, 1943–1948. [CrossRef]
14. Wehtje, E.; Adlercreutz, P.; Mattiasson, B. Formation of C-C bonds by mandelonitrile lyase in organic solvents. *Biotechnol. Bioeng.* **1990**, *36*, 39–46. [CrossRef] [PubMed]
15. Okrob, D.; Paravidino, M.; Orru, R.V.A.; Wiechert, W.; Hanefeld, U.; Pohl, M. Hydroxynitrile Lyase from *Arabidopsis thaliana*: Identification of Reaction Parameters for Enantiopure Cyanohydrin Synthesis by Pure and Immobilized Catalyst. *Adv. Synth. Catal.* **2011**, *353*, 2399–2408. [CrossRef]
16. Torrelo, G.; van Midden, N.; Stloukal, R.; Hanefeld, U. Immobilized Hydroxynitrile Lyase: A Comparative Study of Recyclability. *ChemCatChem* **2014**, *6*, 1096–1102. [CrossRef]
17. Costes, D.; Wehtje, E.; Adlercreutz, P. Hydroxynitrile lyase-catalyzed synthesis of cyanohydrins in organic solvents Parameters influencing activity and enantiospecificity. *Enzym. Microb. Technol.* **1999**, *25*, 384–391. [CrossRef]
18. Hanefeld, U.; Gardossi, L.; Magner, E. Understanding enzyme immobilisation. *Chem. Soc. Rev.* **2009**, *38*, 453–468. [CrossRef] [PubMed]
19. Bauer, M.; Griengl, H.; Steiner, W. Parameters influencing stability and activity of a *S*-hydroxynitrile lyase from *Hevea brasiliensis* in two-phase systems. *Enzym. Microb. Technol.* **1999**, *24*, 514–522. [CrossRef]
20. Paravidino, M.; Sorgedrager, M.J.; Orru, R.V.A.; Hanefeld, U. Activity and Enantioselectivity of the Hydroxynitrile Lyase *Me*HNL in Dry Organic Solvents. *Chem. Eur. J.* **2010**, *16*, 7596–7604. [CrossRef] [PubMed]
21. Little, C.J.; Dale, A.D.; Whatley, J.A.; Wickings, J.A. Methyl tert.-butyl ether: A new chromatographic eluent. *J. Chromatogr.* **1979**, *169*, 381–385. [CrossRef]
22. Naito, M.; Radcliffe, C.; Wada, Y.; Hoshino, T.; Liu, X.; Arai, M.; Tamura, M. A comparative study on the autoxidation of dimethyl ether (DME) comparison with diethyl ether (DEE) and diisopropyl ether (DIPE). *J. Loss Prev. Process Ind.* **2005**, *18*, 469–473. [CrossRef]
23. Simons, C.; Hanefeld, U.; Arends, I.W.C.E.; Sheldon, R.A.; Maschmeyer, T. Noncovalent Anchoring of Asymmetric Hydrogenation Catalysts on a New Mesoporous Aluminosilicate: Application and Solvent Effects. *Chem. Eur. J.* **2004**, *10*, 5829–5835. [CrossRef] [PubMed]
24. Hanefeld, U.; Straathof, A.J.J.; Heijnen, J.J. Study of the (*S*)-hydroxynitrile lyase from *Hevea brasiliensis*: Mechanistic implications. *Biochim. Biophys. Acta* **1999**, *1432*, 185–193. [CrossRef]
25. Van Langen, L.M.; van Rantwijk, F.; Sheldon, R.A. Enzymatic Hydrocyanation of a Sterically Hindered Aldehyde. Optimization of a Chemoenzymatic Procedure for (*R*)-2-Chloromandelic Acid. *Org. Process Res. Dev.* **2003**, *7*, 828–831. [CrossRef]

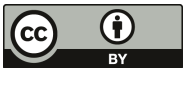

© 2018 by the authors. Licensee MDPI, Basel, Switzerland. This article is an open access article distributed under the terms and conditions of the Creative Commons Attribution (CC BY) license (http://creativecommons.org/licenses/by/4.0/).

MDPI
St. Alban-Anlage 66
4052 Basel
Switzerland
Tel. +41 61 683 77 34
Fax +41 61 302 89 18
www.mdpi.com

Catalysts Editorial Office
E-mail: catalysts@mdpi.com
www.mdpi.com/journal/catalysts

MDPI
St. Alban-Anlage 66
4052 Basel
Switzerland

Tel: +41 61 683 77 34
Fax: +41 61 302 89 18

www.mdpi.com

ISBN 978-3-03897-319-5